



CISM COURSES AND LECTURES NO. 406
INTERNATIONAL CENTRE FOR MECHANICAL SCIENCES

AMST '99

ADVANCED MANUFACTURING SYSTEMS AND TECHNOLOGY

FIFTH INTERNATIONAL CONFERENCE ON
ADVANCED MANUFACTURING SYSTEMS
AND TECHNOLOGY
PROCEEDINGS

EDITED BY

ELSO KULJANIC



Springer-Verlag Wien GmbH

CISM COURSES AND LECTURES

Series Editors:

The Rectors of CISM
Sandor Kaliszky - Budapest
Mahir Sayir - Zurich
Wilhelm Schneider - Wien

The Secretary General of CISM
Giovanni Bianchi - Milan

Executive Editor
Carlo Tasso - Udine

The series presents lecture notes, monographs, edited works and proceedings in the field of Mechanics, Engineering, Computer Science and Applied Mathematics.

Purpose of the series is to make known in the international scientific and technical community results obtained in some of the activities organized by CISM, the International Centre for Mechanical Sciences.

INTERNATIONAL CENTRE FOR MECHANICAL SCIENCES

COURSES AND LECTURES - No. 406



AMST '99

ADVANCED MANUFACTURING
SYSTEMS AND TECHNOLOGY

PROCEEDINGS OF THE
FIFTH INTERNATIONAL CONFERENCE

EDITED BY

ELSO KULJANIC
UNIVERSITY OF UDINE



Springer-Verlag Wien GmbH

La presente pubblicazione è stata stampata
con il contributo del Consorzio Universitario del Friuli

This volume contains 485 illustrations

This work is subject to copyright.
All rights are reserved,
whether the whole or part of the material is concerned
specifically those of translation, reprinting, re-use of illustrations,
broadcasting, reproduction by photocopying machine
or similar means, and storage in data banks.

© 1999 by Springer-Verlag Wien
Originally published by Springer-Verlag Wien New York in 1999
SPIN 10729169

In order to make this volume available as economically and as
rapidly as possible the authors' typescripts have been
reproduced in their original forms. This method unfortunately
has its typographical limitations but it is hoped that they in no
way distract the reader.

ISBN 978-3-211-83148-9 ISBN 978-3-7091-2508-3 (eBook)
DOI 10.1007/978-3-7091-2508-3

**MATERIALS SCIENCE AND THE SCIENCE
OF MANUFACTURING - INCREASING PRODUCTIVITY
MAKING PRODUCTS MORE RELIABLE AND LESS EXPENSIVE**

ORGANIZERS

University of Udine - Faculty of Engineering - Department of
Electrical, Managerial and Mechanical Engineering - Italy
Centre International des Sciences Mécaniques, CISM - Udine - Italy
University of Rijeka - Technical Faculty - Croatia

CONFERENCE VENUE

CISM - PALAZZO DEL TORSO
Piazza Garibaldi, 18 - UDINE - Italy

PREFACE

Manufacturing a product is not difficult, the difficulty consists in manufacturing a product of high quality, at low cost and rapidly.

Profound changes will occur in manufacturing in the near future. The competitive environment for manufacturing will be significantly different in the next twenty or thirty years. Major changes will occur in a number of different areas such as education, customers, economics-global and national, agreements and relationships among nations, the workforce and social conditions.

The International Conference on Advanced Manufacturing Systems and Technology – AMST is held every third year. The First International Conference on Advanced Manufacturing Systems and Technology AMST'87 was held in Opatija (Croatia) in October 1987. The Second International Conference on Advanced Manufacturing Systems and Technology AMST'90 was held in Trento (Italy) in June 1990, the Third International Conference on Advanced Manufacturing Systems and Technology AMST'93 was held in Udine (Italy) in April 1993 and the Fourth International Conference on Advanced Manufacturing Systems and Technology AMST'96 was held in Udine in September 1996.

The Fifth International Conference on Advanced Manufacturing Systems and Technology – AMST'99 aims at presenting up-to-date information on the latest developments- research results and industrial experience- in the field of machining of conventional and advanced materials, high speed machining, forming, modeling, nonconventional machining processes, new tool materials and tool systems, rapid prototyping, life cycle of products and quality assurance, thus providing an international forum for a beneficial exchange of ideas and furthering a favorable cooperation between research and industry.

Elso Kuljanic

FOREWORD

The dilemma between detailed scientific work and system approach should be overcome.

The aim of Taylorism, now 100 years old, was to increase productivity, reduce process time and reduce time for learning by job division and job simplification. 200 years ago Beckmann, a scientist in Gottingen Germany, differentiated between fine arts and useful arts and described the different crafts in useful arts, calling this description `technology`. The world was split into a cultural and technical world. In this last years a specialist has been created who is able to go deeper and deeper in understanding and creating new insight and knowledge in his limited world.

To have competition and to pressure the communication comparisons have mainly taken place among one kind of specialists in this area of activity and interest. By this procedure, which is also necessary in the future, we are able to achieve more and more knowledge and new solutions in special areas. There are scientific communities, faculties who do not communicate among each other to a remarkable extent. Our organization in enterprises, in governmental administration, at universities and colleges is referring to this perception. Furthermore, our education and training is also referring to this perception. We are creating competing individuals and specialists speechless to their outside world.

In manufacturing, for example, we were concentrating on technology, machines, tooling, processes and materials achieving by this an increasing productivity, cost cutting, quality increase, high income and buying power.

In the 80`s disadvantages came up, when besides cost, price and quality and to some extend flexibility, speed in customer need`s response and ability to learn and adapt were required. The world became global and turbulent.

The specialists were concentrated in departments and many interfaces along the value-added chain were too time and information consuming. Each interface is a loss in time, information, knowledge and know-how. We have explicit and implicit knowledge; the last one can only be raised in direct cooperation and teamwork.

This acknowledgment changed the perception how to manage, structure and organize. The specialist able to communicate with other disciplines is required. It will influence the education at universities and colleges. A professional engineer e.g. should be educated 60% in his specific profession, at least 20% in neighboring discipline and 20% in cultural and ethic questions.

Because of an increasing knowledge in the world, the individual person is losing the understanding of the world; therefore, confidence in the specialists is needed. The former requirements in manufacturing remain valid but speed, innovation, saving of resources and protections of the environment are added.

Management must understand to guide and structure that creativeness and innovation can break through.

An individual and each enterprise must focus on becoming a leading specialist in its field and simultaneously must be able to cooperate with other specialists to form groups for system approach. This must be managed efficiently and effectively in networking and project management.

A manufacturing enterprise will only survive in improving the main factors humane resources, machines, tools, materials, processes, organization, methods, control simultaneously.

A vision (target) and at least one competence (know-how) in a specific field are needed with continuous improvement. For this knowledge management is an ability that is more and more required.

Hans-Jurgen Warnecke

HONOUR COMMITTEE

R. ANTONIONE, President of Giunta Regione Autonoma
Friuli - Venezia Giulia
M. STRASSOLDO DI GRAFFEMBERGO, Rector of the
University of Udine
J. BRNIC, Rector of the University of Rijeka
S. CECOTTI, Mayor of Udine
G. BIANCHI, General Secretary of CISM
S. DEL GIUDICE, Dean of the Faculty of Engineering,
University of Udine
C. MELZI, President of the Associazione Industriali della
Provincia di Udine

SCIENTIFIC COMMITTEE

E. KULJANIC (Chairman), University of Udine, Italy
F. MIANI (Secretary), University of Udine, Italy
N. ALBERTI, University of Palermo, Italy
P. BARIANI, University of Padova, Italy
A. BUGINI, University of Bergamo, Italy
R. CEBALO, University of Zagreb, Croatia
G. CHRISOLOURIS, University of Patras, Greece
M.F. DE VRIES, University of Wisconsin Madison, U.S.A.
R. IPPOLITO, Polytechnic of Torino, Italy
F. JOVANE, Polytechnic of Milano, Italy
I. KATAVIC, University of Rijeka, Croatia
H.J.J. KALS, University of Twente, The Netherlands
F. KLOCKE, T.H. Aachen, Germany
W. KONIG, T.H. Aachen, Germany
F. LE MAITRE, Ecole Nationale Supérieure de Mécanique, France
E. LENZ, Technion, Israel
R. LEVI, Polytechnic of Torino, Italy
B. LINDSTROM, Royal Institute of Technology, Sweden
G. MARINSEK, Centro Ricerche Fiat, Italy
J.A. Mc GEOUGH, University of Edimburg, UK
M.E. MERCHANT, IAMS, Ohio, U.S.A.
G.F. MICHELETTI, Polytechnic of Torino, Italy
B. MILCIC, INAS, Zagreb, Croatia
T. NAKAGAWA, University of Tokyo, Japan
S. NOTO LA DIEGA, University of Palermo, Italy
J. PEKLENIK, University of Ljubljana, Slovenia
H. SCHULZ, T.H. Darmstadt, Germany
G. SPUR, T.U. Berlin, Germany
N.P. SUH, MIT, Mass.. U.S.A.
H.K. TÖNSHOFF, University of Hannover, Germany
K. UEDA, Kobe University, Japan
C.A. VAN LUTTERVELT, University of Delft, The Netherlands
A. VILLA, Polytechnic of Torino, Italy
B.F. VON TURKOVICH, University of Vermont, U.S.A.
H.J. WARNECKE, Fraunhofer Gesellschaft, Germany

ORGANIZING COMMITTEE

E. KULJANIC (Chairman)

F. MIANI (Secretary)

C. BANDERA, G.D. BIANCHI, E. CUM, F. DE BONA, S. FILIPPI,

A. GASPARETTO, M. GIOVAGNONI, S. MIANI, P. PASCOLO,

A. STELLA, C. TASSO, G. CUKOR

SUPPORTING ORGANIZATIONS

Giunta Regione Autonoma Friuli - Venezia Giulia

University of Udine

Fraunhofer Gesellschaft, Germany

Consorzio Universitario del Friuli

Danieli

Comitato per la promozione degli studi tecnico scientifici

Centro Convegni e Accoglienza

ANSALDO

CONTENTS

	Page
Preface	
Foreword <i>by H.J. Warnecke</i>	
Trends in Manufacturing 20th Century Evolution of Basic Machining Technology - an Interpretive Review <i>by M.E. Merchant</i>	1
Machining the Present and the Future <i>by E. Kuljanic</i>	11
Machinery and Systems: a Competitive and Sustainable "High-Tech" Mechatronic Product for Europe. The Role of Research <i>by F. Jovane</i>	25
Product Development Must Consider Environmental Aspects <i>by H. Schulz, A. Atik and E. Schiefer</i>	39
Recent Developments in the Design and Control of Cold Forming Processes <i>by N. Alberti and F. Micari</i>	53
Evaluation of Fully Parallel and Hybrid Kinematics for Advanced Manufacturing Systems <i>by H.K. Tönshoff, G. Gunther and H. Grendel</i>	65
The Concurrent Ecodesign Methodologies Eco Sustainable Technologies for Product and Processes <i>by G.F. Micheletti</i>	81
Dynamic Analysis of Production Processes by Planned Experiments <i>by D. Romano, A. Bertagnolio, and R. Levi</i>	97
Part I - Machining Processes	
Hard Turning with PCBN Tooling <i>by E.J. Brookes, R.D. James, and X. Ren</i>	107
Manufacturing of Magnesium Parts - Machining and Forming <i>by H.K. Tönshoff, B. Karpuschewski and J. Winkler</i>	117
High-Speed Continuous and Discontinuous Machining of Hardened Steel and Hard Cast Iron Using Submicrometer Ceramics on the Basis of Al ₂ O ₃ <i>by A. Krell, P. Blank, L.-M. Berger and V. Richte</i>	125

Influence of the Grinding Process on the Process Behaviour of Cutting Tools <i>by K. Weinert and M. Schneider</i>	137
Chip Formation in Orthogonal Cutting FEM Simulations and Experimental Evidence <i>by E. Ceretti, B. Karpuschewki and J. Winkler</i>	145
Performances of Three Layered Ceramic Composites Inserts for Steel Cutting <i>by S. Lo Casto, V.F. Ruisi, E. Lucchini, O. Sbaizero and S. Maschio</i>	155
Minor Cutting Edge Wear in Finish Turning Operations <i>by C. Borsellino, M. Piacentini and V.F. Ruisi</i>	163
Effect of Microstructure in Ultraprecision Machining of Copper Beryllium Alloys <i>by N.P. Hung, S.W. Lim and Z.W. Zhong</i>	171
Ductile Regime Machining of Metal Matrix Composites <i>by N.P. Hung and Z.W. Zhong</i>	179
Vibration Monitoring and Classification in Centerless Grinding <i>by R. Ippolito, L. Settineri and M. Sciamanda</i>	187
Grind-Hardening Modeling with the Use of Neural Networks <i>by K. Tsirbas, D. Mourtzis, S. Zannis and G. Chryssolouris</i>	197
High Performance Gears Hobbing <i>by S. Durante, M. Comoglio and F. Rabezzana</i>	207
Part II - Optimization and Process Planning	
Automatic Part Geometry and Material Removal Recognition to Optimize the Cutting Conditions along Tool Paths in NC-Milling <i>by K.D. Bouzakis and R. Paraskevopoulou</i>	215
An Integrated Model for Cutting Parameters Optimization and Shop-Floor Scheduling <i>by E.P. Henriques and R.M.D. Mesquita</i>	223
A New CAM/CNC Interface for High Speed Milling <i>by R. Ippolito, L. Iuliano and E. Vezzetti</i>	231
CAPP Software for Tool Selection, Optimization and Tool Life Data Base Adaptation in Turning <i>by G. Cukor and E. Kuljanic</i>	241
Time Weighted Petri Nets for Optimization of a Refrigerator Manufacturing Plant <i>by O. Sawodny and E.P. Hofer</i>	249

Economic Design of Control Charts Considering the Influence of the Tool Wear <i>by C. Gardini, E. Ceretti, G. Maccarini and A. Bugini</i>	257
Optimization of Turning Tool Geometry by Nonlinear Programming <i>by G. Cukor and M. Jurkovic</i>	265
Classification of Features Considering their Machinability and Factory Facilities for Computer Aided Process Planning <i>by K.D. Bouzakis and G. Andreadis</i>	273
Use of Manufacturing Features for Computer Aided Process Planning and Manufacturing System Design. Application to Furnitures Parts of Solid Wood <i>by P. Martin and P.J. Meausoone</i>	281
A Multiple-Criteria Scheduling Method for Planning of Continuous Manufacturing Processes: a Food Industry Case Study <i>by D.A. Mourtzis, E.D. Xeromerites and G.M. Chryssolouris</i>	289
Automatic Extraction of Manufacturing Features from CAD Models for Capp: a Simple and Logical Approach <i>by A.S. Deshpande, K.K. Appunkuttan and V.K. Kustagi</i>	301
A Virtual Lathe for Part Program Verification <i>by E. Lo Valvo</i>	309
A Selection Method of Process Plans Set for Part Types Mix Production <i>by J. Ljubetic and G. Cukor</i>	315
Part III - Forming	
Hot Workability Studies of Nimonic 80A Applied to the Net-Shape Forging of Aerofoil Blades <i>by P.F. Bariani, T. Dal Negro and M. Fioretti</i>	323
Influence of Extrusion Processing Variables on the Microstructure and Mechanical Properties of Aluminum-Lithium Alloy Extrusions <i>by J. Fragomeni</i>	329
Comparison of Measured and Computed Contact Pressure Distribution in Cold Sheet Rolling Process <i>by J. Brnic, M. Canadija and G. Turkalj</i>	337
Optimal DIE Design for Cold Extrusion Processes <i>by R. Di Lorenzo and F. Micari</i>	345
Effectiveness of Numerical Simulation in Avoiding Defects in Hot Extrusion Forging Products <i>by D. Antonelli and A. Barcellona</i>	353

Validation of Predictive Approaches for Ductile Fracture in Cold Extrusion <i>by C. Borsellino and V.F. Ruisi</i>	361
Development of a Design Procedure for Bending Operations <i>by R. Di Lorenzo and L. Fratini</i>	369
Rubber Forming Processes of Thin Sheets <i>by A. Castro, L. Fratini and S. Lo Casto</i>	377
The Use of Artificial Intelligence Techniques to Optimise and Control Injection Moulding Processes <i>by V. Basile, L. Filice and F. Micari</i>	385
Hardness Tests on Damaged Metals <i>by D. Antonelli and D. Romano</i>	393
Analysis of the Tool Loading During Forward Steel Extrusion <i>by V. Stoiljkovic and S. Randjelovic</i>	401
Improving Steel Formability by Cyclic Heat Treating <i>by B. Smoljan</i>	411
Influence of Microstructural Factors on Fatigue Behaviour in HSLA Steel Laminates <i>by M. Dabalà, G. Vedovato and M. Magrini</i>	417
Increased Efficiency Resulting from a Detailed Analysis of the Interface Between Forging and Manufacturing <i>by O. Krimmel, K. Martinsen, K. Tonnessen and F.O. Rasch</i>	427
An Intelligent System for the Determination of the Required Setups and the Associated Clamping Points and Clamping Devices in Milling <i>by K.D. Bouzakis and G. Giannopoulos</i>	437
Stabilization of a Milling Machine Against Chatter <i>by A. Gasparetto M. Giovagnoni E. Kuljanic and F. Miani</i>	445
Automation of a Production Line for Flashless Precision Forging <i>by J. Pilgrim, B. Mussig and B.C. Schmidt</i>	453
Study of A Decision Support Tool for the Automatic Configuration of a Modular Plant <i>by E. Ceretti, C. Giardini and G. Maccarini</i>	461
Part IV - Flexible Manufacturing Systems	
Management of Instant Processes in the Shopfloor <i>by H.K. Tönshoff and G. Masan</i>	469

From Functional to Cellular Manufacturing Systems: Evaluating of Attractiveness <i>by A. De Toni and A. Meneghetti</i>	477
Possibilistic Programming and Gas for Aggregate Production Planning under Vague Information. <i>by S. Fichera, A. La Spada, G. Perrone, V. Grasso and U. La Commare</i>	485
Cost/Benefit Analysis of Implementation of Total Quality Program in Manufacturing <i>by J. Mrsa and B. Smoljan</i>	493
Managing the Buyer-Supplier Interactions the Boundaries of Cooperation <i>by G. Nassimbeni</i>	499
High-Accuracy Postprocessor for Milling Machines <i>by K. Sorby</i>	507
Uncertainty and Information in Cell Formation Problems <i>by A. Donnarumma and M. Pappalardo</i>	515
A Neural Network Approach in Cellular Manufacturing <i>by T. Mikac, M. Jurkovic and Z. Pekic</i>	521
New Mechanisms and New Technologies for the Machine Tools <i>by B. Milcic, T. Udiljak and S. Jakupec</i>	529
Integrated Information System for Order Planning, Control and Cost Estimation in Laser Job Shops <i>by H.K. Tönshoff, A. Ostendorf and C. Peper</i>	537
Part V - Rapid Prototyping and Nonconventional Machining	
An Approach to Selective Laser Sintering (SLS) of Pre-Coated Sands for Shell Moulding <i>by G. Dini, M. Lanzetta, M. Santochi, G. Tantussi and A. Franco</i>	545
Reverse Engineering: from Computer Tomography to Rapid Prototyping <i>by G. Marinsek and S. Paolasini</i>	557
Application of Rapid Tooling for Sheet Metal Forming <i>by A. Gatto</i>	565
Experiences in Rapid Prototyping: Voice Devices for Patients who have Undergone Total Laryngectomy <i>by C. Miani, A.M. Bergamin, A. Staffieri, S. Filippi, F. Miani and M. Zanzero</i>	573
Parametric Investigation of Sheet Laser Bending by Experimental and Numerical Analysis <i>by G. Casalino and A.D. Ludovico</i>	583

A Technological Approach for Selective Laser Sintering by <i>F. Miani, E. Kuljanic and G. Marinsek</i>	591
Optimization of the Process of Laser Cutting of Steel by <i>J. Grum and D. Zuljan</i>	603
A Study on the Correlations Between Machining Parameters and Specimen Quality in WEDM by <i>C. Borsellino, L. Filice, F. Micari and V.F. Ruisi</i>	611
Residual Stresses After Laser Surface Remelting by <i>J. Grum and R. Sturm</i>	619
Surface Strengthening by Water Jet Peening by <i>B.M. Colosimo and M. Monno</i>	627
Robust PID Controller for Continuous Casting Mold Level Control by <i>F. Blanchini, F. Miani, S. Miani and U. Viaro</i>	635
Automatic Alignment of Workpieces for Robotic Manipulation Using a Conveyor Belt and Fixed Flat Fences by <i>R. Caracciolo, P. Gallina and A. Gasparetto</i>	643
A Convergent Algorithm for L2 Optimal MIMO Model Reduction by <i>A. Ferrante, W. Krajewsky, A. Lepschy and U. Viaro</i>	651
Analytical Determination of the Position Loop Gain for CNC Machine Tools by <i>Z. Pandilov and V. Dukovski</i>	659
Part VI - Measuring Data Acquisition, Robotics and Control	
Computer Aided Tolerance Charting by <i>A. Del Taglia and S. Perugini</i>	667
A Data Acquisition System to Monitor and Improve the Pinch and Roll Process of Compressor Blade Manufacture by <i>R.A. Belinski and J.S. Gunasekera</i>	677
The Harmonic Fitting Approach for CMM Measurements Optimization by <i>E. Capello and Q. Semeraro</i>	687
Vision System Calibration and Sub-Pixel Measurement of Mechanical Parts by <i>M. Lanzetta and G. Tantussi</i>	695
Analysis of the Accuracy of the CAD Model Reconstruction of Spiral Bevel Gears by CMM's Digitisation by <i>V. Carbone, E. Savio, J. Yang and L. De Chiffre</i>	703

On a Methodology for Plasma Sprayed Ceramic Coatings Microhardness Measurement by <i>T. Gutema, P. Bracali and R. Groppetti</i>	711
Principles of Torque Measurements for Rotating Microsystems by <i>W. Brenner, G. Haddad, G. Popovic, A. Vujanic, E. Chatzitheodoridis, R. Duffait and P. Wurmsdobler</i>	721
Low-Cost Visual Control For Handling and Assembly of Microsystems by <i>M. Jakovljevic, D. Petrovic, W. Brenner, G. Popovic, E. Chatzitheodoridis, A. Vujanic, R. Martins and E. Fortunato</i>	729
Part VII - Materials and Mechanics	
Stability Analysis of Rotating Discs: the Circular Saw Case by <i>P. Chabrier and P. Martin</i>	737
On the Pressure Distribution at the Contact Between Small End of a Conrod and Gudgeon Pin by <i>F. De Bona, A. Strozzi and P. Vaccari</i>	745
Fatigue in Hard Metals and Cermets - an Important Damage Process in Tool Life Limiting by <i>H.G. Sockel, P. Kindermann, P. Schlund, S. Kursawe, U. Schleinkofer, W. Heinrich and K. Gorting</i>	753
Residual Stresses after Induction Surface Hardening and Grinding by <i>J. Grum</i>	763
Micro-Dynamic Behaviour of as Nanometer Positioning System by <i>S. Zelenika and F. De Bona</i>	771
Employment of Fuzzy Logic Modelling in Quenching of Steel Rods for Reinforced Concrete after Hot Rolling by <i>F. Memola Capece Minutolo, B. Palumbo and V. Sergi</i>	781
High Precision Rotation Mechanism Based on Cross-Spring Pivots: Mathematical Modelling and Laser Triangulation Measurements by <i>F. De Bona, A. Strozzi and S. Zelenika</i>	791
Part VIII - Quality	
End-Of Life Evaluation of Products by <i>T. Andes and W.A. Knight</i>	799
A Method for Estimating the Profitability of a Product Disassembly Operation by <i>S. Das</i>	807
Establishing the Ecodesign Strategy by <i>M. Kljajin</i>	815

Quality Improvement and Design of Experiments: an Industrial Application <i>by E. Gentili, M. Formentelli and G. Trovato</i>	825
Quality Methods for Design of Experiments <i>by F. Galetto</i>	833
Dynamic Inspection Policy in Manufacturing Systems Subjected to Linear Wear Process <i>by M. Braglia, C. Festa and E. Gentili</i>	843
An SPC Approach to the Analysis of Process Capabilities of a Flexible Manufacturing System <i>by M. Russo, D. Freguia, R. Guggia and R. Meneghello</i>	851
Partial Mixed Effects Split-Plot Design under Unknown Spatial Dependence <i>by R. Guseo</i>	859
Some Comments about Run Orders in Performing Two-Level Factorial Designs <i>by C. Mortarino</i>	867
Statistical Economic Design of an X Control Chart <i>by G. Celano and S. Fichera</i>	875
Influencing Factors and Case Studies in Design for Quality Manufacturability <i>by S.K. Das and B. Veerapanini</i>	883
Virtual Learning Environment Based on Advanced Information Technologies: a New Approach Toward Human Empowerment for Total Quality <i>by A. Alto and M. Dassisti</i>	891
Author Index	903

20TH CENTURY EVOLUTION OF BASIC MACHINING TECHNOLOGY
AN INTERPRETIVE REVIEW

M.E. Merchant

Institute of Advanced Manufacturing Cincinnati, OH, USA

KEY WORDS: Machining Technology, Empirical Technology, Science-based Technology, Computer-based Technology

ABSTRACT: Although the machining process came into use in industry at the very beginning of the Industrial Revolution in the late 1700's, no technology capable of describing the physics or mechanics of that process came into being until over 200 years later. Yet such technology is essential to establishment of an engineering basis for determining proper machining parameters for obtaining predictable, high productivity in applying the machining process in practice. Finally, during the 20th century, such technology did begin to evolve. In that period, it has gone through three main stages, namely, development of empirical technology, of science-based (predictive) technology and of computer-based technology. Empirical technology can be said to have had its beginning as an organized process in the late 1890s to early 1900s. Science-based technology began to emerge in the 1940s and computer-based technology in the 1970s. Each of these three stages was ushered in by a key event. The first originated with F. W. Taylor's pioneering engineering research and development of empirical methodology (and empirical equations) for estimating reasonably economic machining conditions. The second stage was initiated largely by Merchant's physics-based modeling and analysis of the basic force system acting between cutting tool, chip and workpiece in a machining process. The third (and major) stage was the "watershed" event of the advent of digital computer technology and its application to manufacturing in general. That enabled computer-based engineering of the machining process and its integration with all of the databases of the full system of manufacturing

Published in: E. Kuljanic (Ed.) *Advanced Manufacturing Systems and Technology*,
CISM Courses and Lectures No. 406, Springer Verlag, Wien New York, 1999.

1. INTRODUCTION

This paper presents a brief overview, of an interpretive nature, of American contributions to the evolution of the basic technology of machining during the 20th century. Such technology is of very considerable importance to the world's manufacturing industry, since machining is by far the most widely used machine-performed process in the manufacture of mechanical products in industrialized countries today. Its economic impact is tremendous. This is due to the fact that today, in those countries, the cost of machining now amounts to more than 15 percent of the total value of all products produced by their entire manufacturing industry, whether or not these products are mechanical.

Industrial performance of the process of the machining of metals came into being with the application of that process during the advent of the Industrial Revolution in the late 1700's. In fact, the prime catalyst of the advent of that Revolution was the development, by Wilkinson, in Britain in 1775, of the capability to bore a large cylinder to an accuracy equal to the thickness of a worn shilling. That made it possible for James Watt to actually produce the steam engine that he had earlier invented.

Initially, of course, machining was an art. No technologies existed that were capable of describing even the rudiments of the physics or mechanics of the machining process. Furthermore, and more importantly at that time, no technologies existed that could provide an engineering basis for determining proper machining parameters (such as cutting speed, feed rate and cutting tool characteristics) for obtaining predictable and high productivity in applying the machining process in practice. The only methods present for the selection of such parameters were the non-technological "trial-and-error-based" ones developed by each individual machinist.

As could be expected, this situation resulted in the average productivity of machining operations being quite low in practice. Fortunately, this fact was of no serious economic consequence at first. However, one would have expected that, by the middle of the 19th century, as machine tools began to be manufactured in significant numbers and machining began to become one of industry's major manufacturing processes, significant efforts would have been instituted to develop technology capable of engineering of efficient machining. Surprisingly enough, however, this did not really begin to evolve for almost another 40 years.

2. EVOLUTION OF MACHINING TECHNOLOGY

In the 20th century, basic technology for engineering of the machining process finally did begin to evolve, going through three main stages in that period. These were:

1. Development of empirical technology, beginning in (or just prior to) the early 1900s.
2. Development of science-based (predictive) technology, beginning in the 1940s.
3. Development of computer-based technology, beginning the 1970s.

Each of these stages was triggered by a key event and, interestingly enough, all three of these stages today co-exist and synergize each other. We will describe and interpret the main character of each of these three stages and discuss the key event that ushered in each.

3. EMPIRICAL TECHNOLOGY

The main characteristic of the machining technology driving this early stage is that it was limited to use of experimental data as its basis. That meant, of course, that the technology was not, by its very nature, truly predictive. Thus it was limited to situations where the ranges of the parameters of the operation to be dealt with closely mimicked those prevailing during the experiments from which the original data was derived.

The pioneering figure who stepped forward to institute successful basic technology for engineering of the machining process was F. W. Taylor. In 1880, he launched and then carried out a massive, wholly factory-based research program at a company known as the Midvale Steel Works -- a program that lasted 26 years. The primary aim of his research, as stated by him, was to establish technology that could answer three main questions asked by machinists, namely:

1. What cutting speed shall I use?
2. What feed shall I use?
3. What cutting tool shall I use ?

That research produced (in addition to much empirical understanding of machining operations) a whole series of empirical equations suitable for use by machinists in the form of slide rules.

4. SCIENCE-BASED TECHNOLOGY

The basic characteristic of science-based technology for the engineering of machining is that it draws on the established natural sciences, and particularly the science of physics, to provide reliable *predictive* tools for such. Such tools can then be used to carry out reliable engineering calculations of the expected behavior or characteristics of a machining process, independent of empirical information.

Development of capability for science-based machining technology was quite dependent on the knowledge and understanding of the nature of the machining process developed by the research on empirical machining technology. A good example of such was the research done by the Ernst-Merchant team at Cincinnati Milling Machine Company (now named Milacron) in the period from 1936 to 1957, which culminated in the creation by Merchant of the initial science-based model of the machining process.

Hans Ernst was the company's Director of Research at that time. He was an inquisitive and imaginative inventor and researcher. Among other things, he was particularly curious about the mechanism by which a cutting tool removes metal from a workpiece; i.e. the process of chip formation. To investigate this, he had previously carried out such activities as studying the action of chip formation through the microscope during cutting and taking high-speed motion pictures of such. He also made photomicrographs of sections through chips still attached to workpieces (obtained by suddenly stopping a cut while in process) such as that shown in Fig. 1. He published the findings of his research in a variety of technical papers, of which his classic paper titled "Physics of Metal Cutting" [2] is typical. As a result of this type of empirical research, he arrived at the concept of the "shear plane" in chip formation, i.e. the very narrow plastic zone ("plane") between the body of the workpiece and the body of the chip that is being removed by the cutting tool.

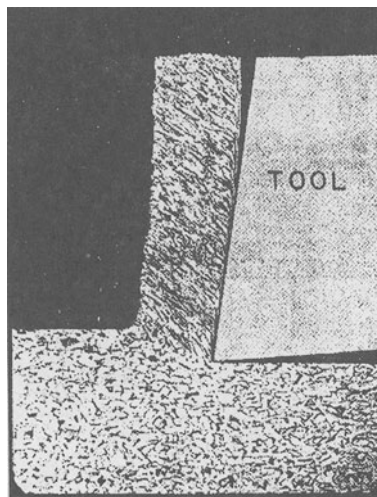


Fig. 1. Photomicrograph of chip formation in machining (Ernst, 1936)

Merchant joined Ernst's staff (as a graduate student in a unique post-graduate cooperative education program at the University of Cincinnati) in 1936, having just graduated from the University of Vermont in Mechanical Engineering.. Ernst asked him to undertake research on the mechanism of chip formation and, in particular, on the mechanism of the sliding friction between the chip and the cutting tool in chip formation.

As Merchant's friction research progressed (resulting, incidentally, in his theory of the nature of friction between chemically clean metal surfaces that is still in use today), he studied, considered and discussed with Ernst the latter's thoughts about chip formation and the empirical "shear plane" model. This led Merchant to reason that the chip could well be considered to be a body in stable mechanical equilibrium between the shear plane and the tool face. He therefore tried applying the science of the mechanics of solid bodies to such a concept. This resulted in the model of the equilibrium force system acting in the chip-tool-workpiece system shown in Figure 2. Combining ("condensing") the two equal and opposing sets of forces into one (based on the equality of the two opposing resultant forces) resulted in the diagram shown in Figure 3. That made it possible to derive the mathematical relationships governing such, as set forth in Merchant's paper "Basic Mechanics of the Metal Cutting Process" [3]. The outcome was thus a science-based, predictive model of the basic process of chip formation – the first of its kind. That made possible engineering calculation of such quantities as the friction force acting between chip and tool, the coefficient of friction there, the shear stress at the shear plane, etc

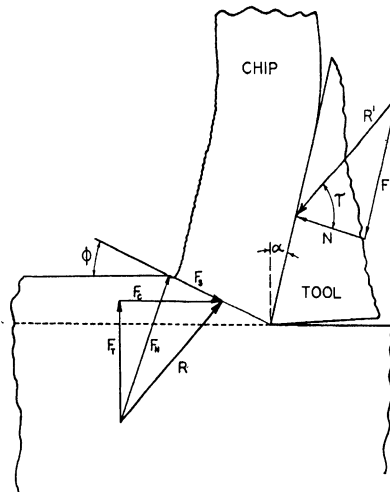


Fig. 2. Equilibrium force system acting on chip during cutting (Merchant, 1944) [3]

The best known and most widely used of these was the equation:

$$VT^n = C \quad (1)$$

where V = cutting speed (m/min)

T = tool life (min)

n = exponent whose value varies somewhat with machine and work material parameters

C = empirical constant whose value depends on the specific machine and work material parameters of the particular operation

This relationship is still widely used today, even though no scientific basis for it appears to have yet been established.

Taylor kept the results of his research secret for 26 years, handling them as proprietary technology that he licensed to client or sponsoring manufacturing companies. Then, in 1906, he published the results of his research in his mammoth paper entitled "On the Art of Cutting Metals." This he presented, in his role as president of the American Society of Mechanical Engineers (ASME), in the form of the President's Annual Address at that Society's 27th Annual Meeting in New York, on December 4, 1906. It was printed in full in the Transactions of the Society [1]. It comprises 248 printed pages, 24 huge foldouts containing tables and curves, and 64 pages of discussion, ending with the author's closure. Some 1,300 persons attended that meeting, requiring the use of the New York Edison Company's auditorium to accommodate the crowd of attendees. Thus the results of his massive research program finally became generally available to the entire manufacturing industry. In the meantime, their application at Midvale, and at his licensed clients and sponsors, had resulted in an increase, on average, of 200-300 percent in the productivity of their machine tools and of 25-100 percent in the pay of their machinists!

As a result of the publication of Taylor's work, a strong effort to continue the development of a broad base of empirical technology for the engineering of the machining process emerged, and then continued unabated through the 1940s. During all of the period from 1906 on, substantial progress was made. In contrast with Taylor's work, the effort was no longer confined almost wholly to industry, but quickly spread to universities as well. Further, and also in contrast with Taylor's work, the effort was marked by increasingly close cooperation between industry and academia. A substantial empirical understanding developed of how to engineer efficient and economic applications of the metal cutting process in practice. A sizable contingent of proficient researchers in this field evolved, in both academia and industry, with their "rallying point" eventually becoming the ASME Research Committee on the Cutting of Metals, organized in 1923. This contingent of researchers could be said to have been the "hard core" of the contributors to the development of this empirical understanding. Then, beginning in the 1940's, a new type of basic machining technology began to evolve, namely science-based technology.

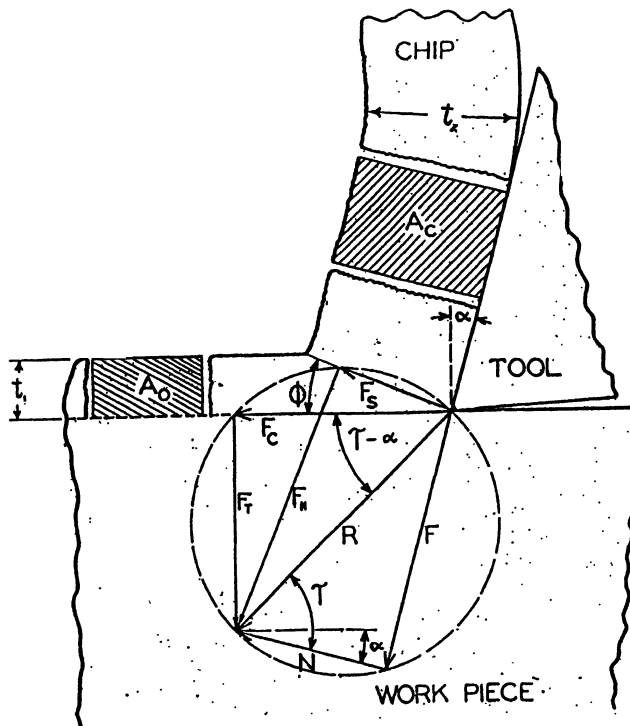


Fig. 3. Condensed form of tool-chip-workpiece force system showing geometrical relationships between force components (Merchant, 1944) [3]

Publication of this initial, basic model suddenly made it clear to those engaged in manufacturing research that a new approach to engineering of the machining process was actually possible, namely that of science-based, predictive, modeling. That discovery thus opened the door to a new era in metal cutting research, that which Komanduri [4] has characterized as “the golden age of metal cutting and grinding research”, lasting from about 1940 to 1960. As a result, a worldwide effort to develop a substantial scientific basis for the engineering of the machining process gradually emerged, and then continued unabated through that whole period. In particular though, it was the academic community that responded, with research on science-based machining technology blossoming handsomely among manufacturing-oriented university researchers and faculty. During the period, substantial progress in developing that science base was made.

5. COMPUTER-BASED TECHNOLOGY

Then, in the 1950s, a watershed event occurred that, in due time, added a still another dimension to the field of basic technology for the engineering of machining operations. This was the advent of digital computer technology. This technology gave the first strong hint of its potential to bring about radical change in the field of machining, by its application to digital control of machine tools in the 1960s. Soon thereafter, it demonstrated powerful capability for engineering the machining process. One of the most important strengths of this new technology, as applied to machining, was its capability to combine both empirical and science-based technology in the engineering of machining operations. In particular, it proved able to simulate the actual ongoing performance of such operations; i.e. it could create "dynamic" models of such. However, of even broader significance was the fact that it provided powerful capability to *integrate* these dynamic models of machining performance with the performance of all of the other components of the overall system of manufacturing, as first envisioned by Merchant [5] (Fig.4).

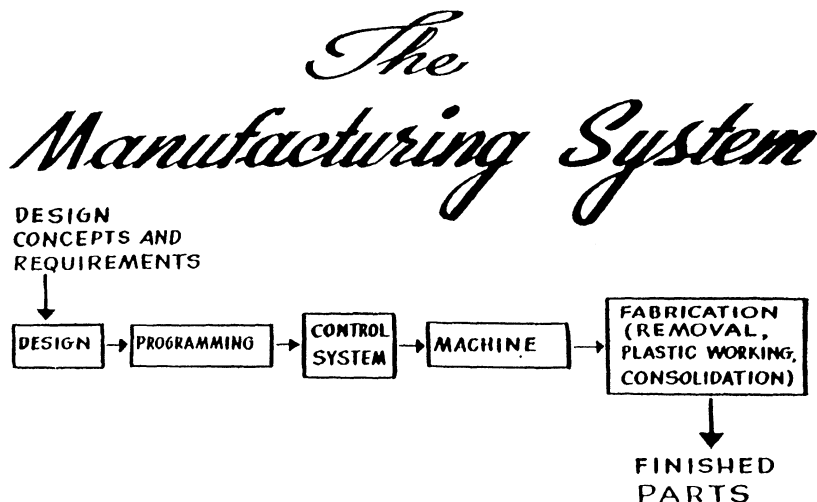


Fig. 4. Initial concept of the computer integrated machining system (1961) [4]

Accomplishment of such integration in industry (which was well along by the early 1970s) enabled the process of performing simulation of machining operations to have full online access to all of the total database of the full system of manufacturing. Such capability greatly enhanced both the accuracy and the speed of computer-based engineering of machining operations. Currently however, the status of computer-based machining simulators is still somewhat rudimentary, generally utilizing a combination of empirical and science-based technology, in the form of empirical data in combination with finite element analysis (FEA). Nevertheless, this does at least enable them to handle fairly complex tool and work material properties, tool/chip interactions and non-linear

geometric boundaries, such as the surface of the chip. It is evident, though, that much more research must be done before the full potential of computer-based engineering of the machining process can be realized.

Finally, it is worthy of note that one further and very important result of the integration of machining process technology with the database of the full system of manufacturing was its enablement of the development of fully automated, integrated systems of machine tools, (which soon came to be known as “flexible manufacturing systems”). This advance, in itself, has already enabled the machining process and its technology to become much more productive than was ever possible in the past.

6. TODAY

Today, the synergistic combination of the three types of basic machining technology is resulting in the rapid development of engineering capability that considerably outstrips that which any one of the three types would be capable of on its own. This is fortunate however, since the rapid development of advanced manufacturing technology, based on digital computer technology, is presenting many new challenges to the practice of machining. These challenges take many forms. Just one example of such is the challenge posed by the fact that, in today's proliferating computer integrated manufacturing enterprises, machine tools are becoming required to run ever more autonomously. Thus, they must become able to autonomously avoid or even correct processing errors or failures while machining is underway. Basic to advancement of such capability is significant increase in the accuracy and realism of machining process engineering. Accomplishment of this will require both increased utilization of the fundamental knowledge, empirical or science-based, created by past research on the basic technology of machining and the creation of new fundamental knowledge of such through continued research on the subject.

REFERENCES

1. Taylor, F. W.: On the Art of Cutting Metals, Transactions, American Society of Mechanical Engineers 28 (1906) 70-350
2. Ernst, H.: Physics of Metal Cutting, Machining of Metals, American Society for Metals, Cleveland, (1938) 1-34
3. Merchant, M.E.: Basic Mechanics of the Metal Cutting Process, Journal of Applied Mechanics 11 (1944) A 168-A 175
4. Komanduri, R.: Machining and Grinding: A Historical Review of the Classical Papers, Applied Mechanics Reviews 46 (1993) 80-132
5. Merchant, M.E.: The Manufacturing System Concept in Production Engineering Research, Annals of the CIRP 10 (1961) 77-83

MACHINING
THE PRESENT AND THE FUTURE

E. Kuljanic
University of Udine, Udine, Italy

KEY WORDS: Machining trends, Near-net-shape, Tool monitoring, Small-scale production

ABSTRACT: This paper discusses the present and the future of machining with a visionary approach in manufacturing challenges. The competitive environment for manufacturing will be significantly different in the near future. Some research trends and developments in tool and tool monitoring, machinability of conventional and new materials, machining for near-net-shape parts, new approach in machining titanium based alloys, high speed machining – high speed hobbing and high speed broaching, nonconventional processes, microfabrication and submicron manufacturing – nanofabrication are presented.

*Which new machining and fabrication
processes will be used depend on
man's imagination.*

The author

1. INTRODUCTION

Nowadays the most advanced and the most expensive machining systems apply the principle of chip formation used 25000 years ago. The tools in Stone Age had a wedge

Published in: E. Kuljanic (Ed.) *Advanced Manufacturing Systems and Technology*,
CISM Courses and Lectures No. 406, Springer Verlag, Wien New York, 1999.

angle β as our modern tools do, Figure 1. Thus nothing has changed in the principle of chip formation.

After milleniums it seems that we can expect revolutionary changes in this field in the next century.

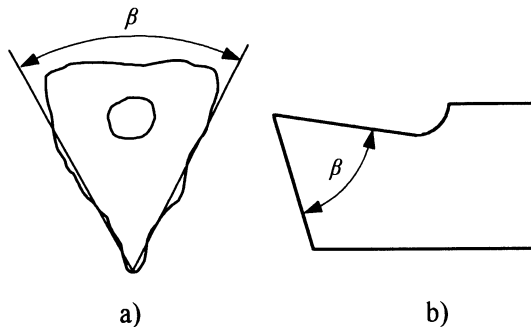


Figure 1. Wedge angle of the a) stone age tool, and b) modern tool

Some research approaches and developments in tool and tool monitoring, machinability of conventional and new materials, machining for near-net-shape parts, new approach in machining titanium based alloys, high speed machining, nonconventional processes and small-scale production and new processes are discussed.

2. TOOL AND TOOL CONDITION MONITORING

The tool has been so important for mankind that a period of time (the Stone Age) was named after the tool. The importance of the tool could be seen from the following maxim:

The profit of a factory "hangs" on the cutting edge.

G. Schlesinger

The effect of tool material on cutting speed is given in Figure 2. It can be seen that the increase of the cutting speed has been approximately thousandfold in the last ninety years. Such an increase of the cutting speed, due to tool material, has had a significant effect on machining cost and product price, i.e. in the standard of living.

Besides tool material the geometry and the concept of the tool affect the efficiency of the machining system. Chip control is very important for efficient operation of unmanned machining systems. Therefore, the research in chip formation, tool geometry, and chipbreaker are of significant importance. Chip grooves control the size and direction of

chips produced during cutting. The inconvenient chip form is the continuous chip, which could roll around the workpiece and tool (turning) and stop the machining. The chip should break away from the workpiece and cutting tool.

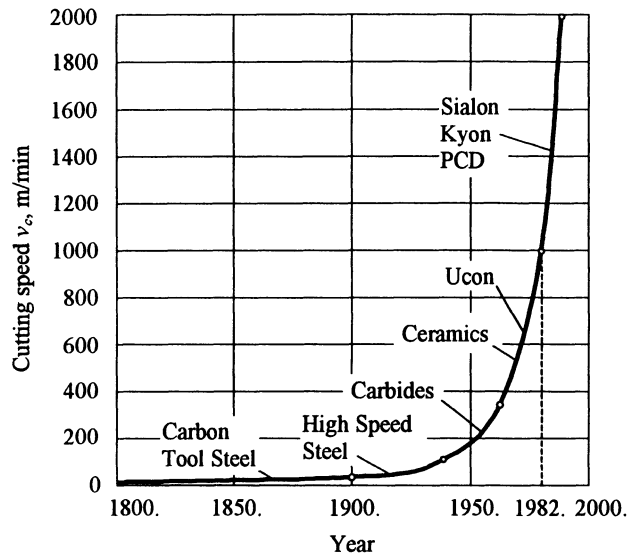


Figure 2. Effect of tool material on cutting speed

By applying grooves as a chip breaker the effective rake angle increases. Since the shear angle increases the chip thickness decreases, and that reduces the cutting force, the generated heat, thus the total energy required in the cut. The cutting temperature is reduced too and the tool life increases.

A significant research is undertaken in the field of substrates, coatings and edge preparation. The cutting edge could be constructed to meet performance criteria set by a new workpiece material or to tackle a particular automotive or aerospace part.

A system approach and optimization of some parts of tool system can be applied [1].

2.1. TOOL CONDITION MONITORING

At present the need to apply tool condition monitoring is more critical than it was once because of the use of unmanned machining systems, where the tool monitors are key elements in the automation package.

Sensors are the front-line troops [2] in this "war" to make a product of high quality at low cost and in a short time. There are different sensors such as laser, vibration, acoustic

emission, horsepower, torque and force sensor in order to indirectly detect disturbances in machining [3]. Unfortunately, after more than thirty years of research into sensor's field, we still do not have a reliable and simple sensor for industrial application, for direct on-line measurement or detection of one of the most important parameter – tool wear.

A new sensor approach based on thin film sensor integration into the coating of a coated carbides insert for turning operation is currently being developed [4]. On Figure 3 is shown the concept of intelligent tool. By applying this concept it is possible to measure the tool wear and the cutting tool temperature during cutting. The approach is based on the development of new thin film sensors, which are integrated into the wear protection coating of a cutting insert.

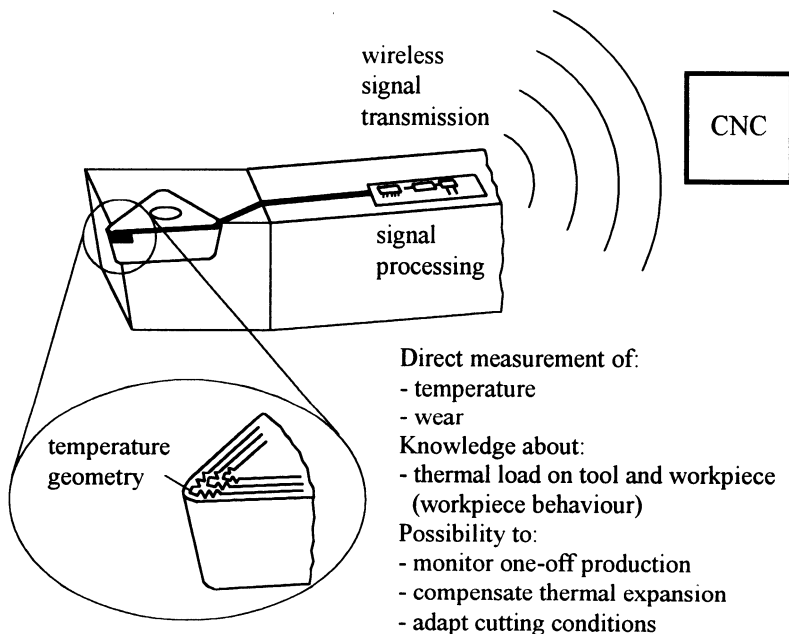


Figure 3. Concept of intelligent tool [4]

The dimensions of the wear zone are monitored on-line using geometrically adapted mesh of strip conductors. The electrical resistance of these structures during the signal processing correlated with their location gives evidence of the wear geometry on the coated carbides insert. Schematics of the sensor layout for the intelligent tool is given on Figure 4, [5], which was developed in Fraunhofer Institute for Coating and Surface Technology (FhG-IST) in Braunschweig in cooperation (consortium) with Fh-IPT in Aachen, Fh-IZM in Berlin and with the Chair of Manufacturing Technology at the Laboratory of Machine Tools and Production Engineering (WZL) at the Technical University Aachen.

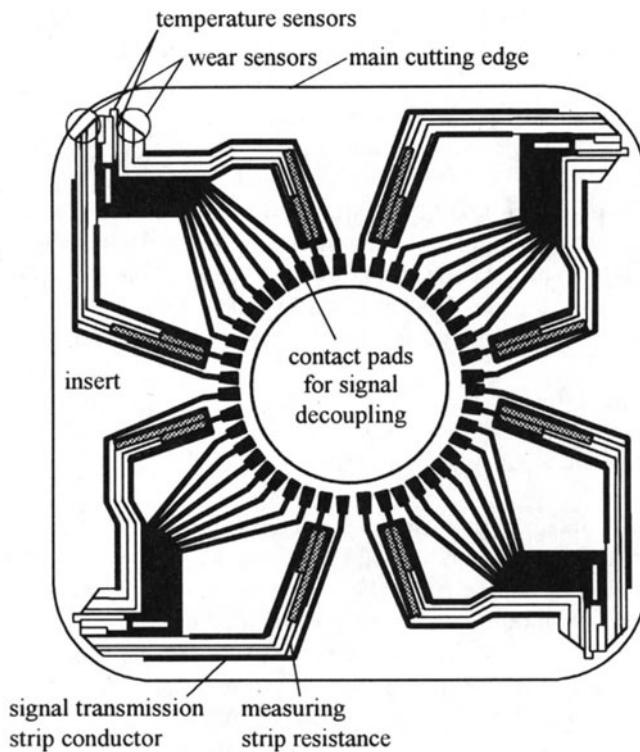


Figure 4. Schematics of the sensor layout for the intelligent tool [5]

To make such a sensor is very difficult since the conditions close to the cutting edge are very severe: rubbing surfaces chip-insert-workpiece at high temperature and high specific pressure could be more than 15000 N/mm^2 . To make such a sensor the solutions have to be found in different fields such as thin-film and surface technology, micro structuring, bonding technology, system and circuit design, signal transmission and processing, cutting technology and cutting process monitoring.

The solution of such intelligent tool would be very practical due to the direct on-line tool wear and temperature measurement, and the possibility for direct on-line process monitoring – optimization and adaptive control.

3. MACHINABILITY OF CONVENTIONAL AND NEW MATERIALS

The old approach used to be to choose a high quality material, i.e. to make a product of high quality regardless of its cost. In our competitive age such an approach is not possible.

Since there are different materials with similar mechanical properties and different machinability, it is better to choose a material with greater machinability. However, there are not many machinability data available due to expensive and long laboratory testing procedures. Also, the reliability of the data is rather low. To increase the reliability, to decrease the testing cost, and to make machinability data more comparable the author, as a chairman of "Milling" W. G. of Scientific Technical Committee "Cutting" of CIRP (Collège international pour l'étude scientifique des techniques de production mécanique) – Paris, proposed to standardize milling testing through CIRP and ISO. The results of this work are two ISO documents: Tool Life Testing in Milling Part 1 – 8682/1 – face milling, and Part 2 – 8682/2 – end milling, 1985. In order to transmit the knowledge in milling from the scientific world to industry the way through ISO was the right one.

In the meantime the conditions in industry have changed rapidly in the last fifteen years that the methodologies given in the ISO documents are not anymore sufficient. There is a need to change the concept in machinability testing.

The author proposed an Integrated Machinability Testing concept – IMT [6] which was presented at MIT (Massachusetts Institute of Technology) in 1997. The IMT concept is an approach in which tool life data and/or tool wear, tool wear images, cutting temperature, machining conditions and significant data as dimensions of the machined workpiece, surface roughness, chip form etc. are registered and analyzed in an intelligent machining system. In practical use all mentioned variables are not indispensable, for example, for rough operation the surface roughness, the dimension changing of machined workpiece and some other variables might not be important to register automatically and to be analyzed. Thus the needed data will be obtained from the machining process in industrial conditions. The reliability of the machinability data will be greater than the data obtained in laboratory conditions. The stiffness of the machining system and other real variables are included. The cutting conditions: cutting speed, feed and depth of cut will be chosen by a computer applying the design of experiments [7]. The tool wear and tool life will be determined by intelligent sensor systems with decision making capabilities as described in [4].

The information obtained from the data analysis can be used for in-process optimization of machining conditions and adaptive control, and for on-line machinability data bank with more reliable data. Such machinability data bank would be self-regenerative and small factories could have a proper machinability data bank.

4. SOME TRENDS IN MACHINING

There are no changes without applying a force. The pushing force to change the machining and manufacturing is the strong competition, i.e. to make a product of high quality at low cost and in a short time.

4.1. MACHINING FOR NEAR-NET-SHAPE PARTS

The emphasis on cost control in manufacturing has led to an increasing use of near-net-shape forgings and castings. Notable examples are found in auto industry.

Near-net-shape parts offer sharply reduced material waste, machining time, energy consumption, i.e. ensuring a product at low cost and to make it in shorter time. The tendency is to use higher quality materials – more expensive materials, hence the reduction of material waste is very important too.

However, machining near-net-shape parts is much more difficult than machining a part from a bar. The main difference between conventional machining and the machining of near-net-shape part is in the shape of cross-section of the chip. The ratio depth of cut a and feed f is different as follows:

- $af \simeq 10$ conventional turning [8],
- $af \ll 10$ machining of near-net-shape part.

The depth of cut is much smaller in near-net-shape machining, and feed could be greater in order to reduce the machining time. Due to the smaller cross-section area of the chip in near-net-shape, the chip bends easily but does not break easily. Also, higher cutting speed can be applied and the heat generated is greater. Therefore, the chip temperature is higher and the chip does not break. Also, the surface roughness or surface irregularities of the near-net-shape part are much greater, and the hardness of the workpiece surface is greater due to the cooling effect etc.

All these factors make the machining near-net-shape parts more difficult. The problem can be solved with the selection of an adequate tool, particularly with special insert geometry, groove geometry and with stronger insert material in order to provide the edge strength needed to handle higher feed rates and withstand part surface irregularities.

4.2. NEW APPROACH IN MACHINING TITANIUM BASED ALLOYS

Low machinability materials such as titanium and nickel based alloys are used for blades, wheels and housing components in the cold and hot sections of gas turbines and aircraft engines. The titanium and nickel based alloys are some of the most difficult materials to be machined due to physical and mechanical properties. Machining is usually done with high speed or carbides tools at low cutting speeds.

According to F. Klocke et al [9] for turning titanium based alloys an alternative is Polycrystalline Cubic Diamond – PCD. Ceramics and Polycrystalline Cubic Boron Nitride – PCBN for nickel based alloys. They can be used at higher cutting speeds than carbides owing to greater hardness and wear resistance. The reliable application in turning these materials depends on the knowledge of machining conditions, cutting speed, feed and depth of cut and the wear and performance behavior.

Milling is tricky and more difficult operation than turning in general. Milling with diamond tools is more difficult due to interrupted cut – entrance and exit conditions of the tooth. The following example shows a great possibility of milling titanium blade with PCD cutter [10, 11].

The workpiece was a very "slim" compressor blade of a gas turbine: 191 mm long, 172 mm wide, and the thickness of the blade was from 1,26 mm to 5,30 mm. From these dimensions it can be seen that the stiffness of the blade was extremely low, thus the stiffness of the machining system was low too. The workpiece material was TiAl6V4 titanium alloy heat treated to 400 HB.

The aim of the research was to determine whether it was possible to use PCD cutter for finishing milling of a "slim" TiAl6V4 compressor blade. The result was unexpected. The tool life of the PCD cutter was $T = 381$ min at cutting speed $v_c = 108$ m/min, feed $f_z = 0,135$ mm, radial depth of cut $a_r = 5$ mm with cooling. The tool life of carbide cutter was approximately $T = 20$ min for the same milling operation of this blade at much lower cutting speed. An explanation for such a long tool life and research results on surface roughness, inclination of the cutter, chip formation and the application of cooling lubricant is given in [11].

This example proves that PCD cutter can be used successfully for milling TiAl6V4 at very low stiffness of the machining system. Also, it is evident that some solutions in machining materials with low machinability could be found by applying new tool materials.

4.3. HIGH SPEED MACHINING

The advantage of high speed machining is well-known and a lot of research is going on in this field. The common opinion is that high speed machining is usually applied in milling and turning. However, high speed machining can be used, for example, in hobbing and in broaching.

High Speed Hobbing

Hobbing is an operation in which the geometrical accuracy is very important. High speed hobbing is dry – without applying coolant due to the protection of the carbides hob. Namely, at the exit of a tooth the coolant can cause damaging thermal shock on the carbides cutting edge.

It is known that chips absorb high amount of heat generated during machining in high speed machining. In hobbing chips absorb more than 80% of the process energy [12]. Approximately 15% of the heat flows into the workpiece and only 5% is taken by the hob. There are some problems that have to be solved in high speed dry hobbing. For example, chips have to be removed from hobbing machine as quick as possible in order to prevent negative effects of the heat, such as distortion of different parts.

The main advantages of high speed dry hobbing are higher productivity and a clean process. Oil mist can cause environmental problems. It is certain that the cost for getting rid of old oil and contaminated chips will increase in the future.

The increase of the cutting speed is approximately tenfold than the cutting speed in conventional hobbing.

High Speed Broaching

Twenty-five years ago the cutting speed was approximately $v_c = 3$ m/min for broaching a gear steel. Today the cutting speed could be $v_c = 60$ m/min using cermets and more.

The comparative performance of High Speed Steel (HSS), micrograine carbides and cermet in broaching prove that cermet is a suitable tool material [13]. Chip formation is much better and without built-up edge in dry broaching with cermet tool at cutting speed $v_c = 66$ m/min. A better surface roughness is obtained as well. The comparison of tool wear of HSS-TiN coated, cemented carbide WC6Co-TiN and cermet uncoated in dry broaching is given in Figure 5. It can be seen that cermet has much longer tool life. The wear resistance of coated tools after resharpening is much lower since the coated layer is taken away. Thus a cermet broach – uncoated has an advantage in comparison with coated tools.

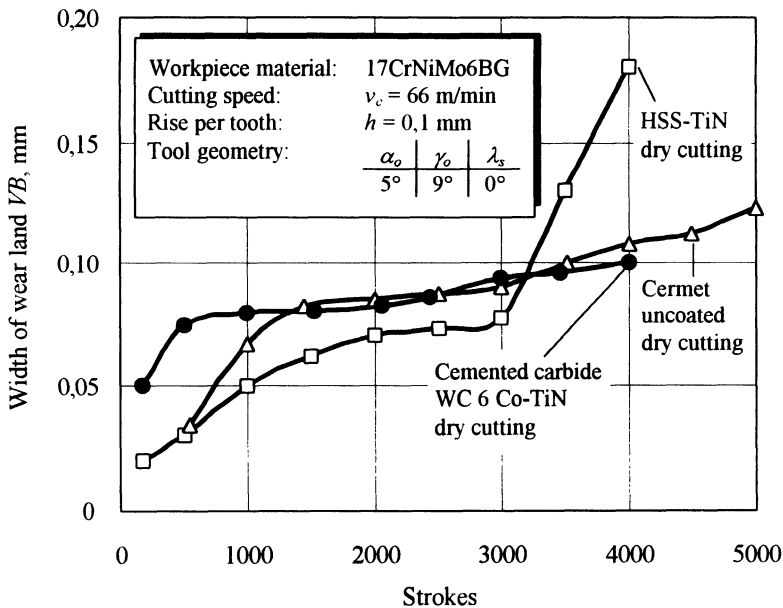


Figure 5. Long tool life of cermet tool in broaching [13]

High speed machining has a great promise for die and mold makers as well as for large workpiece machining in aerospace manufacturing.

5. NONCONVENTIONAL PROCESSES

Some applications of nonconventional processes seem unreal. For example, it is possible to make thousand relief holes on a sealing ring in one second by laser [14]. Laser-based processes can be applied in different areas. At present small companies find some difficulties to use CO₂ and Nd: YAG high-power lasers as machining tools due to complexity, cost and sizes of laser systems. The conditions of the application of high-power lasers may change in the near future.

Controlled metal building (CMB) combines laser deposition welding and high-speed milling [14]. The laser deposition generates near-net-shape buildings of metallic materials. Milling follows the generation of each layer. The laser deposition and milling are performed on the same machining system automatically.

The first hot machining research was done by Max Kronenberg in Cincinnati Milling Machine Co. at the present Cincinnati Milacron in Cincinnati USA approximately sixty years ago. Different heat sources for heating the workpiece can be used such as laser, hot plasma etc. Laser heats the workpiece material locally that has to be removed by cutting. This operation is called laser assisted hot machining – LAM. The increase in temperature softens the material, making it easier to machine. The needed cutting power is lower and cutting speed could be much higher.

Laser assisted hot machining can be used for machining materials with low machinability, for example, advance ceramics. A prototype precision lathe with an integrated high-power diode laser – HPDL has been developed in Germany in close collaboration with industry and Fraunhofer Gesellschaft. The first lathe will be brought onto the market this year.

Each nonconventional process will be suitable for machining some materials and some operations.

6. SMALL-SCALE PRODUCTION AND NEW PROCESSES

The trend toward small-scale production components is already present. Microfabrication and nanofabrication processes will evolve from laboratory to production processes in the near future. Extremely small-scale process building blocks that allow for synthesizing or forming new material forms and products will emerge [15]. Molecular assembly of complex precise functional structures will lead to the development of microdevices, such as sensors, computational elements, medical robots, and macroscopic devices constructed from fundamental building blocks.

An example of microfabrication is deep x-ray lithography using synchrotron radiation [16]. It is possible to make different microstructures made of polymethylmethacrylate – PMMA, such as microgear "negative" shape, Figure 6. Electrodeposition should be used in order to obtain the final "positive" metallic gear. The diametric pitch is 200 μm , the thickness of the gear is 100 μm and the tooth thickness is approximately 20 μm .

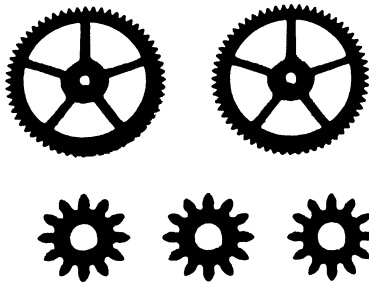


Figure 6. Negative shape of microgear made by deep x-ray lithography using synchrotron radiation [16]

Processes that transform materials into products have changed a little in the last twenty years. The need for revolutionary processes will be driven by the competitive reality in the near future, when the primary differences between manufacturing enterprises will be their ability to create and produce new products rapidly to meet the high expectations and constantly changing demands of customers [15]. The integration of multiple unit processes into a single operation will significantly reduce capital investment, inspection time, handling, and processing time.

Processes that are completely programmable and do not require hard tooling will enable the customization of product and rapid switching from one product to another. Manipulation at the molecular or atomic level will lead to the creation of new materials, eliminate separate joint and assembly operation, and allow material composition to be varied throughout a single part.

Nanofabrication technology includes the following types of processes: nanomachining – in the 0,1 to 100 nm range – to create nanoscale structures by adding or removing material from macroscale components, and molecular manufacturing to build systems from the atomic or molecular level [17].

In the near future revolutionary changes will occur in larger-scale production components too

7 CONCLUSION

In the light of the considerations presented in this paper, we may draw some conclusions.

A system approach and optimization of some parts of the tool as a system should be applied. By application of new substrates, coatings and edge preparation, the tool performance could be improved. The result of new sensor approach based on thin film sensor integration in the coating of a coated carbides insert could be the intelligent tool. With the application of such a tool it would be possible to direct on-line process monitoring – optimization and adaptive control, as well as tool wear and temperature measurements. The application of Integrated Machinability Testing concept – IMT [6] would be much easier with intelligent tool.

Since the application of new materials depends on manufacturing processes, an extensive research in manufacturing processes is needed for such materials.

Near net-shape-parts offer reduced material waste, machining time and energy consumption. The conditions of chip formation in machining near net-shape-parts are more difficult than in conventional machining. Thus a stronger tool material and a particular tool geometry and groove geometry are needed.

Machining of low machinability materials such as titanium based alloys could be expensive and time consuming. Finishing milling titanium based alloys with Polycrystalline Cubic Diamond – PCD cutter on low stiffness machining system gives very good results. The tool life of PCD cutter has increased nineteenfold in comparison to the tool life of a carbides cutter at much lower cutting speed. The application of new tool materials might be a solution for machining some low machinability materials.

High speed machining can be used not only in milling and turning but also in hobbing, broaching and some other operations. The increase of the cutting speed is approximately tenfold when using carbides hob for dry hobbing in comparison to conventional wet hobbing with HSS hob. High speed broaching can be successful by using cermet broach. The cutting speed could be $v_c = 60$ m/min and more compared with $v_c = 3$ m/min for HSS broach twenty-five years ago. High speed machining has a great promise for large workpiece machining, for example, in aerospace manufacturing and for die and mold makers.

Each nonconventional process will be suitable for certain operations and for machining some materials. At present EDM (Electro Discharge Machining) is the best method for machining carbide parts, laser to make thousand relief holes on a sealing ring in one second, laser assisted hot machining for machining advanced ceramics, etc.

In small-scale production – microfabrication and nanofabrication processes will become production processes. Revolutionary changes will occur in large-scale production components too.

REFERENCES

1. Katbi, K.: The Insert as a Cutting System, *Manufacturing Engineering*, Vol. 119/8, 1997, 84-92
2. Meredith, D.: Practical Tool Condition Monitoring, *Manufacturing Engineering*, Vol. 120/1, 1998, 34-39
3. Byrne, G., Dornfeld, D., Inasaki, I., Ketteler, G., König, W., Teti, R.: Tool Condition Monitoring (TCM) – The Status of Research and Industrial Application, *Annals of the CIRP*, Vol. 44/2, 1995, 541-576
4. Klocke, F., Rehse, M.: Intelligent Tools through Integrated Micro Systems, *Production Engineering*, Vol. IV/2, 1997, 65-68
5. Löhken, T.: Unpublished Research Report, Fraunhofer Institute for Coating and Surface Technology (FhG-IST) Braunschweig, 1996
6. Kuljanić, E.: Machinability Testing in the 21st Century – Integrated Machinability Testing Concept, In: *Advanced Manufacturing Systems and Technology*, CISM Courses and Lectures No. 372, Kuljanić, E. (Ed.), ISBN 3-211-82808-7, Springer Verlag, Wien New York, 1996, 23-36
7. Kuljanić, E.: Random Strategy Method for Determining Tool Life Equations, *Annals of the CIRP*, Vol. 29/1, 1980, 351-356
8. Kronenberg, M.: *Machining Science and Application*, Pergamon Press, 1996
9. Klocke, F., König, W., Gerschwiler, K.: Advanced Machining of Titanium – and Nickel-Based Alloys, In: *Advanced Manufacturing Systems and Technology*, CISM Courses and Lectures No. 372, Kuljanić, E. (Ed.), ISBN 3-211-82808-7, Springer Verlag, Wien New York, 1996, 7-21
10. Beltrame, M., Kuljanić, E., Fioretti, M., Miani, F.: Titanium Alloy Turbine Blades Milling with PCD Cutter, In: *Advanced Manufacturing Systems and Technology*, CISM Courses and Lectures No. 372, Kuljanić, E. (Ed.), ISBN 3-211-82808-7, Springer Verlag, Wien New York, 1996, 121-128
11. Kuljanić, E., Fioretti, M., Beltrame, M., Miani, F.: Milling Titanium Compressor Blades with PCD Cutter, *Annals of the CIRP*, Vol. 47/1, 1998, 61-64
12. Sulzer, G.: High-Speed Dry Hobbing, *Manufacturing Engineering*, Vol. 119/5, 1997, 46-52

13. Klocke, F., Pöhls, M.: Broaching with Cermets – Exploiting the Potentials of Modern Cutting Materials, *Production Engineering*, Vol. V/1, 1998, 13-16
14. Bergs, T., Heineman, S.: Laser Claim New Roles in Manufacturing, *Manufacturing Engineering*, Vol. 121/4, 1998, 46-51
15. Visionary Manufacturing Challenges for 2020, National Research Council, Washington D.C., 1998
16. De Bona, F., Matteucci, M., Mohr, J., Pantenburg, F.J., Zelenika, S.: Microfabrication at the Elettra Synchrotron Radiation Facility, In: *Advanced Manufacturing Systems and Technology*, CISM Courses and Lectures No. 372, Kuljanić, E. (Ed.), ISBN 3-211-82808-7, Springer Verlag, Wien New York, 1996, 487-494
17. Nelson, M., Shipbaugh, C.: *The Potential for Nanotechnology for Molecular Manufacturing*, MR-615-RC, Santa Monica, California, Rand Corporation, 1995

**MACHINERY AND SYSTEMS: A COMPETITIVE AND SUSTAINABLE "HIGH-TECH"
MECHATRONIC PRODUCT FOR EUROPE.
THE ROLE OF RESEARCH**

F. Jovane

Institute of Industrial Technologies and Automation (CNR-ITIA), Milan, Italy

KEY WORDS: Manufacturing, Machinery and Systems, Competitive and Sustainable Production

ABSTRACT: Europe is faced with challenge of maintaining its standard of living and welfare in the era of globalization. This calls for competitive and sustainable industrial growth.

Manufacturing Industry has an important role to play for maintaining and generating jobs, directly and through services. It also impacts on sustainable development.

For European Manufacturing Industry, mainly SMEs, -which sustains 120 million jobs- to be competitive and sustainable, products and process innovation is required.

Advanced Machinery and Systems (M&S) can play a very important role. They ensure the competitiveness and sustainability of all Manufacturing sectors and are high-tech "mechatronic" products, holding a leading position on the world market.

The European Machinery and Systems Industry: has a turnover close to that of motor vehicles and parts and much higher than aerospace; is the third in terms of added value; employs, in small and medium size enterprises (SMEs), people - mainly knowledge workers - whose number is as high as that of car industry.

All this calls for an enlightened and strategic research and innovation policy.

To this end a reference model for manufacturing is presented. It shows that strategic innovation of such a diversified "world" as Manufacturing may be achieved by investing in M&S Research on critical transectorial technologies and their sectorial applications.

M&S European Industry is composed of SMEs. It is difficult for them to act strategically, although European and National R&ST Programmes ask for and enable such approach.

At this time it is critical for the strategic survival of M&S European Industry that Research Institutes and Universities play a fundamental role as the M&S "innovation motor", integrated and embedded within the M&S Industrial "fabric" of Europe. An Observatory Network may be a first step.

1. INTRODUCTION

The industrialised world is faced with the challenge of maintaining its high quality of life and welfare in the globalisation era.

A competitive and sustainable industrial growth must be pursued if we want to face, effectively, this challenge.

This requires controlled qualitative and quantitative changes of industrial capacity, which must take place within pervasive mutations in the economic, trade, social world framework.

For instance: appropriate actions must be performed to be competitive, retain employment and reverse its decline in the value generating industrial production sector (MANUFACTURING). This should take place while globalisation leads to opposite changes: economic strategies of companies, as well as their operations, transcend national boundaries.

Manufacturing Industry - products and related processes - has indeed an important role to play. In USA, it has been recognised as:

- fundamental for keeping jobs and generating new ones;
- a source for generating services and, hence, jobs.

This has become a policy guideline and as result of the consequent actions:

- new jobs have been created;
- Machinery Industry is again a great world competitor.

The new policies adopted in USA related to Manufacturing have contributed a new and powerful impulse to world competitive industrial growth.

Manufacturing Industry is, on the other hand, very important in relation to sustainability as it deals heavily with the life cycle of products and related processes (from design, to production, to maintenance and recycling).

To contribute to sustainability, Manufacturing Industry must:

- move towards a closed life cycle of products and its optimisation, a better use of resources (materials, energy, knowledge and skills) and cleaner technologies;
- apply the same concepts to the processes sustaining the life cycle of products (i.e.: from design process to recycling process) and optimise it all.

Manufacturing Industry may thus contribute, by a great deal, to a sustainable development.

2. EUROPE AND MANUFACTURING

The European Manufacturing Industry, covering a high number of sectors, accounts for 40 million jobs. It moreover sustains services employing 80 million people. The added value curve of European Industrial Production, fig. 1, is flat since 1990, whereas the USA curve is rising and the Japan curve is undergoing some problems, but following a long standing rise.

European competitiveness on global market is challenged both by low labour cost and technologically advanced countries

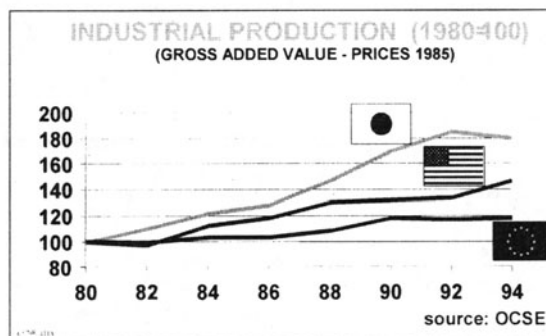


Fig. 1: Evolution of industrial production in the main industrialised regions

To improve the competitiveness of production processes Europe has turned mainly to technology. The positive role of organization and logistics, skills (knowledge workers) is increasingly being exploited.

With reference to products, while USA and Japan show, respectively, computers and consumer electronics as their strongest specialization in export, Europe export specialization shows, high quality and style traditional goods (leather goods and fashion) followed by technological goods (petrochemical and mechanical engineering).

For the European Manufacturing Industry- from large companies to SME - to remain competitive and ensure sustainable growth, products and processes must be, increasingly, innovated. Advanced Machinery and Manufacturing Systems (M&S) can play a very important role. They ensure the competitiveness and sustainability of all Manufacturing sectors. Beside this strategic role, they are "high-tech" mechatronic products, holding a leading position on the world market.

The European Machinery and Systems Industry:

- is the third in terms of added value;
- is the "driving force for technical progress in its customer industry" (as stated in a EU Study);
- has a turnover close to that of motor vehicles and parts and much higher than aerospace, table 1. It employs, in small and medium size enterprises(SMEs), skilled

(knowledge) workers whose number is higher than that of assembly of motor vehicles and parts;

- was born in Europe during the first Industrial Revolution;
- is producer of mechatronic medium-high technology products;
- will help European Manufacturing Industry not delocate.

All this calls for an enlightened and strategic research and innovation policy, in close co-operation between University, Research Institutes and Industry.

New generations of Machines and Systems should be developed covering all manufacturing sectors: from mechanical to wooden, leather, plastic products, from car to white goods, etc. They would be competitive and sustainable European “high-tech” mechatronics products for global, as well, internal market.

To contribute to the definition of the R&TD activities required a reference model has been developed and is presented hereafter.

Manufacturing sub-sector	Production		Employment	
	(billion EURO)	(% Manufact.)	(employess)	(% Manufact.)
Motor Vehicles and parts	308.0	10,8	1.604.576	8,4
Machinery	183.1	6,4	1.565.118	8,2
Aerospace	41.8	1,5	345.795	1,8
TOTALS	532.9	18,7	2.936.982	18,4

Source: Panorama of EU Industry 97

Table 1: Production and Employment in three relevant sectors: motor vehicles and parts, machinery, aerospace

3. A REFERENCE MODEL FOR MANUFACTURING

ITIA-CNR Technological Observatory has developed a model (fig. 2), composed of two interrelated parts:

- the reference model for Production;
- the reference model for Research and Development.

3.1 The Reference model for Production

Manufacturing is composed of many sectors. Each of them, in turn, is composed of classes of similar Products and related Processes and Organisation. Hence, three levels must be considered:

- product
- sector
- meta-sector (Manufacturing Industry)

At *product level* a reference model (fig. 2 right side) has been developed based on:

- Product Matrix. It relates the product sustainable quality (market expected performances and compliance with eco-requirements) to its sw-hw structure (fig.3).
- Product-processes life cycle Matrix. Each product shows a life cycle involving various phases, going from design to recycling (fig.4). Each product phase is implemented by a process (including technology, organisation, skills), showing its own sustainable quality (performances and compliance with eco-requirements). Any process, in turn, shows a life cycle going from design to implementation, use, recycling. The combination of product and processes life cycles, i.e. the PPLC Matrix is shown in fig. 5. At each phase corresponds a transformation. Using the IDEF presentation, this implies: input, output, tools, controls. Each phase will be "structured" according to product complexity and will be related to the external context i.e. economy (market), society (eco-requirements), technology (state of the art).
- Actors. Each phase requires one or more "structured" actors, from shop floor to extended company level, involving three main areas: technology, organisation and logistic competence (fig. 6).

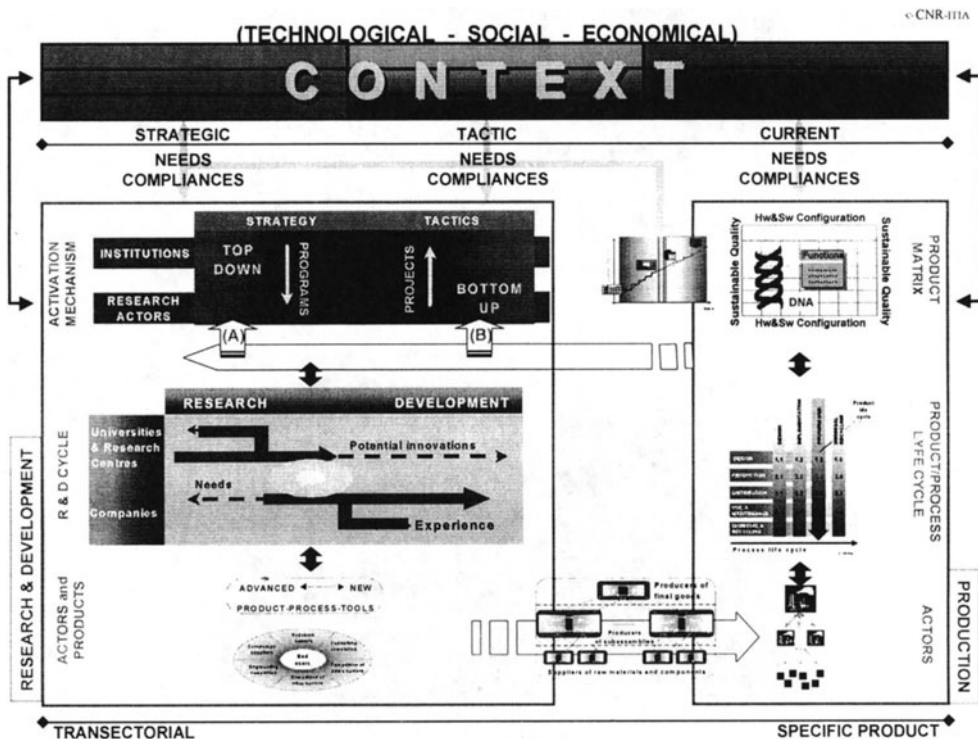


Fig. 2: Reference model for dynamic and strategic Manufacturing

The above model enables a "manageable" representation -at product level- of:

- a given product and its PPLC;
- transformations taking place at each PPLC phase and their relationship with the economical, social and technological context;

- “actors” performing the various phases and, hence, bearing such needs.

For a given product the above “ methodology Matrix ” enables to single out needs emerging from context changes in terms of, competitiveness and sustainability, and innovative responses required.

If representative products, within a sector, are chosen, the use of the above “ technology Matrix ” and “common features” approach enables to “represent” a sector in terms of needs and requested “responses” showing common features. By applying a similar procedure to sectors, we may represent Manufacturing, in terms of common transectorial needs and requested “responses”.

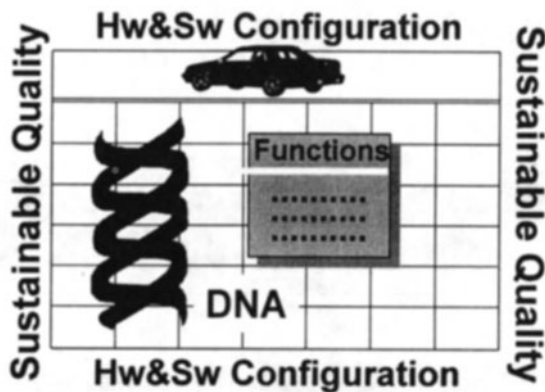


Fig. 3: The product Matrix: sustainable quality vs Hw&Sw configuration

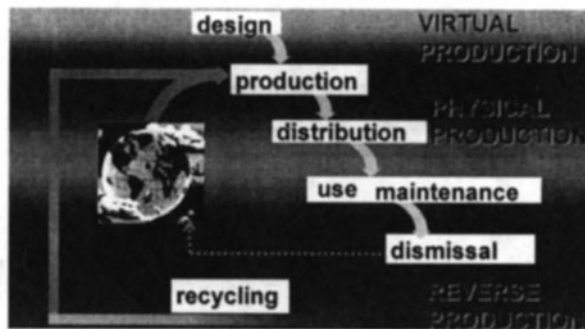


Fig.4: Product life cycle

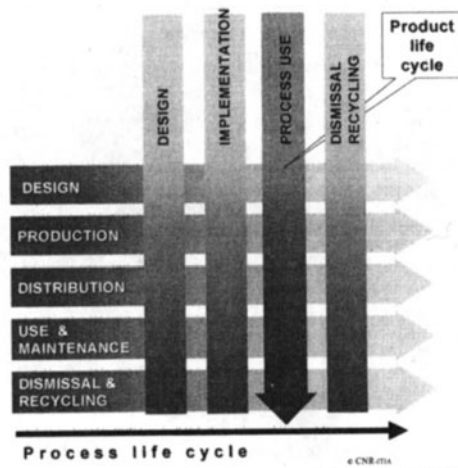


Fig. 5: The product and related process life cycle (PPLC) Matrix

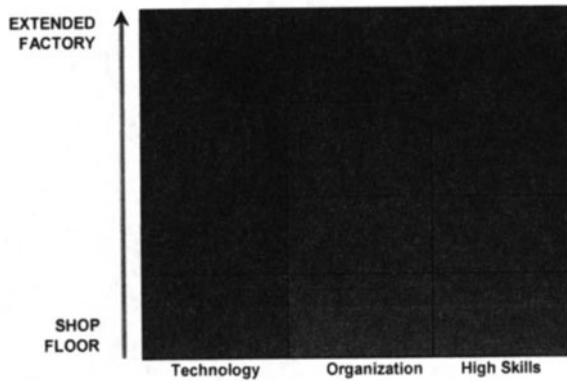


Fig. 6: The "Factory" structure and content

3.2 The reference model for Research and Development

The reference model for R&D is shown in fig. 2, left side. It shows:

- the "activation mechanisms": R&TD Programmes(top down approach) and Initiatives(bottom up approach) as conceived by Institutions following strategic forsigthing;
- the R&TD proposal approach by Research Actors;
- the (schematic) research to production cycle and its results;
- the actors involved at micro (fig. 7) and macro level;
- the network structure (fig.8) bridging production (Physical Factory) and R&D (Virtual Factory) within each factory and along the supply chain(extended factory).

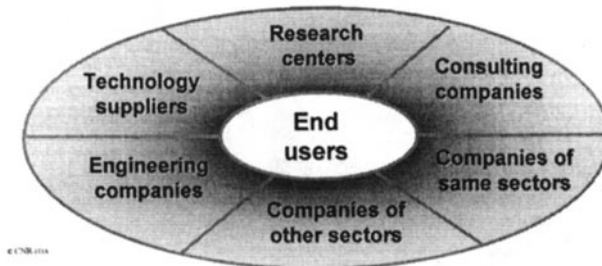


Fig.7: Research-Innovation "Actors"

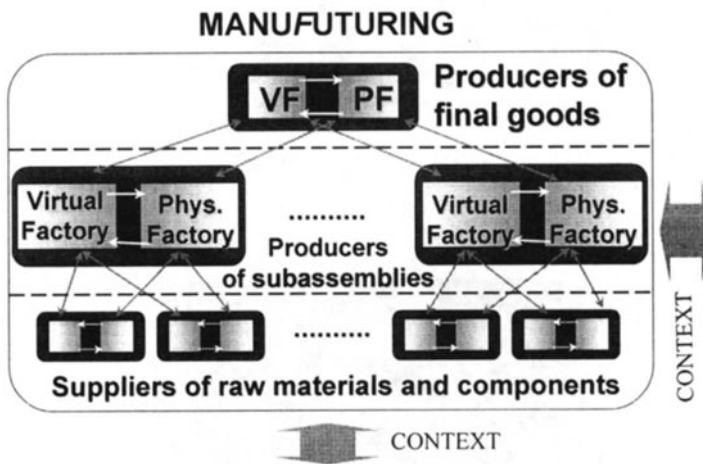


Fig. 8: Production-Innovation Networks: VF=R&D, PF=Production: the new industrial "fabric"

4. USE OF THE REFERENCE MODEL FOR MACHINERY AND SYSTEMS R&TD

The proposed reference model (fig.2) is a "dynamic" representation of Manufacturing - as a Meta-sector, evolving through time by a proactive approach involving from Institutions to Industry. It may be used by Institutions and R&TD Actors involved, according to their needs.

Institutions are concerned, see par. 3.2, with the launch of Programmes and Initiatives to implement political goals considering:

- the evolution of the strategic context in terms of economical and social needs;
- the technology required to respond to those needs.

Research actors, fig.7, are concerned with the development - through R&TD projects - of a new product or process to respond to future needs. Going from Institutions to Research Actors we move from strategy to strategic/tactic R&TD actions.

In the following paragraphs we will consider the use of the model for both, needs and technological responses, as seen by Institutions and research Actors.

4.1 Priority needs for competitiveness and sustainability in Manufacturing

To single out product and processes needs in relation to competitiveness and sustainability it is necessary to introduce:

- Sustainable Quality (SQ) demand curve, (fig.9). This results from changes in the economical and social context through time;
- product and/or processes sustainable quality evolution to respond to it (fig. 7)
- consequent incremental or radical innovation in products and/or processes hard/soft configuration (fig.3).

For a given product (and Matrix) and consequent PPLC Matrix:

- considering the above demand curves
- using the procedure previously presented

we may single out *Sustainable Quality* (SQ) demand curve trends and, hence, the needs of improvement of products/processes SQ.

If representative products within each sector are chosen and the "Matrix methodology" and "common features" approach are applied, first to each product and then to each sector, it is possible to individuate, respectively, specific (to the product) and common (to the sector and hence to the sectors) needs for competitiveness and sustainability. The transectorial needs –getting across sectors and, hence, Manufacturing- may be assumed as strategic and hence having priority for R&D in Manufacturing.

Off course, the above procedure could also be applied to expected new strategic products.

Priority needs related to competitiveness and sustainability, -calling for innovation in technology, organisation and logistics, skills, from shop floor to extended company (fig.6)- will arise from any PPLC Matrix phase i.e. from design to recycling.

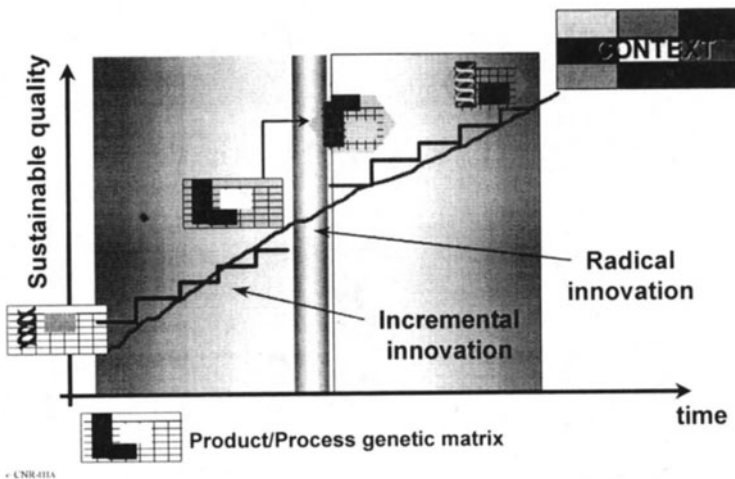


Fig. 9: Product/Process Response to Sustainable Quality Demand

4.2 Innovative technological responses to *Sustainable Quality* (SQ) needs.

To respond to needs of improvement in *Sustainable Quality* (SQ) of Product and/or Processes, technological as well organisational innovation is required.

This, in turn calls for appropriate R&D activities leading to new technologies (hard and soft), for products and processes within tactic and strategic horizons.

At product level, for given:

- product and related processes;
- *Sustainable Quality* (SQ) improvement needs

the state of art of technology must be assessed and technologies to be developed through R&D must be singled out.

To single out new technologies to be developed and related R&D activities to launch, we may make use of the methodology and approach, previously presented.

If the above procedure is used for each representative product within a sector, we may obtain the sectorial technologies to be developed. Having done this for the sectors chosen to represent Manufacturing, by using the “common feature” approach, we may determine the “distribution” of transectorial technologies and sectorial technologies.

If we apply the above procedure to the production phase (fig. 5) of the PPLC Matrix for various manufacturing sectors we find the distribution of transectorial technologies (bars) and sectorial technologies (squares). This is shown by the synergic and strategic Machinery and Systems Innovation Matrix (fig. 9).

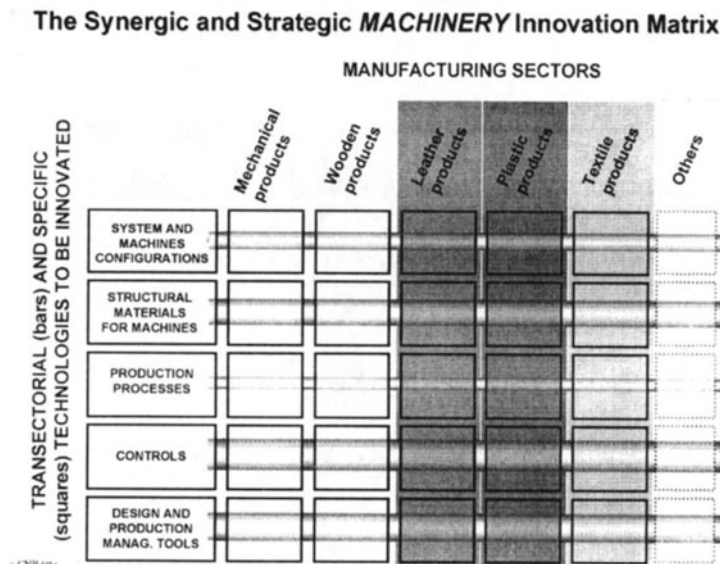


Fig. 9: The Synergic and Strategic MACHINERY & SYSTEMS Innovation Matrix

Investing in R&D of transectorial technologies may lead to high savings in R&D costs, more efficiency in R&D, high impact on Manufacturing industry as a whole.

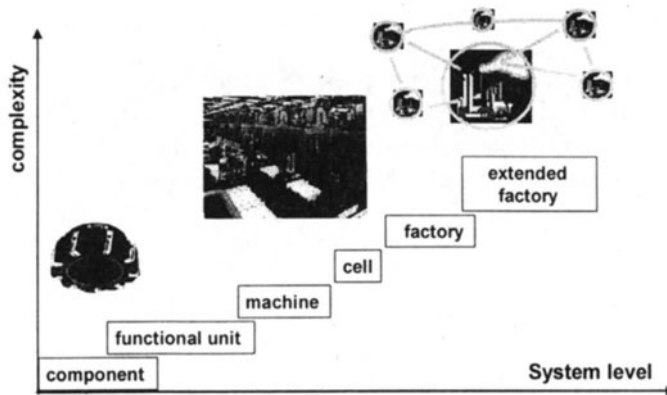


Fig. 11: Manufacturing system from components to extended factory

5. A FUTURE FOR MACHINERY AND SYSTEMS: THE ROLE OF RESEARCH AND CONCLUSIONS

Machinery and Systems (M&S):

- contribute to the competitiveness and sustainability of European Manufacturing Industry;
- are "high-tech" mechatronic products, holding a leading position on the world market.

A dynamically and strategically innovating M&S Industrial "fabric" must be implemented. It may comply with the reference model presented. For this to happen Institutions as well as Research Actors must provide their active contribution.

At Institutions level:

- the European Commission has addressed the above problem in the FP5 through the Key Action "Innovative Products, Process, Organization"(Thematic Programme: Competitive and Sustainable Growth). This is coherent with the reference model discussed and the transectorial approach discussed. The new problem solving approach adopted by FP5 transfers to the Actors the definition of strategic needs and technological responses;
- Eureka Factory, through the strategic Project DNA, is addressing the M&S innovation problem with particular reference to a sectorial approach.

At Actors level we must say that:

- M&S European Industry is composed of SME. They, often, show an incremental innovation approach. In general they are not developing M&S based on new technological processes or for new products or for the various life cycle phases of current and incoming products.

All this may lead to a decline of European M&S Industry. Because of its relevance for Europe such a decline would be a disaster. To solve this European problem, M&S Industry should strategically innovate: its products, its processes, its "industrial fabric".

Focusing on M&S products and considering the system approach - from components to extended factory (fig.11) - at each system level we should promote the Research-Development cycle, shown in fig. 2, to develop new tools and methodologies, configurations.

As shown by the proposed reference model unifying approach, strategic innovation of M&S may come from large R&D investments on transectorial technologies linked to sectorial applications. This would require from strategic foresight, to R&D critical mass: both difficult to find in the M&S Industry "fabric", composed of SMEs.

Although Institutions at European and National level have provided Programmes, Initiatives, Funds which may allow such a strategic move - as FP5 and Eureka Factory show - we may end up with small scattered projects although they may be clustered.

At this time it is fundamental for the strategic survival of M&S European Industry that research institutes and Universities become the driving force of the M&S strategic innovation process, the strategic "heart" of the Machinery and System Industry. To do this Research Institutes and Universities must take a strategic problem solving approach as:

- foresee and single out the critical M&S transectorial technologies;
- carry out research on them in co-operation with innovative Technology Suppliers;
- work on sectorial application with M&S Industry, mainly SMEs;
- networking to become the strategic "fabric" for innovation, embedded in the European M&S Industrial "fabric".

To play such a strategic role - between Institutions political goals and SME strategies - a common effort on studying future needs and technological answers is required. An Observatory network may be an answer. This Conference is a relevant occasion for discussing such an initiative for Europe.

6. REFERENCES

1. Jovane, F.: Advanced production systems: an european asset for global competitiveness, Proceedings of the Brite-Euram conference on Industrial Technologies, Toulouse Oct. 1997
2. Boër, C.R. and Jovane, F.: Towards a new model of sustainable production: ManuFuturing, Annals of the CIRP, 46th CIRP General Assembly, Como Aug. 1996

3. Fifth RTD Framework Programme(E.C.) 1998-2002, Decision N° 182/1999/EC, 22nd Dec. 1998
4. Towards a EUREKA FACTORY Ambitious Project for Advanced Machinery and Production Systems, Eureka Factory Working Meeting, Lisbon, 23/24 Apr. 1998
5. Programma Nazionale di Ricerca e di Formazione sui Sistemi di Produzione Innovativi, MURST, Jan. 1994

PRODUCT DEVELOPMENT MUST CONSIDER ENVIRONMENTAL ASPECTS

H. Schulz, A. Atik and E. Schiefer

Technical University of Darmstadt, Darmstadt, Germany

ABSTRACT: The incorporation of methods and tools for the development of environmentally sound products into design processes is frequently not sufficient. The authors present a solution that integrates a computer aided system into a usual design environment. Product and process data coming from a CAD System are aggregated to an ecological index-score using fuzzy sets. This index-score supports the designer as a simple and certain aid to accompany decision-making.

1. INTRODUCTION

Current activities in the area of environment protection primarily relate to the elimination of existing environmental damage and to the reduction of harm to the environment caused by existing products. However, the most significant impact comes from preventive action minimising or avoiding right from the start any harm to the environment caused by new products in all phases of their entire life cycle from production through use and recycling to final disposal. The current type of product development merely considers partial aspects of environmental soundness. In particular, there is a lack of easy-to-use methods for holistic and prospective evaluation of products and processes with respect to the environmental harm to be anticipated.

Within a special research project ¹ at the Darmstadt University of Technology, engineers, scientists and sociologists from nine different institutes are working together on methods, means and instruments for holistic development of environmentally proper products, on integrating these into current design engineering methods and on implementing a computer-aided design environment. The objectives are

- to recognise and evaluate the environmental harm potential of a product already during the phase of product development, prospectively for all phases of its useful life;
- to identify, evaluate and make preventive use of the potential for environmentally proper designing possibilities in all phases of design engineering;
- to develop from a combination of ecological, technological and economical criteria future-oriented products appropriate both environmentally and commercially (Fig. 1).

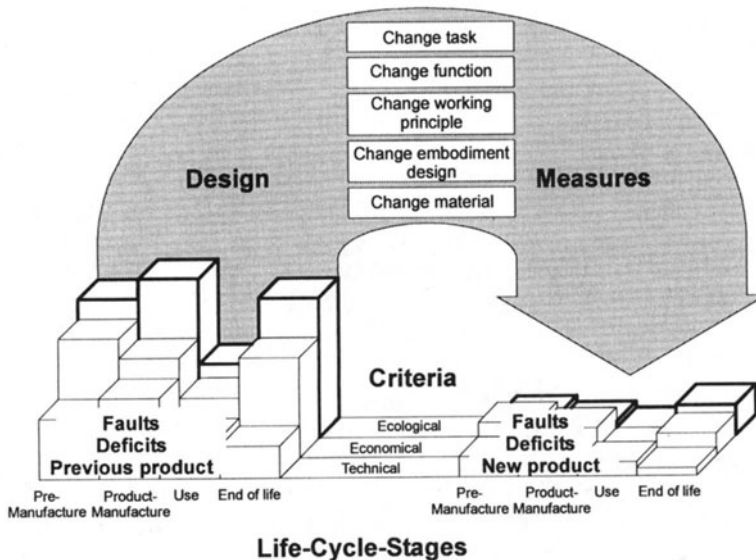


Figure 1: Integral Product Development

2. INTEGRATED DESIGN ENVIRONMENT

Today the design engineer is supposed not only to think in terms of value-addition (Fig. 2), but also to consider the entire life cycle of a product (Fig. 3).

¹ Granted by the German Research Foundation (DFG)

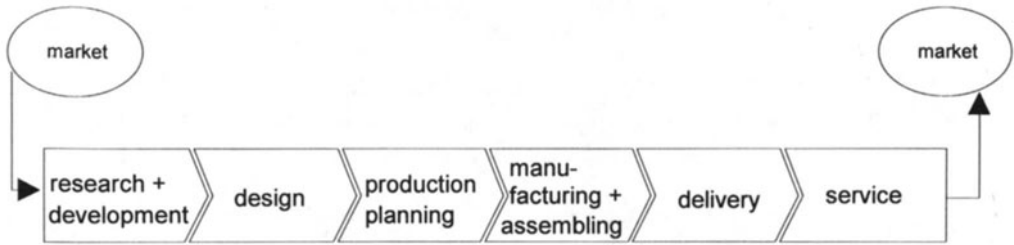


Fig. 2: Value-addition scheme in manufacturing a product

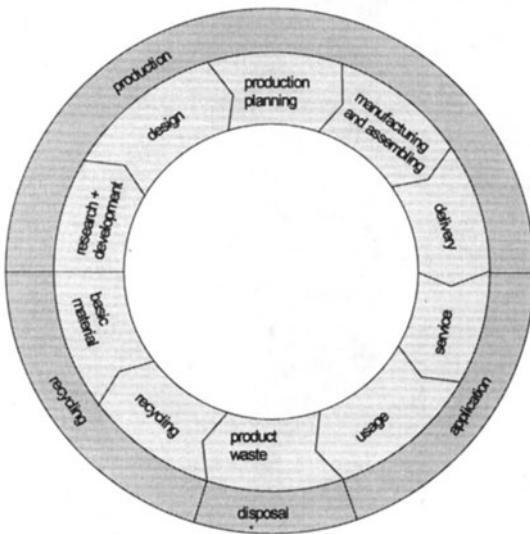


Fig. 3: Entire life cycle of a product

This is why in the future a computer-integrated product development environment composed of a CAD and PDM (product data management) system as well as an information system providing ecological data must be available. The latter system will comprise:

- a *life-cycle modeller* specifying the product life cycle co-operatively by attribution of (partially predefined) processes to the product life phases and thus forming the basis for an ecological evaluation to be performed;
- an *evaluation system* for performing an ecological assessment of the product and for conditioning the results specifically for use by the product developer while permitting identification of ecological weak points as well as of tools for efficient optimisation;
- an *information system* providing hypertext-based information on environmentally relevant standards or guidelines as well as supporting the user by application of knowledge-

based methods in decision-making (for instance in the environmentally proper choice of materials);

- *an object-oriented data bank system* providing, apart from organisational and administrative product data, also the possibility of representing fuzzy set based functional relationships required for integration of input/output balance data into the data bank [1].

Fig. 4 shows an example of what such a product development environment may look like.

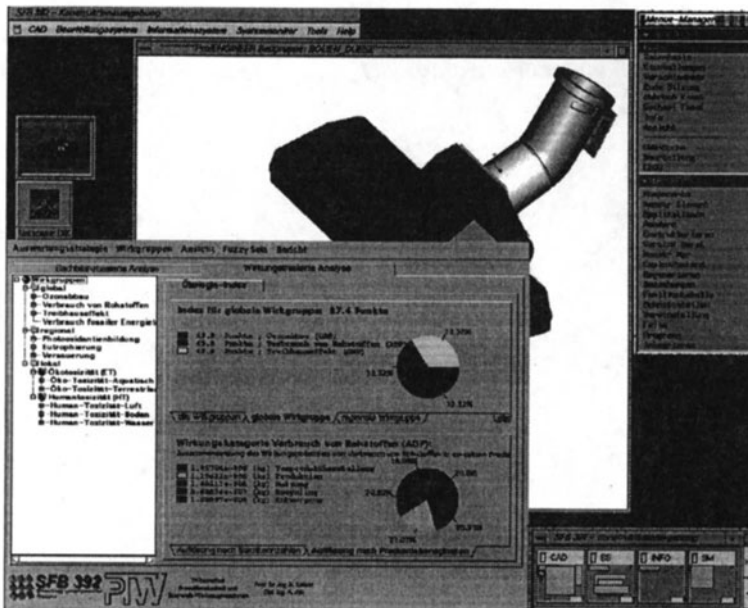


Fig. 4.: Screenshot of product development environment

Internal functionalities of the evaluation system can be activated from the CAD system. This has made handling of the product development environment much easier.

3. METHOD FOR ECOLOGICAL EVALUATION

The ecological evaluation model of the German Federal Environmental Service (UBA) has been adapted to the design-related specifications existing within the overall concept while considering national and international standardisation efforts [2, 3, 4, 5]

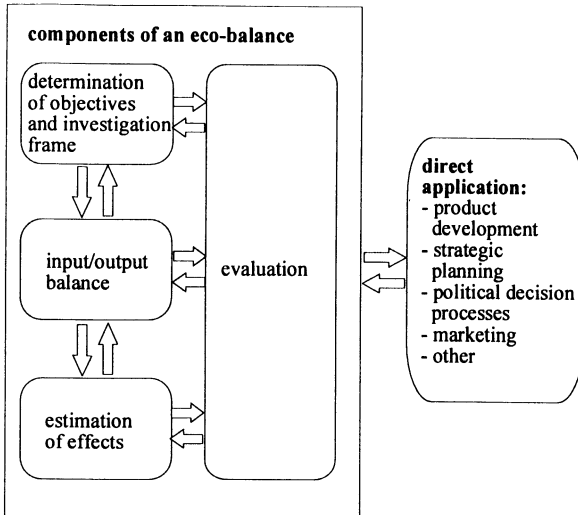


Fig. 5: Outlines of an ecological balance as per ISO 14040 [4]

The core of the eco-balance (Fig. 5) is represented by the input/output balance which lists all input and output amounts (referred to as index scores below) over the entire product life. Examples of such index scores are data on emissions into the air, input of resources, input of energy or waste output. Within the assessment of effects, the index scores determined within the input/output balance are at first attributed to the respective effect categories on which they have an environmentally harmful impact (step: classification). By multiplication with the respective equivalence factors accounting for the variously important harmful effects different materials have on the environment, the so-called effect contributions are determined whose unit is the reference substance of an effect category, such as CO₂ as reference substance for the greenhouse effect. When summing up the effect contributions of the various materials, the result is the effect potential of the various effect categories:

$$\text{effect contribution } i_{,CE} [\text{kg}] = m_i [\text{kg}] \cdot EF_{i,CE} [-] \quad (1)$$

$$\text{effect potential } CE[\text{kg}] = \sum_i^n \text{effekt contribution } i_{,CE} [\text{kg}] \quad (2)$$

wherein m_i : mass index score type i ; EF : equivalence factor; CE : category of effects.

From the results of input/output balancing and effect assessment, appropriate recommendations can be derived such as for the solution alternative to be preferred.

4 INPUT/OUTPUT BALANCING OF PRODUCTS

Known studies of metal cutting processes under ecological aspects deal primarily with subsequent or preventive action to protect the environment. Preventive action is in particular aimed at environmentally relevant partial improvements, in most cases regarding the reduction of coolant use [6, 7, 8, 9]. Until now, metal cutting processes have rarely been subjected to comprehensive ecological studies. First approaches to balancing, except for one [10], are primarily energy balances [11, 12, 13, 14, 15]. Frequently, the studies are restricted to the area of the point of chip generation [10, 13]. In other cases, the extent of the balance is based either on the machine tool [11, 12] or on an area not clearly identified [14]. A systematic effort of balancing the energy and material inputs, waste outputs and emissions in metal cutting operations supported by valid data do not yet exist.

A new concept now is the description of the relationships between product configuration and harmful effects on the environment with consideration of plant-related fringe conditions so that the design engineer already can, in a properly cause- and product-related manner, assess the energy and material inputs, waste outputs and emissions to be anticipated during production [16].

5 ENVIRONMENT/PROCESS RELATIONSHIPS

In metal cutting operations, a great variety of processes are interlinked in a plant. These can be attributed to the three balancing sectors of chip generation point, machine tool and process peripherals (Fig. 6).

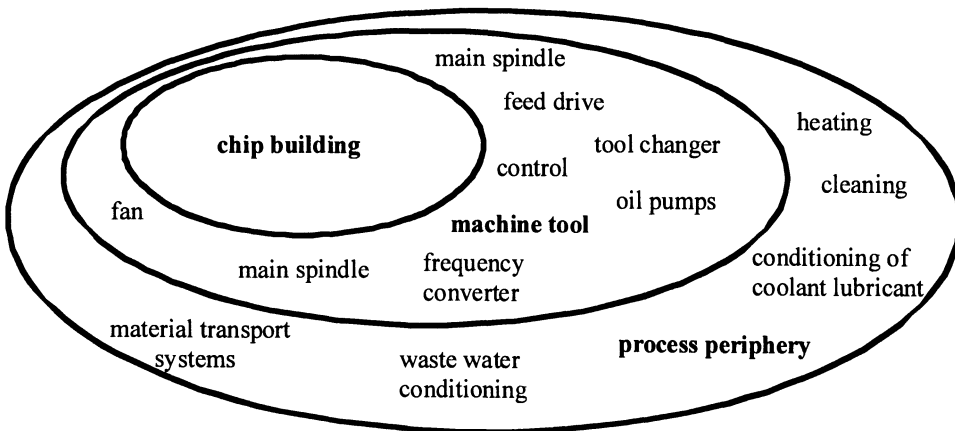


Fig. 6: The balancing sectors of chip generation point, machine tool and process peripherals [16]

The essential relationships for the area of the chip generation point can be derived from the metal cutting theory or taken from literature [13, 17, 18]. For determining the inputs and outputs for the machine tool and the process peripherals it is required to perform energy and material flow analyses specifically for the plant involved. For this purpose, a balance of the energy and material inputs and outputs is made by taking plant-related fringe conditions into account. Many data required for balancing are already available in a plant, such as in the purchasing, work planning and production control departments or in maintenance plans or controlling. Important factors for a subsequent detailed ecological evaluation are precise information and data about the quantity and quality of energy, materials and emissions, the utilisation of any by-products generated, as well as information about processes affected such as recycling. In order to allow product-related assessment of the anticipated energy and material flows in the metal cutting operations, environmental characteristics specific to process and/or configuration are determined for each input and output. By way of functional environmental process relationships, these inputs and outputs are attributed to the product involved with proper consideration of the causes [16].

The energy requirement at the chip generation point can be calculated from the specific cutting force k_c and the metal removal volume V [13, 18]. Determination of the machine tool's energy requirements beyond the metal removal energy is made by means of power characteristics which by multiplication with production or machine utilisation time result in corresponding energy inputs for the product. For the process peripherals (such as coolant supply system, exhaust system, lighting and heating of the building), power characteristics specific to the machine location are determined and, also by multiplication with machine utilisation time, give the amount of energy required by the machine peripherals and specific to the product involved.

On the basis of the chip volume obtained, the material usage and waste amounts occurring during the same period are used for calculating usage and waste characteristics related to the chip volume for a particular machine location.

As to the relevant emissions from metal cutting operations, these are primarily coolant aerosols occurring due to turbulence and evaporation at the point of chip generation. Since modern machine tools are encapsulated and equipped with exhaust systems, merely local effects are produced by the amounts of aerosols released into the immediate surroundings. Since actual concentrations in the air cannot be predetermined, they have to be measured specifically for each plant around the machine involved or must be estimated from the product information furnished by the coolant manufacturer [16].

Fig. 7 shows an example of calculating the energy requirements for a turned workpiece. The metal removal energy contributes merely about 5 %, while the machine tool's energy requirements beyond metal removal energy amount alone to about 60 % of the energy total. Investigations have shown that in metal cutting operations the great majority of the energy is consumed, regardless of load, by the machine tool and the process peripherals [17].

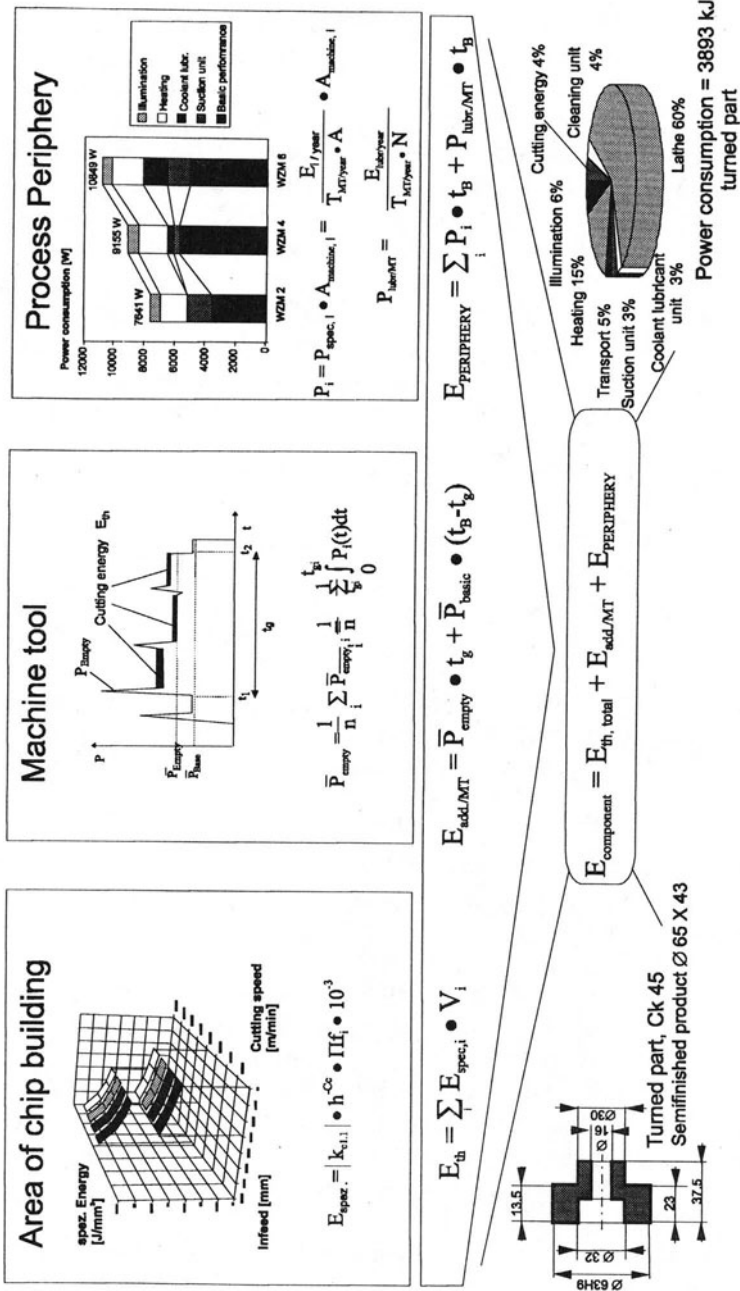


Fig. 7: Determination of energy required for metal removal on a workpiece according to [17].

6 RELATIONSHIP OF ENVIRONMENT AND PRODUCT CONFIGURATION

As a rule, machining operations and process control are not yet known during the design phase. For this reason the relationships of environment and product configuration have to be developed (Fig. 8) based on the functional environment/process relationships which include plant-specific attribution of workpiece and machine tool, plant-specific reference data sets for process parameters [18] as well as a rough estimate of production times.

These environment/configuration relationships are modelled based on features in an object-oriented partial model by means of systematic attribution of machining elements. This partial model is an important part of the information model.

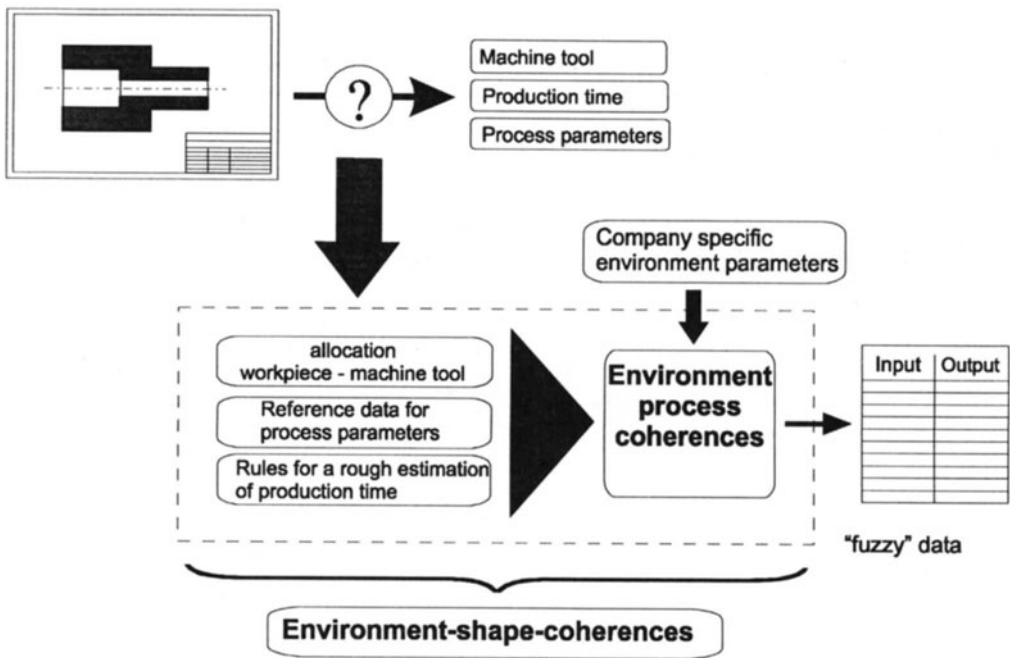


Fig. 8: Estimate of input and output data in product development via environment/ configuration relationships

7 FUZZY MODELLING OF UNCERTAIN ECOLOGICAL DATA

Ecological data required for eco-balance based evaluation frequently are available in highly inexact form only [19]. Viewed over the entire product life, such inexactness can cumulatively result in wide variations of the final results of such a balance or evaluation [20]. For

this reason it is necessary to consider also fuzzy data for ecological evaluation. These will provide the product developer with valuable information as to the plausibility of a result.

The evaluation system must therefore be capable of processing exact figures, intervals and fuzzy sets [21, 22].

8 APPLICATION OF INFORMATION SYSTEM

In order to make an evaluation comprising the entire life cycle of a product, it is required to model the product life. The objective of the product life modeller is to specify product life by fast and easy attribution of processes to product life phases and thus to furnish the basis for ecological evaluation [23]. By transfer of the process information describing product life (product life modeller) and of the configuration information describing the product (CAD system) to the object-oriented data bank, it is possible to generate dynamically the specific index scores based on the information model. These index scores represent the input data of the evaluation system.

The design engineer thus can perform a comparative ecological evaluation accompanying product development, to find solution alternatives. He can evaluate these alternatives by comparison and can obtain the results in the form of aggregated index scores. Thus, the product developer has a fast, easy-to-handle and accurately aimed decision-making aid regarding the environmental soundness of the solution alternatives considered (Fig. 9).

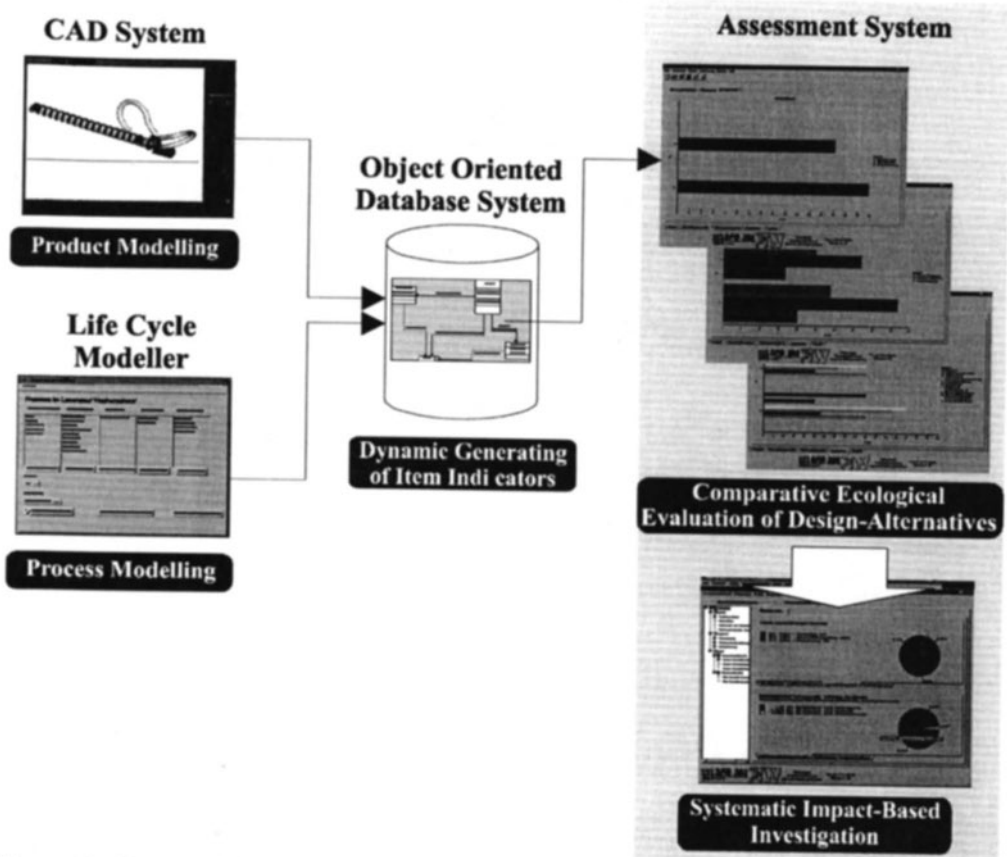


Figure 9: Course of the ecological evaluation embedded into integrated design environment

This result permits conclusions to be made as to the causes of environmental harm. The possibility of systematically tracing back the results contributes substantially to transparency. Furthermore, actual weak points can be revealed. Investigation for the causes can be made either by input/output balance analyses or by means of effect-based analyses.

Input/output-based analyses furnish a structured representation and analysis of the index scores acquired, specifying all input and output flows by types (such as resources, emissions etc.). Moreover there is the possibility of retrieving information about their occurrence in the various product life phases.

Effect-based analysis, in contrast to input/output-based analysis, does not furnish index scores but their potential effect on the environment. Since different substances usually have different effects on the environment, it is indispensable for ecological evaluation to include effect-based considerations.

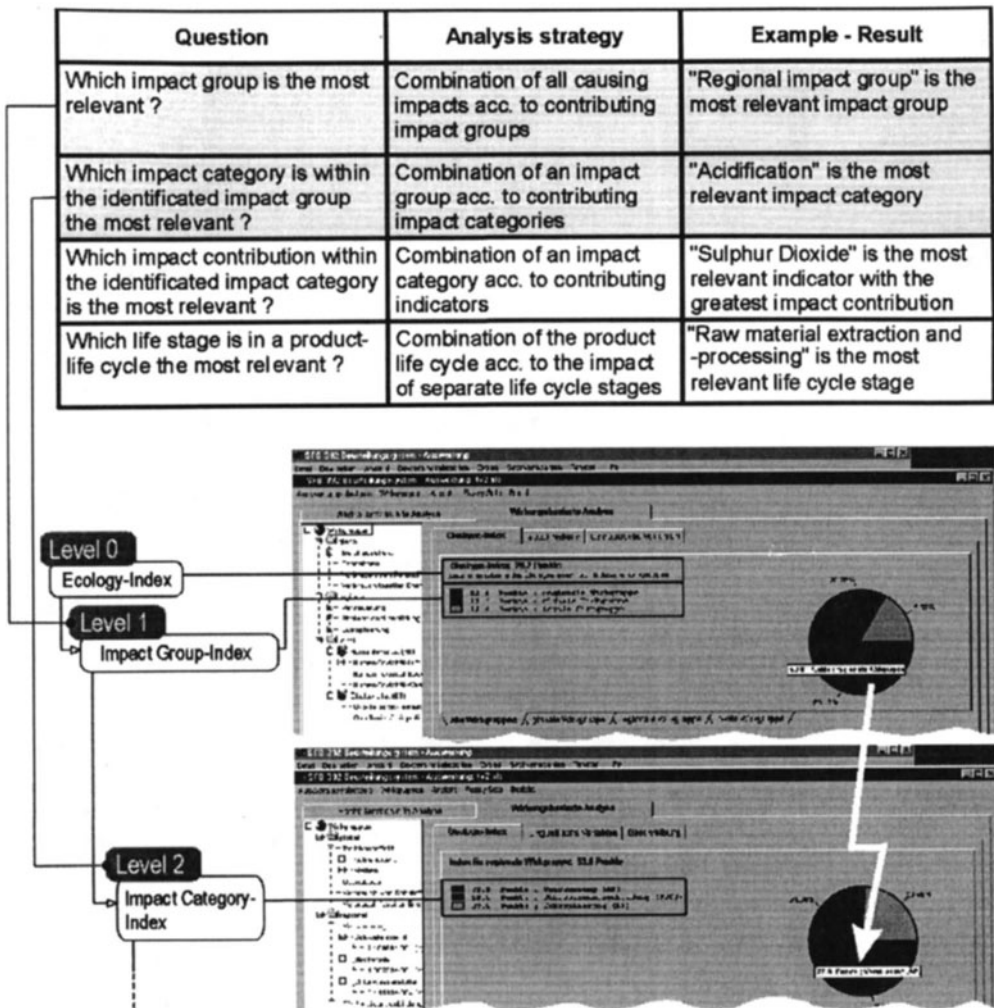


Fig. 10: Systematic effect-based investigation of causes by means of the evaluation system

Based on the resulting ecology index (Fig. 10, level 0), the design engineer has the opportunity of determining step by step the effect categories, index scores and product life phases representing causes. Their relative contributions are visualised, and the different contributions can be activated directly by mouse click. Colour marking of the most important contribution in each case enables the user to identify relevant aspects fast. Activation of these contributions then leads to the next lower level so that the causes responsible for each index score become transparent.

6. CONCLUSION

Systematic investigation of causes thus will permit the ecological weak points in each product life phase to be determined. From the ecologically relevant substances and/or product life phases identified, „eco drivers“ can be recognised. This way it is possible to find out immediately which of the various processes are responsible for the environmental harm caused or which of the various components and/or machining elements within a sub-assembly are critical under ecological aspects.

REFERENCES

1. Anderl, R.; Daum, B.; John, H.; Pütter, Ch. (1997): Entwicklung einer Umweltdatenbank für eine rechnergestützte Konstruktionsumgebung, in: Geiger, W.; u.a. (Hrsg.): Umweltinformatik '97, Straßburg 1997, Marburg: Metropolis, S. 56-69
2. Umweltbundesamt (Hrsg.) (1995): Ökobilanz für Getränkeverpackungen, Berlin (Texte 52/95)
3. Umweltbundesamt (Hrsg.) (1997): Materialien zu Ökobilanzen und Lebensweganalysen – Aktivitäten und Initiativen des Umweltbundesamtes, Berlin (Texte 26/97)
4. DIN – Deutsches Institut für Normung (Hrsg.) (1997): Umweltmanagement – Ökobilanz – Prinzipien und allgemeine Anforderungen (DIN EN ISO 14040), Berlin: Beuth
5. Neitzel, H. (1997): Stand der Diskussion um Ökobilanzen im Rahmen der ISO- und DIN/NAGUS-Arbeiten zur Methodenentwicklung, in: FGU Berlin (Hrsg.): Produktbezogene Ökobilanzen V, (UTECH Berlin '97, S. 15-23
6. König, W.; Gerschwiler, K. (1997): Trockenbearbeitung – Grundlagen, Grenzen, Perspektiven, in: VDI-Gesellschaft Produktionstechnik (ADB) (Hrsg.): Umweltfreundlich zerspanen, Tagung Aachen 23./24. Juni 1997, Düsseldorf: VDI-Verlag (VDI-Berichte 1339)
7. Schulz, H.; Kalhöfer, E. (1996): Umweltfreundliches Produzieren durch Trockenbearbeitung möglich?, in: Thema Forschung 2/96, S. 16-23
8. VDI-Gesellschaft Produktionstechnik (ADB) (Hrsg.) (1997): Umweltfreundlich zerspanen, Tagung Aachen 23./24. Juni 1997, Düsseldorf: VDI-Verlag (VDI-Berichte 1339)
9. Tönshoff, H.K.; Karpuschewski, B.; Lierse, T. (1996): Potentiale und Grenzen umweltgerechter Fertigung, in: Neue Möglichkeiten umweltgerechter Fertigung, Seminar Universität Hannover, IFW
10. Munoz, A.; Sheng, P. (1995): An Analytical Approach for Determining the Environmental Impact of Machining Processes, in Journal of Materials Processing Technology 53 (1995) 3-4, S. 736 - 758
11. SFB 144 RWTH Aachen (Hrsg.) (1996): Energie- und Rohstoffeinsparung – Methoden für ausgewählte Fertigungsprozesse, Düsseldorf: VDI-Verlag (VDI-Z Integrierte Produktion, Sonderpublikation)
12. Eversheim, W.; Schmetz, R. (1992): Energetische Produktlinienanalyse, in: VDI-Z 134 (1992) 6, S. 46-52

13. Reeber, R. (1980): Der Energiebedarf bei trennenden Fertigungsverfahren, in: Werkstatt und Betrieb 113 (1980) 2, S. 109-113
14. Hartmann, D.R. (1996): Simulation des kumulierten Energieverbrauches industrieller Produkte, Herrsching: E&M
15. Degner, W. (1996): Rationeller Energieeinsatz in der Teilefertigung, Berlin: VEB Verlag Technik (Betriebspraxis)
16. Schulz, H.; Schiefer, E. (1999): Methode zur Bilanzierung der Umweltbeeinträchtigungen von spanenden Fertigungsverfahren, erscheint in: wt Werkstattstechnik 89 (1999)
17. Schulz, H.; Schiefer, E. (1998): Analyse der Zusammenhänge zwischen Prozeßführung und Energiebedarf bei spanenden Fertigungsverfahren, in: Zwf – Zeitschrift für wirtschaftlichen Fabrikbetrieb 93 (1998) 6, S. 266-271
18. Schulz, H.; Schiefer, E.; Irion, J. (1997): Abschätzen des Zerspanungsenergiebedarfs aus der Werkstückgestalt, in: Zwf – Zeitschrift für wirtschaftlichen Fabrikbetrieb 92 (1997) 11, S. 596-599
19. Salski, A. (1993): Fuzzy-Sets-Anwendungen in der Umweltforschung, in: Reusch, B. (Hrsg.). Fuzzy-Logic – Theorie und Praxis, Heidelberg: Springer
20. Pohl, Ch.; Roš, M. (1996): Sind Ökobilanzen zu präzise?, in: Ranze, C. (Hrsg.): Intelligente Methoden zur Verarbeitung von Umweltinformationen, 2. Bremer KIPfingstworkshop, Marburg: Metropolis, S. 121-136
21. Pant, R.; Jager, J.; Atik, A.; Schulz, H. (1998): Methoden und Instrumente zur Einbindung einer vergleichenden ökologischen Beurteilung von Lösungsalternativen in den Produktentwicklungsprozeß, in: VDI (Hrsg.): Markt- und Kostenvorteile durch Entwicklung umweltverträglicher Produkte, Tagungsband, Tagung Fellbach 09./10.06.1998, Düsseldorf: VDI-Verlag
22. Altrock, C. von; Zimmermann, H.J. (Hrsg.) (1993): Fuzzy Logic Band 1: Technologie, München; Wien: Oldenbourg
23. Schott, H.; Birkhofer, H.; Grüner, C.; Dannheim, F. (1997): Sustainable Life-Cycle Engineering – A Challenge for Design Science, in: Life Cycle Networks '97, 4th International CIRP Seminar on Life Cycle Engineering

RECENT DEVELOPMENTS IN THE DESIGN AND CONTROL OF COLD FORMING PROCESSES

N. Alberti

University of Palermo, Palermo, Italy

N. Alberti and F. Micari

University of Calabria Arcavacata di Rende (CS), Italy

ABSTRACT

In the paper some problems of process design and control in metal forming are taken into account. In particular as far as the former aspect is concerned, the problem of the preform design in cold forging is analyzed: the contributions offered by several researchers are presented and an innovative design procedure is proposed. As well, the suitability of closed-loop control systems for metal forming applications is discussed with particular reference to sheet stamping operations; again, after an overview of the state of the art, the advantages offered by the application in this field of Artificial Intelligence techniques is pointed out.

1. INTRODUCTION

Process design plays a fundamental role in the modern metal forming industry. The high level of competition which nowadays characterizes the global market forces the companies to reduce costs and time to market of any new product: in this context the development of effective design procedures assumes a dramatic importance for the company success.

In the recent years the availability of powerful and reliable finite element codes, as well as the application of Artificial Intelligence tools and statistical methods, has allowed a valuable improvement in process design. In the next sections the approaches proposed by some groups of researchers will be presented: their studies have permitted to determine the

optimal set of operating parameters, i.e. the set which allows to obtain the final desired component free of defects, for several bulk and sheet forming processes.

It is worth pointing out that the design of the forming process is generally carried out on the basis of some assumptions about the process conditions: material properties, frictional conditions, tools temperatures are generally fixed and assumed as constants in the design activity. As a consequence the design is insensitive to variations of process conditions and the selected operating parameters sometimes could result ineffective.

Due to the above considerations two fundamental research activities are currently developed. The former is aimed to a further improvement of the design procedures mainly focused on the robustness of the procedure itself: the idea is to make the forming process as robust as possible, i.e. allowing for some variation of the process conditions. The latter, on the contrary, is aimed to the development of closed-loop control systems: in this case one or more relevant operating parameters are automatically adjusted during the process in such a way that some representative forming variables follow, as closely as possible, a prescribed trajectory. Obviously the latter approach requires a continuous monitoring of these variables.

In the next section some applications of process design will be firstly presented, with particular reference to the activity carried out by the authors; in particular the problem of preform design in cold forging will be discussed. In the second part of the paper the status of the research in the field of closed-loop control systems will be presented: after a detailed review of the methods proposed in the literature, the attention will be mainly focused on the advantages offered by the application in this framework of Artificial Intelligence tools.

2. PROCESS DESIGN - THE PROBLEM OF PREFORM DESIGN IN COLD FORGING

Cold forging is aimed to modify the initial shape of a billet into an useful product, which generally presents a rather complex shape. As a consequence a complete sequence of operations is required, since one or more intermediate steps are necessary in order to ensure a proper material flow and final properties conform to the design specifications.

The design of the forging sequence comprehends several activities: first of all the process designer has to select the initial state of the material and the lubricant type. Moreover, even in the simplest case of a sequence made by only two operations, he has to select and optimize the shape of the tools to be utilized in the former step which supply the preform (or "blocker") for the finishing step. Actually the design of preform is of critical importance: such design, in fact, has to guarantee that in the finishing step the desired product is obtained without shape defects such as underfilling or folding and with a minimum material loss into the flash.

In the companies preform design is mainly carried out on the basis of the skill and the experience of the process engineer, according to some empirical basic guidelines [1]. Sometimes the effectiveness of the design is verified by means of advanced finite element codes, which are certainly able to analyze in detail the process mechanics and therefore to predict the insurgence of defects. However numerical models can be utilized only to verify

and to validate completed designs, while the design phase is still carried out almost manually and requires time consuming and expensive trial and error procedures.

In the last two decades some researchers all over the world started to focus their attention on the development of effective approaches to automate and optimize the preform shape design.

The first attempt is probably due to S. Kobayashi and his coworkers, who proposed the so called "backward tracing method" [2]: the desired final component is assumed as the starting point for the simulation, which is carried out on the reverse forging process. Obviously the contacting sequence has to be inverted in the reverse simulation, i.e. at each step reverse displacement have to be imposed to the nodes which are assumed to be in contact with the tools. By this way a suitable preform shape has been obtained for simple forging and rolling [3] processes. Nevertheless the application of this approach for an industrial forging process appears very difficult: it is well known, in fact, that such processes are characterized by complex contact conditions, with some part of the workpiece coming into contact or releasing the contact during the punch stroke. Actually the evolution of the contact conditions depends on the process mechanics, which, in turn, is largely affected by the preform shape. In other words the effectiveness of Kobayashi's approach depends on the suitability of the assumed contact history, i.e. on the choice of the nodes on which the displacements are imposed during the reverse forging simulation; consequently it decreases when the process complexity increases. Very recently Chang and Bramley [4] proposed a new reverse simulation approach for the optimal design of forging preforms; in order to determine the boundary conditions they utilized a geometric criterion based on the concept of material distribution measurement.

Oh and Yoon [5] applied a different approach to design the blocker in an axisymmetrical rib-web type closed die forging operation. They found that the blocker geometry can be generated by eliminating high frequency modes from the finisher geometry and consequently developed a procedure which uses low pass filters to convert the finisher into the preform geometry. The effectiveness of the method was proved using FEM simulations.

Osman and Bramley [6] proposed an upper bound modeling based technique to design preforms for forging of rotationally symmetric parts; their approach was applied to the precision forging of bevel gears and allowed an improved metal flow as well as a reduction of the energy required in the final stages of the process.

Finally Fourment et al. [7,8] tackled the preform shape design as an optimization problem: they assumed an objective function (the prescribed shape to be obtained at the end of the process or the forming energy which has to be minimized) and calculated its gradients as a function of the preform shape, using a BFGS algorithm. The approach was applied to an axisymmetrical rib closed die forging process and allowed to obtain a satisfactory preforming tool design after few iterations of the optimization procedure.

In a couple of recent papers [9,10] the authors took into account the closed die forging process of an axisymmetric rib-web component and utilized an inverse approach to optimize the preform design. The basic idea was to find out, utilizing proper statistical techniques, the analytical linkage between the preform design parameters and a variable

representing the “quality” of the obtained final component: in particular the occurrence of underfilling was assumed as the most important defect to be minimized. More details about this approach are presented in the next paragraph.

3. APPLICATION OF AN INVERSE APPROACH TO PREFORM DESIGN

As above mentioned the effectiveness of the proposed design procedure has been tested taking into account the closed die forging process of an axysymmetrical rib-web component. Actually the forging process of such type of components presents much more difficulties than a similar operation aimed to the production of spherical or blocklike shapes. The governing parameter is in fact the surface to volume ratio: the higher this ratio, the stronger friction effects. As a consequence the achievement of a proper metal flow able to ensure the complete die filling is more and more difficult.

Due to the above considerations one or more intermediate forging steps are necessary in order to obtain the final desired component. Furthermore the intermediate steps must be optimally designed because the preform shape plays a very relevant role in the success of the final operation.

The main difficulty in designing preform shape is to determine an explicit relation linking the preform geometry and the objectives to be pursued in the closed die forging process. Together with the complete die filling, in fact, preform design should guarantee a defect free metal flow, suitable mechanical properties of the final component and a minimization of metal losses into the flash and of die wear in the finish forging operation. On the basis of these considerations it is quite obvious that the empirical guidelines available in the technical literature are ineffective for an optimal preform design, even if they are very useful to define the “*direction*” of any optimization procedure. As regards the production of a rib-web part, for example, the industrial experience [1] suggests that the cross sectional area of the preform must be equal to the final part one augmented by the area necessary for the flash; moreover all corner and fillet radii of the blocker should be larger than the final component ones and finally an upsetting type metal flow is preferred to an extrusion type one. Thus the dimension of the preform in the forging direction has to be larger than the final part one: in this way in fact in the finishing operation the material is squeezed towards the die cavities, reducing material sliding at the die-workpiece interface and consequently frictional effects, total forging load and die wear.

The investigated problem was a typical closed die cold forging process with flash aimed to the production of an AA5052 C-shaped axysymmetrical rib-web component. In particular, the geometry of the part was characterized by a rib height vs. rib width ratio larger than two, so that a preliminary forging operation is necessary according to the technical literature [1].

The goal to be pursued in the investigation here addressed was the complete filling of the finishing die cavity through the optimal choice of the preform shape, i.e. the part obtained at the end of the preliminary forging step. Such shape is fully defined by means of the following set of operating parameters (fig.1):

❖ W_p (preform rib width);

- ❖ t_p (preform web thickness);
- ❖ R_{fp} (preform fillet radii);
- ❖ R_{cp} (preform corner radii).

The optimization procedure was based on a statistical procedure aimed to determine the analytical expression which links the above mentioned preform parameters to a variable expressing the satisfaction of the selected goal. The unfilled volume of the finishing die cavity was assumed as the proper indicator of the final “quality” of the component: then once the analytical linkage between the design parameters and the unfilled volume was obtained, a minimization procedure was carried out to determine the optimal values of the preform parameters which ensure the complete filling.

It is worth pointing out that the above mentioned analytical function was obtained applying a quadratic regression model on a knowledge base built up by means of a set of numerical simulations of the process. The numerical investigations plan was designed according to an effective design of experiment method commonly known as Central Composite Design (CCD) [11]: this technique allowed the definition of a four dimensions testing hyperspace identifying the set of combinations of the input parameters (W_p , t_p , R_{fp} , R_{cp}) to be utilized in each simulation.

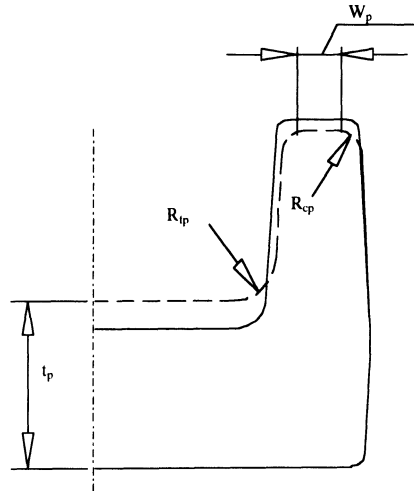


Fig. 1 Preform geometrical parameters

Once the knowledge base was built up, the quadratic regression model was applied on the available data and allowed to determine the following response function:

$$y = 586.51 + 0.826t_p^2 + 6.688W_p^2 - 0.027R_{fp}^2 + 2.075t_pW_p + 0.406t_pR_{fp} + 4.484W_pR_{fp} - 33t_p - 117W_p - 30.3R_{fp}$$

where y is the unfilled volume percentage. The variable R_{cp} is no more involved in the final response function, because a low significance of this variable on underfilling was found

out. Finally the analytical function was minimized allowing to determine the optimal preform parameters. The optimal preform shape and the final component obtained at the end of the forging process are shown in fig.2.

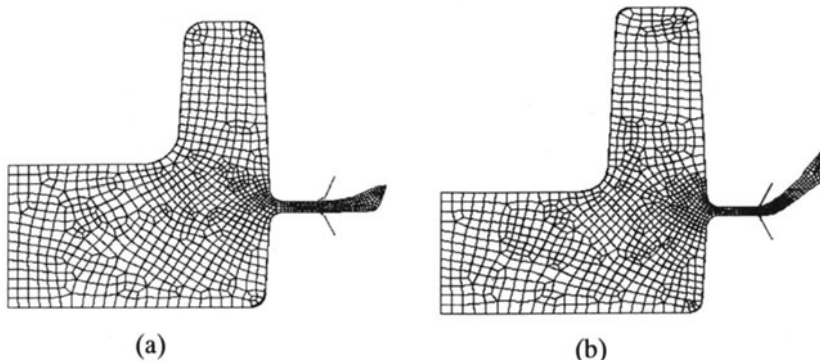


Fig.2 The optimal preform (a) and the final component (b)

The robustness of the obtained solution was tested at varying the friction coefficient (i.e. hypothesizing different lubricating conditions): again a satisfactory filling of the finishing die cavity was found out. A further most relevant test of the solution robustness was performed carrying out the whole design procedure (i.e. construction of the knowledge base, application of the quadratic regression model and minimization of the analytical response function) for different friction conditions. The obtained new optimal solutions were only slightly different from the one corresponding to the initially fixed friction coefficient proving again the robustness of the solution itself.

4. DEVELOPMENT OF CLOSED-LOOP CONTROL SYSTEMS FOR FORMING PROCESSES

In the previous sections the importance of an effective process design has been pointed out. In particular the representative case of preform design in closed die cold forging has been described more in detail. Other typical design problems are for instance the die profile design in extrusion [12-15], the pass schedule design in multi-pass extrusion and drawing and so on.

Some interesting applications of process design can be found also in the field of sheet forming. As far as deep drawing is concerned (i.e. the basic sheet forming process), the analysis has been mainly focused on a couple of operating parameters, the blank-holder force (BHF) and the use of a drawbead. Both of them determine the restraining actions on the flange: as a consequence a too low blank-holder force may lead to wrinkling occurrence. On the other hand, a too high blank-holder force (or an excessive drawbead penetration) may determine excessive restraining forces on the flange and a consequent stop of the metal flow which may induce ductile fractures.

Furthermore both the blank-holder force and the drawbead should introduce in the process mechanics a certain amount of the so called “stretching effect”, in order to reduce the springback phenomenon at the end of the forming process.

The considerations above reported justify the large number of investigations which have been carried out in the recent years on the definition of optimal blank-holder force histories and drawbead positioning patterns aimed to the optimization of stamping operations.

As far as the former are concerned, recent reports showed that drawability can be improved utilizing a variable blank-holder force, function of the punch stroke. In particular Yossifon et al. [16] experimentally predicted the acceptable blank-holder force range in an axisymmetrical deep drawing process determining the curves which respectively bound the wrinkling locus and the fracture one. Moreover they implemented a variable blank-holder force system able to vary the BHF over the punch stroke following a predetermined curve. In this way they improved the quality and the repeatability of the drawn parts.

Ahmetoglu et al. [17] investigated the deep drawing process of rectangular boxes, with particular reference to the analysis of the effects of the blank shape and the blank-holder force: either numerical simulations and experimental tests were developed in order to determine BHF trajectories able to improve the drawn part height.

Finally, a pulsating blank-holder force was experimentally utilized by Siegert et al. [18] in order to improve the formability obtaining a wider acceptable blank-holder force range.

On the other hand the definition of optimal drawbead positioning patterns was investigated by Xu and Weinmann [19]; Michler and Weinmann [20], Weinmann and Kernosky [21] and finally Michler et al. [22] focused their attention on the research of the relation linking the resulting restraining force and the drawbead positioning during the stamping process.

The effectiveness of any design procedure strongly depends on the accuracy of the utilized data as far as the process variables are concerned. In other words, if during the process the frictional conditions vary with respect to the assumed ones, or if the material properties or the initial workpiece or die temperatures are different than the design ones, the selected operating parameters could result unsuitable and bring to the failure of the process.

As far as the frictional conditions are concerned more in detail, any design procedure is based on numerical simulations. Actually in FEM codes frictional phenomena are taken into account by means of simple friction models, which require the choice of a suitable friction coefficient: an incorrect choice of this coefficient could largely affect the validity of the numerical simulation of the process. What is more, the friction coefficient is generally assumed as constant both during the process and along the blank-tools interfaces. On the contrary the lubricant behavior strongly depends on its thickness which may change during the process and can locally vary according to the relative pressure value and to the surface roughness.

These considerations have given rise to a new research line, aimed to the development of closed loop control systems able to carry out a continuous process monitoring and to adjust the process parameters if the actual conditions differ from the design ones.

Osakada et al. [23] implemented a proportional control logic based on thinning and wrinkling criteria. They found out an initial optimal BHF history and applied the control logic on the FEM simulation of an axisymmetrical deep drawing process.

Siegert et al. [24] utilized the draw-in of the blank edge in a non-axisymmetric deep drawing process as indicator of the material flow into the die cavity, so that it was an effective index of the stamping process itself. In this way they set up a proportional controller working on the scraps between the target draw-in curve and the actual one. Furthermore, since the process mechanics is characterized by an uneven metal flow in the different regions of the blank, a segmented blank-holder was utilized in order to develop an individual control for each region of the component.

In some recent papers [25-28] the authors proposed a new integrated approach based on the use of Artificial Intelligence techniques to establish the logic of the closed-loop control system. Such techniques in fact are characterized by a proper knowledge representation and by self-learning capability and consequently represent very effective tools to control sheet stamping processes. In particular, fuzzy logic provides reliable results since its ability to deal with uncertainty in process knowledge representation [29].

In the next paragraph some results obtained applying a control system based on neuro-fuzzy reasoning to the deep drawing process of rectangular boxes are presented.

5. APPLICATION OF AN AI-BASED CONTROL SYSTEM TO THE DEEP DRAWING PROCESS OF RECTANGULAR BOXES

The investigated process was a typical deep drawing operation aimed to the production of rectangular ASTM A622M steel boxes with dimensions 50 x 33.3 x 16 mm. Proper punch and die radii were chosen on the basis of previous investigations, while the initial blank was designed according to the procedure proposed by Lange [30].

In the process here addressed, an uneven material distribution arises due to the variation of metal flow rates along the straight walls and around the corners of the deforming flange. Thus the process mechanics at the corners is very different from the one occurring at the straight sides: in the former zone wrinkling may occur due to the compressive hoop stresses so that a suitable blank-holder force is needed to prevent wrinkles; at the flat wall, on the contrary, no hoop stresses occur so that the process mechanics can be referred to as a bend and straighten one and it is slightly influenced by the blank-holder action. For these reasons a segmented blank-holder represents the most suitable solution in order to control the process; in particular a segmented blank holder, made of eight independent segments (4 corners and 4 flat edges, respectively), was assumed in the research here presented. Fig.3 reports the utilized model: according to obvious symmetry considerations only one quarter of the total setup was taken into account.

First of all the so called design conditions were selected, i.e. the most suitable combination of the blank-holder forces (BHF) for the hypothesized frictional conditions was determined: such combination was able to ensure the achievement of a final sound box, avoiding both wrinkling and excessive thinning occurrence.

Nevertheless the lubricating conditions can undergo some variations during the forming process, making ineffective the selected BHF. As a consequence the blank-holder forces control is highly requested since a proper adjustment of these variables allows to regulate

the restraining forces applied to the sheet, balancing the process mechanics and taking the process under control.

Actually the variations in the process conditions determine an uncertainty which can be usefully managed by fuzzy reasoning tools. In particular a fuzzy logic based control system permits to overcome the drawbacks of the classical control techniques: it is quite difficult in fact to formulate a mathematical and crisp model to govern the controller since it is not possible to express deterministic linkages among process variables. On the contrary, fuzzy logic allows a linguistic formulation of such relations which is rather useful in order to build up a control system.

The developed system was based on the continuous monitoring of some process variables and on the comparison of their paths with the prescribed, “target” paths; if any variation is detected, the new process conditions were recognized and the fuzzy controller provided to adjust the BHF on each segment in order to balance the process mechanics and take back the process in control. In particular the draw-in was assumed as the process variable able to monitor the material flow: due to the process geometry draw-in was measured along three directions, i.e. along the short and the long edges and at the corner of the deforming flange (D_1 , D_2 , D_c , respectively in fig.3).

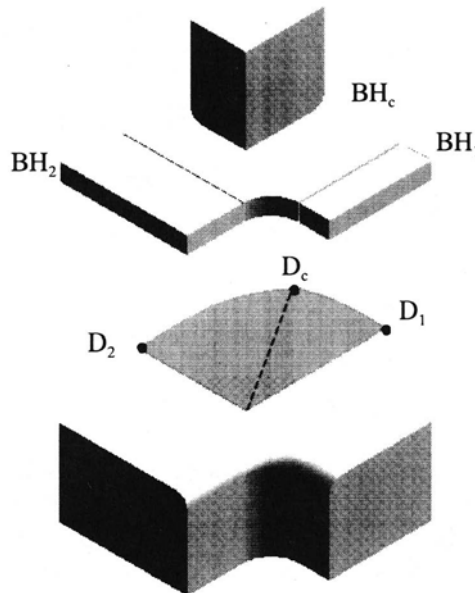


Fig.3 The utilized model

The fuzzy controller development required the linguistic translation of the input variables (the draw-in values) and of the control parameters (the BHF) as well as the determination of the degree of support (DoS) of the If-Then rules (which are the core of the fuzzy inference process). The latter task was carried out utilizing a learning procedure based on a

neural network approach: the behavior of an ideal controller (i.e. the one able to provide a straight adjustment of the BHF's to the most suitable values for the new recognized process conditions) was defined and utilized to train the controller.

The effectiveness of the developed system was tested applying the controller on the FEM simulation of the deep drawing process. Once the initial "target" conditions had been fixed, the occurrence of a lubricant film breakage was simulated by means of an artificial and sudden variation of the friction coefficient value. In particular after a punch stroke equal to 8 mm, the friction coefficient was varied from 0.1 to 0.3. Four different conditions were investigated corresponding to the film breakage on the whole blank-holder or on each segment of the blank-holder.

In particular fig.4 reports the BHF's paths associated to the occurrence of a film breakage on the whole blank-holder: the system was able to ensure an effective and quick adjustment of the blank-holder force on each segment. These paths permitted to produce a sound box (according to the numerical simulation results), avoiding excessive thinning or tearing.

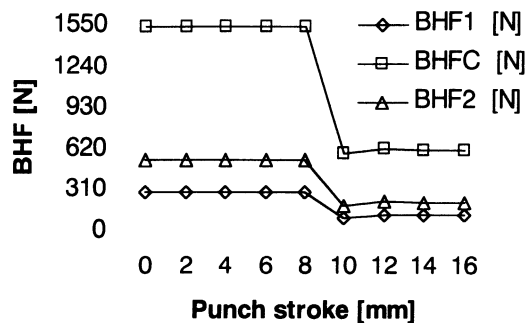


Fig. 4 BHF vs. punch stroke paths associated to film breakage on the whole blank-holder

CONCLUSIONS

In the previous paragraphs an hopefully detailed overview of the state of the research in some basic process design and control problems has been presented.

The most important research lines are nowadays focused on the development of effective and robust design procedures, as well as on the setup of closed-loop control systems. Taking into account the specific features of the two approaches, the authors believe that the former line presents a better suitability from the point of view of industrial applicability. It is difficult to imagine, in fact, that the companies could be available to equip their presses with complex and expensive monitoring instruments. Nevertheless the development of closed-loop control systems still maintains its own theoretical validity and could result very effective for the production of particularly complex and expensive components.

REFERENCES

1. Altan, T., Oh, S.I., Gegel, H., 1983, Metal Forming: Fundamentals and Applications, A.S.M..
2. Park, J.J., Rebelo, N., Kobayashi, S., 1983, A new approach to preform design in metal forming with the finite element method, *Int. Jnl. Tool Des. Res.*, vol.23, n.1, 71-79.
3. Hwang, S.M., Kobayashi, S., 1984, Preform design in plane-strain rolling by the finite element method, *Int. Jnl. Tool Des. Res.*, vol.24, n.4, 253-266.
4. Chang, C.C., Bramley, A.N., 1998, A new forging preform design approach using reverse simulation, *Annals of CIRP*, vol.47/1, 193-196.
5. Oh, S.I., Yoon, S.M., 1994, A new method to design blockers, *Annals of CIRP*, vol.43/1, 245-248.
6. Osman, F.H., Bramley, A.N., 1995, Preform design for forging rotationally symmetric parts, *Annals of CIRP*, vol.44/1, 227-230.
7. Fourment, L., Balan, T., Chenot, J.L., 1995, Shape optimal design in forging, *Proc. of NUMIFORM '95*, 557-562.
8. Fourment, L., Balan, T., Chenot, J.L., 1995, Shape optimization for the forging process, *Proc. of IV COMPLAS Conference*, 1369-1381.
9. Di Lorenzo, R., Micari, F., 1998, An inverse approach for the design of the optimal preform shape in cold forging, *Annals of CIRP*, vol.47/1, 189-192.
10. Di Lorenzo, R., Micari, F., 1998, Optimization of the preform design in closed die forging: a new approach based on statistical methods and numerical simulations, proposed for presentation and publication on the *Proc. of the XXVII NAMRC Conference*.
11. Box, G.E.P., Hunter, W.G., Hunter J.S., 1978, Statistics for experimenters, John Wiley & Sons.
12. Chen, Ming-Fa, Maniatty, A.M., 1995, An inverse technique for the optimization of some forming processes, *Proc. of NUMIFORM '95*, 545-550.
13. Joun, M.S., Hwang, S.M., Application of finite element method to process optimal design in metal extrusion, *Proc. of NUMIFORM '92*, 619-624.
14. Kusiak, J., Thompson, E.G., 1989, Optimization techniques for extrusion die shape design, *Proc. of NUMIFORM '89*, 569-574.
15. J. S. Chung, S. M. Hwang, 1997, Application of a genetic algorithm to the optimal design of the die shape in extrusion, *J. of Material Processing Tech.*, vol.72, 69-77
16. Yossifon, S., Sweeney, K., Ahmetoglu, M, Altan, T., 1992, On the acceptable blankholder force range in the deep drawing process, *Journal of Materials Processing Technology*, vol.33, 175-194.
17. Ahmetoglu, M, Broek T. R., Kinzel, G., Altan, T., 1995, Control of blankholder force to eliminate wrinkling and fracture in deep-drawing rectangular parts, *Annals of CIRP*, vol.44/1, 247-250.
18. Siegert, K., Dannenmann, E., Wagner S., Galaiko A., 1995, Closed-loop control system for blank-holder forces in deep drawing, *Annals of CIRP*, vol.44/1, 251-254.

19. Xu, S.G., Weinmann, K.J., 1996, An investigation of drawbead control in rectangular box forming by finite element modeling, *Transaction of the Namri/SME*, vol.24, 137-142.
20. Michler, J.R., Weinmann, K.J., 1995, Experimental and finite element study of sheet metal flow in a strip test apparatus with controllable drawbead penetration, *Transaction of the Namri/SME*, vol. 23, 45-50.
21. Weinmann, K.J., Kernosky, S.K., 1996, Friction studies in sheet metal forming based on a unique die shoulder force transducer, *Annals of CIRP*, vol.45/1, 269-272.
22. Michler, J.R., Kashani, A.R., Bohn, M.L., Weinmann, K.J., 1995, Feedback control of the sheet metal forming process using drawbead penetration as the control variable, *Transaction of the Namri/SME*, vol.23, 71-76.
23. Osakada, K., Wang, C.C., Mori, K., 1995, Controlled FEM simulation for determining history of blank holding force in deep drawing, *Annals of CIRP*, vol.44/1, 243-246.
24. Siegert, K., Ziegler, M., 1997, Pulsating blank-holder forces in the deep-draw process, *Annals of CIRP*, vol.46/1, 205-208.
25. Alberti, N., Fratini, L., Micari, F., Noto La Diega, S., Provenzano G., Riccobono R., 1997, Application of fuzzy logic to the control of an axisymmetric deep drawing process, *Proc. of the CIRP Int. Symposium on Advanced Design and Manufacture in the Global Manufacturing Era*, 695-701.
26. Alberti, N., Di Lorenzo R., Fratini L., Micari F., Perrone G., 1997, Application of fuzzy logic to control the drawbed penetration in the axisymmetrical deep drawing process, *Proc. of the CIRP Conference of Design and Production of Dies and Molds*, 249-254.
27. Di Lorenzo, R., Fratini, L., Lo Nigro, G., Micari, F., Noto La Diega, S., 1997, Development of a closed loop control system of a deep drawing process based on a neuro-fuzzy approach, *Proc. of III AITEM Conference*, 319-326.
28. R. Di Lorenzo, G. Perrone, S. Noto La Diega, 1998, Design of a fuzzy controller for the deep drawing process by using GAs, *Proc. of the 2nd Int. Conf. on Knowledge based intelligent electronic system*, 102-108
29. Mamdani, E. H., 1977, Application of Fuzzy Logic to approximate reasoning using linguistic synthesis, *IEEE Trans. Computers*, vol.26, 1182-1191.
30. Lange, K., 1985, Handbook of metal forming, McGraw Hill.

EVALUATION OF FULLY PARALLEL AND HYBRID KINEMATICS FOR ADVANCED MANUFACTURING SYSTEMS

H. K. Tonshoff, G. Gunther and H. Grendel
University of Hannover, Hannover, Germany

KEY WORDS: Parallel Kinematics, Hybrid Kinematics, Hexapod, System Design

ABSTRACT: owing to the increasing interest in parallel kinematics different parallel and hybrid Systems were proposed and realized in recent years. Due to the different structures and drive principles there are a lot of design possibilities. In order to enable a comparison between the systems among each other and with the conventional systems the criteria of comparison have to be adapted to the parallel kinematics. Already a comparison between fully parallel kinematics and hybrid kinematics appears difficult due to their different characteristics such as workspace, stiffness, isotropy and so on. Also, there are a lot of possibilities of construction. For example, the chosen drive type and the applied joints affect the comparison criteria.

In the paper an overview of the existing parallel kinematics and their applications is given. After that, two different systems and their properties are introduced. Thereby different boundary conditions (drive system, joint angles, strut arrangement) are taken into account and their influence onto the system characteristics is examined. As criteria for the comparison the resulting workspace and stiffness were chosen because, on the one hand, the ratio between the workspace and the size of the machine is considered as the main disadvantage of parallel kinematics, on the other hand, the high stiffness is the main advantage of these systems.

1. INTRODUCTION

Parallel kinematics have become one of the most interesting research areas in production engineering in the last years. The main property of parallel kinematics systems is the existence of a closed kinematics chain within the structure. Hence the possible application area for parallel kinematics is not limited and includes robotics, machine-tools, position devices, measurement machines and other special elements or components for production or related fields.

New systems with a different kinematics structure as conventional robots or machine tools have been proposed and designed. The axes are connected in a parallel way, which offers new system characteristics like improved stiffness caused by the parallel strut arrangement or higher dynamics due to the lower masses to be moved.

In the robotics parallel kinematics are well known for special applications like high speed pick and place tasks. The Hexapod-structure is also used in simulators for a long time. However the investigation in parallel kinematics has become a new stimulating impact for the machine tool as well as the robotics sector in the last years. The choice of the system structure that fits to the foreseen application is one of the most important tasks for the system designer. This means not only the characteristics of the system components but also the structure itself e.g. the arrangement of struts and drives.

New machines have been developed for many different applications. Research institutes, laboratories and companies are working on further developments in order to build machines, which are competitive to conventional machines in speed, stiffness, accuracy and costs.

In the first part a survey of the state of the art of existing parallel kinematics and their fields of application is given. In the second part a comparison of different structure designs for these new machines will point out that a careful design is always necessary.

2. ADVANTAGES AND DISADVANTAGES

Taking all theoretical and design basics into consideration, many different designs of parallel kinematics are conceivable or have already been realised. All of them have the same goal: to achieve some advantages compared to serial robots and/or machine-tools. The structural advantages were discussed in many papers before [1,2,3,4]. The main characteristics can be summarised as follows :

advantages:

- only compression and tension in the struts; no bending forces,
- parallel strut construction leads to greater rigidity and better stiffness,
- low masses to be moved enable high dynamics,
- many equal parts and therefore the possibility of modular design as well as
- favourable ratio between masses to be moved and load capacity.

disadvantages:

- unfavourable ratio of system size to workspace,
- limited dexterity and small tilting angels ($\pm 15^\circ \dots \pm 30^\circ$) as well as
- inherent danger of strut collision; singularities in workspace.

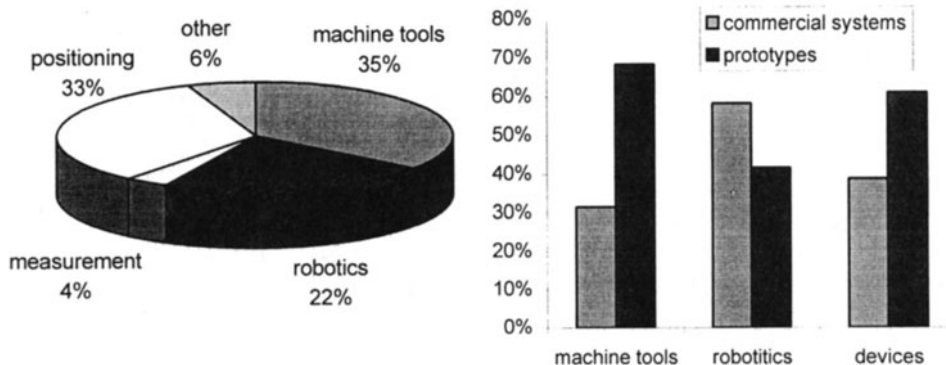
There are some more drawbacks due to the low practical experience in this new technology and the lack of standardised components and calibration procedures.

However optimisation steps to design parallel kinematics have the target to support one of the listed advantages as far as possible or to avoid one of the disadvantages in special.

Therefore an evaluation of the listed characteristics is absolutely necessary in relation to the planned application. An universal solution offering the best performance for all applications is not realistic. In this field a configuration tool could be very helpful for the system designer [5].

3. FIELDS OF APPLICATION IN THE PRODUCTION TECHNIQUE

The IFW, Hannover, has built up a database that contains the data of 58 different parallel kinematics for various applications in production engineering. The following statements are based on this database. In figure 1a the distribution of different applications is shown.



a)

b)

Figure 1: Applications of parallel kinematics systems

This figure refers to the number of different systems and not to the total number of manufactured systems. It is obvious that the most parallel kinematics applications are machine tools, positioning devices or robots. The highest percentage belongs to the machine tool sector. But it has to be pointed out that in this field the number of prototypes is much higher than the number of commercial systems (figure 1b). Up to now there are only few systems in industrial use. In most cases only one prototype of each machine has been built. Only in the field of robotics the number of marketable systems is higher than the number of prototypes. One reason for the different ratio of prototypes to marketable systems in the

mentioned applications is caused by the longer experience with parallel kinematics in the robotics.

The IFW database contains about 20 different machine tools. Of only five of them an amount of more than one item has been set up. In total about 30 machine tools based on parallel kinematics are built. Details of different parallel kinematics machine tools, robots and devices are listed in [6].

In the robotics several systems with over fifty sold items are on the market. This means that the total number of all manufactured parallel robot units is about 10 times higher than the number of parallel kinematics machine tools.

In the field of positioning devices it is very difficult to list the existing systems because many research activities in parallel kinematics start with a hexapod based positioning platform, but not all of them are presented in papers. But also in this field some positioning platforms are commercially offered.

4. HYBRID KINEMATICS STRUCTURES

Some mechanisms consist of a combination of parallel kinematics and serial kinematics. Those mechanisms are called hybrid kinematics structures. In addition to the classical Hexapods also Tripods and Tripod-based hybrid kinematics [7], as well as different other hybrid structures were analysed in regard to their adequacy for special applications.

In figure 2 the ratios of fully parallel to hybrid kinematics structures are presented for all known systems and separately for the three main sectors of applications. The figure shows that over 80% of the various parallel kinematics systems are fully parallel. This structures are mainly Hexapods (6 DOF) but there are also fully parallel systems with 3 DOF.

If the system needs a higher dexterity, the system designer has to take into consideration the advantages of hybrid structures. Hybrid systems improve the ratio of system size to workspace, mainly caused by the increased tilting angle of the end-effector. On the other hand the aimed advantages of the parallel systems especially the stiffness has to be checked carefully. This could be one reason, why in some sectors, where high stiffness is necessary like in machine tools or devices, the percentage of fully parallel systems is over 90%.

In the field of robotics the situation is different. Here the hybrid structures have an amount of nearly 42%. This higher percentage of hybrid structures is caused by the need of a higher dexterity in the robotics. Furthermore robots require less stiffness than machine tools. The scope of application aims at more than the simple handling and assembling. Different companies and research institutes try to construct parallel kinematics for the application area between robots and machine tools. This means that the use of parallel kinematics is applicable for tasks where serial robots do not ensure enough stiffness or accuracy, a machine tool's workspace is not big enough or a conventional machine tool is too expensive to be constructed in the needed size. Here hybrid kinematics have a good chance on market, because they have higher dexterity compared to hexapod-systems. The Tricept of Neos Robotics for deburring and assembling with high forces in Z-axis, the robot Multi-

Craft 560 for deburring and grinding [8] and the prototype Georg V. for laser cutting, developed at Hannover University [9] have already proven their advantages.

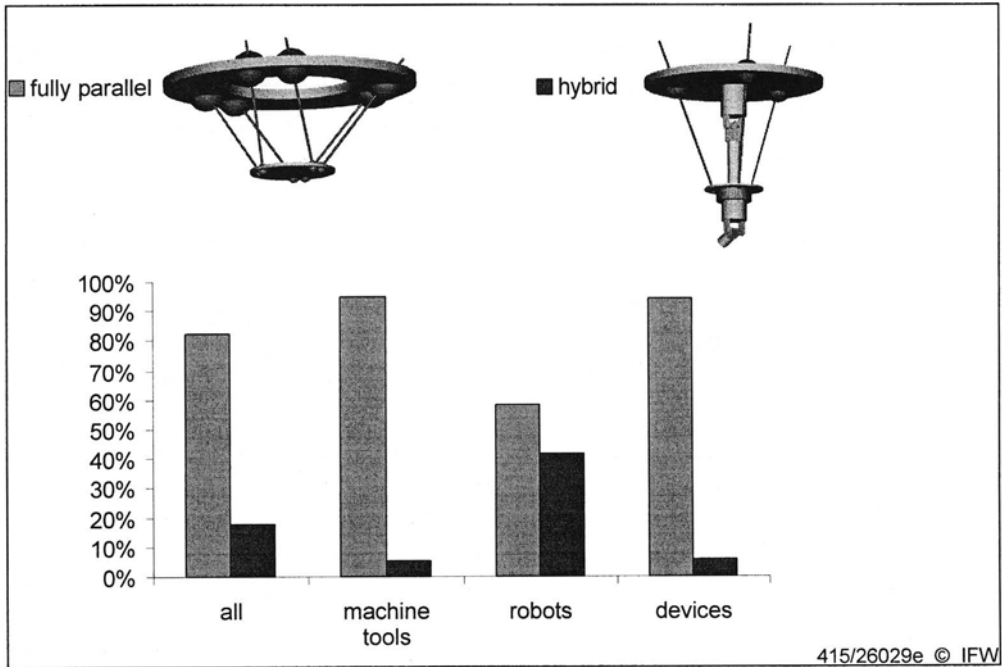


Figure 2: Various parallel kinematics structures in different production sectors

The high number of sold Tricepts TR 600 (over 80 items) and MultiCraft 560 robots (over 50 items) indicate that a market exists for such robots and machines respectively. With the new version of the Tricept called TR 805 the gap to the machine tool performances will become smaller once again. However the tripod based hybrid structures are only one possible solution to build hybrid mechanisms.

5. WORKSPACE AND MOVEABILITY

Generally, the determination of the workspace is more difficult for spatial parallel kinematics than for serial kinematics [10]. The workspace is the set of all poses which according to the kinematics can be reached beginning from the zero position. The difficulty is that in contrast to serial tool machines the workspace can not be split up into two independent workspaces describing the possible position resp. orientation. In case of parallel kinematics the orientation ability depends on the position. The workspace is completely embedded in \mathcal{R}^6 which can not be conceivably represented. Thus, illustrations of results are restricted to cuttings and projections of the workspace into \mathcal{R}^3 or \mathcal{R}^2 .

Often, an intersection through the workspace is used in which the orientation and one space co-ordinate is fixed or a cutting of the workspace is applied in which certain orientations are possible.

The workspace is restricted by various boundary conditions. These are restrictions due to the limited traverse path of the axes, possible internal collisions between struts and limited angles of the passive joints. Also, the workspace can be restricted by singular positions.

6. SINGULARITIES

When applying parallel kinematics there are two types of possible singularities. The first type of singular positions, also known from serial robots, results in the loss of a degree of freedom of the end-effector. A demanded velocity of the end-effector can not be reached with finite velocity of the axes. Close to singularities of this type high velocities of the machine axes appear. In this position the determinant of the Jacobi matrix is zero $\det(\mathbf{J}) = 0$.

The other type of singularity occurs if the determinant of the inverse Jacobi matrix is zero $\det(\mathbf{J}^{-1}) = 0$. This position results in an additional degree of freedom. A force onto the end-effector can not be compensated with finite forces of the drives. Close to these singularities high forces onto the axes appear.

These types of singular positions in the workspace have to be avoided at the design stage of the structure. The calculation of the inverse Jacobi matrix can not always be solved analytically and to find the roots of the determinant in a closed form is very costly. Thus, often numerical or geometrical methods are used in order to find the singular positions [11]. These problems of singular positions are well known in the robotics, but up to now uncommon in the field of machine tools.

7. USABLE WORKSPACE

In order to clarify whether a certain task can be performed by kinematics a determination of the workspace is not sufficient. Beside the fact that the demanded positions are within reach other characteristic parameters have to be taken into account. For example, these parameters might be the required stiffness and velocity. Thereby, either the absolute values or the conformability in the different space directions (minimal anisotropy) are required.

8. STIFFNESS

Similar to serial robots the stiffness of parallel kinematics is much more dependent of the position compared to conventional machine tools. Flexibility is located mainly in the joints, motors and struts. The frame can be made relatively stiff. To calculate the complete stiffness of kinematics with length variable struts the stiffness of each single component

has to be taken into account. With the stiffness k_i of the struts including the joints and drives, the over-all compliance matrix \mathbf{C} can be calculated via the Jacobi matrix \mathbf{J} to

$$\mathbf{C} = \mathbf{J} \mathbf{K}^{-1} \mathbf{J}^T. \quad (1)$$

Thereby, \mathbf{K} is the diagonal stiffness matrix in the machine coordinate system (MCS) which consists of the stiffness of the different struts k_i .

$$\mathbf{K} = \text{diag}(k_i). \quad (2)$$

With the function $f(\mathbf{q})$ the position vector \mathbf{q} (MCS) is transformed into the position vector \mathbf{x} in the Cartesian base coordinate system (BCS)

$$\mathbf{x} = f(\mathbf{q}). \quad (3)$$

The Jacobi matrix \mathbf{J} can be described by applying the partial derivation of the transform function f with respect to q_i (MCS) as

$$\mathbf{J}(\mathbf{q}) = \frac{\partial f}{\partial \mathbf{q}^T} = \begin{bmatrix} \frac{\partial f_1}{\partial q_1} & \dots & \frac{\partial f_1}{\partial q_{n1}} \\ \vdots & \ddots & \vdots \\ \frac{\partial f_m}{\partial q_1} & \dots & \frac{\partial f_m}{\partial q_n} \end{bmatrix}. \quad (4)$$

The above relation can also be formulated when using the inverse Jacobi matrix \mathbf{J}^{-1} , which for parallel kinematics can be easier determined as the Jacobi matrix \mathbf{J} .

The eigenvectors of the compliance matrix \mathbf{C} is orientated in the direction of the maximal and minimal compliance of the structure. The value of the respective compliance can be derived from the related eigenvalues.

For kinematics with moveable base points the procedure needs more effort. In this case, on the one hand, the stiffness of the drives and, on the other hand, the stiffness of the struts including the joints have to be transformed to BCS by using the two separated Jacobi matrices \mathbf{J}_A and \mathbf{J}_S . In the next step they have to be superimposed. The compliance matrix \mathbf{C} in the Cartesian reference system results in

$$\mathbf{C} = \mathbf{J}_A \mathbf{K}_A^{-1} \mathbf{J}_A^T + \mathbf{J}_S \mathbf{K}_S^{-1} \mathbf{J}_S^T. \quad (5)$$

A comparison of the different drive principles is given in [12].

9. ANISOTROPY

Generally, the stiffness of the parallel kinematics in one operating point varies for the different spatial directions. Thus, it shows an anisotropic behaviour. This means in practice that a force onto the end-effector leads to a displacement which not exactly follows the direction of this force.

The ratio between maximal and minimal stiffness for a point in the workspace is the condition number c of the Jacobi matrix \mathbf{J} . If the stiffness is equal for all spatial directions the condition number is $c = 1$. For anisotropic stiffness, c increases to $c > 1$. Mathematically the condition number c is the ratio between the maximal and minimal singular value σ_i of \mathbf{J}

$$c = \frac{\sigma_{\max}}{\sigma_{\min}} \rightarrow \min. \quad (6)$$

In turn, the singular values are the square roots of the eigenvalues λ_i of $\mathbf{J}^T \mathbf{J}$

$$\sigma_i = \sqrt{\lambda_i(\mathbf{J}^T \mathbf{J})}. \quad (7)$$

In general an anisotropic stiffness is acceptable within certain limits or when the application is suitable for the anisotropic system behaviour.

10. COMPARISON OF HYBRID AND FULLY PARALLEL SYSTEMS

In order to compare a hybrid and a fully parallel kinematics system a hexapod and a tripod system with a serial wrist joint were investigated. Starting point for the layout was a traverse path of 900mm for each leg of both systems, with the zero position in middle of the traverse path. The hexapod was designed for an optimal isotropy with a method introduced in [13]. The radius of the fixed platform is $r_A=2204.5\text{mm}$. The radius ratio of the fixed to the mobile platform is 2:1. The length of a strut in the zero position amounts to 2700mm. The tool length between the platform and TCP was fixed to 200mm. For the tripod equal struts and platforms were applied. The Tripod is equipped with a passive central strut avoiding a twist of the moveable platform. The swivelling axis in the wrist joint is limited to an angle of $\pm 110^\circ$ which, usually can be accomplished by robot wrist joints (for example, Neos Tricept TR600: 120°). The intersection point of the wrist axes is 200mm below the moveable platform. Also, the end-effector itself has the length of 200mm.

The stiffness of the joints is determined with $k_G=200\text{N}/\mu\text{m}$. This accords roughly to the stiffness reached by joints with two or three degrees of freedom [14]. Often ball screw drives are applied in order to transform the rotational movement of the motor into a linear movement. The stiffness of the drives, for example, received by the flexibility of the nut of the ball screw drive, is determined to $k_A=50\text{N}/\mu\text{m}$. For the length variable struts the product

of the elasticity modulus and the cross-sectional area is $EA=130000\text{kN}$. Thus, the length depending stiffness of $50\text{N}/\mu\text{m}$ for each single strut is reached when the strut length equals $u=2600\text{mm}$. The total stiffness of a single strut k_i is composed of the summing-up of the stiffness of the two joints, the length depending stiffness of the strut itself and the stiffness of the drive

$$k_i = \left(\frac{2}{k_G} + \frac{l}{EA} + \frac{1}{k_A} \right)^{-1} \quad (8)$$

The design for a minimal anisotropy results in restrictions regarding the workspace and, especially, the orientation capability. An other possible design goal is an optimal workspace [15]. However, the design for a minimal anisotropy was chosen because the small anisotropy of adequate Hexapods is a special advantage over other kinematics. Due to the many different design possibilities the used kinematics can not be seen as typically representatives of their classes. However, they enable a comparison of the respective system with one another by using the same components.

10.1. COMPARISON OF WORKSPACE

Figure 4 shows the workspaces of both kinematics depending on the demanded orientation of the TCP and on the limited angle of the passive joints.

It is conspicuous that the hexapod requires larger joint angles ($\pm 40^\circ$) than the hybrid kinematics ($\pm 15^\circ$) in order to cover the complete workspace.

However, the workspace of the hexapod depends more on the demanded orientation of the TCP than the workspace of the hybrid kinematics structure. When the demanded TCP orientation is already $\pm 20^\circ$ the workspace is reduced to the half, when $\pm 30^\circ$ it is reduced to the twentieth part.

The workspace of a hexapod when the TCP is vertical orientated does not change even when reducing the joint angle to $\pm 30^\circ$. However, in this case the workspace is heavily reduced if a set angle of the TCP is demanded. This trend is obvious looking at the orientation $\pm 30^\circ$, which can not be reached by the chosen hexapod structure with a limit of $\pm 30^\circ$ for the passive joints (see figure 4b).

This shows clearly the necessity of considering the mechanical boundary conditions when designing a parallel kinematics structure.

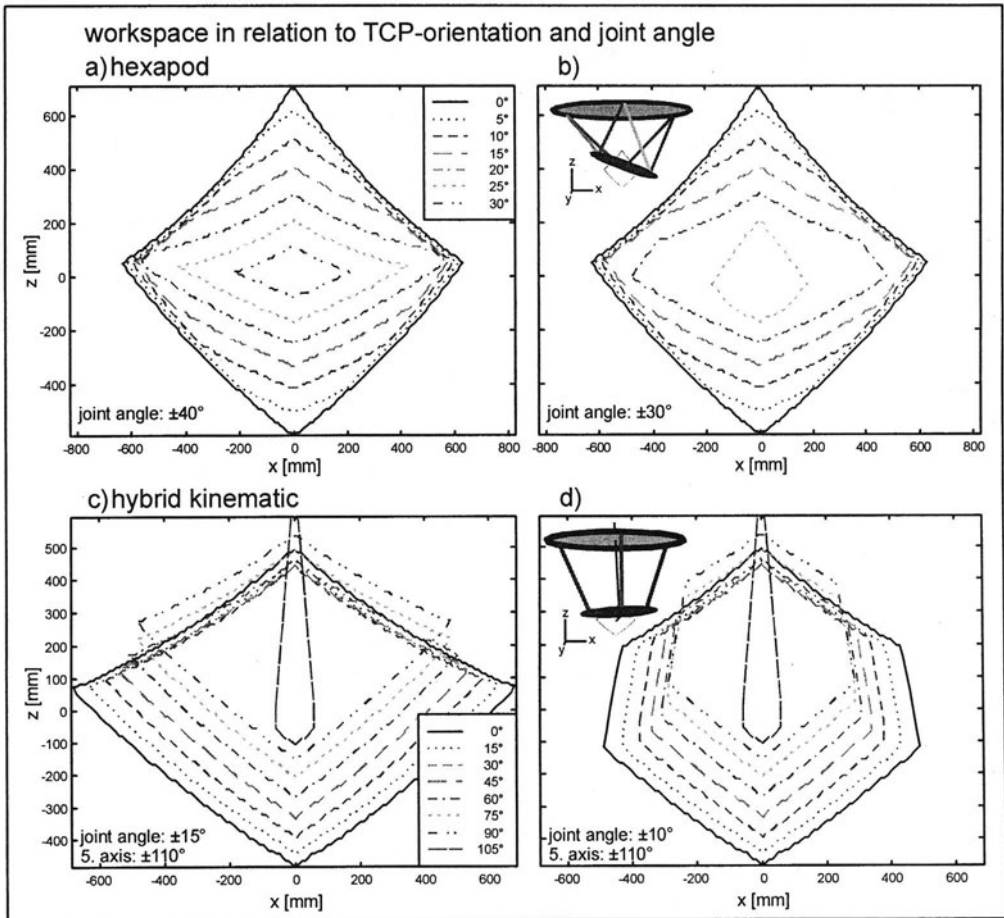


Figure 4: Comparison of the workspaces of a hexapod and a tripod with a serial wrist joint. $r_A=2204,5\text{mm}$, $r_B=1102,3\text{mm}$, traverse path $u=\pm 450\text{mm}$, average length of the struts $L_1=L_2=2700\text{mm}$

As expected, the workspace of the hybrid kinematics structure is only slightly limited up to the orientation of $\pm 30^\circ$ due to the wrist joint. There are no limitations of the workspace for the chosen system when the joint limits are $\pm 15^\circ$ (figure 4c).

If the joint limit is set to $\pm 10^\circ$ the workspace is clearly reduced by the joint limits. In turn, this limitation depends on the demanded orientation of the TCP. For a vertical orientation of the TCP the joint limit results in a shorter travel path in x-direction mainly. This leads to a 10% smaller hexagonal-shaped workspace (figure 4d).

Generally, it can be seen that for a hybrid kinematics structure, up to a demanded set angle of the tool of $\pm 90^\circ$, a workspace is existing which shows an advantageous ratio between height and width.

The achievable workspace of the hexapod for a vertical orientation of the TCP is bigger (ca.15%) than the one of the tripod structure with a serial joint. Comparing both structures it is also obvious that beginning with a demanded TCP orientation of $\pm 15^\circ$ the workspace of the hybrid structure is bigger than the one of the hexapod. The workspace of the hybrid structure in figure 4c for a demanded orientation of $\pm 90^\circ$ is even bigger than the workspace of the hexapod shown in figure 4a for a demanded orientation of $\pm 20^\circ$.

Thus, it is obvious that regarding the orientation capability in applications which require a flexible tool orientation, a hybrid kinematics has its advantages to a pure hexapod structure.

10.2. COMPARISON OF STIFFNESS AND ANISOTROPY

In the following figures the kinematics in the zero position and the limit of the workspace are shown. The length and direction of the arrows illustrate the displacement of the moveable platforms caused by a force in x- and z-direction, respectively. Only when forces taking effect in the direction of the main axes of the compliance matrix the structure evades only in the direction of the effective force.

The hexapod structure is shown in figure 5. The stiffness varies between $20.01\text{N}/\mu\text{m}$ and $69.93\text{N}/\mu\text{m}$. The stiffness vector with the maximum norm is located at the lower edge of the workspace in the vertical (z) direction. At this point also the lowest stiffness occurs in the horizontal (x) direction. In the upper area of the workspace the ratio between maximal and minimal stiffness is balanced with $c=1$ due to the system design for optimal anisotropy. Towards the margin and downwards this ratio increases up to $c=3.5$.

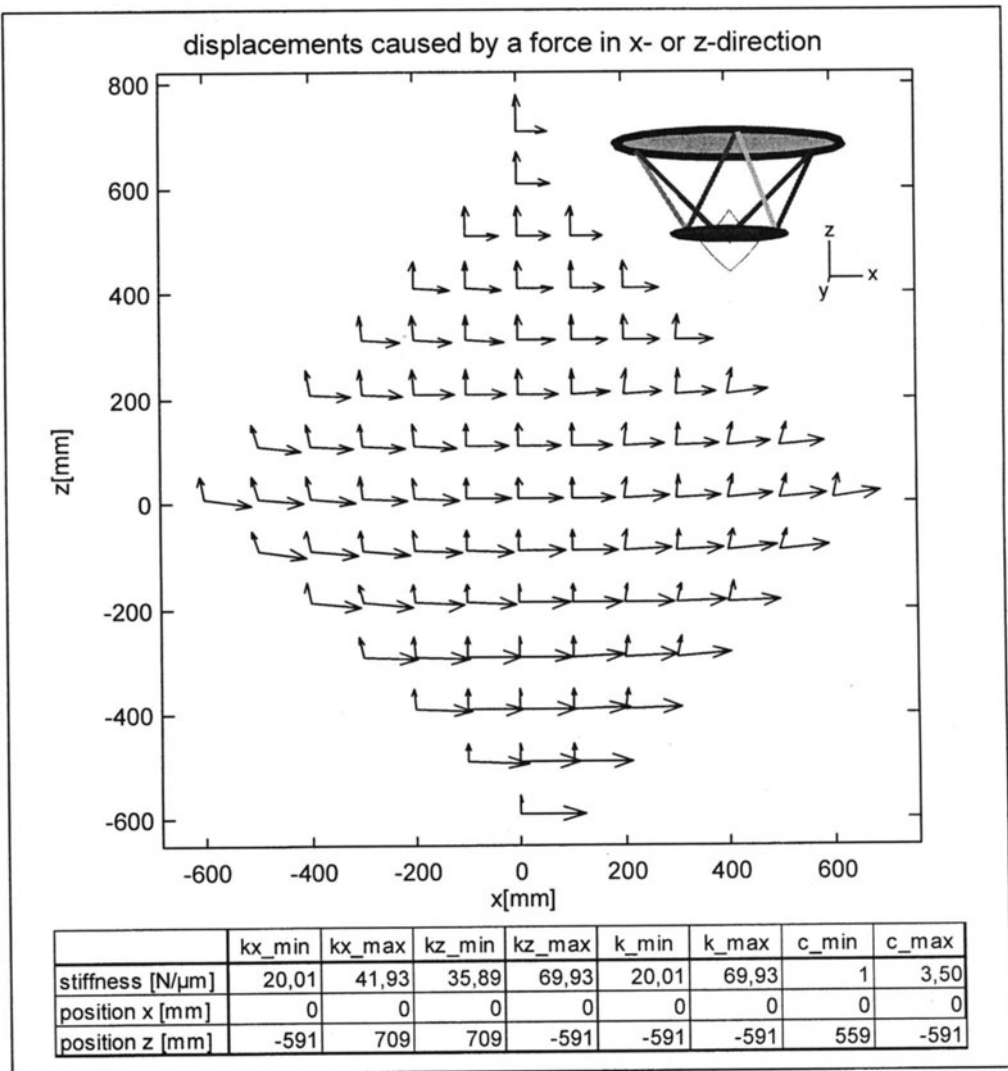


Figure 5: Hexapod structure. The traverse path from the marked zero position $u=\pm 450$ mm, average length of the struts $L_1=L_2=2700$ mm, stiffness of the joints $k_G=200$ N/ μ m, stiffness of the struts $k_S=EA/l$ with $EA=130E6$ N, stiffness of the drives $k_A=50$ N/ μ m.

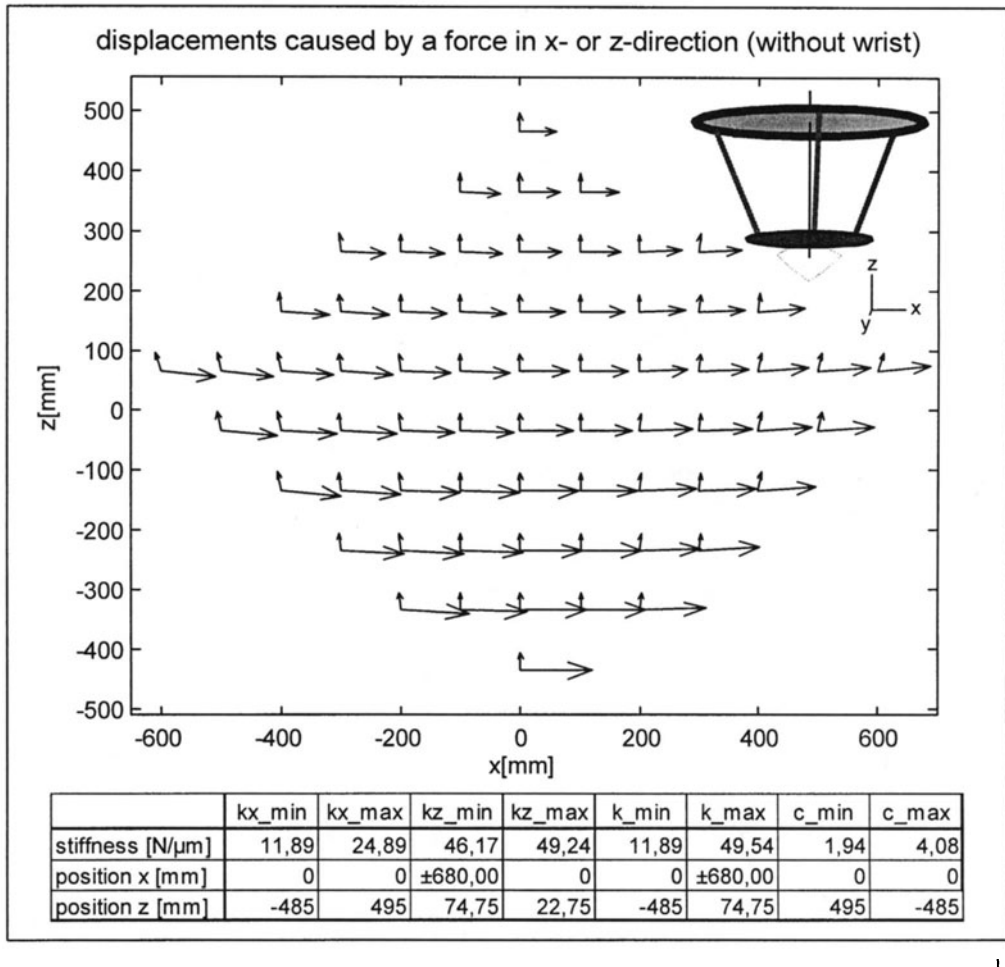


Figure 6: Hybrid structure with stiff wrist. The traverse path from the marked zero position $u=\pm 450$ mm, average length of the struts $L_1=L_2=2700$ mm, stiffness of the joints $k_G=200$ N/ μ m, stiffness of the struts $k_s=EA/l$ with $EA=130E6$ N, stiffness of the drives $k_d=50$ N/ μ m.

Figure 6 shows the stiffness characteristics of the tripod structure with a stiff wrist. The stiffness varies in the workspace between 11.89N/ μ m and 49.54N/ μ m. Due to the steep arrangement of the struts the stiffness values in x-direction are lower and the variations are stronger than in z-direction. Thus, the ratio between the maximal and minimal stiffness is minimal $c=1.94$ at the top of the workspace. Towards the bottom this ratio increases up to $c=3.5$.

The stiffness vector with the maximum norm is located at the left and right edge of the workspace in a nearly vertical direction. The stiffness vector with the minimum norm

$k_{\min} = 11,89\text{N}/\mu\text{m}$ is located at the lower edge of the workspace directed in the horizontal (x) direction.

In an additionally investigation it was proven that the maximum and minimum value of the stiffness of the chosen hexapod occurs in the margins of the workspace. This is quite different to the analysed hybrid structure. Normally the maximal stiffness in the z-direction is located, like in the hexapod structure, at the bottom of the workspace. This behaviour is caused by an optimal angle between the direction of the elongated struts and the vector of the z-force at the lower boundary of the workspace. But for the analysed tripod, the length variable stiffness of the strut reduces the total stiffness more than the strut direction increases the total stiffness of the system.

The maximal stiffness of the hexapod is higher due to the simple fact that the six struts in a parallel arrangement are more stiff than three. Moreover, the anisotropy in the workspace is higher for the hybrid system compared to the hexapod system.

It has to be pointed out that the stiffness comparison of the two systems are made for a vertical orientation of the end-effector. The influence of the end-effector itself (of both systems) as well as the influence of the wrist of the tripod was ignored for the stiffness calculation. Thus in practice, the mounted wrist at the tripod will lead to a significant decrease of the total stiffness mainly in the horizontal direction.

11. SUMMARY

Parallel kinematics were first developed and used in the 40's to 60's. These platforms were mainly used as simulators. Within the field of the robotics parallel kinematics were developed for fast handling tasks at the end of 1980's.

The first experiments, to utilise parallel kinematics for machining and especially for milling led to intensive discussions and reports in research and industry. Until now many different research institutes and commercial providers developed parallel kinematics for different applications. There are over fifty different build machines, robots and devices. The number of build items depends on the application sector. Most of the parallel kinematics in the machine tool sector are prototypes. Only few companies have build more than one unit of their machines. In the robotics there are commercially available systems with higher numbers of build items. In this sector also hybrid kinematics are used.

Fully parallel systems and hybrid kinematics systems have different characteristics. This was clarified in the examination of main system parameters like workspace, stiffness and isotropy. A general comparison between the different kinematics is affected by the diverse possibilities of realising such structures. The comparison of parallel and hybrid structures was restricted to kinematics with similar geometry and the same drive principle. In this comparison the workspace of a fully parallel and a hybrid structure were examined with

varying TCP orientations. Thereby, it was shown that the workspace of the considered hexapod is slightly bigger than the one of the hybrid kinematics system for a vertical TCP orientation. However, the workspace of the hexapod decreases significant for increasing tilting angles. Thus, the workspace of the hexapod with an orientation of $\pm 20^\circ$ is already smaller as for the considered hybrid kinematics structure with an orientation of $\pm 90^\circ$. Moreover, the requirements on the joint angles of the parallel part of the hybrid are less. Thereby, it has to be taken into account that the achievable stiffness of a tripod (only three struts) is lower than the stiffness of a hexapod system. Furthermore the anisotropy is higher for a hybrid kinematics system, which mean these systems often have a preference axis of stiffness.

System characteristics of fully or partial parallel systems can be calculated at the design stage already, when the characteristics of the mechanical components are known. In the investigation both mechanical boundary conditions (like joint limits and stiffness of components) and requirements on the machine (orientation capability) are covered. System characteristics have a strong dependence on the mentioned criteria. However, the systems suit to different tasks. The orientation capability and stiffness are the main features to distinguish the different fields of application. The investigation points out the necessity to develop the system design according to the user requirements.

REFERENCES

1. Hesselbach, J.; Thoben, R.; Pittschellis, R.: Parallelroboter für hohe Genauigkeiten, *wt-Produktion und Management* 11/12, 1996, S. 591-595
2. Zirn, O.; Preu, H.-J.; Hebsacker, M.; Honegger, M.: Potentiale paralleler Kinematik, *Steuerung und Antriebe parallelkinematischer Werkzeugmaschinen, Werkstattstechnik*, 88, No.1/2, S. 53-56, 1998
3. Weck, M.; Giesler, M.; Pritschow, G.; Wurst, K.-H.: Den hohen Anforderungen gerecht. *Neue Maschinenkinematiken für die HSC-Bearbeitung, Schweizer Maschinenmarkt*, 45, S. 28-35, 1997
4. Neugebauer, R.; Wieland, F.: *Neue Werkzeugmaschinenstrukturen, Zwf*, 7/8, S. 363-366, 1996
5. Pritschow, G.; Wurst, K.-H.: *Systematic Design of Hexapods and other Parallel Link Systems, Annals of the CIRP Vol. 46/1/1997*, pp. 291-295
6. Tönshoff, H.K.; Grendel, H.: *A systematic comparison of parallel kinematics, Draft proceedings of the first European-American-Forum on parallelkinematic machines, 1998*
7. Tönshoff, H.K.; Soehner, C.; Isensee, G.: *Vision-Guided Tripod Material Transport System for the Packaging Industry, Robotics & Computer-Integrated Manufacturing, Vol. 13, No. 1, pp. 1-7, 1997*
8. Kochan, A.: *Parallel robots perfect propellers, Industrial Robot, Vol. 23, No.4, pp. 27-30, 1996*

9. Tönshoff, H.K.; Soehner, C.; Ahlers, H.: A new machine tool concept for laser machining, Proc. Int. Seminar on Improving machine tool performance, San Sebastian, pp. 119-124, 1998
10. Gosselin, C.; Ricard, R.; Nahon, M.A.: A comparison of architectures of parallel mechanisms for workspace and kinematic properties; DE-Vol. 82, Design Engineering Tech. Con. Vol. 1, ASME, 1995
11. Takeda, Y.; Funabashi, H.: Kinematic and Static Characteristics of In-Parallel Actuated Manipulators at Singular Points and Their Neighborhood, JSME (Japan Society of Mechanical Engineers) International Journal, Series C, Vol. 39.No. 1, 1996
12. Tönshoff, H.K.; Günther, G; Grendel, H.: Vergleichende Betrachtungen paralleler und hybrider Strukturen, VDI Berichte Nr. 1427, S. 249-270, 1998
13. Huang, T; Whitehouse, D.J.; Wang, J.: The Local Dexterity, Optimal Architecture and Design Criteria of Parallel Machine Tools, Annals of the CIRP Vol. 47/1/1998, pp. 347-351, 1998
14. Bode, H.; Heisel, U.: Gestaltung und Bewertung von Gelenkeinheiten für Maschinen mit Hexapod Kinematik Teil II, Chemnitzer Parallelstruktur-Seminar, Tagungsband, S.41-49, 1998
15. Merlet, J.-P.: The importance of optimal design for parallel structures, Draft proceedings of the first European-American-Forum on parallelkinematic machines. 1998

THE CONCURRENT ECODESIGN METHODOLOGIES
ECO SUSTAINABLE TECNOLOGIES FOR PRODUCT AND PROCESSES

G.F. Micheletti
Polytechnic of Turin, Turin, Italy

KEY WORDS: Ecodesign, Life Cycle Analysis, Life Cycle Engineering, L.C.A

ABSTRACT: Life Cycle has and shall play an increasing role in the future, by influencing industrial management and eco-management putting together producers, suppliers, customers to properly face the environment needs. Concurrent ecodesign enables, at design level, to anticipate, many of the problems that arise at the end of a product life. Eco-sustainable technologies shall be faced with a global monitoring as a summa of sub-monitoring and pre-monitoring activities, together with “ad hoc” simulation tools. New methods of costs auditing should be structured, involving the whole product life cycles where likely new business areas could arise.

1. INTRODUCTION

A paper has been presented by the Author of this key-note paper at the AMST Conference (Udine, September 1996)¹, in which the investigation of the role of Ecodesign was made, along four main guidelines in the area of Life Cycle:

Life Cycle Analysis - Engineering - Assessment - Development Concept

¹ Role and Influence of Ecodesign on new products conception, manufacturing and assembly” by G.F. Micheletti, AMST’96 (September 1996 Udine Italy)

taking into account also the bases of the required ethical and psychological attitudes towards products friendly conceived in respect of the environment. It was already used the expression “*concurrent design strategy*”, derived from “*concurrent engineering strategy (CE)*”, this one being a concept very well known since several years², and yet currently applied in industrial production. The *concurrent engineering strategy* emphasises a better integration within the results and a fruitful stimulation, through the establishment in the company of groups involving experts from different areas, sustained by their personal experience and inclined to investigate together many issues of different nature. The Working Groups, put in action by “*concurrent engineering strategy*”, include designers, production engineers, quality and planning responsables, market operators a.s.o.

2. THE ECODESIGN STRATEGY

The evolution of the concept moving from *concurrent engineering strategy* to *concurrent design strategy* and now to *concurrent ecodesign strategy* requires that eco-experts are included in the teams together with ecoauditors, and ecodesigners who assure to the teams their sensibility to the environment problems. The ecodesigners, being active since the first start of the design phase (conception of the product), avoid subsequent corrections that bring to time delays and additional costs. The core of this methodology is a flexible composition of the teams (Enrolling Everyone), where various competencies integration is accomplished both acting inside the company and from outside the company (f.i. suppliers and customers issues). **Now AMST'99 presents a profitable occasion to verify the subject enhancement during the past three years time.** Without any doubt, design of new products is more and more addressed to prepare better perspectives in respect of the environment, to day mostly affected by industrial processes. Similarly, more and more urgent is the challenge on how industry is required to increase the integrated approach to such a complex scenario in creating environmentally compatible products. I would like to underline firstly the word **create** because, implicitly in the importance to recover and recycle as much as possible the dismissed industrial goods, there is the necessity to go up again to the source: the **product design phase**. Secondly, I underline the word **integrate**: the integrated approach is in fact a key-factor, since it involves managers, experts, disciplines, materials, manufacturers, users, recyclers that are requested to cooperate together along a continuous path, whose goals are strongly conditioned by the quality and intensity of the integration itself.

3. CONCURRENT ECODESIGN (CED)

To better illustrate this interaction, let's have a look on Fig. 1 showing the diagram of Concurrent Engineering (CE) and the loop of Concurrent Ecodesign Strategy (CED); Prospect 1 and Prospect 2 respectively reproduce the definition of each term.

² Since its adoption in USA after 1989.

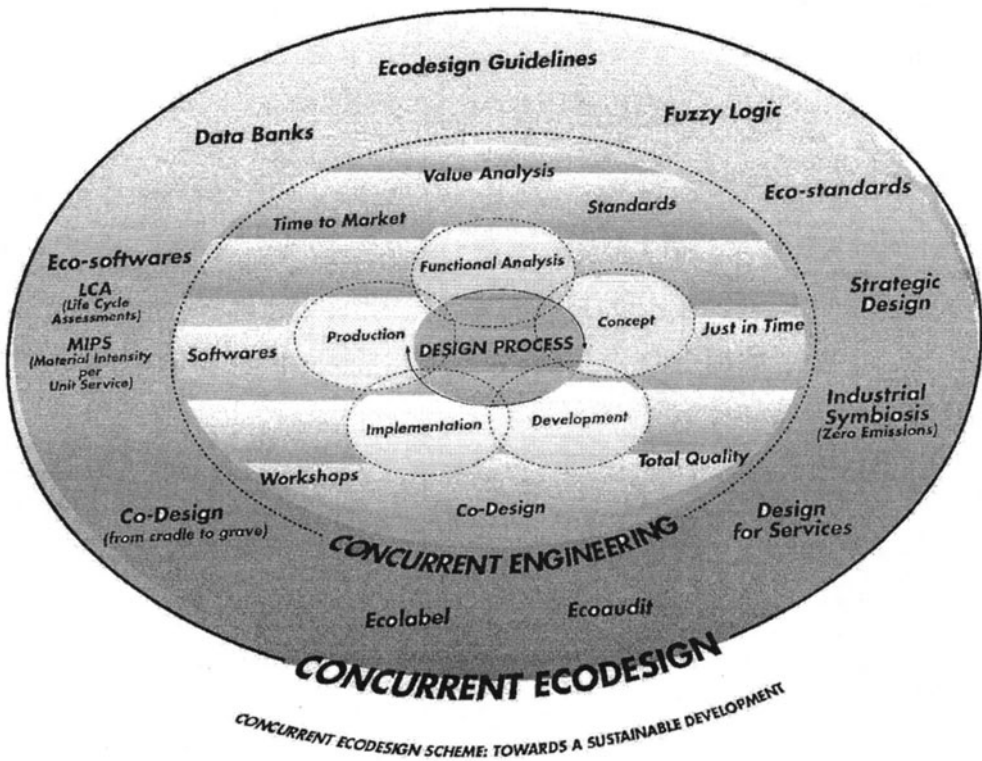


Fig.1: Diagram of Concurrent Engineering and Concurrent Ecodesign towards a sustainable development

<p>Concurrent Engineering (CE)</p> <p>The core is identified in the Design Process</p> <p>Usual procedures connected with it are: <u>Functional Analysis, Concept, Development, Implementation, Production;</u></p> <p>that involve:</p> <p>Software: Tools and programmes appropriate and customised for the company, product and manufacturing process;</p> <p>Standards: following the norms (f.i. UNI ISO 8402; UNI EN ISO 9000; UNI EN ISO 9001) and Protocols (f.i. STEP, Standard for Exchange of Product Model Data - ISO 10303 ...);</p> <p>Value Analysis: evaluation of the activities finalised to optimise the quality level and the costs reduction;</p> <p>Time to Market: time (and costs) reduction between design and dispatching;</p> <p>Just in time (JIT): analysis to minimise the quantity of material or components or products at the warehouse and to assure their punctual delivery</p> <p>Total Quality: conformity to the principles of Quality Assurance and Quality System.</p>	<p>Prospect 1</p>
--	--------------------------

Prospect 2

The concurrent Ecodesign (CED)

The core doesn't change, being the **Design Process**.

Ecodesign Guidelines: Rules and suggestions to be applied since the beginning of conception activity for designing new products, paying attention to the eco-system.

Data Banks: collecting and memorising data and information both for considering the requirements of the product, and for a proper use of the resources (materials, processes, a.s.o.).

Eco-Software's: info-techniques to support the design and to evaluate the environment requirements of the products, processes, materials; there are software tools allowing quantitative evaluations of environmental impacts of the product system all Life Cycle long; they can be grouped in two main categories: LCA (Life Cycle Assessment) and LCI (Life Cycle Inventory)*.

Another important software tools category is given by: DFX (Focused Analysis Tools, or Dedicated Instruments), for special strategies (f.i. to minimise the Use of toxic materials, to Design for recycling, to Design for disassembly**).

Co-Design (from cradle to grave): a system involving the use of Internet and Intranet in order to include, in the design phase, designers placed in different part of the world, connected by terminals; all the actors involved in the design join their competence sharing the elaboration and the common responsibility; the connection of all participants in real time cancel and overtake the concept of the physical distance between end-users, designers, producers of components and dismantlers.

Eco-standards: The way to follow the international and national Standards (f.i. EMAS standard in EU; ISO 14000 and UNI EN ISO 14001 all over the world)

Eco-Label: specific quality label for environment (to assure that a product has a better environmental approach);

Eco-Audit: certifications issued to industrial plants following certain standards;

Design for Services: the identification and the planning of activities accompanying the productive process; it can be extended to companies that offer - for instance - consultancy, organisational strategies, softwaring programmes research & development addressed to key aspects of ecodesign.

Industrial Symbiosis: plants proper localisation in order to optimise strategically the productions (it may happen that the waste of a company can become raw material for another placed in the same area), the same symbiosis could be planned in spite of geographical distances, depending on the material volume.

Strategic Design methodology for analysing alternative solutions to the system complexity, with the help of finalised hypothesis based on a mix of Design, Management, Technologies, Human Resources; it could assist in managing not only products and technologies, but also the philosophy and decision making of the companies: for instance should be possible to optimise the results instead of product itself, reaching the goal to simplify the consumers world, increasing the design for services and the efficiency of the performance.

Fuzzy Logic: it is a chapter of logics-mathematics, allowing to attribute a sort of artificial intelligence to components, through the use of interactive microprocessors; Fuzzy Logic regards to environment acts in two ways: optimising product complexity management during their use; proposing a longer product life through a friendly behaviour-sharing between product and product-owner (better care in the use of product).

Factor 4,4+ and 10: tend to reach the same results in terms of welfare, products and services with a reduction of materials used, according to the indexes indicated.

This doesn't sound to penalise the industrial enterprises, but to assure an help because it should give the opportunity to continue the Sustainable Development, reducing the negative aspects especially linked to the materials world.

* Among them: Boustead Model, Buwal 250, ECO-it, EcoScan 2.0, SimaPrò, TEAM/DEAMs, LEADS

** Design for environmental software tool, ECODESIGN TOOL, Idemat, LAsER, P2-EDGE, RECOVERY, RECREATION, ReGrEd/DisPlay, ReStar, RONDA e.s.o.

Apparently, could appear an easy one the extension from CE to CED, that significantly includes the environmental factors; but in fact, should induce several difficulties, because both the two methodologies are merged in the Concept Design: the first one, limited to the

Design Process using the engineering tools interacting with this, while the second one aims at introducing information that could become compulsory to manage the complexity of the environmental problems. Both CE and CED seem to perform the function of an “umbrella”, guesting inside many other functions capable to encourage and foster products “willing to react” to the environmental requirements. In fact, CED generates Ecodesign, and Net Co-Design techniques, Strategic Design, Design for Services, extended to the whole cycle of the product. Life Cycle Assessment, Industrial Symbiosis, MIPS (Material intensity per unit service) represent the further developments to accomplish the objective, that is “closing the loop”.

The afore mentioned list of procedures must be enriched by “eco-need” additional definitions, as made clear in Prospect 2.

4. RUNNING PILOT INITIATIVES

Some very interesting pilot initiatives have been set out, still running and spread in many different industrialised countries: mainly in West Europe, USA, Japan. The pilot initiatives demonstrate that undoubtedly the core of the problem is placed, and must be faced, during the initial phase of the product birth: how it is conceived and made feasible for the manufacturing processes, taking into account the concrete reality, the technical constraints, the management requirements, the economical parameters and, at least, the recycling that is the link to soundly and correctly close the environment compatible loop.

An “ad hoc” Project has been submitted and approved by the European Commission (DG XII-C-1 Brite-Euram), following the Proposal of a significant number of partners (among them, the Politecnico di Torino) in the area of Industrial and Materials Technologies Programme for Thematic networks. The subject of the Programme - entitled ECOLIFE - is “*Closing the Loop of Electr(onic) Products and Domestic Appliances - From Product Planning to End-of-Life Technologies*”. The Programme will be developed within 3 years duration and involves 28 Partners, from the three main areas of Industries, Universities, Research Institutions.

Life Cycle is the starting point that gives the possibility to select and manage the successive stages of the product flow: *design, manufacturing, packaging, distribution, use, disposal*. For each stage it’s interesting to identify and evaluate the parameters involved as energy, water consumption, solid waste, water emission, air emission, raw materials.

End-of-life aspects should be considered as a prosecution of the chain, the last ring of which is reached when closing the cycle; i.e. where are set up the solutions profitably and efficiently found. Therefore ecodesigners suggest a reformulation for the existing products, to minimise their actual impact on life cycle: some others emphasise the urgency an entirely “thinking new”, keeping in mind that recycling must become a function not only equal, but in some cases even predominant among design specifications.

It's undoubtfull that components and design selection are conditioned by the convergent flow of engineering requisites, manufacturability, energy, performance, usage, environmental effects due to hazardous materials, beside cost and time: among them a sort of creative compromise will be found. The point is to know in advance the dimensions (range, feasibility, efficiency) of each contribution, so that decisions agreed and made at the design stage affect a positive impact on the subsequent recycling process.

In addition, the problem is how to put ecodesign also in business perspective, after having evaluated the right priorities towards the biggest outstanding issues on implementation.

5. FROM DESIGN AS "DRAWING AND STYLING" TOWARDS ECODESIGN AND INDUSTRIAL FUNCTIONALITY

In the Politecnico di Torino is very active an interdisciplinary group of professors, researchers, designers working with their students on focusing "ecodesign" (the members of the team belong to both Faculties of Engineering and Architecture). They have discussed and agreed a sort of dodecalogue as interrelated guidelines, that can be synthesised as follows:

1. to forecast firstly the entire product's life cycle, including the components, and consequently adopting a design which optimises the production processes and progressively all the other phases, taking into account the re-use, the disposal, a well-balanced obsolescence and life-time of all the parts (or at least for some of the more relevant group);
2. to adopt a design aimed at simplifying the object shape, giving preference to modularity rather than a rigid standardisation of various elements;
3. to reduce, where and if possible, the dimension and therefore the materials quantity;
4. to address the design, since its origin, towards disassembly, defining in advance the failure area, compacting symmetric parts, adopting modularity, simplification, rationalisation and preferring a design conceived "by components";
5. to encourage as much as possible the use of the same materials or at least similar, easily compatible and recyclable, marking each material for a complete identification;
6. to aim at a design, able to minimise the manufacturing processes and the energy consumption;
7. to adopt lean technologies, reducing also as much as possible the energy non-renewable sources;
8. to low the noise itself, in order not to add too much of insulating materials;
9. to elaborate eco-budget before the manufacturing stage, improving a progressive optimisation;
10. designing the packaging together with the product itself (parallel design to avoid risks in the phase of transport and stocking);
11. to rethink the results within the frame of an aesthetic image (configuration) of an attractive styling;
12. finally to inspire the breath of a new ethics addressed to both the producers and the user/consumers.

It is evident, but not easy to put in action, the “orchestration” of the 12 points together.

6. FUNDAMENTAL MODES FOR ENGINEERING THE PRODUCT TOWARDS AN ECO-COMPATIBLE CONCEPT

Once agreed that design and engineering should share together the path, it starts the product venture within CE and CED frameworks. Connected with the adaptation of the product to production exigencies (i.e. engineering), during the phase in which the product is assessed from the original design to the version ready for production, two more needs arise, namely *Design for Manufacturing (DFM)* and *Design for Assembly (DFA)*, extended to ecological requirements.

The key phases for manufacturing are:

1. *Selection of materials*, that must be based on the various parameters and not only on the costs, which are affected by weight, energy consumption to produce the material, contaminant substances, and possibility of subsequent re-use;
2. *Number of the components* that must possibly be minimised to improve the maintenance operations and the whole quality of the products; in addition, to reach better assembly conditions since products with a small number of components are those not having a wide variety of materials, not relative motions between the parts and finally not requiring disassembly operations for the maintenance;
3. *Machining process*: must be reduced at a minimum, simplified and performed on a restricted number of machines; similarly the semi-manufactured materials from which the parts are made must be chosen to minimise the depth of cut;
4. *Assembly operations* are closely connected to the shape of the components; for instance, a symmetric piece does not require orientation; a piece without holes or groove doesn't face the danger of hooking in the automatic feeders; on the contrary, chamfers and fitting facilitate the flow;
5. *Connections*: better to use screws, if a reversibility is required, or welding and gluing, or riveting (if reversibility is not needed);
6. *Disassembly and recycling* are connected with the exigencies to plan since the very beginning, to allow the convertibility and the re-use of the product at the end of life.

7. AN EXPLORING-PRAGMATIC PROPOSAL DEVELOPED AT MIT

At the opening of this paper integration was mentioned as the predominant postulate. Some integration methodologies have been studied and adopted to get, in short times, models and analytical tools allowing the designers to correlate the traditional technical parameters with the environment corollaries. The Massachusetts Institute of Technology (MIT) turned into an experimental way, starting from a CAD programme already set for the design of a PC body and investigated how to implement it according the Life Cycle requirements.

Though the existing programme was divided into segments in order to manage each segment separately, giving each one the same level of importance. Each segment has the chance to flow along following iterative paths: times are increased, but it is possible to proceed with sub-optimal solutions reached step by step, each of them in a balanced contest there the modules are conceptually separated, but can be later evaluated simultaneously by experts with dedicated competencies.

Mathematical models support the preparation of the product programmes, inclusive of Life Cycle requirements. The resulting strategy of a modular integrated production, where every module is visible to other modules by means of standard interfaces, allowing to transfer information and exchange. The methodology, once applied, can be saved and taken again for similar designs.

An advanced software, based on a virtual configuration, can be adapted on two well defined systems: *a logic system* and a *physical system*:

- the *logic system* relates the production activities: design, planning and management;
- the *physical system* includes the real entities as materials, machines, jigs and fixtures, transportation and
- *computers* and their *network connections*.

The integration between virtual and real infrastructure, using data available in the data base, allows a continuous updating both for the new technology at disposal, and for the users expectations. To ensure a valuable Life Cycle Assessment it is necessary, beside the general data base, to set up a personalised software suitable and compatible with an hardware properly connected to the production systems. In other words, the available virtual model - by simulating the real paths of production processes - enables additional logical structures, open to the introduction of data never considered before, pertaining chemical, physical, metallurgical properties of materials, and toxicity, biodegradability etc.

8. RECENT TRENDS FOR LIFE CYCLE STUDIES: THE ROLE OF SIMULATION

Could the Life Cycle Simulation become a resolute factor towards feasible acquisition?

The introductory aspect of this procedure is represented by intending the maintenance as the prediction of potential deterioration of the product components, induced by operational and environmental stress. An evaluation of the resultant functional degradation can be derived. I refer to methods such as FTA (Failure Tests Analysis) and FMEA (Failure Mode and Effect Analysis) widely used for Quality Assessment.

Life cycle simulation represents an essential tool for life cycle configuration, whose function is to estimate how aging processes with specified tasks could be performed under specified conditions and constrains. Simulation can be employed in various phases of the

life cycle: in **the design phase** it is effective for reliability and maintainability design; in **the operation phase**, it is useful for maintenance planning.

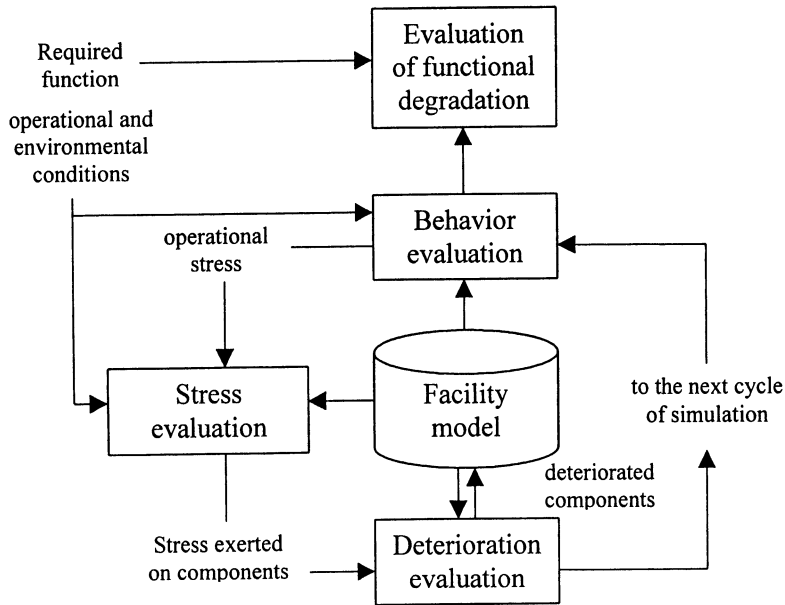


Fig. 2: General procedure of life cycle simulation (S. Takata)

Operational parameters: torque, speed, temperature

Stress evaluation: stress exerted on facility components during the operation

Deterioration evaluation: induced by exerted stress and resultant changes in the properties

Facility model: reflecting the results

Behavior model based on deteriorated facility evaluation

Evaluation of functional degradation: by repeating the procedure, to evaluate the progress of the degradation, checking position accuracy and end-effectors

A three years research has been carried out at Waseda and Kyoto Universities (Japan), focused on a life cycle simulation system for robot manipulators. The significance of the research arises from the checked methodology that can be profitably transferred to other industrial items of home appliances. Starting objective: to identify and check a method enabling a quantitative evaluation of the facility, when it operates in a particular environment and performs a task with specific conditions.

The Fig. 2 gives evidence to the simulation procedure, set up by S. Takata and other co-Authors, referred to a robot example. Since operational and environmental stress are acting on the components, perhaps it becomes evaluable the deterioration process, and the resultant functional degradation can be identified: that is the main purpose, because it is ex-

tremely important to individuate the level of the deterioration as a sort of break-even-point, not to be overtaken due to the risk to nullify all successive revenues.

A robust help has been assured to the researchers by an existing “manipulators failure history” elaborated between 1993-96 to check the modes and effects, using appropriate algorithms, formulas and geometric representation. The components subjected to a faster wear being statistically evaluated, modifications have been suggested in respect of used materials and design improvements. Unfortunately deterioration is a very complex phenomenon: though a high number of factors must be considered, lubrication included.

Next step forecast: “for making quantitatively accurate prediction of facility life via life cycle simulation, we need to establish a procedure to obtain the data during the operation; therefore, to feed them back for improving models parameters to be used in the simulation” (S. Takata). A new approach has been recently tried at the University of Tokyo by F. Kimura³ presenting his interesting interpretation of the “closed loop of the product life cycle” (Fig. 3).

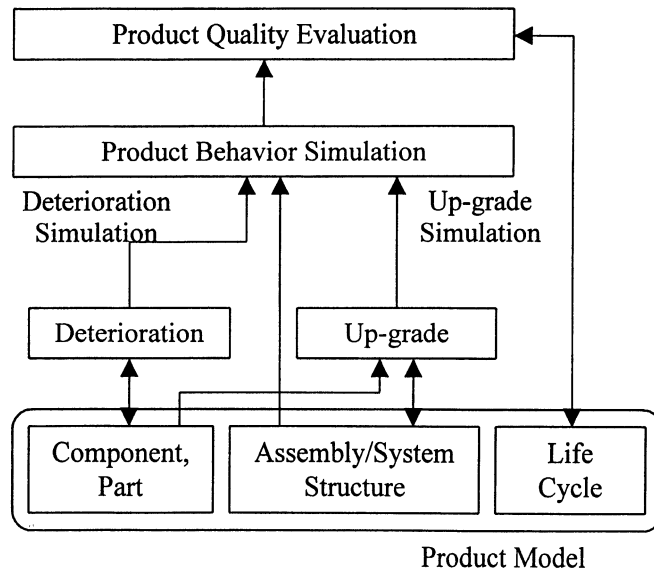


Fig.3: Scheme to illustrate the simulation model structure (F. Kimura)

Looking at his scheme, a close flow of the product is considered, which envisages the possibility to re-use the product or part of the product by means of small repair or refurbishment. In this sense, the product maintenance during operation together with a periodical up-grading, facilitate parts/product reuse, giving a sound contribution to reduce the product

³ “Product quality Evaluation Based on Behaviour Simulation of Used Products“ by F. Kimura, T. Hata, H. Suzuki, Annals of CIRP Vol. 47/1/1998

flow and the volume of the materials. Kimura and his co-Authors gave to this concept the name of *inverse manufacturing*. The methodology has been largely discussed during the experimentation. Theoretically, promising results seem to be achievable.

The reasons why it seems rather strong the practical application come from outside the logic and physical simulation, due to prevailing variables as:

1. the rapid development of technology that make parts quickly obsolete;
2. the difficulty to make an identifiable quality assurance of old parts;
3. modular or standardised design allowing parts re-use, that is somehow redundant;
4. the cost of collecting and repairing old parts, higher than fabricating new parts.

Another different approach has been proposed by Kimura, using a *rapid product life cycle technique*: (Fig. 3) that considers deterioration and up-grade simulation in order to deduce a simulated product behaviour (in the case of a copying machine as a reference sample), ready for the taking-back products or components to the factory before their total breakdown or functional obsolescence. This way could modify the current attitude of the consumers (especially in respect of their household appliances), inclined to keep the product until the moment when severe (say *dramatic*) breakdown will occur: the product is then so old and obsolete to block any reused perspective.

9. ECODESIGN COSTS NEED AN ACCOUNTING STRUCTURE EVOLUTION

Basic question advanced by researchers, designers and producers: How to compare the technically defined proposals and needs, in respect of the operating costs, involving the effects of restrictive environment regulations? The Fraunhofer⁴ Institute in Stuttgart developed a new method to calculate the life cycle cost of capital goods as machines and manufacturing systems (costs of production, installation, usage disposal). The target aimed to anticipate the potential life cycle costs, deriving the approaches from the cost structure when covering the **entire product durability**, that includes also post-sales services (extended to teleservices and teleoperations) and disposal activities.

First consideration: "the traditional accounting methods are not qualified to cover new demands in order to optimise the cumulative benefits" (E. Westkämper).

- How to consider the post-sales various types of service and of disposal?
- Can they represent for the producers new and economical successful business areas, or merely negative expenditures?
- How to conciliate the only ones benefits for the producer and the benefit due to a prolonged working life of the product when correctly maintained and up-graded by assistance services?

⁴ E. Westkämper, O.v.D. Osten-Sacken, Fraunhofer Institute (IPA), Stuttgart

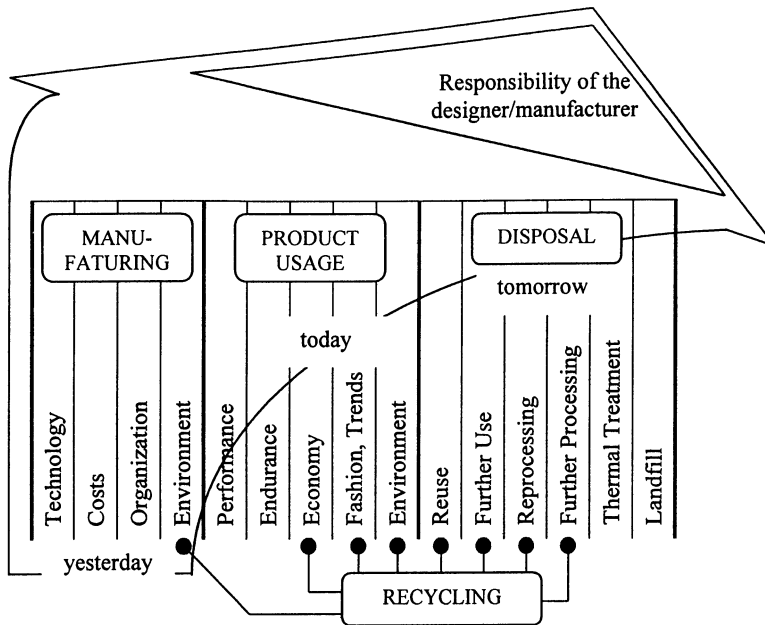


Fig. 4: Responsibility of the Designer/Manufacturer (E. Westkämper)

The environmental protection of course claims the second part within the economical correct confrontation, being now a day available efficient monitoring supports, that lead to operate the product much more effectively, than traditionally done, and to assume the maintenance as the prevailing strategy due to its crucial impact on revenue. A new word appear after the product service-usage: **deproduction**, that is the phase of decreasing expenditures (see Fig. 4, elaborated by Westkämper, giving evidence to the evolutionary process). Clearly, the new basis in costs allocation requires three stages: production, usage and services, recycling and reuse (these last ones induced by the residual value).

The conclusion of the Fraunhofer Institut research is evident: *"the life cycle cost accounting has to prove the thesis that longevity of products including the permanent up-grading of the operating system is ecologically and economically useful, (justifying) innovative products, new operation and maintenance concepts, new financing models and cooperation forms"*.

10. PRODUCERS ATTITUDE

The advancements made in the areas of ecolife simulation, rapid product life cycle, costs confrontation certainly will be put under pressure during the next three years: the results are essential and their diffusion will mark the success of ecodesign. My experience among research departments, brain storming stylists or designers, public rulers and private

uncertainties, makes myself partially comprehensive in respect of producers, that could be grouped along three basic profiles:

- mainly medium sized enterprises: suspicious and rather intolerant in respect of legal and administrative environment regulations, whose costs are very high, not fully allowed to be absorbed in the production costs, and therefore acting as cuts of profits; just the compulsory interventions are executed, mainly addressed to pollution macro-effects:
- the following profile includes large and powerful industrial groups, often transnational, where some researches addressed to concurrent ecodesign is starting and whose some significant examples are pointed-out; certainly the main pioneering task will lay upon the shoulders of large companies, as whose responsible for the most important steps to enforce such strategies that could induce a sort of “cloning process”;
- the remaining profile (small sized companies) corresponds to the area where no effective studies are carried out on the subject, except the case of consultancy groups, expressly focusing Product Life Cycle techniques, ecodesign, models and simulation: mainly services than manufacturing.

11. AESTHETIC ASPECTS WILL FIND THEIR APPEAL.

Let me take into account the two basic factors such as *shape and matter*, recalled from the philosophy of art. The former predominates in manufacturing world practice. The new eco-life addresses this concept in a revolutionary fashion. Material should no longer be considered as passive entities used merely to be processed and turned into consumer products. The intrinsic vitality of a material is recognised as a lasting property permitting subsequent transformation and re-use.

The **design strategy** is tailored to this postulate; it gives evidence of renewed value ensuing from transformation and can forecast its further effects. Paradoxically, the principle of “refusing refusals” should be adopted, in the sense of accepting the possibilities extant in a refusal as stimulation by industrial creativity towards successfully attainable re-use later on. This is what we should do to promote the aesthetics of re-creative duration, instead of destructive elimination. It also is what the world requires of design team activity, through economic, social and political pressure. It has been quite rightly said “ the scenario of producing doesn’t only mean making but undoing to remake as well”. What the producers acting as system head actually do? They mostly put parts together in conformity with some technical or safety rule, package them into a shell, and deliver them to the end user. Better still if the shell is attractive, when the market requires it as the result of a cosmetic surface capable of positioning the item within the imagined expectations created around the market itself. In many instances, the shell itself becomes the only support of a message and saves the item in question from the indistinct chaos of available commodities, by making it prominent and readily identifiable by the consumer, as often happens with domestic appliances and leisure goods for example.

I would like to draw attention to this interface. The shell should no longer exercise its external appeal that reduces its technical content to a sort of hidden black box unintelligible to consumers. If we follow this logic to the design philosophy we all hope for, manufacture of the product is confined to its outside skin, as a precious package and “decor” requiring no technical description or conformity with eco-compatibility. Conversely, the skin should reward the clean technology contained inside the package, with an immediately perceivable aesthetic message stimulating identity between the concept of “green” and “beautiful” products, that is between *form* and *matter*.

We know the industrial world’s hardware requires being explored, before transferring the center of gravity of today’s economic and production interest towards progressive refinement focused on interaction and mutual functionality versus both use and re-use. Logic itself will no doubt be reshaped. Despite the centuries-old tradition of aggregating and combining internal parts alone, design and production will have to enter today’s “desegregating for recombining” approach respecting each component’s individual nature and combinability for the respective properties, that reject the fate to live and die merely as a function of product’s life.

12. CONCLUSION

My wish, that I know is shared by the AMST’99 audience, is that next Conference within 3 years will enjoy a key-note Paper in which encouraging advancements will be described together with a wider consciousness that the efforts have, and will spread benefits from an individual to a planet scale, because this auspice is right, is good, is attractive. Specialists are linked in real time, working on a common goal in different countries and continents; virtual technique will significantly facilitate major design changes, because it is highly interactive, allows fascinating representation and navigation; anyone is a part of the decision experimenting innovative changes in real time, ensuring a trouble-free virtual solution. New approaches flow together for interpreting environmental protection, stimulating creativity.

Once again, the world of culture confirms its links and positive interaction powers, when sketching the messages of a magmatic scenario, that marks today and condition tomorrow. I would like to renew the auspices: *an environmental New Age needs the breath of science, technology, fantasy and faith*.

REFERENCES

1. Alting, L.; Legarth, J.B.: *Life Cycle Engineering and Design*, Annals of CIRP, Vol.44/2, 1995
2. Kimura, F.; Suzuki, H.: *Product Life Cycle Modelling for Inverse Manufacturing*, 1995

3. Krause, F.L.; Jansen, H. (Ed.): *Life Cycle Modelling for Innovative Products and Processes*, Chapman & Hall, London 80-89
4. Micheletti, G.F.: *The concurrent ecodesign methodologies: eco-sustainable products and processes*, International Conference on Production Technology (PTK'98), 29 -30 October 1998, Berlin
5. Kimura, F.; Hata, T.; Suzuki, H.: *Product Quality Evaluation Based on Behaviour Simulation of Used Products*, Annals of CIRP Vol. 47/1, 1998.
6. Takata, S.; Yamada, A.; Kohda, T.; Asama, H.: *Life Cycle Simulation Applied to a Robot Manipulator - An Example of Aging Simulation of Manufacturing Facilities*, Annals of CIRP Vol. 47/1, pg. 397-400, 1998.
7. Westkämper, E.; Osten-Sacken, D.: *Product Life Cycle Costing Applied to Manufacturing Systems*”, Annals of CIRP vol. 47/1, 1998
8. Krause, F.L.; Selinger, G. (Ed.): *Product Life Cycle Design based on Deterioration Simulation*, 1997, “*Life Cycle Networks*” 4th CIRP Int. Seminar on Life Cycle Eng., Chapman & Hall, London 59-68.
9. Takata, S.; Shiono, H.; Hiraoka, H.; Asama H.: *Case-Based Evaluation of Potential Deterioration for Facility Life Cycle Management*, Annals of CIRP vol. 46/1, 385-390, 1997
10. NN: *Information infrastructure for Life Cycle Maintenance*, Proc. of CIRP Design Int. Seminar 133 - 142, 1997
11. Alting, L.; Hauschild, M.; Wenzel, H.: *Environment Assessment in Product Development*, on Phil.Trans. R. Society, London 355, 1373-1388, 1997
12. Bistagnino, L.: *Ecodesign dei componenti*, in Meccanica e Automazione, Gruppo Editoriale Futura, Milano, 1998
13. Micheletti, G.F.: *The Individual Vitality of Materials and Components as a Key to Ecodesign*, in Krause, F.L./ Uhlmann, E.; Carl Hanser Verlag, München, Wien 1998, pp 437-444

DYNAMIC ANALYSIS OF PRODUCTION PROCESSES BY PLANNED EXPERIMENTS

D. Romano

Polytechnic of Turin, Turin, Italy

A. Bertagnolio

Minerali Industriali SpA, Masserano Biella, Biella, Italy

R. Levi

Polytechnic of Turin, Turin, Italy

KEY WORDS: Dynamics, Process Improvement, DOE, Time-Frequency Transforms.

ABSTRACT: An experimental investigation was performed on a plant providing selected raw material to ceramic and tile industry. Sizable single and combined effects of a number of factors were observed, and valuable information relevant to process planning and control was obtained, leading to improved production rate and energy conservation. Dynamic aspects of process mechanics were also investigated, since under given conditions vibration induced fatigue loading affects critical component integrity. Dependence of critical spectral components from process parameters was therefore investigated; data obtained include maps of safe operating regions within a broad sample space, allowing trouble free operation without impairing production rate.

1. INTRODUCTION

Process improvement is perhaps the more natural and consolidated field of application of design and analysis of experiments in industry. Classic experimental designs have been mostly applied on processes assuming that they are inherently stationary, namely that variables involved in the experiment are time-invariant. Yet some difficulties occur when this assumption has to be relaxed for some signals measured on the process. However, applying a Fourier transformation a time signal may often be summarized in terms of a small number of spectral components, which account for a large fraction of signal's total energy. These components in turn lend themselves readily to statistical analysis, provided that two source of random variability are considered, namely one related to short term repeatability and the other with long term fluctuations in amplitude as well as in frequency of the dominant components along time due to non-stationarity.

Published in: E. Kuljanic (Ed.) *Advanced Manufacturing Systems and Technology*,
CISM Courses and Lectures No. 406, Springer Verlag, Wien New York, 1999.

An analysis of the nature of these peculiar responses and their relevant statistical treatment is given in the next section of the paper. The aim is to turn these responses into ordinary ones pooling the additional variability due to non-stationarity in the experimental error of the statistical model.

In the remainder an investigation on the dynamic behavior of a mill system for the production of fine sand by intergranular grinding of hard minerals by factorial experimentation is discussed, where both stationary and transformed non-stationary responses are present. The mill's drive train undergoes under particular circumstances sizable torsional vibrations, severe enough to entail permanent damage to critical components, and eventually catastrophic failure; only some frequency components however were found to correspond to potentially damaging oscillating stresses. Response surface methodology was resorted to in order to map safe operating regions in the experimental space and evaluate risk of fatigue induced failure elsewhere. Furthermore, parsimonious empirical models were arrived at providing practical information for economic control of production process.

2. SPECTRAL COMPONENTS AS EXPERIMENTAL RESPONSES

Spectral analysis is a primary technique for the study of system dynamics. Describing a time-signal in the frequency domain is very revealing for many purposes, like energy localization, modal characteristics, system identification and control, detection of non-linearity. Now some implications will be outlined when a spectral component is taken as a response in a planned experiment.

Consider a time-signal coming from a measurement instrument, either analog or digital. It can be mathematically modeled as an instance of a random process. A continuous-time (discrete-time) random process is a signal $\xi(t)$ (sequence ξ_n) defined on some probability space. For any time-instant t^* (index j) the distribution function for the random variable $\xi(t^*)$ (ξ_j) has to be provided, together with all the possible joint distribution functions. In the general case a complete definition is practically prohibitive. To deal with the majority of real world applications two important sub-classes are defined: stationary and cyclostationary processes. Stated in a few words, stationarity means that all the probabilistic properties do not depend on time origin but only on the time lag between involved RVs; one of the consequences is that all RVs $\xi(t^*)$ (ξ_j) are identically distributed. In particular their mean and variance are time invariant. For cyclostationary process probabilistic properties do not change when the time origin is shifted by a multiple of a period T ; mean and variance of all RVs $\xi(t^*)$ (ξ_j) are periodic function of time too. In the study of frequency transformed signals, cyclostationary time signal can be seen as the counterpart of every frequency component.

We focus now on gaussian random processes, which are the more frequently encountered in the applications. If a linear transformation is applied to a gaussian process, stationary or not, the resulting process is still gaussian. Now Fourier transform is a linear operator, being the expansion of a signal in terms of a linear combination of orthogonal harmonic functions. Therefore every frequency component extracted from the Fourier transform is a complex normal RV. If the amplitude spectrum is considered, in principle normality would be lost; however it can be easily retained by mirroring the time signal about the y -axis or the origin. This modification produces an even or odd signal having a purely real or imaginary Fourier transform, so that amplitude is affected by a sign change at the most. On

the other hand mirroring the signal has a very little effect on the frequency spectrum which is only multiplied by a constant factor. Hence real part, imaginary part and amplitude of Fourier transform of a gaussian random process are still normal RVs. This consideration matches perfectly the assumption of normality ordinarily stated for an experimental response. Now we will look for an efficient estimate of the response variance, exploiting the peculiar nature of the response, which is a spectral component extracted from the huge amount of information contained in the observed time window of the signal. The idea is to resort to a more informative transformation, capable of capturing the frequency content of a signal along time. Such a transformation is known under the general name of time-frequency transformation (TFT).

2.1 Time-frequency transformations

The Fourier transform and its inverse establish a one-to-one relation between the time domain and the frequency domain. These constitute two alternative way of looking at a signal. Although Fourier transform allows a passage from one domain to the other, it does not allow a combination of the two domains. In particular, most time information is not easily accessible in the frequency domain. While the spectrum $X(f)$ shows the overall strength with which any frequency f is contained in the signal $x(t)$, it does not generally provide easy-to-interpret information about the time localization of spectral components, which is embedded in the phase spectrum in a very entangled way. On the contrary, a TFT is a joint function of time and frequency and gives a clear picture of time localization of spectral components producing a surface over the time-frequency plane. Note that this concept resembles a musical score, which indicates which notes (spectral components) are present at which time in a piece of music. Obviously additional information provided by this bi-variate transformation is paid with an increase of the computational burden. Among existing TFT, linear, quadratic, otherwise non-linear, the first will be considered for the desirable property which was previously mentioned.

The simplest linear TFT is the Short Time Fourier Transform. It is obtained by doing a sequence of Fourier transforms on windowed adjacent portions of the time signal. Of course the window width determines the time resolution of the spectrum and the frequency resolution is accordingly determined on the basis of the uncertainty principle: improving the time resolution (by using short a window) results in a loss of frequency resolution and viceversa.

Wavelet transformations, the other important linear TFT, uses the trade-off between time and frequency resolution in a flexible way. Here the windowing functions have a variable time duration, giving rise to the so called multiresolution analysis. Thus a series of increasing time resolutions corresponds to a series of decreasing frequency resolution. For the purpose of this paper the first transformation seems more adequate. Basic notions on this topic can be found in [4].

2.2 Use of TFT in the analysis of spectral experimental responses

The main utilization of TFT in our problem is detection of non-stationarity and estimation of random variability on spectral components. Relying upon the Fourier transform only can be very misleading for the interpretation of non-stationary signals. Fourier transform provides an averaged spectral description, which is only a piece of the information; the other piece is variability along time of frequency components. Obviously any conclusion drawn from the analysis of the average spectral content is, to a different extent, wrong. Remind that in case of strong departure from stationarity, observation of only a small

portion of the signal leads to an exceedingly inaccurate analysis. Only when peculiar features are to be investigated a restriction of the signal to quasi-stationary time intervals can be adopted. TFT just provides the missing information: random variation in the statistical model of a frequency component is inferred using the sample counterpart evaluated on the TFT units along time at the frequency of interest. Note that this technique, compulsory when dealing with extreme non-stationary signal, is useful in general, even for stationary signal, as it provides an efficient estimate of the random variability of the statistical model.

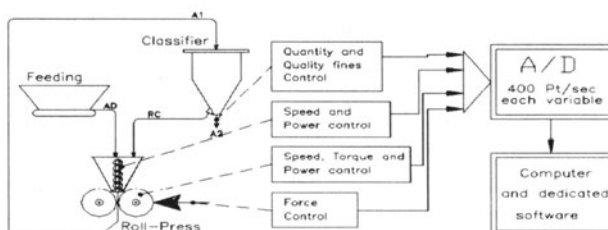
3. CASE STUDY

Minerali Industriali S.p.A. is one of the 13 production units of Gruppo Minerali S.p.A., an Italian company involved in extracting, processing and trading raw materials supplied to ceramic and glass manufacturers. The philosophy of the Group is aimed at continuous improvement by investing in technology. In particular Minerali Industriali has developed the roll-press to break silica sand down to $45\mu\text{m}$ dispensing with the traditional ball-mill. The process of grinding is to have a machine which breaks the grains (ball-mill or roll-press) and one (classifier) separating the fine from the coarse as required ($45, 63, 100\mu\text{m}\dots$). Treatment is easy with soft materials (kaolin, talk, calcium carbonate, pumice), but becomes more complex with hard raw materials like feldspar, silica flour, zirconium.

The principle of the roll-press was already known in Roman times but it had never been developed for an energy intensive process like grinding hard sand. Two rotating horizontal rolls forced one against the other break up the raw material fed into the gap by a cochlea. Usually the raw material is composed by sand with 2mm grain size and the output of the machine (in open-circuit) is made up by a sand mix with a range of grain sizes. If the finished material has to be (for example) all under $75\mu\text{m}$ it is ground in closed circuit. Fig. 1 shows a block diagram of the system in closed circuit operation. The roll-press grinds fresh and recycled material and sends it to the classifier where fine sand is extracted and the coarse is sent back for recycling.

This outline of the process underlines some of the difficulties in appraising the influence of the different parameters on system's performance on a theoretical basis. Systematic experimental approach was therefore resorted to in order to collect information. Roll-press system design caters for flexible parameter setting, rolls and cochlea being controlled by a converter and applied force by an ad hoc device. One plant was fitted with a comprehensive instrumentation system exceeding requirements for regular plant operation, thus coping with the more exacting demands of specific investigations.

Fig. 1: Schematic diagram of roll-press system.



Troubles arose in the course of initial operation of the prototype plant as the process is an intensive energy one, and insufficient knowledge about the complex pattern of interaction among variables led occasionally to abusive loading of components. The roll-press system proved successful right from the startup, since it was definitely cost effective even after making allowance for the limited service life of some heavily stressed parts. Something had to be done to prevent unplanned downtime for repair from upsetting regular production flow; such a consideration prompted the study described below.

4. EXPERIMENTAL INVESTIGATION

Recognition of both static and dynamic phenomena among those governing plant performance, which could not be properly modeled for want of key information, was a major factor in suggesting initiation of a systematic testing program. Existence of a complex pattern of interactions of substantial magnitude was furthermore suspected in the light of preliminary investigations, as results of "one factor at a time" tests were inconclusive. Provision for routine data logging during test runs as well under production conditions for trouble shooting purposes was made, a precaution more than justified in the light of accumulated experience.

Selection among a host of factors affecting operation was made aiming at parsimony in model building, balancing the advantages of concise description against the uncertainty entailed. Theoretical considerations based upon energy content as well as priorities suggested by practical experience helped to single out, among others, four main factors, related to roll force and speed, feeding cochlea speed and control pressure. Steady state test results showed that single and combined effects of these factors account for over 90 % of corrected sum of squares, a performance deemed adequate for the investigation at hand. Along with production rate and power requirement dynamic loading of the instrumented drive shaft was retained as one of the main responses, as evaluated by the output of the strain gauge bridge fitted on the torque tube. Slip rings were dispensed with using inductive coupling for both bridge excitation and signal transmission; provision was made for output amplification and signal conditioning on board of rotating shaft with dedicated circuitry, thus enhancing substantially signal to noise ratio. Contactless operation, catering for rapid drive shaft assembly and disassembly, was a distinct advantage since instrumented shafts came to be requested on short notice as the value of torque monitoring for trouble shooting purposes became appreciated over a number of plants in different locations.

Experimental design in the form of a complete 2^4 factorial plan, plus a star for squared term estimation, was eventually retained, taking into account the requirements of both steady state and dynamic investigations. Main factors considered were roll and cochlea rotational speed, applied force and control pressure. Control of drift was obtained by blocking and center point replication within blocks, with provision for analysis of covariance if need be. Operating factor range was as usual a compromise between clustering around actual operating values, thereby increasing precision at expense of generality, and spacing levels wide apart in order to cover a broad sample space.

5. MAIN RESULTS

Results are depicted as normalized response surfaces in cube plots [2], in terms of

normalized variables (main factors). The normalized output rate ranges in a one to two ratio within the sample space showing sizable room for improvement of productivity. A clear rise can be observed moving from the lower left to upper right corner in the cube plots of Fig. 2, meaning that, by and large, all factors considered entail an increase of productivity when present at upper level, whereas two interactive terms involving applied force are responsible for the curvature in the isolevel surfaces. Two covariates are also effective, frequency of the ventilation system and product between control pressure and elapsed plant lifetime. Productivity increases linearly with frequency and decreases along time if a high control pressure is used. These effects are not explicitly accounted for in the cube plots shown, which are referred to given levels of covariates for reference purposes. The energy absorption cube plot for control pressure level = -1 (Fig. 3) degenerates to a planar contour plot owing to the interaction between applied force and control pressure. Cochlea speed and control pressure are energy dissipating factors, as opposed to cylinder speed and ventilation frequency.

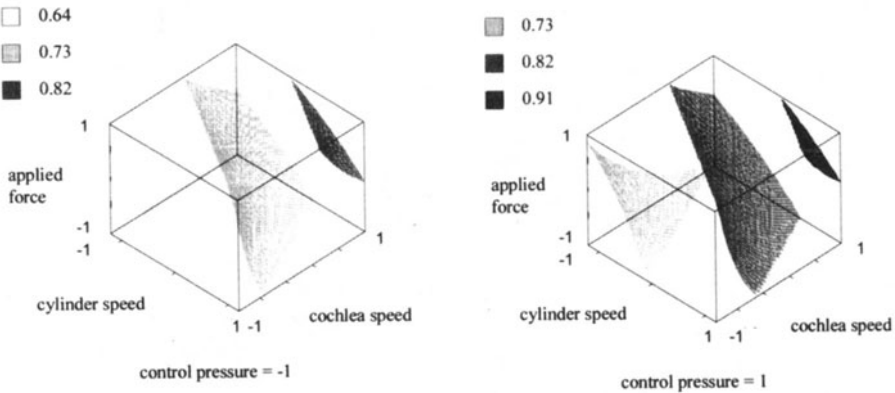


Fig. 2: Cube plots for productivity, at lower and upper level of control pressure.

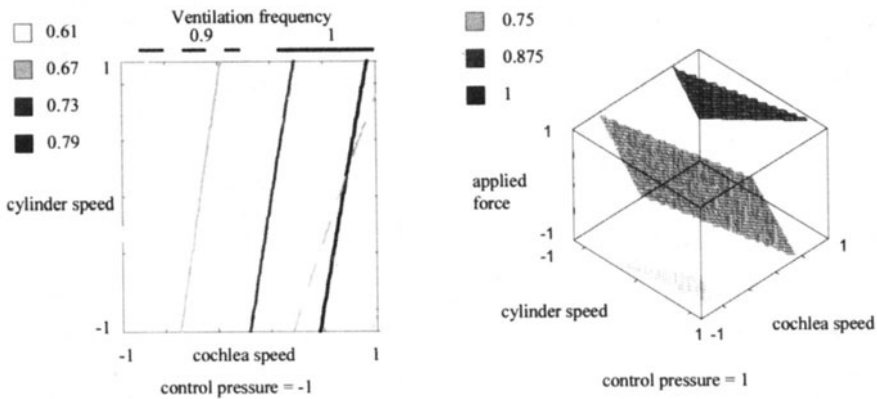


Fig. 3: Cube plots for energy absorption, at lower and upper level of control pressure.

Reliability analysis is based upon data collected on torque on transmission shaft, where fatigue failures were sometimes experienced in the past; risk of fatigue failure under

assigned process operating conditions was accordingly assessed on a probabilistic basis. Classical analysis of fatigue induced by a number of harmonic loads at different frequencies was used, assuming a 1/3 variation coefficient, quite a substantial value justified by the large scatter typical of fatigue test results and the additional variability (compared with laboratory tests) due to non-stationary loading conditions during real machine operations.

Typical waveforms sampled for two experimental settings and their FFT amplitude spectra are depicted in Figs. 4 and 5. Data acquisition was routinely performed with a .5 kHz sampling rate on 40 s blocks of observation.

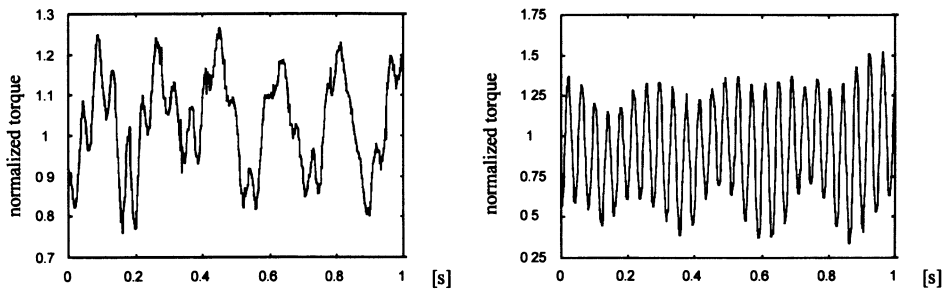


Fig. 4: Typical torque waveforms as measured by strain gauge bridge in one second observation window. Torque is normalized dividing by the static signal component. Note the different features exhibited by the two signals.

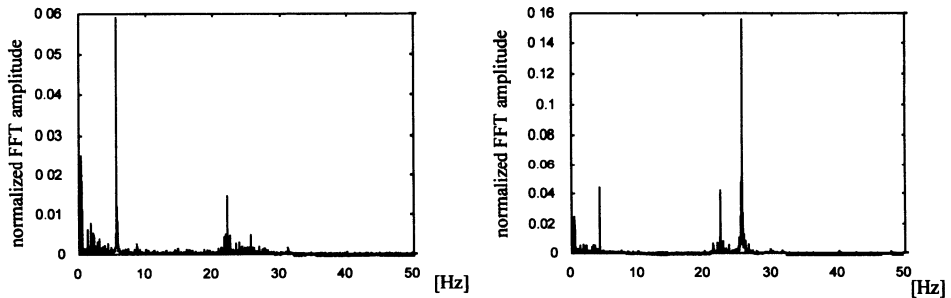


Fig. 5: FFT normalized amplitude spectra of the waveforms of Fig. 4, computed on the full 40 s observation time. Static component (unit) is not shown.

Apart from the static component three dominant frequency lines appear. The first two frequencies are strictly correlated to the rotation speed of cochlea and cylinders respectively, as might be expected. The third one, unrelated to systematic driving terms in the process, appears to be a structural resonance frequency. This conclusion is supported by the fact that the energy carried by this component is nearly always small in the experiment but for a few runs where it resolutely peaks, see Fig. 5. Resonance is initiated as soon as a sufficient energy enters the resonance bandwidth. A closer observation of the waveform reveals that vibrations at the suspected resonance frequency start rather irregularly, however after some energy is injected in the vicinity of that frequency. A short-time frequency transform shows these events more clearly in Fig. 6.

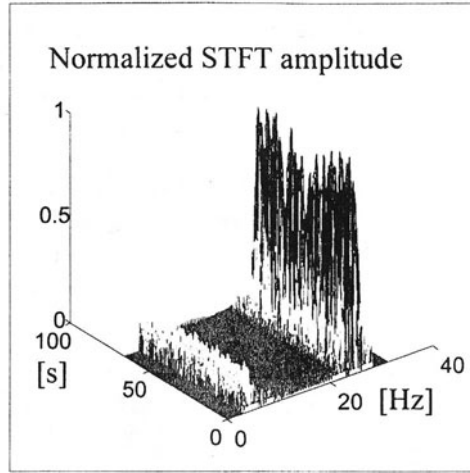


Fig. 6: STFT of the second signal in Fig. 4, observed over about 60 s.

Failure risk was estimated modeling the fatigue response of the material of the transmission shaft when an equivalent torque T_{eq} made up of the dominant components is applied:

$$T_{eq}(t) = A_0 + A_1 \sin(2\pi f_1 t) + A_2 \sin(2\pi f_2 t) + A_3 \sin(2\pi f_3 t) \quad (1)$$

Components A_0 through A_3 are extracted from the amplitude spectra of STFT applied on the set of sampled signals corresponding to treatment combinations examined. The von Mises equivalent stress σ corresponding to strain gauge bridge output signal ΔV is calculated as:

$$\sigma = 2(3)^{1/2} G k^{-1} \Delta V / V_0 \quad (2)$$

where G is the shear modulus of the material, k the calibration factor of the strain gauges and V_0 the excitation voltage.

To evaluate the cumulative damage produced by the different sinusoidal terms in the above equation the Miner hypothesis was used. If N_1 , N_2 , N_3 are the durations (expressed as number of cycles) corresponding to equivalent stresses σ_1 , σ_2 , σ_3 the fatigue failure occurs after a time

$$D = n_1/f_1 = n_2/f_2 = n_3/f_3 \quad (3)$$

where the cycle numbers n_1 , n_2 , n_3 are determined, according to Miner, so that the following holds:

$$n_1/N_1 + n_2/N_2 + n_3/N_3 = 1 \quad (4)$$

This technique is admittedly a rather crude approximation, however adequate in the light of the large scatter affecting fatigue phenomena. Combining eq. (1) and (2) yield for duration D :

$$D = f_1^{-1} / (N_1^{-1} + f_2/f_1 N_2^{-1} + f_3/f_1 N_3^{-1}) \quad (5)$$

It is straightforward to verify that fatigue life is indefinite only if N_1 , N_2 , N_3 are all ∞ . Hence it is sufficient to check that fatigue life is indefinite for the maximum of the

equivalent von Mises stresses obtained using eq. (2) on the voltage signals related to the three sinusoidal torque components.

Graphical representation of whether the fatigue life is indefinite or not is provided on the Goodman diagram. A widely used display for fatigue analysis, it is easy to build and to interpret, and provides, in a plane where a generic alternate stress load is represented, a closed region within which indefinite life is predicted for a given material at hand. Load is defined in terms of static and cyclic stress components σ_m and σ_a , material is characterized by yield stress σ_s , ultimate tensile strength R and fatigue limit σ_0 , the latter corresponding to a sinusoidal load with a zero static component. Fig. 7 shows experimental points plotted with Goodman contour lines plotted at different risk levels according to an elliptical approximation to the classic polygonal diagram. Cube plots shown in Fig. 8 depict where indefinite life regions are located in the sample space; limit surfaces and corresponding risk levels are also shown.

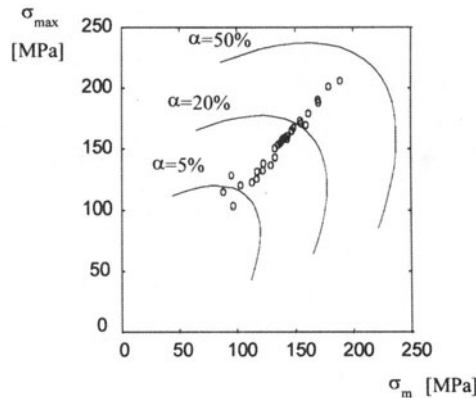


Fig. 7: Goodman diagrams at three risk levels, showing experimental points ($\sigma_{max}=\sigma_m + \sigma_a$). The most energetic sinusoidal component in each run has been considered.

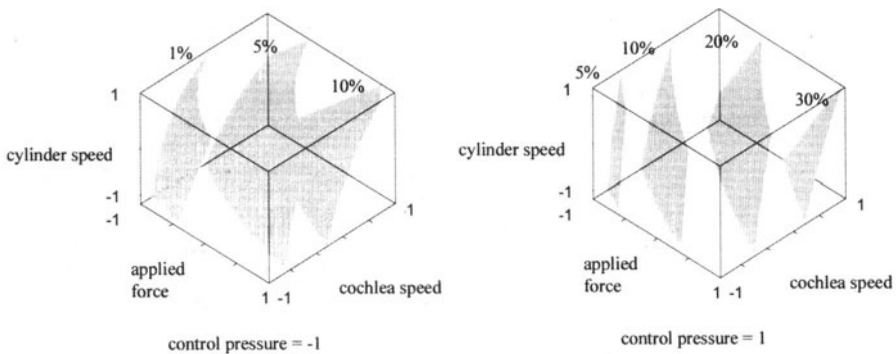


Fig. 8: Cube plots of probabilistic limit surfaces for indefinite endurance. Surfaces refer to given risks; cubes correspond to lower and upper level of control pressure.

6. DISCUSSION

Results obtained relate expected component endurance to operating conditions within a comprehensive parameter range, and show clearly within the sample space considered which regions lend themselves to safe exploitation and which on the other hand must be avoided. By controlling production process accordingly trouble free operation was effectively obtained while boosting production at the same time; no more failures occurred and regular maintenance proved adequate to keep the machinery operating day in, day out. Cube plots proved their worth once again in conveying effectively information to personnel quite capable on the job but unacquainted with statistical analysis. By providing the information required in a clear, intelligible format, yet unencumbered with forbidding mathematics, plant foremen were empowered and actually encouraged to steer their processes along creative, yet inherently safe paths.

Identification of origin and mechanism of potentially disruptive phenomena enables also selection of inexpensive, readily replaced components as mechanical fuses, designed to protect expensive pieces of inventory from crippling damage just in case some control went berserk. Apparently a kind of reverse Murphy law went into effect since the investigation was performed, since no more failures were experienced over one year of operation of several plants, against a previous record of frequent disruption of production schedule due to unplanned downtime.

Independent tests were resorted to in order to validate main conclusions, and to extend their field of application to cover several kinds of raw material; incidentally, the basic process mechanics were found to be but marginally affected by substantial variations of material specification.

ACKNOWLEDGMENTS

Support and encouragement provided by Minerali Industriali S.p.A in the course of this work, and permission to publish part of results obtained during the investigation performed on their behalf, are gratefully acknowledged.

REFERENCES

1. Box G.E.P., Hunter W.G., Hunter J.S. (1978), *Statistics for Experimenters: an Introduction to Design, Data Analysis and Model Building*, Wiley, New York
2. Kinzer, G.R. (1985), *Application of Two-Cubed Factorial Designs to Process Studies*, in: "Experiments in Industry", Snee, R.D., Hare, L.B. and Trout, J.R. ed., ASQC Press, Milwaukee
3. Romano, D. and Levi, R. (1998), *Sperimentazione su cilindraia ad alta compressione, mirata all'ottimizzazione delle prestazioni produttive in condizioni di affidabilità controllata*, Parts 1 & 2, unpublished technical reports for Minerali Industriali S.p.A., DISPEA – Politecnico di Torino
4. Hlawatsch, F., Boudreaux-Bartels, G.F. (1992), "Linear and Quadratic Time-Frequency Signal Representations", IEEE SP Magazine, April, pp. 21-67
5. Boashash, B. (1990), "Time-Frequency Signal Analysis", chapter in *Advanced in Spectrum Estimation*, ed. S. Haykin, Prentice-Hall, Englewood Cliffs
6. Daubechies, I. (1992), *Ten Lectures on Wavelets*, SIAM, Philadelphia

HARD TURNING WITH PCBN TOOLING

E.J. Brookes, R.D. James and X. Ren
University of Hull, Hull, UK

KEYWORDS: Machining, hard-facing, PCBN, quick-stop

ABSTRACT: Material removal, at economic rates, from hardened workpieces has always presented a challenge and, until quite recently, abrasive machining processes were the only option for hard-facings. However, cutting tools based on polycrystalline cubic boron nitride (PCBN) have opened up the possibility of turning and milling as attractive alternatives for abrasion-resistant workpiece materials. This paper describes work carried out at the University of Hull to investigate the interaction between a high CBN content cutting tool material when turning an iron-based welded hard-facing material. Results of machining trials are reported and SEM photographs are presented, which show the failure mode of CBN. The behaviour of large carbide particles in the workpiece is of particular interest and has been studied using a modified 'quick-stop' procedure.

1. INTRODUCTION

Iron-based hard-facings are widely used to provide resistance to abrasive wear in industries ranging from mining to food processing [1]. Abrasion resistance is achieved by producing a microstructure comprising hard carbides dispersed in a relatively soft matrix [2]. Alloys forming chromium carbides are popular because these carbides tend to exist as relatively large micro-constituents and present large surface areas to the abrasive material. Weld-deposited layers of hard-facing, several millimetres thick, are typical and subsequent machining is almost invariably necessary to achieve required standards of dimensional accuracy and surface finish. This presents a dilemma because a material offering good abrasion resistance will, almost invariably, be difficult to machine. Indeed, until quite recently, abrasive machining was the only material-removal option for hard-facings. However, cutting tools based on polycrystalline cubic boron nitride (PCBN) have opened up the possibility of turning and milling as alternatives.

Cubic boron nitride (CBN) is the second hardest material in the world after diamond and polycrystalline CBN tools, unlike diamond, are suitable for machining hard ferrous materials. The superior performance of CBN tools, in terms of higher material removal rate, has been shown in many areas [3]. Materials suitable for machining with CBN tools include hardened alloy steel, cobalt-based alloys, nickel-based alloys and tool steels. In addition, cast irons and nickel/chromium cast iron can be machined at very high speeds. The ability of CBN to cut these hard materials at high speeds is due to the retention of strength at higher temperatures compared with other tool materials, combined with excellent abrasion resistance and resistance to chemical reaction with ferrous workpieces. CBN tools can also be used to machine very tough materials including Ni-hard [4], tungsten carbide and other engineering ceramics [5].

CBN tools have been successfully used in machining nickel-based and cobalt-based hard-facing alloys at a speed of 200-250 m/min and feed of over 0.2 mm/rev [4]. Round, chamfered inserts were used with a depth of cut sufficient to penetrate into the material below the very abrasive as-deposited alloy skin. Machining of iron-based hardfacing materials has only recently been investigated. Bieker [6] reported an application of CBN in milling welded die materials. In this work, welded alloy F41 (56 NiCrMoV) with a very irregular surface and varying hardness was successfully machined by a milling process and it was shown that the CBN materials used offered considerable benefits.

CBN tools have great potential for replacing grinding processes in the machining of some hard-facings with high hardness but the high price of CBN material implies very high tooling cost. CBN tooling products were designed for difficult-to-machine ferrous workpieces but none was specifically intended to cope with carbide-containing hard-facings. Thus the availability of tools for this particular application was limited. Lack of understanding of the machining process, especially the deformation process of the

workpiece material and the interaction between the tool insert and the workpiece, has restricted the application of ultra-hard materials in this field.

The work reported here is concerned with assessing the ability of a high CBN content (>95%) cutting tool material for turning chromium carbide based hard-faced workpiece. The investigation included cutting trials and detailed examination of the tool/workpiece and tool/chip interfaces using a 'quick-stop' device.

2. EXPERIMENTAL DETAILS

The materials for the cutting tests were prepared from a chromium carbide based hard-facing layer, nominally 6mm thick, deposited on a mild steel bar ($\phi 100$, L300mm) using a flux cored arc welding (FCAW) machine. The hardness of the welded layer was HRC 55-58. The sample was pre-turned to remove the rough welded skin, prior to the cutting tests. The tests were conducted, without a coolant, using a Churchill 'Computurn' 290 CNC lathe and the cutting conditions were: S70 m/min, F0.25 mm/rev, depth of cut of 0.65 mm. The tools used were RNGN070400 solid indexable inserts (7mm diameter with a 0.1mm edge chamfer) held in a matching tool holder to give a negative rake of 6° . A tail-stock was used in all the tests in order to make the system more rigid. Stages in the wear of the flank and rake faces of the cutting tool were monitored and cutting was stopped when an insert was observed to have lost its ability to cut effectively.

A 'quick-stop' technique was used to preserve the tool:chip interface, formed under controlled cutting conditions. In this test, the tool holder was pivoted and supported by a shear pin. Once steady state cutting was established, the cutting action was suddenly stopped by firing a captive bolt gun to break the shear pin and to accelerate the tool holder away from the workpiece. The chip, still attached to the work-piece sample, was then sectioned, prepared for metallographic examination and etched in Vyella's reagent (5ml HCL, 1ml picric acid, 100ml ethyl alcohol), to reveal the carbides and the matrix. Sections normal and parallel to the cutting direction on the transient plane of the work-piece material were prepared and examined using optical and scanning electron microscopy.

3. MATERIALS

The structure of the hardfacing alloy is complex, determined by the processing conditions [2]. The basic microstructure of the workpiece was a coarse, hypereutectic of primary carbides in a eutectic matrix. The large primary carbides, identified as $(Cr, Fe)_7C_3$ [7, 8] formed during the welding process. The majority of these were columnar with hexagonal cross section, due to preferential cooling from the mild steel base.

Tools with high CBN content were considered to offer the best chance of success for machining hard-facing materials. The tooling selected for this work was a tough, coherent, high strength and chemically stable compact comprised of a rigid network of small sized (5-8 μ m) cubic boron nitride particles with an AlN intergranular phase. Under processing conditions, penetration of the spaces between particles was complete ensuring a fully dense material with no voids or cavities. The material hardness was HK36.5.

4. RESULTS

Figure 1a is a general view of a cutting tool insert after machining for 15 minutes. Significant deterioration in the tool geometry has occurred, most obviously in the form of flaking of the rake face. This has resulted in a reduction in cutting ability and would, ultimately, lead to tool failure. Closer examination (Figure 1b) reveals small-scale chipping damage concentrated at the lower edge of the chamfer. It is probable that cumulative chipping damage of this type has resulted in the flaking of the rake face.

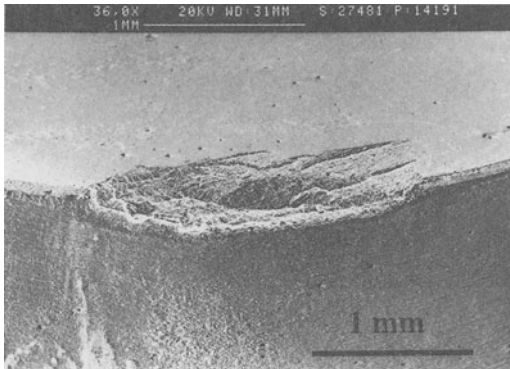


Fig 1a General view of insert after 15 minutes cutting

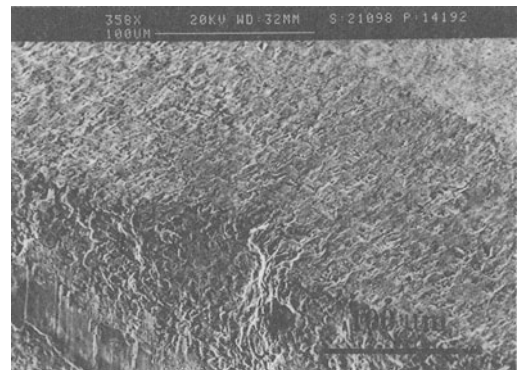


Fig 1b Edge chipping in early stages of cutting

A detailed examination of worn tools (Figure 2a) revealed that, within the zone of contact on the flank face, cracks propagated around the primary CBN particles. Therefore, the chipping damage to the near edge region appears to have been due to the removal of individual grains or aggregates. The flaking process on the rake face, however, was the result of transgranular fracture. Cleavage cracks (Figure 2b) have propagated across CBN particles, with limited deflection.

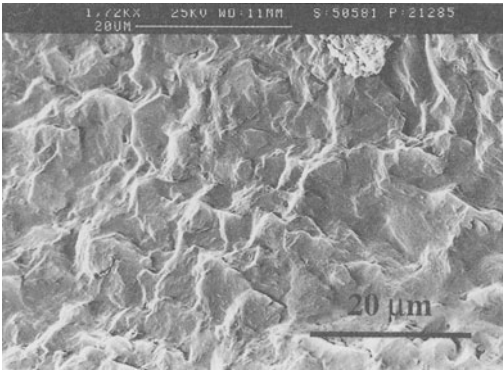


Fig 2a Close up view of the edge region

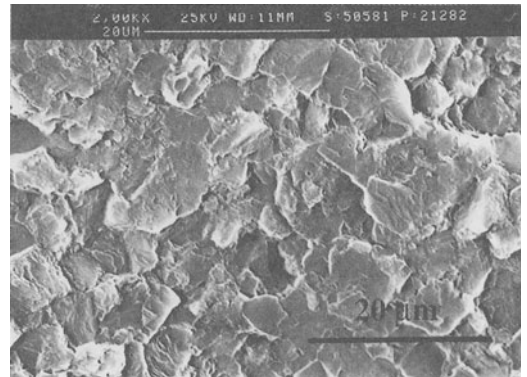


Fig 2b Flaking by transgranular fracture

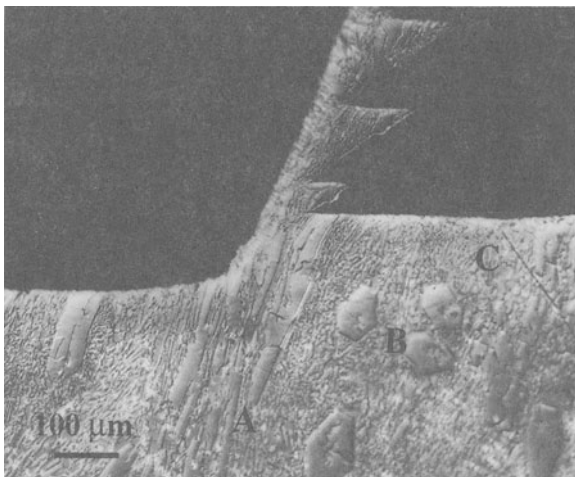


Fig 3a Quickstop specimen



Fig 3b Chip detail

The 'quick stop' specimen, shown in Figure 3a, resulted in a clean detachment of the cutting tool and retention of the chip to the workpiece. The large, columnar $(\text{Cr, Fe})_7\text{C}_3$ carbides (A) can be clearly seen, roughly perpendicular to the cutting edge. The hexagonal grains (B) are representative of those roughly parallel to the cutting edge and show some defects, in the form of inclusions, at the centre. The region marked C is the eutectic matrix.

The hard-facing chips were typically saw-toothed, semicircular and severely serrated on the side near the minor cutting edge. The tool face side was regular and no apparent flow of the workpiece was observed. Saw-tooth chips of varying segment size were formed, due to the microstructural heterogeneity of the workpiece. It is apparent that both the morphology and the quantity of the carbide particles inhibit the chip formation process and the deformation within the chip segment (Figure 3b).



Fig 4a Cleavage cracks in the carbides

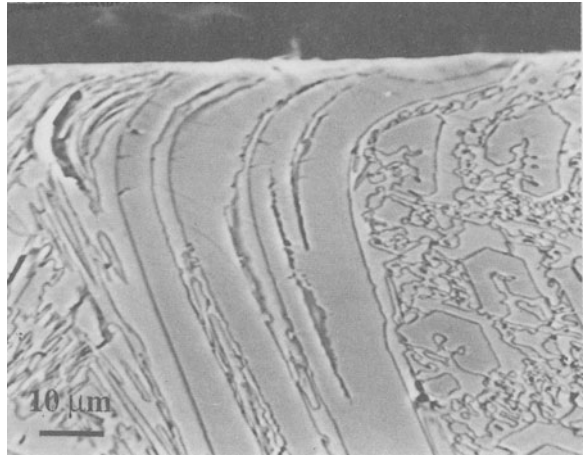


Fig 4b Deformation of carbides

Cleavage fracture of the large, columnar, primary carbides ahead of the cutting edge was observed (Figure 4a) but cracking of the eutectic matrix was not seen. In some cases, separation of the carbide and matrix has occurred along the boundary with a chromium-depleted zone. After fracture, fragments of the carbide have moved into the chip in the subsequent chip formation process and no other movement, e.g. rotation, of these large fractured segments of the carbide was observed. A cross-section of the transient surface (Figure 4b) revealed the deformation of carbides and the matrix beneath the surface in contact with the flank face of the tool during cutting. Cracking and bending of columnar primary carbides was evident near the surface region and it is clear that plastic deformation of the carbides has occurred during the cutting process. When a cluster of columnar primary carbides with short free distance has been encountered by the tool, the carbides have been severely cracked and bent. In general, the cracks are parallel to the cutting direction and have propagated about half way through the carbide crystals. Separation of the carbides and matrix, due to bending of the carbides, can be observed.

5. DISCUSSION

Chromium-carbide based hard-facings are very difficult to machine because of the presence of large discrete carbides. Cutting forces were not measured in this work but it was obvious that the lathe was subjected to higher loading when machining hard-facings than when machining hardened steel or a titanium alloy. An important aspect of machining hard materials is the generation of sufficiently high temperatures to soften the workpiece material whilst the tool material retains its strength. It is well established that CBN cutting tools retain their hardness at high temperature [9] but so do carbide-containing hard-facing materials [10]. Thus, the beneficial effects of thermal softening cannot be fully achieved.

From the quick-stop samples and subsequent metallurgical analyses, four distinct areas of workpiece deformation were identified. In addition to the usual three deformation zones associated with homogeneous metals [11,12], a further large deformation zone has been identified ahead of the cutting edge and extending deep into the workpiece. In this region, large columnar carbides have cleaved and the subsequent segmented chip-formation process has actually occurred within the eutectic matrix and the fractured carbides. The fragments and the eutectic carbides inhibit further deformation within the chip segment, so that the shearing and cracking process to form the chip segment was limited to a narrow region extending from the tool edge to the free surface of the workpiece.

Two possible processes may have contributed to the formation of this region. Firstly, in metal cutting processes, there is a steep stress gradient in advance of the tool and a strong stress concentration at the relatively sharp cutting edge [12]. When the matrix is not strong enough to absorb the energy, the large carbide particles are subjected to bending moments, which, if sufficiently large, will cause cracking. The second possible source of energy input to the matrix is associated with the cutting chamfer. When the insert is forced into the workpiece, a stress pattern is generated around the edge region, with the maximum stress at the chamfer [13]. The hard-facing matrix in this region will be highly strained due to its high workhardening ability and will transfer the energy to the discrete carbides, which are of lower fracture toughness.

The existence of the primary carbides and the eutectic carbide within the microstructure of this hard-facing will also increase the energy consumption in the other three deformation regions. In the primary zone, the matrix has been effectively strain hardened to fracture the eutectic carbides which are perpendicular to the chip formation plane. The eutectic carbides parallel to the plane can separate from the matrix along the interface and large carbide fragments may be pulled out. A much greater energy would be needed to achieve this removal of carbide fragments compared with a simple shearing or crack formation process. In the secondary deformation zone, the matrix is not sufficiently continuous to form a protecting layer and contact with the under side of the chip with fractured carbides will exert high mechanical and thermal loading condition to the rake face. In the tertiary

deformation zone, interaction of the fractured carbides and the flank face of the insert occurs when these two surfaces move at very high relative speed and further deformation of the carbide indicates high mechanical and thermal loading. The brittle ductile transition temperature (BDT) of many ceramic materials, including carbides, is exceeded at operational temperatures above 600°C (0.3 T_m for single crystals [14]). It is clear that the carbide particles are capable of significant plastic deformation prior to fracture.

In most metal cutting operations, tool life is a major consideration because of its impact on the continuity of production. Earlier work by the Authors [15] has demonstrated the ability of the high CBN-content tool material used here to perform well in cutting trials when turning carbide-containing hard-facings. Its performance was explained, in part, by reference to its reluctance to adhere to the workpiece material in quasi-static adhesion tests. However, its progressive damage mode, which directly influences tool life, appears to be closely related to small grain size and structural density.

6. CONCLUSIONS

1. Chromium carbide based hard-facings can be effectively machined by turning and high CBN-content tool materials are particularly suitable for this task.
2. The relatively poor machinability of chromium carbide based hard-facing materials is strongly related to specific features of their microstructure. The machining process involves fracture of large carbides ahead of the cutting edge and this requires more energy than with less complex materials.
3. Progressive, small-scale chipping of the cutting edge, leading to flaking of the rake face, is the predominant mode of tool failure.
4. Structural density and grain size are important factors in determining tool failure mechanisms and, hence, life.

7. REFERENCES

1. Gregory, E N, 1980, Weld Surfacing and Hardfacing, The Welding Institute, pp11-22
2. Menon, R, 1995, The Welding Journal, Vol. 75, No.2, pp43-49
3. Roebuck B, 1995, Technologies and markets for cutting tool materials, National Physical Laboratory

-
4. Heath, P J, 1986, 14th North American Manufacturing Research Conference Proceedings, pp66-80
 5. Kitagawa T and Maekawa K, 1990, *Wear*, Vol.139, pp251-267
 6. Svensson L E, Bhadeshia H K D H, Gretoft B and Ulander B, 1986, *Journal of Mater. Sci.*, pp1105-19
 7. Bieker R, 1995, *Industrial Diamond Review*, Vol. 55, No. 564, pp1-3
 8. Atamert S and Bhadeshia H K D H, 1990, *Material Science and Engineering*, A130, pp101-111
 9. Brookes C A and Hooper R M, 1981, *Towards Improved Performance of Tool Materials: Proceedings of the international conference organized jointly by the National Physical Laboratory and the Metals Society, Teddington*, pp32-35
 10. Weinert K, 1994, *Annals of the CIRP*, Vol 43, pp97-101
 11. Trent, E M, 1991, *Metal Cutting (Third edition)*, Butterworths, London
 12. Shaw, M C, 1984, *Metal Cutting Principles*, Clarendon Press (Oxford)
 13. Konig W, Berktold A, Liermann J and Winands N, 1994, *Industrial Diamond review*, No.3, pp127-132
 14. Kosolapova, T I, 1971, *Carbides: properties, production, and application*, Plenum Press (New York)
 15. Brookes E J, James R D and Ren X, 1998, 4th International Conference on Behaviour of Materials in Machining: Opportunities and prospects for Improved Operations, Strafrod-upon-Avon (UK), pp. 189-198

MANUFACTURING OF MAGNESIUM PARTS - MACHINING AND FORMING

H.K. Tonshoff, B. Karpuschewski and J. Winkler
University of Hannover, Hannover, Germany

KEY WORDS: Magnesium Alloy, Turning, Burnishing, Surface Modification

ABSTRACT: When machining magnesium, the part quality is related to adhesive effects between workpiece and cutting tool. In addition, the danger of chip ignitions exists when unsuitable cutting tool materials and coatings, respectively, are chosen for dry machining. The effect of different tool materials and coatings in turning therefore is investigated.

Burnishing operations are useful to improve surface and subsurface properties of the machined part. The effect of the rolling force being the most influencing rolling parameter is presented. Rolling-in ceramic particles in the surface is discussed for improving wear resistance.

1. CUTTING EXPERIMENTS

Sand cast bars with a diameter $d = 150$ mm and a length of $l = 320$ mm were machined. The alloy used was AZ91 HP with approx. 9% Al, 0.7% Zn and 0.2% Mn. All tests including burnishing experiments were carried out on a CNC inclined-bed lathe Gildemeister MD10S with a main power $P = 50$ kW and a maximum number of revolutions of $n = 10,000$ min⁻¹. A Kistler 9257 B dynamometer was integrated in the machine tool to investigate machining forces. Surface roughness R_z and R_a were measured with a contact stylus instrument Hommel T1000 with a tip radius of 5 μ m and a tip angle

of 90°. The effect of different machining conditions on the surface formation was detected by scanning electron microscopy (SEM).

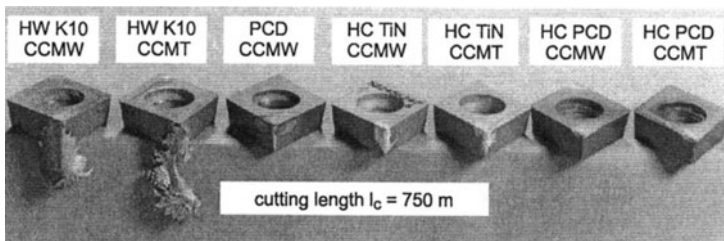
Uncoated carbide tools and tools with polycrystalline diamond (PCD) tips as well as TiN and PCD-coated carbide tools CCMW 120408 and CCMT 120408 were used in a tool holder SCMCN 3225 P12. Resulting angles at the cutting edge (tip radius 0.8 mm) were a flank angle of $\alpha = 7^\circ$, a rake angle of $\gamma = 0^\circ$ and a tool angle of $\kappa = 50^\circ$. The rake for the CCMT-geometry is $\gamma = 5^\circ$. Tools with solid PCD tips that are soldered to a carbide body were only available with a rake of $\gamma = 0^\circ$.

The influence of different cutting tool materials and coatings, respectively, on adhesive effects is shown in Fig.1. Cutting conditions were a cutting speed $v_c = 900$ m/min, a depth of cut $a_p = 1.5$ mm, a feed rate $f = 0.4$ mm and a cutting length $l_c = 750$ m. Flank build-up can be observed if uncoated and TiN-coated carbides are used. The variation of the rake does not show a significant influence. If PCD-tipped tools are used, adhesive effects can not generally be avoided as workpiece material gets into contact with the carbide body. PCD-coated tools show a superior behaviour. No magnesium build-up on the flank is observed. However adhered workpiece material is found on the rake of all tools.

Prerequisites for the formation of flank build-up seem to be

- a certain affinity between cutting tool material and workpiece material,
- the existence of a sufficient temperature in the tool-workpiece contact,
- a soft material component in which a hard phase are embedded [1, 2] as well as
- high mechanical stresses.

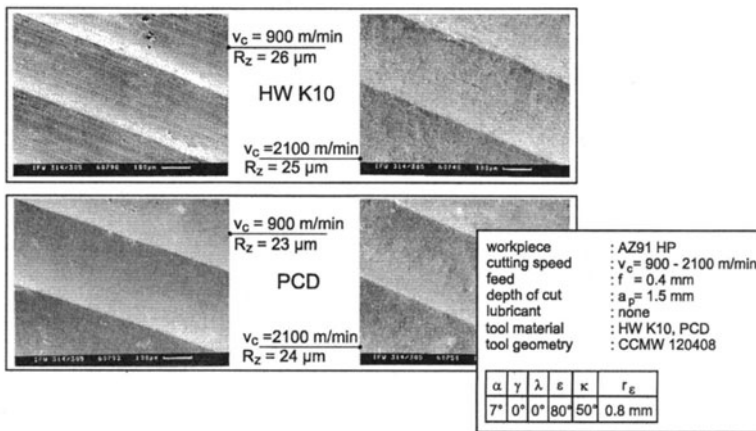
workpiece	: AZ91 HP	tool	: HW, HC, PCD
cutting speed	: $v_c = 900$ m/min	geometry	: CCMW 120408
feed	: $f = 0.4$ mm		: CCMT 120408
depth of cut	: $a_p = 1.5$ mm	α	γ
cooling lubricant	: none	λ	ε
		κ	r_g
		7°	0°
		5°	0°
		80°	50°
			0.8 mm



314/19017 © IFW

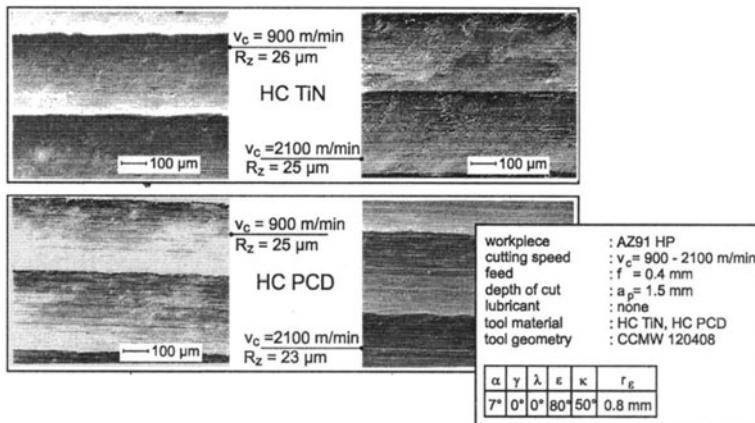
Fig.1: Influence of cutting tool materials and coatings on adhesive effects

Adhesive effects between cutting tool material and workpiece material do not only have a negative influence on machining forces, but also lead to an inferior surface quality. Fig.2 shows SEM photographs of machined surfaces after a cutting length $l_c = 10$ m. Grooves caused by the tool feed can be observed. If cemented carbides are used at a cutting speed of $v_c = 900$ m/min additional grooves are caused by the tool material's grains. At a cutting speed $v_c = 2100$ m/min magnesium particles are torn out of and welded on to the workpiece surface forming flank build-up. Subsequently the microstructure of the flank build-up, in contrast to chips and subsurface of the machined element, shows strong plastic deformation [2].



314/19004 © IFW

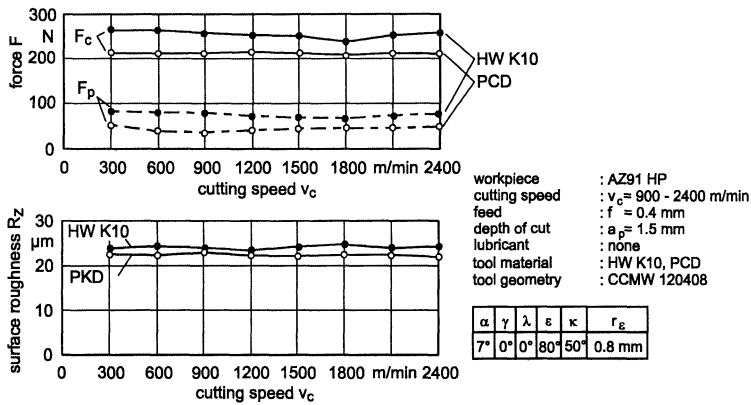
Fig.2: Influence of the cutting tool material on the machined surface



314/19005 © IFW

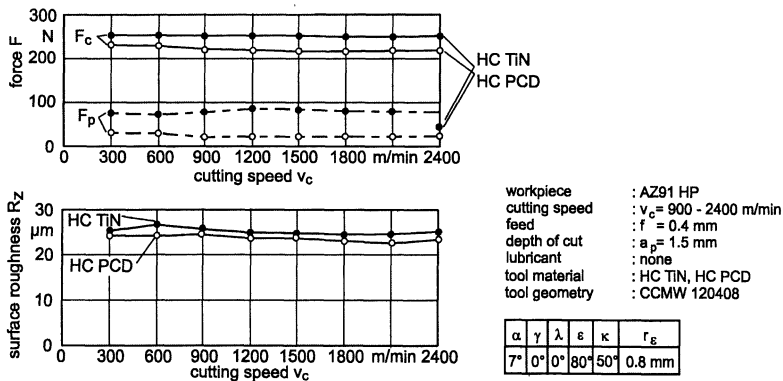
Fig.3: Influence of the tool coating on the machined surface

According to [fig.2](#), photographs of surfaces machined with TiN and PCD-coated cutting tools are shown in [fig.3](#). Adhesive effects can be observed when machining with TiN-coated tools even at a cutting speed of $v_c = 900$ m/min. Molten workpiece material can be found at $v_c = 2100$ m/min. PCD-coatings are an adequate mean to suppress adhesion, but tracks caused by the pyramidal structure of the coating can be observed within the workpiece surface.



314/19002 © IFW

Fig.4: Influence of the cutting tool material on machining forces and surface quality



314/20516 © IFW

Fig.5: Influence of the tool coating on machining forces and surface quality

Fig.4 and 5 show the machining force components cutting force F_c and back force F_p for carbide tools and PCD-tipped tools and coated cutting tools, respectively for cutting speeds from $v_c = 300$ m/min up to 2400 m/min ($a_p = 1.5$ mm, $f = 0.4$ mm, $l_c = 10$ m). PCD tools, either tipped or coated, show lower machining forces and a better surface roughness R_z . As machining forces are decreasing, the thermal load on the chip is reduced resulting in a lower danger of chip ignition when using PCD tools. TiN-coated cutting tools should be avoided in production processes.

Compared to aluminium, machining forces are reduced to approx. 50% when machining magnesium, tool wear for this reason can hardly be observed [3].

2. BURNISHING EXPERIMENTS

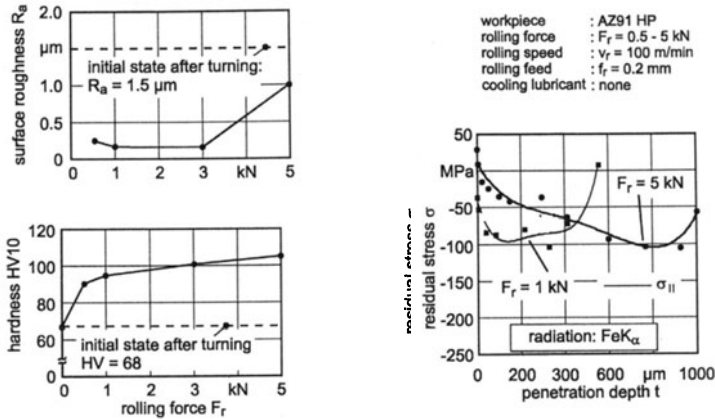
An Ecoroll EG14 burnishing tool was used to carry out burnishing tests on the named AZ91 HP bars. All specimens had been prepared by identical turning operations before burnishing. Fig.6 shows the influence of the rolling force on surface quality, hardness and the residual stresses in the subsurface layer. Rolling speed and feed rate had only minor effect on the experimental results.

The average roughness R_a can be reduced to approx. 15% of the initial state after turning ($R_a = 1.5$ μ m). However, if the rolling force is chosen too high (e.g. $F_r > 3$ kN), the surface is damaged resulting in increasing R_a values. In spite, the gain in surface hardness is most significant for highest rolling forces (108 HV10 for $F_r = 5$ kN compared to 68 HV10 after turning). Residual stresses parallel to the rolling direction for both rolling forces $F_r = 1$ kN and $F_r = 5$ kN are compared in the right section of fig.6. It can be shown that

- compressive residual stresses can be induced in the workpiece subsurface by rolling operations,
- the maximum of residual stresses moves towards the workpiece centre for higher rolling forces,
- the maximum value of residual stresses is independent of the rolling force and
- for the rolling force $F_r = 5$ kN tensile residual stresses can be detected in the workpiece surface.

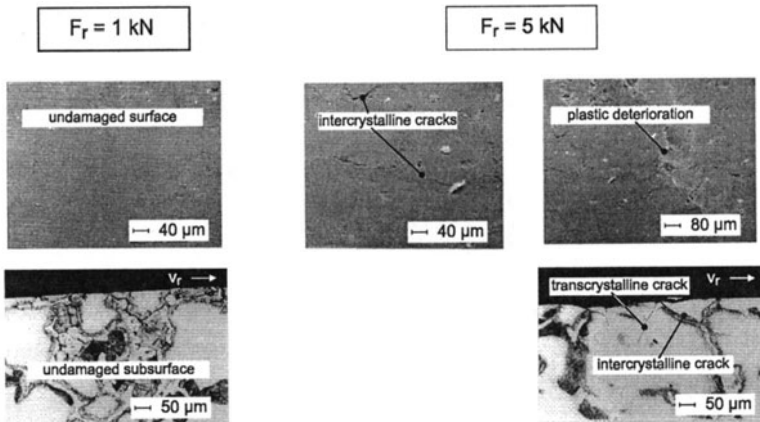
Tensile stresses in the workpiece surface can cause damages to the workpiece and may decrease its working life [4].

Surface damage caused by high mechanical loads ($F_r = 5$ kN) are shown in fig.7. Whereas surface and subsurface layer appear smooth and undamaged for a rolling force of $F_r = 1$ kN, intercrystalline and transcrystalline cracks as well as a plastic deterioration can be observed in SEM photographs of the surface and in photographs of the ground section of the subsurface for $F_r = 5$ kN. However, no grooves caused by the feed of the cutting tool in the previous machining process can be detected (compare to fig.2 and fig.3) for both rolling forces.



314/22220 © IFW

Fig.6: Influence of the rolling force F_r on surface roughness, hardness and residual stresses



314/22219 © IFW

Fig.7: Influence of the rolling force F_r on damage in surface and subsurface

Additional experiments have been carried out to roll-in a ceramic reinforcement component in a cylindrical functional surface to improve the tribological properties of the workpiece by adding a reinforced top layer. Blocky shaped SiC-particles with mean diameters of $d = 5 - 7 \mu\text{m}$ and $d = 50 - 56 \mu\text{m}$, respectively, were directly applied to the burnishing roller-workpiece contact. The work piece had been prepared by turning operations before. Parameters for rolling-in were chosen according to prior broaching experiments ($F_r = 1 \text{ kN}$, $v_r = 100 \text{ m/min}$, $f_r = 0,2 \text{ mm}$). SEM pictures show SiC-particles of both sizes being embedded in the workpiece (Fig. 8, left hand side). Whereas particles of the mean diameter

of 50 - 56 μm can be crushed by the roller, comparatively small particles remain undestroyed. Compared to the machined surface ($R_a = 1.5 \mu\text{m}$), achievable surface roughness is improved for small particles ($R_a = 1.0 \mu\text{m}$) and slightly reduced for the coarser particles ($R_a = 2.2 \mu\text{m}$).

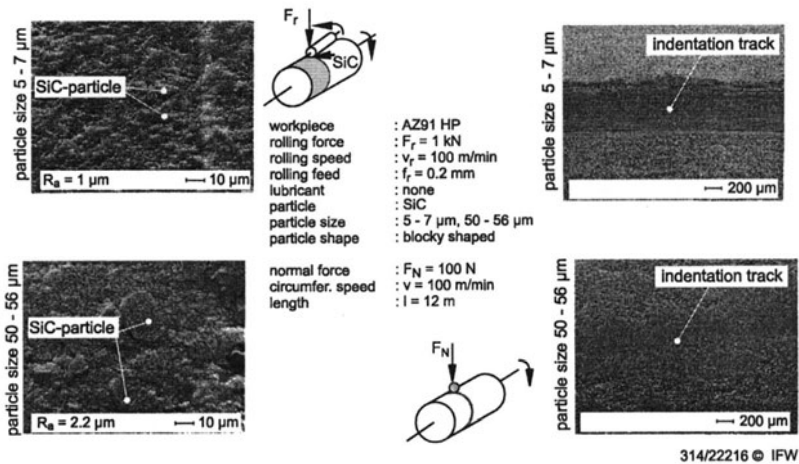


Fig.8: Rolled-in ceramic particles and tribological testing

Prepared surfaces have been subjected to tribological tests. A fixed cemented carbide ball (diameter $D = 6 \text{ mm}$) is pressed onto the rotating surface (circumferential speed $v = 100 \text{ m/min}$) with constant load ($F_N = 100 \text{ N}$). The indentation tracks caused by the sliding contact are shown in Fig. 8, right hand side, for a length of $l = 12 \text{ m}$ (close type tribological system). For small particles of $d = 5 - 7 \mu\text{m}$, plastic deformations can be observed, the reinforced layer is destroyed. The coefficient of friction is raising from $\mu = 0.2$ ($l = 0 \text{ m}$) to $\mu = 0.5$ ($l = 12 \text{ m}$) whereas for the layer of particle size $d = 50 - 56 \mu\text{m}$ $\mu = 0.3$ it remains constant. The latter also shows a good wear resistance.

3. CONCLUSION

To observe the interactions between the workpiece material AZ91 and tool materials and coatings, respectively, turning experiments have been carried out. When machining magnesium dry adhesion between cutting tool and workpiece can lead to flank build-up at cutting speeds of $v_c = 900 \text{ m/min}$ and more if uncoated or TiN-coated carbides are used. Also the danger of chip ignition exists in dry machining if the materials melting point of approx. 600°C is exceeded which is especially significant for small depths of cut and small feed rates [3].

Tools with PCD insert or CVD diamond coating can be used to reduce friction and adhesion in the tool-workpiece contact resulting in low machining forces, low chip

temperature as well as a superior workpiece surface quality even at high cutting speeds of $v_c = 2400$ m/min. Diamond coatings can also be applied to tools with complex geometries.

Furthermore, burnishing operations are a useful mean to improve surface quality, surface hardness and to induce compressive stresses in the subsurface if adequate machining conditions are chosen. For AZ91 HP a rolling force of $F_r = 1$ kN gives good results whereas $F_r = 5$ kN leads to serious damage in the surface and subsurface, respectively. The rolling-in of a ceramic reinforcement in the top layer of a cylindrical surface can be used to increase its wear resistance. Good results were found for SiC-particles of coarse grain (mean diameter $d = 50 - 56$ μm).

4. ACKNOWLEDGEMENT

The work described in this paper has been undertaken with support of the German Research Council (DFG) in a Special Research Programme on magnesium technology (SFB 390).

5. REFERENCES

1. Tomac, N., Tønnessen, K.: Formation of Flank Build-up in Cutting, Magnesium Alloys, Annals of the CIRP 40 (1991) 1, 79-82
2. Tönshoff, H.K., Karpuschewski, B., Winkler, J.: Trockenbearbeitung von Aluminium- und Magnesiumlegierungen, Industrie Diamanten Rundschau, 4/1997 357-363
3. Winkler, J.: Spanende Bearbeitung von Magnesiumwerkstoffen, DGM-Seminar „Magnesium - Eigenschaften, Anwendungen und Potentiale“, Clausthal-Zellerfeld, 1997
4. Broszeit, E., Steindorf H.: Mechanische Oberflächenbehandlung, DGM Informationsgesellschaft-Verlag, 1996

HIGH-SPEED CONTINUOUS AND DISCONTINUOUS MACHINING OF HARDENED STEEL AND HARD CAST IRON USING SUBMICROMETER CERAMICS ON THE BASIS OF AL₂O₃

A. Krell, P. Blank, L.-M. Berger and V. Richte

Fraunhofer Inst. Keramische Tech. Und Sinterwerkstoffe, Dresden, Germany

KEYWORDS: Cutting ceramics, Discontinuous cutting, Dry cutting, Hardened steel

ABSTRACT: The performance of very hard and strong pure Al₂O₃ ceramics with grain sizes of 0.5-0.7 μm is investigated on machining *hardened* steel (HRC ≈ 60) and globular *hard* cast iron (HRC ≈ 43). These ceramics are successfully applied even at high speed (300 m/min) or with a high feed rate (0.3 mm/rev) and depth of cut (2 mm). Surprisingly, the new ceramics surpass CBN tools on discontinuous and interrupted conditions.

The behaviour of pure submicrometre alumina tools is compared with new Al₂O₃/Ti(C,O) composites of the same grain size and with advanced commercial grades.

1. INTRODUCTION

Grinding is most common for machining functional surfaces of *hardened* steel, e.g. in ball bearings. In spite of the recent progress in ceramic grits with a submicrometre microstructure [1], grinding is time consuming, the equipment is expensive, and deposition or recycling of the grinding silt is ecologically and economically difficult. Even without a complete substitution of grinding, the working time can be cut to 2/3 if first turning steps are combined with final grinding [2].

If turning shall be used for the *final* finish, important tool life criteria are the surface roughness of the machined workpiece and the stability of the cutting tip position (which determines the accuracy of the machined measure). Tools with low thermal conductivity may be preferred to obtain high process temperatures at the cutting tip for softening the hard metal surface but, on the other hand, it is imperative to keep a constant (high) hardness on *final*

machining. A high wear resistance in dynamic contact with the abrasive carbide particles of hardened steel microstructures requires a high hardness combined with a sufficient creep resistance at high temperatures and a high chemical stability (preventing oxidation and reactions with constituents of iron-based workpieces). With the present understanding of *microstructural influences on hardness* [3], wear [4], and the power of ceramic grinding materials [1], an average grain size of less than 1 μm and a low frequency of flaws are imperative for new cutting ceramics. Additional measures may be required to balance the increasing high-temperature creep rate usually associated with small grain sizes.

If the wear resistance is increased by decreasing the grain size, an additional advantage comes from an improved quality of the ground cutting edges. For example, reduced wear of submicrometre alumina is associated with a decreasing amount of grain pull-out [4], and with a constant grinding procedure in finishing alumina cutting inserts the roughness of a ground 0.6 μm alumina ceramic is about one half of the value on a ground 3.6 μm microstructure [5]. The improved quality of cutting edges increases the life-time of the tool at low cutting forces and gives a small roughness of the machined surface.

At present, cubic boron nitride (CBN) is preferred for turning hardened steel, and polycrystalline diamond can be used for some applications with hard cast iron [6]. Looking for alternatives, the industry has focused investigations on fine-grained $\text{Al}_2\text{O}_3/\text{Ti}(\text{C},\text{N})$ composites, and a first commercial grade claimed "submicronstructured" appeared on the European market in 1997. Compared with conventional Al_2O_3 , such composites may give advantages in strength and hardness, but for machining *hard* materials the technical significance of the lower oxidative and chemical stability of $\text{Ti}(\text{C},\text{N})$ phases (compared with corundum) is not known a priori. Also, surprisingly few attention is given to possible toughness shortcomings of the submicrometre composites the K_{IC} of which may drop to values less than known for pure sintered alumina [7].

Contrary to the use of advanced $\text{Al}_2\text{O}_3/\text{Ti}(\text{C},\text{N})$ composites for machining *hardened* steel, first studies with pure, submicrometre sintered Al_2O_3 inserts did not investigate this application but were focused on basic wear mechanisms [8][9]. The objective of the present work, however, was machining alloyed *hard* cast iron and *hardened* steel. For this application we developed new ceramics which are more fine-grained than in previous investigations [4][7][10] and which may promote the substitution of grinding by turning.

2. MATERIALS AND METHODS

Most manufacturers have started to develop submicrometre composite tools on the basis of Al_2O_3 with TiC or $\text{Ti}(\text{C},\text{N})$, but the covalent nature of the carbides prevents pressureless sintering at temperatures of 1600 $^\circ\text{C}$ or less, and the most fine-grained of new (laboratory) composites with TiC concentrations of 25-35 % exhibit average sizes of Al_2O_3 and TiC subregions of about 0.8 - 1 μm (associated with a hardness HV_{10} up to 23 GPa, measured at a testing load of 10 kgf) [11]. On the other hand, with *oxygen* introduced into the covalent phases of TiC or $\text{Ti}(\text{C},\text{N})$ much more fine-grained composites with a higher hardness can be produced associated with a different milling behaviour of these powders [7]. Therefore, the performance of these new composites was investigated in the present experiments, Fig. 1 gives the microstructure.

Two commercial ceramics were used as references. SH1 is a well known $\text{Al}_2\text{O}_3/\text{Ti}(\text{C},\text{N})$ composite manufactured by CeramTec (Plochingen, Germany). Additionally, a

"submicronstructured" composite introduced into the market with special emphasis to the machining of hardened steel was investigated. Its major microstructural merit is the elimination of slightly agglomerated carbide structures which are not perfectly avoided in other grades.

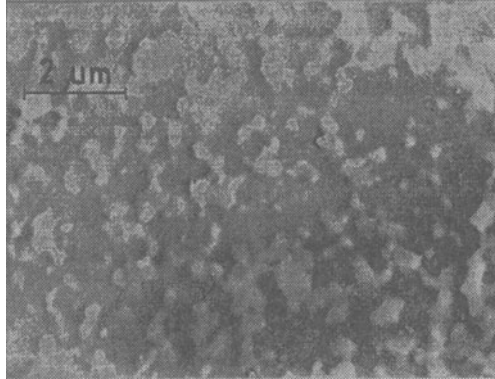


Fig. 1: Microstructure of composite AT60A. The scanning electron micrograph gives an average size of single phase subregions of $0.44 \mu\text{m}$ ($\text{Ti}(\text{C},\text{O})$) and $0.84 \mu\text{m}$ (Al_2O_3) [average size = $1.56 \cdot$ average intercept length]. Additional TEM studies have shown that alumina subregions are typically composed of about 1.5-2 grains. Hence, the size of individual grains is about $0.4\text{-}0.5 \mu\text{m}$ for both the alumina matrix and the $\text{Ti}(\text{C},\text{O})$ crystals.

It is not clear if carbide-reinforced tools will meet the thermodynamic and chemical demands for turning hardened steel. On the other hand, pure sintered corundum ceramics associate the advantage of highest chemical and oxidation resistance with a hardness that after *pressureless* sintering is in no way inferior to *hot-pressed* carbide-reinforced *composites* [3], and their strength of $800\text{-}900 \text{ MPa}$ [10] equals or even exceeds the strength of composites. Such cutting inserts were prepared from a high-purity powder of 99.99% Al_2O_3 by cold isostatic pressing and pressureless sintering, the microstructure is given by Fig. 2.

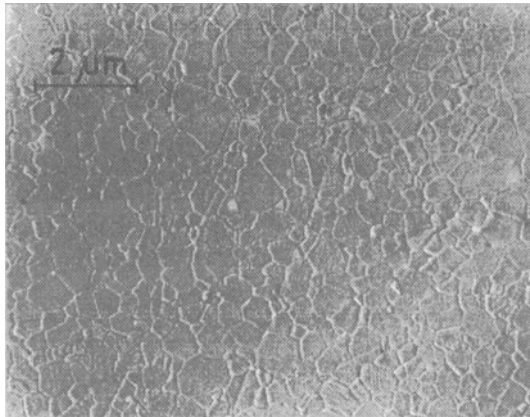


Fig. 2: Microstructure of pure Al_2O_3 inserts with submicrometre grain size.

The investigated ceramic inserts are characterized by Table I; all data were measured in our laboratory. Commonly, the hardness is evaluated on *polished* surfaces, and these data are given here to enable a wide comparison. However, the surfaces of technical ceramic tools are *ground* and exhibit a *different* hardness [4][7]. Therefore, in Tab. I the data for *ground* surfaces are more representative to illustrate the cutting behaviour.

Tab. I. Ceramic tool materials for machining hard cast iron and hardened steel.

Composition		Density absolute (relative) [g/cm ³] [%]	Grain size [μm]	Vickers hardness (testing load = 10 kgf) [GPa] [GPa]	
		(for composites [cp. Fig. 1]: size of single phase subregions [average of all phases])		polished	ground
<i>Pure alumina</i>					
AC41	Al ₂ O ₃	3.96 (99.3%)	0.56	20.2 ± 0.2	22.1 ± 0.9
<i>Composites</i>					
AT60A	Al ₂ O ₃ + 33 vol-% TiC _{0,73} O _{0,14}	4.325 (100 %)	0.70	20.8 ± 0.2	22.8 ± 0.8
AT62	Al ₂ O ₃ + 33 vol-% TiC _{0,42} O _{0,23} N _{0,35}	4.355 (100 %)	0.70	20.2 ± 0.3	21.1 ± 0.6
<i>Commercial references:</i>					
SH1	Al ₂ O ₃ + 33 vol-% Ti(C,N)	4.352	1.52	19.6 ± 0.3	21.2 ± 0.2
"submicron"	Al ₂ O ₃ + 33 vol-% Ti(C,N)	4.356	1.63	19.6 ± 0.2	21.2 ± 0.5

The cutting performance of inserts SNGN120412 (12.7·12.7·4.76 mm³, radius 1.2 mm, 20° chamfer / width 0.2 mm) was tested on a 35 kW CNC lathe (NILES, Chemnitz, Germany, 1990) with a feed rate $f = 0.1$ mm/min and a depth of cut $a = 0.2$ mm in most of the tests. The plates were positioned with a rake angle $\gamma = 6^\circ$, an inclination angle $\lambda = -4^\circ$, and a large entering angle $\kappa = 45^\circ$ chosen to maximize the selectivity of the tests (related to the tool materials) by high loads at the cutting tip. In some additional experiments with an entering angle $\kappa = 75^\circ$ it was shown that κ does not affect the flank wear width, but it is clear that the choice of $\kappa = 45^\circ$ result in a larger roughness. Three parameters were measured:

- (1) The *flank wear width VB* is the usually evaluated wear parameter at the primary cutting edge.
- (2) The *cutting edge displacement CED* determines the degree of precision in machining a hard metallic workpiece. It was measured optically as an independent parameter at that point of the insert radius where the normal direction of the cut metal surface meets the radius of the cutting tool perpendicularly.

(3) The *quality of the cut metal surface* is an important criterion for the value of tools on *precise-machining* hard cast iron or hardened steel. Two parameters are important:

(i) The *roughness* was measured as a function of the cutting time with R_a as the statistical average depth of the profile and R_{ZD} as the arithmetic average of a number of measurements that assess the maximum depth for some measuring distance.

(ii) On turning hardened steel at high velocities > 250 m/min there is a significant input of heat not only into the chips but also into the cut surface of the shaft. Depending on the state of wear of the tool, cutting forces and process temperatures increase and cause a softening of the hardened steel. Therefore, the decrease of the hardness was recorded as an additional parameter in such tests, and an intermittent machining operation at a low velocity (180 m/min) was required to restore a surface with the original hardness before every new experiment with $v > 250$ m/min.

The tools were run up to an upper flank wear width $VB \approx 0.15\text{--}0.25$ mm. A minimum of two tests series at least were performed with each grade.

Two different iron-basis workpieces were machined (German standard notations):

- alloyed globular hard cast iron G-X300CrMo153 (0.3 wt-% C, 15 wt-% Cr, 3 wt-% Mo) with an average Rockwell hardness $HRC = 42.9 \pm 1.3$ (controlled after each cut),
- hardened steel 90MnCrV8 (0.86 wt-% C, 0.2 wt-% Si, 1.98 wt-% Mn, 0.43 wt-% Cr, 0.14 wt-% Cu, 0.10 wt-% Al, 0.08 wt-% V) with $HRC = 58.4 \pm 1.5$.

The rough, macroscopically uneven surfaces of the as-delivered shafts had to be pre-machined to get equally prepared surfaces exposing constant conditions for all tested inserts. This preparation is difficult for shafts of hard cast iron or hardened steel because it associates the high hardness of the counterpart and discontinuous cutting conditions with a changing frequency and power of impacts. Cubic boron nitride inserts (dreborid[®], Lach company, Hanau/Germany) failed on machining the hard cast iron, and hardmetal inserts (WC + 6 % Co, Vickers hardness ≈ 16 GPa, $K_{Ic} \approx 9$ MPa \sqrt{m}) were not able to cut the rough outer shell of the hardened steel shaft (neither at $v = 50\text{--}100$ m/min nor at higher velocities). The same negative result applied for both commercial ceramic composites. Therefore, the new laboratory grade ceramics designed for *precise machining* had to be used for this severe cutting operation.

3. RESULTS

3.1 Machining hardened steel

3.1.1 Discontinuous cutting

It is commonly assumed that Al_2O_3 ceramics with toughness values $K_{Ic} < 4$ MPa \sqrt{m} cannot be used for interrupted machining or with high feed rates. With the failure of all commercial tools, however, the submicrometre alumina and $Al_2O_3/Ti(C,O)$ inserts *had* to be applied and were used at $v = 120$ m/min with a large feed rate $f = 0.3$ mm/rev and a depth of cut $a \approx 1.5$ mm. In regions with substantial deviations from circular cross-sections, $a \approx 1.5$ mm is an average value because some parts of the circumference were not cut at all whereas the depth of the first cut was more than 2 mm at other positions. Such interrupted conditions are associated with severe thermal shock indicated by the fluctuating appearance of the red colour at the cutting tip and documented by video recording.

The number of two rough shafts (hardened, 1350 m long) in the investigations determined the number of interrupted tests. To increase the significance of individual data, similar results obtained with the composites AT60A/AT62 were pooled to enable a qualitative comparison between the different *groups* of ceramics (composites - pure Al_2O_3).

Fig. 4 gives the flank wear. Both commercial grades (SH1, submicrometre) failed by fracture within 1-2 min, the roughness of the cut metal surface was $R_a = 4-5 \mu\text{m}$ at $t < 1 \text{ min}$.

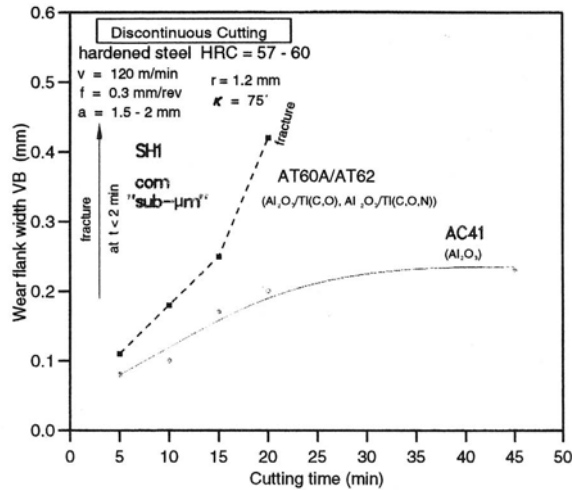


Fig. 4. Severe discontinuous cutting of hardened steel with submicrometre tool ceramics.

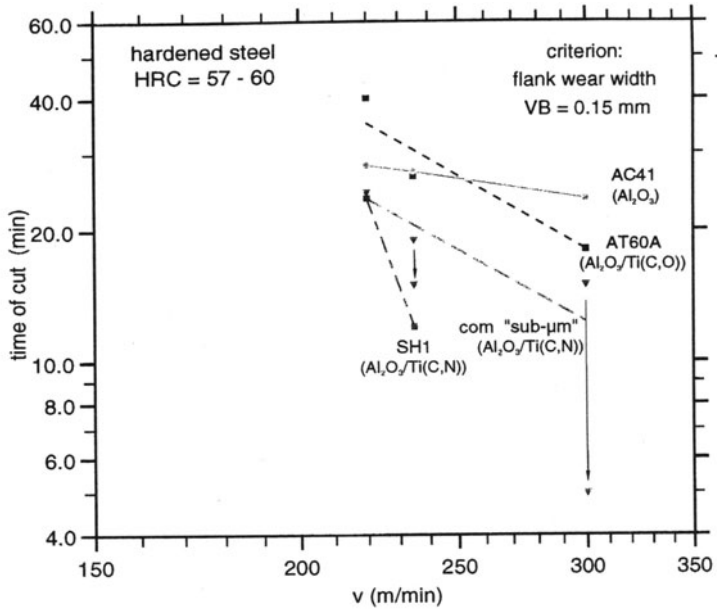
On the contrary, both the pure alumina insert (AC41) and the submicrometre composites AT60A/AT62 were successfully applied. The new, submicrometre alumina tools did not only not fracture *macroscopically* during one hour of severe cutting (with *one* tip) but retained microscopically nearly perfect cutting edges providing a high surface quality of the hardened shaft in the first cut ($R_a \leq 2 \mu\text{m}$ for $t \leq 30 \text{ min}$).

Fig. 4 gives the flank wear. Surprisingly, under these severe conditions the general performance of pure alumina ceramics (AC41) is even more prospective than the behaviour of the new submicrometre composites AT60A and AT62.

3.1.2 Continuous cutting: Fracture behaviour and wear at $v = 200-250 \text{ m/min}$

Figs. 5-7 give the results for continuous cutting hardened steel. The high hardness of the steel and the low thermal conductivity of the tool materials cause a large input of heat into the metal chips which appear rather flaming than red-glowing.

For the references (SH1 and the commercial submicrometre composite), this feature is associated with a critical influence of the cutting velocity between 200 and 250 m/min: the flank wear was small at 220 m/min, but already at 235 m/min a greater crater-wear was observed. At this higher velocity, more than 50 % of the commercial inserts exhibited a sudden, strong increase in the flank wear during the first 10-20 minutes of cutting accompanied by local or global fracture at the cutting edge, and it was difficult to record the flank wear continuously up to $\text{VB} = 0.2 \text{ mm}$. As a consequence, it was impossible to measure the cutting edge displacement of the reference tools on turning hardened steel with



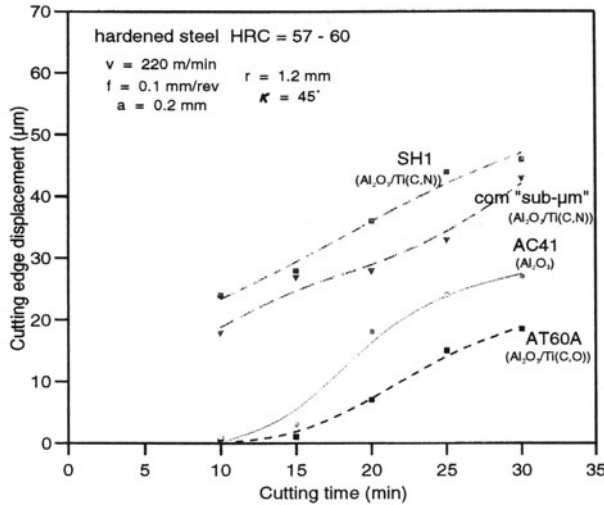


Fig. 6. Cutting edge displacement on turning hardened steel at 220 m/min.

same ranking as also observed on machining hard cast iron (Fig. 8), and also the *smaller* influence of the cutting velocity on the wear of *alumina* inserts compared with composites (Fig. 5) was similarly noticed on cutting hard cast iron.

Contrary to the new laboratory grade tools, most commercial "submicrometre" inserts fractured within the first 5-10 minutes at $v = 300$ m/min (Fig. 7).

At $v = 300$ m/min, increasing with time wear deteriorates the cutting edge, increases the cutting forces and the input of heat into the surface of the machined steel. The resulting decrease of the hardness of the workpiece is given as an additional parameter in Fig 7.

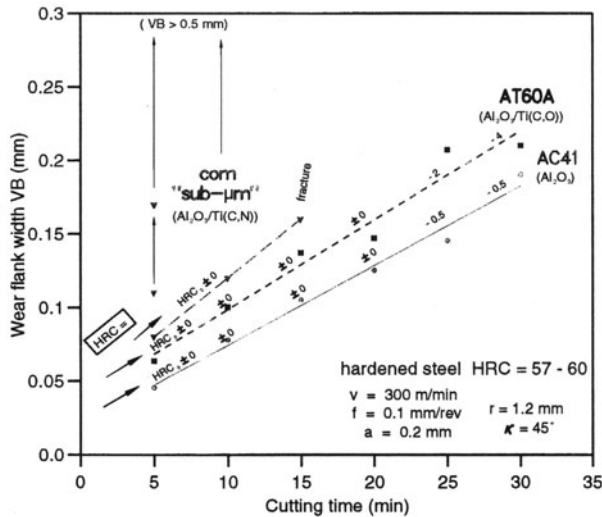


Fig. 7. Flank wear width VB on turning hardened steel at $v = 300$ m/min. HRC₀ is the original hardness of the steel surface in the cut region *before* the test.

3.2 Moderate demands: Machining globular hard cast iron

In Fig. 8 the composites show a fair ranking with their grain sizes: The *commercial* "submicrometre" tool exhibits less wear than the other reference SH1, and wear is further reduced in the new Ti(C,O) reinforced submicrometre composite AT60A, apparently due to its higher hardness (Tab. I). When nitrogen is introduced into the covalent oxycarbide phase (AT62), the hardness drops to the same level as also observed for SH1 (Tab. I), and AT62 exhibits a similar wear behaviour in spite of its reduced grain size (Fig. 8).

Much more surprising is the leap of decreasing wear of pure alumina (AC41). This leap is not explained by the hardness which is just intermediate between the (lower) hardness of the commercial composites and the (higher) value of the AT60A composite. Also, the grain size of the sintered corundum material (Tab. I) is not very different from the microstructural data given in Fig. 1 and Tab. I for the $\text{Al}_2\text{O}_3/\text{Ti}(\text{C},\text{O})$ composite AT60A.

At a lower cutting speed of 150 m/min, the advantage of the pure alumina tools (AC41) compared with the commercial composites was about the same as given in Fig. 8 (220 m/min), and the behaviour of the new submicrometre composite AT60A was close to AC41. Unfortunately, the composite deteriorates at $v > 200$ m/min (Fig. 8).

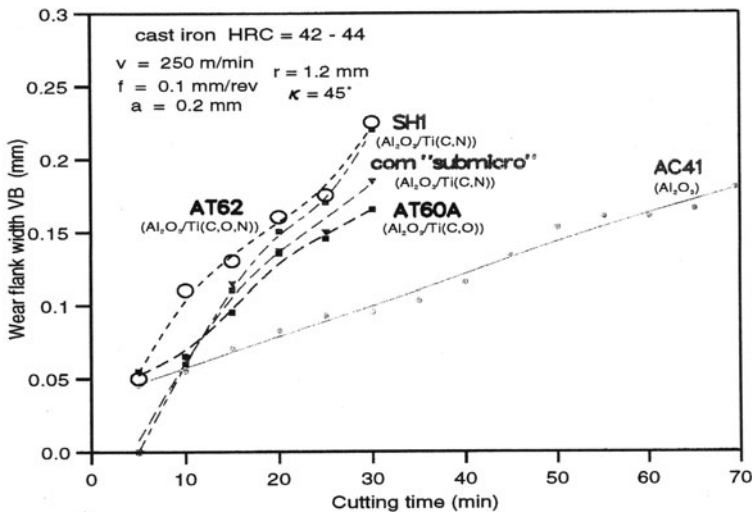


Fig. 8. Flank wear VB on turning globular hard cast iron at 250 m/min.

Another important criterion for the quality of tools in precision turning of hard materials is the obtained roughness of the cut metal surface. Fig. 9 describes the time dependent increase of the average roughness R_a . A fixed ratio $R_{ZD}/R_a \approx 5$ between the statistically averaged *maximum* depth of roughness and R_a was observed in all of the tests and is given as a note to Fig. 9. The arbitrary scatter of roughness data was rather large, and no significant difference was observed between the surfaces cut by SH1 or by the commercial "submicrometre" tool. However, all other inserts show the same ranking as observed for the flank wear in Fig. 8: improved results are provided by the (very hard) oxycarbide-reinforced composite AT60A, but a more significant progress results from the use of the pure submicrometre alumina insert AC41.

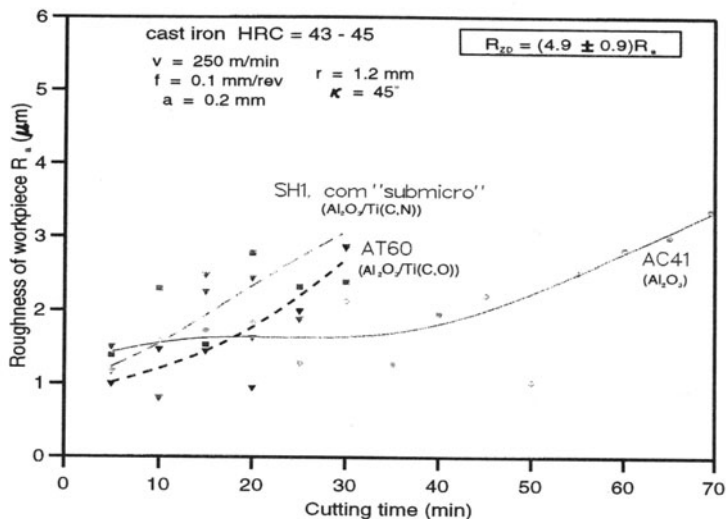


Fig. 9. Surface quality on turning hard cast iron with different ceramic tool materials.

4. DISCUSSION

Different results are obtained on machining globular hard cast iron and hardened steel. For hard *cast iron*, the wear rates of composites reinforced by Ti(C,N), Ti(C,O) or Ti(C,O,N) and the qualitative leap to reduced wear of pure submicrometre alumina tools suggest:

- Reducing the grain size of composites with TiC, Ti(C,N) or Ti(C,O) increases the hardness and may reduce the wear on turning hard cast iron, but the effect is not large.
- The reason is indicated by the much higher wear resistance of pure, thermodynamically highly stable alumina (which does *not* offer a higher hardness!). Probably, tribochemical interactions between the iron and the carbide phases at the cutting tip of composites increase the wear.

In fair agreement with this idea, the advantage of the very hard $\text{Al}_2\text{O}_3/\text{Ti}(\text{C},\text{O})$ composite compared with the commercial $\text{Al}_2\text{O}_3/\text{Ti}(\text{C},\text{N})$ tools decreases at higher cutting velocities (i.e: with increasing process temperatures at the cutting tip), whereas the pure alumina tool retains its advantage over the whole range of cutting velocities investigated here.

On turning hardened *steel*, again both the pure alumina (AC41) and the laboratory grade composite AT60A exhibited less wear than the commercial cutting tools, but the ranking of AC41 and AT60A ceramics shows interesting changes. Without investigations of microscopic wear mechanisms, this is not the place for speculations, but it is obvious that the technical behaviour of the two ceramics is affected by some important basic properties:

- (a) It has been shown for $\text{Al}_2\text{O}_3/\text{TiC}$ composites that even at room temperature and with almost inert conditions (e.g. dry air, fretting wear against alumina) chemical interactions cause preferential (local) wear of the covalent carbide constituents of the composite - with the consequence that at equal crystallite sizes pure sintered corundum is more wear resistant than the composite [12][13]. The same ranking was observed here on turning hard cast iron (Fig. 8).
- (b) On machining hardened steel, flaming chips indicate a much higher process temperature

than on turning hard cast iron at similar speed. Whereas pure submicrometre alumina exhibits intense creep at $T > 1100\text{ }^\circ\text{C}$, a continuous network of covalent crystals reduces the creep rate in composites with more than 25 vol-% of TiC, Ti(C,N) or Ti(C,O). Indeed, comparing at $v \leq 250\text{ m/min}$ the machining of hard cast iron and hardened steel, the increasing temperature increases the wear of the alumina tool more than the wear of the best composite AT60A. This feature changes their ranking in a way that on machining hardened steel it is now AT60A which (at a similar submicrometre grain size as AC41) exhibits the smallest wear (Fig. 6).

- (c) This advantage of composites is lost when at yet higher temperatures oxidation of the Ti(C,O,N) phases or more intense chemical reactions start. On machining hardened steel, high cutting speeds $> 250\text{ m/min}$ cause a more intense deterioration of the wear resistance of even the best composite AT60A than observed for pure alumina (AC41): already at 235 m/min both ceramics exhibit the same wear (Fig. 5), and at 300 m/min sintered corundum shows the best performance (Fig. 7).

The same behaviour of a stronger influence of the cutting velocity on the flank wear (Fig. 5) was also observed on machining hard cast iron.

The influence of *high-velocity* turning on the *hardness* of the workpieces (Fig. 7) is important for different aspects in the development of new machining technologies. With a high velocity, the softening of the steel promotes high material removal rates even at small feed rates, and turning of hardened steel with cutting ceramics that are less expensive than cubic boron nitride (CBN) becomes possible. On the other hand, final precision machining has to conserve a *constant* high hardness of the cut surface. This feature defines critical limits for the cutting velocity ($\leq 250\text{ m/min}$ in the present investigations) or, at higher speed, for the tolerable tool wear (Fig. 7: $VB \leq 0.15\text{ mm}$ at $v = 300\text{ m/min}$).

The *fracture* behaviour of cutting edges is affected by *time dependent wear* processes. Hence, the high frequency of fracture of commercial inserts on turning hardened steel at $v \geq 220\text{ m/min}$ and the surprising lack of such events with the new laboratory grades even on pre-machining rough shafts for about one hour (with *one* cutting tip / discontinuous conditions!) cannot be compared readily with the bending strength at room temperature. For the commercial grades, the manufacturer gives a strength of 600 MPa for SH1 (no data for the submicrometre grade available). The bending strength of the new composite AT60A is about 800 MPa, and about 900 MPa were reported for AT62 [7]. A lower strength of about 650-700 MPa was observed for the submicrometre Al_2O_3 ceramic [10]. The fracture toughness of all of the laboratory grades is 3.3-3.8 $\text{MPa}\sqrt{\text{m}}$, whereas surprisingly high values of 5.5 $\text{MPa}\sqrt{\text{m}}$ (SH1) and 6.6 $\text{MPa}\sqrt{\text{m}}$ (submicron commercial composite) are given by manufacturer's information for these reference tools. None of these data explain the fracture risk of the commercial tools and the extremely high reliability of the new laboratory grades on machining hardened steel. Complex wear-induced processes of flaw-generation will have to be investigated to understand the high global and microscopic stability of the new submicrometre ceramics.

It is the unique message from these results that the leap to cutting ceramics on the basis of alumina which stand *both* the high temperature on high-speed machining *and* the mechanical impacts of hardened steel on discontinuous cutting comes with the submicrometre grain size and the thermodynamic stability of these tools. A grain size $< 0.7\text{ }\mu\text{m}$ seems to be the first, most important requirement, probably associated with a strength $> 600\text{ MPa}$. The

fracture toughness K_{Ic} and the creep resistance give additional influences but, surprisingly and contrary to the common opinion, their influence is of only secondary importance.

5. CONCLUSIONS

Advanced submicrometre ceramics can be successfully applied to machine hard cast iron and hardened steel. Properly adjusted microstructures improve the cutting performance of covalent-phase reinforced composites and give rise to a qualitative leap obtained with pure sintered alumina. Associated with different advantages and limitations in important basic properties (chemical stability, creep resistance, hardness), the ranking of these two groups of tool ceramics is different depending on the microstructural properties of the machined materials and on the process temperatures that develop at the cutting tip.

The surprising excellence of pure sintered alumina compares with recent advances in the grinding efficiency enabled by the same corundum microstructure [1]. Conventional Al_2O_3 tools disappeared from the market 25 years before and were totally replaced by composites reinforced with ZrO_2 and $Ti(C,N)$. On the contrary, the present investigations indicate that new submicrometre alumina tools can be successfully applied not only for the *precision*-machining of hard materials on *continuous* cutting with small feed rates, but likewise under severe *discontinuous* conditions with high feed and depth of cut.

REFERENCES

- [1] Krell, A., Blank, P., Wagner, E., Bartels, G.: Advances in the Grinding Efficiency of Sintered Alumina Abrasives, *J. Am. Ceram. Soc.*, 79 (1996) 3, 763-9
- [2] Wellein, G., Fabry, J.: Hartdrehen ist mehr als der Einsatz von CBN (Cutting of hard materials is more than the application of CBN, in German), *Werkzeug-Technik*, 45 (1996) 9/10, 7-10
- [3] Krell, A., Blank, P.: Grain Size Dependence of Hardness in Dense Submicrometer Alumina, *J. Am. Ceram. Soc.*, 78 (1995) 4, 1118-20
- [4] Krell, A.: Improved Hardness and Hierarchic Influences on Wear in Submicron Sintered Alumina, *Mater. Sci. Eng. A*, 209 (1996) 1-2, 156-63
- [5] Krell, A.: Fracture origin and strength in advanced pressureless sintered alumina, *J. Am. Ceram. Soc.*, 81 (1998) 7, 1900-1906
- [6] Xiao, H.: Wear Behaviour and Wear Mechanism of Ceramic Tools in Machining Hardened Alloyed Steel, *Wear*, 139 (1990) 2, 439-51
- [7] Krell, A., Berger, L.-M., Blank, P.: Submicrometer $Al_2O_3/Ti(C,O,N)$ Composites for Tool Applications, Proc. 22nd Annual Conference on Composites, Advanced Ceramics, Materials, and Structures, The American Ceramic Society, Westerville (OH), 1998, xxx-xxx
- [8] Goh, G.K.L., Lim, L.C., Rahman, M., Lim, S.C.: Effect of Grain Size on Wear Behaviour of Alumina Cutting Tools, *Wear*, 206 (1997) 1/2, 24-32
- [9] Takahashi, T., Katsumura, Y., Suzuki, H.: Cutting Performance of White Ceramic Tools having High Strength, *J. Japan. Soc. of Powder and Powder Metall.*, 41 (1994) 1, 33-37
- [10] Krell, A., Blank, P.: The Influence of Shaping Method on the Grain Size Dependence of Strength in Dense Submicrometre Alumina, *J. Europ. Ceram. Soc.*, 16 (1996) 11, 1198-1200
- [11] Krell, A.: Fortschritte in der spanenden Metallbearbeitung durch Keramiken mit Submikrometer-Gefüge (Advances in Machining Metals Using Ceramics with Submicron Microstructures, in German), Hartstoffe (Proc. of the Hagen Symposium on Powder Metallurgy, 13-14 Nov. 1997), Werkstoff-Informationsgesellschaft, Frankfurt, 1997, 57-76
- [12] Krell, A., Klaffke, D.: Effects of Grain Size and Humidity on Fretting Wear in Fine-Grained Alumina, Al_2O_3/TiC , and Zirconia, *J. Am. Ceram. Soc.*, 79 (1996) 4, 1034-40
- [13] Koinkar, V.N., Bushan, B.: Microtribological Studies of Al_2O_3 , Al_2O_3-TiC , Polycrystalline and Single-Crystal Mn-Zn Ferrite, and SiC Head Slider Materials, *Wear*, 202 (1996) 1, 110-22

INFLUENCE OF THE GRINDING PROCESS ON THE PROCESS BEHAVIOUR OF CUTTING TOOLS

K. Weinert and M. Schneider
University of Dortmund, Dortmund, Germany

KEY WORDS: Tool-Grinding, Finite Element Method, Cemented Carbide, Cermet

ABSTRACT: In the context of this paper the results of grinding and the subsequent use of basic and complex cutting tools such as drills should be acquired. Apart from investigating the grinding of cemented carbides, tools manufactured from cermet are also included in the studies. In order to determine the thermal and mechanical stresses on the cutting material when tools are ground, the finite element method is employed. This involves demonstrating connections between the grinding of tools on different conditions and the later wear behaviour of the tools when in use.

1. INTRODUCTION

In the machining processes used at the moment (e.g. HSC, dry machining) the tool is subjected to high thermal, mechanical and chemical loads. In order to deal with this collection of stresses adequately the highest demands must be placed on the cutting tool with respect to the cutting tool material, the geometry of the tool and the quality of the grinding process.

When tools are being ground, dimensional and geometrical accuracy are of the utmost importance. Aspects such as surface quality, surface near-zone characteristics and surface texture play an important role with respect to the application behaviour of the tools [1]. A central problem during the grinding process is especially the thermal stress on the tools. If the process temperatures are too high, certain application properties of the tool can be changed and under certain conditions lasting damage to the tool, such as microstructural changes or microcracks, can be caused [2-4].

¹Published in: E. Kuljanic (Ed.) *Advanced Manufacturing Systems and Technology*,
CISM Courses and Lectures No. 406, Springer Verlag, Wien New York, 1999.

In order to describe the fundamental relationships between grinding conditions and the application behaviour of geometrically determined cutting tools, both cemented carbide and cermet tools were used. Cermet is characterised by a higher wear resistance than conventional cemented carbides [5, 6]. However, at present there are still some significant problems associated with the production of tools such as drills in cermet [7]. In the investigations cutting tips were used as model tools. Single-edge gundrills and short drills were also employed. The tool grinding process was basically completed by varying the process parameters (e.g. cutting speed, feed rate) and the specifications for the grinding wheel (e.g. grain size, bonding). In order to evaluate the grinding process the process forces and temperatures were ascertained. To determine the grinding temperatures measurements and basic analytical calculations were employed. Furthermore, the thermal stress on the tool during the grinding process was simulated by the finite element method. The quality of the ground tool was determined on the basis of the state of stress, the surface topography, the surface near-zone influences (e.g. formation of cracks) and the quality of the edge. The ground tools were then used in cutting tests where the process forces, the wear behaviour and chip formation were evaluated. Metallographic analyses of the tools complemented the investigations that were undertaken. In the following sections, and based on specific examples, the important parameters affecting the quality of a cutting tool, which result directly or indirectly from the grinding process, will be explained.

2. INFLUENCE OF THE GRINDING PROCESS PARAMETERS

In the investigations single-edge gundrills made of cemented carbide and cermet were used. It must be mentioned here that up to now no cermet gundrills have been commercially available. The fabrication of the cermet gundrills proved to be extremely difficult. To produce them first the grinding processes and the grinding process parameters applied when producing conventional cemented carbide gundrills were used. This meant that the grinding of the rake face was achieved by lateral grinding. This resulted in drill-head breakage during the grinding process (Fig. 1). Cracks also appeared on the rake face of the tool.

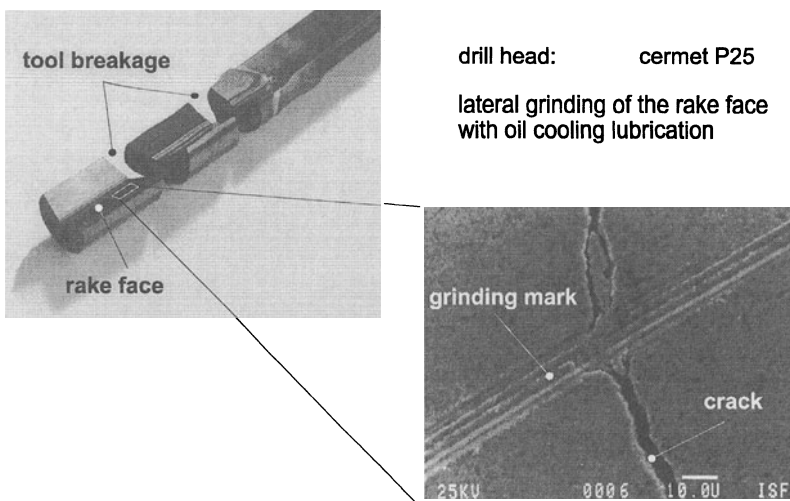


Fig. 1: Tool breakage of cermet single-edge gundrills

Crack formation or tool breakage can be mainly traced back to the stresses present in the tool material. Since cermet has a lower thermal conduction value than conventional cemented carbide, the result is that the heat induced in the tool is concentrated in the surface near-zone, which means that large temperature gradients arise. Through the combined action of the larger thermal coefficient of expansion for cermet compared to cemented carbide and the hindering of expansion, greater stresses are induced in the surface near-zone of the tool. Therefore, the fabrication of these cermet drills was possible only because the process parameters were drastically reduced and the lateral grinding of the rake face was replaced by peripheral grinding. The smaller process parameters and the shorter contact length of the grinding wheel during peripheral grinding resulted in a lower tool temperature. The formation of cracks on the surface could in this way be reduced, but not however completely suppressed. Because of this damage the cermet tools were destroyed directly at the beginning of the subsequent drilling process.

Similar effects could be observed at the cutting tips. Basically two types of both cemented carbide and cermet were at the centre of these investigations. The application groups P10 and P25 were employed for both cutting tool materials. The grinding of these cutting tips was accomplished by, among other things, as mentioned above, varying the cutting speed and the specific material removal rate. The cutting tips were then used in turning experiments. Fig. 2 shows paradigmatically the dependence of the crater depth K_T on the grinding conditions of the cutting tips.

Compared to cemented carbide cutting tips the cermet cutting tips show substantially less wear. This can be explained by the greater temperature hardness, better oxidation stability and lower tendency to diffusion relative to steel. These characteristics are a result mainly of the high percentage of TiC and TiN in the tool material [8].

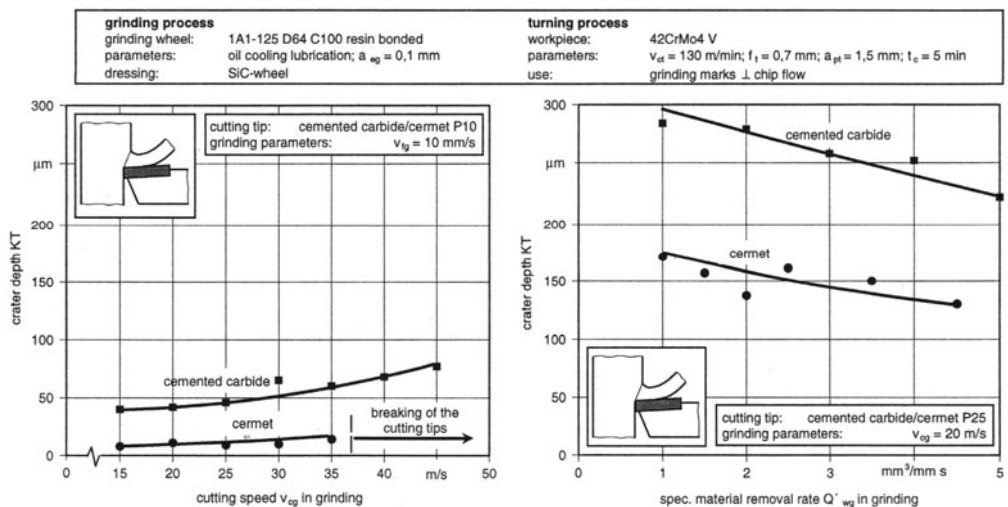


Fig 2: Wear behaviour of ground cemented carbide and cermet cutting tips

While grinding cermet during the course of the experiments, the specific material removal rate could be increased from 1 mm³/mms to 5 mm³/mms through specifically applied measures. Above the latter value however tool breakage occurred. It should be mentioned

here that the measures essential mainly responsible for this increase were the use of shoe jets for cooling the grinding contact zone as well as the use of grinding wheels having high thermal conductivity.

With an increase in the specific material removal rate during grinding of the tools a slight decrease in tool wear could be observed. In the case discussed here the feed rate also increased proportionately relative to an increase in the material removal rate. A greater feed rate leads to a lower surface temperature and to a smaller penetration depth of the process heat that is produced. During the tests compressive stresses in the immediate vicinity of the surface could be detected at the cutting tips after the grinding process. These compressive stresses increased with an increase in the material removal rate, a fact which can be explained by the lower surface temperature. The result was at first a greater wear resistance of the cutting tool material, which had been ground with a high material removal rate. An increase in the material removal rate and thereby in the feed rate also led however to a greater stress gradient in the material, whereby, however, the danger of crack formation increased.

When the grinding cutting speed increases, an increase in crater depth for both cermet and cemented carbide tools can be noticed. An increase in cutting speed during grinding leads to greater thermal stress on the whole tool. A thermal overload can have a harmful effect on the surface (e.g. crack formation). This damage accelerates the wear progress – especially abrasive wear – when the cutting tips are used in turning.

Similar to the situation described for gundrills above breakage can occur during the grinding process when there is a thermal overload of the cutting tool material cermet. A three-dimensional simulation of the grinding process shows interesting correspondences between the temperature distribution and the forms of damage noted on the cermet cutting tips (Fig. 3). The cracks run parallel to the simulated isotherms, whereby a u-formed crack, which has often been observed, on the runout edge encloses the area of maximum temperatures. This reinforces the assumption that above the temperatures as well as their distribution in the tool are mainly responsible for the development of cracks.

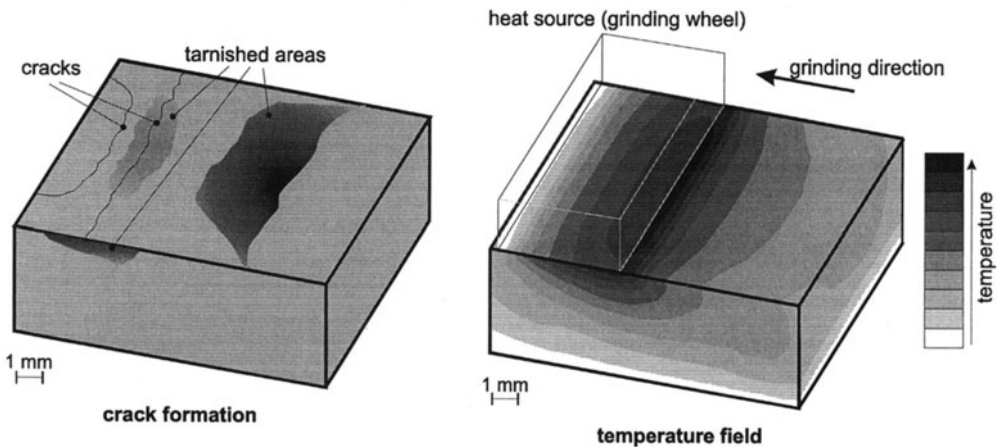


Fig 3: Forms of damage when grinding cermet cutting tips

3. INFLUENCE OF THE GRINDING WHEEL SPECIFICATION

In the investigations various grinding wheel specifications were employed and their effect on the wear behaviour of the cutting tools was analysed. Fig. 4 shows the influence of various abrasive grain sizes on the process forces when ground cutting tips are employed. For cutting tips that were ground using a grinding wheel having a small grain size (D46) the process forces were substantially smaller than when the grinding was done with grinding wheels having medium-sized or large-sized grains (D64 or D91). This fact can be attributed to the surface roughness which increases with an increase in the grain size of the grinding wheel. In use an increase in surface roughness leads to a greater hindrance of chip flow and thus to an increase in the mechanical stress on the tool. The least amount of tool wear was observed however when the grinding was done using medium-sized grains. Several simultaneous effects have to be mentioned here. A small grinding wheel grain size results in high thermal stress on the tool during grinding. This can be attributed to a greater role played by friction due to the smaller penetration depth of the individual grain tips during grinding. A greater thermal stress on the tool during grinding can result in tool damage, which can then lead to more intensive tool wear when the tool is later used. On the other hand, a large grain size leads to intense and increased tearouts on the cutting edge of the tool as well as to a lower edge stability. Further tearouts that occur when the tool is being used give rise to an automatic grooving of the tool and thereby increase the wear. A large-sized grinding wheel grain should therefore only be used in rough grinding. Optimal results with respect to application behaviour of the tool were observed during the tests when a grinding wheel grain size D64 was used for both cermet and cemented carbide tools. These findings could be confirmed in talks with tool manufacturers.

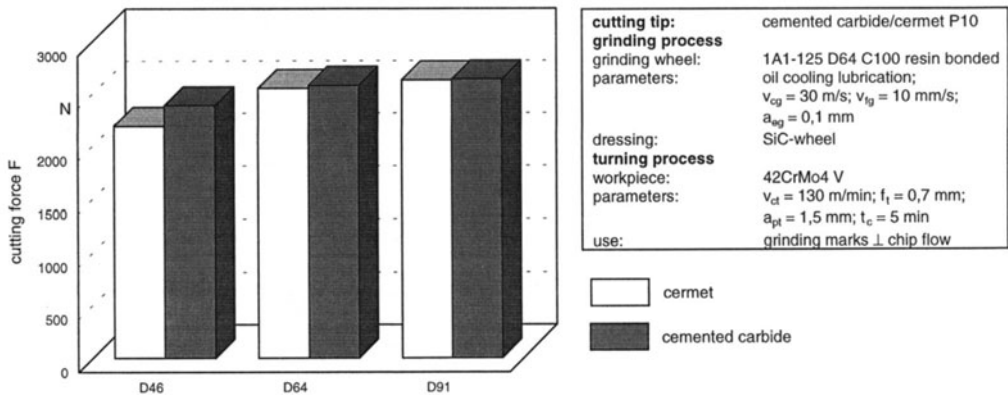


Fig. 4: Influence of various abrasive grain sizes on the process forces of ground cutting tips

A further important parameter is the thermal conductivity of the grinding wheels. In our studies resin bonded grinding wheels with a high percentage of Cu/Si resulted in the lowest tool temperatures during grinding. A small thermal load on the tool during grinding leads to, as already described above, high tool quality and thus to good wear and application behaviour.

4. INFLUENCE OF SURFACE TOPOGRAPHY

During the investigations it was noticed that the texture of the grinding marks plays an important role on influencing the wear behaviour of the tool. In the tests ground cutting tips having different orientations of the grinding marks to chip flow were employed during longitudinal turning (Fig. 5).

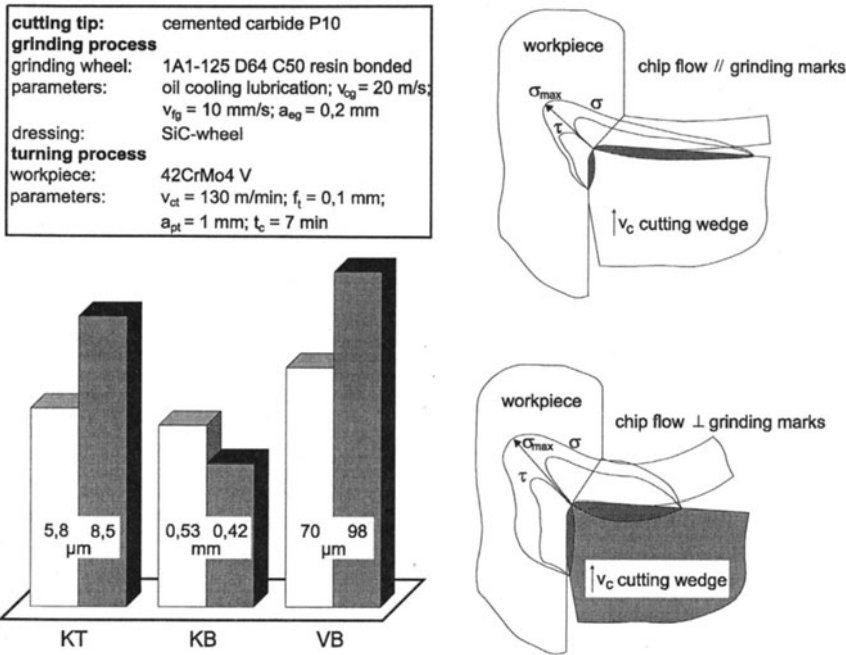


Fig 5: Influence of the grinding mark direction on the wear behaviour of ground cutting tips

When the grinding marks were perpendicular to chip flow a greater crater depth KT and width of wear land VB of up to 30 % more could be observed depending on the cutting tool material used and the application conditions than when the direction of the grinding marks was parallel to chip flow; the crater width KB however was smaller by the same amount.

The chip flow is hindered when the grinding marks are perpendicular to the direction of movement, meaning that a poorer sliding off of the chips is the result. The consequence of this is increased chip compression, which then in turn leads to greater mechanical and thermal stress on the cutting wedge. The process temperatures favour the diffusion conditions existing between the cutting tool material and the workpiece material and thereby the tribochemical wear processes, which manifest themselves in increased crater depth.

In the case of grinding marks perpendicular to chip flow, as mentioned above, the mechanical load on the cutting wedge is increased. This can be seen by an increase in the shearing and normal stresses in the contact area between the chip and the rake face, which has an effect extending deep into the workpiece material. Since the workpiece material is

deformed not only plastically but also elastically, the stress on the flank face also increases, which can be seen by an increase in the width of wear land.

In order to study the influence of the direction of the grinding marks on the machining process various model tests were made using a tribological testing stand. The construction of the model testing stand is based on the kinematics of longitudinal turning. A test body is pressed against a rotating counter body. In order to realise an open systems structure found in real machining processes a translational feed motion is added so that areas of the material that have not been stressed can be constantly brought into contact with the test body.

Fig. 6 shows scanning electron microscope pictures of the contact area which was ground parallel or perpendicular to the direction of the friction motion and subsequently used on the model testing stand. While in the photo on the left only very small deposits in the wear area can be seen, the photo on the right shows that the whole contact area is marked by pick-ups. Here too we can see that the grinding marks oriented perpendicular to the direction of movement offer greater resistance to the material sliding away over them. This is also substantiated by the values for the coefficient of friction from both tests. In all the tests considered the values for the coefficient of friction for grinding perpendicular to the direction of movement are 2-7 % above those values for parallel grinding.

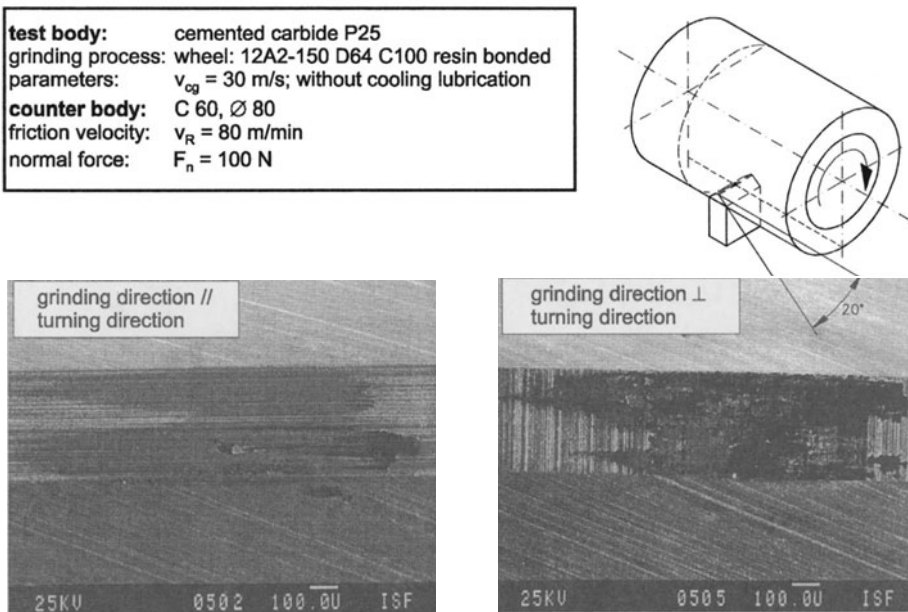


Fig 6: Tribological tests of grinding mark direction

5. CONCLUSIONS

During the course of numerous experiments the basic correlations between grinding conditions and the application behaviour of geometrically determined cutting tools were ascertained. In this context, the influence of the grinding process on cemented carbide and cermet cutting tools was investigated.

In structuring the tool grinding process one has to pay special attention to the choice of appropriate process parameters and grinding wheel specifications. In addition to these aspects the surface topography has also proven to have an important influence on the wear behaviour of the tool.

REFERENCES

1. Weinert, K.; Johlen, G.; Schneider, M.: Experimental and Numerical Studies of the Grinding Process on Tool Life, Annals of the German Academic Society for Production Engineering, Vol V/2 (1998)
2. Lowin, R.: Schleiftemperaturen und ihre Auswirkungen im Werkstück, Dissertation RWTH Aachen 1980
3. König, W.; Hönscheid, W.; Lowin, R.: Untersuchung der beim Schleifprozeß entstehenden Temperaturen und ihre Auswirkung auf das Arbeitsergebnis, Forschungsbericht NRW Nr. 2648, Westdeutscher Verlag GmbH, Opladen, 1977
4. Iwanow, W.; Postnych, A.; Kotow, A.; Iwankin, W.; Tschekalkin, A.; Chronusow, W.: Beitrag zur Temperatur- und Spannungsberechnung beim Schleifen, In: Jahrbuch Schleifen, Honen, Läppen und Polieren, Hrsg. Saljé, E. und Westkämper E., 57. Ausgabe, Vulkan-Verlag, Essen, 1993, 1-19
5. Christoffel, K.: Cermets beim Reiben: Genauigkeit bei hohen Schnittgeschwindigkeiten, Werkstatt und Betrieb, 123 (1990) 5, 359-362
6. Kolaska, H.; Dreyer, K.: Hartmetalle und ihr Einsatzfeld, DGM-Seminar „Werkstoffgefüge und Zerspanung“, Hannover, 1992
7. Weinert, K.; Adams, F.-J.: Trockenbohren von Stahl mit Cermet, VDI-Z Special Werkzeuge, (1995) 9, 24-26
8. Tönshoff, H.K.; Wobker, H.-G.; Cassel, C.: Wear Characteristics of Cermet Cutting Tools, Annals of the CIRP, 43 (1994) 1, 89-92

CHIP FORMATION IN ORTHOGONAL CUTTING FEM SIMULATIONS AND EXPERIMENTAL EVIDENCE

E. Ceretti

University of Brescia, Brescia, Italy

B. Karpuschewki and J. Winkler

University of Hannover, Hannover, Germany

KEY WORDS: Orthogonal Cutting, FEM simulations, Experimental comparison

ABSTRACT: This paper is the result of a cooperation between the Institute for Production Engineering and Machine Tools (IFW), University of Hannover, Germany and the Department of Mechanical Engineering of the University of Brescia, Italy. The aim of the work is to validate the reliability of a Finite Element code in simulating orthogonal cutting operations. Experimental tests on orthogonal cutting have been realized at the IFW while FE simulations were carried out at the University of Brescia. The collected data have been used to define the input variables of the FE code and to analyze the FE outputs. The experimental data in terms of cutting forces and chip morphology have been compared with the FEM results. The good agreement between experiments and simulations shows that FEM can be a valid help in tool designing and in identifying the process parameters also for the study of cutting operations.

1. INTRODUCTION

In cutting processes, the final part quality is influenced by changes in tool geometry, chip flow, temperature generation, heat flow and tool wear. The understanding of these interactions during the cutting process is a fundamental task. In fact, this knowledge enables the manufacturer of cutting tools to evaluate the performance of the cutting tool design prior to manufacturing and expensive field testing. It also enables the users of cutting tools to evaluate the effects of the working conditions on tool life and on the quality of the final part.

Published in: E. Kuljanic (Ed.) *Advanced Manufacturing Systems and Technology*,
CISM Courses and Lectures No. 406, Springer Verlag, Wien New York, 1999.

Finite element codes have proved to be effective for simulating large elastic-plastic deformation problems including temperature dependent material properties and high strain rates (e.g. forging, extrusion, bending). Attempts to apply Finite Element techniques to machining have been made by many researchers. Most of these studies deal with a static situation and not with the problem of chip formation and breakage, of friction in the contact zone between tool and material, of temperature increase, and of cutting speed [1, 2]. Other models are able to consider the above defined parameters but require the use of non-commercial, ad hoc FE codes [3-9].

The model proposed to simulate the cutting process uses the commercial code DEFORM 2D. To simulate continuous chip formation the default remeshing procedure has been changed.

The advantage of using a commercial FE code consists in the input model definition and in the analysis of the output variables. To validate the FE model a real orthogonal cutting process has been studied. Several experimental tests have been conducted changing cutting speed and tool material. Experimental data, in terms of cutting forces, chip morphology, normal and shear stresses (friction) and temperature, have been collected and compared with the simulation results [10]. The obtained results are in good agreement with experiments.

2. THE EXPERIMENTAL SETUP

For analysing the temperature distribution on the rake of a cutting tool, the use of new developed sensors is required due to the small extensions of the contact zones in orthogonal turning. Furthermore, the contact zones are not accessible during the cutting process using standardised measuring devices without influencing chip formation, chip flow and thermal and mechanical behaviour of the cutting tool. In the past, devices making use of thermal-electric effects, chemical and thermal reactions of the cutting tool or an indicating material and thermal radiation were used. These methods are either not suitable to determine temperature distributions, they influence the contact characteristics or can only be used at elevated temperatures.

At the IFW sensors have been developed using thin film technology. The principle of measurement makes use of the effect that conducting materials change their electric resistance at the presence of changing thermal or mechanical load. If temperature is raised, usually the electric resistance of a conducting material increases as well, whereas an increasing mechanical load results in a decreasing electric resistance. These effects, however, are strongly depending on the used material. Pure metals usually are very little sensitive to changes in mechanical load. The thin film sensors for this reason are made of platinum, to ensure that only the influence of thermal load is detected. Calibrations have shown, that the sensors output influenced by mechanical load can be neglected for the used application.

The thin film sensors are applied to standard cutting tools made of $\text{Al}_2\text{O}_3\text{-ZrO}_2$ ceramics (Figure 1) by PVD processes. The sensors size is $0.2\ \mu\text{m}$ in thickness and $25\ \mu\text{m}$ in width. Due to their small extension, up to twelve sensors can be arranged in the contact zone between cutting tool and chip without changing the cutting tools mechanical and thermal properties. To protect the sensors against abrasion, to avoid short circuits when machining

conducting materials and to ensure that contact characteristics between tool and workpiece are not influenced, the sensors are covered by an Al_2O_3 layer of 2 μm in thickness. Compared to other measuring devices, the use of the presented thin film sensors avoids the disadvantages named above.

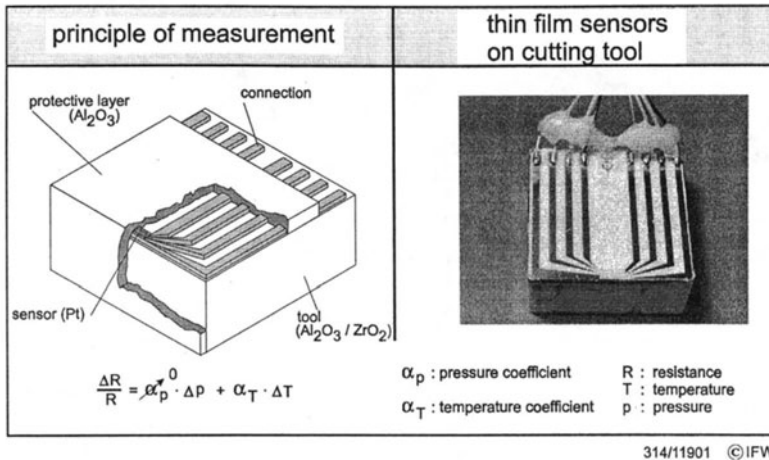


Figure 1: Thin film sensor

The change in electric resistance of each sensor caused by variations in temperature is used to calculate the local temperature from calibration tests performed in advance. If the temperature at up to twelve locations placed along the contact zone is known, the temperature distribution can be evaluated.

In order to describe the mechanical load on the rake face, in our investigations a split tool is used (Figure 2): A gap divides the tool into two elements, one including the rake face only, the other including the flank and part of the rake face. The tool elements consist of cemented carbide inserts. Forces normal and parallel to flank and rake face can be measured directly, as the wedge angle is 90° and the clearance angle of 6° is neglected. The resulting cutting force F_z is split into the components normal and shear force on the rake (F_{ny} , F_{sy}) as well as normal and shear force on the flank ($F_{n\alpha}$, $F_{s\alpha}$). Therefore the cutting force F_c equals the normal force on the rake F_{ny} plus the shear force on the flank $F_{s\alpha}$. Accordingly, normal force on the flank $F_{n\alpha}$ and shear force on the rake F_{sy} both form the feed force F_f . In orthogonal cutting the passive force F_p equals the feed force F_f . Interactions between the two cutting tool elements are determined by a calibration that has to be performed before each experiment.

The position of the gap on the rake face can be changed by using different flank elements. Differences within the forces after varying the gap position are then related to the difference of the contact area belonging to the rake face element (Figure 2). It is assumed that the cutting process is not affected by the gap. Due to small contact lengths between flank and

new machined workpiece surface, the use of the split tool is restricted to measurements for stress distributions in the rake face only.

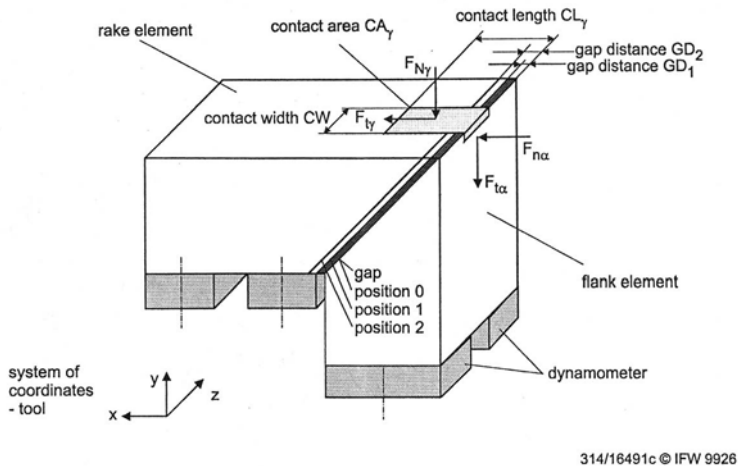


Figure 2. Split cutting tool

3. THE FEM MODEL

To study the cutting process with DEFORM 2D [11] it was necessary to modify the remeshing module of the FE code [1, 2].

To represent the experimental tests, the orthogonal cutting process is modeled with plane strain deformation and non-isothermal (Figure 3), while the simulation type is incremental (the step increment is defined to cut 1 mm with 100 steps). Two objects, the workpiece and the tool (Figure 4) are defined. Their parameters are reported in Table 1. The flow stress of the workpiece material (σ) is assumed to be strain, strain rate and temperature dependent. Since σ values were not available for large strains, in this range σ is assumed to remain independent of strain (Table 1).

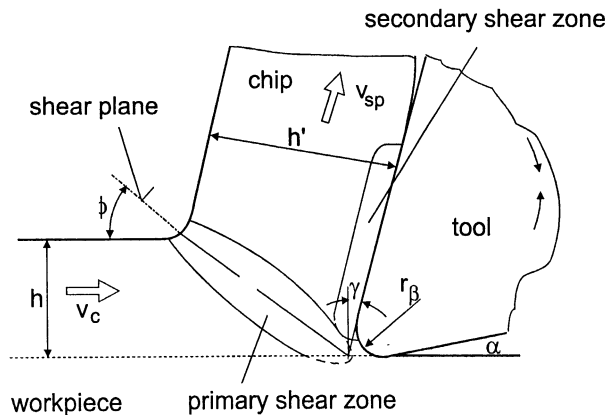
The workpiece and the tool are characterized by non-uniform mesh distributions, as illustrated in Figure 4. Very small elements are required in the contact area between tool and workpiece because of the very large temperature gradients that will develop in this region. Larger elements are tolerable in the area of the workpiece and of the tool not affected by the cutting process.

4. COMPARISON OF PREDICTIONS WITH EXPERIMENTS

To evaluate the cutting model, the experimental data provided by the IFW are compared to the results of the simulations using the same cutting conditions (friction, workpiece material and tool geometry). In these comparisons, the effect of temperature is also considered.

Parameter	Workpiece	Tool
Model for the object:	Plastic	Rigid
Geometry	Height = 5mm Width = 20mm	Rake angle $\alpha = - 6^\circ$, Clearance angle $\theta = 6^\circ$, Tool Tip Radius $r = 0.05\text{mm}$
Material	Aluminium Alloy AlCuMgPb	$\text{Al}_2\text{O}_3 - \text{ZrO}_2$
Number of elements	1800	600
Thermal Properties:		
Thermal Conductivity:	204 W/(m K)	28 W/(m K)
Heat Capacity:	879 J/(Kg K)	850 J/(Kg K)
Emissivity:	0.75	0.75
Interface Heat Transfer Coef.:	10 kW/(m ² K)	10 kW/(m ² K)
Friction:	Variable friction law (experimental)	
Cutting Feed:	0.2 mm	
Cutting Speed:	200, 400, 600, 800 m/min	
Initial Temperature:	20°C	20°C
Flow Stress Law $\sigma = 311.5 \epsilon^{0.18} \text{ MPa} \quad (\vartheta = 20^\circ\text{C})$ $\sigma = 74.4 \epsilon^{0.695} \text{ MPa} \quad (\vartheta = 300^\circ\text{C})$ $\sigma = 51.6 \epsilon^{0.11} \text{ MPa} \quad (\vartheta = 400^\circ\text{C})$ $\sigma = 35.1 \epsilon^{0.155} \text{ MPa} \quad (\vartheta = 500^\circ\text{C})$		

Table 1: Parameters of the simulation



after G.Warnecke

0/18791c © IFW 0389

Figure 3: Chip formation in orthogonal turning

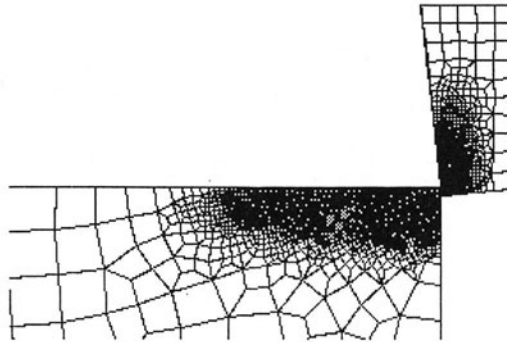


Figure 4: Geometry and mesh of piece and tool in the realised model

Figures 5 - 9 give the plots of the computed and experimental results for cutting and feed forces, contact length between tool and chip, cutting ratio (the ratio between the undeformed chip thickness t and the chip thickness t_c , Figure 3), and tool and chip temperatures. The agreement between experiments and simulations is obvious. The difference between the calculated forces and the forces obtained in experiments is about 10% and due to the simplifying assumptions (friction condition, property of the workpiece material, limited workhardening, strain rate, and temperature effects). Only for the cutting ratio (figure 8) the difference between experiments and simulation is evident (20% for 200,400 and 600 m/min and 50% for 800 m/min), but it must be considered that at high cutting speed the influence of strain rate and temperature on flow stress is consistent and it is difficult to find reliable input data for the simulation program (we did a simple linear interpolation), thus the comparison is not significant .

The influence of cutting speeds was evaluated, a review of the results, presented in Figures 5-11, indicates that with varying cutting speed:

- The total cutting force remains almost constant. It is possible to see a slight increase in the cutting force as the cutting speed decreases, this is due to the thermal softening of the workpiece material (Figure 5).
- The maximum temperatures of chip and rake face of tool are increasing with increasing cutting speed (Figure 9). In fact the energy required for cutting increases. Figure 10 shows the temperature distribution in the workpiece and in the tool for a cutting speed of 800 m/min. A comparison between experimental and calculated temperatures as in simulation a steady state was not reached.
- The shape of the mesh presents an increase in chip curling as the cutting speed increases, which results in a decrease in the contact length between tool and chip. This is due to the increase of temperature which affects the deformation and encourages the curling of the chip [12] (Figure 11).

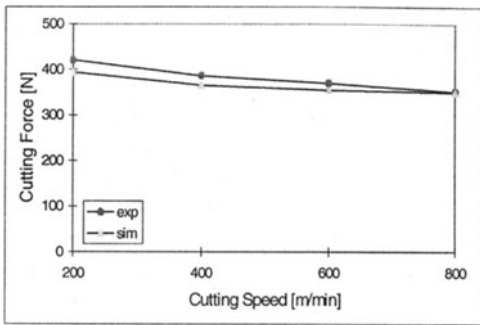


Figure 5: Cutting force vs Cutting Speed (tool path 6 mm)

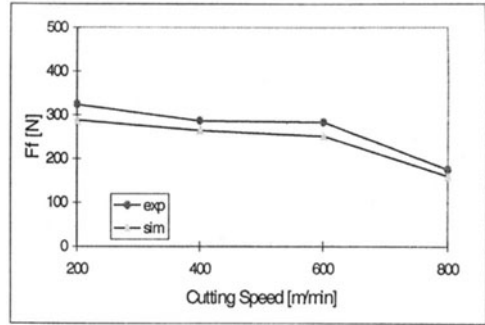


Figure 6: Feed force vs Cutting Speed (tool path 6 mm)

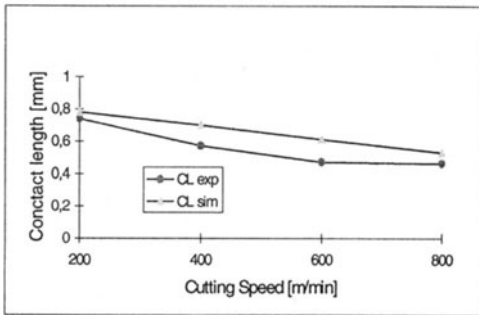


Figure 7: Contact Length vs Cutting Speed (tool path 6 mm)

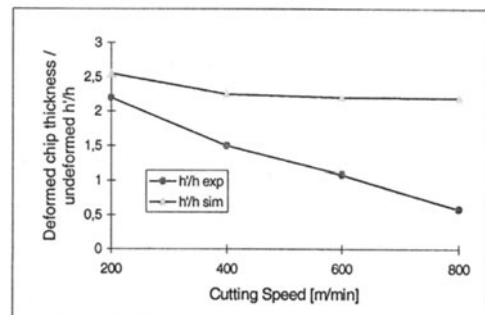


Figure 8: Cutting ratio vs Cutting Speed (tool path 6 mm)

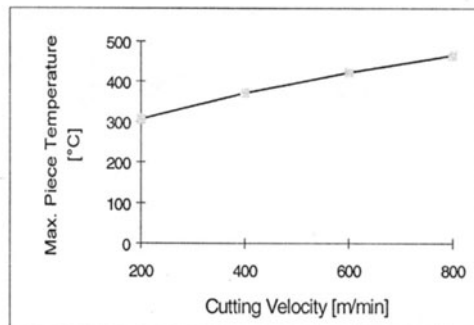


Figure 9: Max. Temperature vs Cutting Speed (simulation, tool path 6 mm)

The results obtained with the 2D FEM code DEFORM so far seem to indicate that the implemented model can simulate the orthogonal cutting process and predict the reality with satisfactory accuracy.

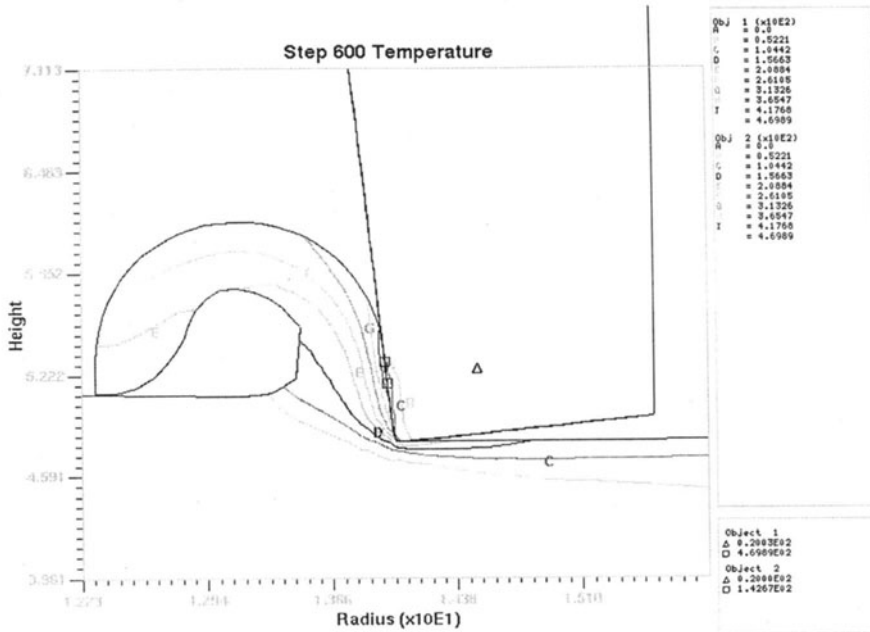


Figure 10: Temperature distribution (cutting speed 800 m/min, tool path 6 mm)

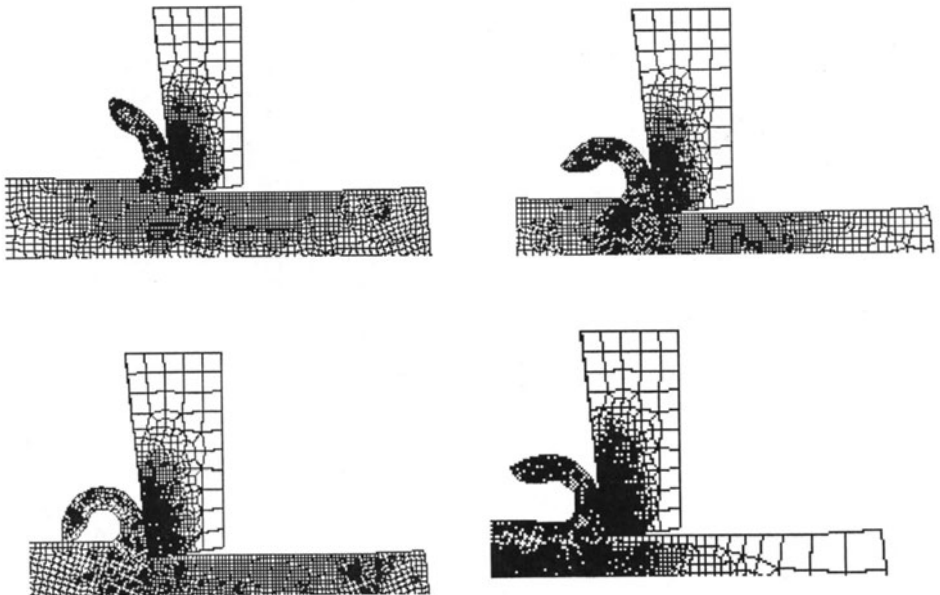


Figure 11: Influence of cutting speed (200, 400, 600 and 800 m/min) on chip geometry (tool path 6 mm)

5. CONCLUSIONS

The model presented aims to understand the mechanics of the cutting process and to identify how critical cutting parameters effect the chip flow, cutting forces, and temperatures.

In the simulations the chip flow is continuous i.e. the chip is deformed plastically without breakage. It is suitable for the simulation of cutting ductile materials and for all cutting conditions under which the chip does not break. The simulation results in terms of cutting forces, temperature and chip morphology have been compared with experiments.

The results indicate that:

The simulation of cutting by FE code is possible. The prediction of cutting forces is within an acceptable range of accuracy of 10%. Additional comparisons with experiments are planned to evaluate the validity of the FEM model under various cutting conditions.

The results are in good agreement with experiments in terms of estimating chip geometry and tool workpiece contact length.

To estimate chip and tool temperatures it is necessary to run longer simulations or to increase the heat transfer coefficient between chip and tool to reach a steady state within an acceptable cutting length.

It is possible to study the influence of cutting parameters upon cutting forces and heat generation. This capability could be useful in designing cutting tools (manufacturer of cutting tools) or in defining process variables (user).

REFERENCES

1. E. Ceretti, P. Fallböhmer, W. T. Wu, T. Altan, "Application of 2D FEM to chip formation in orthogonal cutting", *JMPT*, vol. 59, pp. 169-180, 1996.
2. E. Ceretti, E. Taupin, T. Altan, "Simulation of metal flow and fracture Applications in orthogonal cutting, blanking and cold extrusion", *Annals of the CIRP*, Vol. 46/1/1997.
3. Hashemi, J., Tseng, A. A., & Chou, P. C., (1993). Finite element modelling of high speed orthogonal cutting process *Int. Conf. on Processing Materials for Properties*, pp. 49-52.
4. Heinstejn, M., Yang, H. Y. T., Shih, J. M., (1989). Adaptive 2D finite element simulation of metal forming processes, *Int. Jou. for Numerical Methods in Engineering*, vol 28.
5. Iwata, K., Osakada, K., & Terasaka Y., (1984). Process Modeling of Orthogonal Cutting by the Rigid-Plastic Finite Element Method, *Trans. of the ASME, J. of Engineering for Industry*, vol. 106, pp. 132-138.
6. Lin, Z.C., & Liu, C.C. (1996). Analysis of Orthogonal Finish Machining Using Tungsten Carbide and Diamond Tools of Different Heat Transfer Coefficients. *Int. J. Mach. Tools Manufact.*, Vol. 36, No. 1, pp. 73-88
7. Marusich, T. D., Ortiz, M. (1995). Finite element simulation of high speed machining, *NUMIFORM '95, (Simulation of Materials Processing: Theory, Methods & Applications)* Shen&Dawson, eds., pp. 101-108.

8. Shaw, M. C., Vyas, A. (1993). Chip formation in the machining of hardened steel, *Annals of the CIRP* vol. 42, pp. 29-33.
9. Strenkowski, J. S., Mitchum, G. L., (1987) An improved finite element model of orthogonal metal cutting, *Proc. N. Am. Manufacturing Res. Conf.*, pp. 506-509.
10. Tönshoff, H.K., Karpuschewski, B., Winkler, J. (1996). Analysis of the Effect of Thermal and Mechanical Stress on Tool Wear in Continuous Cutting, *Society of Tribologists and Lubrication Engineers, Annual Meeting*
11. DEFORM, Scientific Forming Technologies Corporation. (1993), *Metal Forming FEM code*. Columbus, OH.
12. Jawahir, I, Zhang, J.(1995). An Analysis of Chip Curl Development, Deformation and Breaking in Orthogonal Machining. *Transactions of NAMRI/SME*, Vol. 23, pp. 109-114

PERFORMANCES OF THREE LAYERED CERAMIC COMPOSITES INSERTS FOR STEEL CUTTING

S. Lo Casto and V.F. Ruisi

University of Palermo, Palermo, Italy

E. Lucchini and O. Sbaizero

University of Trieste, Trieste, Italy

S. Maschio

University of Udine, Udine, Italy

KEY WORDS: Alumina zirconia, Layered ceramics, Steel cutting, Wear

ABSTRACT: Sandwich-structured three-layered ceramic inserts were made with the aim of obtaining ceramic cutting tools with an increased useful life.

Alumina was chosen for the external layers because of its high hardness and chemical inertness. Mixtures of Al_2O_3 and tetragonal ZrO_2 were used for the inner layer since it is possible to predetermine the tensile stresses on the rake faces by varying the ratio between the two oxides of the inner layer. The fired compacts were machined in order to obtain cutting tools with the desired geometrical dimensions. Tests were performed by cutting an AISI 1040 steel at speeds ranging from 1.7 to 7.8 m/s. The performances of three-layered composites were similar to those of monolithic Al_2O_3 - ZrO_2 commercial inserts. In particular, the prestressed layered ceramics exclude the "chipping" caused by metal infiltration during, and by thermal stresses after, cutting. Scanning electron microscope investigation of the used inserts confirmed that all wear mechanisms can be related to Al_2O_3 plastic deformation during turning tests.

1. INTRODUCTION

In previous works, studies were made of the wear performances of commercial ceramics when cutting carbon-steels [1,2]. Specifically, it was demonstrated that alumina-zirconia inserts perform better than carbide tools at high cutting speeds. These performances are due to the chemical inertness of alumina and zirconia against the workmetal. When cutting speeds exceed 5.5 m/s, the temperature on the rakeface can rise above 1500°C [3] so that chemical reactions between steel and some components of the inserts may occur.

From this point of view, alumina and zirconia are very interesting because they exhibit negligible solubility in iron [4]. They are however sensitive to high temperatures. In particular, two wear mechanisms related to thermal effects were established.

The first is related to plastic deformation of alumina grains above 1000°C when a sufficient load is applied [5]. This phenomenon was observed in the crater zone of some alumina-zirconia inserts. In use, this is the area where the temperature is highest and at the same time the metal chips exercise heavy shear stresses on the ceramic surface. Brandt proposed a wear mechanism based on the formation of "ridges" which are broken cyclically by subsequent chip flows [5].

The second wear mechanism is a consequence of thermal stresses induced by the temperature gradients across the inserts. Ceramics have low thermal conductivity and low toughness. The resulting tensile stresses are located on the flank of the insert and can often exceed the material strength [6]. Microcracks are generally not catastrophic but the resulting flaws are then filled by the steel, which oxidizes at high temperatures. The volume of metal increases when it is transformed into oxide and causes detachment of small ceramic particles (chipping) [6].

Analysis of these wear mechanisms prompted us to develop new ceramic composites in order to avoid these shortcomings [7]. Laminated composites were considered for this purpose. In such materials, the outer surfaces can be prestressed in compression by using an inner layer with a thermal expansion coefficient higher than that of the outers. During cooling, outer surfaces are therefore stressed in compression. The compressive stresses are a function both of the mismatch between the thermal expansion coefficients and of layer thickness. In this paper, we present the preliminary results regarding the wear performances of "laminated" inserts when cutting steel.

2. MATERIALS AND METHODS

The hardness of alumina is higher than that of zirconia so additions of zirconia to pure alumina lowers tool hardness. Since hardness is one of the most important properties required by all cutting tools, it was decided to use pure alumina for the outer layers.

Sintered Al_2O_3 has lower toughness than $\text{Al}_2\text{O}_3\text{-ZrO}_2$ compacts but it was assumed that the increase in toughness caused by compressive stresses in the three-layered monolithic materials would be sufficient to offset the toughening effect of the tetragonal-monoclinic transformation of zirconia.

The inner layer contained 60 % vol Al₂O₃ and 40 % vol ZrO₂ (partially stabilized with 12% mol CeO₂). In view of the higher thermal expansion coefficient of zirconia, rake faces of the tools were prestressed in compression after the sintering process; the resulting compressive stress can be calculated by the following equation [7]:

$$\sigma_1 = -\frac{E_1 E_2 d_2 \Delta \epsilon_0}{(1 - \nu)(2E_1 d_1 + E_2 d_2)}$$

Where E₁ and E₂ are respectively the outer and inner layer elastic modula, d₂ is the inner layer thickness, ν is the Poisson ratio and Δε₀ is the thermal expansion mismatch.

Layer thicknesses were maintained constant. The inner layer was set to 1.5 mm and the two symmetric outers were set to 2.7 mm. With this geometry, the residual compressive stress in the outer layers of our samples was calculated to be 150 MPa whereas the inner had a tensile stress of 450 MPa. The global rupture strength of the samples was 350 MPa and toughness was 6.3 MPa m^{1/2}. The hardness of the outer layer was 17GPa, which is similar to the value of unstressed pure alumina.

The production process used for the inserts is described elsewhere [7]. In the present work the green samples were fired 2 h at 1550°C.

The sintered bodies were machined in order to obtain cutting tools complying with insert number SNUN 12 07 08. The rake faces were polished with a 12 mm diamond paste.

The tools were tested in continuous dry turning on AISI 1040 steel whose characteristics are reported in table I.

Chemical composition:
C=0.43%, Mn=0.76%, Si=0.28%, S=0.027%, P=0.016%
Tensile strength R=620 MPa
Hardness HBN(2:5/187.5)=182

Table I. Properties of AISI 1040 steel.

All tests were carried out with a Boehringer DM 550/1000 lathe and the tools were mounted on a commercial tool holder with the following geometry.

rake face $\gamma = -6^\circ$

clearance angle $\alpha = 6^\circ$

side cutting edge angle $\psi = 15^\circ$

inclination angle $\lambda = -6^\circ$

The tools were tested under the following cutting conditions:

depth of cut, $d = 2.20$ mm - feed, $f = 0.25$ mm/rev. - speeds $V = 5.5$ m/s and 7.8 m/s.

The flank wear criterion ($VB_B = 0.3$ mm) was chosen to evaluate tool life.

Tools and chips were examined after testing using an Assing Stereoscan Scanning electron microscope (SEM) coupled with an EDAX apparatus.

3. RESULTS AND DISCUSSION

The VB_B criterion was adopted because preliminary tests showed that the rakeface did not suffer severely from the chip flow. These results were confirmed by measurements made by a profilometer. At present, we are unable to explain the better performances of the laminated inserts with respect to wear on the rake face for the compressive stresses do not increase the hardness of the Al_2O_3 outer layers. Fig. 1 shows the aspect of a laminated tool tested at 7.8 m/s for 200 s. It is possible to observe that, in spite of the high cutting speed, wear in the crater zone is modest. No cracks, microcracks or chipping phenomena were observed in flank zones after the tests. This is an important result because these wear mechanisms were observed on alumina-based commercial tools tested under similar cutting conditions [1]. It therefore seems reasonable to assume that the compressive stresses of the outer layers inhibit the formation and propagation of cracks.

Examination of flank wear after the tests revealed the presence of plastic deformation. Fig. 2 shows the aspect of the flank after a test at 7.8 m/s for a period of 200 s. This kind of wear was observed in alumina-based commercial tools at cutting speeds below 5.5 m/s. Above this value, only chipping phenomena were present. Probably both plastic deformation and chipping actually occur but damage caused by chipping hides deformed alumina grains. In the case of inserts with a laminated structure, compressive stress excludes chipping and Al_2O_3 deformation is evident.

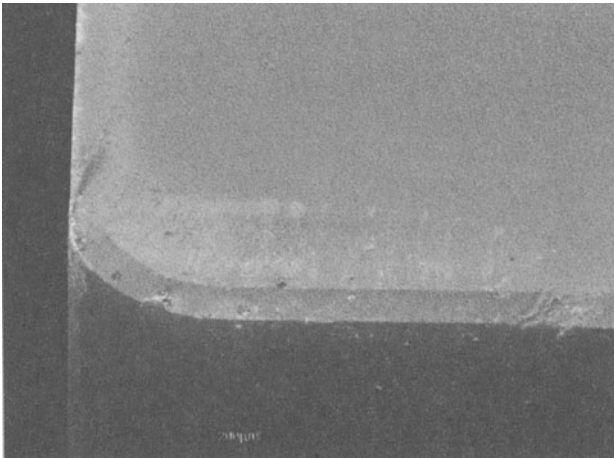


Fig. 1. Aspect of laminated ceramic insert after testing at 7.8 m/s: cratering is negligible.

In spite of the better resistance of laminated tools to the chipping, they exhibited a life (VB_B criterion) 30% - 40% shorter than commercial tools tested under the same cutting conditions. It is therefore possible to infer that they are more sensitive to the plastic deformation wear mechanism in the flank. The significance of this result is not clear.



Fig. 2. Aspect of flank tool after testing at 7.8 m/s for 200 s. Alumina plastic deformation is evident.

Two hypotheses may be put forward. The first is related to the different preparation methods used. Commercial inserts are machined out from hot pressed large compacts whereas our tools are pressureless sintered in air. The hot pressed alumina bodies have small grains whereas laminated compacts exhibit coarser microstructures. It follows that, in commercial

inserts, sliding of the crystallographic planes is partially inhibited by the high number of grain boundaries.

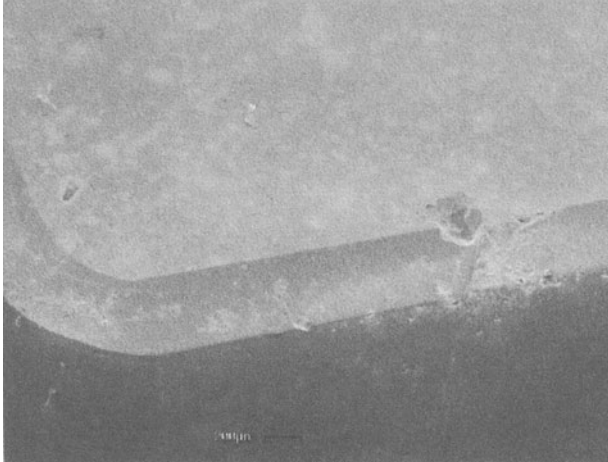


Fig. 3. Brittle fracture in cut zone depth after turning test.

The second hypothesis is related to the different compositions of the tools. Commercial tools contain tetragonal zirconia inclusions whose pinning effects reduce alumina deformation. Work is now in progress to explain such different behaviour in similar inserts.

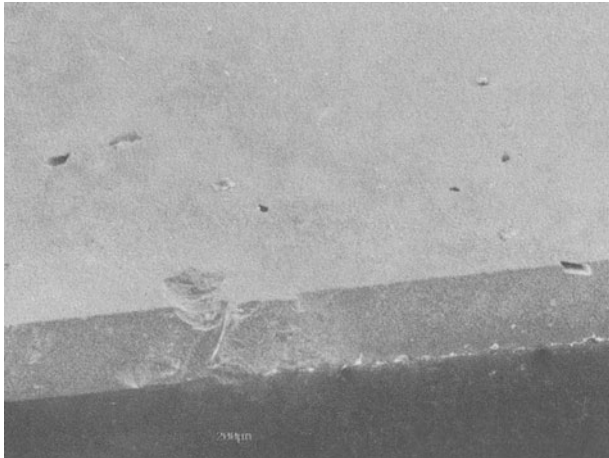


Fig. 4. Voids on surface of laminated insert. The evident brittle fracture in the D. O.C. was probably caused by a similar defect.

Some of the tools failed during the cutting operations in the depth of the cut zone (see fig. 3). SEM observations revealed that this shortcoming may be due to the presence of surface flaws, which are evident in fig. 4.

These defects derive from the incomplete sintering process or from over-energetic grinding. This drawback can be avoided by using a hot pressing preparation technique. However the cost of inserts will rise correspondingly.

4. CONCLUSIONS

Ceramic inserts with outer layers in compression are promising tools for machining steel or other materials. Chipping and cratering are drastically reduced. Some drawbacks, such as high plastic deformation in the flank and random breakages in the depth of cut zones, could be removed using hot pressing techniques and/or alumina containing some toughening agents with low solubility in the metals.

REFERENCES

1. Lo Casto S., Lo Valvo E. , Ruisi V.F. , Lucchini E. and Maschio S. "Wear Mechanisms of Ceramic Tools" *Wear*, 160 (1993) 227 - 235.
2. Lo Casto S. , Lo Valvo E. , Lucchini E. , Maschio S. and Ruisi V.F. "Wear Rates and Wear Mechanisms of Alumina Based Tools Cutting Steel at Low Cutting Speed" *Wear* 208 (1997) 67 - 72.
3. Lo Casto S. , Lo Valvo E. , Lucchini E., Maschio S., Piacentini M. and Ruisi V.F., in I. M. Low and X. S. Li (Ed.), *Advanced Ceramic Tools for Machining Applications-II, Key Engineering Materials*, Trans.Tech Publications, Vol. 114, Chap. 3, pp 105 - 134 (1995).
4. Kiamer M. and Judd P.K. " Computational Design of Wear Coatings" *J.Vac. Sci. Technol. A* 3 (6), (1985) 2439 - 2444.
5. Brandt G. "Flank and Crater Wear Mechanisms of Alumina Based Cutting Tools When Machining Steel", *Wear* 112 (1986) 39 - 56.
6. Tonshoff H.K. and Bartsch S. " Wear Mechanisms of Ceramic Cutting Tools", *Ceramic Bulletin* vol. 67, No, 6 (1988) 1020 - 1021.
7. Burelli S. , Maschio S. and Lucchini. E. in E. Kuljanic (Ed.) *New Advanced Ceramics for Cutting Steel. AMST'96 Proc. of 4th International Conference on Advanced Manufacturing Systems and Technology.* (1996) 747 -752, Springer Verlag Wien New York

MINOR CUTTING EDGE WEAR IN FINISH TURNING OPERATIONS

C. Borsellino, M. Piacentini and V.F. Ruisi
University of Palermo, Palermo, Italy

KEYWORDS: Roughness, Wear minor cutting edge, Sintered carbide and Ceramic tools.

ABSTRACT: In finish turning operation, it has already shown, that for the sake of control the dimensional accuracy and the micro-geometry of the worked surface, the wear parameters employed in rough turning operations are not suitable. In the present work the study of wear in finish turning operations, is carried out, employing a particular groove survey methodology, already proposed in a previous paper, that is based on the techniques of acquirement and processing of images. In order to verify the applicability of the proposed technique two kind of alumina-based inserts and two kind of sintered carbide inserts have been tested. The experimental tests have confirmed the validity of the technique in the prediction of tool lifetimes for several couples tool-workpiece materials.

1. INTRODUCTION

The employ of new materials in turning operation is the main factor that has determined improvements in industrial production.

Nowadays in machining operation the choice of new geometries and materials for cutting tools is oriented to the optimisation of the single cutting operation.

Particular attention has been dedicated on materials able to resist at high temperature gradients due to the increased cutting speed. Between them alumina-based materials has shown good attitude to be employed in cutting operations. Alumina-based tools offer high wear resistance, very good resistance to high cutting temperatures, thermal stability and chemical inertia [1,...,4].

Actually the best results can be obtained with the proper choice of the tool geometry and of the couple tool/workpiece material, depending on the particular step of the working schedule, on the machine performances, etc...

With the use of alumina based tools in finish turning operations, a valid alternative to the grinding of hardened materials is obtained. This operation, in fact, is more versatile than grinding because of the wide range of complex shapes that is possible to obtain and

Published in: E. Kuljanic (Ed.) *Advanced Manufacturing Systems and Technology*,
CISM Courses and Lectures No. 406, Springer Verlag, Wien New York, 1999.

because of the higher productivity due to the reduced setting times. Moreover, by this way, it's possible to realize high quality products with lower costs related to machines and tools, and lower machining times.

In finish turning operation, it has already shown, that for the sake of control the dimensional accuracy and the micro-geometry of the worked surface, the wear parameters employed in rough turning operations (i.e. crater wear-KT/KM and flank wear-VB_B) are not suitable [5,6].

The value of the theoretical roughness depends on tool geometry, on tool position with respect to the workpiece and on feed [7,8]. The value of the actual roughness can be greater than the theoretical one because of several factors, between them one of the most significant is the wear of the minor cutting edge [9].

Depending on the couple tool-workpiece material these kind of wear can manifest itself with the generation and growth of equally spaced grooves perpendicularly to the secondary cutting edge. The number of grooves and their depth influence heavily the actual roughness of the workpiece surface [10].

The survey of the geometrical characteristics of the workpiece or of the tool wear plays a very important role in the automated machining systems. Actually, the in-process [11] or on-line [12] measurement techniques employed until now, need great times and costs for the measurement of the roughness for the employment of complex software or expensive instruments (profilometers, tool-room microscopes, SEM, etc...).

In a recent paper the Authors proposed a technique for on-line survey and analysis of the grooves on the minor cutting edge in finish turning operations [13]. Actually, in the present work, the study of wear in finish turning operations for several tool materials (sintered carbide and alumina-based materials) during the machining of some kind of structural steel is carried on, for sake of verify the applicability of the proposed technique.

2. TOOL WEAR EXPERIMENTS

2.1 The grooves survey methodology

The grooves survey methodology employed is based on the techniques of acquirement and processing of images [13].

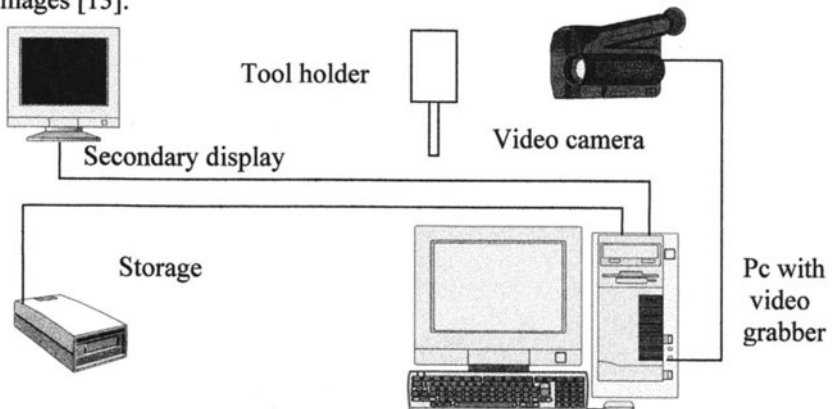


Figure. 1. Experimental set-up.

At the end of the cut the image of the part of the insert showing both the minor cutting edge and a part of the radius between the edges, is acquired with the system showed in figure 1.

This image is processed to obtain the highlighting of the grooves generated during the cutting operation. In this way with appropriate software it's possible to count the number of grooves, to store and compare it with the one found at the previous cut.

The suggested methodology indicates the moment in which the tool has to be changed because the values of Ra exceed the tolerance limits, as the one where the number of grooves starts to decrease.

2.2 Experimental Set-up

The finish turning tests have been carried on two different kind of structural steel: AISI 1040 and 39CrMo4 (their characteristics are reported in table 1), employing two kind of alumina based inserts and two kind of sintered carbide inserts; their composition and their geometry are reported in the following table.

	AISI 1040	39CrMo4
Chemical composition	C = 0,43%, Mn = 0,76%, Si = 0,28%, P = 0,016%	C = 0,42%, Cr = 1,1%, Mo = 0,22%, Mn = 0,78%, Si = 0,28%, P = 0,016%
Hardness	HBN _(2,5/187,5/30) = 208	HBN _(2,5/187,5/30) = 390
Tensile strength	R = 700 N/mm ²	R = 1150 N/mm ²

Table 1. Characteristics of the employed materials.

The commercial materials selected for the tests, according to the insert number TNGA160408, were as follows:

- Zirconia-toughened alumina (Al₂O₃ -7vol%ZrO₂), in the following called with its commercial name **CC620**.
- Mixed-based alumina (Al₂O₃ -TiN.TiC-ZrO₂), in the following called with its commercial name **CC650**.
- Sintered carbide grade **S1P** (WC-TiC-Co).
- Sintered carbide grade **SM30** (WC-TiC-TaC-Co).

For each kind of insert and each workpiece material several cutting parameters have been used, namely the ones reported in table 2.

Geometry	Cutting parameters
Rake angle $\gamma = -6^\circ$	Depth of cut: $d = 0,5 \text{ mm}$
Clearance angle $\alpha = 5^\circ$	Feed: $f_1=0,05 \text{ mm/rev}, f_2=0,1 \text{ mm/rev}$
Side cutting edge angle $\psi = 0^\circ$	Cutting speed $V_{c1}=3,3 \text{ m/s}, V_{c2}=4,16 \text{ m/s}, V_{c3}=5 \text{ m/s}$
Inclination angle $\lambda = -6^\circ$	

Table 2. Geometry and cutting parameters employed during the tests.

The finish-turning tests were performed on a NC lathe, at the end of each cut the image of the insert was acquired using the system showed in figure 1. By means of a television camera CCD the image of the insert, that is positioned on a support of an optical bench, is acquired and sent to a personal computer where it can be processed; subsequently the determined value of VB_B and the number of grooves are stored. At the same time the roughness of the workpiece was measured on six longitudinal profiles in different radial positions by means of a profilometer (Taylor – Hobson, Series Form Talysurf).

3. ANALYSIS OF THE RESULTS

For all the couples of the cutting parameter above mentioned the tool lifetimes are reported in tables 3a,b for both sintered carbide and alumina based inserts working AISI 1040 and 39CrMo4 steels respectively. The lifetimes are evaluated on the base of a limit roughness of 3.5 μm .

AISI 1040								
tool	S1P		SM30		CC620		CC650	
$V_c \backslash f$	0,05	0,1	0,05	0,1	0,05	0,1	0,05	0,1
3,33	95	120	45	60	290	310	315	340
4,16	95	71	45	40	203	215	265	285
5	80	60	38	28	184	202	250	230

Table 3a. Inserts lifetimes working AISI 1040.

39CrMo4								
tool	S1P		SM30		CC620		CC650	
$V_c \backslash f$	0,05	0,1	0,05	0,1	0,05	0,1	0,05	0,1
3,33	36	40	15	27	93	105	98	120
4,16	32	38	10	18	70	85	80	100
5	10*	6*	8*	6*	42	53	50	60

Table 3b. Inserts lifetimes working 39CrMo4.

For the two kinds of tools working both AISI 1040 and 39CrMo4 steels, for all the cutting parameters, it has been observed that the roughness reaches the imposed limit when the number of grooves on the secondary edge decreases. This behaviour is shown in figure 2 where the roughness and the number of grooves are reported versus the cutting time.

In the same figure the trend of the flank wear (VB_B) is reported to show that its value is lower than 0,3 (suggested as the critical one in [14]). For this reason the technique proposed to determine the lifetime has shown to be the most suitable to be applied.

For all the cases the lifetime is estimated employing the proposed technique of groove survey and counting.

In table 3b the values marked with (*) are the lifetimes evaluated for $VB_B=0,3$ mm; in this conditions, i.e. working at higher cutting speed, the sintered carbide tools showed a

different behaviour finishing 39CrMo4 steel. Actually, a relevant flank wear is generated and its presence causes the increasing of the roughness and it overcomes the imposed limits before that the number of grooves decreases; see figure 3.

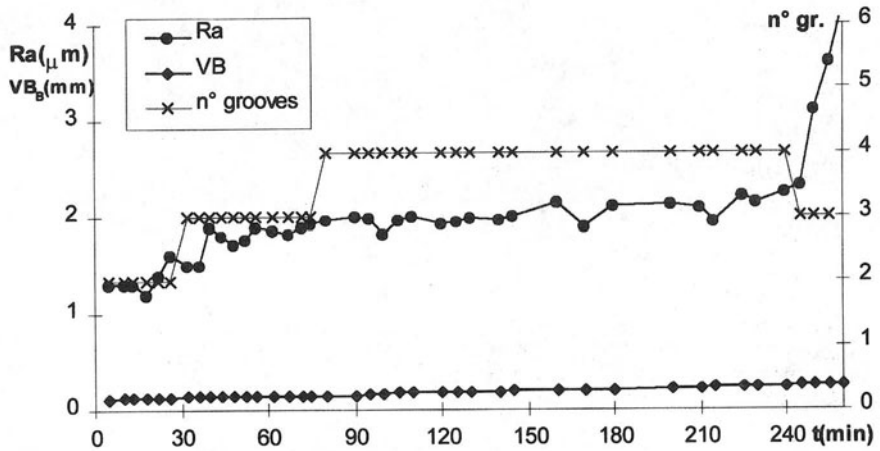


Figure 2. Roughness, number of grooves and flank wear versus cutting time for CC650 insert working AISI 1040 steel. ($V_c=5\text{m/s}$, $f=0,05\text{ mm/rev}$).

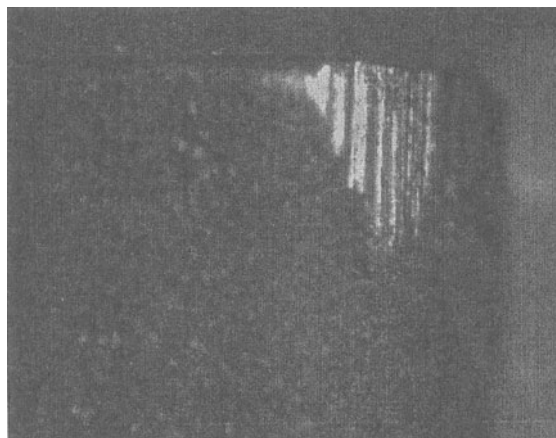


Figure 3. The S1P insert after 6 min working 39CrMo4 steel. ($V_c = 5\text{m/s}$, $f = 0,1\text{mm/rev}$).

In the following the sequence of images 4a,...d, shows the generation of the grooves on the minor cutting edge during the cut of AISI 1040 steel employing CC650 tools ($V_c=5\text{ m/s}$, $f=0,05\text{ mm/rev}$) and their counting realised on the correspondent binarized image by the appropriate software.

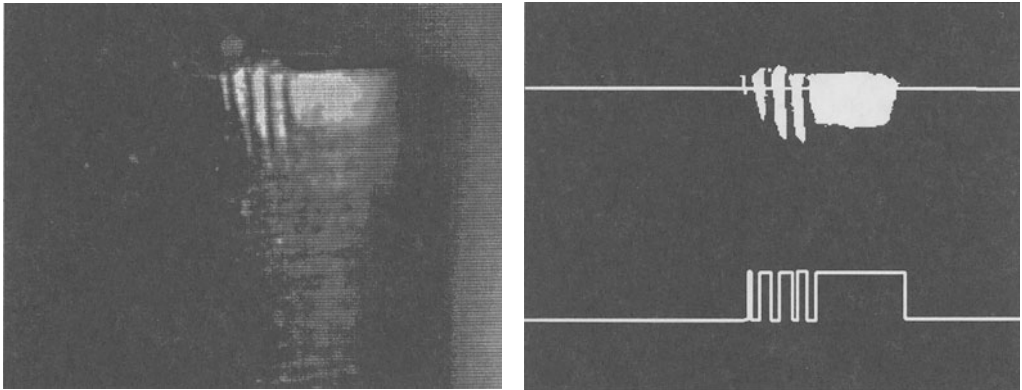


Figure 4a – Minor cutting edge and the correspondent binarized image.
 $V_C = 5 \text{ m/s}$, $f = 0,05 \text{ mm/rev}$, cutting time = 45 min.

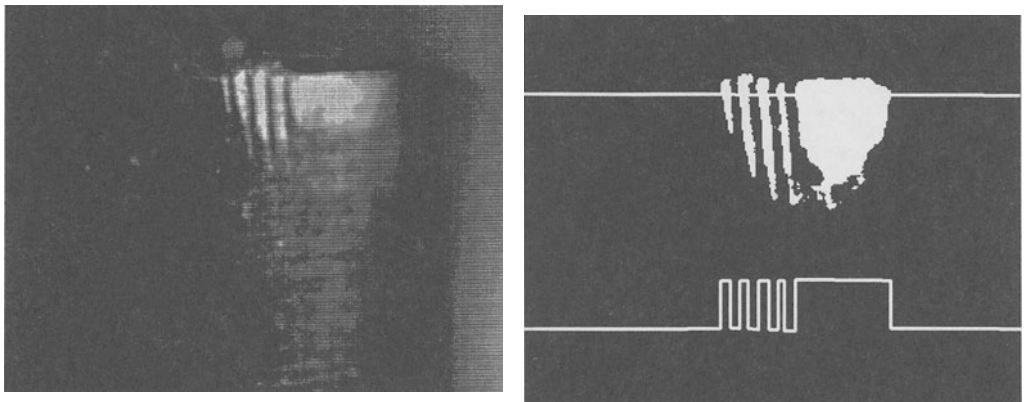


Figure 4b – Minor cutting edge and the correspondent binarized image.
 $V_C = 5 \text{ m/s}$, $f = 0,05 \text{ mm/rev}$, cutting time = 110 min.

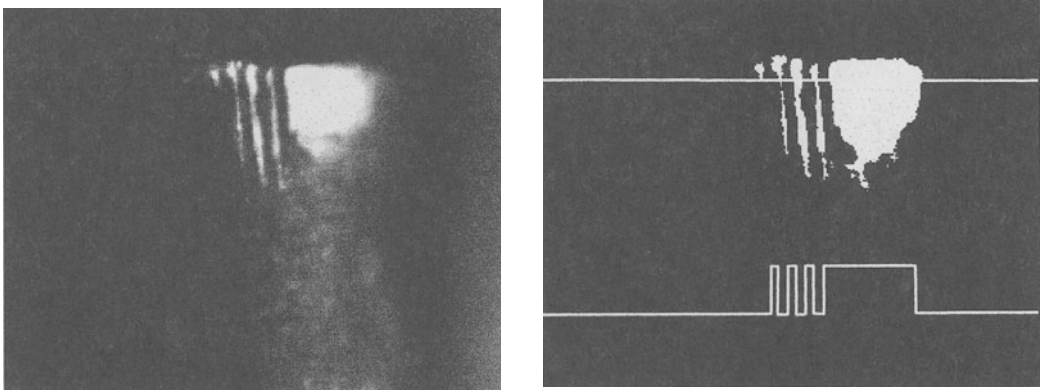


Figure 4c – Minor cutting edge and the correspondent binarized image.
 $V_C = 5 \text{ m/s}$, $f = 0,05 \text{ mm/rev}$, cutting time = 215 min.

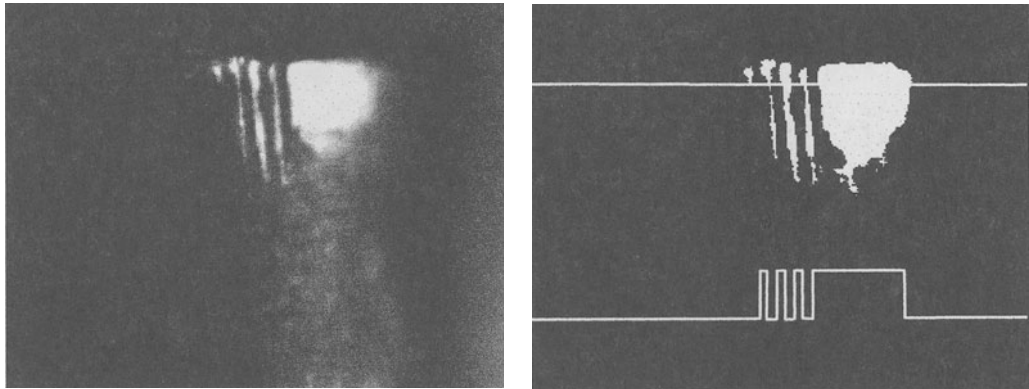


Figure 4d – Minor cutting edge and the correspondent binarized image.
 $V_C=5$ m/s, $f=0,05$ mm/rev, cutting time = 250 min.

It's important to notice that, during the cutting of not alloyed steel (see table 4), the Zirconia-toughened alumina tools and Mixed-based alumina tools show much greater lifetimes than the sintered carbide ones. This occurrence offers the possibility to reduce the machining times and the associated costs related to machines and tools.

The alumina tools can be utilised in the working of steels with high hardness where, instead, carbide tools have very short lifetimes; thus they can be employed in finish and super-finish turning offering an alternative to grinding operations.

4. CONCLUSIONS

On the basis of the above reported results it's possible to reach the following conclusions:

- The proposed methodology can be properly implemented as on-line survey of the wear reached by the tool and consequently of the micro-geometry of the worked surface.
- The control is performed in real time, by this way a great reduction of the costs is attained compared to other techniques usually applied to achieve the data on the tool wear and on the roughness of the workpiece.
- This methodology has been tested both on different workpiece materials and on several kind of tools (alumina based and sintered carbide inserts). All the tools exhibit the same wear mechanism which permit to apply this kind of survey when working alloyed and not alloyed steel.
- During the tests the alumina based tools showed much greater lifetimes than the carbide ones that brings the reduction of machining times and the associated costs related to machines and tools.

ACKNOWLEDGEMENTS This work has been supported by MURST 60% (Italian Ministry of University and Scientific Research).

REFERENCES

1. Lo Casto S., Lo Valvo E., Lucchini E., Maschio S., Piacentini M., Ruisi V. F.: Machining of steel with advanced ceramic cutting-tools, *Key Engineering Materials*, vol. 114 (1996), Chapter 3, pp. 105-134.
2. Lo Casto S., Lo Valvo E., Lucchini E., Maschio S., Ruisi V. F.: Wear rates and wear mechanism of alumina-based tools cutting steel at a low cutting speed, *WEAR*, 208 (1997), pp. 67-72.
3. Lo Casto S., Lo Valvo E., Lucchini E., Maschio S., Micari F., Ruisi V. F.: Wear performance of ceramic cutting tool materials when cutting steel, 7th Int. Conf. On computer-Aided Production Engineering, 13-14 August 1991, Cookeville, Tennessee, printed on *Journal of Materials Processing Technology*, September 1991, pp. 25-36.
4. Calzavarini R., Settineri L.: Utensili ceramici avanzati, prove di lavorabilità sui materiali di difficile lavorazione, Istituto lavorazione metalli del CNR.
5. Galante G., Piacentini M., Ruisi V.F.: Elaborazione dell'immagine dell'utensile per il controllo della finitura superficiale, X Congresso AIMETA, Pisa, (1990), vol. II, pp.501-504.
6. Galante G., Piacentini M., Ruisi V.F.: Surface roughness detection by tool image processing, *Wear*, 148 (1991), pp.211-220.
7. Lonardo P.M.: Relationships between the Process Roughness and the Kinematic Roughness in Turned Surfaces, *Annals of the CIRP*, 25 (1976), pp.455-459.
8. Lonardo P.M. Lo Nostro G.: Un criterio di finibilità dei materiali per le operazioni di tornitura, *Industria Meccanica- Macchine Utensili*, Anno IV n°4, aprile 1977.
9. Pekelharing A. J. Hovinga H. J.: Wear at the end cutting edge of carbide tools in finish and rough turning, *M.T. D.R.*, 1 (1967), pp.643-651.
10. Yao Y. Fang X. D., Arndt G.: On-Line Estimation of Groove Wear i the Minor Cutting Edge for Finish Machining, *Annals of the CIRP*, 40 (1991), pp.41-44.
11. Lonardo P. M., Bruzzone A. A., Melks J.: Tool wear monitoring through the neural network classification of diffraction images, *Atti II Convegno AITEM*, Padova (1995), pp.343-352.
12. Giusti F., Santochi M., Tantussi G.: On-Line Sensing of Flank and Crater Wear of Cutting Tools, *Annals of the CIRP*, 36 (1987), pp.41-44.
13. Borsellino C., Lo Valvo E., Piacentini M., Ruisi V.F.: A New On-line Roughness Control in Finish Turning Operation, 4th International Conference on Advanced Manufacturing Systems and Technology, AMST'96, Udine (1996), pp.661-668.
14. Ente Nazionale Italiano di Unificazione, Rugosità delle Superfici, UNI 3963.

EFFECT OF MICROSTRUCTURE ON ULTRAPRECISION MACHINING OF COPPER-BERYLLIUM ALLOYS

N. P. Hung, S.W. Lim and Z.W. Zhong
Nanyang Technological University, Singapore

KEYWORDS: Microstructure, Ultraprecision Machining, Copper Beryllium, Chip Formation, Diamond Turning, Surface Finish.

ABSTRACT: This paper investigates the micromachinability of Cu-Be alloys and the effect of microstructure. The material temper, tool material, lead content, and machining parameters were varied to assess their effects. Similar chip formation mechanisms were found when the depths of cut varied from few millimeters to submicron levels. Good agreement between predicted and measured data was obtained providing grain boundaries were visible on a machined surface. A flatness of 20 nm over the 9.5 mm diameter rod, and roughness of 2 nm R_a and 8 nm R_t were achieved. Beryllide inclusions and the precipitates degraded the micromachinability, while the lead particles improved it.

1. INTRODUCTION

The effect of surface quality of a diamond-turned metal surface on its optical performance (e.g., reflectivity) is known [1]. Copper alloys, such as copper beryllium (Cu-Be), are used in electronics industry as connectors, springs... for their high conductivity, modulus, and strength. The alloys are also used in optical industry for laser or infrared applications since the materials exhibit the highest damage thresholds for the long wavelength and high energy beams [2].

Limited studies on micromachining of copper alloys were found. Simulation works were performed to study the ultraprecision machining of coppers [3-6]. The materials within a grain deformed along the slip systems, and a noticeable change of cutting force across a grain boundary was found. Other experimental works were also published. Most of the researchers used oxygen-free (OF) copper that might include silver and boron [7,8]. Others used Cu-0.55wt% Te alloy [9] and Cu-0.04 O alloy [10] in their studies.

Arnold *et al* micromachined OF coppers and Cu-Be alloys [11,12]. A machined OF copper sample retained residual stresses with magnitudes from -27.3 to +4.1 MPa. Depths of cut, ranging from 1.27 to 38.1 μm , did not affect the resulting surface finish. Three commercial Cu-Be alloys were machined: C17200 (Berylco 25: Cu, 1.9 wt% Be), C17300 (Berylco 33-25: Cu, 1.9 Be, 0.4 Pb), and C17500 (Berylco 10: Cu, 2.5 Co, 0.6 Be). These authors used single-crystalline diamond tools with 3.175 mm nose radius, feed rate of 5.08 $\mu\text{m}/\text{rev}$ (0.16% of the nose radius). Some samples machined well while others caused "excessive tool wear" and produced a poor surface quality. The peak-to-valley surface roughness, R_t , of those successfully machined samples were measured to be in the range 20-41 nm. The C17500 samples exhibited an orange-peel texture for all tempering conditions, while the C17200 samples showed the grain boundaries for all tempering conditions.

With limited published information on micromachining of copper alloys and the popularity of Cu-Be alloys, there was a need to understand the effect of secondary processes and microstructure on micromachinability. The objectives of this study were to (i) obtain the best possible surface quality of Cu-Be alloys by micromachining, and (ii) study the effects of tempering and microstructure on the surface quality.

2. EXPERIMENT

Two main alloys were used in this study. The same processes were applied to fabricate and ultraprecision machine samples from both alloys. The CA17200 was the unleaded version of the C17300. The later had the composition of Cu, 1.84 wt% Be, 0.23 Co, 0.02 Ni, 0.04 Fe, 0.1 Si, 0.03 Al, 0.24 Pb. Large rods were solutionized at 790°C then water quenched. Their diameters were reduced 37% to 9.525 mm in a cold drawing process to attain the full-hard (H) temper. One rod was then peak-aged at 316°C for 2 hrs (HT temper). Microhardness across the cross section of a rod was measured along different radial directions such that all measured points were at least 10 indentation apart. Short coupons were cut and mounted with wax on a fixture, then were faced in either continuous or interrupted modes on a ultraprecision machining system (Precitech 2800). Compressed air or a mixture of air and baby oil was used to blow the microchips away from a machined surface. A factorial engineering experiment was design, and relevant machining parameters and tooling were tabulated in Tables 1 and 2.

After being machined, a sample surface was analyzed with a scanning-probe microscope (SPM, Digital Instrument Nanoscope IIIa), a profilometer (FT, Form-Talysurf 120L), a phase-shift interferometer (PSI, WYCO NT2000), a laser interferometer (Zygo GPI-XP) and a scanning-electron microscope (SEM, Leica S360). The Energy Dispersive X-ray technique was used to identify inclusions or elements on a sample surface. At least two

areas per sample were analyzed: at 0.5 mm and at 4.0 mm from the center of the sample. All physical scans were performed in the direction perpendicular to the feed marks. All feedrates were normalized to a percentage of tool nose radii. In this way, different tools could be used and a comparison with published data can be made. Tool edge sharpness (edge radius) and tool crystallographic orientation were measured with a SPM. The crystallographic orientation of a rake face was measured twice on a X-ray diffractometer (Philips X'Pert-MPD) using Cu K_{α} radiation.

Table 1. Details of tested diamond tools.

Tool	Tool geometry*	Edge radius (nm)	Crystallographic orientation, rake face
O	-25 \rightarrow +5, 0, 5, 5, 30, 0, 0.03 \rightarrow 2.00 mm	20 \rightarrow 80	(100)
C	-25 \rightarrow 0, 0, 7, 7, 30, 0, 0.64 \rightarrow 0.77 mm	20 \rightarrow 80	N/A (synthetic)
S	0, 0, 7, 7, 30, 0, 0.30 \rightarrow 0.50 mm	500 \rightarrow 750	N/A (polycrystalline)

* American Standard Association's tool nomenclature

Table 2. Machining parameters for facing operations.

Parameter	High value	Low value
Circumferential speed (m/min)	75	30
Coolant	air	oil mist
Depth of cut (μ m)	1.0	0.2
Feed (% tool nose radius)	5.0	0.5
Material temper	HT	H
Material	C17300	C17200

3. RESULTS AND DISCUSSION

Results of surface finish measurement were collected by different techniques and compared. Since the contact-type surface measurement was probe dependent, the optical-based PSI was the preferred technique.

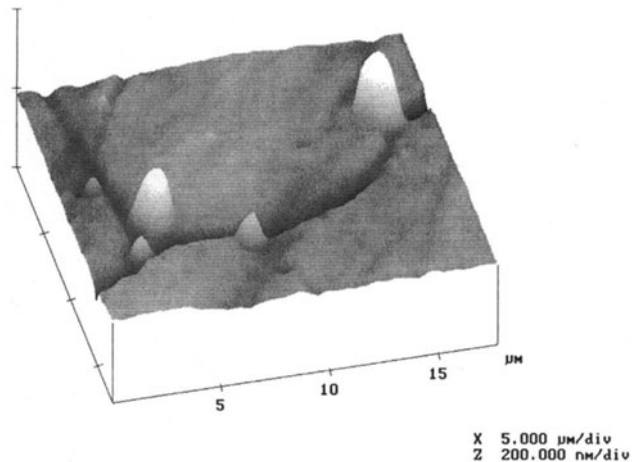
The cold-drawing process changed the mechanical and crystallographic properties of a rod. Different crystallographic orientations of workpiece grains contributed to different ultraprecision machining characteristics [4,5]. The crystallography of Cu-Be alloy was studied and found to be similar to that of brass [13]. Depending on rod size and drawing parameters, a cold-drawn rod could be subjected to severe plastic deformation near the surface, but had less deformation near the center. Excessive cold drawing of a rod promoted a preferred orientation of copper's FCC lattices along its axis (fiber texture). Complex pole figures, obtained by tedious X-ray diffraction technique, were normally used to verify the orientation of the lattices. The dual fiber textures of cold drawn copper rods were reported to be the $\langle 111 \rangle$ and $\langle 100 \rangle$ directions [13-16]. The ratio of the two types varied due to addition of alloying elements, the amount of cold work, the radial distance from the axis, and the ratio ζ /Gb (where ζ is the stacking fault energy, G is the shear modulus, and b is the Burger's vector) [15].

Assuming a uniform distribution of the alloying elements in a Cu-Be rod, the fiber texture would depend only on the amount of cold work and the radial distance. Because of the dependence of microhardness and the amount of cold work, it was postulated that there was an indirect relationship between hardness and fiber texture. The same microhardness levels of the tested rods and similar surface integrity from inside to outside of a rod indicated (i) the uniformity of cold drawing and (ii) a uniform fiber texture across the rods. The result of this study was valid for full-hard cold drawn rods with diameters less than 9.525 mm.

Cobalt and nickel were added to the material to promote a fine-grained structure in Cu-Be alloys [17]. These elements, however, combined with beryllium during solidification to form the beryllide inclusions. Large beryllides were broken up during extrusion, but were not completely dissolved during the solutionizing process. As the consequence, the microstructure of an unaged sample was made up of fine alpha grains with uniform distribution of beryllides and lead particles. Scanning probe microscopy showed the preferred formation of this beryllide phase at the grain boundaries (Fig. 1). The microstructure of aged Cu-Be was similar to that in Fig. 1, with an exception of the additional γ' precipitates forming at grain boundaries and along slip planes. The beryllides still remained in the microstructure after aging.

Fig. 1.

Concentration of beryllides (spikes) at the grain boundaries of C17300-H. SPM tapping mode; 0.3 Hz scanning rate.



The presence of micron-size beryllides degraded the micromachinability of Cu-Be. In a collision with a single-crystalline diamond tool, the beryllides were broken and either embedded in the chip (Fig. 2) or smeared along the machined surface. It was postulated that such collisions also chipped a sharp and brittle diamond cutting edge. Tool chipping and smearing/ploughing of broken beryllides worsened the surface finish of a machined sample. The effect of particle size on micromachinability is shown (Fig. 3). Perhaps this was the reason for the random "excessive tool wear" seen when machining different batches of Cu-Be [12].

Fig. 2. Embedding of broken beryllide at the chip. The arrow points at the sharp cleavage fracture of a brittle beryllite.

Dry facing C17300-HT; 1 μm depth; 5 μm /rev feed; 30 m/min circumferential speed; tool "O" (-15° back rake; 0.5 mm nose radius).

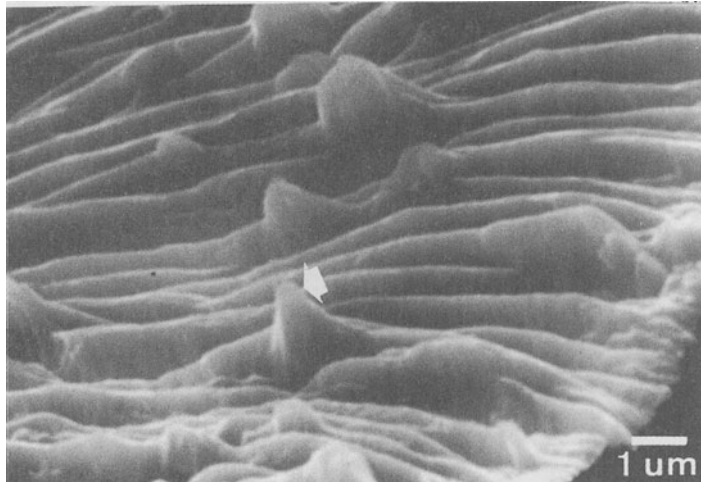
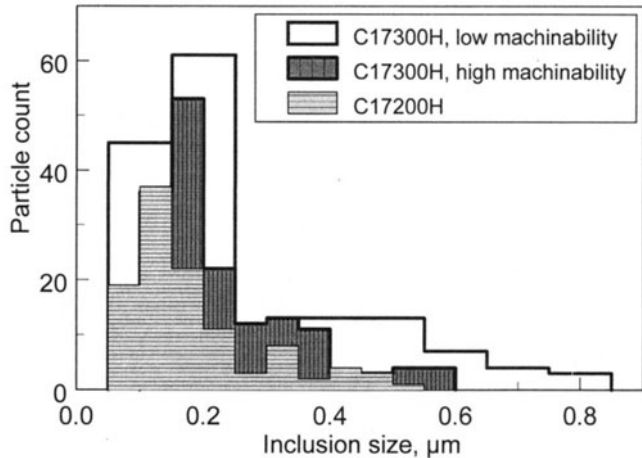


Fig. 3. Distribution of beryllides and lead particles in different batches. Low machinability refers to the material batch that had poor surface finish. Image analysis on SEM, 2000x.



Micro and macro chips were analyzed. A chip root of the C17300-H showed severe plastic deformation above the shear plane and stretched the grains in the direction 45° from the horizontal plane (shear angle). When an aged C17300-HT sample was machined, the presence of the γ' precipitates along the slip planes and grain boundaries reduced the material ductility. The instability in the secondary shear zone, adiabatic shear, or stress concentration at the interface of beryllides caused inhomogeneous shear. Broken chips were caused by excessive grain-boundary sliding where a high density of precipitates was found.

Continuous chips were seen when machining the H-tempered alloys for all depths of cut ranging from 0.2 μm to 1 mm. However, segmented macro/micro chips (~1-2mm) were observed for the HT-materials in macro/micro-machining. Microchips from both the aged and unaged materials, nevertheless, appeared the same at magnifications above 1000x. The microchips showed similar features (but at different scales): (i) smoothed chip due to rubbing at the tool rake face, and (ii) inhomogeneous shear causing the shear bands. The

shear band (microlamellar structure), about 0.5 μm in this study, is much thinner than that in macromachining. Such microlamellar structures were also observed when ultraprecision machining plated copper [18]. The same chip forming mechanism, therefore, prevailed for both macro- and micro-machining of copper alloys including Cu-Be.

Recall from the discussion above that a heavily cold-drawn rod possessed a dual $\langle 100 \rangle$ and $\langle 111 \rangle$ fiber texture along the rod axis. Such textures were assumed to be similar from inside to outside of a heavily cold drawn rod as those in this study. It was expected, and verified, that the surface finish results were not significantly different at different measured locations for all samples in this study.

The feedrate, normalized as percentage of tool nose radius, affected the surface finish the most. Results of this study showed that the best flatness was about 20 nm (RMS) over the entire 9.5 mm diameter sample, and the best surface finish was in the range 1.5 -2.0 nm R_a . Reasonable agreement between the theoretical surface finish and the measured data (Fig. 4). The theoretical surface finish was calculated from [19]:

$$R_a \approx 0.03155 \frac{f^2}{R} \quad (1)$$

Given a material with so many inclusions of both lead and beryllides, and fine grain sizes (more grain boundaries), it was difficult to obtain a very consistent roughness measurement on random locations of a machined surface due to such material defects. Tool chipping was also evident from SPM scanning of a machined surface or from grooving of a chip under SEM examination. All these artifacts worsened the surface finish and explain the deviation of measured and theoretical surface finish machined.

Extreme care was exercised to avoid contamination of ultraprecision machined Cu-Be surfaces. The oil mist was not using as cutting fluid because of a severe surface contamination. A single crystalline diamond tool (SCD) cut the materials cleanly while a polycrystalline tool (PCD) ploughed and roughened a surface. Part of the problem was the shallow depth of cut compared to the large edge sharpness of a PCD tool (Table 1). The surface finish from the C17300 samples was better than that of C17200 due to the lubricating property of lead. The lead particles (i) reduced friction at the tool chip interface (ii) helped to break the chip easier, and (iii) lowered energy to remove materials as chips. The non-soluble lead particles reduced the effect of the γ' precipitates, that pinned dislocations and increased the resolved shear stress on a slip plane. An increasing of surface roughness was measured on the unleaded C17200-HT samples. The change was only $\sim 10\%$ for samples cut with a SCD tool, but was $\sim 20\%$ for those machined with a PCD tool (Fig.5).

4. CONCLUSIONS AND RECOMMENDATIONS

Micromachinability of Cu-Be alloy was studied. This paper showed:

1. Within the range of parameters explored, the microfaceting process produced a mirror surface with good flatness (20nm over 9.5 diameter rod) and surface finish (2 nm R_a and 8 nm R_t). The roughness of 8 nm R_t was an improvement over the published data of 20-41 nm R_t for similar material.

2. The beryllide inclusions reduced the micromachinability of C17300 because of tool chipping and surface smearing. Effort to reduce the size and improve the distribution of beryllides is recommended. The surface finish of an inclusion-free copper alloy, such as brass, can be used to compare with that of the improved Cu-Be alloys.
3. Lead particles improved the material machinability in micro/macro-scale machining. This could be deduced from the fact that the chip formation mechanisms were similar for both cases. An improvement of 10-20% on surface finished was seen.
4. Although more expensive, a single crystalline tool with a much sharper cutting edge outperformed a polycrystalline tool when micromachining Cu-Be.
5. Although consistent within a surface measuring technique, variation of measured surface finish data was found for different techniques. The contact type measurement left a residual track on the surface work piece. Both the contact mode and tapping mode techniques were probe dependent, and were much slower than the optical technique. A reference surface of nanometric scale is needed for equipment calibration.

Fig. 4. Comparison between theoretical and experimental surface finish values.

Dry facing of C17300-H and C17300-HT; 0.2-1.0 μm depth; 1-5%R $\mu\text{m}/\text{rev}$; -25° to 5° back rake; 509-641 μm nose radius.

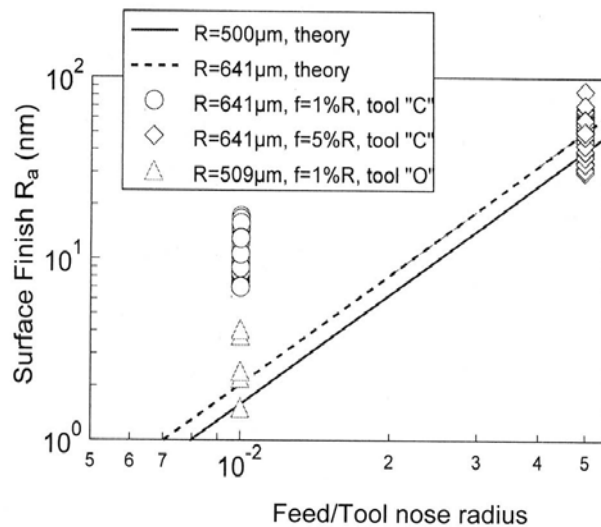
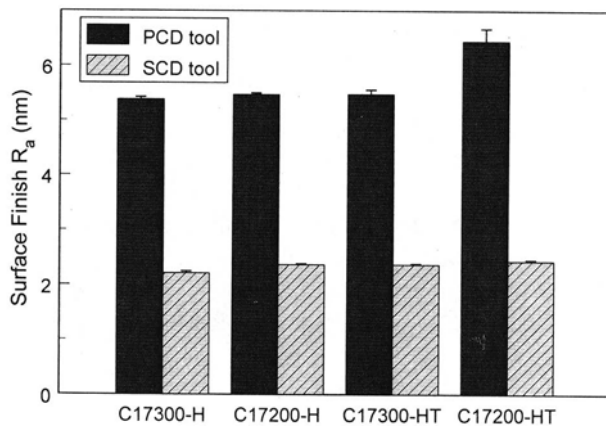


Fig. 5. Differences in surface finish due to tool material, material temper, and lead content.

Plot of mean and standard deviation of four surface finish measurements for each group.



REFERENCES

1. Decker D.L., Bennett J.M., and Soileau M.J.: Surface and Optical Studies of Diamond Turned and Other Metal Mirrors, SPIE Advances in Precision Machining of Optics, 93 (1976), 71-80.
2. Walter J.S.: The Art of Metal Polishing, J. SPIE, 65 (1975), 35-41.
3. Inamura T. and Takezawa N.: Atomic Scale Cutting in a Computer Using Crystal Models of Copper and Diamond, Annals of the CIRP, 41 (1992) 1, 121-124.
4. Liang Y., Moronuki N., and Furukawa: Calculations of The Effect of Material Anisotropy on Microcutting Processes, J. Precision Engineering, 16 (1994), 2, 132-138.
5. Moronuki N., Liang Y., Furukawa Y.: Experiments on The Effect of Material Properties on Microcutting Processes, J. Precision Engineering, 16 (1994) 2, 124-131.
6. Moriwaki T., Sugimura N., and Luan S.: Combined Stress, Material Flow and Heat Analysis of Orthogonal Micromachining of Copper, Annals of the CIRP, 42 (1993) 1, 75-78.
7. Brinksmeier E., Preuß, and Riemer O.: From Friction to Chip Removal: An Experimental Investigation of The Microcutting Process, Proceedings, 3rd Int. Conf. Ultraprecision in Manufacturing Engineering, Germany, 1994, 393-399.
8. Carr J.W. and Feger C.: Ultraprecision Machining of Polymers, J. Precision Engineering, 15 (1993) 4, 221-237.
9. Lucca D.A., and Seo Y.W.: Effect of Tool Edge Geometry on Energy Dissipation in Ultraprecision Machining, Annals of the CIRP, 42 (1993) 1, 83-86.
10. Burnham M.W.: The Mechanics of Micromachining, SPIE Advances in Precision Machining of Optics, 93 (1976), 38-45.
11. Arnold J.B., Steger P.J., and Morris T.O.: Machinability Aspects of Diamond-Turned Metal Optics, SPIE Metal Optics, 65 (1975), 108-117.
12. Arnold J.B., Morris T.O., Sladky R.E., and Steger P.J.: Machinability Studies of Infrared Window Materials and Metals, SPIE Advances in Precision Machining of Optics; 93 (1976), 96-103.
13. Geisler A.H., Mallery J.H., and Steigert F.E.: On the Mechanism of Precipitation in Copper Beryllium Alloys, J. of Metals, 5 (1952), 307-306.
14. Hibbard W.R. Jr. and Yen M.K.: Wire Texture of Copper and Its Binary Alpha Solid Solution Alloys With Aluminum, Nickel And Zinc, Metals Technology, TP 2334, Feb. 1948.
15. Backofen W.A., Deformation Processing, Addison Wesley Inc., 1972.
16. Barrett C.S, Structure of Metals, 2nd edition, McGraw Hill Inc., 1952.
17. Harkness J. and Guha A.: Metallographic Techniques for Beryllium Copper and Beryllium Nickel Alloys, Brush-Wellman company, undated brochure.
18. Arcona C. and Dow T.A.: A New Technique for Studying The Chip Formation Process in Diamond Turning, J. Precision Engineering, 18 (1996) 2/3, 157-160.
19. Whitehouse D.J., Handbook of Surface Metrology, IOP publishing, UK, 1994.

DUCTILE REGIME MACHINING OF METAL MATRIX COMPOSITES

N. P. Hung and Z.W. Zhong
Nanyang Technological University, Singapore

KEYWORDS: Microstructure, Ultraprecision Machining, Metal Matrix Composites, Diamond Turning, Surface Finish, Ductile Regime.

ABSTRACT: This paper presents research results on ultraprecision machining of metal matrix composites (MMCs) reinforced with either SiC or Al₂O₃ particles. Ductile-regime machining of both SiC and aluminum was applied to improve the surface integrity of the composite. Both polycrystalline diamond (PCD) and single crystalline diamond (SCD) tools were used to ultraprecision machine the composites at the depth of cut ranging from nearly 0 to 1.0 μm. A SCD tool removed the MMC as chips while a PCD simply smeared the surface. The critical depths of cut were found to be 1 μm and 0.2 μm for MMCs reinforced with Al₂O₃ and SiC, respectively. Both depth of cut and crystallographic direction of the ceramic particle were the sufficient conditions for ductile-regime machining. Because of the random orientation of the reinforcing particles, some were fractured due to the cutting action while others were machined in ductile mode at the same depth of cut. A measured surface finish, therefore, varied significantly depending on the measured areas.

1. INTRODUCTION

Metal matrix composites were known for their synergistic properties; however, sensitive cost and fabrication challenges including machining were to be overcome for successful

Published in: E. Kuljanic (Ed.) *Advanced Manufacturing Systems and Technology*,
CISM Courses and Lectures No. 406, Springer Verlag, Wien New York, 1999.

applications of these composites. The surface finish and surface integrity were important for surface sensitive parts such as optical lenses or parts subjected to fatigue or creep. Since both common conventional and unconventional machining processes generated subsurface damages of machined MMC sample, efforts were emphasized to improve the surface integrity. Literature survey showed that finishing processes such as grinding and abrasive blasting were utilized to marginally improve the surface integrity of machined MMC samples. Despite the research efforts, fracture of the brittle ceramic reinforcement in MMCs due to machining was still a serious challenge to manufacturing engineers. Although ultraprecision grinding could be used as a finishing process, grinding was limited to certain geometry due to the limited shape of grinding wheels. A more versatile process such as ultraprecision diamond turning was investigated as an alternative technique for finish machining. This project studied how ultraprecision machining using diamond tools affected the surface integrity of MMCs reinforced with SiC or Al₂O₃ particles. The objectives of the research were to (i) implement the ductile regime machining technique to both the matrix metal and the reinforcing ceramic for a high quality surface, and (ii) compare the ductile-regime conditions for SiC and Al₂O₃.

2. LITERATURE REVIEW

There were limited published papers on ultraprecision machining of MMCs, and on ductile-regime machining of brittle materials. When a material was machined in such a fine scale that satisfied ductile-regime conditions, then the chip was removed in a ductile manner despite the brittle nature of the material. A model for the critical depth associated with ductile-regime in micromachining was proposed [1]:

$$d_c \alpha \frac{\text{plastic flow energy}}{\text{fracture energy}} = 0.15 \left(\frac{E}{H} \right) \left(\frac{K_{cs}}{H} \right)^2 \quad (1)$$

Where d_c : critical depth of machining E : Young's modulus
 K_{cs} : critical surface fracture toughness H : material hardness

A shallow depth of cut, therefore, would energetically promote plastic flow rather than brittle fracture in the substrate and the chips. Using equation (1), the critical depth of cut, d_c , for Si, SiC, and Al₂O₃ were calculated to be 0.4, 0.6, and 1.0 μm respectively. Further investigation showed that grinding speed had insignificant effect on d_c , but there was a dramatic change of d_c when using water or alcohol as grinding fluids. The study suggested that such change was due to a chemical reaction that modified the surface properties of the materials.

Ultraprecision machining of as-cast and extruded 6061/SiCw was studied [2]. The MMCs were machined with SCD tools at pre-selected depths of cut in the range 10-40 μm . Higher speed, lower feed, shallower depth of cut, and low volume fraction of reinforcement improved the surface finish of the samples. Further study using transmission electron microscopy showed the high-density dislocation in the soft aluminum matrix below a machined surface. The reinforcing SiC whiskers were either "cut directly," rotated, or pulled out during the machining process.

Milling and grinding of aluminum-based MMCs reinforced with SiC or Al₂O₃ particles/whiskers were experimented [3]. Depth of cut was selected at 15 μm. Examination of the machined surfaces by electron microscopy showed the brittle fractures and evidences of pulled-out reinforcements. Grinding of A359/SiCp and 2618/Al₂O₃p were also experimentally performed [4,5]. Fine grinding using 3000-grit diamond wheel at 1 μm depth produced ductile-regime cutting of the Al₂O₃ particles but micro fracture on the brittle SiC particles.

Although precision turning and grinding of MMCs was conducted as shown in the literature survey, the ductile-regime machining of MMC was yet to be fully explored. The following section presents how depth of cut affecting the ductile-regime machining, and then compares the results with the published data.

3. EXPERIMENT

The cast A359/SiC/10p and extruded 6061/Al₂O₃/20p composites were kindly provided by Duralcan. Some of the as-cast samples were hot-isostatically pressed and/or aged to enhance the matrix properties. Although no coolant was used during machining, compressed air was directed to blow the chip away from a machined surface. Both SCD tools and PCD tools were used for the facing operations. Tool crystalline orientation was measured using a x-ray diffractometer (Philips X'Pert-MPD). The cutting edge radii (tool edge sharpness) were measured on an atomic force microscope (AFM, Digital Instrument Nanoscope IIIa). Tables 1 and 2 provide more relevant information of the materials and cutting tools.

Table 1. Details of the materials.

MMC	Details
A359 /SiC /10p	Matrix: Al, 9.27 wt% Si, 0.15 Fe, 0.55 Mg. Reinforcement: SiC, median $9.3 \pm 1.0 \mu\text{m}$ Processes: – Permanent-mold cast to $\phi 18$ mm bars. Pouring temperature 700-710°C, average stirring rate 175 rpm. – Hot isostatic pressing by heating in argon at 550°C for 1 hour, isostatically pressed at 150 MPa for 1 hour, oven-cooled to 300°C, then air-cooled. – Solution heat-treated at 540°C for 14 hours, water quenched, peak aged at 155°C for 5 hours to obtain the T6-temper
6061 /Al ₂ O ₃ /20p	Matrix: 6061 aluminum (Al, 0.72 wt% Si, 0.27 Cu, 0.90 Mg) Reinforcement: Al ₂ O ₃ , median $21 \pm 2 \mu\text{m}$ Processes: extrusion at 427°C, extrusion ratio 35/1, speed 6.1m/min.

Short coupons of MMC samples were mounted on a precision fixture using wax, which melted at 80°C, to avoid the undesirable effects of mechanical clamping. Both continuous and interrupted facing of short MMC coupons was performed on an ultraprecision system (PeciTech Optimum2800) that had 9 nm positioning accuracy. All feedrates were

normalized at 0.5% of tool nose radii. The samples were machined at constant depths of cut in the range 0.2-1.6 μm at an increment of 0.2 μm , or a taper cut to vary the depth of cut continuously from ~ 0.0 to 0.2 μm . The cutting speed was chosen in the range 10-200 m/min as part of a factorial experiment design.

Machined surfaces were analyzed with an AFM, a profilometer (Form Talysurf 120L), and with a scanning-electron microscope (SEM, Cambridge S360). The as-machined samples were observed/scanned in the as-machined condition, then repeated again after etching the samples in Keller's etchant (190 ml H_2O , 5ml HNO_3 , 3 ml HCl , 2ml HF) to dissolve the smearing aluminum on the surfaces. Selected samples were sectioned, mounted, hand ground, polished then etched to show the microstructure at the subsurface. Energy Dispersive X-ray technique was used to identify different phases and elements on a sample.

Table 2. Details of cutting tools.

PCD	Polycrystalline diamond: 0.5 μm grain size, ASA* tool geometry $0^\circ, 0^\circ, 9^\circ, 5^\circ, 60^\circ, 30^\circ$, 0.33 mm; edge sharpness 500-750 nm.
SCD	Single crystalline diamond: (100) rake plane, ASA tool geometry ($\pm 5^\circ$ & 0°), $0^\circ, 5^\circ, 5^\circ, 30^\circ, 0^\circ$, 0.51-2.06 mm; edge sharpness 20-80 nm.

* American Standard Association

4. RESULTS

4.1. Surface Integrity

The average roughness R_a was used to characterize the surface finish. The surface integrity was further assessed by micro-examination of the as-machined or sectioned surfaces before and after etching. Machining at a feedrate that was small compared to the nose radius, the theoretical surface finish of the machined surface was given by [6]:

$$R_a = K(f, R) \frac{f^2}{R} \approx 0.03155 \frac{f^2}{R} \quad (2)$$

The calculated R_a would be in the sub-nanometer surface finish using $f = 0.5\%R$ for the tools detailed in Table 1. A parallel study showed that a mirror surface of $R_a = 1-2$ nm was achieved by ultraprecision machining of copper alloys. Such surface finish, however, was not achievable for MMCs although the same machining conditions and tooling were used. Shattering of the $\text{SiC}/\text{Al}_2\text{O}_3$ particles and tool wear degraded the surface finish of MMC samples. A consistent measurement result was seen when measuring the surface finish with a profilometer or an AFM when measuring away from the eutectic phases where the SiC particles concentrated in the A359/SiCp (Fig. 1).

The effect of ultraprecision machining parameters was investigated. The surface finish of single crystal metals or semiconductors was sensitive to the environment, tooling, and machining parameters. However, the surface finish of MMCs was not that responsive in ultraprecision diamond machining. The results showed that surface finish measurements were indifferent for tools with $\pm 5^\circ$ or 0° rake angles; or between as-cast, HIPped, or different tempering conditions. The effect of cutting speed on surface finish was also

minimum when varying the cutting speed in the range 10-200m/min. This was not a surprise since all the measurements were confined in the aluminum phases. The surface integrity of the machined surface must be evaluated to assess the effectiveness of the process.

Examination using SEM and AFM showed that surfaces of the samples were smeared with the soft aluminum matrix, which covered most of the broken SiC/Al₂O₃ particles when machined with a PCD tool. The rubbing and smearing of a PCD tool were inevitable since a PCD tool edge sharpness was in the range 0.50-0.75 μm (Table 1) which was comparable or, in some cases was greater than, the depth of cut. In contrast, different phases and more broken SiC particles in the eutectic zones were more visible on the A359/SiC/10p when machined with a SCD tool (Fig. 2). Due to the broken silicon dendrites and SiC reinforcements in the eutectic phase, the surface roughness varied greatly depending on whether the measurement was confined within a smoother aluminum phase or in the rougher SiC-containing eutectic phase. The dependent of measured area, however, was not an issue for the extruded 6061/Al₂O₃/20p since the alumina particles distributed uniformly in the matrix.

Fig. 1. Surface finish in the aluminum phase of A359/SiC/10p after ultraprecision machining. Facing at feed = 0.5% nose radius (μm/rev). The sample's nomenclature indicates Temper /Cutting speed (m/min) /Depth of cut (μm) /Tool material/ Tool radius (mm).

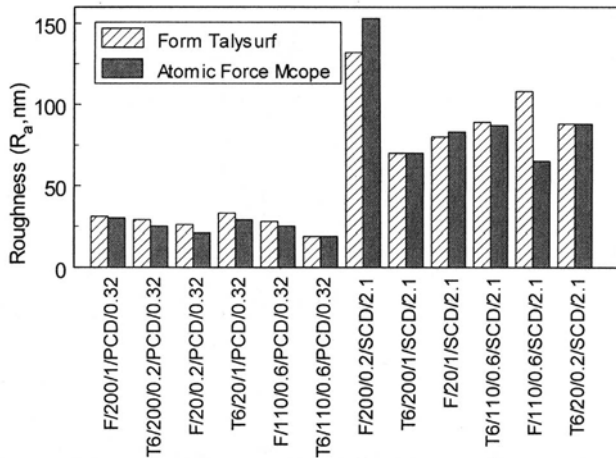
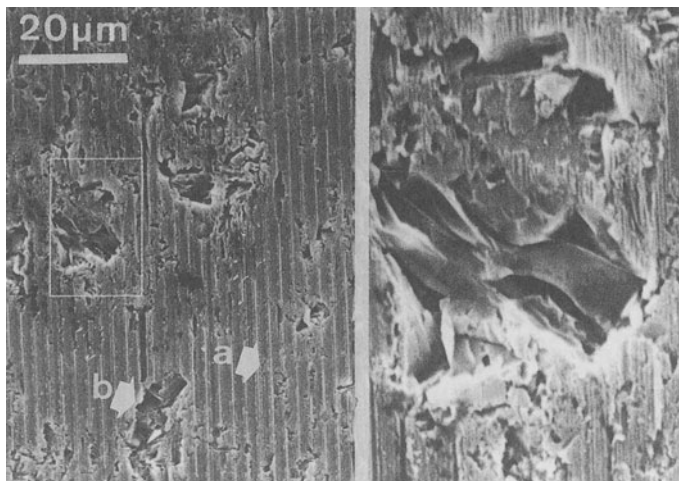


Fig. 2. Surface integrity of as-machined A359/SiC/10p-F after ultraprecision machined with a single-crystalline diamond tool. Notice (a) the ductile feed marks in the aluminum phase, and (b) broken SiC particle. Facing at 9.6 m/min speed, 0.2 μm depth, 2.55 μm/rev feed using SCD tool (0° rake, 0.51 mm radius).



4.2. Ductile-Regime Machining

Ductile regime machining of the hard particles was confirmed by examining the as-machined surface, the sectioned subsurface, and the etched surfaces. The selected physical and mechanical properties, required in equation (1) for SiC and Al₂O₃ are tabulated in Table 3. Thus, the calculated ranges for the critical depth of scratching using equation (1) were $d_c = 0.023\text{-}0.059 \mu\text{m}$ for SiC and $d_c = 0.08\text{-}0.25 \mu\text{m}$ for Al₂O₃. This range for micro-scratching, however, did not agree with the published critical grinding depth $0.6 \mu\text{m}$ for SiC [1] and $1 \mu\text{m}$ for Al₂O₃ [1,4]. Using the properties of Al₂O₃ in Table 3 and $d_c = 1 \mu\text{m}$, equation (1) gave the value of the proportional constant $A \approx 0.6$. With this new constant A , the adjusted critical depth of cut for SiC should be in the range $0.092\text{-}0.236 \mu\text{m}$. This result agreed with the experimental depth of cut $0.2 \mu\text{m}$ at which the transition of ductile-brittle machining of SiC was observed (Fig. 3). Facing the 6061/Al₂O₃/20p at $1.0 \mu\text{m}$ depth of cut re-confirmed this critical depth of cut (Fig. 4). Equation (1), therefore, should be modified as following for ultraprecision machining of MMCs reinforced with either SiC or Al₂O₃ reinforcement:

$$d_c = 0.6 \left(\frac{E}{H} \right) \left(\frac{K_{cs}}{H} \right)^2 \quad (3)$$

Table 3. Selected properties of common reinforcements for MMCs [7]

Ceramics	Young's modulus (GPa)	Fracture toughness (MPa.m ^{0.5})	Knoop hardness (GPa)
α -Al ₂ O ₃	275-393	3.85-5.90	19.6-20.1
SiC	382-475	2.50-3.50	24.5-25.0

At a depth of cut below those critical depths of cut, some particles were machined in the truly ductile-regime mode, some in a pseudo-ductile mode, but some were shattered in a brittle fashion. Shattering of a particle by a diamond tool was probably due to a deeper effective depth of cut, unfavorable orientation of that particle with respect to the cutting tool, or defects in the particles. A deeper effective depth of cut was possible due to a minute rotation of a particle when first engaged with the cutting tool. Preliminary experiment to measure the force using a high sensitive piezo-dynamometer showed that the forces were in the sub-Newton range. Although small, such cutting force might be enough to separate and rotate those partially wetted particles from the matrix, rotated it, thus effectively increased the depth of cut beyond the critical threshold. Plastic deformation of the matrix, loosened particles from previous cut, and defects in the particles also contributed to this problem.

Since the crystallographic orientations affected the critical depth of cut of semiconductor materials [8-9], it was reasonable to assume that ductile-regime machining of SiC and Al₂O₃ also affected by the crystalline orientation as well as its physical and mechanical properties. The SiC reinforcement had either diamond structure (β -SiC), hexagonal or rhombic structure (α -SiC), while the common α -Al₂O₃ reinforcement had a hexagonal structure. The critical resolved shear stress, on a crystalline plane of the reinforcement due to the cutting action, was directly proportional to the Schmid factor $\cos\lambda\cos\phi$, where ϕ and λ were the orientations of the slip plane and slip direction. It was

postulated that an ideal ductile mode happened when the cutting shear stress was parallel to both the slip plane and the slip direction, otherwise a pseudo ductile mode with micro cleavages would be seen. Equations (1) and (3), therefore, lacked the contributing factor of the crystalline orientation. This probably was the principle reason for the variation of published critical depths for ductile-regime machining of SiC and Al₂O₃.

Since a random distribution of the ceramic reinforcing particles in a MMC was obtained, it was impractical to characterize or control the crystalline orientation of all these micro particles. This explained why some particles, on the same machined surface, were ductile-regime machined but others were machined with micro cleavages or even fractured. Ultraprecision machining at a depth of cut below the critical threshold, as predicted in equation (3) was only the necessary condition for ductile-regime machining. Thus, it was very difficult, if not impossible, to obtain the true ductile-regime turning of MMCs reinforced with particles or whiskers.

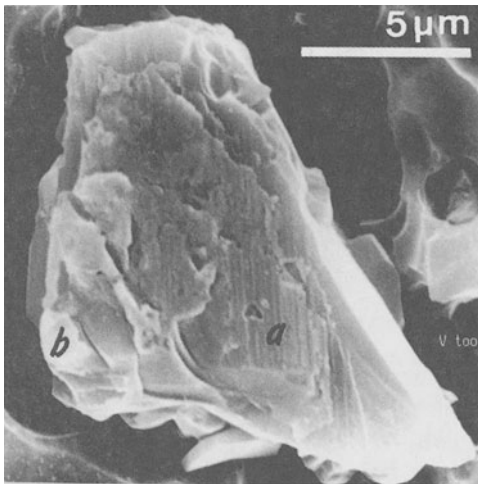


Fig. 3. Pseudo-ductile mode of a SiC particle. Notice (a) the ductile feedmarks, and (b) the micro-cleavages. Vertical cutting direction. Facing A359/SiC/10p-F then etching with Keller's etchant; 6.7 m/min speed; 2.55 μm/rev feed; 0.1 μm depth of cut; SCD tool (0° rake, 0.51 mm radius).

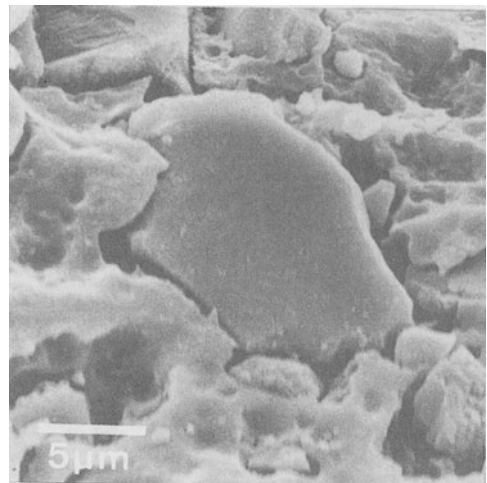


Fig. 4. Ductile mode of an Al₂O₃ particle. Notice the absence of cutting marks. Horizontal cutting direction. Facing 6061/Al₂O₃/20p then etching with Keller's etchant. 50 m/min speed, 1 μm depth of cut; SCD tool (-25° rake, 0.03 mm radius).

5. CONCLUSIONS

Ultraprecision machining of A359/SiC/10p and 6061/Al₂O₃/20p was studied. This investigation showed:

1. Equation (3) was recommended to calculate the critical depth of cut for MMCs reinforced with SiC and Al₂O₃. The critical depths of cut of 0.2 μm and 1.0 μm were calculated and verified with experimental data, for SiC and Al₂O₃ respectively. At such depths of cut, most metal matrices would be machined in the truly ductile-regime.
2. When machining below the critical depth of cut, the reinforcements were not only machined in the ductile mode, but also in pseudo-ductile mode, or in a brittle mode. The depth of cut was only the necessary condition for ductile-regime machining. The contributing factor of particle crystallographic orientation should be considered.
3. Surface finish of machined MMCs alone did not fully quantify the surface integrity. The matrix could be machined in ductile mode, but the particles could be shattered and significantly degraded the surface finish.
4. The blunt cutting edge of PCD tool (500-750 nm) rubbed and smeared the aluminum on the machined surface, but the sharp cutting edge of a SCD tool (20-80 nm) cut the surface effectively to reveal different phases.

REFERENCES

1. Bifano, T.G., Dow, T.A., and Scattergood, R.O.: Ductile-regime Grinding of Brittle Materials: Experimental Results and the Development of a Model, *Advances in Fabrication and Metrology for Optics and Large Optics*, SPIE 966, (1988), 108-115.
2. Yuan, Z.J., Geng, L., and Dong, S.: Ultraprecision Machining of SiCw/Al Composites, *Annals of the CIRP*, 42 (1993) 1, 107-109.
3. Chandrasekaran, H. and Johansson, J.O.: Influence of Processing Conditions and Reinforcement on the Surface Quality of Finish Machined Aluminum Alloy Matrix Composites, *Annals of the CIRP*, 46 (1997) 1, 493-496.
4. Zhong, Z.W., Hung, N.P., Loh, N.L., and Sano, T.: Grinding of Aluminum-Based Metal Matrix Composites, *Proc. of the International Conference on Mechanics of Solids and Materials Engineering*, Singapore, A (1995) 274-279.
5. Hung, N.P., Zhong, Z.W., and Zhong, C.H.: Grindability of Metal Matrix Composites, *Proc. of the Fourth Conference on Composites Engineering*, Hawaii, (1997) 459-460.
6. Whitehouse D.J., *Handbook of Surface Metrology*, IOP Publishing, UK, 1994.
7. Ratterman E. and Cassidy R.: Abrasives, *Engineering Materials Handbook: Ceramics and Glasses*, ASM, 4 (1991) 329-335.
8. Leung, T.P., Lee, W.B., and Lu, X.M.: Diamond Turning of Silicon Substrates in Ductile Regime, *J. Materials Processing Technology*, 73 (1998) 42-28.
9. Shibata, T., Fujii, S., Makino, E., and Ikeda, M.: Ductile-Regime Turning Mechanism of Single Crystal Silicon, *J. Precision Engineering*, 18 (1996) 2/3, 129-137.

VIBRATION MONITORING AND CLASSIFICATION IN CENTERLESS GRINDING

R. Ippolito, L. Settineri and M. Sciamanda
Polytechnic of Turin, Turin, Italy

KEY WORDS: Centerless grinding, Vibrations, Neural Networks, Entropy, Time series

ABSTRACT: In centerless grinding operations, grinding wheel and workpiece regenerative chatter can affect the accuracy of the surface finish as well as the workpiece roundness. An algorithm for automated classification of chatter by type is needed to develop closed-loop vibration control systems. In this paper, three approaches are compared for vibration signal classification applied to regenerative chatter monitoring in centerless grinding: neural network, time domain K-L and entropy function approach. Such methods have been compared in their classification performances and computational loads.

The results show the better performances of the neural network approach, that outruns the others also in flexibility, due to the particular network typology adopted.

1. INTRODUCTION

In recent years one of the sectors of the machining technology on which a major research effort has been applied is the machining with abrasives, due to the necessity to machine more and more resistant materials with higher precision, productivity and automation level [1]. The main machining operation in this area is grinding, one of the most complex technological processes. Several studies have been carried out to explain the physical and chemical aspects of the process; however, it is not yet available a model able to forecast the process evolution starting from the setting parameters.

During the grinding process, the growth of chatter is usually governed by regenerative

Published in: E. Kuljanic (Ed.) *Advanced Manufacturing Systems and Technology*,
CISM Courses and Lectures No. 406, Springer Verlag, Wien New York, 1999.

effects. In centerless grinding, regenerative chatter may occur either on the workpiece surface or on the wheel surface. The chatter mechanisms in centerless grinding and the existence of unstable regions have been explored, but the practical chatter behaviour cannot be explained yet [2].

For the optimal selection of grinding wheels and process parameters, the operators are sometimes assisted by Artificial Intelligence systems created for the storage and management of information relevant to the process and the tools. Furthermore, systems able to monitor the process conditions have been introduced, capable of giving useful information for possible corrective actions. Such systems are essentially based on contact sensors or power sensors to detect burns, grinding wheel chattering and wear [3]. Some of them are today commonly adopted, like automatic wheel balancing and wear compensation in the NC machines [4].

Recently, however, the possibility to use Acoustic Emissions (AE) and vibrations in the grinding process to monitor the evolution of the process has been explored [5]. Such methods, however, have the disadvantage of being very sensitive to changes on the environmental conditions and need sophisticated signal processing techniques.

In the present paper an automatic method based on vibration analysis for performance monitoring of a grinding machine is presented, able to distinguish normal from abnormal working conditions, even if such operating conditions are unprecedented.

Three signal processing approaches have been compared, new-generation neural networks, time-domain techniques and extraction of signal attributes. The neural network approach gives a more accurate classification of the damage conditions. Furthermore, such method allows for considerable time and resource savings with respect to the other methodologies, due to the limited learning time of the network and to the possibility for the system to work unattended.

2. MACHINE TOOLS VIBRATIONS

The different components of a machine tool contribute to the vibrations that can be observed in any part of the structure. Two main classes of vibration signals can be individuated: vibrations directly connected with the cutting process and vibrations caused by the various moving parts of the machine tool, the latter being due to periodical disturbances like misalignments of shafts, bearings, hydraulic systems. The induced vibrations measured in any part of the machine show frequencies similar to those of the sources or to their harmonics and their intensity depends on the amplitude of the original vibration and on the compliance (or dynamic deformability) of the machine tool at that particular frequency.

Vibrations related to the cutting process can be due to non-homogeneous part surface or to variations on the chip thickness that causes sudden changes of the cutting forces. In some cases, when the transient phases don't decay rapidly enough between the pulses, such variations can cause self-excited vibrations and sometimes resonance phenomena.

In case of vibrations between the grinding wheel and the working part the variations on the cutting forces tend to change the wheel characteristics, creating fractures or packing of the chip. This causes a fluctuation on the normal force and as a consequence, the process tends to become dynamically unstable [6], the stability condition being expressed as follows:

$$\frac{|\text{Re}_m|}{k_m} < \frac{1}{2k_c} \left(1 + \frac{v_w}{v_s \cdot G} \right) + \frac{1}{k_s}$$

where: Re_m real part of the frequency response; k_m static rigidity; k_s contact zone rigidity; G grinding ratio; k_c cutting rigidity; v_w part speed; v_s grinding wheel speed.

3. CLASSIFICATION TECHNIQUES

There are several methods for signal classification, most of them belonging to three main typologies: time-domain techniques, extraction of some signal attributes and neural networks.

Each of these typologies presents advantages and limitations therefore, since the available signal was not known *a priori*, we have tested methods belonging to all of them.

3.1 Time-domain techniques

Among the several methods belonging to this category, parametric techniques have been used, that present some advantages with respect to the others [7]. In particular AR (AutoRegressive) models have been adopted in order to process the vibration signals, thought as time-series, since the computation of the parameters involves in this case the solution of only linear equations.

For classification purposes, the NN (Nearest Neighbour) rule has been used, that consists in assigning a sampled data batch to the most similar class among some reference classes. It is therefore necessary to have reference observations for the comparison with the experimental data and to select a similarity criterion.

The used similarity criterion has been the K-L (Kullback and Leibler) criterion, that can be applied to the experimental observation if a normal distribution for the population is assumed [8]. If $x^{(0)}$ is the sampled data batch to be assigned to a reference class, and $x^{(m)}$ a data batch observed and stored as reference, the K-L distance between the two series is given by:

$$d(x^{(0)}, x^{(m)}) = \frac{1}{2} \log \left(\frac{\hat{\sigma}_m^2}{\hat{\sigma}_0^2} \right) + \frac{1}{\hat{\sigma}_m^2} \sum_{i=0}^{P_m} \sum_{j=0}^{P_m} a^{(m)}(i) a^{(m)}(j) C^{(0)}(j-i) - 1 \quad (1)$$

where:

$C^{(0)}(j-i)$ is the estimated covariance function for the time series; $a^{(m)}(i)$ is the estimated parameters' vector; $\hat{\sigma}_m^2$, $\hat{\sigma}_0^2$ are respectively the estimated dispersions of the observed and reference populations.

3.3 Extraction of the main signal attributes

An effective method able to classify the sampled signals is the extraction of some features that can represent the signal in their basic characteristics. Most of these features are extracted from the power spectrum of the signal, but some are extracted directly from the pure signal. Some authors propose, as representative parameters, the spectrum area, the frequencies of the maximum amplitude, of the maximum area or of the half-area peaks of the spectrum, and the spectrum entropy [9], but other features are suitable, like the Root Mean

Square (RMS) of the pure signal and the mean value of the spectrum [10].

As regards the entropy function, traditionally used in thermodynamics, it was first introduced by Claude Shannon in 1948 for measurement of uncertainty in information theory [11]. Applied to the power spectrum of a signal, it gives an indication on the spectrum complexity. If $p = (p_1, p_2, \dots, p_n)$ is a probability distribution with: $p_i \geq 0 \quad \forall i \in [1, n]$ and

$$\sum_{i=1}^n p_i = 1, \text{ the entropy function is defined as follows: } En(p) = -\sum_{i=1}^n [p_i \cdot \ln(p_i)], \text{ with}$$

$p_i \cdot \ln(p_i) = 0$ if $p_i = 0$, by definition.

It is necessary a preliminary analysis of the signal in order to individuate the most significant features for its classification. To this purpose a *representativity parameter* can be defined for each feature, as the ratio between variance and average value of the i-th feature: $\psi_i = \frac{\sigma_i}{\mu_i}$.

The features for which $\psi_i \leq 0.1$ have been considered, to our purposes, suitable for signal classification [12]. In our case, only spectrum entropy (S), pure signal root mean square (RMS) and spectrum mean value (m), passed this representativity test.

3.2 Neural Networks

Neural Networks (NN) are today extensively used in signal processing, due to their flexibility and adaptability to different problems. Nevertheless, their need for a great number of examples in order to be “trained” limited their diffusion. Such problem can be overridden by using networks able to carry out self-learning and self-updating, like the ART2 networks that are used in the present paper.

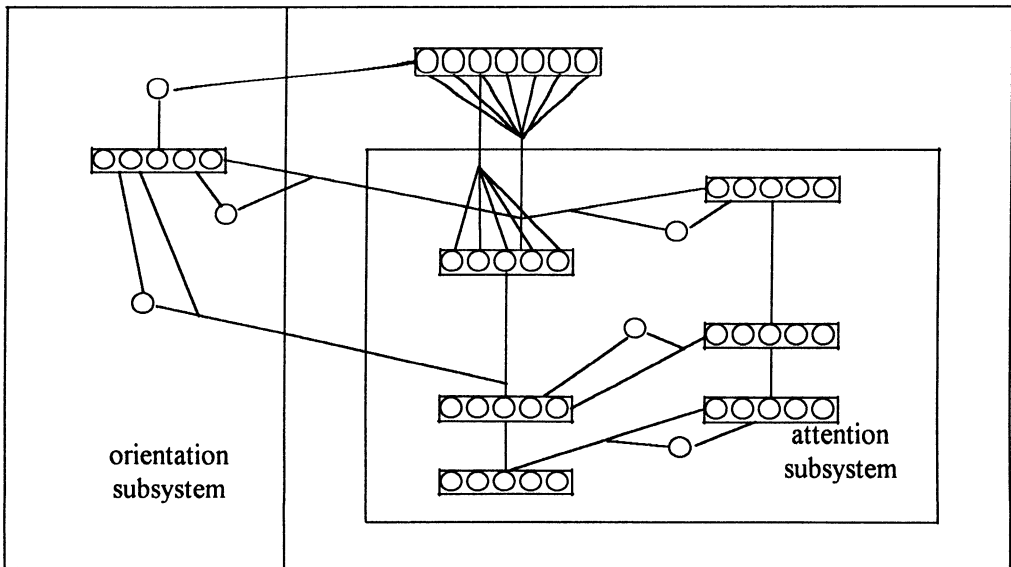


Figure 1 - Structure of the ART2 Neural Network.

The ART (Adaptive Resonance Theory) networks belong to the match-based back-propagation NN typology [13, 14], i.e. the internal memory is modified only when the external input meets internal expectations or appears completely new. Such characteristics, along with the intrinsic stability, makes the ART networks a very good instrument for the analysis of continuously evolving phenomena with a noticeable number of data. There are several typologies of ART networks, being the ART2 nets used for analog inputs. The basic schema of the ART2 network is represented in figure 1. Two subsystems are present: the *orientation* subsystem and the *attention* subsystem [14], each of them formed by one or more levels. The adopted learning criterion has been a delta rule, with a learning rate of 0.9, while the stopping criterion was the reaching of a minimum for the classification error, with a threshold level of 0.05. The number of eves between two phases has been set at 10000.

4. COMPARISON BETWEEN THE DIFFERENT TECHNIQUES

4.1 Experimental set-up

The experimental system has been designed to compare the performances of the presented techniques in classifying chatter by type. The experimental tests have been carried out on a centerless grinding machine, on which two acceleration transducers have been installed. The classification results are separately obtained with the proposed algorithms and then compared.

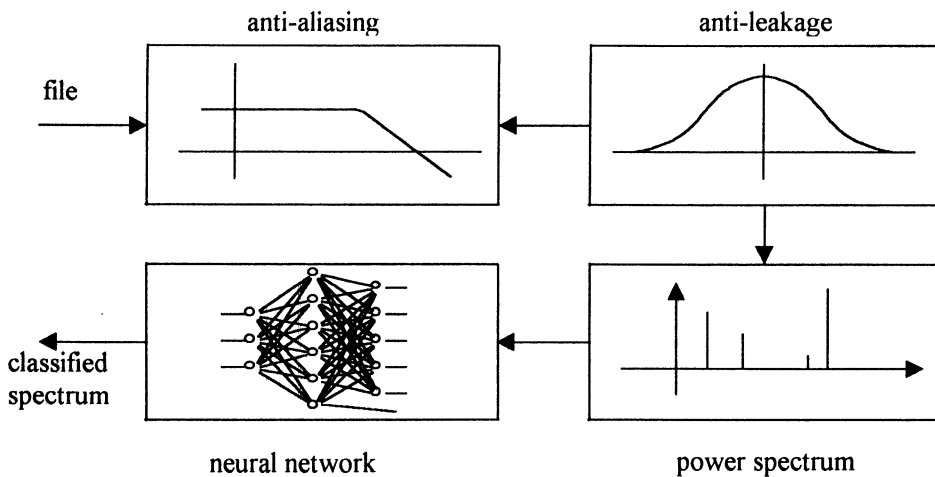


Figure 2 - Schema of the signal processing system.

Vibration data have been processed by using a Butterworth low-pass filter of the 6th order with cutting frequency of 15 kHz, in order to avoid aliasing phenomena. Afterwards, an anti-leakage Hanning window on the whole data batch has been applied and the power spectrum has been computed. In figure 2 the schema of the processing system for the neural network approach is represented.

The operating conditions are reported in the following table:

Table I - Operating conditions.

Grinding wheel	White corundum WA120M7V, 40050, dia. 400 mm, width 50 mm
Workpiece material	38 Ni Cr Mo 4
Machining conditions	Wheel speed 30 m/s
Accelerometer	Brüel & Kjær, mod. 4332
Charge Amplifier	Brüel & Kjær, mod. 2634
Acquisition Board	National Instrument AT-MIO-16E-10

The three considered vibration conditions are:

a) normal conditions; b) wheel regenerative chatter; c) workpiece regenerative chatter.

A comparison has been carried out among the different classification techniques indicated in section 3, using a 180 sample test data set (60 samples for each vibration condition), while for the system tuning 30 sample training data sets (10 samples for each vibration condition) have been used.

4.2 Neural network

The neural network was trained with 30 sample training data sets (10 samples for each vibration condition). The used ART2 neural network gave the following results:

Table II - Classification performances of the Neural Network.

Training cycle	Classification error	
	(No of error samples/Total no. of samples)	
	Training data set	Test data set
30	14/30	62/180
60	5/30	4/180
120	1/30	1/180
180	0/30	0/180
300	0/30	0/180
900	0/30	0/180

4.3 K-L distance measurement

As a first step, the optimal AR model order for the parameter identification has been defined: to this purpose, the Akaike AIC (Akaike's Information Criterion) method has been used [8] over the 30 sample training data sets; this yielded an average order value of $p=35$. A parameter set for an AR model of order $p=35$ has then been computed for each one of the three reference classes (normal conditions, wheel regenerative chatter, workpiece regenerative chatter). During the cutting operations the sampled vibration signals have been assigned to one of the reference classes by filtering them with the computed AR models and the forcing error computed:

$$\varepsilon^{(0,m)}(t) = \sum_{i=0}^p a_i^{(m)} x^{(0)}(t)$$

Then, the covariance is estimated by:

$$C^{(0)}(k) = \frac{1}{n} \sum_{t=1}^{n-k} [x^{(0)}(t+k) - \bar{x}] [x^{(0)}(t) - \bar{x}], \quad \text{for } k \leq p_0$$

$$C^{(0)}(k) = \sum_{i=1}^{n-k} [\alpha_i^{(0)} C^{(0)}(k-i)], \quad \text{for } k > p_0 + 1$$

The K-L distance can now be computed with eq. (1) and the sampled vibration signal assigned to the reference class for which the smaller distance results.

Such method has been able to classify correctly 172 over 180 test data sets, with an error percentage of 4.4 %.

4.4 Attribute extraction method

The observed value of each extracted attribute has been assumed normally distributed around his medium value. The attributes with an “acute” distribution will be assumed to be more significant. Such aspect has been numerically evaluated by means of the representativity parameter previously introduced. In figure 3 some distributions of signal attributes selected after the representativity test are shown. A second condition to be satisfied was that the normal distributions should be sufficiently distant to be not superimposed. Such conditions have been verified over the proposed signal attributes and then only the signal spectrum entropy was selected for classification purposes:

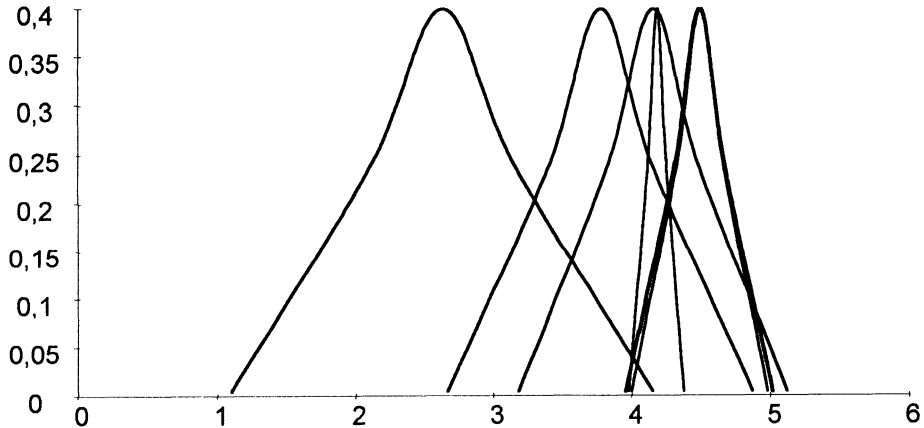


Figure 3 - Probability distributions of the entropy function for some sampled signals.

The adopted classification criteria, tuned over the 30 sample training data sets, were as follows:

- If the entropy value falls in $[A1, +\infty)$ the grinding condition is classified as normal;
- If the entropy value falls in $\{A2, A1\}$ the grinding condition is classified as wheel regenerative chatter;
- If the entropy value falls in $\{-\infty, A2]$, the grinding condition is classified as workpiece regenerative chatter.

With $A1$ and $A2$ threshold levels respectively set at 1.352 and 0.885, using the following

criteria:

- $A1 = (\text{lowest entropy value in normal condition} + \text{highest entropy value in wheel regenerative chatter})/2$;
- $A2 = (\text{lowest entropy value in wheel regenerative chatter} + \text{highest entropy value in workpiece regenerative chatter})/2$.

The error percentage of such approach has been of 6.7 %, having classified correctly 168 over 180 data sets.

4.5 Discussion

Though all the proposed techniques performed quite well in classifying chatters, the neural network approach shows the best classification performances: 0% classification error on the test data set, along with an acceptable computational load.

By using a back-propagation ART2 neural network, the training data set has been enormously reduced with respect to the training data needed for the forward-propagation networks; besides, the ART2 network shows noticeable self-updating possibilities in case of changes on the operating conditions.

On the other end, while showing the lowest classification performances, the attribute extraction method seems to be the simplest to implement and the one requiring the lowest computational load if adopting an FFT algorithm to extract the signal power spectrum.

Finally, the time-series approach, with the computation of the K-L distance between the AR-filtered sampled data sets and some reference AR polynomial classes, shows satisfactory classification performances, but the higher computational load and response time.

If a final classification is to be made, the neural network approach with the proposed network structure shows the best overall performances along with the flexibility given by the self-learning and self-updating capabilities.

5. CONCLUSION

In this paper, three methods have been used to monitor regenerative chatter in centerless grinding: Neural Networks, time-domain K-L distance measurement and attribute extraction method. Vibration signals sampled during grinding operations were used as input of the three methods, whose performances have been compared. The results show better classification performances for the neural network approach, along with an acceptable computational load. The worst classification performances were shown by the entropy extraction approach, but with the lowest computational load, while the K-L distance method showed the higher computational load and response time.

REFERENCES

1. Rowe W. B.: *Centerless grinding research and its application in advanced manufacturing technology*, Annals of CIRP, Vol. 38/2, 1989.
2. Hashimoto, F., Miyashita, M.: *Growing Mechanism of Chatter Vibrations in Grinding Processes and Chatter Stabilisation Index of Grinding Wheel*, Annals of the CIRP, Vol. 33/1, 1984.

3. Rowe W., Li Y., Inasaki I., Malkin S.: *Application of Artificial Intelligence in Grinding*, Annals of CIRP, Vol. 43/2, 1994.
4. Rowe W., Li Y., Mills B., Allanson D.R.: *Application of Intelligent CNC in Grinding: Computers in Industry* Vol. 31, pp. 45-60, 1996.
5. Junkar M., Filipic B.: *Grinding Process Control through Monitoring and Machine Learning*: Proc. of 3rd Int. Conf. On Competitive Perform. through Adv. Techn. pp. 77-80, 1992.
6. Malkin, S.: *Grinding Technology*, Ellis Horwood Limited, 1991.
7. Kay S.: *Fundamentals of statistical signal processing*, Prentice-Hall International edition, 1993.
8. Scharf L.: *Statistical signal processing, detection, estimation and time-series analysis*, Addison-Wesley Publishing Company, 1991.
9. Junkar M., Filipic B., Bratko I.: *Identifying the grinding process by means of inductive machine learning*, Computers in Industry, by Elsevier, Vol. 17, pp. 147-153, 1991.
10. Ippolito R., Settineri L., Andorno L.: *Tool Conditions Monitoring by Means of a Neural Network*, Proc. of the ICME'98 CIRP Int. Seminar on Intelligent Computation in Manufacturing Engineering, Capri, Italy, July 1-3 1998.
11. Martin N.F.G., England J.W.: *Mathematical Theory of Entropy*, Addison-Wesley Publishing Company, 1981.
12. Fu J.C., Mori K., Yokomichi M.: *Application of Entropy Functions in On-line Vibration Classification for Cylindrical Plunge Grinding*: Int. J. Of Prod. Research, Vol. 32/6, 1994.
13. Freeman J.: *Simulating Neural Networks*, Addison-Wesley Publishing Company, 1994.
14. Hecht-Nielsen R.: *Theory of back-propagation Neural Networks*, Proc. of the Int. Joint Conf. on Neural Networks, 1989.

GRIND-HARDENING MODELING WITH THE USE OF NEURAL NETWORKS

K. Tsirbas, D. Mourtzis, S. Zannis and G. Chryssolouris
University of Patras, Patras, Greece

KEY WORDS: Grind-Hardening, Neural Networks, Process Modeling & Simulation.

ABSTRACT: This paper describes the modeling procedure and results of a non-conventional process, called grind-hardening. The main idea of the grind-hardening process is that the heat dissipation in the cutting area is used for the heat treatment of the workpiece. Grind hardening is a complex manufacturing process governed by a multiplicity of parameters.

In order to satisfy the need for industrial exploitation of the process, it must first be thoroughly investigated and optimized. This goal can be achieved by efficient modeling. For this purpose, artificial intelligence methods were used, namely Neural Networks. This advanced simulation method is highly efficient in the case when relationships among parameters are non-linear, which is the case in grind-hardening.

The case studied in this paper is a double-face grind-hardening process. The part in question is a punched disk simultaneously ground and hardened on both sides. Quantitative and qualitative parameters are used to describe the process. The qualitative parameters are modeled using vector representation. Experimental data taken from this process are used to train the network.

After the network training stage has been completed, the network is then used to determine the impact of the process parameters on the working result, namely the surface hardness on both sides of the part. The network results, concerning the level of accuracy of its predictions for different combinations of process parameters, have been obtained and evaluated as satisfactory.

1. INTRODUCTION

A large amount of research in manufacturing has been dedicated to the modeling and optimization of the grinding process. In [1] there is a wide collection of different models concerning this process. In particular, there are empirical and semi-empirical models, which concern the grinding wheel topography, the chip thickness, the grinding forces and energy, the surface integrity, the surface roughness and finally the temperature. In addition, in [2] some more empirical models are presented and the main parameters of grinding are identified.

Despite the high quality of work done in this area, two major limitations seem to hinder the efficient modeling of the process: The high non-linearity of the process and the large number of assumptions that are included in the empirical and semi-empirical models already mentioned. In an attempt to overcome these limitations, Artificial Intelligence (AI) techniques have been widely used for this purpose, not only for grinding but also for many other processes. The application of AI techniques in grinding is extensively discussed in [3], where different AI approaches, such as Expert Systems, Fuzzy Logic and Neural Networks are used and evaluated for modeling a grinding process. Almost the same subject is covered in [4], using a multi-agent approach to the problem, namely case-based reasoning, neural network reasoning and rule-based reasoning. Furthermore, in [5] there is a comparison between statistical and AI methods in machining processes, indicating the great advantage of the AI processes in such problems.

Neural Networks in particular have been used in various areas of manufacturing. For example, they are used for modeling purposes of processes, such as cutting tool wear monitoring [6] and tool condition monitoring [7]. Moreover, Neural Networks have been reported to be very efficient for scheduling different processes [8], specifically for decision making on grinding [9] and many other manufacturing processes [10][11], yielding remarkable results.

Due to the fact that grind-hardening is an innovative process, it has not been thoroughly investigated yet. In [12], only the concept of grind-hardening and some preliminary experiments and their results are described. In addition, it is reported to be highly non-linear. Based on the success of using Neural Networks for modeling complex and non-linear processes, the same method has been selected for the modeling of the grind-hardening process as well.

2. PROBLEM DEFINITION

Grind-hardening is a special grinding process which utilizes the friction generated heat flux, in order to achieve high surface hardness of the ground part. This is achieved, as the dissipated heat induces martensitic phase transformation to the workpiece material and thus, increasing its hardness. The main process parameters are the workpiece speed, the depth of cut, the cutting speed, the feed rate, the workpiece material and the grinding wheel type; while the process result is described by the hardness penetration depth and the surface

hardness. This one-step operation can be used for concurrently heat treating and surface finishing of high quality parts. The main benefits from such a process are the lower machining costs, the reduction of machining cycle times, the higher process flexibility, and the low energy consumption and environmental impact.

As stated in [12], the surface hardness and the hardness penetration achieved is dependent on the process conditions. In particular, the material removal rate Q'_w and the properties of the workpiece material are reported to be among the most influential parameters on the process result. However, the correlations between parameters are described in [12] as complex and not yet clarified. On the grounds that this process should be further investigated and optimized, in order to be incorporated into production, these correlations should be investigated through a modeling procedure.

3. METHODOLOGY

As already stated, Neural Networks have been widely used for modeling purposes and especially for grinding processes. Therefore, the same method was used for the grind-hardening process as well.

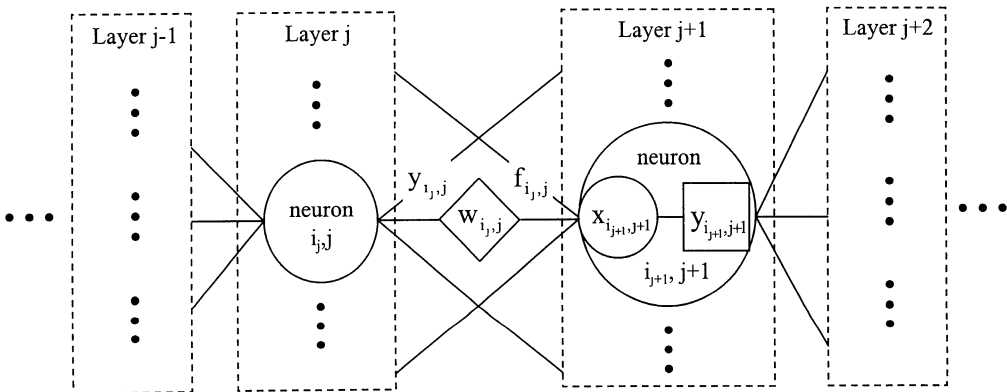


Figure 1: Schematic layout of network architecture.

A neural network consists of many non-linear computational elements operating in parallel. Computational elements, or neurons, are connected via weights, which are adapted through a learning or training process in order to improve performance. The neurons are arranged in layers. Each neuron in a specific layer takes input from all neurons of the previous layer and gives its output to all neurons of the next layer [13].

A typical neural network architecture is shown in fig.1. The network is composed of J layers and layer j ($j=1,2,\dots,J$) includes I_j neurons. Each of these neurons is represented as (i_j, j) , where i_j ($i_j = 1,2,\dots,I_j$) is the neuron number within layer j . Three types of functions exist in a neural network: connection functions f , neuron input functions x and neuron output functions y . Each link between two neurons possesses a connection function, while the input functions and output functions are included in each neuron.

The following analysis is based on two consecutive neurons, (i_j, j) and $(i_{j+1}, j+1)$, and their connection. The connection function receives the output $y_{i_j, j}$ of the source neuron (i_j, j) and transforms it into an input $f_{i_j, j}$ for the destination neuron $(i_{j+1}, j+1)$. The connection function implemented is:

$$f_{i_j, j} = y_{i_j, j} \cdot w_{i_j, j} \quad (1)$$

where $w_{i_j, j}$ is the weight value associated with the link.

The neuron input function x combines the inputs $(f_{i_j, j})$ of a neuron. The input function used in most cases simply sums up the values of the neuron's I_j inputs:

$$x_{i_{j+1}, j+1} = \sum_{i_j=1}^{I_j} f_{i_j, j} \quad (2)$$

The neuron output function determines the relationship between the combined neuron input $x_{i_{j+1}, j+1}$ and the neuron output $y_{i_{j+1}, j+1}$. Output functions are non-linear functions, which usually generate values between 0 and 1. The sigmoid function used in most neural network applications is shown below:

$$y_{i_{j+1}, j+1} = \sigma(\text{net}_{i_{j+1}, j+1}) = [1 + e^{-(\text{net}_{i_{j+1}, j+1})}]^{-1}, \quad \text{where } \text{net}_{i_{j+1}, j+1} = x_{i_{j+1}, j+1} - b_{i_{j+1}, j+1} \quad (3)$$

The quantity $b_{i_{j+1}, j+1}$ is the neuron bias, and marks the value of the combined input $x_{i_{j+1}, j+1}$ at which the neuron output $y_{i_{j+1}, j+1}$ “jumps” from near 0 to near 1. Changing the value of this bias modifies the computational behavior of the neuron.

The application of a neural network requires a learning procedure, which gradually adjusts the network's weights and biases, until the network correctly maps all of the training inputs onto the corresponding training outputs. The most commonly used learning algorithm is called backpropagation. Using this algorithm, the output error is determined by performing the forward computations in the network and comparing the results with the desired output. The error is propagated backwards through the network, and the weights and biases are changed in order to reduce the local error fraction δ . The link weight adaptation formula is:

$$\Delta w_{(i_j, j)(i_{j+1}, j+1)} = \eta \cdot \delta_{i_{j+1}, j+1} \cdot y_{i_j, j} \quad (4)$$

where $w_{(i_j, j)(i_{j+1}, j+1)}$ is the weight of the link from neuron (i_j, j) to neuron $(i_{j+1}, j+1)$, η is the learning rate, $\delta_{i_{j+1}, j+1}$ is the local error fraction at neuron $(i_{j+1}, j+1)$, and $y_{i_j, j}$ is the output value of neuron (i_j, j) . The local error fractions for the neurons in the output layer are computed using the following relationship (sigmoid functions are assumed):

$$\begin{aligned} \delta_{i_{j+1}, j+1} &= (d_{i_{j+1}, j+1} - y_{i_{j+1}, j+1}) \cdot [\partial \sigma(\text{net}_{i_{j+1}, j+1}) / \partial \text{net}_{i_{j+1}, j+1}] = \\ &= (d_{i_{j+1}, j+1} - y_{i_{j+1}, j+1}) \cdot y_{i_{j+1}, j+1} \cdot (1 - y_{i_{j+1}, j+1}) \end{aligned} \quad (5)$$

where $d_{i_{j+1}, j+1}$ is the desired output of neuron $(i_{j+1}, j+1)$, $y_{i_{j+1}, j+1}$ is the computed output, $(d_{i_{j+1}, j+1} - y_{i_{j+1}, j+1})$ is the error and $\sigma(\text{net}_{i_{j+1}, j+1})$ is the sigmoid output function of neuron $(i_{j+1}, j+1)$. The local error fractions for non-input-layer neurons are calculated as:

$$\begin{aligned}\delta_{i,j} &= [\partial\sigma(\text{net}_{i,j})/\partial\text{net}_{i,j}] \cdot \sum_{l_{j+1}=1}^{I_{j+1}} (w_{(i,j)(i,j+1,l_{j+1})} \cdot \delta_{(i,j+1,l_{j+1})}) \\ &= y_{i,j+1} \cdot (1 - y_{i,j+1}) \cdot \sum_{l_{j+1}=1}^{I_{j+1}} (w_{(i,j)(i,j+1,l_{j+1})} \cdot \delta_{(i,j+1,l_{j+1})})\end{aligned}\quad (6)$$

Bias changes are computed as:

$$\Delta b_{i,j+1} = -\eta \cdot \delta_{i,j+1} \quad (7)$$

Before the training starts, the initial weights and biases of the network are randomly selected. Then the training algorithm, during the training process, constantly changes the weights and biases until the optimum values are reached. The procedure of selecting the initial weights and biases is called *initialization* and is critical for the training process as mentioned in the following section.

When modeling various processes, there are usually quantitative and qualitative parameters taken into consideration. The quantification of the qualitative parameters is performed using two different approaches: Number notation and vector notation. Number notation is performed by assigning a simple number to each parameter level. In general, when number notation is used, the required number of network inputs N is given by the formula

$$N = p_t + p_l \quad (8)$$

where p_t is the number of quantitative parameters and p_l is the number of qualitative parameters. On the other hand, when vector notation is used, N is expressed by the following equation:

$$N = p_t + \sum_{k=1}^{p_l} L_k \quad (9)$$

where L_k is the number of levels of the k -th qualitative parameter.

4. PILOT CASE – IMPLEMENTATION

The case studied in this paper is a double-face grind-hardening process. The part in question is a punched disk, made of 16MnCr5 steel and it is ground and hardened at the same time on both sides with a cutting speed of 30m/sec. The process parameters and their levels are summarized in table 1. It must be noted that all the other parameters that affect the process, mainly the workpiece material and the cutting speed, were kept constant throughout the experimental process. There were 62 experiments carried out, measuring the surface hardness of each part ground-hardened under different process conditions.

In order to model the procedure of grind-hardening, Neural Networks were used. Firstly, the parameters and their respective levels to be investigated were defined (table 1). Appropriate experiments were then performed and the results were collected in order to be used for the training process of the network. These results were then divided into two parts. The first part was used for training the network, while the second was used for verification

purposes. In our case 56 sets were used for training, while 6 sets were used for verification. In addition, the data had to be normalized before they were presented to the network. Through the normalization procedure, the values included in the data sets are all brought within a certain interval, usually $[0,1]$ or $[-1,1]$. This helps the training algorithm to handle the data more easily and to converge quicker and more efficiently. In our case, the $[-1,1]$ interval was used.

	Work- Piece speed (v_n) (m/min)	Depth of cut (a_e) (μm)	Feed rate (v_{ae}) (mm/min)	Cooling Method	Work- piece side	Punching	Grinding wheel
Levels	3	200	0.90	Dry	Up	Yes	Soft
	15	300	1.30	Aircooling	Down	No	Hard
		500	2.75	300-200			
		6.00	Coolant				
Number notation				1,2,3,4	1,2	1,2	1,2
Vector notation				[1 0 0 0]	[1 0]	[1 0]	[1 0]
				[0 1 0 0]	[0 1]	[0 1]	[0 1]
				[0 0 1 0]			
				[0 0 0 1]			

Table 1: Quantitative and qualitative parameters and their levels used for the grind-hardening experiments. Number and vector notation of the qualitative parameters.

During the training stage, the network tried to map the correlation between input and output by altering internal parameters. After the network was successfully trained, the input values of the verification data set were presented to the network, and the corresponding output values were obtained. Then the error was calculated, namely the difference between network output and the anticipated value. When the error was considered acceptable, the training procedure stopped.

It has been observed that the initialization of the network plays a critical role for the network error. During different initializations of the same network using the same data, a considerable variation in the error percentage was found. In order to be able to determine the best alternative between the number and vector notation, a set of different initializations were performed for each notation. The Mean Error Percentage (MEP) of the corresponding trained networks was considered as the overall network error percentage. This value was used to compare the efficiency between the number and vector notation (fig.2).

The next step is to use the network with the minimum error percentage to simulate the process. This is performed by building data sets in which only the parameter under investigation varies, while all other parameters are kept constant. The occurred data sets

were presented to the trained network. Their output shows the impact of the parameter in question on the process result.

5. RESULTS

The training data set was first formed using the number notation, since this produced the minimum number of input parameters for the neural network ($N=7$). Nevertheless, the network performance was very poor, since the MEP reached the value of 28%. However, when the vector notation was used ($N=13$), there was a significant improvement of approximately 40%. The MEP of the network was less than 17%, while the best individual error percentage was 4.28% (fig.2). This is due to the fact that the number notation of the qualitative parameters does not accurately describe the process. For example, in the case of the "cooling" parameter, the "aircooling" level is represented by number 2, while the "coolant" level is represented by level 4 (table 1). During the training process, the network will probably consider level 4 more significant than level 2, or even consider the level "coolant" as the equivalent of the level "aircooling" multiplied by 2. Such correlations are obviously wrong and misleading for the network. On the other hand, by using the vector notation, the different levels are completely independent and the network does not differ between values. Hence, the process is more efficiently represented. However, the drawback of this technique is that the number of the input parameters rises significantly, along with the computational burden, during the training process.

The results of the process simulation are shown in figures 3 to 8. The impact of each parameter on the process output, namely the surface hardness, is evaluated by the variation of the parameter within its specified range, while keeping all other parameters constant at their nominal values (table 2). In addition, the Depth of Cut (DC) was set at three different values (200, 300 and 500 μm) in order to visualise its effect on the surface hardness. Finally, the impact of DC on the surface hardness is also depicted in figure 5 for different values of the Feed Rate (FR).

Parameter	Nominal value
Workpiece speed (m/min)	15.00
Depth of cut (μm)	500.00
Feed rate (mm/min)	2.75
Cooling	[1 0 0 0] (dry)
Workpiece side	[1 0] (up)
Punching	[0 1] (no)
Grinding wheel type	[1 0] (soft)

Table 2: Nominal values of the process parameters.

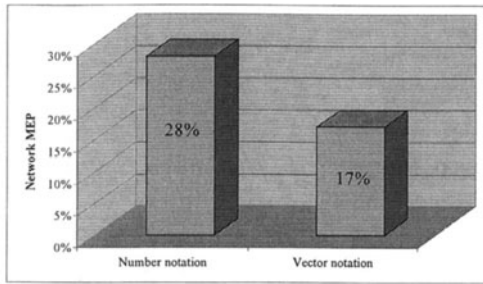


Figure 2: Comparison of performance between number and vector notation.

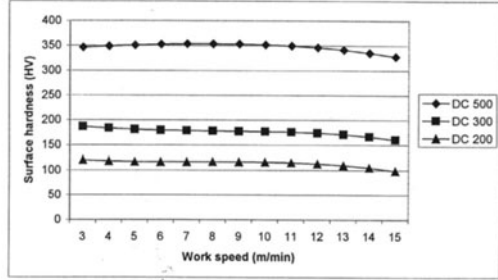


Figure 3: Surface hardness vs. work speed

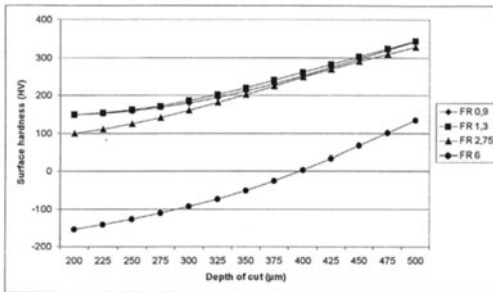


Figure 4: Surface hardness vs. depth of cut

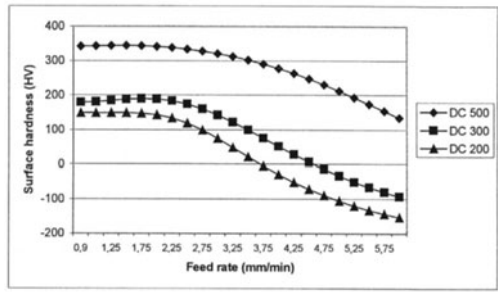


Figure 5: Surface hardness vs. feedrate

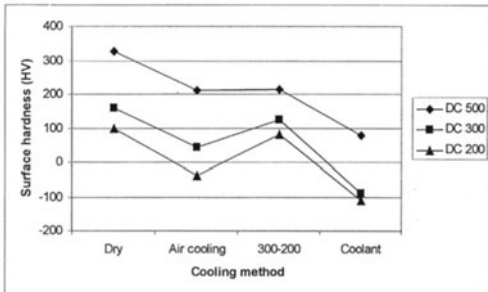


Figure 6: Surface hardness vs. cooling method

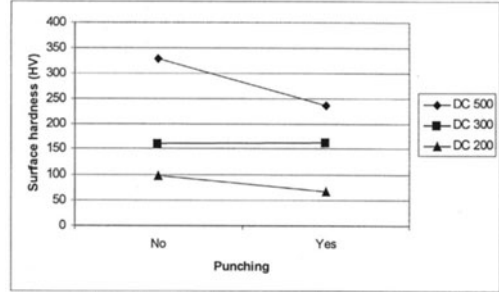


Figure 7: Surface hardness vs. existence of punching

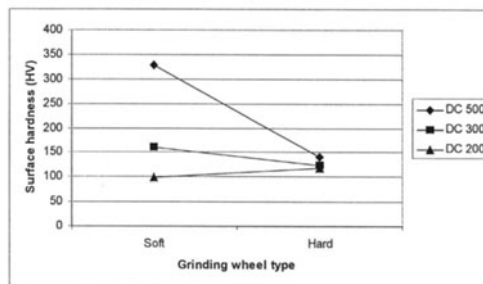


Figure 8: Surface hardness vs. grinding wheel type

6. DISCUSSION

From the figures 3 to 8, conclusions can be deduced concerning the impact of each parameter on the surface hardness. In figure 3, the surface hardness vs. the work speed is depicted. It is clear that the surface hardness shows a decrease, as the work speed increases. This is due to the fact that higher work speeds do not allow for enough interaction time between the grinding wheel and the workpiece. Another point that derives from figure 3 is that, as the depth of cut increases, there is also an increase of the surface hardness. This conclusion is better observed in figure 4, where a rise in the depth of cut produces an increase of the surface hardness, due to higher heat production. In addition, it is shown in the same figure that for high feed rates and low depth of cut, negative surface hardness is predicted. This can be interpreted as the inability of inducing phase transformations to the workpiece when large feed rates are used. The same phenomenon is depicted in figure 5, where the model predicts negative surface hardness for high feed rates and low depth of cut.

Concerning the qualitative parameters, the different cooling methods yield different surface hardness. The highest hardness is achieved when using no coolants, as observed in figure 6. This result is reasonable, as any use of coolants would absorb heat, which is crucial for the heat treatment of the workpiece. The negative values of surface hardness when using lower DC values express the fact that no grind-hardening is possible when using any cooling method with low depths of cut, except when the process is performed dry. This is mainly due to the fact that coolants absorb the heat produced.

Figure 7 shows that the surface hardness achieved near punched areas is usually lower than in other areas, since the hole allows heat to be dissipated into the coolant or the atmosphere. The effect of DC on the surface hardness is also clear. Finally, figure 8 indicates that a hard grinding wheel does not have great effect on the hardening depth irrespective of the DC setting, in contradiction to the soft grinding wheel.

7. CONCLUSIONS

As already stated, preliminary experiments have shown a strong dependency between the material removal rate Q'_w and the surface hardness [12]. This hypothesis has been verified by the simulation results obtained and discussed in the previous section, since the material removal rate depends on the workpiece speed and the depth of cut. It is evident that, since the workpiece speed shows small impact on the surface hardness, compared to that of the depth of cut, the behavior of the material removal rate is mainly influenced by the depth of cut. As the increasing depth of cut increases the surface hardness, then we can reach to the conclusion that as Q'_w rises the surface hardness increases.

In addition, the fact that the simulation results verify the experimental observations indicates the reliability of the model. The network can be used for further investigation of parameter dependencies.

The workpiece material is also reported to be an important parameter concerning the surface hardness [12]. Thus, future work should include this parameter in the experimental process and in the neural network modeling process, in order to determine its impact on the process result.

REFERENCES

1. Toenshoff, H.K., J. Peters, I. Inasaki and T. Paul: Modeling and Simulation of Grinding Processes, 1992, CIRP Annals, V.41 n. 2: 677-688.
2. Brinksmeier E., H.K. Toenshoff, I. Inasaki: Basic Parameters in Grinding, 1993, Annals of the CIRP, Vol 42.
3. Rowe, W.B., Li, Y., Inasaki, I., Malkin S.: Applications of Artificial Intelligence in Grinding, 1994, CIRP Annals, V. V.43/2: 1-11.
4. Rowe, W.B., Y. Li, X. Chen and B. Mills: An Intelligent Multiagent Approach for Selection of Grinding Conditions, 1997, CIRP Annals, V.46 n. 1: 233-236.
5. Chryssolouris G.: A comparison of statistical & AI approaches to the selection of process parameters in intelligent machining, May 1990, Transactions of the ASME-Journal of Engineering for Industry, vol. 112, pp 122-131.
6. Leem, C. S., Dornfeld, D. A., Dreyfus, S. E.: A customized neural network for sensor fusion in on-line monitoring of cutting tool wear, May 1995, Transactions of the ASME-Journal of Engineering for Industry, vol. 117, pp 152-159.
7. Rangwala S., D. Dornfeld: Sensor Integration Using Neural Networks for Intelligent Tool Condition Monitoring, Journal of Engineering for Industry, August 1990, Vol 112.
8. Chryssolouris G., M. Lee, J.Pierce, M. Domroese: Use of Neural Networks for the design of Manufacturing Systems, Manufacturing Review, Vol 3, September 1990.
9. Sakakura M., I. Inasaki: A neural network approach to the decision-making process for grinding operations, 1992, Annals of the CIRP Vol.41.
10. Fan, H. T., Wu, S. M.: Case studies on modeling manufacturing processes using artificial neural networks, August 1995, Transactions of the ASME-Journal of Engineering for Industry, vol. 117, pp 412-417.
11. Schutz G., D. Fichtner, A. Nestler, J. Hoffman: An Intelligent Tool for the Determination of Cutting Values based on Neural Networks.
12. Brinksmeier E.: Utilization of grinding heat as a new heat treatment process, 1996, Annals of the CIRP Vol.45.
13. Chryssolouris G.: Manufacturing Systems Theory & Practice, 1992, Springer Verlag, New York, pp 275-276 & 306-311.

HIGH PERFORMANCE GEARS HOBBING

S. Durante and M. Comoglio

Centro Ricerche FIAT, Orbassano (TO), Italy

F. Rabezzana

METEC Tecnologie, Turin, Italy

KEY WORDS: Machining, Hobs, Coating, Gear, Methodology, Mills

ABSTRACT: A new collaboration activity between Fiat Research Centre, Metec, and Iveco truck manufacturer has been conducted in order to improve durability and machining performances of HSS cutting tools for hobbing operation on high performance steel engine gears.

Hobs are very critical tools, in fact they show complex geometry which needs difficult thermal treatments, expensive technologies and precious materials for substrate and coatings. For this reasons the hobs are very expensive and it is mandatory to increase their life.

1. INTRODUCTION

In order to improve the life of the hobs and their machining performances, an integrated activity between laboratory research and industrial experience has been conducted.

So two big phases can be individuated in this activity:

- laboratory testing and analysis;
- field production final tests;

the first one concerning in the development and set-up of a rapid methodology able to explore a wide range of coating/substrate coupling solutions, so in order to reduce the number of possible combinations for production tests.

So a new methodology has been developed in order to explore rapidly a wide range of solutions.

Published in: E. Kuljanic (Ed.) *Advanced Manufacturing Systems and Technology*,
CISM Courses and Lectures No. 406, Springer Verlag, Wien New York, 1999.

2. APPROACH AND METHODOLOGY

The need to develop a new methodology comes from the need to reduce the costs connected to the hobs experimentation: production, coatings, machining costs.

As we said above, hobs are very expensive tools for the following reasons:

- selected materials, powder metal characterised by high value of hardness and resistance;
- high performance coatings, with good adhesion and high tribological behaviour;
- complex geometry, obtained from grinding operation, carried out by using high precision machines. Grinding operations are always very critical phases for residual stresses and tolerances.

In the next picture (fig.1) it is possible to appreciate the complex geometry of a hob.

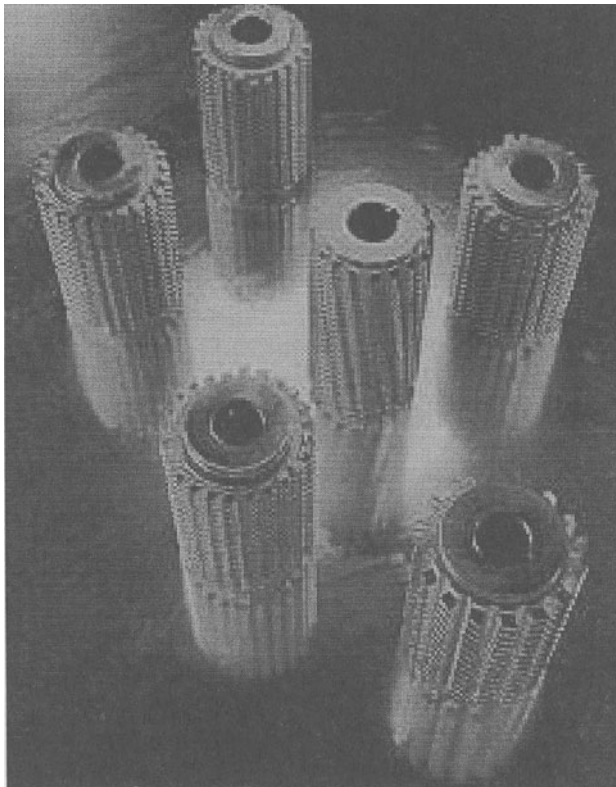


Figure 1- Hobs coated by Titanium Nitride.

The developed methodology, as shown in next illustration (fig.2), starts from the **Machining process analysis** and from the **Used hobs analysis**.

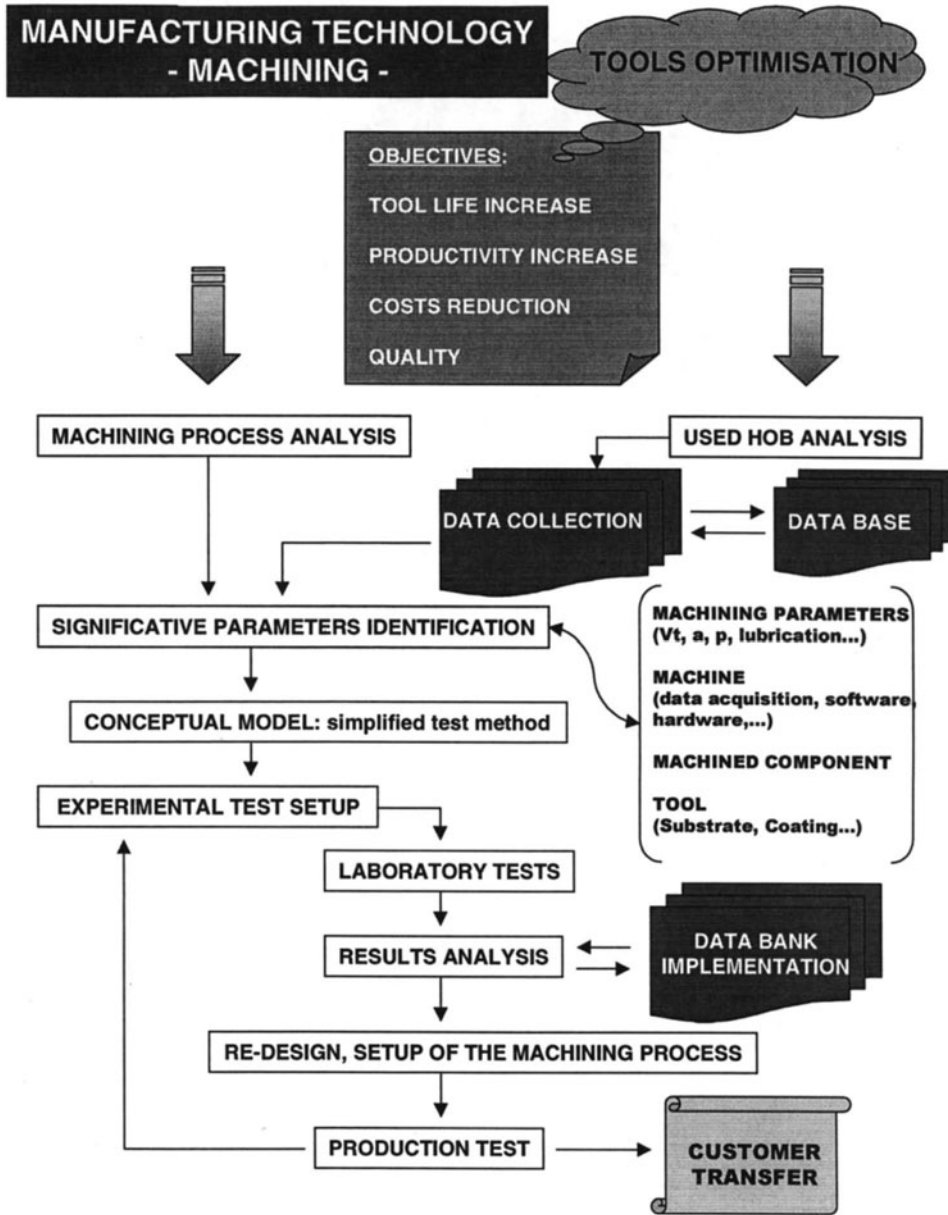


Figure 2- The developed methodology.

The results of the used tools analysis have been implemented on an important **Data collection**. The data collected have been then compared within our **Data base** and are completed by the Machining process analysis results in order to obtain a **Significant parameters identification**.

The analysed hob has been manufactured in TiN coated HSS-PM (Powder Metal High Speed Steel).

In particular, the Significant parameters identification includes the following data:

- machining parameters: cutting speed, feed rate, depth of cut, shifting, lubrication (dry), etc.;
- tool parameters: geometry, substrate (materials, manufacturing process, thermal treatment, previous machining operations, structural defects), coating (materials, substrate preparation, deposition process, multilayer synergy, adhesion, possible structural defects);
- machine parameters: software, hardware, data acquisition, vibrations, tool fixing, workpiece positioning, workpiece fixing);
- workpiece: geometry, material, production process, thermal treatment, previous machining operation, possible structural defects.

The following step is the creation of a **Conceptual model** for experimental tests set-up. This step is the most critical phase of the entire methodology, in fact it is necessary to overhaul a **Simplified test method** considering all the significant parameters find before.

In our case, the most effective method consist in use modular mills. These mills have the same profile geometry of the hobs, but are very easy to produce and to test.

Of course this simplified test method not permit to evaluate some characteristics machining parameters like shifting. Anyway these mills are able to accurately simulate the wear behaviour of the hobs, and allow us to compare several combination substrate-coating at low costs.

The experimental methodology has been developed during the **Experimental test set-up**: the experimentation success comes from a good planning and a careful selection of materials, tools, machine.

So, the **laboratory machining test** have been conducted using modular mills mounted in a five-axis milling machine. The machining parameters and the workpiece materials were the same used in production for hobbing the high performance gears and has been tested in wet and dry cutting conditions.

During the session of machining on a parallelepiped specimen, the adsorbed mill machine energy has been monitored, then the wear rate of the tool was measured and analysed on the computer.

The obtained results, in terms of wear behaviour of the different combination substrate-coating, have been analysed and introduced in our **data bank**.

The analysis of the results of the experimental test have been used as input for the hobs **re-design activity**, and for the **machining process set-up**.

The hobs were modified as follows:

- the geometry of the tooth of the hob has been modified in order to reduce possible vibration phenomena;
- a new substrate material has been used, with better characteristics in terms of toughness and chipping reduction;
- new coating solution has been adopted.

The machining process parameters have been optimised on the ground of the hobs modifications.

The final phase, which is still running, is the **production field testing**, where all the previous results should be confirmed.

3. LABORATORY MACHINING TESTS

The machining tests have been carried out using a five axis milling machine.

The milling tools have been manufactured using different HSS-PM steel materials. In the next table the compositions of the substrate materials are illustrated:

Materials	Chemical Composition							
	C	Cr	Mo	W	V	Co	Mn	Si
MAT A	2.3	4.0	7.0	6.5	6.5	10.5		
MAT B	1.55	4.0		12.25	5.0	5.0	0.3	0.3

Table 1- Substrate materials composition

Different types of coating were used during our investigation.

The coating materials characteristics are shown in the next table.

	TiN	TiCN M.P.	Ti ₂ N	TiAlN	TiAlCN
Opt. Thickness (µm)	1-20	1-8	1-5	1-5	1-5
Hardness (HV 0,01)	2.200-2.400	3.000-4.000	2.400-2.700	2.400-2.800	3.200-3.400
Critical Load on HSS (N)	60-80	50-70	50-70	-	-
Friction Coefficient against 100C6	0,67	0,57	-	-	-
Oxidation resistance (T°C ¹ hour in air)	450-500	450-500	450-500	700	600

Table 2- Characteristics of hard Ti-based coatings produced with the Cathodic Arc technology

A brand new type of coating was applied: MOVIC. This coating is a particular MoS₂-based coating, able to drastically reduce the friction coefficient between the tool and the workpiece, during the machining operations and it has been applied in addition to the Ti-based coatings.

The following table shows its mechanical properties:

Characteristic	Values
Friction Coefficient against steel	in vacuum : 0,01- 0,04 in dry air : 0,01 - 0,04 in wet air : 0,2 - 0,3
Temperature Resistance	800°C
Hardness	1-2 MOHS (25-40 HV)
Deposition Temperature	≤ 150°C
Coating thickness	0,5 - 1 micron
Microstructure	lamellar hexagonal
Laminar Dimension	Submicronic

Table 3- Characteristics of MoS₂-based coatings produced with the PLATIT technology.

The milling tools used have been shaped in order to exactly reproduce the hob geometry. The machine used in the tests, has been selected because of high rigidity, in order to reduce possible tools damage due to vibration phenomena.

The machining parameters adopted during the test were the same hobs parameters used in the production field.

The machined materials was the same as the material of the gear workpiece.

4. TEST PROCEDURE

A parallelepiped specimen has been fixed in the milling machine and a series of parallel milling cuts have been performed on it.

All the mills Ti-based coated have been tested in wet cutting conditions (oil emulsion), while all the tools Movic coated tools have been tested in dry cutting conditions. The reason of this choice is that MoS₂-based coatings are soluble in water, so they are unable to work in oil emulsion, but they can only work in mineral oil or dry environment.

After every session of machining, a microscope analysis of the milling cutting edge has been carried out, so it has been possible to draw the wear curve.

In the next picture (fig.4) is possible to appreciate the wear on a teeth. In this case is possible to observe a coating detachment. In fact, the typical sollicitation on the top zone of the teeth is a shear stress.

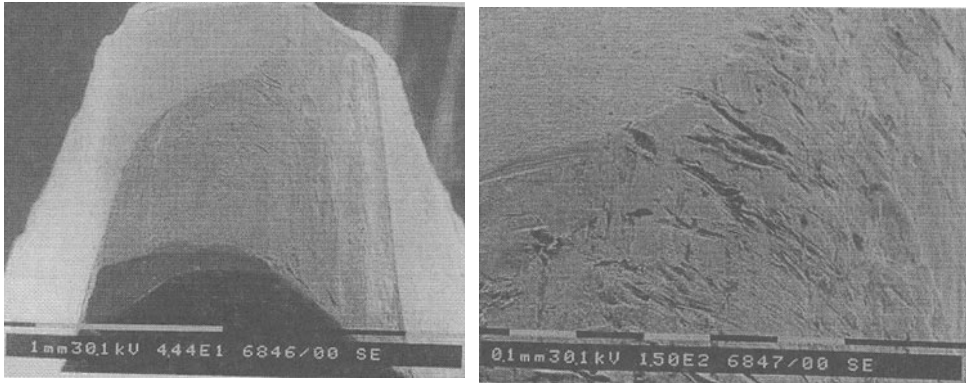


Figure 4- Wear on a teeth: coating detachment-44X

Figure 5- Wear on a teeth: interface zone between the not-damage coating and the damage-substrate -150X

In particular, increasing the magnification (fig.5), is possible to examine the interface zone between the not-damage coating and the damage-substrate. In this case it is possible to appreciate the anti-wear properties of the coating: the zone where the coating comes off is characterised by high value of wear.

The bigger zoom permit to evaluate, in the following pictures, the detachment mechanism of the coating:

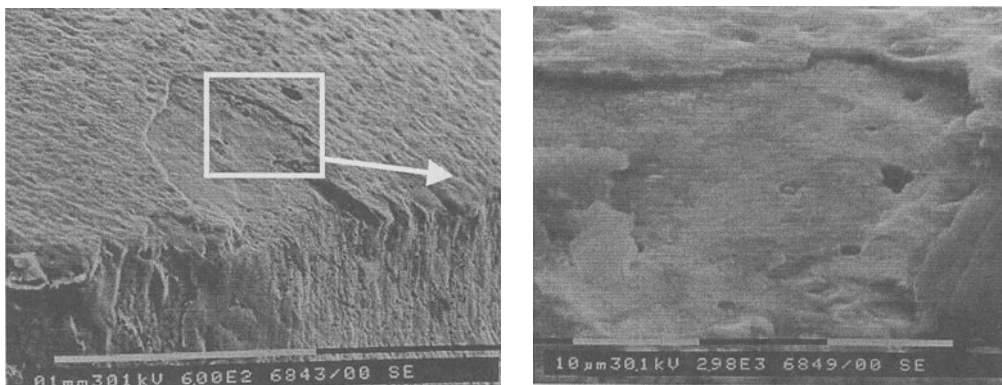


Figure 6- Wear on a teeth: detachment mechanism of the coating-600X

Figure 7- Wear on a teeth: detachment mechanism of the coating-3000X

We have found fragile fracture on the top of the teeth of the tool. The crater wear has been contained.

In particular chip off phenomena has been found in the coating, due to low adherence between coating and substrate.

5. CONCLUSION

The first results of different machining tests, started in dry cutting conditions at standard cutting speed, show the advantages of using innovative duplex TiAlN + MoS₂ PVD coated hobs rather than standard TiN coated hobs.

In particular the duplex TiAlN + MoS₂ PVD coatings tested in hobbing operations show the following indications:

1. In hobbing operations with HSS hobs, good tool life increments are gained by using TiAlN + MoS₂ coatings compared with standard TiN coated tools.
2. The reason for this improvement is the high “autolubricant” property of the soft coating combined with the high hardness of TiN, and the good resistance to temperature of external MoS₂ coatings.
3. In comparison with standard TiN coated hobs, with the duplex TiAlN + MoS₂ coated hobs have increased the tool life due a lower crater and flank wear, which means a strong decrease of flank wear at the same tool life productivity.

AUTOMATIC PART GEOMETRY AND MATERIAL REMOVAL RECOGNITION TO OPTIMIZE THE CUTTING CONDITIONS ALONG TOOL PATHS IN NC-MILLING

K.D. Bouzakis and R. Paraskevopoulou
Aristotle University, Thessaloniki, Greece

KEY WORDS: milling, workpiece shape recognition, cutting strategies and conditions optimization

ABSTRACT: A computer-supported procedure to create NC-code with optimum paths and cutting conditions in 2 ½ axis NC milling is introduced. The raw material and the final workpiece shape are derived from an IGES file created by means of the used CAD system. Various tool motion strategies with optimized cutting conditions are checked, that one leading to a minimum cutting time is selected and the corresponding NC-code is generated. The optimum values of feedrate and cutting speed for every region of the examined tool path are calculated considering cutting forces, tool wear, machine tool power and tool deflection.

1. INTRODUCTION

The automatic selection of cutting conditions is an essential step for the creation of a computer integrated manufacturing environment and affects greatly the machining efficiency and the cost of the machined components [1]. However, the commercial CAM systems are mainly geometrically oriented and they do not offer facilities for a technology based optimization, which is necessary to improve the manufacturing accuracy and time.

In the present paper, a computer supported procedure for the automatic recognition of part geometry and material which has to be removed, as well as for the optimization of the cutting conditions in 2 ½ axis NC-milling is presented. The raw material shape and the final workpiece geometry of a machining setup are derived from a neutral file, as for

Published in: E. Kuljanic (Ed.) *Advanced Manufacturing Systems and Technology*,
CISM Courses and Lectures No. 406, Springer Verlag, Wien New York, 1999.

example an IGES one, created by the used CAD system. The workpiece is considered to be intersected by parallel machining planes, perpendicular to the cutting tool axis, as shown in [Figure 1](#). The distance between two successive machining planes is, generally, equal to the used axial depth of cut, while horizontal planes containing initial part features derived from the IGES file are automatically defined as ‘machining planes’. The initial, the final workpiece shape (external part outline and machining features if any exist) and the material, which has to be removed on each machining plane, are recognized through developed algorithms [2,3]. These algorithms, as well as the determination of an optimum tool motion strategy are described in the next paragraphs. The optimization of the cutting conditions along a tool path is conducted according to a procedure introduced in [4,5].

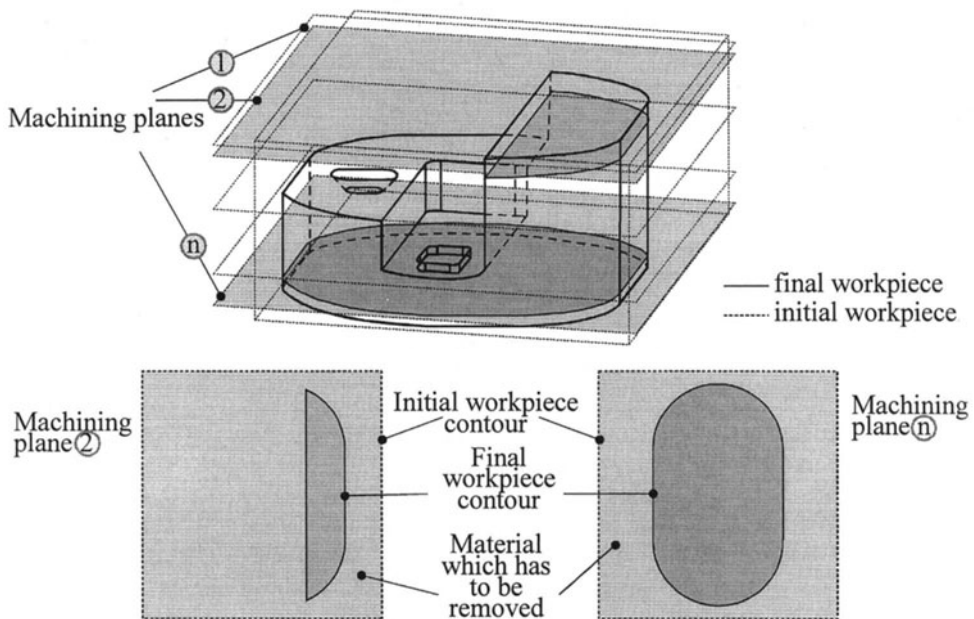


Figure 1: Definition of machining planes and of the raw material to be removed, on each of them

2. DETERMINATION OF MATERIAL TO BE REMOVED ON MACHINING PLANES

In order to determine the material, which has to be removed on every machining plane, it is necessary to define the initial and final workpiece geometry on each of them. Using a CAD system, commonly, the part geometry is described, without calculating intersections with the machining planes. For this reason, an appropriate procedure has been developed, which moreover recognizes the material to be removed on the successive machining planes. The steps of this procedure are:

- determination and classification of horizontal planes containing initial part features,

- non horizontal edges correlation to the horizontal features, as well as machining planes definition and
- determination of workpiece intersection shape with every machining plane.

2.1 DETERMINATION AND CLASSIFICATION OF HORIZONTAL PLANES

The geometrical model of the workpiece can be accomplished using any commercial CAD software, offering wire-frame possibilities and having an IGES output translator. The geometrical elements of the contours are supposed to be straight lines or circular arcs, considering the common control facilities of a 2 ½ milling machine.

After the recognition of the entities ‘line’ and ‘circle’, the entities which do not lay on horizontal planes (‘non horizontal entities’) are separated and acquire specific direction. The direction is defined in such a way that the Z coordinate value of every non horizontal entity final point is smaller than the Z coordinate of its initial point. The horizontal entities are sorted on horizontal planes according to their Z coordinate value. By this way, all the horizontal planes containing features are recognized and classified in descending order. Furthermore, all the horizontal plane entities are recognized, oriented and herewith the final point of an entity is the initial point of the next entity. Wherever this connection is not possible, a new shape is created. By means of this procedure, all features on every plane and all the elements of every feature are determined, classified and numbered as illustrated in Figure 2.

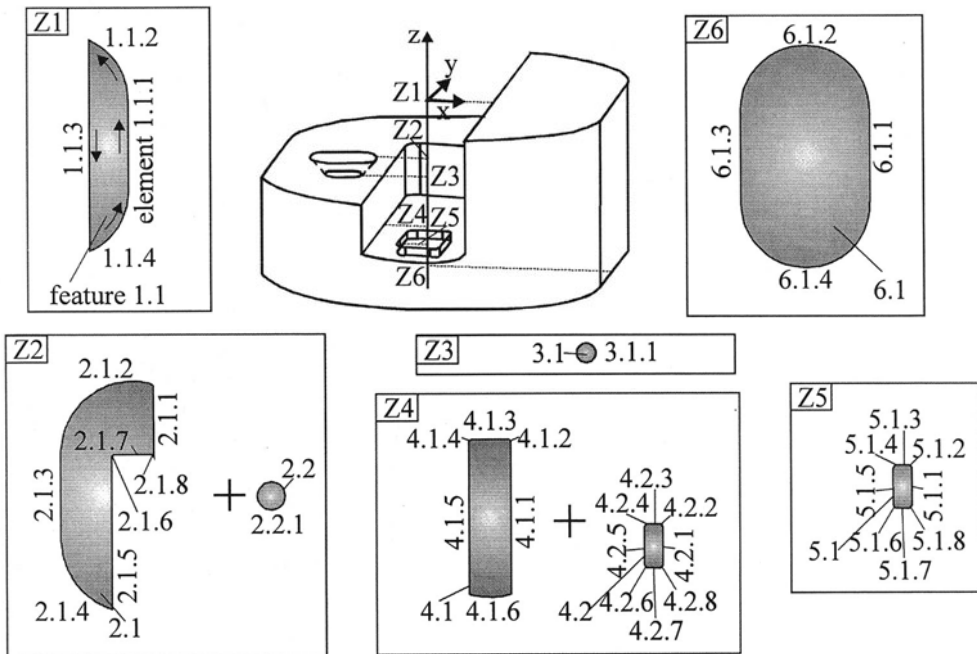


Figure 2: Determination and classification of horizontal planes, features and elements

2.2 MACHINING PLANES DEFINITION

The initial point of every non horizontal entity (as for example the line NE1 in Figure 3) is identical with the initial point of a specific horizontal element (in the examined case, the line E2.1.5). This horizontal element has already been classified and belongs to a specific feature (2.1), that in turns lays on a specific horizontal plane (Z2). The same procedure is repeated for all the final points of every non horizontal entity. Using this approach, as presented in figure 3, the non horizontal edges are correlated to the horizontal features.

Furthermore, the workpiece is intersected by horizontal machining planes. To define the machining planes, the user determines the axial depths of cut. Considering these values it is examined if the horizontal planes containing features, which have to be machining planes, are already selected. If this is not the case, modifications of the axial depth of cut values are required and carried out automatically, to make them machining planes. If more than one features exist on the same machining plane, the user can define different axial depth of cut for each specific feature.

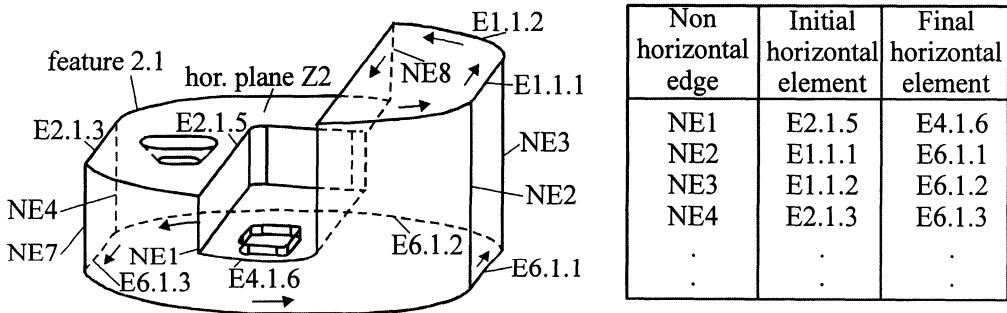


Figure 3: Non horizontal edges correlation to the horizontal features

2.3 WORKPIECE SHAPE RECOGNITION ON MACHINING PLANES

On every machining plane the intersection points with the non horizontal edges are calculated. These points are the vertices of the features describing the workpiece shape on the specific machining plane. The part geometry on a particular machining plane is conducted by means of the following procedure. The vertex having the maximum X coordinate value (point P1 at the upper left of the Figure 4) is determined and located on a non horizontal edge (NE2), associated with the related horizontal feature element (E.1.1.1). The next horizontal element (E1.1.2) of the specific horizontal feature is considered, in order to define the corresponding non horizontal edge (NE3). Hereby, two cases are distinguished:

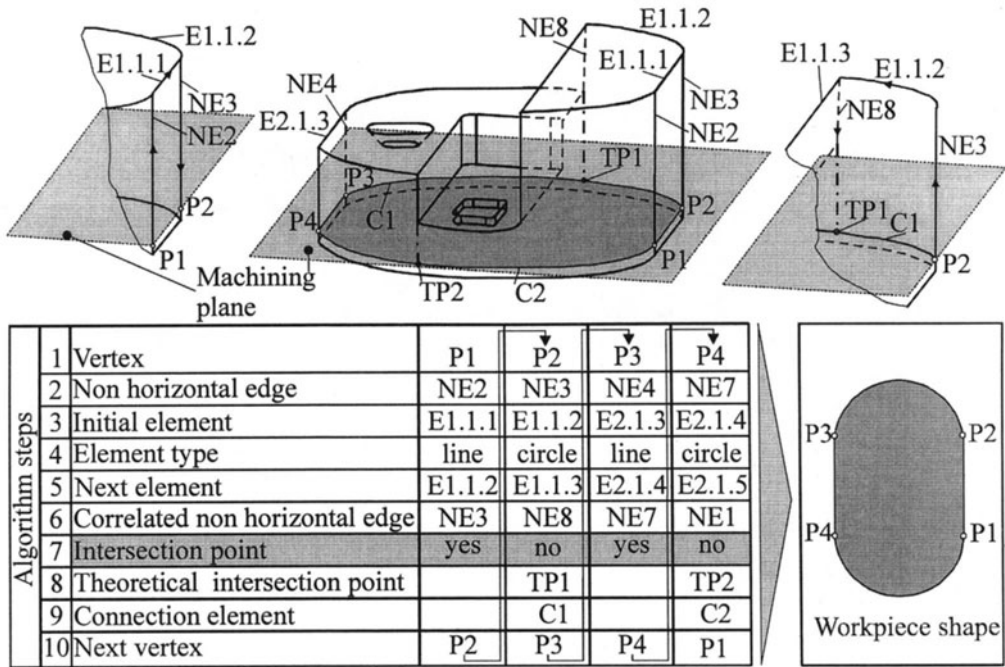


Figure 4: Algorithm steps for the workpiece shape recognition on every machining plane

If there is an intersection point between the horizontal plane and the specific non horizontal edge (as for example point P2), this is considered to be the next vertex of the workpiece shape on the specific machining plane. The two vertices are connected through an entity of the same type (line P1P2) as the horizontal feature entity (E1.1.1), where the first intersection point is located, as shown in figure 4.

If none intersection point exists (as shown at the upper right of the figure 4), considering the type of the horizontal feature element with which the first vertex has been associated, the following algorithm is applied. If the horizontal feature element (E1.1.2) is a circular arc the methodology is as follows: The non horizontal edge (NE8), to which the next element has been corresponded, is extended and the intersection point with the horizontal machining plane is calculated (TP1). This point and the previous vertex, belong to a circle, which has as center the projection point of the corresponding horizontal feature element (E1.1.2). Furthermore is examined which of the rest intersection points (P3 and P4) belongs to this circle. This point is the next vertex of the workpiece shape on the specific machining plane.

A similar methodology is followed, if the horizontal element is a straight line. This procedure is repeated for every intersection point between the non horizontal edges and the machining plane (as presented in figure 4).

If the workpiece shape is complex, consisting of more than one closed contours, it is examined whether each of the closed contours corresponds to an external geometry, pocket or island. This is accomplished by checking if the contour's vertices are situated inside of other closed contours placed on the same horizontal machining plane and the appropriate conclusion is arrived. The above presented methodology is applied twice, once for the raw material shape and once for the final workpiece's shape recognition for every set-up.

3. TOOL PATH STRATEGY SELECTION AND CUTTING CONDITIONS OPTIMIZATION

Considering the initial and final workpiece shape in every set-up, the raw material volume, which has to be removed on all machining planes, is defined, as shown in figure 1. The raw material removal can be accomplished using various strategies, related to the tool movement mode. Hereby, three most common strategies are considered: tool motions are either parallel to the axis X, or to the axis Y or parallel to the workpiece contour. For each of them, the tool paths on a particular machining plane, using a prescribed radial depth of cut are determined and the optimum cutting conditions for every tool path region are calculated. Tool path regions are distinguished according to a procedure introduced in [4,5]. The cutting strategy is selected, which leads to the shortest cutting time.

The developed methodology for the determination of the optimum cutting conditions uses process simulation algorithms [4,5,6] which enable the calculation of the chip geometry, of the cutting force components, as well as, of the tool wear behavior, required for the determination of optimum cutting conditions, with regard to the manufacturing cost.

Considering, as optimization criteria, the maximum available machine power, as well as the maximum permitted cutting edge load for roughing and an allowed maximum tool deflection for finishing, the maximum permitted force and the corresponding feedrate value for every tool path region are determined. Furthermore, regarding as optimization target the achievement of minimum manufacturing cost, the optimum values for the cutting speed in each of the introduced regions are also defined. The determined optimum values may be limited by the machine tool capabilities. For every tool path, the cutting time, with optimized cutting conditions in all its regions, is calculated. The cutting strategy leading to the shortest manufacturing time is selected, and the corresponding NC-code is automatically generated.

An application of the developed procedures is demonstrated in the case of a test part presented in figure 2. Twenty machining planes have been defined by means of an initial axial depth of cut, selected by the user. The designation of the horizontal planes containing features (shown in figure 2) as 'machining planes' is conducted automatically. After the workpiece geometry recognition, the required data for tools, cutters overlapping on every machining plane and initial cutting conditions are also selected by the user.

In [Figure 5](#), the tool paths for the roughing of the feature 1 on the machining plane $Z=-45$ are illustrated, according to the three strategies, which have been considered. The corresponding cutting time with initial and optimized cutting conditions for each strategy has been calculated and is inserted in figure 5, too. The machining of the feature 1 will be

realized with tool motions parallel to the workpiece contour, because this strategy leads to the shortest cutting time. The reduction of the cutting time achieved between the worst cutting strategy with initial cutting conditions and the best tool motion strategy with optimized cutting conditions is about 33 %. Similar results are concluded for every machining plane. Figure 5 shows moreover a section of the NC-code for the machining of contour 1, on the specific machining plane, according to the selected tool movement strategy and the optimized cutting conditions. This NC-code section corresponds to the tool path regions indicated by wider solid line on the upper right part of figure 5.

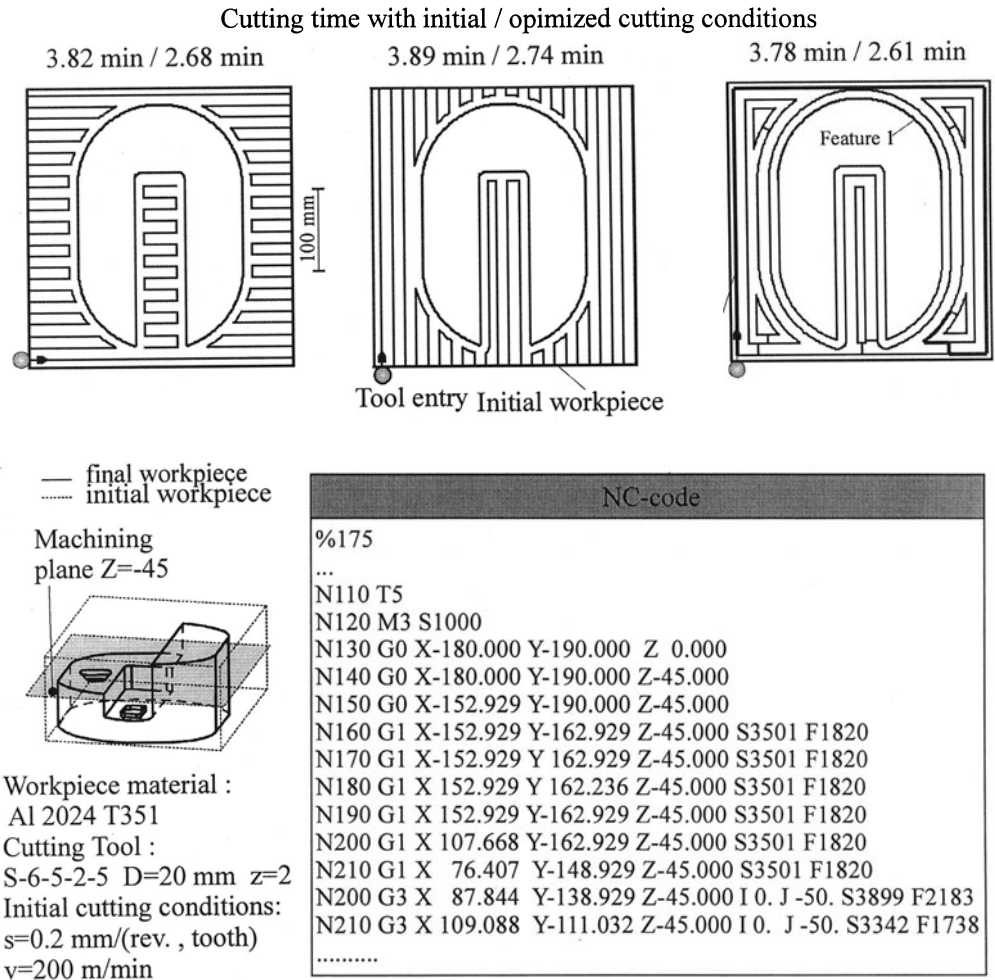


Figure 5: Tool motion strategies for the machining of feature 1 and NC-code with optimum cutting conditions

4. CONCLUSIONS

The presented methodology to select the appropriate tool motion strategy and create NC-code with optimum cutting conditions, considering the IGES part file, can be used to reduce the manufacturing cost and time. The methodology includes the steps:

- Machining planes definition and recognition of the initial and final workpiece shape on every machining plane.
- Selection of the tool movement strategy so that a minimum cutting time is achieved.
- Optimization of the cutting speed and of the feedrate for every tool path region and NC-code generation.

REFERENCES

1. Armarego, E. J. A., Smith A. J. R., Wang J. : Computer- aided constrained optimization analyses and strategies for multipass helical tooth milling operations, *Annals of the CIRP*, vol. 43/1/1994, pp. 437-442.
2. Bouzakis, K.-D. and Paraskevopoulou, R. : Feature - based cutting conditions optimization on the tool path in 3-axis milling, *CIRP International seminar on intelligent computation in manufacturing engineering, Capri, 1998*, pp. 531-538.
3. Paraskevopoulou R. : Optimization of the cutting conditions along tool paths during NC milling based on geometrical workpiece data derived from a CAD neutral file and on the automatic determination of the cutting tool paths, Ph. D. Thesis, Aristoteles University, Thessaloniki.
4. Bouzakis, K.-D. Efstathiou, K. and Paraskevopoulou, R. : NC-Code Preparation with Optimum Cutting Conditions in 3-Axis Milling, *Annals of the CIRP*, vol. 41/1/1992, pp. 513-516.
5. Bouzakis, K.-D. Efstathiou, K. and Paraskevopoulou, R. : NC milling with optimum cutting condition in CIM environment, *25th CIRP seminar on manufacturing systems, Bled-Slovenia, 1993*, pp. 197-210.
6. Bouzakis, K.-D. and Methenitis, G : Determination of the technological parameters, which are used to describe the time course of cutting force components in milling, *Annals of the CIRP*, vol. 34/1/1985, p.p. 141-144.

AN INTEGRATED MODEL FOR CUTTING PARAMETERS OPTIMIZATION AND SHOP-FLOOR SCHEDULING

E.P. Henriques and R. M. D. Mesquita
Instituto Superior Tecnico, Lisboa, Portugal

KEY WORDS: Dynamic Process Planning, Machining Optimisation

ABSTRACT: Trends towards the reduction of batch sizes and decreased throughput times determined the need for improved process and production planning activities. This paper presents a new contribution for the integration of process planning and production scheduling and control, towards the development of a fully dynamic shop floor control system. It is presented also a new methodology and model for dynamic process planning and machining parameters optimisation. In our approach, at the detailed process planning level, information on the shop-floor load status is retrieved from a scheduling system. This information is used to enable the selection of available machine tools, as well as cutting tools, and to allow the optimisation of cutting parameters considering the available machining time at every workstation.

1. INTRODUCTION

Trends towards the reduction of batch sizes and decreased throughput times determine the need for improved process and production planning activities. Full utilisation of production resources requires an integrated approach for process and production planning, to avoid excessive machine-tool downtime, unbalanced lines, increased waiting times, the selection of non-optimal or unavailable routings. Optimal selection of machine tools, cutting tools and cutting parameters must consider the current status of the shop floor. The processes, operation sequences, fixtures and cutting tools required to produce the part, are identified in the process plan. Traditionally, process planning is performed considering a static approach; the generated plans are compatible with the capability of the shop-floor resources but an infinite capacity of these resources is assumed. However, the competition of simultaneous jobs to use the limited manufacturing resources, together with some unpredictable events (machine breakdowns, rush orders, lack of tools, delays, etc.), contributes to an environment characterised by a dynamic behavior. Quite often the process plans

generated with reduced information from production scheduling contribute to an unbalanced loading of resources. This fact is a main contribution to the poor performance of conventional shop floor scheduling, in what concerns the control of work-in-progress or the achievement of due dates, in small batch-type manufacturing. The resultant improvised re-planning at the shop floor, with little assistance from a process planning system, may lead to a non-optimal process plan and consequently to decrease manufacturing efficiency.

During the last few years some effort has been put on the development of methodologies aiming an efficient integration of process planning with shop floor scheduling and control functions. In an industrial environment, characterised by small and medium sized batches, several approaches have been developed mainly oriented towards the generation of alternative process plans for different sets of machine tools enabling the dispatching of alternative routings when required [1,2,3,4]. However, the generation of process plans foreseeing alternative manufacturing routes involves a redundancy of planning work performed through several alternatives that will not be used.

In previous work, the authors developed a prototype of an integrated CAD/CAPP/CAM/TMS system [5]. Some process planning functions, such as, feature recognition, identification of elemental turning operations, tool selection, cutting parameters optimisation and manufacturing cost and time estimation, were completely automated.

The present work aims to extend the existing platform (Figure 1), presenting a new contribution for the integration of process planning and production scheduling and control, towards the development of a fully dynamic shop floor control system. It will be presented also a new methodology for dynamic process planning and machining parameters optimisation. In our approach, at the detailed process planning level, information on the shop floor load status is retrieved from a scheduling system. This information is used to enable the selection of available machine tools, as well as cutting tools, and to allow the optimisation of cutting parameters considering the available machining time at every workstation.

2. DYNAMIC PROCESS PLANNING

Two information flows between the process planning and the scheduling systems are considered in our approach to dynamic process planning (Figure 2). The first one is related with the machine-tool selection module. To achieve a more realistic selection, both technological and load criteria should be introduced. For turning operations one should consider: (1) maximum length and diameter of the work area; (2) minimum achievable tolerance and surface roughness; (3) average load of machine tools within the time horizon defined by internal or external due dates. The second one is a bi-directional flow and is related to the cutting conditions optimisation module, based on machining cost criteria and considering several technological constraints as well as an additional shop floor constraint – maximum available time in the shop floor, at every machine tool.

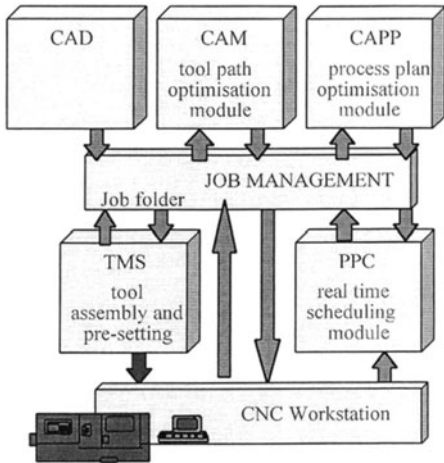


Figure 1 – Computer Integrated Manufacturing platform: manufacturing functions and information flow

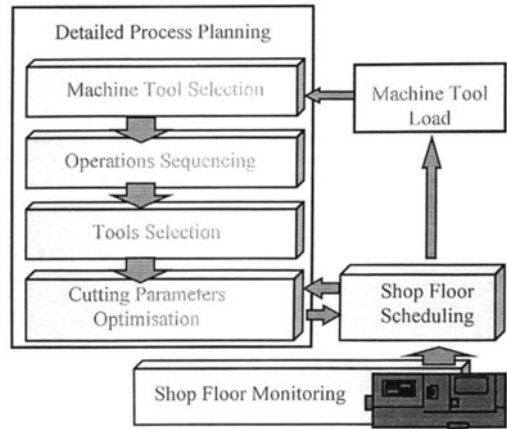


Figure 2 - Integration of process planning and shop floor scheduling and monitoring

The process planning system is automatically informed about the real shop floor conditions at two levels (Figure 2):

1. During the machine tool selection to achieve a more uniform resources load;
2. During the tool selection and cutting parameters optimisation to calculate, if required by the particular shop floor status, cutting conditions in accordance with the available time to perform the job.

The process plan optimisation module calculates the cutting parameters (cutting speed, feed rate and depth of cut) for the minimum manufacturing cost, as well as for the minimum manufacturing time [6,7]. Several technological constraints, related to part geometry and required quality, workpiece material, machine tool, cutting tool and fixture devices, are considered.

Two process plans are generated, one for minimum cost and another for minimum time, being automatically sent to a shop floor scheduling system. The first one, the so-called active plan, is the one that is considered for scheduling purposes. The second one, is a constraint plan, since it contains the information concerning the minimum time required to machine the part (Figure 3).

In case of an unbalanced load or an expected event (overload of the particular resource, breakdown, due date not met), an alternative process plan is requested (Figure 4). Depending on the particular situation, this alternative plan can convey another machine tool, cutting tool or a new set of cutting conditions to meet the available time for the job at a particular machine tool. In this situation the optimisation module must be informed about

the maximum time available on the machine tool to process the job. It is important to remark that this maximum available time has threshold values and is limited by the manufacturing time for minimum cost (active plan) and by the manufacturing time for maximum production rate (constrain plan).

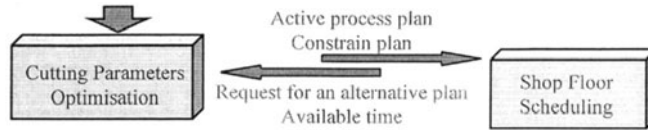


Figure 3 - Information flow between the scheduling system and the optimisation module

Considering this new load constraint, the optimisation module determines the new optimal cutting parameters and issues a new plan, which is the minimum cost plan compatible with the particular scheduling conditions. Although the manufacturing cost is superior than the one previously calculated in the first active plan, a decrease in the manufacturing throughput time is achieved.

To support the information flow between both, the scheduling and the process planning (which include the cutting parameters optimisation module) systems, a dynamic scheduling module, based on heuristic rules derived from Kusiak [8], was developed. It is able to: (1) carry out shop floor scheduling, (2) retrieve real-time information about machine-tool status and order progression, (3) ask for new plans if a due date is not met or a better load balance is required, and finally (4) to perform re-scheduling every time a new job is released or the deviations between the planned and the executed job determine such a need.

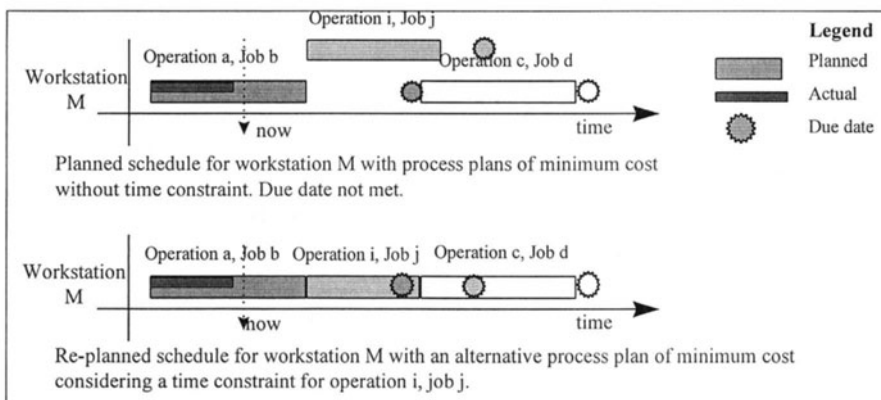


Figure 4 – Initial scheduling and final scheduling with an alternative process plan

The scheduling system receives real-time information on the shop floor status (resources and jobs progression) from a production monitoring system. When a new job is released, or when some variance between the real and the planned jobs determines that the current schedule is no longer valid, all pending jobs are re-scheduled. If any “non-conformity”

concerning the resources load balance or due dates is detected, an alternative process plan is requested and generated for the particular shop floor situation. This new alternative process plan can involve an alternative workstation, a modification in the sequence of the required manufacturing processes, the selection of a new cutting tool or a new set of optimal cutting parameters considering a newly introduced manufacturing time constrain.

3. CUTTING CONDITIONS OPTIMISATION

If we take into consideration the new constrain – available time, the technological / economical models that have been reported in the literature pertaining to cutting parameter optimisation, such as the one developed by one of the authors [7] should be modified. In the “conventional” models, the search for the optimal parameters is performed, for every elemental operation, in an independent way, being the total part machining time the addition of optimal machining time for every elemental operation (using the minimum cost or minimum time criteria or both). However, the authors consider that, if the actual machine tool load constraint determines that the total available time is smaller than the machining time for minimum cost, the solution must be found in a different context. In this situation, all the operations required to produce the part (considering productive and unproductive times) must be aggregated. The required reduction on part machining time must be reflected on every operation. This reduction on machining time cannot be evenly distributed in every elemental operation, since the cost associated with each operation has different sensibilities to time changes (and consequently to optimal machining parameters). The optimal cutting parameters for all operations become dependent from each other and the optimisation process must cover all of them simultaneously.

In our system, a new cutting parameter optimisation module was developed using the Sequential Quadratic Programming method. The system aims the optimisation of an operation-aggregated cost function for complete part manufacturing subjected to a set of technological constraints for every elementary operation as well as to a maximum part machining time constraint.

In the proposed optimisation model, the objective function is the sum of the machining cost for every elemental operation, C_i , each one depending on three decision variables: cutting speed, v_i , feed rate, f_i , and depth of cut, a_i :

$$\min \left[\sum_{i=1}^{n^{oper}} C_i(v_i, f_i, a_i) \right]$$

A set of technological constraints related to the part geometry, part material and part quality, tool geometry, tool quality and tool life, machine tool and fixture devices are considered for each operation:

$$g_{ij}(v_i, f_i, a_i) = 0 \quad \text{where } j = 1, \dots, k; \quad i = 1, \dots, n, \text{ operations}$$

$$g_{ij}(v_i, f_i, a_i) \leq 0 \quad \text{where } j = k+1, \dots, n; i = 1, \dots, n. \text{ operations}$$

Finally a shop floor constraint is introduced, when required, by a load criterion:

$$\sum_{i=1}^{n^{oper}} g_{i,n+1}(v_i, f_i, a_i) - t_{max} \leq 0$$

where $g_{i,n+1}$ is the machining time for operation i and t_{max} is the maximum available time on the machine tool to produce the part.

4. CASE STUDY

One of the first steps to generate a process plan is the elemental operations recognition. Figure 5 presents a rotational part with 6 elementary operations automatically identified by the CAPP system. To perform tool selection and cutting parameters optimisation machine-tool information is required. Table 1 presents some technological, economical and time data for a typical CNC lathe. For every operation a set of tools is selected. The optimisation of the cutting parameters allows the identification of the minimum cost tools for each operation (Table 2).

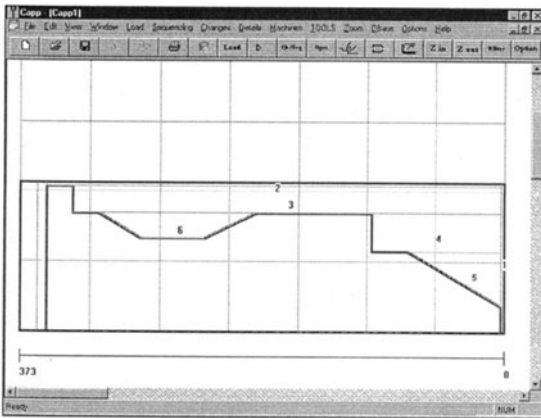


Figure 5 - Elementary operations automatically generated by the CAPP system

Max. Power	-- 50 KW
Max. Speed	-- 3000 rot/min
Min. Speed	-- 200 rot/min
Max. Power Speed	-- 800 rot/min
Rapid Traverse	-- 5000 mm/min
Max. Clamp. Force	-- 100000 N
Setup Time	-- 35 min
Tool Change Time	-- 0.5 min
Adjust Time	-- 0.02 min
Workstation. Cost	-- 48 USD/h

Table 1 - Data for Gildmeister workstation

Under these cutting conditions, the minimum machining cost is 41.8 USD, and the correspondent machining time is 41.1 min. Considering a batch size of 22 units, a 1min clamping and unclamping time cycle, 35min machine set-up time, the machining time required at the workstation to perform the complete job (Job 014) is 962 min. This time frame is not available at the workstation, considering current shop floor scheduling (Figure 6), making the due date for the job not possible. The maximum available time on the workstation (Gildmeister) enabling all due dates is 900 min.

Operation	Tool	Speed (m/min)	Feed (mm/rot)	Depth (mm)	Tool life (min)
1	PSKNL2020K09 SNMG090312-QM 425	272.29	0.50	2.50	9.84
2	PSBNL2020K09 SNMG090312-QM 425	272.29	0.50	2.50	9.84
3	MTJNL2020K16 TNMM160412-QR 435	184.02	0.53	4.85	14.25
4	MTJNL2020K16 TNMM160412-QR 435	173.81	0.60	5.40	14.25
5	PTTNL2020K16 TNMM160412-QR 435	173.81	0.60	5.40	14.25
6	PSBNL2020K12 SNMM120416-QR 435	162.77	0.76	6.68	11.91

Table 2 - Tools for minimum machine cost and optimal cutting parameters

An alternative process plan including new cutting conditions, constrained by the shop floor particular conditions is generated (Table 3). The newly optimised cutting conditions are calculated and the maximum available time to perform the job at the machine is considered. This procedure could be used to generate alternative process plans accommodating up to a 20% decrease on machining time.

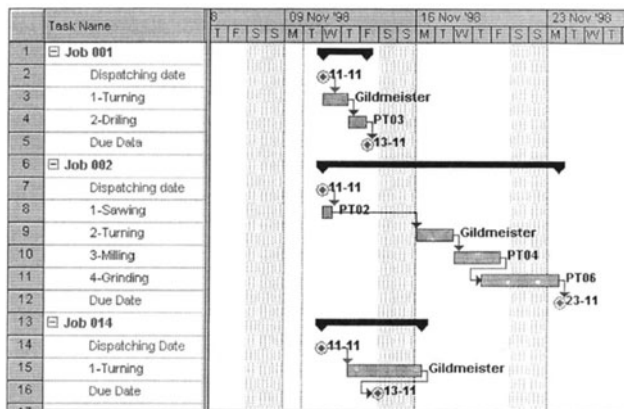


Figure 6 – Shop floor scheduling with simultaneous jobs. Due date for Job 014 is not met.

Operation	Speed (m/min)	Feed (mm/rot)	Depth (mm)	Tool life (min)
1	299.19	0.50	2.50	6.75
2	299.19	0.50	2.50	6.75
3	203.50	0.53	4.85	9.53
4	192.18	0.60	5.40	9.53
5	192.18	0.60	5.40	9.53
6	179.50	0.76	6.68	8.05

Table 3 - Cutting conditions for minimum cost constrained by the maximum machining time

The new plan satisfies the shop floor constrain, since the unit machining time is 38 min. The unit machining cost is now 42.4 USD, which is the minimum cost for the particular shop floor available time.

5. CONCLUSIONS

In this paper it is shown that the selection and optimisation of cutting parameters should not be determined only by cost, technological or quality measures but also by shop floor available capacity. We propose an integrated process and production planning methodology to develop process plans for a real shop floor scenario, aiming to identify and correct any deviation on planned jobs, to avoid less than optimal process planning and to optimise machining parameters, in real time, using the Sequential Quadratic Programming method. Considering this approach, a new variable is introduced for shop floor scheduling and re-scheduling - the part machining time, which can range from the time for maximum production rate to the time for minimum machining cost. Through this variable, adjustments can be made on every optimised running or planned job.

The reduction of manufacturing lead-time can be achieved by integrated process planning and production planning methodologies, where resources allocation are sustained by real-time information on the shop floor behaviour.

6. REFERENCES

1. Usher, J. and Fernandes, K.: Dynamic Process Planning - The Static Phase, *Jour. of Material Processing Tehnologies* 61 (1996), 53-58
2. Wiendahl, H. and Schimdt, B.: A System Solution to Integrated Process Planning and Workshop Scheduling using Manufacturing Alternatives, *Production Engineering*, Vol. II/2, (1995), 149-154
3. Mamalis, A., Malagardis, I., Kambouris, K.: On-Line Integration of a Process Planning Module with Production Scheduling, *Jour. of Adv. Manuf. Techn.* 12, (1996), 330-338,
4. Zhang, H-C.: IPPM - A Prototype to Integrated Process Planning and Job Shop Scheduling Functions, *Annals of the CIRP*, 42(1), (1993) 513-518
5. Mesquita, R., Henriques, E., Ferreira, P.S. and Pinto, P.: Computer Integrated and Optimised Turning, *Proc. AMST'96*, 1996, Italy
6. Mesquita, R. and Henriques, E.: Modelling and Optimisation of Turning Operations. *Proc. 30th Int. MATADOR Conf.*, UMIST, Manchester, 1993, 599-607
7. Mesquita, R., Krasteva, E. and Doytchinov S.: Computer-Aided Selection of Optimum Machining Parameters in Multipass Turning, *Jour. of Adv. Manuf. Techn.*, 10 (1995) 1, 19-26
8. Kusiak, A.: *Intelligent Manufacturing Systems*, Prentice Hall, 1990

A NEW CAM/CNC INTERFACE FOR HIGH SPEED MILLING

R. Ippolito, L. Iuliano and E. Vezzetti
Polytechnic of Turin, Turin, Italy

KEY WORDS: Computer Aided manufacturing, non linear, High speed milling

ABSTRACT: Nowadays the market of good is becoming more and more instable and so the industries must answer to its request in a very short time. This aspect shows the necessity to produce dies and moulds, with flexible and automatic manufacture system, that could grant a good quality also on parts with complex geometry and high speed milling could be an answer to reduce the machine time. The actually CAM/CNC solutions have some limitations with this high speed philosophy because it is difficult to calculate the tool path on real translated surfaces. The CAM system, in fact, gives like information control tool path a number of points starting from an algorithm that maintains the chordal error under a value decided by the operator. This kind of methodology is to much heavy for the CNC computer and can give problems of approximation with the feed rate required, which is in term of m/min. Even if now the CNC system are developing new kind of interpolations with systems that use not only linear mathematical function, but also quadratic and cubic ones, the actual CAM systems continue to give in the post - processor ISO file, punctual information derived from polyhedral approximation. In the paper is presented a possible solution to this problem through the development of an interface between CAM output and the cubic interpolation of CNC machine tool. This interface is tested on an industrial CAM software to control the dimensional coherence between the designed and the manufactured product. Moreover machining tests are performed on a spline CNC interpolation to evaluate the performance of the developed interface in terms of dimensional accuracy and computational costs.

1 INTRODUCTION

Designers use Cad systems to design parts for visual and theoretical analysis. On the basis of the CAD model, the numerical control (NC) programmer uses the CAM system to

Published in: E. Kuljanic (Ed.) *Advanced Manufacturing Systems and Technology*,
CISM Courses and Lectures No. 406, Springer Verlag, Wien New York, 1999.

generate an NC toolpath for a computerised numerical control (CNC) machine so that it can produce the part. The surfaces are usually represented in CAD systems in unitless form via parametric curves. However, these unitless curves need to be converted back into the time domain to relate the surfaces to real machining process with specified machining parameters such as the feed rate. On the basis of the desired feed rate the tool position along a designated tool path needs to be specified in terms of time. These successive tool positions, called commands, are input into the position servo control system, and act as reference-position input, the servo control system sends the control signal, as voltage, to servo driver, and then drives the actuator in the machine tool to follow the desired trajectories. This process of command generation is usually performed via a device called interpolator that is located in the controller of the CNC machine.

The conversion, made by the CAM system, of the unitless curves in the time domain cause, in the phase of NC code processing, the generation of a great number of information, that the CNC machine will respect connecting them with linear segments to generate a finite NC toolpath. This method creates many short linear move commands with sudden changes in direction. Toolpath created in this way induce problems for the CNC machine during the machining process, and this can affect the finished quality of the part. Moreover the dimension of the files that the CAM transfer to CNC control machine are big and this dimension improve with the complexity of the CAD model. This research work wants to develop an interface between the CAM systems and the CNC machines to permit the use of the non linear interpolation in the CNC control system. The final part of the work consists in the measure of a simple object, manufactured with the different methodologies developed in the work, to analyse the performance of the interface.

2 HIGH SPEED MACHINING

High speed milling would introduce the philosophy to improve both cutting speed and feed rate in the cutting operation but this wants also to mean that it must maintain or improve the accuracy of the traditional operation. Improving the feed rate is connected to the necessity to have the possibility to control, in real time, the position of the tool during the machining operation while the machine control is computing the new move command. If in the traditional cutting operation this was possible because the feed rate along axis was only of mm/min, now it is more complex. In fact the feed rate along the machine axis is became of m/min while the information of the move command are remained about mm to maintain the chordal error, of the manufacturing operation, under a certain value. The first problem that is the too high number of information that the machine must compute in real time, while the machine is working[1]. To resolve this problem some CNC developers have decided to improve the Hardware features. But this solution cannot solve the problem of sudden redirection connected with high speed[2]. This problem in fact is so strong in the philosophy of the improved feed rate because of the great acceleration and deceleration that the machine structure must bear in the singular points. Even if the structure of the machines used for high speed machining is rigid the accuracy of the manufactured is not assured like what the operator wants. The solution that we want to present is the realisation of an interface and we have decided to work on the field between the CAD/CAM and the CNC as displayed in Fig. 1.

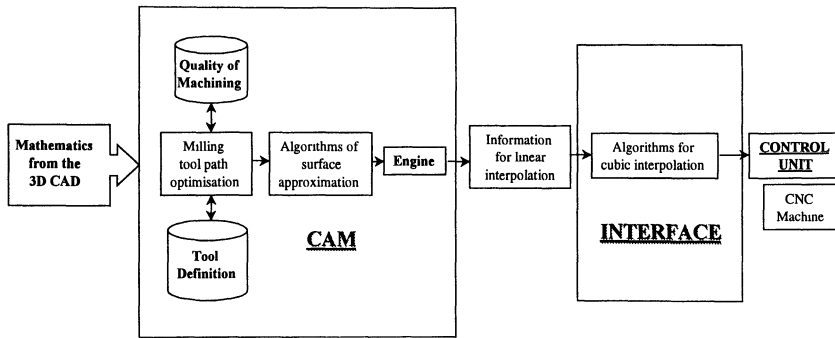


Figure 1: Interface Scheme

This interface could avoid the bottleneck of the linear interpolation, and starting from the punctual information could give in output what the CNC control asks in term of not linear interpolation. In our situation the CNC machine needs, for Bezier interpolation, the interpolated points and the control points that makes part of the tangency of the real function in the same interpolated points. This experimentation was developed using the Visicam SURF5 CAM software and the a 3 axis CNC milling machine Prolight1000.

3 CHOICE OF THE INTERPOLATION METHOD

Actually the only used philosophy of interpolation for the machining of complex geometry is the linear interpolation, this kind of mathematical algorithms near a given non linear curve by a set of line segment trying to satisfy a desired machining tolerance and feed rate. Two methods are commonly used to evaluate these cutter location. A bisecting step size algorithm and a variable step-size algorithm. In each these method the philosophy is based on the intent of maintaining the maximal chordal error under a certain value, that is in every manufacturing operation under the value of 0.001 mm. This error is the maximal distance between the real curve of the object and the segment that is its approximation.

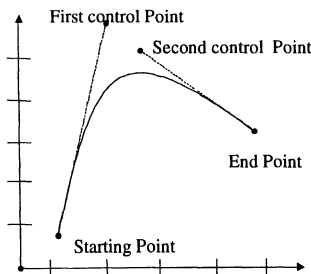


Figure 2: Non linear interpolation

Using the linear interpolation method to generate a tool path on a large and overdetermined data set, the CAM post processor is obliged to generate too many short linear move commands[3]. This may causes the data buffer in the CNC controller to underflow and in addition, the linear moves in the toolpath are tangentially discontinuous from one move to

the next. This tangential discontinuity causes a sudden change of direction at each point along the toolpath and affect the quality of the finished surface.

In order to reduce the number of data points with minimal alteration of original profile it could be used an arc spline, that is a curve made of circular arcs and straight line segments. A spline curve is continuous with a continuous unit tangent. A toolpath generated with an arc spline consists of both linear and circular interpolation commands. The problems induced by a sudden change of cutting direction are eliminated because of the continuity of the unit tangent. The importance of the circular-arc cutting path has been addressed by the manufacturing industries. Furthermore, when applying a tolerance constraint to the arc spline, the redundant points within the tolerance are excluded from the NC toolpath.

An arc spline segment is composed of a pair of circular arcs, called biarc, and two tangents at the two end points of the segment (Figure 2)

The non linear interpolation methodology choiced is based on NURBS curves, and in particular on Bézier curves. This kind of interpolation is codified in the ISO program of the machine centre with the sign G101. The command line of this kind of interpolator is:

G101 x y I J AB

where X and Y explain always like in the traditional linear interpolation the end point of the tool path interpolation I and J are the values of a point on the tangent line to the curve at the starting point of the movement, while A and B are the coordinates of a point of the tangent line to the curve in the end point, of the move command[4].

The tangent information is necessary to assure that the entire tool path is without interruption and sudden changing of direction. This situation permits to the machine tool path to not need strong variation of velocity. To obtain the required information we have analysed two interface methodologies namely:

3.1 REVERSE BEZIÈR PROCEDURE

As previously said the goal of research project is to develop an interface between the CAM system and the CNC control machine, and so we must analyse the output of the CAM system and the input of the CNC control system[5]. This analysis is important because the interface must give the right parameters to the CNC control system to use the non linear interpolation, starting only from the information obtained by the CAM post processing.

The CNC control system, used, needs, like command information, the interpolated point and two control points. These two control points make part, the first of the tangency on the curve in the movement starting point, while the second of the tangency on the curve in the end point of the move command. To obtain the information about the tangency to the curve in the interpolated points, starting only from the punctual CAM output, we have realised the following approximation methodology.

Starting from a number of points $n+1$ of the CAM tool path

$$(X_{i-1}, Y_{i-1}) \quad (X_i, Y_i) \quad (X_{i+1}, Y_{i+1})$$

for every three points we compute the ordinal connecting segments using these mathematical formalisation:

$$Y - Y_{i-1} = [(Y_i - Y_{i-1}) / (X_i - X_{i-1})] * (X - X_{i-1}) \quad Y - Y_{i+1} = [(Y_{i+1} - Y_i) / (X_{i+1} - X_i)] * (X - X_{i+1})$$

Because of the inclination of the two lines, that we have obtained, is also expressed like tangency of an angle, we must remind that this function is not linear and so we cannot compute the average of these two inclination to obtain an average value.

In relation with this problem we must evaluate the angle, connected with this inclination, and make the average of this. We can obtain these parameters using the common trigonometry

$$\Phi_1 = \text{TAN}^{-1} [(Y_i - Y_{i-1}) / (X_i - X_{i-1})] \quad \Phi_2 = \text{TAN}^{-1} [(Y_{i+1} - Y_i) / (X_{i+1} - X_i)]$$

$$\Phi_m = (\Phi_1 + \Phi_2) / 2 \quad K_m = \text{TAN} (\Phi_m)$$

The parameter K_m represents the inclination on the average angle and also the approximation of the tangency in the interpolated point[6].

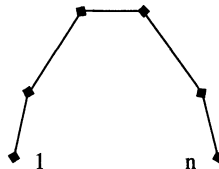


Figure 3 : Phase n

The procedure proceeds computing, for every point, the value of the intersection between the tangency of the point X_i and of the point X_{i+1} (Fig. 3).

$$\begin{cases} Y_i = K_i x + h_i \\ Y_{i+1} = K_{i+1} x + h_{i+1} \end{cases}$$

Computing on every $n+1$ points the value of the intersection of the tangency with its nearest, we obtain other n points that represent the phase n . We consider, at first, the n phase because we develop a reverse procedure and so the counter starts from the highest value and decrease to lowest. The following representation of the variable wants only to explain with the apex ($n-j$) the current phase of the procedure and with the pedice i the connotation of the point.

$$(X_i^{n-j}, Y_i^{n-j}) \quad \text{with} \quad j: 0 \dots n-2$$

When we have obtained these information we can start with the phase $n-1$. In this phase we must construct a vector obtained from the connection of the points i of the phase $n-1$ with the point $i+1$ of the phase n (Fig.4)[7].

This procedure is also explained using three geometrical conditions:

1. Parallelism of vectors
2. Coincidence between the end point and the starting point of vectors
3. Value of the module of the starting vector equals to the value of the end vector

In general we can compute the points of all the phase $n-j$ with $j : 1 \dots n-2$ using these equations:

$$i: 0 \dots n-j \quad j: 1 \dots n-2 \quad \Delta X = (X_{i+1}^{n-j} - X_i^{n-(j+1)}) \quad \Delta Y = (Y_{i+1}^{n-j} - Y_i^{n-(j+1)})$$

Only in the first step of the phase $n-1$ the value (X, Y) coincides with the starting

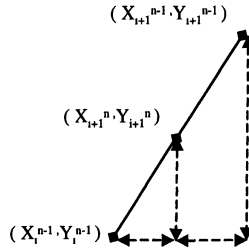


Figure 4 : Doubling of the vectors in the phase $n-1$

interpolated points $X_0^{n-1} = X_0$ and $Y_0^{n-1} = Y_0$. Proceeding with the methodology we obtain in general the new points of the phase $n-(j+1)$ [8]:

$$X_{i+1}^{n-(j+1)} = 2\Delta_X + X_i^{n-(j+1)} \quad Y_{i+1}^{n-(j+1)} = 2\Delta_Y + Y_i^{n-(j+1)}$$

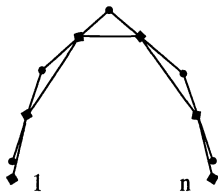


Figure 5: Phase $n-1$

First Control Point Second Control Point

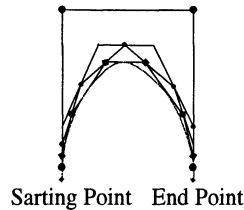


Figure 6 : Phase 0

If we want to understand geometrically this procedure we can analyse the following figures that represent some of the $n-2$ phases developed with the procedure (Fig 5). The last phase, the 0 phase, ends the procedure giving only two control points and maintaining the starting and the end point interpolated by the tool path[9]. We can see the end phase of the procedure in the Figure 6.

3.2 INTERSECTION PROCEDURE

The procedure just explained is not the only available. Starting at the same from an approximation of the tangency to the curve with the method explained before we can also use another interpolation method. If we have a minor number of points, for example using, in the CAM definition, a chordal error of 1 mm or more, we obtain a less number of points during the scanning procedure used by the CAM system to realise the tool path for the CNC machine[10]. Remembering that the CNC control system use a Cubic Bezier interpolation it needs four points: two interpolated points and two control points. Using this philosophy (Fig.7) the control system can trace a curve with the use of a mathematical interpolation that relate the intersection point of the tangency, estimated in the interpolation points, to the control points.

The relation are :

$$X_{P1} = (X_{P0} + 2X_{P*})/3 \quad X_{P2} = (X_{P3} + 2X_{P*})/3 \quad Y_{P1} = (Y_{P0} + 2Y_{P*})/3 \quad Y_{P2} = (Y_{P3} + 2Y_{P*})/3$$

In these equations (X_{P1}, Y_{P1}) and (X_{P2}, Y_{P2}) represent the value of the two control points that the control machine needs to use the non linear interpolation. The values (X_{P0}, Y_{P0}) and (X_{P3}, Y_{P3}) represent the value of the interpolated points, the starting and the end move command points [11].

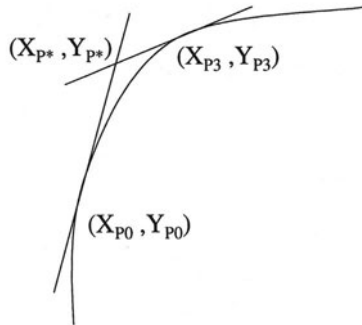


Figure 7 : Intersection procedure

4 EXPERIMENTAL WORK

The experimentation[12] has been carried out using the interface, developed in Turbo Pascal language, in the machining of a semisphere with a ball end mill tool with a diameter of 10mm.



Figure 8: Semisphere $\Phi_{0T}=40$ mm. $\xi_c=0.05$ mm. a) Linear interpolation b) Reverse Bezièr



Figure 9: Semisphere $\Phi_{0T}=40$ mm. $\xi_c=1$ mm. a) Linear interpolation b) Intersection

To make a right comparison work we have also machined the part with linear interpolation. The parameters imposed or chosen into the CAM for this milling operation are: a chordal tolerance $\xi_c = 0.05$ mm, and a distance between the different z positions 1.5 mm. This last parameter is not adapted to obtain a semisphere with a low roughness but we want to understand the effects on the curves, and for this motive the parameter is not so important (Fig.9a). At first the comparative study is realised making the same semisphere with a diameter $\Phi_{0T}=40$ mm, with the use of the non linear interpolation (G101 Reverse Bezièr) and with the linear interpolation. Using the non linear interpolation the NC code obtained by the CAM has been past trough the interface. The interface, Reverse Bezièr, makes a points reduction, and then a reduction of the line of the ISO code (Tab.1) used by the CNC control to realise the semisphere (Fig.8b). Then the experimentation follows using both linear interpolation and the second G101 interface, intersection, with a chordal error of 1 mm, to produce the same semisphere (Fig.9).

Procedure	Chordal Error (mm.) ξ_c	Number of program lines
Linear interpolation	0.05	2000
Reverse Bezièr	0.05	400
Linear interpolation	1	200
Intersection	1	200

Table1: Comparison of interpolation procedures

This last operation has been made to accentuate the strong difference on geometrical tolerance obtained[13] using a reduced number of points with a linear and the non linear interpolation as displayed in Table 1 and in Fig.9.

At last we have measured the object obtained from the different interpolation procedures, using a coordinates measure machine. The diameter Φ_{0T} and the sphericity ξ_ϕ of the object were measured using 50 points on the manufactured object to obtained a sure analysis of the semisphere and the results are displayed in the Table 2

5 CONCLUSION

From the results obtained from the experimental application we can show the following consideration:

- Using the reverse Bezièr procedure, we can obtain a semisphere starting from the same chordal error but with a computational cost reduced. While in fact in the first linear interpolation we have 2000 in the non linear procedure we use only 400 points obtaining a comparative tolerance result.
- Using the intersection procedure, with a chordal tolerance of 1mm. and so a little number of points we obtain at the same an object with a correct dimensional tolerance, while using the linear interpolation with the same chordal error of 1mm. the dimensional tolerance is not respected.

Moreover for a non linear interpolator, the memory size required is proportional to the number of individual segments while for a linear interpolator, the number of segments needed to approximate a given curve depends on the curvature of the curve [14].

Type of machining operation	ξ_c [mm]	Φ_{0M} [mm]	Φ_{0T} [mm]	$\Phi_{0T}-\Phi_{0M}$ [mm]	ξ_ϕ [mm]
Linear interpolation	0.05	39.85	40	0.15	0.04
Reverse Bezièr	0.05	39.80	40	0.20	0.05
Intersection	1	39.85	40	0.15	0.06
Linear interpolation	1	38.49	40	1.51	0.99

Table 2: measures of the manufactured objects

Using a non linear interpolation we can also reduce the strong acceleration or deceleration due to the sudden change of direction present in the segmentation of the linear interpolation. This is a strong advantage in the introduction and development of the High speed machining philosophy.

At the end of the work developed, training to realise an interface to use the non linear interpolation in the milling operations, we can affirm that the non linear interpolation represents a significant improvement in the cutting operation especially in High speed machining philosophy. From the results of this preliminary experimentation we can say that the second procedure is better than the first, but now we must continue our study to know which procedure is better working on more complex configurations. This interface in fact represents only a first experimental approach and the research activity is developing a study on more complex geometrical figures more connected with the moulds for the plastic injection.

REFERENCES

1. Dumur D. Boucher P., "New predictive solutions to very high speed machining" CIRP 1994, 363-366
2. Schulz H. Hock S.T., "High Speed Milling of dies and moulds cutting conditions and technology", CIRP 1995, 35-38
3. Bezier P., "Numerical Control", Wiley, 1972
4. Duc E., Lartigue C., Thiebaut F., "A Test Part for the machining of Free-form surfaces", International Seminar on Improving Machine tool performance, San Sebastian, SPAIN July 6-8, 1998, 423-434
5. Barry J. Wenping W. Fuhua C., "Reduced-Knot NURBS representation of rational G1 composite Bèzier curves", Computer Aided Design Volume 26 Number 5 May 1994, 393-399
6. Mortenson M.E., "Geometric Modelling" John Wiley & Son, 1985
7. Hopkins T. & Phillips C., "Numerical Methods in practice", International computer series.
8. Visicam Surf 5, User Manual
9. Prolight 1000, User Manual

-
10. Tarng Y. S. Chang W.S., “ *Dynamic NC simulation of milling operation*”, Computer Aided Design Volume 25 Number 12 December 1993, 769-775
 11. Tsay D. M. Wei H. M., “ *Design and machining of cylindrical CAMS with traslating conical followers*” Computer Aided Design Voulme 25 Number 10 October 1993, 655-661
 12. Hwang J.S. ,”*Interference – free tool-path generation in the NC machining of parametric compound surfaces*”, Computer Aided Design Volume 24 Number 12 December 1992, 667-676
 13. Xiuzi Ye, “*Generating Bèzier points for curves and surfaces from boundary information*”, Computer Aided Design Volume 27 Number 12 December 1995, 875-885
 14. Juhász I., “*Approximating the helix with rational cubic Bèzier curves*” , Computer Aided Design Volume 27 Number 8 August 1995, 587-593

CAPP SOFTWARE FOR TOOL SELECTION, OPTIMIZATION AND TOOL LIFE DATA BASE ADAPTATION IN TURNING

G. Cukor

University of Rijeka, Rijeka, Croatia

E. Kuljanic

University of Udine, Udine, Italy

KEY WORDS: Computer Aided Process Planning, Tool Selection, Tool Life Modeling, Multi-Criteria Optimization

ABSTRACT: The presently developed Computer Aided Process Planning (CAPP) systems suffer from a very important practical deficiency: tool life data gathered from machinability experiments performed under isolated laboratory or shop floor conditions are not directly transferable to the actual industrial conditions, owing to the complex nature of machining process. Therefore, there is a need for CAPP software that is capable to adapt the tool life model parameters to a given machining system. In this paper a modular approach to such organized CAPP is proposed. Furthermore, the developed interactive program system for turning operations consisting of modules for tool selection, cutting conditions optimization and tool life data base adaptation is presented.

1. INTRODUCTION

The most important part of a *Computer Aided Process Planning* (CAPP) system is the cutting process itself, i.e. how to select proper tools and to determine optimum cutting conditions (cutting speed, feed and depth of cut) for each scheduled cutting operation. This selection is particularly important because it affects the productivity and production cost, i.e. the efficiency of very expensive advanced machining systems such as

machining cells, flexible machining centers and unmanned machine tools in general. However, owing to the complex nature of machining process, it is impossible to establish a reliable and generally valid machinability data base that holds for process optimization on different machining systems. Thus it emphasizes the imperative of CAPP software capable to adapt the machinability model parameters to the particular machining environment for which the data are needed. Also, it is of a great importance to have an appropriate statistical procedure which can be used to establish a reliable machinability data base for a given system.

The interactive program system for turning operations described herein consists of modules for tool selection, cutting conditions optimization and tool life data base adaptation.

2. SYSTEM ARCHITECTURE

The basic idea of concept was presented in [1]. The framework and information flow of the system are shown in Figure 1. The output of *Tool Selection (TS)* module includes the candidate tool assemblies able to perform the operation along with the associated data required for optimization. The optimum cutting conditions in a constrained environment,

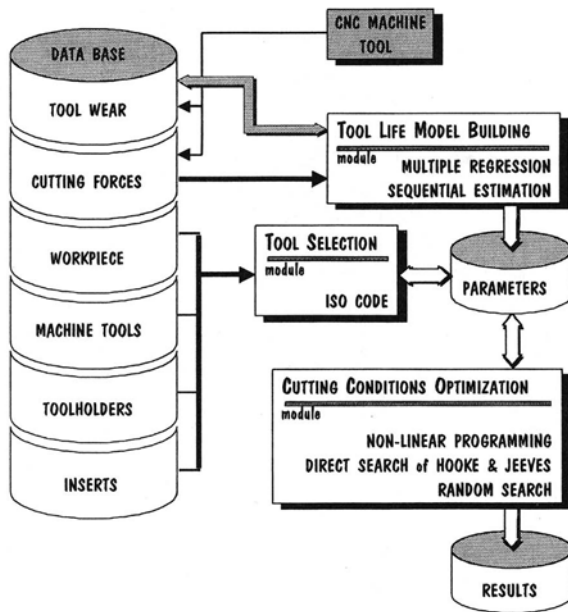


Figure 1. System framework and information flow

considering a compromise solution of two economic objective functions - minimum unit machining cost and minimum unit machining time, are determined for each candidate tool by *Cutting Conditions Optimization (CCO)* module. Finally, the candidate tool with the best economic performance is selected for a given operation. The initial solution is derived on the basis of previously documented tool life model parameters estimates. The actual tool life in the on-going machining process will serve as additional data to gain a better set of parameters estimates out of *Tool Life Model Building (TLMB)* module. The updated estimates for tool life model parameters will be used in the optimization procedure recursively to obtain a better solution. After a few iterations, the tool life model will adapt to the on-going process and the solution will reach the optimum. In the following, each module will be briefly described.

Tool Selection Module. For a given operation toolholder, insert geometry and material should be determined. The selection of these features is based on the series of screenings through several levels which represent checks for fulfillment of compatibility and suitability requirements between workpiece material, specified workpiece geometry, the amount of material to be removed, the direction of machining, availability of tools, tool materials and the machine tool on which the cutting is to be performed [2], Figure 2.

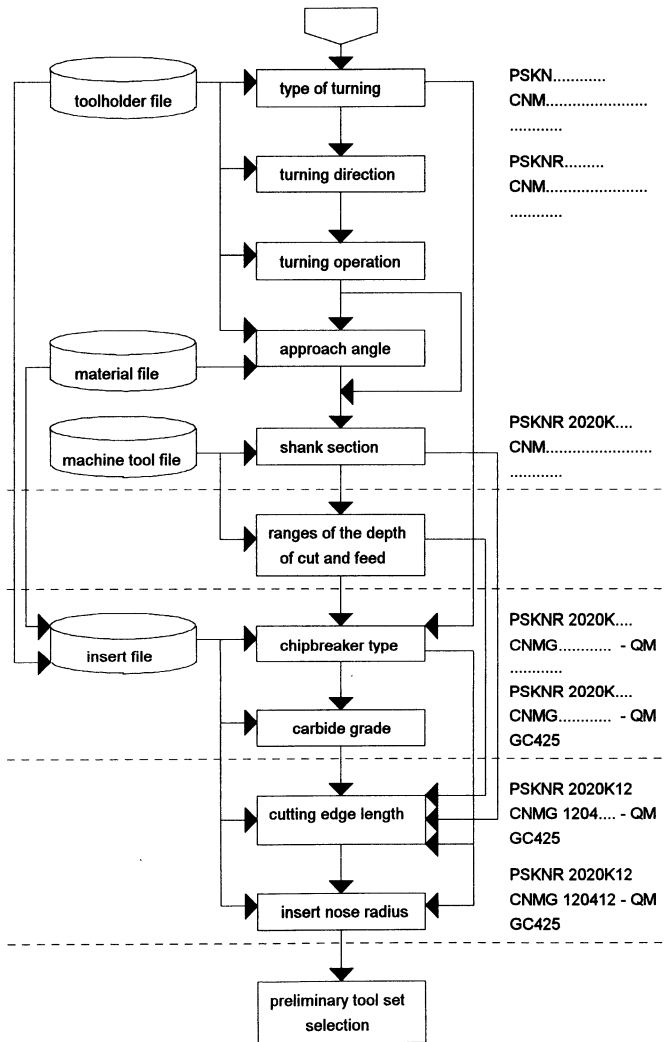


Figure 2. Flow diagram of tool selection procedure

The tool class is determined as a group of tools produced by a given manufacturer for a specific turning operation, with specific design and clamping system. The selection is progressive and relatively straightforward at the first level, while later is more complex. At each level the procedure is decomposed in selection steps. A part of toolholder or insert ISO code is determined at each step.

Cutting Conditions Optimization Module. In principle, the cutting conditions are usually selected either from the viewpoint of minimizing unit machining cost or from the viewpoint of minimizing unit production time if cost is neglected. It has also been recognized that between these two criteria there is a range of cutting conditions from which an optimum point could also be selected in order to increase profit in the long run. In fact, this is the major goal in industry.

In order to obtain a compromise solution between the criteria both the minimum unit machining cost $y_1(x)$ and minimum unit production time $y_2(x)$, the following *two-criteria objective function* is adopted [3]:

$$y(x) = \frac{w}{y_1^*(x)} y_1(x) + \frac{1-w}{y_2^*(x)} y_2(x) \quad (1)$$

where w is the weight coefficient, $y_1^*(x)$ and $y_2^*(x)$ represent minimum values of the corresponding criterion when considered separately. It should be noted that two-criteria optimization becomes one-criterion optimization from the viewpoint of minimum unit machining cost or time for $w = 1$ or $w = 0$ respectively. A compromise solution to obtain an optimum economic balance between the unit machining cost and time yields for $0 < w < 1$. Hence, the cutting conditions, at which this occurs, will theoretically result in maximum profit rate.

The objective function (1) should be minimized within the feasible region of cutting conditions bounded by the numerous operation constraints [4]. For handling the constraints, the *modified objective function method* is implemented. The constraints are incorporated into the objective function (1) which leads to an unconstrained model of the form:

$$\text{minimize } \left\{ y(x) + C_F \sum_{j=1}^m k[g_j(x)] \right\} \quad (2)$$

where C_F is correction factor, m is the total number of non-linear constraints $g_j(x)$ and the *exterior penalty function* is of the form:

$$k[g_j(x)] = \begin{cases} 0 & g_j(x) \geq 0 \\ g_j(x) & g_j(x) < 0 \end{cases} \quad (3)$$

Penalty function is used in order to apply a penalty to the objective function at non-feasible points, thus forcing the search process back into the feasible region.

Since the optimization model is non-convex, non-linear and multi-variable model of a complex nature, the care must be taken to apply an appropriate optimization method. To find such a method, a comprehensive literature survey has been carried out and some methods have been tested. Although many of tested general non-linear programming methods can achieve acceptable results, it has been concluded that the combination of techniques both the *Direct Search of Hooke and Jeeves* and *Random Search* [5, 6] is the quickest approach for solving the above minimization problem.

A computer program in Fortran programming language was developed and the flow diagram of direct search routine of Hooke and Jeeves is given in Figure 3. Direct search is performed three times at different starting points chosen with respect to feasibility and criterion values out of randomly generated points.

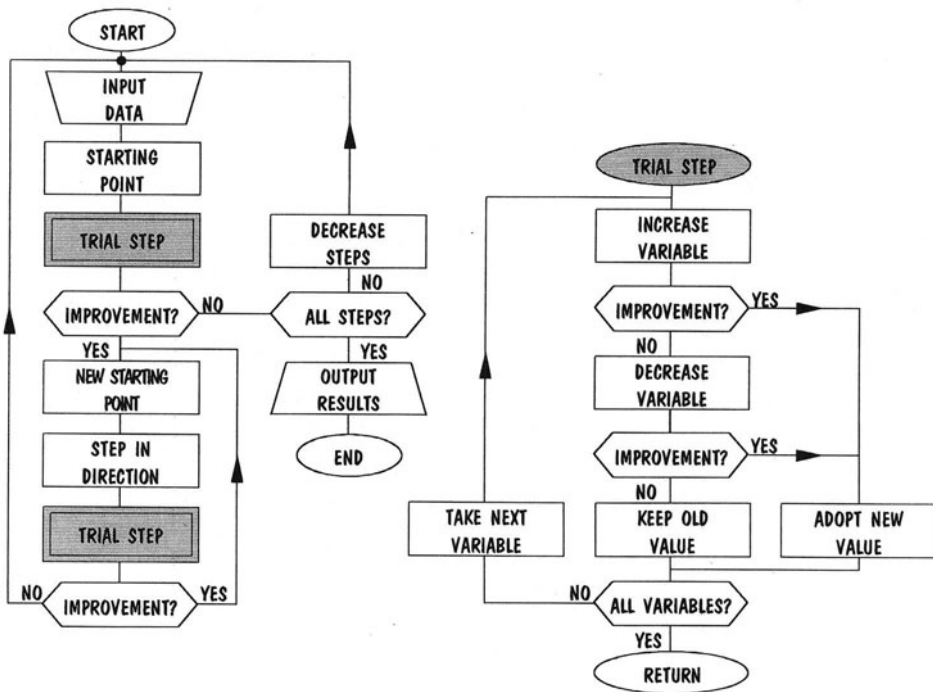


Figure 3. Flow diagram of direct search procedure of Hooke and Jeeves

Tool Life Model Building Module. It has been shown that tool life can be predicted successfully on the basis of some polynomial form of the following model [7]:

$$\hat{y} = f(x_k, b_k), \quad k = 0, 1, 2, \dots, p, \quad x_0 = 1 \quad (4)$$

where \hat{y} is the tool life prediction, b_k are the estimated tool life model parameters and p is the number of cutting conditions x_k . It should be noted that the capabilities of TLMB module are being enhanced since its presentation in [1]. Namely, only linear tool life models represented by the first order polynomials were considered in the previous version. Moreover, in 1975 E. Kuljanić [8] proposed to include significant interactions in tool life equation called *New Tool Life Equation*. Accordingly, in order to predict the responses with increased reliability over a wider range of cutting variables, i.e. to take into consideration the non-linearity, the second order polynomial models with included significant interactions are introduced. The estimating model is as follows:

$$y = b_0 + \sum_{k=1}^p b_k x_k + \sum_{k=1}^p b_{kk} x_k^2 + \sum_{k<l}^p b_{kl} x_k x_l \quad (5)$$

The model (5) is determined by applying design of experiments, obtained experimental data and multiple regression analysis. However, in small batch production, the cost of conducting lengthy off-line experiments can well exceed any savings gained from experimentation for a batch. Even on-line testing can be costly if a group of data is collected and analyzed together because of limited total available testing points and unknown stopping point in the test. Moreover, regression analysis can not be used with subjective prior information, since every time the model parameters are to be updated, all the previous data have to be retrieved and used along with the new feedback data. Thus, the *sequential estimation* [9] is implemented too.

The method of sequential estimation enables to update the existing tool life model parameters considering new measuring results. The parameter values are stabilized after a sufficient number of evaluated measurements, depending on the number of the independent tool life model parameters. Nevertheless, the estimates converge reasonably quickly. The sequential estimation procedure is based on following newly developed equations:

$$A_{u,i+1} = \sum_{k=0}^p x_{k,i+1} P_{uk,i} + \sum_{k=1}^p x_{k,i+1}^2 P_{u(p+k),i} + \sum_{k<l}^p x_{k,i+1} x_{l,i+1} P_{u(2p+m),i}, \quad m = 1, 2, \dots, n-1-2p \quad (6)$$

$$\Delta_{i+1} = \sigma_i^2 + \sum_{k=0}^p x_{k,i+1} A_{k,i+1} + \sum_{k=1}^p x_{k,i+1}^2 A_{p+k,i+1} + \sum_{k<l}^p x_{k,i+1} x_{l,i+1} A_{2p+m,i+1} \quad (7)$$

$$e_{i+1} = y_{i+1} - \sum_{k=1}^p x_{k,i+1} b_{k,i} - \sum_{k=1}^p x_{k,i+1}^2 b_{kk,i} - \sum_{k<l}^p x_{k,i+1} x_{l,i+1} b_{kl,i} \quad (8)$$

$$b_{u,j+1} = b_{u,j} + A_{u,j+1} \frac{e_{i+1}}{\Delta_{i+1}}, \quad u = 0, 1, \dots, p \tag{9}$$

$$b_{vv,j+1} = b_{vv,j} + A_{u,j+1} \frac{e_{i+1}}{\Delta_{i+1}}, \quad v = 1, 2, \dots, p, \quad u = p + 1, \dots, 2p \tag{10}$$

$$b_{vz,j+1} = b_{vz,j} + A_{u,j+1} \frac{e_{i+1}}{\Delta_{i+1}}, \quad v = z = 1, 2, \dots, p, \quad v < z, \quad u = 2p + 1, \dots, n - 1 - 2p \tag{11}$$

$$P_{uv,j+1} = P_{uv,j} - A_{u,j+1} \frac{A_{v,j+1}}{\Delta_{i+1}}, \quad u = v = 0, 1, \dots, n - 1 \tag{12}$$

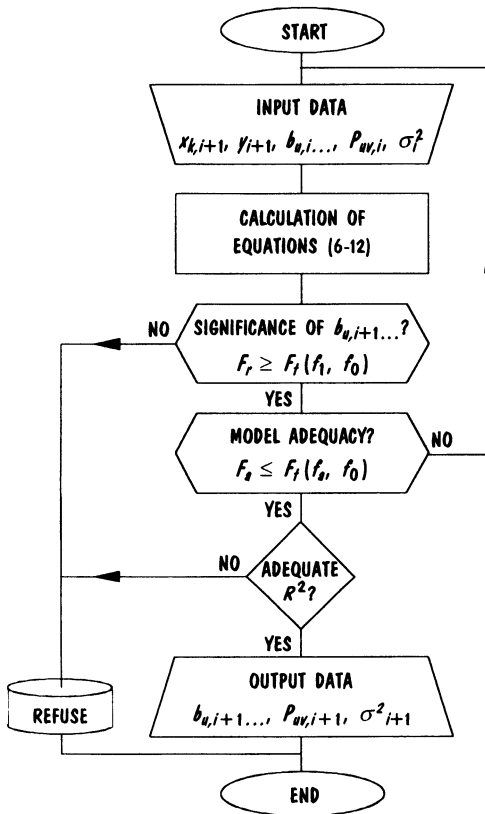


Figure 4. Flow diagram of sequential estimation procedure

where A_s , Δ , and e are intermediate variables, P_s are the estimated covariance of the b_s , and σ^2 is the variance of tool life y_i (prior information). A computer program in Fortran for the estimation of model parameters sequentially according to equations (6–12) was developed and the flow diagram of routine is given in Figure 4. In terms of computation time, this is a very fast procedure since only one new data entry is introduced at a time.

3. CONCLUSION

Based on the modular approach with the introduction of CAPP functions, the interactive program system for tool selection, cutting conditions optimization and tool life data base adaptation in turning is developed. The program can be readily implemented on the main frame computer for larger manufacturing systems as well as on the microcomputers for smaller systems or systems using a distributed computing structure. The described program system provides an environment for its friendly use by experienced process planners and

tooling engineers with no ground expertise in optimization or even in computer science. The system is flexible and expandable enabling to create a customized data base from which the tool selection and cutting conditions optimization, according to user defined criteria and algorithms, could be carried out. Further research will attempt to enhance the capabilities of the program by adding new routines for other machining operations and CAPP functions.

ACKNOWLEDGEMENTS

This research is financially supported by the Ministry of Science and Technology of the Republic of Croatia, projects no. 069015 and no. 069103.

REFERENCES

1. Cukor, G., Kuljanić, E.: An Interactive Program System for Turning Operations Tool Selection and Optimization, Proceedings of 9th International DAAAM Symposium, Cluj-Napoca, Romania, Katalinić, B. (Ed.), ISBN 3-901509-08-9, DAAAM International, Vienna, Austria 1998
2. Mesquita, R. M. D., Cukor, G.: An Automatic Tool Selection Module for CAPP Systems, Proceedings of 3rd International Conference on Advanced Manufacturing Systems and Technology AMST'93, Kuljanić, E. (Ed.), Vol. I, Udine 1993, 155-165
3. Cukor, G., Kuljanić, E.: Multi-Criteria Optimization in Multi-Pass Turning, In: Advanced Manufacturing Systems and Technology, CISM Courses and Lectures No. 372, Kuljanić, E. (Ed.), ISBN 3-211-82808-7, Springer Verlag, Wien New York 1996, 221-227
4. Cukor, G.: Computer-Aided Optimization of Cutting Conditions for Multi-Pass Turning Operations, Proceedings of 3rd International Conference on Production Engineering CIM'95, Cebalo, R. (Ed.), ISBN 953-96501-2-7, Croatian Association of Production Engineering, Zagreb 1995, D27-34
5. Hooke, R., Jeeves, T. A.: Direct Search Solution of Numerical and Statistical Problems, Journal of the Association for Computing Machinery, 8 (1961) 2, 212-229
6. Osyczka, A.: Multicriterion Optimization in Engineering with Fortran Programs, Ellis Horwood Ltd, New York 1984
7. Cukor, G.: Tool Life Models for Advanced Machining Systems, Proceedings of 4th International Conference on Production Engineering CIM'97, Cebalo, R. (Ed.), ISBN 953-97181-0-4, Croatian Association of Production Engineering, Opatija 1997, B35-42
8. Kuljanić, E.: Effect of Stiffness on Tool Wear and New Tool Life Equation, Journal of Engineering for Industry, Transactions of the ASME, Ser. B, (1975) 9, 939-944
9. Balakrishnan, P., DeVries, M. F.: Sequential Estimation of Machinability Parameters for Adaptive Optimization of Machinability Data Base Systems, Journal of Engineering for Industry, Vol. 107 (1985), 159-166

TIME WEIGHTED PETRI NETS FOR OPTIMIZATION OF A REFRIGERATOR MANUFACTURING PLANT

O. Sawodny and E.P. Hofer
University of Ulm, Ulm, Germany

KEY WORDS: Process Planning and Control, Simulation, Petri nets

ABSTRACT: In a flexible manufacturing plant handling systems, transportation vehicles, manufacturing stations, and workpieces in process have to be coordinated well in order to guarantee the desired output of the manufacturing plant. Especially, using driverless transportation vehicles in a complex manufacturing area the optimization of the manufacturing structure has to be supported by simulation of the manufacturing process prior to the implementation of expensive hardware. Therefore, a program module has been developed for the flexible simulation of any time weighted petri net structure.

The efficiency of the optimization tool will be demonstrated for a manufacturing plant in home appliance industry. The manufacturing plant consists of up to 12 manufacturing stations, a station for the foaming of the appliance housing, two manufacturing stations which combine the necessary components for the preceding processes, and several stations for the plastification of the foam under definite temperature and time conditions. Each workpiece has to be machined in three stations.

By calculating the necessary operating frequency the optimal number of stations for the foam plastification is determined. Next, the optimized number of driverless transportation vehicles is computed and evaluated. Simulations prove that the number of workpieces in process has a relevant effect on the output of the manufacturing plant. Finally, the number of workpieces in process is optimized to reach a high performance of the manufacturing plant.

As a result of previous optimization a considerable reduction of manufacturing stations and driverless transportation vehicles was possible and the output of the manufacturing plant could be further increased.

1. INTRODUCTION

The considered home appliances are manufactured in four main manufacturing steps. One of these steps is the foaming of the appliance housing for isolation which is a bottleneck process in the manufacturing structure, where different types of appliances have to be manufactured at the same time. Therefore, the plant needs a maximum of flexibility combined with short total processing time. The workpieces in process are transported by driverless transportation vehicles. In order to increase capacity the manufacturing structure was redesigned. To guarantee high performance of the plant, optimal flow of material and high productivity concerning to the following assembly lines, the number of stations, vehicles and workpieces in process are optimized, and the results proved by simulations.

2. MANUFACTURING STRUCTURE

The foaming plant is connected to previous and subsequently plants by two handling station (HS) in which the already foamed and plastified housing is changed with a non foamed housing of the previous assembly line. Therefore, the already foamed housing is put out of the mould and the next to be foamed one into the mould. The transport of the moulds with the housing in the plant is done by driverless transport vehicles (DTV) on a given parcourse. The next station in process is the foaming station (FS) which can be divided into three process parts. With the foaming process the plastification of the foam starts. The necessary plastification time varies about 50 %. For plastification the moulds are unloaded at plastification stations (PS) where the plastification process is running under definite temperature conditions. After leaving the already foamed mould in the PS the DTV picks up an already plastified mould out of the buffer of the PS and brings it back to the HS where the plastified housing is changed with a to be foamed one and the process starts again.

As possible modification of manufacturing plant two alternative structures were discussed. The difference between these two structures is the algorithm for the allocation to the PS's after the mould leaves the foaming station. In one case it is a defined sequence in order to guarantee as possible equal station utilization (fig. 1) and in the other case it is a fixed connection between PS and subsequent manufacturing lines which is then directly related to the type of the appliance, and number of mould and DTV (fig. 2).

The other manufacturing structure (fig. 2) has only a maximum of 5 stations but with a higher mould capacity. Instead of a unique path from the PS to the handling stations, PS1 and 2 is fixed connected to handling station 1 and PS 3,4 and 5 to handling station 2. The PS's are directly connected with the following manufacturing assembly lines of the different appliance types.

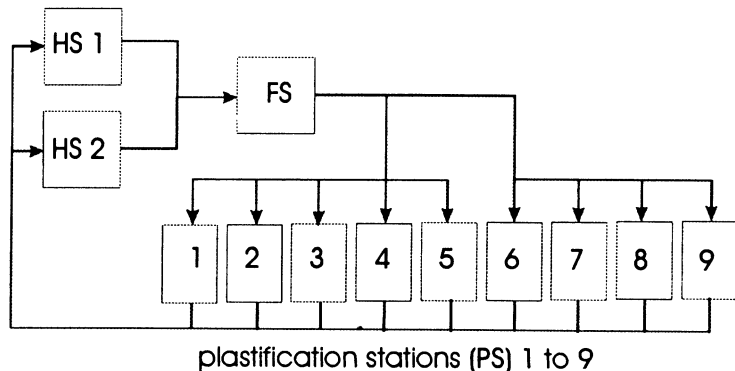


Fig. 1: Sequence oriented manufacturing structure.

To minimize the risk of low plant productivity a simulation [3] in combination with an optimization [4] of the plant by evaluating the optimal number of PS's, capacity of these stations, number of DTV's, and moulds in process was done for these alternative manufacturing structures.

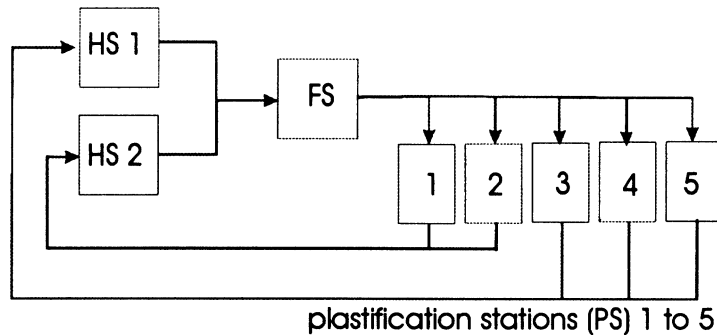


Fig. 2: Type oriented manufacturing structure.

For simulation an effective tool is the modeling of the plant with time weighted petri nets. The simulation tool proves the results of the analytical optimization.

3. TIME WEIGHTED PETRI NETS AND SIMULATION TOOL

Petri nets are used for the model description of time discrete event systems. In petri nets the actual partly state of the system is represented by the so called places or conditions which are one type of nodes in the net [1]. Each condition or place follows at least one transition or event which are the other type of nodes in petri nets. The structure of the net is given by directed edges which connect transition and places. Initially a petri net does not mirror the time dependence of the given time discrete system. Therefore, an edge weighting which represents the time of the transition process is introduced. Active places are marked by a token. For distinguishing different types of tokens different colors can be used which leads to the so called colored petri nets.

In the present problem the places are track sections of the DTV parcour or the process stations like the foaming station.

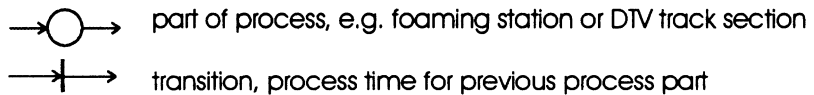


Fig. 3: Assignment of places, and transition to the given problem.

The transitions indicate the necessary process time for the previous place (fig. 3). The unloaded driverless transport vehicles are tokens of green color, the moulds tokens of blue color, and the mould loaded vehicles have a violet color. For modeling petri net structure systems can be reduced to the following elementary modules. The decision for the following process progression can be represented by forking from one place with more than one outgoing edges to transitions. The merging to one line of process progressing is expressed by leading edges from more than one transition to one place (fig. 4).

In the present problem these elements are used to mirror e.g. the switches on the DTV parcour. Next basic element is the splitting up of a process in parallel processes, and the synchronization again to one process. This occurs here by leaving a mould in the PS and picking up an already plastified one. The manufacturing structure according to fig. 1 as the resulting petri net is shown e.g. in fig. 5.

For simulation of time weighted petri nets a software package was developed. This programm allows the definition of a petri net structure via a initialization file. In a list the places are defined with the transition time to the following nodes and the type of structure element according to fig. 4. As well the decision for the route of the vehicles according to the algorithm for the allocation of the PS

is given by the initialization file. In this file also the number of tokens which are in the example the moulds and DTV's and the initial state of the net by setting the starting nodes of moulds and DTV's are determined.

After reading the initialization file the programm runs into the simulation loop. Each node of the net is being proofed whether or not it is occupied by a vehicle or mould. If there is a occupied node the identification number of mould or vehicle is read. After requesting the target of the mould or vehicle the next transition in the net structure tree is evaluated. If the conncted timer to this transition is already started the actual time is read. If the process time is over the next place is proofed whether or not it is occupied. In case it is occupied the token stays at the actual place otherwise it is put to the next following place. After evaluating the new allocation of tokens the screen will be actualized. For protocolling counter can be defined at each place in the net to prove system output. A function to change time scaling during simulation runs complete the functionality of the simulation tool.

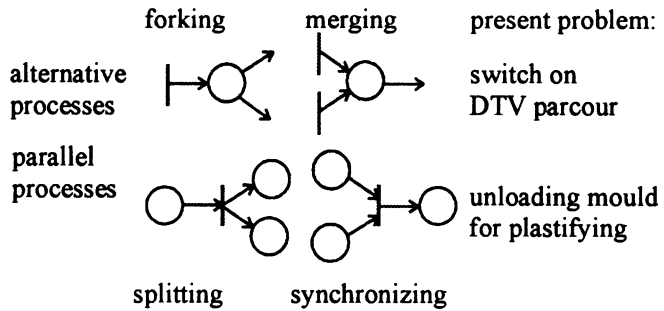


Fig. 4: Basic modeling elements for petri nets and their application at the present problem.

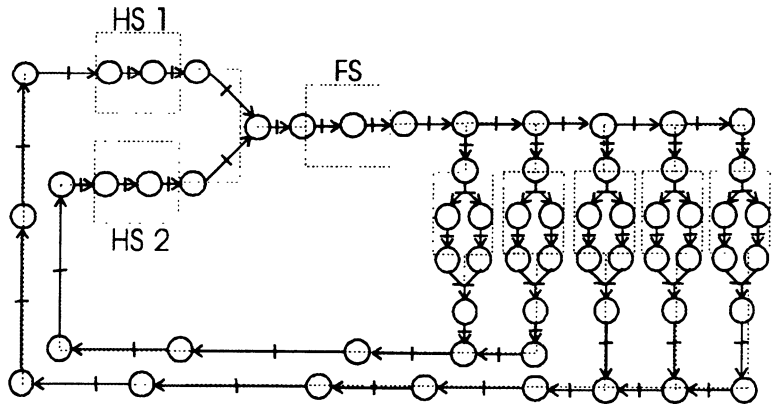


Fig. 5: Manufacturing structure according to fig. 2 modeled as a petri-net.

4. OPTIMIZATION OF THE MANUFACTURING PLANT

4.1 Optimization of the sequence oriented plant

An optimal output of the plant is given if the plastification time of each foamed housing is exactly kept. Due to the increasing travelling time of the DTV's to the more distantly stations the remaining plastification time t_{ream} in the PS's is decreasing. In the plant the bottle-

neck is the foaming station. So another condition for optimal plant output is the constantly utilization of the foaming station. This results in a necessarily definite cycle of leaving DTV's for plastification at the end of the FS determined by the cycle time t_{cyc} of the station. So there can be a necessary serve frequency for each station defined which is the next lower natural number of the quotient of t_{ream} and t_{cyc} . In the present problem the serve frequency for the stations of the manufacturing structure according to fig. 1 are given in table 1.

PS	1	2	3	4	5	6	7	8	9	10
Serve frequency	8	8	8	8	7	6	6	6	6	6

Table 1: Necessary serve frequency

That means, in case of 10 PS's the cycle time of the foaming station is not sufficient to serve all 10 stations in time. Because of the plant layout it is not possible to realize 8 stations with a serve frequency of 8. So the optimal station number is 7. 4 stations in the block of station 1 to 5 with a serve frequency of 8 and 3 stations in the second block of station 6 to 10. A station sequence is then determined which exactly guarantee the above calculated serve frequency (table 2).

$$1, 6, 2, 7, 3, 8, 4, 6, 1, 7, 2, 8, 3, 6, 4, 7, 1, 8, 2, 6, 3, 7, 4, 8, 1, 6, 2, \dots$$

Table 2: Sequence of target PS's for DTV's leaving the foaming station.

Next is the optimization of the number of vehicles and moulds in process. For the number of DTV's based on matrix operations of petri net theory the time of the desired vehicle back at the buffer in front of the foaming station is calculated. As seen in table 3 after 506s the DTV No. 1 of cycle 1 is back at the foaming station buffer. So it could be used for new cycle 14 at $t=650s$. DTV No. 1 is then back at the foaming station buffer at $t=1274s$ and will be utilised at cycle 28 and so on. This calculation proves that 13 DTV's are needed to avoid idling cycles of the foaming station.

cycle	Leaving FS at	DTVNo.	PS No.	HS No.	Buffer FS	DTV for new cycle
1	0	1	1	1	506	14
2	50	2	6	1	674	16
3	100	3	2	2	606	15
4	150	4	7	1	780	18
5	200	5	3	1	708	17
6	250	6	8	2	856	20
7	300	7	4	1	896	19
8	350	8	6	1	976	22
9	400	9	1	2	928	21
10	450	10	7	1	1078	24
11	500	11	2	1	1006	23
12	550	12	8	2	1156	26
13	600	13	3	1	1126	25
14	650	1	6	1	1274	28
15	700	3	4	2	1230	27
16	750	2	7	1	1378	30
17	800	5	1	1	1306	29

Table 3: Calculation of optimal number of DTV's.

At last, the number of necessary moulds are determined. The time for the distance of foaming station to PS back to the handling station should be for optimal plant output exactly the plastification time t_{plast} . The time needed for the distance of handling station to foaming station t_{cf} is also well defined. So it can be calculated that in case of no idling cycles at the foaming station a minimum of 21 moulds is necessary which is the next natural number to the quotient of the sum of t_{plast} and t_{cf} to t_{cyc} . Because in this calculation no dynamic influences like occupying of one track section by two vehicles the results of the optimization was proved by time weighted petri net simulations. The desired output of the optimized manufacturing plant with 7 PS's, 13 vehicles, and 21 moulds was exactly reached. The sensitivity of these result was investigated by further simulations. So increasing of number of vehicles does not increase the output significantly. As well 22 moulds instead of 21 does not have an noticeable effect on the plant output. Further, simulations show the output of the optimized configuration was 17 % higher than the output of the initial plant configuration with 10 stations, 16 DTV's, and 20 moulds. Due to this investigation one can perceive the importance of exact tuning of station number, vehicle number, and moulds in process.

4.2 Optimization of the type oriented plant

As simulations show, a future decreasing of the cycle time of the foaming station causes a back-up of the vehicles in front of the handling stations. Due to the programming of the DTV's this has the effect that the vehicles does not leave the PS's. So the output dramatically decreases. Also the organizing structure of manufacturing where the plant has to supply three subsequent assembly lines with different types of appliances with different plastification times this leads to the manufacturing structure according to fig. 2. Instead of a sequence oriented distribution of the DTV's to the PS's these stations are connected to the appliance types. Because of 3 assembly lines at once maximum 3 different types can be manufactured simultaneously. Each appliance type has its own specific type of mould. Due to the segmentation of 50% of type 1, 40% of type 2, and 10% of type 3 the 5 PS's are connected as follows (table 4) where the different plastification times are considered. Because the number of PS's and the connection between type and station is given the optimization problem is reduced to the evaluation of number of DTV's and number of moulds. Due to fixed connection of PS and type implicit a fixed connection of vehicle, mould, and PS is given. To get the optimal number of vehicles it is assumed that in front of the foaming station there is in average always one vehicle in the buffer. So the times needed for one complete cycle from foaming station to PS to handling station and back to the foaming station can be evaluated. This value is divided by the complete production time of the plant. So the number of vehicle cycles per shift can be evaluated.

appliance type (assembly line)	PS
1	1,2
2	4,5
3	3

Table 4: Connection of appliance type and PS of manufacturing plant.

PS	1	2	3	4	5
Vehicle cycles per shift	78	93	84	80	76

Table 5: Vehicle cycles per shift depending on the PS.

For the moulds a mould cycle per shift value can be determined by dividing complete production time and cycle time of the mould which is plastification time plus traveling time from handling station to foaming station including one foaming station cycle time waiting in the buffer of the foaming station. A suitable tuning of number of moulds and vehicles is given if the quotient of for output necessary number of moulds multiplied with cycle time of mould per shift and cycle time of vehicle is rounded. So a tuning table of number of moulds and number of vehicles can be calculated (table 6).

Number of moulds	PS 1		PS 2		PS 3		PS 4		PS 5	
2					1	1				
3	1.85	2	1.93	2	1.5	2	1.95	2	2.05	2
4	2.47	3	2.58	3	2	2	2.6	3	2.73	3
5	3.09	3	3.22	3	2.5	3	3.25	3	3.4	4
6	3.71	4	3.87	4	3	3	3.9	4	4.1	4

Table 6: Tuning table of number of moulds and resulting number of vehicles.

From table 6 a schedule table for the plant operator can be derived in which he looks for the desired output on the production line and gets the value of necessary number of vehicles and moulds. The steps of the table are defined as the allowed shift batches (table 7). As a secondary condition only the total plant capacity has to be considered. As an example the schedule table of the production line of type 1 is presented.

To prove the results of the optimization different scenarios were simulated by time weighted petri nets. Fig. 6 shows a typical screenshot of a simulation of the manufacturing plant. The number under the nodes identifies the vehicle and mould which actually occupy the place. On the right upper corner there is the foaming station. Following the DTV path in the center and to the left edge of the screenshot the PS are located. In the lower right corner the handling stations are placed. The bottom of the screenshot shows the counter of specific places, the simulation time, the time scaling factor, and in this specific case of simulation the resulting cycle time of the complete plant.

Shift batch	PS1		PS2		Total	
	Mould No./DTV No.		Mould No./DTV No.		Mould No./DTV No.	
192	5	3			5	3
230	6	4			6	4
268	4	3	3	2	7	5
306	5	3	3	2	8	5
344	6	4	3	2	9	6
382	5	3	4	3	10	6
420	5	3	5	4	11	7
458	6	4	5	4	12	8

Table 7 : Schedule table for plant operator to evaluate optimized number of DTV's and moulds for appliance type 1 on PS1 and PS2 of production line 1.

The simulations meet exactly the predicted output of the plant by the optimization procedure. The sensitivity of the solution was investigated by increasing the number of vehicles by introducing an additional vehicle to the optimal number of vehicles. Depending on the PS

where the additional vehicle is set at starting of simulation the output decrease because of back-ups, is 0, or is only increasing very low. The maximum increase of output was in the case of increasing the number of vehicles of 8 % less than 1 %. Also additional moulds in process has no effect on output as simulations proof.

5. CONCLUSION

In the paper after introducing the procedure of manufacturing home appliances the bottleneck plant of

foaming the housings of the appliances was presented. Due to capacity increasing redesign of manufacturing structure was done. Two alternatives were discussed. Because the tuning of number of plastification stations (PS), number of driverless transportation vehicles (DTV), and number of moulds in process has an high influence on the output of this flexible manufacturing plant an optimization of these variables has great relevance. To prove the results of the analytical optimization the plant was dynamically simulated by time weighted petri nets. Therefore, after introducing time weighted petri nets, a simulation tool was developed to reproduce time event discrete systems. After modeling present problem the simulation meets the predicated results of the optimization and fortify the optimization results by sensitivity investigations in case of changing number of vehicles and moulds and comparing the resulting productivity. Result was that in flexible manufacturing systems the exact tuning of number of manufacturing stations, number of transportation vehicles, and moulds or workpieces in process are highly important to guarantee high productivity of the plant.

REFERENCES

- [1] Abel D.: Petri Netze für Ingenieure, Springer Verlag, Berlin, 1990
- [2] Moßig K., Krebs V.: Control design for timed petri nets with the max-plus algebra; in Proceedings of the 1. Asian Control Conference, Vol. 2, 1994, 889-892
- [3] Tatikonda M., Croscheck M.: A case study on FMS capacity determination; in: Stecke K., Suri R.: Flexible Manufacturing Systems, Proceedings of the 3. ORSA/TIMS Conference, Elsevier, Amsterdam, 1989, 73-78
- [4] Tempelmeier H., Kuhn H.: Flexible Fertigungssysteme, Springer Verlag, Berlin, 1992

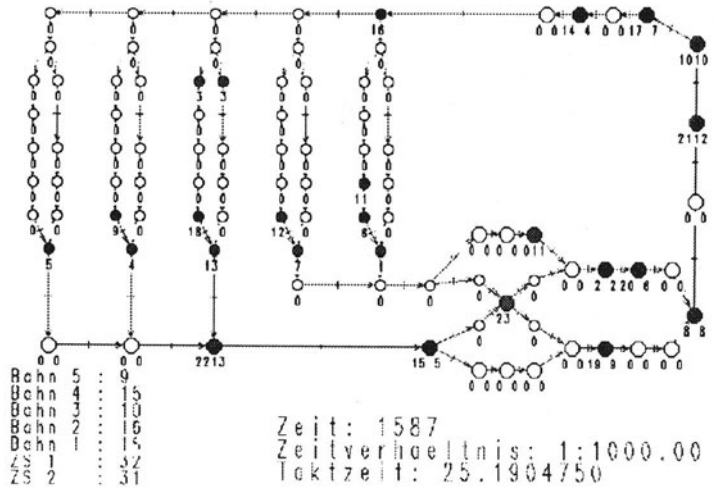


Fig. 6: Screenshot of simulation tool with modeled plant by time weighed petri nets.

ECONOMIC DESIGN OF CONTROL CHARTS CONSIDERING THE INFLUENCE OF THE TOOL WEAR

C. Giardini, E. Ceretti and G. Maccarini

University of Brescia, Brescia, Italy

A. Bugini

University of Bergamo, Bergamo, Italy

KEY WORDS: *optimal tool substitution, statistical analysis, shift phenomenon, x charts*

ABSTRACT: *Statistical analysis, within the quality control technique, allows us to evaluate the reliability of the processes under consideration by means of: control charts (x-R, n-p, ...) and suitable parameters (c_p , c_{pk} , ...), especially when a great number of pieces is worked. In particular, the x-R charts make the analysis of the production behaviour possible, allowing the immediate identification of various process irregularities, such as: out-of-control pieces and the shift phenomenon. These phenomena can be strictly correlated to either regular or accelerated tool wear. The data for monitoring the process are taken at regular intervals. The basic idea of the present work is to consider the influence (in terms of cost) of the intermediate check of the work-piece condition (according to the process statistical analysis) on the tool substitution and management policy.*

1. INTRODUCTION

When a great number of pieces is worked, it becomes very important to identify those parameters which allow the reliability of the process to be evaluated. The statistical analysis, within the quality control technique, allows us to overcome this problem by means of: control charts (x-R, n-p, ...) and suitable parameters (c_p , c_{pk} , ...) [13,14,15,16,17].

In particular, the x-R charts make the analysis of the production behaviour possible, allowing the immediate identification of various process irregularities, such as: out-of-control pieces (out of upper and lower control limits) and the shift phenomenon (i.e., the trend of a given piece dimension to increase or decrease) as shown in figure 1.

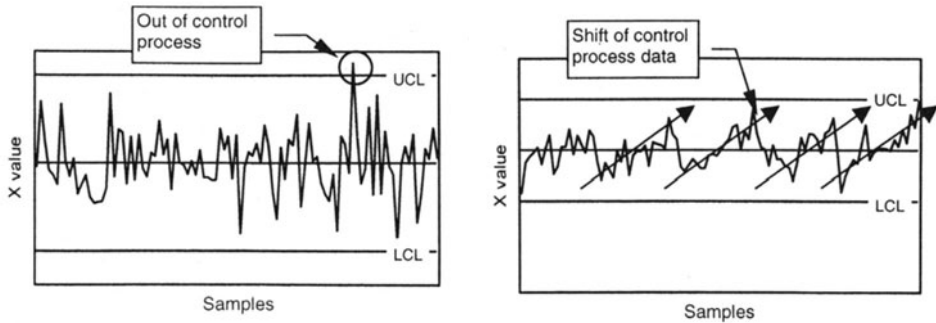


Figure 1 - Examples of X charts showing out control processes

In cutting processes these phenomena can be correlated with the tool status which can be monitored in many ways. The tool status can be correlated with the flank wear VB (either regular or accelerated) and it is generally described as a stochastic figure for given VB value [1,2,3,11]. Figure 2 shows, as an example, the experimental results obtained turning carbon steel (C40 annealed) with TPGN 160304 SIP IN sintered carbide tool tips with: s 215 m/min, f 0.2 mm/rev, d 2 mm [4,5,6,8].

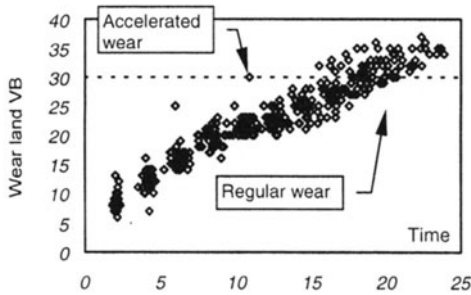


Figure 2 - Wear land distribution vs. time (50 tools monitored) [4,5,6,8]

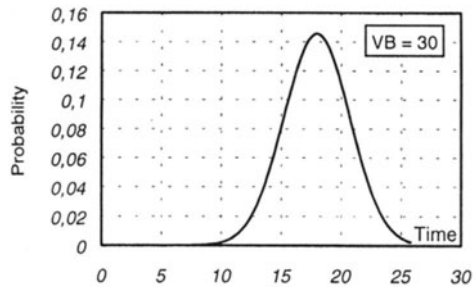


Figure 3 - pdf for the monitored tools at VB equal to 30 [4,5,6,8]

Tool status can be described by means of a suitable pdf (probability density function), which represents the probability that a tool could perform its task (i.e.: it is not broken or too worn) at a given time (figure 3). The function parameters can be evaluated by executing a set of experimental tests, and are correlated with the tool and work-piece material and the cutting parameters [1,3,9,11].

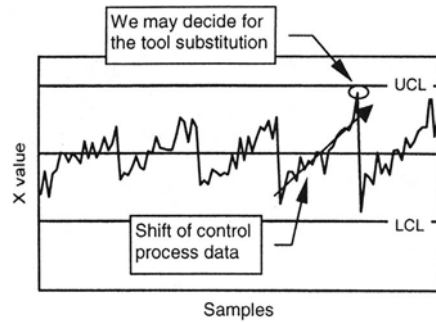
From literature it is possible to find out how to calculate the optimal cutting conditions as a function of the various costs and penalties, when the objective function is to minimise the cost per piece produced, suggesting, also, an optimal tool substitution interval (namely the expected tool life) [7,10,12].

The basic idea of the present work is to consider the influence (in terms of cost) of the intermediate check of the work-piece dimensions (according to the process statistical analysis) on the tool substitution and management policy. In fact, when the checking frequency of the work-pieces is

greater than the tool substitution rate, some intermediate controls on the tool status are carried out, before the substitution time has been reached.

The checks correspond to each point drawn on the control chart. When out-of-control pieces are produced or when strange behaviour is noticed, the tool can substituted before the expected time, so giving a different tool performance.

Several re-working policies can be adopted for the out-of-control pieces, which can also be definitively scrapped. These intermediate inspections affect the cost per piece calculus which, obviously, depends on both the checking time interval and the consequent tool reliability. The identification of this influence, the new cost per piece and the tool reliability are the objectives of the present work.



2. THE PREMATURE BREAKDOWN IDENTIFICATION CASE

When we speak about *production time*, we refer to T_p defined as:

$$T_p = T\alpha \cdot R\alpha + T_R \cdot (1 - R\alpha) \tag{1}$$

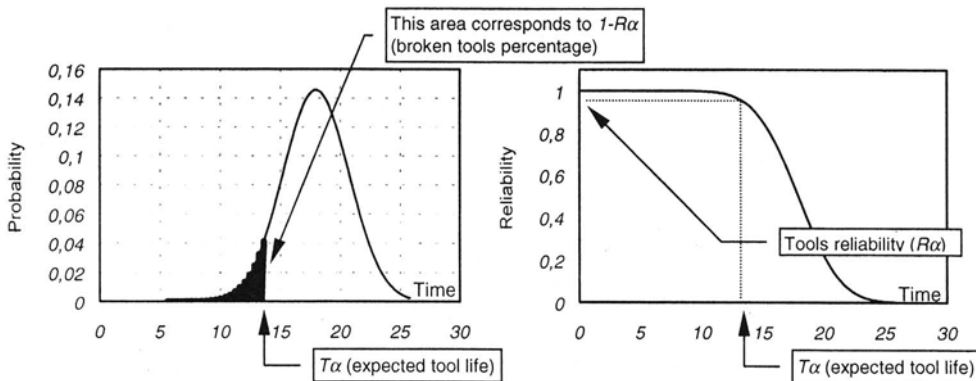


Figure 4 - Meaning of the several parameters involved in formula (1)

where (see figure 4):

- $T\alpha$ is the *expected tool life* i.e. the time at which the tool must be substituted
- $R\alpha$ is the *tool reliability* i.e. the probability that the tool is able to reach $T\alpha$
- T_R is the *breakage mean time* i.e. the time at which, on average, those tools that do not reach $T\alpha$ break down

This means the mean number of pieces worked by each tool tip can be expressed as:

$$\bar{N}_p = \frac{T_p}{T_c} \tag{2}$$

where T_c is the cutting time.

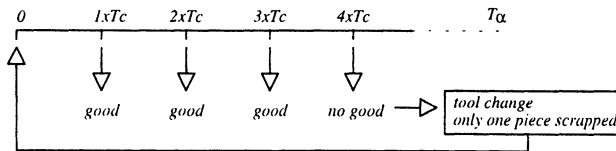
It is well known that the cost per produced piece C_p can be written as:

$$C_p = C_o \cdot T_c + \frac{C_o \cdot t_c}{\bar{N}_p} + \frac{C_a}{\bar{N}_p} + \frac{(1 - R\alpha) \cdot (Rw + Rt)}{\bar{N}_p} \tag{3}$$

where:

C_o is the operator cost per minute	Rw is the penalty cost
C_a is the tool cost	Rt is the penalty time, i.e. the cutting time lost in working the broken piece
t_c is the tool changing time	

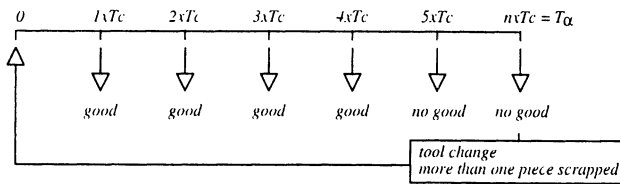
This formula is valid under the hypothesis that at the end of each cutting operation the tool is checked in order to decide if it is still able to continue the cutting process and if the workpiece must be scrapped.



Commonly it can be said that formula (3) represents the cost per piece when the premature break-down of the tool can be identified.

3. IN CONTROL AND OUT OF CONTROL PIECES

A different tool substitution policy can be outlined.



If no intermediate checks on the pieces produced are carried out, the tool will continue the cutting operation until T_α is reached, and it will be substituted only at T_α scrapping more than one piece.

It can be easily noticed how the predefined \bar{N}_p represents the number of *in control* pieces and does not change with respect to the previous policy. On the other hand, the number of *out of control* pieces (produced by those tools which break down before T_α) varies and can be evaluated as:

$$\bar{N}_o = N_{tot} - \bar{N}_p = T_\alpha / T_c - \bar{N}_p = (1 - R\alpha) \cdot \left(\frac{T_\alpha - T_R}{T_c} \right) \tag{4}$$

Referring to the control chart analysis, in this case we can obtain the well known *shift phenomenon* for which a behaviour similar to that presented in chapter 1 can be outlined.

4. THE COST IN THE CASE OF THE SHIFT PHENOMENON

The total production cost corresponding to each tool tip (C) considers both the cutting of \bar{N}_p and \bar{N}_o . As a consequence, C can be written as follows:

$$C = C_o \cdot T_c \cdot (\bar{N}_p + \bar{N}_o) + C_a + C_o \cdot t_c + Rw \cdot \bar{N}_o \tag{5}$$

Considering that: $C_p = C / \bar{N}_p$ we can derive a new expression for C_p :

$$C_p = C_o \cdot T_\alpha \cdot \frac{T_c}{T_p} + C_a \cdot \frac{T_c}{T_p} + C_o \cdot t_c \cdot \frac{T_c}{T_p} + Rw \cdot (1 - R\alpha) \cdot \frac{T_\alpha - T_R}{T_p} \tag{6}$$

This expression must be compared with that obtained from formula (3). As an example, figure 5 shows the T_c and R_w influences on C_p values according to shift or no shift policy. The calculus are carried out considering: log-normal distribution ($\mu = 2.35$; $\sigma = 0.20$), $Ca/Co = 5.0$, $t_c = 0.5$.

From the analysis of figures 5 and 6, several considerations can be made:

1. in the case of no shift, the T_c time does not influence the calculus of the cost because the basic hypothesis is that the tool status is checked at the end of each cutting operation (the control is extended to every piece);
2. when $T\alpha$ is not much greater than T_c (say max. 10 times), the shift phenomenon is not so evident in terms of costs and the number of scrapped (out of control) pieces is low; in this case, the sampling interval can coincide with $T\alpha$;
3. on the contrary, when $T\alpha$ becomes very high compared to T_c , the number of out of control pieces can increase significantly (and, consequently, the cost per piece produced): this means that either we control all the produced pieces or work a very short time with a very high tool reliability (corresponding to the minimum in the cost curves).

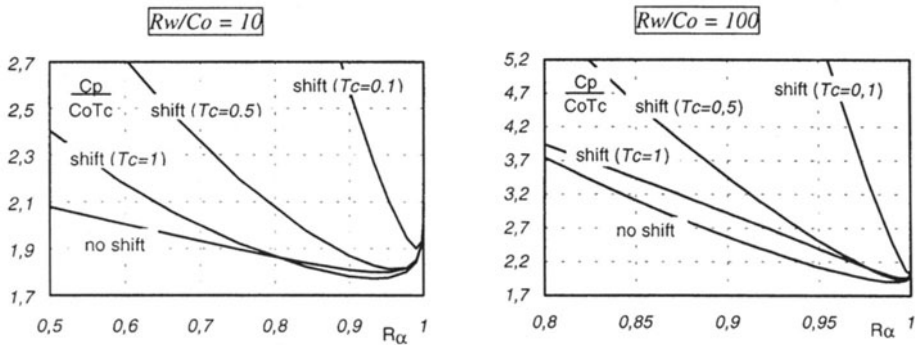


Figure 5 - Behaviour of $C_p/(CoT_c)$ according to formula (3) and formula (6) vs. T_c value

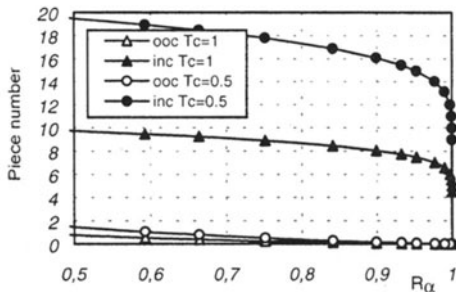


Figure 6 - Behaviour of the in control (inc) and out of control (ooc) pieces vs. T_c

The solutions to this problem can be found by reducing the penalty term ($R_w \cdot \bar{N}_o$), that is, making intermediate controls as the production continues.

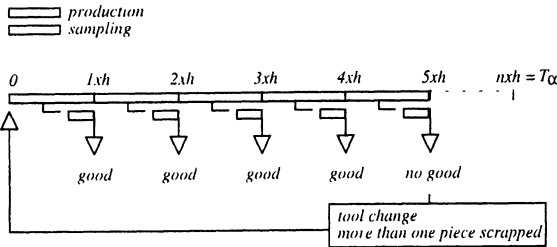
When we refer to a system in which SPC is commonly employed, these controls can coincide with the sampling interval necessary to conduct statistical analysis on the pieces produced. This means dividing $T\alpha$ into equal intervals performing the controls on the sampled pieces in correspondence to these stops.

This policy allow us to reduce the number of scrapped pieces (out of control) substituting the tool tip as soon as a shift takes place.

It is important to determine these intervals h (or their number n) correctly in order to find the optimum solution both in terms of inspections scrapped piece cost.

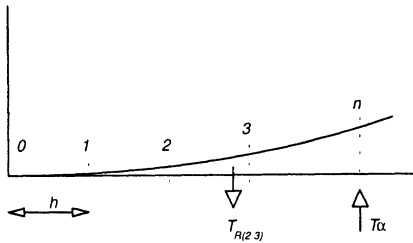
5. THE CASE OF INTERMEDIATE CHECKS

As already said, it is possible to perform intermediate checks on the tool status by controlling the pieces produced and deciding to substitute the tool tip when a shift occurs.



In this case the expected time $T\alpha$ is divided into n , long h , intervals.

The figure at the side shows the new adopted policy. In this case a new cost per produced piece can be identified starting from the new expression of out of control pieces $\bar{N}o$ (refer to formula (4)).



This value must be recalculated considering that for each interval the number of out of control pieces is equal to the difference between the upper limit of the interval (h_i) and the mean time at which the tool breaks within the interval ($T_{R(i-1,i)}$), divided by Tc , and multiplied by the probability that the breakage actually takes place ($R\alpha_{i-1} - R\alpha_i$) in this interval. Extending the calculus to the whole $T\alpha$, we have:

$$\bar{N}o = \sum_{i=1}^n (R\alpha_{i-1} - R\alpha_i) \cdot \left(\frac{i \cdot h - T_{R(i-1,i)}}{Tc} \right) \tag{7}$$

As a consequence the number of in control pieces $\bar{N}p$ becomes:

$$\bar{N}p = \sum_{i=1}^n \frac{R\alpha_{i-1} \cdot h}{Tc} - (R\alpha_{i-1} - R\alpha_i) \cdot \left(\frac{i \cdot h - T_{R(i-1,i)}}{Tc} \right) \tag{8}$$

This means that the cost expressed by formula (5) becomes:

$$C = Co \cdot Tc \cdot (\bar{N}p + \bar{N}o) + Ca + Co \cdot tc + R_w \cdot \bar{N}o + Cm \cdot (1 + \sum_{i=1}^{n-1} R\alpha_i) \tag{9}$$

where $\bar{N}p$ and $\bar{N}o$ are derived from formula (7) and (8) and Cm is the single sample control cost.

NO intermediate checks						Intermediate checks						
Interval	$T_{R(i-1,i)}$	$R\alpha$	$\bar{N}o$	$\bar{N}p$	Total	Interval	$T_{R(i-1,i)}$	$R\alpha_{i-1}$	$R\alpha_i$	$\bar{N}o$	$\bar{N}p$	Total
Unique	78.93	85.04	6.35	193.65	200.00	0-1	9.22	100.00	100.00	0.00	20.00	20.00
						1-2	18.07	100.00	100.00	0.00	20.00	20.00
						2-3	26.92	100.00	99.97	0.00	20.00	20.00
						3-4	36.19	99.97	99.80	0.01	19.98	19.99
						4-5	45.77	99.80	99.23	0.05	19.91	19.96
						5-6	55.52	99.23	98.03	0.11	19.73	19.84
						6-7	65.36	98.03	96.01	0.20	19.41	19.61
						7-8	75.25	96.01	93.12	0.29	18.91	19.21
						8-9	85.17	93.12	89.42	0.38	18.25	18.63
						9-10	95.11	89.42	85.04	0.45	17.43	17.88
						Total				1.49	193.62	195.11

Note how we can obtain the same number of in control pieces, working a lower number of pieces; in particular the number of out of control pieces becomes smaller.

The term: $1 + \sum_{i=1}^{n-1} R\alpha_i$, represents the average number of controls carried out per tool tip.

First of all it is important to note how the number of out of control pieces obtained when no intermediate controls are carried out is greater than when they are carried out. As an example, the tables report the results obtained when considering $\mu = 5.124$, $\sigma = 0.50$, $T_c = 0.5$, $T\alpha = 100$, $h = 10$.

6. OPTIMISATION CONSIDERATIONS

Dividing the expression number (9) by $\bar{N}p$, we can obtain the cost per piece produced which must be minimised, firstly with respect to $T\alpha$ and then with respect to h .

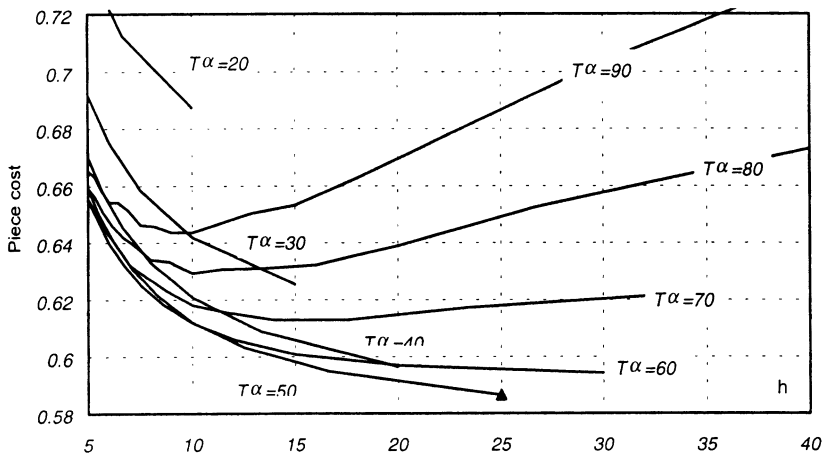


Figure 7 - $C/(CoNp)$ vs. $T\alpha$ and h with intermediate controls (formula 9)

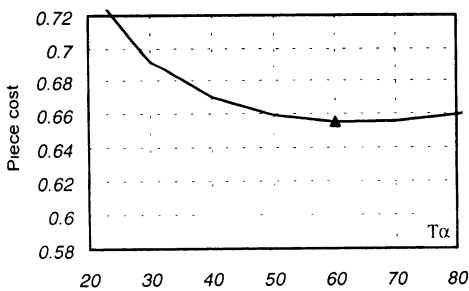


Figure 8 - $C/(CoNp)$ vs. $T\alpha$ without intermediate controls (formula 6)

The influence of the several figures involved in this formula make it evident that:

- if the cost of the rough pieces is high compared to the single sample control cost, it is better to carry out a greater number of intermediate checks ($h \downarrow$) in order to identify the occurrence of the shift phenomenon as soon as possible;
 - on the other hand, if the cost of the rough pieces is low compared to the single sample control cost, a lower frequency check will be made ($h \uparrow$);
- the final number of in control and out of control pieces is also affected by the T_c value with respect to h .

As an example, figure 7 shows the influence of h (for constant values of $T\alpha$) on the cost per piece produced as derived from equation number (9). The comparison must be drawn with respect to figure 8 where no intermediate checks are considered. It is evident how, if $T\alpha$ is low (i.e. the tool works with an high final reliability), no many intermediate checks are needed (the minimum cost is

reached for the higher h values). On the contrary, when $T\alpha$ is high (i.e. the tool works with a low final reliability), the minimum cost corresponds to intermediate values of h . The absolute minimum found is lower than the one obtained without intermediate controls. The signs \blacktriangle represent the two minimum conditions.

The calculus are carried out for the following values: $C_d/C_o = 5$, $t_c = 0.5$, $R_w/C_o = 10$, $C_m/C_o = 1$.

7. CONCLUSIONS

In the present work the authors have showed how it is possible to optimise the tool substitution interval together with the inspection frequency on the production carried out. A new formula for the calculus of the cost of the pieces produced, able to consider the influence of both these figures, is suggested. Finally, the influence of tool substitution interval and inspection frequency, during the optimisation phase, is also outlined.

8. REFERENCES

1. Ramalingam S., Watson J. D., "Tool-life distributions - Part 1: single-injury tool-life model", *Jou. Of Eng. for Ind.*, August, 1977.
2. Rossetto S., Levi R., "Fracture and wear as factors affecting stochastic tool-life models and machining economics", *Jou. Of Eng. for Ind.*, February, 1977.
3. Rossetto S., Zompi A., "A stochastic tool-life model", *Jou. of Eng. for Ind.*, vol. 103, 1981.
4. Pacagnella R., Giardini C., Restelli G., Bugini A., "The effects of the statistical nature of tool life on the economics of machining: experimental results", *Int.Conf. on CAD of Machinery 91*, Beijing, 1991.
5. Giardini C., Pellegrini G., Pacagnella R., Bugini A., "The stochastic nature of tool life: experimental results in continuous turning", 6th Int. Conf. CAD-CAM, Robotics, Fact. of Future, London, 1991.
6. Giardini C., Pellegrini G., Pacagnella R., Bugini A., "Experimental results in continuous turning: the feed influence on tool wear", *ICIM '91*, Turin, 1991.
7. Makis V., "Optimal control of a tool-wear process", *proc. of 13th ICPR*, Jerusalem, 1995.
8. Ceretti E., Giardini C., Maccarini G., "A new method of representing the tool life data: the mixtures", *proc. of 14th ICPR*, Osaka, 1997.
9. Quesenberry C.P., Kent J., "Selecting among probability distributions used in reliability" *Technometrics*, Vol. 24, n. 1, 1982.
10. Bugini A., "La distribuzione di frequenza della durata utensili ed il costo di lavorazione" (in italian), *La Meccanica Italiana*, n. 174, 1983.
11. Bugini A., Pacagnella R. "La durata attesa di un utensile" (in italian), *La Meccanica Italiana*, n. 166, 1982.
12. La Commare U., Noto La Diega S., Passannanti A. "Optimum tool replacement policies with penalty cost for unforeseen tool failure", *Int. J. Mach. Tool Des. Res.* Vol. 23 n. 4, 1983.
13. Bowker A.H., Lieberman G.J, "Engineering statistics", 2nd ed., Prentice Hill, Englewood Cliffs, N.J., 1972.
14. Chiu W.K., "Economic design of attribute control charts", *Technometrics*, Vol.17.
15. Grant E.L., Leavenworth R.S., "Statistical quality control", 5th ed., McGraw Hill, New York, 1980.
16. Montgomery D.C, Heikes R.G., "Process failure mechanism and optimal design of fraction defective control charts", *AIIE Transaction*, vol.8, 1976.
17. Douglas C., Montgomery D.C., "Economic design of an x control chart"; *Jou. Of quality technology*, vol. 14, n. 1, 1982.

OPTIMIZATION OF TURNING TOOL GEOMETRY BY NONLINEAR PROGRAMMING

G. Cukor and M. Jurkovic
University of Rijeka, Rijeka, Croatia

KEY WORDS: Tool Geometry, Tool Life Models, Turning, Optimization

ABSTRACT: This paper deals with the determination of optimal tool geometry for longitudinal turning. A tool life is usually the main machinability factor and, as such, the basic optimization criterion of tool geometry. The establishing of tool response function is done by the second order central composite design of experiment. Since the criterion function is inherently nonlinear in this case, i.e. besides linear contains quadratic elements and two-factorial interactions, the care must be taken to employ an appropriate optimization method for solving such function. Therefore, the optimization procedure based on nonlinear programming methods is proposed. Furthermore, the testing example of developed algorithm is presented.

1. INTRODUCTION

The first step in the optimization of cutting process is the definition of mathematical model that is given as the functional dependence of measured value on influencing parameters. The establishing procedure of reliable mathematical model still remains an extremely complex problem because the influencing process parameters, except their particular influences, may have also their mutual interactions. Therefore, the process modeling includes computer assistance and, because of its rationality, is based on the design of

Published in: E. Kuljanic (Ed.) *Advanced Manufacturing Systems and Technology*,
CISM Courses and Lectures No. 406, Springer Verlag, Wien New York, 1999.

experiment. There are different ways of model generating, but the basic question is how adequately it describes the real process conditions. Nevertheless, in many experimental investigations of cutting process where extreme responses are expected, the second or the third order polynomial models are satisfying.

The determination of optimal parameters starts after defining the optimization criterion based on the some form of mathematical model. As a result of optimization, the extreme value of optimization criterion can be determined. However, the obtained result is depended to a great extent on the optimization method used.

This study has been developed under the assumption that an optimum tool geometry will result as a consequence of maximum tool life criterion. A solution using the nonlinear programming methods is introduced.

2. TOOL LIFE MODELING

It has been shown that tool life can be predicted successfully on the basis of some polynomial form of the following model [1]:

$$y = f(x_i, b_i), \quad i = 0, 1, 2, \dots, k, \quad x_0 = 1 \quad (1)$$

where y is the tool life prediction, b_i s are the estimated tool life model parameters and k is the number of influencing parameters x_i s. Although the first order polynomials, that is linear tool life models are still, directly or indirectly, widely used both in industry and research, however the accuracy reached by these models can be insufficient since the data sometimes clearly show the existence of non-linearity (saddle shaped functions) which cannot be ignored. In that case, more sophisticated ones have to be used if the optimization is to be carried out under more realistic conditions.

In order to predict the tool life response with increased reliability, i.e. to take into consideration the non-linearity, the second order polynomial with included significant interactions is selected. Its definition is based on the statistically designed experiment and multiple regression analysis. Accordingly, the adopted algorithm of tool life modeling is given in Figure 1.

The best experimental design to use will depend on the selected form of tool life model. Using the second order central composite design of experiment [2], it is possible to establish the tool life response function in the second order polynomial form:

$$y = b_0 + \sum_{i=1}^k b_i x_i + \sum_{i=1}^k b_{ii} x_i^2 + \sum_{i < j}^k b_{ij} x_i x_j \quad (2)$$

where regression coefficients b , b_{ii} , b_{ij} denote linear, quadratic and the effects of two-factorial interactions respectively, and x_i s are the coded values of input physical parameters p_i s in accordance with:

$$x_i = \frac{p_i - \frac{p_{i \max} + p_{i \min}}{2}}{\frac{p_{i \max} - p_{i \min}}{2}} \tag{3}$$

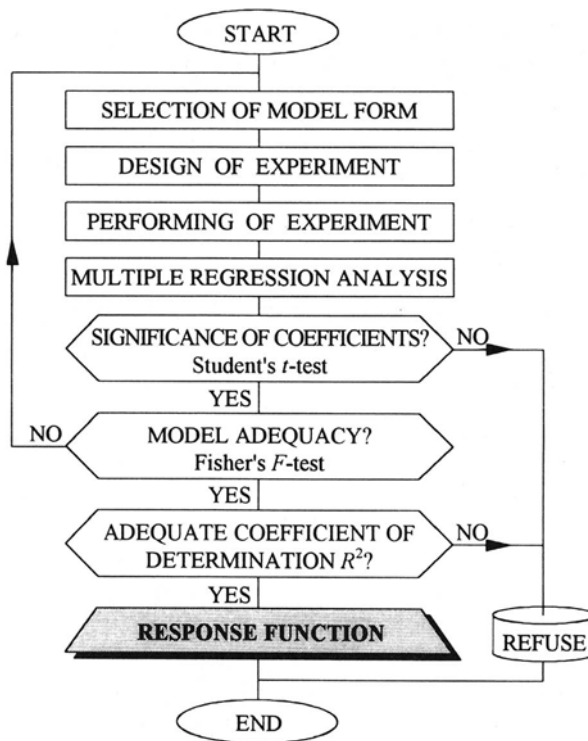


Figure 1. Algorithm of tool life model establishing

3 OPTIMIZATION PROCEDURE

The tool life T is the basic optimization criterion of tool geometry. If the selected input tool geometry parameters are clearance angle α , nose angle ε and approach angle κ , as it is shown in Figure 2, the following maximum tool life criterion can be postulated [3]:

$$T_{\max} = y(\alpha, \varepsilon, \kappa)_{\text{opt}} \tag{4}$$

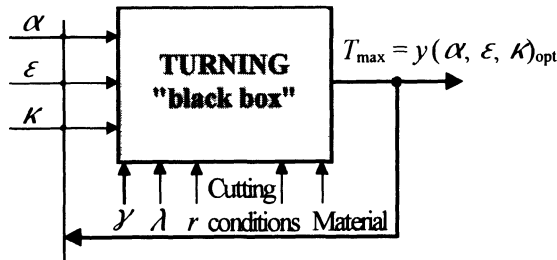


Figure 2. Scheme of input/output parameters

The optimization criterion (4) should be maximized within the feasible region of the space of tool geometry parameters. Hence, for handling the boundaries of parameters, the *modified criterion function method* is implemented [4]. The boundaries are incorporated into the criterion function which leads to a boundless model of the form:

$$\text{maximize } \left\{ y + C_F \sum_{m=1}^n g[h_m(x)] \right\} \quad (5)$$

where C_F is correction factor, n is the total number of boundaries $h_m(x)$ and the *exterior penalty function* is of the form:

$$g[h_m(x)] = \begin{cases} 0 & h_m(x) \geq 0 \\ h_m(x) & h_m(x) < 0 \end{cases} \quad (6)$$

Penalty function is used in order to apply a penalty to the criterion function at non-feasible points, thus forcing the search process back into the feasible region.

Since the optimization model developed herein is non-convex, nonlinear and multivariable model, the care must be taken to employ an appropriate optimization method for its solving. To determine such a method, a comprehensive literature survey has been carried out and many methods have been tested. Although many of general non-linear programming methods tested can achieve acceptable results, it has been concluded that in order to ensure finding global optimum, a combination of methods both the *Direct Search of Hooke and Jeeves* and *Random Search* [5, 6] is the most efficient for solving the maximization problem presented.

A computer program using Fortran programming language was developed and the algorithm of direct search routine of Hooke and Jeeves is given in Figure 3. Direct search is performed three times at different starting points chosen with respect to feasibility and criterion values out of randomly generated points. A minimum installation needed for the program is PC/486.

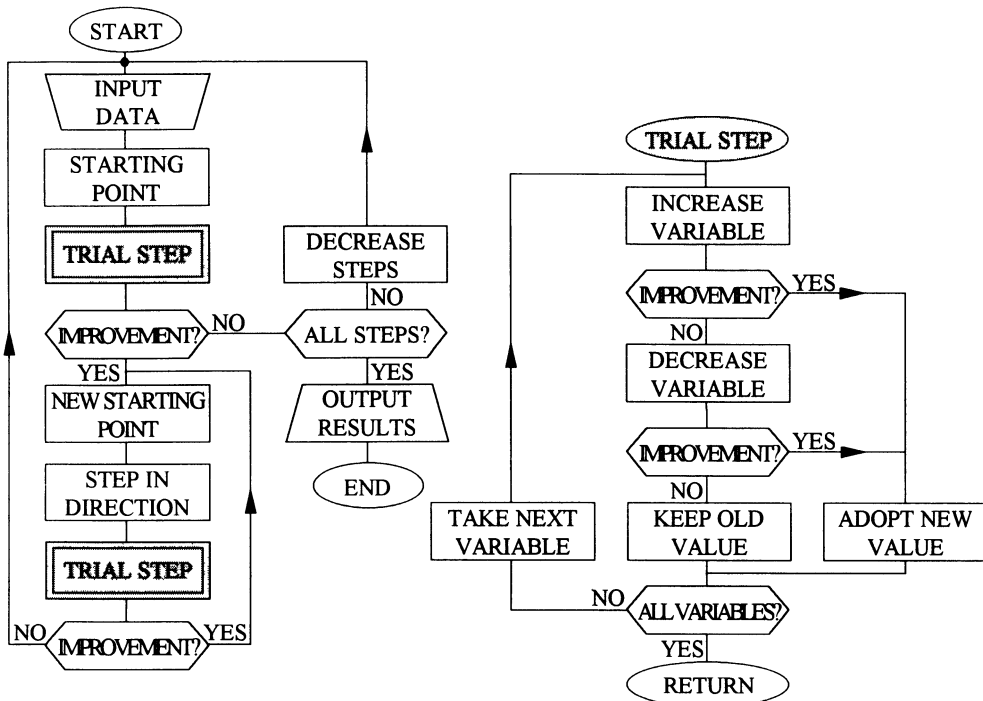


Figure 3. Algorithm of direct search procedure of Hooke and Jeeves

4. EXPERIMENT RESULTS

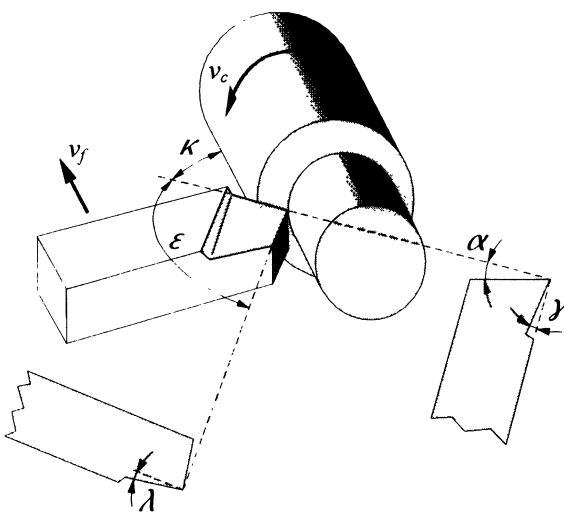


Figure 4. Tool geometry

The experiments were performed on universal lathe TS-200 with tool grade P30 (ISO). Longitudinal turning in Figure 4 was conducted dry and performed at constant cutting speed $v_c = 3$ m/s, feed $f = 0,125$ mm per revolution, depth of cut $a_p = 2$ mm, rake angle $\gamma = 6^\circ$, inclination angle $\lambda = 4^\circ$ and nose radius $r_\epsilon = 1$ mm. The workpiece material was quenched and tempered steel C 60 (DIN) with Brinell hardness 260 HB. The tool life criterion was planned to be $VB = 0,3$ mm and tool wear was measured on the tool micrometer microscope Carl Zeiss (0,01 mm).

By means of mathematical model (2) and using the second order central composite design of experiment $N = 2^k + n_0 + n_\alpha = 2^3 + 6 + 6 = 20$, the tool life was modeled ($x_1 = \alpha$, $x_2 = \varepsilon$, $x_3 = \kappa$) by varying all the factors on five levels (-1.682, -1, 0, 1, 1.682) as shown in table 1.

Table 1. Review of observed tool life results

Test no.	Coded values			Variables			Measured T	
	N_j	x_1	x_2	x_3	α°	ε°	κ°	y_j [min]
1	1	-1	-1	-1	5	75	35	23.0
2	2	1	-1	-1	11	75	35	22.0
3	3	-1	1	-1	5	95	35	28.0
4	4	1	1	-1	11	95	35	26.0
5	5	-1	-1	1	5	75	55	25.0
6	6	1	-1	1	11	75	55	24.0
7	7	-1	1	1	5	95	55	31.0
8	8	1	1	1	11	95	55	28.0
9	9	0	0	0	8	85	45	29.2
10	10	0	0	0	8	85	45	28.5
11	11	0	0	0	8	85	45	29.0
12	12	0	0	0	8	85	45	27.5
13	13	0	0	0	8	85	45	28.5
14	14	0	0	0	8	85	45	28.3
15	15	-1.682	0	0	3	85	45	25.0
16	16	1.682	0	0	13	85	45	26.0
17	17	0	-1.682	0	8	68	45	20.0
18	18	0	1.682	0	8	102	45	32.0
19	19	0	0	-1.682	8	85	28	21.0
20	20	0	0	1.682	8	85	62	32.0

The calculated values of regression coefficients and the review of their significance are given in table 2.

Table 2. Regression coefficients

b_0	b_1	b_2	b_3	b_{11}	b_{22}	b_{33}	b_{12}	b_{13}	b_{23}
28.5167	-0.3892	2.86826	2.01314	-1.0828	-0.9060	-0.7293	-0.375	-0.125	0.125
✓	✓	✓	✓	✓	✓	✓	✗	✗	✗

✓ - significant at level $\alpha_t = 0.05$; ✗ - not significant

Significance evaluation of calculated coefficients was done according to Student's t -test for the condition $|b_i| \geq \Delta b_i = \pm t_{s_0} \sqrt{\alpha_{ij}}$, where $f_0 = n_0 - 1 = 6 - 1 = 5$ and a level of significance $\alpha_i = 0.05$ (i.e. 5%). Considering only significant regression coefficients, the following mathematical model of tool life was obtained:

$$y = 28.5167 - 0.389 x_1 + 2.868 x_2 + 2.013 x_3 - 1.083 x_1^2 - 0.906 x_2^2 - 0.729 x_3^2 \quad (7)$$

The verification of model adequacy was done according to Fisher's F -test for the condition $F_a < F_t(f_a, f_0) = F_t(8, 5)$ with probability $P = 0.99$. Since $F_a = 9.339 < F_t(8, 5) = 10.30$, the dependency of tool life on tool geometry has been well explained. According to coefficient of determination $R^2 = 0.8778$, the tool life has been described sufficiently accurate by the functional dependence (7) in the tested area. After decoding, the final form of fitted polynomial was determined:

$$T = -91.77 + 1.79 \alpha + 1827 \varepsilon + 0.857 \kappa - 0.12 \alpha^2 - 0.009 \varepsilon^2 - 0.0073 \kappa^2 \quad (8)$$

Finally, using the optimization procedure described in previous section, the optimum values of tool geometry parameters were obtained from the tool life model (8). Hence, the optimum tool geometry was defined by the following angles:

$$\begin{aligned} \alpha_{\text{opt}} &= 7^\circ 27', \\ \varepsilon_{\text{opt}} &= 101^\circ 30', \\ \kappa_{\text{opt}} &= 58^\circ 42'. \end{aligned}$$

5. CONCLUSIONS

Based on the performed research and the obtained results, the following conclusions can be drawn:

- the adopted methodology of tool life modeling as well as the recommended tool life model can be successfully used for the optimization of tool geometry according to maximum tool life criterion;
- the proposed optimization procedure based on nonlinear programming can be successfully applied for defining and selecting the optimal tool geometry;
- for the presented example, it is shown that tool life is on the increase with the increasing of angles $\varepsilon > 90^\circ$ and $\kappa > 45^\circ$ up to their optimal values ε_{opt} and κ_{opt} , also with the decreasing of angle $\alpha < 8^\circ$ down to its optimal value α_{opt} , which can be explained by better withdrawal of heat for the angles ε_{opt} and α_{opt} , that is by the decreasing of cutting force for the angle κ_{opt} .

Therefore, the definition of optimal tool geometry is strongly suggested whenever is possible since it is proved that tool life can be increased significantly.

ACKNOWLEDGEMENTS

This research is financially supported by the Ministry of Science and Technology of the Republic of Croatia, projects no. 069017 and no. 069103.

REFERENCES

1. Cukor, G.: Tool Life Models for Advanced Machining Systems, Proceedings of 4th International Conference on Production Engineering CIM'97, Cebalo, R. (Ed.), ISBN 953-97181-0-4, Croatian Association of Production Engineering, Opatija 1997, B35-42
2. Montgomery, C. D.: Design and Analysis of Experiments, Wiley, New York 1984
3. Jurković, M., Časni, N.: Mathematical Modeling and Optimization of the Elements of Tool Geometry for Turning, Proceedings of 3rd International Conference on Production Engineering CIM'95, Cebalo, R. (Ed.), ISBN 953-96501-2-7, Croatian Association of Production Engineering, Zagreb 1995, D47-55, (in Croatian)
4. Cukor, G.: Optimization of Machining Process, Master of Science Thesis, Faculty of Engineering, University of Rijeka, Rijeka 1994, (in Croatian)
5. Himmelblau, D. M.: Applied Nonlinear Programming, McGraw-Hill, New York 1972
6. Osyczka, A.: Multicriterion Optimization in Engineering with Fortran Programs, Ellis Horwood Ltd, New York 1984

CLASSIFICATION OF FEATURES CONSIDERING THEIR MACHINABILITY AND FACTORY FACILITIES FOR COMPUTER AIDED PROCESS PLANNING

K.D. Bouzakis and G. Andreadis
Aristotle University, Thessaloniki, Greece

KEYWORDS: IGES, feature machinability, process planning.

ABSTRACT: The present paper deals with the classification of workpiece features, considering their machinability and factory facilities, in order to determine automatically the workpiece process plan. Starting from the corresponding IGES file of a part, recognition of all features included in its geometry is conducted. Furthermore based on these features using eligible manufacturing criteria, a reorganisation and grouping of them is derived. Finally the classification of these features is accomplished and with the aid of the features normal vectors, the necessary set-ups as well as the process plan of the workpiece are determined.

1. INTRODUCTION

The process planning is a very significant stage in the manufacturing procedure of a product. For this purpose many intermediate procedures must be derived [1].

The main objective of the present paper is the creation of a flexible process plan algorithm independent from the design procedure. An appropriate computer-supported procedure, will be introduced in the following paragraphs. The data needed for the recognition of the predefined features are extracted from a neutral file (IGES), in order to develop a CAPP procedure, independent from the used CAD one, and capable to be integrated into any CAD/CAM system. Hence there are no restrictions regarding the design process and there

is a significant capability for final control of the results. The developed system is modular structured, enabling later on the completion or replacement of any of its criteria.

The structure of the developed algorithm is shown in [figure 1](#). Using an IGES file, as an interface, the whole system is autonomous from the various CAD programs. From the included in an IGES file information, only the necessary is selected and transformed into a convenient format. Moreover with the aid of the workpiece's entry faces, all the features are derived [2,3].

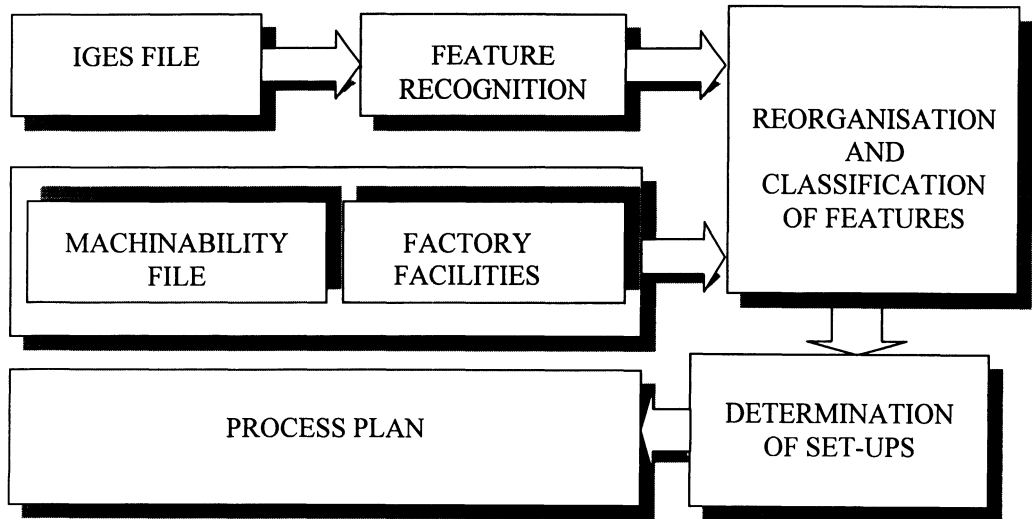


Figure 1: Structure of the developed algorithm

The results of the feature recognition procedure are stored into a further file (Feature.dat) containing all the extracted features, with their corresponding entry, base and side surfaces. Due to eligible manufacturing criteria, these features are reorganised and classified considering the existing machinability file and factory facilities database. A determination of the set-ups is finally conducted, based on the normal vector of the feature surfaces and the process plan of the workpiece is derived.

2. CLASSIFICATION OF FEATURES AND EXTRACTION OF THE WORKPIECE PROCESS PLAN

The results of a feature recognition procedure have in generally two weak points for process planning purposes. The recognised features are in random order, because no manufacturing criteria have been taken into account, and furthermore each feature is associated to many entry surfaces, thus no decision for possible set-ups can be derived. To overcome these problems the following procedure has been developed.

Using eligible machinability criteria, stored in a corresponding data file, as well as the factory facilities database, a reorganisation and classification of the extracted features is conducted.

These criteria have a certain hierarchy and their application affects in two ways the previous mentioned “Feature.dat” file. The sequence of the features is modified and a deletion of some of the possible entry faces is fulfilled. Hereby machinability criteria are applied, as for example the following:

- Selection of the machining surface of the workpiece according to the number of features.

The workpiece’s (orthogonal) raw material volume has 6 sides. The side in which the maximum number of features appears, is considered initially as the machining surface. For example in [figure 2](#), the front side of the workpiece is selected, due to the fact that this side contains the maximum number of features.

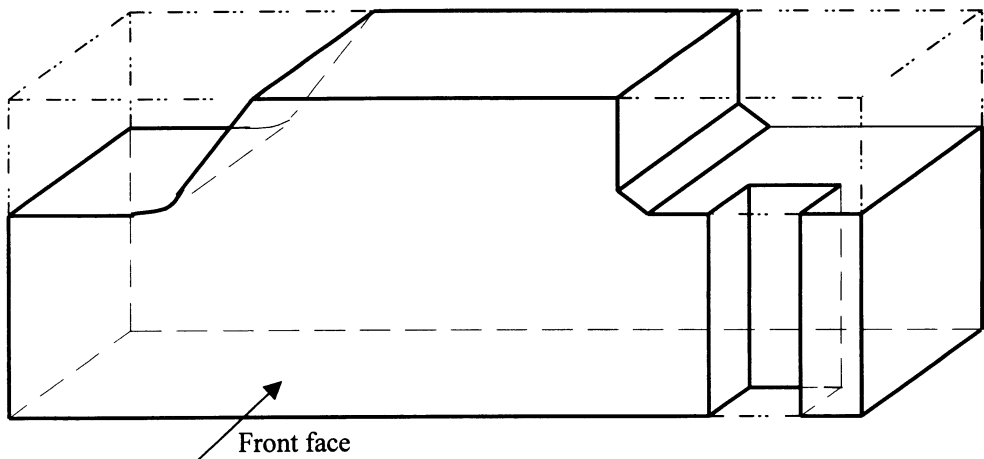


Figure 2: Workpiece example for the selection of the side with maximum number of features

- Intersection of holes.

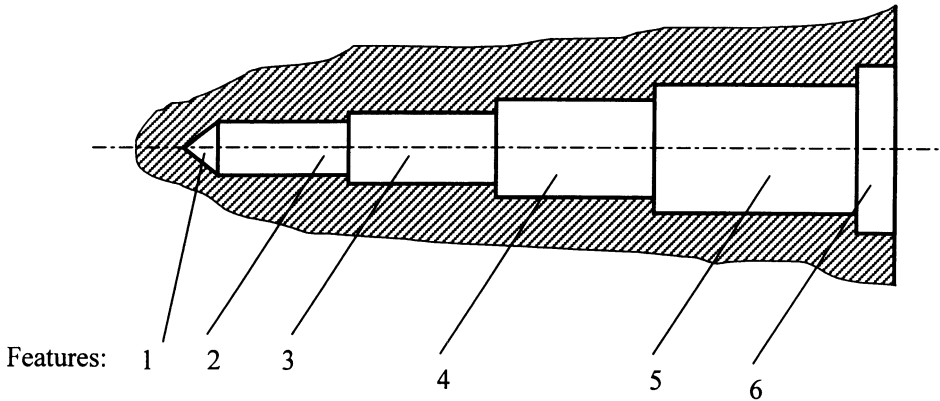
If two intersected holes are existing, that with the maximum diameter is selected, to be machined first. This sequence of cutting procedures minimises the impact loads and the possible risk of breaking the drilling tool.

- Holes with changeable diameters.

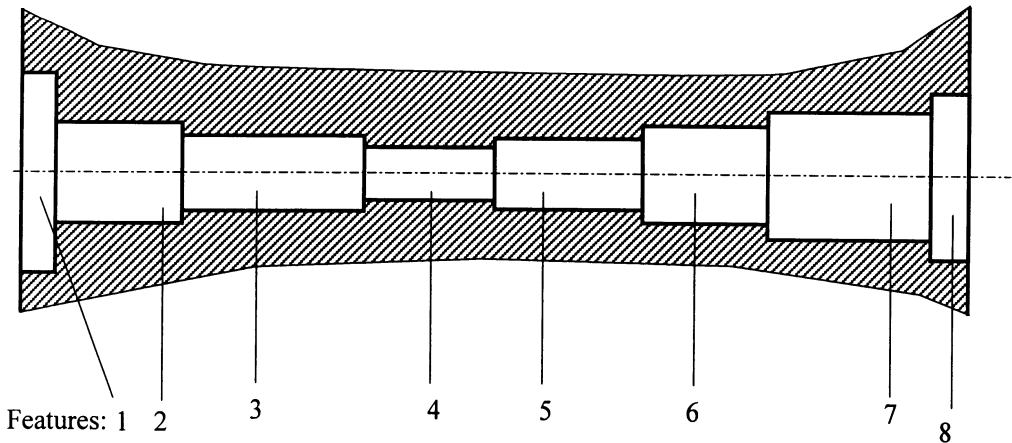
In the case of a hole with many changes of its diameter, the feature recognition procedure, recognises each different diameter as a separate feature. Thus it is necessary to unify these features into a contiguous hole. For example the recognised features 1 through 6 in the workpiece illustrated in [figure 3](#) compose one hole.

Additionally to this criterion, in the case of a through hole consisting of successive cylindrical entities with decreasing diameters, if the diameter starts increasing again, a new feature (through hole) is defined.

For example in the workpiece demonstrated in [figure 4](#), there are two holes, one consisting from features 1 through 4 and the other consisting from features 5 through 8.



[Figure 3](#): Hole with changeable diameters



[Figure 4](#): Through hole with changeable diameters

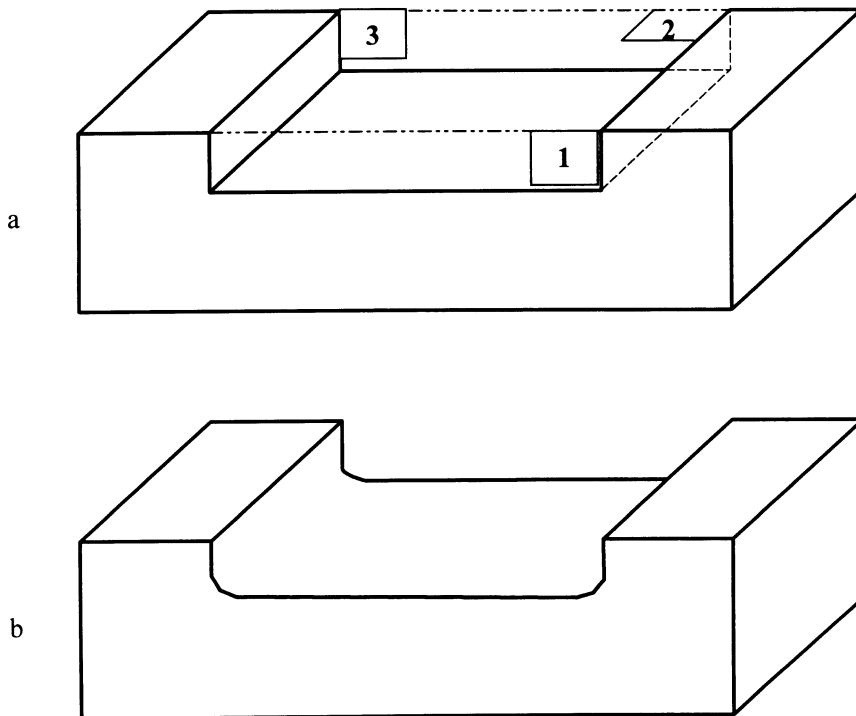
- Maximum length of holes.

This criterion is related to the maximum length of a hole that can be machined. For this reason if the length of a hole is bigger than a maximum value, then a through hole has to be divided into two parts, and two set-ups are required. In the case of a blind hole, a specific process is needed (deep drilling).

- Avoidance of a feature's curvature formation.

According to this criterion the entry faces of a feature leading to the formation of unexpected curvatures are detected and rejected. For example in the workpiece shown in [figure 5\(a\)](#) if the cutting tool uses as entry faces the 1 or 3, the curvature indicated in figure 5(b) will be formed. For this reason the faces 1 and 3 are rejected and the face 2 is selected as an appropriate entry face of the cutting tool.

Apart from the above-mentioned machinability criteria, the factory facilities database offers further information regarding the capabilities of the available machine tools, the cutting tools and the accuracy, which can be achieved.



[Figure 5](#): Avoidance of a feature's curvature formation

Moreover criteria as the minimisation of the tool motion are also applied. This is accomplished according to the following procedures. For each feature an indicative point is determined (for example the centre of a hole). Starting from another specified point, as for example the corner of each side of the raw material of the workpiece, all the connecting distances are calculated and the shortest path is selected. For instance in the workpiece shown in [figure 6](#) the selected path is illustrated in the lower part of this figure.

Using all these criteria the classification of features in a proper manufacturing order is carried out. The sequence of the appropriate machining processes of the workpiece is detected, trying to accomplish the minimum number of set-ups. Moreover according to features normal vector directions, the process plan of the workpiece is derived. Hereby each of the classified features in the reorganised "Feature.dat" file is checked regarding of its entry surfaces normal vector direction and all features are grouped concerning these (six) directions. The occurring groups are sorted with respect to the number of the included features. The group with the temporary maximum number of features

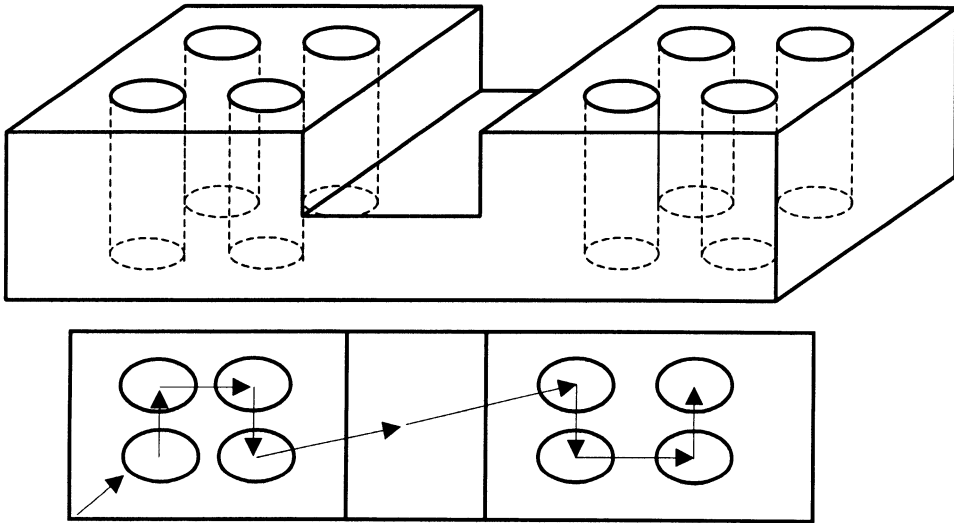


Figure 6: Workpiece example for the minimisation of the cutting tool path

determines the direction for the first set-up [4]. Finally a process plan including all the set-ups, and for each set-up all the required machining processes is derived.

The whole algorithm has modular structure, enabling an efficient inserting, deleting or editing of criteria. The holding of the workpiece is also examined, whether it satisfies some criteria (a minimum value for each side's area is required), otherwise the sequence of the machining processes is modified.

3. AN APPLICATION EXAMPLE

An application of the developed procedures is demonstrated in the case of the test part shown in figure 7. This part includes various geometrical features, like holes, slots, steps etc. The features are recognised and classified by the described developed algorithm. The results are written in a structured mode. A section of that file is illustrated in figure 8.

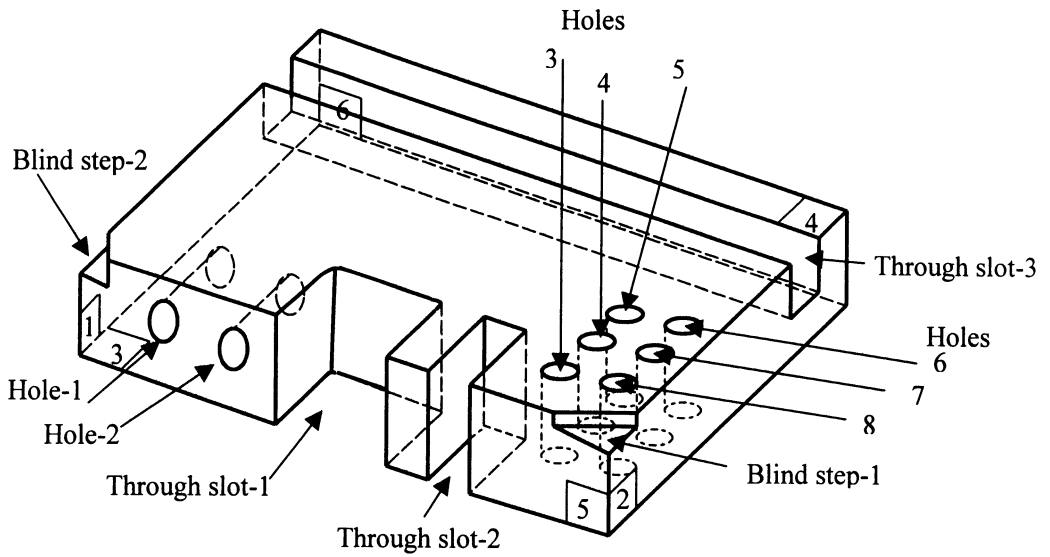


Figure 7: An application example

Machine Tool	Machining centre: FQH 50a (Sinumerik 8M)	
Set-up 1	Machining Process: milling	
	Features	Through slot-2
	Machining Surface	5
	Reference surface	6
Set-up 2	Machining Process: drilling	
	Features	Hole-1, hole-2
	Machining Surface	5
	Reference surface	6
Set-up 2	Machining Process: milling	
	Features	blind step-2, through slot-1, blind step-1, through slot-3,
	Machining Surface	4
	Reference surface	3
	Set-up surfaces	5,6
	Machining Process: drilling	
Features	Hole-3, Hole-4, Hole-5, Hole-6, Hole-7, Hole-8	
Machining Surface	4	
Reference surface	3	
Set-up surfaces	5,6	

Figure 8: The process plan of the application example

The structure of the file "Process-plan.dat" is the following: for each machine-tool selected, a number of set-ups has derived and each set-up consists of the data: machining, reference and set-up surfaces, as well as the features that are going to be manufactured with the appropriate order.

In this application example, 2 set-ups are needed for the machining of the part. In the first set-up Through slot-2, Hole-1 and Hole-2 are processed and in the second set-up Blind step-2, Through slot-1, Blind step-1, Through slot-3 and Hole-3 through Hole-8 will be processed.

4. CONCLUSIONS

CAPP systems are typically referred to machining features such as slots, holes and pockets, and therefore require as input a feature-based part representation.

The present paper deals with the classification of features included in the geometry of a workpiece taking into account machinability criteria. The developed methodology applies these criteria in the extracted features from the information of a CAD database, in order to classify these features for the determination of the process plan of the workpiece. The developed procedure provides independence from any CAD program.

REFERENCES.

1. Elinson A., Hermann J. W., Nau D. S. and Singh G., Toward Hybrid variant/generative process planning. In Proc. of DETCY97: 1997 ASME Design Engineering Technical Conferences, September 14-17 1997.
2. Bouzakis K.-D. & Andreadis G. (1998), Feature Recognition based on Iges files. CIRP International Seminar on Intelligent Computation in Manufacturing Engineering - ICME 98, Capri, pp 447-454.
3. Bouzakis K.-D., Efstathiou K., Andreadis G., Giannopoulos G., and Paraskevopoulou R., (1996). Implementation of a CAD/CAPP/CAM System into a Small Size Enterprise. Proceedings of the 28th CIRP International Seminar on Manufacturing Systems, Johannesburg, South Africa, pp. 256-260.
4. Bouzakis K.-D. & Andreadis G. (1998), A feature-based algorithm for computer aided process planning of prismatic parts, 4th International Seminar "Intelligent Manufacturing Systems – Theory and Practice", Belgrade, pp 19-26.

**USE OF MANUFACTURING FEATURES FOR COMPUTER AIDED PROCESS
PLANNING AND MANUFACTURING SYSTEM DESIGN
APPLICATION TO FURNITURES PARTS OF SOLID WOOD**

P. Martin

ENSAM, Metz, France

P.J. Meausoone

University of Nancy I, Nancy, France

KEYWORDS: Computer aided process planning, manufacturing features, furniture

ABSTRACT: Nowadays the market fluctuation and the fashion ask for designing and manufacturing with reducing delays. So it is necessary to design product by taking into account of the manufacturing requirements and sometimes to design product and manufacturing system simultaneously. We propose, in this paper, an approach of this concept to a particular domain, that of the second transformation of wood manufacturing industry. This domain closely is linked with market requirements, the added value of the product is quite low and the productivity must be high.

For this objective it is necessary to use structured data bases which can be used by the designer and the manufacturer. We have developed a description model of solid wood furniture pieces. We defined manufacturing features as geometric shapes and a set of specifications for which a machining process is known. The features we have selectionned correspond either to a given cutting operation or to a male female feature or a set of features in accordance to the customs of process planning. The formalization of knowledge is made by using tables, rules, flow charts. A workpiece is defined by a set of manufacturing features.

At first a workpiece is defined by its reference surfaces and some attributes (material, hardness, moisture constant, initial shape, ...). Then manufacturing features are defined.

The data base organization is defined by entity-relation formalism. So after that it is easy to deduce workpiece drawings or several sequence operations which take into account all the production constraints.

In the case of wood industry we have a close connection between manufacturing features and fonctionnal features. So by using the same manufacturing features it is possible to design the structure of the manufacturing line which allows to machine the workpieces.

Published in: E. Kuljanic (Ed.) *Advanced Manufacturing Systems and Technology*,
CISM Courses and Lectures No. 406, Springer Verlag, Wien New York, 1999.

We have developed a prototype software based on a relational data base (MS-ACCESS) which allows to get process planning. From our experience of wood manufacturing we choiced an up-bottom approach using an algorithm treatment based of a mixed system made up of variant and generative methods.

1. INTRODUCTION

Nowadays the market fluctuation and the fashion ask for more and more new and different patterns, the batch size decreases, it is necessary to design and manufacture with reducing delays. So the concept of concurrent engineering [1] must be used. The design of the parts, the process planning, even the production system must be made quite simultaneously. So the design and development cycle is reduced and the manufacturing constraints are taken into account as soon as possible.

Usually in furniture industries the manufacturing systems performances are known and the design aim is to create a new product which have to be manufactured on the workshop equipments with the firm knowledge and at the best price. So in the frame of concurrent engineering the design phase must take into account of manufacturing constraints but these ones must not restrict designer creativeness.

For industry, computer aided process planning must allow:

- to generate quickly new process plannings (main one and substitution ones),
- to know quickly the new product price,
- to define several prototypes and to compare them ,
- to design new product which would be manufactured without any problem,
- the production management must use directly the processes which are obtained.

So the followed questions must be solved:

- what kinds of datas are necessary for designing and manufacturing.
- how to follow a logical thread between design and manufacturing,
- how to get the part process planning,
- how to define and memorize the useful datas for process planning,
- how to catch and structure knowledge.

If we want to generate process planning automatically it is necessary to extract the knowledge of the designer and the manufacturer, to formalize it, to compute it in order to obtain one or several solutions and to validate. The main problem is due to the non formalization of knowledge and the great number of possible solutions.

For this purpose we have developed a methodology which allows to get process planning of furnitures parts by using manufacturing features. A prototype software based on a relational data base (MS-ACCESS) has been developed in order to show the validation.

2. PROCESS PLANNING

The problem of process planning has advanced through the changes of the manufacturing concepts. Classically about twenty years ago, process planning is reduced toward the production tasks and must prepare the elements for a production of quality without incidents. It was a problem of planning and one tried to solve it with automatic systems, particularly expert systems. For a use by less experienced engineers, it was necessary to include the definition of machining features into the process planning system. It was the age of feature recognition which did not change the problem of planning. The big change is due to the emergence of the concurrent engineering which requires the process planner's role to be thought. The duty of co-operation between the actors of the product life cycle imposes the process planner's activity and tools to be revised. The integration of product design and process planning consists in ensuring that a part has the intrinsic possibility of being manufactured.

Here is the challenge of nowadays for the process planning research area. In France, the GAMA group gathers the research laboratories in process planning domain. They worked first on automatic process planning and proposed several systems developed in cooperation with industry [2]. The group is now also working on the integration problem. Elaborating a process plan for a part under consideration consists in proposing an ordered set of actions to be performed in order to transform a roughed part to a finished part. The process plan is suggested from the finished part definition, the technology for the initial part to be obtained (it allows to have an approximate representation of the roughed part), the production context and the production capabilities which are considered used. An action can be performed only if the resources necessary for its complete success are defined and available.

It is the matter of a planning problem which can be classically expressed: what is the sequence of actions which allows the initial state of the part (the roughed part) to be transformed in the expected state of the part (the finished part) ? It is a non linear planning problem, the subgoals which can be considered are dependent on themselves. This first problem is coupled with a problem of allocation and sharing out of resources. An action becomes effective when a cutting tool, a fixture and a machine-tool belonging to the capable and available resources are allotted to it. The difficulty lies in the fact that the capability of the resource to achieve the required quality for the action to be performed is difficult to evaluate and that the economic objective imposes the maximum use of each resource. As this problem is a planning problem, it is normal to search an automatic process planning system.

Numerous ways have been tested and it is not the matter to be exhaustive here: let you see [3-4-5-6] for a review on process planning and features.

Several approaches can be used :

- a variant approach is used when the parts are quite similar, a process planning which covers each part type is defined, group technology can be used to define each part family.
- in a generative approach a new route sheet is deduced for each new part from its geometrical datas and specification attributes. This process is obtained from the manufacturing knowledge which is described by algorithms or by artificial intelligence rules. The approach can be made up to bottom, i.e. from the rough board to the finished

part or by bottom-up approach. From our experience of wood manufacturing we choiced an up-bottom approach using an algorithm treatment based of a mixed system made up of variant and generative methods.

3. OUR APPROACH FOR AUTOMATIC PROCESS PLANNING

3.1 features approach

We define a feature as a semantic group defined by a set of parameters, describing an object and used in the reasoning of activities linked with product design, use these products, manufacturing systems design. A machining feature is a geometric shape and a set of specifications for which a process planning is known. This planning is nearly-independent from the others [2].

From this later definition the following remarks can be made:

- a geometric shape is a set of surfaces or volumes made by tool displacement and tool shape,

- a set of specifications means technological datas,

- a known process planning means that several solutions can exist and it can be defined previously or generated in each case.

We have defined seven basic features [7]. These features are reference surfaces (plane, groove, tenon) or link surfaces (hole, cylinder, groove, tenon) or aesthetic surfaces (moulder, plane, complex shape).

3.2 entity-relation formalism

In order to have a larger view and to allow to new developments the data base structure is defined by entity-relation formalism.[8]. The conceptual data model (fig.1) allows to define the organisation of the data base, the relations between the different tables and their coherence. The conceptual treatment model (fig.2) allows to define the steps of the procedure and the requirements which allow to generate the process plan.

3.3 Part design and part description

The designer describes the part with functional features. They allow to define the fonctionnal requierements of the product (link, kinetic, strenght...). Remember that functional features are not functions but technical solutions which fulfil it, some funtions are not fulfilled by some other componants, functions can be split into several pieces, a function can be linked with several funtionnal features. Fonctionnal constraints are linked to them: tolerances proper to each surface, tolerances of position between surfaces, topology between features. The designer use fonctionnal features and the manufacturer machining features, the link between them is not bijective usually and it is necessary to have a mapping between the different kinds of features. But for wood manufacturing it is possible to do it easily, and to define a global feature or manufacturing feature (fig.3) which gathers the attributes of each one. So the designer for who function approach is usual, can have a feature library, but have to be take into account of all the workpiece context.

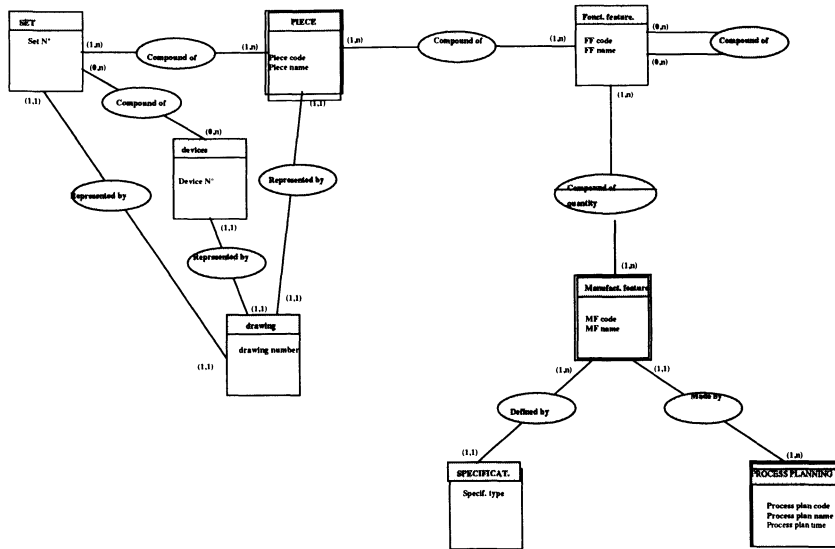


Figure 1 : Partial conceptual data model

3.2 Part design and part description

The designer describes the part with functional features. They allow to define the functional requirements of the product (link, kinetic, strength...). Remember that functional features are not functions but technical solutions which fulfil it, some functions are not fulfilled by some other components, functions can be split into several pieces, a function can be linked with several functional features. Functional constraints are linked to them: tolerances proper to each surface, tolerances of position between surfaces, topology between features. The designer uses functional features and the manufacturer machining features, the link between them is not bijective usually and it is necessary to have a mapping between the different kinds of features. But for wood manufacturing it is possible to do it easily, and to define a global feature or manufacturing feature (fig.3) which gathers the attributes of each one. So the designer for whom a function approach is usual, can have a feature library, but has to take into account of all the workpiece context.

So the part is described by a list of manufacturing features, the relations between these ones, the rough board, the specifications. Position of each feature is defined in the board references faces and axis. As the usual shape of a board is a parallelepiped, these ones are defined by its primary and secondary faces, primary and secondary edges, primary and secondary ends. In order to get the whole piece, it is necessary also to define the rough faces which are the final faces with an added thickness.

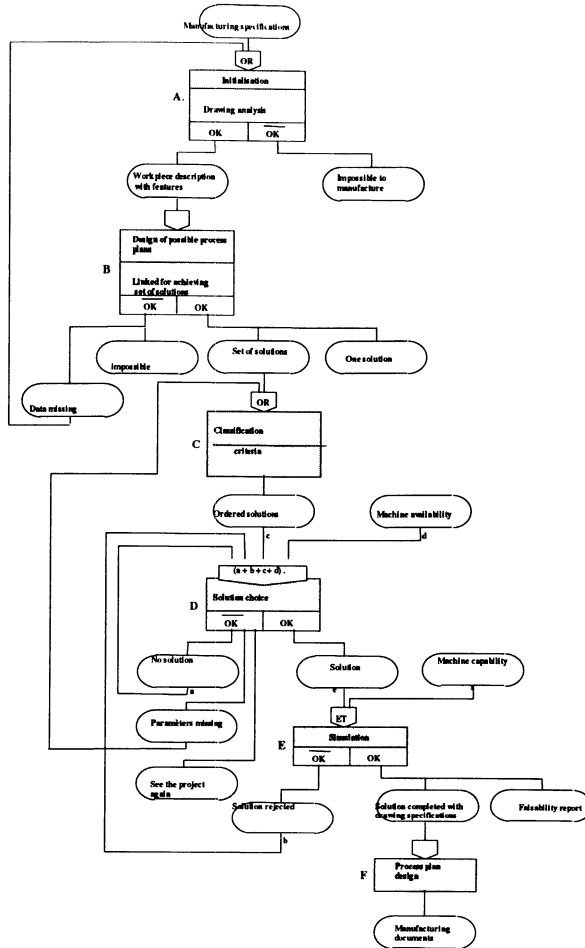


Figure 2 : Partial conceptual treatment model

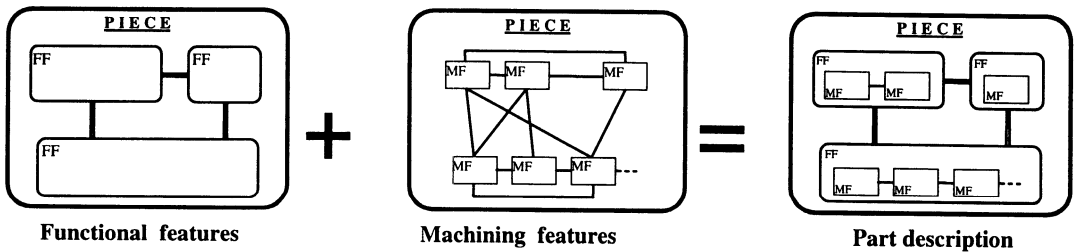


figure 3: Models used for designing and manufacturing parts

3-4 Process planning

For each feature the system searches for the operation sequences and the machine tools which are allow to machine it. Tables (feature process table) defining the machine-tools type which are able to do each feature are used for this purpose. Then the grouping of features is made by using the firm know-how (relation-feature table). A feature E1 in P1 position can be machined in the same time that the E2 feature in P2 position on the machine tool TM if the conditions of their operation sequences Pr1 and Pr2 are fulfilled. The knowledge formalization is defined by a rule IF..THEN..ELSE.. .At this level a list of possible solutions for one part is obtained..Operations sequences are arranged in order by taking into account of the wood machining state of art (risk of splinters, surface tolerances and surface roughness..). An envelope process plan has been defined for each part family and each feature position relatively to board's references. This process plan gives the list of possible operations, machines and tools which allow to machine a part belonging to a part family. So it is an union of the different possibilities of route sheets for each part family. The system grades the solution according to the number of groupings in terms of cost, machine tools availaibility, machining time... The operation sequence are choosen and substitution operation sequences can also be obtained. After acceptance by the production management, the scheduling is obtain. Then the validation of the route sheet in terms of machining accuracy, dimension..; is made. Part dimensions for machining must be calculate from the draw dimensions by taking into account of the operations sequences and the machine tools accuracy. If it is impossible to machine the part a new solutions must be search for. Then the documents (scheduling, route sheet, job order..) which are necessary to perform manufacturing are made out.

4. CONCLUSION

An automatic process planning system has been developped for solid wood furniture parts. As furniture parts are more simple that mechanical parts [9] it is possible to develop a general purpose system. This method necessitates the formalization of two kinds of knowledges: professionnall skill and knowledge on one hand and firm itself knowledge on second hand. The use of relational data bases seem to be the best way to developp this kind of application and il can be use now by SME.

The use of manufacturing features appears as the best concept to define parts for design and manufacturing points of view. Now the context of concurrent engineering imposes that the process planner is one of the actors which participate to the product definition. The process planner, as the product engineer does for his own objective, gives the constraints due to the machining process of the part. The problem of process planning becomes a problem of designing for process planning and can be asked like that : is the part under design machinable ? If not, what are the obstacles which prevent the part from machining ? If yes, can part improvements be proposed for a less expensive solution ? The most important change with this new process planning problem is the fact that process planning activity becomes an activity with a creation of part geometry. More the concept of machnining feature can be use also for designing the manufaturing system itself [10].

REFERENCES

- 1-Sohlenius G. - Concurrent engineering - Royal Institute of Technology, Stockholm - Annals of the CIRP - 41/2 - 1992- p645-655
2. Groupe GAMA - La gamme automatique - Editions HERMES - Paris - 1990-
3. ElMaraghy H.A. (1993), Evolution and future perspectives of CAPP, Annals of the CIRP, Vol.42/2.
4. Leung H.C. (1996), Annotated bibliography on computer-aided process planning, Int. Journal of Advanced Manufacturing Technology, Vol.12.
5. Shah J.J., Shen Y., Shirur A. (1994), Determination of machining volumes from extensible sets of design features in Advanced in feature based manufacturing, Shah, Mantyla, Nau editors, Elsevier.
6. Lenau T., Mu I. (1993), Features in integrated modelling of products and their production, Int. Journal of Computer Integrated Manufacturing, vol.6 n°1&2.
7. Meausoone P.J. - Approche en ingénierie concourante pour les industries du bois - Thèse de doctorat de l'université Henri Poincaré-Nancy I - 15 Novembre 1996
8. Collonges A., Hugues J., Laroche B., MERISE : Méthode de Conception - Collection Dunod Informatique - Editions Dordas - Paris - 1986
9. Martin P. , Bois et productique - Collection automatismes et production - Editions CEPADUES, Toulouse, 1992.
10. Brady G., Martin P., Charpentier P., "Utilisation du concept d'entités d'usinage dans un contexte multi-utilisateurs. Application à la seconde transformation du bois". Computer Integrated Manufacturing and Automation Technology, CIMAT'96, Laboratoire d'automatique de Grenoble, pp. 193-198, Grenoble, 29-31 May

A MULTIPLE-CRITERIA SCHEDULING METHOD FOR PLANNING OF CONTINUOUS MANUFACTURING PROCESSES

A FOOD INDUSTRY CASE STUDY

D.A. Mourtzis, E.D. Xeromerites and G.M. Chrysolouris
University of Patras, Patras, Greece

KEYWORDS: Production planning, schedule synchronization, Food industry

ABSTRACT: The main objectives of Food Industry nowadays, are to insure the high quality of their products, to provide uninterruptedly the market with products, as well as to reduce production costs.

The large number of final products, the continuous manufacturing processes and the non-interruptible order processing, together with the sensitivity of raw materials/products and the very short product life-span, are the most common planning problems faced by the Food Industry, especially in the field of dairy production.

This paper describes the application of a scheduling and synchronization method to the production planning problem of a Typical Food Factory. The objective of this work is to develop a method for supporting the scheduling procedures and for synchronizing the schedules of the different production stages. This method, based on a multiple-criteria decision making technique, provides a complete resource allocation schedule for each one of the production stages, as well as a set of performance indices for each of them in order for the schedule evaluation to become feasible. A set of static, dynamic and combined dispatching heuristics has also been incorporated in this method. An algorithm for the synchronization of the partial schedules for the production departments has been developed.

A set of experiments was designed and carried out in order to evaluate the method. The multi-criteria scheduling method is compared with the dispatching heuristics applied to a simulated environment and the results are discussed. For these experiments realistic data coming from the Food industry is used.

Published in: E. Kuljanic (Ed.) *Advanced Manufacturing Systems and Technology*,
CISM Courses and Lectures No. 406, Springer Verlag, Wien New York, 1999.

1. INTRODUCTION

This paper describes the application of a scheduling and synchronization method to the production planning problem of a Typical Food Factory (TFF). The method is applied to a Greek industrial firm, in the sector of dairy products.

In this work, a hierarchical model is used in order to deal with the resource allocation problem, referring to the assignment of production resources to the manufacturing processes over the time. Furthermore, in this paper, the problem of synchronizing the different production stages is faced.

2. THE FOOD INDUSTRY PLANNING PROBLEM

The work presented in this paper is a part of the development and implementation of a Decision Support System for the production planning and control procedures for one of the TFF plants of a Greek industrial firm. This paper is concerned with the production scheduling at various levels of the factory hierarchy [1] [2] in the Yogurt and Desserts Production (YDP) area. The overall objective is to integrate the production planning phases in the production sections and to make them flexible enough, so as to increase the operational and decisional capability. At the same time, all the product and process constraints are considered.

2.1. PRODUCTION SYSTEM DESCRIPTION

The under study Production System consists of three separate sections or production areas, namely the Raw Material Preparation, the Production, and the Packaging sections. It is well known that a manufacturing system can be defined as a combination of humans, machinery, and equipment, bound by a common material and information flow. This definition will be used to describe all three above mentioned sections (Fig. 1).

Raw Material Preparation Section: The first step for the production of yogurt and desserts is the preparation of raw materials. The preparation is the main operation performed in this section, together with the mixing of raw materials with additives when an order process begins. The material input in this section is milk, cream and additives. The information input is the type, the quantity, the composition of the milk, the cream and the additives, the time that the raw materials will be available, as well as the inventory control information for these materials. The main processes performed within this section, are the heating, the temporary storage and cooling of milk and cream, the mixing of milk with additives, as well as a number of non-productive operations, such as the cleaning in place (CIP) of tanks, valve clusters, pipelines and mixers (Table 2).

Production Section: The second step is the production of the semi-final products in a number of different product types with a different composition for each one of them. The products in this section are not yet packed in their commercial packages. The material input is the required quality and quantities of milk and cream from the production section. The information input is the product type to be produced, the quantity required as well as the time the semi-final products should be available to the next section. The main processes performed within this section are pasteurization, feeding with milk, heating,

cooling, fermentation, straining of the yogurt, homogenizing and temporary storage of the semi-final products. In this section the non-productive processes of cleaning in place are also performed.

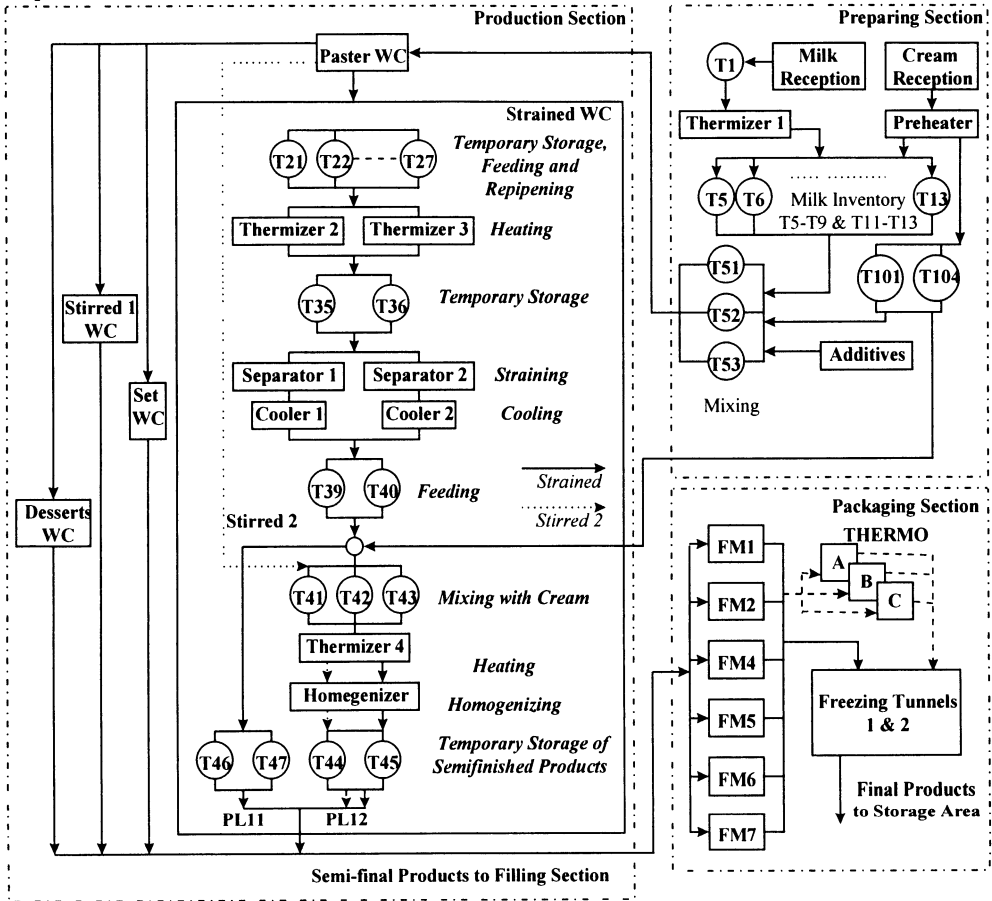


Fig. 1. The overall manufacturing diagram for the Typical Food Factory

Packaging section: The third step is filling and packing of the final products in their commercial packages. The products are bottled and then are packed in boxes to end up in pallets. The material input is the semi-final products, the fruit juice and preserved fruits to be added in some of the 48 different final products, as well as the packaging materials. The information input is the required quantity for each one of the final products to be produced and the delivery time. The main processes performed in this section are, the filling of plastic pots, the mixing with fruits or juice, the packaging, the heating and cooling of the final products as well as the non-productive processes of cleaning in place (Fig. 1).

2.2. PLANNING REQUIREMENTS AND PROBLEM DESCRIPTION

The point to be taken into consideration when planning a manufacturing system of this type, should be the satisfaction of customers, the accurate determination of due dates, the

low production costs, the high and constant product quality.

In a TFF, a large number of constraints have to be considered by the production manager, in order to draw up the daily schedule for the production. The most common planning problems faced by the field of dairy production are the large number of final products, the continuous manufacturing processes, the non-interruptible order processing. Moreover, the sensitivity of raw materials and products and the very short product life-span lead to almost no-inventory keeping among the production stages.

2.3. PROBLEMS WITH CURRENT PLANNING PRACTICE

Currently, the production planning is carried out based on the experience of the production manager and on some information about the state of the factory.

The weekly demand, with daily resolution, comes from the sales department of the company, to the production manager at the end of each week. This weekly demand is analyzed, taking into consideration the inventory of final products. The output to the production department is a daily production schedule with hourly resolution (Fig. 2).

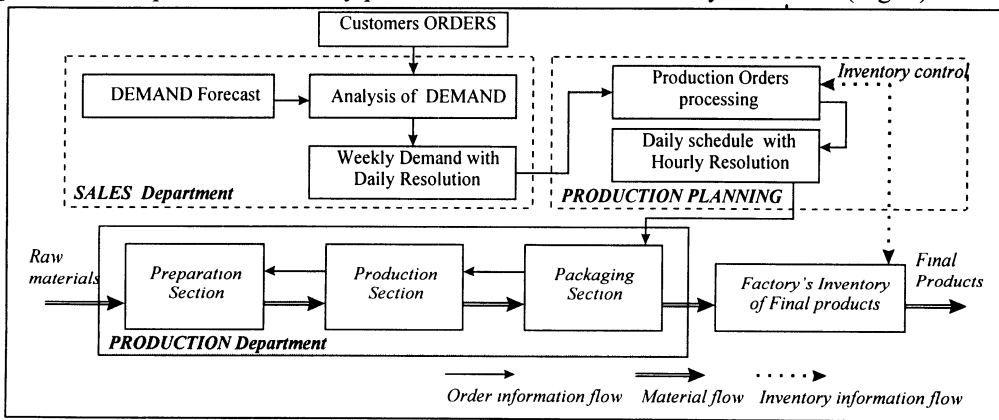


Fig. 2. The information flow diagram for the production orders

The problems with the current planning practice are the following:

Large number of final products: The number of the alternative resources at the different production stages is large, especially in the packaging section. Thus, the number of alternative solutions becomes large. This number of production scenarios must be created and evaluated, in order for the production manager to select a satisfactory one to follow.

Continuous and non-interruptible order processing: The sensitivity of raw materials and products does not allow for inventory keeping between the production stages, nor the interruption of an order process. Thus, the need for synchronizing the production sections, comes out.

Non-productive operations: The quality standards of the products and the sensitivity of raw materials lead to a large number of time consuming non-productive operations which must be performed. Such operations include the cleaning in place (CIP) of all the production resources after every order processing, as well as the sterilization of tanks.

Short product life span: The short life span of the final products leads to short inventory

keeping, so, the batch size of the production orders is small. This fact, together with the large number of the final products, leads to a great number of orders to be scheduled weekly.

3. PROPOSED METHODOLOGY

The proposed methodology consists of both the scheduling method and the synchronization algorithm.

3.1. THE SCHEDULING METHOD

The resource allocation problem, referring to the assignment of a set of resources to a set of tasks over time, is of utmost importance to many industrial activities, particularly to the planning and controlling of manufacturing systems. In actual facilities the number of resources and tasks is large enough, so as to make the problem combinatorial explosive [2]. For this work, the following hierarchical model will be used. The manufacturing system consists of a set of job shops, each producing a family of final or semi-final products with similar characteristics. Each job shop is further partitioned into work centers, consisting of resources with similar, sequential and/or complementary manufacturing functions. A resource is defined as an individual production unit, which can represent either a single machine resource (tanks, pumps, valve clusters, pipelines etc.) or a human resource. The imposed scheduling method assigns the available resources to pending production tasks, following a number of steps that a human undertakes, when making a choice:

1. Determine a set of relevant decision making criteria.
2. Determine a set of alternative solutions.
3. Determine the consequences of the alternatives with respect to the different criteria.
4. Apply decision making rules in order to select the best alternative.

This scheduling method faces some of the special characteristics of the continuous manufacturing systems. Such characteristics are, sequences of production tasks which must be assigned to a specific resource, and groups of resources which cannot be allocated simultaneously to pending tasks.

In addition to the multiple criteria decision making, a set of dispatching heuristics [1] is incorporated in the scheduling method.

3.2. THE SYNCHRONIZATION ALGORITHM

The problem of synchronizing the partial schedules of different production sections is quite often in multi job-shop manufacturing systems. This problem becomes essential in cases such as that of the under study TFF, in which there is no possibility of inventory among the sequential production stages, and the order processing cannot be interrupted.

This algorithm combines the backward and forward planning techniques. The planning procedure begins from the last section which serves the customers and the due dates ought to be respected. The output is a detailed time schedule for the allocation of the production resources to the production tasks in terms of Start, Completion and Slack Time or Tardiness for each job order of the section.

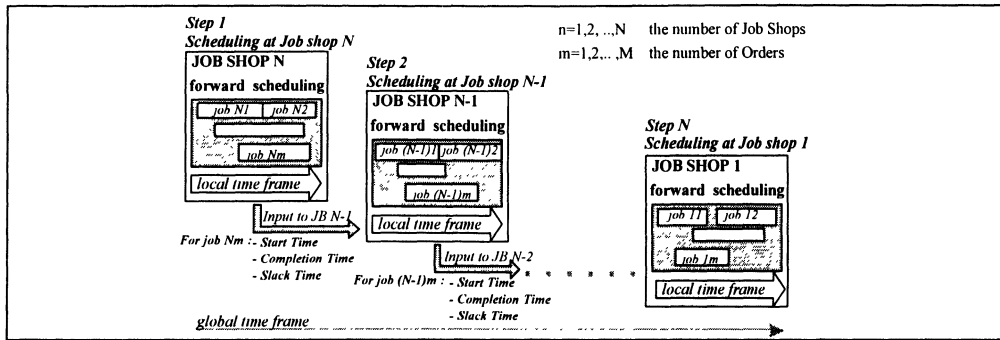


Fig. 3. The stepwise scheduling and synchronizing procedure

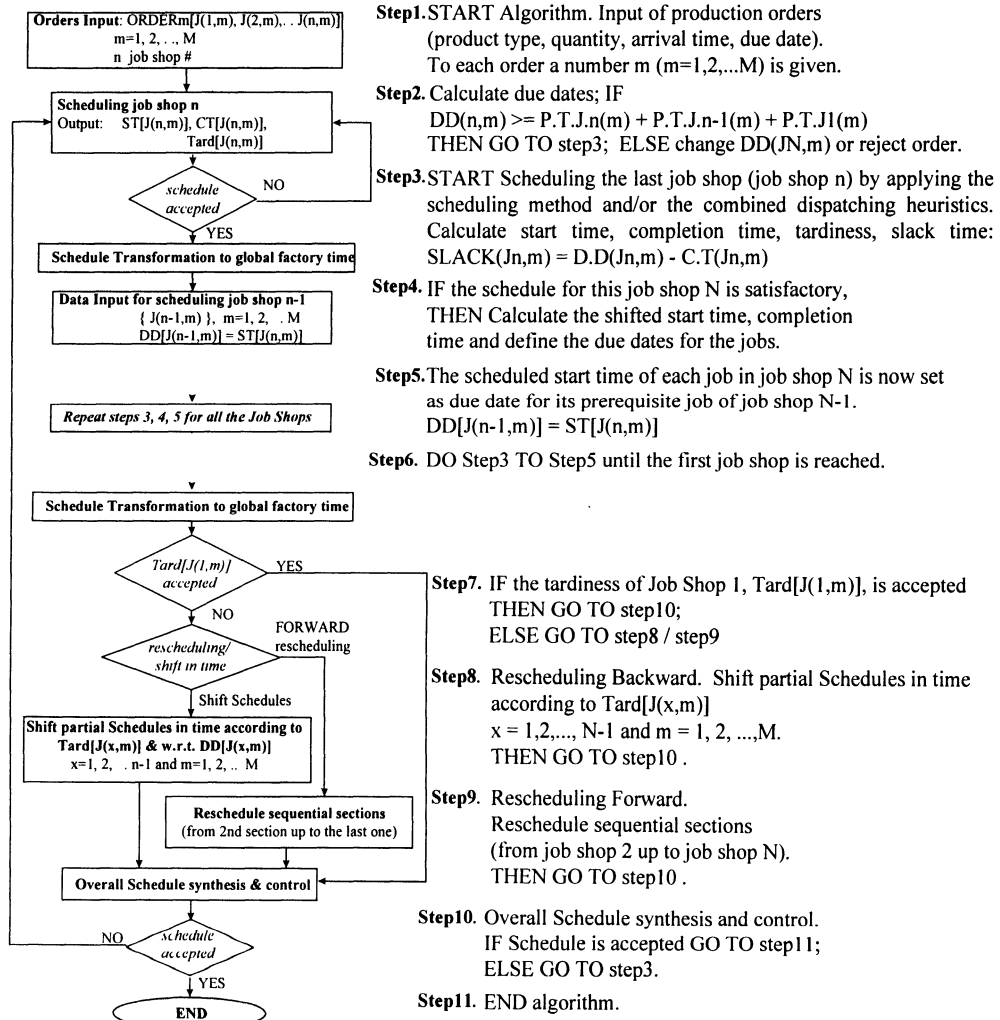


Fig. 4. The basic steps of the synchronization algorithm

The scheduling procedure at the previous section in sequence, is performed as soon as the scheduling of the last section is finalized. Dealing with sequential job orders, the start time of each job of the last section becomes due date for the corresponding one of the previous section. These steps are repeated until the first production section is reached. The algorithm and the stepwise synchronization approach are presented in Fig. 3 and 4.

The above described synchronization procedure was applied to the TFF case. The procedure starts from the Packaging section. The scheduling at the Production section is performed as soon as the scheduling of the Packaging section has been completed. The start time of each job of the Packaging section becomes due date for the corresponding job of the Production section. The same procedure is also followed for the Preparing section.

4. THE PRODUCTION SYSTEM MODEL

The food factory, being under study, consists of different production lines and as defined in paragraph 2, this paper is concerned with the YDP line scheduling. The planning tool data entry phase is divided into three categories: *Facilities* which include the Factory and Job-shop model, the Work center and Resource definition, *Work load* which includes the Job and Work load definition as well as the Arrival profiles, and the *Operating policy*.

Operating Policy is the decision-making logic used to assign manufacturing system’s resources to various production tasks. The scheduling method allows the definition and use of a criteria combination or some dispatching heuristics [1] as the operating policy. The criteria defined in the scheduling method used are Mean Flowtime, Tardiness, Cost and Mean Quality. The implemented dispatch rules are presented in Appendix.

4.1. FACTORY MODEL

Each one of the three sections of the TFF can be modeled as a job shop, which consists of a number of Work Centers (Table 1).

Table 1. The factory model

Job shop - ID	Process - ID	Number of Work centers
Preparation - JB	Milk and Cream Preparation for production	3
Production - JB	Yogurt and desserts production	5
Filling - JB	Filling of cups, packaging and freezing	2

4.2. JOB SHOP MODEL

In sequence, every section of this factory can be modeled with the help of a Work Center and Resource hierarchy (Tables 2,3,4): The *Preparation Section* is modeled as a job shop consisting of three work centers; the *Production Section* is modeled as a job shop with five work centers; the *Packaging Section* is modeled as a job shop with two work centers.

Table 2. Job Shop model - Preparation Section

Work Center-ID	Process-ID	Resource #	Resource-ID
Silo - WC	Milk storage and initial preparation	13	T5, T6, T7, T8, T9, T11, T12, T13, CC109, CC115, CC118, PL1, PL2
Cream - WC	Cream preparation	6	R2, T101, T104, CC407, DISP2, PL3
Mixers - WC	Mixing with additives	4	T51, T52, T53, CC505

Table 3. Job Shop model - Production Section

Work Center ID	Process-ID	Resource #	Resource-ID
Paster - WC	Milk Pasteurization	4	P1, P2, P3, P4
Strained - WC	Strained & Stirred2 production. Straining Cream mixing Homogenizing	37	T21, T22, T23, T24, T25, T26, T27, TH2-3, T35, T36, SEP1, SEP2, C1, T39, T40, T41, T42, T43, TH4, T44, T45, T46, T47, CC308, CC311, CC315, CC613, T33, T34, T102, T103, T106, T107, T108, T109, T110, T111
Stirred 1 - WC	Stirred 1 production. Homogenizing	11	T55, T56, T57, T61, T62, C4, T63, T64, T65, CC1111, CC2502
Set - WC	Set production.	5	T66, T67, T68, T69 CC530
Desserts - WC	Desserts' production.	7	T115, T116, T118, T119, CC206, CC207, CC508

Table 4. Job Shop model - Packaging Section

Work Center ID	Process-ID	Resource #	Resource-ID
Filling - WC	Bottling, packaging	5	FM1, FM2, FM4, FM5, FM6
Thermo- WC	Heating, freezing of final products	5	THERMOA, THERMOB, THERMOC, TUN1, TUN2

4.3. WORKLOAD MODEL

In the manufacturing system under study, five different product types are produced. Every production order consists of three sequential jobs, one to be processed in each job shop.

Job definition: Each job arrives at every section of the TFF accompanied by a process plan, namely, a set of instructions that determine the sequence of the different tasks as well as their technological constraints.

Work Load model: The generic job model is $JX\text{-}yyyy$, where X indicates the Job Shop ID, namely, P for the Preparation, R for the Production, and F for the Packaging Section, $yyyy$ indicates the product type, namely, DE for the Desserts, SE for the Set, SR for the Strained, ST for the stirred 1 and STB for the stirred 2.

The generic task model is $TX\text{-}yyyy\text{-}rrrrrr\text{-}zz$, where X and $yyyy$ are as previously defined, $rrrrrr$ is the code name of the resource which can be assigned to the specific task, and zz indicates the task type, namely, S for setup, P for processes, F for filling up, E for emptying tanks, and C for cleaning.

Work Load Definition: The work load consists of 16 production orders, which contain yogurt and desserts to be produced in different types, packages, and quantities. The definition of the implemented workload is presented in Table 5, while its precise definition is given in [3].

Table 5. The workload definition

Section	# of Orders	# of Jobs per section	# of Tasks per section
Preparation		16	184
Production		16	238
Packaging	16	16	115
Total	16	48	537

4.4. PROBLEM APPROXIMATION

In order for the above described problem to be solved, the approach was as follows:

Planning for the entire manufacturing system, using as input in the packaging section the

orders coming from the sales department. Furthermore, continuing the planning by using the result of the packaging section scheduling, as input to the production and preparation sections. This way, the due dates for the tasks of a job shop are chosen in relation to the start times of the related jobs in the next job shop.

The scheduling of the manufacturing system under study, has been implemented using a number of different policies. These different policies are combinations of four conflicting criteria, namely, job tardiness, flowtime, cost and quality. In addition, nine dispatching heuristics, have been applied. Two cases were simulated as regards the due dates; one with loose and one with tight due dates [4] (Table 7). Let $n=1,2,\dots,N$ the number of Job Shops, $m=1,2,\dots,M$ the number of orders, and $PT(J_n,m) = \sum_{i=1}^I P.T(T_{i,n,m})$, thus,

$$DD(J_n,m) = AT(J_n,m) + c \times PT(J_n,m) \tag{1}$$

where DD the due date, AT the arrival time, PT the processing time, $T_{i,n,m}$ the tasks of job J_n,m . Simulation results have been obtained in Gantt charts and alphanumeric form.

5. RESULTS AND DISCUSSION

At the end of each run or at any point during a simulation process, statistically calculated performance measures can be reported. Mean Job Tardiness (MJT), Mean Job Flowtime (MJF), Mean Job Cost (MJC), Mean Capacity Utilization (MCU) and Mean Job Wait time (MJW) form the basis for the conclusions, regarding the operating policies performed onto the predetermined workload. As it comes out from the arithmetic results (Table 6) and the graphs (Fig. 5-9), the results from the experiments are as follows:

For planning with *loose due dates* (Table 7), the multi-criteria planning method (PM) gave better results than the heuristics for the MJT, except for LPT, which resulted in slightly lower MJT. As regards MJF and MJW, the planning method gave better results than the heuristics did, except for SPT, SPT-T(a) and LPT. The lowest value for MJC was achieved by the planning method. As regards the MCU, the method was better than most of the heuristics; SPT-T(a), LPT, and FOPNR resulted in better MCU.

When planning with *tight due dates* (Table 7), the method gave the best results regarding the MJT, MJF, MJW and MJC. As regards the MCU, the method was better than that of the heuristics, except for LPT, which gave a slightly better result.

As is can be inferred from these results, the planning method proved to be better than the heuristics, in the case of planning with tight due dates, which is the most realistic case. The comparison of the results from the dispatching heuristics shows, that SPT-T(a) was the best among them, when planning with loose due dates, while LPT's performance was the best when planning with tight due dates. The static dispatching heuristics, gave exactly the same results in both cases of planning with loose and tight due dates, except for MJT. The dynamic heuristics, DS and S/PT, improved their performance in terms of MJF, MJW and MCU when planning with tight due dates.

As far as job orders are concerned, detailed schedules for each job order are listed. Each schedule includes information about each task in the job order, such as the resource it was processed on, its arrival, start, due and completion date. Summary data on times for an

entire job, are also available.

Table 6. The results from the experiments (PM stands for Planning Method, MJC in monetary units)

	Loose Due Dates					Tight Due Dates				
	MJT (h)	MJF (h)	MJC	MCU (%)	MJW (h)	MJT (h)	MJF (h)	MJC	MCU (%)	MJW (h)
PM	0,19	12,53	112,64	48,33	8,12	2,72	12,19	111,30	49,18	7,70
SPT	0,35	12,26	113,45	44,92	8,00	2,93	12,26	113,45	44,92	8,00
LPT	0,18	12,29	113,48	49,39	7,81	3,17	12,29	113,48	49,39	7,81
FOPNR	0,22	13,35	116,67	48,70	8,30	3,80	13,35	116,67	48,70	8,30
LWKR	0,38	13,28	114,32	46,40	8,59	3,31	13,28	114,32	46,39	8,59
MWKR	1,73	22,21	114,37	45,48	20,12	11,60	22,21	114,37	45,48	20,12
P+WKR(α)	0,38	13,01	114,32	45,70	8,29	2,94	13,01	114,32	45,70	8,29
DS	1,63	21,76	114,96	40,24	18,31	7,24	18,76	113,24	43,43	14,16
S/PT	1,41	21,68	114,96	45,94	19,63	6,45	17,57	115,85	48,55	12,89
SPT-T(a)	0,19	12,17	113,45	49,65	7,90	2,96	12,28	113,45	44,92	8,03

6. CONCLUSIONS

This work demonstrates a new approach to scheduling and synchronizing the production stages of a typical food factory. The results from simulation applied to the packaging section are presented, as this is the most important of the three sections.

The planning method propounds the combination of different criteria for the planning of the food factory. Every time a decision is required, a set of feasible alternatives is produced and evaluated, and a good alternative is selected. Static, dynamic and combined dispatching heuristics are incorporated into the method and a synchronization algorithm is developed in order for the integration of the manufacturing phases to become more effective. The application of the method to the packaging section TFF test case shows that the overall method brings about reasonable and satisfactory results in terms of Mean Job Tardiness, Flowtime, Wait time, Cost and Capacity Utilization, especially when planning with tight due dates.

7. REFERENCES

1. Chryssolouris, G., (1992) *Manufacturing Systems: Theory and Practice*. Springer-Verlag, New York.
2. Mourtzis D., Papakostas N., Chryssolouris G., (1995) *An Approach to planning of textile manufacturing operations: a scheduling method*. IFIP WG5.3 International Conference on life-cycle modeling for innovative products and processes, Berlin, Germany.
3. Mourtzis D., Xeromerites S., Ellinikos D., (1998) *Modeling of the manufacturing system*. Project report, RETEX No 10830155.
4. Vollman T., Berry W., Clay Whybark D., *Manufacturing Planning and Control Systems*. IRWIN, Boston, 3rd edition 1992.
5. Chryssolouris G., J. Pierce, and K. Dicke (1991) *An Approach for Allocating Manufacturing Resources to Production Tasks*. Journal of Manufacturing Systems, Vol. 10, No. 5, 368-382.
6. Chryssolouris, G. and M. Lee (1994) *An Approach to Real-Time Flexible Scheduling*. International Journal of Flexible Manufacturing Systems. Vol. 6, 235-253.

Fig. 5. The Mean Job Tardiness

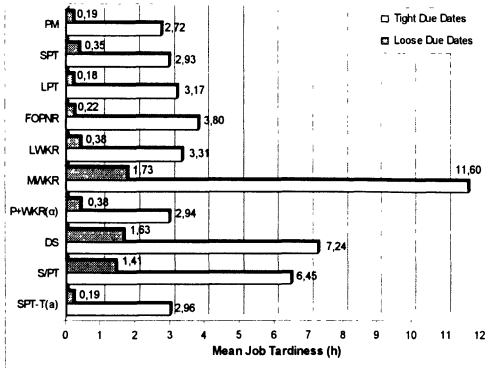


Fig. 6. The Mean Job Flowtime

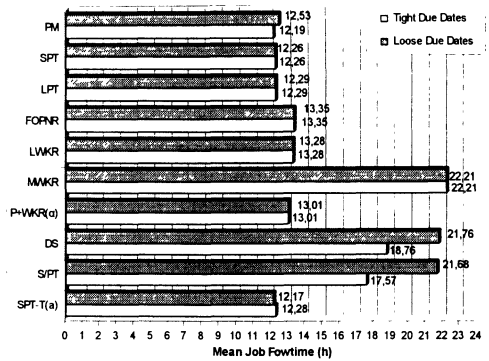


Fig. 7. The Mean Job Wait time

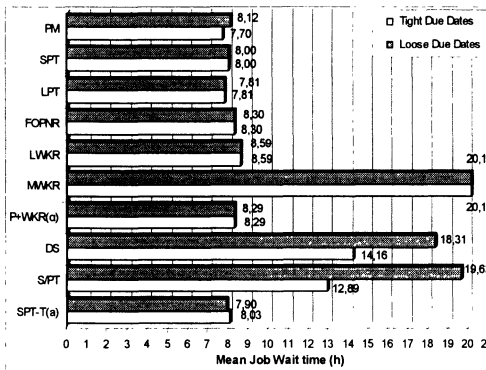


Fig. 8. The Mean Job Cost

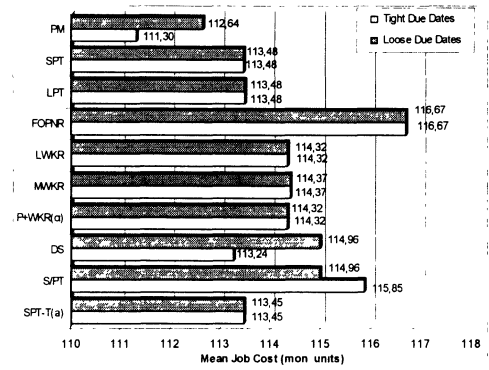


Fig. 9. The Mean Capacity Utilization

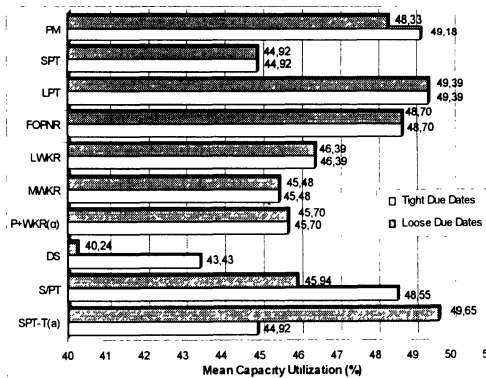


Table 7. The tight and loose due dates used for the simulation

Job ID	P.T (h)	Due Dates(h)	
		tight	loose
JFDE1	3,55	4,44	24
JFDE2	1,72	2,15	24
JFSE1/1	14,09	17,61	24
JFSE1/2	14,09	17,61	24
JFSE2/1	13,66	17,08	24
JFSE2/2	13,66	17,08	24
JFSE3	14,25	17,81	24
JFSE4/1	11,57	14,46	24
JFSE4/2	8,00	10,00	24
JFSE5/1	13,17	16,46	24
JFSE5/2	8,93	11,16	24
JFSR2	3,72	4,65	24
JFST1	8,82	11,03	24
JFST2	8,82	11,03	24
JFSTB1	4,07	5,09	24
JFSTB2	7,06	8,83	24

APPENDIX

A short description of the Dispatching Heuristics used for the experiments is given in the following table

<i>Rule</i>	<i>Description</i>
SPT	Job is selected which has the shortest operation processing time.
LPT	Job is selected which has the longest operation processing time.
FOPNR	Job is selected which has the fewest operations remaining to be performed.
LWKR	Job is selected which has the least work remaining to be performed.
MWKR	Job is selected which has the most work remaining to be performed.
S/PT	Job is selected which has the least ratio of slack time divided by remaining processing time.
DS	Job is selected which has the least slack time determined by due date less the remaining expected flow time minus the current date (dynamic slack).
P+WKR(a)	Job is selected which has the smallest weighted sum of next processing time and work remaining. 'a' is a weighting constant which is greater than 0.
SPT-T(a)	This is the truncated version of SPT. As long as no job in the queue from which selection is made has waited more than 'a' time units in this queue, normal SPT selection is made. When a job has waited too long, it is given dominating priority.

AUTOMATIC EXTRACTION OF MANUFACTURING FEATURES FROM CAD MODELS FOR CAPP

A SIMPLE AND LOGICAL APPROACH

A.S. Deshpande K.K. Appunkuttan and V.K. Kustagi
Gogte Institute of Technology, Belgaum, India

KEYWORDS: CAD, CAPP, Feature Extraction

Abstract: Automatic Feature-s recognition is likely to be an essential requirement for future integrated design & manufacturing systems and in the development of fully *Automated* process planning systems. A CAPP system essentially provides an effective platform for an integrated CAD-CAM system. Majority of the current design and manufacturing data used on shop floors , is associated with CAD models. The present paper discusses in brief about the role of CAD in CAPP. Also, an overview of research in extraction of feature-s from CAD models is taken. Most of the systems suggest complex algorithms which, new developers find difficult to implement . Hence, the development such a system for 2-D CAD models has been described completely.

1.INTRODUCTION

The first step in process planning is to understand the engineering design. Manufacturing aspects in product development expect a precise and detailed model of the component to be produced. The way in which the part description is input to the process planning system has a direct effect on the degree of automation that can be achieved.[1] Traditionally, engineering drawings have been used to convey part descriptions.

Since the invention of computer graphics in the year 1950, CAD models are being used extensively for engineering applications and have become popular because of clarity,

accuracy and improved "Quality" etc. It encourages concurrent engineering i.e. a systematic approach to the integrated current design of products and related processes including manufacturing and support.

Wire frame , surface and solid models are most commonly used by the CAD modellers. To ease the modelling difficulty, in recent years a feature based modelling has been proposed. A feature based design system is a front end to a solid modeller.[2]

Manufacturing or CAM modules expect the complete geometrical as well as technological information from CAD models in a form acceptable to them. An overall review indicates that, very few CAD modellers satisfy this major requirement in the CIM environment.

2. ROLE OF CAD IN CAPP

CAPP systems usually serve as a link between CAD and CAM. However, this is a partial link, because most of the existing CAD drafting systems do not provide part feature information, which is the essential data for CAPP. The clear and complete information of geometrical and technological aspects of the FEATURE_S of the CAD models is important for CAPP decisions.

Feature extraction plays an important role in manufacturing and design systems as well. Feature extraction acts as a bridge between CAD and CAM, this is because the entities incorporated in a component during the design stage are recognised by a feature extraction system before the part is actually forwarded for the various manufacturing operations.

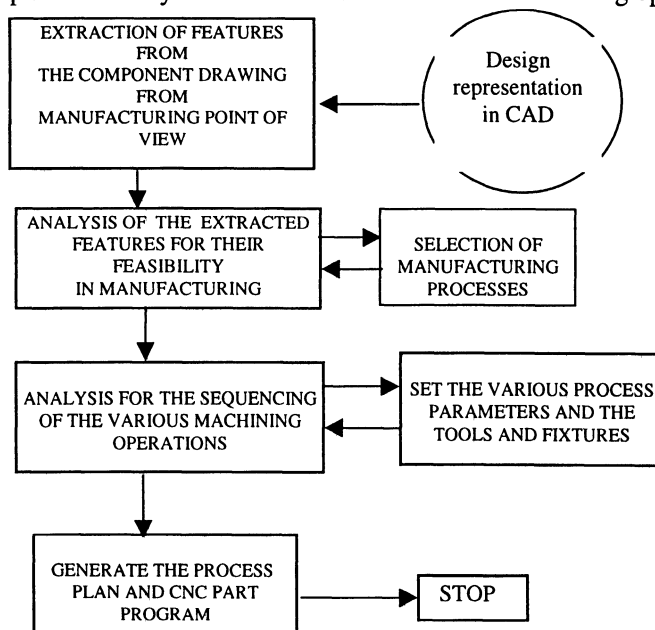


Fig.1

Systems for feature extraction provide feature based user interface for the designing processes and in case of manufacturing, they help in determining the appropriate operations in process planning.

Any Computer Aided Process Planning system involves the procedures as shown in the flowchart below. The importance of feature extraction in CAPP can be thus assessed by viewing at the depiction shown in Fig.no.1

Thus one can infer from the above diagram that feature extraction forms the foundation part of the entire structure of a Computer Aided Process Planning system.

Some of the CAD interfaces available for the interpretation of CAD models are DXF, IGES,SAT,STEP etc. Most of the CAD systems support one or more ,from these interfaces.

3. BRIEF LITERATURE REVIEW.

An overall glance through the research in feature extraction indicates that , many researchers have focussed their attention on automatic feature-s extraction from CSG as well as B-rep based solid models. Although these techniques are mathematically sound and robust, , they contrast with the engineers FEATURE based view of the component.[3]

A number of approaches to part feature recognition for rotational as well as prismatic components. They include syntactic pattern recognition[3],geometry decomposition ,expert system rule logic[1] ,graph based approach [4] and set theoretic [5].

Feature extraction techniques employed in rotational part feature recognition systems are mainly based on the syntactic and/or expert logic approach.[1]

The logic for feature recognition in prismatic parts is complex and need a proper representation of generic model. Most of the systems take the CAD interface file as the input and is analysed for feature interpretation in the program. In general, artificial intelligence based systems are being extensively used for this task.[7]

Much of the research is currently in progress on the augmentation of such models with technological and other lifecycle data which is referred to as product model .

4. PRESENT WORK.

The review indicates that ,not much work has been reported on feature recognition of 2 D drawings, which the form in which the majority of design data currently exist[6].Also, the manufacturing drawings used on shop floor, are in 2 D only. In the perspective of these, arguments , present work is designed for 2 D models.

Concepts of Artificial Intelligence (AI), have been used in the algorithm and architecture which incorporates the function of extracting features for prismatic as well as rotational parts. An interactive and user friendly software has been developed in Turbo Pascal V7. DXF interface has been used in the program.

The component drawings are represented in 2-D configuration. This part drawing is generated in a CAD modeller.(AUTOCAD has been used in the present work)

To determine type of feature which comprise the part, the part model must be evaluated. A DXF interface is created for the part drawing in CAD modeller. The required information is available in 'ENTITIES' section of the DXF file. This section gives the detailed information about the different entities viz. Lines , Circles and Arcs etc. The details of a line are given in the form of its end co-ordinates .The details about an arc is available in terms of radius and the end points. These details are in random order and hence, the different entities have been grouped separately under each of the orthogonal view. The separation of these views has been done based on an intelligent and simple logic as under. (Refer Fig.3)

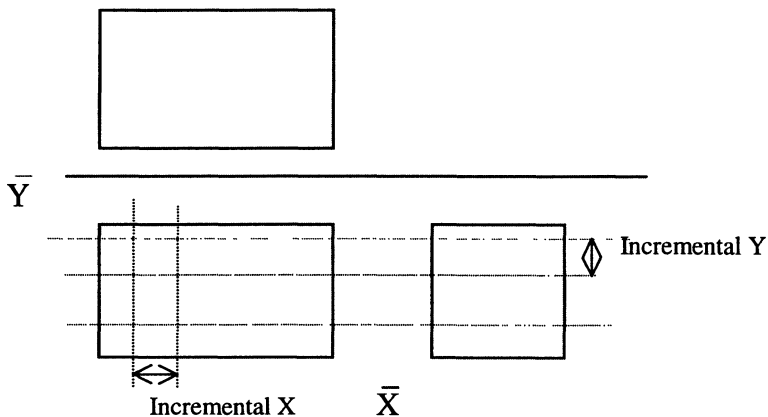


Fig 3 Separation of views.

- The minimum X and Y co-ordinates are identified. [$\min(x)$]
- Keeping X - co-ordinate of this point same, the Y- co-ordinate is incremented by a small value. A horizontal line is drawn from this incremented position. If this line does not intersect any of the lines, then this separates the top view. If it intersects any of the lines, then again the Y co-ordinate is incremented until it separates the top view from other views.
- Now keeping Y co-ordinate of the $\min(x)$ same, the X- co-ordinate is incremented by a small value. A vertical line is drawn from this incremented position.. If this line does not intersect any of the horizontal or vertical lines, this separates the side view from the front view, otherwise, again the X- co-ordinate is incremented till it separates the side view.

Once the views are separated, the entities are put in the respective views by using following logic.

IF the Y co-ordinate of an entity is greater then incremented y-value THEN
the entity belongs to Top view
ELSE

IF the X co-ordinate of the entity is greater than the incremented x-value THEN
the entity belongs to Side view

ELSE
the entity belongs to Front view.

Identification of the features, which otherwise, is a task requiring an intelligent and complex algorithm, has been done by using a basic conceptual logic used in reading the engineering drawings. Following paragraphs discuss about some of these features.

After view separation, each view is searched for circles. If in any view a circle is found then the other view is searched for the corresponding lines representing the hole. If the lines are hidden, then they represent the hole, the length of the hidden lines being the depth of hole.(Fig 4)

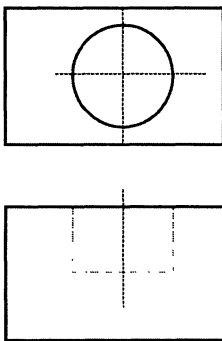


Fig.4

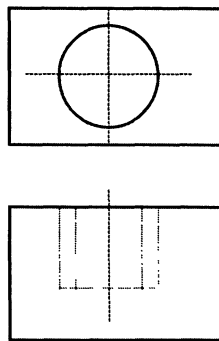


Fig.5

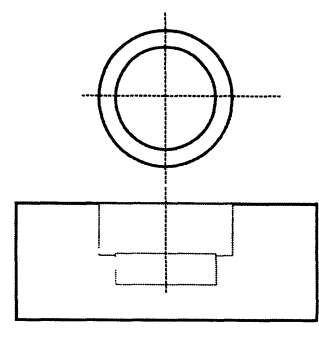




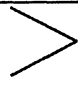

Fig.6

If there exist another pair of hidden lines within these lines then they represent tapping. (Fig 5)

If there are two circles with same centre and different radii, then they represent the hole with counter hole. (Fig 6)

To identify the features of the prismatic components, a separate method of coding has been developed as shown in table 1.

Table-1

Angle between Lines	Code	Example
90	1	
270	0	
>270	2	
<90	3	

In each view, from minimum X co-ordinate value, the scanning is done in clockwise direction. Each point representing the intersection of two lines gets a code assigned depending on the angle between those lines. The codes are assigned as below. (Angles measured in clockwise direction) Refer Table-1.

```

IF the angle between the lines is 90 deg THEN code=1
ELSE
If the angle between the lines is 270 deg THEN code=0
ELSE
If the angle between then >270 deg THEN code=2
ELSE
If the angle between lines <90 deg THEN code=3
ELSE
code=4

```

Using these codes, each feature is identified by a definite code sequence. The code sequence for different features is shown in the Table-2.

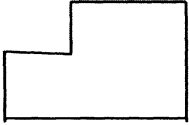

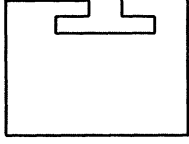
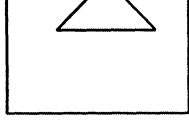
Code sequence in the model is checked in the program for the interpretation of , the features and their dimensional details .

7.CONCLUDING REMARKS

Trends in CAPP technology have been changing from GT based approaches in the past through Generative at present to Automatic in the future. Automatic approach needs CAD model to be interpreted automatically for accuracy and completeness. Automatic Feature-s

recognition is likely to be an essential requirement for future integrated design & manufacturing systems and in the development of fully automated process planning systems.

Table-2

Feature	Representation	Code sequence
Step		0-1-0
Rectangular slot		0-1-1-0
T-slot		0-0-1-1-1-1-0-0
Dovetail		2-3-3-2

8. REFERENCES

1. Joshi,S.,Vissa, N.,Chang,T.C.,“Expert Process Planning System with Solid Model Interface” , Int.J.Prod.Res.Vol. 26/5/1988, PP 863-885.
2. Chang, T.C.,”Expert ProcessPlanning for Manufacturing”,Addison-Wesley USA,1990.
3. Kulkarni, V.S., Pande,S.S.,"A system for automatic extraction of 3D part features using syntactic pattern recognition techniues", Int.J.Prod.Res.Vol. 33/6/1995, PP 1569-1586.
4. Joshi S., and Chang T.C.,”Graph based heuristics for recognition of machined features from a 3Dsolid model”,Computer Aided Design.20(2):PP58-66.

5. Perng D.B., Chen Z. and Li R.K., "Automatic 3D machining extraction from 3D solid CSG input.", *Computer Aided Design*.22(5):PP285-296.
6. Meeran.S. and Pratt.,M.J., "Automatic feature recognition from 2D drawing", *Computer Aided Design*.25(15):PP 7-17.
7. Deshpande, A.S., Kustagi,V.K. , Balaji rao L.V., " Computer Aided Process Planning for Manufacturing: Need of an Integrated & Intelligent Approach", *Proc. Int.conf.on CAD ,CAM & Auto.fact. Jamia,Delhi, Dec.1996.*
8. Kripa Shanker , "Computer Aided Process Planning", *Notes of Intensive Course Advances in Automated Manufacturing Systems,IIT,Kanpur*

A VIRTUAL LATHE FOR PART PROGRAM VERIFICATION

E. Lo Valvo

Univeristy of Catania, Catania, Italy

KEYWORDS: Turning, Graphic Simulation, Virtual Reality

ABSTRACT: The simulation and verification of NC codes for CNC machining is very important in the highly competitive and automated industries no matter if the codes are generated by conventional programming [1-4]. In fact, a succession of long and complex preliminary actions is needed to use this kind of machine tool, increasing the costs of the production process as a whole.

The aim of this work is to provide the operator with a rapid and effective tool to visualize the result of a turning operation with the intent of saving time, human resources and money.

In the paper a proper software, written in C language, is presented which through a polygon clipping algorithm and some OpenGL techniques, is able to simulate the machining using the numerical control verification module in a CN lathe.

Since the rendering image of simulated results can closely mimic the machined part, this research provides a better approach for a very fast NC simulation and verification on an inexpensive personal computer. In addition the model can also be displayed from different viewpoints and it can be manipulated for further applications.

This software can be used also as a visual postprocessor allowing the user to visualize the workpiece obtained from a part program produced from a CAM system.

Published in: E. Kuljanic (Ed.) *Advanced Manufacturing Systems and Technology*,
CISM Courses and Lectures No. 406, Springer Verlag, Wien New York, 1999.

1. INTRODUCTION

The development of the so called *Virtual Reality* technology (VR), together with its industrial applications, gave origin to an interesting research field concerning the development of a fictitious workspace aided by a personal computers. It enables the user to operate within it as a real workspace.

The following are the most relevant features of this technology:

- The availability of VR models of the different working equipment allow their use as a “test stand” to provide information about the production process that otherwise could be obtained only from expensive and time consuming real tests.
- VR can also support the operator during the learning process by the use of machine tools and virtual workpiece allowing also to simulate emergency or unusual operating conditions, by the use of production system’s models.
- VR can also allow to quickly test and verify some operating procedures before their real employ in the actual productive system

In the field of simulation of machining processes, modern CAD/CAM systems enable both to automatically generate the NC code and to visualize the toolpath to check the program before sending it to the machine tool. Anyway it is often necessary to check a priori the working on machine tool thus consuming both human and productive resources that obviously are very expensive.

Graphic simulation of machine tool’s workings gave rise a peculiar interest [1-4]. Recently some commercial software among which 3Dview, MachineWorks, NCSimul, RapidCam, VRMill, NCVerify, VeriCut have been developed, that are able to visualize the toolpath. This feature is obtained making use of the most recent 3D visualization techniques based on widespread software named OpenGL [5-6].

Loading and unloading step, setup of machine tool, execution of NC program and some other operations can be easily off-line verified before it is used on the machine tool. Fixturing systems can be also designed and checked simulating the working process using VR techniques. Moreover machining times can be computed and the running of the machine tool can be analyzed.

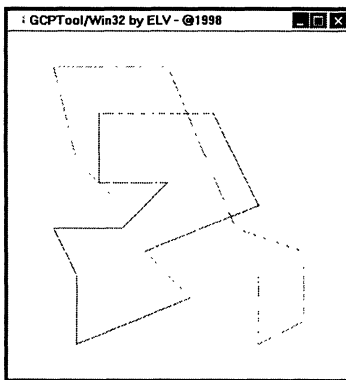
A simple but effective example describing such techniques has been realized in Windows 95 environment on a common Personal Computer. Starting from an NC program, the realized software allows to generate a dynamic three-dimensional visualization of an NC lathe machined workpiece by showing a revolving solid with given profile in a window of the screen.

2. OPENGL, GLUT AND GLE TOOLKITS.

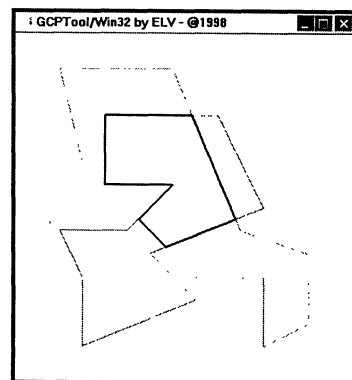
The OpenGL is a 2D and 3D graphics API (Application Programming Interface) developed by Silicon Graphics in 1991. This programming interface provides many graphics functions, including modeling, transformations, color, lighting and smooth shading, as well as advanced features like texture mapping, NURBS, fog and other for developing portable, interactive 2D and 3D graphics applications. OpenGL is supported by most 3D accelerator manufacturers and software developers (including Sun and Microsoft) [6].

Moreover some OpenGL-based toolkits, among which GLUT e GLE, have been provided to the scientific community.

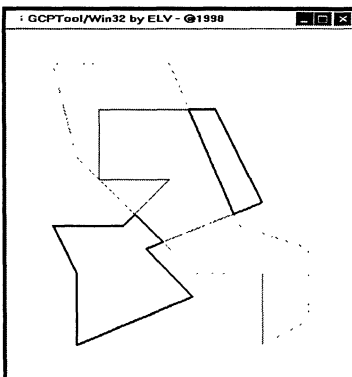
GLUT is the OpenGL Utility Toolkit, developed by M. Kilgard that implements a simple windowing application programming interface for OpenGL [7]. Moreover the version 3.6 includes another toolkit named “*GLE Tubing and Extrusion Library*” [8]. This toolkit, developed by L. Vepstas, is a graphics application programming interface able to perform the actual drawing of the tubing and extrusion. This toolkit include a specific subroutine named *gleLathe* that sweeps an arbitrary contour along a helical path, then it can be used to obtain a revolution solid starting from the knowledge of its cross section.



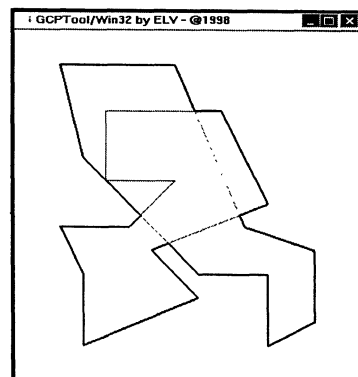
a) Two sample polygons



b) Intersection operation



c) Difference operation



b) Union operation

Fig.1- The boolean operation on polygons

3. GPC (GENERIC POLYGON CLIPPER)

To carry out the realization of the above mentioned visualization software, a public library, available on Internet, has also been utilized. It allows to perform clipping operations, i.e. boolean operations like union, intersection, difference and XOR on polygons, convex or concave, as complex as desired (fig. 1). The polygons may be comprised of multiple disjoint contours. The contours can be convex, concave or self-intersecting and may be nested (i.e. the polygons may have holes).

This toolkit, developed by A. Murta [9], is based on the algorithm proposed by Vatti [10]. This library has been utilized both for compatibility with OpenGL language and above all for its effectiveness and quickness. In fig. 1 an example of the possible operations performed with this library is reported.

4. THE SIMULATION OF CUTTING PROCESS

The cutting process is the consequence of the interference between the tool and the workpiece and it can be simulated by some boolean operations between primitives.

The software here developed, reads the part program of a generic CNC lathe and uses solid modeling to graphically simulate the material removal process by updating the stock shape as the cutter moves along the toolpath producing then the final piece.

This is directly obtained by reading the NC files. Every instruction contained into part program is read, and, if recognized as a working instruction, it is interpreted and represented as a proper polygon. This polygon therefore can be subtracted, with a boolean operation, from a previous polygon representing the section of workpiece. Sweeping the resulting polygon, the 3D representation of virtual workpiece can be obtained.

In order to get the above described operations, first of all a polygon representing the initial cross section of the stock is drawn, then the polygon traveled by the tool along its working movements is obtained. Since the GPC makes only use of polygons made of linear segments, it was necessary to approximate circumference-arcs with a polygonal line made by n edges, where n depends on the requested visualization mode. Such a polygon is every time subtracted from the polygon representing the cross section of the piece under work.

This procedure enables then a real time visualization and check of the writing operations of the part program, moreover relevant information pertaining to the machine process is continuously displayed. The tool path and the workpiece section are displayed in proper window and at any time during the simulation, the user can rotate and zoom into the part in another window. The user can use a NC program editor to modify the NC file and rerun the simulator. So it is possible to repeat the cutting simulation changing geometric parameters in few seconds, in order to optimize the editing stage.

In fig. 2 an example of verification and editing stage is reported; in it is possible to see the four windows showing the dynamic rendered image display (the model can be dynamic rotate, pan, zoom), the cross-sectional display of stock, the machining conditions and finally the part program for editing respectively.

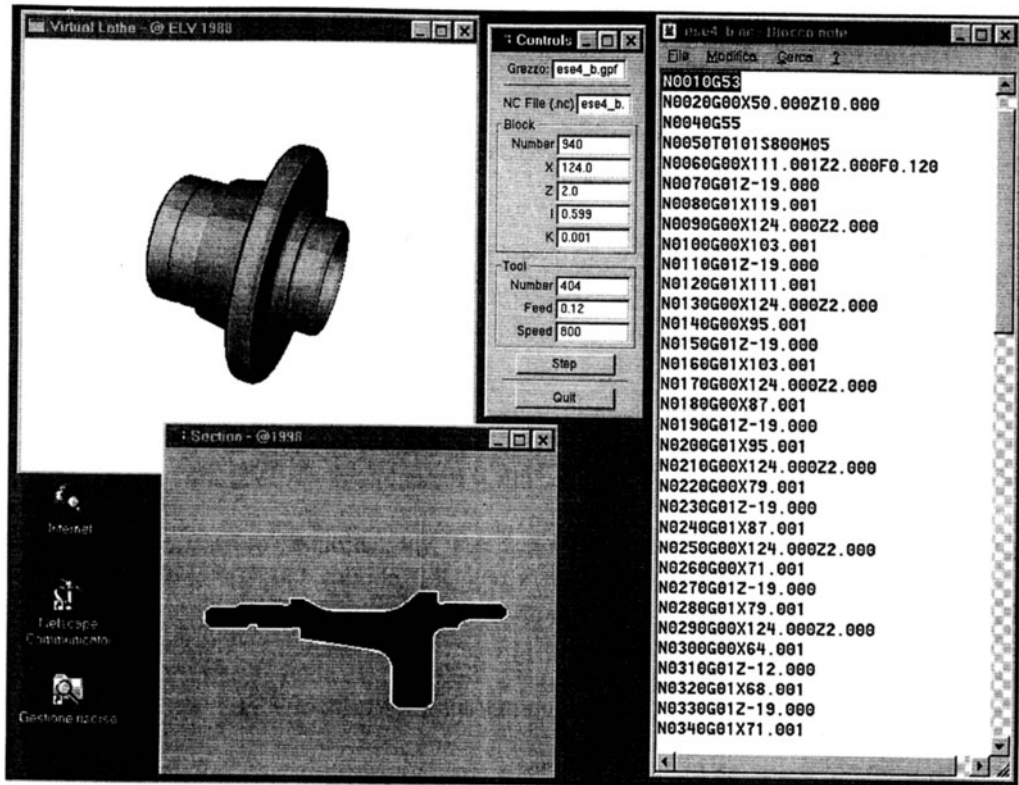


Fig. 2 – A snapshot of developed software

5. CONCLUSIONS

The part program check is very expensive in terms of time and human resources if it is manually performed. The possibility to correct programming mistakes after the post-processing stage involves the elimination of many cutting tests and a better functional use of the machine.

The developed software is a valid support to easily and quickly check the part program. In fact, the operator is able to immediately see both the piece and the mistakes of the shape of the cutting process. This is particularly useful for those machine tools, recently appeared on the market, which use a standard personal computer as numerical control.

Moreover, since the rendering image of simulated results can closely mimic the machined part, this software provides a better approach for NC simulation and verification on a personal computer, allowing:

- To increase of machine tool utilization and productivity;
- To significantly reduce both the cost and the time to produce parts;
- To improve quality and reduce scrap material;

- To eliminate expensive and time consuming proofing and dry runs;
- To visually compare of “as manufactured” with “as designed” part;
- To train new programmers, operators and students.

ACKNOWLEDGMENTS

This work has been performed with funding from Italian Ministry for University and Scientific Research.

REFERENCES

1. Voelcker, H.B., Hunt, W.A., The Role of Solid Modeling in Machining-Process Modeling and NC Verification”, SAE Technical Paper Series 810195, 1981
2. Sungurtekin, U.A., Voelcker H.B., “Graphical Simulation & Automatic Verification of NC Machining Program”, Proc. IEEE Int. Conf. on Robotics and Automation, 1986, 156-165
3. Appleton, E., Tool Path Simulation – Software Enables Engineers to Visualize Machining Processes in Advance, Computer Graphics World, 1990, 85-91
4. Kim, C.B., Yang, M.Y., Park, S., Tool Path Verification and NC Program Editing under a Multi-Window Environment, JAPAN/USA Symposium on Flexible Automation, Vol. 1 1992, 409-414
5. Segal, M., Akeley K., The OpenGL Graphic System: A Specification (version 1.2) – Silicon Graphics, March 23, 1998
6. The OpenGL, <http://www.opengl.org>
7. Kilgard M., Programming OpenGL for the X Window System, Addison-Wesley, 1996
8. Vepstas L., GLE Tubing and Extrusion Library, ver. 2.3 (1997), <http://linas.org/gle/index.html>
9. Murta, A. : A Generic Polygon Clipping Library, 1998, <http://www.cs.man.ac.uk/aig/staff/alan/software/gpc/gpc2.html>
10. Vatti, B.R.: A Generic Solution to Polygon Clipping, Communications of the ACM, 35(7), July 1992, 52-63

A SELECTION METHOD OF PROCESS PLANS SET FOR PART TYPES MIX PRODUCTION

J. Ljubetic and G. Cukor
University of Rijeka, Rijeka, Croatia

KEY WORDS: Flexible Manufacturing System, Alternative Process Plans, Part Types Mix, Production Time Load Optimization

ABSTRACT: The being of alternative process plans for each component of part types mix of a certain working order is an important ground of Flexible Manufacturing System's (FMS) efficiency in frequently changeable production surrounding. Hence, there is a need for identification and selection of such their set by which the realization of working order with minimal time occupation of FMS is ensured. The foundations of developed method for the selection of an optimal or sub-optimal set from all available alternative process plans are presented. Furthermore, based on the survey of obtained results from a concrete example, a premise for the evaluation of method's validity is given.

1. INTRODUCTION

An inherent characteristic of Flexible Manufacturing System (FMS) is its high production efficiency. It is so even in the conditions of dynamic production environment with the frequent structure modifications of working orders according to types and number of parts that are to be produced on the same FMS in a determined production period. However, the need for process flexibility is revealed.

Published in: E. Kuljanic (Ed.) *Advanced Manufacturing Systems and Technology*,
CISM Courses and Lectures No. 406, Springer Verlag, Wien New York, 1999.

The basic assumption for process flexibility is the being of alternative process plans by which the production of each component of part types mix at different number of operations and with different use of machines is foreseen [1, 2]. The alternative process plans enable different ways of transforming an input raw material n' into the final part type n of specified construction characteristics, Figure 1.

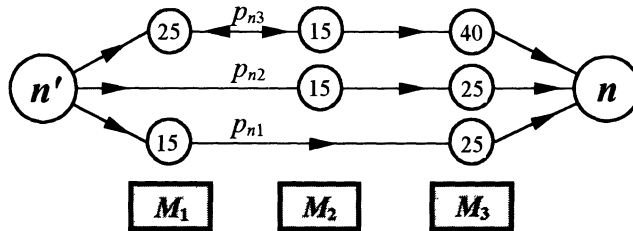


Figure 1. Alternative process plans for the part type n

In the following, the selection method of an optimal set from all developed alternative process plans which is based on the fundamental postulates of Seo and Egbelu [3], but with modified approach in the phase of solution evaluation is presented. For that purpose the modified model of process plans set selection is developed.

2. MODEL OF PROCESS PLANS SET SELECTION

The problem formulation has the following elements:

Input data: the alternative process plans of part types mix to be produced according to specified working order, which assign operations to machines and determine machining and transport times;

Output decision: the optimal set having only one process plan of each component of part types mix in the working order;

Objective: minimizing the total time load of FMS;

Constraints: complying with the exploitation characteristics of FMS, structure of working order and available alternative process plans.

The problem data of model are as follows:

- the set N of part types in working order to be produced, $N = \{1, 2, \dots, n, \dots, |N|\}$;
- the set M of machines in FMS, $M = \{1, 2, \dots, m, \dots, |M|\}$;
- the set Q of the number $q(n)$ of parts that must be produced for each part type $n \in N$, $Q = \{q(n) | n \in N\}$;
- the sets $P(n)$ of the number $r(n)$ of developed alternative process plans $p(n, i)$ for each part type $n \in N$, $P(n) = \{p(n, i) | i = 1, 2, \dots, r(n) \text{ and } n \in N\}$ while $p(n, i)$ can be

represented by $p(n, i) = \{ \langle d_{ab}[p(n, i)], t[p(n, i), m] \rangle, \dots, \langle d_{yz}[p(n, i)], 0 \rangle \}$ where $d_{ab}[p(n, i)]$ is the input path segment between nodal points a and b that a pallet has to pass before required operation on machine m , $d_{yz}[p(n, i)]$ is the output path segment between nodal points y and z after last operation is done and $t[p(n, i), m]$ is the operation time required to machine a part type n on machine m according to the alternative process plan $p(n, i)$;

- the speed v_p of automatic transport.

Since the production cycle is consisted from machining and transport times, the i -th selected alternative process plan $p(n, i)$ for part type n can be valued by the total time load $\tau[p(n, i)]$ of $q(n)$ parts that have to be produced, that is:

$$\tau[p(n, i)] = q(n) \left\{ \sum_{m \in M} t[p(n, i), m] + \frac{1}{v_p} \sum_{ab}^{yz} d_{jk} [p(n, i)] \right\} \tag{1}$$

From the number $i = 1, 2, \dots, r(n)$ of developed alternative process plans $p(n, i)$ **only one** is to be joined to each part type $n \in N$. Hence, the total time load of each machine $m \in M$ as well as the total time load of transport system for complete set N can be obtained respectively by:

$$T_M(m) = \sum_{n \in N} q(n) t[p(n, i), m], \quad \forall m \in M \tag{2}$$

$$T_t(N) = \frac{1}{v_p} \sum_{n \in N} \left\{ q(n) \sum_{ab}^{yz} d_{jk} [p(n, i)] \right\} \tag{3}$$

For achieving the optimal results, it is of a great importance to balance at the utmost the time loads among the machines of FMS. The measure of time load diverse is expressed by the magnitude Δm as a difference between the bottleneck-machine time load and the average time load of other machines in the FMS according to equation:

$$\Delta m = \frac{|M| [T_M(m)]_{\max} - \sum_{m \in M} T_M(m)}{|M| - 1} \tag{4}$$

Moreover, it is important that transport system does not create a waiting queue on the momentary bottleneck of FMS, i.e. eventual waiting on bottleneck has to be the least possible. The influence of transport system on the performance of FMS is represented by the magnitude Δh in the following way:

$$T_t(N) \leq [T_M(m)]_{\max} \Rightarrow \Delta h = 0 \tag{5}$$

$$T_i(N) > [T_M(m)]_{\max} \Rightarrow \Delta h = T_i(N) - [T_M(m)]_{\max} \quad (6)$$

Model formulation: as the goal of process plans set selection is to ensure the least time load of FMS together with the best possible balance between the time loads of both the machines and automatic transport system, the general form of the model may be stated as follows;

$$\text{minimize} \quad \left\{ \sum_{n \in N} \sum_{i=1}^{r(n)} \tau[p(n,i)] x[p(n,i)] \right\} + \Delta m + \Delta h \quad (7)$$

$$\text{subject to} \quad x[p(n,i)] = \begin{cases} 1, & \text{if the } p(n,i) \text{ is selected,} \\ 0, & \text{otherwise,} \end{cases} \quad \forall x[p(n,i)] \quad (8)$$

$$\sum_{i=1}^{r(n)} x[p(n,i)] = 1, \quad \forall n \in N \quad (9)$$

With the proposed model, the selection of only one process plan of each component of part types mix is ensured as well as the possibility of selecting any of developed alternative process plans.

3. PROCEDURE OF PROCESS PLANS SET SELECTION

Searching of all possibilities and finding the optimal solution at large number of components of part types mix and large number of alternative process plans for a single part type seeks for large volume of activities. The solution area is defined by the expression $\prod_{n \in N} r(n)$. Using the convenient heuristic algorithm, the procedure is made practically applicable at various structures of working orders. For this purpose, the tabu search technique [4, 5] is used which considerably shortens the selection procedure of process plans set S_O that represents the optimal solution $S_O = \{p_1, p_2, \dots, p_n, \dots, p_{|N|}\}$ where the process plan number p_n denotes selected process plan $p(n, i)$ for the part type $n \in N$ and posses an integer value between 0 and $[r(n) - 1]$, that is $p_n = i - 1$.

For procedure performing, it is necessary to associate a code mark to every searched solution S_C . Each code mark represents the unique number in the solution area. The code of solution is obtained by summing up the position values of selected process plans. At this, the position value of selected process plan $p(n, i)$ for the part type $n \in N$ is equal to the product of related number p_n from 0 to $[r(n) - 1]$ and the total numbers of variant processes of successive parts from $n + 1$ to $|N|$ in ordered set S_C . Accordingly, the code of solution S_C can be expressed as:

$$C(S_C) = \sum_{n=1}^{|N|-1} p_n \prod_{n+1}^{|N|} r(n) + p_{|N|} \quad (10)$$

The favorableness rate of solution S_C is obtained in accordance with the objective function (7) as a value of merit function $f(S_C)$, in the following way:

$$f(S_C) = \sum_{n=1}^{|N|} \tau(p_n) + \Delta m(S_C) + \Delta h(S_C) \tag{11}$$

where $\tau(p_n)$ is the sum of machining and transport time for $q(n)$ parts of type n obtained by the equation (1) according to the process plan p_n selected in solution S_C , while $\Delta m(S_C)$ and $\Delta h(S_C)$ represent the influence of time load diverse of machines and the influence of automatic transport on the value of merit function respectively. In the following the developed searching algorithm will be briefly described, Figure 2.

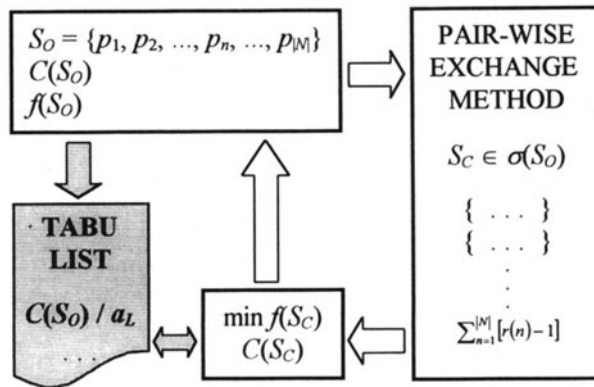


Figure 2. The structure of selection procedure

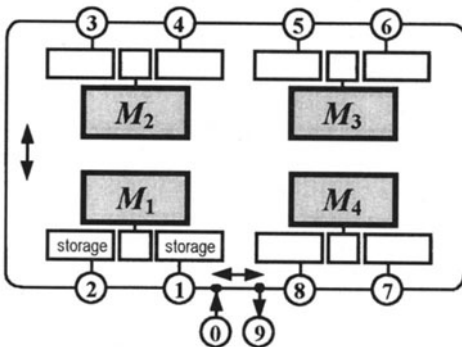
Searching algorithm starts from the solution S_0 which $p_n = 0$ for all $n \in N$ and establishes the solution value by calculation of function $f(S_0)$. At the same time, the solution S_0 is an initial best solution. In every following step, the set of solutions $\sigma(S_0)$ is generated using the pair-wise exchange method [3] which results with $\sum_{n=1}^{|N|} [r(n)-1]$ new solutions S_C . In every new solution S_C , the selection among the others of developed alternative process plans is varied by altering the value p_n for one. The momentary best solution S_C is the one with the least value of merit function $f(S_C)$ satisfying the condition that it is not on tabu list TL, thus becoming new best solution S_0 for the next step. All previously considered solutions are set on tabu list, thus being excluded from repeated selection and consideration in the following steps. This restriction is not activated if the value $f(S_C)$ of momentary best solution S_C is less than value $f(S_0)$ in the previous step. As the case stands, the value $f(S_0)$ in the previous step is to be joined as the aspiration value a_L to the solution S_0 on tabu list.

4. TESTING EXAMPLE

The application of proposed selection method was tested on a concrete example. For the working order containing four part types $N = \{1, 2, 3, 4\}$ in given lot sizes $Q = \{50, 20, 80, 60\}$, the alternative process plans defined by the sets of parameters were developed:

- Part 1 $p_{11} = \{(d_{01}= 2, t_{111}=30), (d_{23}= 8, t_{112}=15), (d_{45}= 4, t_{113}=35), (d_{67}= 8, t_{114}=30), (d_{89}= 2)\}$
 $p_{12} = \{(d_{03}=10, t_{122}=35), (d_{47}=13, t_{124}=28), (d_{81}= 6, t_{121}=45), (d_{29}= 5)\}$
 $p_{13} = \{(d_{03}=10, t_{132}=35), (d_{45}= 4, t_{133}=20), (d_{67}= 8, t_{134}=60), (d_{89}= 2)\}$
- Part 2 $p_{21} = \{(d_{05}=14, t_{213}=10), (d_{67}= 8, t_{214}=40), (d_{83}=15, t_{212}=25), (d_{41}=10, t_{211}=15), (d_{29}= 5)\}$
 $p_{22} = \{(d_{01}= 2, t_{221}=22), (d_{27}= 8, t_{224}=30), (d_{83}=15, t_{222}=32), (d_{49}=14)\}$
 $p_{23} = \{(d_{05}=14, t_{233}=25), (d_{61}=15, t_{231}=18), (d_{27}= 8, t_{234}=30), (d_{89}= 2)\}$
 $p_{24} = \{(d_{01}= 2, t_{241}=42), (d_{27}= 8, t_{244}=45), (d_{89}= 2)\}$
- Part 3 $p_{31} = \{(d_{05}=14, t_{313}=20), (d_{63}= 6, t_{312}=30), (d_{41}=10, t_{311}=40), (d_{27}= 8, t_{314}=15), (d_{89}= 2)\}$
 $p_{32} = \{(d_{05}=14, t_{323}=58), (d_{61}=15, t_{321}=52), (d_{29}= 5)\}$
- Part 4 $p_{41} = \{(d_{07}= 5, t_{414}=18), (d_{81}= 6, t_{411}=12), (d_{23}= 8, t_{412}=25), (d_{49}=14)\}$
 $p_{42} = \{(d_{05}=14, t_{423}=20), (d_{61}=15, t_{421}=42), (d_{29}= 5)\}$
 $p_{43} = \{(d_{05}=14, t_{433}=10), (d_{63}= 6, t_{432}=18), (d_{41}=10, t_{431}=15), (d_{27}= 8, t_{434}=12), (d_{89}= 2)\}$

The above processes were developed for use in FMS with four machines and automated transport system, Figure 3.



Matrix of transport times:

		target stations				
		1	3	5	7	9
starting stations	0	2	10	14	5	0
	2		8	13	8	5
	4	10		4	13	14
	6	15	6		8	11
	8	6	15	10		2

$$t_{03} = \frac{d_{03}}{v_p} = \frac{10}{1} = 10 \text{ t.u.}$$

Figure 3. FMS with four machines and automatic transport along with the survey of matrix of transport times

For problem solving the application of pair-wise exchange method was conducted in 12 steps. Optimal solution $S_O = \{2310\}$ with the value of merit function $f(S_O) = 27247$ was already found in the third step, consisting of the set of process plans $\{p_{13}, p_{24}, p_{32}, p_{41}\}$. The solving procedure is represented in table 1 showing first 4 steps.

Table 1: Survey of the solving procedure on the example

Step No.	S_O	$C(S_O)$	$f(S_O)$	$S_C \in \sigma(S_O)$	$C(S_C)$	$f(S_C)$	TL $C(S_O) / a_L$					
1	{0000}	0	29413	{0001}	1	30453	0 / ∞					
				{0002}	2	30313						
				{0010}	3	29040						
				{0100}	6	28860						
				{0200}	12	28687						
				{0300}	18	27953						
				{1000}	24	30597						
				{2000}	48	29700						
2	{0300}	18	27953	{0301}	19	30333	18 / 29413					
				{0302}	20	28853						
				{0310}	21	28660	0 / ∞					
				{0200}	12	28687						
				{0100}	6	28860						
				{0000}	0	29413						
				{1300}	42	29137						
				{2300}	66	28093						
				3	{2300}	66		28093	{2301}	67	28620	66 / 27953
									{2302}	68	28813	
{2310}	69	27247	18 / 29413									
{2200}	60	28887										
{2100}	54	29170										
{2000}	48	29700										
{1300}	42	29137										
{0300}	18	27953										
4	{2310}	69	27247	{2311}	70	29567	69 / 28093					
				{2312}	71	28260						
				{2300}	66	28093	66 / 27953					
				{2210}	63	28280						
				{2110}	57	28260						
				{2010}	51	28927						
				{1310}	45	30093						
				{0310}	21	28660						
											18 / 29413	
						0 / ∞						

etc. until 12th step

At the best solution identified, the time load of FMS is represented by the following time load structure of isolating elements (in time units): $T_{M1} = 5720$, $T_{M2} = 3250$, $T_{M3} = 5640$, $T_{M4} = 4980$ and $T_t = 6140$. From these data the following quantities arise: $\Delta m(S_O) = 1097$ and $\Delta h(S_O) = 420$. These quantities point at the significant unbalance of time load of FMS. The bottleneck of the system is the automatic transport since its time load value T_t exceeds the maximum time load value of momentary bottleneck among machines, i.e. T_{M1} . It should be noted that in case of accelerated transport of 17,5% for instance, transport is not anymore the bottleneck of the system and the solution $S_O = \{2310\}$ still remains the

most favorable one with the value of merit function $f(S_0) = 25757$. Thus, together with the same time loads of machines the quantity $\Delta m(S_0)$ remains unvaried, while $T_t = 5070$ and $\Delta h(S_0) = 0$.

5. CONCLUSION

The need for alternative process plans in concurrent production of part types mix on the same FMS has been pointed out. Also, the model of minimizing the total time load of FMS has been formulated based on which the selection method of an optimal set of process plans was developed. The implemented searching algorithm is founded on the tabu search technique. By the proposed method, the high level of reliability in finding the most acceptable solution as well as fast executing in tasks which are characterized by comparatively higher number of variables are ensured. The results of testing example with less number of variables have supported the application of method since the optimal solution was already found in the very early phase of procedure executing. Nevertheless, it is real to expect that more complex working orders will demand procedure executing with a greater number of steps. Even then, with the use of a computer, fast procedure executing is ensured.

REFERENCES

1. Ljubetić, J.: Sequence Proceeding of Working Orders and Structure of FMS - Influence on Efficacy, Bulletins for Applied Mathematics, Budapest BAM 1191/'96 (1996), 125-134
2. Katalinić, B.: Industrieroboter und flexible Fertigungssysteme fuer Drehteile, VDI Verlag, ISBN 3-18-401027-9, Duesseldorf 1990
3. Seo, Y., Egbelu, P.J.: Process Plan Selection Based on Product Mix and Production Volume, International Journal of Production Research, 34 (1996) 9, 2639-2655
4. Glover, F.: Tabu Search - Part I, ORSA Journal on Computing, 1 (1989) 3, 190-206
5. Glover, F.: Tabu Search - Part II, ORSA Journal on Computing, 2 (1990) 1, 4-32

HOT WORKABILITY STUDIES OF NIMONIC 80A APPLIED TO THE NET-SHAPE FORGING OF AEROFOIL BLADES

P.F. Bariani, T. Dal Negro and M. Fioretti
University of Padua, Padua, Italy

KEY WORDS: Hot Forging, Turbine Blades, Nimonic 80A, Workability

ABSTRACT: Real material based physical-simulation experiments are carried out on Nimonic 80A samples with the aim of investigating the workability exhibited by the material under the process conditions that occur during multi-step hot forging of a gas turbine blade. On the basis of workability data, expressed in terms of rheological behaviour, sensitivity of the flow strength to temperature and strain rate variations during deformation and final microstructure, opportunities for redesign and optimisation of process parameters are analysed.

1. INTRODUCTION

Modelling the forging of turbine blades can be approached in different and complementary ways, according to the particular aim of the analysis. Analytical methods, such as slab method and slip-line theory, prove to be effective in predicting loads, optimum die profile, preform position and minimum stock volume for complete filling of cavities in the aerofoil region of the turbine [1,2]. Physical simulation techniques based on soft model materials deformed by using cheap tools have been extensively applied to investigate both 2D and 3D flow patterns [3-5]. In the most sophisticated applications, these techniques enable forging loads and pressure distribution at interfaces to be evaluated as well [6]. Exclusive capability of the Finite Element method is the coupled thermal and mechanical analysis of forging operations with quantification of local values of strain, strain rate, stress and temperature in the whole volume of the workpiece and dies [7-9].

Nett-shape forging of Nickel-alloy turbine blades is a complex operation to model. Due to the high sensitivity of the flow strength of the material to temperature and, for some alloys,

to strain rate and the thin section in the aerofoil region, filling of the die cavities is dominated by the response of the material to the straining and temperature histories that are determined by the geometry, heat transfer and friction at the material-workpiece interface. Accordingly, knowledge of the instantaneous response of the material to the thermal and mechanical cycles is a prerequisite to accurate modelling and effective design of the forging process.

To this aim, physical-simulation experiments have been set up by the authors [10-12] where the thermal and mechanical events of the forging process are reproduced on real-material samples.

This paper refers to the application of the above physical simulation experiments to Nimonic 80A samples with the aim of investigating the workability exhibited by the material under the process conditions that occur during multi-step forging of a gas turbine blade. On the basis of workability data, expressed in terms of rheological behaviour, sensitivity of the flow strength to temperature and strain rate variations during deformation and final microstructure, opportunities for redesign and optimisation of process parameters are then analysed.

2. THE APPROACH

The approach followed in investigating the workability of Nimonic 80A and in evaluating opportunities to improve the forging process consisted of three main steps:

- (i) analysis, through isothermal and constant strain-rate uniform compression tests, of the sensitivity of the flow strength to temperature, strain and strain rate;
- (ii) evaluation, through physical simulation experiments carried out under control of temperature and strain-rate, of microstructure evolution and instantaneous flow strength exhibited by the material during the thermal and mechanical cycles of the forging process;
- (iii) identification, on the basis of workability data, of opportunities for redesign and optimisation of process parameters.

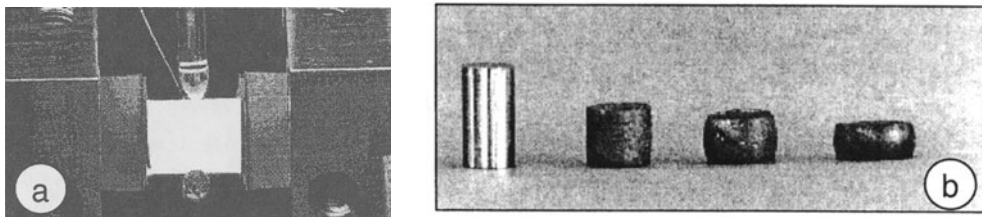


Fig. 1: Heating of a specimen on the Gleeble system (a), specimen before and after deformation (b)

3. FLOW STRESS TESTS AND PHYSICAL SIMULATION EXPERIMENTS

Flow stress tests

According to section (i) of the approach, a set of isothermal and constant strain rate uniform compression tests have been carried out with the aim of evaluating the sensitivity of the flow strength of Nimonic 80 A to temperature, strain and strain rate. Five values of temperature have been tested in the range of 1000-1200°C for three different values of the

strain rate ($\dot{\epsilon}' = 15, 36, 45 \text{ s}^{-1}$)

The flow stress tests have been carried out on the computer-controlled dynamic system Gleeble 2000[®]. It can be programmed to reproduce thermal and mechanical events under control of temperature, force, strain and strain rate. The specimen is resistance heated by thermocouple feedback controlled a.c. current (Fig.1) that produces uniform temperature distribution in the diametrical planes. Temperature is uniform also along the axis of the specimen thanks to multi-layered interfaces between specimen and punches that consist of a sandwich of two alternate foils of graphite and tantalum.

Physical simulation experiments

According to section (ii) of the approach, a set of physical simulation experiments have been carried out on the Gleeble system with the aim of evaluating the instantaneous flow strength exhibited by Nimonic 80 A during the real forging process. In these tests, cylindrical specimens are cycled through a multi-stage upsetting in uniform compression conditions. Under the control of time, temperature, strain and strain rate, these tests replicate accurately the forging cycle of the blade. Fig. 2 shows the temperature-time diagram for the 3-steps cycle reproducing the current forging process.

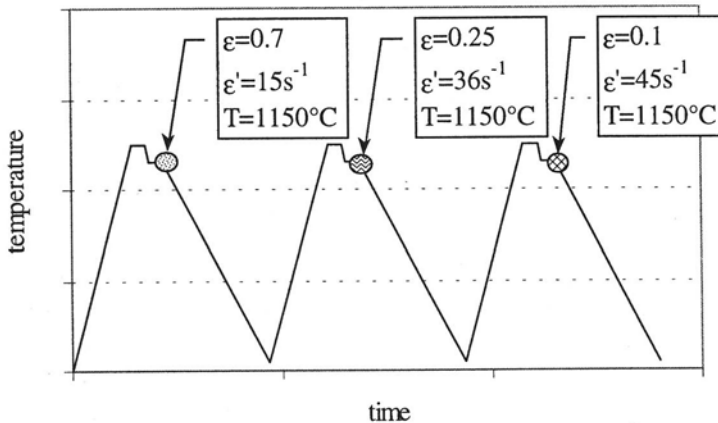


Fig.2: Temperature – time diagram for the physical simulation experiment

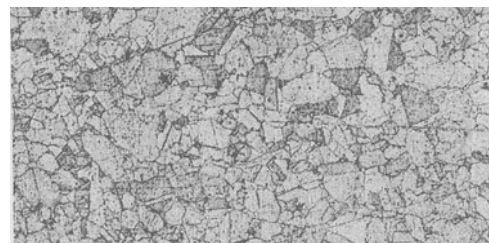
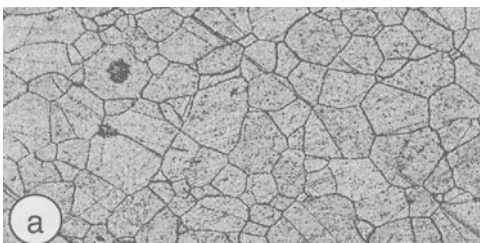


Fig.3: Microstructure of Nimonic 80 A specimens in flow stress test with total strain $\epsilon=0.7$ and strain rate $\dot{\epsilon}'=15 \text{ s}^{-1}$, (a) $T=1150^\circ\text{C}$, (b) $T=1050^\circ\text{C}$

4. RESULTS AND DISCUSSION

Fig.4 shows the true stress-true strain curves relevant to five temperatures at the constant strain rate of 15 s^{-1} . In all testing conditions the material exhibits a high sensitivity of the flow strength to temperature, whereas sensitivity to strain rate is always negligible. The high sensitivity to temperature is also evident from the two microstructures of Fig. 3.

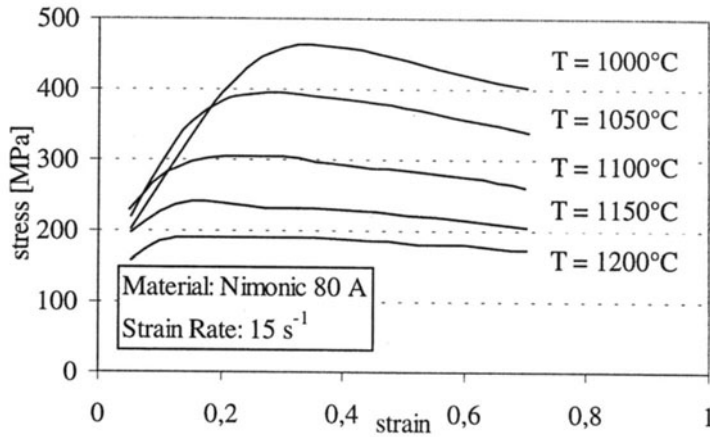


Fig.4: Flow curves for five different temperatures

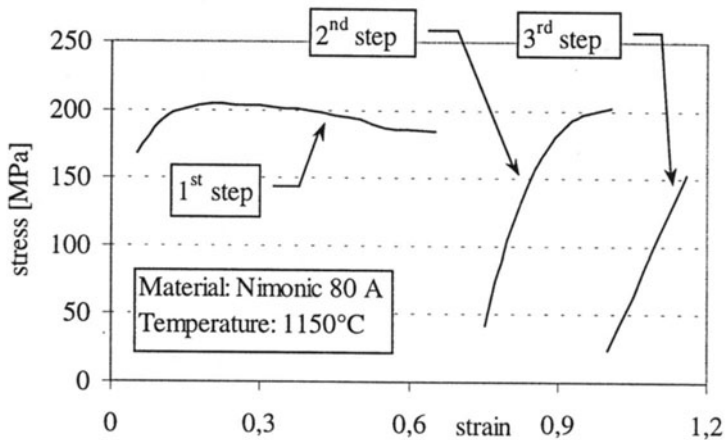


Fig.5: Instantaneous flow strength in the multi step test of Fig.2

Fig. 5 shows the instantaneous flow strength during physical simulation experiments of Fig.2. In the second and third step, the deformation is performed with a flow strength that is fairly lower than that of the first step. In Fig. 6 the flow strength in the second deformation step of Fig.5 is compared with the corresponding flow strength evaluated in the flow stress test at $\dot{\epsilon} = 36 \text{ s}^{-1}$. The flow strength in the multi step deformation is 25% lower than that evaluated in flow stress tests, the better workability being due to the softening activated during the first step.

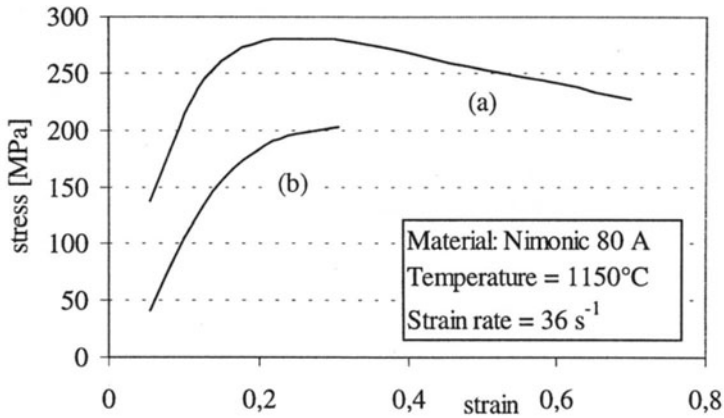


Fig.6: Flow strength in flow stress test (a) and in the second step of the multi step test (b)

The high material workability at the highest testing temperatures together with the reduction of the flow resistance due to the static and dynamic softening suggested a redesign of the forging process reducing from three to two the number of forging steps, with the advantage of shortening the mechanical and thermal cycle. The two process are compared in Fig.7 in terms of final microstructure at three different locations of the blade section. The different grain size in the three locations are due to the different levels of the accumulated strain, while the lower grain size measured in the blade forged in two steps is mainly due to a lower number of re-heating cycles.

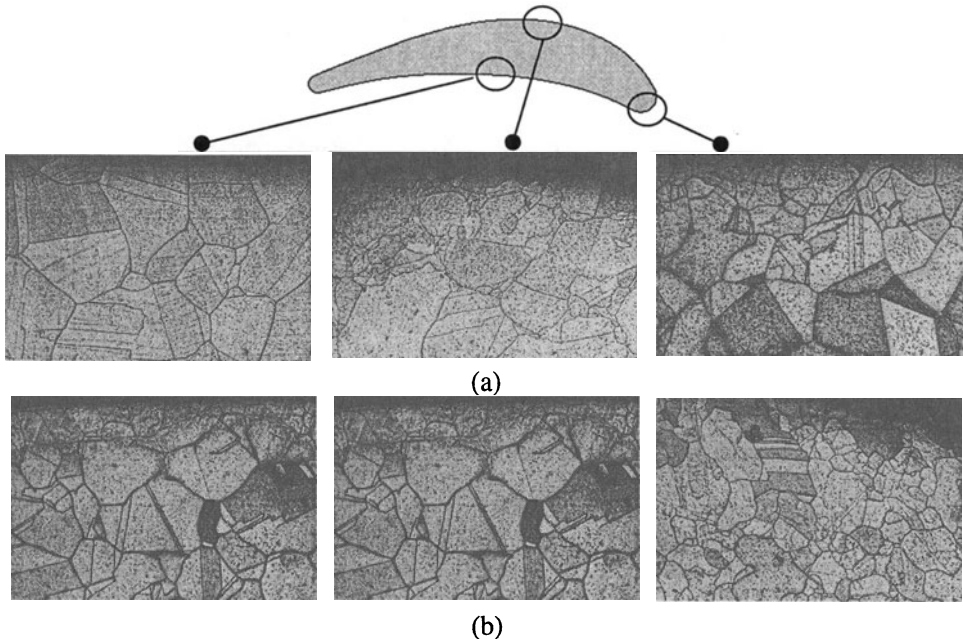


Figure 7: Microstructure at three locations of the airfoil section forged in 3 steps (a) and in 2 steps (b)

5. CONCLUDING REMARKS

Main achievements in investigating the workability of Nimonic 80 A are (i) the quantification of the sensitivity of the flow strength to temperature and strain rate, as well as its reduction during the forging process due to static and dynamic softening, and (ii) the evaluation of the influence of thermal and mechanical cycles on the final microstructure. On the basis of the workability data, the forging process has been successfully re-designed reducing from three to two the number of forging steps, with the twofold advantage of shortening the production cycle and improving the microstructure as a consequence of the removal of one re-heating operation.

6. ACKNOWLEDGEMENTS

The work on which this paper is based is part of a scientific co-operation between PIETRO ROSA TBM and DIMEG – University of Padua. The authors wish to thank Mrs S. Bruschi, PhD student at DIMEG, for the co-operation in conducting the tests.

7. REFERENCES

- [1] Altan T. and Akgerman N., Application of CAD/CAM in Forging Turbine and Compressor Blades, *J. of Engineering for Power*, 98 (1976), pp.290-296
- [2] Aksenov A.B., Chitkara N.R. and Johnson W., Pressure and Deformation in Plane Strain Pressing of Circular Section Bar to Form Turbine Blades, *Int. J. of Mech. Sci.*, 17 (1975),
- [3] Altan T., Henning H.J. and Sabroff A.M., The Use of Model Materials in Predicting Forming Loads in Metalworking, *J. of Eng. Ind.*, 92 (1970), pp.444-452
- [4] Wanheim T., Maegaard V. and Danckert J., The Physical Modelling of Physical Working Forming Processes, *Int. Conf. of Advanced Technology of Plasticity*, Tokyo, 2 (1984), pp
- [5] Boer C, Rebelo N, Rydstad H. and Schroder G, Process Modelling of Metal Forming and Thermomechanical Treatment, Springer-Verlag, Berlin, 1986, pp.109-140
- [6] Ou H. and Balendra R., Modelling Techniques for Net-Forging of Turbine Blades, *Int. Conf. on Forging and Related Technology*, Birmingham, 1998, pp.63-72
- [7] Dean T.A. and Brooks J.W., An Exercise in the Investigation of Boundary Conditions and Evaluation of Numerical Simulation Applied to the Net-Shape Forging of Ti-6Al-4V Aerofoil Blades, *Int. Conf. on Forging and Related Technology*, Birmingham, 1998, pp.73-
- [8] Soltani B., Mattiasson K. And Samuelsson R., Implicit and Dynamic Explicit Solutions of Blade Forging Using FEM, *Int. J. of Material Processing Technology*, 45 (1994) pp 69-74
- [9] Cho J.R., Lee N.K. and Yang D.Y., A Three-dimensional Simulation for Non-isothermal Forging of Steam Turbine Blade by the Thermoviscoplastic FEM, *J. of Engineering Manufacturing*, ImechE, 207 (1993), pp.263-273
- [10] Bariani P.F., Dal Negro T., Guggia R. and Fioretti M., Designing the Forging Process of a Nimonic 80A Turbine Blade Through the Physical Simulation of Thermal and Mechanical Operations, *Int. Conf. on Forging and Related Technology*, Birmingham, 1998, pp.83-91
- [11] Bariani P.F. and Dal Negro T., Hot Deformation Studies on a Micro-alloyed Steel: the Influence on the Flow Stress of the Varying Process Conditions, 1st Int. Conf. ESAFORM, Sophia Antipolis, 1998.
- [12] Bariani P.F, Dal Negro T. and Fioretti M., Joint Use of Physical and Numerical Simulation Techniques in Predicting Process Parameters Evolution and Final Microstructure in Nimonic 80 A Turbine Blade, accepted for presentation at 2nd Int. Conf. ESAFORM, 1999.

INFLUENCE OF EXTRUSION PROCESSING VARIABLES ON THE MICROSTRUCTURE AND MECHANICAL PROPERTIES OF ALUMINUM-LITHIUM ALLOY EXTRUSIONS

J. Fragomeni

Ohio University, Athens, OH, USA

KEY WORDS: Extrusion, Aluminum, Microstructure, Zener-Hollomon

ABSTRACT: Extrusion temperature, strain rate, extrusion ratio, billet temperature, and extrusion geometry were varied, and correlated with the microstructure of the alloy, and the heat treating times and temperatures. The extrusion processing variables were related to the microstructure through the Zener-Hollomon parameter i.e., the temperature compensated strain rate. Based on optical and transmission electron microscopy studies it was found that regardless of the extrusion conditions, the various microstructures were for the most part were unrecrystallized for both the as-extruded and the solution heat treated conditions. Smaller grain sizes were correlated to smaller Zener-Hollomon parameters. The extrusion temperature and ratio did not significantly effect the strength or elongation. The section geometry did effect these mechanical properties.

1. INTRODUCTION

The extrusion of a material is a very complex process since it involves the interaction between the material properties and the processing variables. The extrusion process is often used to produce a section geometry that must satisfy strict geometric, microstructural, and property specifications. There are several processing variables which can be controlled during an extrusion process. These variables include the extrusion ratio, the extrusion temperature, the strain rate, and the ram speed. However, the extrusion ratio is often pre-determined by the product specifications so that only extrusion temperature and ram speed are controllable. Most metals are extruded at elevated temperatures since the deformation resistance is low and therefore less force and energy are required to force

the extruded billet through the die orifice. The extruded billet is forced through the die orifice by a ram with a dummy block or pressure plate at the end of the ram in direct contact with the billet. On addition to changing the shape of the material, the extrusion process also has a substantial influence on the microstructure and properties. The plastic deformation that occurs during the extrusion process alters the grain size, texture, subgrain size, dislocation density and various other microstructural features. Often the material being extruded is not homogeneous so therefore variations in the microstructure and properties occur across the cross-section of the final extruded product. The mechanical properties and microstructure can also vary with length since the temperature is hard to maintain constant throughout the extrusion process. The extrusion temperature often varies from the heat generated during the extrusion process. Heat is conducted from the billet to the extrusion container, tools, and ram.

The demonstration material that was extruded for this study was an aluminum alloy containing 2.6wt.% lithium and 0.09wt.% zirconium. This alloy was strengthened by heat treatment causing the nucleation, growth, and coarsening of coherent metastable δ' (Al_3Li) precipitates in the microstructure. The δ' precipitates which are a consequence of artificial aging the Al-Li alloy, are spherical, ordered, and coherent with the aluminum matrix and impede the dislocation glide motion during plastic deformation. The δ' particles grow homogeneously in the matrix, and have the Cu_3Au (L1_2) superlattice crystal structure. Aluminum-lithium alloys are used primarily for aerospace structural applications since they have attractive properties such as a lower density and higher elastic modulus than conventional 2XXX and 7XXX alloys.

2. MATERIAL PROCESSING

An aluminum-lithium alloy having a composition of 2.6wt.% lithium and 0.09wt.% zirconium was cast by the Aluminum Company of America, ALCOA laboratories, in the form of a rolling ingot slab. One large ingot was cast having the dimensions of 30.5 cm (12 in.) X 96 cm. (38 in.) X 30.5 cm. (12 in.). The ingot was later preheated in a gas fired furnace at the ALCOA Extrusion Works, Lafayette, Indiana, for eight hours in the temperature range of 482-500 °C (900-925 °C) followed by 12 hours in the temperature range of 527-538 °C (980-1000 °F). Several smaller billets were then machined from the one preheated larger ingot to be used for the extrusion processing.

3. EXTRUSION PROCESSING

From the preheated ingot, billets 15.25 cm (6 in.) diameter by either 25.4 cm. (10 in.) or 50.8 cm (20 in.) were machined. The aluminum-lithium billets were direct extruded by the ALCOA Lafayette Extrusion and Tube Division, Lafayette Indiana, after being reheated to temperatures of either 466°C (870°F) or 290°C (555°F). Six product geometries, three round rods and three rectangular sections, were extruded from the billets using an instrumented 2500 ton press in the direct mode.

4. EXTRUSION POST-PROCESSING

The Al-Li alloy was machined into standard ASTM tensile samples from the extruded product. All of the tensile samples were oriented in the longitudinal grain direction. The tensile specimens were first solution heat treated (SHT) for one hour at 550 °C (1022 °F) in a molten sodium nitrate salt solution followed by a cold water quench to room temperature. Following the solution heat treatment, the tensile samples were artificially aged for various lengths of time in a molten sodium nitrate (NaNO₃) salt bath, followed again by a cold water quench. Different artificial aging treatments were utilized by varying both aging time and the aging temperature. Most of the tensile samples were aged at temperatures of 185 °C (365 °F) and 193 °C (379 °F). The molten salt solution was continuously stirred throughout the solution heat treatment and aging process to insure a uniform temperature distribution throughout the salt bath.

5. METALLOGRAPHY AND MICROSTRUCTURE

In order to study the grain structure of the alloy, light optical microscopy (LOM) was performed on samples that were fine ground and mechanically polished to 0.05 μm. The sequence of the mechanical polishing was as follows; (1) 240, 320, 400 and 600 grit SiC paper; (2) 600 grit alundum; (3) 0.5 μm alumina and (4) 0.05 μm MgO slurry. The specimens were anodized and then observed under polarized light to reveal the grain structure. Anodization was performed in a solution containing 948 ml deionized H₂O, 55 ml HBF₄, and 7 grams H₃BO₃ (Boric Acid) for one minute at 18 volts and -32 °C. Polarized light micrographs were then taken of the partially recrystallized grain structure in the peak-aged condition of 48 hours aging time at 185 °C aging temperature (see Figure 1).

The particle size distribution and particle morphology were examined and photographed using transmission electron microscopy (TEM) from thin foil specimens obtained from samples aged at 185 °C for various aging times ranging from 24 to 225 hours. The thin foil specimens were sliced with a diamond saw cutter and then polished to foils approximately 0.05 mm thick. Disks approximately 3 mm in diameter were then punched from the foils. The thin foil disks were then electropolished using a twin jet polisher, with the disks submerged in a 3:1 methanol-nitric acid solution (the electrolyte) and cooled by liquid nitrogen to around -20 to -35°C. The thin foil disks were observed and photographed using a JEOL-200 CX microscope operating at 200 KV for various specimen inclinations. Centered dark field images were used since they gave good contrast between images of the δ' particles and the matrix phase (see Figure 2). Particle size measurements of both the Al₃Li precipitates and composite Al₃Li-Al₃Zr precipitates were performed directly from TEM negatives. A semiautomatic eyecom II image analyzing system was used to measure the particle sizes. The average particle size was measured for each aging time. Particle size distributions of over 500 particles were constructed for each aging time. Two particle diameters were measured for each particle in order to determine the aspect ratio of each

particle, and thus quantitatively describe the spherical morphology of the particle size distributions.

6. THEORETICAL CONSIDERATIONS

6.1 DETERMINING THE MEAN EQUIVALENT EXTRUSION TEMPERATURE

The relative motion between the billet and the container wall which cause heat to be generated during direct extrusion, also causes some plastic deformation. Thus the exit temperature of the extruded product will often be greater than the initial temperature of billet prior to extrusion. The rise in temperature causes the variations in the temperature of material perpendicular to and transverse to the ram travel. Transverse variations in temperature produce variations in structure, and hence in properties, across to extruded geometry. Therefore, in order to accurately represent the extrusion temperature for the given extrusion process, an average equivalent extrusion temperature, developed by Farag and Sellers [1], is often used to show this relationship and is expressed as

$$T_{eq} = (2 T_o T_f)/(T_o + T_f) \quad (1)$$

Where T_o is the initial billet temperature, T_f is the exit extrusion temperature or the final billet temperature, and T_{eq} is the average equivalent extrusion temperature. Thus the general rise in temperature during extrusion can cause variations in the internal structure and properties of the extruded product. Thus, based on the exit extrusion temperatures and the initial billet temperatures, the equivalent extrusion temperatures were calculated and are summarized in Table 1. Based on the equivalent extrusion temperatures, the Zener-Hollomon parameters were determined and used to establish the relations between extrusion processing and microstructure and mechanical properties.

6.2 DETERMINING THE MEAN EQUIVALENT STRAIN RATE

There are several factors that can influence the strain rate of a material during extrusion such as lubrication and temperature. Both the strain and strain rate during extrusion are not constant nor independent of position [2,3]. Investigators making use of partially extruded billets clearly show that the microstructure is inhomogeneous with a heterogeneous strain distribution across the cross section. Due to the heterogeneous strain distribution it is necessary to calculate a mean or average equivalent strain rate in order to relate the processing variables to the microstructure and bulk properties of the extruded product. The most common approach used to calculate this value was developed by Feltham [4], who suggested a time-averaged method based on the relationship given by

$$\varepsilon = \text{total strain/time to produce the strain} = E/t \quad (2)$$

with the total strain E given by

$$E = \ln (\chi R_e) \quad (3)$$

Where R_e is the extrusion ratio, and χ is the shape factor for noncircular extruded product. The time required to yield the total strain is expressed as

$$t = D / \{6 V \tan \alpha\} \quad (4)$$

where V is the ram speed, α is the semiconical die angle, and D is the billet diameter. Combining equations (2) through (4) gives the approximate expression for the mean equivalent strain [5]

$$\varepsilon = \{6 V \tan \alpha\} \{\ln (\chi R_e)\} / D \quad (5)$$

where ε is the average equivalent strain rate. A semi-conical die angle α based on the extrusion geometry of the round rods was chosen for this study. Since not all the geometries produced in this study were circular, the notion of a semi-conical angle α is not valid and can only be considered as an approximation for the non-axisymmetric extrusions. Table 1. summarizes the calculated values for the average equivalent extrusion rate for the values of the extrusion parameters corresponding to the Al-2.6wt.%Li-0.09wt.%Zr alloy.

6.3 DETERMINING THE ZENER HOLLOMON PARAMETER (Z)

The flow stress during plastic deformation depends on the applied processing variables. These variables include the strain rate or rate of deformation and the temperature of plastic deformation, and can be related to material constants by the Zener-Hollomon parameter. Mathematically the Zener-Hollomon parameter or temperature compensated strain rate can be expressed by the expression given by [1,8]

$$Z = \varepsilon \exp \{ Q_{\text{flow}} / RT \} = A [\sinh(\beta \sigma)]^n \quad (6)$$

where ε is the mean equivalent strain rate, Q_{flow} is the activation energy for deformation or plastic flow, R is the universal gas constant, T is the extrusion temperature, σ is the flow stress, and A , β , and n are empirical constants. The calculated Zener-Hollomon parameters are summarized in Table 1 for the extrusion processing of the Al-2.6wt.%Li-0.09wt.%Zr alloy.

6.4 DETERMINING THE ACTIVATION ENERGY FOR PLASTIC FLOW

The activation energy for plastic flow, Q_{flow} , is the activation energy necessary for plastic deformation and is dependent on the particular metal or alloy. The activation energy for plastic flow or deformation is approximately equal to the activation energy for self diffusion in high stacking fault alloys [6]. The activation energy is to a small extent a function of the alloy composition. However, Castle and Sheppard [2] determined that Q_{flow}

ranged from 156 to 164 KJ/mole for a large range of compositions of aluminum alloys, and concluded that it does not appear necessary to obtain a highly accurate value of the activation energy for the study of high temperature deformation. For commercially pure aluminum, Farag and Sellars [1] derived an activation energy value of 150 KJ/mole. Other investigators [7,8] determined a value for the activation energy to be approximately equal to 155 KJ/mole. For the Al-2.6wt.%Li-0.09wt.%Zr alloy used in this investigation, an average value of the activation energy of 160 KJ/mole was used throughout this study for the calculations of the temperature compensated strain rate.

6.5 CORRELATION OF Z WITH MICROSTRUCTURE

The Zener-Hollomon parameter can be related to the subgrain size of the high temperature deformed aluminum alloy. By relating the Zener-Hollomon parameter to the development of the subgrain structure a correlation can be made to the material processing parameters such as the billet temperature, extrusion ratio, ram speed, and exit extrusion temperature. The smaller the subgrain size in the as-extruded condition, the smaller will be the Z value. The subgrain size of hot worked aluminum is found to be uniquely related to Z by equations of the form [9,10,11]

$$d_{sg}^{-1} = a_{sg} + b_{sg} \ln Z$$

where d_{sg} is the average subgrain size, Z is the Zener-Hollomon parameter, and a_{sg} and b_{sg} are empirical constants. Using linear regression techniques and the examination of subgrain sizes along with the calculated values of Z, the constants a_{sg} and b_{sg} can be determined. Thus, for the Al-2.6wt.%Li-0.09wt.% demonstration alloy in the as-extruded condition $a_{sg} = -1.178$, and $b_{sg} = 0.055$. For the Al-2.6wt.%Li-0.09wt.% demonstration alloy in the solution heat treated condition $a_{sg} = -0.533$, and $b_{sg} = 0.029$. Thus, increases in the subgrain size with solution heat treating as compared with the as-extruded resulted in higher Z values and less stable substructure. The equilibrium δ phase can in part play a role in the change in subgrain size for high Z, low temperature, extrusions. Both the presence of this equilibrium phase and the Al_3Zr phase control the development of the substructure and during solution heat treating they dissolve which permits subgrain boundary migration to occur.

7. SUMMARY AND CONCLUSIONS

The Zener-Hollomon parameters for the Al-2.6wt.%Li-0.09wt.% demonstration alloy were determined from the extrusion processing variables and correlated to the average subgrain sizes. The average equivalent temperatures were determined for the various extrusions and used for the calculations of the Zener-Hollomon parameters. The values of the activation energy for deformation and the equivalent extrusion temperatures were determined and used for the estimations of Z. The subgrain sizes were in general found to increase with the solution heating. For any given extrusion temperature there was an inverse relationship between the subgrain size and the $\ln(Z)$. Smaller grain sizes were correlated to smaller

Zener-Hollomon parameters. The extrusion temperature and ratio did not significantly effect the mechanical strength or ductility measured as percent elongation. The section geometry of the extruded product, either round or rectangular, did effect these particular mechanical properties.

8. ACKNOWLEDGEMENTS

This work was supported by the National Science Foundation under Grant CDR 8803017. The aluminum-lithium alloy used for this study was provided by the Aluminum Company of America (ALCOA) and cast by the ALCOA Technical Center in Pittsburgh Pennsylvania, USA. The Al-Li alloy was extrusion processed by the ALCOA Lafayette Extrusion and Tube Division in Lafayette, Indiana, USA. The composition analysis for the Al-Li alloy was also performed by the ALCOA Extrusion Facility, Lafayette, Indiana, US.

9. REFERENCES

- [1.] M.M. Farag and C.M. Sellars, "Flow Stress in Hot Extrusion of Commercial Purity Aluminum, *Journal of the Institute of Metals*, Vol. 101, pp. 137-145, 1973.
- [2.] A.F. Castle and T. Sheppard, "Pressure Required to Initiate Extrusion in Some Aluminum Alloys", *Metals Technology*, pp. 465-475, Oct. 1976.
- [3.] D. Raybould and T. Sheppard, "Axisymmetric Extrusion: The Effect of Temperature Rise and Strain Rate on the Activation Enthalpy and Material Constants of Some Aluminum Alloys and Their Relation to Recrystallization, Substructure, and Subsequent Mechanical Properties"" *Journal of the Institute of Metals*, Vol. 101, pp. 65-72, 1973.
- [4.] P. Feltham, "Extrusion of Metals: A Simple Theory of Criteria of Press Design and Extrusion Efficiency in the Industrial Extrusion of Metals", *Metal Treatment and Drop Forging*, Vol. 23, pp. 440-444, 1956.
- [5.] G.E. Dieter, "Extrusion", *Mechanical Metallurgy*, McGraw-Hill, Inc., Third Edition, pp. 616-635, 1986.
- [6.] T. Sheppard, "Temperature and Speed Effects in Hot Extrusion of Aluminum Alloys", *Metals Technology*, pp. 130-141, April 1981.
- [7.] C.M. Sellars, "Hot Working Operations", *Aluminum Transformation Technology and Applications*, American Society for Metals, pp. 405-440, 1978.
- [8.] H.J. McQueen and J.J. Jones, "Recent Advances in Hot Working Fundamental Dynamic Softening Mechanisms", *Journal of Applied Metal Working*, Vol. 3, No. 3, pp. 233-241, 1984.
- [9.] C.M. Sellars, *Aluminum Transformation Technology and Applications*, pp. 405-440, 1978.
- [10.] H.J. McQueen and J.J. Jones, *Treatise on Material Science and Technology*, Academic Press, New York, Vol. 6, p. 404, 1975
- [11.] H.J. McQueen and J.J. Jones, *Plastic Deformation of Materials*, edited by R.J. Arsenault, ed., Academic press, New York.

Table 1: Calculated Parameter for the Extrusion of the Al-2.6wt.%Li-0.09wt.% alloy.

Extrusion Geometry	Equivalent Extrusion Temperature (°C)	Total Strain (cm/cm)	Equivalent Strain rate (cm-per-cm/min)	Zener Hollomon Z (10^{11} s^{-1})
2.54X8.9	308	2.2	26.2	1058.7
5.3 dia.	303	2.2	30.3	1663.4
0.635X8.9	324	3.6	40.0	661.6
2.69 dia.	332	3.6	46.8	517.9
0.318X8.9	319	4.3	39.4	874.8
1.91 dia.	339	4.3	47.8	367.0
2.54X8.9	469	2.2	26.2	0.82
5.3 dia.	468	2.2	30.3	0.97
0.635X8.9	456	3.6	40.0	1.97
2.69 dia.	421	3.6	46.8	8.73
0.318X8.9	433	4.3	39.4	4.58
1.91 dia.	451	4.3	47.8	2.82

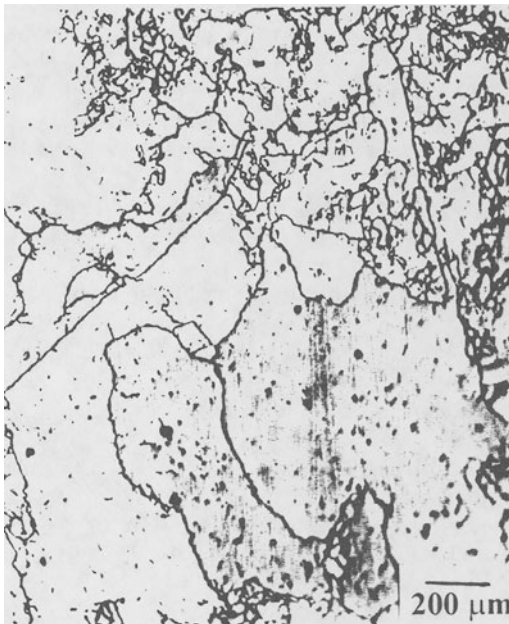


Figure 1: Polarized Light optical micrograph showing the transverse grain structure for the peak-aged condition of the Al-2.6wt.%Li-0.09wt.%Zr alloy extruded at 451 °C with a 73:1 extrusion ratio.

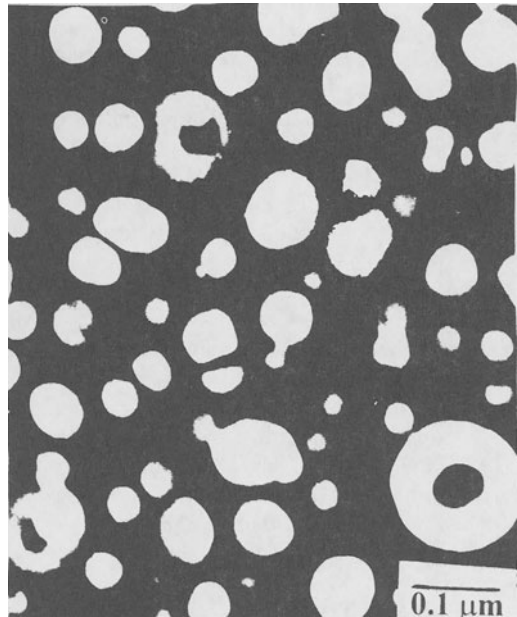


Figure 2: Dark field TEM electron micrograph showing the microstructure of the Al-2.6wt.%Li-0.09wt.%Zr alloy in the peak-aged condition extruded at 451 °C with a 73.0:1 extrusion ratio.

COMPARISON OF MEASURED AND COMPUTED CONTACT PRESSURE DISTRIBUTION IN COLD SHEET ROLLING PROCESS

J. Brnic, M. Canadija and G. Turkalj
University of Rijeka, Rijeka, Croatia

KEY WORDS: Sheet Rolling Process, Finite Element Modelling, Computer

ABSTRACT: Cold rolling process belongs to the oldest deformation processes in metal-working industry. Opposite to the massive forming processes, this paper deals with the numerical modelling and computer simulation of the sheet – metal forming process. According to the used boundary conditions, this forming process can be treated as a cold rolling process with plane-strain conditions. This workpiece is a part of sheet, e.g., it is narrow thin plate. The numerical procedure is based on the finite element technique. Large strain elastoplastic updated Lagrangian Hencky formulation is used. Computer program using numerical algorithm is made and tested comparing by the well-known results as well as by numerical investigations

1. INTRODUCTION

In present time the applications of computer-aided techniques (engineering, design, manufacturing) for process design and process simulation in metal-forming industry increased considerably. Namely, in metal-forming technology the determination of deformations as well as the knowledge about the change of material properties, workpiece geometry, etc., according to the manufacturing process optimization are required. With the mentioned knowledge it would not be possible to design the dies and the equipment adequately as well as it would not be possible to predict the product life or to prevent the occurrence of defects [1]. The approximate methods of many metal-forming processes

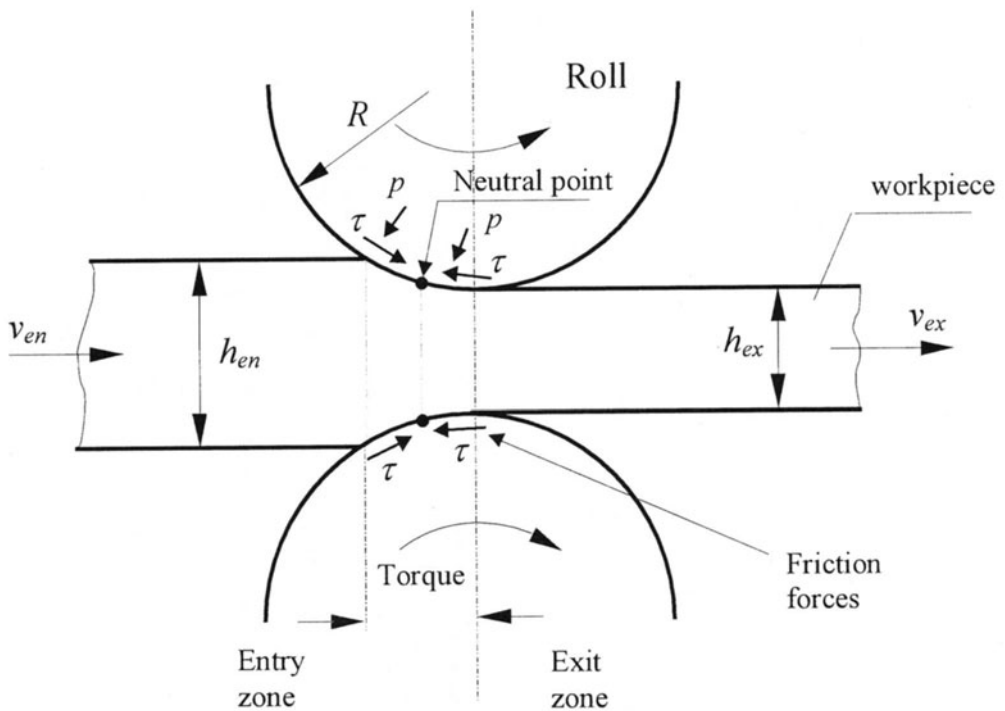
Published in: E. Kuljanic (Ed.) *Advanced Manufacturing Systems and Technology*,
CISM Courses and Lectures No. 406, Springer Verlag, Wien New York, 1999.

have been developed, but more recently method today is finite element method (FEM). Also, in present time very useful technique is finite volume method (FVM).

Metal - forming processes, such as rolling processes, forging process, etc., are using increasingly sophisticated mathematical modelling techniques [2]. One between these techniques is mentioned finite elements technique. The problem considered in this paper is cold sheet-rolling-flattening process which can be numerical modelled as a plane-strain problem. The starting material is a flat-rolled product. There are no limitations width-to-thickness ratios. Sheet metal-forming process can be treated as a process of choice for relatively thin products. Cold rolling process is a producing process for all of metal products to very tight tolerances and controlled surface finish [3].

2. FINITE ELEMENT FORMULATION, IMPLEMENTATION AND ANALYSIS OF COLD ROLLING-FLATTENING PROCESS

The problem under consideration in a basic concept in Fig. 1. is presented.



(a)

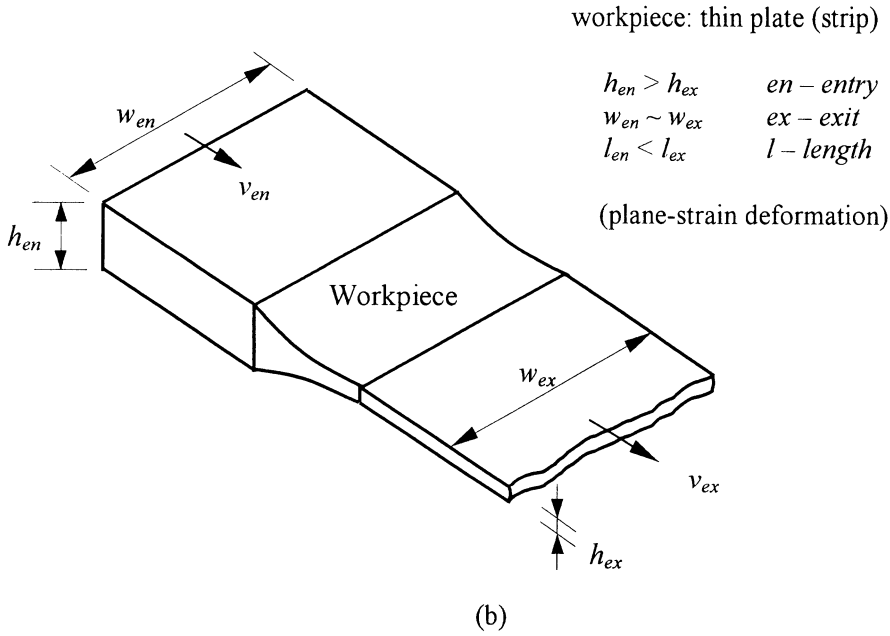


Figure 1. Basic concept of cold rolling process of thin plate (strip): a) workpiece between rolls, b) workpiece (strip)

Cold rolling process can be made at room temperature, so, the temperature effects can be neglected. This process will be considered as an isothermal process.

Starting from updated Lagrangian formulation (UL) [4, 5, 6]:

$$\int_{V'} {}^{t+\Delta t} S_{ij} \delta {}^{t+\Delta t} \epsilon_{ij} dV = {}^{t+\Delta t} \mathfrak{R} \tag{1}$$

where all variables are referred to the last calculated configuration, after some mathematical operations, the following linearized equilibrium equation can be written:

$$\int_{V'} {}^t C_{ijrs} e_{rs} \delta {}^t e_{ij} dV + \int_{V'} {}^t \tau_{ij} \delta {}^t \eta_{ij} dV = {}^{t+\Delta t} \mathfrak{R} - \int_{V'} {}^t \tau_{ij} \delta {}^t e_{ij} dV \tag{2}$$

There are:

Stresses:

$${}^{t+\Delta t} S_{ij} = {}^t \tau_{ij} + {}^t S_{ij} \quad ; \quad {}^t S_{ij} = {}^t \tau_{ij} \tag{3}$$

Strains:

$${}^{t+\Delta t} \epsilon_y = {}^t \epsilon_y \quad ; \quad {}^t \epsilon_y = {}^t e_y + {}^t \eta_y \tag{4}$$

$${}^t e_y = \frac{1}{2} ({}^t u_{i,j} + {}^t u_{j,i}) \quad ; \quad {}^t \eta_y = \frac{1}{2} {}^t u_{k,i} {}^t u_{k,j} \tag{5}$$

and:

$${}^t S_{ij} = {}^t C_{ijrs} {}^t e_{rs} \quad ; \quad \delta {}^t \epsilon_y = \delta {}^t e_y \tag{6}$$

Equation (2) in incremental displacements based updated Lagrangian formulation, in matrix form can be given as follows:

$$\left(\int_V {}^t \mathbf{B}_L^T {}^t \mathbf{C} {}^t \mathbf{B}_L d^t V + \int_V {}^t \mathbf{B}_{NL}^T {}^t \boldsymbol{\tau} {}^t \mathbf{B}_{NL} d^t V \right) \hat{\mathbf{u}} = \int_{S_f} {}^t \mathbf{H}^S {}^{t+\Delta t} \mathbf{f}^S d^{t+\Delta t} V + \int_V {}^t \mathbf{H}^T {}^{t+\Delta t} \mathbf{f}^B d^{t+\Delta t} V - \int_V {}^t \mathbf{B}_L^T {}^t \hat{\boldsymbol{\tau}} d^t V, \tag{7}$$

or:

$$\left({}^t \mathbf{K}_L + {}^t \mathbf{K}_{NL} \right) \mathbf{U} = {}^{t+\Delta t} \mathbf{R} - {}^t \mathbf{F}, \tag{8}$$

where:

- ${}^t \mathbf{K}_L, {}^t \mathbf{K}_{NL}$ - linear and nonlinear strain incremental stiffness matrix
- ${}^{t+\Delta t} \mathbf{R}$ - vector of externally applied nodal point loads at $t+\Delta t$
- \mathbf{U} - vector of increments in the nodal points displacements
- ${}^t \mathbf{F}$ - vector of nodal point forces (equival. to the element stresses)
- \mathbf{H}^S, \mathbf{H} - surface-and volume-displacement interpolation matrices
- ${}^{t+\Delta t} \mathbf{f}^S, {}^{t+\Delta t} \mathbf{f}^B$ - vectors of surface and body forces
- ${}^t \mathbf{B}_L, {}^t \mathbf{B}_{NL}$ - linear and nonlin. strain-displacement transformation matrices
- ${}^t \mathbf{C}$ - incremental stress-strain material property matrices
- ${}^t \boldsymbol{\tau}, {}^t \hat{\boldsymbol{\tau}}$ -matrix and vector of Cauchy stresses.

Friction between roll and workpiece is modelled with friction layer technique [7]. This technique is based on experimental observations which have shown that shear stresses at the contact of die-workpiece is essentially equal to material yield shear stress multiplied by material-dependent constant m . In order to simulate mentioned behaviour, fictitious layer of finite elements is placed at the die-workpiece interface. Stiffness matrix of each fictitious finite element is multiplied with the stiffness matrix multiplier β :

$$\beta = m/(1 - m) \quad (9)$$

Well-known incompressible behaviour of metals during plastic deformation cannot be modelled with satisfactory accuracy with displacement based FEM. So, in this model mixed finite element formulation is used, with both displacement and pressure as variables [8]. Spherical part of stress tensor is calculated from pressure which is an independent variable, preserving in that way volume constancy. If 9/3 isoparametric planar finite elements are considered, no locking behaviour occurs.

3. EXAMPLE

Program Rolling was developed and used for the simulation of cold rolling of aluminium workpiece. Used geometrical and material properties are presented in Tab. 1.

Table 1. Geometrical and material properties

Property	Symbol	Value
Initial height	h_{en}	6.274 mm
Output height	h_{ex}	5.385 mm
Roll radius	R	79.775 mm
Initial workpiece length	ℓ_0	16 mm
Elasticity modulus	E	70 GPa
Friction factor	m	0.25
Yield stress	σ_{y0}	50.3 MPa
Poisson's ratio	ν	0.30

Stress – strain behaviour in elastoplastic range is described with equation:

$$\sigma = 50.3 \left(1 + \frac{1}{0.05} \varepsilon_p \right)^{0.26} \quad (10)$$

Finite element mesh consisted of 126 finite elements with 555 nodes. Gauss integration rule was used, with 5x5 gauss points per element. Initial FE mesh is presented in Fig. 2.

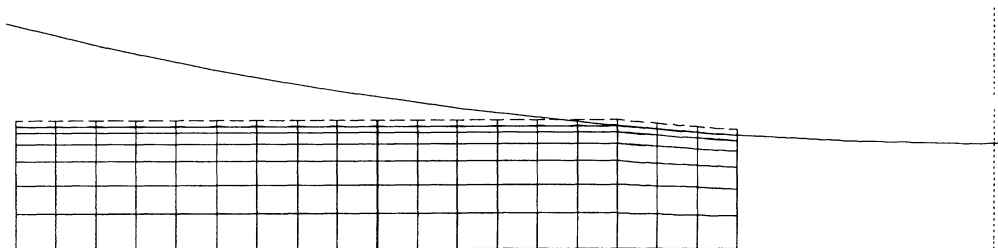


Figure 2. Initial finite element mesh

The obtained pressure distribution is presented in Fig. 3. If these results are compared to the known experimental values [9], one can conclude that results are in good agreement with measured values. If greater values for friction factor are used [10], calculated pressure also obtains greater values and discrepancy between two curves is smaller. Furthermore, analytical method fails to give characteristic two-hill type of curve. Clearly, with wide range of details which can be obtained, numerical methods like FEM have superior performance over the analytical methods.

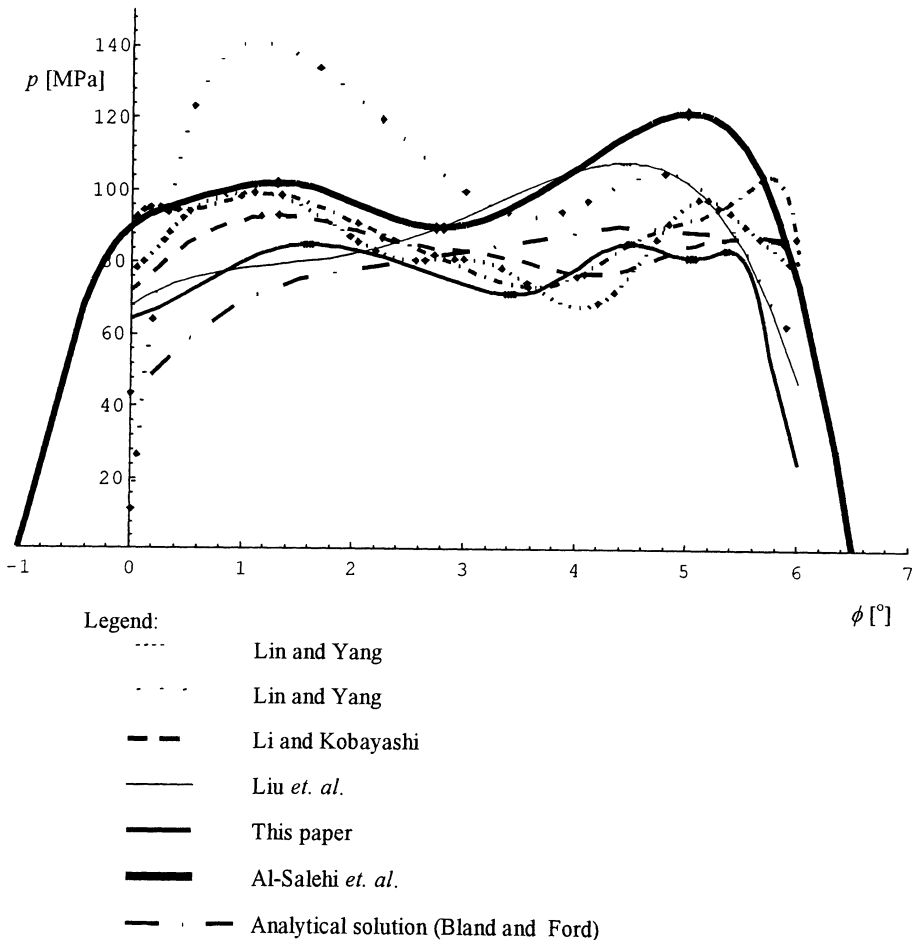


Figure 3. Pressure distribution

When velocities are considered, one can say that velocities at the exit from roll gap are greater than velocity of roll at contact. Contrary, at the entrance to the roll gap, velocities are smaller than roll velocity. This gives rise to the existence of the so-called neutral point, in which roll and workpiece velocities are equal. This phenomenon is clearly visible at Fig.

4. where velocity fields relative to the neutral point velocity in different stages of rolling process obtained by the program Rolling are presented.

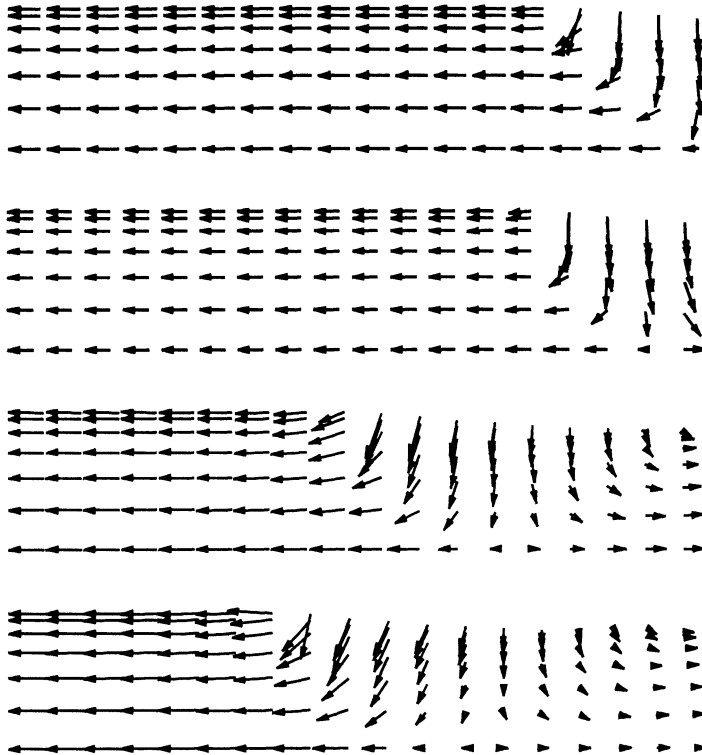


Figure 4. Relative velocity fields in workpiece during rolling

4. CONCLUSIONS

Using large strain elastoplastic updated Lagrangian Hencky formulation the Rolling program is made. The results obtained by mentioned program are compared by well known numerically and experimentally obtained results and their agreement are very good. Further improvements can be achieved by introducing temperature effects to simulate hot rolling and with considering fracture theory for prediction of material damage.

REFERENCES:

1. Kobayashi, S., Oh, S.I., Altan, T.: Metal Forming and the Finite-Element Method, Oxford University Press, New York, 1989.
2. Simo, J.C., Hughes, T.J.R.: Computational Inelasticity, Springer – Verlag, New York, 1998.

3. Schey, J.A.: Manufacturing Processes and Their Selection, In: ASM Handbook – Materials Selection and Design, Vol. 20, ASM International, USA, 1997.
4. Brnić, J., Čanadija, M.: Nonlinear Modelling of a Special Forming Process, Proceedings of the 9th DAAAM Symposium, Vienna – Cluj – Napoca, Oct. 22-24, 1998, 75-76.
5. Brnić, J.: Elastoplasticity and Elastoviscoplasticity, PAMM Centre, Budapest, 1988.
6. Bathe, K.J.: Finite Element Procedure, Prentice Hall, New Jersey, 1996.
7. Hartley, P., Sturgess, C.E.N., Rowe, G.W., Friction in Finite-Element Analysis of Metalforming processes, International Journal for Mechanical Sciences, 21 (1985), 301-311
8. Sussman, T., Bathe, K.J.: A Finite Element Formulation for Nonlinear Incompressible Elastic and Inelastic Analysis, Computers & Structures, 26 (1987), 357-409
9. Al-Salehi, F.A.R., Firbank, T.C., Lancaster, P.R.: An Experimental Determination of the Roll Pressure Distributions in Cold Rolling, International Journal for Mechanical Sciences, 15 (1973), 693-710.
10. Liu, C., Hartley, P., Sturgess, C.E.N., Rowe, G.W.: Elastic-Plastic Finite-Element Modelling of Cold Rolling of Strip, International Journal for Mechanical Sciences, 27 (1985), 531-541

OPTIMAL DIE DESIGN FOR COLD EXTRUSION PROCESSES

R. Di Lorenzo

University of Palermo, Palermo, Italy

F. Micari

University of Calabria, Arcavacata di Rende (CS), Italy

KEY WORDS: Process Design, Cold extrusion, Optimization

ABSTRACT: The design of cold extrusion processes requires the optimisation of several process variables in order to obtain a defect free product. The fulfilment of different objectives, such as the minimisation of forming loads or the homogeneity of the deformations, is highly requested. Nevertheless, several other relevant aspects of extrusion processes have to be taken into account and require a suitable optimisation of the process parameters and in particular of the die shape. In this paper, tool life has been assumed as the most relevant goal and an effective die design procedure as been setup. It is well known that fatigue cracking of the dies is the principal cause of dies failure in cold extrusion and that fatigue cracking is related to the stress/strain distribution in the zone of highest loading; thus the proposed approach is aimed to the research, through statistical techniques, of the function linking the die profile and the radial stress distribution in the die itself. By this way the most suitable die shape has been designed able to ensure the minimisation of the stress peak and an almost uniform pressure distribution at the specimen-die interface.

1. INTRODUCTION

Cold extrusion represents one of the most important and diffused net-shape processes, the purpose of which is to produce a finished component with an high dimensional accuracy.

Published in: E. Kuljanic (Ed.) *Advanced Manufacturing Systems and Technology*,
CISM Courses and Lectures No. 406, Springer Verlag, Wien New York, 1999.

Since the process is characterized by extremely high pressures at the tool-workpiece interfaces and the material has undergone to large strains, an effective process design is absolutely necessary: in particular the process designer has to select the most suitable combination of press, tools material, geometry and structure, lubrication and material properties in order to make the operation successful.

As far as the tools are concerned, in cold extrusion fatigue cracking of the die is the most important cause of failure [1,2]. Generally tool life is much more constrained by fatigue cracking than by wear. On the other hand it is quite obvious that a significant economical effect could be achieved through an increase in the service time of tool elements: it has been calculated, in fact, that tooling costs represent a percentage ranging between 5 and 30% of the total manufacturing costs [3,4]. Actually the greatest problem in the preliminary estimation of tool life is the large dispersion of tool life itself, even for the same tool geometry, material and construction.

The above consideration justify the large research effort aimed to the definition of effective methods for the prediction of the tool life: Lange et al. [5] proposed a Fatigue Analysis Concept to estimate tool life during the process and tooling design phase; Hansel et al. [6] utilized numerical FE simulations to follow the growth of a fatigue crack in cold extrusion dies; Engel [7,8] proposed a statistical approach, hypothesizing effective distributions with reference both to the forging load and to the die strength.

It is worth pointing out that in cold extrusion die life is fundamentally affected by the pressure distribution along the die shoulder: in the most common case of conical dies, crack initiation is generally located in the transition radius at the shoulder entrance, where the pressure peak occurs. Kocanda [9] provided strain-life data for the AISI M2 high speed steel at room and elevated temperatures: he pointed out that the number of cycles (i.e. the number of forged parts) to crack initiation is strongly linked to the total radial strain amplitude in the die and consequently to the pressure peak at the transition radius. Osakada [10] showed an interesting relation between forming pressure and tool life: tool steels for cold forming can sustain about 3000 Mpa in a compression test without being plastically deformed, but the tool life is very short when a pressure of such a level is applied repeatedly.

Actually the pressure distribution along the die shoulder is strongly affected by the die geometry. In the recent years several researchers have proposed different approaches aimed to optimize the die shape taking into account different objectives: Kusiak and Thompson [11] investigated three different optimization techniques, namely one direct-search and two gradient methods, to determine the optimal die shape design able to minimize the total ram force; Joun and Hwang [12] assumed as objective the homogeneity of the strain distribution in the extruded component and applied their approach to the pass schedule design in multi-pass extrusion too; finally Chung and Hwang [13] utilized an integrated approach between genetic algorithms and finite element simulations to determine the optimal die shape, both taking into account the minimization of the punch load and the minimization of the effective strain variations.

Very recently the authors have proposed a new approach to the optimal design of cold forming processes based on the integration of numerical simulations and statistical tools:

the basic idea is to determine the analytical linkage between the process target and the set of the process parameters. Such approach has been successfully applied to the preform design in a couple of closed die forging processes [14], since it has allowed to determine the optimal preform shape able to ensure a complete filling of the finishing die cavity.

In this paper the authors apply a similar approach to cold extrusion: according to the above considerations the achievement of a suitable “smooth” pressure distribution along the die shoulder, avoiding any pressure peak, has been considered as the most important objective and the optimal die shape able to fulfill this requirement has been determined.

2. THE INVESTIGATED EXTRUSION PROCESS

An axisymmetric extrusion process with a reduction in area equal to 75% has been investigated assuming as workpiece material an aluminum alloy, namely the AA5052 alloy forged at room temperature, whose flow stress law is reported in (1):

$$\sigma = 210 \varepsilon^{0.13} \text{ [Mpa]} \quad (1)$$

A typical cold extrusion die material has been utilized in the numerical simulations of the process, namely AISI D2 steel (1.5C, 12Cr, 1Mo). Furthermore, the utilization of a proper lubricant at the die-workpiece interface has been assumed with a constant friction coefficient equal to 0.2.

In order to find out the optimal profile a class of shapes including flat, conical, parabolic and sigmoidal dies has been taken into account. It is worth pointing out that for each shape the shoulder length has to be selected too. Actually, the latter topic is not new: already Avitzur [15] for the simple conical die, investigated the optimal value of the cone angle (α) and proposed a solution based on the Upper Bound method. The optimal α value is the one able to minimize the total forming energy i.e. the one which lets the best compromise between the energy dissipated by friction (which decreases at increasing α) and the redundant work (which increases at increasing α).

For these reasons, in the research three different lengths of the die deformation zone have been considered and for each one the conical profile together with some parabolic and sigmoidal shapes have been examined; in particular the three lengths are the ones that in the case of a conical profile correspond to values of the cone angle equal to 30°, 45° and 60° respectively.

A polynomial form has been selected to describe the die profile, able to comprehend the conical shape as well as the parabolic and the sigmoidal ones. This function can be expressed as follows:

$$F(z) = r_0 + \frac{(r_1 - r_0)}{(z_1 - z_0)}(z - z_0) + (z - z_1)(z - z_0)[P_n(z)] \quad (2)$$

where $(z_0; r_0)$ and $(z_1; r_1)$ are the coordinates of the points of the profile corresponding to the die entry and exit respectively, while $P_n(z)$ indicates an n degree polynomial.

The above reported function guarantees that the entry and exit points of the die belong to the chosen profile. Furthermore, it is worth noticing that in order to represent the above mentioned die shapes a degree of P_n equal to 1 is enough.

By this way in fact, the degree of $F(z)$ is equal to 3, thus a sigmoidal form is fully described and by assigning proper values to the coefficients of P_n even the parabolic (degree equal to 2) and the conical (degree equal to 1) profile are included.

As a consequence, the function $F(z)$ can be expressed as follows:

$$F(z) = r_0 + \frac{(r_1 - r_0)}{(z_1 - z_0)}(z - z_0) + (z - z_1)(z - z_0)(mz + p) \tag{3}$$

Among the die shapes belonging to the sigmoidal “family” (i.e. degree of $F(z)$ equal to 3) a particular attention has been focused on the so called “double tangent” profile, that is a profile which is tangent to the cylindrical part of the die both at the entry and at the exit section. The qualitative shape of the “double tangent” sigmoidal profile is reported in Fig. 1(a), while the parabolic profile and the conical one are reported in Fig. 1(b) and Fig. 1(c) respectively, for a length of the die shoulder corresponding to a cone angle of 45° .

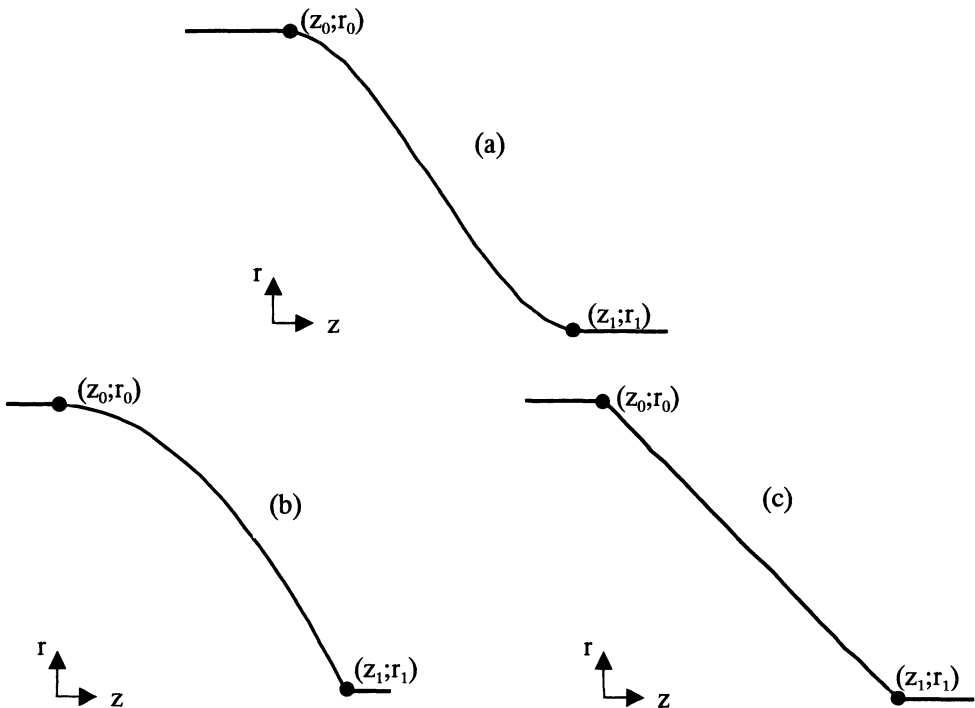


Fig. 1: (a) the “double tangent” die profile, (b) the parabolic die profile, (c) the conical die profile

3. THE DESIGN PROCEDURE

As above reported the aim of this paper is to find out a die profile which leads to a minimization of the pressure peak at the die-workpiece interface and consequently to a relevant reduction of the stresses in the die; thus it has been necessary to find out the analytical function able to express the linkage between the design variables of the optimization problem (i.e. the coefficients m and p) and the variable representing the output of the model for different lengths of the die shoulder (i.e. the difference between the z coordinates of the exit and the entry sections, z_1-z_0). As far as the output variable is concerned, the maximum radial stress in the die has been utilized according to the above considerations.

In this way, several numerical investigations have been carried out, testing different forms of the die profile at varying the coefficients of P_n and finding out the corresponding values of the maximum radial stress.

It has to be underlined that the profiles which assume values out of the range $[r_1, r_0]$, have been excluded from the test class in order to avoid physically meaningless shapes.

Thus, for each investigated value of the die shoulder length, a set of data has been obtained relating the design variables m and p to $\sigma_{r(max)}$ in the die. The obtained data sets have been structured as follows:

m	p	$\sigma_{r(max)}$
m_1	p_1	$\sigma_{r(max)1}$
m_2	p_2	$\sigma_{r(max)2}$
m_n	p_n	$\sigma_{r(max)n}$

Tab. 1 The knowledge base structure

A regression model has been applied on the data belonging to the knowledge base, for each value of the die shoulder length, to determine the desired function. In particular a regular behavior of the above mentioned function has been hypothesized and a quadratic expression has been assumed, which can be represented as follows:

$$\sigma_{r(max)} = b_0 + b_1p + b_2m + b_{11}p^2 + b_{22}m^2 + b_{12}pm \quad (4)$$

where p and m are the input parameters in this application and $\sigma_{r(max)}$ represents the output variable.

The definition of this response function is fully obtained by the determination of its coefficients, namely the zero order coefficient b_0 , the first order coefficients (b_1 ; b_2), the second order pure ones (b_{11} ; b_{22}) and the second order mixed one (b_{12}) [16,17].

Once the response function has been obtained a local minimum has been determined whose coordinates are the optimal value of m and p .

4. RESULTS

The die profiles obtained with the proposed procedure have been tested in order to verify the validity of the results. In particular three different optimum points have been found out for each one of the analyzed die shoulder length.

It is worth observing that the parabolic profile resulted the favorite one in each case: the lower pressure peaks have been obtained in fact, by utilizing those values of the parameters m and p corresponding to a degree of $F(z)$ equal to 2.

This general conclusion is confirmed by some results shown in the next figures 2, 3 and 4.

All the reported results are referred to the die shoulder length corresponding, in the case of the conical die, to a cone angle $\alpha = 45^\circ$.

In particular, in Fig. 2 the distribution of σ_r on the die with the simplest conical profile is reported: the value of $\sigma_{r(max)}$ in this case is equal to 396 [N/mm²].

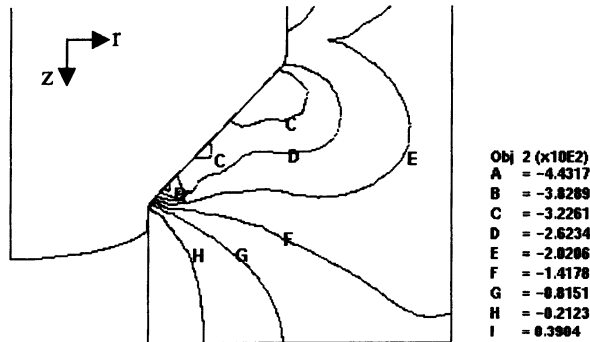


Fig. 2 The radial stress distribution for a conical die profile

The "double tangent" profile for the same length of the die shoulder presents a slight worsening in terms of the maximum value of the radial stress with respect to the conical shape, with a peak equal to 413 [N/mm²] (see Fig. 3).

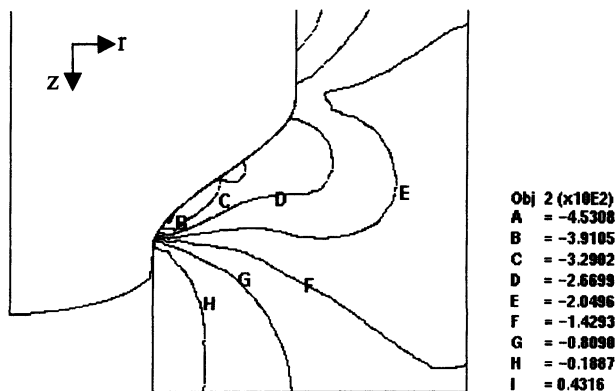


Fig. 3 The radial stress distribution for a "double tangent" die profile

The application of the statistical techniques on the available knowledge base has permitted to individuate the optimal die design in a parabolic profile. A numerical simulation of the process has been carried out by utilizing such profile and it has led to the radial stress distribution shown in Fig. 4: the maximum value of the radial stress detected on the die shoulder is equal to 332 [N/mm²] proving the validity of the optimization procedure.

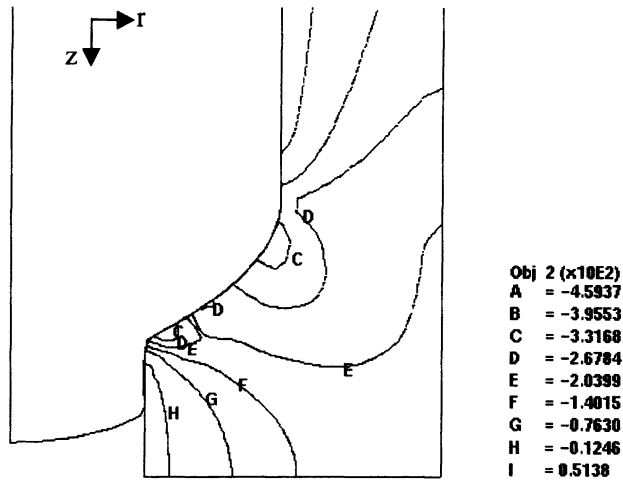


Fig. 4 The radial stress distribution for a parabolic die profile

The same kind of optimal die profile, namely a parabolic one, has been obtained by carrying out the optimization procedure at the varying of the die shoulder length, confirming the robustness of the acquired solution.

It is worth pointing out that the achieved result is in very good agreement with the one reported by Kusiak et al. in [11]; these authors in fact, developed an optimization procedure aimed to the minimization of the total ram force and found that the optimal die profile had a "trumpet shape" for frictionless extrusion while it became a parabolic one as the friction increases; the latter condition being very similar to the one considered in this paper.

5. CONCLUSIONS

In the paper a statistical based optimization procedure for the die shape design in cold extrusion has been presented. The objective pursued in the proposed research is related to die life improvement since the design procedure has been aimed to find out the die profile which leads to a reduction in the pressure peaks along the die shoulder which is directly connected to fatigue cracking occurrence.

The proposed optimization procedure has been developed on the basis of a knowledge base built up by numerically investigating different die profile behaviors. Moreover the obtained

results have been numerically tested in order to prove the effectiveness of the proposed approach.

ACKNOWLEDGEMENTS

This work has been performed with funding from MURST (Italian Ministry for University and Scientific Research).

REFERENCES

- [1] K. Lange, L. Cser, M. Geiger, J.A.G. Kals,: Tool life and tool quality in bulk metal forming, Keynote paper STC Forming 42nd General Assembly of CIRP, 1992
- [2] T. Altan: Design and manufacture of dies and molds, *Annals of CIRP*, 38 (1991) 2
- [3] Small quantity production in cold forging ICFG Document n° 7, 1988
- [4] P.F. Bariani, G. Berti, L. D'Angelo: Tool cost estimating at early stages of cold forging process design, *Annals of CIRP*, 42 (1993) 1, 279-282.
- [5] K. Lange, M. Knoerr, T. Altan: A fatigue analysis concept to avoid failure of forging tooling, *Proc. of the 27th Plenary meeting of the ICFG*, 1994, 1-10
- [6] U. Engel, M. Hansel: FEM Simulation of fatigue crack growth in cold forging dies, *Proc. of the 3rd ICTP*, Kyoto, 1990
- [7] U.Engel: Tool life and tool reliability in bulk metal forming, *Proc. of the Int. Conference and Exhibition on Design and Production of dies and molds*, 1997, 321-327
- [8] U. Engel: Prediction of tool failure from a probabilistic point of view, *J. of Material Processing Technology*, 42 (1994) 1, 1-13
- [9] A. Kocanda: Die steel for warm forging – An evaluation of resistance to cyclic loading, *Advanced Technology of Plasticity*, 1, (1990), 349-354.
- [10] K. Osakada: Outline of precision forging, *Proc. of the JSTP Int. Seminar on Precision Forging*, 1997, 1-10
- [11] J. Kusiak, E. G. Thompson: Optimization techniques for extrusion die shape design, *Proc. of Numiform '89*, 1989, 569-574
- [12] M. S. Joun, S. M. Hwang: Application of finite element method to process optimal design in metal extrusion, *Proc. of Numiform '92*, 1992, 619-624
- [13] J. S. Chung, S. M. Hwang: Application of a genetic algorithm to the optimal design of the die shape in extrusion, *J. of Material Processing Technology*, 72, (1997), 69-77
- [14] R. Di Lorenzo, F. Micari: An inverse approach for the design of the optimal preform shape in cold forging, *Annals of CIRP*, 47 (1998) 1, 189-192.
- [15] B. Avitzur: *Metal forming: processes and analysis*, McGraw-Hill Book Company, 1968
- [16] G.E.P. Box, W.G. Hunter, J.S. Hunter: *Statistics for experimenters*, John Wiley & Sons 1978
- [17] G.E.P. Box, N.R. Draper: *Empirical model building and response surfaces*, John Wiley & Sons, 1987

EFFECTIVENESS OF NUMERICAL SIMULATION IN AVOIDING DEFECTS IN HOT EXTRUSION FORGING PRODUCTS

D. Antonelli

Polytechnic of Turin, Turin, Italy

A. Barcellona

University of Palermo, Palermo, Italy

KEY WORDS: Hot forging, Numerical simulation

ABSTRACT: The hot extrusion forging, in the production of an half shaft of a motorcycle engine, has been analysed by means of finite element simulations. The severe mesh distortion occurring in the simulation has been overcome with the aid of a code provided with automatic remeshing techniques. The study is aimed to promote the use of FEM not only in the designing phase but also as a tool able to investigate defects occurring at the production level.

1. INTRODUCTION

Hot Extrusion forging is a well known and assessed production technique employed in manufacturing a large medley of mechanical parts, like gears, engine shafts and bolts.

A significant benefit of this process can be attributed to the easiness of manufacturing two different parts: the extruded shaft and the forged head. In this way, welding operations are not required. It leads to considerable cost saving, because of the reduction in die and operation number and of a significant improvement of mechanical properties.

Unfortunately there are some drawbacks connected to the conflicting technological requirements in two different processes. As a matter of fact, fillet radii should be chosen differently in extrusion than in forging, the lubricant should be different and even preferred material flow directions should be otherwise oriented. Therefore, technological variables have to be selected as a compromise between opposite demands.

Numerical analysis, namely the Finite Element technique, is usually employed in order to improve the choice of process parameters. The simulation of the process is especially effective when employed just in the first stage of the process design, to assist the die dimensioning. It allows for the comparison and evaluation of a wide number of different productive options on a base of knowledge obtained by simulation. Thus it makes possible to study the influence of changes in the operative parameters on the productive goals, avoiding the necessity of expensive prototypes.

Numerical analysis of an hot forging process must cope with some peculiar difficulties such as non accurate operative parameter assessment, partially unknown material characteristics and eventually the great deformation of material fibers leading to severe mesh distortion.

As a matter of fact, to produce an effective numerical simulation, process data should be known with a good accuracy and kept under strict control. This is hardly to be seen in a common industrial environment, where seldom the characterisation of material and process data exceeds the specification by the customer demand. Besides, tolerances on a hot worked part are low enough to justify a simplified in-process control.

This work aims to prove that, even when some important material and processing data are incomplete or lacking, it is possible to realise a simulation able to reproduce the principal process features with a level of accuracy compatible with engineering design requests. Moreover, simulation can be employed not only during process optimisation, but also in order to identify productive defect causes and test possible solutions.

2. THE INDUSTRIAL PROCESS

The selected case study is the half shaft of a two-stroke motorcycle engine. The employed material is a 39NiCrMo3 steel. The components is represented in fig.1 after the first forging step. This shaft is heavily stressed during its operating life by composite torsion and bending loads.

The most stressed points lay on the fillet between the crank and the shaft. This fact has been a strong incentive to the choice of an extrusion forging process. The productive cycle is made up of the processes described in fig.2.

This work stresses on the blocking stage in the extrusion forging process, because it is the activity in which the greatest number of defect may arise. The employed machine is a vertical mechanical press with a nominal working force of 6500kN and a stroke of 200mm.

Forging temperature is assessed with a poor accuracy, due to unpredictable elapsed time between the workpiece extraction from the induction oven and its positioning under the die. Moreover die temperature is uniformly distributed only in the initial phase, after the pre-heating.



Fig.1 – The forged part after the blocking stage

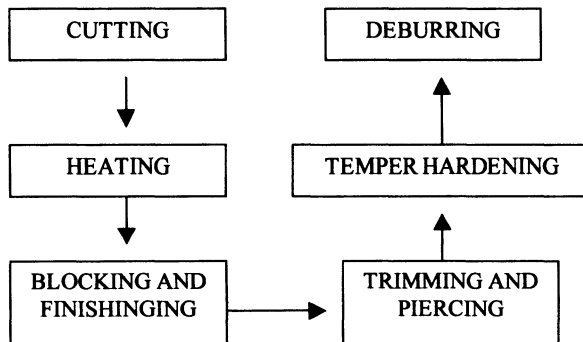


Fig.2 – Flow chart of the production process

During forging the heat flow from the workpiece to the die induces a non uniform temperature distribution. This fact, together with the lubrication type, has a deep influence on the insurgence of many production defects. Average temperature of the workpiece is 1150°C. Die temperature is taken nearly to 300°C before the starting of the production. After 50 strokes it can be assumed that die temperature reaches a steady state with increased temperature inside narrow cavities and decreased near the external border. Not only the temperature, but also the constitutive law of the material and the friction conditions at the boundary interface are of uncertain definition. This is due not only to the

effective difficulty in experimental measurements but also to the great variation of values inside the production environment.

The employed lubricant is a graphite-based oil mixed with water, Lubrodal type F24W. The fluid acts both as a coolant and as a lubricant and is applied by mist lubrication. Oil is sprayed on the die by means of a spray gun fed by a pneumatic pump.

3. EXPERIMENTAL ANALYSIS

The studied process is subjected to a number of production problems, related to the heavy extrusion ratio combined with the length of the extruded shaft, both imposed by design constraints [1].

The most serious defects due to the forging process are the folding originated close to the fillet radius. This defect is a starting point for the propagation of cracks. Often folding dimensions are small and hardly visible by bare eyes, so that a control by magneflux is made necessary on every piece. An typical cause for this defect is the wrong positioning of the workpiece on the die.

Another defect is the underfilling of the stem, due to lack of material, or to a wrong positioning of the workpiece on the die. Yet another defect is the overheating of the stem because of excessive temperature or too long permanence time in the oven. During the forging they produce surface tearing. All of these defects are originated with an apparent accidental sequence and cannot be predicted or avoided. Control charts showed that the most of the rejected pieces belong to the starting phase of work. Moreover, the folding develops independently from the shape of flash, that should have revealed a positioning error. Therefore the attention has been transferred to the temperature distribution and to the lubrication, both variables assuming values substantially different at the start-up.

A number of tests has been executed on both damaged and undamaged parts. The most significant have been the forging force measurement, the fiber flow, HRB hardness, final geometry measurements [2].

The forging force has been measured on the press during the blocking stage. The force has been induced by the deformation of press columns detected by strain gauges mounted on them. Because of uncertainties, measures have been repeated several times. The average maximum force is 4000 kN.

It is possible to see the fiber folding on themselves due to a flaw near the fillet between shaft and the head. The test has been executed by plunging the workpiece for 10 minutes in a boiling solution of 50% chloridric acid.

The fiber flow is represented in fig.3a for an undamaged part. It is evident the lack of uniformity in the fiber flow along the stem, due to the asymmetry in the head. In fig.3b it is highlighted the above mentioned folding defect, that is the most frequent cause of reject. Rockwell B hardness tests have been performed on the half section of a forged piece before any thermal treatment to detect possible heat-hardening due to non-uniform cooling. Hardness has a uniformly distributed value, leading to give up the hypothesis that folding defects were induced by non uniform temperature distribution.

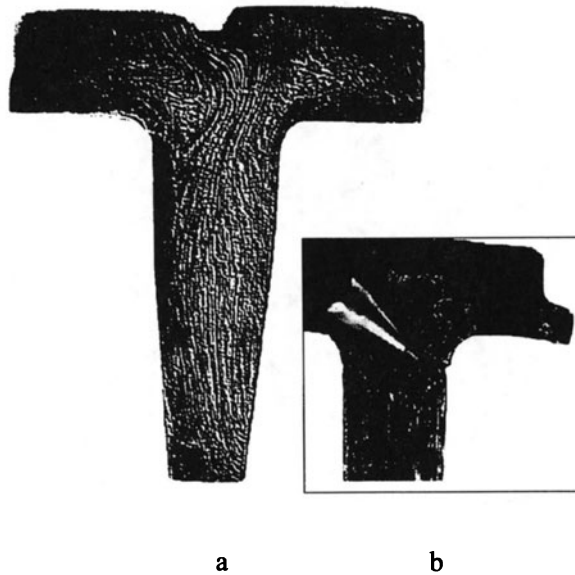


Fig. 3 – a) Fiber flow for the undamaged part after blocking . b) Highlight of the folding defect in the final part

4. THE NUMERICAL SIMULATION

By means of the finite element DEFORM code [3], the axisymmetric hot extrusion forging process has been simulated.

An initial number of 630 axisymmetric isoparametric quadrilateral elements interconnected in 688 nodal points was used to model the workpiece. Dies were also meshed with rigid elements in order to perform a thermal mechanical analysis of the workpiece and a thermal analysis of the dies. The model is shown in fig. 4. An average number of 12 remeshings was required by the simulation due to the presence of a very narrow flash. The actual velocity has been assigned to the upper die; the plastic flow properties of the material, as a function of strain, strain rate and temperature, have been employed.

Frictional effects at the interface workpiece-dies have been taken into account by means of the constant shear friction model:

$$\tau = m \frac{\sigma_{eq}}{\sqrt{3}}$$

where τ is the frictional shear stress, m is the friction shear factor and σ_{eq} the equivalent flow stress. The value of m has been chosen equal to 0.3 [4]; this value was obtained by means of comparison between experimental and numerical profile.

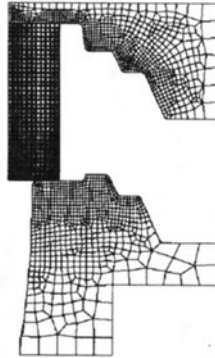


Fig. 4 – The numerical model

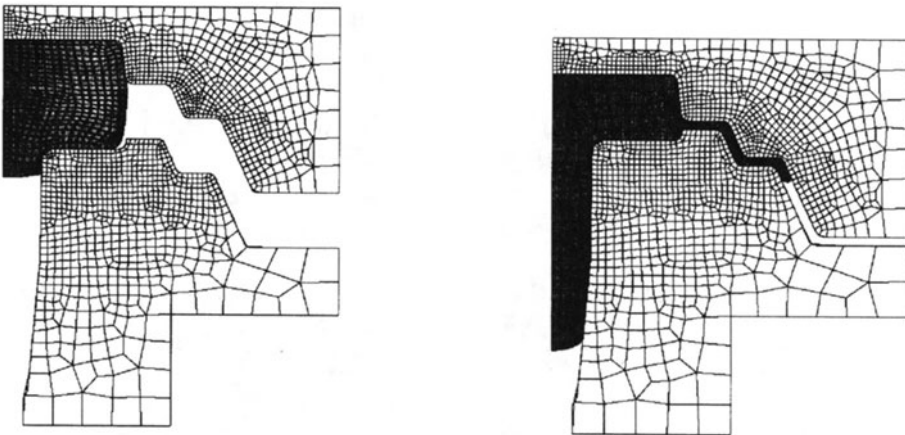


Fig. 5 – The deformed mesh for a punch stroke of 17 mm and the final configuration

In order to correctly follow the geometrical profile of the dies, containing small fillet radii, a very high value of the penalty function has been chosen for contact management. The simulations have been carried out on a IBM Risc 6000 workstation, with a mean CPU time of 600 seconds for each run. The numerical simulation supplied the results reported in fig. 5 in which it is possible to see the deformation pattern for a punch stroke of 17 mm and at the end of the operation. Fig. 6 shows a comparison between numerical and experimental forging loads with respect to the forging stroke. An excellent overlapping with the experimental results has been obtained both with respect to the final geometry and to the predicted loads, despite the approximations in input data.

Once the validity of the numerical model has been assessed, the model itself has been employed as a powerful CAE tool to assist the analyst in the process design.

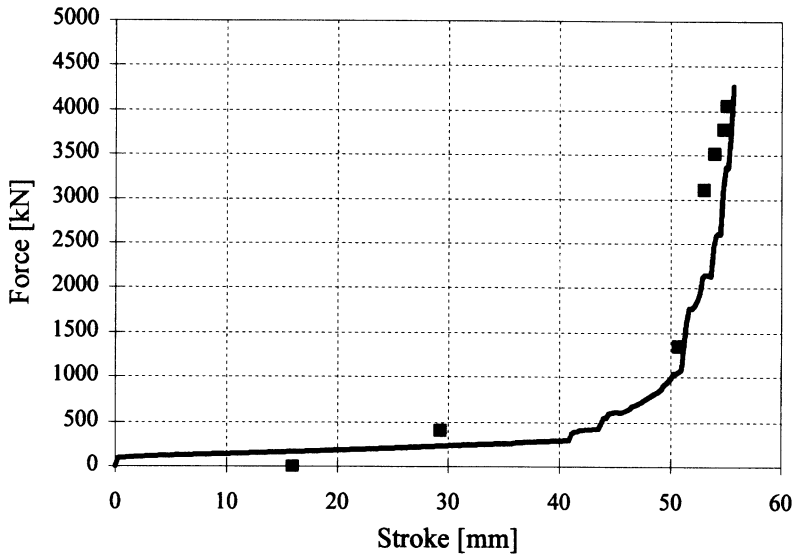


Fig. 6 – Experimental (dotted) and numerical (continuous line) loads

In particular, the numerical analysis has been carried out in order to analyse defect occurrence in terms of flow distortion and localised pressure peaks.

Therefore, a sensitivity analysis has been performed, by varying the parameters whose control can be still improved. Among these, the most significant are the lubricant conditions and the average die temperature. Since, in the actual industrial process, the lubricant is sprayed on the die surface from a lateral side, its distribution is not uniform and it is possible to assume that only a small fraction of lubricant fits the stem cavity of the die. It has been assumed that this could concur to the occurrence of the above mentioned folding defect. In order to study this effect by means of numerical analysis, friction factor has been assumed a different value both in the stem or in the head. With respect to the condition of uniform lubrication, the results showed a quite different flow pattern, as can be seen in fig. 7. In the figures the detailed zone of the fillet corner is shown; it is clearly visible that the neutral fiber is more far from the stem in this latter case. This position of the neutral fiber induces more bent flow lines nearest the fillet corner, thus leading to the folding.

With regards to the contact pressure on the dies, that is responsible for die wear, a sensible increasing has been observed. Namely, the peak pressure on the corner varies from 580MPa in the uniformly lubricated case to a maximum of 830MPa when only the head is well lubricated.

Variations in the working temperature of the dies, bring to worst values of all the considered parameters. The fiber flow is less regular while the peak pressure reduces

slightly for large increasing of die temperature (100 MPa reduction when dies reach the temperature of 700°C as experimentally observed).

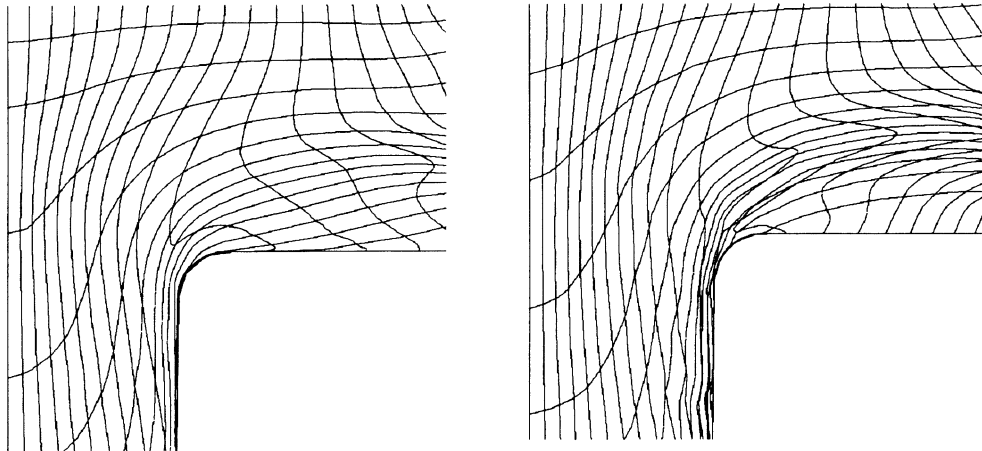


Fig. 7 – The fiber flow pattern for the uniform and non uniform lubrication case

CONCLUSIONS

A sensitivity analysis of an extrusion forging process has been realised by means of FE simulations. The goal was the determination of defect causes, avoiding expensive trial and error experimental methods. The simulation has been made more compelling by the necessity of reproducing the actual industrial process, characterised by a limited possibility of determining and controlling the operative parameters. Nevertheless, the simulation showed a fairly good correspondence to the reality. Moreover, the sensitivity analysis was able to give precious indications for the assessment of the process parameters.

REFERENCES

1. Basuc D., Ghiban N., Antonelli D., Romano D.; 1996, An Analysis of Billet Dimensions Influence on a Combined Upsetting and Extrusion Process, Junior-Euromat '96, Lausanne (Switzerland).
2. Sasia A.; 1996, Studio di un processo di extrusion forging: integrazione tra prove sperimentali ed analisi numerica, M. Sc. Thesis, unpublished, Politecnico di Torino.
3. Oh, S.I., Wu, W.T., Tang, J.P. and Vedhanayagam, A.; 1991, Capabilities and Applications of FEM code DEFORM: the Perspective of the Developer, J. Of Mat, Processing Technology, vol. 27, pp. 25-42.
4. Barcellona, A., Cannizzaro, L., Forcellese, A., Gabrielli, F.; 1996, Validation of frictional studies by double-cup extrusion test in cold-forming, Annals of the CIRP, Vol. 45/1/96, pp. 211-214.

VALIDATION OF PREDICTIVE APPROACHES FOR DUCTILE FRACTURE IN COLD EXTRUSION

C. Borsellino and V.F. Ruisi
University of Palermo, Palermo, Italy

KEYWORDS: Extrusion, Ductile fracture, Central bursting.

ABSTRACT: Cold extrusion is sometimes accompanied by some typical internal defects, known in the technical literature as “central bursts”, which dramatically could affect the component behaviour during its service life. Several researchers, following both analytical and numerical approaches have attempted central bursting prediction in extrusion. Among the latter several approaches have been proposed in the literature, namely the ones based on the use of ductile fracture criteria and the ones founded on the damage mechanics analysis. Each one of these approaches presents some advantages and drawbacks. In the paper the authors analyze a set of cold extrusion processes on AISI 1040 specimens at varying the most relevant process parameters. The occurrence of central bursting has been predicted utilizing all the classes of approach previously mentioned and the goodness of the predictions has been validated through a set of experimental tests. On the basis of this validation the usefulness and the industrial suitability of each approach is discussed.

1. INTRODUCTION

The prediction of ductile fractures insurgence during metal forming processes has constituted one of the matters of greatest interest for the researchers during the last decade. Such interest is justified fully by the economic consequences connected to the formation of ductile fractures, particularly when these last are not visible with a simple external examination of the forged component and they are been revealed in exercise subsequently. Such characteristics are for instance present in the case of the typical defect of central bursting during cold extrusion processes [1,2]: such defects in fact occur inside the component, and only in few cases they arrive until on the surface.

Several approaches have been proposed in the recent years to predict ductile fractures. Actually it is possible to consider these approaches as belonging to two main groups [3]: the former is based on the use of ductile fracture criteria, which utilize the calculated strain and stress fields in order to evaluate a properly defined damage factor to be compared with

the critical value [4-8]; the latter, in turn, try to achieve a better insight of the mechanisms of damage insurgence and to take into account the influence of damage on the plastic behaviour of the material [9-12].

It is worth pointing out that the use of ductile fracture criteria represents a relatively simple approach: these criteria, in fact, generally have a simple incremental form and sometimes are available in the commercial finite element codes. On the other hand the models based on the analysis of damage mechanics surely allow a better comprehension of the damage phenomenon; nevertheless they are much more complicated from the mathematical point of view, require properly defined yield conditions and associated flow rules for damaging materials and finally the definition of a set of material parameters.

In a recent paper the authors had presented the results obtained carrying out a wide experimental analysis of cold extrusion processes on AISI 1040 specimens [13]. The tests were performed at varying the most relevant process parameters (i.e. the reduction in area and the semicone die angle) and had allowed to determine for which combinations of the process parameters the insurgence of central bursting was more frequent.

In this paper the authors verify the effectiveness of both the above mentioned approaches: in particular, as far as the methods based on ductile fracture criteria are concerned, two of the most important and widely utilized criteria have been taken into account, namely the Cockroft and Latham [4] and the Oyane [5] criterion. On the other hand, the damage mechanics formulation has been founded on the Tvergaard and Needleman [12] yield criterion for damaging materials and on the model proposed by Chu and Needleman [14] for the nucleation of microvoids. All the material data involved in the formulation have been determined through an inverse approach.

The predictive capability of both the approaches has been verified all over the available experimental data: the obtained results are presented and discussed in detail.

2. EXPERIMENTAL TESTS

The investigated process parameters are all the combinations obtained for reductions in area $RA = 15, 20, 25, 36, 42\%$ and semicone die angle $\alpha = 15, 20, 25^\circ$, while the mechanical and chemical properties of the utilized material are summarized in table 1.

Chemical composition: C 0,4%; Si 0,32%; Mn 0,71%; P 0,023%;	
Hardness:	HBN _(2,5/100/30) = 260 Kg/mm ² ;
Tensile strength:	955 N/mm ²

Table 1. Mechanical and chemical properties of AISI 1040.

In particular the AISI 1040 specimens had an initial diameter of 25 mm; on each of them four consecutive reductions, were carried out with the same geometrical parameters of the die. The extrusion operations were conducted on a Universal Testing Machine by MetroCom Engineering Spa, properly equipped. Before each test the specimens were lubricated by applying a film of Molybdenum Disulphide on the surface. For each sequence 10 tests have been performed. The presence of the Central Bursting defect has been discovered by the steep decay of the extrusion load, which occurs each time that a "burst" appears inside the material.

Table 2 reports the most important results of the experimental tests: in particular, for each combination of the geometrical parameters, the eventual occurrence of Central Bursting is pointed out, together with the step at which the defect has been discovered.

RA% \ α°	15°	20°	25°
15%	No defects	No defects	C. B. 3 rd step:
20%	No defects	C. B. 3 rd step	C. B. 2 nd step
25%	No defects	C. B. 4 th step	C. B. 3 rd step
36%	No defects	No defects	No defects
42%	No defects	No defects	No defects

Table 2. The experimental results.

Some typical Central bursting defects are shown figure 1.



Figure 1. Central bursting

3. THE DUCTILE FRACTURE CRITERIA -THEORETICAL REMARKS

3.1 The Cockcroft and Latham criterion

The Normalized Cockcroft e Latham criterion assumes that fracture arises when the tensile plastic strain energy reaches a critical value:

$$\int_0^{\bar{\epsilon}^F} \frac{\sigma}{\bar{\sigma}} \bar{\sigma} d\bar{\epsilon} \leq C_3 \quad (1)$$

where $(\sigma^*/\bar{\sigma})$ is the maximum normalized tensile stress defined as the ratio between the maximum tensile stress, σ^* , and the equivalent one, and C_3 is the critical value. The latter is determined by upsetting a cylindrical specimen under sticking conditions at the punch-specimen interface until the first cracking appears on the external surface. By simulating the same operation and stopping the process at the same value of height reduction experimentally determined, the critical value is the maximum damage value reached on the external surface of the specimen [15].

3.2 The Oyane criterion.

This criterion was derived by Oyane from the plasticity theory for porous materials and is based on the assumption that fracture incomes when the volumetric strain, ϵ_v , reaches a critical value depending on the characteristics of the material and on the strain path. [8]:

$$\int_0^{\epsilon_v^F} f_v^2 \rho^{2p-1} d\epsilon_v = \int_{\bar{\epsilon}^i}^{\bar{\epsilon}^F} \left(A + \frac{\sigma_m}{\bar{\sigma}} \right) d\bar{\epsilon} \quad (2)$$

where ρ is the relative density of the material, f_v is a function of the relative density and p is a constant, the integration limits are respectively: ε_v^F , volumetric strain, $\bar{\varepsilon}^F$ equivalent strain at fracture, $\bar{\varepsilon}^i$ equivalent strain at the voids arising.

Oyane supposed that after the beginning of the fracture the material still follows the plasticity law for porous material and that, for given material, the quantity at first member is constant at fracture; Osakada et al. shown that the strain at which the voids arise depends on the pressure, firstly Shima e Oyane assumed that this value of strain is constant at atmospherical pressure and $\bar{\varepsilon}^i = 0$ consequently the criterion assumes the form:

$$\int_0^{\bar{\varepsilon}^F} \left(A + \frac{\sigma_m}{\bar{\sigma}} \right) d\bar{\varepsilon} = B \quad (3)$$

where A and B are constant at fracture characteristics of the material.

It is worth pointing out that in the latter criterion the influence of the hydrostatic stress on the occurrence of ductile fracture is pointed out with larger evidence than in the Cockcroft and Latham one.

The previous expression can be written as: $\varepsilon_{eq}^F = \frac{B}{A} - \frac{1}{A} \int_0^{\varepsilon_{eq}^F} \left(\frac{\sigma_m}{\sigma_{eq}} \right) d\varepsilon_{eq}$ (4)

that in the plane $\left(\int_0^{\varepsilon_{eq}^F} \left(\frac{\sigma_m}{\sigma_{eq}} \right) d\varepsilon_{eq}, \varepsilon_{eq}^F \right)$ describes a linear function where B/A is the

intersection with the y-axis and $-(1/A)$ is the angular coefficient.

Thus, the values of the constants can be determined by means of a set of upsetting processes on cylindrical specimens with different height/diameter ratios. The equivalent strains reached at the moment in which the first fracture arises on the external surface allow, in fact, to construct the function (4) and then to determine the values A and B

3.3 The Tvergaard and Needleman model

The former approach to develop an yield function for a solid with a randomly distributed volume fraction of voids, "f", was proposed by Gurson [10]:

$$\Phi = \frac{\sigma_{eq}^2}{\bar{\sigma}^2} + 2f \cosh\left(\frac{\sigma_{kk}}{2\bar{\sigma}}\right) - (1 + f^2) = 0 \quad (5)$$

where σ_{eq} is the macroscopic equivalent stress, σ_{ij}' is the macroscopic stress deviator, and $\bar{\sigma}$ is the yield stress of the matrix (void-free) material. The Gurson equation (5) clearly shows the effect of the mean stress on the plastic flow when the void volume fraction is non-zero, while for $f=0$ the Gurson criterion reduces to the von Mises one.

The components of the macroscopic plastic strain rate vector can be calculated applying the normality rule to the yield criterion above written: in fact as shown by Bishop and Hill the validity of the normality rule for the matrix material implies the validity of a

macroscopic normality rule. Following these considerations the components of the macroscopic plastic strain rate vector can be expressed as: $\dot{\epsilon}_{ij} = \dot{\lambda} \frac{\partial \Phi(\sigma_{ij})}{\partial \sigma_{ij}}$ (6)

where the parameter $\dot{\lambda}$ can be calculated if monoaxial stress conditions are assumed. Tvergaard [11] and Tvergaard and Needleman [12] introduced other parameters, q_1 and f^* , obtaining the following expression:

$$\Phi = \frac{\sigma_{eq}^2}{\bar{\sigma}^2} + 2f^* q_1 \cosh\left(\frac{\sigma_{kk}}{2\bar{\sigma}}\right) - \left[1 + (q_1 f^*)^2\right] = 0 \quad (7)$$

The first parameter, q_1 , permits to take into account the interactions between neighbouring voids: Tvergaard in fact obtained the above criterion analysing the macroscopic behaviour of a doubly periodic array of voids using a model which takes into account the nonuniform stress field around each void. Tvergaard assumed the value of q_1 equal to 1.5. The second parameter $f^*(f)$ was introduced in substitution of f in order to describe in a more accurate way the rapid decrease of stress-carrying capability of the material associated to the coalescence of voids: in fact $f^*(f)$ is defined as:

$$f^*(f) = f \quad \text{for } f \leq f_C \quad \text{and} \quad f^*(f) = f_C + \frac{f_u^* - f_C}{f_F - f_C} \cdot (f - f_C) \quad \text{for } f > f_C \quad (8)$$

where $f_u^* = 1/q_1$, f_C is a critical value of the void volume fraction at which the material stress-carrying capability starts to decay very quickly and finally f_F is the void volume fraction value corresponding to the complete loss of stress-carrying capability. Again the constitutive equations associated to the Tvergaard and Needleman yield criterion can be determined by means of the normality rule.

The Tvergaard and Needleman damage model has been implemented in a finite element code based on an Updated Lagrangian formulation; an incremental procedure has been employed in order to follow the transient process from the workpiece input phase to the achievement of steady state conditions. In fact to evaluate the possibility of a ductile fracture insurgence, it has been necessary to follow the whole deformation path for each point of the material.

Depending on the stress conditions, both the existing voids can grow and new voids can nucleate. Then, at the end of each step of the deformation process the values of the void volume fractions calculated at the integration points within each element must be updated.

The increasing rate of the void volume fraction can be considered partly due to the growth of the existing voids and partly to the nucleation of new voids: $\dot{f} = \dot{f}_{growth} + \dot{f}_{nucleation}$ (9)

As far as the first aspect is concerned the rate of changing of the void volume fraction is related to the volumetric strain rate $\dot{\epsilon}_V$ by the relation: $\dot{f}_{growth} = (1 - f)\dot{\epsilon}_V$ (10)

On the other hand, several models have been proposed in order to evaluate the nucleation of new voids; in these models the void nucleation rate is assumed as depending on the matrix equivalent plastic strain rate and on the rate of increase of the hydrostatic stress, following the expression: $\dot{f}_{nucleation} = A\dot{\epsilon}_{eq} + B(\dot{\bar{\sigma}} + \dot{\sigma}_m)$ (11)

where A and B are material dependent constants. In particular Chu and Needleman suggested to calculate A and B assuming that the void nucleation follows a normal distribution and have distinguished two different cases: the case of plastic strain controlled nucleation (B=0) and the case of stress controlled nucleation (A=0). In the first case the proposed expressions for A [14], Chu and Needleman have introduced the parameter f_n , which is the volume fraction of voids potentially able to nucleate if sufficiently high strains are reached; the void nucleation follows a normal distribution about a mean equivalent plastic strain ϵ_{mean} with a standard deviation s ; in the form reported below:

$$\dot{f}_{nucleation} = \frac{f_n}{s\sqrt{2\pi}} \exp\left[-\frac{1}{2}\left(\frac{\epsilon_{eq} - \epsilon_{mean}}{s}\right)^2\right] \dot{\epsilon}_{eq} \quad (12)$$

The application of the damage mechanics model requires the determination of the parameters involved in the yield condition and in the nucleation model. Such task has been carried out applying an inverse identification algorithm with reference to the load vs displacement curve in the tensile test [16]. This algorithm is an optimization procedure, which determines the set of parameters, that allows the best matching between the numerical and the experimental results, and consequently supplies a suitable material characterisation

3. THE NUMERICAL SIMULATIONS

All the simulations were carried out utilizing the following flow stress law for the material:

$$\bar{\sigma} = 985 \cdot \bar{\epsilon}^{0.12} \text{ [MPa]}$$

The simulations were performed at varying the above mentioned combinations of the geometrical parameters as reported [17, 18]. A constant friction law has been assumed and the shear factor was determined by means of the double cup extrusion tests which supplied $m=0,2$.

As far as the material constants required in the fracture criteria are concerned, they have been determined on the basis of the upsetting tests, according to the considerations reported above. The material constants required by the damage mechanics approach were determined, on the contrary, applying an inverse approach on the results of the tensile test. All these data are reported in the next table.

Tvergaard and Needleman damage model	$f_n = 0,025$; $f_c = 0,03$; $\epsilon_{mean}=0,15$, $s= 0,05$
Cockroft and Latham criterion	$C_3= 0.47$.
Oyane criterion	$A=-1.96$ and $B=0.68$.

Table 3. The constants characterizing the damage model and the fracture criteria.

Figures 2a, b, c, report the trends of the maximum values of the three damage variables, (i.e. the two fracture criterion and the damage model) for a semicone die angle $\alpha=25^\circ$ and for all the reductions in area to predict if and when the fracture should occur. In particular Figures 2a, b, and c show the trends obtained utilizing the damage variable, “d”, calculated utilizing the Cockroft and Latham criterion; the one, “b”, calculated utilizing the Oyane criterion and finally the void volume fraction, “f”, from the Tvergaard and Needleman model respectively.

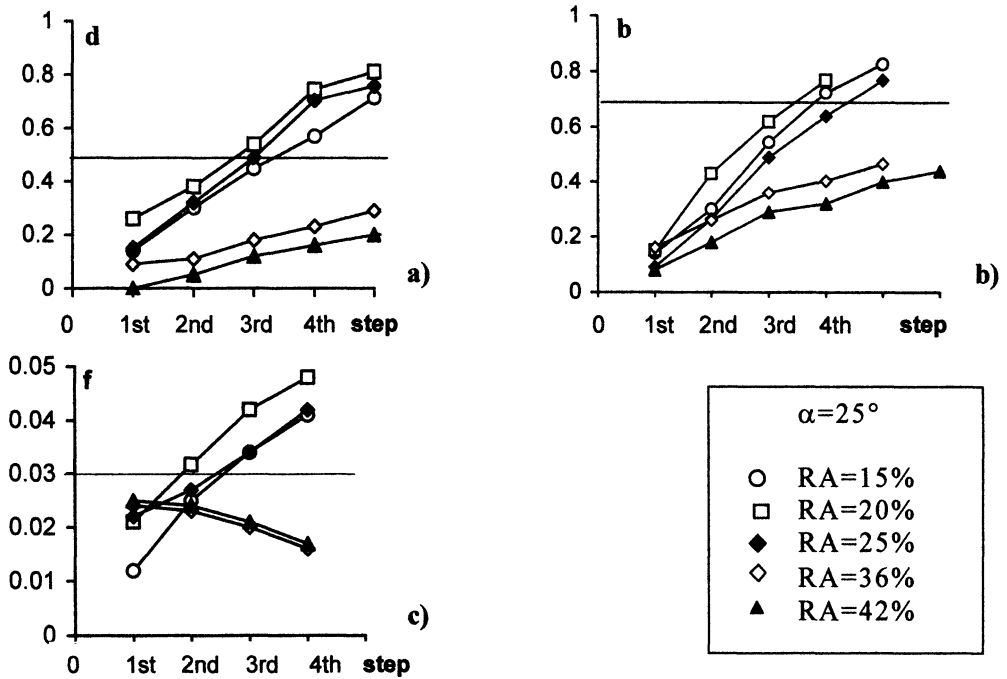


Fig. 2a, b, c. Maximum value of the damage variable at the end of each extrusion step.

3. DISCUSSION OF THE RESULTS

In the following tables all the numerical results are summarized: the extrusion step at which the insurgence of central bursting is predicted (i.e. the value of the damage variable overcomes the critical one, depending on the particular criterion adopted) is pointed out. The evaluation of the ductile insurgence is reported in table 3, respectively employing the Cockroft and Latham criterion, the Oyane criterion and, finally, the Tvergaard and Needleman damage model.

		RA=15%	RA=20%	RA=25%	RA=36%	RA=42%
Cockroft-Latham Criterion	$\alpha=15^\circ$			4		
	$\alpha=20^\circ$		3	3		
	$\alpha=25^\circ$	3	2	3	5	
Oyane Criterion	$\alpha=15^\circ$			4		
	$\alpha=20^\circ$		5	4		
	$\alpha=25^\circ$	5	4	4		
Tvergaard and Needleman Model	$\alpha=15^\circ$					
	$\alpha=20^\circ$	5	3	3		
	$\alpha=25^\circ$	3	2	3		

Table 3. Numerical results.

Actually the latter model has shown to be the most suitable instrument to describe the process mechanics and predict the insurgence of defects since the damage effects are

introduced directly in the constitutive equations of the material; on the converse, it needs a more detailed material characterisation. The determination of the critical damage value for the two ductile criteria is, instead, very easy to realize, in particular the Cockroft and Latham one. The comparison with the experimental results shows that the information supplied by the Cockroft and Latham criterion are in a better matching with the experimental data than the Oyane ones, even if both the ductile fracture criteria fail in suggesting the possibility of ductile fracture at the 4th extrusion ($\alpha=15^\circ$, RA=20%). Thus it's possible to conclude that the Cockroft and Latham criterion is the most suitable tool for industrial applications.

ACKNOWLEDGEMENTS: This work has been made using MURST 40% funds.

REFERENCES

- [1] Kalpakjian, S., Manufacturing Processes for Engineering Materials, Addison-Wesley Publishing Company.
- [2] Kobayashi, S., Oh, S. I., Altan, T., 1989, Metal Forming and the Finite Element Method, Oxford University Press.
- [3] Alberti, N., Micari, F., Forming Processes Design Oriented to Prevent Ductile Fractures, *Advanced Manufacturing Systems and Technology*, 4th AMST'96, pp.47-61, 1996.
- [4] Cockroft, M. G., Latham, D. J., Ductility and the Workability of Metals, *J. Inst. Metals*, vol.96, pp.33-39, 1968.
- [5] Oyane, M., Sato, T., Okimoto, K., Shima, S., Criteria for Ductile Fracture and their Applications, *J. of Mech. Work Tech.*, vol.4, pp.65-81, 1980.
- [6] Osakada, K., Mori, K., Kudo, H., 1978, Prediction of Ductile Fracture in Cold Forging, *Annals of CIRP*: 135-139.
- [7] Brozzo, P., De Luca, B., Rendina, R., A New Method for the Prediction of Formability Limits in Metal Sheets, *Proc. 7th Conf. of the Int. Deep Drawing Research Group*, 1972.
- [8] Shima, S., Oyane, M., Plasticity Theory for Porous Metals, *Int. J. of Mech. Sci.*, vol. 18, pp. 285, 1986.
- [9] Aravas, N., The Analysis of Void Growth that Leads to Central Bursts during Extrusion, *Jnl. Mech. Phys., Solids*, vol.34, no.1, pp.55-79, 1986.
- [10] Gurson, A. L., 1977, Continuum Theory of Ductile Rupture by Void-Nucleation and Growth: Yield Criteria and Flow Rules for Porous Ductile Media, *J. of Eng. Mat. Tech.*, vol.99: 2-15.
- [11] Tvergaard, V., 1982, Influence of Void Nucleation on Ductile Shear Fracture at a Free Surface, *J. Mech Phys. Solids*, vol. 30, no. 6: 339-425.
- [12] Needleman, A., Tvegaard, V., An Analysis of Ductile Rupture in Notched Bars, *J. of Mech. Phys. Solids*, vol. 32, No. 6: 461-490, 1984.
- [13] Borsellino, C., Micari, F., Ruisi, V.F., Extrusion of Steel Rods: a Numerical Simulation Aimed to the Prediction of Central Bursting Defects, 3rd AITEM, Sept. 1997, pp. 67-74.
- [14] Chu, C.C., Needleman, A., *Jnl. Eng. Mat. Tech.*, vol.102, pp.249-262, 1980.
- [15] Altan T.Ceretti E, Taupin E.:Simulation of metal flow on fracture applications in orthogonal cutting, blanking and cold extrusion, *Annals of the CIRP 1997*, vol 46/1/97, pp. 187-190.
- [16] Fratini, L., Micari, F., Lombardo, A., Material characterization for the prediction of ductile fractures occurrence: an inverse approach, *J. of Mat. Proc. Tech.*, vol.60, pp.311-316, 1996.
- [17] DEFORM (Design Environment of Forming) User's manual. Release 5.2.
- [18] ABAQUS User's manual. Rel. 5. 4. 1. Hibbit Karlsson and Sorensen, Providence, (1994).

DEVELOPMENT OF A DESIGN PROCEDURE FOR BENDING OPERATIONS

R. Di Lorenzo and L. Fratini
University of Palermo, Palermo, Italy

KEY WORDS: Sheet Bending, Process Design, Optimization

ABSTRACT: Springback can be considered as one of the most important shape defect in sheet stamping. Such effect results relevant even when simple bending operations are taken into account. In the paper the authors present a design procedure able to provide the proper value of the punch stroke to be applied in order to compensate for elastic springback. In particular two approaches have been followed: firstly an inverse design technique has been utilized in order to find out the response function governing the investigated phenomenon; furthermore neural network techniques have been applied in order to represent the logical link between the input data and the aimed output, i.e. the proper punch stroke able to compensate the springback effect. The set up models have shown a very good attitude to the process design.

1. INTRODUCTION

Optimisation of sheet metal forming operations is mainly focused on the metal flow control with the aim to obtain sound components free from both shape defects and fractures. As far as sheet bending operations are regarded, the product optimisation has to be aimed to the determination of the best values of the operative parameters, such as material properties, sheet thickness, punch radius and so on. Moreover, once the final

Published in: E. Kuljanic (Ed.) *Advanced Manufacturing Systems and Technology*,
CISM Courses and Lectures No. 406, Springer Verlag, Wien New York, 1999.

product has been fixed, i.e. the bent component material, its thickness and the final bending angle, the forming process has to be developed in order to avoid discrepancies between the designed product and the obtained one. In particular such processes are strongly affected by the elastic springback which makes the final component shape different from the desired one. Actually springback occurs after the pressure of the forming tool is removed and results from the change in strain produced by elastic recovery when the load is released [1][2][3][4][5].

It should be observed that the increasing demand of low weight - high performance materials in advanced manufacturing, such as in the automotive and aerospace ones, emphasises the need for continuous investigations on elastic springback in order to foresee and overcome the occurrence of shape deviations from the original design of the final components. In this way, finite element method based techniques have been widely used to simulate the sheet stamping processes. Their excellent predictive capabilities regarding material flow, strain and stress states, forming loads and so on, permit significant cost reductions in the manufacturing process planning. In particular a few different procedures aimed to the simulation of the elastic springback have been proposed, based on implicit models, explicit ones or mixed ones [6][7][8].

As well, several models have been proposed to reduce or to compensate springback effects. The most conservative ones are based on the application of an overbending to compensate for springback the bending angle. In other words in the bending process the punch stroke is artificially increased with respect to the one necessary to obtain the desired bending angle; in this way as the bent part is removed from the forming tools and springback occurs, the bending angle returns to a value close to the desired one.

In the paper the authors present a design procedure able to provide the proper value of the punch stroke to be applied in order to compensate the occurring elastic springback in a V-bending process of AA 5083 aluminum alloy sheets. In particular two approaches have been followed: firstly, an inverse design technique has been employed in order to find out the response function governing the investigated phenomenon; furthermore a neural network has been set up and optimized in order to represent the logical link between the punch stroke and the final bending angle.

Both the design techniques have been widely tested on several bending operations aimed to the production of fixed angle V-parts. The effectiveness, the advantages and the usefulness of the two methods are compared and will be discussed in next paragraphs.

2. THE INVESTIGATED PROCESS

The 90° V-bending process of AA 5083 aluminum alloy 90 x 110 mm sheets has been taken into account (fig. 1, left). In particular three different thicknesses, namely 2, 4 and 6 mm, and three different punch nose radii, namely 4, 8 and 15 mm, have been investigated. Detailed descriptions of the theoretical aspects of bending can be found out in references [9][10]; it should be observed that as the forming tools are removed the internal stress state of the bent part is no more in equilibrium and a deformation occurs till a new equilibrium configuration is reached.

Several investigations on the bending process were performed in order to study the effects of the punch nose radius and of the sheet thickness on the elastic springback; the simulations have been interrupted for several different values of the punch stroke, obtaining a wide set of data linking these parameters to the springback ratio defined as follows:

$$K = \alpha_r / \alpha \quad (1)$$

where α_r and α are the bending angles after and before unloading respectively.

In fig. 1 (right) the predicted springback ratio versus the punch stroke is reported for a fixed punch nose radius equal to 4 mm and for the three different investigated sheet thicknesses.

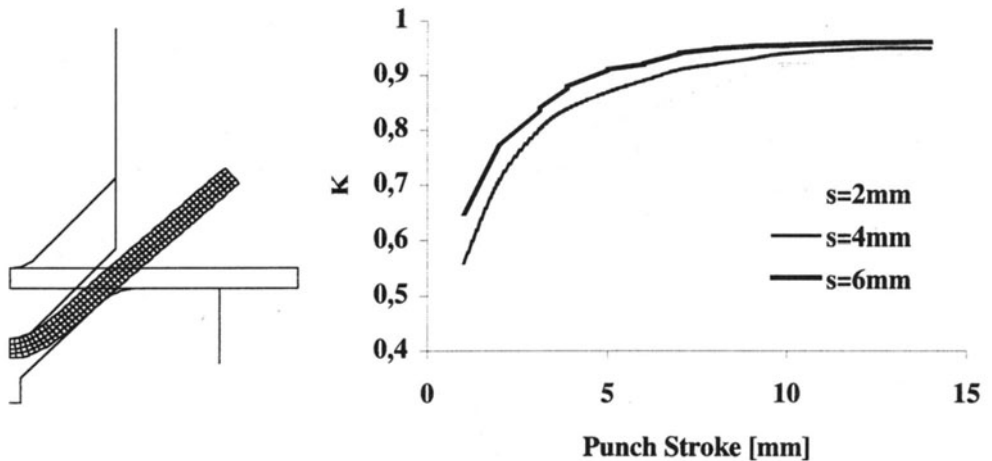


Fig. 1 - The 4 mm thick sheet V-bending process (left); the springback ratio vs. the punch stroke for a 4 mm punch nose process (right)

It is worth pointing out that a strong dependence of the springback ratio on the sheet thickness has been observed; on the other hand a weaker dependence of the springback ratio on the punch nose radius has been found. Anyway all the variables have been utilized in order to build up the knowledge base for the design procedure. On the basis of the very good overlapping between the numerical predictions and the experimental verifications [9][10] such knowledge has been built up basing on the numerical results.

As far as the numerical simulations are regarded, a mixed procedure, already tested with experimental verifications [10], has been developed; in particular an explicit model has been utilized to simulate the loading phase, while an implicit one has been used in order to develop the elastic step occurring in the releasing stage [8][11].

3. THE DESIGN PROCEDURE

The task to be pursued in the proposed design procedure is the compensation of the elastic springback in the taken into account V-bending operations. In order to reach this objective, the proper value of the punch stroke to be applied has to be fixed. In this way an optimal design problem has to be faced: once the punch geometrical parameters (namely punch nose radius) and the sheet thickness are available, and the desired bending angle is chosen as well, the optimal punch stroke has to be determined, in order to give an overbending to the bent part compensating the springback phenomenon.

Two different knowledge based design approaches have been followed to reach this aim, namely a statistical regression procedure and an Artificial Neural Networks based approach. The developed knowledge base has been built up associating a punch stroke value to each combination of the design parameters; the obtained data set has been structured as follows:

α <i>desired bending angle</i>	r_p <i>punch nose radius</i>	t <i>sheet thickness</i>	s <i>punch stroke</i>
α_1	r_{p1}	t_1	s_1
α_2	r_{p2}	t_2	s_2
...			
α_n	r_{pn}	t_n	s_n

Tab. I - The knowledge base structure.

On the basis of such a kind of knowledge the two proposed approaches have been utilized in order to obtain design tools able to provide as an output the proper value of the punch stroke basing on the input parameters (α , r and s).

It is worth observing that neither for the statistical approach performance nor for the ANN training the whole data set has been exploited, on the contrary, a certain percentage of the available data has been used to test the quality of the responses provided by both the design methods. Furthermore, the results obtained by the statistical approach have been compared with the ones provided by the neural network in order to verify the applicability, the advantages and the usefulness of each method in particular design problems, namely at varying the wideness of the available knowledge.

The accuracy of the obtained results, has been measured for both the procedures, by calculating a synthetic index measuring the fitness of the output with respect to the values stored in the test data set neglected in the preceding phase; in particular the mean square error has been utilized which is defined as follows:

$$\frac{\sum_{i=1}^N (s_i^* - s_i)^2}{N} \quad (2)$$

where s_i^* is the output supplied by the design tools for a fixed combination of the input variables, s_i is the desired value of the punch stroke recorded in the test data set and N is the number of test data the mean square error is calculated upon.

As far as the statistical approach is regarded, it has to be pointed out that it consists of two phases: a design of experiments and a regression model application [12][13].

Regarding the design of experiments, a complete space of variables combinations has been built up with the available values of the inputs, i.e. desired bending angle, sheet thickness and punch nose radius. Subsequently, the application of the regression procedure has allowed to determine a response function which expresses the analytical relation between the punch stroke variable and the set of input parameters (desired bending angle, punch nose radius and the sheet thickness).

In particular a regular behavior of the above mentioned function has been hypothesized and a quadratic expression has been assumed, which can be represented as follows:

$$y = b_0 + b_1 x_1 \dots + b_j x_j + b_{11} x_1^2 \dots + b_{jj} x_j^2 + b_{12} x_1 x_2 \dots + b_{(j-1)j} x_{(j-1)} x_j \quad (3)$$

where $x_1 \dots x_j$ are the input parameters and y represents the output variable ($x_1 = \alpha$; $x_2 = r$; $x_3 = t$ and $y = s$ respectively, in this application).

The definition of the response function is fully obtained by the determination of its coefficients, namely the zero order coefficient b_0 , the first order coefficients ($b_1 \dots b_j$), the second order pure ones ($b_{11} \dots b_{jj}$) and the second order mixed ones ($b_{12} \dots b_{(j-1)j}$), whose values have been deduced on the basis of the available knowledge.

It has to be observed that since in the proposed application three input variables have been considered there are ten unknown coefficients to be determined following this procedure, i.e. ten degrees of freedom have to be managed performing the regression model application.

As regards the application of the ANN to the design problem here addressed, it has to be underlined that a supervised multilayer feedforward network based on a backpropagation algorithm has been built up [14]. In particular, the chosen network architecture consists of three layers: an input layer, in which three neurons are used representing the three input parameters, an hidden layer with three neurons and an output layer in which one neuron is present corresponding to the output variable (s).

Each layer is fully connected to the successive one and according to the backpropagation rule, the weights of the connections linking a neuron belonging to a certain layer with a neuron belonging to the succeeding one are adjusted with the aim to minimize the error between the desired output (D_j) and the calculated one (O_j):

$$E = 1/2 \cdot [\sum_j (D_j - O_j)^2] \quad (4)$$

Let us define $x_j^{[s]}$ the current state of the j -th neuron in the s -th layer and $w_{ji}^{[s]}$ the weight of the connection between the i -th neuron in the layer $(s-1)$ and the j -th neuron in the layer s : each element transfers its input according to a particular transfer function (F) as follows:

$$x_j^{[s]} = F(\sum_i (w_{ji}^{[s]} x_i^{[s-1]})) \quad (5)$$

Furthermore the adjustment of the connections weights is calculated as follows:

$$w_{ji}^{[s]}(t+1) = w_{ji}^{[s]}(t) + \nu \cdot \delta_j^{[s]} \cdot x_i^{[s-1]} + \phi \cdot [w_{ji}^{[s]}(t) - w_{ji}^{[s]}(t-1)] \quad (6)$$

where ν is the learning coefficient (varying between 0 and 1), ϕ is the momentum (whose action is to fast the convergence) and δ is the error at the j -th node in the layer s [15].

It has to be underlined that the topology of the utilized network has been defined on the basis of a optimization procedure aimed to improve the network performances [16]. Furthermore, in order to perform the above mentioned comparison between the statistical procedure and the NN, it has been necessary to deal with the same number of unknown parameters (degrees of freedom); as a consequence, a network topology which presents a maximum of three neurons in the hidden layer has been chosen since the number of connections (whose weights are the parameters for the network definition) are the "degrees of freedom" of the network.

4. THE OBTAINED RESULTS

On the basis of the available data it has been possible to choice 3 values both of the punch radius and of the sheet thickness and 24 values of the bending angle in order to build up a complete space of experiments both for the statistical analysis and for the neural network approach. In this way, 216 combinations have been generated: 180 of them have been randomly chosen and utilized to apply the regression procedure and to train the neural network, while the remaining 36 have used as test data for the obtained models.

The function determined with the procedure described above shows a very good fitness with respect to the available data providing a mean square error calculated on the test data set lower than 3%. In the same conditions, the mean square error calculated on the test data set of the neural network has shown a slightly higher value with respect to the former one, i.e. 3.33%.

These results have been verified in terms of error on the final bending angles: namely, once a desired bending angle has been fixed, the punch strokes suggested by the two models have been tested, introducing them in two further numerical simulations. In particular the lowest values of the desired bending angles have been investigated since in this cases the error on the punch stroke has the strongest influence on the final bending angle. In this way errors in the final bending angles lower than 8% have been measured.

Furthermore the described design procedures have been repeated at the varying of the wideness of the data set available for learning, i.e. the deduction of the statistical function and the training of the neural network. In particular starting from the complete knowledge

base of 216 data, 108, 54 and 27 combinations have been randomly extracted, in order to implement the proposed procedures, while the remaining data have been utilized for the testing phase. In figure 2 the mean square error versus the number of learning data is reported, showing a progressive worsening of prediction for both the models at the decreasing of the available knowledge. In particular, as expected, the neural network approach (NN) shows a greater sensibility to the number of learning information with respect to the statistical method (SA). Anyway, the latter is founded on the assumption of a quadratic behavior of the investigated phenomenon: such hypothesis makes the model effective just in a limited range of the input variables domain.

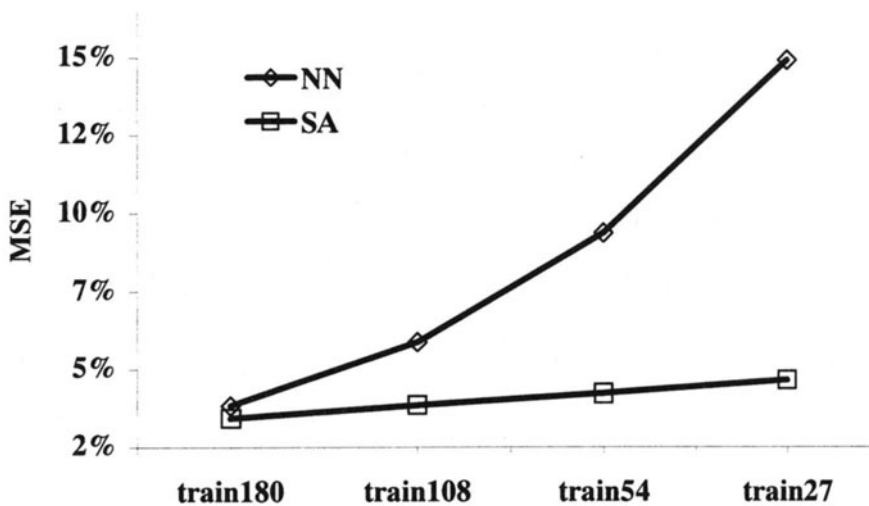


Fig. 2 - The mean square error vs. the number of learning data

With the development of the presented models it is possible to skip the quite long trial and error procedure which is required in order to determine the right overbending utilizing just the FEM techniques. In particular, the developed statistical tool allows a straight reduction in the design time of the taken into account V-bending process since even with a very reduced knowledge it remains a powerful tool. On the other hand, an equivalent design model founded on a totally experimental knowledge, i.e. the actual industrial know-how, should be based on NN techniques, due to their ability to manage the implicit knowledge form typical of the experimental data.

5. CONCLUSIONS

In the paper a design procedure for the determination of the overbending in a V-bending operation is proposed. In particular two different approaches have been presented, namely a statistical procedure and a neural network technique, showing a good fitting of the investigated phenomenon. It should be observed that the statistical approach provides a

more robust tool, regarding the wideness of the available knowledge, while the neural network technique shows a better capacity to manage large ranges of the design variables.

ACKNOWLEDGEMENTS

This work has been performed with funding from MURST (Italian Ministry for University and Scientific Research).

REFERENCES

- [1] He, N., Wagoner, R.H.: Springback simulation in sheet metal forming, Proc. of Numisheet '96, 1996, 308-315
- [2] Huang, M., Gerdeen, J.C.: Springback of doubly curved sheet metal surface - an overview, SAE Conference, Detroit Michigan, 1994, 125-138
- [3] Joannic, D., Gelin, J.C.: Accurate simulation of springback in 3D sheet metal forming processes, Proc. of Numiform '95, 1995, 729-729
- [4] Mickalich, M.K., Wenner, M.L.: Calculation of springback and its variation in channel forming operations, GMR - 6108, General motors research publication, General Motors research lab, Warren, MI, 1988
- [5] Schmoekkel, D.: Springback reduction in draw-bending process of sheet metals, Annals of CIRP, 42 (1993) 1, 339-342
- [6] Makinouchi, A.: Sheet forming simulation in industry, J. of Materials Proc. Technology, 60, (1996), 19-26
- [7] Makinouchi, M., Nakamachi, E., Onate, E., Wagoner, R.H., (eds.): Numisheet '93 - Second International Conference On Numerical Simulation of 3D Sheet Metal Forming Process - Verification of Simulation with Experiments, Tokyo (Japan), 1993
- [8] Mattiasson, K., Strange, A., Thilderkvist, P., Samuelsson, A.: Simulation of springback in sheet metal forming, Proc. of Numiform '95, 1995, 115-124
- [9] Forcellese, A., Fratini, L., Gabrielli, F., Micari, F.: Sheet bending modelling for AA 5083 aluminium alloy, Proc. of 31st MATADOR Conference, 1997, 377-382
- [10] Forcellese, A., Fratini, L., Gabrielli, F., Micari, F.: Computer aided engineering of the sheet bending process, J. of Materials Proc. Technology, 60, (1996), 225-232
- [11] Onate, E., Agelet de Saracibar, C.: Alternatives for finite element analysis of sheet in metal forming problems, Proc. of Numiform '92, 1992, 79-88
- [12] Box, G.E.P., Hunter, W.G., Hunter J.S.: Statistics for experimenters, John Wiley & Sons, 1978
- [13] Box, G.E.P., Draper, N.R.: Empirical model building and response surfaces, John Wiley & Sons, 1987
- [14] NeuralWorks Professional II/Plus, NeuralWare inc., Pittsburgh, PA, 1993
- [15] Fu, L.: Neural Networks in computer intelligence, McGraw Hill, 1994
- [16] Fratini, L., Lo Nigro, G.: Neural network application in laser bending process: direct and inverse approaches, Proc. of II AITEM Conf., 1995, 11-20

RUBBER FORMING PROCESSES OF THIN SHEETS

A. Custro, L. Fratini and S. Lo Casto
University of Palermo, Palermo, Italy

KEY WORDS: Sheet Metal Drawing, Rubber Forming, Numerical Simulations

ABSTRACT: In the last decade flexible media have been increasingly utilized in sheet metal drawing processes in order to reduce the tooling cost and to improve the product quality. In the present paper an axisymmetric deep drawing process of thin steel sheets is taken into account: in particular a flexible pad is utilized in order to simplify the tooling set. The process mechanics is investigated through numerical simulations and experimental tests with the aim to find out a proper set of operative parameters allowing the stamping of sound components and to highlight the particular deformation path of the drawing cup. The comparison between the numerical predictions and the experimental verification has shown a very good overlapping.

1. INTRODUCTION

Nowadays the competitive arena of the metal-working industry requires innovation, high qualitative products and low costs. In this way, in order to get up to date, modern companies have to aim to high flexibility, to new product design and to processes research. In particular the latter should be focused either on the optimization of the classic metal forming processes or on the development of innovative forming operations and procedures aimed to the improving of the forming limits and to the reduction of the production stages.

Published in: E. Kuljanic (Ed.) *Advanced Manufacturing Systems and Technology*,
CISM Courses and Lectures No. 406, Springer Verlag, Wien New York, 1999.

As far as sheet metal stamping is regarded, in the last decades innovative solutions have been introduced such as tailored blanks, laser forming or flexible media as forming tools [1]. Pointing the attention on such flexible tools, the hydroforming or aquadraw processes have to be mentioned [2][3][4][5][6], in which fluid counter pressure is utilized as female die. The stamping process is developed fulfilling the die cavity with an incompressible fluid (generally water or oil); as the blank enters the die, the hydraulic pressure increases and acts on the drawing component, flowing out beneath the blank and the die: in this way a sort of dynamic equilibrium between the blankholder pressure and the fluid one is established. As a consequence an increase in the friction at the punch-workpiece interface is obtained and subsequently a reduction in the axial stresses is observed. Since the limiting drawing ratio is strongly affected by the reached level of axial stresses during the deep drawing process, hydroforming processes allow higher drawing ratios or, more generally, increased forming limits. Furthermore, it should be observed that in the sheet metal processes one of the most important targets is the reduction of thinning phenomena; in hydroforming processes a more uniform thickness along the drawn cup is obtained due to the hydrostatic pressure acting on the external surface of the blank.

On the other hand, the hydroforming processes are characterized by complex tooling sets and slow ram speeds which make them quite expensive. Anyway, in hydroforming processes the process mechanics is strongly affected by a large number of operative parameters even for very simple geometries of the stamped parts, and they still represent a subject of study and scientific interest.

The other kind of flexible medium which is commonly utilized in the sheet metal stamping operations is rubber. Actually, the first applications of rubber to forming processes can be found out in the latter 19th century, when it was utilized over metal dies to eliminate scratching of the sheet metal surface; then at the beginning of the 20th century rubber was used in bulging tests and during the second world war the Guerin process was industrially developed but it was just in the sixties with the introduction of polyurethanes, much more resistant to wear and chemical attacks given by the lubricants, that this kind of medium started to be utilized in the common industrial practice [7][8].

Today rubber forming is performed through a flexible pad, confined into a rigid container, which is coupled with a rigid die: this permits to overcome possible alignment problems between the dies and to utilize a single block of rubber for the production of several different components. In particular, rubber forming processes can be developed coupling to the flexible pad a rigid male: in this case no blankholding action is given at the beginning of the process and, as the punch stroke starts, the rubber pad tends to fill the tool set giving rise to a reaction which pushes the blank towards the punch reproducing its profile. Generally such configuration determines a rather insufficient support to the blank during the process and wrinkles insurgence is expected due to geometrical instabilities.

On the contrary, when a rigid female is utilized as the process starts the reaction of the rubber pad determines both the forming action on the unsupported blank corresponding to the die cavity and the blankholding one on the sheet metal beneath the die collar and the flexible medium, which avoids the insurgence of wrinkles. Furthermore, it should be observed that the rubber forming action determines a biaxial tensile stress state, very

different from what observed in a common deep drawing process, which favors the process mechanics permitting higher limiting drawing ratios and generally higher forming limits.

In the paper the rubber forming process for the stamping of axisymmetric steel cups is analyzed. Either the rigid male configuration or the rigid female one are investigated with the aim to highlight the process mechanics and the influence of the most important operative parameters. As far as the rigid female configuration is regarded, a bottomless die has been utilized in order to focus the process mechanics and the rubber actions upon the sheet; moreover a closed die has been chosen in order to compare the investigated process with an equivalent classic deep drawing process. Two different kinds of steel have been taken into account, i.e. an EN 10130-Fe P01 mild steel for deep drawing and a tinplate, and two different urethanes have been tested, characterized by a Shore hardness equal to 50A and 90A, respectively.

A set of numerical simulations have been developed and an explicit commercial code has been used; the hyperelastic behavior of the utilized urethane has been taken into account implementing the Mooney and Rivlin constitutive equation and a balanced master-slave contact algorithm has been chosen in order to properly take into account the interactions at the urethane-sheet metal interface [9][10][11]. A set of experimental tests has been carried out in order to verify the numerically predicted results, obtaining a very good overlapping.

2. THE INVESTIGATED PROCESS

A simple axisymmetric deep drawing process has been taken into account in order to investigate the process mechanics which characterizes a rubber forming process and to compare it with what happen utilizing two rigid dies. As shown the urethane pads have been confined into a rigid container with the aim to avoid lateral deformations favoring the fulfilling of the dies. The elastomers have been received as 13 mm thick disks with a diameter equal to 78 mm. In order to properly characterize the urethane hyperelastic behavior, several uniaxial compression tests have been developed using pads of the same dimensions of the ones utilized in the deep drawing processes; in this way it has been possible to take into account the shape factor affecting the elastomer elastic modulus [8].

A drawing ratio equal to 1.67 has been chosen in order to avoid the insurgence of fractures; in particular a rigid male configuration has been investigated with a punch radius equal to 3 mm: in this case the forming process has been developed pushing the rigid punch against an urethane cushion on which the sheet had been placed. What is more, two rigid females configurations have been investigated, utilizing a bottomless and a closed die respectively, characterized by a die radius equal to 3 mm.

The experiments have been developed using 0.5 mm thick EN 10130-Fe P01 steel blanks and 0.17 mm thick tinplate blanks, with an initial diameter of 77 mm. In order to obtain the flow stress expressions to be introduced in the numerical analyses, tensile tests have been previously carried out on the two materials, obtaining the following flow stress equations:

$$\begin{aligned}\sigma_{eq} &= 665 \varepsilon_{eq}^{0.331} \text{ [N/mm}^2\text{]} && \text{(Fe P 01 mild steel)} \\ \sigma_{eq} &= 982 \varepsilon_{eq}^{0.28} \text{ [N/mm}^2\text{]} && \text{(tinplate)}\end{aligned}$$

Several tests have been developed at the varying of the sequence of the urethane pads of different Shore hardness and of the lubricating media in order to obtain the best process conditions, i.e. the best reaction forces distribution of the flexible die on the blank.

As far as the numerical simulations are regarded, an explicit commercial code has been utilized [12]; in particular in order to take into account the non linear elastic stress-strain behavior of the urethanes the Mooney and Rivlin constitutive relation has been chosen [13]. Such a law is obtained from the polynomial form of the strain energy per unit of volume, what is called the strain energy potential $U(\epsilon)$, taking into account just the linear terms as follows [9]:

$$U = C_{10}(I_1 - 3) + C_{01}(I_2 - 3) \quad (1)$$

where C_{10} and C_{01} are material parameters determined on the basis of the uniaxial compression test experimental data, while I_1 and I_2 are the first and the second deviatoric invariants of the Green-Lagrange strain tensor [11][13].

Since the process mechanics is strongly affected by the reaction forces on the sheet metal special care has to be taken on the contact and friction modellization at the urethane blank interface. The rubber pad and the steel blank are two formable bodies and in this way a balanced master slave contact algorithm has to be utilized in order to deal with such a contact condition. Furthermore in order to avoid penetrations of one body on the other a fast local track contact option has been neglected, improving the process analysis but increasing the CPU time [9]. As regards frictional condition, the Coulomb model has been utilized choosing friction coefficients in the range 0.2-0.4 at the rubber-blank interface on the basis of the referring lubricant condition.

3. ON THE PROCESS MECHANICS

First of all the possibility to utilize a rigid male former has been investigated. In this case no blankholding action is given to the drawing blank; as the process starts the circumferential stresses rise and determine the insurgence of geometrical instabilities, namely wrinkles, in all the unconstrained blank. As a consequence the no sound components can be obtained utilizing such a configuration. In fig. 1 both the experimental result and the numerical prediction are shown regarding the EN 10130-Fe P01 steel: a good overlapping is obtained.

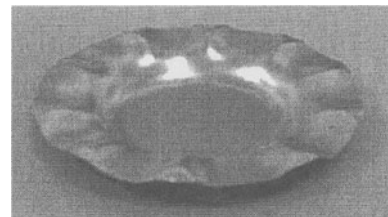
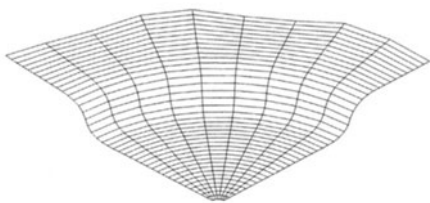


Fig. 2 - The wrinkling phenomenon

As far as the rigid female is regarded in figure 2 the sound Fe P 01 steel components are reported for both the bottomless die configuration (a) and for the closed die one (b). In particular, in order to develop a comparison between the investigated rubber forming process and a classic deep drawing process characterized by the same drawing ratio, a 15 mm deep closed die has been chosen.

In this case the process mechanics which govern the drawing operation is much more complex: actually both frictional actions and rubber reactions have to be taken into account. During the process, the frictional forces at the interface between the sheet metal and the flexible pad are directed towards the inner part of the tool, i.e. the bottom of the cavities. These frictional forces contribute to the deforming action of the rubber, decreasing the needed pressure to complete the stamping process [14]. Furthermore, the rubber reactions determine a biaxial stress state which can be highlighted analyzing the deformation paths all along the drawing component.

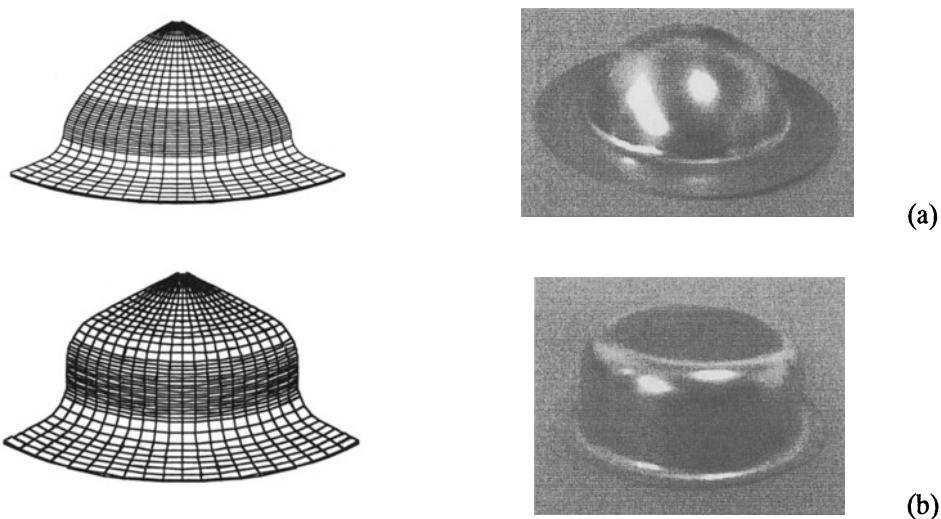


Fig. 2 - The sound components obtained using the bottomless die (a) and the closed die (b) respectively

Let the process mechanics be compared with the one occurring during a classic deep drawing process regarding the EN 10130-Fe P01 steel and characterized by the same drawing ratio: actually during the deep drawing process the total drawing force, which is the sum of the forces required to compress the sheet in the flange circumferentially, to overcome friction and finally to bend and unbend the sheet around the punch and the die radii, is applied by the punch on the base of the cup and transmitted through the wall which consequently undergoes tensile axial stresses and compressive circumferential ones. A few numerical deformation paths along the cup wall for the classic deep drawing process are reported in figure 3 (curves A, B and C), in which the minor and major strains are

compared to the Forming Limit Diagram of a mild steel for deep drawing [15]. It is worth pointing out that the deformation paths are all characterized by negative minor strains and in particular it should be observed that a relevant danger of localized thinning occurs nearby the punch nose where the conditions of uniaxial tensile stress state are reproduced due to the very low level of circumferential strain (curve A). These considerations are confirmed in figure 4 (left) where the average values of several experimental tests are reported, showing the thickness distribution of a classically drawn cup. Even for the utilized soft drawing ratio a 14% thinning is observed in proximity of the punch nose.

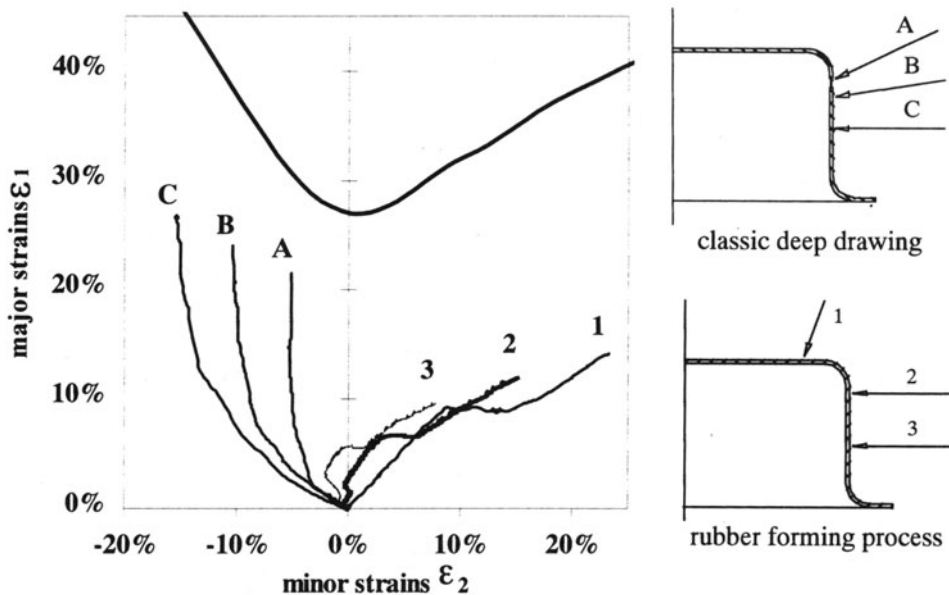


Fig. 3 - A few deformation paths in the cup wall of the classically deep drawn component (A, B, C) and along the drawn part obtained through the rubber forming process (1, 2, 3)

As far as the rubber forming process is regarded, the insurgence of a biaxial stress state in the drawing cup is highlighted in figure 3 where three deformation paths are reported (curves 1, 2 and 3); it should be observed that the referring points on the component have been chosen all along the drawn part since even at the bottom of the cup deformations occur during the stamping process. The reported curves are characterized by positive minor strains, confirming the biaxial stress state, and indicate a level of stretching conferred to the drawn part. Moreover lower maximum values of major strain are observed with respect to the classic deep drawing process and anyway the worst conditions are reached at the bottom of the cup in which the maximum thinning level is reached even if no localized thinning is highlighted, as shown in figure 4 (right). Furthermore, it should be observed that the deformation paths in figure 3 (curves 1, 2 and 3) are characterized by a few peculiarities: regarding curve 1, referred to an element at the bottom of the cup, as the blank reaches the bottom of the die cavity a large flat zone is highlighted in which no

significant increment of the major strain is observed. In this phase the fulfilling of the die cavity is developed. As the lateral wall of the drawing part reaches the die wall, the major strain restart to increase with a lower slope with respect to the first part of the curve; in this phase both the completing of the drawing process and the fulfilling of the die cavity is obtained. The same considerations can be developed for curve 2, even if the highlighted phases are less evident since the referring element is placed in the side of the component and then the flat zone of curve 2 results shorter.

Finally, as far as curve 3 is regarded, it is referred to an element placed at the beginning of the process underneath the die external collar and the urethane pad. Such elements in the first stages of the process undergo typical strain paths which characterize the flange movement in a deep drawing operation, i.e. with negative minor strains. Subsequently, as the sheet metal enters the die cavity the rubber action determines the biaxial stress state in such elements and the strain paths follows the behavior described before.

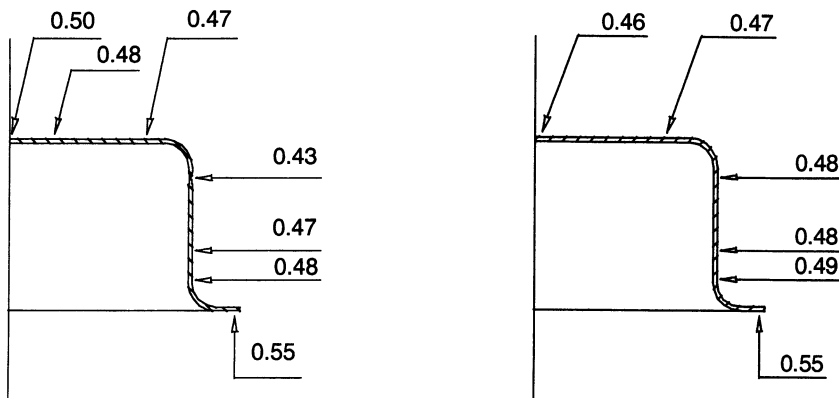


Fig. 4 - The thickness distribution in the classically drawn cup (left) and in the component obtained through the rubber forming process (right)

As far as the tinplate steel is regarded the same numerical predictions and experimental verifications have been carried out, and the same behavior has been highlighted. In particular in order to investigate the insurgence of geometrical instabilities, i.e. wrinkles, further investigations will be performed in the next.

4. CONCLUSIONS

On the basis of the previous considerations and of the above reported results the following statements can be assumed:

- numerical simulations, based on the Mooney and Rivlin model and a proper contact algorithm, are able to supply a good prediction of the elastomers behaviour;
- a rigid male former does not provide a blankholding action giving rise the insurgence of wrinkles all around the unsupported blank area;

- in rubber forming processes with a rigid female die coupled with an urethane pad a level of stretching is given to the drawing blank; in this way a biaxial stress state is determined in the sheet metal avoiding localized thinning phenomena and allowing increased forming limits with respect to a classic deep drawing process characterized by the same drawing ratio.

ACKNOWLEDGEMENTS

This work has been performed with funding from MURST (Italian Ministry for University and Scientific Research).

REFERENCES

- [1] Nakagawa, T.: Recent developments in auto body panel forming technology, *Annals of CIRP*, 42 (1993) 2, 717-722
- [2] Gelin, J.C., Delassus, P.: Modelling and simulation of the aquadraw deep drawing process, *Annals of CIRP*, 42 (1993) 1, 305-308
- [3] Gelin, J.C., Ghouati, O.: Modelling and control of hydroforming processes for flanges forming, *Annals of CIRP*, 47 (1998) 1, 213-216.
- [4] Nakagawa, T., Nakamura, K., Amino, H.: Various applications of hydraulic counter-pressure deep drawing, *J. of Materials Proc. Technology*, 17 (1997), 160-167
- [5] Nakamura, K.: Reverse deep drawing with hydraulic counter pressure using the peripheral pushing effect, *Annals of CIRP*, 35 (1986) 1, 173-176
- [6] Nakamura, K.: Sheet metal forming with hydraulic counter pressure in Japan, *Annals of CIRP*, 36 (1987), 1, 191-194
- [7] Thiruvarudchelvan S.: Free forming of near-hemispherical shells using a urethane pad, *J. of Materials Proc. Technology*, 18 (1989), 5-15
- [8] Thiruvarudchelvan S.: Elastometers in metal forming: A review, *J. of Materials Proc. Technology*, 39 (1993), 55-82
- [9] ABAQUS/Explicit, User's Manual, HKS, 1997
- [10] Onate, E., Agelet de Saracibar, C.: Alternatives for finite element analysis of sheet in metal forming problems, *Proc. of Numiform '92*, 1992, 79-88
- [11] Tabaddor, F.: Rubber elasticity models for finite element analysis, *Computer & Structures*, 26 (1987), 33-40
- [12] Rebelo, N., Nagtegaal, J.C., Taylor, L.M., Passmann, R.: Comparison of implicit and explicit finite element methods in the simulation of metal forming processes, *Proc. of Numiform '92*, 1992, 99-108
- [13] Sussman, T., Bathe, K.J.: A finite element formulation for nonlinear incompressible elastic and inelastic analysis, *Computer & Structures*, 26 (1987), 357-409
- [14] Alberti, N., Forcellese, A., Fratini, L., Gabrielli, F.: Sheet metal forming of titanium blanks using flexible media, *Annals of CIRP*, 47 (1998) 1, 217-220
- [15] Numisheet '99 - Benchmark materials specifications, 1998

THE USE OF ARTIFICIAL INTELLIGENCE TECHNIQUES TO OPTIMISE AND CONTROL INJECTION MOULDING PROCESSES

V. Basile

University of Calabria, Arcavacata di Rende (CS), Italy

L. Filice

University of Palermo, Palermo, Italy

F. Micari

University of Calabria, Arcavacata di Rende (CS), Italy

KEYWORDS: Injection moulding, Process optimisation, Neural Network, Fuzzy logic.

ABSTRACT: In the paper a typical injection moulding process on a single-screw extrusion machine aimed to the production of axisymmetric polypropylene dishes for alimentary use has been investigated. First of all the most important process parameters have been individuated; subsequently a wide testing hyperspace has been investigated, at varying the process parameters in a large range. For each combination both some geometrical characteristics of the obtained component have been measured and the occurrence of defects has been verified. The largest part of the available data have been used to train a neural network aimed to explain the process dynamics. Furthermore an off-line control system, based on fuzzy logic reasoning, has been developed. If a defect is detected the system is able to suggest the most effective adjustment of the process parameters in order to take the process back in control. The validity of the controller has been assessed through several experiments on the available equipment.

1. INTRODUCTION

Injection moulding of thermoplastics probably represents the most important and diffused process among the plastic forming technologies. The process exploits some basic properties of plastics: i) they melt at relatively low temperatures; ii) they do not loose the

initial properties in the melting process, making possible to carry out a new injection moulding cycle on recycled parts. As well as in any other manufacturing technology, process optimisation is a fundamental aim in plastics manufacturing [2][3][4]. In many cases the optimisation criterion may be represented by the minimisation of production discards, i.e. products whose quality is not conform to the required specifications. It is worth noticing that a substantial contribution to this aim could be supplied by the development of effective and accurate models able to explain the relations existing between process parameters and products features: by this way, in fact, it would be possible to increase the reliability of the production system and to decrease the Time to Market of the product [1][5]. Unfortunately in injection moulding these relations are not completely known: even the use of numerical models and FE codes oriented to this type of problem (CFLOW, MOLDFLOW etc.) can permit to achieve only a partial knowledge of the process [5][6]. Furthermore the process conditions variability is so large that a deterministic approach (like the numerical FE one) does not appear as the most suitable. In this paper an integrated approach to the optimisation of a typical injection moulding process is proposed, based on the synergetic use of a couple of Artificial Intelligence tools. In particular an accurate model of the process has been established utilising a properly trained Neural Network, i.e. an identification technique well suitable to deal with problems characterised by a stochastic behaviour. By this way the influence of the most important process parameters on the occurrence of some common defects has been identified. Furthermore an off-line control system has been developed, based on Fuzzy Logic. As it is well known, Fuzzy Logic is a very powerful tool to introduce the knowledge acquired by an expert in the control system, making such knowledge available where it is required. In this way an effective controller, based on a large set of fuzzy rules, has been designed: if a defect is detected, the controller provides to suggest the most effective adjustment of the process parameters in order to remove the defect reason and to take the process back in control.

2. PROCESS IDENTIFICATION – MODELLING WITH NEURAL NETWORK.

During a typical injection moulding process several complex physical phenomena occur: change of state of the plastics, heat transfer between melted plastics and mould, very high values of the injection pressure are only some of the most important. These phenomena demonstrate the complexity and the strong non-linearity of the process; furthermore injection moulding is characterised by a large variability of the process conditions. For these reasons a Neural Network has been utilised to model the process: these AI tools are in fact very powerful and effective to cope with problems characterised by non linear behaviour and stochastic nature. A large testing hyperspace has been investigated, at varying the process parameters in a large range. For each combination both some geometrical characteristics of the obtained dish have been measured and the occurrence of defects has been verified. These data have been utilised to train a neural network aimed to explain the process dynamics.

2.1 THE EXPERIMENTAL TESTS

The tests were carried out on a single-screw extrusion machine, the main features of which are reported in the next table:

CONSTRUCTOR	METALMECCANICA
EUROMAP	95/250
MAX. INJECTION	110 bar
MAX. INJECTION RATE	16,6 cm/s

Table 1.

The process was aimed to the production of axisymmetric dishes for alimentary use; the material was polypropylene MH 113. The first task was to define the set of process parameters which affect the process mechanics; in this research the following group of most relevant parameters has been considered:

1. Injection Pressure (IP);
2. Barrel Temperature (BT), temperature of the material during the injection;
3. Injection Rate (IR), generally defined as a percentage of the maximum injection rate available on the machine (reported in the above table);
4. Cooling Time after injection (CT);
5. Holding Pressure (HP), pressure still applied on the dish inside the mould during the cooling phase after the injection, in order to compensate shrinkage;
6. Holding Pressure Time (HPT), time of application of the holding pressure.

All these parameters strongly affect the process and consequently determine the quality of the obtained dish. As far as the latter item is concerned, the success of the injection moulding process mainly depends on the avoidance of some typical defects, among which the most important are:

1. Insufficient Filling of the mould cavity (IF), due to the so called short injection;
2. Flashes (F) or long injection;
3. Wrinkles (W);
4. Streaks (S), visible veinings on the product due both to the colour distribution in the plastic and to the injection conditions; generally streaks occur along the radial direction, according to the flow of the melted material;
5. Sink Marks (SM), surface defect mainly discernible touching the disk; the surface presents furrows and has an irregular profile.

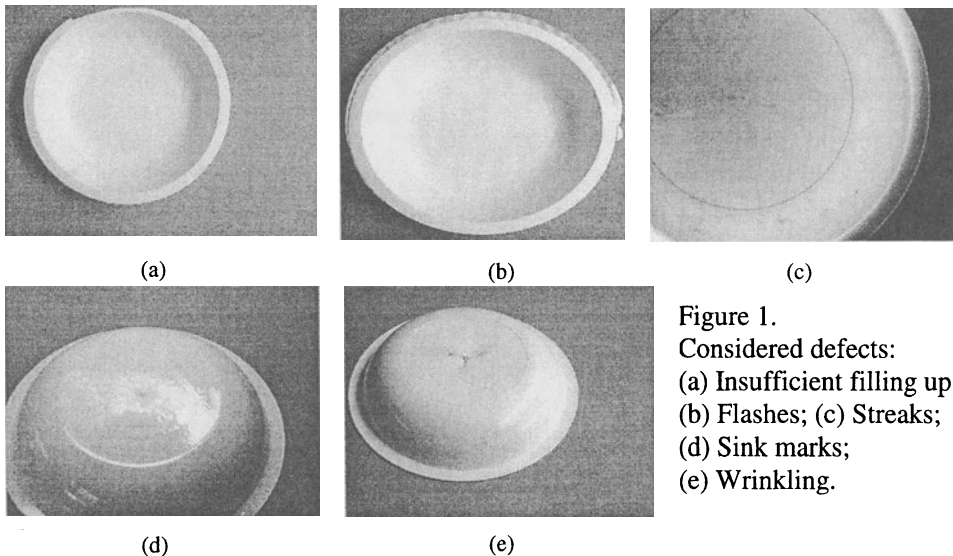


Figure 1.

Considered defects:
 (a) Insufficient filling up;
 (b) Flashes; (c) Streaks;
 (d) Sink marks;
 (e) Wrinkling.

The aim of the this part of the research is to find the linkage between process parameters and defects occurrence. For this reason an accurate experimental campaign has been carried out on the available extrusion machine, at varying each process parameter in a wide range. The next table reports the considered range for each parameter; a total number of 600 different combinations of the process parameters has been tested.

PARAMETERS	RANGE
INJECTION PRESSURE	55 – 85 bar
BARREL TEMPERATURE	220 – 275 °C
INJECTION RATE	50 – 99 %
COOLING TIME	0,5 – 2,5 sec
HOLDING PRESSURE	5 – 70 bar
HOLDING PRESSURE TIME	0,1 – 0,3 sec

Table 2.

The dishes so obtained were carefully controlled to verify some physical features and the eventual occurrence of defects. As far as the former are regarded, the weight and the thickness distribution along the dish radius have been measured, without noticing any significant variation with respect to the target values. For this reason the study has been limited to the analysis of the defects detected on the products.

It is worth pointing out that in order to supply the defects data to the Neural Network, these data have been codified utilising a binary elements array: the array has five components as the number of considered defects, and each component has value 1 if the defect occurs and 0 if it doesn't occur. Some results are shown in the next table 3. Fig.2 shows the strong influence of the injection pressure and temperature on the insufficient filling defect (short injection).

Table 3.

N°	PROCESS PARAMETERS						DEFECTS				
	IP (Bar)	BT (°C)	IR (%)	CT (s)	HP (Bar)	HPT (s)	IF	F	W	S	SM
1	70	250	99	1,8	35	0,1	0	0	0	0	0
2	55	250	99	1,8	35	0,1	1	0	0	0	1
3	85	250	99	1,8	35	0,1	0	1	0	1	1
4	70	250	99	1,8	25	0,1	0	0	0	1	0
5	70	250	99	1,8	45	0,1	0	0	0	1	0
6	70	220	99	1,8	35	0,1	1	0	0	1	0
7	70	275	99	1,8	35	0,1	0	1	1	1	0
8	70	250	50	1,8	35	0,1	1	0	0	1	0
9	70	250	60	1,8	35	0,1	1	0	0	1	1
10	70	250	99	1,8	35	0,2	0	0	1	0	1

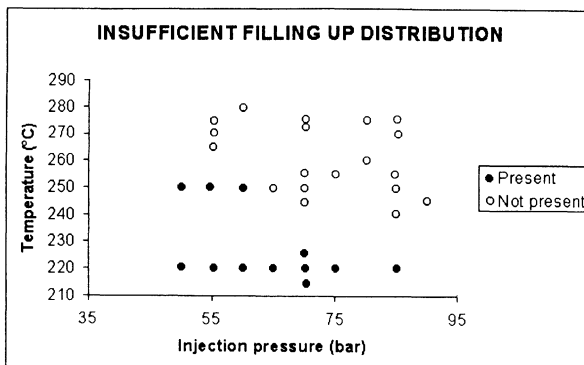


Figure 2.

2.2 THE NEURAL NETWORK.

The largest part of the experimental data were utilised to train a Neural Network, with the following main features:

- 6 neurones of the input layer (i.e. the number of considered process parameters);
- 1 hidden layer, with 30 neurones;
- 5 neurones on the output layer (i.e. the number of considered defects, codified as described before).

The training algorithm was based on the Error Back Propagation method. In particular the experimental data corresponding to 400 different combinations of the process parameters were utilised to train the Network; training required about 100000 iterations and a total CPU time of about 20 hours on a Pentium 233 MHz based platform.

The predictive capability of the Neural Network has been assessed testing its behaviour on the remaining 200 experimental data set. The following table 4 shows only some of the results: for each combination of the process parameters, both the experimental data and the predictions furnished by the NN are presented..

Table 4.

INJECTION MOULDING PARAMETERS							EXPERIMENTAL					NN PREDICTION					
N°	IP (bar)	BT (°C)	IR (%)	CT (s)	HP (bar)	HPT (s)	IF	F	W	S	SM	IF	F	W	S	SM	
1	70	249	99	1,8	35	0,1	0	0	0	0	0	0	0	0	0	0	0
2	55	249	99	1,8	35	0,1	1	0	0	0	1	1	0	0	0	0	0
3	85	249	99	1,8	35	0,1	0	1	0	0	1	0	1	0	0	0	0
4	70	249	99	1,8	25	0,1	0	0	0	0	0	0	0	0	0	0	0
5	70	249	99	1,8	45	0,1	0	0	0	1	0	0	0	0	0	0	0
6	70	221	99	1,8	35	0,1	1	0	0	1	0	1	0	0	1	0	0
7	70	274	99	1,8	35	0,1	0	1	1	1	1	0	1	1	1	1	1
8	70	249	50	1,8	35	0,1	1	0	0	1	0	1	0	0	1	0	0
9	70	249	60	1,8	35	0,1	1	0	0	1	1	1	0	0	1	0	0
10	70	249	99	1,8	35	0,2	0	0	1	0	1	0	1	1	0	1	1

The comparison between the experimental data and the NN predictions gave good results: a satisfactory predictive capability about the insurgence of defects has been found out, as shown in the following table.

Table 5.

	Ins. filling	Flashes	Wrinkling	Streaks	Sink marks	TOTAL
Number of tests	200	200	200	200	200	1000
Errors	19	24	21	28	44	136
Success	181	176	179	172	156	864
Errors %	9,5	12	10,5	14	22	13,6
Success %	90,5	88	89,5	86	78	86,4

This analysis allows to conclude that a confidence level equal to 86,4% has been achieved. This value increases to 90% when the most dangerous defects (insufficient filling up, wrinkling and flashes) are considered.

3. PROCESS CONTROL – DEVELOPMENT OF A FUZZY LOGIC CONTROLLER

An off-line control system of the injection moulding process has been developed. The system is based on fuzzy logic reasoning and more in particular on the Mamdani approach, i.e. the control structure is based on a set of IF-THEN rules linking input and output variables [7][8][9].

The aim of the controller is to bring back the process in control properly modifying one or more process parameters if any defect is detected. Thus the problem consists in determining the most suitable set of process parameters at the time $t+\Delta t$, once the process parameters and the output of the system at the time t is known. The input of the controller is then the 6-component array of the operating variables and the 5-component array of the considered defects; in the latter the i -th component has value equal to 1 or 0 depending on the occurrence of the defect, as above described. The next step is the definition of Fuzzy partitioning, i.e. the definition of the levels that each variable can assume in the assigned range. As far as the process parameters are regarded a proper linguistic set has been associated to each one of the variables, namely Injection Pressure (IP), Barrel Temperature (BT), Injection Rate (IR), Cooling Time (CT), Holding Pressure (HP), Holding Pressure Time (HPT). The linguistic values have been defined as follows:

- IP={VH Very High, H High, M Medium, L Low, VL Very low};
- BT={VH Very High, H High, M Medium, L Low, VL Very low};
- IR={H High, M Medium, L Low};
- CT={H High, M Medium, L Low};
- HP={H High, M Medium, L Low};
- HPT={H High, M Medium, L Low}.

On the other hand a defect may occur or not occur; thus for each defect only two linguistic values were defined:

- IF, F, S, W, SM = {P Present, NP Not Present}.

The number of linguistic levels for each set has been chosen in order to properly reproduce the variation of the corresponding variable. As well, suitable membership functions have been selected for each variable: in particular triangular functions were used for the process variables, while trapezoidal functions are more appropriate for the defects. Taking into account the mentioned linguistic sets and membership functions, as well as the expert skill, a set of 340 IF-THEN rules has been built up. Some basic rules provided by the experience are summarised in table 6.

DEFECT	ACTION
INSUFFICIENT FILLING UP	Increase Injection Pressure, Increase Holding Pressure, Increase Temperature, Increase Holding Pressure time, Increase Injection Rate.
FLASHES	Decrease Injection Pressure, Decrease Holding Pressure, Decrease Temperature, Decrease Holding Pressure time.
STREAKS	Increase Temperature, Decrease Injection Rate, Increase Cooling Time.
WRINKLES	Increase Injection Pressure, Increase Holding Pressure, Decrease Temperature, Increase Holding Pressure Time, Increase Injection Rate, Increase Cooling Time.
SINK MARKS	Increase Injection Pressure, Decrease Temperature, Increase Temperature, Decrease Injection Rate.

Table 6.

Finally a proper degree of support (DoS) has been assigned to each rule: in particular the highest values has been assigned to the ones involving the injection pressure and the temperature due to their influence on process.

The defuzzification method used to obtain the output values has been the centroid method. The effectiveness of the controller has been verified through several experimental tests on the available extrusion machine. Some results are reported in the next tables: in particular table 7 shows some input parameters combinations and the corresponding detected defect; the adjustments suggested by the controller and the obtained results are reported in the next table 8.

Table 7.

N°	INPUT PARAMETERS						RESULTS				
	IP	BT	IR	CT	HP	HPT	IF	F	W	S	SM
1	55	250	99	1.8	35	0.1	1	0	0	0	1
2	55	250	99	1	35	0.1	1	0	1	0	0
3	70	270	99	1.8	35	0.1	0	1	1	1	1
4	70	250	99	1.8	50	0.1	0	0	0	0	0
5	70	250	70	1.8	35	0.1	1	0	0	1	0

Table 8.

N°	INPUT PARAMETERS						RESULTS				
	IP	BT	IR	CT	HP	HPT	IF	F	W	S	SM
1	70	250	99	1.8	35	0.17	0	0	1	0	0
2	62.5	250	99	1	35	0.1	0	0	0	0	0
3	70	255	99	1.8	35	0.1	0	0	0	0	0
4	70	250	99	1.8	35	0.1	0	0	0	0	0
5	77	250	99	1.8	35	0.17	0	0	0	0	0

The controller corrected almost all the defects previously detected. If these data are furnished again to the controller a complete correction is achieved (table 9).

Table 9.

N°	INPUT PARAMETERS						RESULTS				
	IP	BT	IR	CT	HP	HPT	IF	F	W	S	SM
1	70	250	99	1.8	35	0.1	0	0	0	0	0
2	70	250	99	1.8	35	0.1	0	0	0	0	0
3	70	250	99	1.8	35	0.1	0	0	0	0	0
4	70	250	99	1.8	35	0.1	0	0	0	0	0
5	70	250	99	1.8	35	0.1	0	0	0	0	0

4. CONCLUSIONS

In the paper a typical injection moulding process on a single-screw extrusion machine aimed to the production of axisymmetrical polypropylene dishes for alimentary use has been taken into account.

- Several experimental tests have been executed with different parameters configurations in order to train a neural network. The aim is to achieve a model able

to describe with good accuracy the process dynamics and the occurrence of defects. The validation phase highlighted a confidence level of 90%.

- An off-line controller based on fuzzy logic reasoning and on the expert skill has been developed. The controller is aimed to take in control the moulding process when a single or multiple defect occurs. The accuracy guaranteed by the controller was verified with experimental tests. The parameters tuning suggested by fuzzy controller gave an appropriate effect on process behaviour so that all defects have been avoided in a single cycle or in the worst cases in two moulding cycles.
- This quality control approach led to satisfactory results and could be applied with success in production. The advantages gained with this method are: i) Discards reduction; ii) Products quality improvement; iii) Local decision making with knowledge duplication. In this manner a non specialised manpower is able to conduct the process. The relevance of these advantages increases more and more, taking into account the low costs linked to the implementation of the proposed approach.

REFERENCES

1. Demirci H.H., Coulter John P., Güçeri S.I.: A numerical and experimental investigation of neural network based intelligent control of moulding processes, *Transactions of the ASME*, 119 (1997), 88-94
2. Wortberg J., Walter A., Al Haj Mustafa M.: On line quality and process optimisation in plastics processing, *Proceeding First ESAFORM Conference on Material Forming, Sophia Antipolis (F) 1998*, 433-436
3. Covas J., Cunha G.A., Oliveira P.: An optimisation methodology using genetic algorithms for solving polymer single screw extrusion problems, *Proceeding First ESAFORM Conference on Material Forming, Sophia Antipolis (F) 1998*, 429-432
4. Kwong C.K., Smith G.F., Lau W.S.: Application of case based reasoning in injection moulding, *Journal of Materials Processing Technology*, 70 (1997), 258-263
5. Shelesh Nezhad K., Siores E.: An intelligent system for plastic injection moulding process design, *Journal of Materials Processing Technology*, 63 (1997), 458-462
6. Seow L.W., Lam Y.C.: Optimising flow in plastic injection moulding, *Journal of Materials Processing Technology*, 72 (1997), 333-341.
7. Mamdani E.H.: Application of Fuzzy Logic to approximate reasoning using linguistic synthesis, *Proceeding IEEE Trans Computers* 26, 1977, 1182-1191.
8. Mamdani E.H., Efstaphiou H.J.: *Expert systems optimisation in process control*, Unicorn series Technical Press, 1986.
9. Babuška R., Verbruggen H.B.: An overview of fuzzy modelling for control, *Control Eng. Practice* 4 (1996) 11,1593-1606.

HARDNESS TESTS ON DAMAGED METALS

D. Antonelli and D. Romano
Polytechnic of Turin, Turin, Italy

KEY WORDS: Hardness Test, Damage, Quality Insurance, Computer Experiments

ABSTRACT: The development of cracks inside the material is usually investigated on the entire production by means of non destructive inspection techniques. Unfortunately, the progress of ductile damage cannot be observed with these techniques because of the small dimensions of the single cavity. In the present study we propose to employ a micro-hardness test to induce the presence and evolution of damaging inside the material. The influence of damage on the material hardness was assessed by Finite Elements numerical experiments. The study shows that changes in material porosity give rise to sensible changes in the hardness value.

1. INTRODUCTION

Hardness and micro-hardness tests are widely used in the mechanical industry, because they are non-destructive, easy to execute and not expensive. In metalworking processes the hardness is routinely measured on samples from production, as its changes after manufacture can be indirectly related to a modification of a number of material properties, like strain-hardening, residual stresses, crystalline grain modification. We propose to extend the scope of micro-hardness to another microstructural property, namely the internal damage in ductile materials.

The authors already proposed to link hardness to damage evolution, using an approximate model, in a study on multipass wire drawing [1]. As far as now, a reference framework for

this application is still to be outlined. Like in the case of thermal treatments, where tables exist to set the equivalence between the degree of quenching and Vickers hardness, it would be useful to get quantitative information on damage evolution from micro-hardness data.

The relationship between hardness and void density was investigated by using Finite Element numerical experiments. The experimental plan was set up to take also into account the possible interaction of damage with other material properties: yield strength and strain hardening exponent.

In the next section, the model for void insurgence and propagation in ductile material is described. In the third section, the Finite Element model of the hardness test is showed. The fourth section deals with the methodology used to guarantee accuracy in the empirical models drawn from the FE experiments; the fifth presents the experimental plans adopted and the resulting empirical models.

2. CONSTITUTIVE EQUATIONS FOR THE DAMAGED MATERIAL

Defect insurgence in highly deformed ductile materials is the effect of an evolutive process developing globally, though crack initiation usually takes place in a small portion only. A number of observations, dating back since the fifties, have definitely established the mechanism governing ductile failure.

The most consolidate model that embodies the inherently microscopic damage mechanism into elasto-plastic constitutive equations has been proposed by Gurson [2] and subsequently modified by Tvergaard [3]. They derived a new yield criterion from the Von Mises one, to be applied to "damaged" materials:

$$\Phi = \left(\frac{\sigma_{eq}^2}{\sigma_0^2} \right) + 2q_1 f \cosh \left(\frac{q_2 \sigma_m}{2\sigma_0} \right) - (1 + q_3 f^2) = 0 \quad (1)$$

where Φ is the yield function, σ_{eq} is equivalent stress for damaged material, σ_0 the yield stress of sound material, σ_m the mean normal stress and f the relative void volume fraction. The constants q_1 , q_2 , q_3 are parameters introduced by Tvergaard to obtain a better agreement with experimental data. For f values different from zero, the yield condition depends not only on the equivalent stress but also on hydrostatic pressure and void volume. It is worth noting that hydrostatic pressure and void volume interact with each other because positive mean stress causes dilatation while negative shrinks cavities; conversely variations in void volume affect yield function and hydrostatic pressure.

The study of deformation of a ductile damaged material is a coupled problem of mechanical equilibrium and void propagation. The void propagation law is:

$$\dot{f} = \dot{f}_{gr} + \dot{f}_n \quad (2)$$

where the subscript gr stands for void growth and n for nucleation of new voids. Void growth must comply with mass conservation law, written as:

$$\dot{f}_{gr} = (1 - f) \cdot \dot{\epsilon}_m^{pl} \quad (3)$$

in which $\dot{\epsilon}_m^{pl}$ is the sum of the three principal strain-rate components, i.e. the volumetric strain rate. The cavitation rate is ruled by a probabilistic strain controlled law, assuming that the critical strain at which voids nucleate follows a normal distribution around a mean value:

$$\dot{f}_n = \frac{v_n}{s_n} \frac{1}{2\pi} e^{-\frac{(\epsilon_{eq}^{pl} - \epsilon_n)^2}{2s_n^2}} \cdot \dot{\epsilon}_{eq}^{pl} \tag{4}$$

where v_n , ϵ_n , s_n are, respectively, the percentage in volume of void nucleating particles, the mean and the standard deviation of the critical strain.

Mechanical equations can be derived from the force equilibrium equations and the elastoplastic constitutive relations. The plastic part of these latter expresses the plastic strain rate tensor $\dot{\epsilon}^{pl}$ as a function of the stress tensor $\underline{\sigma}$ through the flow potential, that, actually, coincides with the yield function (1). Calling $\dot{\lambda}$ the derivative of the plastic hardening modulus, the plastic flow equation can be stated as:

$$\dot{\epsilon}^{pl} = \dot{\lambda} \frac{\partial \Phi}{\partial \underline{\sigma}} \tag{5}$$

In order to solve simultaneously the damage and the mechanical problems, it is necessary to introduce a further equation due to Gurson: the microscopic equivalent strain rate is assumed according with the plastic work rate expression:

$$(1 - f) \sigma_0 \dot{\epsilon}_{eq}^{pl} = \underline{\sigma} : \dot{\epsilon}^{pl} \tag{6}$$

To solve the fully coupled problem, we resorted to the numerical Finite Element simulation.

3. THE NUMERICAL MODEL

The simulation of the Brinell test was accomplished by indenting a cylinder with an infinitely rigid spherical body. Because of the axial-symmetry of the geometry, a two-dimensional model made up of quadrilateral axisymmetric elements was adopted (see Fig. 1).

Testpiece size was selected in order to avoid end-effects due to the borders. Brinell test specifications recommend a minimum distance of 2.5 times the indentation diameter between the impression and the border and a minimum thickness of 8 times the impression depth. Some preliminary simulations indicated that plastic strains are confined in a quite smaller area than elastic strains. So, a 20mm large and 20mm high cylinder (about 6 times the impression diameter) was used, far beyond the recommended limit values. The bottom of the cylinder is fully constrained, which is a consistent assumption when the testpiece's height is large compared with the impression's height. The challenging aspect of the simulation is the very small contact area compared with the large volume of the cylinder. As a matter of fact, stress gradients inside the material are very high and, even using a very dense mesh, only a small number of elements are subjected to plastic deformation.

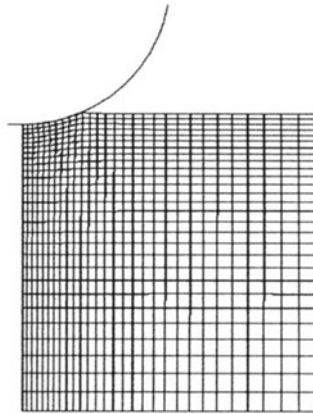


Fig. 1 - Mesh of the testpiece for the simulated Brinell test

The contact pressure, and consequently the contact profile, has to be predicted accurately because it is responsible for void closure. Biquadratic elements would have matched better with a spherical shape, but they have the drawback of a poor reproduction of contact pressure: as there are more normal vectors for a single element surface, small numerical errors in the interpolation of the contact normal induce a large error on the calculated contact pressure. For this reason bilinear full integrated elements were chosen, with a very fine discretization in the contact area.

Despite all the precautions, it was verified that the mesh density had still a not negligible influence on the simulation results; this problem is far more critical in Finite Element experiments where the mesh represents a very severe disturbance that can corrupt the reliability of estimates drawn from experimental results. Countermeasures to this problem are provided by the methodological approach described in the following section.

An elastic-plastic material with strain hardening was used. The plastic stress-strain law is:

$$\sigma_0 = K \cdot (\varepsilon_{eq}^{pl} + \varepsilon_0^{pl})^n \quad (7)$$

K is a material constant, n the strain-hardening exponent and ε_0 the residual pre-strain. When the equivalent plastic strain is null, the law (7) gives the yield stress Y , which is one of the factors considered in the experiment.

In order to guarantee comparability among different tests, the ratio between impression and indenter diameter is kept constant, imposing a fixed displacement in every simulation run and measuring the resulting load. The norm recommends an optimal ratio of 0.375, which is also the value that provides the geometrical similarity between Brinell and Vickers tests. The influence of contact friction is very peculiar. Even a small friction between the two surfaces modifies the distribution of the stress under the indenter, thus affecting the distribution of voids (see Fig. 2); nevertheless, the amount of friction does not modify significantly the hardness value, as some preliminary simulations showed. As a consequence the friction coefficient was not included in the experiment.

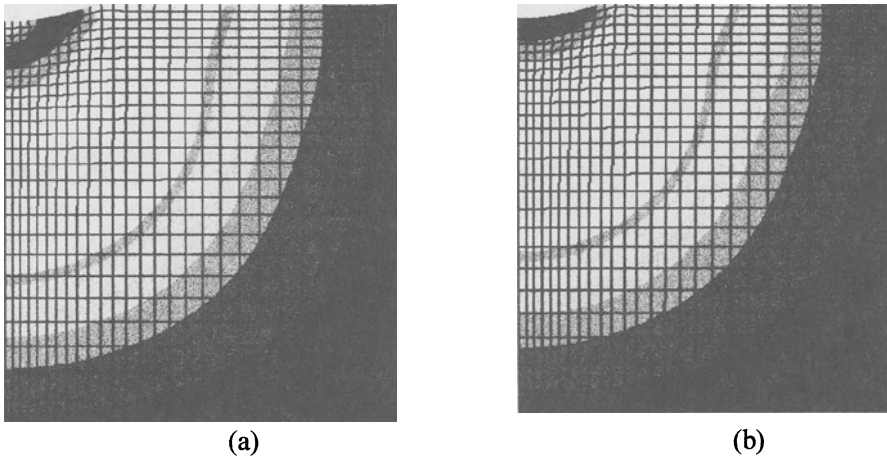


Fig.2 - Equivalent stress in the case a) with friction and b) without friction (dark gray in the bottom right corner stands for 50MPa, in the upper left for 900MPa)

Fig.3 shows the distribution of voids after one hardness test, starting from an initial void density of 4%. As can be expected voids close almost completely under the indenter, with a maximum closure rate slightly under the surface.

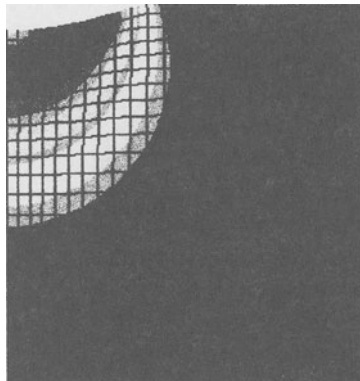


Fig.3 - Void distribution under the indenter (bottom right corner stands for 4% void density, dark gray in the upper left for 3%)

4. METHODOLOGY FOR THE NUMERICAL EXPERIMENTS

Increased computational power and availability of more accurate simulation codes make the numerical experimentation a valuable tool in many technical fields, from modeling of very complex systems to product/process design and optimization. *Design and Analysis of Computer Experiments* (DACE) [4] is a recent research sector, aimed at applying to

computer experiments the statistical methods used for physical experiments. The main objection to the application of DOE in numerical experiments is that outputs of a deterministic computer program are not subject to random variability, unlike the response of a physical test. However, in complex codes, like FEM codes, there are many parameters that affect the output in an unpredictable way. Examples are different solution algorithms (i.e. implicit or explicit solvers), elementary discretization intervals, convergence thresholds for iterative techniques. They are definite sources of uncertainty out of the user's control. This provides a strong conceptual foundation to the statistical treatment of numerical data coming from computer experiments.

One of the main sources of disturbance in FEM analysis is the discretization of the model's geometry. Both mesh's density and topology produce effects on the response which can be even more significant than engineering factors. The problem is sharpened because non linear contacts occur, where results are sensitive to the number of contacting elements.

Like every experimental disturbance, the noise due to the mesh can deteriorate accuracy of results either inflating the experimental error or, more dangerously, distorting the estimated effects of those engineering factors, which it has an interaction with. In general two options are available to protect the reliability of the estimates. The first is including the mesh as a random factor in the experiment. This means using the following model for the experimental response y :

$$y = \mu + \alpha(x_1, x_2, \dots, x_n) + \beta(x_1, x_2, \dots, x_n; \xi_1, \xi_2, \dots, \xi_m) + \varepsilon \quad (7)$$

where μ is the mean effect, the function α contains the deterministic effects of the control factors x_1, x_2, \dots, x_n , β contains the effects of mesh factors $\xi_1, \xi_2, \dots, \xi_m$, and conjoint effects between mesh and control factors, ε is the experimental error. The model (7) is very accurate but also very expensive due to the large number of factors (simulation with engineering factors at the same level should be repeated using different mesh).

The other possibility is to keep the mesh disturbance out of the model using some precautions to protect reliability of the estimates. In this case the model is :

$$y = \mu + \alpha(x_1, x_2, \dots, x_n) + \varepsilon \quad (8)$$

so that no additional experimental effort is required. Yet the error variance σ_ε^2 will be inflated and the estimated effects of x_1, x_2, \dots, x_n distorted by their possible interactions with the mesh. Two countermeasures can be taken: $\sigma_{y(\xi)}^2$ can be estimated through some *ad-hoc* initial simulations letting the mesh factors to vary; protection of reliability of estimated effects of engineering factors can be done by randomization of mesh factors, within a given range, in the experimental runs. Usefulness of the latter technique was demonstrated in [5].

5. RESULTS

The numerical experiments were aimed at two purposes. The first was determining the sensitivity of material hardness to porosity, compared with the well acknowledged effects of yield stress and strain-hardening. The second, consequent to the first, was to build an accurate empirical model able to predict the reduction in hardness due to material damage.

Computational complexity grows with the number of elements and this problem is even more critical for FEM experiments. Hence, the number of elements in the experiment's runs was kept under control.

A preliminary study on the effect of mesh density allowed to determine the mesh size which meets the accuracy requirements in the two experiments. Running a number of simulations where only the mesh density was varied an estimate of $\sigma_{HB(\xi)}^2$ for different mean levels of mesh density was obtained. The estimate of the variation coefficient $\sigma_{HB(\xi)}/\mu_{HB(\xi)}$ was 3.5% for a mesh size within the values 25x25 and 30x30 (horizontal x vertical element number). The first experiment was a central composite design with three factors (see table I), randomly selecting the mesh in the former selected range. Levels for void percentage are selected using a quadratic transformation in order to obtain a better accuracy around low values of void density. Results are summarized in a polynomial model where only statistically significant terms were included; the model is written using normalized variables so to evaluate directly the priority in statistical significance of the terms:

$$HB = 249 - 15.5 f + 52.8 Y + 7.56 n Y - 6.67 f n Y \tag{9}$$

The experimental variation is satisfactorily captured by the model having an adjusted determination coefficient $R_{adj}^2 = 0.96$.

Table I - Factors and levels in the first experiment

Factors	Levels				
	(-1.68)	(-1)	(0)	(1)	(1.68)
Yield stress, Y [MPa]	400	562	800	1038	1200
Strain-hardening, n	0	0.12	0.3	0.48	0.6
Voids percentage, f	0	0.16	1	2.54	4

Hardness sensitivity to void fraction is, as expected, quite high. Also the combined effect of void fraction with yield stress and strain-hardening is reasonably explicable. Effectiveness of voids in decreasing material hardness should increase in material with both a larger strain-hardening and a larger yield stress.

Taking for sure the presence of a substantial void effect, the following experiment was aimed at predicting in a more accurate way the expected decrease in hardness experienced by a damaged material. In the second experiment only two levels were taken for Y and n , given the lack of quadratic single effects in model (9), while keeping the five former levels for f . To provide a better accuracy a 5x2x2 complete factorial plan was used and more refined meshes were employed, so as to have a smaller $\sigma_{HB(\xi)}/\mu_{HB(\xi)}$, now below 1.7%. Once more, to protect the results of the experiment against possible interactions of the mesh disturbance with engineering factors, a randomization of the mesh size (within the range between 40x25 and 50x30 elements) was adopted. The following equation gives, for non coded variables, the expected relative decrease in hardness ($(HB(f) - HB(f=0)) / HB(f=0)$):

$$\Delta HB [\%] = (-6.47 + 3.86 n + 0.00101 Y) f \tag{10}$$

This model has $R_{adj}^2 = 0.95$ and a standard deviation of the estimate around 1.5; the statistical significance of each term is presented in Fig.4, left. The outstanding result is that the percentage reduction in hardness is far larger than the percentage void volume fraction in the material before the test (Fig.4, right). This implies that micro-hardness is a very sensitive indicator of the ductile damage. A set of experimental Vickers micro-hardness data are now being evaluated in the light of the previous model with interesting results.

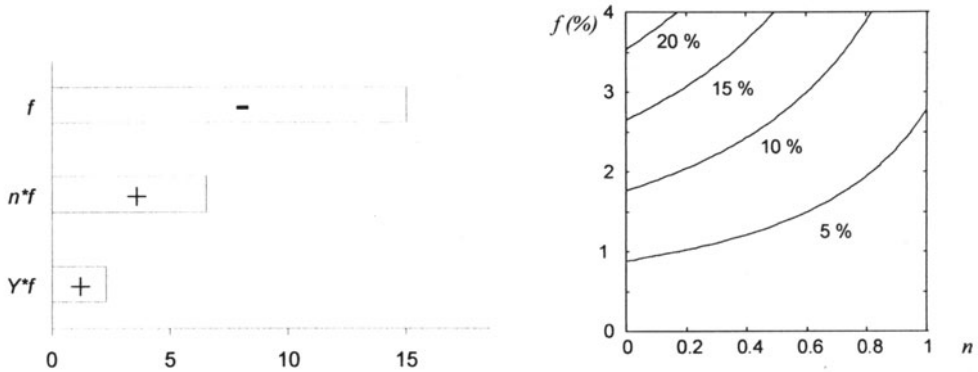


Fig.4 - Left: Pareto chart of calculated T values of the regression model (10).

Right: contour plot of ΔHB [%] as a function of f and n ($Y = 800$ MPa).

6. CONCLUSIONS

The study highlights the influence of material damage on the result of a hardness test. The purpose is to promote the use of the micro-hardness test as a reliable, sensitive and non intrusive inspection method to signal the presence of micro-porosity inside ductile materials. Numerical experiments show a significant relation between hardness and void density, and an empirical model is proposed, to be evaluated on an experimental basis in the future.

REFERENCES

1. Romano D., Antonelli A., Peuto A.M., Pettorruso S.; 1997, Evoluzione delle porosità dei fili di acciaio nella trafilatura multipla, Atti XXVI Conv. Naz. AIAS, Catania: 39-46.
2. Gurson, A. L.; 1977, Continuum Theory of Ductile Rupture by Void Nucleation and Growth: Part I - Yield Criteria and Flow Rules for Porous Ductile Media, Journ. Eng. Materials and Technology, 99: 2-15.
3. Tvergaard, V.; 1982, Ductile Fracture by Cavity Nucleation between Larger Voids, J. Mech. Phys. Solids, 30: 265-286.
4. Sacks J., Welch W.J., Mitchell T.J., Wynn H.P.; 1989, Design and Analysis of Computer Experiments, Stat. Science, 4, 4: 409-435.
5. Romano D., Vicario M.G.; 1997, Studio dell'attendibilità delle stime in esperimenti numerici non lineari agli elementi finiti, Atti Conv. SIS, Torino: 325-332.

ANALYSIS OF THE TOOL LOADING DURING FORWARD STEEL EXTRUSION

V. Stoiljkovic and S. Randjelovic
University of Nis, Nis, Yugoslavia

KEYWORDS: Extrusion process, Measurement sensor

Abstract

An accurate and precise analysis of any plastic metal deforming process implies excellent knowledge of the very technology of the process in question. It implies, first of all, an analysis of the parameters affecting the metal yield process as well as the possibilities of their changes in addition to the anticipated range in which the given parameters will be found. In order to define as well as present the given process as best as possible, it is necessary to choose an appropriate procedure as well as the measuring equipments and ways. This is directly conditioned by the knowledge of design and the technology of making the tools needed for the given procedure, as well as the procedure and the way of measuring the required parameters, in addition to their analysis and mutual dependence.

Published in: E. Kuljanic (Ed.) *Advanced Manufacturing Systems and Technology*,
CISM Courses and Lectures No. 406, Springer Verlag, Wien New York, 1999.

1. MEASURING METHOD DESCRIPTION

The analysis of the uni-direction extrusion process has been studied by many authors. First of all, this is a process of volume deforming in which the workpiece material, throughout the whole process, is subjected to overall pressure. Due to high surface pressure upon the extruder head and on the rigid matrix walls, the material flows (that is, it is extruded) towards the opening on the conical matrix surfaces. During the extrusion process the greatest forces occur in the extrusion axis direction, that is, upon the extruder head and on the matrix walls.

The satisfying matrix hardness and annulling of high pressure in the radial direction can be achieved in two ways. One of them is to increase the matrix wall thickness up to a certain limit thus getting the required matrix rigidity. The other solution comes up to the clamping ring application thus bringing the matrix body into a pre-stress state of the opposite sign with respect to the stresses occurring during the extrusion process itself. If, in the first case, we regard the matrix as a fairly thick pipe, of outer diameter D_1 , stressed by high inner pressure [1,5,6], then its walls are subjected to radial stress of pressure σ_r and tangential extension stress σ_t whose greatest value is on inner matrix diameter D_0 :

$$\sigma_r = -p \quad \text{and} \quad \sigma_t = \frac{a^2 + 1}{a^2 - 1} \cdot p = C \cdot p \quad (1)$$

where $a = D_1 / D_0$.

By superposing these two stresses, according to the plastic yield hypothesis, the following overall stress is obtained:

$$\sigma_u = \sqrt{\sigma_r^2 + \sigma_t^2} = p \cdot \sqrt{1 + C + C^2} \quad (2)$$

Assuming that, for instance, the outer matrix diameter is four times larger than inner diameter [36], that is $a = 4$ it is obtained that:

$$C = \frac{17}{15} = 1,13 \quad \text{and} \quad \sigma_u = p \cdot \sqrt{1 + 1,13 + 1,28} = 1,85 \cdot p \quad (3)$$

Along with further increase of the outer diameter the overall stress reduction in the matrix walls is not adequate. In the case that $a=10$, which is not quite justified in real exploitation conditions, it is obtained that $C = 1.02$ and $\sigma_u = 1,75p$, that is, the overall stress reduction is for 9,5% along with the outer matrix dimension increase for 2,5 times [3,5,6]. Since the matrix must remain in the elasticity range, that is, since there must be no lasting deformation ($\sigma_u < \sigma_e$) throughout the process, we can loosely determine the greatest value of the working pressure in the matrix made of alloyed tool steel which was subjected to heat treatment by quenching:

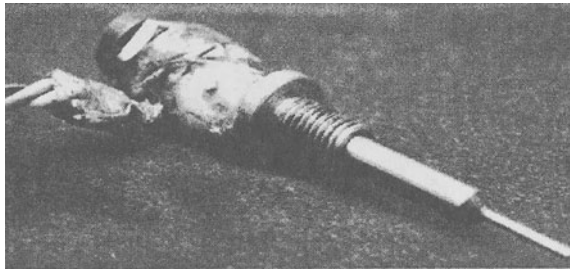


Fig. 2a. Sensor for measurement

The extrusion force upon the extruder can be measured in many ways. In this paper the choice is made of the measurement procedure by means of the universal pickup (200 t) which can be placed either in the upper or the lower part of the tool, as is the case here, through which the overall loading is transmitted along the extrusion axis. For the measurement of radial

forces, the measuring means of pin load cell method [2, 7] as the most suitable for this kind of the plastic metal deforming process (Fig. 2a, b).

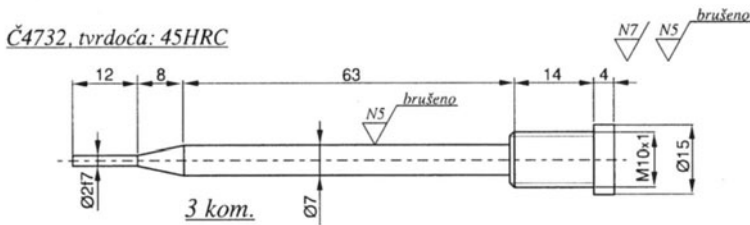


Fig. 2b. Pin load cell

In order to obtain complete information about magnitude and kind of stress throughout the extrusion process, the measuring sensors distribution is defined by the matrix geometry as well as the workpiece size. For these reasons, there are three sensors placed in the radial way in the extrusion matrix body at an angle of 120° with a measuring sensors that is in direct contact with the workpiece during the extrusion process. In order to obtain complete information about the loading magnitude during the process the measuring sensors are placed at various heights in the material receptor (Fig. 1b).

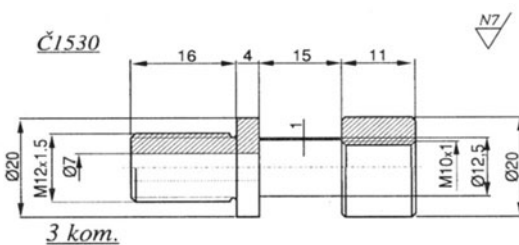


Fig.3 Measuring pipe

The loading due to the contact between the workpiece and three measuring sensors is transmitted to the measuring pipes (Fig. 2a and Fig. 3) placed on the outer matrix wall. Following of the extension of the wall which is 1mm thick, due to radial forces, will actually represent the loading magnitude on the matrix walls. On each pipes wall there are two measuring bands [8]

(measurement and compensation ones) glued and joined into a semi-bridge (Wheatstone).

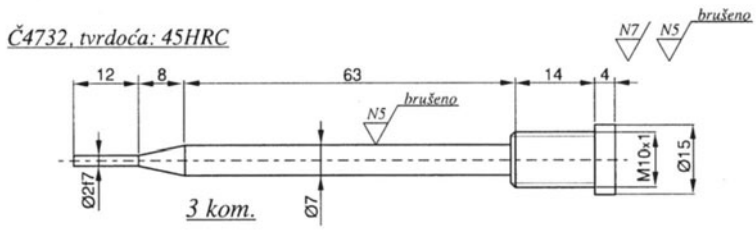
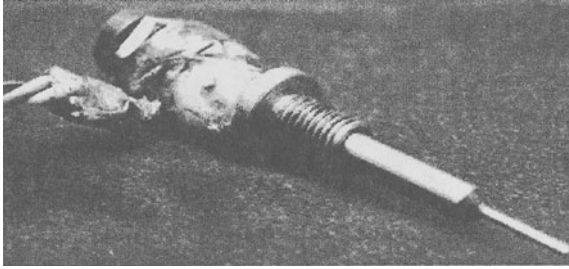


Fig. 2b. Pin load cell

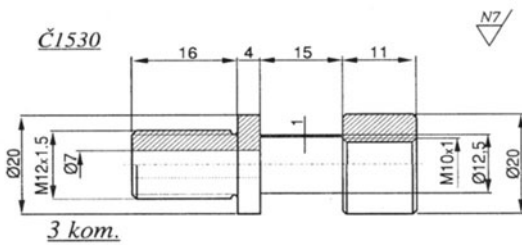


Fig.3 Measuring pipe

Since improvised sensors are dealt with, namely those whose characteristic is not known, it is necessary to carry out their calibration with known loading and thus to set up a relation between the pipe wall elongation and the force being transmitted. The calibration is done on the breaker machine at which it is possible to follow the exact loading increase. In order to record this characteristic as well, the data file with force magnitudes and respective number of micro deformations in the bush material elasticity area has been recorded.

In order to provide for variants of the presented tool solution, the very deformation focus (conical matrix part) and calibration zone are made in special inserts introduced (Fig. 4a, 4b) into the matrix body (tight fit, lap of 0,02 mm). The characteristic conical surface, upon the given inserts, has three values of the angle, namely 60° , 90° and 120° , which will directly affect both the extrusion forces and the radial forces in the tool.

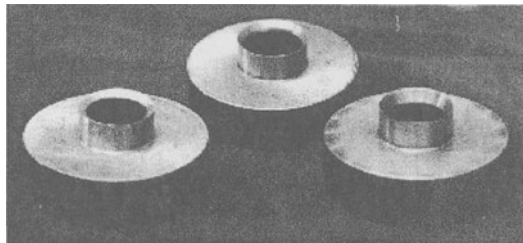


Fig. 4a.

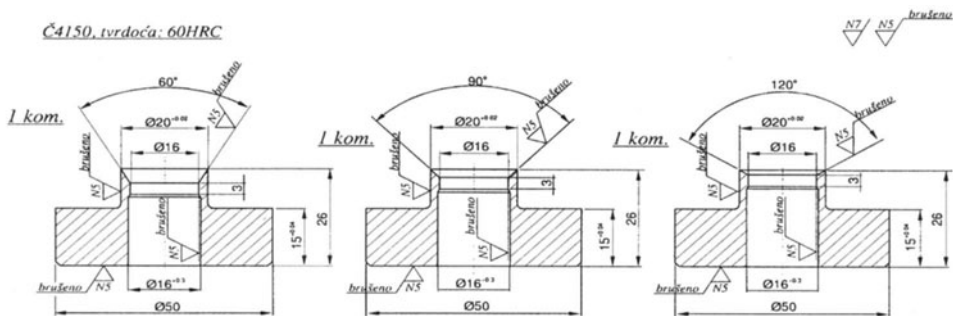


Fig. 4b. Extrusion inserts with various cone angles in the deformation focus

2. MEASUREMENT RESULTS

The described design solution has been used as an experimental tool upon which the measurement is done on the hydraulic press that provides for the force of 200 kN upon the extruder. The necessary tool elements needed for the metal extrusion process, namely, the extruder, the ejector, the connecting plates and the plates for the pressure transmission to the force pickup, have been provided from universal tool sets that have already withstood the exploitation conditions.

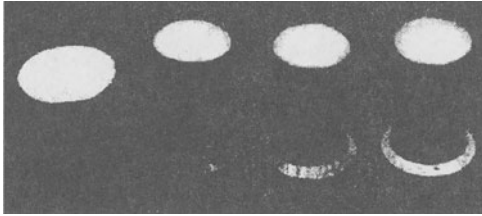


Fig.5. Workpiece and finished parts with various cone angle

The workpiece material is low-carbon steel C1220 that shows high plastic properties in the deforming process. The friction effect is lowered by the workpiece bonderizing procedure (placing of the film by the chemical procedure based on plant oils that tightly adhere to the metal surface and serves for better lubrication oil adherence during the deforming process). As the bonderizing layer itself reduces the friction effect in the process, some of the workpieces are

extruded with such a surface while a certain number of the workpieces being covered with an oil film that has further reduced friction in the deforming process (Fig. 5).

The coordinate system for presenting the results comprises a time x-axis at which the number of readings has been introduced, 800, together with a step, that is, a time interval between two signals from 0,003 seconds as well as y-axis at which the force in kN has been introduced. At x-axis one of its parts has been singled out at which the workpiece extrusion process and the extruded part ejection process have been marked.

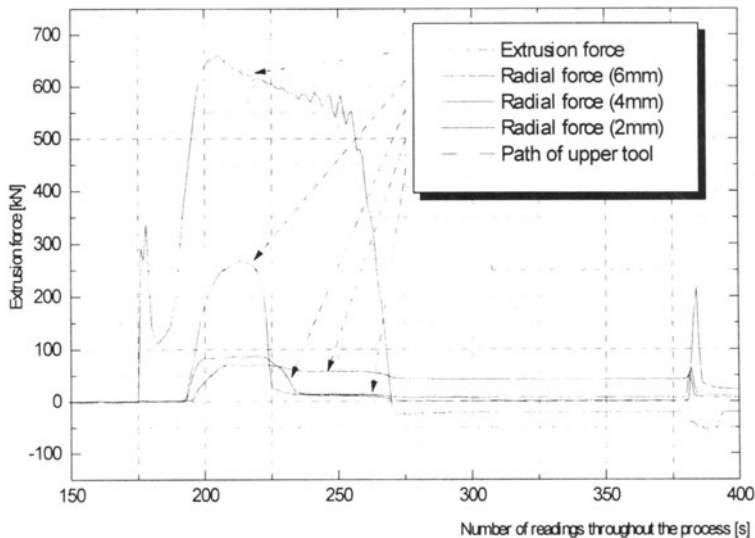


Fig.6. Force alteration for the case of uni-direction extrusion (cone angle $\alpha = 60^\circ$, without lubrication)

The measurement results show certain regularity so that similar effects (Fig. 6. 7. 8) can be noticed in all the extrusion processes. The force upon the extruder shows, before the very extrusion process, a marked instability as well as a very high increase after which it drops to its minimal value throughout the overall deforming process. The force instability as well

as its increase can be explained by taking the most favorable initial position of the workpiece in the tool as well as by the needed - quite high - force for the very beginning of the material flow on the matrix insert walls [4]. A marked force drop shows that the first phase has been completed, that is, that the material has filled up the input part of the cone; after that the force rapidly starts increasing reaching its maximum after which the material flow on the conical tool parts begins. The maximal value has a marked increase along with the matrix angle increase, while it slightly changes with alternation of the lubricant; it should be also stated that, in both the cases - when only the bonderized surfaces are oil-lubricated - there is a decrease of the friction coefficient. During the extrusion process, that is, throughout the material flow, the maximal force on the extruder has a slight drop with respect to the achieved maximal value, with smaller oscillations of the force when the extrusion process is about to end.

At all the diagrams the radial forces are denoted by the height at which they were measured. Namely, as there is a difference regarding the height of the place at which the sensors makes a contact with the workpiece; at every 2 mm from the upper edge of the matrix insert, at mutual angles in the matrix of 120° , there has been a different increase of the given forces recorded. In the beginning of the process, the maximal radial force is achieved at the highest sensor with respect to the matrix insert at the moment when the extrusion force achieves its maximal value, that is, when the initial unstable phase has been completed and the material flow has already started. This is explained by the very workpiece itself at this particular moment (barrel-like form in the receptor) and immediately after it, when the workpiece material has filled up the whole material receptor volume and when its "maximal diameter slides" along the matrix walls. After reaching its maximal value as well as its retention, this force drops to almost zero value. A less distinct maximum is reached by the radial force on the second sensor, at the height of 4mm from the matrix insert, but in almost identical period of time when the first radial force reaches its maximum. The lowest sensor with respect to the matrix pickup records almost the same magnitude of the radial force as that on the second sensor, but it can clearly be seen that it preserves this value, with some slight decline, till the end of the extrusion process since the non-extruded volume of the material from the receptor also remains at its height.

The extrusion force on the extruder has values ranging from 560 to 600 kN in the matrix with the smallest cone angle of 60° , that is, 660 to 690 kN for the matrix with the cone angle of 90° , or to 720-790 kN in the matrix with the cone angle of 120° . Reduced to the cross-sectional area of the workpiece, over which this force is transmitted, working pressures of 1900 - 2500 N/mm² occur in the extrusion process. The radial force on the matrix wall, depending on the cone angle, moves in the interval from 0.5 to 2.3 kN for 60° , that is, from 0.7 to 2.3 kN for 90° and 1 - 3.5 kN for 120° . The force increase follows the increase of the measurement place heights in the matrix wall. In the radial direction there are considerably smaller pressures and they move within the limits from 160 N/mm² to 320 N/mm².

On the right side of all the diagrams, there is a marked instability of all the forces associated with the ejection phase of the extruded piece from the insert and the matrix itself.

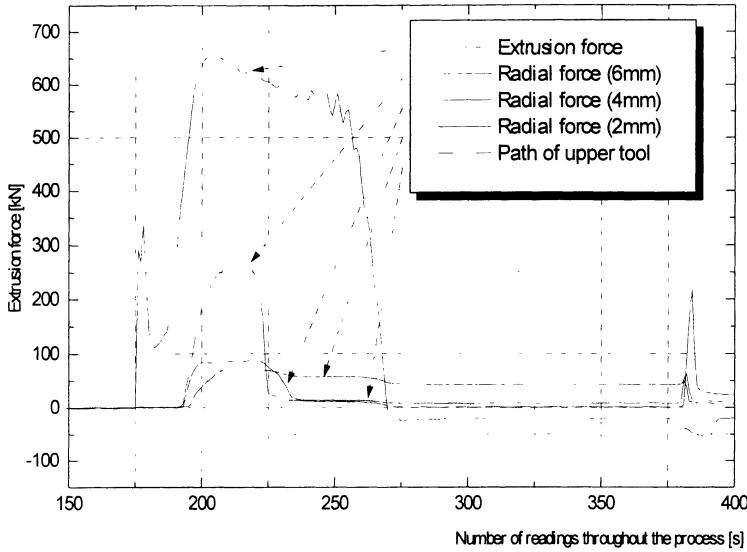


Fig. 7. Force alteration for the case of uni-direction extrusion (cone angle $\alpha = 90^\circ$, Without Lubrication)

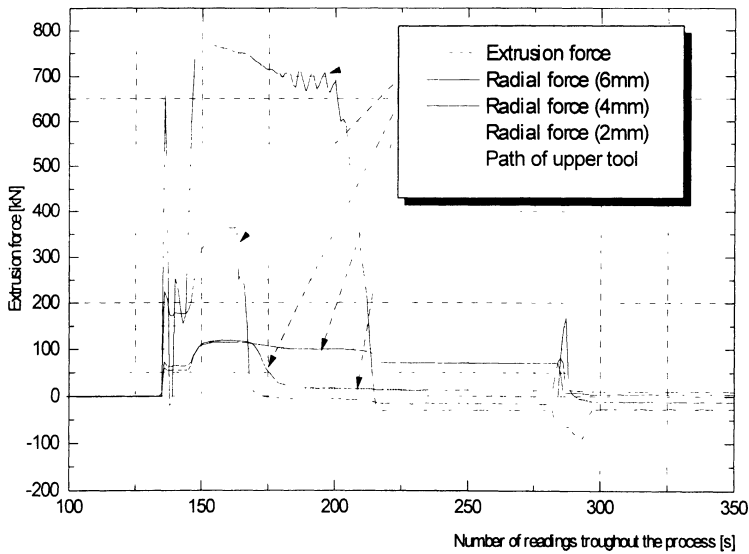


Fig. 8. Force alteration for the case of uni-direction extrusion (cone angle $\alpha = 120^\circ$, without lubrication)

3. CONCLUSION

The analysis of the tool loading points to the order of the loading magnitude as well as the force effect distribution in time during the process. The tool loading is of variable character and the order of the magnitude directly depends on the workpiece diameter, the finished part diameter and the extrusion angle in the deformation focus. The measurement itself aims at pointing to the loading magnitude at the contact surfaces while, in further work, this could serve as input data for solving the stress distribution equations with respect to the extruded part volume.

REFERENCES:

- [1] Johnson W., Mellor P. B., *Plasticity for Mechanical Engineers*, Van Nostrand Reinhold Company, London, 1962.
- [2] Jurkovic M., Jurkovic Z., Direct determining of stress and friction coefficient on the contact surface of tool and workpiece, *International conference on industrial tools*, pp. 127 - 132., Maribor, 1997,
- [3] Kanetake N., Lange K., Metal flow in the rod extrusion of rate sensitive materials, Nagoya University, Japan, pp. 493 - 498, *Advanced Technology of Plasticity*, Stuttgart, 1988.
- [4] Lange K., *Lehrbuch der Umformtechnik, Band 2, Massivumformung*, Springer - Verlag, 1974.
- [5] Musafija B., *Primjenjena teorija plasticnosti I i II*, Sarajevo 1973.
- [6] Musafija B., *Obrada metala plasticnom deformacijom*, Sarajevo 1988.
- [7] Plancak M., *Odredjivanje napona u procesima hladnog istiskivanja metodom vizioplasticnosti*, *Jugoslavenski casopis za obradu materijala deformisanjem*, Novi Sad, 1985.
- [8] Stoiljkovic V., *Merenje mehanickih velicina elektricnim putem*, Univerzitet u Nisu - Masinski fakultet, Nis 1980.

IMPROVING STEEL FORMABILITY BY CYCLIC HEAT TREATING

B. Smoljan

University of Rijeka, Rijeka, Croatia

KEY WORDS: Heat Cycling, Formability, Strain Hardening Parameters

ABSTRACT: The steel formability improving by cyclic annealing has been investigated. The performance of cyclic annealing in formability improving has been evaluated by the comparison with ordinary annealing. Better mechanical properties are obtained by the appropriate cyclic heat treatment than by isothermal annealing.

1. INTRODUCTION

Steel with good formability has small strength properties and high plasticity and toughness. Good formability can be obtained by the isothermal or cyclic heat treatment. Making the steel structure finer and more uniform is the most effective way of improving the plastic properties of steel [1].

One of the effective methods of the prior austenitic grain size refinement is temperature cycling. Grain size refining of steel, by temperature cycling could be based on repeated $\alpha \rightleftharpoons \gamma$ phase transformations [2][3].

Phase transformation, phase and thermal micro-deformation, which are developed during the temperature cycling are interactive processes, they affect each other, so that they by separate and by interactive manner can change mechanical properties of steel. However, in all these processes, the dislocation density increases, and strength coefficient can increase and formability of steel can be worsened.

Published in: E. Kuljanic (Ed.) *Advanced Manufacturing Systems and Technology*,
CISM Courses and Lectures No. 406, Springer Verlag, Wien New York, 1999.

The heating condition in temperature cycling is determined essentially by heating rate and maximum cycle temperature. The rate of heating depends on the mode of a heating, specimen dimension, and on the heat medium. Rates of specimen cooling and specimen heating should be undertaken in limits in which the dislocation density is not increases. Repeated cooling and heating should be done in furnaces for many steel kind. This kind of heat cyclic treatment is named cyclic annealing.

2. DEFINITION OF HEAT TREATMENTS

The investigations were done on steel Ck 35, Ck 45 and Ck 60 (DIN). Elemental compositions of investigated steels are shown in table 1.

Table 1. Elemental composition of investigated steel

Steel	C, %	Si, %	Mn, %	S, %	P, %
Ck 35	0.35	0.18	0.36	0.011	0.008
Ck 45	0.42	0.19	0.30	0.014	0.009
Ck 60	0.61	0.22	0.27	0.009	0.010

Heat treatments were done on bars with a circular cross section and with a specimen diameter of 16 mm and length of 60 mm. The specimens were treated by two different treatments, by ordinary isothermal annealing and by cyclic aneling. The investigated heat treatments are shown in Fig. 1.

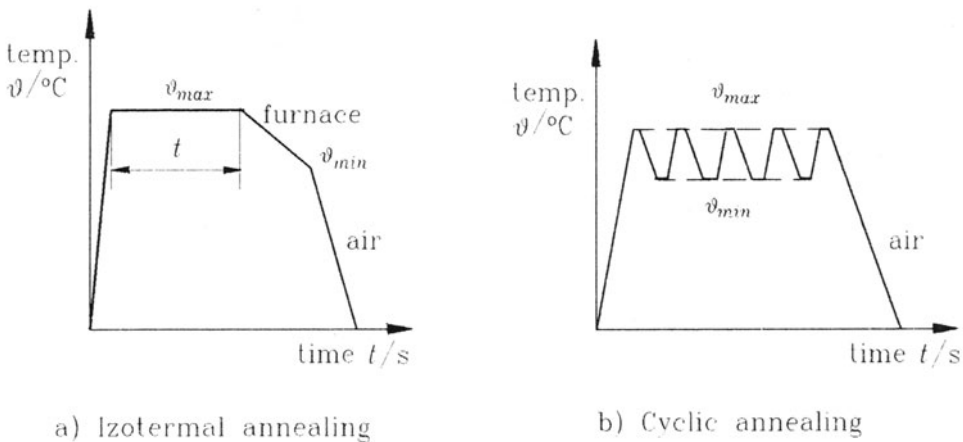


Fig. 1. Heat treatments

Heat treatments parameters are shown in table 2.

Table 2. Heat treatment parameters

Heat treatment	Maximum temperature $\vartheta_{max}/^{\circ}\text{C}$	Time at ϑ_{max} . t/min	Minimum temperature $\vartheta_{min}/^{\circ}\text{C}$	Heating rate $v_H/^{\circ}\text{Cmin}^{-1}$	Cooling rate $v_C/^{\circ}\text{Cmin}^{-1}$	Cycles number n
Isothermal annealing	830	60	600	5	2	1
Cyclic annealing	780	5	680	5	3	5

5. PERFORMANCE OF STEEL FORMABILITY IMPROVING BY CYCLIC HEAT TREATMENT

The true strength-strain curve is fundamental property that determines the steel formability [4].

The description of the stress-strain curves and strain-hardening of metals by mathematical expressions is frequently used approach. This is because it allows the plastic part of the curve to be treated by certain parameters that can be applied to the study of formability [4].

The most important and widely used application is the evaluation of stretch-formability by the n value, which is the exponent of the equation [4][5]:

$$\sigma = K\varepsilon^n$$

where:

σ - true stress, Nmm^{-2}

ε - true strain

K - strength coefficient, Nmm^{-2}

n - strain hardening exponent

The increase of steel formability released by cyclic heat treatment was estimated by comparing with the increase of steel formability released by isothermal annealing. The steel formability has been estimated on the base of true strength-strain curve. The true stress-strain curve has been determined by compression test by using the specimen with circular cross section. The used specimen in investigation is shown in Fig. 2. Holes with a diameter of 13 mm and deepness of 1 mm were filled-up by paraffin for reduction of

friction forces.

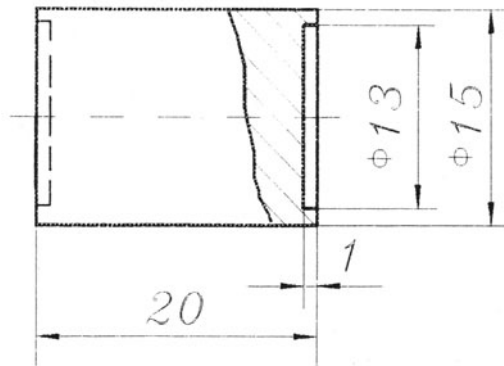


Fig. 2. Specimen

Results of strength coefficient and strain a hardening exponent released by different heat treatment of investigated steels are given in Table 3. Stress-strain curves are shown in figure Fig. 3.

Table 3. Strength coefficient and strain hardening exponent

Steel	Heat treatment	Strength coefficient K / Nmm^{-2}	Strain hardening exponent, n	Regression coefficient, r
Ck35	Isothermal annealing (IA)	915	0.18	0,962
	Cyclic annealing (CA)	844	0,225	0,966
Ck45	Isothermal annealing (IA)	1008	0.16	0,927
	Cyclic annealing (CA)	952	0,21	0,961
Ck60	Isothermal annealing (IA)	1120	0.155	0,948
	Cyclic annealing (CA)	1030	0,21	0,934

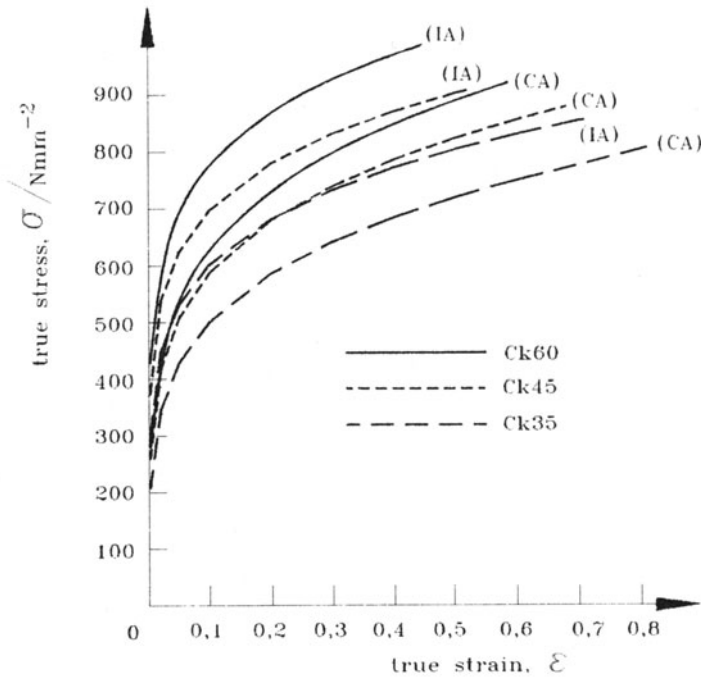


Fig. 3. Stress-strain curves

4. CONCLUSION

A steel with minimum carbon content has the best formability properties. All investigated steels have had better formability properties by application the cyclic heat treatment than by application of isothermal annealing. Plasticity and strain-hardening exponents are increasing and strength coefficients are decreasing.

REFERENCES

- [1] Anashkin, A. et all: Heat Cycling of Carbon Steel Wire, Metal Science and Heat Treatment of Metals, 1987, vol. 2, pp. 10-14.
- [2] Fedyukin, V.: Cyclic Heat Treatment of Steels and Cast Irons, Leningrad State Univ., Leningrad, 1984, pp. 51, (in Russian).
- [3] Konopleva, E.: Thermal Cycling Treatment of Low-Carbon Steel, Metal Science and Heat Treatment of Metals, 1989, vol. 8, pp. 617-621.
- [4] Kleemola, H.: On the Strain-Hardening Parameters, Metallurgical Transactions, 5,

1973, p. 1863-1866.

[5] ..., ASTM E646-84, Tensile strain-hardening exponents of metallic sheets materials.

[6] Rose A. et al: Atlas zur Wärmebehandlung der Stähle I, Verlag Stahlesen, Düsseldorf, 1958, pp. 128-134.

[7] Barsom J. and Rolfe S.: ASTM STP 466, American Society for Testing and Materials, 1970, pp. 281.

[8] Smoljan B.: Thermal Cycling Treatment of Steel for Quenching and Tempering, Amst'93, Udine, 1993, pp. 183-189.

INFLUENCE OF MICROSTRUCTURAL FACTORS ON FATIGUE BEHAVIOUR IN HSLA STEEL LAMINATES

M. Dabalà, G. Vedovato and M. Magrini
University of Padua, Padua, Italy

KEY WORDS: fatigue strength, HSLA steels, microstructures, spring steels

ABSTRACT: The high resistance to yielding of micro-alloyed HSLA steels (high strength low alloy) and their low cost, make attractive to use them to substitute spring steels, in applications where high strainings are required.

In the present paper it is evaluated the practicability of using Nb-alloyed HSLA laminates in the manufacturing of flat springs subjected to elevated cycles of straining.

The microstructural factors, influencing the fatigue resistance, are consequently analysed. It was found out that the strong anisotropy of the microstructure (caused by the distortion of ferritic grains during the rolling process), in presence of an high content of inclusion, influences the fatigue resistance. This was found to change strongly with the direction relative to the direction of lamination. The tests conducted demonstrated that the use is possible, but the inclusion content must be checked. Furthermore the greatest stress must be oriented transversally respect to the direction of lamination.

1. INTRODUCTION

Construction steels have not high mechanical proprieties, but they are cheap and they can be used at the «supply state» (without any thermal treatment).

Special steels have instead excellent mechanical characteristics, that can be obtained only after a series of thermal treatments, made by the purchaser. They have an elevated final price.

HSLA steels [2-4] are construction steels. They were developed to have mechanical properties comparable (even if not equal) to special steels. They have a good strength (yield point $\sigma_y = 350-700$ MPa) and they can be used without thermal treatments, with a final price just lightly higher than the normal construction steels.

The strength of these steels is increased altering their microstructure with the addition of microalloying elements (in quantity lower than 0,1%). These, after a thermomechanical rolling process, arise to a higher strength by means of the precipitation of their carbides and carbonitrides and of the refining of the grain.

A further increasing can be obtained with a strain-hardening by means of a cold rolling mill process [5], during the last phases of manufacturing. In this way the yield point is raised, but the grains are strained. This morphology induces an anisotropy of the mechanical properties. In the direction transversal respect the lamination direction, the steels present an higher yield point and a better tensile strength.

Also the fatigue ratio (ratio between fatigue limit and tensile strength), can change with the direction: these steels usually have the worst resistance to fatigue in the direction transversal respect to the lamination sense.

The anisotropy of the fatigue limit is originated by the presence of inclusions of lengthened shape that can be originated by the lamination process. The concentration of the stresses in proximity of these is higher when an inclusion, lengthened in the operations of lamination, is oriented transversally respect to the highest tension of traction.

2. AIM OF THE PAPER

Aim of the paper was to verify if it were possible to use HSLA steel in the manufacturing of flat springs, subjected to dynamic stresses. The modulus of resilience U_R of these steels is in fact so high, that they can substitute spring steels in many applications (some typical resilience modules are shown in tab. 1). Respect to spring steels, the HSLA steels have the advantage of a better formability, a better corrosion resistance and, above all, of a lower cost. Nevertheless, the behaviour in elastic field is affected by a greater number of structural variables and (as it was told) they don't have a perfect isotrope behaviour because they do not have a final thermal treatment.

Some cold flattened strips of Nb micro alloyed HSLA steel were tested; the influence of microstructural proprieties on their fatigue resistance was examined, with a special regard to the effects of anisotropy.

	U_R , kPa
Medium carbon steel	300
Spring steel	2200
HSLA steel (longitudinal direction)	900
HSLA steels (transversal direction)	1200

Table 1: Comparison of typical resilience modules of different types of steel

3. EXPERIMENTAL PROCEDURE

Three different strips of Nb microalloyed HSLA steel were examined. They were obtained with a driven cold flattening milling process. All the strips had a thickness lower than 0,5 mm.

Their compositions were analysed and the results are shown in table 2.

To characterise the material the following proprieties and characteristics were examined.

- *Ferritic grains.* A metallographic analysis was performed. The ferritic grains always resulted very elongated (fig. 1). Sizes and shape of ferritic grains were measured, according to the prescriptions of standard ASTM 112. In the strip 3 the dimensions of the ferritic grains resulted slightly bigger.

Strip	C %	Mn %	Si %	P %	S %	Nb %
1	0.066	0.340	0.014	0.012	0.004	0.056
2	0.056	0.347	0.009	0.010	0.004	0.055
3	0.054	0.351	0.011	0.010	0.004	0.056

Table 2: Weigth composition of the strips of HSLA steel

Strip	Longitudinal	Normal	Transversal
1	11±0.8	5.2±0.4	2.3±0.1
2	12.5±0.8	6.2±0.1	2.78±0.2
3	13±0.6	6.6±0.4	3±0.3

Table 3 Sizes and shape of ferritic grains

- *Inclusions.* The metallographic analysis revealed the presence of inclusions homogeneously distributed across the thickness of the samples, with a maximum diameter of 20 µm (figure 2). In the strip 3 a greater quantity of inclusions were detected.
- *Microhardness.* The values of microhardness were measured on three different planes (parallel, longitudinal and transversal respect to lamination plane). The medium values were 215, 210 and 216 HV₁₀₀. In the section normal respect to lamination plane, a remarkable increasing of the hardness in correspondence of the surface was observed.

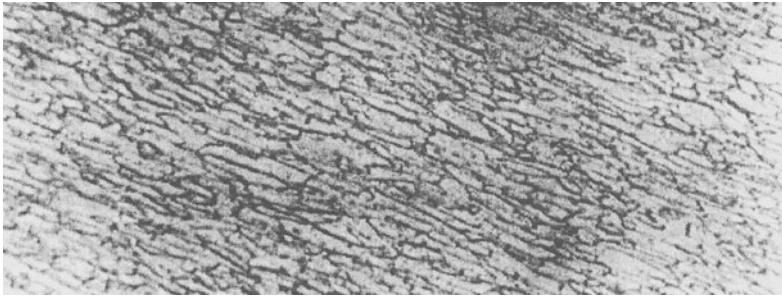


Figure 1: micrograph of the strip 3 (500×). Longitudinal section, normal to the lamination plane

- *Residual stresses.* The residual stresses were evaluated by means of X ray diffractometry. Their values were low and were homogeneous between the different strips.

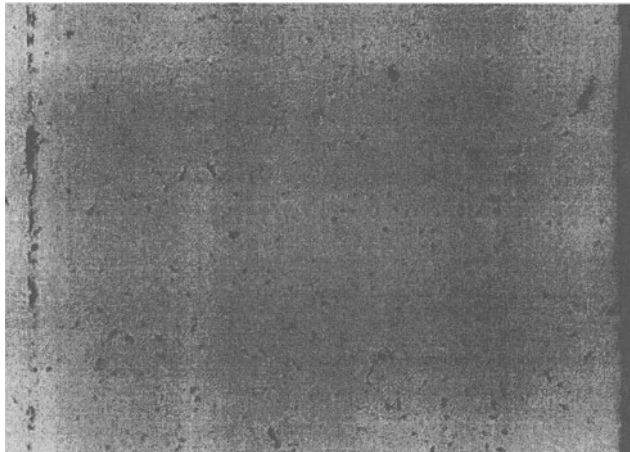


Figure 2: Micrograph of the strip 3. The high inclusional content is evident (200×). The sample is not attacked to evidence inclusions.

- *Mechanical proprieties.* To evaluate the strength of the steel the yield point and the tensile strength were measured. The results are shown in tab. 3. We remember that high yield point values can determine a good resilience (that is a typical propriety of spring steels).

Strip	Tensile strength [MPa]		Yield point 0.2% [MPa]	
	Transversal	Longitudinal	Transversal	Longitudinal
1	649	732	633	685
2	651	729	632	705
3	641	732	617	701

Table 4: tensile strength an yield point of the examined steels

After the characterisation of the steels, the fatigue tests were conducted: 15 samples were prepared (five for each strip) as in figure 3. A ferromagnetic core of soft iron was inserted in the central hole with a cold plastic deformation. During the fatigue tests the core (and thus the sample) was subjected to a vibration by means of an high frequency magnetic field. The force F_1 is originated by the magnetic field, the force F_2 is a force of elastic returning that was added in order to make asymmetric the load condition and to change the stresses with the direction. These were measured installing two estensometric washers in two points at 90° respect to the centre (fig. 3).

All the samples were fatigue tested for a total of 30 million of fatigue cycles.

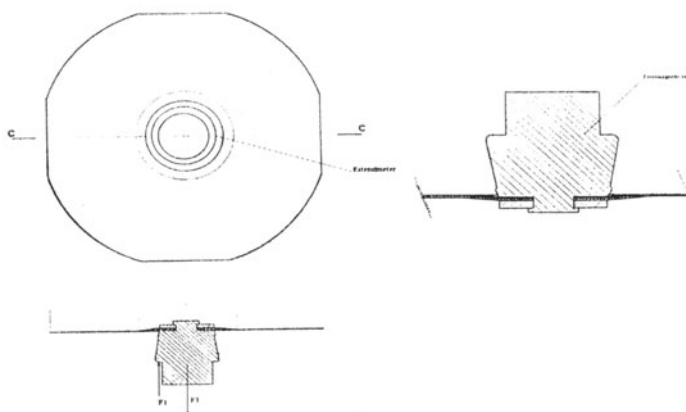


Figure 3: Test sample after the application of the ferromagnetic core. The points of application of the estensimeters and the applied forces are indicated

The temperature of the samples were maintained between the 15 and 30°C with to a current of air of 10 m/ s. The samples had different orientations respect the direction of lamination. The samples of the strip 3 (unlike the others) , did not overcome the test and were both broken. Both were this samples were disposed to be mainly stressed in the diagonal direction (respect to the direction of lamination). We remember that the strip 3 presented a higher number of inclusions and a lightly higher grain size (both these decrease fatigue resistance).

4. EVALUATION OF THE BREAKING CAUSES

Further tests were executed to evaluate the breaking causes. The so called «external factors» (such us load conditions, environment, temperature, etc.) were constant between the different samples and were not considered.

4.1 INTERNAL FACTORS

The following «internal factors» that influence the fatigue were analysed:

- *Sizes*

The sizes were the same between the different samples. The only uncertain size (the thickness) was measured and resulted homogeneous.

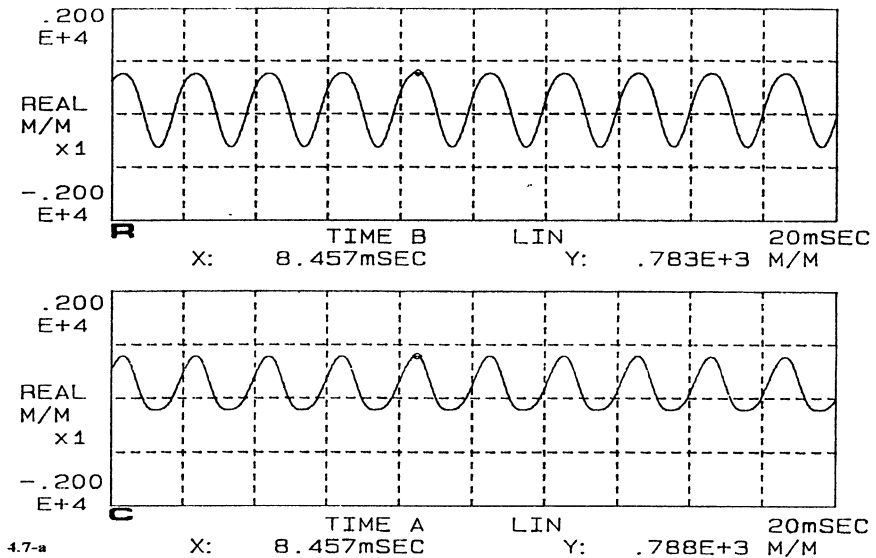


Figure 4: example of stress course in point A and B (sample 1). Radial and circumferential stresses are shown

- *Residual stresses*

As it was just told, there was not a remarkable differences between the different samples. They were considered to be not influent

- *Surface finishing*

It was the same for all the sample, it was considered to be not influent.

- *Material Drawn embrittlement [7]*

Laminates are very sensitive to drawn embrittlement [7], so it was verified that this was not the breaking cause. This is aroused by the presence of phosphor (that tends to segregate in

the grain edge), in this case the crack is intercrystalline. From the micrographic analysis the crack is instead resulted intracrystalline, that exclude the hypothesis.

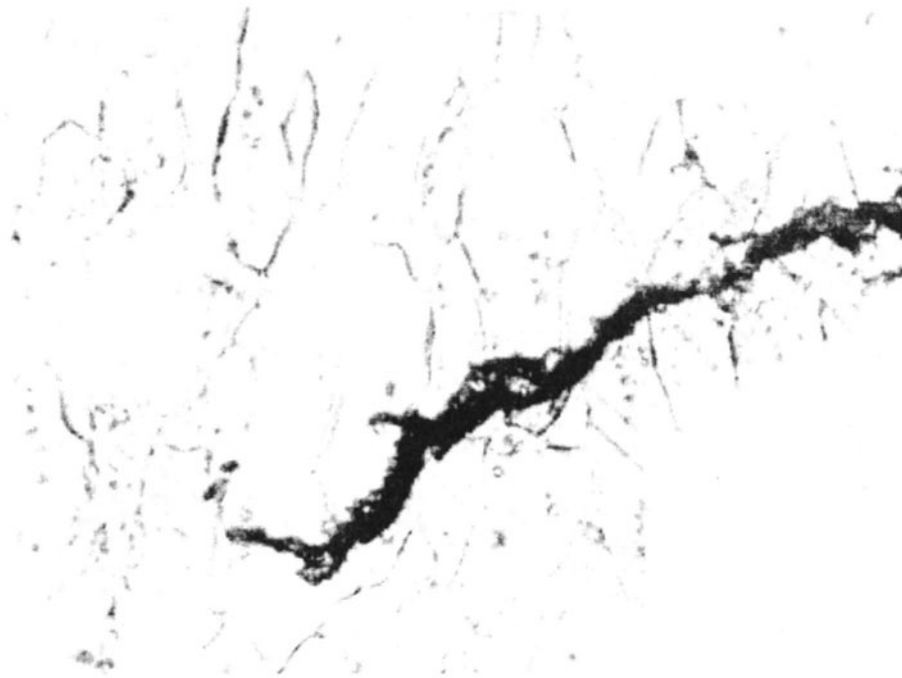


Figure 5: Micrography of a crack tip.

Chemical variability

The chemical composition was already measured, but the C e N and S content was controlled in each sample. The C e N content influences the interstitial content, and consequently the strength limit. It was higher in the first sample, but about equal in the two other, so it was not considered relevant.

The S content resulted low in all the samples an can be neglected.

	Strip 1	Strip 2	Strip 3
C wt%	0,080-0,110	0,050	0,050-0,060
N wt%	0,013-0,014	0,014-0,016	0,011-0,012
S wt%	0,005	0,005	0,004-0,005

Table 5: range of the C, N e S contents, measured in different samples of each strip

- *Microhardness*

A new relieve of the microhardness was effected along the diameter of the sample. The results were again homogeneous.

- *Grain sizes and shape*

As it was remarked the strip 3 has lightly higher size, but in a too small way to be relevant.

- *Inclusional content*

Regard to the inclusion content: there is no difference of shape and size between the three strips. The third strip has an higher inclusion content. The latter is the only remarkable difference between the different samples.

As a concluding remark the only parameter that can influence the fatigue strength is the inclusional content. Thus it is evident that the different behaviours were originated by the low transversal fatigue limit, the latter one is due by the high concentration of inclusions in this strip.

The effects of these inclusions, with the elevated plastic deformation, determine that the samples oriented transversally resist only 5,000,000 cycles, whilst the samples oriented longitudinally overtake with no problem 13,000,000 cycles.

5. CONCLUSIONS

The effected tests demonstrate that the HSLA cold laminated steels can replace the spring steels, in the applications where there is an elevated fatigue resistance. Some simple contrivance must be nevertheless used.

In fact the fatigue limit, in direction transversal respect to lamination direction, tend notably to decrease at the increasing of the inclusions content. Thus, the inclusion content must be checked; anyway the laminated must be oriented to have the maximum stress in a direction transversal respect the direction of lamination.

REFERENCES

1. Pickering F. B., in *Material Science and Technology*, Cahn R. W. *et al.* (Ed.), Weinheim, New York, Basel, Cambridge, Vol. 7, 1992, 335
2. Kohzazu I., Ouchi C. Sampei, T. Okita, in *Microalloying 75*, Korchynsky, M. (Ed.), New

York, Union Carbide Corp., 1977, 100

3. Le Bon A. B. de Saint Martin T., L. N., in *Microalloying 75*, Korchynsky, M. (Ed.), New York, Union Carbide Corp., 1977, 72

4. Tanaka T., Tabata N., Hatomura T., Shinga C., in *Microalloying 75*, Korchynsky M. (Ed.), Metals Park (OH), ASM International, 1986, 243

5. Hudd R. C., in *Material Science and Technology*, Cahn R. W. *et al.* (Ed.), Weinheim, New York, Basel, Cambridge, Vol. 7, 1992, 218

6. Dieter, G.E. *Mechanical Metallurgy*, Mc Graw Hill, London, 1988, 282

7. Honeycombe R. W. K., in *HSLA Steels – Metallurgy and Applications*, Gray J. M. *et al.* (Ed.), Metal Park (OH), ASM International, 1986, 24

INCREASED EFFICIENCY RESULTING FROM A DETAILED ANALYSIS OF THE INTERFACE BETWEEN FORGING AND MANUFACTURING

O. Krimmel

Norwegian University of Science and Technology, Trondheim, Norway

K. Martinsen

Raufoss Technology AS (RATEC), Raufoss, Norway

K. Tonnessen

SINTEF, Trondheim, Norway

F.O. Rasch

Norwegian University of Science and Technology, Trondheim, Norway

KEY WORDS: Quality Assurance, Optimisation, Machining, Forming, Tolerances, Process Control

ABSTRACT: The efficiency of a production chain that includes different processes is strongly influenced by the quality of the parts delivered from one production process to the next. In the present case, the machining costs for forged parts in multispindle chucking automatics are strongly influenced by their dimensional variations. Quality assurance of forged parts is challenging because of their complex shape. Acceptance criteria for dimensional variations that can be accepted by production departments succeeding forming are difficult to describe and to measure. Consequently, there exists only little knowledge about process capabilities for forged parts in general. Often, machining and assembly can not even give sufficient information about their requirements and therefore experience disturbance of their production. A discussion and case study about this will be presented in this paper.

1. INTRODUCTION

The article is a discussion about the optimisation problems of two subsequent production departments in large series production including forming processes and a subsequent process like e.g. machining. It is based on experience gained from the production of forged workpieces. A method of approach to solve existing problems in the production chain is presented which starts from the oral definition of a problem. Assuming that the problems are caused by unexpected dimensional variations, the relevant dimensions are identified and their process capabilities are quantified. Then, all the possible ways of improvement

for the incapable processes are discussed. The particularities of process control in metal forming processes are described. A case study of a problem solving process is provided.

The quality of formed parts strongly influences the costs in the forming as well as in the machining department and therefore the total production costs. Loosely estimated tolerances may cause problems in succeeding operations, while unnecessarily tight tolerances escalate the manufacturing costs in forming. This is illustrated in Figure I, which shows that there is an optimum quality level (100%) that leads to minimum costs. It has been tried to find optimum tolerances by calculating the costs during the production process for the simpler case of machining operations (/11/, /16/). In this paper however, it is assumed that finding tolerances that are acceptable for all the production departments is very close to the economic optimum. The article concentrates on geometric tolerances; not quantifiable criteria like optical and metallurgical criteria e.g. cracks will not be discussed. It is assumed that total costs can be significantly reduced by clearly defining an interface between forming and machining and thereby increasing the overall equipment efficiency (OEE) /17/.

$$\text{OEE [\%]} = \text{Quality Rate} * \text{Performance Rate} * \text{Availability} (1)$$

This can be done by:

1. Reducing the number of defect parts
2. Increasing the production speed to the limit of the capability of the machine tool (reduce idling due to insufficient part quality).
3. Reducing downtime (Set-up time, disturbance etc).

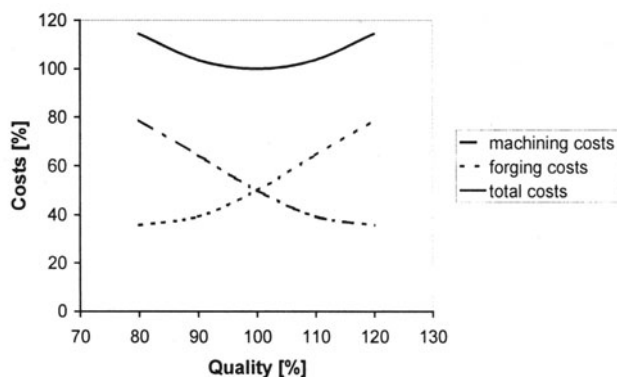


Figure I: Total costs as a function of the quality of the parts

The quality of parts is specified by the requirements that are documented in the technical drawings, i.e. the interface between forming and machining, and the degree of their fulfilment.

Most of the relevant acceptance criteria for forged parts are covered by simple linear measures /1/. However, these often do not reveal the behaviour of forged parts during further production steps or of the finished product. Even if the parts have been produced within the tolerances, disturbance occurs, e.g. difficulties during clamping of the forged parts in machining. In this case, the specification of the part is insufficient. Especially,

The next step is to take sample parts from the production and to measure these criteria in order to determine the appropriate approach to solve the quality problem. Process capability values are calculated from the distribution of the measures. The c_m - and c_p - values have been used to describe the capability (/2/, /15/). The c_m - value, i.e. the machine capability, is a measure for the short-term process variation whereas the c_p - value shows the long-term variation including wear, changing operators, different raw materials etc. By its nature, the process capability varies more than the machine capability. In our case, the c_{pk} - value would be misleading. A low c_{pk} - value can be due to bad centring or to too large variation of the process. Whereas centring is simply solved by adjusting the size of the tool, process variation needs different approaches:

1. $c_p > 1,3$: The problem hasn't been defined properly. Either wrong dimensions or wrong tolerances have been chosen. The quality problems might even be of a totally different nature and not even due to the formed parts (e.g. the assembly process).
2. $c_p < 1,3$ and $c_m > 1,3$: If the relevant dimension can be controlled by the operator, the necessary measurement facilities should be provided, e.g. gauges. As the here tested dimensions often have never been measured before, the operator or the die maker often simply never adjusted the process according to the requirements.
3. $c_m < 1,3$: The forming process is not capable of producing the required quality. Nevertheless, the objective of the process capability is now clearly described and relevant measures can be taken.

Monitoring an incapable process doesn't help much /5/ if the dimensions have been measured previously but not documented. More precisely, the definition of relevant criteria solves the problem, not the documentation. Keeping within tolerances with the required process capability requires even more than just to produce with zero defects /3/.

Three ways to attain the required process capability can be seen from formula (2). USL and LSL are the upper and lower specification limits and σ is the standard deviation of the characteristic /13/:

$$c_p = \frac{USL - LSL}{6 \times \sigma} \quad (2)$$

1. The tolerance has to be wider, i.e. the difference USL-LSL must be increased.
2. The variation of the process capability has to be reduced.
3. Alternation of the process, i.e. additional production steps like a 100% control, rework for the incapable dimension, or the application of different technology, e.g. machining instead of forming.

The objective can be reached by only taking one of the three measures or by a combination of them. After the process capability has reached a satisfactory level, no disturbance in the succeeding production steps should occur anymore. Under such an optimisation process, the following should be provided to the operators in the forming department:

- Special drawings that reflect only the set-up and running criteria of the parts regarding machining, assembly and function.
- Facilities for measurement and control.

form and positional tolerances like roundness or squareness have to be measured in addition to the linear measures.

2. METHOD OF APPROACH

The starting point for the optimisation is an existing problem in a production department subsequent to forming e.g. in the machining department. This problem is mostly only described orally. As the first step to solve this kind of problem, the relevant dimensions and the acceptable tolerances have to be defined. Making an orally formulated problem measurable generates facts and is the basis for the solution of a problem it has so far been accepted to live with. The method is visualised in Figure II.

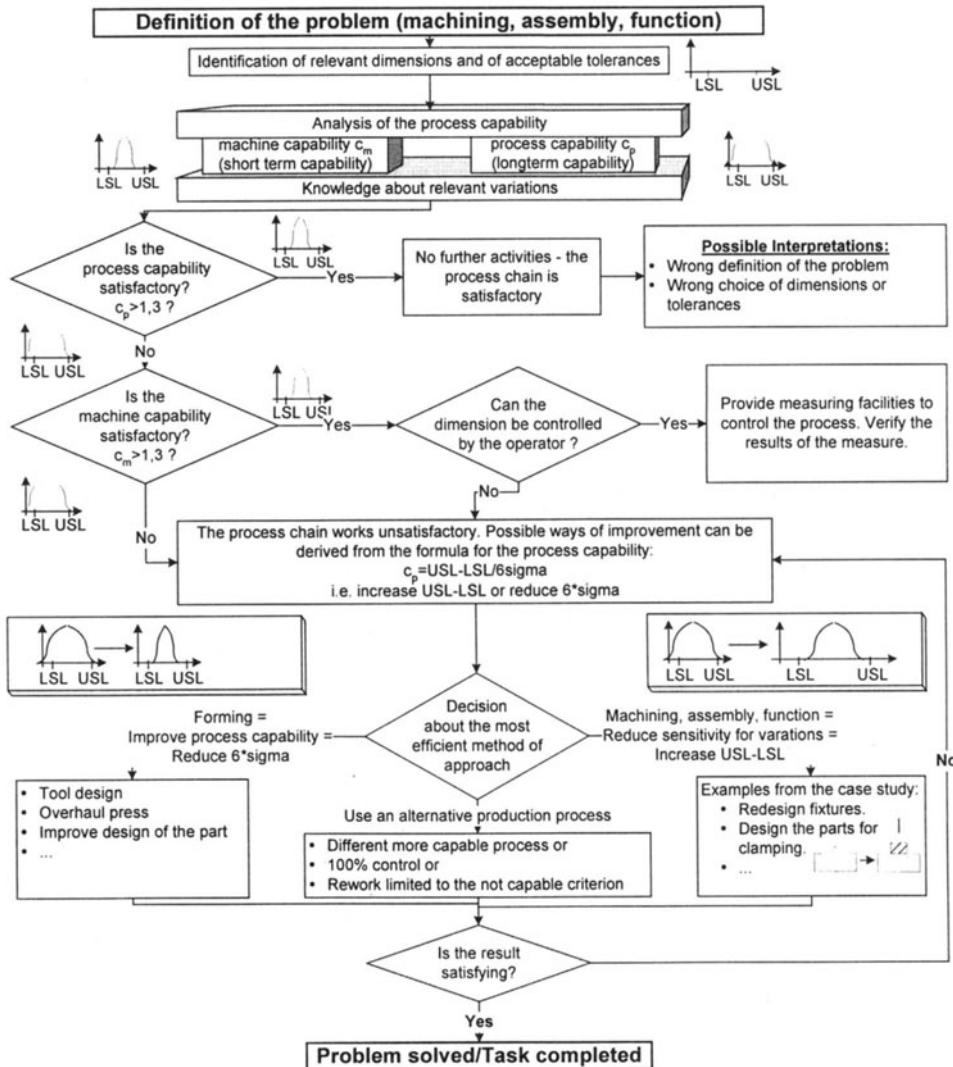


Figure II: Method to improve the process chain

Following the method described above, the following steps have been taken:

- Tolerances, that are assumed to be acceptable for the forming department and for the clamping fixtures have been estimated. They have to be estimated, because the true requirements of the fixtures are not known. The dimensions that are relevant for the clamping are the diameter, the roundness and the matching of upper and lower die.
- The measurements have been done on a co-ordinate-measuring machine.
- The data have been analysed statistically.

Tolerating in forming is often based on experience and can be supported by standards, e.g. DIN 17673 /14/. If the tolerating has been done properly, the tolerances should be neither too wide nor too narrow with respect to the variation of the process. The machine capability for a diameter of the workpieces is shown in Figure III. Obviously, it is satisfying ($c_m = 4,191$) but not centred.

Figure III: Machine capability of a diameter – histogram and probability paper

As stated by many other authors, c_p - or c_{pk} -values can't describe the process capability of single sided tolerances. These are based on the standard distribution, which is symmetric (and have a tail that goes to infinity in both directions). Single sided criteria have a range from $[0;\infty[$. To handle the distributions, which can be observed for single sided criteria, one can either calculate the process capability values from single sided distributions like the Weibull or the gamma distribution /3/ or compensate for the skewness of the distribution as if the range would be $]-\infty;\infty[$. Although the theory for a compensation for the skewness of the distribution has been discussed in literature (/8/, /9/, /10/), this is applied in industries only to a limited extent. Neither are process capability studies that are based on other distributions than the standard distribution widely applied.

Dimensions that are not important for the operator must be excluded to keep the drawing as simple and as easy-to-follow as possible. For example, dimensions given by the geometry of the tool or with wide tolerances need not to be controlled by the operator, only by the die maker. The criteria are therefore also called equipment maintenance parameters /2/.

3. PARTICULARITIES OF PROCESS CONTROL IN FORMING

Controlling a process requires both effective control parameters for the process and quantified control criteria, i.e. measurable dimensions. Both are much more difficult to handle than for machining processes. This is explained in the following tables. See Table I for a structured analysis of the processes forming and machining.

Differences between forming and machining processes	
Machining	Forming
Control of the process to achieve the required the dimensions	
<p>Control parameters:</p> <ul style="list-style-type: none"> • Depth of cut influences directly the relevant dimension. • No cross influence – the depth of cut influences only one dimension, which in turn isn't influenced by other parameters. • All relevant dimensions can be controlled separately. • Short adjusting time, the result is visible at once. • Automatic control possible because of the simple relation between parameter and effect. 	<p>Control parameters:</p> <ul style="list-style-type: none"> • Travel in feed direction (excenter press) or force (hydraulic press). • Lubrication. • Dimensions and mechanical properties of the parts. • Adjustment of the forging tool (expensive solution, takes a long time, additional tests of the forging tools might be required). • Unclear relation between control parameters and effect. <p>Technical particularities:</p> <ul style="list-style-type: none"> • Delayed effect of the control action, e.g. annealing for forging. • Variations depend on the material flow, i.e. it is influenced by strains and tensions of the deformation of the workpiece. • The effect of variations of process parameters is not clearly defined. Side effects on other characteristics are common. • Variations in preproduction and material properties influence the variations of the finished product, i.e. casting and heat treatment:
Obstacles for improvement	
<ul style="list-style-type: none"> • Low costs for measuring devices. • Measuring devices are easy to operate. • Statistical process control is widely used and benefits of SPC are undoubtedly accepted 	<ul style="list-style-type: none"> • Often more expensive measuring equipment required. • In some cases difficult to operate measuring equipment (e.g. coordinate measuring machines). • Traditions in the field of quality control. • Improvement takes a long time and demands a considerable effort. • Many additional criteria have to be controlled (e.g. cracks, surfaces etc).

Table I: Characteristics for the control of machining and forming processes

The manufacturing of formed workpieces is of sophisticated nature. To be able to assure good quality, extensive pre-production trials, the use of high quality raw material for the workpieces and the measurement of some dimensions that give an instant impression about the condition of the forming process are methods commonly used. This is supported by the regular inspection of the tool and preventive maintenance of the facilities /1/. Extensive measurements during the production in forming are not common because of the differences in measuring of formed and machined workpieces as illustrated in Table II.


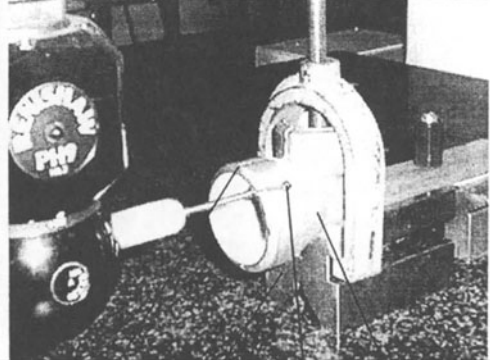
Machined workpiece, e.g.: turning	Formed workpiece, e.g.: forging
	
<p>(1) (2)</p> <ul style="list-style-type: none"> • Small measurement error due to good interface between the measuring device and the workpiece. E.g. a test table can be a satisfying reference area for the workpiece as well as for a probe (1). • The result depends only to a minor degree on the measuring position (2). • The measurement can easily be described by referring to a standard. • The repeatability is therefore satisfying and independent of the person who measures as long as he measures according to the description/standard. • The measurement can often be as simple as the distance between two points. 	<p>(1) (2) (3) (4)</p> <ul style="list-style-type: none"> • Burr strongly influences the measurability (1). • Often inappropriate interface between measuring equipment and workpiece (2). • Influence of the measuring position due to form errors due to blast cleaning and polishing (3). • Most surfaces are conical or inclined and are therefore difficult to measure (4). • Many tolerances are set in technical drawings, some of which are irrelevant for the operator. • Inappropriate qualification of operators. • Hot workpieces. • Heavy workpieces. • High production speed limits quality control

Table II: Characteristics for the measurement of machined and formed parts

4. CASE STUDY OF TODAY'S SITUATION AT RATEC

At RATEC the parts are forged from extrusions and afterwards machined in multispindle chucking automatics. Some of the most important problem areas today are:

- Clamping.
- Air machining, i.e. machine goes often at cutting feed velocity to reduce the consequences of unexpected tool-workpiece contact.
- Parts contain unnecessary material that either has to be machined or is delivered to the customer although the material is not necessary for the function of the product.

This case study is focused on the clamping problem. Two jaws that have a shape similar to the forging tool clamp the workpiece. The part is supposed to be in contact with the jaws over wide areas of the entire surface. However, for some parts sudden movements of the part in the fixtures are observed. This leads to tool breakage or faulty parts despite careful set-up. An analysis of the contact areas between workpiece and jaws by colouring the workpiece with touching ink showed that the clamping points are very few, not evenly distributed and always different from part to part. This is due to dimensional variations.

For the machining processes, the tolerances are not kept satisfactorily for the existing set of clamping fixtures. The dimensions are generally badly centred with low variations (satisfying c_p / unsatisfying c_{pk}). In order to achieve an economic solution, it seems appropriate to focus on making the fixtures more tolerant towards variations of the forged parts. The dimensional variations that have been found allow redesigning the fixtures with the following characteristics:

- Elastic jaws with some degrees of freedom
- Clear definition of the contact points.
- The fixtures should be less sensitive to wear; i.e. the wear of the jaws should not alter the behaviour of the fixture.

The second approach, i.e. to reduce the standard deviation σ of the forging process will not be regarded during this project. Nevertheless, the forging department is in a constant improvement process and the improvement of the process capabilities of the forging tools has been observed.

5. RESULTS

Deleryd has analysed the use of process capability studies in Swedish companies /4/.

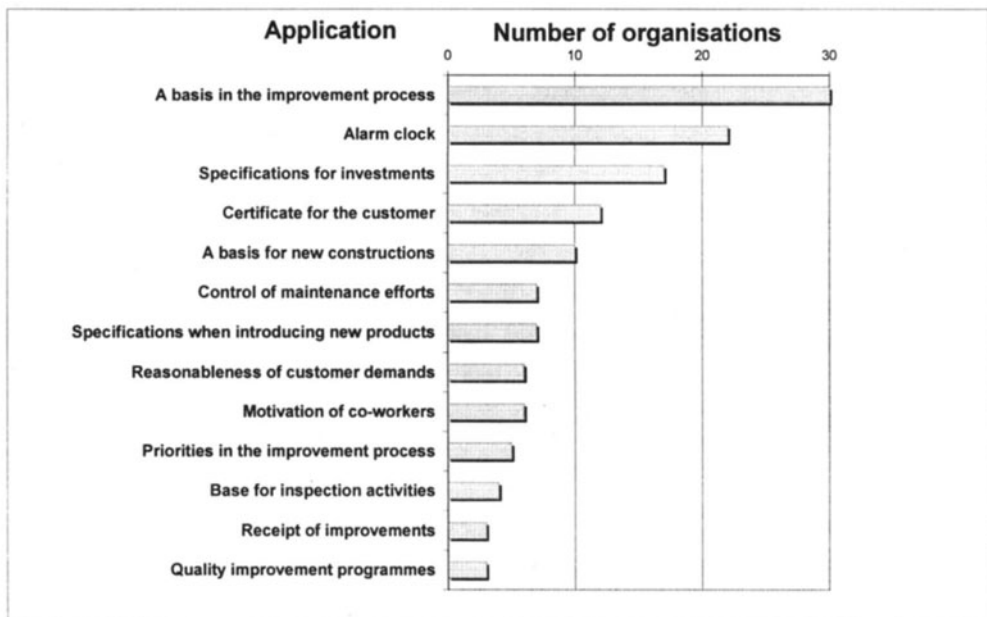


Figure IV: Benefits of the information gained from process capability studies /4/.

The quantity of the quotation of the different applications provides a good structure of the benefits of process capability studies, which helps to structure the results of this project:

- The study is the basis to improve the machining process. Only a thorough understanding of the quality of the preproduction process can provide the ability to adapt to these conditions.

- The studies can serve as an alarm clock. If anything is going dramatically wrong in forging, it will be discovered by measuring the critical acceptance criteria.
- The variations observed for one workpiece allow predicting variations of newly developed products. Tolerances can be set before the first production.
- It is motivating for the operators to feel safe about the products that they deliver. Surprising rejections become rarer.
- Preference for improvement will be given to processes with low process capability.
- Presses and forming dies are inspected in case of deteriorating process capability.
- The project is part of a quality improvement program.

Some of the points listed above require establishing a constant process control of the dimensions. The economic benefit has to be assessed for the specific cases.

6. CONCLUSION

1. Problems that arise due to the interface between forming and machining can only be solved by carefully defining the geometric tolerances of the parts. By doing this, a production chain including a forming department can be optimised.
2. In the case of an inefficient process chain three different ways of approach to improve the process chain are basically possible.
3. Technical drawings used in forming should only contain set-up and running criteria, which would provide the necessary overview over the requirements to the operator.
4. The geometric tolerances have to include form and positional tolerances.
5. Special measuring equipment might be necessary to control the relevant dimensions.
6. For many criteria, dimensional inspection will have to be carried out with the help of co-ordinate measuring machines, fixtures equipped with automatic data acquisition, or manual inspection with gauges /6/. Any of these solutions requires considerable investments.
7. Process capability indices are often misleading for single sided criteria /3/. A solution for this is either a compensation for the skewness of the distribution or the application of indexes that are based on single sided distributions.

The proposed method requires considerable resources. It takes a long time to investigate problems and to carry out the process capability studies. Then, taking the required measures, that should solve the problem, consumes both lots of time and money. The benefits can be derived from formula (1) for the overall equipment efficiency (OEE):

- The quality rate can be increased.
- The production speed can be increased.
- The availability of the machine tools can be increased.

What the method requires most of all, is constant self-motivation to really carry such a project to its hopefully successful end. The project will be continued at Raufoss Technology AS.

ACKNOWLEDGEMENTS

We thank the Research Council of Norway and Raufoss Technology AS for the support of this project.

LITERATURE

- /1/ Onodera, S., Sawai, K., 'Modern cold forging applications for the manufacture of complex automotive parts', *Journal of Materials Processing Technology*, vol. 46, 1994, pp. 169-183
- /2/ Juran, J.M.; Gryna, F.M., 'Juran's Quality Control Handbook', MacGraw-Hill, Inc., New York, 1974
- /3/ Gunter, B., 'The use and abuse of C_{pk} ', part 1-4, *Quality Progress*, vol. 22, 1989, part 1: no.1, pp.72-73, part 2: no. 3, pp. 108-109, part 3: no.5, pp.79-80, part 4: no.7, pp. 86-87
- /4/ Deleryd, M., 'A Pragmatic View on Process Capability Studies', *International Journal of Production Economics*, In Press
- /5/ Deleryd, M., 'On the Gap between Theory and Practice of Process Capability Studies', *International Journal of Quality and Reliability Management*, vol. 15, no.2, 1998, pp. 178-191
- /6/ Boyles, R., 'Exploratory Capability Analysis', *Journal of Quality Technology*, vol. 28, 1996, no.1, pp. 91-98
- /7/ Ondera, Shinsaku, 'ISO 9000 conformance in respect of precision cold forging manufacturing', *Journal of Materials Processing Technology*, vol. 71, 1997, pp. 71-75
- /8/ Polansky, A., 'A Smooth Nonparametric Approach to Process Capability', *Quality and Reliability International*, vol. 14, 1998, pp. 43-48
- /9/ Youn-Min, C., Polansky, A., Mason, R., 'Transforming Non-Normal Data to Normality in Statistical Process Control', *Journal of Quality Technology*, vol. 30, no. 2, April 1998, pp. 133-141
- /10/ Clements, J., 'Process Capability Calculations for Non-Normal Distributions', *Quality Progress*, September 1989, pp. 95-100
- /11/ Yu-Cheng, L., Chiu-Chi, W., 'Process Capability-Based Tolerance Design to Minimise Manufacturing Loss', *International Journal of Advanced Manufacturing Technology*, vol. 14, 1998, pp. 33-37
- /12/ Yu-Cheng, L., Chiu-Chi, W., 'Determining the process tolerances based on the manufacturing process capability', *International Journal of Advanced Manufacturing Technology*, vol. 10, no. 6, 1995, pp. 187-192
- /13/ Pearn, W., Kotz, S., Johnson, N. 'Distributional and Inferential Properties of Process Capabilities', *Journal of Quality Technology*, vol. 24, no. 4, 1992, pp. 216-231
- /14/ DIN 17673 Part 4, 'Drop Forgings of Copper and Wrought Copper Alloys – Permissible Variations', Beuth Verlag GmbH, Berlin, 1974
- /15/ Porter, L., Oakland, J., 'Process Capability indices – an overview of theory and practice', *Quality and Reliability Engineering International*, vol. 7, 1991, pp. 437-448
- /16/ Wei, C., 'Tolerance design with concurrent optimisation of quality loss and process capability', *International Journal of Industrial Engineering*, vol. 5 (2), 1998, pp. 169-174
- /17/ Nakajima, S., 'TPM development program: Implementing total productive maintenance', Productivity Press Inc., Cambridge, MA, 1989

AN INTELLIGENT SYSTEM FOR THE DETERMINATION OF THE REQUIRED SETUPS AND THE ASSOCIATED CLAMPING POINTS AND CLAMPING DEVICES IN MILLING

K.D. Bouzakis and G. Giannopoulos
Aristotle University, Thessaloniki, Greece

KEY WORDS: Milling, clamping, expert systems, CAM

ABSTRACT: The paper presents a rule based expert system, developed to predict the necessary setups as well as the fixturing points and the corresponding clamping devices, necessary to support a prismatic part during milling. The procedure is conducted in two steps. Initially, the geometrical and topomorphical information including all the machining features of a prismatic part are recognized and introduced into the developed expert system. In the first step the expert system determines the essential setups needed to machine the part on a particular machine, while in the second step the prospective clamping edges are located and the possible clamping points are determined. Moreover, the developed system regarding the cutting data, the specifications of the available supporting devices, and the geometry of the machine tool used, defines the required standard clamping and supporting structural elements, needed to support the part during milling

1. INTRODUCTION

In order to manufacture a particular part in an actual CIM environment the part geometric model must be described in terms of features, which represents shapes and technological attributes associated with manufacturing operations and tools [1]. Moreover it is necessary to define the part positioning, orientation and clamping with respect to the available machine tools. Just like any other machining procedure the setup and clamping of a workpiece must combine many sources of design information. Both the geometry of the

Published in: E. Kuljanic (Ed.) *Advanced Manufacturing Systems and Technology*,
CISM Courses and Lectures No. 406, Springer Verlag, Wien New York, 1999.

workpiece with the associated features, and the machining conditions combined with heuristic knowledge are used in order to accomplish these tasks. Moreover clamping must satisfy certain knowledge-based rules for the machining, considering the tool paths and the setups of the part. Taking into account these rules, and the machining parameters, the design goals are concluded. Particularly the design goals must consider the following [2]:

- Hold firm the workpiece on the machine tool table, taking into account that the number of the clamping points must be proportional to the magnitude of the developed forces during cutting.
- Position of the clamps about the part considering the part's axis of symmetry, so that the bending moment produced by the cutting tool are minimized, and the pressure exerted by the clamps will be more uniformly distributed. Both the above results to the reduction of the parts distortion due to cutting.
- The clamping of the part must be carried out quickly and accurately.
- To minimize the clamping development cost and installation time, standard parts as far as possible are used.

This paper presents a rule based expert system, which considering the above design rules and goals, determines the necessary setups, clamping points and the associated clamping devices. The functional diagram of the developed system is shown in [Figure 1](#). It consists of three modules. The input module feeds information, derived from a number of sources, into the inference engine of the expert module, after they have been subjected to an initial processing from the setup identification and clamping determination modules.

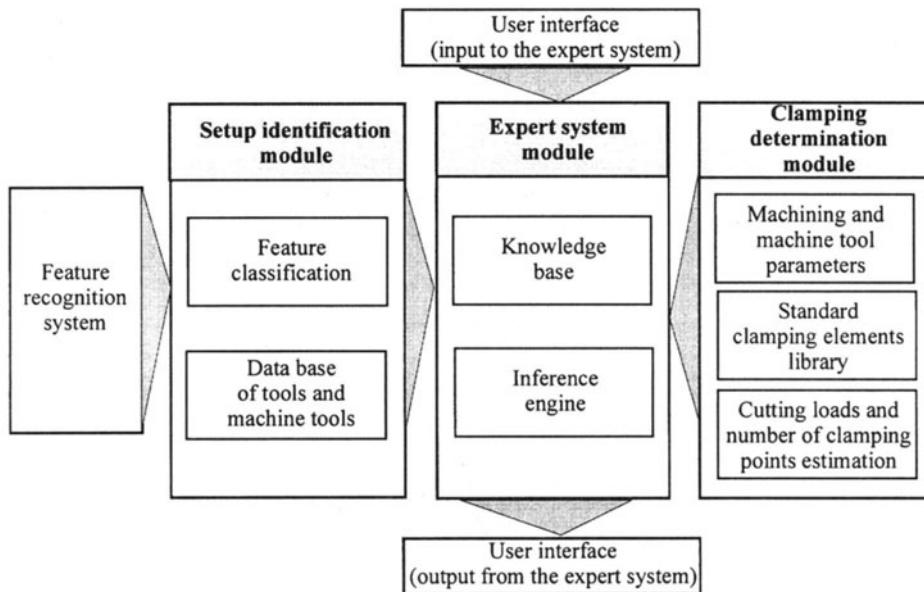


Figure 1: Structure of the developed intelligent system

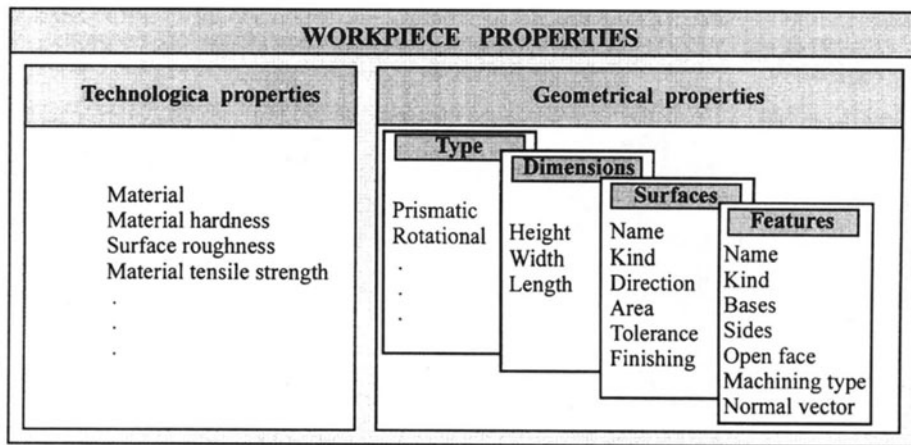


Figure 2: Geometrical, topological and technological properties used in the developed intelligent system

The inference engine combines this information with the rules contained in the system's knowledge base [3]. If a rule is true then a conclusion comes up, which is then presented through the output module of the user interface. These three system modules are described in more details in the following sections.

2. AUTOMATIC SETUP IDENTIFICATION

The developed system uses as input a file, created by a feature recognition system [3,4] and containing data that express the characteristics of the surfaces and the describing a part features (see Figure 2). Such data are the direction of a surface (normal vector), the type of surface (flat cylindrical, etc.) the type of feature (step, slot pocket, etc.), the number of its sides, the open face surface etc. In addition some other data are created after certain calculation have been conducted e.g. the area of a surface. Another input is the information concerning the cutting tools and the machine tools, which create new data. Such data are the type of the cutting tool, the number of machine tool axis, the maximum dimensions of its table, etc.

An important parameter influencing the setup identification, is the initial stock, from which the final part is machined. The stock has certain properties, like the number of surfaces, the corresponding areas, tolerances etc. The surface of the stock must have all the characteristics of the final part. In case that this is not fulfilled, then proper machining must create these characteristics. The dimension of the stock, unless these are given, are calculated using the dimension of the final part i.e. the maximum height, length and width. The reasoning that is followed in order to determine the setups is to begin from the stock and through intermediate steps, if parts are created, to end up with the final part. This may be achieved by rotating the intermediate part around the x, y, z axis successively and by applying the set of rules. In case that in a particular rotation, the rules do not produce a conclusion, means that this specific orientation does not correspond to a setup and hence it

is discarded and the procedure will continue. The results of the evaluation are a list with all the necessary setups that are needed to carry out the machining. For every setup the reference surface, the open face, the clamping surface and the feature to be machined are given.

3. THE CLAMPING DETERMINATION MODULE

As indicated in figure 1, a further module of the developed system is the clamping determination module. The purpose of this module is to extract data that are necessary to determine the position and the number of the clamping points, from the input information and a number of databases. The data concerns the optimum position of the workpiece into the machine tool table, the maximum cutting force developed during the milling operation and the determination of the clamping elements necessary to realize the clamping devices. As the workpiece moves on the machine tool table in a direction perpendicular to the table guides, the clamping characteristics such as the clamping position, the contact area etc. are changed (Figure 3). It is therefore essential to define the optimum distance between the workpiece zero point and a reference table guide, considering as criterion the minimization of the clamping region distance from a guide.

Another essential factor needed in order to calculate the number of clamping points is to estimate the maximum cutting force developed during milling. This is conducted using parameters like chip cross-sections, number of simultaneously engaged cutting edges and tool wear, as it has been suggested by [3].

For the determination of the clamping elements necessary to realize the clamping devices the system considers the conclusion list of the expert system, and attempts to locate the proper washers, studs, clamps, etc. from the clamping element database. The results are given in a list of recommended clamping elements.

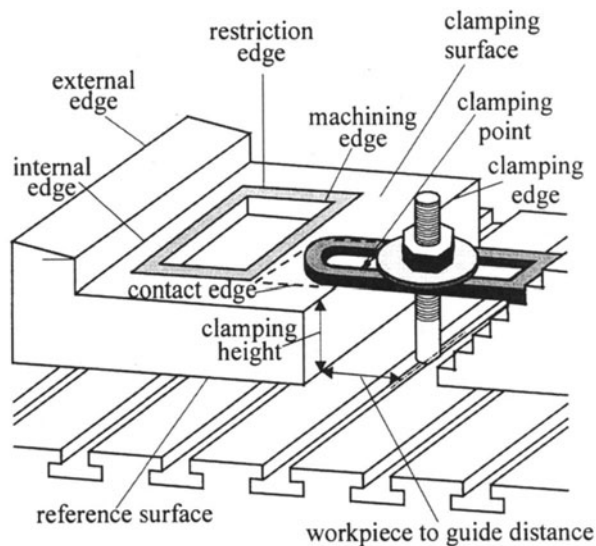


Figure 3: Concepts and nomenclature of a clamping system

4. THE KNOWLEDGE BASE OF THE EXPERT SYSTEM

The expert system knowledge base consists of a number of rules logically separated into three groups (see Figure 4). To the first group belong rules that determine the reference surface and proposes a list of surfaces appropriate for clamping. The second group contains rules suitable to determine on which surface with a given orientation a particular feature will be created. The third group contains heuristic rules with purpose to select from the number of prospective clamping points, that points that are located on the right position with respect to the machining area. The selection is based on a number of criteria, described below, attempting to define which points of the part geometry can be considered as clamping points. In brief these criteria are:

- The surface must be a plane surface and have to be parallel to the reference surface or have a slope less than 3°.
- The clamping point belong to an external edge, i.e. the edge is the intersection of two surfaces that form a convex angle.
- Suitable studs and supports must exist in the clamping element database, for the clamping point's height.
- The clamp must be at an appropriate distance from the machining area, to prevent stresses due to thermal plastic deformation.

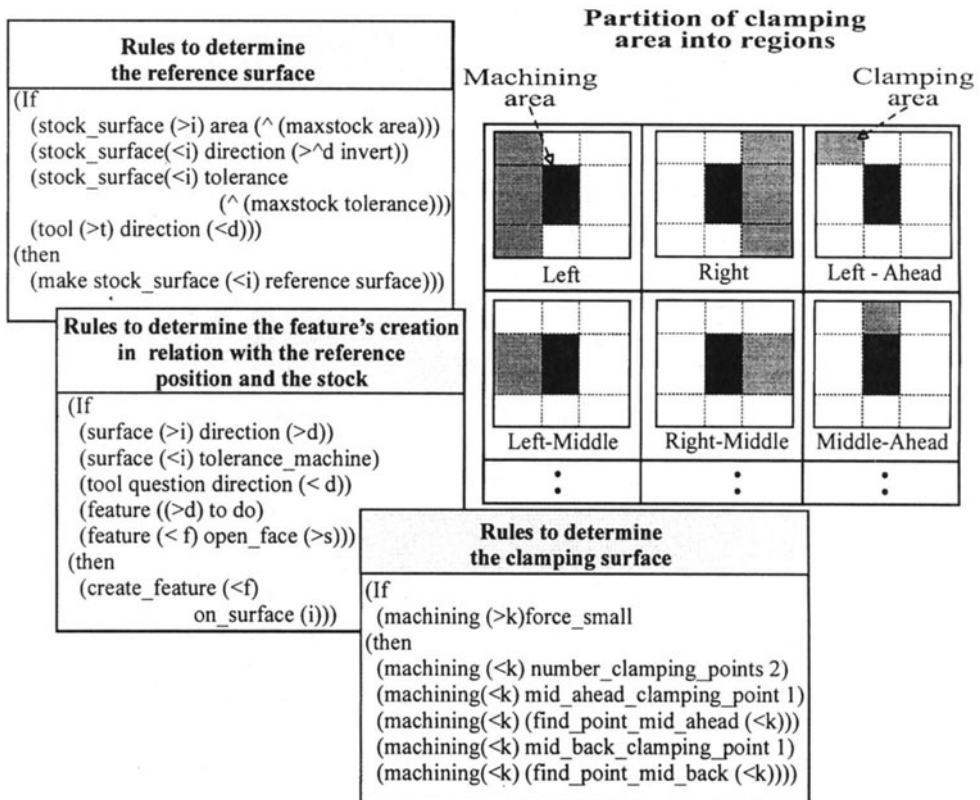


Figure 4: Representation scheme of the knowledge Base

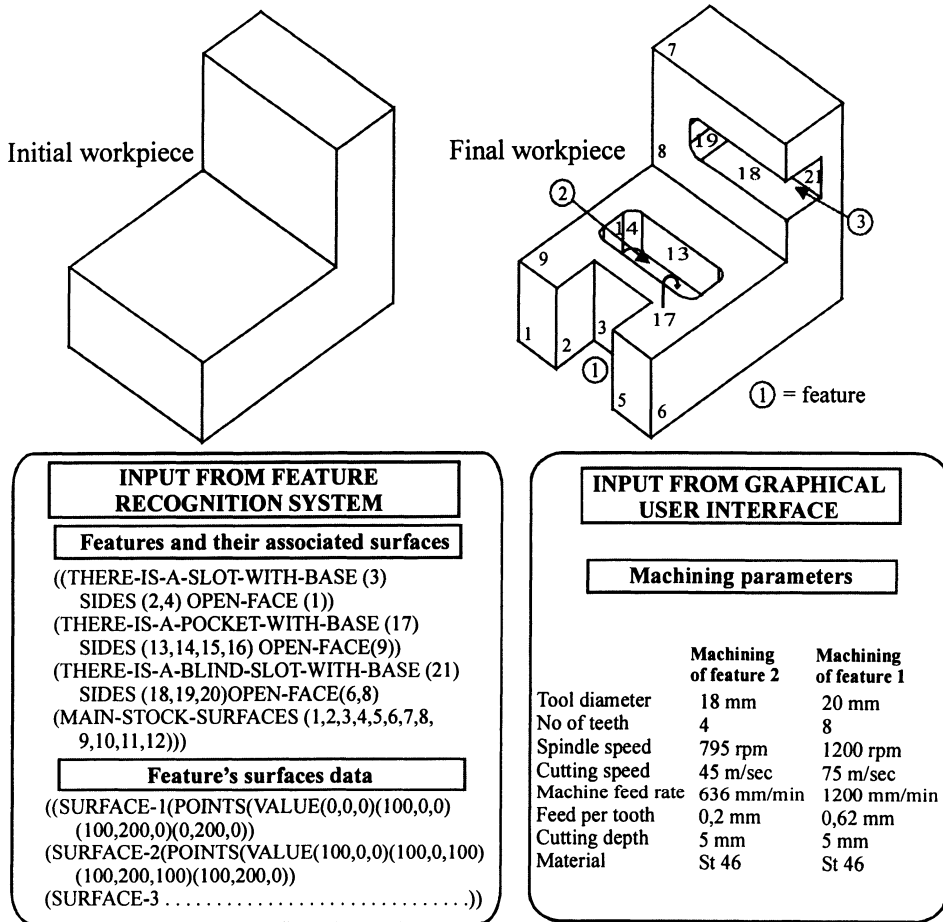


Figure 5: A workpiece to be machined and the input information

The edges fulfilling the above criteria are characterized as “prospective clamping edges” and the point belonging to them as “prospective clamping points”. The selection of the “actual clamping points” is accomplished by using rules which divide the clamping surface into regions with respect to the machining area (see figure 4). The rules determine the area where the proper clamping points must be located. After the location of the proper area, the rules try to verify if there exist prospective clamping edges and consequently clamping points in that area. If exist, then the system selects the middle point as the actual clamping point, otherwise it attempts to determine the clamping point using a predefined sequence of rules. If for example, the rule does not locate prospective clamping edges at the area “middle ahead” then tries to locate first at the area “right ahead” and then at the area “left ahead”.

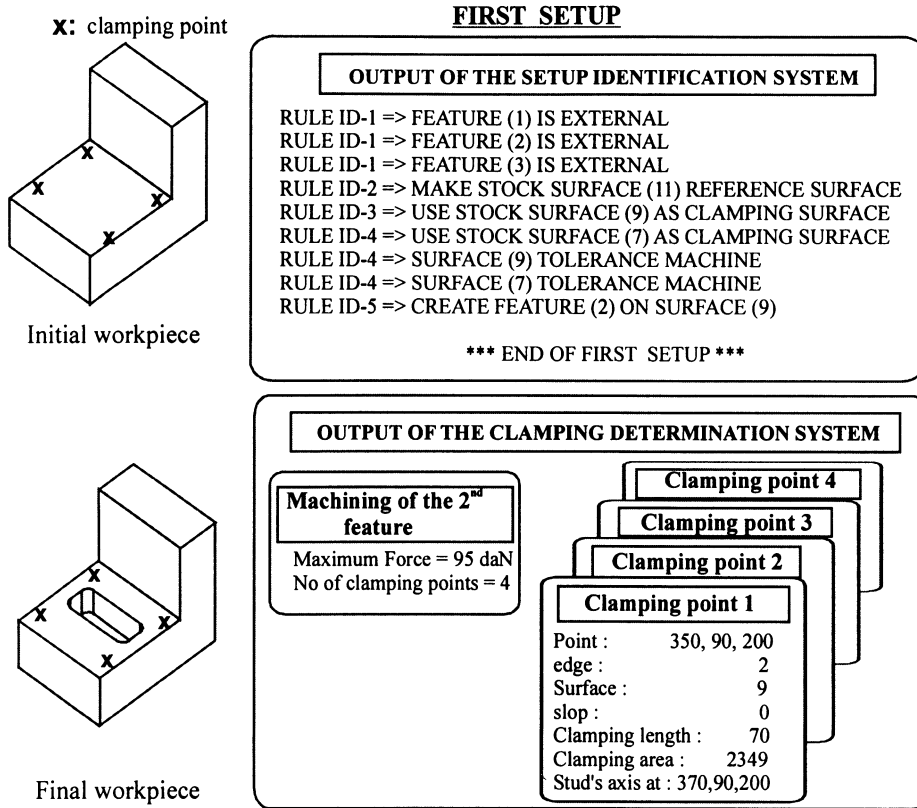


Figure 6: Intelligent system output for the first setup

5. AN APPLICATION EXAMPLE

The above procedure is demonstrated using the workpiece shown in Figure 5 together with the inserted input information. The initial workpiece originates from a manufacturing procedure. There are three features to be machined, a through slot a pocket and a blind slot (feature 1, 2 and 3 respectively). The machining will be carried out in two setups, corresponding to the first and fifth orientation of the workpiece while it is rotated. The calculated maximum forces for the machining of feature 2 and features 1, 3 are shown in Figures 6, 7 together with the clamping points. Figure 7 shows also the required standard clamping elements for every clamping point, as well as the total bill of clamping elements.

5. CONCLUSION

The developed system can be used to predict the necessary setups, the fixturing points and the corresponding clamping devices, necessary to support a prismatic part during milling, considering the geometrical and topomorphical information of a workpiece model.

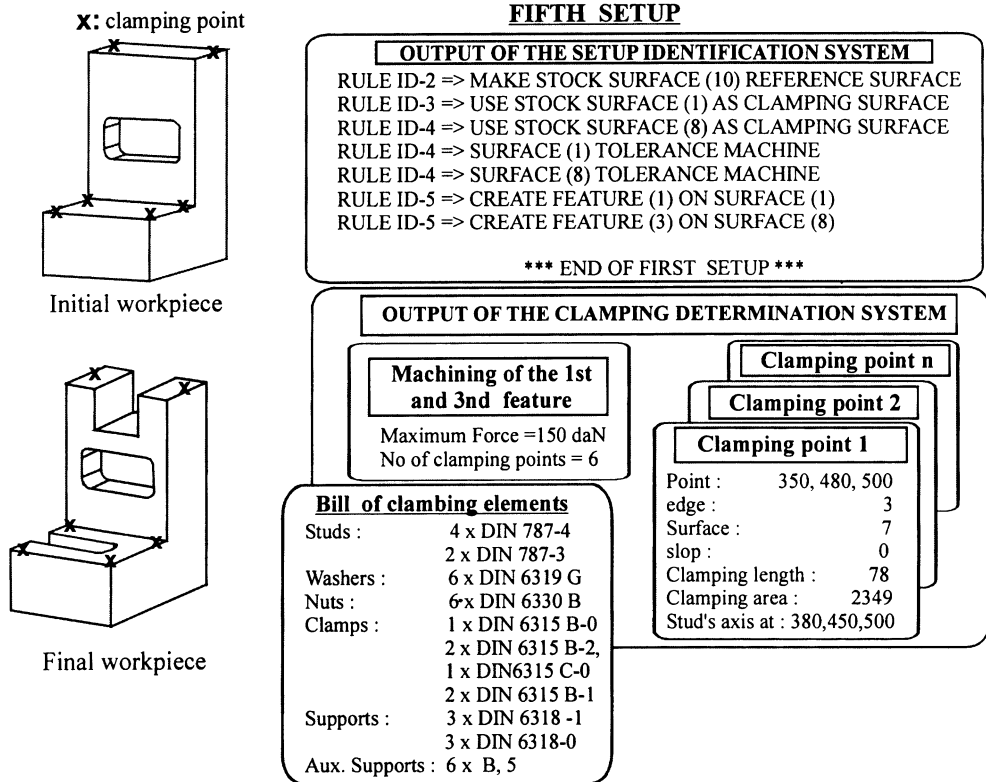


Figure 7: Intelligent system output for the fifth setup, and the bill of clamping elements required for the implementation of the clamping

REFERENCES

1. Shah, j. Assessment of feature technology, CAD, Vol. 23, No 5, 1991, pp. 331-334
2. Bouzakis, K., Giannopoulos G., Development of an expert system for automatic feature recognition and the determination of the manufacturing sequence. 10th International Conference on Computer Aided Production Engineering, Palermo, Italy, 1994, pp.241-250.
3. Bouzakis, K., Giannopoulos G., A rule based expert system for the determination of the optimum clamping in milling. CIRP International Seminar on Intelligent Computation in Manufacturing Engineering, Capri, Italy, 1998, pp. 539-545.
4. Bouzakis, K., Giannopoulos G., Development of an expert system for automatic feature recognition. 3rd Conference of the Laboratory of Machine Tool and Machine Dynamic, Thessaloniki, Greece, 1993, pp.85-106.

STABILIZATION OF A MILLING MACHINE AGAINST CHATTER

A. Gasparetto, M. Giovagnoni, E. Kuljanic and F. Miani
University of Udine, Udine, Italy

KEY WORDS: Mode Coupling Chatter, Milling Machine, Stabilization

ABSTRACT: This work analyzes a phenomenon of self excited vibrations (mode coupling chatter) that was observed in a machine for wood cutting during the milling of a chair back. The configuration of the system for which chatter occurs is first illustrated. It is then recognized that the most crucial factor affecting the stability of the system is the angle γ between the cutting force acting on the tool and one of the degrees of freedom of the structure. As a matter of fact, when γ becomes smaller than a certain negative value, chatter occurs. An effective way to stabilize the milling machine is presented, consisting in changing the orientation of the tool with respect to the feed direction of the workpiece, so that the value of γ is positive during the whole milling operation, and the instability zone is never entered. Tests carried out on the available milling machine proved the effectiveness of the stabilization. Finally, a theoretical framework is presented, which explains with more details how the stability of the system is affected by the value of γ . Moreover, a simple stability condition which can be useful for practical stabilization purposes is also defined.

1. INTRODUCTION

Mode coupling chatter is an undesired phenomenon of self excited vibrations occurring in many machining operations, in particular configurations of the machine tool with respect to the workpiece. The occurrence and the amplitude of mode coupling chatter depend on many

Published in: E. Kuljanic (Ed.) *Advanced Manufacturing Systems and Technology*,
CISM Courses and Lectures No. 406, Springer Verlag, Wien New York, 1999.

factors, such as the type of operation performed, the orientation between the workpiece and the tool, the chip width. Extensive research on chatter has been carried out for many decades, establishing the classical theory of chatter [1,2,3,4].

In this paper, an occurrence of mode coupling chatter in a machine for wood cutting during the milling of a chair back is described and analyzed. The factors causing the onset of vibrations in the milling machine are then evaluated, focusing on the reciprocal orientation between the tool and the workpiece. Then, an effective stabilization of the machine is proposed and successfully tested. Finally, theoretical considerations are made, that explain the vibratory phenomenon by studying the eigenvalues and the eigenvectors of the system. This allows to define the stability borderline of the system and consequently to evaluate the zones of stability and instability of the system.

2. THE OBSERVED OCCURRENCE OF CHATTER

An occurrence of mode coupling chatter was observed in a machine for wood cutting, used to make chair backs (Figure 1). During the milling of a chair back, it was noticed that chatter occurred when milling the end part of the internal side of the workpiece. Chatter seriously damaged the workpiece, which should be discarded and could not be used for chair production. Several attempts to eliminate or at least reduce vibrations were made, namely increasing the overall stiffness of the machine and reducing the spindle speed. In this way some chatter reduction was observed; however, the problem was not completely overcome because vibrations still occurred, and the workpiece still showed several marks due to chatter. Moreover, reducing the spindle speed led to an increase of the machining time for each workpiece, thus lowering the efficiency of the overall machining operation.

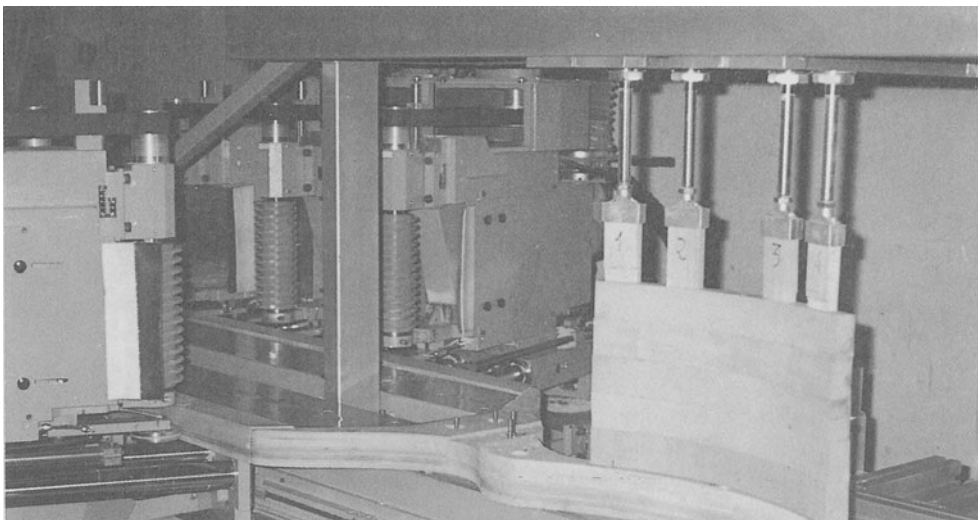


Figure 1 - The milling machine for wood cutting and a chair back to be machined

3. STABILIZATION OF THE MILLING MACHINE AGAINST CHATTER

A more effective way to stabilize the system against chatter had thus to be found, preserving also the overall efficiency of the machining operation. To this end, a model of the machine - tool - workpiece system has to be first established.

The tool - machine system can be considered as a vibratory system with two degrees of freedom, which are aligned among two perpendicular axes (X_1, Y_1), characterized by stiffnesses K_x and K_y respectively. The value of K_y is very low compared with the value of K_x , since K_y is the stiffness of the pneumatic actuator connecting the tool to the machine, whereas K_x is the stiffness of the structure.

Another reference system should be defined, with the X_2 axis parallel to the direction of the cutting force acting on the tool (see Figure 2). In this way the angle γ expressing the relative orientation of the two reference systems can be defined. It will be shown that the angle γ between the cutting force acting on the tool and the degree of freedom of the system along the X_1 axis is the most crucial factor affecting the stability of the system.

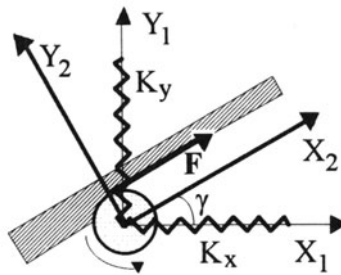


Figure 2 - The model of the system

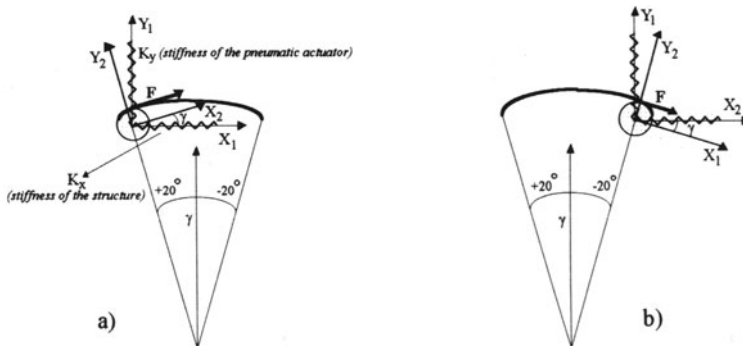


Figure 3 - Non-stabilized milling at the beginning and at the end of a chair back

During the milling operation that is being analyzed, the value of γ changes, ranging from +20 to -20 degrees (Figure 3). As a matter of fact, when more than half of the chair back

has been machined, i.e. when γ reaches some negative value γ^* , strong vibrations are originated, and the internal end part of the chair back is seriously damaged.

In order to prevent the occurrence of chatter, thus stabilizing the system, we changed the reciprocal orientation of the tool with respect to the workpiece, so that to have γ ranging from +40 to 0 degrees (Figure 4). Several machining sessions were then performed with this new orientation, and no more chatter was observed. This means that the angle γ strongly affects the occurrence of vibrations. In the following section, a theoretical framework will be built, so as to explain how the value of γ affects the occurrence of mode coupling chatter. In this way it is also possible to define a practical method to stabilize the system against chatter.

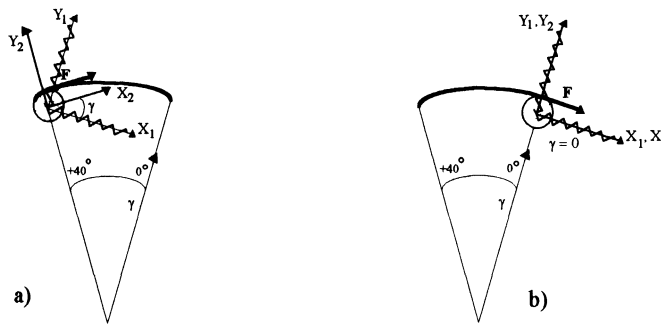


Figure 4 - Stabilized milling of a chair back at the beginning and at the end of a workpiece

4. THEORETICAL FRAMEWORK

The classical chatter theory already recognized that mode coupling chatter depends on many factors, among which the mutual orientation between tool and workpiece has to be taken into account. However, this paper presents a new approach, based on the system theory, that can provide a simple stability condition and therefore a practical way to stabilize the system with no need to increase the stiffness of the system.

Referring to Figure 2, the cutting force F acting on the tool, according to Merchant [5], is assumed to be proportional to the depth of cut in the direction orthogonal to the force. The equation expressing the components of the force vector F in the reference frame 2 is then:

$$\begin{bmatrix} F_x \\ F_y \end{bmatrix}_2 = \begin{bmatrix} 0 & k \\ 0 & 0 \end{bmatrix} \begin{bmatrix} u_x \\ u_y \end{bmatrix}_2 \quad (1)$$

where $\mathbf{u} = [u_x, u_y]^T$ is the displacement vector of the tool and k is a coefficient named "static directional cutting stiffness", that is directly proportional to the depth of cut. Moreover, if the tool rotates counterclockwise (refer to Figure 2), the cutting force acting on the tool is oriented along the positive direction of the X_2 axis, so $k > 0$. Conversely, if the

tool rotates clockwise, then $k < 0$. In the following we will assume that the tool rotates counterclockwise, so we will consider $k > 0$.

Eq.(1) can be expressed in the reference frame 1 using a rotation matrix \mathbf{R}_{21} , defined by:

$$\mathbf{u}_1 = \mathbf{R}_{21} \mathbf{u}_2 = \begin{bmatrix} \cos\gamma & -\sin\gamma \\ \sin\gamma & \cos\gamma \end{bmatrix} \mathbf{u}_2 \tag{2}$$

Hence, Eq. (1) can be rewritten as:

$$\begin{bmatrix} F_x \\ F_y \end{bmatrix}_1 = \begin{bmatrix} \cos\gamma & -\sin\gamma \\ \sin\gamma & \cos\gamma \end{bmatrix} \begin{bmatrix} 0 & k \\ 0 & 0 \end{bmatrix} \begin{bmatrix} \cos\gamma & \sin\gamma \\ -\sin\gamma & \cos\gamma \end{bmatrix} \begin{bmatrix} u_x \\ u_y \end{bmatrix}_1 = \begin{bmatrix} -k \sin\gamma \cos\gamma & k \cos^2\gamma \\ -k \sin^2\gamma & k \sin\gamma \cos\gamma \end{bmatrix} \begin{bmatrix} u_x \\ u_y \end{bmatrix}_1 \tag{3}$$

A 2 DOF, undamped vibratory system is considered in our model. Damping is not taken into account in order to simplify the resulting equations. According to this model, the equations of the system in the reference frame 1, are:

$$\begin{bmatrix} M & 0 \\ 0 & M \end{bmatrix} \begin{bmatrix} \ddot{u}_x \\ \ddot{u}_y \end{bmatrix} + \begin{bmatrix} K_x & 0 \\ 0 & K_y \end{bmatrix} \begin{bmatrix} u_x \\ u_y \end{bmatrix} = \begin{bmatrix} -k \sin\gamma \cos\gamma & k \cos^2\gamma \\ -k \sin^2\gamma & k \sin\gamma \cos\gamma \end{bmatrix} \begin{bmatrix} u_x \\ u_y \end{bmatrix} \tag{4}$$

where M is the mass of the cutting system, and K_x, K_y are the stiffnesses of the system along the two degrees of freedom (X_1, Y_1).

Eq. (4) can be rearranged to give:

$$\begin{bmatrix} \ddot{u}_x \\ \ddot{u}_y \end{bmatrix} = \begin{bmatrix} -\frac{K_x + k \sin\gamma \cos\gamma}{M} & \frac{k \cos^2\gamma}{M} \\ -\frac{k \sin^2\gamma}{M} & -\frac{K_y - k \sin\gamma \cos\gamma}{M} \end{bmatrix} \begin{bmatrix} u_x \\ u_y \end{bmatrix} = \mathbf{H} \begin{bmatrix} u_x \\ u_y \end{bmatrix} \tag{5}$$

The stability of the system can be analyzed by studying the eigenvalues of the matrix \mathbf{H} . The eigenvalues can be obtained from the characteristic equation of the system:

$$\lambda^4 + \left(\frac{K_x + K_y}{M}\right) \lambda^2 + \frac{K_x K_y + (K_y - K_x) k \sin\gamma \cos\gamma}{M^2} = 0 \tag{6}$$

From Eq. (6) we obtain two values for the squared eigenvalues λ^2 :

$$\lambda^2 = \frac{1}{2M} \left[- (K_x + K_y) \pm \sqrt{\Delta K (\Delta K + 2k \sin 2\gamma)} \right] \tag{7}$$

having set: $\Delta K = K_x - K_y$, i.e. the difference between the stiffnesses of the two degrees of freedom of the system. For the milling machine considered, $K_x > K_y$, so $\Delta K > 0$.

Now, two cases are possible, depending whether λ^2 is a real negative number or a complex number, with negative real part. It will be shown that if λ^2 is a real negative number, then the system is stable. Conversely, if λ^2 is a complex number, with negative real part, then the system is unstable, i.e. chatter occurs in the machine.

Moreover, a simple stability condition can be written, expressing the borderline between the two cases, as a function of the argument of the square root in Eq. (7).

Hence, assuming $\Delta K > 0$ and $k > 0$, the limit condition of stability is given by:

$$\Delta K + 2k \sin 2\gamma = 0 \tag{8}$$

which can be rewritten as:

$$\sin 2\gamma = -\frac{\Delta K}{2k} \tag{9}$$

Now, when $\sin 2\gamma > -\frac{\Delta K}{2k}$, i.e. when the value of γ is greater than a certain negative value

$\gamma^* = \frac{1}{2} \arcsin(-\frac{\Delta K}{2k})$, then the squared eigenvalues of the system are two real negative numbers and the system is stable. In fact, if the squared eigenvalues are two real negative numbers, then the four eigenvalues of the system are located on the imaginary axis, and are symmetric with respect to the real axis. The eigenvectors associated with the two squared eigenvalues are two real eigenvectors. Hence, it can be shown that the tool motions are two straight lines (Figure 5). The modes depicted in Figure 5 are purely oscillatory, so the system is stable in a BIBO sense. Moreover, we have to remember that we did not consider damping in our model. The structural damping of the real system will shift the eigenvalues of the system towards left in the complex plane, therefore giving exponentially decaying modes.

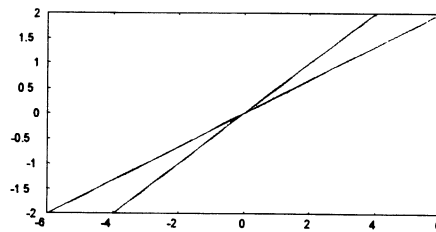


Figure 5 - Tool motions in the stable case

On the other hand, when $\sin 2\gamma < -\frac{\Delta K}{2k}$, i.e. when the value of γ is smaller than a certain negative value $\gamma^* = \frac{1}{2} \arcsin(-\frac{\Delta K}{2k})$, then the squared eigenvalues of the system are two complex conjugated numbers with negative real part, thus the system is unstable.

In fact, if the squared eigenvalues (named $\lambda_A^{2''}$ and $\lambda_B^{2''}$) are two complex conjugated numbers, then the four eigenvalues of the system (λ_1'' , λ_2'' , λ_3'' and λ_4'') are located as shown in Figure 6, symmetrically with respect both to the real and the imaginary axis. Then, the eigenvectors associated with the two squared eigenvalues are two complex conjugate eigenvectors. Hence, it can be shown that the tool motions are two ellipses, multiplied by an exponential (Figure 7).

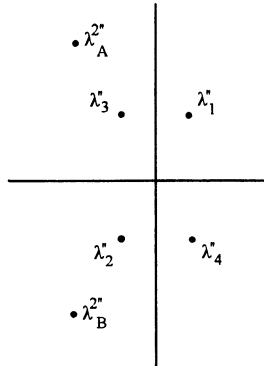


Figure 6 - Location of the eigenvalues in the complex plane (unstable case)

This means that the tool motions are given by two elliptical spirals with frequency $\omega = \text{Im}(\lambda_1'')$. In Figure 7 only one spiral appears because the graphical representations of the two motions totally overlap. One of the ellipses corresponds to an unstable motion, because the coefficient of the exponential, given by the real part of the eigenvalues λ_1'' and λ_4'' , is a positive number. This means that the correspondent mode increases exponentially. The other ellipse corresponds to a stable motion, because the coefficient of the exponential, given by the real part of the eigenvalues λ_2'' and λ_3'' , is a negative number. This means that the correspondent mode decays exponentially. However, the system as a whole results unstable.

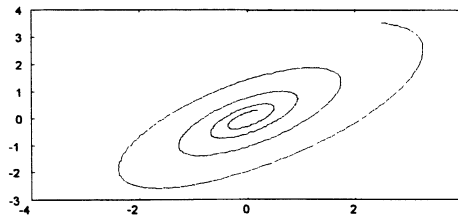


Figure 7 - Tool motion in the unstable case

From the above considerations it follows that the stability of the system depends on three factors, namely the static directional cutting stiffness k , the difference ΔK between the stiffnesses of the two mutually perpendicular degrees of freedom of the system, and the angle γ between the direction of the cutting force acting on the tool and the degree of freedom of the system along the X direction. Assuming that ΔK is constant for all milling operations performed on the considered machine, the value of γ^* for which instability

occurs depends on the coefficient k , which is taken positive or negative depending whether the tool rotates counterclockwise or clockwise respectively, and whose value is affected by the characteristics of the workpiece (mainly by the type of wood and the height of the chair back, that corresponds to the chip width). In fact, the higher the chair back, the smaller the absolute value of the angle γ^* for which the unstable zone is entered.

Therefore, it is clear how stabilization of the system could be obtained by just changing the orientation of the tool with respect to the feed direction of the workpiece, so as to make the angle γ range from +40 to 0 degrees. In this way, the value of $\sin 2\gamma$ is always positive, and the unstable zone is never entered.

5. CONCLUSIONS

The occurrence of mode coupling chatter in a machine for wood cutting during the milling of a chair back has been analyzed in this paper. It has been recognized that the most crucial factor affecting the stability of the system is the angle γ between the cutting force acting on the tool and one of the degrees of freedom of the structure. An effective way to stabilize the milling machine has then been presented, consisting in changing the orientation of the tool with respect to the feed direction of the workpiece, so as to keep the value of γ greater than zero during the whole milling operation. Tests carried out on the machine proved the effectiveness of the stabilization. Finally, a theoretical framework has been presented, which explains how the system stability depends on the value of γ , thus enabling one to formulate a simple stability condition.

REFERENCES

1. Koenigsberger, F. and Thusty, J.: *Machine Tool Structures*, Pergamon Press, 1971.
2. Merritt, H. E., *Theory of Self-Excited Machine Tool Chatter*, ASME Journal of Engineering for Industry, 87 (1965) 4, 447-454.
3. Thusty, J. and Ismail F.: *Basic Non-Linearity in Machining Chatter*, Annals of the CIRP, 30 (1981), 229-304.
4. Thusty, J. and Ismail F.: *Special Aspects of Chatter in Milling*, ASME Journal of Vibration, Stress and Reliability in Design, 105 (1983), 24-32.
5. Merchant, M. E.: *Basic Mechanics of the Metal-Cutting Process*, ASME Journal of Applied Mechanics, 11 (1944) A, 66-168.

AUTOMATION OF A PRODUCTION LINE FOR FLASHLESS PRECISION FORGING

J. Pilgrim

Weidmuller ConneXt GmbH, Detmold, Germany

B. Mussig and B.C. Schmidt

University of Hannover, Hannover, Germany

KEY WORDS: Automation, Precision forging, Decentralised control system, Finishing accuracy

ABSTRACT: Automation is an important approach to achieving more economical production systems. But most automated production lines are inflexible. Flexibility is an essential topic for manufacturing lines which have high machine costs and whose various products are made on variably combined aggregates such as forging lines for example. For the innovative technology of flashless precision forging an automated production line has been developed at the IPH - Institut für Integrierte Produktion Hannover to demonstrate a new concept of flexible automation in forging. With the flashless forging process gearwheels are produced in one forming step with such precision that only final grinding after forging is necessary.

All aggregates needed for the complete process chain such as material handling, heating system, forging piece handling, die cooling and lubrication system, forging press, heat treatment and clipping press are inter-connected via a field bus and controlled by decentralised CAN-Bus-components located directly at the machines.

One advantage of the decentralised CAN-Bus-technology compared to conventional central control is the possibility of fast changes of manufacturing aggregates without new wiring of sensors and actors. Another advantage is the possibility of integrating the existing machine controls. Both factors contribute a deal to a flexible production line at a favourable price.

All process parameters are controlled in almost real-time by an on-line monitoring system since they have to be maintained in a very small range of tolerances for the demanded precision. The visualisation and data processing of the process parameters and process steps allow fast reaction to problems and enable an effective quality assurance.

1. INTRODUCTION

New and innovative methods for massive forming combined with considerable improvement of finishing accuracy require high-technology manufacturing concepts. Today, forging parts can be produced with such precision that functional surfaces are ready for installation. This requires a high constancy of the quality relevant process parameters and extremely small tolerances of tools and handling systems. A solution for this problem is a fully automated and reproducible production process which ensures an improvement of the process stability and thus manufacturing with higher accuracy.

Furthermore, production lines should be flexible and easy to configure to be able to fulfil the customers' wishes such as just-in-time-delivery and wide product variety, together with low batch sizes. Because of the otherwise high investment costs it makes sense to use existing equipment and its installed controlling systems as far as possible. The opportunity to install and exchange parts of the production line must exist. A non-central concept for a controlling system shall meet the demands mentioned above.

The first step for introducing automation is an analysis and an assessment of the existing production line. According to that, the interfaces will be determined. The second step is the compilation of a detailed list of requirements which contains the necessary steps based on the analysis of the production process. Starting from there, the automation is designed in order to achieve a flexible solution which is compatible with the existing controlling systems. The last step is the implementation, the commissioning and the testing of the production system.

2. OBJECTIVES

The subject of this research is the automation of a flashless precision forging line for gearwheels. The gearwheels are formed in one step. The demands on the automated forging line are flexibility, easy adjustment of parameters via PC-based monitoring, reasonable price by integrating of existing machinery and resistance against adverse workshop conditions. Moreover, the automation shall assure the required reproducibility and accuracy of the forging process. The prerequisite is an automated handling device for the exact positioning of workpieces in the die and the monitoring of relevant parameters that influence the process, for example forming temperature and force. The accuracy of the forging parts, the defined material characteristics as well as high productivity can only be gained by controlled heating combined with automatic selection of incorrectly warmed workpieces. During the start-up of the line most workpieces do not reach the correct temperature. They have to be separated. After the forming process the material gains its desired characteristics by controlled heat treatment on a cooling conveyor. Pieces that are submitted to an incorrect march of temperature while being cooled down, have defective material characteristics and must also be separated.

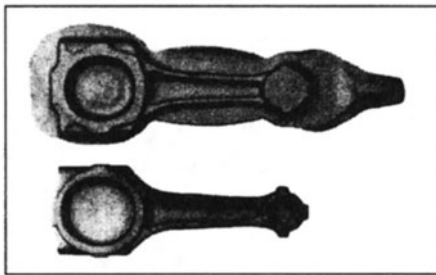
Working cycles of about 15 to 20 seconds and process transparency for trouble shooting are demanded for economic production. Because just-in-time-delivery will be required more often in the future, it can be expected that the batch size of forging parts will

decrease. This circumstance demands high flexibility of the production line as well as an easy and quick configuration and programming of the control system. For a quick set-up of single manufacturing components or for trials, it is also necessary to operate parts of the manufacturing system separately and manually. In addition to the normal production the automated forging line at IPH must fulfil the requirements regarding its use as research machinery, process development and prototype producing system.

3. THE FORGING PROCESS AND ITS REQUIREMENTS FOR AUTOMATION

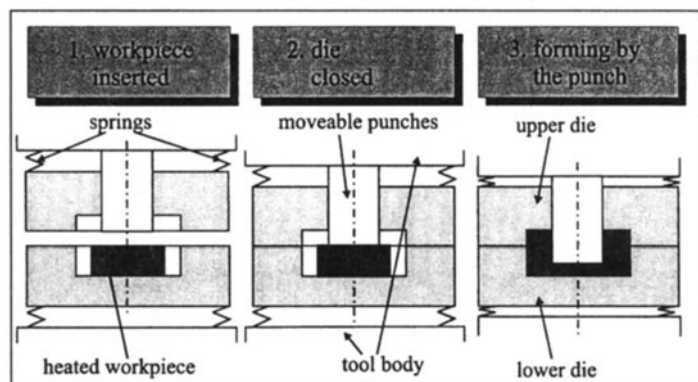
An important prerequisite for the automation of a manufacturing process is the detailed knowledge about the process chain and about the requirements on the process chain. In the following, a description of the forging process, its manufacturing equipment and the influencing variables, which have to be controlled, is given.

The forging process in a die is a shape building method. Material is formed between an upper and a lower die under high pressure so that the die is filled and the surplus material flows into a flash. Therefore it is necessary that sufficient raw material be supplied to obtain a fully filled form. In the conventional forging process the share of the material that flows into the flash can reach up to 50%, depending on the complexity of the forging part. To save costs on raw material, heating energy and waste, efforts have been made to decrease the amount of flash. Another way to save costs is the elimination of process steps, e.g. machining operations. Near



Pic. 1: Conventional and flashless precision forged connecting rod

net shape forging and precision forging have the advantage that functional surfaces are ready-to-be-installed after fine machining. In Hannover a method for precision forging has been developed that almost eliminates flash (Pic. 1). Tools are constructed where the material is inserted into the die cavity, the tool is closed and then punches form the material to the final forging part (Pic. 2). While the downward movement of the press with the punches continues, the tool is held closed by

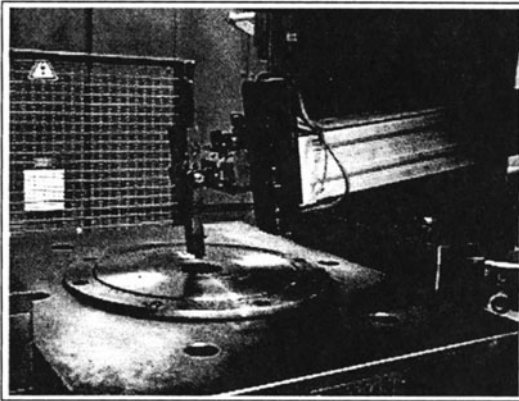


Pic. 2: Tool concept for a flashless precision forged gearwheel

compressed springs.

Condition for a successful flashless precision forging process is a very exact mass of the raw parts, a controlled temperature of the raw parts and the dies and controlled handling and forming of the workpiece. Therefore a press and other manufacturing components that achieve very small tolerances regarding geometric deviations are needed.

Currently, the developed automated production system is equipped with a tool system for single step precision forging of helical gearwheels developed at IFUM (Institut für Umformtechnik und Umformmaschinen, Hannover) which is integrated into the tool changing system (Pic. 3).



Pic. 3: Tool for gearwheels

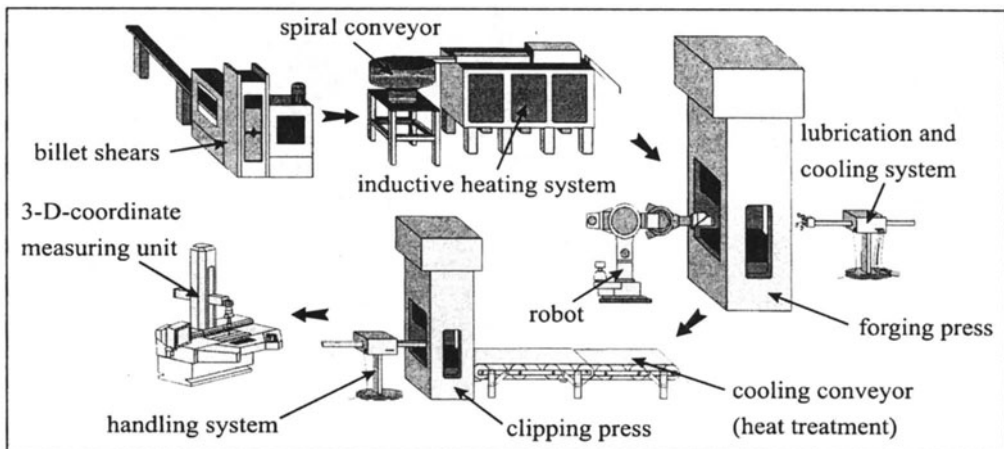
The modular construction of the die allows the production of varying gearwheels and other, mainly rotationally symmetric parts up to a weight of 1.5 kg simply by the exchange of the inner die. The bore hole of the gearwheel is formed as a cup and pierced later in a cold punching operation. The accuracy of the gearwheels is high enough that only the functional areas have to be fine machined after the forging process.

Future steps are the automation of complex processes like the multistage

forging of connecting rods. Reproducible handling and process control is essential for these products to reach the goal of flashless precision forging.

4. DESCRIPTION OF THE MANUFACTURING COMPONENTS

The different steps of the manufacturing process are performed on components shown in



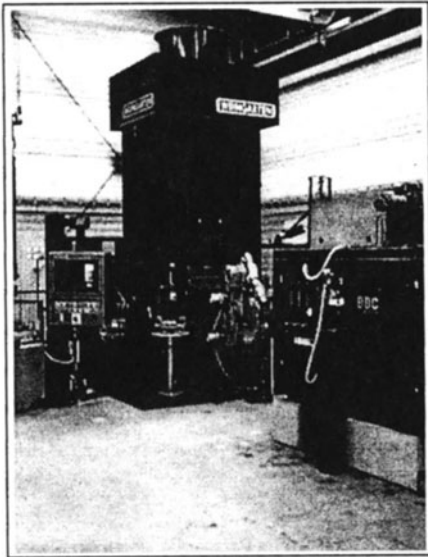
Pic. 4: Process chain of flashless precision-forged gearwheels

Pic. 4. They have to be connected to implement an automated manufacturing line. For the production of the raw parts, a pair of billet shears (max. diameter of rod respectively length of billets: 100 mm; accuracy about 2%) with a hydraulic gripper feed is used. The cycle time of the billet shears is shorter than the cycle time of the press. Accordingly it is not directly connected with the rest of the production line.

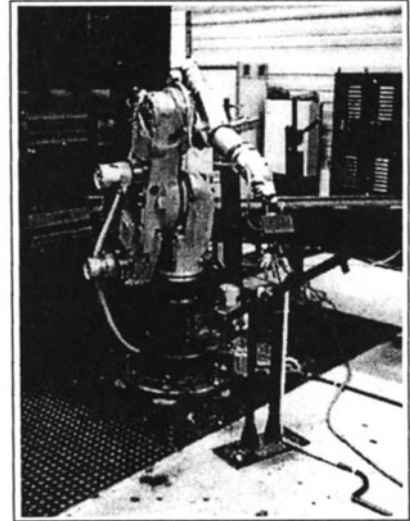
From a buffer storage container the sheared billets are continuously fed via an oscillating spiral conveyor to the induction heater that is equipped with a pyrometric temperature control. After heating, a 6-axis robot (made by KUKA) places the heated billets into the die cavity (Pic. 5). Because of its versatility, the robot is able to manage the handling of different workpieces in a multistage process as well as the separation of incorrectly warmed parts, which are thrown into a scrap bin.

The handling by the robot is made independent of the billet geometry by exchangeable grippers. The robot has a RCM3-controlling system.

The centre of the manufacturing system is a screw press ($F_{max} = 14.000 \text{ kN}$ by Müller Weingarten) in which tools up to 940 mm length as well as multistage forming tools can be installed (Pic. 6). Additionally, the machine is equipped with a tool changing system that allows fast exchange of different tool systems. The press is equipped with an internal Siemens S5 control that needs to be interfaced to and triggered by the overall control system for the entire automated line.



Pic. 6: Screw press



Pic. 5: 6-axis robot

The removal of the forging, the combined air-cleaning, cooling and lubrication of the die are carried out by pneumatically driven linear units with a stop position sensor. The action of the feeding, cleaning, cooling, lubrication and removing is overlapping. The water-graphite suspension, necessary for cooling and lubrication, is sprayed time- and quantity-controlled by two separated nozzles, one on the upper and one on the lower die side.

The pneumatic unit for removing the forged parts

is also equipped with interchangeable grippers. It transports the forged parts to a cooling conveyor belt.

The velocity of the belt can be varied according to the process cycle and the necessary thermal treatment. After the parts have been cooled down on the conveyor belt, they are placed in the workroom of the clipping press by another automatic feeding system. Pneumatically activated slide bars position the forged gearwheels for the piercing process. The clipping press is a normal gap-frame eccentric press ($F_{\max}=500$ kN). Alternatively it can be placed next to the main forging press for hot piercing or hot flash removal. It is activated by a foot switch. The connection of this mechanic press to the automated line is implemented by triggering the switch with a pneumatic cylinder which is controlled by one of the decentralised control boxes. Finally, a quality control of the forged gearwheels is performed with spot checks on a 3-D co-ordinate measuring unit.

5. CONCEPT FOR THE CONTROL SYSTEM

First step to control an automated manufacturing system is to develop a concept for the control system and for the communication between the machines. Primary goals of this control system are the simple, reliable and fast operation of the system. The parameters of the system such as e.g. the forming force or the temperatures of the raw parts and dies have to be configurable easily in the workshop. Other important goals are flexibility in order to exchange, integrate and adapt components of the existing manufacturing system. The control components require a high resistance against adverse environmental influences such as dirt, heat, vibrations and electromagnetic fields by the induction heater.

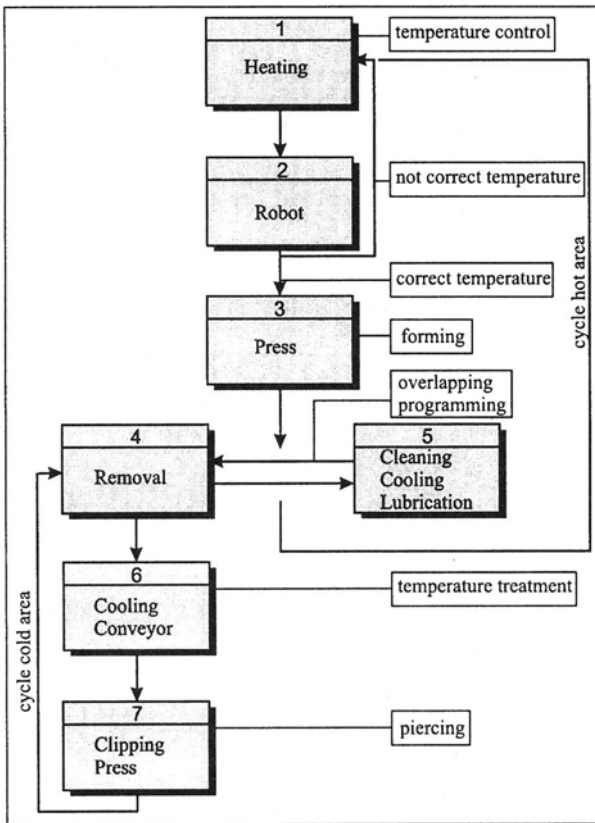
Many demands on the system result from the different ways of use at IPH as research machinery, as process development tool or for prototype production.

Because of the high modularity and flexibility of the line with changing combination of components the CANopen-Network (Controller Area Network) and a decentralised controlling intelligence seems advisable to co-ordinate the single operations heating, forming, handling, cooling and piercing.

CANopen allows the realisation of a flexible and decentralised control of the given input and output systems and interconnected sensor and actor systems. With this system, existing or already implemented machine controls can be connected. Compared to a centralised control system there is no need for a new cabling, what saves work and time. Therefore the decentralised control system is cheaper than a centralised one.

For the realisation of the many encountered individual control tasks, a concept was developed in co-operation with Weidmüller ConneXt, a company from Detmold, Germany. The developed concept bases on a CANopen network. Considering the adverse environmental conditions, under which the electronic components have to function reliably in forging industry, the developed system is an interesting alternative to conventional concepts. The CANopen network consists of seven spatially divided stations with eleven modules of the WINblocCAN family from Weidmüller ConneXt. Five of the stations are directly located at the components of the manufacturing system, such as induction heater or cooling device. The remaining two stations are directly integrated into the switch boards

for the press and the robot, and ensure their optimal use in the overall concept. The seven stations correspond to the seven manufacturing steps which are combined in two sub-processes, the 'hot area' with the heating and forging, and the 'cold area' with cooling and piercing (Pic. 7).



Pic. 7: Seven linked stations of the control system

The programming of the automation is realised with four interacting software-tools (Pic. 8). The locally arranged intelligent SPS-modules are programmed with a software according to IEC1131-3. The configuration and mapping of the network is carried out with a second software tool. It uses graphic elements with drag-and-drop-function, which are easy to handle. The third software package controls the communication among the modules. In addition to that, it controls the connection with the visualisation software. The process data are graphically presented with the help of the fourth software for visualisation. This software is also able to adjust certain process parameters, for example the threshold temperature for the selection of the warm slugs. The function of the CANopen network with the I/O modules and pre-processed programmable modules is to combine and to co-ordinate independent controls and

components of the manufacturing system in a way, that the operator can monitor and control the process from the heating of the slug to the piercing of the forging part via the PC. The decentralised programmable CANopen-modules include:

1. the ability to co-ordinate the individual manufacturing components, which have their own stored program system (SPS) in two cases. The exchange of data is accomplished by physical I/O channels which transfer information of status and receive start/stop orders.
2. SPS-programs that control simple process steps. The pneumatically driven cooling or handling devices are for example controlled by their own modules which can operate independently.

3. the pre-processing logic that delivers filtered and compressed data to the network and to the visualisation. The data are firstly analogue ones that give information about certain parameters as temperature of the slug and the die. Secondly there are digital data which provide information about the status of the readiness of all the machines for the next forging cycle.

4. The ability to integrate the touch screen input by the operator into the process. For

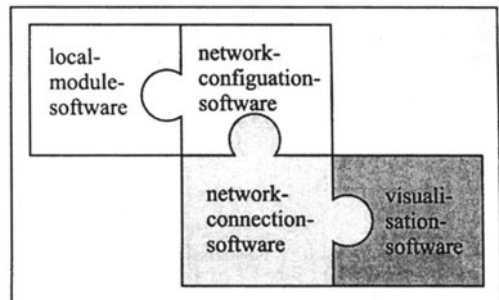
example, the operator feeds data of rated values of the heating temperature into the computer via the touch screen. This information is transmitted to the respective module and is taken into the course of the active program.

The PC-based process visualisation system can be surveyed and controlled by every PC-network connection. This offers the possibility of manipulating the process via internet or intranet. Online data collection for quality assurance or data management or even training of operators can take place spatially separated from the actual machinery .

6. CONCLUSION

At IPH, the automation of a flashless precision forging process has been realised in partnership with Weidmüller ConneXt and IFUM. Objectives are high flexibility in exchange, integration and adaptation of manufacturing components as well as simple operation of the automation control during configuration, testing and production. The objectives are now gained. The solution is a decentralised controlling system with PC-based visualisation and flexible handling devices, sensors and actors. The automated forging line is able to produce differently sized products at a high quality level, combined with the possibility of fast exchange of dies to enable just-in-time-delivery with small lot sizes. It is also possible to integrate existing manufacturing components with their own internal control system. Since that an investment in a completely new forging line is not necessary for the introduction of the automation.

One technical problem was encountered with the induction heater. It is a pusher type heater that is positioned in the forging line with a fixed cycle time. Because of the fixed cycle time the slugs stay too long in the heater at a temperature of about 1250°C. The slugs glue together randomly, cannot be transported by the robot and go into the reject bin. There are two possible solutions. Either the cycle time of the process becomes shorter or the slugs must be pushed separately through the heater by a pneumatically driven rod. Efforts have to be made to develop grippers with less wear. The less wear the grippers have the more accurate is the positioning of workpieces. Also gripper changing systems for a fast change-over as well as new gripper techniques like vacuum grippers for complex forging parts have to be developed.



Pic. 8: interaction of software modules

STUDY OF A DECISION SUPPORT TOOL FOR THE AUTOMATIC CONFIGURATION OF A MODULAR PLANT

E. Ceretti, C. Giardini and G. Maccarini
University of Brescia, Brescia, Italy

KEY WORDS: Simulator – Configurator program, Versatile Manufacturing Line

ABSTRACT: This work has been developed in cooperation with a company (STREPARAVA SpA – Brescia) to realise a tool for the automatic configuration of a modular plant which is made of a set of identical machines. These machine setups are different and the type and number of the operations performed by each module can be varied as the productive mix and the available resources vary. The scope of the research is to study a production line made of:

- a number of machines with the same structure but with the possibility of realizing different operations depending on the tool mix available on the machine itself;
- several pallets, which mount different pieces, able to exchange information with the machine and to decide whether it is better to occupy that working station or not;
- a loop transport system to connect and move the pallets;
- a single loading /unloading station operator assisted.

In this production system the definition of the set of operations performed by each machine depending on the production mix is fundamental. In fact, each entity can execute several operations and the production system can be varied. Obviously, this configuration must consider the uncertainty due to machine reliability, tool availability, and when necessary, production mix.

The simulative program realized will reconfigure the production system when a failure or malfunction occurs. It is evident that this reconfiguration must depend on the production mix. Otherwise, it will be possible to change the production mix temporarily depending on the active machines and on the tool availability.

1. INTRODUCTION

The aim of the present paper is the study of the dimensioning and the configuration of a system, different from the classic production layout. In fact, it can be considered as a

Published in: E. Kuljanic (Ed.) *Advanced Manufacturing Systems and Technology*,
CISM Courses and Lectures No. 406, Springer Verlag, Wien New York, 1999.

“hybrid” from two production typologies the “Transfer Line” and the “FMS”, which are well known in the field of mechanical manufacturing (figure 1).

The transfer lines have a very poor flexibility; this is not relevant for high production volume and low mix of parts but it is an important restriction when there is a continuous reduction of the product life and a large production mix.

On the other hand, the development of the FMS is very difficult, due to: the complexity of the system management, the difficult integration of the machine components and the elevated cost of the system itself.

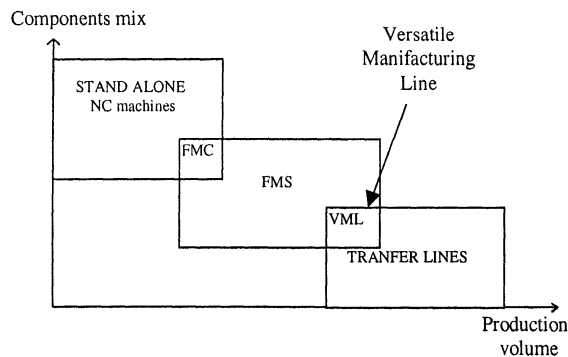


Figure 1 - Classification of the production system based on components mix and production volume

The system realized by the Strepavara SpA can be defined as a “Versatile Manufacturing Line” and it is able to realize high production volume while maintaining characteristics of flexibility and reconfigurability at low cost.

The plant in this study, in its complete configuration, consists of a maximum of 33 working modules disposed in a rectangular layout, all the modules are furnished by means of a central loop transport system (figure 2).

In the system only two different types of CNC working modules are present:

- roughing module with 3 working axes and a tool magazine able to store 12 tools;
- finishing module with 5 axes.

There are also measuring modules, which perform all the dimensional controls necessary to check the work pieces.

One of the peculiarities of this system is the capability of the pallet to store, in a proper electronic circuit, the information required in order to correctly work the part. These data are: the work piece type, the setup parameters of the pallet and the state of the working cycle (the next operation to be performed on the work piece). Obviously these data are updated during the productive cycle. In this way, the system has a distributed knowledge and doesn't need a supervision computer to control the line.

The pallet runs on the central loop transport system and, when it is in front of a module, exchanges information with the module itself. If, in the tool storage of work machine, there are the tools able to perform the next needed operation and if the buffer before the work machine is free, then the pallet fills the module, otherwise it continues to the next module.

When the work piece ends the cycle its data are updated, it leaves the module and returns on the central loop transport system, where it runs until a new machine, able to perform the necessary operation, is found. At the end of the work cycle the pallet goes to the unload station.

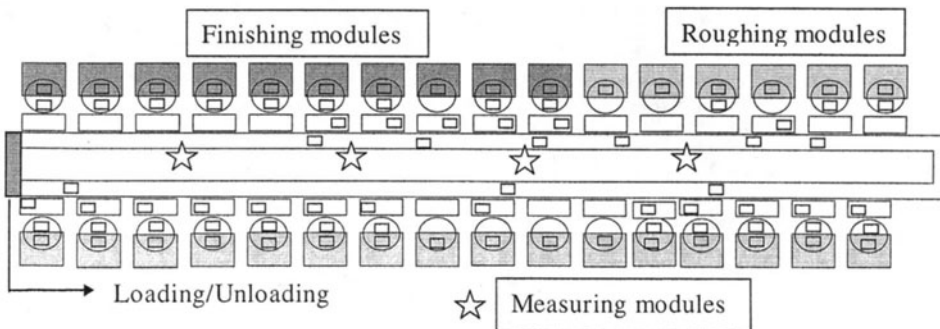


Figure 2 - Layout of the plant

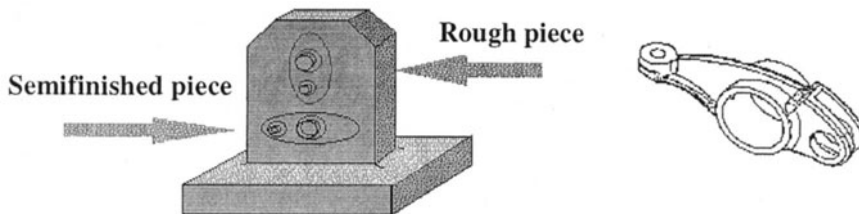


Figure 3 - Pallet and final piece

2. THE PRODUCT

The production line in this study produces a mechanical group made of three different rocker arms, which are assembled on a diesel engine. The technological cycle has 12 roughness operations and 5 to 7 finishing operations. On the pallet, two pieces of the same type are fixed so that two different sides can be worked. In the upper part of the pallet a rough piece is fixed and side A can be worked, while in the lower part a piece is fixed with side A already worked and side B exposed to the tool.

The Pert diagram of the working cycle is in figure 4; it is easy to identify the priorities and the constraints of the operations.

3. THE SIMULATOR AND CONFIGURATOR

With this system, object of our studies, we have to solve two principal problems:

- how many modules are necessary to achieve the wanted productivity ?
- how are the single operations shared between the modules ?

Considering the two objectives of system dimensioning and configuration, and observing that the system is characterized by a very large number of variables, we have found that the best tool to solve the problem is the simulation.



Figure 4 - Technological cycle

Unlike the analytical approach, where the extreme complexity of the problems discourages its use or, in order to have a solution, it is necessary to introduce drastic simplifications, the simulation approach is a valid tool for creating a model of the system in order to study its behavior.

We have to underline that this tool doesn't find an optimal solution if this is not within the alternative solutions analyzed. Furthermore the very *innovative nature* of the system doesn't allow the utilization of classical methods found in literature. The simulation approach is very useful when the system has limited dimensions and all the possible alternatives can be studied. For a medium large system it isn't possible to study all the alternatives, in a reasonable time. So, an heuristic algorithm has been developed in order to help the simulator in its work.

The design of the simulator has been taken into account that it must be used in the process to configure the initial layout but also to reconfigure all the system when one or more work machines are not available (ordinary or special maintenance etc.). The simulation language used is ARENA © which can describe: productive system, assembling line, automated storage, etc.

The simulator is able to:

- design the system, balancing the use of the resources i.e. the available roughing and finishing modules;
- configure the line in a way that correctly shares the various operations between all the modules with the aim of optimizing the line saturation.

This program allows Streparava to reproduce the operative conditions of the system. Moreover when the qualitative and quantitative characteristics of the technological cycle of the items change, the specific parameters of the tools can be considered too (tool life, tool reliability, etc.).

An appropriate user friendly interface, written in VISUAL BASIC© for EXCEL©, allows the easy input of all the data necessary to describe the system. These data, correctly

elaborated, are stored in a file which is then read from by a user routine, written in C programming language, linked to the simulator. The results are shown, at the end of the simulation, using Microsoft EXCEL© (figure 5).

4. PRODUCTION SYSTEM DIMENSIONING AND CONFIGURATION

The production system dimensioning problem is related to the definition of the optimum working module numbers, so as to balance the available resources (roughing and finishing machines); in fact, the overall system efficiency depends on the balance between these two resources. On the contrary, system configuration means the correct tool setup on each machine so as to maximize the production.

As first, a macro dimensioning of the system was created, taking into consideration the *cycle time*, the *production mix*, and the *working machine saturation*. In fact, the number of roughing modules (r) to supply one finishing module can be obtained by dividing the average cycle time (T_{wc}) by a saturation coefficient (s), for roughing and finishing.

$$r = \frac{T_{wc_{rou}}}{s_{rou}} \times \frac{s_{fin}}{T_{wc_{fin}}}$$

Varying the number of finishing modules and using the upper and lower integer value of r , several plant configurations with different dimensions can be obtained. The user will choose the plant dimension which best suits the available resources and the desired production mix. After the system macro dimensioning, it is possible to improve it using the scheduling technique. The configurations analyzed are: parallel and series.

In the parallel configuration, each working module can perform all the operation sets, in a series configuration, the 12 operations are realized by different modules.

<i>Scheduling</i>	<i>Advantages</i>	<i>Disadvantages</i>
<i>Parallel</i>	1 loading / unloading operation	Normal maintenance
<i>Series</i>	Hidden maintenance	+ loading / unloading operations

In the parallel configuration, the part is loaded and unloaded only once, in the series configuration there are several loading / unloading operations, which means longer penalty time. While, in the parallel configuration the tool substitution time affects the overall working time, in series, the presence of 2 identical tools in the machine tool storage allows the worn or broken tool substitution in hidden time.

To identify whether the series or parallel configuration is best, several variables have been defined:

System Variables

Cinematic parameters of the transport system (transport time), This is the time needed to unload a pallet from the working machine and to load it onto the following module. It was observed, from the simulation results, that reducing the transport time by half the series configuration becomes more competitive than the parallel.

Tool storage capacity, Increasing the tool storage capacity decreases the series advantages and the parallel configuration becomes more convenient.

Technological variables

Tool life and tool substitution time, Increasing or decreasing this time will change the effect of the substitution time on the working time, making it necessary to change the scheduling strategy.

The simulation of these variables must be understood:

- When parallel is better than series
- The criterion of assigning operations to the working modules, so as to identify one or more series solutions. These results have been used to write the micro dimensioning algorithm.

Some of the analyzed variables become constraints for the algorithm. The criterion for working module operation allocations states that each machine has a tool number, so that the sum of the operation times is higher than the transport time. The maximum number of equal tools must be defined, so as to consider the system maintainability equal to zero.

This first part of the algorithm is necessary to dimension the cell (the number of roughing modules). The identified set of cells is divided on the basis of production plant availability, that is, the number of the plant working modules.

For each cell module, the average working time is calculated considering its tool set up. Having considered the technological constraints and the above variables, it is possible to reallocate the operations between the cell machines, so that the cumulated working time is closer to the average estimated time.

The second part of the algorithm is repeated several times, on the basis of the number of possible cells, and a series solution set is produced. This solution set is filtered through a system balance indicator. Finally, the best solutions are simulated and compared with the reference case, that is, the parallel solution.

5. VARIABLE ANALYSIS

This simulator configurator program has been used to study the rocker arms line in different working conditions, with the aim of identifying those parameters which affect the process performance. To tune these parameters, it is fundamental to ensure that the system does not work in a sub-optimal way. The identified variables are:

- Working time of the loading unloading station,
- Number of pallets in the system.

The working time of the loading unloading station is the time needed by the operator, who works at the beginning of the line, to unload a finished part and to load a rough piece.

From the simulations it is evident that the production increases as the number of working modules increases. The working time goes from 60 sec to 30 sec. That means that the working time of the loading unloading station has to be comparable with the system theoretical throughput.

The number of pallets in the line represents the system work in progress. If there are few pallets, only a part of the line is working, while increasing the pallet numbers, the interference situations increase. In both cases, the working modules produce in sub-optimal conditions. Several simulations have been conducted for different system configurations. For each configuration, the pallet number which optimizes the production had been

identified (figure 6). The slope of the number of pallets, which maximizes the production, versus the number of working modules is linear (figure 7).

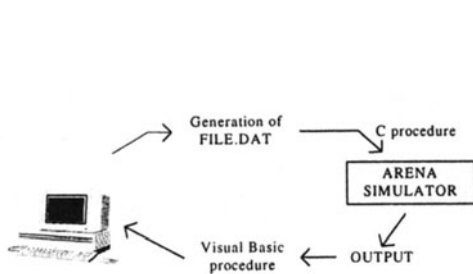


Figure 5 - The realised interface.

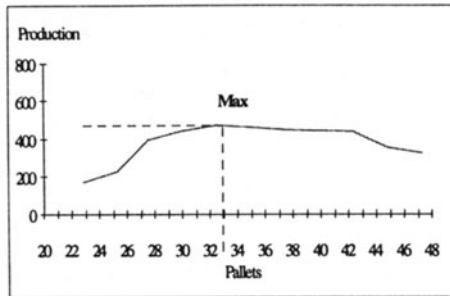


Figure 6 - Production variation when changing the number of pallets in the system.

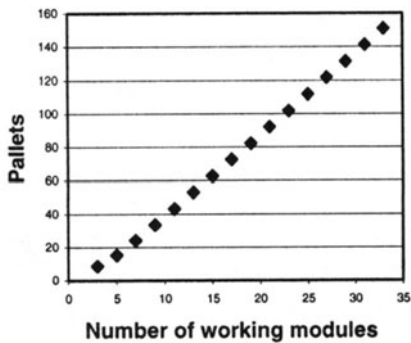


Figure 7 - Number of pallets maximizing the production vs. plant configuration.

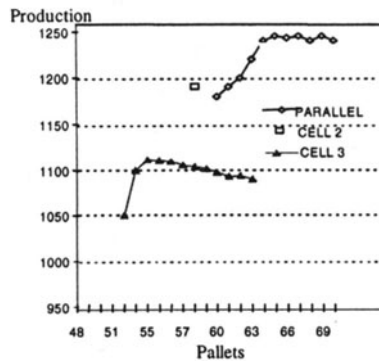


Figure 8 - Production variation vs. number of pallets.

The line interpolating these points gives good approximations for big systems but much worse for small plants. Therefore, an exponential factor has been introduced which estimates the pallet numbers better, as the number of working modules increases (figure 7).

$$Y = 4,91 \cdot X + 22,249 \cdot (0,6028)^X - 10,9081$$

The series scheduling needs other considerations. In fact, using the simulation, it was clear that the pallets- production curve moves left. The magnitude of this shift is proportional to the degree of the plant serialization. Thus, in a series scheduling, the system needs fewer pallets to reach the maximum production (figure 8).

6. FINAL CONCLUSIONS AND PROPOSED SOLUTIONS

From the simulations it is clear that the plant average saturation value decreases as the plant dimension increases. This can be due to a transient state and to the frequency, with which the interference state happens.

The transient state is determined by:

- The physical distance of the downstream modules from the loading unloading station.
- Non homogeneous rough and unfinished part flow.

The interference state happens each time a pallet which has to be unloaded from the working module comes into conflict with an other pallet coming from the transport loop. If this happens, the first pallet must wait on the internal line and the working module starves (the machine stops working).

Interference and transient states increase frequency as the system dimensions increase.

To decrease the transient and interference effects, two solutions have been identified:

1. Introduction of an additional loading – unloading station.
2. Use of smaller plants instead of a big one.

The introduction of a new loading unloading station, baricentral with the rough modules, improved the part flow of the downstream modules and increased the production by 2% (figure 9).

Using two small plants instead of one (with the same number of working machines: 22 roughing and 10 finishing modules) improved the transient state and decreased the interference frequency. In this case the production increase was 7% (figure 10).

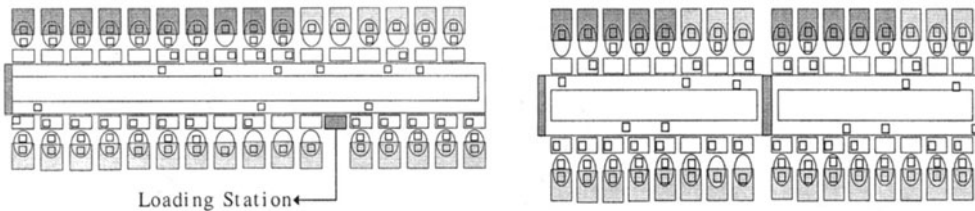


Figure 9 - Solution with baricentral loading station. Figure 10 - Solution with two smaller plants.

In conclusion, the studied plant is a system where it is possible to control the module feeding only by using the information stored in the pallets and the dynamic features of the line. That means, the plant scheduling does not need a supervision computer. These aspects mean an easy plant management, but, at the same time, they determine a non saturation of the line itself, which is difficult to eliminate.

REFERENCES

1. Sianesi A.: *FMS sistemi di produzione per la fabbrica automatica*, Ed. Il Rostro.
2. Mikell P. Groover: *Automation, production systems, and computer integrated manufacturing*, Prentice Hall.

MANAGEMENT OF INSTANT PROCESSES IN THE SHOPFLOOR

H.K. Tonshoff and G. Masan
University of Hannover, Hannover, Germany

KEY WORDS: INSTANT PROCESS, MAINTENANCE, PROCESS PLANNING, DYNAMIC PLANNING, INFORMATION SYSTEMS, SYSTEMATIC NONLINEAR PLANNING.

ABSTRACT: Modern approaches to manufacturing and maintenance management request quick decisions and fast response. Both targets rely on a sound information management. This paper presents a process-oriented approach to information management for the shopfloor with a focus on maintenance. Based on the idea of process-oriented information management, the concept of *instant processes* is presented. These processes are adaptive to the current situation. To support these processes, an information infrastructure is developed.

1. INTRODUCTION

The objective of modern production management is manufacturing goods at a constant quality level. Hence, it is desired to keep the conditions of production constant. This includes the conditions of production processes as well as the production facilities. Quality management has the duty to keep process and product quality at level. Maintenance keeps the expensive production equipment ready to use.

Due to the complexity of production facilities, especially maintenance cannot be fulfilled by just one person. Many experts, for example electricians, mechanics or software specialists, have to work together. Cooperative work requires rapid information sharing between people and all involved information systems.

Nowadays, information is extensively collected and stored in various information systems throughout the enterprise (Fig. 1). But information often lacks accessibility through

networked systems or the source is just unknown to the potential user [1,2]. The unavailable information delays the execution of processes, since much time is spent for information retrieval and evaluation. If information needed for decision making is rapidly supplied, process execution will be accelerated.

Decision Support Systems use the storage and processing capacity of computers to interactively give decision-makers the relevant information at the right place and time, accelerating the whole process. This requires a process model with special focus on decision making and its demand of information. Furthermore, it is necessary to have the ability to adapt the process to the rapidly changing context. Neither a method nor a software system to provide with these problems is known.

This paper presents a process-oriented approach to information management for the shopfloor with a focus on maintenance. It shows how business processes with inherent dynamics can be supported with a flexible planning procedure and a powerful information retrieval.

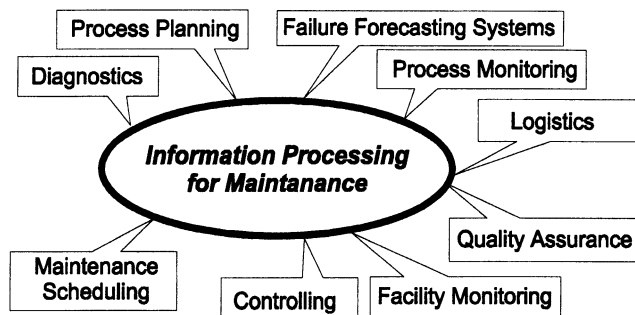


Fig. 1: Application systems involved in maintenance

2. INSTANT PROCESSES

Every business process consists of a sequence of activities and transitions between the activities. After every activity a decision is made. Decisions describe the sequence of activities. Decisions are made either by a human manager or an automatic, computerised system. It is important that the process can be handled automatically, since this leads to better usage of automated systems. Traditional workflow management systems are constructed in a way, that information is retrieved and presented to the user by the system. This implies, that the system has to know about the *arising* need of information. The beforehand known need of information is called *deterministic*. The concept of determinism applies to activities as well as to transitions.

In opposite to determinism stands creative behaviour. An activity or transition is called creative if knowledge is applied in an unconventional way. A closer look on the transitions of business processes in maintenance reveals three different classes of processes (Fig. 2).

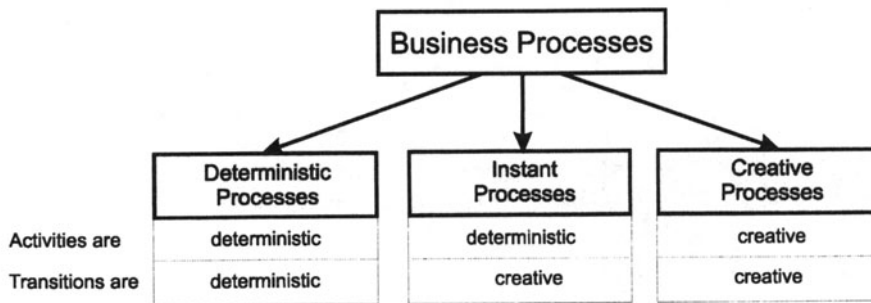


Fig. 2: Classes of business processes

Deterministic processes are business processes completely defined before the process starts. Such processes appear in administration, usually using files as media. This class of processes is well known both to research and practice. Modelling, planning and management of deterministic processes is supported by workflow-systems.

Creative processes typically appear in research. Activities are carried out for the first time, decisions are made step by step. The sequence of activities relies on the expertise and experience of the processor, who is human most times. Hence, scheduling creative processes is very difficult.

Instant processes consist of recurrent, well-known activities. But the sequence of activities is new every time they are executed. This rearrangement of activities distinguishes instant from deterministic processes and makes them tricky to handle in information systems. The transitions between activities are non-deterministic.

The class instant process is typical for maintenance activities. During process execution the need for further activities grows, as the following example illustrates: A detailed plan for repair cannot be given until the exact cause for failure has been traced. The result of the diagnosis process is indispensable for planning any further activities. The progress and the activities to execute depend directly from the result of one activity. The progress of the whole process cannot be foreseen in every possible branch. A net-plan would grow beyond any utilisable size [3].

We propose the following definition for the term instant process:

Definition 1: *A business process containing non-deterministic transitions is called an instant process.*

A closer look on instant processes reveals, that partial recur in various contexts. Reappearing sequences of deterministic transitions identify the partial process chains. For example, while scheduling a maintenance action, the partial chain „booking the maintenance team“ recurs unmodified regardless of the failed facility. These parts of instant processes are called modules:

Definition 2: *A module is a deterministic section of an instant process.*

A module can be described with methods like IDEF-0 or event-driven process chains. In opposition to complete business process, which are focussed on the present problem, modules are reusable in various contexts. The crucial task in managing instant processes is to find the right sequence of modules for the given case.

3. DYNAMIC SEQUENCING OF MODULES

The dynamic, case-based sequencing of modules during execution is not contained in the presented model.

The sequence of modules depends on the context of the present problem. The idea of context can be illustrated with the knowledge domains necessary for solving the problem. A process travels this domain during execution. Regularly the ongoing execution reaches points of decision (Fig. 3). These points can be identified as the module transitions of an instant process.

Although transitions to be managed are non-deterministic, an algorithm quickens the decision making by lowering the number of alternatives. A suitable algorithm was presented by McAllester et. al. : *Systematic Non-linear Planning* (SNLP) [4,5]. With the application of SNLP, two targets of managing instant processes are reached:

Complete examination of the knowledge domain

Each alternative path in the domain is checked for application. It is not necessary to know about each possible process sequence, because the system keeps track of this data. Thus, decisions are made on a base of sound information, because the whole present information is taken into account.

Reduced number of alternatives

SNLP is capable of deleting the improper search paths by considering the context during work. The result is a rather small list of alternatives.

The output of the calculation is presented to the executing instance, e.g. maintenance personnel, which chooses between the available alternatives. The basic SNLP algorithm runs as follows:

```

GOALS ← set of goals to achieve.
while GOALS ≠ ∅
  choose g ∈ GOALS.
  OPS ← set of operators achieving g.

```

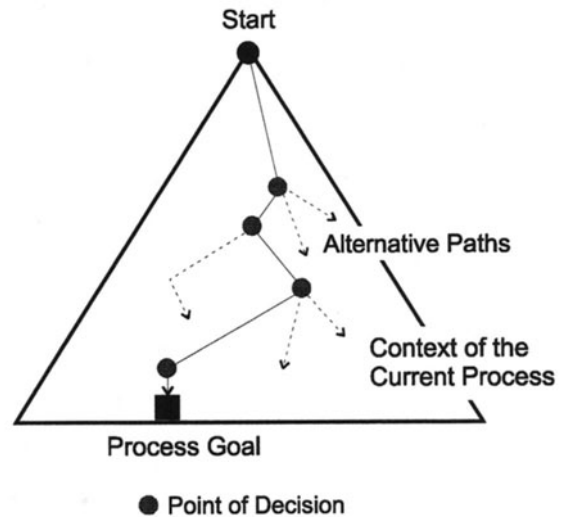


Fig. 3: Travelling the knowledge domain

```

if OPS ≠ ∅, start backtracking
else choose o ∈ OPS.
GOALS = GOALS ∪ { preconditions of o}.

```

Make plan consistent. If impossible, start backtracking.

To employ this condensed representation, interpretation is essential. The structure elements of instant processes must be matched with the structure elements of SNLP. These elements are operators, casual links and threads.

Operators: Every planning domain contains a set of operators. If an operator is executed, the assigned goal is achieved. An operator may require some preliminary steps which are also represented by operators. Different operators may have the same goal, but require different prerequisites or vice versa.

The operator of SNLP is equal to a module of an instant process. Each operator is described by parameters. The most important parameters are the goal of an operator and his prerequisites. If the execution requires some actions before, the necessary goals are listed as preconditions. Additionally, every operator has the attribute costs resembling required resources like manpower, time or machining capacity.

Threads: During planning, SNLP takes threads to operators in account. Every process or activity which endangers the flawless execution of an operator is called a thread. The concept of threads presented by McAllester has been extended to meet the requirements of business process planning. Three subtypes of threads have been identified.

1. *Internal Threads* occur during the planning process as shown by McAllester. Usually the algorithm solve these threads by altering the sequence of operators
2. *Standard Threads* apply to every link. Such threads can be solved with the maintenance assistant shown by Tönshoff [1]. If a standard thread cannot be solved, the planner deletes the threaded operator and the resulting branch from the process tree.
3. *External Threads* are caused by operations carried out outside the actual context. Any other running process is a potential thread to an operator. For example, if a maintenance operation requires special trained staff, this staff must be usually shared with others.

Casual Links: Casual links are the key element in supporting instant processes. They represent the non-deterministic transitions between modules. If a module is a possible succession to the given context, a link is established. Casual links are revealed by matching the present context with the prerequisites of known modules. After calculation, the found casual links are presented to the user.

4. APPLICATION OF THE CONCEPTS TO EVENT-DRIVEN PROCESS CHAINS

We applied the described concepts to event driven process chains, a modelling technique common to industrial and administrative applications [5].

The first task of application is to generate modules from ordinary business process models. Event-driven process chains consist of the basic elements *event*, *activity*, *information*

object and connector. To verify if a given model is a module, all these elements, except events, have to be deterministic. If one of the following rules fails, the failing element should be checked for non-deterministic behaviour.

[R1] *The decision made in connectors are deterministic.*

This rule is met, if the foundations of the decision can be completely named: the decisive factors as information objects, the decision logic and the expected results.

[R2] *Each information object has an assigned data source.*

If an information object has no assigned source, it will be retrieved by a non-standard way or from outside the knowledge domain. Therefore an information object with no source assigned will behave rather unpredictable and may hide creative activities.

[R3] *Each activity has an assigned executing resource class or process plan.*

If the processor or the behaviour of an activity is unknown, the behaviour will be unpredictable. Such an activity may hide creative decisions.

These rules are implemented in an support system called the information broker. To verify the properties of a module, the information broker tries to assign a method to every element of the process chain (Fig. 4). A method is an atomic and deterministic description of the element and its behaviour. For example, the method assigned to an activity names the process plan necessary to complete. It is noteworthy, that a method may be a process module by itself.

If an element cannot be assigned to any method, two solutions are suggested. The first is declaring a new method. This is a sound check for deterministic behaviour. The second solution is splitting the model two modules. This choice indicates, that alternatives in the process execution are selected case-based.

Obviously, decisions are made in connectors. But they are also hidden in activities, as function may yield different events. For example, the decision to replace or to fix a broken part of a machine are taken inside an activity. This decision requires complex evaluation and assessments on the alternatives, but seems purely deterministic at the first glance.

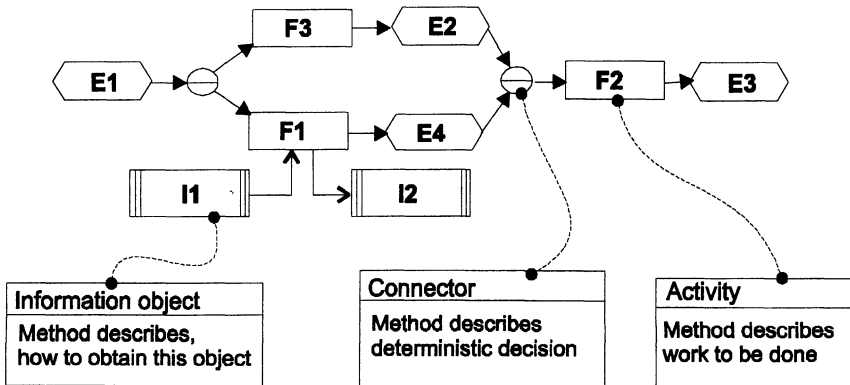


Fig. 4 : Assignment of methods to elements of process modules

During execution of the instant process, the information broker calls the assigned methods. At the moment methods are implemented using the programming language JAVA. The information broker maintains them as mediator software agents [7]. This form enables maximum flexibility, because with an agent the widest potential for adapting to legacy systems is given [8].

Figure 5 depicts the resulting architecture of the information broker. It consists of two components: the planning component, the associated module base and the execution component with the associated method base. Module base and method base are coupled by the assignments of methods and modules as shown in figure 4. The execution component requests the required methods from the method base. Since methods are programmed using JAVA, they can be directly transmitted via the agent interface.

The interactive interface between planning and execution component enables the user to review the suggestions made by the information broker. This feature is indispensable since a non-deterministic behaviour is contained in every instant process.

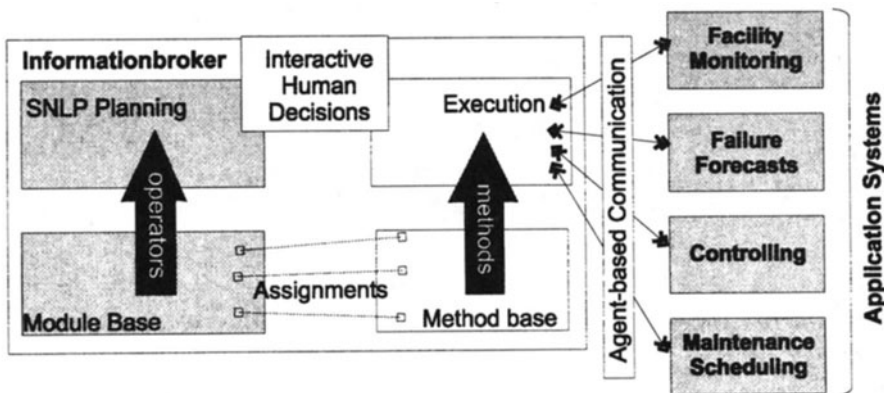


Fig. 5: Outline of the support system for instant processes

5. CONCLUSIONS

Research has shown, that modern information management has to add some complexity to business process descriptions [9]. The presented approach enriches established modelling techniques for information management. Event driven process chains were adopted for more flexible handling of process chains.

Investigations of business processes revealed three different classes. The classification of processes led to a natural, but still very strict, way to divide a process into modules. By dividing a process into modules flexibility is enhanced. The extra effort needed for modelling can be saved by reusing modules in various contexts. The instant concatenation of modules eliminates the need to build process models for every single application context. Thus, module-oriented modelling in conjunction with SNLP handles unforeseen cases. This feature is very important in the area of maintenance, because breakdowns are often unpredictable.

Working with the system, a worker gets a comprehensive list of abilities of the information system. Hence, decisions are made faster and process lead time is reduced. Moreover, efficiency of information management grows due to the better utilisation of available information. Without losing time by organisational barriers, information can be transferred throughout the departments of a company by using the support system for instant processes. The powerful information broker allows complex standard processes to be run efficiently.

This research was supported by the German Research Council (DFG), Special Research Department SFB384, Project D4 „Information Broker for the Systems of High-Availability Production Facilities“.

REFERENCES

1. Tönshoff, H. K.; Seufzer, A.: Simultaneous Planning of Maintenance Tasks. *Annals of the German Academic Society for Production Engineering*, Vol. V/1, S. 103-106, 1997.
2. Tönshoff, H. K.: Annual report of SFB 384. University of Hannover, IFA, 1998.
3. Schmidt, B. C.; Kreutzfeld, J.: FLEXPLAN: Integrated Process Planning and Workshop Scheduling. *Proceedings of IFIP WG 5.3 Conference PROLAMAT 1992*, Tokyo, June 24-26, p. 699-709.
4. Munoz-Avila, H.: A Case Study on Mergeability of Cases with a Partial-Order Planner. In: Steel, S; Alami, R.: *Recent Advances in AI Planning*. *Proceedings of ECP-97*, Springer, 1997.
5. McAllester, D.; Rosenblitt, D.: Systematic Non-linear Planning. In *Proceedings of the AAAI-91*, p634-639. Also: AI-Memo 139, Artificial Intelligence Laboratory, Massachusetts Institute of Technology, Boston 1991.
6. Scheer, A.-W.: *Wirtschaftsinformatik: Referenzmodelle für industrielle Geschäftsprozesse*. 6. Aufl. - Berlin [u.a.] : Springer, 1995.
7. Rothermel, K.: *Internet - von der Technologie zum Wirtschaftsfaktor / Deutscher Internet-Kongress '97 Düsseldorf*. Heidelberg: dpunkt, 1997.
8. Harrison, C. G.; Chess, D. M.; Kerschenbaum, A.: *Mobile Agents - Are they a good idea?* IBM Research Report, IBM Research Division, Rep. No. 1995.
(<http://www.research.ibm.com/massive/mobag.ps>)
9. Klarmann, J.; Becht, M.; Muscholl, M: *Modellierung flexibler Workflows mit teilausführbaren Aktivitäten*. DCSCW'98 Workshop "Flexibilität und Kooperation in Workflow-Management-Systemen", Universität Stuttgart, IPVR, Bericht 18/98-I.
(<http://www.informatik.uni-stuttgart.de/ipvr/vs/Publications/Publications.html#1998-klarmann-01>)

FROM FUNCTIONAL TO CELLULAR MANUFACTURING SYSTEMS

EVALUATION OF ATTRACTIVENESS

A. De Toni and A. Meneghetti
University of Udine, Udine, Italy

KEY WORDS: group technology, machine dedication, multiple class system

ABSTRACT

In the last decade some case and simulation studies showed how moving from a traditional functional layout to a group technology cellular one could be disadvantageous, opening a debate about the actual attractiveness of such a conversion.

Basing on a simple analytical queueing model, we compare a work shop performance to a partitioned system one, obtained by dedicating some machines to a family of products. We recognise how four parameters that describe both the unpartitioned and the new system characteristics can affect the value of a proper indicator, which measures the convenience of changing the manufacturing system and it is function of the lead times of the two manufacturing environments.

A simulation model is built to verify what the analytical model suggests; results confirm how the four parameters actually affect the convenience indicator; particularly interesting is the relevance of the factor which counts for the different process time of the various products and that distinguishes this research from previous studies.

1. INTRODUCTION

During the last three decades Group Technology principles have spread all around the world asserting the convenience of moving from a traditional functional layout to cellular manufacturing. Nevertheless, at the beginning of '70s some researchers as Leonard and Rathmill [1] expressed their doubts about the effective reduction in flow times and work-in-process achievable by cells. They claimed that several successful applications of cellular

manufacturing were not compared to efficient job shops, but to the poor performing functional layout which many firms started with. Successive simulation studies, as Flynn and Jacobs [2], Morris and Tersine [3], confirmed how, under many operative conditions, functional laid out systems gain better performance than cells. It was so highlighted what Shambu et al. [4] term the “cellular manufacturing paradox”. More recently published articles try to explain this paradox by developing analytical models that can overcome the particularity of simulation experiments and give a more general understanding. In particular Suresh [5], [6] and Suresh and Meredith [7] represent the original system and the new partitioned one, formed by cells and a remainder system, by queuing models in which all the products are supposed to have the same process time (the so termed “single-class” products) and only a single production step is considered. They deduce a deterioration of performance in the remainder system due to a loss of pooling synergy that erodes the advantages associated with the cells and often make the change not so attractive. The flexibility required to job shops makes the hypothesis of single-class products quite restrictive; we believe, instead, that the “multi-class” characteristic of the most functional laied out systems, i.e. the presence of very different process times, plays an important rule on determining the success of any cellular transformation. Thus, we introduce a multi-class factor in our analytical model to count the possibility that very different items have to be processed in the original system. The survey of Wemmerlov and Hyer [8] reports that the 43% of the respondents implemented cellular manufacturing as a machine dedication without moving the equipment to create cells. Therefore we decided to investigate how a multi-server work shop performs when some machines, which form a production step of the virtual cell, are formally assigned to a part family. The basic idea is to express the performance of the partitioned system as a function of the characteristics of the original work shop and some proper factors describing the type of change. Then we used simulation experiments to validate what our analytical model suggests about the cellular paradox.

2. ANALYTICAL INSIGHTS

We consider a typical work shop (marked by sub-index w) with m machines and describe it as a queueing system with m servers and both the interrarrival and process times belonging to a Markovian distribution, i.e. we use a $M/M/m$ queueing model. Since actual systems have often to manage different products, each with its own processing time and arrival rate, we try to extend Suresh’s analysis to the multi-class problem.

Following Whitt [9] and Bitran and Tirupati [10] approach, first an “aggregate product” is formed by properly combining the data of the different items. This aggregate product is then used to replace all the parts that have to be processed in the work shop; in this way the multi-class problem can be brought back to a single-class one, which is more easy to manage. Several assumptions are made for reason of tractability.

Let $\lambda_i = D_i / q_i$ be the mean arrival rate of the i -th part, supposed to follow a Poisson process, where D_i and q_i are its demand rate and lot size respectively. The arrival rate of the aggregate product to the work shop is still Poisson with a mean $\lambda_w = \sum_i \lambda_i = \sum_i D_i / q_i$. Its unit process time is supposed to be exponentially distributed, with a mean equal to a weighted

average of all part unit process (run) time: $t_w = \sum_i \lambda_i t_i / \sum_i \lambda_i$. The service rate will be $\mu_w = 1/(\tau_w + q_w \cdot t_w)$, where τ_w is the average setup time per batch and q_w the lot size of the aggregate product in the work shop, while utilisation is $\rho_w = \lambda_w / \mu_w$.

We can now obtain the lead time W_w and the minimum lot size $(q_w)_{\min}$ for stability [9] in the work shop, analysed at an aggregate level:

$$W_w = \left[\sum_{n=0}^{m-1} \frac{\rho_w^n}{n!} + \frac{\rho_w^m}{m!(1 - \rho_w/m)} \right]^{-1} \frac{\rho_w^m \mu_w^{-1}}{(m-1)!(m - \rho_w)^2} + \mu_w^{-1} \quad (1)$$

$$(q_w)_{\min} = \frac{D_w \cdot \tau_w}{(m - D_w \cdot t_w)} \quad (2)$$

where $D = \sum_i D_i$ is the total demand rate, q_w the lot size of the aggregate product and τ_w its average setup time per batch.

Suppose now to dedicate a certain fraction β of the m machines to some parts, which can be considered a family in a Group Technology philosophy. A “cell” and a “remainder system” can so be recognised.

Let k, γ be the fraction of the total demand rate and the fraction of the aggregate mean process time that can be assigned to the cell respectively. Denoting by sub-indexes c and r the cell and the remainder system, we have:

$$\begin{aligned} m_c &= \beta \cdot m & m_r &= (1 - \beta) \cdot m \\ D_c &= k \cdot D_w & D_r &= (1 - k) \cdot D_w \\ t_c &= \gamma \cdot t_w \end{aligned}$$

The aggregate process time in the remainder system can be evaluated as following:

$$D_w t_w = D_c t_c + D_r t_r \Rightarrow D_w t_w = k D_w \gamma t_w + (1 - k) D_w t_r \Rightarrow t_r = \frac{1 - k\gamma}{1 - k} t_w$$

As regards setup times we introduce a reducing factor δ to account for advantages in the cell due to similarity of items, while we consider the aggregate setup time in the remainder system unchanged with respect to the original work shop:

$$\tau_c = \delta \tau_w \quad \tau_r = \tau_w$$

Even the cell and the remainder system have so been brought back to a single-class multi-server case and relations (1), (2) can be used to evaluate time-related performance in terms of the original work shop data (D_w, t_w, τ_w, m) .

Since we want to avoid that a comparison between the original work shop and the partitioned one could be distorted by the poor performance related to non-optimised systems, we determine for each system the lot size which leads to the minimum lead time. Since Karmarkar et al. [11] have demonstrated that lead time is a convex function of the lot size, we calculated the optimal value of lot size by progressively increasing the minimum lot given by relation (2) until lead time starts to grow.

An indicator has to be properly created to evaluate the convenience of moving from a traditional work shop to a partitioned one. Since a time-based competition approach is supposed to be coherent to market characteristics, we believe that the faster the deliveries the higher the price a customer is inclined to pay, so that, if W is the lead time and P a

proper constant, the unit price is $P_u = P/W$ [£/units]. The partitioned system has to be preferred if the related revenue in a time period T is greater than the unpartitioned one in the same period, i.e. if:

$$R_c + R_r - R_w > 0 \tag{3}$$

The dedication of some machines in a work shop may be associated to parts strategically important and therefore benefits expected from improving their lead time are greater than those obtained by increasing the performance of the others. Thus, we introduce a weight s to possibly increase the revenue associated to items diverted to the cell whether their strategic rule has to be considered.

Relation (3) can be rewritten as:

$$\begin{aligned} s(P/W_c)D_cT + (P/W_r)D_rT - [s(P/W_w)D_cT + (P/W_w)D_rT] > 0 &\Rightarrow \\ s(P/W_c)kD_wT + (P/W_r)(1-k)D_wT - [s(P/W_w)kD_wT + (P/W_w)(1-k)D_wT] > 0 &\Rightarrow \\ s \cdot k \left(\frac{1}{W_c} - \frac{1}{W_w} \right) + (1-k) \left(\frac{1}{W_r} - \frac{1}{W_w} \right) > 0 &\tag{4} \end{aligned}$$

If we denote with R the left-hand side of the above inequality, we obtain a proper indicator to compare the original work shop to the partitioned system. R is a function of the original work shop data and the type of change introduced into the system; the four factors β, k, γ, δ , in facts, describe the new partitioned system in terms of number of original machines and demand rate devolved to the cell, characteristics of the portion of products processed in the cell and the expected setup time reduction due to similarity. Thus, given a work shop, it is possible, on the basis of the values assigned to the four factors, describe different potential cellular layouts and evaluate if the related change is advantageous from a time-based competition point of view.

3. RESULTS FROM THE ANALYTICAL MODEL

In general we can observe how partitioning the original work shop leads to an improvement of the cell performance but a deterioration in the remainder system. Thus, the change looks convenient only if cell improvement can overcome the worse performance obtain in the remainder system due to what Suresh and Meredith [7] define a loss of pooling sinergy.

Varying one factor at a time it is possible to draw the behaviour first of the lead time in the cell and in the remainder system, as showed for example in figure 1, and then the values assumed by the indicator R , measuring the opportunity of a system change (see figure 2).

From the analytical model we can deduce the existence of proper combinations of the four factors leading the partitioned system to perform better than the original work shop ($R > 0$).

Varying the four design factors outside this optimal four-dimension region leads to a poorly performing system (see the negative values of R assumed in figure 2); it is so underlined that partitioning a work shop is not always correct and cellular manufacturing has to be carefully adopted.

As expected, the strategic weight of cell products s is able to enlarge the region of factors' variation which ensure the opportunity of partitioning the original work shop.

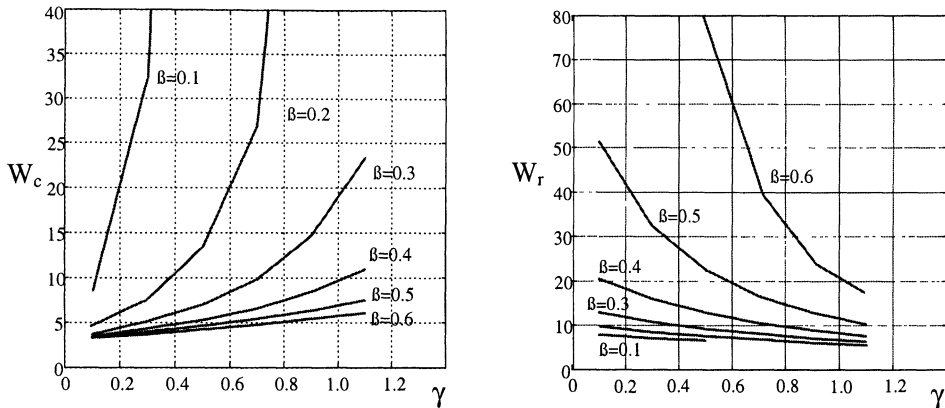


Figure 1 Lead time [h/batch] W_c in the cell and W_r in the remainder system varying β and γ

Particularly interesting is how the multi-product factor γ , which has been introduced to describe the multi-class characteristic of the analysed systems, can really affect their performance and consequently the opportunity of a change. This suggests that if the chance for a work shop to process products with very different run times is ignored, i.e. a single-class model is adopted, wrong decisions can be taken.

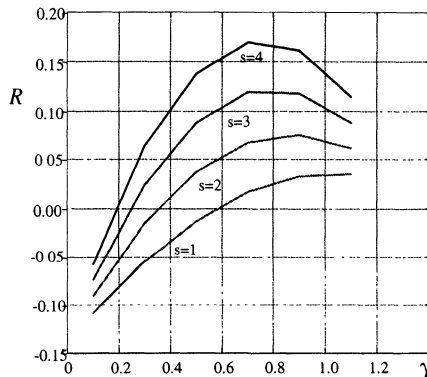


Figure 2 The indicator R varying the multi-class factor γ and the strategic weight s .

4. SIMULATION EXPERIMENTS

The analytical model suggests that partitioning a work shop not always leads to an improvement of performance; the four factors introduced to describe the type of change applied to the original system seem to play an important rule for a successful result. Thus, it is reasonable to deduce that before bringing any transformation to the system, attention has to be paid to decide the number of machines to be moved, the portion of demand rate devolved to the cell, to which items, in term of processing times, the cell is going to be dedicated and finally how much setup reduction can be made due to part similarity in the family. Since the analytical model is simplified for tractability, we

conducted simulation experiments to validate the conclusions it leads to, i.e. to verify if the four factors can really explain a successful or unsuccessful system change.

We simulated first a work shop made by 10 machines that processes 13 products for a total demand rate of 400 units/hour, with Poisson arrivals and different exponentially distributed process times. As the original work shop has to be optimised for a proper comparison, we chose the lot size of every item to ensure system stability and a low work-in-progress level. After calculated the lead time associated to this original work shop, we partitioned it dedicating a certain fraction β of machines to some products that can naturally form a family in a Group Technology meaning. The items diverted to the “cell” amount for a portion k of the total demand rate and their mean run time is γ times the mean run time of all the products. Also, due to similarity in the family, a setup reduction δ is applied in the cell. Then we varied the values of the four factors to measure deterioration or improvement of performance in the partitioned system by the indicator R . Items devolved to the cell are not recognised to be strategically relevant; therefore, $s = 1$.

We performed a 2^4 factorial design, considering for each of the four factors β, k, γ, δ only a low and a high level of variation, as showed in Table 1; 10 replications of experiments are made.

Factors	Description	Low level	High level
β	fraction of machines	0.4	0.6
k	fraction of demand	0.3	0.5
γ	fraction of process time	0.8	1.1
δ	setup reduction	0.6	0.9

Table 1 Levels for the 2^4 factorial design

5. SIMULATION RESULTS

The main effects, which represent the change induced on R if a factor moves from is low level to his high level, and the two-factor interaction ones statistically significant ($\alpha=0.1$) are shown in Table 2.

The three major effects are related to factors k, γ and the interaction of β and γ . Increasing the portion of demand rate devolved to the cell has a positive impact on R and therefore on the convenience of a system change; it may be deduced that dedicating some machines to particular items is worth-while only if there is a sufficient volume to be processed and conversely a low amount of demand has to face a loss of pooling synergy in the remainder system. This impact is strengthened if a setup reduction can be expected, as underlined by the negative interaction effect of k and δ (remember that a high level of δ is related to a low setup reduction and so a negative effect means a deterioration of performance if setup times are poorly reduced). In this case, in facts, a greater amount of demand can benefit by the shorter time spent in queue waiting for machines being set up. It has to be underlined how the relative small effect of δ on R can be associated to its quite small range of variation chosen for simulation experiments; this agrees with [5], [6] and [7] which recognised how a great reduction on setup times is required to face the loss of pooling synergy.

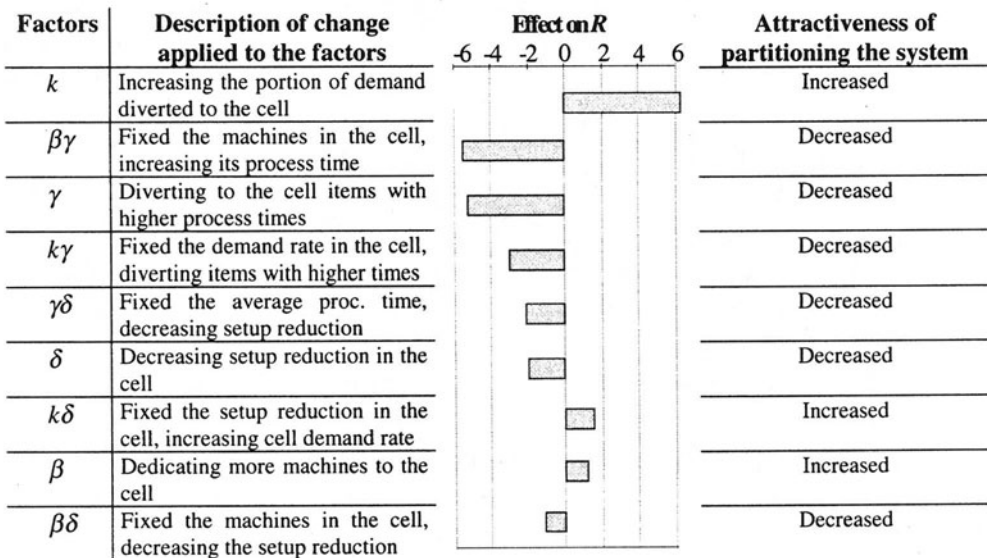


Table 2 Main and two-factor interaction effects on R statistically significant (W_c , W_r and W_s are expressed in seconds and effect values are E-06)

The remarkable negative effect of the multi-product factor γ attests what the analytical model suggests: the multi-class characteristic of a work shop cannot be disregarded while partitioning the system, because the longer the processing times of items diverted to the cell compared to the overall average processing time (i.e. the higher the value of γ), the greater the loss of pooling synergy. The interaction effect between β and γ shows, in facts, agreeing with the analytical model, how for a given β , i.e. a given number of dedicated machines, the advantage of partitioning the system decreases as the lead time of the cell grows due to the high run times of those items that cannot rely on the less loaded machines of the remainder system.

6. CONCLUSIONS

The analytical model and the simulation experiments shows that partitioning a work shop is not always advantageous. Attention has to be paid particularly to the portion of demand rate diverted to dedicated machines and to its processing times. It so underlined how a distorted expectation of improvement can be taken if the work shop is analysed as a single-class system. The cellular paradox stands out our study; it can be recognised, in facts, that successful changes in the system are made only if the relative factors fall in a proper region. This work can be regarded as a first step to better understand the effective attractiveness of moving from a functional to a cellular manufacturing system, when Group Technology is implemented as a machine dedication problem, without moving the equipment. Further analysis can be made to understand how several partitioned work

shops, that belong to a part family routing, interact and affect the overall production system performance.

REFERENCES

1. Leonard, R. and Rathmill, K., "The group technology myths", *Management Today*, January 1977, pp. 66-9;
2. Flynn, B. B. and Jacobs, F. R., "A simulation comparison of group technology with traditional job shop manufacturing", *International Journal of Production Research*, Vol. 24, 1986, pp. 1171-92;
3. Morris, J. S. and Tersine, R. J., "A simulation analysis of factors influencing the attractiveness of group technology cellular layouts", *Management Science*, Vol. 36, No. 12, 1990, pp. 1567-78;
4. Shambu, G., Suresh, N. C. and Pegels, C. C., "Performance evaluation of cellular manufacturing systems: a taxonomy and review research", *International Journal of Operations and Production Management*, Vol. 16, No. 8, 1996, pp. 81-103;
5. Suresh N.C., "Partitioning work centers for group technology: insights from an analytical model", *Decision Sciences*, Vol.22, No. 4, 1991, pp. 772-91;
6. Suresh, N.C., "Partitioning work centers for group technology: analytical-extension and shop-level simulation investigation", *Decision Sciences*, Vol. 23, No. 2, 1992, pp.267-90;
7. Suresh, N.C. and Meredith, J.R., "Coping with the loss of pooling synergy in cellular manufacturing systems", *Management Science*, Vol. 40, No. 4, 1994, pp. 466-83;
8. Wemmerlov, U. and Hyer, N. L., "Cellular manufacturing in the US industry; a survey of users", *International Journal of Production Research*, Vol. 27, 1989, pp. 1511-30;
9. Whitt, W., "The Queueing network analyser", *Bell System Technology Journal*, Vol. 62, No. 9, 1983, pp. 2779-2815;
10. Bitran, G. R. and Tirupati, D., "Multiproduct queueing networks with deterministic routing: decomposition approach and the notion of interference", *Management Science*, Vol. 34, No. 1, 1988, pp. 75-100;
11. Karmarkar, U. S., Kekre, S., Kekre, S. and Freeman, S., "Lot-sizing and lead time performance in a manufacturing cell", *Interfaces*, Vol. 15, No. 2, 1985, pp. 1-9.

POSSIBILISTIC PROGRAMMING AND GAS FOR AGGREGATE PRODUCTION PLANNING UNDER VAGUE INFORMATION

S. Fichera

University of Catania, Catania, Italy

A. La Spada

University of Palermo, Palermo, Italy

G. Perrone

University of Basilicata, Potenza, Italy

V. Grasso and U. La Commare

University of Palermo, Palermo, Italy

KEY WORDS: Production planning, possibilistic programming, genetic algorithm

ABSTRACT: In production planning activities, aggregate planning is surely the phase where the lack of information is more relevant. The reasons for that can be summarised in: a) the planning product is an aggregate one, very often not corresponding to actual products; b) the delay from the actual production is relevant so that information regarding actual production resources availability and performances are vague; c) the planning activity is often based on forecasts. On the other hand, all the subsequent production planning activities are based on the result of aggregate planning. In the paper a research going on at the Workgroup for Soft Computing Application in Manufacturing is presented. A Decision Support System (DSS) for assisting the decision maker in Aggregate Production Planning decisions in a vague environment has been developed using possibilistic formulation. First results are presented and discussed.

1. INTRODUCTION

The concept of *fuzzy production systems* has arisen recently in manufacturing research. Conceptually, a fuzzy production system is a production environment that contains vague information. Vagueness is a kind of uncertainty that is not based upon frequency of event occurrence as is statistical characterisation. Vagueness is more related with the definition of the event, therefore it is not manageable by using statistical tools.

Examples of vagueness in manufacturing can be encountered in:

- Ishii et. al. [1] and Ishibuchi, et al. [2]; in the papers the authors stress that the due date is not a simple number, but is a concept, more precisely an agreement between the

customer and the supplier. Agreements are subject to human imprecision, therefore concept such due dates are more properly described by using fuzzy linguistic variables.

- Inuigushi, et al. [3] and Kuroda, et al. [4]; in the paper the authors generalise the vagueness concept in production systems stating that it can concern both data, such service times, job availability etc..., and requirements or constraints, such as cost requirements, due dates, production volumes.

The data vagueness is due to the approximate knowledge of the process especially when humans are involved. Service times, especially in small and medium enterprises, are an example of vagueness concerning data. In such environments is very difficult to foresee service times for several reasons such as: humans are very involved in production activities; the production is very dynamic and changeable so that production lots are not standardised; there are no resources and time for collecting data and historical series analysis. For all the above reasons and others, data such processing times and job availability are expressed through approximate expression such as "*about X units of time*", or "*the job will be available in approximately Y units of time*". Such vague concepts can easily turned into fuzzy numbers and treated by using fuzzy algebraic operators. Requirements and constraints are often the result of a human decision process. Due dates are the result of an agreement; production quantities are the result of a trade-off among marketing requirements and production resources availability; cost requirements are the result of a decision process involving budget consideration and production resources utilisation. The result of human decision processes is never a crisp requirement, because it is human in nature, then vague. Such vagueness is usually linguistically expressed. Traditional models force this vagueness to became crisp, while fuzzy models leave the vagueness there giving a more adequate description of the reality. Several applications have been proposed so far in the field of production management by using fuzzy methods. Among other the following are the most relevant: Inuigushi, et al. [3] have proposed to use fuzzy possibilistic programming for planning fuzzy production systems; McCahon et al. [5], Hong et al. [6], Kuroda et al, [4], Ishibuchi et al. [7] have proposed several algorithms to schedule job and flow shop within Fuzzy Production Systems; Ishi et al. [1] and Ishibuchi et al. [2] have proposed method to deal with fuzzy due dates in job shop scheduling; Negi et al. [8] have proposed the extension of fuzzy mathematics to Queue Theory; finally, Perrone et al. [9] have proposed fuzzy methods for processing fuzzy information within a discrete event simulation process.

This paper takes start from the work of Inuigushi et al. on fuzzy possibilistic programming for production planning and proposes models for aggregate production planning under vagueness information. The paper advocates the use of genetics algorithm as optimisation tool for such models.

2. POSSIBILISTIC FORMULATION OF THE "ANTICIPATE OR CHASE" MODEL

This paper proposes the extension of the classical "*anticipate or chase*" model. Such a model concerns the formulation of the master production schedule in front of cyclical

demand variation. In fact, in front of seasonal demand changes the model proposes two alternatives:

- anticipate production utilising stock to deal with demand peaks;
- chase demand by utilising overtime work.

Having indicated with:

$t = 1, \dots, T$ period index; T number of planning periods;

$D(t)$ demand of the product over the period t ;

$e(t)$ inventory of the product at the end of the period t ;

$W(t)$ hours of direct and regular manpower in the period t ;

$S(t)$ hours of direct and overtime manpower in the period t ;

h number of manpower hours needed for a unit of product;

w unit cost per hour of regular manpower;

s unit cost per hour of overtime manpower;

m unit direct production cost (energy + raw part);

i unit inventory cost;

$MAXW(t)$ hours of direct and regular manpower available in the period t ;

$MAXS(t)$ hours of direct and overtime manpower available in the period t ;

$x(t)$ number of products to be produced in the period t ; this is the decision variable;

the "anticipate or chase" model can be stated as it follows:

$$\text{Min}(C_t) = \text{Min} \left(\sum_{t=1}^T [(m \cdot x(t)) + (i \cdot e(t))] + [(w \cdot W(t)) + (s \cdot S(t))] \right) \text{ cost minimisation} \quad (1)$$

subject to

$$x(t) + e(t-1) - e(t) = D(t) \quad \text{balance equation among stock, demand and production;} \quad (2)$$

$$h \cdot x(t) \leq W(t) + S(t) \quad \text{total capacity production constraint;} \quad (3)$$

$$0 < W(t) \leq MAXW(t) \quad \text{regular manpower hours capacity constraint;} \quad (4)$$

$$0 < S(t) \leq MAXS(t) \quad \text{overtime manpower hours capacity constraint;} \quad (5)$$

$$e(t) \geq 0 \quad \text{stockout and backlog are not allowed.} \quad (6)$$

In the classical formulation of the "anticipate or chase" model the demand is precisely known. This is one of the most relevant limits of classical models, in fact, often only an approximate evaluation of the period demand is available. The other limitation concerns the estimation of h ; in fact, specially in manual manufacturing systems the exact estimation of h is very difficult and it is an information that in small and medium enterprises is very difficult to find. What, indeed, is generally available is again an approximate estimation of h . Here a model where the vagueness within $D(t)$ and h is addressed by using fuzzy numbers is proposed. In particular, triangular fuzzy numbers are very widely used to model situation affected by approximate and imprecise knowledge.

In our approach the vagueness related with the knowledge of $D(t)$ and h is expressed through the triangular fuzzy numbers $\tilde{D}(t) = (a_D, b_D, c_D)$ and $\tilde{h} = (a_h, b_h, c_h)$.

Such a choice imposes a possibilistic formulation of constraints (2) and (3). Constraint (2) has the following formulation:

$$x(t) + e(t-1) - e(t) = \tilde{D}(t) \quad (7)$$

Figure 1 shows the possibilistic formulation of the above constraint and how its satisfaction, $\Pi_{\tilde{D}(t)}$, is computed by using possibility theory. Constraint (3) has the following formulation:

$$\tilde{h} \cdot x(t) \lesssim W(t) + S(t) \tag{8}$$

Figure 2 shows the possibilistic formulation of the above constraint and how its satisfaction, $\Pi_{\tilde{h}(t)}$, is computed by using possibility theory.

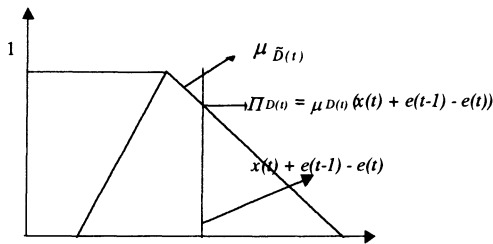


Figure 1. Possibilistic formulation of constraint (2)

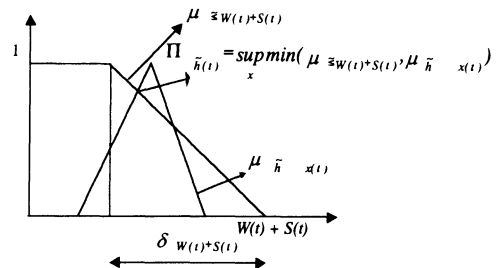


Figure 2. Possibilistic formulation of constraint (3)

Figure 2 shows how a fuzzy relaxation accounting for production inefficiency has been introduced in constraint (3). In fact, a constraint satisfaction function, $\mu_{\tilde{z}(W(t)+S(t))}$, has been introduced expressing that if the amount of production required for the period t , $\tilde{h} \cdot x(t)$, is lower than $W(t) + S(t) - \delta_{\tilde{z}(W(t)+S(t))}$, then the production can be effectively performed; if $\tilde{h} \cdot x(t)$ is comprised in the range $[W(t) + S(t) - \delta_{\tilde{z}(W(t)+S(t))}, W(t) + S(t)]$ due to possible production inefficiency, it is not sure that the production can be effectively performed and, therefore, the satisfaction is decreasing; finally, if $\tilde{h} \cdot x(t)$ is greater than $W(t) + S(t)$, the constraint is violated and the satisfaction is zero. With the introduced possibilistic formulation of constraints (2) and (3), the "anticipate or chase" model is formulated as follows:

$$\text{Min}(C_t) \quad \text{total cost minimisation} \tag{1}$$

$$\text{Max}(\Pi_{\tilde{D}(t)}) \quad \text{maximisation of the satisfaction of demand constraint} \tag{2bis}$$

$$\text{Max}(\Pi_{\tilde{h}(t)}) \quad \text{maximisation of the satisfaction of total production constraint} \tag{3bis}$$

subject to

$$0 < W(t) \leq \text{MAX}W(t) \quad \text{regular manpower hours capacity constraint;} \tag{4}$$

$$0 < S(t) \leq \text{MAX}S(t) \quad \text{overtime manpower hours capacity constraint;} \tag{5}$$

$$e(t) \geq 0 \quad \text{stock-out and backlog are not allowed.} \tag{6}$$

As the reader can notice the introduction of the fuzzy constraints leads to a multiple objective formulation of the model. It is to be stressed that, only objective (1) does not vary within a $[0, 1]$ interval, so that this objective needs to be scaled within this interval. For this purpose, let us define with C_t^+ and C_t^- respectively the maximum and the minimum value

of the cost function obtained with only constraints (4) to (6). The scaling of the objective (1) is given by the following satisfaction function:

$$\Pi_{C_i} = \begin{cases} 1 & \text{if } C_i \leq C_i^- \\ \frac{C_i^+ - C_i}{C_i^+ - C_i^-} & \text{if } C_i^+ \leq C_i \leq C_i^- \\ 0 & \text{otherwise} \end{cases} \quad (9)$$

therefore the final formulation of the "anticipate or chase" model is:

$$\text{Max}(\Gamma(t)) = \text{Max}(\Pi_{C_i} \wedge \Pi_{\bar{D}(t)} \wedge \Pi_{\bar{h}(t)}) \quad \text{maximisation of the global satisfaction} \quad (10)$$

subject to (4), (5) and (6), where the symbol \wedge is a intersection operator such as minimum or product one. The optimisation of the above model is particularly complex. Our approach consists in applying a genetic algorithm for the optimisation of possibilistic models.

The chromosome is a vector consisting of $\xi(t) = [x(t), e(t), W(t), S(t)]$ while the algorithm structure is the following:

1. generate a random initial population \mathbf{P} of chromosomes $\xi(t)$;
2. the population \mathbf{P} goes under selection based on the reproduction of the better individuals method;
3. selected chromosomes go under crossover with probability p_c ;
4. selected chromosomes go under mutation with probability p_m ;
5. as result of steps 3 and 4 a new population \mathbf{P}' is generated;
6. the stop criterion is evaluated; if it is satisfied the process ends, otherwise restart from step 2.

3. THE DSS FOR POSSIBILISTIC AGGREGATE PRODUCTION PLANNING

The research here presented belongs to a wider project that aims to develop a Decision Support System (DSS) for assisting production planner. This software will codify different aggregate production planning models and focuses its peculiarity on giving the possibility to formalise fuzzy information. While the "anticipate or chase" model is the only codified one up to now, other functionality of the DSS have already been codified. In particular this functionality concerns:

- the user front-end module;
- the optimisation module (the genetic algorithm);
- the post processor module.

The above modules have been developed in JAVA++ in order to be platform independent for a company intranet utilisation. A numerical example will clarify the potentiality of the approach and of the DSS developed. Figures 3-5 show some of the potentialities of the developed modules. In particular:

- Figure 3 shows the user front-end module characteristics; as the reader can notice, the menu allows the analyst to introduce several kind of company data concerning the demand, the production, such as technological routing, service times and production costs, and the number of planning periods;

- Figure 4 shows the front-end of the optimisation model in which the analyst can introduce the data concerning the genetic algorithm control parameters;
- Figure 5 shows the result post processor in which several aggregations of the results are available.

4. NUMERICAL EXAMPLE AND CONCLUSIONS

As numerical example, the proposed model and software has been applied to a simple case of study. A product is to be planned in a six months period. The production data are:

$$w = 10 \text{ UM/hr};$$

$$s = 17 \text{ UM/hr};$$

$$m = 2 \text{ UM/part};$$

$$i = 0.5 \text{ UM/part};$$

$$\text{MAXW} = 120 \text{ hr/day};$$

$$\text{MAXS} = 40 \text{ hr/day};$$

$$\tilde{h} = (10, 12, 13) \text{ hr/part}.$$

As the reader can notice the vagueness concerning the service time has been modelled by using a triangular fuzzy number. Furthermore, the vagueness in the period demand knowledge has been modelled by using the triangular fuzzy numbers depicted in Table 1.

Period	a	b	c	day/period
1	90	100	110	22
2	360	400	440	22
3	270	300	330	22
4	90	100	110	22
5	90	100	110	22
6	370	450	470	22

Table 1. Period demand

The decision variable for the problem are:

$x(t)$ production at the period t , for $t = 1, \dots, 6$;

$e(t)$ inventory at the period t , for $t = 2, \dots, 6$; the inventory available is 50 units ($e(1) = 50$), while the inventory for the period $t+1$ will be zero;

$W(t)$ regular manpower at the period t ;

$S(t)$ overtime manpower at the period t .

This problem has been codified and solved by using the proposed DSS. Due to the difficulty to find an initial random feasible solution, the proposed DSS system is able to provide an initial feasible solution. Such solution is the one reported in Table 2, while in Table 3 are reported the satisfaction for objectives (2) and (3) and the plan cost. The satisfaction indexes of objectives 2 and 3, reported in Table 3, are obtained computing the minimum satisfaction among the periods; the cost satisfaction index is computed knowing that the maximum with $C_i^+ = 335.920 \text{ UM}$ and $C_i^- = \sum_t D_a(t) \cdot h_a \cdot w = 122.00 \text{ UM}$, being

$D_a(t)$ and h_a respectively the lowest values of the triangular numbers $\tilde{D}(t)$ and \tilde{h} ; finally, the global satisfaction is the minimum among the single objective satisfaction, i.e. the chosen intersection operator is the minimum.

Period	Initial plan				Optimal plan			
	x	e	W	S	x	e	W	S
1	280	50	2640	880	280	50	2616	827
2	220	230	2640	0	217	230	2616	97
3	250	50	2640	360	250	50	2640	440
4	200	0	2400	0	200	0	2407	53
5	220	100	2640	0	220	100	2606	106
6	200	220	2400	0	196	220	2423	53

Table 2. Initial plan and optimal plan

	Initial plan Satisfaction	Optimal plan Satisfaction
Demand constraint satisfaction	1.0	0.9
Capacity constraint satisfaction	0.62	0.73
Cost	178.365 UM	183.710 UM
Cost Satisfaction	0.73	0.71
Global satisfaction	0.62	0.71

Table 3. Plans performance

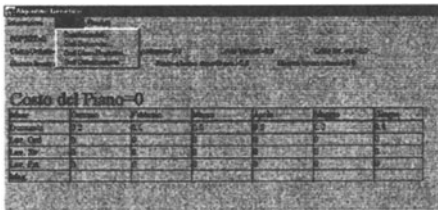


Figure 3. The user front-end module

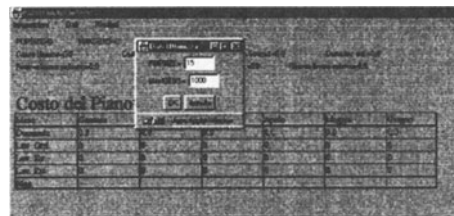


Figure 4. The optimisation module

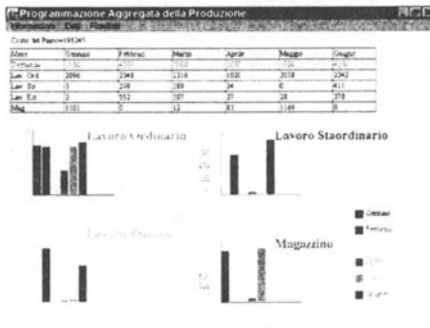


Figure 5. The post processor module

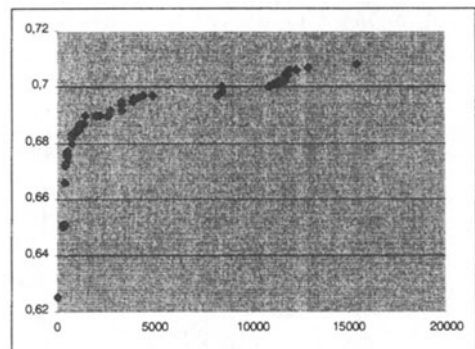


Figure 6. The optimisation process

The initial solution has been improved by using a genetic algorithm with the following characteristics:

- averaged sum as crossover operator [10];
- population size of 20 individuals;
- crossover probability 40%;
- mutation probability 7.5%;
- maximum number of generation 20.000.

Figure 6 shows the improvement obtained by the genetic algorithm, while Tables 2 and 3 report respectively the best solution and the related satisfaction. As the reader can notice the genetic algorithm improves the initial solution of 14%.

In conclusion this paper presents a first result of a research going on at the Workgroup for Soft Computing Application in Production Engineering. This research concerns the extension of aggregate production planning algorithm to case affected by vagueness by means the utilisation of fuzzy set theory and evolutionary optimisation. In particular the paper presents the possibilistic formulation of the "anticipate or chase" model for single product production planning. Furthermore, the basic characteristics of the Decision Support System for production planner assistance when vagueness affects production data.

ACKNOWLEDGEMENT

This research has been supported by MURST.

REFERENCES

1. Ishii H., Tada M., and Masuda T., (1992). Two scheduling problems with fuzzy due date. *Fuzzy Set and Systems*, **46**, 339-347.
2. Ishibuchi H., Yamamoto N., Misaki S., and Tanaka, H., (1994). Local search algorithms for flow shop scheduling with fuzzy due dates. *Int. J. of Production Economics*, **33**, 53-66.
3. Inuiguchi, M., Sakawa, M., Kume, Y., (1994). The usefulness of possibilistic programming in production planning problems. *Int. J. of Prod. Econ.*, **33**, 45-52.
4. Kuroda, M., and Wang, Z., (1996). Fuzzy job shop scheduling. *Int. J. of Production Economics*, **44**, 45-51.
5. McCahon, C. S., and Lee, E. S., (1992). Fuzzy job sequencing for flow shop. *European J. of Operational Research*, **62**, 294-301.
6. Hong, T.-P., Huang, C.-M., Yu, K.-M., (1995). A fuzzy LPT algorithm for scheduling. *Proc. of Int. Conf. on Systems, Man and Cybernetics*, Vancouver, CANADA.
7. Ishibuchi, H., Murata, T., Lee, K.-H., (1996). Formulation of fuzzy flowshop scheduling problems with fuzzy processing times. *Proc. of the fifth IEEE Int. Conference on Fuzzy Systems*, 8-11, New Orleans, Louisiana – USA.
8. Negi D.S. and Lee, E. S., (1992). Analysis and simulation of Fuzzy Queues. *Fuzzy Set and Systems*, **46**, 321-330.
9. Perrone G., Noto La Diega S., Zinno A., (1998a) "A Fuzzy Discrete Event Simulator for Fuzzy Production Environment Analysis", *Annals of CIRP* **98**, 405-408.
10. Michalewicz, Z., (1996). *Genetic Algorithms + Data Structures = Evolution Programs*, 3rd edition, Springer, New York.

COST/BENEFIT ANALYSIS OF IMPLEMENTATION OF TOTAL QUALITY PROGRAM IN MANUFACTURING

J. Mrsa and B. Smoljan
University of Rijeka, Rijeka, Croatia

KEY WORDS: Quality Costs, Quality Management,

ABSTRACT:

The optimization of quality costs in manufacturing was investigated and efficiency of a total quality program was analyzed. Traditional view of optimal distribution of quality costs has been abandoned. It has been found out that optimal quality costs respond to total quality control or to the zero defect level. Quality management cannot be successful without quality cost management. The activity of manufacturing quality system as cost centers have been defined. The manufacturing quality costs have been classified in categories. In total quality control there is a reduction in all quality cost categories and quality is increased. A ratio between the prevention costs and failure costs as measure of efficiency of an achievement of a total quality program is decreased in accordance of implementation of a total quality program.

1. INTRODUCTION

Total quality management is management approach of an organization centered on quality, based on the participation of all its members and aiming at long-term success through customer satisfaction, and benefits to all members of the organization and to society [1].

Quality management cannot be successful without quality cost management. Cost of quality could be viewed as having two components, prevention costs and failure costs. The first of these, prevention costs, includes all costs of quality assurance efforts. Prevention costs could be named as prevention costs plus appraisal costs. These include inspection, statistical process control, self-life programs to prevent spoilage, and the like. Any cost that is incurred to detect incipient failure of a product or to ensure the acceptability and effectiveness of a service is prevention cost. Prevention costs also include quality control measures to keep incipient failures from developing at all, such as design reviews, vendor certification programs, and quality orientation training. Prevention keeps customers from becoming dissatisfied with the goods and services they receive from the organization. Prevention costs are also incurred in the production of intermediate products such as parts and subassemblies, and earlier phases of product design and service or project planning. The now accepted practice of forming design teams that include suppliers with production or operating personnel ensures that failures of the ultimate product are prevented even before the product goes into prototype production [2].

Another group of quality costs is the cost of failure, i.e., internal and external failure costs. These costs are the costs of making a bad product that does not do as required in the customer's hands, or of doing services that do not meet the customer's requirements. Such costs include in-field repair, warranty, scrap, and reworks. All such costs are incurred because some process created an output that did not meet specifications [2].

Sometimes third class of cost of quality elements could be shown as the opportunity cost of sales because of customer's poor experience or because of poor reputation in the market. It is easy to see why this aspect is seldom addressed directly, since no one can tell precisely how much customers might have bought if quality had been better. Even harder is an appraisal of lost revenue that results from accepting lower prices than might have been commanded in the marketplace by a premium product or service. To estimate the cost of lost revenue from lost volume or from lower pricing requires trusting the marketing department, a source that is alien to most accountants. Such data is based on estimates and conclusions that accountants often find hard to swallow because they are not usually based on past events that are observable and measurable in objective ways. Calculating the value of lost sales is exceedingly difficult and involves a number of factors [2].

2. CLASSIFICATION OF COST OF QUALITY

Realistic cost/benefit analysis in terms of the effort needed or justified obtaining the desired levels or assurance of quality can be successfully done on the base of: a true factory man hour rate about overhead and salary, quality/quality control activity costs both about man hours and money and quality related costs of any care study item.

The quality cost figures are quite straightforward in respect of: prevention costs, appraisal costs, internal failure costs, external failure costs (Table 1) in any costs center:

Table 1. Quality costs

<p><u>Prevention costs</u> Quality engineering Quality training Quality planning Quality audits Design reviews Quality circles</p>	<p><u>Appraisal costs</u> Inspection of row materials Packing inspection Product acceptance Process acceptance Field testing Supplier verification</p>
<p><u>Internal failure costs</u> Scrap Rework Delay Reinspection Retesting Design changes</p>	<p><u>External failure costs</u> Lost sales Return/allowances Warranties Repair Product liability Complaint adjustment</p>

Prevention costs are incurred to prevent defects in the products or services being produced.

Appraisal costs are incurred to determine whether products and services are conforming to their requirements. Appraisal costs are in terms of product acceptance and process acceptance.

Internal failure costs are incurred because non conforming products and services are detected prior to being shipped to outside parties.

External failure costs are incurred because products and services fail to conform to requirements after being delivered to customers.

3. NUMERICAL VERIFICATION

During the accomplishment of a quality program, for every quality cost category questionnaire must be completed. The questionnaire consists of following data: activity, people number, time in hours, a sum paid for items and services and other costs. The quality cost report and cost analysis should be issued for every accounting period and if it is necessary, a quality program should be improved. In table 2 the trends for each individual quality cost category of concrete manufacturing are presented.

Table 2, Quality costs trend

Accounting period	Prevention, %	Appraisal, %	Internal failure, %	External failure, %	Σ
0	5.0	3.5	3.5	6.2	18.2
1	8.1	4.9	3.6	5.5	23.1
2	5.7	3.6	3.1	4.9	17.3
3	4.1	2.4	2.0	1.3	9.8
4	2.1	1.4	1.1	0.6	5.2

In a phase of intensive activity of quality level improvement, quality costs increase. As quality improves, savings can be realized by having fewer workers to correct the mistakes made initially. Rework people will disappear when there are no more reworks. Warranty costs will stop when there are no failures in the field, inspections of incoming raw materials will be to cut back, company will reduce the level of product acceptance activities, and so on. In total quality control there is a reduction in all quality cost categories and quality is increased.

The good measure of correctness improvements of implementation of a total quality program is the ratio between the prevention costs and failure costs. This ratio should increase during the total quality program period implementation in one side, but in same time total amount of costs of quality should decrease:

$$\text{efficiency of TQP implementation} = \frac{\text{prevention costs} + \text{appraisal costs}}{\text{failure costs}}$$

In table 3 the trend for ratio between the prevention costs and failure costs are presented.

Table 3, Efficiency of implementation of a total quality program

Accounting period	0	1	2	3	4
Prevention costs + appraisal costs	8.5	13.0	9.3	6.5	3.5
Failure costs	9.7	9.1	8.0	3.3	1.7
Ratio between prevention and failure costs	0.87	1.42	1.16	1.96	2.05

According to the trend for ratio between the prevention costs and failure costs it is visible that the timing of involving the total quality program is caused in quite a right manner.

4. CONCLUSION

Investment in quality and management responsibility for measuring and reporting quality costs must be monitored in responsibility costs centers. The quality cost figures are quite straightforward in respect of: prevention costs, appraisal costs, internal failure costs, external failure costs in any cost center.

In a first phase of activity of quality level improvement, quality costs increase. As quality improves, savings can be realized by having fewer workers to correct the mistakes made initially, rework people will disappear, warranty costs will stop when there are no failures in the field, inspections of incoming raw materials will be to cut back, the level of product acceptance activities will be reduced, and so on. In total quality control there is a reduction in all quality cost categories and quality is increased.

An analysis of quality costs in concrete manufacturing plant shows that in a phase of intensive activity of quality level improvement, quality costs increase, but in total quality control there is a reduction in all quality cost categories.

REFERENCES

- [1] ..., ISO 8402: 1994.
- [2] Woods, M, Total Quality Accounting, Jon Wiley & Sons, 1994.
- [3] Dale, B. and Plunkett, J., Quality Costing, Champan and Hall, London, 1991.
- [4]. ..., ISO 9002, The International Organization for Standardization, 1994.
- [5] Moyes, E. and Rogerson J., Reduction of Quality Related Costs in the process Plant Industry, NEDO Books, London, 1985.
- [6] Mrša, J., Reporting and Using Quality Cost Information, 30th Symposium HZRFR'95, Zagreb, 1995. (In Croatian)
- [7] Mrša, J and Smoljan, B., Measuring Quality related Costs, Advanced Manufacturing Systems and Technology, AMST' 96, Ed. by E. Kuljanić, Springer Verlag, 1996.

MANAGING THE BUYER-SUPPLIER INTERACTIONS THE BOUNDARIES OF COOPERATION

G. Nassimbeni

University of Palermo, Palermo, Italy

KEY WORDS: Sourcing Policies, JIT Purchasing, Co-design, Empirical research

ABSTRACT: On the basis of an empirical research on a sample of Italian plants, this study analyses the relationships between advanced buyer-supplier operational interaction practices (JIT, CE and TQM Approaches) and the basic options of the buyer's purchasing strategy, such as: sources selection criteria, supply base reduction policies, long-term supply perspectives. In addition, the study compares these operational practices and purchasing policies in different performing plants.

1. INTRODUCTION

The new current interest in the different forms of buyer-supplier exchange is to a large extent promoted by the diffusion of new approaches to operations. Management and production systems such as "Just in Time", "Total Quality Management" and "Concurrent Engineering" promote the adoption of quality control tools spread along the supply chain, integrated coordination of production flows, cooperation between all those units (inside or outside the firm's boundaries) involved in the product development. The new innovative "lean production practices" need to be implemented along the full production and logistic chain for full exploitation, in order to synchronise the flows at the upper and lower end of the supply pipeline [1] In this context, Transaction Cost Economy (TCE) theorists would predict a failure of the traditional market-based exchange, that is, a failure of procurement logic based on "multiple sourcing", on a priced-based mechanism in the sources selection, on short term horizons [2,3]. In fact, the buyer-supplier operational synchronisation and design synergy promoted by new approaches are associated to higher level assets specificity [4]. For example, JIT and TQM Systems can require the development of specific

quality assurance practices, the acquisition of specific tools, training of personnel, development of compatible procedures to meet the partner's idiosyncratic requirements. In addition, the contractual incompleteness associated to the buyer-supplier exchange becomes higher, due to the higher amount of environmental and behavioural uncertainty. In other words, the exchange becomes more difficult to define ex-ante, since it involves the supply not only of an "object" alone, but also of complex bi-direction logistics, design, informative services. Moreover, it is also more difficult to measure ex-post, given the difficulty to circumscribe the respective responsibility and the performance evaluation (and valorisation) ambiguity.

According to TCE, in order to protect transaction-specific assets from opportunistic appropriation, and to cope with the effects of exchange uncertainties, buyers will choose to internalise the transaction or otherwise arrange to increase the extent of hierarchical control over the other party. An exchange structure arises which is an intermediary solution between the integrated manufacturer and the "market", in that, suppliers and buyers agree to co-operate with one another to form a long-term, co-operative relationship guided by expectations of repeated transactions. This type of relationship is characterised by "relational contracting". Anyway, "relational-exchange" (=long term, exclusive) constitutes a risky alternative to the market, because the buyer becomes more vulnerable to opportunistic behaviour of sources. Furthermore, the sources engaged in a relational exchange escape from direct market competitive pressure: in the long run this can produce a worsening of their performances. Both empirical research and theoretical debate exhibit contrasting positions about the advantages of long-term, stable supply relationships and about the diffusion of a true "relational" buyer-supplier exchange in western context [5]. Waters-Fuller [6] following extensive review of JIT Purchasing literature, synthesises this diversity of positions by comparing two lines of thoughts: the "sceptical school" and the "advocate school". The first school asserts that exclusivity and longevity are associated to higher switching costs (i.e. lower source replacement possibilities), higher risks of supply disruptions and technological obsolescence. Therefore, the "cooperative" supply relationship produces in the long run an inefficient form of sourcing. The second school considers the advantages of JIT sourcing (development of a congruent logistic network with consequent lower inventories, higher delivery reliability, improvements in product quality and delivery lead-times, ...) prevailing over risks. In spite of the abundant literature on this topic, few contributions document on an empirical basis the actual evolution in buyer-supplier relationships, especially through comparative analysis, whether by cross national comparison of industrial change or sectoral transformation [7, 8].

2. THE OBJECTIVES

This study considers the three main operational buyer-supplier [4, 9]: a) design link, consisting in the involvement of suppliers in buyer's product development activities; b) logistic link, which is accomplished when the supplier's deliveries are frequent and therefore small-lot sized, perfectly respondent to the buyer's quantity and quality requirements, rigorously synchronised with the buyer's production schedules; c) the quality link, which is accomplished when the buyer and the supplier exchange information concerning quality aspects (joint definition of quality specifications, transmission of quality tests and charts, transfer of statistical process control data).

On the basis of empirical research on a sample of Italian plants, this study: a) analyses the relationships between advanced buyer-supplier operational interaction practices (design link, logistic link, quality link) and the basic option of the buyer's sourcing policies, such as: sources selection criteria, supply base reduction policies, long-term perspectives (stability of procurement) granted to suppliers; b) compare those operational interaction practices and sourcing policies in different performing plants. The underlying hypothesis, which summarises all the detailed hypotheses which will be presented in the next section, is that the development of an operational link between buyer and supplier modifies the buyer's sourcing policies, in particular the basic choices: 1) Which supplier to select? (selection criteria); 2) How many suppliers to utilise? (number of sources); 3) What kind of relationship (short or long term) to develop with sources? (Procurement stability).

HYPOTHESES 1

The traditional supply relationship is "price-dominated": price is the dominant sources selection criteria in the "arm's length" approach. The limitations of this approach are essentially two. First, price is only a component of the actual total procurement cost: delays, qualitative or quantitative unreliability, packaging modes, post-sales assistance are examples of cost elements which are usually not included in the purchasing price. Second, traditional "price-dominated" relationship reduces the source selection to the choice of a single economic parameter and encourages a limited uni-dimensional improvement. It is largely argued that the development of an advanced operational link with sources generates the need for multi-dimensional sources evaluation and enhances the importance of "non-price" selection criteria [10,11]. In fact, the buyer needs sources able to sustain more qualified and involving interaction, that is, suppliers endowed of those design, production/logistic and quality relational skills required by new approaches. In addition, an accurate multi-dimensional rating can reduce the "contractual hazard" associated with the possible buyer specific investment. Finally, according to transaction cost theory, supplier evaluation and monitoring constitute a rational control instrument over the supplier's behaviour: in absence of market-based control mechanisms, an accurate rating system can restore a competitive pressure inside the pool of suppliers by monitoring and comparing the suppliers improvement over time. The first hypothesis can be expressed in these terms: H1a - *"The weight given to price in the source selection is negatively correlated to the buyer-supplier operational link"*; H2b - *"The weight given to "non-price" factors in the source selection is positively correlated to the buyer-supplier operational link"*.

HYPOTHESES 2

Several authors argue that modern buyer-supplier design and logistic interaction renders its recourse difficult to achieve [12,13]. JIT deliveries coming from different multiple sources seem to involve logistic integration, production planning, quality homogeneity, time synchronisation problems. Similarly, co-design seems to permit the participation of only few suppliers and the earlier (=nearer to product concept) is their involvement in the product development activities, the more difficult it is for the buyer to maintain different procurement alternatives. Assuming that the establishment of a buyer-supplier operational link is associated to the reduction of the number of sources, a major point of discussion then regards the entity of that supply base reduction, that is: the adoption of

single-sourcing practices. Some authors hold that single-sourcing is important for the realisation of a JIT link with the suppliers (see: 14). Others maintain that the competition among suppliers, even if restricted to a selected group of sources, is of critical importance if the costs are to be kept low and the quality of the supplies raised [8,13]. A further hypothesis is then the following: Our second hypothesis are therefore the following: Hp. 2a. - *“The adoption of supply base reduction policies is positively correlated to the buyer-supplier operational link”*; Hp. 2b. - *“The adoption of single-sourcing policies is positively correlated to the buyer-supplier operational link”*.

HYPOTHESIS 3

According to the TCE theory, the time horizon of the relationship depends on the kind of exchange. When the exchange is characterised by specific investments, a failure of the traditional market-based ("spot transaction" where price is the main contracting element) will arise for two basic reasons [2,3]. First, because the specific investment can be justified only for medium to long term supply relationships. Second, because the party which carries out the specific investment is exposed to the risk of opportunistic behaviour by the other party. This happens, for example, when the buyer decides unilaterally to lower the price of supplies once the supplier has made specific investments, thereby becoming dependent on the buyers itself. Thus, only the expectation of stable (long-term) relationships provides the incentive for specific investment and mitigates the risks of opportunistic behaviour. As discussed in the previous section, the operational interactions considered in this study (on design, logistic and quality) are associated to several kinds of assets specificity.

The third hypothesis can be expressed in this terms: Hp3 - *“The adoption of long-term sourcing policies is positively correlated to the buyer-supplier operational link”*.

HYPOTHESIS 4

The possible advantages and disadvantages of the traditional and of the cooperative buyer-supplier exchange are several: the arguments of both the "sceptical school" and the "advocate school" are numerous. Thus, only empirical evidence can decree the performance superiority of one model over the other. Unfortunately, as Zaher and Venkatraman [15] observe, investigating the performance implications of the different exchange governance structures is another important gap in current research. This study has therefore analysed the relationships between: buyer-supplier operational (design, logistic, quality) interaction practices, buyer's sourcing policies and plant performances. The corresponding hypothesis is the following: Hp4 - *“Better performing plants exhibit higher use of advanced buyer-supplier operational practices and cooperative sourcing policies”*.

4. THE METHODOLOGY

To test these hypotheses, a survey was carried out using structured questionnaires sent to a sample of 52 Italian plants. We chose the plant as unit of analysis since the JIT-P practices analysed are implemented at the plant level. The sample was selected at random from plants employing more than 100 people and was stratified into "traditional" and "world class reputation" plants. By "world class reputation" we mean

Table 1 reports the results of the regression analysis. Discriminant analysis was then utilised to compare the use of the operational practices and sourcing policies analysed in low and high performing plants. Results are reported in table 2.

	MEANS		Univariate F-statistics	Standardised discriminant coefficient
	"traditional" plants	"WCM" plants		
OPERATIONAL LINKS				
• design links	-0.412	0.543	p=0.004	0.878
• logistic link	-0.302	0.399	p=0.016	0.687
• quality link	-0.042	0.056	p=0.730	0.103
MULTIVARIATE F TEST: p=0.000				
Percent of grouped cases correctly classified: 71.15%				
SOURCING POLICIES				
• Importance of price in supplier select.	0.000	-0.088	p=0.784	-0.392
• Importance on non-price select. criteria	-0.124	0.254	p=0.234	0.354
• Supplier base reduction	-0.182	0.214	p=0.217	0.054
• Single sourcing	-0.180	0.088	p=0.353	0.379
• Long term perspective	-0.423	0.577	p=0.000	0.912
MULTIVARIATE F TEST: p=0.009				
Percent of grouped cases correctly classified: 76.74%				

Table 2. Results of the discriminant analysis

The results of the statistical analysis point out two main elements of discussion. The first element concerns the relationship between the sourcing policies and the overall set of operational links examined. The second element consider the relationship between the sourcing policies and each single operational (design, logistic, quality) link.

As far as the first element is concerned, the following results emerge:

- among the sourcing policies analysed, three variables ("importance of non-price selection criteria", "supplier base reduction" and "long-term perspective") are significantly correlated to the presence of an operational link with suppliers. The variable "long-term perspective" shows the highest (p=0.000, table 2) relationship;
- two other variables ("importance of price in supplier selection" and "single sourcing") are not significantly related to the operational links examined. Evidently, when developing an advanced operational link with sources, the buyer reduces the supplier base avoiding however a total exclusive rapport. Similarly, if non-price factors assume higher importance when an operational link arises, the weight given to price doesn't shows any significant changes. Thus, price still continues to play an important role (average value = 4.58 in corespondent 5-point Likert scale).

Summarising, the establishment of design, logistics or quality interactions with sources modifies the buyer's sourcing options, imposing an exchange government structure different from the "market-based" one. However, such a change does not foresee single sourcing practices and the denial of price-related factors in supplier selection.

The second element of discussion concerns the relationship between the sourcing policies and each single operational (on design, logistic, quality) dimensions. The following results emerge:

- the quality link reveals a less committed buyer-supplier interaction. It is associated to a long-term perspective (p=0.012, table 2), but is not accompanied by supplier base reduction policies or by clear valorisation of non-price supplier selection criteria.

those which are reputed to have higher than average performances in the sector. "Traditional" plants were selected from the Kompass (1992) list of firms belonging to the two sectors; "World Class Manufacturing" (WCM) plants from a master list compiled using experts in industry as source (consultants and managers). The sectors analysed are those of electronics and machinery in which JIT implementation and the interaction with the suppliers are competitive variables of increasing importance. The data and their elaboration refer to a sample of 52 units, 25 in the electronic and 27 in the machinery sectors. The principal characteristics of the sample are the following: sales: 88.2 millions \$, number of employees: 613; production process: one of a kind (20.2 %), small batch (40.4 %), large batch (20.8 %), semi repetitive (27.2 %), repetitive (1.7 %). Prior research was reviewed to identify existing objective and perceptual measures of the practices analysed. When available, existing measures were then adapted to facilitate their use in this study. For non existing measures, new perceptual ones were then developed using 5-point Likert-scales; the score was determined as the non-weighted mean of the values of each single item. The greater part of these questions was addressed to the Purchasing, Plant and Production Managers. Some of the questions were also directed to the Quality Manager, Process Engineer, Information System Manager, two supervisors and four workers to make a total of 12 respondents per plant. In all, 497 respondents were involved. All measures were subjected to reliability and validity assessment. Content validity was verified through a review of the literature, the theoretical revision used by the authors, a comparison with some managers of the firms sampled. Construct validity was verified by using factor analysis to test the uni-dimensionality of multi-items perceptual measures [16].

4. THE RESULTS

Hypotheses H1-H3 were verified using regression analysis, assuming the three operational (design, production-logistic and quality) links as independent and the three sourcing policies (supplier selection criteria, supplier base reduction and long-term perspective) as dependent variables.

	Importance of price in supplier selection	Importance of non-price selection criteria	Supplier base reduction	Single sourcing	Long term perspective
Hypotheses	<i>1a</i>	<i>1b</i>	<i>2a</i>	<i>2b</i>	<i>3</i>
adjusted R ²	0.009	0.119	0.120	0.033	0.396
F	0.862	3.199*	3.345**	1.521	11.930***
Signific. of F	0.468	0.032	0.027	0.222	0.000
INDEPENDENT VARIABLES					
• design link	b=0.131	b=0.386**	b=0.389**	b=0.019	b=0.298**
• logistic link	b=0.195	b=0.049	b=0.201	b=0.268	b=0.513***
• quality link	b=-0.038	b=0.147	b=0.072	b=0.146	b=0.285*

b: standardised regression coefficients p: significance: * p<0.05 ; ** p<0.01; *** p<0.001

Table 1. Results of the regression analysis

Evidently, the importance of quality in present competition has determined a wide diffusion of TQM practices almost at each step of the supply chain. Therefore, the ability to adequately interact with the buyer about quality-related topics is now an indispensable component of the supply offer, rather than a differentiation element;

- comparing the design and the logistic link, we discover that only the design link is associated to supplier base reduction policies and to a supplier selection which emphasises non-price criteria. Both links play instead a significant role in committing the buyer to a long-term relationship. In general, the empirical evidence shows that the design link is generally more exclusive and binding than the logistic link.

From the results of the discriminant analysis, better performing plants have more advanced design ($p=0.004$, table 3) and logistic links ($p=0.016$) with sources. The quality doesn't show any discriminating effect ($p=0.730$).

As extensively argued in the literature, buyer-supplier design and logistics interactions can reduce the product development, production and delivery time, can improve quality and lower costs. As expected, these results confirm the strong relationship between plant performances and co-design or JIT purchasing practices. Is not surprising that quality interaction doesn't discriminate on plants. Two of the items used to measure the quality link have values that are among the highest. Thus, the practices regarding the management and control of quality on entry flows are by now widespread: the ever more exacting market demand for quality call these practices to the attention of even the less well performing plants.

As far as the sourcing policies are concerned, only the "long-term perspective" exhibits a discriminating effect ($p=0.000$, table 3). It is thus confirmed that the perspective of lasting relationship is a necessary element of partnership: it justifies the transaction-specific investment, allows the "continuous improvement" logic, mitigates opportunistic temptations. Instead, the importance of price in the supplier selection and the use of single sourcing doesn't differ in traditional and WCM plants. Therefore, the best performing supply systems (evaluated through their impact on plant performances) are not characterised by total exclusivity of relationship and a supplier selection not governed by price (cost) consideration.

6. CONCLUSIONS

The results of this study raise several issues. First, it is demonstrated that the creation of an advanced link with sources modifies the basic options of the supply strategy of the buyer. In particular, operational inter-dependencies at the design, production-logistic or quality level orientate the buyer towards the long term convincing him to invest in integrated sources (for example thorough assistance and training). Thus, as predicted by TCE theory, advanced operational buyer-supplier interaction practices, like those promoted by JIT and Co-design approaches, seem to be inoperable under traditional, pure market-based mechanisms. Even where there is a strong operative collaboration, however, single sourcing remains an unused policy and price remains one of the principle criteria for monitoring sources. The buying strategy that is created follows a sort of compromise between the need to abandon traditional buying procedures and the need to avoid the dangers of excessive dependence on sources. The second important element which arises from the research is that the hypothesised relationship between sourcing policies and buyer-supplier operational link depends also on the latter. Design interaction seems to be the most exclusive and binding form of collaboration. This is

presumably justified by the higher specificity of the contribution and the greater difficulty in substituting the sources involved in this form of interaction. Vice versa, the quality link reveals the less committed buyer-supplier interaction: the ability to adequately interact with the buyer over quality-related topics seems at present to be an indispensable component of the supply offer, rather than a differentiation element.

The third element concerns the factors discriminating plants, that is, the impact of operational practices and sourcing policies on performance. This study demonstrates that better performing plants exhibit a higher level of design and logistic interactions and a better use of long-term supply agreements with sources. Thus, co-design and JIT purchasing practices, together, with the stability of procurement, influence to a significant extent plant performance. However, the best performing supply systems do not exhibit total exclusivity of relationship and a supplier's selection not governed by price (cost) considerations, that is, do not exhibit all the elements which ideally characterise the "cooperative" approach.

REFERENCES

1. Lamming, R., 1996, Squaring Lean Supply With Supply Chain Management, *International Journal of Operations and Production Management*, 16 (2), 183-196.
2. Williamson, O. E., 1979. *Markets and Hierarchies: Analysis and Antitrust Implications* (New York, Free Press).
3. Williamson, O. E., 1985, *The Economic Institutions of Capitalism*. (New York, Free Press).
4. De Toni, A., and Nassimbeni, G., Buyer-supplier operational practices, sourcing policies and plant performances: Results of an empirical research, *International Journal of Production Research* (forthcoming)
5. Helper, S., 1991, How Much Has Really Changed between U.S. Automakers and Their Suppliers?, *Sloan Management Review*, Summer, 15-28.
6. Waters-Fuller, N., 1995, Just-In-Time Purchasing and Supply: a Review of the Literature, *International Journal of Operations and Production Management*, 15 (9), 200-236.
7. Kalwani, M. U., and Narayandas, N., 1995, Long-Term Manufacturer-Supplier Relationships: Do They Pay Off for Supplier Firms?, *Journal of Marketing*, 59, 1-16.
8. Imrie R., Morris J., (1992), A Review of Recent Changes in Buyer-Supplier Relations, *Omega*, Vol. 5, No. 6, pp. 641-652.
9. Nassimbeni, G., 1996, Factors Underlying Operational JIT Purchasing Practices, *International Journal of Production Economics*, 42 (3), 275-288.
10. Willis, T., and Huston, C.R., 1990, Vendor Requirements and Evaluation in a JIT Environment, *International Journal of Oper. & Production Management*, 10(4), 41-50.
11. Weber, C., Current, J., and Benton, W., 1991, Vendor Selection Criteria and Methods, *European Journal of Operation Research*, 50 (1), 2-18.
12. Ansari, A., and Modarress, B., 1987, The Potential Benefits of Just-in-Time Purchasing for U.S. Manufacturing, *Production and Inventory Management*, 28 (2), 30-36.
13. Turnbull, P., Oliver, N., and Wilkinson, B., 1992, Buyer-Supplier Relations in the UK Automotive Industry: Strategic Implications of the Japanese Manufacturing Model, *Strategic Management Journal*, 13, 159-168.
14. Hall, R. W., 1983. *Zero Inventories* (Homewood, Il, Dow Jones-Irwin).
15. Zaheer, A., and Venkatraman, N., 1995, Relational Governance as an Interorganizational Strategy: an Empirical Test of the Role of Trust in Economic Exchange, *Strategic Management Journal*, 16, 373-392.
16. Zeller, R. A., and Carmines, E. G, 1980. *Measurement in the social sciences* (London, Cambridge University Press).

HIGH-ACCURACY POSTPROCESSOR FOR MULTI-AXIS MILLING MACHINES

K. Sorby
NTNU Trondheim, Norway

KEY WORDS: Multi-axis machines, Postprocessing

ABSTRACT:

This paper investigates the accuracy achieved when cutter location data is postprocessed for multi-axis milling machines. A recursive linearisation algorithm and a feed rate control algorithm are presented, and the problem of singular configuration is discussed. It is explained how a postprocessor can be used to optimise the workpiece clamping position in order to minimise the machining time, and how the postprocessor can compensate for inaccuracies in workpiece clamping.

1. INTRODUCTION

The accuracy of a workpiece that is machined in a multi-axis machine is affected by the accuracy of several actions that are performed before the tool starts to cut. Examples are the accuracy of the cutter location data (CL data) generated by the CAD/CAM system, the accuracy of the postprocessor that transforms the CL data into a NC file, and the accuracy of the workpiece clamping in the machine. This paper discusses how a postprocessor can be designed and used to improve the accuracy of tool paths in multi-axis machines.

Algorithms for linearisation and feed rate control in postprocessing have been described earlier [1]. It has also been described how postprocessing can compensate for mechanical

inaccuracies of the machine tool [2]. In this paper, a new linearisation algorithm is presented. The new algorithm is based on the same principle as the algorithm in [1], but the new algorithm is recursive. The accuracy of the principle for the algorithms is investigated. The problem of singular configuration is solved for a particular five-axis milling machine. An algorithm for feed rate control is presented, and it is shown how the postprocessor can be used to optimise the fixture design for a specific workpiece in order to minimise the machining time. It is also shown how the postprocessor can compensate for inaccuracies in the clamping of the workpiece.

2. FORWARD AND INVERSE KINEMATICS

The postprocessor developed for this study generates NC data for a five-axis milling machine that consists of a vertical-milling machine with an additional tilt-rotatory table.

The input data for the postprocessor is CL data generated on a CAD/CAM system. The CL data is presented on the format $[x \ y \ z \ i \ j \ k]$, where x , y and z are the position of the tool centre point and i , j and k are the tool axis orientation. The CL data is relative to the workpiece coordinate system.

The orientation and position of a coordinate system located in the table centre can be described relatively to the tool by the homogenous transformation

$$T_1 = \begin{bmatrix} c_B & s_B & 0 & -X \\ -c_A s_B & c_A c_B & -s_A & (c_A - 1)d_F - s_A d_E - Y \\ -s_A s_B & s_A c_B & c_A & (c_A - 1)d_E + s_A d_F - Z \\ 0 & 0 & 0 & 1 \end{bmatrix}, \quad (1)$$

where s_A , c_A , s_B and c_B are the shorthand notations for $\sin(A)$, $\cos(A)$, $\sin(B)$ and $\cos(B)$. X , Y , Z , A and B are the positions of the machine tool's axes, and d_E and d_F are offsets of the rotational axes.

If the workpiece is clamped so that the workpiece coordinate system is coincident with the coordinate system of the table, Eq. (1) expresses the orientation and position of the workpiece relative to the tool. If, however, the workpiece is clamped in an arbitrary orientation and position on the table, a transformation T_2 from the table centre to the workpiece coordinate system must be applied;

$$T_2 = \begin{bmatrix} r_{11} & r_{12} & r_{13} & l_x \\ r_{21} & r_{22} & r_{23} & l_y \\ r_{31} & r_{32} & r_{33} & l_z \\ 0 & 0 & 0 & 1 \end{bmatrix}. \quad (2)$$

The matrix T_2 can be found from measurements of the workpiece position and orientation after clamping, or from the fixture design.

The inverse kinematics of the five-axis machine is found by solving the equation

$$T_1 T_2 \begin{bmatrix} \cdot & \cdot & i & x \\ \cdot & \cdot & j & y \\ \cdot & \cdot & k & z \\ 0 & 0 & 0 & 1 \end{bmatrix} = \begin{bmatrix} \cdot & \cdot & 0 & 0 \\ \cdot & \cdot & 0 & 0 \\ \cdot & \cdot & 1 & 0 \\ 0 & 0 & 0 & 1 \end{bmatrix}. \quad (3)$$

Elements indicated by dots in the equation represent the orientations of the tool's x - and y -axis, which are not specified.

From solving Eq. (3) we get

$$B = \arctan 2(- (r_{11}i + r_{12}j + r_{13}k), (r_{21}i + r_{22}j + r_{23}k)) \quad (4)$$

$$A = \arctan 2(- (s_B r_{12}j + s_B r_{11}i - c_B r_{21}i + s_B r_{13}k - c_B r_{23}k - c_B r_{22}j), (r_{33}k + r_{32}j + r_{31}i)) \quad (5)$$

$$X = c_B y r_{12} + c_B x r_{11} + c_B l_x + c_B z r_{13} + s_B x r_{21} + s_B y r_{22} + s_B z r_{23} + s_B l_y \quad (6)$$

$$Y = c_A c_B x r_{21} + c_A c_B y r_{22} + c_A c_B z r_{23} + c_A c_B l_y - c_A s_B z r_{13} - c_A s_B l_x - c_A s_B y r_{12} - c_A s_B x r_{11} \\ + c_A d_F - s_A d_E - s_A l_z - s_A z r_{33} - s_A y r_{32} - s_A x r_{31} - d_F \quad (7)$$

$$Z = c_A y r_{32} + c_A l_z + c_A z r_{33} + c_A d_E + c_A x r_{31} + s_A c_B x r_{21} + s_A c_B y r_{22} + s_A c_B z r_{23} \\ + s_A c_B l_y - s_A s_B z r_{13} - s_A s_B l_x - s_A s_B y r_{12} - s_A s_B x r_{11} + s_A d_F - d_E \quad (8)$$

The range of the A-axis (tilt axis) is $0^\circ - 95^\circ$. This must be taken into account when the machine tool axes are calculated, as described in Algorithm_1:

```

1  Algorithm_1
2      calculate B    Special case: If B = arctan2(0,0), then B := 0
3      calculate A    If A < 0, then A := -A and B := B + 180°
4      calculate X, Y and Z
5  end Algorithm_1

```

3. LINEARISATION

When generating CL data, the CAD/CAM system presupposes that the tool movement between two points specified in the CL data file will be rectilinear (straight-lined) in the *workpiece coordinate system*. However, on a machine tool, the motion of the cutting tool is linear interpolated in the *absolute coordinate system*. Due to the rotational axis of a multi-axis machine, a tool movement that is rectilinear in the absolute coordinate system will not be rectilinear in the workpiece coordinate system. Therefore, the ideal tool movement

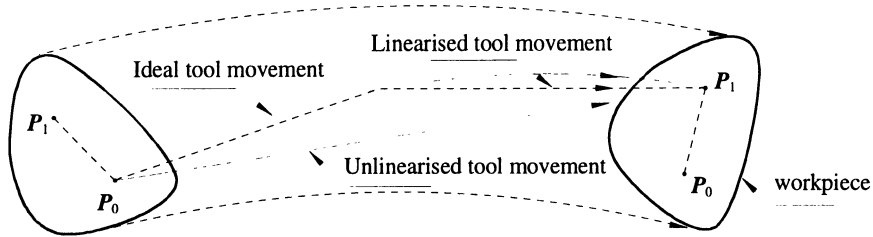


Figure 1. Movement of the tool between P_0 and P_1 .

should **not** be rectilinear in the absolute coordinate system. The ideal tool movement between two points (P_0, P_1) can be approximated by a linearised tool movement (Figure 1).

P_0 and P_1 are tool positions and orientations specified in the CL data file,

$$P_0 = [x_0 \quad y_0 \quad z_0 \quad i_0 \quad j_0 \quad z_0] \quad (9)$$

$$P_1 = [x_1 \quad y_1 \quad z_1 \quad i_1 \quad j_1 \quad z_1] \quad (10)$$

By using Algorithm_1 we obtain positions of the machine axes at the start point and end point of the tool movement,

$$Q_0 = Q_0(P_0) = [X_0 \quad Y_0 \quad Z_0 \quad A_0 \quad B_0] \quad (11)$$

$$Q_1 = Q_1(P_1) = [X_1 \quad Y_1 \quad Z_1 \quad A_1 \quad B_1] \quad (12)$$

To identify the need of linearisation, we must calculate the deviation between the ideal movement and the unlinearised movement with respect to both tool position and tool axis orientation. The position deviation at a point $P' = [x' \quad y' \quad z' \quad i' \quad j' \quad k']$ between P_0 and P_1 is

$$\delta = \sqrt{(x' - x^*)^2 + (y' - y^*)^2 + (z' - z^*)^2}, \quad (13)$$

where

$$P' = (1 - \tau) \cdot P_0 + \tau \cdot P_1, \quad 0 < \tau < 1, \quad (14)$$

$$\begin{bmatrix} \cdot & \cdot & i^* & x^* \\ \cdot & \cdot & j^* & y^* \\ \cdot & \cdot & k^* & z^* \\ 0 & 0 & 0 & 1 \end{bmatrix} = [T_1(Q^*)T_2(Q^*)]^{-1}, \quad (15)$$

and

$$Q^* = (1 - \tau) \cdot Q_0 + \tau \cdot Q_1, \quad 0 < \tau < 1. \quad (16)$$

The orientation deviation is

$$\alpha = \arccos(i^i \cdot i^* + j^j \cdot j^* + k^k \cdot k^*). \quad (17)$$

A linearisation procedure is listed in Algorithm_2. The algorithm is recursive; it calls itself until the accuracy of the approximated tool movement is within the specified tolerances.

```

1   Algorithm_2 ( $P_0, P_1$ )
2     if position deviation at the midpoint > TOL_P
3       or orientation deviation at the midpoint > TOL_A, then
4         calculate new  $P'$  between  $P_0$  and  $P_1$  ( $P' = 0.5 \cdot P_0 + 0.5 \cdot P_1$ )
5         calculate new machine axis values  $Q' = Q(P')$ 
6         call Algorithm_2 ( $P_0 = P_0, P_1 = P'$ )
7         print  $Q'$  to NC file
8         call Algorithm_2 ( $P_0 = P', P_1 = P_1$ )
9   end Algorithm_2

```

In Algorithm_2 the point that is used to identify the need of linearisation is the midpoint between P_0 and P_1 (50% of the distance between P_0 and P_1). The same method is used by [1]. To test the accuracy of this method, a computer program was used to calculate the position deviation and orientation deviation for $6.2 \cdot 10^5$ different tool movements in the machine tool's workspace. Each tool movement was divided into 100 steps. The maximum length of tool movements in the tests was 50 mm.

First, the tool orientation deviation is considered. The point of maximum orientation deviation is found between 37% and 63% of the distance between P_0 and P_1 for all the tested tool movements. The deviation at the maximum point can be up to 12% higher than the deviation at the midpoint. Therefore, if the maximum allowed orientation deviation is TOL_ANGLE, the allowed orientation deviation at the midpoint (TOL_A) must be set to TOL_ANGLE/1.12 to achieve the required accuracy when Algorithm_2 is used.

Next, the tool position deviation is considered. The computer test showed that the point of maximum position deviation is between 24% and 76% of the distance between P_0 and P_1 for all the tested tool movements. Further, the tool position deviation at the maximum point could be up to 62% higher than the deviations at the midpoint. Large difference between the midpoint deviation and the maximum deviation occurs if the tool movement is long and the tool orientation variation within the tool movement is large. If the maximum allowed position deviation is TOL_POSITION, the maximum allowed position deviation at the midpoint (TOL_P) must be set to TOL_POSITION/1.62.

Algorithm_2 is guaranteed to give high accuracy tool path if each tool movement in the CL file is not longer than 50 mm relative to the workpiece, even if the tool orientation variation within the movement is very large. Generally, for CL data generated on a CAD/CAM system the tool movement lengths are significantly shorter than 50 mm, and the tool orientation variation within each tool movement is small. Therefore, we can

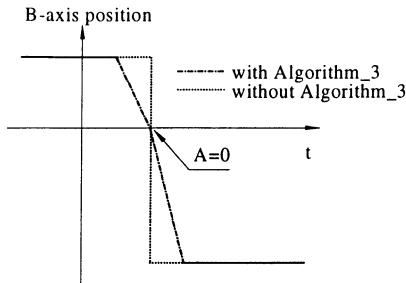


Figure 1. The effect of Algorithm_3.

Table 1. Maximum tool orientation error introduced by Algorithm_3

γ :	5°	4°	3°	2°	1°
error:	3.6°	2.9°	2.1°	1.4°	0.7°
γ :	0.5°	0.3°	0.1°	0.05°	0.01°
error:	0.4°	0.2°	0.07°	0.04°	0.007°

conclude that the algorithm will give high accuracy linearisation for all practical applications.

4. SINGULAR CONFIGURATION

At $A=0$ the solution of B is non-unique, i.e. that the rotational table is in a singular configuration. Near the singular point there could be a discontinuity of the B -axis position; the linearisation algorithm would never reach its stop criteria and the postprocessor would fail. To avoid problems of a tool movement through the singular configuration the following algorithm is suggested to modify the output of Algorithm_1:

```

1  Algorithm_3
2      if  $A < \gamma$ , then
3           $B := B \cdot A / \gamma$ 
4          calculate new values for X, Y and Z
5  end Algorithm_3
    
```

Algorithm_3 will prevent discontinuities of the B -axis position near $A = 0$ (Fig. 1). However, the algorithm will introduce an error in the tool axis orientation, which depends of the size of the γ angle (Table 1). It should be noted that Algorithm_3 is consistent with line 2 in Algorithm_1.

The value of γ could be chosen so small that the required accuracy could be achieved. A reduction of the γ value increases the size of the NC file and the machining time slightly.

5. FEED RATE CONTROL AND ESTIMATION OF THE MACHINING TIME

In a multi-axis machine tool, movement of the rotational axes affects the relative feed rate between the tool and the workpiece. In order to keep a constant relative feed rate, an adjusted feed rate must be calculated for every block in the NC file. Algorithm_4 describes a feed rate control procedure.

1 Algorithm_4

2 calculate the duration of the tool movement:

$$t = \sqrt{(x_1 - x_0)^2 + (y_1 - y_0)^2 + (z_1 - z_0)^2} / F \tag{18}$$

3 if $|X_1 - X_0| / t > \text{maksfeed_X}$, then $t = |X_1 - X_0| / \text{maxfeed_X}$

4 if $|Y_1 - Y_0| / t > \text{maksfeed_Y}$, then $t = |Y_1 - Y_0| / \text{maxfeed_Y}$

5 if $|Z_1 - Z_0| / t > \text{maksfeed_Z}$, then $t = |Z_1 - Z_0| / \text{maxfeed_Z}$

6 if $|A_1 - A_0| / t > \text{maksfeed_A}$, then $t = |A_1 - A_0| / \text{maxfeed_A}$

7 if $|B_1 - B_0| / t > \text{maksfeed_B}$, then $t = |B_1 - B_0| / \text{maxfeed_B}$

8 calculate new feed:

$$F' = \sqrt{(X_1 - X_0)^2 + (Y_1 - Y_0)^2 + (Z_1 - Z_0)^2} / t \tag{19}$$

9 end Algorithm_4

The duration of the tool movement is increased if the maximum feed rate is exceeded for one or more of the machine axes. By adding all the movement durations for the whole tool path, the total machining time can be estimated. The machining time is used in the next section to optimise workpiece clamping position.

6. OPTIMISATION OF THE WORKPIECE CLAMPING POSITION

As described earlier in this paper, the travel of the A-axis is restricted to $0^\circ - 95^\circ$. As a result, the B-axis sometimes will have a 180° turn near $A=0^\circ$. The 180° turn will take some time, and it is therefore unwanted.

The workpiece can be clamped so that the position and orientation of the workpiece coordinate system is different from the coordinate system of the machine tool table. Then, the A-axis may never reach 0° , and the problems with the 180° turn can be avoided. The optimal workpiece clamping position can be found by postprocessing the CL data with different values for the elements of Eq. (2).

The machining time is estimated for a tool path for a specific workpiece with different clamping orientations (Table 2, Fig. 2). The estimated machine times are verified at the

Table 2. Estimated machining time

θ	t [s]
0°	175
30°	115
60°	115
90°	not possible (upper limit of A-axis position is exceeded)

$\gamma = 0.06^\circ$

Nominal feed: 1000 mm/min

Max feed: X, Y and Z-axis: 28000mm/min,

A-axis: 1000 °/min, B-axis: 2000 °/min

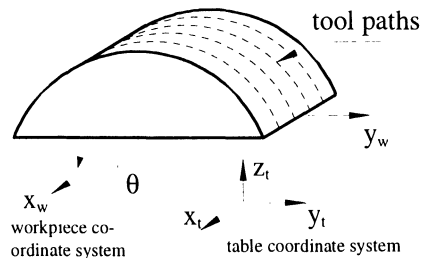


Figure 2. Workpiece orientation.

machine tool. At $\theta = 0^\circ$ the B-axis will have multiple 180° turns near $A = 0^\circ$, but at $\theta = 30^\circ$ and 60° the A-axis will never reach 0° , and the machining time is reduced.

Sometimes, there will be problems with collision between the tool and some other part of the machine tool system. Besides, there can be problems because of limited travel of the machine tool axes. These problems may be solved by a new clamping position and orientation, which can be found by postprocessing with different values of Eq. (2).

7. COMPENSATING FOR INACCURACIES OF WORKPIECE CLAMPING

When a workpiece is clamped in a multi-axis milling machine, it is usually very important to position the workpiece coordinate system as supposed by the postprocessor. Small deviations in the clamping position may cause large dimensional errors of the workpiece. Accurate clamping is especially important if the workpiece has to be machined in several setups.

To compensate for clamping inaccuracy, the workpiece position can be measured in the machine after clamping, and the position information can be put into Eq. (2) before the CL data is postprocessed. Then, the kinematics of the postprocessor will compensate for any position and orientation error.

8. CONCLUSION

- The maximum deviation between an ideal tool movement and an unlinearised tool movement will generally not be at the midpoint of the tool movement. This fact must be taken into account if the midpoint is used to identify the need of linearisation.
- Problems with tool movements near a singular configuration can be avoided by using a algorithm that will introduce a small tool orientation deviation.
- Postprocessing can be used to optimise the workpiece clamping position in order to reduce the machining time. Inaccuracies in workpiece clamping can be compensated.

ACKNOWLEDGEMENTS

I thank the Research Council of Norway for supporting this work.

REFERENCES

- 1 Y. Takeuchi and T. Watanabe, Generation of 5-axis control collision-free tool path and postprocessing for NC data. *Ann. CIRP* **41**(1), 539-542 (1992).
- 2 R. MD. Mahbubur, J. Heikkala, K. Lappalainen and J. A. Karjalainen, Positioning accuracy improvement in five-axis milling by post processing. *Int. J. Mach. Tools Manufact.* **37**(2), 223-236 (1997).

UNCERTAINTY AND INFORMATION IN CELL FORMATION PROBLEMS

A. Donnarumma and M. Pappalardo
University of Salerno, Salerno, Italy

KEYWORDS: Cell Formation, Possibility, Cross-Entropy, Optimisation, MaxEnt

ABSTRACT: In applying group technology to cell formation, information on product volume, machine capacity processing time, and many other parameters, on similar manufacturing operations or handling cost, are of great importance. In this paper is proposed an approach based on information for estimating parameters' data so that different factors can be considered. The analysis of the data has been performed using the functions between machines and parts in terms of membership functions. The measure of the possibility of quality loss is estimated in terms of information measuring the distance of the real solution from an ideal solution on the basis of the *MinxEnt* principle of Kulbach and Leibler. The optimum solution is found analysing objective functions using the Jaynes' *MaxEnt* principle of maximum entropy.

1. INTRODUCTION.

The analysis of a manufacturing system $S = \{U, D\}$ involves a set of elements processed under external constraints. The fundamental condition to get a successful analysis is the dependence of the system on a finite and limited set of appropriate parameters. The reduction of the parameters involves a lowest value of the entropy, the stability and the reproducibility of the same system. The set D of features of the system can be divided in the two subset $D = A \cup Q$ in which A is a set of parameters of design and Q is the set of parameters of ma-

Published in: E. Kuljanic (Ed.) *Advanced Manufacturing Systems and Technology*,
CISM Courses and Lectures No. 406, Springer Verlag, Wien New York, 1999.

chines. D is used as input data for designing the cellular manufacturing system. In analysing the process of parts to the set A of parameters of design corresponds a set B of characteristics of the machines. On the basis of set B a set C of machines is chosen. Formally

$$A \Rightarrow M \text{ is true iff exist } B \text{ such that } A, B \vdash C \quad (1)$$

Many parameters, such as machine capacity, product volume, processing time, handling cost are used in the formation of a cellular manufacturing system. All these factors are studied using many different procedures. The possibility of getting the design's quality on the processed parts has a significant impact on the performance of the system. In this approach is applied the factor of quality to cell formation. The relation between $N = \{x_1, \dots, x_n\}$ parts and $C = \{y_1, \dots, y_m\}$ machines are used to form an incidence matrix X , whose entry X_{ij} ($i = 1, \dots, n; j = 1, \dots, m$) has a membership value $\mu(x_i, y_j)$ indicating the possibility of getting the quality of the part i processed by the machine j . The degree of possibility $\pi(x_i, y_j)$, on the basis of the Consistence Principle, is greater or equal to the degree of probability $p(x_i, y_j)$ then every part i processed by machines j has the degree of membership $\mu(x_i, y_j) = \pi(x_i, y_j) \wedge p(x_i, y_j)$. In the similarity between two machines, close the number of common features is necessary to add the parameters on the quality of the processed parts. Many clustering algorithms have been developed for cell formation, but the control of quality, or the probability to lose quality, is esteemed, very often, in a separate phase.

Using the theory of the sets, the rules and the logic relationships, that tie the different elements of S in design and production, can be defined. The traditional control of quality is a measure of features of the products, with reference to the design's specifications and statistical processing of data. The analysis with statistical functions involves results not very logic: under the same variations, in external points, we can have low variations of quality and in central points we can have large variations. In the use of a product the ideal quality is quite different from technological definitions: it is not a crisp correspondence of measures of data, on product's features, from the data of design. The definition of quality is quite soft. Taguchi's definition of ideal quality is soft and he involves the customers whom must receive the target performance each time the product is used:

- The ideal quality is that which gives full satisfaction to the customers during performance, in operating conditions and etc
- The quality level can be measured in terms of satisfaction loss.

In most situation a quadratic functions gives data on quality loss.

The philosophy of design is:

- Definitions of parameters of design on product.
- Definitions of influence design's parameter on product's performance: control of quality in running design and development.
- Efficient experimentation to find design parameters that influence target performance.

The quality loss is obtained with the control of average of values and the square deviation from the own mean. The control of average is easy to do while the control of square deviation is more difficult. The quality can be controlled processing the values of membership functions of attributes obtained by confront the ideal data of quality with the real data of product.

2. RELATION OF QUALITY

The reduction of dependence of the system from a finite and limited set of appropriate parameters involves the distribution of probability on a reduced number of elements. The entropy on a reduced system is lower than one with higher numbers of parameter and can more easily controlled. The control of quality loss can be carried on utilising the principle of *MaxEnt*. On a system the probability can have infinite distributions but in conditions of equilibrium the distribution is assigned by Laplace-Bernuilli's Principle of Insufficient Reason. A set M of values of membership functions of attributes can be obtained confronting the data of design quality with the data on parts produced by the available machines. The quality is controlled by using the set M with flexible constraints. The values of membership functions derive from the philosophy of design and control. Let $\mathbf{x} = (x_1, x_2, \dots, x_n)^T$ the factors of design and $\mathbf{y} = (y_1, y_2, \dots, y_n)^T$ the factors of production the function $P(x, y)$ $f(\mathbf{x}, \mathbf{y})$ is the relation of quality. Indicating with:

- U the universe of parameters and $T \subseteq U$ a subset of U .
- $T_I = \{x_i\}$ a subset of values of ideal quality (design) and $T_R = \{y_i\}$ a subset of real quality (machines).
- n_T The cardinality of sets $T_I = \{x_i\}$ and $T_R = \{y_i\}$.
- R a binary relation of quality.
- $P(x, y)$ a proposition of quality.
- M a set of membership functions generated by R with cardinality n_T .

In the space $T_I \times T_R = T \times T$ to each tuple (x_i, y_j) of elements $x_i \in T_I$ and $y_j \in T_R$ corresponds a set M of membership functions $M = \{\mu(x_i, y_j)\}$ with $i \neq j \Rightarrow \mu(x_i, y_j) = 0$

$$M = \{y \in T_R, x \in T_I, i = j : yRx\} \tag{2}$$

where the statements yRx means "the real value y_i is in relation with the ideal value x_i iff the proposition $P(x, y)$ give a non empty set $M = \{\mu(x_i, y_j)\}$ ". The relation yRx of quality involves the conditions: $yRx \neq xRy$ $xRz \neq zRy$ $zRz \forall z \in Z$. The relationship yRx gives the set M while the relationship xRy gives a set G with a different meaning. The sets M and G contain all the membership functions. The values of membership functions give the possibility of achieving the ideal quality.

3. QUALITY EVALUATION

Let a system $S = (C, A) = (C, \{T, V\})$ in which

- C is a non empty set set of machines
- A is a non empty set of design specifications and machine's characteristics.
- T a set of system range.
- V a set of design range.

If M and G a non empty set of values of membership functions $\mu(x_i, y_j)$ and $\gamma(x_i, y_j)$, for the set of machines range $T \subseteq A = \{x_i\}$ and a set design range $V \subseteq A = \{y_j\}$, in the

space $T \times V$ for $x \in X$ and $y \in V$ exist two set A and G .

The set A is the non empty set

$$M = \mu(x, y) = \{y \in T_R, x \in T_I, i = j : yRx\} \tag{3}$$

The set G is the non empty set

$$G = \gamma(x, y) = \{y \in T_R, x \in T_I, i = j : xRy\} \tag{4}$$

Indicating, as in figure 1, the common and the system range the proposition of quality is

$$P(x, y) = |\text{common range}| / |\text{system range}| \tag{5}$$

$$M = \frac{|\overline{AB} \cap \overline{CD}|}{|\overline{CD}|} = \frac{|\overline{FE}|}{|\overline{CD}|} = \{\mu(x, y_i) \in [0, 1]\} \tag{6}$$

$$G = \frac{|\overline{AB} \cap \overline{CD}|}{|\overline{AB}|} = \frac{|\overline{FE}|}{|\overline{AB}|} = \{\gamma(x, y_j) \in [0, 1]\} \tag{7}$$

- If $\mu(x_i, y_j) = 1$ means that the manufacturing system achieves all the specifications of designers
- If $\mu(x_i, y_j) = 0$ means that the manufacturing system cannot achieve the specifications of designers
- If $\mu(x_i, y_j) = z$ and $0 < z < 1$ means that the manufacturing system has the possibility of achieving all the specifications of designers.
- If $\gamma(x_i, y_j) = 1$ means that designers achieve all the manufacturing system's specifications
- If $\gamma(x_i, y_j) = 0$ means that designers cannot achieve the manufacturing system's specifications.
- If $\gamma(x_i, y_j) = z$ and $0 < z < 1$ means that designers have the possibility of achieving all the specifications of manufacturing system.

The elements of M and G measures the probability of success in processing parts. In the relation between the m machines and n parts, the values of $\mu(x_i, y_j)$ and $\gamma(x_i, y_j)$ indicate the probability of achieving the quality of the part i processed by the machine j . If \mathbf{d} is the probability distribution of success that the ranges of the manufacturing system can achieve designer's specifications, and \mathbf{g} is the probability distribution of success that the designer's specifications achieve with the range of manufacturing system, then the distance $D(\mathbf{d}:\mathbf{g})$ between the distributions, measured in Minkowsk's metric, is given by

$$D(\mathbf{d}:\mathbf{g}) = \left[\sum_j (\mu(x_i, y_j) - \gamma(x_i, y_j))^2 \right]^{1/2p} \tag{8}$$

- \mathbf{d} represents the distribution when a priori data is the design range and is running the formation of set of machines (system range).

- \mathbf{g} represents the distribution when a priori data is the system range and is running the formation of the set of design's range.

In the Minkowsk distance where when $p = 1/2$ the value of D is the Hamming's distance and when $p=1$ is Euclidean distance. The distance $D(\mathbf{d}:\mathbf{g})$ in terms of information is given by Kulbak and Leibler definition of *cross-entropy*

$$D(\mathbf{d}:\mathbf{g}) = \sum_i \mu(x_i, y_i) \ln \frac{\mu(x_i, y_i)}{\gamma(x_i, y_i)} \tag{9}$$

When $D(\mathbf{d};\mathbf{g})=0$ means that all objectives have been achieved and the cross-entropy is zero. If in the formation of a system the a priori data is the set of the design's range then we must choose $\mu(x_i, y_j)$ in order to minimise the cross-entropy (principle of *MinxEnt*). Since $\gamma(x_i, y_j)$ are fixed data to minimise $D(\mathbf{d};\mathbf{g})$ it means to make maximum Shannon's entropy

$$S = - \sum_i \mu(x_i, y_j) \ln \mu(x_i, y_j) \tag{10}$$

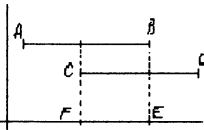
U	System range s_{ij}	Design range	Group 1 $\mu_1(x_i, y_j)$	Group 2 $\mu_2(x_i, y_j)$	Group 3 $\mu_3(x_i, y_j)$	AB= Design range CD= System range EF = Common range 
x_1	s_{11}	d_{11}	0,9	0,9	0,9	
x_2	s_{12}	d_{12}	1	1	0,9	
x_3	s_{13}	d_{13}	0,7	0,9	0,9	
x_4	s_{14}	d_{14}	0,8	0,8	0,8	
x_5	s_{15}	d_{15}	1	1	0,9	
x_6	s_{16}	d_{16}	0,9	0,9	0,9	
x_7	s_{17}	d_{17}	0,6	0,6	0,6	
x_8	s_{18}	d_{18}	0,7	0,7	0,9	
x_9	s_{19}	d_{19}	0,7	0,7	0,9	
x_{10}	s_{110}	d_{110}	0,4	0,7	0,8	
		Entropy	4,206	4,930	5,468	

Figure 1

It is possible to use the principle of the *MaxEnt* of Jaynes in order to optimise the formation of a cellular system using Shannon's definition of entropy or the equivalent definition of Wiener.

A finite soft set $F = \{\mu(x, y), x, y\} \forall x, y \in C$ in different engineering disciplines can to measure the efficiency or quality in a system. The membership function $\mu(x, y) \in [0,1]$ represents quality. An ideal process will be $\mu(x, y) = 1$. The value $\bar{\mu} = (\mu(x, y) - 1)$ represents the quality loss. If $I = \{x, y \in U : \mu(x, y) = 1\}$ is the set in which all elements are ideal and \mathbf{i} is the ideal probability distribution the Euclidean distance are

$$D(\mathbf{d};\mathbf{i}) = \left[\sum_u (\mu(x_i, y_j) - 1)^2 \right]^{1/2} \quad D(\mathbf{g};\mathbf{i}) = \left[\sum_u (\gamma(x_i, y_j) - 1)^2 \right]^{1/2} \tag{11}$$

By the sum of the square of quality loss the term $D = \left(\sum_u (\mu(x_i, y_j) - 1)^2 \right)^{1/2}$ represents a point on surface S_D of a hypersphere of n dimensions. Utilising the statistical terms $D(\mathbf{d};\mathbf{i})$ is given by

$$D = \sqrt{n \left((\alpha - 1)^2 + \frac{n-1}{n} s^2 \right)} \quad \alpha = \frac{1}{n} \sum_i \mu(x) \quad \sigma^2 = \frac{1}{n-1} \sum_i (\mu(x) - \alpha)^2 \tag{12}$$

where α and s^2 are, respectively, the mean and the variance of $\mu(x)$. When n is large the equation can be written

$$D^2 = n \left((\alpha - 1)^2 + \sigma^2 \right) \tag{13}$$

The quality lost is of two terms: $(\alpha - 1)^2$ resulting from the deviation of the average value of $\mu(x)$ from the target $\frac{1}{n} \sum_i \mu(x)$, and σ^2 resulting from the mean squared deviation of $\mu(x)$ from its own mean α .

It is possible to define the entropy of the system for a valuation of quality loss. The entropy is a generic value with very large means not connected to the probabilities. It is possible to define the idea of information for non-probabilistic events. It is possible to define entropy using the definition

$$J(P(.)) \stackrel{\text{def}}{=} -\log_2(P(.)) \quad (14)$$

in all situations. Using Wiener's definition of entropy the expression is

$$H = -\log_2((\alpha - 1)^2 + \sigma^2) \quad (15)$$

The measure of entropy, in probabilistic terms, indicates that in order to reducing the probability of quality loss, we must operate on reducing the deviation of average value or (and) mean squared deviation from own mean. In the figure 1 are reported the result of an example. In accordance to Jaynes' MaxEnt principle, we have the best solution in the third group with the max value of entropy

4. CONCLUSION

In applying the group technology to the cell formation, we have used an approach based on information for estimating parameters so that different factors are considered. The measure of the possibility of quality loss is estimated in term of information measuring the distance of the real solution from an ideal solution on the basis of the MinxEnt principle of Kulbach and Leibler. The quality loss is determined by using a set of memberships functions in soft set logic on the basis of a relation function of quality loss. The measure of entropy, in probabilistic terms, indicates that for reducing the quality loss, we must operate on reducing the deviation of average value or (and) mean squared deviation from own mean. In agreeing with the Jaynes' MaxEnt principle implies that, for having optimisation, the entropy should be maximised. The optimum solution is found analysing objective functions using the principle of maximum entropy.

5. REFERENCES

1. Burbidge, J.R.: The Introduction of Group Technology. John Wiley 1975.
2. J.N.Siddal: Probabilist Engineer Design M.Dekker JHG N.York 1983.
3. Nam P. Suh: The Principles of Design. Oxford University Press New York 1990.
4. Seifoddini H.: A Prob. Model for Machine Cell Formation. J. of Manufacturing Sy., n.1, 1990.
5. N.Kapur K.Kesavan: Entropy Optimization Principles, Academic Press Inc. Boston 1992.
6. Pappalardo M.: Information in Design Process-2nd International Conference on Planned Maintenance, Reliability and Quality - Oxford, England 2nd-3rd April 1998.
7. Donnarumma A., Pappalardo M., Pellegrino A.: Classification And Information Using Fuzzy Design, Int. Conf. on Advanced Production, Warsaw June 1998.

A NEURAL NETWORK APPROACH IN CELLULAR MANUFACTURING

T. Mikac, M. Jurkovic and Z. Pekic
University of Rijeka, Rijeka, Croatia

KEY WORDS: Neural network, Adaptive Resonance Theory, Cellular manufacturing

ABSTRACT: In order to achieve high productivity under the turbulent production environment, production systems have been changed into cellular manufacturing systems. That involves dividing of production system into some cells by collecting similar products and machines in manufacturing process. In this paper, a neural network approach for solving cell formation problem is investigated. We modify the binary self-organizing neural network algorithm (ART1) by changing the weight vector updating equation and using a set of supplementary procedures. The effectiveness of the proposed algorithm is shown by comparing of grouping efficiency with some other well-known approaches like rank order clustering method and ART1neural network (original and another with reversed ones and zeros).

1. INTRODUCTION

Group technology (GT) is an important management philosophy that identifies and exploits the similarities of product design and manufacturing process for improving the productivity of batch manufacturing systems. GT has been used as a technological innovation in small and medium-size batch production systems to achieve the economic advantages realizable in mass production. Cellular manufacturing (CM) is one of the successful applications of GT concept, which aims at harmonious assimilation of a firm's manufacturing facilities to

Published in: E. Kuljanic (Ed.) *Advanced Manufacturing Systems and Technology*,
CISM Courses and Lectures No. 406, Springer Verlag, Wien New York, 1999.

produce similar parts. The fundamental problem in CM is to identify machine cells and component families. To solve the cell formation problem of identifying part families and their associated machine cells, a lot of approaches have been developed. They can be generally classified as visual inspection methods, part coding based procedures or production process based systems. In this paper, we are concerned with the latter approach. A binary machine-part incidence matrix derived from route card data models the machine cell formation problem, and this approach is referred to as a matrix formulation of the GT problem. Columns of an incidence matrix represent parts, rows represent machines. Once the incidence matrix is constructed, a clustering algorithm is required to transform the initial matrix into a solution matrix to help identify clusters. Problem involves a reorganization of the rows and columns of incidence matrix to obtain block diagonal form. Among a lot of suggested approaches to the cell formation problem such as similarity coefficient, array manipulations, mathematical programming, graph theory, heuristics, matrix formulation methods and other clustering algorithms like fuzzy set theory, neural networks, genetic algorithms etc., an artificial neural network approach have been applied. Neural network approaches have been used to reduce the computational complexity, and they show the ability to identify similar patterns at high computational rates. Therefore, several neural network models are studied [1], and models based on Adaptive Resonance Theory (ART) network [2,3] are suggested. The advantages of ART are its speed of calculation and ability of dealing with large problems. In this paper like some other suitable example [4], after describing the cell formation problem, a modified algorithm with ART1 is proposed. Obtained results are compared favorably with popular algorithm proposed in the literature [5] and with original ART1 network as well as ART1 with reversing the zeros and ones. Final results show the effectiveness of the proposed algorithm.

2. CELL FORMATION PROBLEM

The procedure of the machines and parts to form cells in cellular manufacturing is called as the manufacturing cell design, and it is an important step in the development and implementation of cellular manufacturing systems. Performance of cellular manufacturing systems depends heavily on the cell structure. For that reason, the first problem towards the development and implementation of cellular manufacturing systems is that of cell formation. That involves identifying and grouping of machines which process similar components into machine cells and associating the part families that are processed within one cell. A part family consists of those parts requiring similar machine operations. At the same time, the parts that can not be processed within one cell may be identified. Grouping similar parts and associated machines and forming a cell by the parts and machines lead to reduce the parts that need processing in other cells and to increase productivity. To solve the cell formation problem, a lot of approaches have been developed to identify part families and their associated machine cells. In this paper, we are concerned with the direct analysis of process information available in production flow analysis chart. The input to the cell formation problem is the binary machine-part incidence matrix $\{a_{ij}\}$ derived from production flow analysis (PFA) chart. This approach is referred to as a matrix formulation

of the GT problem. Columns of an incidence matrix represent parts and rows represent machines. A matrix element a_{ij} is '1' if machine i is used to process part j , and '0' if otherwise. Table 1 shows an example of PFA chart for 8 parts and 10 machines.

Table 1. PFA chart

		Machines									
		1	2	3	4	5	6	7	8	9	10
P a r t s	1	0	0	0	0	0	1	1	0	0	0
	2	1	0	0	0	0	0	0	0	0	0
	3	1	0	1	0	0	0	0	0	1	0
	4	1	0	1	1	0	0	0	0	1	0
	5	1	0	0	0	1	0	0	1	0	1
	6	0	0	0	0	1	1	1	0	0	1
	7	0	1	0	0	1	1	0	1	0	0
	8	0	1	0	0	1	1	0	1	0	1

Once the incidence matrix is constructed, a clustering algorithm is required to transform the initial matrix into a solution matrix to help identify clusters. Problem involves a reorganization of the rows and columns of incidence matrix to obtain block diagonal form. The best solution is the mutually exclusive block diagonal matrix. It means all part families can be processed within their cells and it is not necessary to move parts among cells. Figure 1 shows an example of block diagonal matrix for the PFA chart shown in Table 1. In most cases as well as in our example, the final grouped cells are not mutually exclusive, and entries outside the diagonal blocks are called exceptional elements.

		Machines									
		10	5	8	1	3	9	4	2	6	7
P a r t s	8	1	1	1					1	1	
	5	1	1	1	1						
	6		1	1						1	1
	4				1	1	1	1			
	3				1	1	1				
	2				1						
	7		1	1					1	1	
	1									1	1

Figure 1. A block diagonal matrix for PFA chart shown in Table 1.

By the treatment of the exceptional parts which do not finish their process within one cell, cell formation problems can be classified by sufficient duplicating machines to form mutually exclusive groups or identifying the clusters of machines or parts without duplicating any of the machines. In this paper we consider latter approach, and exceptional parts that can't be processed completely in any one of machine clusters may be identified.

3. MODIFIED ART1 NEURAL NETWORK ALGORITHM

The topology of the modified unsupervised learning ART1 neural network consists of two layers: input and output layer. The structure of a neural network could be characterized by the interconnection architecture among neurons, the activation function for converse of inputs into outputs, and learning algorithm. The unit in one layer is connected with all the units in the other layer with bottom-up or top-down weight. The top-down weight represents the exemplar pattern of units in the output layer. Neuron x_i in the input layer corresponds to an entry in the incidence matrix. The vector $X = (x_1, x_2, \dots, x_n)$ corresponds to a row of the incidence matrix. Each output node y_k corresponds to a part group. The steps to implement modified ART1 algorithm for cell formation problem are as follows:

- Step 1 Rearrange rows (machines) of incidence matrix in descending order of the number of 1's in the row. In a case of a tie, the machine with the smallest identification number is presented first.
- Step 2 Define the number of neurons in the input layer n and the number of neurons in the output layer m and select a value for the vigilance parameter ρ ($0 < \rho < 1$).
- Step 3 Enable all the output units and initialize top-down weights W^t and bottom-up weights W^b as follows:

$$W_{ij}^t = 1 \quad (1)$$

$$W_{ij}^b = \frac{1}{1+n} \quad (2)$$

- Step 4 Show a binary machine vector X to the input layer (X consists of elements x_i)
- Step 5 Calculate the weight sum of input and bottom-up weight as matching scores for all enable nodes in output layer.

$$net_j = \sum_i W_{ij}^b \cdot x_i \quad (3)$$

- Step 6 Select a node that has the highest level of matching score as a best match exemplar
- Step 7 Implement the vigilance test to verify that input pattern belongs to cluster (cell).

$$V_j = \frac{\sum_i W_{ij}^t \cdot x_i}{\sum_i x_i} \quad (4)$$

The ratio of the nodes whose input and exemplar are matched as '1' is compared with the vigilance threshold. If $V_j > \rho$ there is resonance, go to step 9, otherwise go to step 8.

- Step 8 Disable the best match node and remove it from the future calculation of matching score. Then go to step 5.
- Step 9 Update the best matching examler as follows:

$$W_y^t = f_\theta(\delta_y) \quad (5)$$

$$W_y^b = \frac{f_\theta(\delta_y)}{0,5 + \sum_i f_\theta(\delta_{ij})} \quad (6)$$

where

$$f_\theta(x) = \begin{cases} 1 & \text{if } x > \theta, \quad 0 < \theta < 1 \\ 0 & \text{otherwise} \end{cases} \quad (7)$$

$$\delta_{ij} = \frac{\sum_{i \in j} z_{ip}}{m_j} \quad (8)$$

z_{ip} - element of machine – part matrix

m_j - number of patterns which allocated node j

Step 10 If all input vectors are applied go to step 12, else go to 11.

Step 11 Enable any nodes disabled in step 8 and go to step 4.

Step 12 Allocate the parts to their appropriate machine cells that has the most processes of the part. In a case of a tie, the machine cell with a high percentage of the part processes is selected. In a case of a tie again, the machine cell with the smallest identification number is selected as a associate cell.

4. PERFORMANCE MEASURE

Three performance measures are used to evaluate the quality of proposed solution given by the modified ART1 cell formation algorithm [4,6].

- a) Percentage of exceptional elements (PE). It is obtained by dividing the number of exceptional elements (NE) by the total number of elements having the value of 1 (N) in the final matrix. The smaller the PE , the better the clustering method.

$$PE = NE / N \quad (9)$$

- b) Machine utilization (MU) is the percentage of times the machines with the clusters are used in production. MU can be computed as:

$$MU = NI / \left(\sum_{r=1}^R m_r n_r \right) \quad (10)$$

where: NI - total number of 1's within the groups,

R - the number of groups,

m_r - the number of machines in the r^{th} group,

n_r - the number of components in the r^{th} group.

The higher the MU , the better the machine are being utilized, and the better the clustering method.

- c) Grouping efficiency (GE) is an aggregate performance measure of clustering. It is measure to evaluate exceptional parts and machine utilization, and it is defined as:

$$GE = 0,5 MU + 0,5 \left[1 - NE \left(MN - \sum_{r=1}^R m_r n_r \right) \right] \quad (11)$$

where: MU - the machine utilization as defined before,
 MN - the size of incidence matrix.

As a general rule, the higher the GE , the better the clustering results.

5. NUMERICAL EXPERIMENTS

Table 2. Comparison of algorithms

		NG	NE	PE	MU	GE
Example 1 5x7 matrix	Rank Order Clustering	2	5	0,375	0,909	0,829
	ART1	3	6	0,312	0,917	0,850
	ART1 with inversion	2	2	0,125	0,823	0,856
	Modified ART1	2	2	0,125	0,823	0,856
Example 2 5x7 matrix	Rank Order Clustering	2	3	0,187	0,812	0,846
	ART1	2	3	0,187	0,812	0,827
	ART1 with inversion	3	4	0,250	1,000	0,913
	Modified ART1	3	4	0,250	1,000	0,913
Example 3 6x6 matrix	Rank Order Clustering	3	6	0,400	0,818	0,784
	ART1	3	4	0,266	0,846	0,836
	ART1 with inversion	2	1	0,067	0,778	0,861
	Modified ART1	2	1	0,067	0,778	0,861
Example 4 6x6 matrix	Rank Order Clustering	3	3	0,200	1,000	0,837
	ART1	3	3	0,200	0,857	0,860
	ART1 with inversion	2	0	0	0,750	0,875
	Modified ART1	2	0	0	0,750	0,875
Example 5 8x10 matrix	Rank Order Clustering	2	3	0,111	0,600	0,736
	ART1	4	8	0,296	0,905	0,885
	ART1 with inversion	2	3	0,111	0,600	0,763
	Modified ART1	2	1	0,037	0,619	0,716
Example 6 10x10 matrix	Rank Order Clustering	2	6	0,182	0,540	0,710
	ART1	3	8	0,243	0,735	0,807
	ART1 with inversion	3	6	0,182	0,818	0,864
	Modified ART1	3	6	0,182	0,818	0,864
Example 7 10x15 matrix	Rank Order Clustering	3	9	0,176	0,840	0,875
	ART1	3	8	0,156	0,860	0,890
	ART1 with inversion	3	8	0,156	0,860	0,890
	Modified ART1	3	8	0,156	0,860	0,890
Example 8 15x15 matrix	Rank Order Clustering	3	13	0,260	0,308	0,592
	ART1	4	8	0,160	0,750	0,851
	ART1 with inversion	3	8	0,160	0,500	0,721
	Modified ART1	4	8	0,160	0,677	0,814

In order to clarify the effectiveness of the algorithm proposed in the preceding section, we report on our experiment in solving eight different grouping problems using four methods, rank order clustering [5], original ART1 and ART1 with reversing zeroes and ones [2], and our clustering modified ART1 neural network method. We coded a computer program in Visual C++ and used an IBM compatible Pentium to perform the computations that can be seen in Table 2. *NG* is a number of groups, and other criteria are defined in previous chapter. It has been demonstrated that neural network approaches gives in most cases better quality of grouping than conventional techniques, but all neural networks do not give the same solution. In some cases criteria *MU* and *GE* performs better results, but simultaneously *PE* performs worse results. Reason for that is fact when the number of groups are increased number of zeros within the cells are decreased and simultaneously number of exceptional elements ('1' outside the machine cells) are increased. Because of

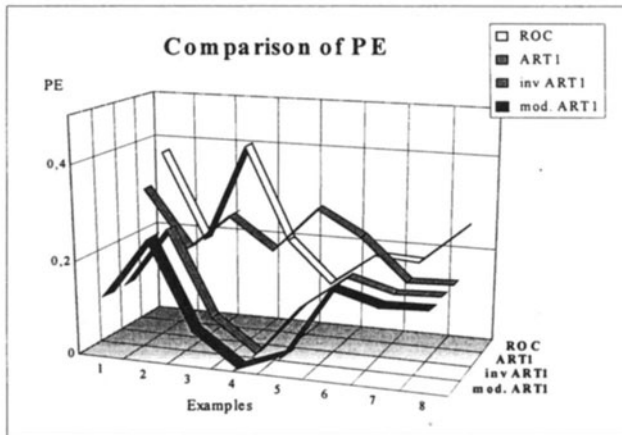


Figure 2. Comparison of *PE* as a result of experiment

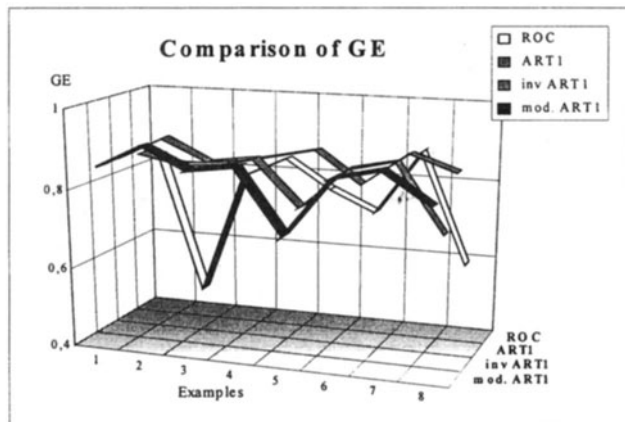


Figure 3. Comparison of *GE* as a result of experiment

that the *PE* and *GE* criteria are taken as a competent measure as can be seen in next figures. With figure 2 where *PE* is shown in dependence of example and applied algorithm, we can claim that the proposed algorithm is not always best but in seven of eight examples reach the best level in comparison with other approaches. Also, as it is shown in figure 3 proposed algorithm six times reach the best level, so we can conclude that is not always best but better then the other approaches in average.

6. CONCLUSION

In this paper, we proposed modified ART1 algorithm as a novel approach for machine cell's formation problems and clarified effectiveness of the approach by numerical experiments. We modify the self-organizing ART1 neural network algorithm by changing the weight vector updating equation and using a set of supplementary procedures. In comparison with some another clustering approaches, we can finally claim that the proposed algorithm has the effectiveness. The results suggest that the modified ART1 could consistently produce a quality result to a cell formation problem in considerably short time. But, it should be mentioned that the paper only deals with the machine cell formation based on the machine-part matrix without considering other manufacturing data such as operation times, production volume and so on. To take these additional factors into account, other neural network models should be investigated.

REFERENCES

1. Zhang, H.C.; Huang, S.H.: Applications of neural networks in manufacturing: a state-of-the-art survey, *International Journal of Production Research*, 33 (1995) 3, 705-728
2. Chen, S.J.; Cheng, C.S.: A neural network-based cell formation algorithm in cellular manufacturing, *International Journal of Production Research*, 33 (1995) 2, 293-318
3. Joshikawa, K.; Fukuta, T.; Morikawa, K.; Takahashi, K.; Nakamura, N.: A neural network approach to the cell formation problem, *Proceedings ICPR 14th International Conference on Production Research 1997, Osaka, 1997*, 1100-1103
4. Vranješ, B.; Grolinger, K.; Jerbić, B.: Modified fuzzy art neural network in group technology, *Proceedings DAAAM 7th International DAAAM Symposium*, ISBN 3-901509-02-X, Vienna, 1996, 471-473
5. King, J.R.: Machine-component grouping in production flow analysis: an approach using a rank order clustering algorithm, *International Journal of Production Research*, 18 (1980) 2, 213-232
6. Malakooti, B.; Yang, Z.: A variable-parameter unsupervised learning clustering neural network approach with application to machine-part group formation, *International Journal of Production Research*, 33 (1995) 9, 2395-2413

NEW MECHANISMS AND NEW TECHNOLOGIES FOR THE MACHINE TOOLS

B. Milcic

INAS-TAS, Zagreb, Croatia

T. Udiljak

University of Zagreb, Zagreb, Croatia

S. Jakupec

INAS-TAS, Zagreb, Croatia

KEY WORDS: Tool Milling Machine, High Speed Machining, Hexapod Mechanisms

ABSTRACT:

As a result of permanent development, and tradition in manufacturing and application of Tool Milling Machine, feasibility study from which we expect answer about possible substitution of 5-axes milling by Machine Tool with HPM (HexaPod Mechanism) carried on. Development of production systems is characterised with tendency to build machining systems with higher degree of automation, flexibility and integration of operations. In production of very complex workpieces like moulds, dies, stamps, turbine blades, prothesis and other workpieces with free formed surfaces we wish by using Machine Tools with HPM and HSP (High Speed Machining), to promote the process of machining, achieve better quality and productivity.

1. INTRODUCTION

Production without development is difficult to exist at the instable and turbulent market. Permanent changes, quick development of technology, technics and informatic sciences as well as significant changes at the world market and orientation to the globalisation of economy and production represent the facts of the present situation. For this reason, the management philosophies change-it has the greatest impact on industry in terms of quality, productivity and competitiveness.

The possibilities of automatisation are such that enable the reduce of labour in the process of production. Recent efforts of experts are related to the increase of quality, to shorten the production process, increase of flexibility as the key for creation of success in the future. The mentioned changes in production significantly influences development of machine tools and related technologies.

2. TOOL MILLING MACHINES

Tool milling machines are very complex machine tools, very often called also universal vertical milling machines, equipped with great number of different facilities which make their significance more universal. Speaking about tool milling machines, special attention has been payed to the working space such as access to the working space and being easy to survey. By regular equipping with vertically main spindle, linear motion on the axes X, Y, Z, tool milling machines are often equipped with:

- horizontally main spindle
- vertically high speed spindle
- dividing head
- circular dividing table
- universal swivel table
- slotting head and great number of accessories, jigs and fixture for workpiece and

tool.

The most frequent solutions are CNC-computer numerical controle for 3- linear axes and the manual controlled axes B and A, is also possible. In case of complete automatization of tool milling machine, the numerical controlled rotated and swible table is built in, and which gives special complexity to the realization of such tool milling machine. The tools, produced by such machines are as follows:

- milling cutter, end mills
- boring tools
- shaped profile cutter
- forging dies
- pressure die castings for metal
- metal mould castings
- glass mould castings
- stamping tools
- bending dies, deep drawing dies
- dies for precision casting
- injection mould for plastics
- model for copying
- electrodes for EDM

On the tool milling machines it is possible, besides mould and dies, the machining of very complex workpieces such as thin compressor rotor blades for gas and steem turbines, water turbines and propellers. Tool milling machines could very successfully perform the machining of parts of fuselage, rockets and other complex parts.

The development of tool milling machines in INAS Machine Tool Company lasts for a long time, so that the first tool milling machine has been introduced to the market in 1954. Its development has been shown on the table 1. On the figure 1. the design of the Tool Milling Machine ALG- 100 C and on the figure 2. Tool Milling Machine ALG 100F are shown.

Table 1. Development and production of Tool Milling Machine in INAS-TAS d.o.o.

Year of production	Type of Tool Milling Machine	Working Surface Width x Length [mm]	Number of CNC Axis
1954.	ALG-100	215 x 600	
1962.	ALG-200	250 x 1030	
1963.	ALG-100 B	215 x 600	
1967.	ALG-100 C	215 x 600	
1967.	G-301	300 x 1100	
1968.	G-301 H-31A	300 x 1100	Hydrocopy
1970.	G-301 D1, D2, D3, D4	300 x 1100	
1971.	G-301 NC	300 x 1100	3
1976.	ALG-100 D	215 x 600	
1977.	ALG-200 B	250 x 1030	
1978.	G-01 NC	300 x 1000	3
1979.	AGBH 500 CNC	500 x 1000	4
1980.	ALG-100 E	215 x 600	
1980.	G-301 HA/400	400 x 1100	
1981.	AG-400 CNC	500 x 800	3, 4, 5
1986.	AG-250 CNC	325 x 500	3, 4, 5
1992.	ALG-100 RE	215 x 600	3
1997.	ALG-100 FR	215 x 600	3
1997.	AG-434 CNC	320 x 600	3
1998.	AG-434V NC/CNC	320 x 600	3, 4
1998.	AG-755VT CNC	500 x 800	3, 4

3. TECHNOLOGICAL ANALYSIS OF TOOL MILLING MACHINE

All, up to the present developed Milling Machines in INAS Machine tool company are characterized by serial feed drive axes. During the last few years, a new trend of Milling machine tools development in the world intensified on the basis of parallel kinematic mechanisms. Milling Machine Tools of Hexapod type and other similar kinematics by their characteristics seems to be more efficient than conventional ones. In the new century, the following characteristics are expected from the machines tools:

- more flexibility
- greater concentration of operation
- high precision of dimension and shapes
- high quality of machining surface
- higher speed of cutting

- higher feed rates and feed velocity
- shorter time for tool exchanges
- higher productivity
- lower purchase price
- less harmful influences on the environment

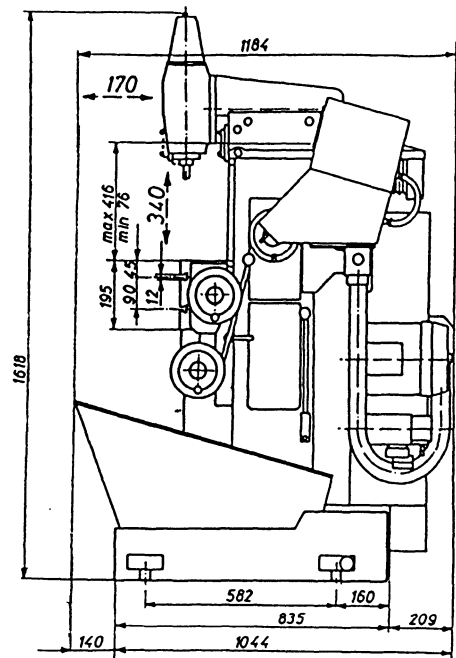
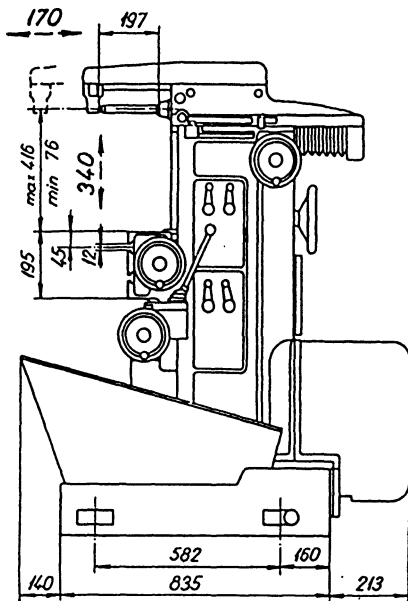


Figure 1. Tool milling machine ALG-100C Figure 2. Tool milling machine ALG-100F

In INAS Machine Tool Company the feasibility study of HEXAPOD is in the course of elaboration. From the study we expect the answer about possible substitution of 5-axes milling with machine type HEXAPOD. The field of its use is in rapid production of prototypes, in high quality and finish machining of steel, hardened steel, cast metal, aluminium and copper.

Characteristic workpieces are moulds, stamps, turbine blades and propellers, prothesis and other workpieces with free formed surfaces. Such workpieces require the use of 5-axes CNC control, especially at complex dies which now are produced by 3-axes CNC control using a great number of technological solutions. Dies are divided in sections using a great number of mechanic accessories and technics of hydrocopying. The final process and finishing are carried out manually. This is a longterm and hard work with great possibilities to fail the workpiece. In other hand, the milling machines with HEXAPOD mechanisms and using the high speed machining undoubtedly represent the advantage. In most cases, it is possible to realize the complete machining on the same machine and in one clamping. Production of dies and moulds don't require models for copying and manual finishing is not necessary or reduced to the minimum.

The expected advantages of Milling machines with HexaPod Mechanism (HPM) in comparison with conventional 5-axes milling machine are as follows:

- machine is mechanically simple
- the system of feed drive motions gives higher precision in positioning and stiffness
- the reduced mass of moving parts enables higher speed of feed drives
- higher stiffness of machine is suitable for high speed machining
- the price of production is lower than of 5-axes convention machine

Because of lack of experience in high speed machining, at the same time, practical investigations are carried on in the field of high speed machining.

4. EXPERIMENTS

The experience of INAS company in building 3-axes machine tools is very reach, while there is a very little experience in building 5-axes machine tools. Therefore, experimental investigation has been conducted trying to establish the influence of cutting toll position in regard to machined surface and feedrate direction, figure 3. It particularly consider machining with high speeds, when surface quality is one of the main goals. The experimental results should help in defining what effects could be expected when HSC is applied for 3-axes milling machine in comaprison when HSC is applied for 5-axes milling machines or HPM based machine tools. The machine tool available for this investigation was 3-axes CNC milling machine, equipped with turbine capable of running up to 40000 *rpm*. The simulation of 5-axes milling (or simulation of inclination angle of cutting tool) was accomplished with workpieces premachined in a manner that machined surface (upper surface of prismatic part) forms an angle of +10 or - 10 with XY plane. The angle of inclination could be defined in the plane containing feedrate vector, figure 3b, and plane perpendicular to feedrate vector, figure 3a.

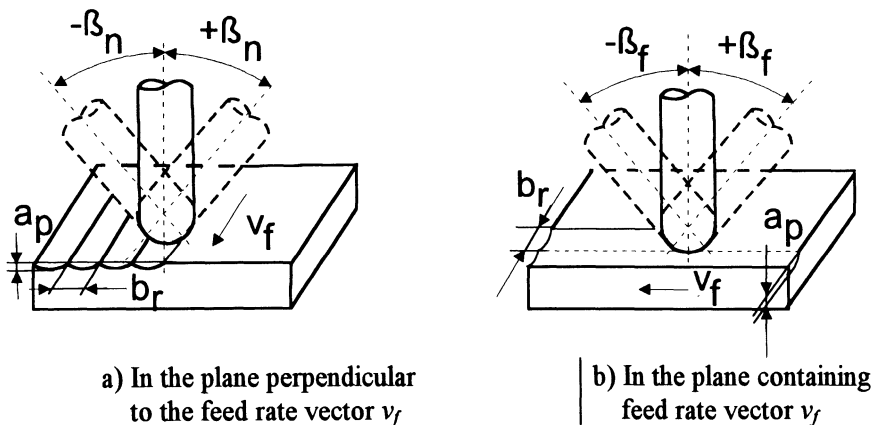


Figure 3. The inclination angle of cutting tool in regards to feed rate direction

Applied cutting tools were ball nose end mills, and measured value was surface roughness. The aim of investigation was to find the mathematical model describing dependence between surface roughness and on feed rate, depth of cut and inclination angle of cutting tool in regards to feed rate direction.

It is to expect that the change of inclination angle from 0° could produce better surface quality because of better cutting condition. At the same time, inclination angle makes cutting tool more sensitive to vibrations. For that reasons the preliminary experiments has been carried on, showing that "side" inclination (figure 3a) generates vibrations and chattering, and unacceptable quality of machined surface. Much better results has been obtained with inclination angle in the plane containing feed rate vector, β_f , and with values in the range $10-20^{\circ}$.

Therefore, factorial experiment have been performed for horizontal surface and for the surface with inclination angle in the plane containing feed rate vector, and under the following experimental conditions:

Machine tool:	CNC milling machine SCHAUBLIN 33-CNC equipped with turbine (up to 40000 rpm)
Workpiece material:	DIN 40 CrNiMo864 or according to ISO 9001 - 1.2738 $R_m=1015 \text{ N/mm}^2$; $A=11.6\%$; $HRC=30$
Cutting tool:	fine graded hard metal ball end mill $\phi=6 \text{ mm}$
Cutting fluid:	dry cutting

Table 2. Measuring results of surface roughness for horizontal and inclined surface

Cutting parameters			Results for horizontal surface			Results for inclined surface		
v_c [m/min]	f_z [$\mu\text{m/t}$]	a_p [mm]	R_a [μm]	R_z [μm]	R_{max} [μm]	R_a [μm]	R_z [μm]	R_{max} [μm]
490	2,5	0,2	3,93	17,17	20,88	0,44	3,30	6,04
698	2,5	0,2	2,97	14,31	17,74	0,60	3,62	4,40
490	10	0,2	3,51	16,43	21,35	1,50	8,30	10,97
698	10	0,2	3,01	15,82	23,45	0,56	3,44	4,17
490	2,5	0,8	0,31	2,17	2,57	4,57	25,29	41,02
698	2,5	0,8	0,62	3,9	5,69	0,52	3,17	3,75
490	10	0,8	2,41	12,98	17,76	3,42	17,82	29,69
698	10	0,8	1,74	10,79	15,92	0,69	3,62	4,40
585	5	0,4	1,49	10,95	28,14	0,38	2,45	3,05
585	5	0,4	1,53	10,86	27,56	0,44	2,48	2,97
585	5	0,4	1,43	10,75	28,22	0,32	2,37	3,12
585	5	0,4	1,37	10,60	28,08	0,41	2,39	2,86

The workpieces have been prepared in order to enable the machining with inclination angle of 0° (horizontal machined surface), and with inclination angle $\beta_f = -10^{\circ}$. For both position of cutting tool, cutting data and measuring results are presented in table 1.

The measuring results were processed by regression analysis, and by applying the mathematical model of following type:

$$R = C \cdot \prod f_i^{p_i}$$

For inclination angle of 0^0 and with linear model (without factor interactions) the following results were obtained:

$$Ra = 12516 f_z^{0.538} a_p^{-0.9072}$$

$$Rz = 353162 v_c^{0.1282} f_z^{0.5162} a_p^{-0.719}$$

$$Rmax = 113346 v_c^{0.452} f_z^{0.5885} a_p^{-0.6859}$$

All models prove to be adequate. The coefficient R is: 0.844 for Ra, 0.848 for Rz, and 0.731 for Rmax, while coefficient R^2 is: 0.713 for Ra, 0.719 for Rz and 0.534 for Rmax.

For inclination angle $\beta_f = -10^0$ (in the feed plane and in the direction of feed rate vector), and with linear model (without factor interactions) the following results were obtained:

$$Ra = 23536 v_c^{-1.483} a_p^{0.3045}$$

$$Rz = 7576.07 v_c^{-3.153} f_z^{0.118} a_p^{0.49}$$

$$Rmax = 68272.79 v_c^{-3.950} f_z^{0.069} a_p^{0.5059}$$

The coefficient R is: 0.56 for Ra, 0.695 for Rz, and 0.734 for Rmax, while coefficient R^2 is: 0.311 for Ra, 0.483 for Rz, and 0.54 for Rmax.

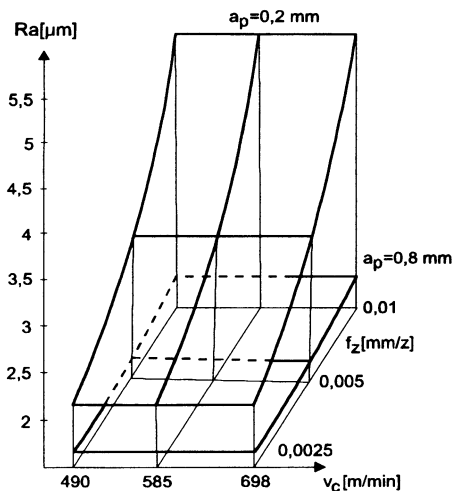


Figure 4. Dependence of Ra on the feed rate and depth of cut

Upon analysis of obtained results it is obvious that inclination angle has a strong impact on results, and on cutting conditions in general. It changes the influence of cutting data on such a way that with $\beta=0^0$, cutting speed shows no influence, figure 2, while with $\beta_f = -10^0$ cutting speed shows the highest influence. Therefore it is possible to conclude that application of HSM with tool perpendicular to machined surface will not produce significant advantage

over the ordinary cutting speed in regards to surface roughness. To accomplish the potential benefits of HSM it is also necessary to ensure the appropriate cutting tool position in regard to machined surface, what is possible with 5-axes milling machines or with HPM (HexaPod Mechanism) based machine tools.

5. CONCLUSION

The judgement on feasibility of HPM based machine tools is subject of numerous analysis, but it is likely to predict that one of the prerequisite for such machines to meet the expectations is to use HSM. The potential benefits of HSM are not obtainable with just high cutting speeds, but are strongly determined with accessible machining strategy in general. This work proves that machining conditions are highly determined with cutting tool position in regards to the feed plane. HSM has initiated many improvements in cutting theory, cutting tools, machine tools design, machine tool controllers and software. Recent commercial achievements obtained with HSM gave a real strong stimulus for further research activities in HSM domain. The combination of HPM machine tool and HSM could bring a significant improvement in machining technologies.

By joining the advantages of HPM machine tools such as:

- increased stiffness
- higher accuracy
- higher speed and acceleration due to reduced moving mass
- reduced production and installation costs due to fewer parts in a hexapod than in a conventional machining center.

With advantages of high speed machining:

- enlarged feed rate speed
- reduced cutting forces
- increase of material removal rate
- improving of surface quality (reduction or elimination of subsequent manual machining)
- enlarged fraction of heat taken away by chips

One could expect to meet a significant improvement in machining technology, and specially for die and mold making industry.

REFERENCES

1. Smith, S. & Tlustý, J. (1997). Current Trends in High-Speed Machining, *Transaction of ASME*, Vol. 119, November 1997, pp. 664-666
2. Schultz, H. & Moriwaki, T. (1992). High Speed Machining, *Annals of the CIRP*, Vol. 41/2/92, pp. 637-643
3. Schultz, H. & Hock, St. (1995). High Speed Milling off Dies and Moulds-Cutting Conditions and Technology, *Annals of the CIRP*, Vol. 44/1/95., pp. 35-38
4. Schultz, H. (1997). Gegenwärtiger Stand und weitere Entwicklungen der Hochgeschwindigkeitsbearbeitung, *Proceedings of 4th International Conference on Production Engineering CIM '97*, Opatija, June 1997, Croatia
5. Cebalo, R.; Schultz, H. & Udiljak, T. (1997). With high speed machining towards 21st century, *Proceedings of 4th Inter. Conf. on Production Eng. CIM '97*, Opatija, June 1997,
6. Jakupec, S. & Milcic, B. (1997). Advanced Approach to the Development and Production of Machine Tools, *Proceed. of the 8th DAAAM Symposium*, 1997. Dubrovnik

INTEGRATED INFORMATION SYSTEM FOR ORDER PLANNING, CONTROL AND COST ESTIMATION IN LASER JOB SHOPS

H.K. Tönshoff, A. Ostendorf, C. Peper
Laser Zentrum Hannover, Germany

KEY WORDS: Laser Job Shops, SME, Integrated Information System, Order Planning

ABSTRACT: Today, laser technology is being used more and more by small and medium sized job shops. Because of their specific company profile, commercially available systems for production, planning and control (PPC-systems) cannot be used. Therefore, a new information system is being developed. To meet the exact needs of laser job shops, six European small and medium sized enterprises (SME) were analysed. In this paper, the results from the survey are presented. Three fields for an optimised order fulfilment system were identified: order planning, order control and cost estimation. A new information system is outlined that provides functionality in these fields. An architecture for an integrated information system is proposed that allows the adaptation of new software modules to existing heterogeneous information systems.

1. INTRODUCTION

Because of their flexibility and high innovative potential, small and medium sized enterprises (SME) are considered an important factor in today's rapidly changing markets. Laser job shops represent an example for such SMEs. In a job shop environment, an efficient order fulfilment system is essential for the economic use of machinery. The commercially available information systems, called "Production, Planning and Control Systems" (PPC-Systems) are often not appropriate for SMEs. The current PPC-Systems

are too complicated and need highly expensive and specialised personnel. These systems often are overqualified for the job, and do not provide the adaptability that is requested by SMEs. Therefore, a new integrated information system is being developed within the scope of a European research project. The goal is to integrate existing software solutions to provide a more effective system for order fulfilment.

2. COMPANY PROFILE OF LASER JOB SHOPS

Laser job shops are generally small companies with up to 50 employees, which provide material treatment services by lasers. Laser cutting and welding of sheet metals are by far the most commonly employed processes [1]. As subcontractors, laser job shops produce components on behalf of a customer order. The customer almost always supplies a drawing or a sample for the product ordered. They are dealing mostly with one-piece products processed in one production stage.

Since products are specified by the customer, there is no stock keeping of articles. Even sheet metals have often to be procured on receipt of the customer order. Most orders are manufactured in small lots of about 10 to 100 pieces.

In laser job shops, 65% of all received orders are new orders [1]. In contrast to repeat orders, where detailed design and cost information is already available, new orders require higher expenditures for the pre-calculation. Because the job shop doesn't have product specific know-how, it competes for every new order with other job shops. Asking for the delivery lead time and the price, the customer typically makes an inquiry of various possible producers. The chances of winning the new order depend on the values for the price and the lead time the job shop can offer. The probability to gain a quotation as a firm order is often lower than 20% [1].

When an order is received, the lead time is mostly shorter than one week. About 15% of all orders must be manufactured within one day [1]. Urgent orders lead to disrupted manufacturing orders, that sometimes lead to tardiness of other orders. Those consequences have to be anticipated in a quotation, since failing to meet delivery promises can result in lost profit. Because of the short lead times and a highly competitive market situation, laser job shops must be highly flexible.

Realisation of short delivery lead times and competitive pricing is crucial for the economic success of laser job shops.

3. RESULTS FROM A SURVEY OF SIX LASER JOB SHOPS: ORDER FULFILMENT CHAINS AND ITS DEFICIENCIES

A survey of 6 laser job shop showed that the chain from the inquiry to the fulfilled order is generally comprised of up to 8 steps. Starting with a *quotation*, the job shop responds to a customer inquiry. The quotation contains the price and delivery lead time. The price is determined by costs and a standard mark-up percentage. Delivery lead times are often determined by the customer.

The *order planning* comprises capacity planning and scheduling. Capacity planning takes into account the total load of a machine, while scheduling specifies the times when the manufacturing starts and ends.

The *design, work-plan generation* and *NC-programming* belongs to the technical part of the order fulfilment chain. It includes all measures to assure a correct and economic manufacturing of the order.

The *manufacturing* stage comprises the actual laser processing. It is often supplemented by a *quality assurance* stage. Most companies perform a *post-calculation* on an irregular basis.

The survey revealed that the companies have different structural organisations (Table 1). Between 2 and 4 departments collaborate during the order fulfilment. Departments can be distinguished by whether they primarily serve the manufacturing part, engineering part or business part of the order fulfilment chain.

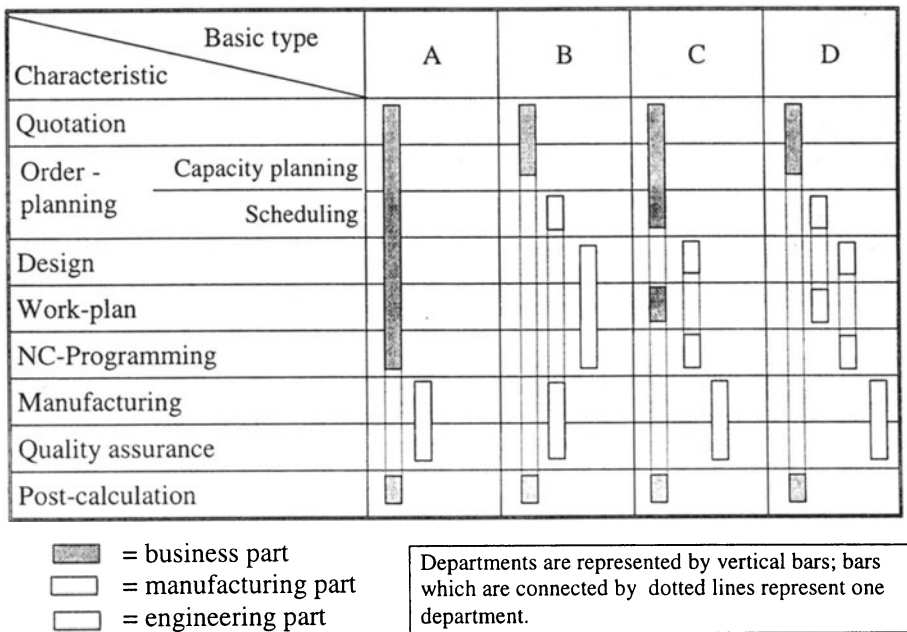


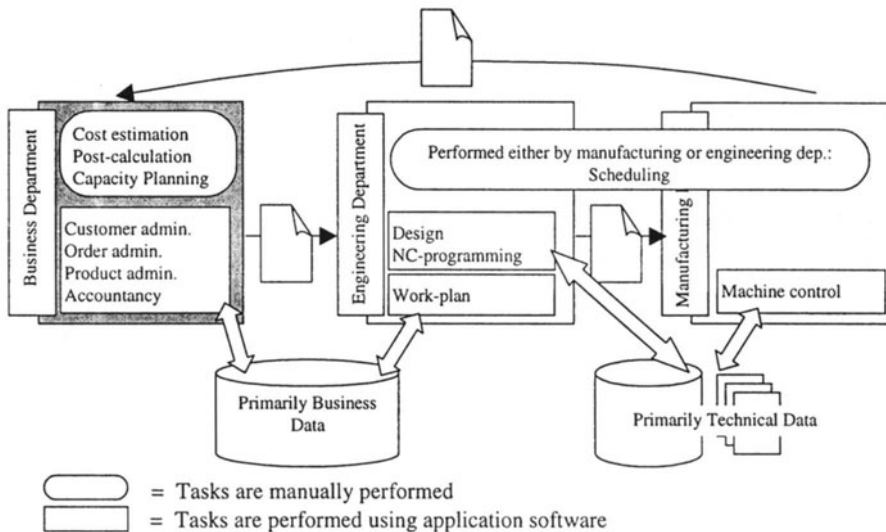
Table 1: Basic types of structural organisations in 6 laser job shops

By defining a department for the business, engineering and manufacturing part of the order fulfilment, a generalised structure for laser job shops is obtained (Figure 1). The business department is accountable for quotations, capacity planning and post-calculation. The engineering department is responsible for design, NC-programming and the generation of the work-plan. The manufacturing department processes the orders and assures product quality. Scheduling is either performed by the foreman in the manufacturing department, or by a production planner in the engineering department.

In addition to the structural organisation, the use of IT-systems was investigated. All examined job shops have at least an IT-system for administration of customer data, order data and product data. Because products consist of just one piece that is manufactured in one production step, work-plan data are simply administrated with the product data.

Besides the administration software, CAD/CAM-systems are used for design and NC-programming. Administration software and CAD/CAM-system have their own separate databases. The situation is depicted in [Figure 1](#).

Most IT-system used by the surveyed companies do not provide functionality in the field of pre- and post-calculation, capacity planning and scheduling. Even isolated spreadsheet solutions are not suitable to provide sufficient functionality in these fields. The reason is that the implementation of these tasks needs information from adjacent departments.



[Figure 1](#): Generalised structure of the order fulfilment in laser job shops

The crux of pre-calculation and production planning

Pre-calculations of a product can be made on the basis of a post-calculation from a similar product. For post-calculations, real processing times from the shop-floor are necessary. To save time, feedback data from the shop floor, which are paper based in most job shops, are often not transferred to the database. Post-calculations are performed irregularly, and thus only a few of them are available for pre-calculations. Therefore, pre-calculations are mostly performed on the basis of calculated manufacturing time. The time is calculated from the contour length and the feed rate.

But neither a post-calculation nor the estimate of the manufacturing time gives reliable costs in a job shop environment. As described in [2], costs also depend on the delivery

time. The shorter the delivery time, the higher are the costs, e.g. double set-up costs if currently processed orders must be interrupted for an urgent one. Furthermore, costs depend on the machine used. Different laser machines can have different processing times and hourly rates. If the business department does not know which machine will actually be used, the cost estimate can be inaccurate.

To save costs, different orders are often manufactured in one job, if sheet metal of the same material and thickness is used. Scheduling data must be available to consider this dependency in the pre-calculation.

To meet promised delivery dates, the business department needs information about actual and planned machine loads. In particular, information is needed about critical delays of orders which would occur if an inquiry becomes order. Scheduling data and functions for IF-THEN scenarios are required for this task. None of them are available in IT-systems employed by the surveyed laser job shops.

4. DIFFICULTIES TO OPTIMISE INFORMATION SYSTEMS

There is no doubt that suitable software is available under the vast amount of commercially IT-systems to solve the problems described above. Job shop specific order planning and scheduling algorithms have also been developed [3, 4]. However, SMEs are faced with specific difficulties in the use of those systems (Table 2).

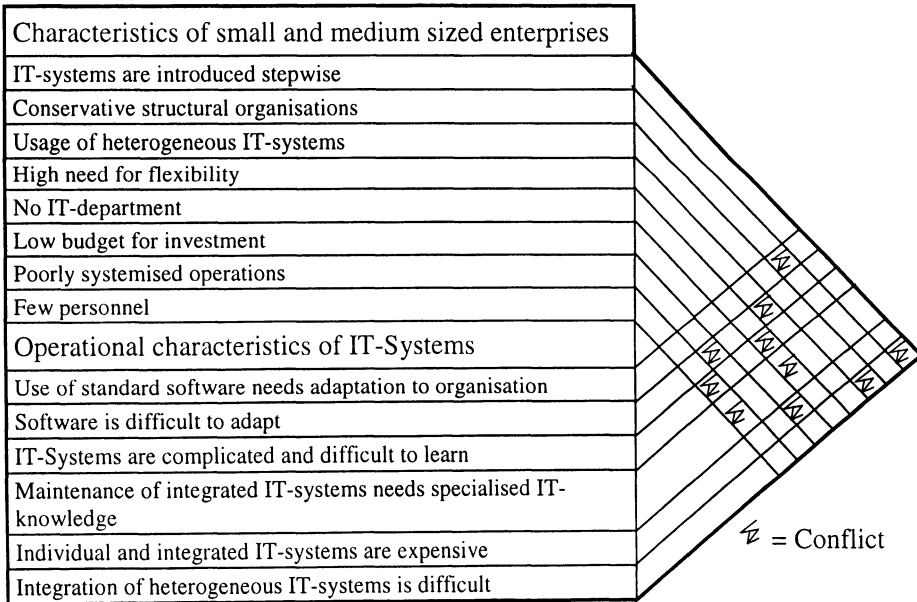


Table 2: Problems of small enterprises to employ IT-system

Most common systems lack sufficient flexibility to adapt easily and quickly to different environments [5]. The specific needs of customers result in more and more complex systems. Only parts of those complex functional capabilities can be used by the end user, since the effort to learn the effective use of those systems is too costly and time-consuming. As monoliths, those systems are mostly designed to replace already existing systems instead of complementing them. This results in high investment costs.

Laser job shops need a branch-specific low-cost solution which is easy to use, easy to maintain and easy to adapt to already existing IT-systems.

5. ARCHITECTURE FOR AN INTEGRATED INFORMATION SYSTEM IN LASER JOB SHOPS

To provide functions for order planning, control and cost estimation in consideration of SME-specific constraints, an integrated information system is proposed (Figure 2). It consists of the following modules:

Database

The centre of the concept is a central, relational database that contains all data relevant to order planning, control and cost estimation:

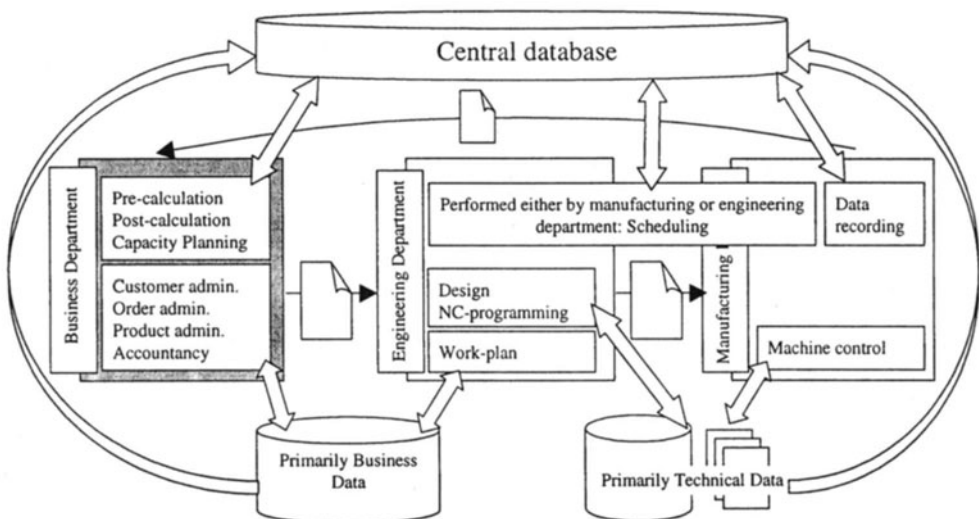


Figure 2: Concept for an integrated information system in laser job shops

- Data for customers, customer orders and products.

- Actual and scheduled data of manufacturing orders; the structure allows modelling the processing of one-piece products including order splits.
- Costs for machining and personnel.
- Machine calendar.

The central database receives data either by transfer from existing databases or by manual input in one of the application modules.

Order Planning and Control Module

The order planning and control module provides actual data about orders and machine loads. Orders are visualised and scheduled in a graphical order sequence sheet. The system provides the user with necessary information to place the order cost and time effective into the order sequence sheet. For instance, orders with similar processes or similar material can be emphasised.

With IF-THEN scenarios, the user can detect how an action affects the observance of promised delivery dates.

Cost-Estimation Module

The cost-estimation module automatically performs a post-calculation when an order is finished. Since post-calculations are based on real processing times, they are useful for the pre-calculation of similar orders.

Shop-Floor Data Recording Module

The order planning and control module and the cost-estimation module rely on data from the shop-floor. Therefore, the machine operator feeds the status of machines and orders into the shop-floor data recording system.

Database Transfer Module

The database transfer module controls data transfer processes between already existent databases and the central database. It can also be used to export data from the central database to common software systems, i.e. for evaluations and graphical representations in a spreadsheet program.

The data transfer module accesses the source database and the target database via the ODBC-interfaces (ODBC: Open Database Connectivity). For non-relational data formats the OLE DB-interfaces are used. ODBC and OLE DB allow universal data access for Microsoft Windows® and Windows NT® operating systems. Using this technology, the data transfer module allows bi-directional data transfer between databases. Therefore, data feedback to already existent databases is possible.

A timer can be set to start update operations periodically.

Hardware and Operating Systems

The new software modules run on a PC basis (Intel-compatible processor x86 upwards) with Microsoft operating systems (Windows®, Windows NT®). Since all ODBC- and OLE DB-compliant data sources independent of the hardware and operating system are accessible via the ODBC- and OLE DB-interfaces, already existent hard- and software systems can be integrated in the new system.

6. CONCLUDING REMARKS

This paper has described the general ideas to aid laser job shops to improve their order fulfilment chain. The goal is to develop an information system to enable laser job shops to become more efficient in scheduling orders time and cost effectively and in responding to customers inquiries. It has been shown that deficiencies in order fulfilment arise mainly from poor information flows between the business, engineering and manufacturing functions. Therefore a system has been proposed that provides integrated functionality in the field of order planning, control and cost-estimation. Since the new software modules fit in already existent, heterogeneous soft- and hardware environments, the specific requirements of SME's for information systems are taken into account. The new software offers a solutions to specific problems of laser job shops.

ACKNOWLEDGEMENT

This research is supported by the European Union within the CRAFT Program (INFOLAS BRST-CT97-5184)

REFERENCES

1. Unpublished Survey among 18 German Laser Job Shops performed by Laser Zentrum Hannover, April 1997
2. Kingsman, B., Worden, L., Hendry, L., Mercer, A. AND Wilson, E.: Integrating marketing and production planning in Make-To-Order companies, *International Journal of Production Economics*, 30-31 (1993), pp. 53-66
3. Tönshoff, H.K., Rotzoll, M.A.: Application of Evolutionary Algorithms for Planning and Improving Manufacturing Systems, *CIRP International Seminar on Intelligent Computation in Manufacturing Engineering, ICME'98, Capri, Italy, 1.7 –3.7.1998*, pp. 97-104
4. Brandimarte, P., Roero, L.: Lead Time Reduction in a Job Shop Environment: Integrating Genetic Algorithms and Simulation Modeling, *CIRP International Seminar on Intelligent Computation in Manufacturing Engineering, ICME'98, Capri, Italy, 1.7 –3.7.1998*, pp. 129-135
5. Augustin, H.: Von Objektorientierung (k)eine Spur, *Arbeitsvorbereitung AV*, 33 (1996), pp. 314-318

AN APPROACH TO SELECTIVE LASER SINTERING (SLS) OF PRE-COATED SANDS FOR SHELL MOULDING

G. Dini, M. Lanzetta, M. Santochi, G. Tantussi and A. Franco
University of Pisa, Pisa, Italy

KEY WORDS: Selective Laser Sintering, Shell-Moulding, Mathematical Model, Heat Transfer

ABSTRACT: The Selective Laser Sintering of pre-coated sands is a promising Rapid Prototyping technique for the construction of sand shells for foundry. In this article, the definition of mathematical simulation concepts and a detailed experimental analysis, performed both with conventional and unconventional techniques, is proposed. In particular, two methods to calculate the temperature distribution within the sand bed and the depth of the heat-affected zone are studied. The results obtained with the experimental methodology and those coming from previous experimental analyses have been used to validate the described mathematical models, that represent a first step for the process comprehension, control and optimisation. Two kinds of pre-coated sands, widely used in shell-moulding, have been considered: zirconia and silica. The guidelines for future simulation refinements are also given.

1. INTRODUCTION

Selective Laser Sintering (SLS) is a process to create solid objects, layer by layer, from plastic, metal, ceramic powders or pre-coated sands that are «sintered» using laser energy. The basic concept, common to all rapid-prototyping techniques, is that any complex shape can be obtained with the superposition of small thickness layers. The inherent material

versatility of SLS technology allows a broad range of advanced rapid prototyping and manufacturing applications to be addressed [1]. In Figure 1. a SLS application for foundry shell construction is schematically described and compared with the traditional process.

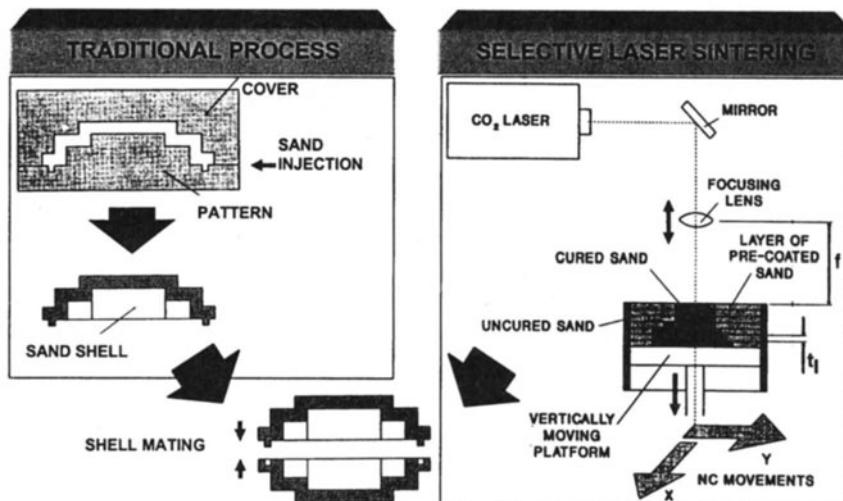


Figure 1. - Comparison between the traditional method and SLS to obtain foundry shells

To achieve parts with acceptable geometry and strength, the following problems should be considered:

- to obtain a reliable adhesion between layers;
- to generate flat surfaces without distortions;
- to obtain a suitable resolution.

Several studies on SLS have been carried out in the last years, but the heat conduction and energy release mechanism, that determines the grain agglomeration, has not yet been completely investigated both on the experimental and theoretical point of view. Only recently, strategies for the simulation of the SLS process related to metallic powders have been developed both in [2] - where Polymer Coated Silicon Carbide Powders as the base material is considered - and in [3-4] - where Polycarbonate is used - but available methods do not provide sufficient details for their application.

In [5], the authors described an experimental facility to investigate the SLS process of pre-coated sands for shell-moulding. The present work continues this analysis, considering the sand thermo-physical properties and the measurement of the real input energy. In addition, two possible mathematical models of the SLS process are proposed and tested.

2. THE PROCESS PARAMETERS

The main technological parameters to control the SLS process are:

- the pre-coated sand and its thermo-physical properties, such as density ρ , specific heat c_p , thermal conductivity k , resin polymerisation temperature range ΔT_p , sand glass-transition temperature T_g , sand energy absorption a , reflection r and transmission τ coefficients, and other properties, such as granulometry and average grain dimension;
- the scan spacing;
- the laser beam power P ;
- the laser spot diameter \varnothing ;
- the scan speed V .

The four sand types under study, belonging to two categories (Table I), are commonly used in shell-moulding as they have a good compatibility to the fused metallic material.

Table I - Commercial sand properties

Sand type	Commercial name	Composition	Density [kg/m ³]	Resin weight [%]	Granulometry [DIN 1171]	Average grain size [mm]
zirconia	Zircon	ZrO ₂ 99.6 %	2810	2.5	61	0.19
silica	DB 40	Si ₂ O ₃ 95%	1600	3.4	79	0.14
silica	LHN 50/70	“	1560	4.0	57	0.20
silica	E 45	“	1555	3.8	108	0.10

The last three process parameters determine the thermal radiant power density, that depends directly on the laser power and inversely on the spot diameter and the scan speed; this latter has a direct impact on productivity.

On the other hand, the shell mechanical resistance is influenced by the depth p of the heat-affected zone (strictly related to the layer thickness t_l of Figure 1.) and by the temperature history determined by the laser radiation, and finally by the process parameters.

In this particular SLS application, the laser beam raises the sand temperature allowing the agglomeration of grains, without local burning. Under the thermal viewpoint, the phenomenon can be schematically described as follows: the energy absorbed by the sand leads the resin into a glass-like state so that grains coalesce into a solid (Figure 2.). The temperature necessary to reach this condition seems lower than the one at which resin polymerisation occurs [5].

It appears that SLS is basically a heat transmission phenomenon in which the input energy, the laser radiation, generates in the sand bed a mixed conduction and convection heat transfer. The grain agglomeration strongly depends on the energy absorbed by the sand bed and on the energy required for the resin polymerisation, as well as on the chemical energy release during the heating process.

To set the optimum thermal radiant power density in order to maximise the productivity and to find a suitable compromise between the quality and the mechanical resistance of shells, a suitable combination of the three parameters should be determined.

A quantitative understanding of the temperature gradient, and of the depth of the heat-affected zone and their dependence on the input parameters allows the generation of quality forms and a thermal control of the working area.

3. THE SLS PROCESS MODELISATION

SLS is a very dynamic process, hence its mathematical description involves the solution of the *unsteady* heat conduction equation. The model should reproduce the thermal history within the sand bed after the radiation incidence starts. As already mentioned, simplified modelisations of the SLS process can be found in the literature, but they are generally related to metallic powder operating at higher temperature range [2-4].

In this paper the application of a heat conduction scheme to the SLS of pre-coated sands and a refinement of the existing models is proposed, having in mind to maintain a simple approach. Moreover, differently with respect to other studies, an attempt to provide a general method that can be simply tested by other researchers with the same or with a different base material has been made.

The material (a pre-coated sand) is considered as homogeneous from the thermal point of view and its thermo-physical properties do not change with temperature. With these hypotheses, the chemical aspects related to the energy absorbed and released during heating are considered.

In our model, as in the majority of those proposed in the literature, the governing equation is the unsteady heat conduction equation. The resulting output data are:

- the temperature distribution and the maximum value on the surface T_{max} ;
- the depth p and the width of the heat-affected zone considered as the penetration of the isothermal front corresponding to the resin glass-transition temperature.

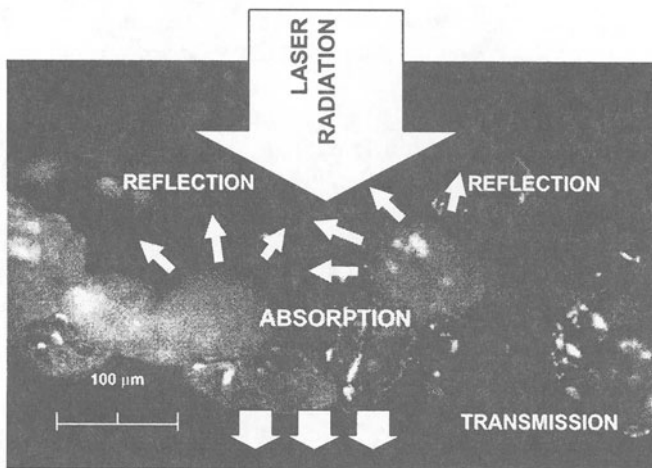


Figure 2. - Energy flow in the SLS general process

This last hypothesis is a direct consequence of the experimental investigation in [5], where it was observed that the sand grain agglomeration occurs before reaching the resin

polymerisation temperature. This kind of model, though simplified, could be a theoretical instrument for preliminary evaluation of the operative parameters in order to avoid unsatisfactory technological results such as high surface temperatures, high polymerisation thickness or burnt sand.

When the laser spot hits the sand bed, the surface interaction with the radiant energy can be described by the coefficients representing the fraction of absorbed a , reflected r , and transmitted energy τ (Figure 2.); of course,

$$r + a + \tau = 1 \quad (1)$$

The three coefficients depend on the sand used, on the resin, and on the radiation itself, but they are very difficult to obtain from the literature. For the pre-coated sands used in shell-moulding, the absorptivity coefficient a is sensibly higher than 0.9 and the reflectivity is lower than 0.01 [6].

As mentioned before, the penetration of the glass-transition temperature front into the sand bed determines the depth and width of the heat-affected zone. However this thermal problem, even if conceptually simple, has not a simple solution for the following reasons:

- the intrinsic complexity of the phenomenon and of its mathematical scheme (three-dimensional thermal conduction with convective surface heat dissipation);
- the difficulties in the characterisation of the sands from a thermo-physical point of view (thermal conductivity, specific heat capacity and thermal diffusivity);
- the difficulties in a correct modelisation of the pre-coated sands from a chemical point of view (polymerisation temperature, energy released during the polymerisation process caused by the breakage of chemical links, etc.).

Moreover it would be necessary to consider the following aspects that are usually neglected in the modelisation:

- the influence of mechanical phenomena, like the sand agglomeration caused by friction and by special thermo-hygrometric conditions;
- the effects of the non-homogeneous material;
- the changes of the pre-coated sand thermo-physical properties with the temperature.

3.1 The analytical solution of the 1D heat conduction equation

A first method to model the SLS process is represented by the one-dimensional heat conduction transfer equation. In this scheme, the heat transfer in a plane perpendicular to the laser radiation incidence is neglected and the heat transfer by conduction is studied only in the direction of the laser beam axis z ; the material is considered as homogeneous.

The phenomenon is governed by the general one-dimensional heat conduction equation in unsteady conditions:

$$\frac{\partial T}{\partial t} = \frac{k}{\rho \cdot c_p} \cdot \frac{\partial^2 T}{\partial z^2} \quad (2)$$

with the following boundary conditions:

$$k \frac{\partial T}{\partial z} \Big|_{z=0} = \dot{q}'' = a \cdot \dot{q} - h(T - T_\infty) \quad t \leq t^* \quad k \frac{\partial T}{\partial z} \Big|_{z=0} = -h(T - T_\infty) \quad t > t^*$$

where h is the convective heat transfer coefficient between surface and surrounding air (that can be conventionally assumed equal to $10 \text{ W/m}^2\text{K}$ for natural convection), \dot{q} is the specific thermal power of laser radiation (in W/m^2) expressed by $P/(\varnothing \times s)$, being s the space hit by laser in the unit of time, T_∞ is the environmental temperature, and t^* is the radiation incidence duration.

A closed solution of the thermal conduction problem expressed by (2) can be obtained by supposing that the thermal influenced zone, exposed since the time $t = 0$ to a heat flux \dot{q}'' , is small with respect to the working area. Until $t = t^*$, the temperature history during the radiation incidence can be expressed as follows:

$$T(z, t) = T_i + 2 \frac{\dot{q}''}{k} \cdot \left(\frac{\alpha t}{\pi} \right)^{1/2} \exp\left(-\frac{z^2}{4\alpha t}\right) - \frac{\dot{q}''}{k} \cdot z \cdot \operatorname{erfc}\left[\frac{z}{2(\alpha t)^{1/2}}\right] \quad (3)$$

where $\alpha = k / (\rho c_p)$ is the sand thermal diffusivity, T_i the initial temperature of the sand bed and erfc is the complementary error function [7].

For $t > t^*$:

$$\frac{T(z, t) - T_\infty}{T_f - T_\infty} = \operatorname{erf}\left[\frac{z}{2(\alpha t)^{1/2}}\right] + \exp\left(\frac{hz}{k} + \frac{h^2 \alpha t}{k^2}\right) \operatorname{erfc}\left[\frac{z}{2(\alpha t)^{1/2}} + \frac{h}{k}(\alpha t)^{1/2}\right] \quad (4)$$

where T_f is the surface temperature at the end of the heating process and erf is the error function [7].

To improve the one-dimensional schematisation, it is possible to consider that the sand temperature T_i in the equation (3) is the environmental temperature at the initial step only. In the next steps, it is necessary to take into account the effects connected with the laser incidence in the adjacent region.

In order to consider the two-dimensional effects of the thermal heat conduction, a different schematisation of the laser incidence is then used: the well known «moving heat source» (that allows the simulation of arc welding and surface hardening as well) [7]. In this way it is possible to evaluate the temperature field deformation, when the heat source moves through the conductive medium, by adjusting the initial condition for the application of (3) and by evaluating the influence of the laser radiation in a plane perpendicular to the z axis to estimate the width of the heat-affected zone also. With a heat source moving in the x direction, the temperature history in the (x, y) plane can be expressed by:

$$T(x, y) = T_\infty + \frac{\dot{q}' \rho c_p}{(4\pi V \alpha x)} \exp\left(-\frac{Vy^2}{4\alpha x}\right) \quad (5)$$

where $\dot{q}' = P / p$ is the *linear* density of the heat flux expressed in W/m . The depth of the heat-affected zone p is adjusted in order to provide the same value of the maximum temperature obtained with the equation (3).

3.2 The numerical solution of the 3D heat conduction equation

To simulate in a more complete way the heat transmission related to SLS, it is necessary to consider the three-dimensional heat conduction problem in a sufficiently large object, made of homogeneous material, with the moving heat source boundary conditions [8].

This problem is not easy to solve and the hypothesis of a small thermal influenced zone with respect to the working area cannot be removed.

An alternative method consists in applying to a finite sand bed volume the three-dimensional time-dependent conduction problem expressed in the classical form as:

$$(9) \quad \rho c_p \frac{\partial T}{\partial t} + \left(\frac{\partial q_x}{\partial x} \right) + \left(\frac{\partial q_y}{\partial y} \right) + \left(\frac{\partial q_z}{\partial z} \right) = \dot{q}_v$$

that is valid for isotropic, heterogeneous media, where $q_v(x, y, z, t)$ is the heat generated per unit of time and space, to be defined from the boundary conditions of the equation (2), and k , ρ and c_p depend on space and time, for their dependence on the temperature. In this case the radiation is considered as one-dimensional but the conduction within the sand is three-dimensional.

Obviously an analytical solution of the equation (6) with this hypothesis is not currently available but a solution based on numerical methods is possible, through the discretisation of the spatial - by means of cubic cells - and of the temporal domains. The solution is a function $T(x, y, z, t)$ and a finite domain is considered.

An attempt to solve the three-dimensional problem represented by the equation (6), transformed in the form of a transport equation for the static enthalpy, has been made in this work by means of a commercial computational code, FLUENT, with the SIMPLER algorithm [9]. With this particular code, the sand porosity can also be considered, by activating the porous media modelling option.

The program flexibility allows a complete schematisation of the thermal phenomenon, including the influence produced by the increase of temperature in the proximity of the radiation incidence point, and consequently it allows a correct definition of the heat-affected zone width, that cannot be considered directly in the one-dimensional model.

While the analytical solution of the equation (2) by means of the equations from (3) to (5) permits to investigate the influence of the laser power, the scan speed and the spot diameter, with the three-dimensional schematisation it is also possible to investigate the influence of the scan spacing. But the modelisation of the moving heat source, representing the laser beam and its transformation in a time-dependent volumetric heat source, is a very critical aspect, with the available options of the numerical code.

4. EXPERIMENTAL TESTS

An experimental investigation was performed to define the real mechanism causing the sand agglomeration, to calculate the sand thermo-physical properties and to determine the actual heat amount absorbed by the sand bed. The obtained data and those coming from previous experimental analysis [5] have been used to validate the described models.

The following analyses have been carried out:

- a) analysis on the SLS process through general tests;
- b) collection of the necessary parameters through the characterisation of the used sands;

- c) determination of the energy transmission coefficients.
- a) In order to test the models and their possibility to simulate the real layer thickness and the temperature values, the experimental facility described in [5] has been used. This analysis permitted to determine the influence of the most important process parameters, described in 2. on some aspects of the process, such as the width and the depth of the heat-affected zone and the temperature distribution. This last variable has been measured through an IR TV camera, whose error assessment is critical, especially at high scan speed.
- b) During tests, two different sands have been used, Zircon and DB40, as the three silica sands in Table I have similar thermo-physical properties. The following thermo-physical sand properties have been determined in laboratory tests: the specific heat, the thermal conductivity and the energy absorption during the heating process. The specific heat was measured by means of calorimetric Peltier analysis using a Calvet calorimeter. It is calculated by comparison with the specific heat of water, by comparing the heat transferred in a definite time to a metallic cell by the two substances, contained inside analogous cells, starting from the same initial temperature. The thermal conductivity k of the pre-coated sands, once that the specific heat c_p was determined, has been extrapolated from the same analysis, starting from the time necessary to cool the sand contained inside the metallic cell and from the knowledge of the reference substance, the water.

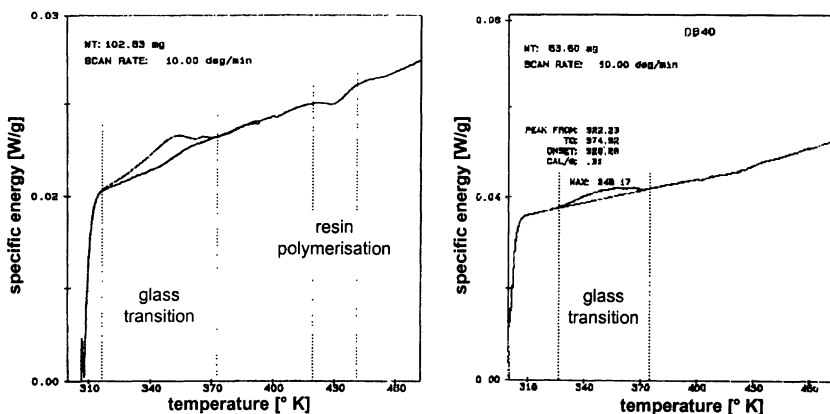


Figure 3. - DSC analysis - a. Zirconia - b. Silica DB40

To investigate in detail the nature of the agglomeration process, both the resin and the sand were exposed to Differential Scanning Calorimetric (DSC) analysis [10], that permitted also to evaluate the energy released during the heating process. In Figure 3.a. and b. the results of the two investigations relatively to zirconia and silica sand are shown. The analysis confirms the validity of one of the basic hypotheses of our modelisation, scarcely considered in the literature about foundry: the most important

transformation evidenced by the analysis takes place at a temperature of about 75-80° C (that can be assumed as the glass-transition temperature T_g) and it is lower than the polymerisation temperature of the phenolic resin, about 155° C. The DSC analysis evidences a small heat release, three or four orders of magnitude lower than the laser beam radiant energy, near the temperature corresponding to the glass-transition, characterised by a decreasing slope of the curves (Figure 3.).

Table II - Sand properties determined in laboratory tests

Sand	c_p [J/kg K]	k [W/m K]	$\alpha=k / (\rho c_p)$ [m ² /s]	T_g [° C]
Zircon	580.7	0.74	$4.53 \cdot 10^{-7}$	78
DB40	774.4	0.53	$4.27 \cdot 10^{-7}$	75

In Table II the main thermo-calorimetric results of the investigated sands are shown. In particular the values of the thermal conductivity k are similar to those provided by other researchers [6]. No reference values are available for the other thermo-physical properties.

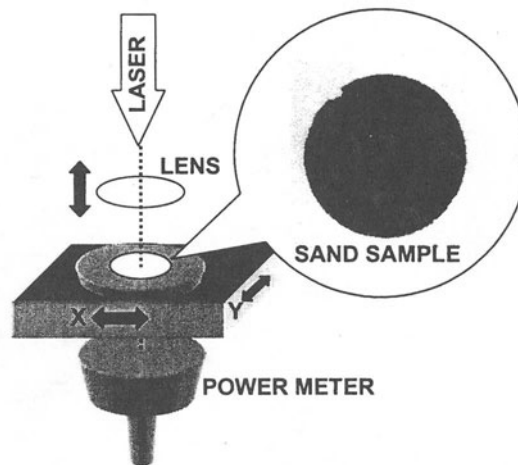


Figure 4. - Experimental configuration for the measurement of the energy transfer

- c) A specific analysis concerning the energy distribution within the sand, to obtain the terms a and τ of the equation (1), has been carried on too. A schematisation of the experimental analysis is shown in Figure 4. The values of the absorption and transmission coefficients, have been obtained with the following method:
- the nominal laser beam power is indicated on a power meter installed on the laser;
 - the effective laser beam power on the sand bed has been measured with a power gauge, based on the thermal balance between incising and dispersed heat;

- the transmitted energy has been measured with the same power gauge, after its positioning under sand layers of different thickness (detail of Figure 4.);
- the reflected energy r is lower than 1%.

The sand absorption coefficient a has been obtained with equation (1). Considering that only a small amount of the energy is reflected and not more than 2-4% is transmitted at higher depth than 0.2 mm, 95% of the radiant energy is adsorbed by the sand, as expected [6]. Finally, for the calculation:

$$a = 0.95-0.97 \quad \tau = 0.02-0.04 \quad r = 0.01$$

5. DISCUSSION OF RESULTS AND CONCLUSIONS

The mathematical models described in 3.1 and 3.2 have been assessed making use of the data provided by the experimental analyses: those provided in [5], concerning the maximum surface temperature $T(z = 0)$ and the depth of the heat-affected zone p , and by using the sand thermo-physical properties acquired in this work. The results, for some combinations of the input parameters, are shown in Tables III and IV for Zircon and DB40 respectively.

Table III - Comparison between experimental results and calculation for Zircon

Nominal Laser Power	1 Watt		3 Watt				5 Watt	
	T_{max} [°C]	p [mm]	T_{max} [°C]	p [mm]	T_{max} [°C]	p [mm]	T_{max} [°C]	p [mm]
Spot diameter [mm]	0.5		0.5	1.2		1.2		
Scan speed [mm/1']	490		1290	740		1180		
Experimental	140	0.6	174	0.5	157	0.4	160	0.6
Analytical	282	0.2	215	0.2	245	0.8	211	0.6
Numerical	370	0.3	350	0.3	207	0.4	277	0.4

Table IV - Comparison between experimental results and calculation for DB40

Nominal Laser Power	1 Watt		3 Watt				5 Watt	
	T_{max} [°C]	p [mm]	T_{max} [°C]	p [mm]	T_{max} [°C]	p [mm]	T_{max} [°C]	p [mm]
Spot diameter [mm]	0.5		0.5	1.2		1.2		
Scan speed [mm/1']	490		1290	740		1180		
Experimental	162	0.8	193	0.6	180	0.6	200	0.6
Analytical	195	0.6	153	0.2	172	0.8	148	0.6
Numerical	560	0.4	551	0.3	327	0.5	422	0.5

From Tables III and IV it can be observed that in most cases both the models tend to *overestimate* the sand bed temperature and to *underestimate* the agglomeration depth.

The experimental measurement of the sand layer depth p , made manually with a microscope, is critical (Figure 2.) and the results can be overestimated about one grain size (Table II). On the other hand, the maximum surface temperature T_{\max} can be underestimated with the used technique. This problem is dealt with in the literature [11].

The best results can be obtained for scan speed higher than 1000 mm/min, in particular for the analytical model. It is necessary to point out that the speed values of this order of magnitude are those interesting for industrial applications.

It is also possible to underline that better results have been obtained simulating the silica sand rather than the zirconia sand.

The three-dimensional numerical analysis provides good results for a laser spot diameter of 1.2 mm and generally overestimates the surface temperature. This effect is probably due to numerical convergence on the boundary cells caused by their small dimension in relation to the high specific input power.

The difference between experiments and simulation for both the heat-affected zone depth p and the temperature T_{\max} may be caused by an incorrect experimental estimation of the laser beam input power \dot{q} , as well as by some of the simplified basic model hypotheses, related to the following aspects:

1. The material has been considered isotropic and its thermal conductivity has been considered not depending on the direction, but the sand grain geometry could determine preferential directions for the heat conduction.
2. The sand thermo-physical properties, mainly the thermal conductivity and the specific heat, could vary according to the increase of temperature and to the resin agglomeration state.
3. Only the thermal diffusion has been considered to reach the glass-transition temperature and consequently for the grain agglomeration. Local phenomena related to chemical reactions could be important too.
4. Even if the energy released during the heating process (Figure 3.) is four orders of magnitude lower than the laser radiation one, it could be important for the process considering that it is a very localised energy. This phenomenon requires further investigations.
5. The mechanical agglomeration of grains is not included in the thermal modelisation.

The discrepancies between the experimental data and the theoretical calculation can be overcome with the following methods:

- a. by introducing corrective parameters determined with specific tests in the interesting range for production purposes;
- b. by changing some basic hypotheses, such as the homogeneous characteristics of the material.

In the last case, this could lead to a very complicated model, making it useless for practical applications.

An alternative approach could be based on an energy balance on a given sand volume between the incident energy and those necessary for the sand heating (calculated by DSC analysis). In this case it would not be necessary to consider the heat conduction problem, in the form of the equations (2) and (6), but the information about the temperature history would be lost.

It seems very probable that further improvements in the theoretical calculation will be possible in short time. However it should be emphasised that the main contribution of the methods provided in the present paper comes from the comprehension of the basic SLS phenomena and not for a strictly quantitative analysis.

ACKNOWLEDGEMENTS

The authors wish to thank Ing. Andrea Pelleriti for his help in the experimental phase, Prof. G. Conti and Prof. G. Levita and A. Marchetti of the Chemical Department and the Chemical Engineering Department respectively and the personnel of the Mechanical, Nuclear and Production Engineering Department of the University of Pisa. Financial support from MURST (60%) is acknowledged.

REFERENCES

- [1] Beaman, J.; Barlow, J.; Bourrel, D.; Crawford, R.; Marcus, H.; McAlea, K.: Solid Freeform Fabrication - A New Direction in Manufacturing, Kluwer Academic Publishers, 1997.
- [2] Nelson, J.C.; Vail, N.K.; Barlow, J.; Beaman, J.; Bourrel, D.; Marcus, H.: Selective Laser Sintering of Polymer Coated Silicon Carbide Powders, *Ind. Eng. Chem. Res.*, n. 34 (1995), 1641-1651.
- [3] Papadatos, A.L.; Ahzi, S.; Paul, F.W.: On Enhancing the Selective Laser Sintering Process: Part I: Simulating the Manufacturing Process, Clenson University Report (1995).
- [4] Papadatos, A.L.; Ahzi, S.; Deckard, C.R.; Paul, F.W.: On dimensional stabilities: modelling of the bonus-z during the SLS process, *SFF Symposium Proceedings*, Austin Texas (1997).
- [5] Santochi, M.; Tantussi, G.; Dini, G.: Laser Sintering of Pre-Coated Sands using Rapid Prototyping Techniques, 41. Internationales Wissenschaftliches Kolloquium, Band 1, Ilmenau Germany (1996), 387-392.
- [6] CIRP Co-operative Research Working Group on Laser Absorption, Paris, Private Communication (1996)
- [7] Bejan, A.: Heat Transfer, John Wiley and Sons Inc., New York, 1993, 151-154, 182-184.
- [8] Eckert, E.R.G.; Drake, R.M.: Analysis of Heat and Mass Transfer, Mc Graw Hill, New York, 1972, 237-238.
- [9] Patankar, S.: Numerical Heat Transfer and Fluid Flow, McGraw Hill, New York, 1980.
- [10] Show, T. L.; Carrol, J. C.: Application of Baseline Correction to the «Ratio Method» of DSC Specific Heat Determination, 13th Symposium on Thermo-physical Properties, Boulder Colorado (1997).
- [11] Ueda, T.; Yamada, K.; Nakayama, K.: Temperature of Work Materials Irradiated with CO₂ laser, *Annals of the CIRP*, Vol. 46 (1997) n. 1, 117-122.

**REVERSE ENGINEERING
FROM COMPUTER TOMOGRAPHY TO RAPID PROTOTYPING**

**G. Marinsek and S. Paolasini
Centro Ricerche FIAT, Orbassano (TO), Italy**

KEYWORDS: Reverse Engineering, Computer tomography, Rapid prototyping

ABSTRACT: The need to speed to market is pushing the engineering design threshold to new levels. Three dimensional digitizing is a common industrial method for capturing complex surface geometry. The most widely used methods are non-contact and contact systems. Each technology comes with its own set of strengths and limitations. The common challenge is to convert the geometrical data into a format acceptable to the CAD software. CT technology proves to be one of the most effective method to reach this target, especially when the shape of the component is very complex or internal features are to be detected. More the CT scanning strategy helps to obtain in a straight-forward way STL files for Rapid Prototyping. Industrial case studies are discussed.

1. INTRODUCTION

In the mechanical industry, designers, engineers and manufacturing people work in a simultaneous engineering environment where the output of one group affects the input of the next group. In such an environment, the total lead time can be drastically reduced by speeding up processes that have the highest impact on lead time.

The product development cycle is nowadays a CAD driven process. It can be split roughly in some main phases, where the CAD model is always the key point.

1. **Concept:** the design process starts by bringing conceptual models into a CAD environment.
2. **Engineering:** the product model undergoes the CAE simulations for the performance evaluation. Parts with no CAD description need to be converted to a digital model for engineering analysis. On the contrary the output of many CAE programs need to be transformed into CAD models.
3. **Tooling:** during the creation of tooling, inaccuracies arise due to misinterpretation of the design intent. The problem here is to verify the accuracy of the tool to the original CAD model and, if necessary, instantly update the CAD model to reflect the inaccuracy.

During prototype build and the approval processes for production parts, there are challenges for time compression, specifically in the areas of:

- Reverse engineering
- Computer-aided verification
- Rapid prototyping

The more complex is the component, the more advantageous the utilization of the above mentioned techniques and the more efficient the time compression.

When the geometry of the part is very complex and internal cavities are present the only digitizing technique available is Computed Tomography.

Developed mainly for medical diagnosis, it was industrially used in the past only for very special projects, like aerospace, when safety reasons were of major importance. Nowadays the dramatic improvement of electronics and the large diffusion of three dimensional CAD models even in the small – medium enterprises alter the conventional methodologies and change the economics. Therefore routes which only few years ago have been considered very expensive, nowadays can be the most convenient solution in terms of cost.

2. WHAT IS REVERSE ENGINEERING?

Since long before the advent of CAD systems, working drawings have been derived from physical models. Not surprisingly, the most common approach today for addressing the need to develop a CAD model from an object is to manually measure pertinent dimensions with calipers, micrometers, rules and any other instrument necessary. Manual methods can work nicely for objects with minimal features, but as the complexity of the part's geometry increases the effort needed to accomplish the task can become prohibitive.

Three-dimensional digitizers of all types are utilized to extract coordinate data from solid objects and drive reverse engineering strategies. The traditional approaches begin by collecting a complete set of (x,y,z) locations that represent the shape of the object. Once collected, these point sets are sent in mass to a CAD system as point data, or, filtered and

manipulated by software products that specialize in preprocessing point data being passed off to the CAD system. The term "point cloud" is used to describe point sets with a high magnitude of points; a high-resolution laser-scanning device will create point clouds with millions of data points. Getting the desired results from the data is a task that can require a tremendous amount of manpower and access to specialized equipment and software. While point clouds are readily meshed with polygons, the development of modifiable CAD models has proven to be more harsh. However a certain number of commercial software are available and integrate 3D digitizers and coordinate measuring machines with CAD.

3. WHAT IS CT IN SIMPLE TERMS?

Most people are acquainted with conventional film radiography. Its applications span a range from medical X-rays to nondestructive testing (e.g., detecting the presence of internal cracks and porosity). A disadvantage of conventional film radiography is that a three-dimensional object is compressed into a two-dimensional image. This can result in critical features being superposed and obscuring one another. Computed tomography employs a finely collimated X-ray beam, a detector package (rather than film), and computer algorithms to inspect planes within the object. CT images correspond to faithful reconstruction of cross-sectional profiles. Internal features are not superposed; valuable information on material properties and dimensional characteristics of the object are preserved. The value of CT in the medical community has been well documented. Medical computed axial tomography (CAT) scans can provide physicians with valuable information such as the presence, location, size and growth patterns of tumours and abnormalities within the body. This information can be used to judge the severity of the problem, aid in removal through surgery and detect the onset of a problem at an earlier stage than might have been possible otherwise. Outside the medical community, CT has been very successful as an NDT modality, such as for the inspection of rocket motors and turbine blades.

By recording the shadow-graphs of an object from many different angles it is possible to mathematically extract the density of each point in a plane of the object. This 2-D density map constitutes a CT slice and gives very accurate positioning information within the plane. The position of the slice is also accurately known due to the accuracy of the positioning mechanism. By creating several slices, a true 3-D volumetric image of the object can be built up. The 3-D volume data can be "sliced and diced" to provide any cutaway view of the object so that both density and position can be analysed.

4. METHODOLOGY TO CREATE A STL AND A CAD MODEL FROM CT DATA

In the following a door reflector case study is discussed (Fig. 1). This part was chosen because of the high complexity of the prismatic surface, which is almost impossible to be detected with CMM methods.

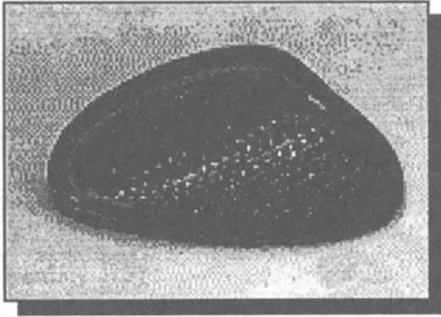


Fig.1 Door reflector

The work done to obtain the CAD model of the part can be split into the following phases:

1. detection of geometrical feature of the component via several CT tomograms along the z axis,
2. generation of the IGES contour data file for each tomogram (software: MIMICS Materialise Belgium),
3. generation of point cloud
4. implementation of the STL file
5. splitting of component in different regions,
6. surface creation of the part without the prismatic part. The creation of surfaces on the prismatic part is a task theoretically possible, but certainly tedious and time consuming,
7. hybrid model generation.

Steps from 3 to 7 were performed with Metris, Belgium software.

Step 1 was accomplished using the industrial CT scanner installed at FIAT Research Centre, supplied by Scientific Measurement Systems, Inc. (Austin, Texas). Its technical specification are as below:

- the *X-ray source* Philips MCN 451 X-ray tube, with 450 kV maximum voltage, 10 mA maximum current and dual beam spot size (1.0 and 4.5 mm);
- the *radiation detector subsystem*, consisting of a linear array detector (63 CdWO₄ scintillators);
- the *object positioning unit* (4 degrees of freedom), which mechanically handles the inspected component, once it is placed on the rotary table; allowing for the inspection of objects with 100 kg maximum weight, 880 mm maximum height and 720 mm maximum diameter.
- the *computer subsystem*, which controls the acquisition, processing and analysis of the experimental information collected; it is comprised of a Pentium personal computer, for data acquisition, and a Sun-Ultra workstation, for computation-intensive reconstruction.

The door reflector was scanned only partially because the ultimate objective is to understand the feasibility of the methodology. Tomograms are taken each 0.5mm and a X ray beam thickness of 0.2mm was chosen. Some of the 80 tomogram are shown in Fig.2.



Fig. 2 – Three of the 80 tomograms included in the whole stack of CT acquisitions on the door reflector.

The Fig. 3, 4, 5, 6 and 7 describe the following steps of the procedure and namely Fig.3 the creation of the point cloud, Fig. 4 the STL file generation, Fig. 5 the manipulation of the point cloud, fig. 6 the reconstruction of surfaces on the point cloud and finally (Fig.7) the final hybrid model realisation.

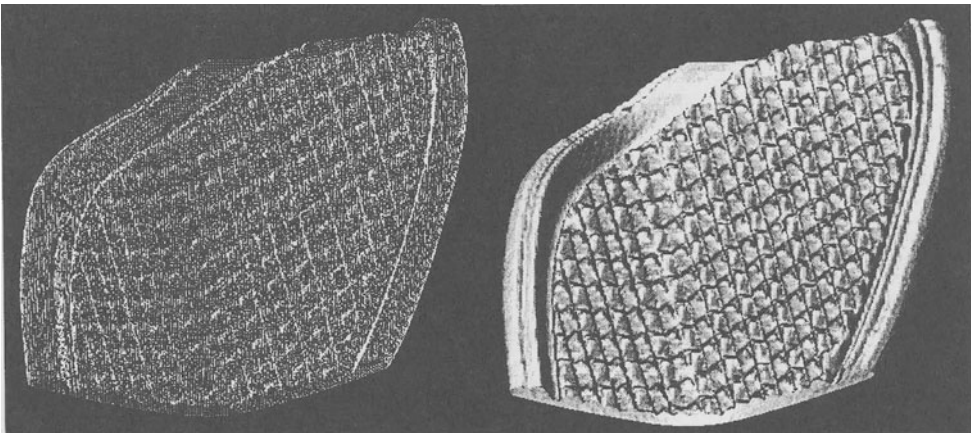


Fig.3 - Creation of the point cloud

Fig. 4 - STL file generation

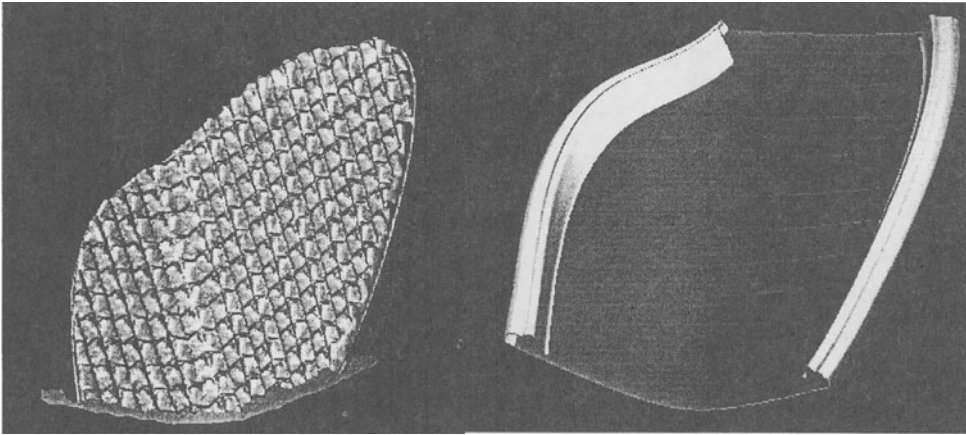


Fig. 5 - Manipulation of the point cloud

Fig. 6 - Reconstruction of surfaces on the point cloud

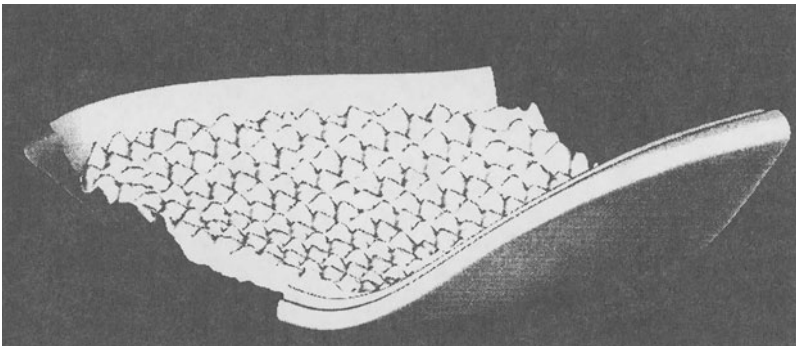


Fig. 7 – Door reflector hybrid model (surfaces for the body and STL for the prismatic outer part)

The scanning time for each tomogram is 3 minutes. However the acquisition procedure is fully automated and can be performed unmanned. As a matter of fact there are no disturbing factors during the scanning that may cause a faulty survey.

The tomogram appears as an image, a matrix of pixels whose grey shades correspond to different levels of material density. To obtain the cross section shape a contouring operation is done setting the right grey shade as threshold value. From the several contours the point cloud is generated and finally the STL file (point cloud meshed with triangles). This two operations can be done in a very marginal amount of time (few minutes), providing a good tomograms quality.

The accuracy of the point cloud is one of the major item. Up to now the out of tolerance error for a small part (within 100mm x 100mm) as the door reflector is around 0.05 mm. However the setting of scanning parameters, the CT system characteristics, the choice of the gray scale threshold may influence the quality of the reconstruction.

5. FROM CT TO RAPID PROTOTYPING

Once the STL file is available, the transfer of the data to any Rapid Prototyping system can be done. In Fig. 8 a prototype of the door reflector, made by the SLS (Selective Laser Sintering) Rapid Prototyping technique, is shown.



Fig. 8 – Door reflector (partial sector) prototype made with the STL file obtained from the CT stack of tomograms

Other examples are a turbine blade, where the internal hole is present, and a sector of an aluminum engine block, whose STL files are shown respectively in Fig. 9 and Fig.10.

6. CONCLUSIONS

Computed Tomography is a well-known NDT method. Its very peculiar characteristics proved to be unique in many industrial applications, where the safety issues of the components are of high concern. However the CT output capability to integrate itself with the electronic data handling opens new alternatives for reverse engineering, computed aided verification and rapid prototyping. Other measurements methods are available and for some aspects (especially cost and speed) they can be for a large part of applications a better choice. However when complexity and internal features are of concern CT can be the only possible solution. It is especially for such cases where the higher benefits in time to market compression can be achieved.

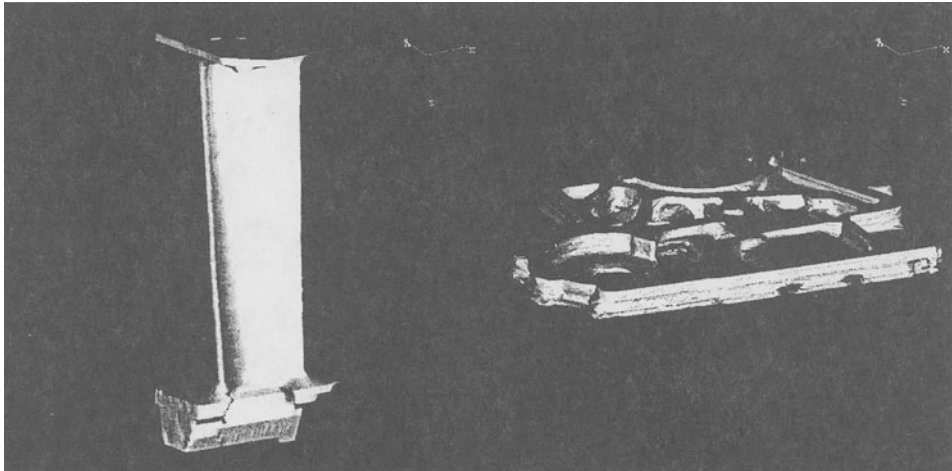


Fig. 9 – STL file of a turbine blade obtained with CT scanning

Fig. 10 – STL file of a slice of an aluminum engine block obtained with CT scanning. The accuracy of the measurement is within 0.2 mm, typical out of tolerance error of sand casting foundry process.

The industrial case studies presented demonstrate the feasibility of CT methodology for reverse engineering linked to rapid prototyping techniques. This is the very beginning of the story: new software for point cloud treatment and better accuracy achievement has to be developed and new detectors may enter the market for a higher quality of tomograms and a reduced scanning time.

7. ACKNOWLEDGMENTS

Part of the results described in this article are obtained in the Project BE-2051 “Process Chains for Rapid Technical Prototypes (RAPTEC)” funded by the European Community under the Brite EuRam Programme.

APPLICATION OF RAPID TOOLING FOR SHEET METAL FORMING

A. Gatto

University of Ancona, Ancona, Italy

KEY WORDS: Rapid Tooling, Sheet Metal Forming

ABSTRACT: The Rapid Prototyping (RP) process is evolving beyond just making three dimensional models and it is beginning to have an impact on tool construction. The Rapid Tooling (RT) process can be considered as a logical development of the Rapid Prototyping process chain but technologies must be successfully integrated into production structure. In this paper the use of a drawing punch built by rapid tooling techniques is evaluated and a drawing die was used to test the punch performances.

1. INTRODUCTION

Technologies by themselves have very little meaning unless they are successfully integrated into a corporate structure: for example, computer software incompatibility causes difficulties in easily integrating Rapid Prototyping technologies into production structure [1-3]. The sheet metal forming and hood industries of the Marche (a region in central Italy with about 1.500.000 inhabitants) have a turnover of 485.000.000 \$ and 2200 employees (1996 data) [4] but only 29% of these industries have over 30 employees. The sheet metal forming and hood industries are reluctant to implement the rapid tooling process until the costs and time effectiveness have been proved; resulting cost cuts over conventional methods can be significant but justifying the necessary equipment can be difficult: the benefits of RP are not always easy to quantify; the financial staff may not understand the need for a new technology that can radically change the way a company produces prototypes [5, 6]. This research was carried out in collaboration with two of

these industries. Usually, a chassis hood component is produced in three steps: drawing; trimming; bending. The combination of prototype drawing dies and laser cutting instead of trimming can answer many questions regarding the development of hood components. At the present the prototype tools or prototype dies for sheet metal forming are built by combining the flexible drawing with tool manufactured using several techniques. In this research, to evaluate the performance of the drawing punch built by RT techniques, a steel blank holder and a steel drawing die instead of a flexible one were used. A hood cap (Fig. 1) was selected as a benchmark to evaluate: the rapid tooling technologies chosen to build snapping tools and drawing dies for small batch or sampling production; drawing dies performances using different materials and thickness; cost and time effectiveness.

2. TOOL MANUFACTURING AND TOOL EVALUATION

EUREKA 8.1 software was used to load the IGES format files of the finished product, blankholder, drawing punch and of the drawing die: the files were generated by a surface modeller (TEBIS).

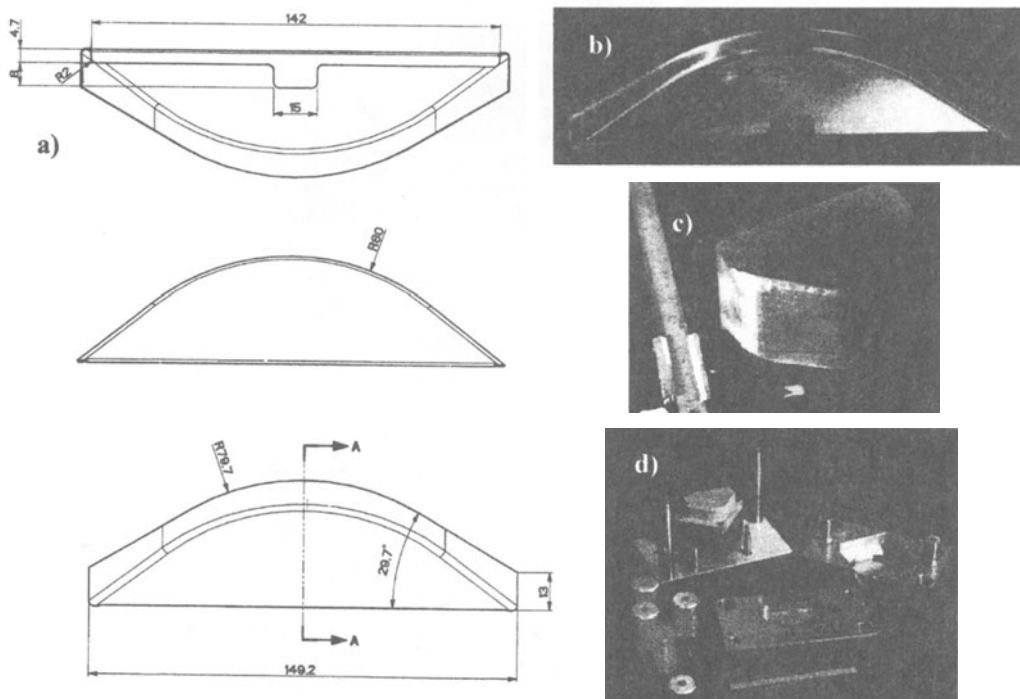


Fig. 1 – a), b) The hood cap selected as benchmark; c) punch model built by stereolithography technique; d) the disassembled modular die.

Information degradation was observed when the files were loaded: no-joined adjacent surfaces; irregular isoparametric curves. The surface to solid conversion was carried out, but despite the repair and surface enclose work, some gaps and overlap problems remained

in the solid model. MAGICS RP (Materialise software) was used to repair the STL file of the object using different faceting tolerance and trial and error methods.

Currently the question for industry is not how to obtain the RP part, but rather how to use the RP to reduce product lead time and investment costs [7]. The application of a sequence of process steps combining conventional manufacturing technologies, composite materials and RP techniques can answer this purpose. At the present the flexible drawing die is used combined with the tool manufactured by the following technologies:

- castable epoxy resins and polyurethane systems [7-9];
- mechanical and abrasive resistant epoxy resins and polyurethane based slab also with filler [10];
- low melting alloy (metal spray or casting) [7, 10-12];
- hard concrete [7];
- high performance cement-based composites [7];
- laminated tooling: horizontal contoured sheet metal stacked and bonded or an array of die laminates each oriented in a vertical plane and clamped together by some means [13];
- discrete tooling which consists of a clamped matrix of equal length pins but with a discrete discontinuous forming surface [13].

The punch model was built by stereolithography SLA 500, 3D Systems, using an epoxy resin and a layer thickness of 0.15 mm. After removal of the supporting structures and post curing, the part was lightly sandblasted and then positioned in a box. A casting polyurethane resin was used to obtain the negative of the SLA part. The RP part and the negative casting were easily drawn without damage. Because of the low polyurethane resin viscosity the zone between the punch and the box is completely filled, the polymerisation (30 minutes) is a slightly exothermic reaction, but no effects due to the temperature were observed on the RP part and it can be reused. A marketing research and a literature data one were carried out to choose the suitable resin for the punch; a quick hardening, cold curing three components resin based on modified polyester was chosen. It air cures in 10 minutes and it has high dimensional stability: about 0.2 % shrinkage after polymerisation. In order to decrease shrinkage, the resin was filled with metallic materials as shown in Table 1: the filler must be thoroughly stirred to ensure homogeneous distribution.

Tab. 1 – Weight and volume composition (%) of the resin with filler.

Specimen	a)		b)		c)		d)	
	Weight	volume	Weight	volume	Weight	volume	Weight	volume
Resin	40	79	40	76	40	78	40	78
Cu powder, 99% ϕ 7–45 μ m	60	21	-	-	40	14	40	14
ASM 1070 steel sphere, ϕ = 3 mm	-	-	-	-	-	-	20	8
ASM 1070, irregular material, length < 2mm	-	-	60	23	20	8	-	-

A simple model of deformation behaviour derived by considering a unit cell was used to evaluate the possibility to predict trends in a composite elastic modulus [15, 16]. The model idealises the microstructure of a two phase material as a periodic arrangement of

cubic inclusions in the second phase. The approach basically involves dividing the unit cell first into parallel and series elements and deducing the composite behaviour from the behaviour of the elements. The elastic modulus of the composite was deduced from the following equation:

$$E_c = \frac{(c \cdot E_p \cdot E_m + E_m^2) \cdot (1+c)^2 - E_m^2 + E_p \cdot E_m}{(c \cdot E_p + E_m) \cdot (1+c)^2} \quad c = \left[\frac{1}{V_p} \right]^{\frac{1}{3}} - 1$$

E_p = elastic modulus of the particle; E_m = elastic modulus of the matrix; V_p = volume fraction.

This model was chosen due to the large differences in the two phase modulus and because microstructural details such as dimensional continuity of phases cannot be considered in predictions [14, 15]. The Young modulus values predicted and measured are reported in Table 2. Cylindrical specimens ($\phi=36$ mm, $h=42$ mm) of the filled resin were compression tested using a 810 MTS test machine (maximum load 250 kN) and a shifting rate of 0.2 mm/s. The trend of predicted elastic modulus is confirmed by experimental data: elastic modulus of the resin reinforced with 60% weight irregular ASM 1070 particle is greater than that reinforced with 60% weight Cu powder and both of them are greater than the elastic modulus of the resin reinforced with 40% Cu powder and 20% steel. It must be taken into account that the powder is uniformly distributed while the steel filler tends to precipitate towards the working surface during casting, but there is no contact between the spheres or the particles due to the resin wettability. The part where the steel filler is present has a higher E value than the one with only Cu powder: the elastic modulus measured depends on this fact. However, the model allows to predict the effect of the filler on the performance trends of the composite materials and this leads to the material design. The resin filled with 40% Cu powder and 20% weight of ASM 1070 sphere was chosen to produce the punch, considering tensile strength and elastic modulus; the use of this filler decreases the resin shrinkage and the tool cost by about 10%.

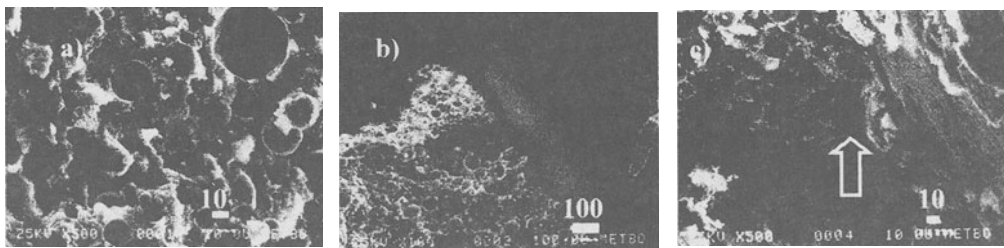


Fig. 2 –Fracture surface of the specimen filled with: a) Cu powder; b) 40% Cu powder, 20% ASM 1070, $\phi = 3$ mm sphere; c) 40% Cu powder, 20% irregular ASM 1070 filler.

The fracture surfaces of the compression test specimen were observed by SEM; in Fig. 2 a) the surface fracture of the specimen filled with Cu powder is shown; no interfacial effects between the filler and the resin and no cracks in the matrix are observed: this is

probably due to crack deflection at the interface matrix-particle. For a weak interfacial bond, a crack in the matrix can lead to debonding at the interface, followed by crack deflection: this energy-absorbing phenomenon leads to enhanced fracture toughness and non catastrophic failure mode. The interface should be strong enough for axial load transfer and strength in the transverse direction, yet weak enough to make a transverse crack deflection along the interface thus providing toughness [17]. The same mechanism was observed on the surface of the specimen filled with Cu powder and ASM 1070 sphere (Fig. 2 b), on the contrary the presence of the irregular ASM 1070 filler causes a different failure mechanism: cracks are visible in the matrix and they start from the corner due to the concentrated stress (Fig. 2 c).

3. DIE MANUFACTURING AND DRAWING TEST

The path chosen consents to build drawing punch within 1-1.5 hours from the RP model; the tool obtained may be machined, drilled and threaded were the steel spheres are obviously absent. The tool was assembled in the modular die after machining (about 1 hour) as shown in Fig. 1 d).

Tab. 2 - E values predicted and measured

Weight %	resin 100%	resin 40% Cu powder 60%	resin 40% ASM 1070 irregular material 60%	resin 40% Cu powder 40% ASM 1070 irregular material 20%	resin 40% Cu powder 40% ASM 1070 sphere 20%
E measured (GPa)	2.70	2.64	3.60	1.70	2.50
E predicted (GPa)	-	3.99	4.23	2.97 ^{a)}	

a) Hypothesis of uniform steel filler distribution.

The die contains all the necessary tool elements (plates, strippers, springs, guiding sets, pins,..) except the special forming elements (punch, blank holder and die holes), but if a flexible drawing die is used only the drawing punch has to be produced. The time required to produce the die from the CAD was about 10 hours (Fig. 3) with 2 hours of unmanned work; using a flexible drawing die there will be about 6 hours of unmanned work but the time required for the die will be the same.

Using RT technique, the time is about 20% and the costs 30% lower than those required using machine-tool (in this case the full work is a manned one). It must be borne in mind that producing a more complex punch with the same height requires the same time as the chosen rapid tooling technique while the time and costs will increase considerably using the machine-tool.

The time required to build the modified punch allows the closed-loop process control concepts to converge upon the appropriate tooling design [13]. In Table 3 the materials used in the drawing test are reported. In Fig. 4 some punched metal sheets are shown: the punched parts surfaces quality is high. Some problems appeared during the deformation of specimen n. 6; they were due to the excessive force used that caused breaking of the sheet

metal with consequent scratching and local punch tear. From specimen n. 7 the spheres marks are visible on the left side impression (Fig. 4), but this local damage allows to punch the metal sheet without leaving marks on the external surface of the part. Using this modular die, an accurate control system of the punching force is required.

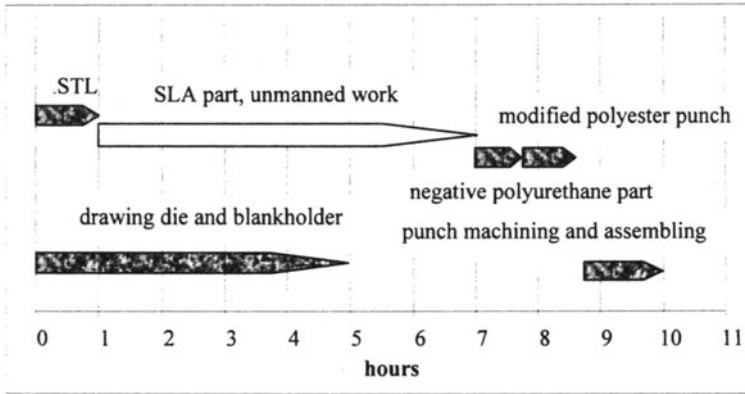


Fig. 3 - Time required to produce the die from CAD model.

Table 3 – Metal sheet used in the drawing test.

Specimen n.	Material	Thickness mm	yield strength MPa	tensile strength MPa	elongation %
1, 2, 3	AISI 304	0.6	195	540-685	45
4	1050 Al	0.6	70	90	11
5	AISI 304	0.7	195	540-685	45
6, 7	AISI 1008	0.5	210	270-350	38
8, 9	AISI 1012	1.0	280	280-410	28
10	AISI 1008	1.2	210	270-350	38
11	AISI 430	0.8	255	440-590	22
12	AISI 1008	2.0	210	270-350	38

1, 2, 3, 4, 5,11 film surface protection, thickness =80 µm; 6, 7, 10, 12 Ra=0.6–1.9 µm; 8, 9 galvanised, thickness=2.5 µm.

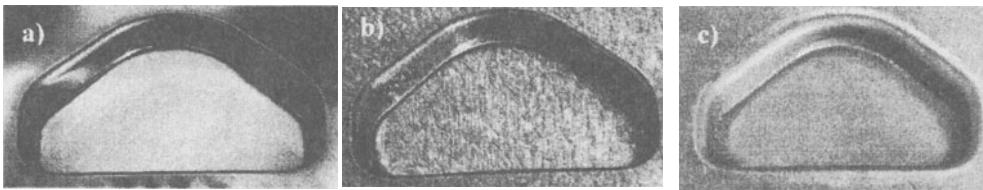


Fig. 4 – a) n. 1, AISI 304, s = 0.6 mm; b) n. 8 AISI 1012, galvanised, s = 1.0 mm; c) n.12, AISI 1008, s = 2.0 mm.

4. CONCLUSIONS

A die for sheet metal was built using a punch produced by the rapid tooling technique to evaluate costs and time effectiveness. The main conclusions of the process are summarised as follows:

- a modified polyester resin filled with metallic materials allows to build a punch for sheet metal forming;
- a simple model of deformation behaviour derived by considering a unit cell allows to predict the trends in composite elastic modulus and the correct filler choice;
- the rapid tooling technique chosen allows to reduce the production die time of 20% and costs of 30%;
- using the described rapid tooling punch it is possible to obtain punched parts with high surface quality.

The next step of the work foresees the use of a flexible drawing die and different polyester resin fillers.

ACKNOWLEDGEMENT

The author would like to express his appreciation to Merloni Elettrodomestici SpA, Fabriano (AN) Italy and Meccanotecnica Centro SpA, Fabriano (AN) Italy, for economic and technical support, and his thanks to Prof. R. Ippolito and Prof L. Felloni for help and encouragement.

REFERENCES

1. F. Breiting: Rapid Tooling for Simultaneous Product and Process Development, *Rapid News*, 5, (1997) 4, 44-50
2. P.R. Sferro: Integrating The Time Compression Technologies Into Existing Management Infrastructure, *Rapid News*, 5 (1997) 7, 16-20.
3. R. Thom: The Top 10 Mistakes With Time Compression Technology: A Practical Guide, *Rapid News*, 5 (1997) 7, 22-27.
4. Industry Yearbook of Ancona, Macerata, Pesaro, Ascoli Piceno District, 1996.
5. T. Sorovetz: Justifying Rapid Prototyping”, *Manufact. Engineering*, 115 (1995), 25-29.
6. Ø. Bjørke, “Layer Manufacturing” Tapir Publishers, 1992.

-
7. H. Muller, U. Berger, K.D. Thoben, D. Steinhauser: Successful Application of Rapid Prototyping Technologies for Advanced Sheet Metal Forming and Investment Casting, Int. Conference on Rapid Product Development, 1994, Stuttgart, Germany.
 8. Ciba Geigy Corporation Technical brochure.
 9. <http://www.urethanetooling.com>
 10. SIKE Chemie GmbH Technical brochure.
 11. MCP Systems, HEK-GmbH technical brochure.
 12. T. Nakagawa: Recent Manufacturing Technologies for Auto Body Panel Forming Tools, J. Mat. Processing Technology, 46, 1994, 277-290.
 13. D.F. Walczyk, D.E. Hardt: A New Rapid Tooling Method for Sheet Metal Forming Dies, 5th International Conference Rapid Prototyping, 1994, Dayton, 275-289.
 14. K.S. Ravichandron: Simple models of deformation behaviour of two-phase composites", High Performance Composites, TMS publication, 1994.
 15. J. Aboudi: Mechanics of Composite Materials, Elsevier Science Publishers, 1991.
 16. H.H. Liu, B. Nauman: On The Micromechanics Of Composites Containing Spherical inclusions", J. Materials Science, 25, 1990, 2071-2076.
 17. K. K. Chawla: Ceramic Matrix Composites, Chapman & Hall, London 1993.

EXPERIENCES IN RAPID PROTOTYPING: VOICE DEVICES FOR PATIENTS WHO HAVE UNDERGONE TOTAL LARYNGECTOMY

C. Miani, A.M. Bergamin
University of Udine, Italy
A. Staffieri
University of Padua, Italy
S. Filippi, F. Miani, M. Zanzero
University of Udine, Italy

KEYWORDS: Rapid Prototyping, Surgical Devices, Concurrent Engineering

ABSTRACT: A preliminary report of a cooperation research experience between a medical research Group and a mechanical engineering Group is reported in designing and developing a prosthesis for patients who have undergone a total laryngectomy surgical operation. The main problem experienced by these patients is the complete absence of voice after the operation, which can be partially restored with the use of one-way valves inserted between the airways and the digestive tract. Up until now, some problems still exist with the use of this valves or voice prosthesis. Two different phases of the project work are presented, consisting of a design stage with a subsequent step in which rapid prototyping is exploited. The advantages of the present approach are discussed, together with an outline of the ongoing work on these research activities.

1. INTRODUCTION

There are two main ways to treat advanced laryngeal cancer: radiotherapy and surgery, namely total laryngectomy. Due to the surgical treatment, the patient is always left with a tracheostoma (plain-diameter tracheal opening at the base of the neck) and loses one of the main laryngeal functions, which is phonation. Voice rehabilitation may be performed in different ways: by using electrolarynx, by esophageal voice, and by surgical/prosthetic voice restoration using artificial voice prostheses or valves. Unfortunately several problems can be encountered in the general use of these kinds of prostheses, mainly coming from their shapes, materials, costs, and so on.

The aim of this paper is to clarify how is possible to ascertain the feasibility of rapid prototyping (RP) for testing and developing of new prosthetic voice devices. We carried out a case study concerning (1) the generation of the solid model of an existing prostheses; (2) the building up of the corresponding RP model; (3) some kinds of evaluation of the prototype; and (4) the process reiteration, taking feedback into the right account.

The paper will start with a section concerning the medical context; a brief dissertation about RP and geometric/solid modeling issues will follow. After that the study will be described and finally a discussion about some context-related topics (Concurrent Engineering, parametric CAD, knowledge fruition/exchange, RP technology) will be presented.

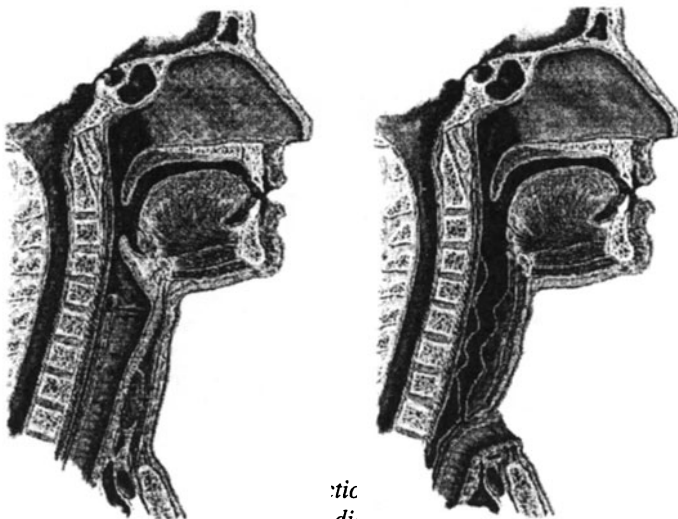
2. MEDICAL ISSUES

2.1. Statistics

Laryngeal cancer involves 8 people out of every 100,000 of the European Union population per year with a crude 10-year survival rate of 50%. Independent of survival rate, all surgically treated patients affected by laryngeal cancer undergo a rehabilitation procedure. Post laryngectomy rehabilitation and controls for recurrent disease will continue for years. This means that after a period of 10 years approximately 150,000-200,000 of the European Union inhabitants will require periodical follow up for restoration. Full rehabilitation enables the patient to resume a satisfactory social and economic life.

2.2. Surgical activities

Total laryngectomy is a very mutilating procedure. This technique is used for recurrence after radiotherapy failures and in very advanced stages of laryngeal cancer. The larynx is completely removed, and airways and esophagus are completely separated one from the other. Patients who have undergone total laryngectomy have lost an organ that simultaneously protects the lower respiratory tract against aspiration of fluid and ensures phonation. Any solution to resolve the problem of aspiration lies in surgery. Indeed the respiratory tract is separated from the digestive tract by surgically opening the tracheal stump at the jugular level (tracheostoma) (figure 1).



Figur
lar.

:tic
di

n with
total

laryngectomy (larynx removed).

2.3. Voice rehabilitation

As said in the introduction, voice rehabilitation may be performed by electrolarynx, esophageal voice, or surgical/prosthetic voice restoration.

The use of the electrolarynx [1], an external vibrator to be applied on the sub-mandibular region, has been practically abandoned, for the extremely poor quality of the voice produced with this method, but it is still used by 15-20% of the patients in the U.S. [2][3]. The use of the esophageal voice, which is something similar to air regurgitation from stomach, allows to produce an intelligible voice in only 50-60% of the patients [1], whereas the surgical or prosthetic voice rehabilitation can reach more than 90% of success [4][5]. Since their introduction in the 70's, tracheo-esophageal voice surgical shunts have gained increasing acceptance in substitution of esophageal voice. By the way, for the poor reproducibility of the surgical approach between different surgical equipes, surgical voice restoration has been progressively substituted by prosthetic voice restoration using artificial voice prostheses or valves [6][7][8].

All these devices work in a similar manner guaranteeing air flow between the trachea and the esophagus while, at the same time, preventing any back flow of liquid or food into the trachea from the esophagus. They all have 4 common elements: 1) an entrance to the trachea which retains the valve to the trachea (tracheal flange); 2) a cylindrical duct, the length and external diameter of which depends on the model (ranging between 2-15 mm and 5-8 mm, respectively), which serves to pass through the tracheo-esophageal shunt (soft tissues space between the trachea and the esophagus); 3) an outlet from the esophagus which is attached to a system for retaining the valve to the esophagus (esophageal flange); and 4) a valve system allowing air to flow between the trachea and esophagus when there is a positive difference in pressure between them and preventing the backflow of liquid (aspiration) when there is a negative pressure differential. This valve system may be located in different sites of the cylindrical duct, depending on the prosthesis type.

During rapid expiration, an increase in pressure is achieved inside the trachea either by closing the tracheostoma with one's finger or by a tracheostomal valve able to close when the expiratory air flow exceeds a certain flow rate. Once the air flow has passed through the voice prosthesis and into the hypopharyngeal-esophageal segment, it flows upward. On its way it passes through an appropriate, muscle membrane-like area called neoglottis, which is prone to vibrate, thus replacing the vocal cords that were removed during surgery [9][10].

2.4. Device related problems

Some problems can be encountered in the general use of voice prostheses [11]. The first one is short device lifetime (4-6 months, some cases less than 20 days) due to partial/total valve blockage (because of biofouling and/or granulation tissue), valve leakage (because of biofouling inside the connecting duct where valve is placed), or valve migration inside esophagus (because of too short valve).

The second one is perivalvular leakage. This is due to progressive enlargement of tracheo-esophageal shunt because of too large diameter of the connecting duct, or too long connecting duct, or poor esophageal flange protection.

The third problem is high airflow resistance during phonation. The factors responsible for this are: valve biofouling (see above); contact between valve and esophageal walls; high resistance of neoglottis (scare or hypertonicity).

The fourth is related to discomfort during valve substitution because of the length of the procedure and/or difficulties in passing valve through tracheo-esophageal shunt.

Finally there are the relatively high cost and the low technological development and testing of

these devices.

2.5. The "Staffieri Pull-out Prosthesis"

"Staffieri Pull-out Prosthesis" [8] has achieved excellent clinical results. This is a permanent or indwelling valve (figure 2) made of molded, medical-grade silicone composed of: a 10 mm diameter tracheal retaining flange; a 4 mm diameter, hollow, cylindrical duct connecting the trachea and esophagus disposable in three different lengths of 5, 7 and 9 mm.; a 22 mm diameter esophageal retaining flange; a dome closing the esophageal area. Approximately half of the circumference (180°) of this part must be incised by the surgeon during fitting.

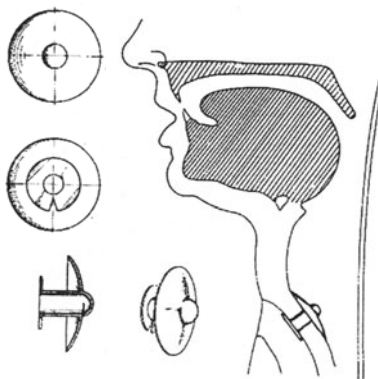


Figure 2. Left: drawing of a Staffieri's prosthesis and its section, together with a scheme of the anatomical site where the valve is placed (right).

The main problems encountered with the use of Staffieri's prosthesis are: unpredictable aerodynamic behavior (due to the hand-made cut for opening the valve); relatively high resistance (due to too small (180°) valve opening); valve leakage (due to 180° device rotation so that the opening becomes directed upward and/or to biofouling); discomfort during valve substitution for the length of the procedure with the risk of valve crash because of extremely thin material, or difficulties in passing valve through tracheo-esophageal shunt, because of backward re-fold of tracheal flange during extraction.

Taking into account problems directly related to Staffieri's valves and those ones of general issues, we tested the possibility of utilizing rapid prototyping for developing a new prosthesis from the old Staffieri's device, as a starting point of a program which is intended to (1) modify the old prosthesis in successive steps with the aid of 3D modeling CAD package; (2) obtain rapid prototypes of 2-4 models chosen; (3) test the mechanical behavior; (4) choose the best material and production process; (5) test medical-use behavior on patients and finally (6) use the new device surgically. So far, only the first two steps have been performed. There description will follow.

3. RAPID PROTOTYPING (RP) ISSUES

3.1. RP approaches and technologies

This is a brief taxonomy about the four main RP technologies actually available on the market. Up to now only one of them has been involved in this study [12].

Stereolithography (SL): stereolithography has been the first technology to be developed. A 3D model is built up out of acrylate photopolymer or epoxy resin, by tracing a low power ultraviolet laser across a vat filled with resin. The material is cured by the laser to create a solid thin slice. The solid layer is then lowered just below the surface and the next slice formed on top of it, until the object is completed.

Laminated Object Manufacturing (LOM): the concept in this case is very simple: the 3D model is built up by adding sheets of paper in a stack, each of them opportunely shaped in advance, using a laser beam.

Selective laser sintering (SLS): the basics of this approach are quite similar to the SL ones. Here, instead of liquid material, the vat is filled with thermoplastic powders that, thanks to the laser beam, are submitted to the sintering treatment. The powder is kept at a temperature very close to the melting point; a high power CO₂ laser fuses the powder in a selective way (only where it is required).

Fused Deposition Modeling (FDM): Fused Deposition Modeling creates 3D models out of heated thermoplastic materials extruded through a nozzle positioned over a computer-controlled z-table. The nozzle is moved in x-y to deposit material until a single thin slice is formed. The next slice is built on top of it until the object is completed. FDM uses several build materials, such as polycarbonate, polypropylene and various polyesters.

3.2. Geometric/Solid modeling

The parametric modeling approach, based on the "form feature" concept [13], has been chosen to build up the 3D model; this one is needed to derive the data for the RP machines to produce the physical prototype. A commercial state-of-the-art modeling package has been used for this purpose (SolidWorks 98) [14].

This kind of approach allows to make the model using a language closed to the engineering issues and transparent for what concerns geometric and other too-low level details. Thanks to form features, it is possible to reach the final configuration by adding new functional characteristics to the model; the modeling package is in charge of converting these characteristics into the corresponding geometry and details automatically.

Features are said to be "parametric" because, during their insertion into the model, it is possible to convert all or part of their dimensions into variables; these variables are modifiable as needed, anytime, without modifying the model structure/description. Nevertheless, the parametric package allows to insert variable relationships; in this way it is quite simple to create an interface with the model based exclusively on the independent parameters. Giving the right values to these parameters time to time, the modeling package automatically re-computes (re-generates) the model; the updated geometry will be a simple consequence. This geometry is then post-processed to obtain the data needed as input for the RP machines.

It is clear how simple is to generate the geometry of a family of parts morphologically similar each other. This characteristic is of real interest in this work, because in the future it will be necessary to realize prototypes belonging to the same family but depending dimensionally upon the surgical needs.

4. ACTIVITIES

Activities started with the generation of the 3D model of the existing Staffieri's valve. The first parametric feature, identifying the main body of the valve, has been obtained by the rotational sweep of a parametric profile. Figure 3 shows this profile with the meaningful

dimensions from a functional point of view.

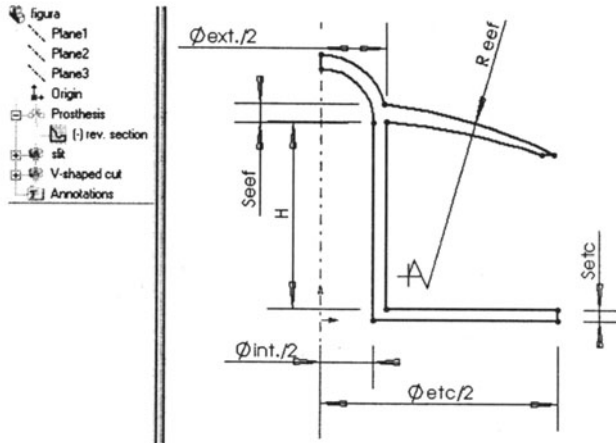


Figure 3. Parametric profile used during the generation of the valve body.

A discrete set of values drives directly to a family of parts; table I shows three different configurations of the valve.

	H	Ext./2	Int./2	Etc/2	S etc	R eff	S eff
Mod. 1	5	2.5	2	9	0.4	20.5	0.7
Mod. 2	7	3	2.5	10	0.4	22	0.8
Mod. 3	9	4	3	12	0.5	24	0.9

Table I. Family of valves expressed in terms of variable sets (eef: endoesophageal flange; etc: endotracheal retention collar)

In figure 4 the result of this first modeling phase is shown.



Figure 4: CAD model of the original Staffieri's valve.

Actually a surgical blade makes the opening in the upper part (dome) of the valve. On the lower disc, in the same way, the surgeons make another cut to identify the position of the first cut so to orient the valve correctly, avoiding liquid passage into the trachea during deglutition. Starting to analyze the possible improvements, a first solution to the problems shown by the original Staffieri's valve could consist in a modification of the lower section, changing from a circular to a 8-like shape. In this way it may be possible to bend the two little wings, join

them with a surgical suture, pull the valve through the tracheo-esophageal shunt, cut the suture and adapt the prosthesis in the correct site without difficulties. Another couple of improvements consists in giving an angle to the superior cut, to reduce at the minimum the possibility of liquid leakage into the trachea, and in adding some ribs to the valve body to avoid rotations during air passage. The updated model, resulted by the application of the described hints and feedback, is shown in figure 5.



Figure 5. Result of the first model upgrade.

It might be observed the relieved arrow indicating the "up" (the opposite side of the cut) of the valve and the greater thickness around the suture-passage holes made in the tracheal flange to avoid breaks during the placing procedure. This model has been used to derive the data file needed by the RP machine to create the physical prototype. In this case an RP machine made by EOS has been used, based on the SLS technology. The result is visible in figure 6.

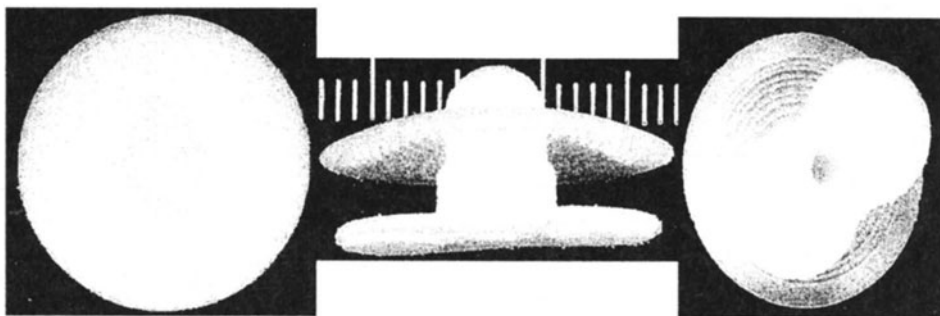


Figure 6. Top, side, and bottom view of the RP model.

Analyzing this prototype, the medical staff decided to modify the model once more. They thought that its dome (the air way to the esophagus) would have been better if drop-like shaped. With this kind of modification, it is foreseen a longer life for the valve (actually the Staffieri's valve has an average life of 6-8 months), due to the fact that the most frequent breaks happen in the hinge section. Moreover, the drop-like shape should help in driving liquid floods down to the esophagus without penetrating into the cylindrical duct. Finally, this shape should avoid resting of any material that usually causes malfunctioning or biofouling.

The last action has consisted in modifying again the lower section, making the shape longer to help the insertion of the valve through the tracheo-esophageal shunt. The resulting model is shown in figure 7. The data file coming from this model has been used to generate the corresponding physical part, using an RP machine made by DTM, based again on the SLS technology. From the starting point to the second model development, no more than 20 days had expired.



Figure 7. Result of the second model upgrade.

5. DISCUSSION

With no doubt, the main interest during the whole study has been focused on the research and development of the valve prototype. Nevertheless some aspects regarding different research areas have risen: the importance of knowledge fruition/exploitation methodologies, some issues about information exchange and about parametric approach in solid modeling and finally some notes concerning the limits of the actual RP technologies. In the following of this paragraph, all this points will be presented briefly.

5.1. Knowledge fruition

Having the model of the valve available in digital format (digital mock-up) allowed its best exploitation from time to time, depending upon goals and users.

First of all, during the whole development the CAD package itself provided to visualize the model graphically, rendering it when required. For this reason, the surgeon, close to the CAD expert, has been able to evaluate the results of his/her choices from a qualitative and quantitative point of view. For example, the CAD package evaluated automatically some global dimensional characteristics starting from the setting of the functional variables of the model. This synergy between medical and computer science domains has had an "off-line" component thanks to bitmap images generation. The surgeon, once that some personal choices have been set and applied to the model, has been allowed to present and discuss these choices with his/her colleagues directly at the hospital with their own times and modalities, because of the availability of the images generated automatically by the CAD package.

Secondly, the RP model generation could be seen as another way to exploit the model knowledge; giving the possibility to handle the physical object users can perform some evaluations bypassing the limits imposed by 2D output devices (displays, printers or plotters, etc.).

5.2. Knowledge exchange

One of the key points of Concurrent Engineering is the information exchange [15]. In this study, the different kinds of knowledge explication have allowed an intensive knowledge exchange, mainly via e-mail messages. Text, images and data files for RP machines have been transferred among the surgeons at the hospital, the CAD expert at the university laboratory and the RP machine operators at the remote sites. All this stuff has required a particular attention for what concerns data exchange standards: e-mail attachments (MIME, binex, etc.) and 2D/3D data transfer (rendered images of the CAD models in GIF format or STL files for what concerns the model description itself).

5.3. CAD: notes about the parametric approach

As said before, the generation of the model of an existing valve has been the first activity of the study. More or less intentionally (thanks to the amount of information available at that time), the modeling task has been conducted without any knowledge about the modifications that would have been carried out by the surgeons throughout all the development. This topic is of particular interest in the parametric modeling context, because one of the classic remark to this kind of approach consists of a scarce flexibility, for what concerns topologic/morphologic modifications applied to an existing model (in opposition to the easiness of re-configuration of the model thanks to dimensioning variable modifications). In effect the model has given a positive answer, minimizing the overload required sometimes by the re-parameterization (when some critical changes have occurred for what concerns the decision about the functional parameters) or when adding or changing some features to the model description. By the way it cannot be forgotten that the model, from a descriptive point of view (feature tree), is quite simple; this could make it of a scarce significance when one would establish the flexibility of the parametric CAD tools quantitatively.

5.4. RP technology related problems

The dimensional attributes and the required precision of the physical RP model have stated a meaningful benchmark to compare the different RP technologies actually on the market. Some of them have been discarded *a-priori* because of their characteristics; the others have been analyzed mostly for what concerns the quality of the result (surface finishing, etc.), meanwhile, because of the dimensions, the aspects related to costs and times have been ignored. By the way, this experience highlighted that some critical components of the valve, from a functional point of view, are not reproducible with any of the RP technologies currently available. In particular, the cut in the upper section of the valve is not producible due to its extremely low thickness. So, even if using the RP technology, a post-processing phase is required (cut made by a surgical blade or a laser beam) in those cases where, for example, the goal is to use the RP model to build up a mold directly.

6. CONCLUSIONS

This paper described a research for what concerns the RP approach applied to the surgical domain. A study has been carried out in developing a new version of the Staffieri's valve, a prosthesis to let the people who have undergone total laryngectomy speak again.

The RP approach allowed the surgeons to consider several solutions on the way, speeding up and simplifying the whole development process. All the operative phases have been illustrated and a mention has been made for what concerns Concurrent Engineering issues (knowledge exchange and fruition), CAD notes (parametric approach remarks), and RP technology problems.

From the research point of view, this experience highlighted many opportunities for what concerns future development; for sure, in the surgical domain it will continue into this direction, going ahead in the four missing phases and in developing new solutions; in the engineering field the methods will be refined and applied, if possible, to different CAD tools and RP technologies. Moreover, this preliminary study has shown the extreme flexibility and the *improving of the possibility of rapid knowledge exchange* between groups of researchers that apply in completely different domains. The obtained goal of the study is an improvement of the mechanical attributes of a medical device.

ACKNOWLEDGMENT

The physical prototypes have been realized thanks to the precious help of CRF (Centro Ricerche FIAT), Turin, for the first model and IN-TECH, Collegno, Turin, for the second. In the first case an EOS machine has been used; in the second a DTM one. Both of them are based on the SLS technology.

REFERENCES

1. Putney FJ., *Rehabilitation of the post laryngectomized patient*. AnnOtol Rhinol Laryngol 1958, 67:544-49.
2. Webster PM, Duguay MJ., *Surgeons' reported attitudes and practices regarding alaryngeal speech*. Ann Otol Rhinol Laryngol 1990,99:197-200.
3. Lopez MJ, Kraybill W, McElroy TH, Guerra O. *Voice rehabilitation practices among head and neck surgeons*. Ann Otol Rhinol Laryngol 1987,96:261-263.
4. Hilgers FJM, Balm AJM, *Long-term results of vocal rehabilitation after total laryngectomy with the low-resistance, indwelling ProvoxTM voice prosthesis system*. Clin Otolaryngol 1993, 18:517-523.
5. van den Hoogen FJA, Oudes MJ, Hombergen G, Nijadam HF, Manni JJ., *The Groeningen, Nijdam and Provox Voice prostheses: a prospective clinical comparison based on 845 replacements*. Acta Otolaryngol (Stockh) 1996,116:119-124.
6. Hilgers FJM, Schouwenburg PF. *A new low-resistance, self retaining prosthesis (ProvoxTM) for voice rehabilitation after total laryngectomy*. Laryngoscope 1990, 100:1202-1207.
7. Singer MI, Blom ED., *An endoscopic technique for restoration of voice after laryngectomy*. Ann Otol Rhinol Laryngol 1980, 89:529-533.
8. Staffieri M, Staffieri A., *A new voice button for post-total laryngectomy speech rehabilitation*. Laryngoscope 1988,98:1027-1029.
9. Omori K, Kojima H, Nonomura M, Fukushima H., *Mechanism oftracheoesophageal shunt phonation*. Arch Otolaryngol Head Neck Surg1994, 120:648-652.
10. Wetmore SJ, Ryan SP, Montague JC, Krueger K, Wesson K, Tirman R, Diner W., *Location of the vibratory segment in tracheo-esophageal speakers*. Otolaryngol Head Neck Surg 1985, 93:355-361.
11. Izdebski K, Reed CG, Ross JC, Hilsinger RL. *Problems with tracheoesophageal fistula voice restoration in totally laryngectomized patients*. Arch Otolaryngol Head Neck Surg 1994, 120:840-845.
12. P. F. Jacob, *Stereolithography & Other Rp&m Technologies : From Rapid Prototyping to Rapid Tooling*, Society of Manufacturing Engineers and Rapid Prototyping Association, ASME Press. 1996.
13. Mantyla M., J. J. Shah, *Parametric and Feature-Based Cad/Cam: Concepts, Techniques, and Applications*. John Wiley & Sons. 1995.
14. R. Wysack, *Designing Parts With Solid Works*. CAD/CAM Pub. 1998.
15. R.C. Dorf (ed.), A. Kusiak (ed.), *Handbook of Design, Manufacturing and Automation*, John Wiley & Sons. 1994

PARAMETRIC INVESTIGATION OF SHEET LASER BENDING BY EXPERIMENTAL AND NUMERICAL ANALYSIS

G. Casalino and A.D. Ludovico
Politecnico di Bari, Bari, Italy

KEY WORDS : Rapid prototyping, Laser bending, Numerical and Experimental Analysis.

ABSTRACT : According to several authors, laser bending is becoming a valid alternative to dies for manufacturing even complex objects from thin metal sheets. The mechanism is based on thermal induced deformations that are produced by a laser source irradiation on a sheet surface that does not need external forces. Nevertheless, the set up process of parameters is both labour and time consuming. The aim of this paper is to contribute to the management and practical use of this process. Therefore some technological and geometrical parameters, as well as material properties dependence on temperature, have been investigated by analysing and experimenting finite elements. This work reports the results of a largely influential investigation of the above mentioned parameters on thin sheet metal bending. Furthermore, the constructed model can be useful for further developments in laser bending investigation.

1. INTRODUCTION

According to the philosophy of rapid prototyping, rapid manufacturing without solid tools affects time and cost. That means avoiding the time and cost consuming operation [1] of designing and manufacturing the die in the case of laser sheet metal forming because the laser is an effective substitute. This process is known as laser bending. It is based on three different mechanisms of deformation [2] which are induced by thermal shrinkage. In this

paper, the Temperature Gradient Method (TGM) is investigated by a parametric numerical and experimental analysis. This mechanism is generated by the thermal gradient through the sheet thickness caused by the interaction of the laser source and sheet surface.

The run feed rate and the power laser source, the sheet's width and the material properties were considered during the set up and testing of the model. The data regarding material properties was improved through preliminary experiments. The numerical results obtained have been compared to those collected during a later experiment.

2. THE LASER BENDING MECHANISM

The bending mechanism known as the Temperature Gradient Method is caused by slow heat conduction into the sheet and rapid heating, from laser irradiation (fig.1), that develops along a linear path on the sheet's surface [3]. From this, a steep temperature gradient is generated along the thickness causing the consequent thermal expansion of the heated metal above. This metal is converted into a deformation of elastic and plastic around the laser's path and along the thickness of the sheet as well because free expansion is restricted by the cold material. The heating of the cold side is negligible and the ratio between the laser's spot (d) and the sheet's thickness (S_0) has to be about one.

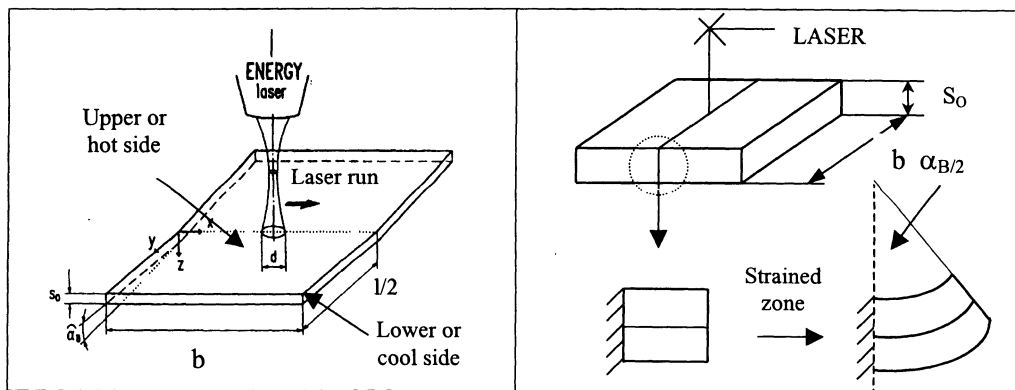


Figure.1 - Laser path

Fig.2 - TGM bending mechanism

The deformation of elastic is called counter bending because during the heating process, the bending angle develops towards the cold side of the sheet due to the increase in length of the irradiated layer. The deformation of plastic depends on the layer near the laser source which shortens after cooling. The difference of length, in respect to the lower layer, develops the compressive plastic deformation which shapes the sheet in the form an angle (α_B) towards the laser beam (fig.2). The rest of the material experiences only rigid rotation. It is noteworthy to say that the temperatures during the process are lower than the melting temperature. In order to increase the bending angle, the irradiation can be repeated during several runs. As a result of the complexity of the above mentioned mechanism, knowledge of the most important operating parameters is crucial in obtaining a large bending angle. They can be classified in three major groups [4], namely :

- *technological parameters* : the power of the laser beam source and the value of the path feed rate;
- *thermal-physical and mechanical parameters* : the values of the coefficients of thermal expansion, thermal conductivity, the heat capacity and energy absorption during irradiation of the sheet material, depends on the temperature of all the above mentioned parameters;
- *geometrical parameters* : the shape of the sheet, it's width and thickness.

One of the major difficulties in the numerical and the analytic simulation of laser bending is to take into account the parameters of the second group. In fact, the size of the heated zone in respect to the cold zone, which determines the compression strain, strongly depends on the thermal-physical and mechanical parameters which vary with temperature. In particular, the absorption is a phenomenon that changes depending on several effects surrounding the material such as, the irradiation wavelength, the temperature, the surface's conditions and roughness, the angle of incidence [5] and many others. Nevertheless, among the mechanical properties the strain hardening of the cold lower layer makes it difficult to calculate the bending angle after several runs.

3. THE MODEL

In this paragraph a model's description is presented along with the parameters' range of investigation. Table 1 contains ranges regarding the technological and geometrical parameters. The path feed ratio (p.f.r.), varies from 300 to 1067 mm/min and the laser power from 1000 to 1500 W. The specimens were 60 mm long, 2 mm thick and from 5 to 30 mm wide. The numerical simulation of bending was performed for every combination showed in table 1.

POWER (W)	WIDTH (mm)			
	5 mm	10 mm	15 mm	30 mm
1000 W	p.f.r. = 300 mm/min	p.f.r. = 400 mm/min	p.f.r. = 500 mm/min	p.f.r. = 600 mm/min
1250 W	p.f.r. = 500 mm/min	p.f.r. = 667 mm/min	p.f.r. = 833 mm/min	p.f.r. = 1000 mm/min
1500 W	p.f.r. = 800 mm/min	p.f.r. = 933 mm/min	p.f.r. = 1067 mm/min	p.f.r. =1200 mm/min

Table 1 - Geometrical and Technological parameters

The Table 2 reports the values of mechanical and thermal-physical parameters of material (SAE 1020), with variation in the temperature's range of investigation [6]. These variations are: the specific heat (c), the thermal conductivity (k), the coefficient of absorption (A), the coefficient of thermal expansion (α), the Young modulus (E) and the yielding stress (σ_y). Referring to the finite element model, a elastic-plastic analysis was performed with the following set up. A fine mesh was placed along as well as close to the laser path and a coarse mesh was used for the rest of the area in order to reduce the computational time and to memorise the allocation of size. Moreover, the geometrical model refers to half the length of the specimen. The dofs of the points of the symmetric plan, which are also those of the laser path, were constrained. Brick elements with 8 nodes were used for the mesh. The laser path develops along the side of the fine mesh.

T (°C)	c (J Kg ⁻¹ °C ⁻¹)	k (W m ⁻³ °C ⁻¹)	A (%)	α (10 ⁻⁶ °C ⁻¹)	E (Gpa)	σ _y (Mpa)
20	474.9	52.7	4.6	7.61	212	
50	484.9	51.8	4.84	8.22	210	329
100	501.6	51	5.24	9.25	201	
150	518.3	49.9	5.65	10.27	195	
200	530.8	48.9	6.05	11.3	189.4	
250	555.9	47.5	6.5	11.75	183.7	328.8
300	572.6	46	6.93	12.4	178.1	234
350	593.6	44.3	7.38	12.85	172.4	
400	627	42.6	7.82	13.3	166.8	167
450	660.4	41	8.3	13.45	161.1	
500	704.3	39.3	8.78	13.6	155.5	105.7
550	748.2	37.4	9.27	13.86	150	
600	796.3	35.5	9.75	14.13	144.2	55.7
650	844.4	33.6	10.26	14.4	138.5	
700	1429.6	31.8	10.77	14.4	132.9	
750	948.9	28.8	11.24	14.4	127.2	
800	879.9	25.9	11.71	13.6	121.6	
850	810.9	26.2	11.8	13	116	
900	810.9	26.55	11.9	12	110.3	
1000	810.9	27.2	12.1	11	99	3.5
1100	810.9	28.45	12.2	11	87.7	
1200	810.9	29.7	12.4	11	76.4	1.44
1400	810.9	29.7	12.5	11	53.8	

Table 2 - Thermal-physical and mechanical parameters of SAE 1020

In this study the continuous mode of function was simulated with the spatial profile of laser beam power being a Gaussian. In this case, the intensity of beam is a function of the distance from the center of the beam itself [7]. Therefore, the nodes along the path were filled with thermal flux loads whose magnitude depended on the position of their nodes and source's running rate. The actual energy input in the material was reduced by the absorption coefficient (A) which varies with temperature, as shown in the table 2, multiplied by a factor of 1.5 on the basis of preliminary experimental trials. The beam spot was 3 mm wide. The mechanical computation was performed with the input of the thermal distribution coming from the thermal analysis. During the mechanical computation, no significant problems were reported.

4. THE NUMERICAL RESULTS

The numerical analysis had two different stages. The first one was to determine the distribution of temperature in the sheet due to laser beam heating. Then the deformation and the bending angle of the specimen were calculated on the basis of the obtained temperatures during the previous step.

The model was able to reproduce the most important steps of the deformation. That being the counter bending (fig. 3) and the bending angle (fig.4), in figure 5 the free deformation

along the z axis is reported. In the case of the formation of sheet metal by die, this deformation is prevented by the die itself.

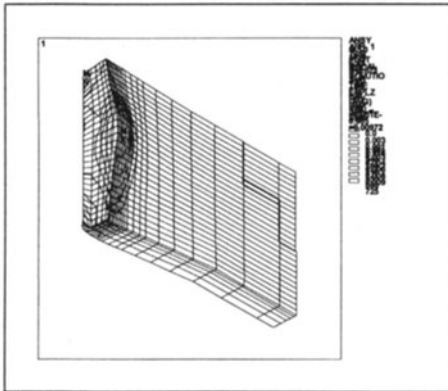


Fig.5 - z-axis deformation

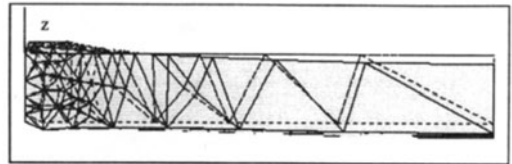


Fig.3 - Counterbending

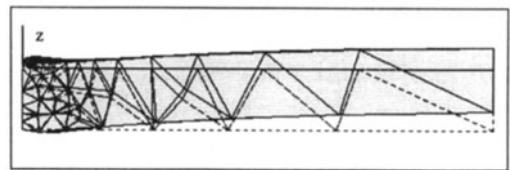


Fig.4 - Bending

The values of the obtained bending angle were plotted against the path feed rate of the laser in the figures from 6 to 9. The following remarks were made :

- an increased path feed rate leads to a lower bending angle for every geometry and power level of laser. The trend for the whole diagrams is linear;
- for one path feed rate an increased laser beam power brought a higher bending angle;
- an increased width leads to a higher bending angle;
- the trend of the bending angle decreasing with the path feed rate lessens with a higher power level. This trend is confirmed for every width.

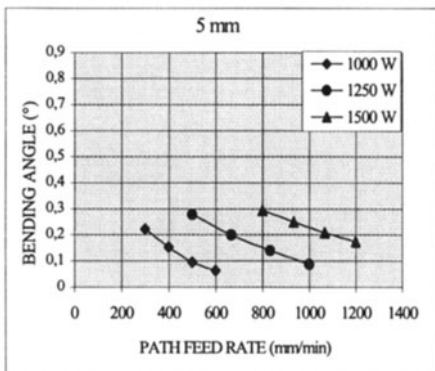


Fig. 6 - Bending angle diagram for 5 mm wide specimen

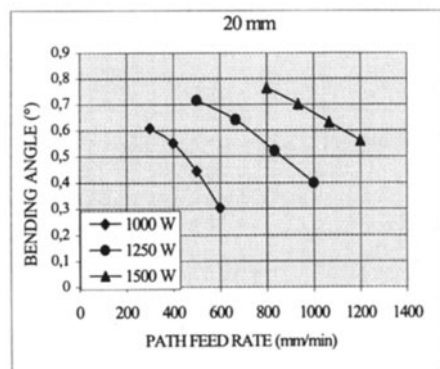


Fig.8 - Bending angle diagram for 20 mm wide specimen

The previous remarks bring us to the conclusion that a higher specific heat input that runs slower and has more beam power, improves the bending angle. The explanation is that the

thermal gradient is steeper because the upper layer is hotter and the thermal conductivity is lower (see table 2 about material's properties). Furthermore, the rise of beam power and longer laser path compensate for the reduction of the bending angle due to low path feed rate. This means that the process strongly depends on the time of the beam-surface interaction.

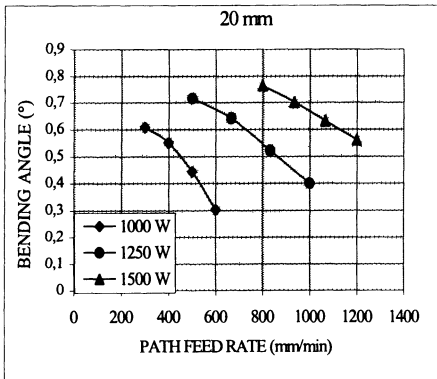


Fig.8 - Bending angle diagram for 20 mm wide specimen

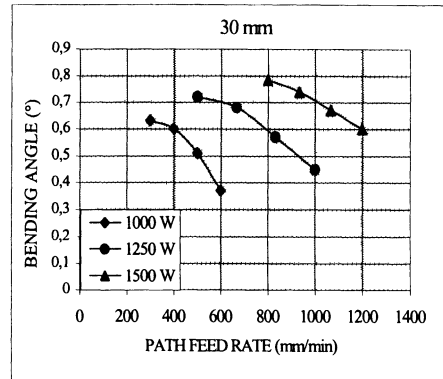


Fig.9 - Bending angle diagram for 30 mm wide specimen

Nevertheless, for one power the bending angle curves against the width of the specimen shows an asymptotic trend for the entire set of investigated speeds (figs 10 and 11). That is due to the opposition in further deformation of the cool area of the sheet. This behaviour shows the limitation of the laser bending process which is unable to create an angle larger than one degree in dimension.

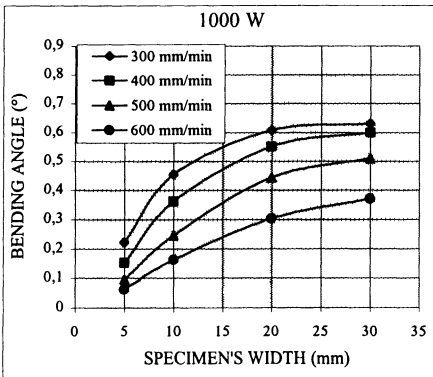


Fig.10 - Bending angle versus width (1000W)

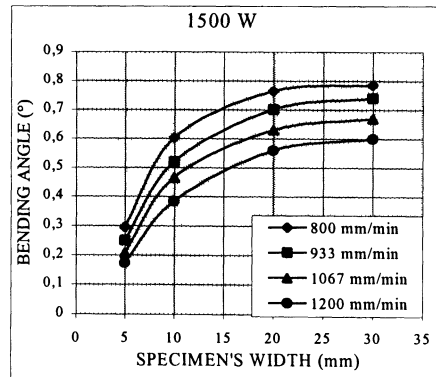


Fig.11 - Bending angle versus width (1500W)

5. THE EXPERIMENTAL RESULTS : MODEL'S VALIDATION.

The experimental plan involved both the 10 mm and 20 mm wide specimens for all the combinations of the beam power and path feed rate. Every experiment was repeated 3 times in order to provide a reliable average of the bending angle. In this way, 72 specimens (12 couples of different speed-powers per 2 different widths each repeated 3 times) were

prepared and processed. The Bystar 4020 BTL 2800 from BYSTRONIC LASER AG was used with a 5" lens and a 4 mm diameter nozzle. In order to obtain the 3 mm beam spot, the fit distance between the nozzle and the sheet was 2.55 mm. The spatial profile of laser beam power was a Gaussian (TEM_{00}). The nitrogen was the inert gas with 0.5 atm pressure and 2.5 Nl/s flow.

The laser beam scanned the sheet along its width with both the path feed rate and the power of beam set on the machine being equal for the numerical simulation. The obtained bending angles were measured by means of an appropriate device that was designed and constructed for this purpose.

The averages of the bending angles for every experiment is provided in figs. 12 and 13 along with the related numerical results. The related numerical results are always lower than the experimental results. Nevertheless, the gap is between 10% and 20% for both the 1250 W and 1500 W cases. In the case of the 1000 W laser power the gap is a bit larger. The explanation for this is that the thermal properties of the material become more difficult to manage as the temperature rises. The influence of the coefficient of absorption and the thermal conductivity must be investigated by trial and error experimental analysis in order to correct the actual thermal input and propagation for every speed and power couple. In particular, the correcting coefficient for absorption has to be arranged for every specifically different energy input.

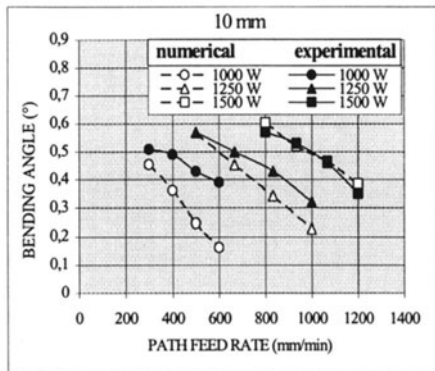


Fig. 12 - Numerical versus experimental results for 10 mm wide sheet

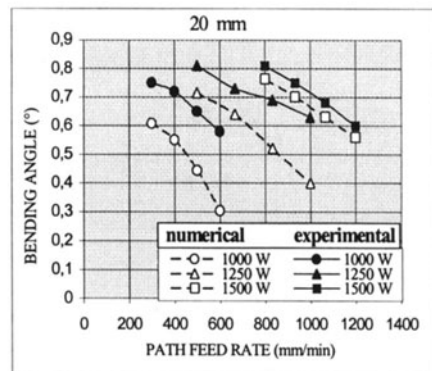


Fig. 13 - Numerical versus experimental results for 20 mm wide sheet

6. CONCLUSION

The parametric FEM analysis, set and validated by experimental trials of the SAE 1020 laser bending performed in this paper, has proved to be quite reasonable. In fact, the characteristic deformation stages of laser bending (counter bending, bending, and z-axis deformation) have all been reproduced. The values of the bending angle have been predicted within a good approximation, while some important parameters of the process were varied. Larger angles have been obtained for wider sheets, according to other authors [8]. The analysis has highlighted that it is very important to consider the variation of material properties with changes in temperature. Moreover, the information available in

the bibliography on thermal and physical properties must be corrected by information coming from preliminary experiments. This is particularly true for the coefficient of absorption and thermal conductivity. These parameters seem to have been influenced by specific heat input which varies with the laser beam power and path feed rate.

On the basis of the obtained results the potential and the innovation of sheet laser bending are both confirmed for application in future years, as well as the capability of the FEM to fairly simulate this non-linear and highly complicated process.

Further developments could be the numerical simulation of several runs bending processes and the automation choice of working parameters for a wide range of applications. In this case, the FEM analysis could be time and cost consuming since the computational time and the computer memory for data allocation rise exponentially. Therefore, the authors are also investigating the use of an artificial neural network [9] as a computational means for predicting process parameters and bending angles.

REFERENCES

1. A. GATTO, L. Iuliano. *Prototipazione Rapida*. Collana Tecnologie, Tecniche Nuove, Milano Italy.
2. F. VOLLERSTEN. Mechanisms and models for laser forming. LANE'94, vol.1 eds: M. Geiger, F. Vollersten; Meisenbach, Bamberg 1994, pag. 345-360.
3. M. GEIGER, H. ARNET, F. VOLLERTSTEIN, Laser Forming, LANE'94, vol.1 eds: M. Geiger, F. Vollersten; Meisenbach, Bamberg 1994, pag. 81-92.
4. N. ALBERTI, L. FRATINI, F. MICARI, Numerical simulation of the laser bending process a coupled thermal mechanical analysis. LANE'94, vol.1 eds: M. Geiger, F. Vollersten; Meisenbach, Bamberg 1994 pag. 327-336.
5. W.M. STEEN. *Laser Materials Processing*. Springer-Verlag, 1991 ISBN 3540196706.
6. S. TOULOKIAN, *Compendium of thermophysical properties of materials*.
7. D. SCHUOCKER, A. KAPLAN. Overview Over Modelling For Laser Applications. SPIE Vol.2207, pag.236-247.
8. F. VOLLERSTEN, S. HOLZER. 3D-thermomechanical simulation of laser forming. *Simulation of Materials Processing : Theory, Meth. and Appl.*, Shen&Dawson (eds), 1995, Rotterdam, Holland.
9. G. CASALINO, A.D. LUDOVICO et al. Neural network application in the field of electron beam welding. ICME'98, July 1-3, 1998, Italy.

A TECHNOLOGICAL APPROACH FOR SELECTIVE LASER SINTERING

F. Miani and E. Kuljanic

University of Udine, Udine, Italy

G. Marinsek

Centro Ricerche FIAT, Orbassano (TO), Italy

Keywords: Rapid prototyping, selective laser sintering, metal powder forming

ABSTRACT

Two of the key factors in the densification of powders properties in sintering processes - the green body density and green body strength - are studied with the purpose of giving appropriate empirical modeling of the laser sintering of uncoated metal powders. Some proposals for the characterisation of technological properties of powders for selective laser sintering of uncoated powders are discussed in this framework for establishing possible standards for the development of new or improved powders. Methods for the production of metal powders are also considered, with a brief discussion of possible benefits or limitations for this specific application. In the case of mechanical forming at low external pressures, some equations are discussed, linking the variables green body density, green strength and applied pressure. Experimental results for powders of iron, nickel and copper allow to estimate the relevant parameters of the empirical equations. The same parameters are proposed for simple modeling that could be helpful in the selection of powders for the process.

Published in: E. Kuljanic (Ed.) *Advanced Manufacturing Systems and Technology*,
CISM Courses and Lectures No. 406, Springer Verlag, Wien New York, 1999.

1. INTRODUCTION.

Selective laser sintering (SLS) is a rapid prototyping (RP) technique, that is steadily growing in these years, and is presently the most interesting technique for rapid tooling applications. The outline of the process has been fully described in many different papers and in a specific recent book on Laser Material Processing [1]. In this paper we want to discuss briefly some technological aspects of the process, with much emphasis on the proper development of the powders for the specific application. The market of powders for SLS applications now has two main products, coated and uncoated metal powders; we shall discuss here some details of uncoated powders, as these materials – and the global process itself- is less sophisticated than the coated counterpart. We observe that one of the main limitations for specific materials selection – cost – does not apply to commercial powders at this stage of the laser sintering process. So one should not just consider metal powder compositions that are successfully employed in the metal powder industry but also some more let's say exotic compositions; in fact, even if less important than in wrought or wrought and cast materials, the cost of the base materials generally speaking is a limitation for sintered products. The second fact we would like to stress is that, while there are more than 50 standards in the PM industry, in the papers that we have in mind on this specific issue – development of materials for the SLS process, for instance [2], no specific procedure or standard is mentioned. According to general references on the sintering process [3] the most important parameters to be considered in the sintering process are - for a specific material - the physical quantities described in next section.

1. PROPERTY SELECTION IN POWDERS FOR RAPID PROTOTYPING – WHICH ONE?

The usual technological characterization of a powder for sintering application [4], let's say an iron based powder is:

- a) chemical analysis, with special attention to the elements that do have influence in further processing (oxygen, carbon, sulphur)
- b) apparent density MPIF 04 (ISO 3923/1, DIN 1980), MPIF 28
- c) flow rate MPIF 03 (ISO 4490, DIN 3927)
- d) compactability MPIF 42 (ISO 2738), MPIF 45 (ISO 3927, DIN 1991)
- e) dimensional variations on restricted sintering conditions MPIF 44 (ISO 4492)
- f) green strength MPIF 15 (ISO 3995, DIN 1991)
- g) particle size distribution MPIF 05 (ISO 4497), MPIF 32 (ASTM B330)

We believe that most of these properties are worth of being considered in developing a powder for SLS applications. Great advantage should also be taken from the experience in sampling (MPIF 01), that may cause different experimental difficulties to the

unaware developer. Properties d), i.e. density on specific uniaxial loads, and f) strength of the compacted body (green body strength) may not be directly exploitable as the pressure ranges employed for quality testing are usually comparable or superior to the yield strength of the base material, we shall see in next section possible developments. On the other hand it's quite surprising that a very simple empirical technique, like the flow through a specific funnel (Hall and Carney flowmeters) has not yet been considered. Particle size distribution is greatly influencing the apparent density, the flowability the green strength and dimensional variations in sintering for any traditional or nontraditional sintering application. We report here, for order of magnitude appraisal, values for two different commercial, copper based, powders for laser sintering applications together with three of the commonest powders for sintering application, atomized iron, electrolytic copper and nickel from nickel tetracarbonyl powders.

Property	Powder A	Powder B	Iron powders	Copper powders	Nickel Powders
Apparent density/full density %	56.4	51.5	38.2	25.8	28.1
Flow rate, s	11	12	25	Not flowing	Not flowing
90 % particles less than μm .	85	55	150	45	8

Table 1. Properties of commercial powders for rapid prototyping (A,B) and for sintering applications.

Particle size distribution measuring is not a simple topic to discuss, at least in sintering applications. It is difficult to extract a number – even a series of number – like in the standard mechanical sieving analysis when the dimensions of the particles, when most of the particles like it's claimed in recent applications – lay below the standard employable sieve, that is 38 μm . A series of books has been written on this topic, we remark here that the use of laser particle size analyser should be the best available tool for development work. So far we have mentioned some relevant properties of metal powders, which might be worth of considering for the SLS powders. We should also recall in the next section the technological processes that could be employed for the production. We have experienced personally some possibilities, but we would like to leave the description of our experiences to a later paper.

2. PRODUCTION ROUTES FOR METAL POWDERS FOR SLS APPLICATIONS.

Raw materials for the metal powder industry are converted into powders with four main processes:

- water atomization
- inert gas atomization
- reduction of pretreated – usually grinded – solids
- electrolytic deposition

Tonnage productions are obtained usually by water atomization or reduction. Electrolytic deposition has been neglected in recent years because of ecological limitations. In principle however, any of this technique could be employed, and there are in any case technological overlaps. For small scale development, water and inert gas atomization have interesting possibilities.

Subsequent treatments – let's call these secondary powder preparations - may be imparted to metal powders, usually:

- reduction/annealing
- mixing
- diffusion bonding

The whole step is not always necessary for a powder, but usually it's applied for powders for sintering applications of elevated performances. We remark here that a powder of the same chemical composition may be just a mechanical mixture of elemental powders, fully alloyed in the liquid state or partially alloyed by the diffusion bonding process. These different processes correspond at different levels of segregation respectively strong segregation, no segregation (all powder particles have very close – even if not identical – composition) and reduced segregation. Also the flowability of powders is greatly influenced by the morphology of the process, as much as low friction effects exist on spherical particles (for instance inert gas atomized) and high friction interactions are present in the flow of irregular particles (for instance electrolytic). So, generally speaking, the best flowing characteristics are obtained for inert atomized powders, and worst flow properties for irregular powders. The flowability of metal powder mixtures is still an art and notwithstanding some possible big specific technological and economic value added no simple model may be used to date. As concerning homogeneity the commercial SLS powders we have examined, consisting of a blend of different metal powders obtained by mixing, seem to have a tendency to segregation: particles of different densities and granulometries tend to float one on the other. In common sintering operations, which in any case have diffusion times of the order of some fraction of hour, segregation is usually detrimental – as detrimental as strong inhomogeneities may be in a material for any mechanical application. As the sintering time is much shorter than traditional sintering operations, it is quite likely that the elimination – or control - of segregation should be of high importance for powder for SLS applications. For what follows here, we believe that it could be interesting to develop a predensification stage, which would be able to aid sintering, with very limited compacting pressures, of the order from some hundredths to a tenth of the pressures applied in press and sintering applications. This pressure could be applied not by dies and moulds like in pressing and sintering but by a roll, as it happens to the process of

the roll compactation of metal powders. Compacting a powder is a standard operation for press and sinter applications. The pressures, usually uni or biaxially imparted, are comparable to the yield strength of the base materials, and could not be applied in a laser sintering apparatus without causing major constructional complexities in the laser sintering machine. Roll compacting of metal powders is a technique, that has been not fully introduced in the metal powder industry, which could be able to pre-densify materials to an appreciable level of green density and green strength. In the following paragraphs, an analysis of the green body density versus applied pressure will be discussed, together with a paragraph on the effects of these two variables on the green strength. Sophisticated first principles or finite elements analysis is not able yet to provide any sound model for traditional, and well established as for powder characteristics, powder pressing applications.

3. DENSITY APPLIED PRESSURE RELATIONS – COMPACTABILITY AT LOW PRESSURE.

We report here the base analysis by German, with a slightly modified terminology. Let it be ρ the density, p the applied pressure and ε the porosity (volume percent of voids). Then to a first approximation to die compaction it will apply:

$$d\varepsilon = -dp \theta \varepsilon \quad (1)$$

where p is the applied pressure and θ a proportionality constant that is linked to the powder properties, mainly base material, particle size distribution, morphology. Integrating and rearranging equation (1) one may obtain:

$$\ln(\varepsilon/\varepsilon_0) = -\theta p \quad (2)$$

where ε_0 is the porosity of the powder in the state of apparent density. This equation has proven to be experimentally useful in the field of compacting pressures of 50 to 700 for powders of iron, nickel and copper. As it is necessary to take into consideration preliminary rearrangements, which are mainly configurational, usually equation (2) is employed as

$$\ln(\varepsilon/\varepsilon_0) = B - \theta p \quad (3)$$

where B is an empirical parameter. German quotes some other 9 equations which have two or more parameters. Equation (3) and similar equations, have been developed however to predict compacting behavior with pressures of the order of the yield strength of the material, in order to obtain a green body density comparable with (70 % or more) the bulk solid density. While equation (3) is applicable to high pressure compacting, at low compacting pressures, equation 2 is extrapolable to the apparent density state, as in this equation results for $p=0$ $\varepsilon/\varepsilon_0=1$.

4. GREEN STRENGTH VERSUS DENSITY AND APPLIED PRESSURE AT LOW COMPACTION PRESSURES.

As in the case of density in function of applied pressure, the green strength – the strength of unsintered, as-compacted powders – is of concern in manufacturing operations in both the microscopic field – for instance microcracks may grow in the sintering process – and even for the movement of the green bodies. Usually this property is tested on the 30X12 rectangular bars employed for the experimental work here, and applying a load on a three point bend test. This parameter is well introduced for testing purposes in the ferrous and copper based production, surprisingly not so well exploited – in the personal experience of the writer- in the hard metal production. One empirical equation that is often used is:

$$\sigma = C \sigma_0 \rho^m \quad (4)$$

where σ is the green strength of the compact, C , σ_0 and m empirical constants, with m usually around 6; ρ is the density of the green body as above. A good green strength in metal powder industry is of the order of 10-15 N/mm². This value depends on obtaining a good interlocking of particles in intermediate and higher pressure (close to the yield strength of the base material); in a sense is opposite to a good flowability of the powders and generally speaking irregular powders do not flow well but have technologically useful values of green strength. Randall quotes some 11 equations for the green strength green density relationships – but stresses the usefulness of an empirical equation relating applied pressure p – green strength directly:

$$\sigma = \beta \sigma_0 p \quad (5)$$

where σ_0 is the strength of the wrought material.

5. EXPERIMENTAL

SETUP

To evaluate some preliminary possibilities, following the standard MPIF42, ISO compatible 3325 and ASTM B 528, three different commercial powders have been compressed in an instrumented press using a hardmetal mould and die, to different compression pressures. Lubricant was admixed to powders (0.8 % Zinc Stearate) in order to allow to use the mould and die at higher loads. The rectangular die and mould have the dimensions of $L=30$ $b=12$ (mm) and a fixed amount of powders (15.5 g.) was used for all powders. Powders employed were: A) commercial atomized and reduced iron 50 - 180 μm ; B) commercial electrolytic Cu 10 45 μm ; C) commercial Ni from

$\text{Ni}(\text{CO})_4$ precursors 4–10 μm . All powders were of irregular shape, to allow a preliminary determination of the green strength at lower loads; as reported in Table 1 powder A) has a flowability (ISO 4490) of 25 s; powders B) and C) do not flow freely as the majority of irregular fine (< 45 μm) powders. These materials are some possible candidate materials (base or strengthening) for future applications in the fields of powders for rapid prototyping.

RESULTS: PRESSURE DENSITY RELATIONSHIP.

For density - compacting pressure relationships, experimental results fit an equation of the type of equation 2 or equation 4. An equation relating linearly relating $\ln(p) - \ln(\rho)$ is the most satisfying of the possible that we tested. However, while equation 2 has a possible physical interpretation and direct material links – as the discussion will report later - we believe that the validity of an equation $\ln(p) - \ln(\rho)$ has to be tested in compacting more different materials.

Table 2 describes the data for iron and the fitted data, for the equation (2) and the linear $\ln(p) - \ln(\rho)$ relation. All experimental data refer to the initial porosity $-\epsilon_0$ in equation (2).

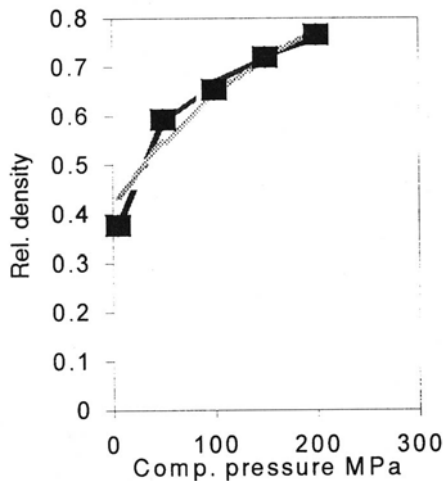


Figure 1 Data of relative density in squares and fitting equation (2) (line); the dashed line is a $\ln p - \ln \rho$. Powders A), atomized and reduced iron.

Table 3 presents the reciprocal of the value θ , that in the data obtained is proportional to R_m (mechanical strength) value of technically pure respective materials, for a factor of 0.85.

p, MPa	A) Fe	B) Cu	C) Ni	Calc. eqn. Fe	Fit (2)	Calc. eqn. Cu	Fit (2)	Calc. eqn. Ni	Fit (2)
50	0.653	0.627	0.708	0.768		0.759		0.782	
100	0.555	0.505	0.643	0.590		0.579		0.654	
150	0.449	0.431	0.582	0.453		0.437		0.524	
200	0.375	0.376	0.409	0.348		0.332		0.427	

Table 2. Data and fitting equation (2)

	Fe	Cu	Ni
1/θ (MPa)	190	183	332
R _m (Mpa)	200	220	320

Table 3. Parameters for equation (2) for the three different materials tested.

We remark that R_m value is strongly influenced by the purity of the metals considered, and we would not consider this specific issue here. In any case, for the sake of the modeling proposed, we believe that looking at the results presented in Table 3, an approximate equation may be considered:

$$1/\theta \approx 0.97R_m \quad (6)$$

transforming equation (3) to:

$$\varepsilon/\varepsilon_0 = \exp(-p/(0.97R_m)) \quad (7)$$

Expressed in density, and with the same limited application to the lower pressures (p < R_m), equation (7) transforms to:

$$\rho/\rho_M = 1 - (1 - \rho_0/\rho_M)\exp(p/R_m) \quad (8)$$

where ρ_M is the full density of the respective metal and ρ₀ has the same meaning of the conditions above for porosity, i.e. is the apparent density. These results are in line for general results for instance as reported by Heckel and James, that the mechanism is related to the material mechanical properties. So for the sake of modeling, an empirical form of the equation (2), θ derived from mechanical properties could be exploitable in a preliminary work for building experimental compositions. From the production route of the primary powders and the possible related morphology one could also estimate the initial (p=0) porosity or apparent density. Even if some experimental work was carried out on mixtures, we believe it's not the time yet not even to outline any simple

RESULTS: PRESSURE GREEN STRENGTH RELATIONSHIP.

Samples prepared as above, where tested following the MPIF 15, in order to obtain green strength values.

P, Mpa	A) Fe	B) Cu	C) Ni
50	0.0218	0.1445	0.6164
100	0.1460	0.7851	1.3843
150	0.3433	1.3493	2.1913
200	9.8424	2.1584	5.3924

Table 4. Experimental results for green strength (MPa) at different compacting pressures.

Equation (4) and (5) have been tested, both proving a fit valid for experimental purposes. Resulting parameters are reported in Table 5.

	A) Fe	B) Cu	C) Ni
$10^3 \beta$ (1/MPa)	3.521	9.514	16.806
$10^3 m$	14.21	9.010	9.12
$\ln(C\sigma)$	-25.50	-15.90	-14.18

Table 5. Parameters for equations (4) and (5).

Here however is more difficult to outline some simple materials properties link. One could just say that the value β in the data reported here is from 1 to $5 \cdot 10^{-5}$ 1/Mpa, and is particularly scattered for the iron powders. Plots of $10^3 \beta$ against pressure however show a linear behavior – that we are not able to investigate here, but that does reduce the difference in a possible estimate of the green strength – green density relation at low pressures in a form:

$$\sigma = \beta_N \sigma_0 p^2 \quad (8)$$

where β_N is now equal to 0.8, 2.6 and 2.4 in units of 10^{-5} (1/Mpa)² in the data considered here, respectively for Fe, Ni and Cu. Again, even some experimental work has already been performed on mixtures, it's too early a stage to quantify these effects.

6. DISCUSSION

The preliminary results reported are encouraging, as exploiting quite simple laboratory techniques it is possible to extract models that might be oversimplified, but have proven to be useful since several decades in the powder metallurgy industry. However, up to date, there was not significant interest in modeling the mechanical behaviour of low pressure compacted powders, as there was no practical application directly exploitable. The field of laser sintering for rapid prototyping application has urgently the need to develop new or improved materials, in both the field of rapid prototyping itself and in the rapid tooling applications. The experimental work on this paper does not consider laser effects – like reflectivity, heat conductivity and enthalpy of fusion effects, but these parameters may be studied and then modelled as well in such a simple fashion, in order to have a deterministic and heuristic model that could be helpful in the selection of the metal powder properties at an intermediate level, avoiding of developing specific powders to be tested in the applications. With some contradiction in term, we would say that rapid prototyping needs rapid testing procedures for the materials applications, and this must be achieved by simple research work.

So if one would consider a powder made of a base metal with mechanical properties $R_m=200$ MPa, a local compactation of 20 MPa would increase the powder density of the 30%. That is, if the powder has an initial relative density of the 40%, it would then increase to 52%. This is depicted in Figure 2.

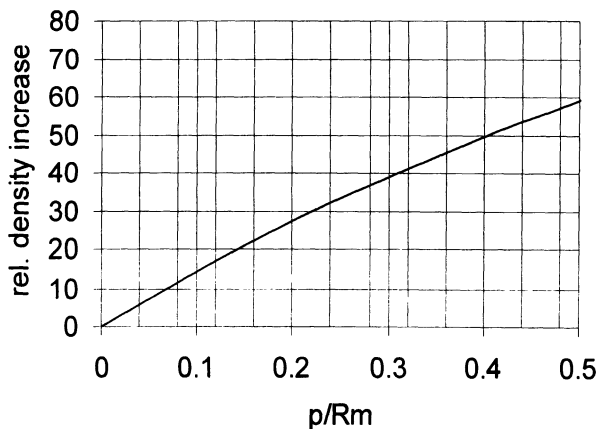


Figure 2. Increase in relative density for an applied pressure p . R_m employed 200 Mpa.

CONCLUSIONS.

The testing procedures for uncoated powders for rapid prototyping that have been discussed, together with some very simple models that may give, for pure metals, the forming characteristic at low pressures in term of forming characteristics. This may be of help in the development of the process suggesting a possible enhancement of the laser sintering set-up with the use of a compacting roll. In this case the green body density pressure relationships and green strength applied pressure relationships could be important for a pre-sintering stage. The empirical parameters, for low applied pressures that are not common and not applicable to normal press and sintering operations, that have been developed, and one of the two equations that have been developed for the green body density and the green strength dependence on applied compaction pressure, could provide appropriate data for the modelling. While an extension of the considerations presented to powder mixtures, provided some experimental data to be analyzed, should enhance the possibility of applying the model, for a thorough simulation program there remain different topics to be investigated, which are in any case deeply linked with the density of the powders, like the thermal conductivity, the heat of fusion, the whole topic of behaviour on sintering.

REFERENCES.

1. German, R.M., Powder Metallurgy Science MPIF 1994, Princeton, New Jersey, 1994
2. Steen, W.M., Laser Material Processing Chapter 7 Rapid Prototyping and Low Volume Manufacture 272-291, Springer Berlin Heidelberg 1998
3. Metal Powder Industry 3. Metal Powder Federation Standard Test Methods for Metal Powders and Powder Metallurgy Materials MPIF, Princeton NJ, 1995
4. ASM Handbook Volume 7 Powder Metal Technologies and Applications Materials Park, Ohio, 1998

ACKNOWLEDGMENTS: One of the authors (F.M.) would like to thank Dr. M. La Raja, G. Lettich and Dr. P. Costa for kind technical help

OPTIMIZATION OF THE PROCESS OF LASER CUTTING OF STEEL

J. Grum and D. Zuljan
University of Ljubljana, Ljubljana, Slovenia

KEY WORDS: Austenitic Stainless Steel, Laser Cutting, Laser Cutting Parameters, Microstructure Analysis, Microchemical Analysis

ABSTRACT: Efficient control of laser cutting processes is closely related to knowledge of heat effects in the cutting front and its surroundings.

The macrographs show that the majority of the cuts shown can be classified in the highest quality class considering the machining conditions specified. This proves that in the case of austenitic stainless steel, the cutting speeds were suitably chosen for the particular material thicknesses. The variation of the HAZ thickness indicate that in the bottom part of the cut more intensive chemical processes are occurring between the molted material and the oxygen gas, hence heat is released. In the bottom part of inclined the cut, due to flow of the melt, heat from the melt is additionally transferred into the cool surroundings of the cut.

1. INTRODUCTION

Numerous studies of the laser cutting process have, therefore, dealt with influences of the varying energy input due to deviation in laser-source power in time as well as influence of the accuracy of workpiece guidance, i.e. cutting accuracy, on cut quality. Nuss et al.[1] studied the deviations in the size of round roundels in laser cutting of different steels with a CO₂ laser in pulsating and/or continuous operation. The deviation was gathered with regard to the precision of NC-table control and direction of light polarisation. Tönshoff

Published in: E. Kuljanic (Ed.) *Advanced Manufacturing Systems and Technology*,
CISM Courses and Lectures No. 406, Springer Verlag, Wien New York, 1999.

and Samrau [2] and Bedrin [3] investigated the quality of the cut by measuring the roughness at varying laser source power and varying workpiece speeds. They also studied the quality of the cut while changing the optical system focus position with respect to the workpiece surface. Thomassen and Olsen [4] studied the effects produced on the quality of the cut by changing the nozzle shape and oxygen gas pressure. Theoretical investigations of temperature in the vicinity of the cutting front were carried out for gas welding by Rosenthal [5] and for laser cutting by Rykalin et al. [6], Schuöcker [7], and Arata et al. [8]. Rykalin analysis was limited to a circular laser source, such as Gaussian source, and to the determination of the temperature on the surface of the cutting front. Olson [9] very carefully analysed the cutting front for which he plotted isothermal lines and then determined the thickness of the molten and heat affected layers of the workpiece material. One of his important findings is that in case of a high temperature gradient, a thin layer of the molten and heat affected material and a small thickness of the heat affected zone are obtained, which assures a good and uniform quality of the cut.

2. EXPERIMENTAL PROCEDURES

Experimental testing was carried out on a laser machining system ISKRA-LMP 600 with a laser power of up to 600 W and with a positioning table speed from 2 to 50 mm/s. A CO₂ laser with Gaussian distribution of light-radiation intensity in the continuous laser beam was used. In laser cutting, cutting oxygen, which permits development of exothermic reactions, was also supplied coaxially to the laser beam. In laser cutting, oxygen was supplied as auxiliary gas. The investigations were carried out by applying a commonly used austenitic stainless steel alloyed with chromium and nickel 18/10 designated A276-82A according to ASTM standard. In order to study the processes in the cutting front and investigate the quality of cut, certain parameters were selected as process constants and other parameters as process variables. Steel is frequently used in chemical processing industry, which requires extraordinary chemical resistance of steel. This kind of steel is frequently an object of investigation in laser cutting since in the remolten and heat-affected layer chemical as well microstructure changes occur and consequently chemical resistance of the steel concerned reduces. By common processes of thermal cutting of high-alloy steels it is difficult to ensure the desired quality of the cut due to a too-low average temperature in the cutting front. In laser cutting, however, oxygen as an auxiliary gas ensures higher average temperatures in the cutting front due to additional exothermic reactions and a highly concentrated laser beam. Plates having a size of 100 x 100 mm² and different thicknesses, i.e. 0.5 - 0.8 - 1.0 - 1.5 mm, were selected as samples for cutting. Machining conditions were selected with regard to a large range of material thicknesses of the samples. Several constant parameters were selected on the basis of some of our previous investigations while other parameters were varied [10-12].

The constant parameters were the following:

- laser power $P = 450\text{W}$
- focal distance of the lens $f = 63.5\text{ mm}$
- focal point/sample-surface distance $z_f = 0.0\text{ mm}$

- nozzle/sample-surface distance $z_n = 2.0$ mm
- nozzle diameter $d_n = 2.0$ mm.

In the selected interval of cutting speeds, i.e. between 25 and 50 mm/min, a linear selection of four cutting speeds for each material thickness was made. Pressure of the auxiliary gas was varied from 2.0 to 5.5 bar, namely by steps 2.0 - 3.0 - 4.0 and 5.0 bar. With regard to the size of the outlet nozzle changes in pressure of the auxiliary gas entailed changes in oxygen flow from 20 to 84 l/min. Changes in the oxygen flow and pressure affected intensity of the exothermic reactions in the cutting front and ejection of the melt and oxides from the cutting front.

3. EXPERIMENTAL RESULTS

In practice the usual procedure is first to assess the cut quality visually. For more detailed assessment numerous researchers describe cut quality by measuring roughness at various points of the cut and their geometrical characteristics. An analysis of macrogeometry of the laser cut may first be made by visual assessment of the cut surface. Visual assessment of the cut may often be very subjective and dependent on criteria of individual assessors and their theoretical knowledge of laser cutting. Because of subjective influences of individual assessors it is recommended to prepare a suitable classification of individual cut characteristics by which to classify them easier and in more detail. Surface topography of the laser cut is most frequently assessed by the standard criteria which are taken into account in quantitative assessment. Practical experiences and results of such systematic assessment of cut quality confirm that such a line of work may be efficient when equal or similar material thicknesses are used. For a demonstration the samples were only partially cut with a laser beam to permit an insight into the cut gap throughout the sample thickness. A step-by-step removal of the sample material along the cut by means of a special, very fine device with a diamond disc made it possible to measure geometrical characteristics of the cut with a measuring microscope with low magnification. Such a technique of preparation of the samples permitted a description of the laser cut in terms of the size and shape of the gap between the left and right faces of the cut. The cuts are extremely accurate and of high quality. A peculiarity is the lower part of the cut where in some cases a slightly groovelike shape containing oxides is obtained. Although a particularly wide range of cutting speeds was selected, it may be stated that with almost all cutting speeds high-quality cuts were obtained. The macrogeometrical analysis of the laser cut is specified by DIN 2310 and includes measurement of the following geometrical characteristics:

- lower laser-cut width,
- upper laser-cut width,
- burr width,
- burr height,
- depth of the heat-affected zone.

The microgeometrical analysis permits a description of a technical surface by means of measurement of the surface profile. This permits determination of various parameters for the description of cut-surface roughness. Deviation of the ideal or theoretical surface from the actual cut surface is an offsize. The deviation of the actual laser-cut surface from the theoretical one is determined by the parameters of roughness and striations. For the microgeometrical description of cut roughness the following were selected:

- measurement of the mean arithmetical roughness R_a ;
- measurement of the mean roughness height R_z ;
- measurement of the maximum roughness height R_y .

The laser-cut surface may be assessed visually and on the basis of the measured parameters of cut roughness. A uniform and sufficiently accurate description of the laser-cut surface may be obtained by measuring the microgeometry of the surface profile at the cut point selected and further digitization of data on the surface profile which permit the determination of individual, well comparable parameters of surface quality. A further description of the cut characteristics includes standard data on the condition of the surface and surface layer, which is in technical terminology referred to as “surface integrity” [6,7]. With the cut surfaces concerned it is usually sufficient to analyse the through-thickness microstructure of the material, i.e. the microstructure in the direction of the remolten and heat-affected zone, and measurement of microhardness at various cut points determined in advance. Owing to extreme conditions in fast heating and fast cooling of the material in the cutting front in laser cutting, the following processes occur:

- melting and oxidation of the material in oxygen cutting,
- ejection of the melt and oxides from the cutting front in oxygen cutting,
- resolidification of a thin surface layer called “remolten layer”,
- diffusion processes inside the remolten and heat-affected layer,
- persistence of oxides at the bottom of the edge of the cut.

In dealing with cutting edges one is usually content with a through-thickness analysis of the microstructure of the material, i.e. the microstructure in the direction of the remolten and heat-affected zone, and measurement of microhardness at various cut levels. With thinner samples the analysis was limited to the upper and lower thirds of the cut while with thicker materials it was made at three levels, i.e. additionally in the middle of the cut. That is to say that with thicker samples another level in the middle of the material had to be added, which is in agreement with the surface macroanalysis and the analysis of the remolten and heat-affected zone.

Fig. 1 shows microstructure of austenitic steel 18/8 with a sample thickness of 1.5 mm. As to the macrostructure of the latter the cut is very nice and smooth but with a non-uniform thickness of the remolten zone. A change in microstructure at the lower part of the cut, where there is a higher temperature due mainly to the presence of the melt and oxides, is strongly emphasized [12].

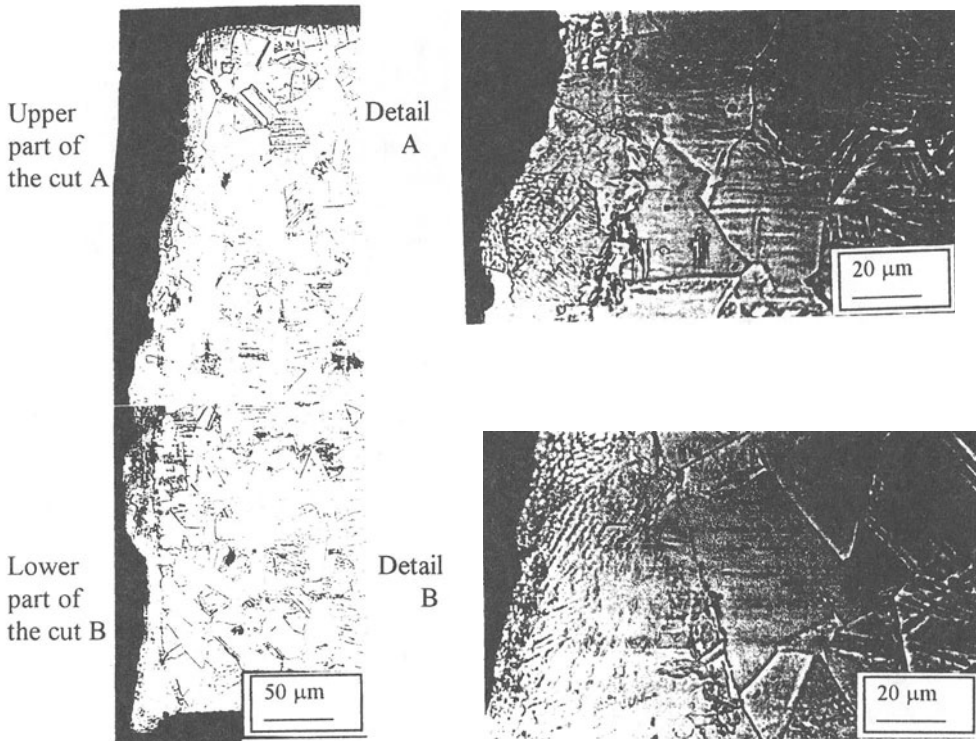


Fig. 1: Micrograph of the remolten and heat-affected zone with a sample thickness of 0.5 mm and cutting speed of 50 mm/s.

In addition to heat effects of the laser beam there are to be found even stronger thermal influences due to chemical reactions between the melt and oxygen as the auxiliary gas and a hydrodynamic influence of the overpressure of oxygen in the molten material inside the cutting front. The upper part of the cut is cooled by the directed oxygen flow while oxygen at the lower part of the cut is consumed to a great extent in combustion of iron, chromium, nickel, titanium and other steel constituents. In the remolten state, with the thin samples a very fine microstructure is obtained due to high velocities of heat removal while with the thick samples columnar crystals are obtained. The microstructure in the thin layer formed is again austenitic, with characteristics found after remelting and fast cooling.

The research work on the description of cut quality can be presented by three different but complementary criteria, i.e.:

- first criterium: macrogeometrical characteristics of the cut,
- second criterium: changes in through-thickness microhardness perpendicular to the cutting front,
- third criterium: microstructure condition at different cut levels complemented by microchemical analyses of the cut surface and the remolten and heat-affected zone.

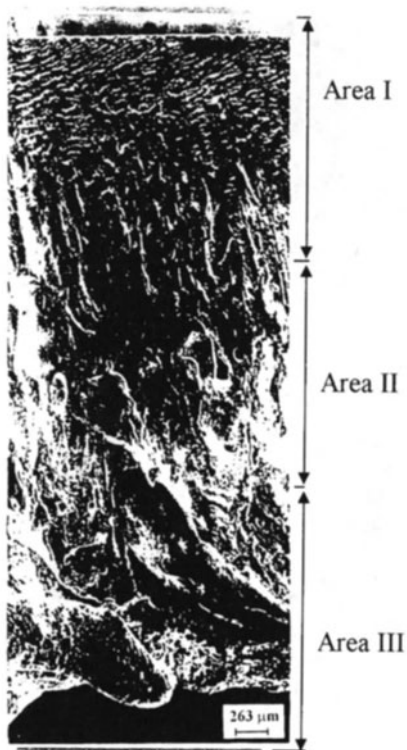


Fig. 2: SEM - Micrograph of the cut surface on stainless steel with a sample thickness of 2.5 mm with a cutting speed v of 13.3 mm/s.

Fig. 2 shows SEM photographs of cut surface topography of a plate with 2.5 mm in thickness obtained with a cutting speed of 15 mm/s. The topographic photograph shows three characteristic areas, which are indicated at the figure by three characteristic cut shapes, i.e. area I (upper part of the cut), area II (middle part of the cut), area III (lower part of the cut).

In Area I extremely high temperature gradients are obtained; therefore, a relatively fine surface, which is rather smooth and has a low level of roughness, is obtained. Area II has a lower temperature gradient; therefore, thermal effects and consequently surface striations are more expressed. In the observation of the cut surface, the directed orientation of striations, which may be described by increased surface roughness with regard to Area I, is very important. In Area III or at the lower part of the cut there is the lowest temperature gradient, which contributed to important increase in striation generation; therefore, the surface at the lower part is essentially rougher.

An increased heat concentration which produces strong overheating of the material at the lower part of the cutting front when there is a flow of oxygen, which produces ejection of a larger mass of the melt than in the middle or upper part of the cut, also contributes to strong striation generation. Moreover the directed orientation of striations at the lower part of the cut indicates the flow of the melt and oxides from the cutting front. This macrograph permits determination of the cutting-front inclination during cutting, which indicates cutting of a sample at the upper cutting-speed limit.

The electronic micrographs of an inclined laser cut (Fig. 3) shows roughness of the cut surface and the oxides present magnified 300-times. The specific X-photographs for Fe, Cr, Ni, Mn and Si show a uniform concentration of individual elements in the oxides, except for iron and chromium. The vicinity of the remolten layer in the oxides is poor in iron and chromium. Particular X-photographs for chromium show that on the oxide surface in the groove there is an increased concentration of chromium. This indicates that owing to a very fast cooling process diffusion of chromium from the remolten layer to the

surface oxide layer in the groove occurred. Powell [13] states that owing to diffusion of chromium from the molten layer to the oxide containing groove the concentration of chromium in the vicinity of the remolten layer reduces. He also states that the thickness of the layer with a reduced concentration in chromium in the remolten layer may be even 50 to 100 μm thick. Unfortunately from the above-mentioned specific X-photographs for chromium this cannot be confirmed although an increased concentration in chromium was observed in the oxide containing groove in the remolten layer. The oxide area on the cut surface has a shape of a continuous layer. In some cases the melt and the oxides merge at the bottom of the edge which is referred to as their burr.

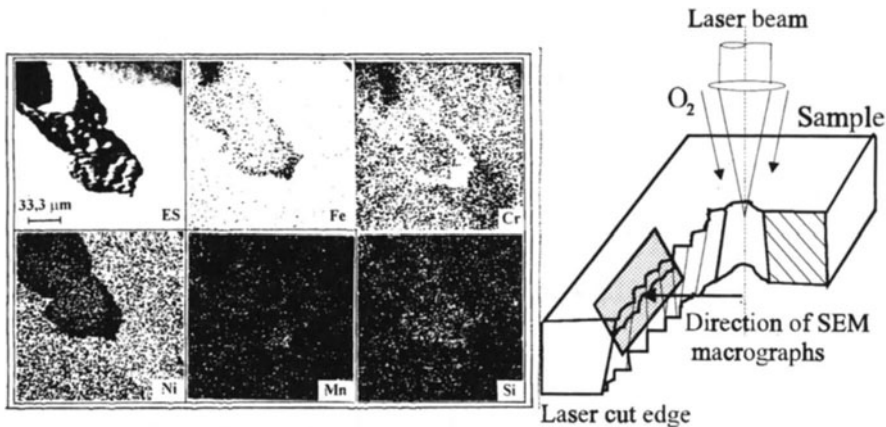


Fig. 3: Microchemical analysis of the laser cut edge on austenitic stainless steel with a sample thickness of 0.6 mm at a laser speed of 33.33 mm/s.

4. CONCLUSIONS

The investigations conducted on macrostructure and microstructure of the cut surface and the surface layer perpendicular to the cutting direction confirm extreme efficiency of cutting, particularly of austenitic stainless having a small thickness. The laser system is reliable enough and has such optical and kinematic properties that it permits good adaptability of machining conditions to different kinds and thicknesses of materials.

The macroanalysis of the cut surface is often very efficient in assessment of laser-cut quality. The visual assessment also permits efficient assessment of the cutting process and, consequently, its optimization. A too-low heat input into the cutting front is indicated first by distinctive curvedness of the cutting front at the lower part of the cut and by increased striation generation at the cut surface. With the highest cutting speeds distinctive and uniform striations generate only at the upper part of the cut while they disappear at the lower part of the cut, which confirms distinctive changes in the process of ejection of the melt from the cutting front. The cut surface at the lower part of the cut is rough and nonuniform when the thickness of the remolten layer is increased and the oxide containing grooves are present. In these cases a conclusion may be drawn that the cutting speed was

considerably higher than optimum cutting speed, which is indicated also by the direction of ejection of the melt and the oxides from the cutting front as well as by the presence of oxide containing grooves in the remolten layer.

Since we want to make a collection of data which would make possible determination of optimum cutting conditions in laser cutting of various kinds and thicknesses of materials, additional experimental investigations had to be conducted in order to establish critical cutting speeds. The experimental results and experience in assessment of laser-cut quality obtained to this day confirm that the critical cutting speed is a very reliable parameter of optimization of laser-cutting.

REFERENCE

- [1] Nuss R., Biermann S., Geiger M.: Precise Cutting of Sheet Metal with CO₂ Laser, Laser Treatment of Materials, Ed.: B.L.Mordike, Deutsche Gessellschaft für Metallkunde, Oberursel, Germany, 1987, 279 -288.
- [2] Tönshoff H. K., Semrau H.: Effect of Laser Cutting on the Physical and Technological Properties of the Surface of Cut, Laser Treatment of Materials, Ed.: B.L. Mordike, Deutsche Gessellschaft für Metallkunde, Oberursel, Germany, 1987, 299 -308.
- [3] Bedrin C., Yuan S. F., Querry M.: Investigation of Surface Microgeometry in Laser Cutting, Annals of CIRP, vol. 37, no. 1, 1988, 157 -160.
- [4] Thomssen F. B., Olsen F. O.: Experimental Studies in Nozzle Design for Laser Cutting, Proc. of the 1st Int. Con. on Laser in Manufacturing, Brighton, UK, 1983, Ed.: M. F. Kimm, 169 -180.
- [5] Rosenthal D.: Mathematical theory of heat distribution during welding and cutting, Welding Journal, 20, 1941, 5, 220-225
- [6] Rykalin N., Uglov A., Kokora A.: Laser machining and welding, Mir Publishers, Moskow, 1978
- [7] Schuöcker D.: The physical mechanism and theory of laser cutting, Industrial Laser Annual Handbook, PennWell Publ., Tulsa, 1987, 65 - 79
- [8] Arata Y.: Dynamic behavior in laser gas cutting of mild steel, Transactions of JWRE, 8, 1979, 2
- [9] Olsen F.: Cutting front formation in laser cutting, Annals of CIRP, 37, 1988, 2, 15 - 18
- [10] Grum J., Zuljan D.: Thermal Response Analysis of Laser Cutting Austenitic Stainless Steel, AMST '96, 4th Int. Conference on Advanced Manufacturing Technology, Udine, Italy, 1996, 495-502.
- [11] Grum J., Zuljan D.: Estimation of the Quality of Cut after Laser Cutting Austenitic Stainless Steel, 6th European Conference on Laser Treatment of Materials, Edited by: F. Dausinger, H. W. Bergmann, J. Siger, ECLAT '96, Stuttgart, Germany, 1996, vol. 2, 1007-1016.
- [12] Grum J., Zuljan D.: Analysis of Heat Effects in Laser Cutting of Steels, Journal of Materials Engineering and Performance, Volumen 5, No 4, August 1996, 526-537
- [13] Powell J.: CO₂ Laser Cutting, Springer-Verlag, London, 1989, 61-63.

A STUDY ON THE CORRELATIONS BETWEEN MACHINING PARAMETERS AND SPECIMEN QUALITY IN WEDM

C. Borsellino and L. Filice

University of Palermo, Palermo, Italy

F. Micari

University of Calabria, Arcavacata di Rende (CS), Italy

V.F. Ruisi

University of Palermo, Palermo, Italy

KEY WORDS: Wire EDM, Material Removal Rate, Roughness

ABSTRACT: Wire electrical discharge machining (WEDM) is widely used in manufacturing, medical, aircraft applications and, virtually, all areas of conductive material machining. The process involves a series of very complex electrical, thermodynamical and electromagnetical phenomena that are still partially unknown. Due to the large amount of parameters involved in the process, a suitable set-up of the variables aimed to obtain the best performance is often very difficult. In the paper the results of a wide experimental analysis are presented: the tests were carried out on high-speed steel and tempered steel specimens utilising brass wires. The influence of the most important process parameters on the material removal rate and on the roughness of the machined surfaces was investigated.

1. INTRODUCTION

Amongst the non-conventional technologies, Electrical Discharge Machining (EDM) is nowadays assuming particular importance in industrial applications. The process is characterised by the erosion of the workpiece material due to a large amount of discrete sparks between the workpiece and the electrode, both immersed in a liquid dielectric

medium. The sparks, in fact, melt and vaporise each time a small amount of the workpiece material which is subsequently removed by the dielectric.

EDM is usually classified into die-sinking EDM, in which the tool shape is reproduced on the workpiece, and wire EDM (WEDM); in this case the shape of the obtained profile depends on the relative movement of the wire and the workpiece.

WEDM is mostly utilised in the die machining industries. Nevertheless the fields of applications of this technology have grown more and more since it was firstly applied about twenty years ago: nowadays, in fact, WEDM is largely utilised in the aircraft, aerospace and medical industries, as well as for high-strength materials cutting and for other precision machining applications.

All these industrial applications fully justify the interest of several researchers all over the world. Currently their attention is mostly focused on the achievement of a higher machining productivity, on the introduction and enhancement of automation in WED machines and, finally, on the improvement of machining accuracy and quality of the machined surface [1,2]. Furthermore, a substantial improvement of the cutting conditions was achieved through the development of innovative wire materials [3]. Based on the experience of die-sinking EDM, the former electrodes were made of copper, which is an excellent conductor. However, under the electro-thermal phenomena that occur during WEDM, copper wears rapidly. In addition its tensile strength is rather poor so that only a limited mechanical tension can be applied on the wire: therefore machining instabilities arise due to a high amount of short circuits. A brass alloy wire (consisting of 63% copper and 37% zinc) was introduced in the early 70s in order to improve cutting speed. Indeed brass, although it is a worse conductor than copper, permits to increase the tension applied on the wire reducing the amount of abnormal sparks.

It is worth noticing that sparks can be classified into three groups [2]: normal sparks, in which ignition delay times are required for the proper generation of effective discharges, arc pulses which do not present any ignition delay time when the gap current is established and short circuits, due to metal bridges between the wire and the workpiece. Usually normal sparks provide better surface roughness and machining stability than arc pulses.

Further improvements of the tensile properties of brass wires were obtained by the addition of 2% aluminium. The resulting alloy possesses a higher tensile stress (over 900MPa).

Finally in the recent years coated wires, composed of a brass core coated with a zinc layer 20-30 μm thick, were introduced [3]. Since the external coated layer of these electrodes is characterised by a lower melting temperature than the core material, when a spark occurs the wire coating is overheated and subsequently evaporated. In other words, the so-called "heat-sink" effect is obtained and thus a cooling of the core material is achieved. By this way the process efficiency is improved, as the cutting speed increases by up of 50%.

Actually the development of an effective WEDM model represents a very difficult aim, since the process involves a large number of complex electrical, electromagnetic and thermodynamical phenomena. Furthermore the model should take into account the influence of a very large amount of process parameters, among which the gap voltage, the pulse current, the pulse-on and the pulse-off time, the wire material and geometry, the mechanical tension on the wire and finally the wire feed speed are the most relevant.

In the paper the authors present the results of a wide experimental investigation on WEDM: in particular such technology was utilised to cut a hard high-speed steel and a tempered steel. The most relevant results in terms of material removal rate and surface roughness at varying some of the most important operating parameters are presented and discussed in detail.

2. THE EXPERIMENTAL TESTS

2.1 Set-up of the experiments

All the tests were carried out on an AEG Electrical Discharge machine. Actually such facility was originally designed and built for die-sinking EDM and has been subsequently modified and equipped for wire EDM. The machine permits to tune the gap voltage into 4 different levels (60-250V), as well as the current peak (maximum 30A), the pulse-on and the pulse-off time. Furthermore the dielectric flux rate, the wire feed velocity and the tensile load on the wire can be selected into a wide range.

Two different materials were utilised in the tests, namely a typical High-Speed Steel with 10% Cobalt content and a tempered steel 38NiCrMo4K. In both cases prismatic rods with rectangular section (width=10mm, height=30mm) were cut. In particular the cutting direction was along the height of the specimen.

As far as the wire material is concerned, several different brass wires were taken into account, characterised by different diameters (0.25 and 0.30mm) and ultimate tensile strength: in particular both soft wires (i.e. $\sigma_R=490\text{Mpa}$) and high strength wires (i.e. $\sigma_R=900\text{Mpa}$) were utilised in the tests.

2.2 Design of the experimental plan

The selection of the process parameters to be investigated, as well as of the output variables to be monitored, has represented a basic task in this research. In particular, after a set of preliminary tests, the plan of experiments reported in the following table was established.

Table 1. Investigated parameters

Pulse-on time [μs]	4			6				10		
Pulse-off time [μs]	9	10	12	13	14	16	18	22	25	31
Stress on the wire [MPa]	130			200				270		

Three different levels were fixed for the pulse-on time, ten levels for the pulse-off time and, finally, three levels for the tensile stress applied on the wire.

The values were selected according to the tuning capabilities available on the machine. It is worth pointing out that the number of pulse-off time levels was very high in order to investigate the influence of the duty factor over a wide range of variation: the duty factor is defined as: $DF = \text{pulse-on time} / (\text{pulse-on time} + \text{pulse-off time})$.

On the other hand the gap voltage (135V) and the wire feed velocity (9m/min) were maintained constant all over the tests. As far as the output variables are concerned, the

3. DISCUSSION OF THE RESULTS

In this paragraph the attention is focused on the influence of some of the most relevant process parameters on the monitored outputs, i.e. the material removal rate and the surface roughness. It is necessary to outline that such influence has been investigated by varying each time only the considered process parameter and keeping unchanged all the other ones.

3.1 The duty factor

First of all the influence of the duty factor was investigated. This parameter, in fact, indicates the percentage of the active spark time over the total time between two

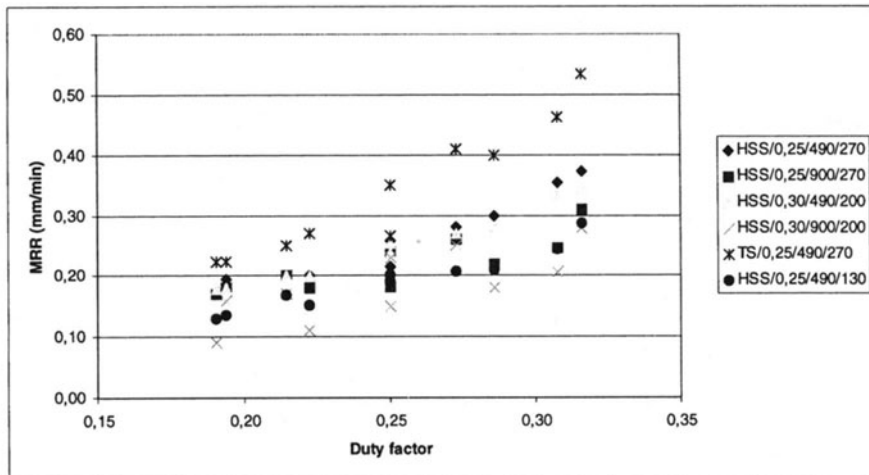


Fig. 1

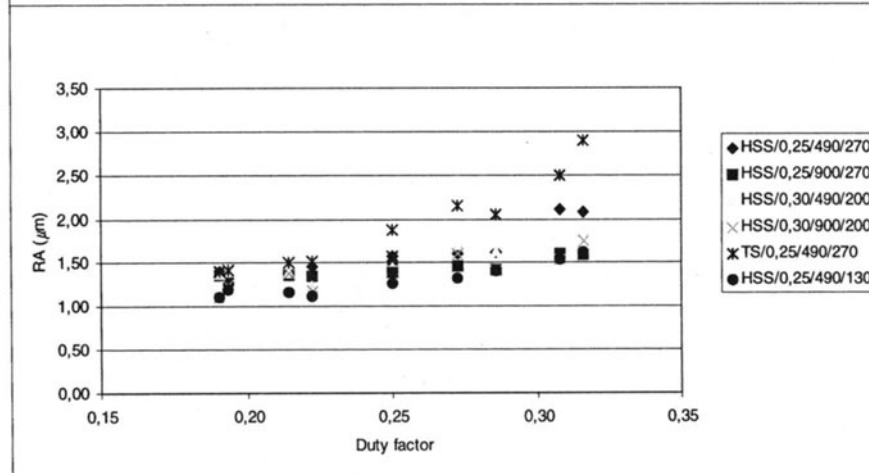


Fig. 2

subsequent sparks, and thus strongly affects the process. Fig. 1 and 2 show that, at increasing the duty factor, a substantial increment of the material removal rate for both the

considered materials is achieved; unfortunately such result occurs together with a relevant worsening of the surface roughness.

The increment of the pulse-on time with respect to the total spark time (pulse-on time + pulse-off time) determines, in fact, an increment of the energy supplied to the material. As a consequence, even if a larger amount of abnormal sparks may occur, the total volume of melt and vaporised material increases. In other words, at increasing the duty factor a progressive movement from roughing to finishing conditions is obtained.

3.2 The pulse-on time

The pulse-on time plays a role on the process mechanics very similar to the one previously described for the duty factor. The analysis of the results reported in Tables 2 and 3, shows in fact that at increasing the pulse-on time, both the material removal rate and the surface roughness increase. At each spark a larger amount of energy is transmitted to the workpiece, and thus larger craters are eroded on the surface.

Actually wire rupture represents a strong limitation to the increment of the pulse-on time. The wire in fact, depending on the diameter and on the material, breaks if the energy grows up to a limiting value. Such risk may be reduced increasing the wire feed velocity.

3.3 The tensile stress applied on the wire

The importance of the tensile stress on the wire during WEDM has been pointed out by several researchers and represents the fundamental reason for the development and application of new wire materials as already described in the introduction.

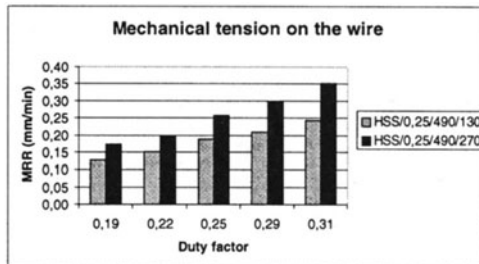


Fig. 3

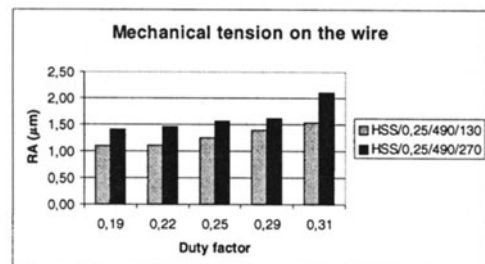


Fig. 4

The fig. 3 and 4 report the results obtained cutting high speed steel with the same brass wire (diameter 0.25mm, $\sigma_R=490$ MPa), but applying two different levels of the tensile stress. It can be easily noticed that, at increasing the tensile stress from 130 to 270 MPa a relevant increment of the material removal rate is achieved, even if, again, the surface roughness undergoes a certain worsening.

These effects can be justified, taking into account that a higher mechanical tension reduces the deflections of the wire due to the electromagnetic forces, as well as the vibrations during the cutting phenomenon. As a consequence, the number of short circuits decreases and the number of normal sparks increases.

3.4 Properties of the wire: ultimate tensile strength and diameter

The considerations reported in the previous point 3.3 justify the development of new wire materials characterised by a higher ultimate tensile stress. In fact the advantages obtained through the application of a higher tensile stress on the wire compensate the worse electrical properties of new materials with respect to the former copper or soft brass wires. On the other hand, if the available WED machine does not permit to increase so much the tensile stress applied on the wire, the use of traditional wires is still more convenient. These considerations are confirmed by the tests reported in figg. 5 and 6. The tests were carried out on high-speed steel, utilising two different brass wires (a soft brass wire with $\sigma_R=490$ MPa and a high strength wire with $\sigma_R=900$ MPa) and applying the maximum tensile stress available on the machine, i.e. 270 MPa.

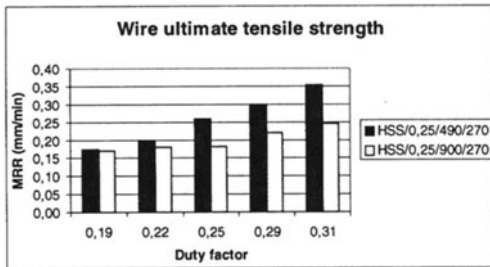


Fig. 5

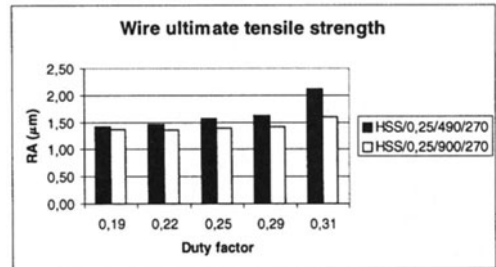


Fig. 6

The obtained results show that with this value of the tensile stress the worsening of the electrical properties has a dominant effect, making most suitable the use of the soft wire. A further set of experimental tests concerned the influence of the wire diameter. In particular the tests were carried out on soft brass wires with a diameter equal to 0.25 or 0.3mm. Actually the effect of the diameter is strictly connected with the tensile stress one. Figg. 7 and 8 report the results obtained applying respectively a tensile stress equal to 200 MPa on the wire with a diameter of 0.3mm, and a tensile stress equal to 130 or 270 MPa on the thinner wire. The thicker wire permits a higher MRR only with respect to the less loaded thinner wire: such result permits to conclude that the use of thicker and more expensive wires is justified only if the available machine permits heavier electrical parameters. Such circumstance occurs, for instance, on some WED machines of the last generation, which allow pulse intensities up to 500A [3].

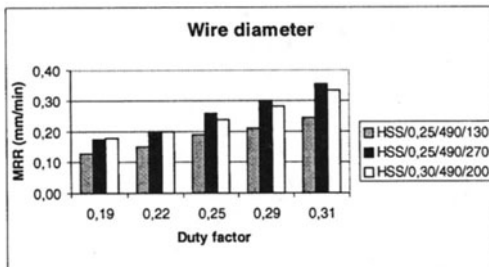


Fig. 7

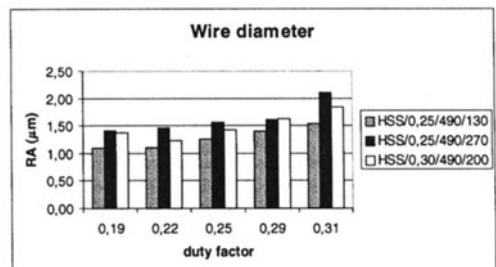


Fig. 8

3.5 Workpiece material

Most of the tests were carried out on a high-speed steel with a 10% Cobalt content, whose hardness has been measured equal to 62HRC. Other tests were performed on the tempered steel 38 NiCrMo4K.

Figs.9 and 10 show that the tempered steel permits a higher removal rate.

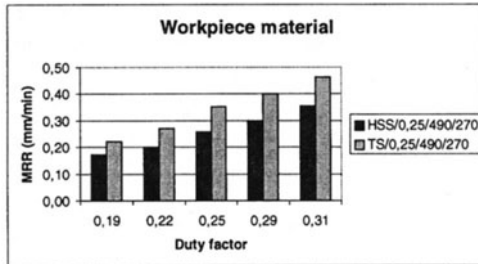


Fig. 9



Fig. 10

Some further interesting considerations can be derived from the SEM analysis of the machined surfaces: the HSS specimen shows a more regular crater distribution, with craters characterised by lower depth and extension (fig.11). The craters are, on the contrary, larger and deeper on the tempered steel specimen (fig.12). These micro-geometrical aspects are confirmed by the surface roughness measurements, which have furnished a value of RA for the tempered steel larger than the HSS one.

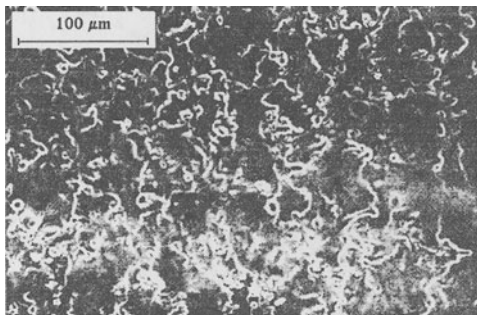


Fig. 11

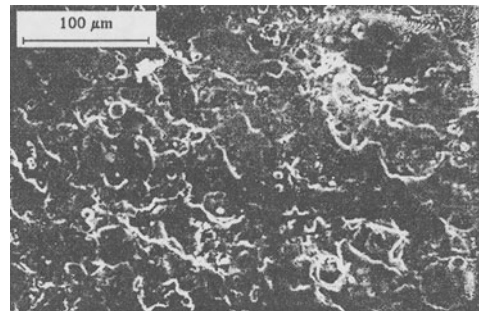


Fig.12

REFERENCES

1. Dauw, D.F., Albert, L.: About the Evolution of Wire Tool Performance in Wire EDM, *Annals of the CIRP*, 41 (1992) 1, 221-225
2. Van Coppenolle, B., Dauw, D.F.: On the Evolution of EDM Research. Part 1: Modeling and Controlling the EDM Process, *Proceeding International Symposium for Electromachining 1995*, 117-131
3. Prohaszka, J., Mamalis, A.G., Vaxevanidis, N.M.: The Effect of Electrode Material on Machinability in Wire Electro-Discharge Machining, *Int. Jnl of Mat. Proc. Technology*, 69 (1997), 233-237

RESIDUAL STRESSES AFTER LASER SURFACE REMELTING

J. Grum and R. Sturm

University of Ljubljana, Ljubljana, Slovenia

KEY WORDS: Remelting, Residual Stresses, Nodular Iron

ABSTRACT: The measurement of residual stresses is very important in exacting dynamically loaded machine parts which have been subjected to different kinds of heat treatment. In designing parts designers very frequently demand the presence of compressive residual stresses after heat treatment and finish grinding of the surface, since this increases the fatigue strength of the material and reduces the danger of fracture. In this investigation of the residual stresses after laser surface remelting, the size and variation of residual stresses were measured as a function of the modified layer depth on flat specimens from nodular iron. Optimal laser remelting conditions were chosen, while only the way of guiding the laser beam over the surface of flat specimens was varied. To measure the residual stresses, the relaxation method was used, including gradual electro-chemical removal of the modified layer in which the deformation of the specimen was measured by resistance strain gauges.

1. INTRODUCTION

Nodular iron is widely used in engineering practice because of low price of the material, good castability and good machinability desirable in the finalization of parts. To increase the wear resistance of the surface of nodular iron parts, a number of heat treatment procedures had been used in industrial applications [1,2]. An advantage of heat treatment procedures is that they achieve desirable structural changes in the modified layer improving the wear and corrosion resistance. Among important of heat treatment procedures we should mention also laser surface melt-hardening [3,4]. The heating up of the workpiece surface material by the laser beam is done very rapidly. The conditions of heating-up can be changed by changing the energy density and relative motion of the

Published in: E. Kuljanic (Ed.) *Advanced Manufacturing Systems and Technology*,
CISM Courses and Lectures No. 406, Springer Verlag, Wien New York, 1999.

workpiece and the laser beam. In surface remelting of cast irons, we have to achieve melting of the material on the surface and austenitization beneath it, followed by rapid cooling down through heat conduction into the cold material. To create a ledeburitic and martensitic structure, the required critical cooling rate has to be exceeded. In laser surface remelting this can be achieved without any additional cooling and is called self-quenching. The properties of the modified layer depend on the microstructure prior to heat treatment and on the amount of energy input transferred into the surface layer of the workpiece. The research work was focused into the study of residual stresses after laser surface remelting of nodular iron.

2. EXPERIMENTAL PROCEDURE

For the experimental laser surface remelting we used a CO₂-laser with a Gaussian power distribution having a maximum power of 1.5 kW which can be suitably adjusted. The experiments were made at a laser source power of 1 kW, defocussing degree from 22 to 34 mm and focal length of the lens 127 mm. The laser beam diameter D_b on the workpiece surface was in the range between 3.3 and 5.1 mm. The workpiece travelling speed was from 15 to 21 mm/s. The absorptivity of the workpieces for the laser light with a wavelength of $\lambda = 10.6 \mu\text{m}$ was increased by an absorption coating of Zn-phosphate. In the tests nodular iron 500-7 (ISO) with ferrite-pearlite microstructure was used. The tests were made with optimal laser treatment conditions so that a 0%, 15% and 30% overlapping of the remelted layer were ensured. By overlapping remelted layer, we achieved a fully and uniformly remelted workpiece surface and a desired depth of the modified layer. The dimensions of the workpieces were adapted to the chosen melt-hardening procedure and the requirements of subsequent residual stress measurements. Figure 1 shows the laser beam guidance on the workpiece and the workpiece dimensions.

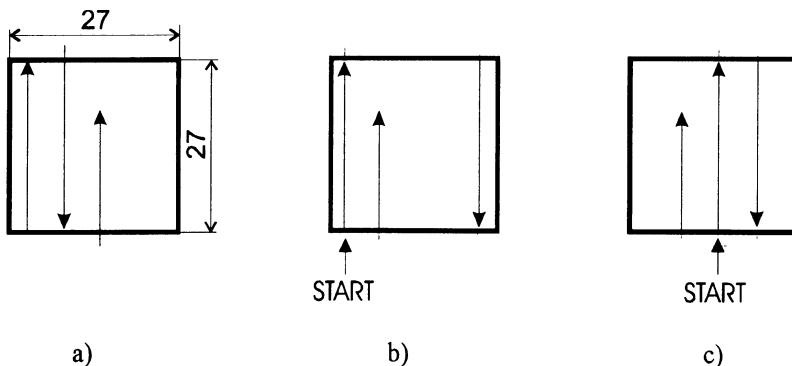


Figure 1. Workpiece geometry and different ways of laser beam travel in laser surface remelting.

3. EXPERIMENTAL RESULTS

3.1 MICROSTRUCTURE

The structure changes in the laser surface remelting of the cast iron are dependent on temperature conditions during surface layer heating and cooling. In all the cases of laser

surface remelting, a modified layer was obtained consisting of characteristic microstructure layers, i.e.: remelted layer and hardened layer [5].

REMELETED LAYER. The structure of the remelted layer is affected by the cooling rates and degree of graphite dissolution in the melt. Because of a short interaction time, the graphite dissolving in the melt is incomplete and may be brought to the surface due to the buoyancy and dynamic forces. The graphite on the surface of the melt may evaporate due to intensive heat or may be blown away by a jet of protective gas. Therefore the carbon content of the liquid may be less than overall carbon content of the alloy, which has an effect on the formation of different structures. By diffraction X-rays [5] in the remelted layer and by means of optic microscopy, it was found that the remelted zone consists of austenite dendrites, ledeburite and martensite and undissolved graphite. The austenite dendrites grow during rapid solidification of the remelted layer in the direction towards the surface, which corresponds to the direction of heat removal.

HARDENED LAYER. In the hardened layer only solid state transformation can be noted. During heating the basic pearlite structure transforms into austenite which in cooling, transforms into martensite with some residual austenite. Ferrite microstructure stays as ferrite.

3.2 MICROHARDNESS

The results of microhardness measurements have confirmed the structure changes in the material and have shown that laser surface remelting can be a successful method [5]. The hardness of the base material in soft state ranges between 200 to 250 HV₁₀₀ and after laser treatment increases onto 800 to 950 HV₁₀₀ in the remelted layer and onto 600 to 830 HV₁₀₀ in the hardened layer.

3.3 RESIDUAL STRESSES

The residual stress variation is very much dependent on the conditions present in the process of remelted layer cooling which can be described by the volume percentage of residual austenite and cementite and concentration gradient of the cementite. With the increase of the amount of residual austenite in the remelted layer, there is a great danger that residual internal stresses will change the direction and will transform from compressive into tensile. A surface with tensile internal stresses is, however, much more likely to develop cracks, which may propagate and grow into a catastrophic failure.

The method [6] for measurement residual stresses consists in removing a thin layer of Δh ; thickness on one face of the sample. A new equilibrium stress state is established involving the sample deformation and a new stress distribution. The principle of the present method is to connect measured strains to the residual stresses relaxed by electro-chemical dissolution. The result of the calculation is expected to represent the original residual stress distribution.

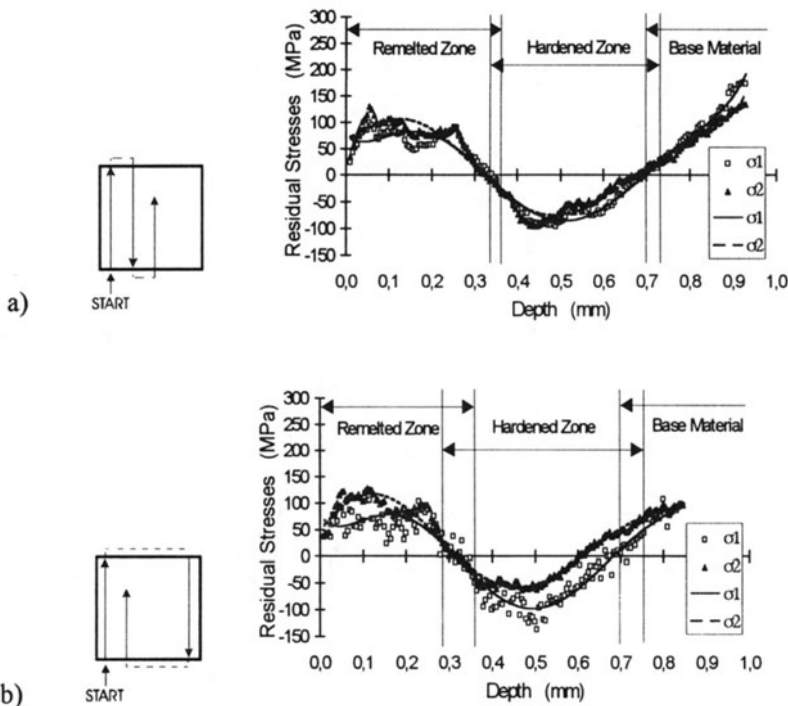
$$\sigma_h^R(j-1,0) = \frac{-(h_{j-1} - \Delta h_j)^2}{2 \cdot (h_{j-1} + 2 \cdot \Delta h_j) \cdot \Delta h_j} \cdot B_j - \sum_{i=1}^{j-1} \left[-3 \cdot \frac{h_{i-1} + \Delta h_i}{(h_{i-1} - \Delta h_i) \cdot (h_{i-1} + 2 \cdot \Delta h_i)} \cdot h_{j-1} + 1 \right] \cdot B_i \tag{1}$$

where

$$B_j = \frac{E}{1 - \nu^2} \cdot (\Delta \varepsilon_{x,j} - \nu \cdot \Delta \varepsilon_{y,j}) \tag{2}$$

E, ν are respectively Young modulus and Poisson ratio, h is the thickness of the sample, Δh the thickness of a layer and $\Delta \varepsilon$ the variation of the microdeformation resulting from layer removal.

Heating and cooling conditions are very much dependent on ways of laser beam travel over the workpiece surface. In Figure 2 we can see the variation of residual stresses as a function of the depth of the modified layer for nodular iron 500-7. Graphs in Figures 2a,2b,2c present two measured curves, i.e. main stresses σ_1 and σ_2 .



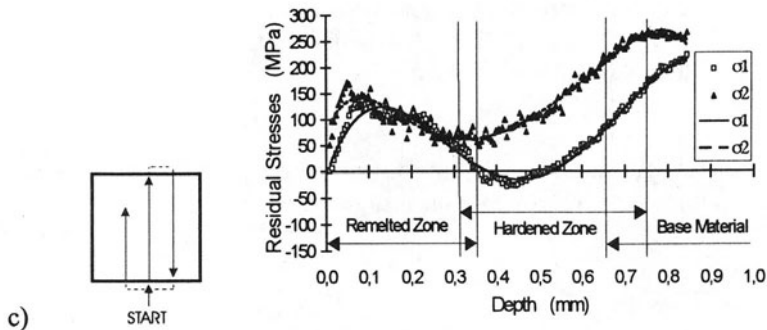


Figure 2. Residual stresses in modified layer of nodular iron 500-7 after different ways of laser beam travel, $P=1$ kW, $z_s=22$ mm, $D_b=3.3$ mm, $v_b=21$ mm/s.

From the graphs we can conclude the following:

- Residual stresses have in all cases of laser beam travel paths a very similar profile differing only in absolute values. In the surface remelted layer, tensile residual stresses were found in a range between 50 and 180 MPa.
- The change from tensile into compressive residual stress takes place in the transition area between the remelted and hardened layer. Maximum compressive residual stress values were found in the middle of the hardened layer in a range between 25 and 150 MPa. But there is one exception. In the case when laser beam travel path starts in the centre of the workpiece (Fig. 2c) no compressive stresses were found.
- The remelted surface layer cracked in the direction of graphite flakes in the gray iron. Our assessment is that during the cooling process, due to high temperature differences, extremely high tensile stresses were generated, exceeding the yield point of the material at increased temperature in the remelted surface layer.

In the cases when the laser beam starts remelting the workpiece surface in the corner of the sample (Figs. 2a and 2b) tensile stresses were found in the remelted layer and compressive stresses in the hardened layer. In the case when the laser beam starts remelting in the centre of the workpiece (Fig. 2c) only tensile stresses were found. The reason for this is in different heating and especially cooling conditions of the workpiece as a whole.

Heating and cooling conditions in a relatively thin workpiece are very much dependent on laser beam power, laser beam diameter on the workpiece surface, interaction time and degree of overlapping of the remelted layers. In Figures 3 and 4 we can see the variation of residual stresses in the modified layer of nodular iron 500-7 as a function of different laser remelting parameters. From the results in Figure 3 we can conclude the following:

- Residual stresses have in all cases at different degrees of overlapping a very similar profile differing only in absolute values. In the surface remelted layer, tensile residual stresses were found in a range between 50 and 200 MPa.

- The change from tensile into compressive residual stress takes place in the transition area between the remelted and hardened layer. Maximum compressive residual stress values were found in the middle of the hardened layer in a range between 25 and 80 MPa.

With laser parameters $P=1$ kW and $D_b=3.3$ mm, degree of overlapping the remelted layers has a very small influence on lowering tensile residual stresses in it.

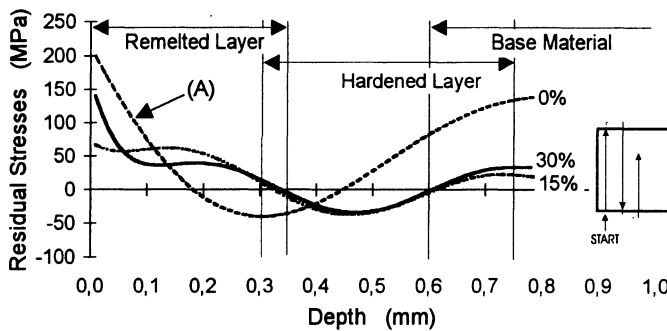


Figure 3. Residual stresses in modified layer of nodular iron 500-7 at different degrees of overlapping of the remelted layers, $P=1$ kW, $D_b=3.3$ mm, $v_b=21$ mm/s.

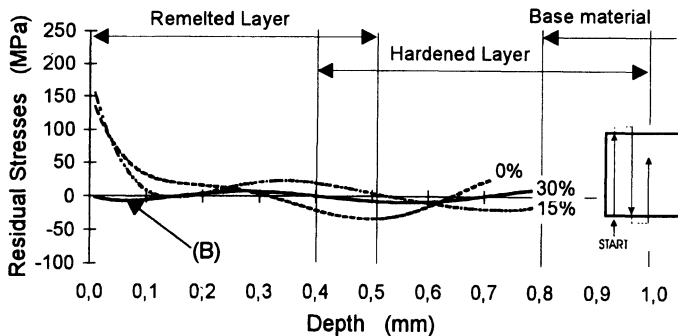


Figure 4. Residual stresses in modified layer of nodular iron 500-7 at different degrees of overlapping of the remelted layers, $P=1.5$ kW, $D_b=5.1$ mm, $v_b=18$ mm/s.

By increasing laser beam power ($P=1.5$ kW) and laser beam diameter on the workpiece surface ($D_b=5.1$ mm) we achieve higher pre-heating. That results in lower cooling gradients which produce such microstructure with almost free residual stresses (Graph B in Fig. 4).

By diffraction X-rays we analyzed the amount of constituents present in the remelted layer. Table 1 presents the results of measured amounts of constituents in the remelted

layer with different laser remelting parameters and different degree of overlapping of the remelted layers.

Table 1. Constituents in the remelted layer in vol. %.

		Overlapping	C_{γ}	$C_{\alpha'}$	Fe_3C	Graphite
Graph A (Figure 3)	P=1 kW $D_b=3.3$ mm	0%	28%	33%	34%	5%
Graph B (Figure 4)	P=1.5 kW $D_b=5.1$ mm	30%	/	55%	42%	3%

From the above results we can conclude that in the case when we are able to produce the remelted surface layer without any residual austenite in the microstructure, tensile residual stresses are minimised. The higher is amount of martensite in the remelted layer, the lower are tensile residual stresses.

4. CONCLUSIONS

On the basis of the results of microstructure analysis and microhardness measurements on the studied nodular iron 500-7, it can be concluded that laser surface remelting can be regarded as a highly successful method for increasing the hardness and wear resistance. With laser remelting procedure a sufficient depth of the modified layer is achieved, in addition to desirable microstructure changes and good microhardness profiles of the modified layer. Great attention has to be given to the selection of laser treatment conditions as different structure of the microstructure matrix can substantially affect the residual stress conductions in the modified layer.

After laser remelting residual stresses are in all the cases of tensile type on the surface and then decrease to the depth of 0.3-0.4 mm when they usually transform into compressive stresses. The relatively great depths of transformation of tensile into compressive stresses confirm that even after fine-grinding it is not possible to achieve the desired stress state in the material with more or less high compressive residual stresses on the surface. The tensile stress state in the surface is possible to achieve with suitable laser beam guidance on the workpiece, which produces the pre-heat treatment effect.

REFERENCES

1. Reinke F.H.: Local Electric Arc Remelting Process for the Generation of Wear - Resistant White Iron Layer on Workpieces of Grey Cast Iron, Especially Camshafts and Cam Followers, AEG Elotherm, Remscheid, 1983

2. Bergmann, H.W., Müller, D., Endres, T., Damascheck, R., Domes, J., Bransden, A.S.: Damascheck R., Domes J., Bransden A.S., Industrial Applications of Surface Treatments with High Power Lasers, materials Science Forum, Volume (1994) 163-165, p. 377-404
3. Bergman, H.W.: Current Status of Laser Surface Melting of Cast Iron, Surface Engineering, Volume (1985) 1, No. 2, p. 137-155
4. Vilar, R., Solgado, F.J., Figuera, Sabino R.: Laser Surface Melting of Cast Iron, Eclat'90, Surface Treatments - Liquid State, (1990) p. 593-604
5. Grum, J., Šturm, R.: Laser Surface Melt-Hardening of Gray and Nodular Iron. Proc. of the Int. Conference Laser Material Processing, Opatija, Croatia, (1995) p. 165-172
6. Hariri, S., Vaucher, R., Flahaut, P., Eyzop, D., Robin, C.: Residual Stresses Measurements by Dissolution Methods, Proc. of the Int. Conference MAT-TEC 96, Paris, France (1996), p. 111-118
7. Yang, Y.S., Na, S.J.: Surface and Coating Technology, Volume (1989) 38, p. 311-324
8. Gravey, D.L., Maiffredy, L., Vannes, A.B.: A Simple Way to Estimate the Level of the Residual Stresses after Laser Hardening, Journal of Mechanical Working Technology, Volume (1988) 16, p. 65-78
9. Grum, J., Žerovnik, P.: Residual Stresses in Laser Heat Treatment of Plane Surfaces, Proceedings of the First International Conference on Quenching & Control of Distortion, Chicago, Illinois, 1992, p. 333-341
10. Guan, Y., Montagnon, J. P., Pantelis, D., Poupeau, Ph., Francois, D.: Laser Surface Treatment of Ferrite-pearlitic Spheroidal Graphite Cast Iron, -Memoires et Etudes Scientifiques Revue de Metallurgie, Volume (1990) 87, No. 1, p. 21-32
11. Grum, J. and Šturm, R.: Characteristics of Laser Surface Melt-Hardening and Possibilities of Optimizing the Process, Proceedings of the 2nd Int. Conf. on Quenching and The Control of Distortion, Cleveland Marriot Society Center, Cleveland, Ohio, USA, (1996), p. 193-200
12. Grum, J., Šturm, R., Žerovnik, P.: Measurement and Analysis of Residual Stresses After Laser Hardening and Laser Surface Melt-Hardening on Flat Specimens, Proceedings of the 2nd Int. Conf. on Quenching and The Control of Distortion, Cleveland Marriot Society Center, Cleveland, Ohio, USA, (1996), p. 181 - 191

SURFACE STRENGTHENING BY WATER JET PEENING

B.M. Colosimo and M. Monno
Politecnico di Milano, Milano, Italy

KEYWORDS: Water Jet, Peening, Surface treatment.

ABSTRACT: Fatigue strength improvement of metallic components can be obtained by generating compressive residual stresses in sub-surface layers, for example by shot peening. The main drawback of conventional shot peening technique is related to surface integrity deterioration. Water Jet Peening is an innovative surface strengthening process which has the main advantage of a negligible influence on surface roughness and texture. Moreover the high accessibility of water jet could also offer the opportunity of processing parts with complex geometry. Since inaccurate choice of parameters could cause erosion, the improvement of fatigue strength could be neutralized by the presence of micro-cracks on the surface. The present study introduces an experimental analysis on water jet peening parameters. Results show that parameters can change in a wide range without affecting surface integrity. This result could be considered as an important step toward industrial application of this new technology. Moreover the paper analyses parameters influence on residual stress induced by the process.

1. INTRODUCTION

Increasing fatigue strength in mechanical component is addressed in the literature as an important opportunity in reducing material cost. Indeed, during the design phase of the component, some important factors that influence fatigue limit, are often fixed. For instance geometry, dimensions and the sequence of processes used to realise the

mechanical part often act as constraints. In this situation, fatigue strength limit can be increased only by selecting a different and generally more expensive, material.

Since the presence of a compressive residual stress layer beneath the metallic surface can increase the fatigue limit, a process able to induce this kind of residual stress could be an opportunity to use the original, less expensive, material.

Traditional processes that induce compressive residual stress are shot peening and rolling. Since the latter is useful only when geometry is regular, the former has many industrial applications when the surface interested by the process is characterised by complex geometry. Since complex geometry is often related to notched components, shot peening could be a profitable process for components that are critical for fatigue behaviour.

Shot peening is a cold working process in which the compressive residual stress layer is realised by small spherical media, the “shots”, striking the material at high speed. Since shot peening media makes a set of dimples on the surface treated (see fig. 1), the deterioration of surface integrity causes a worst roughness. When R_a on the surface is a constraint, we need an additional process, able to reduce R_a without affecting residual stresses close to the surface. Even if a given value of R_a is not required, roughness deterioration caused by shot peening could reduce fatigue limit, thus reducing treatment advantage.

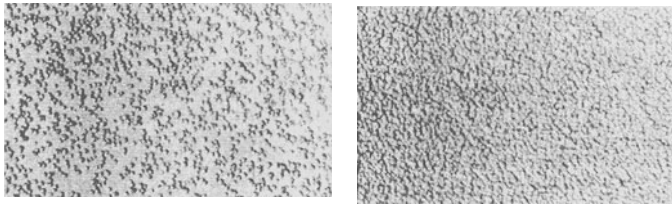


Figure 1: Surface deterioration due to shot peening process [7]

Recent literature [2][5], deals with a new process, Water Jet Peening (WJP) that uses the Water Jet technology for strengthening mechanical surfaces. The idea beneath this new process is to make water drops acting as shots. Compared with the traditional shot peening process, WJP presents the advantage of leaving the surface texture and roughness almost unchanged. The aim of the paper is to go beyond results reported in the literature, by quantitatively analysing influences of parameters on the peened surface. Indeed some authors [2] analyse the effect of parameters on Almen Intensity measured on the peened surface (this kind of residual stress measure is mainly related to the depth of peening than to the value of surface residual stress obtained after the treatment [7]). Other authors only consider results obtained by changing the peening duration (the time the jet insists upon a given area) [5]. Furthermore, both the approaches are devoted to high pressure Water Jet Peening.

The aim of this study is to analyse WJP effects on the treated surface when all relevant parameters change. The objective is to show that the advantageous absence of surface deterioration could be obtained by an accurate control of the technological parameters of the WJP. Indeed if the mechanical action of Water Jet becomes too heavy, residual

stresses begin reducing while erosion rises determining a deteriorated surface. In order to assess WJP as an applicable solution for fatigue strength improvement, the critical range in which parameters can vary while inducing residual stress without causing erosion, has to be wide.

The paper deals with the experimental investigation on this critical range.

2. WATER JET PEENING PROCESS CONTROL.

The possibility of inducing compressive residual stress using Water Jet Peening is related to the general structure of turbulent water jet in air, described in [6]. Depending on the stand off distance, during the travel of a highly coherent jet, there is a main region in which the continuous jet falls into drops. The drops act as small shots striking the surface, thus inducing local plastic deformation obtaining residual compressive stresses.

Compared with traditional shot peening, an advantage of water jet process is relevant to the limited number of process parameters to control. As can be observed in fig. 2a, WJP typical process requires controlling the following process parameters: water pressure P , stand off distance *s.o.d.*, feed rate u , peening angle α , nozzle diameter d_n .

As observed in [2] exiting the water jet by a mixing chamber and a focuser, as usual in abrasive water jet, can enforce the jet break-up into drops. During the experimental phase it has been used such equipment. The stand off distance has been thus measured as the distance of the mixing chamber from the surface. To be able to treat an area, water jet peening has been applied following a path composed by a set of parallel linear passes. The transversal increment (distance between two contiguous passes) is a process parameter that will be referred to as δ . It is also necessary to observe that the jet has been used in working condition with opposite versus passing from one travel to the adjacent one. In fig. 2b a sketch of the path used is reported.

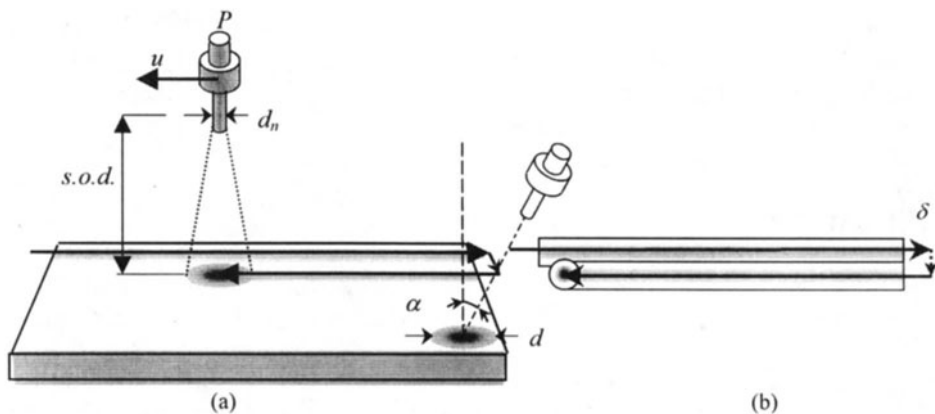


Figure 2: Water Jet Peening Process: relevant parameters.

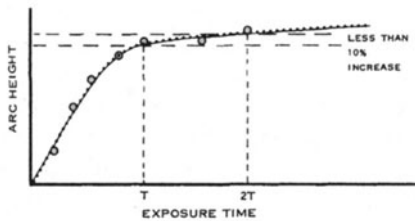
It has to be noticed that path has been defined in order to have an overlapping between two contiguous travels. This coverage effect has been guaranteed during the experimental

phase, by selecting δ having measured the diameter of the peened area, for each set of parameters.

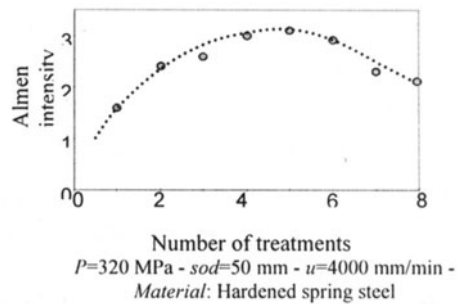
Since the treatment could also be applied more than once on the same surface, another parameter that has to be set is n , the number of treatments.

Compared with conventional shot peening, WJP does not require peening media control (geometry, material and dimensions of shots), thus reducing the number of control parameters.

Another important difference between traditional shot peening and water jet one, is related to the different effect observed when increasing the exposure time on the treated surface (i.e. the number of treatments increases or the traverse speed decreases). When a series of Almen strips are peened with a fixed parameters setting for different exposure times, a saturation curve, represented in fig. 3a [7], can be traced. Saturation is defined as the earliest point on the curve where doubling the exposure time produces no more than a ten percent increase in arc height.



(a)



(b)

Figure 3: Peening effect against treatment duration for shot peening (a) and WJP (b)[7][2]

When the same curve is developed using Water Jet Peening, a different behaviour can be obtained. As it is shown in figure 3b [2], there is a range of exposure time that defines the maximum intensity obtainable with the given set of parameters. This effect could be due to treated surface erosion and must be avoided when the objective is to induce a compressive residual stress avoiding surface topography modification.

3. THE EXPERIMENTAL PROCEDURE

A set of carbon steel specimens (C40: diameter=30 mm; height=11 mm) has been obtained starting from an extruded bar. The specimens have been at first prepared by grinding and then, in order to avoid tensile residual stress, heat treated (2.5 h at $T=600^{\circ}\text{C}$ with slow cooling in oven). Pickling has then been used to remove the oxide surface layer due to the heat treatment. After water jet peening, the residual stress analysis has been performed on an X-ray diffractometer. Compared with traditional Almen Intensity method, traditionally used for shot peened specimens, X-ray measure has the advantage of directly deriving the exact value of residual stress. Indeed the value of Almen Intensity seems to be more directly related to the depth of peening than to the value of surface residual stress [7].

4. EXPERIMENTAL RESULTS ANALYSIS.

In order to understand parameters effect on WJP treated surface, an experimental run has been carried out. The objective of this first step of analysis is to better investigate the influence of the parameters on residual stress.

To study the significance of the considered parameters, reducing the experimental effort, a fractional factorial experimental design with 2_{IV}^{7-3} has been chosen. Details on the used plane regards generators used that, with reference to the notation reported in Table 1, are E=ABC, F=BCD, G=ACD. For every treatment, n=3 replications have been executed.

Factor			low	high
A	Water pressure [MPa]	<i>P</i>	100	200
B	Standoff distance [mm]	<i>sod</i>	40	70
C	Traverse speed [mm/min]	<i>u</i>	4000	8000
D	Number of treatments	<i>n</i>	1	2
E	Nozzle diameter [mm]	<i>d_n</i>	0.17	0.30
F	Angle [degree]	<i>α</i>	0	20
G	Lateral step [mm]	<i>δ</i>	0.4	0.7

Table 1

Results obtained using a family $\alpha = 0.05$ ($\alpha = 0.007$ for each single test), show the statistical significance of pressure (factor A) and nozzle diameter (factor E) on compressive residual stress after water jet peening. Fig. 4 reports the p-values obtained in tests related to principal factors. All the hypotheses at the basis of the ANOVA have been successfully verified.

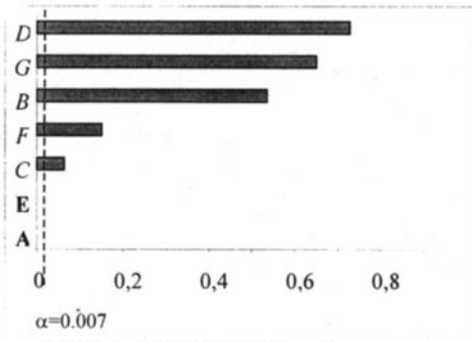


Figure 4: P-values for the different factors investigated

As it can be observed, within the range of variation of the parameters, only *P* and *D* have significant effects on residual stress. Observing p-values in fig. 4 and main effect plots in fig. 5, also *u* seems to be a relevant parameter: it has to be considered with attention since the absence of statistical effect could also be due to the selected levels of *u* considered in the experimental design.

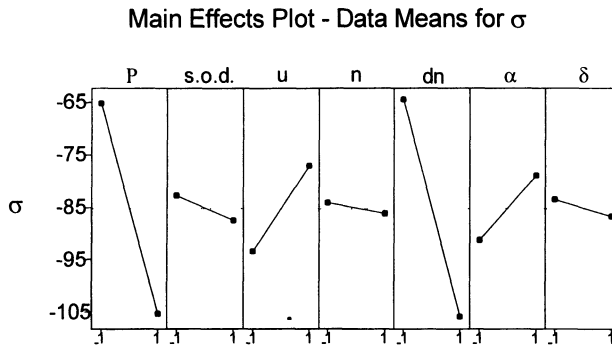


Figure 5: Main effect plot: factors mean against levels.

It has also to be noticed that residual stress on the peened surface can reach nearly a half of $\sigma_{p0.2}$ of material peened ($\sigma_{p0.2(C40)}=420$ MPa, vs. obtained σ_{max} 195 MPa), when all parameters are selected in order to leave the maximum effect. The absence of significance of some considered parameters, although related to the selected levels of the factors in the experimental design, can be interpreted as an interesting result. Since an incorrect selection of parameters could reduce residual stress induced by WJP, causing erosion, parameters have to be carefully selected. However if there is a range in which parameters can vary without causing erosion, industrial applications of WJP seem to be really feasible. Indeed uncontrolled factors, due to shop floor environment, could produce a noise that influences responses in an unpredictable way. If the response, in this case σ , is robust, an accurate selection of controlled parameters could assure desired results. These results are meaningful in order to assess WJP as a real applicable solution in surface enhancement.

5. A CONTRIBUTION TO WJP MODELIZATION.

In order to outline a simple relationship between process parameters and residual stress or erosion, an exploratory investigation has been carried out.

The objective of this analysis is, at first, to assess that the behaviour obtained when increasing the number of treatments (fig.3), can also arise when residual stress on the peened surface are reported against opportune parameters variation. The second objective is to qualitatively investigate the presence of a correlation between residual stress reduction and specimen erosion.

Energetic considerations allow to approximately calculate the specific kinetic energy of the jet exiting from the nozzle as [3]:

$$E_k \propto \frac{1}{2} \frac{\dot{m} v_j^2}{ud} \quad (1)$$

Where:

\dot{m} is the water flow rate, that can be calculated as:

$$\dot{m} \propto \rho_0 \pi d_n^2 v_j \quad (2)$$

- v_j is the jet velocity;
- u is the feed rate [see fig.2];
- d is the surface interested by the jet [see fig.2];
- d_n is the nozzle diameter[see fig.2].

Considering water a compressible fluid, v_j can be derived as:

$$v_j = \sqrt{\frac{2L}{\rho_0(1-c)} \left[\left(1 + \frac{P}{L}\right)^{1-c} - 1 \right]} \tag{3}$$

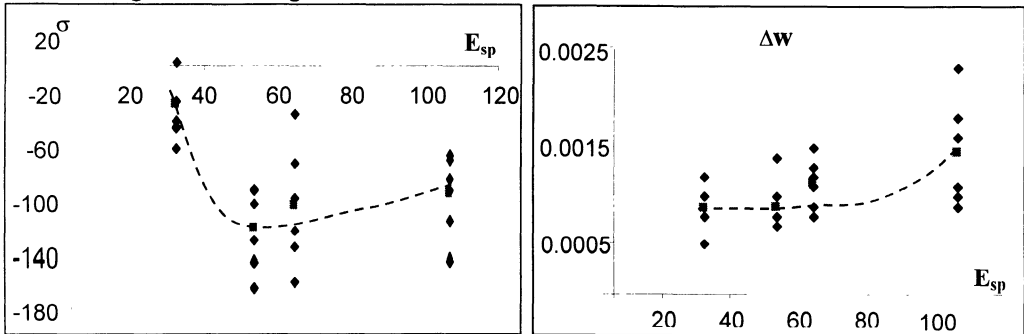
where:

$L=300$ MPa; $C=0.1368$ are constants, $\rho_0=1130$ kg/m³ (t=15° C).

Substituting (2) and (3), (1) becomes

$$E_k \propto \frac{\frac{1}{2} \rho_0 \pi d_n^2 v_j^3}{ud} \tag{4}$$

Two curves have been thus traced when specific energy ($E_{sp} = E_k[d=1 \text{ mm}]$, i.e. once fixed s.o.d.) increases, one depicting erosion, the other reporting residual stress on peened surface (fig. 6). The erosion has been measured by controlling the weight (w) of the sample before and after water jet peening ($\Delta w = w_{\text{before}} - w_{\text{after}}$). Although qualitative, the two curves show that when erosion begins appearing, residual compressive stress on the surface begins decreasing.



(a): Difference in residual stress induced by WJP against jet specific energy.

(b): Difference in weights (before and after WJP) against jet specific energy.

Figure 6: Erosion and compressive residual stress in different conditions

This relationship between residual stress and erosion has been completed by visually analysing the specimens, in order to understand when a difference in weight after and before WJP, is only due to cleaning effects. An example of visual surface changes, due to erosion appearing, is reported in fig. 7, where (a) and (b) are, respectively, an eroded and an intact surface, after WJP.

A second interesting result of this preliminary phase is the link that seems to exist between specific energy and residual stress/erosion. This second relation, once quantitatively investigated, could represent a significant step toward a real understanding of WJP physical mechanism.

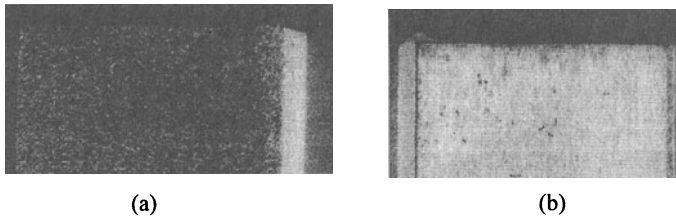


Figure 7: Eroded and not eroded surfaces after WJP.

5. CONCLUSIONS

In order to improve fatigue strength, a new process, the Water Jet Peening (WJP), is considered and characterised. Since the process could induce compressive residual stress without affecting surface integrity, it could be preferred to shot peening when surface integrity is a specific requirement. Since the main problem of WJP is relevant to erosion that could arise if parameters setting is not correct, the paper focuses on the analysis of parameters influence on residual stress left by the treatment. Preliminary results obtained lead to interesting conclusions. Some of the considered parameters can vary in a wide range of values without affecting residual stress. Once defined these ranges, WJP could be considered as a suitable process for surface strengthening applications for shop floor use. Finally the paper reports some energetic relations among parameters which seem to well succeed in foreseeing residual stress induced on peened surface. In the opinion of the authors this seems to be a very promising step toward a deeper comprehension of WJP mechanism.

REFERENCES

1. Baragetti, S.: Shot peening optimisation by means of "DoE": numerical simulation and choice of the treatment parameters, *Int. Journal of Materials & Product Technology*, Vol.12, N.2/3, 1997.
2. Holmqvist G., Öjmertz K.M.: Water Jet Peening at Ultra-High Pressures, submitted to the 14th ICPR, Osaka, Japan 1997.
3. Momber, A., Kovacevic, R.: *Principles of Abrasive Water Jet Machining*, Springer, 1998.
4. Tönshoff, H.K., Kroos, F., Hartmann, M.: Water Peening-An Advanced Application of Water Jet Technology, 8th American Water Jet Conference, Houston, Texas, U.S.A., 1995.
5. Tönshoff, H.K., Kroos, F., Marzenell, C.: High-Pressure Water Peening - a New Mechanical Surface-Strengthening Process, *Annals of CIRP*, vol. 46/1/1997.
6. Yanaida, K., Ohashi, A.: Flow characteristics of water jets in air. *Jet Cutting Technology*, Fourth International Symposium on Jet Cutting Technology, April 12th-14th 1978.
7. *Shot Peening Applications*, published by Metal Improvement Company, Inc., 7th edition.

ROBUST PID CONTROLLER FOR CONTINUOUS CASTING MOLD LEVEL CONTROL

F. Blanchini, F. Miani, S. Miani and U. Viaro
University of Udine, Udine, Italy

KEYWORDS: PID tuning, continuous casting, robust control.

ABSTRACT: This paper is concerned with the problem of controlling the molten metal level in continuous casting processes with particular reference to high-speed slab casters with large-size mold. The main objectives to achieve in these cases are robust stability and good disturbance rejection: the first derives from the rather large plant perturbations caused by the metal flow, whereas the second refers to the sudden drops of clogged material in the mold. To this purpose, the parameters of a standard PID controller are tuned so as to meet the desired time response characteristics and to ensure a sufficient stability margin for all possible plant models. The results obtained show the validity of the proposed procedure.

1. INTRODUCTION

Continuous casting of steel is considered today with increasing attention because it entails a substantial reduction in labor cost and significant improvements in the overall degree of automation of steel-making plants. Other advantages of continuous casting over more traditional techniques are related to the improved efficiency and energy savings: for instance, coupling the continuous casting machine with the direct charge of the cast semis in the rolling, accounts for a 25% reduction in energy consumption with respect to the traditional ingot casting technique. Quality issues are favorable too, even if additional care is required in

Published in: E. Kuljanic (Ed.) *Advanced Manufacturing Systems and Technology*,
CISM Courses and Lectures No. 406, Springer Verlag, Wien New York, 1999.

pouring the liquid steel from the ladle to the tundish and from the tundish to the mold, as well as in the control of the steel level.

Continuous casting of steel involves many and different levels of automation. The crucial point, however, is the control of the metal level in the mold, as this is vital to eliminate surface and sub-surface defects and deviations from the nominal size. For slab and bloom casting, the aim is to keep variations in the final product below 5 mm; for billet casting, where speed is higher, variations up to 10 mm may be tolerated.

Several techniques have recently been applied to solve this problem. In [1] an LQ regulator has been adopted for slow-speed slab casters. The use of an observer for estimating the disturbance caused by the drop of clogged material in the mold has been considered in [2]. Other techniques that have been suggested are: adaptive control [3], H^∞ control [4], predictive control [5], nonlinear control through the identification of the nonlinearities responsible for mold level fluctuations [6]. Expert knowledge based controllers, possibly combined with classic PID design techniques, have been described in [7, 8]. An intuitively simple, yet efficient, technique has been proposed in [9]: it employs a standard PID controller together with a fuzzy controller which replaces the PID controller when severe perturbations occur, like sudden nozzle unclogging.

The variety of mold level control techniques is strictly related to the different approaches for treating system uncertainties and to the different operating conditions (molten steel level fluctuations greatly depend on the casting speed and the mold size). According to [4], stability issues are generally more important for extracting speeds V greater than 1.6 m/min and caster sectional areas C greater than 0.4 m² because of the larger plant parameter perturbations.

This paper is organized as follows. A brief overview of continuous slab caster processes is given in Section 2 where simple models of the component parts are derived. In Section 3 the nozzle clogging/unclogging phenomenon is described together with the model used to simulate this sudden variation [9]. Some basic results on the stability of feedback connections for open-loop uncertain plants are recalled in Section 4; in particular, it is shown how they can be applied to guarantee safe stability margins. Finally, in Section 5 the controller parameters are locally optimized to obtain good unclogging disturbance rejection: the simulated results compare very favorably with those presented in the literature.

2. CONTINUOUS CASTER MODEL

The outline of the considered casting process is shown in Figure 1 together with the relevant control loop.

The molten steel flows from the ladle (a sort of reservoir) to the so-called tundish. A stopper mechanism regulates the molten metal flow to the mold through a submerged nozzle. Here the metal is water-cooled and subsequently extracted at a speed V . It is then moved through the casting machine for further cooling and machining. The main problems facing

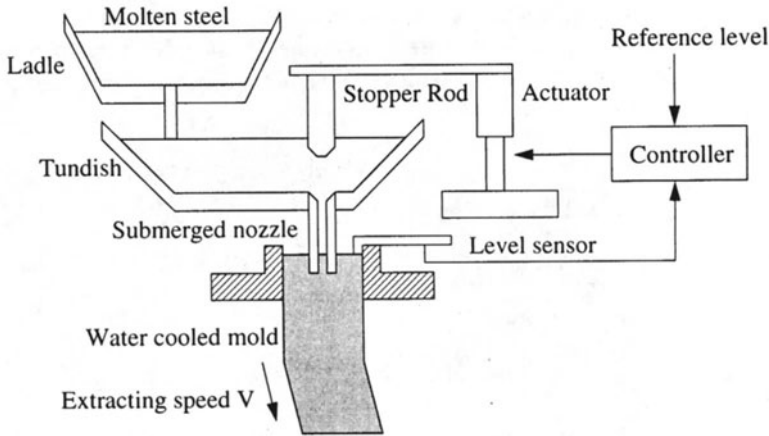


Figure 1: Continuous casting process

the control engineer are essentially two: robust stability and disturbance rejection.

Robust stability is needed because of perturbations caused by many factors, such as unmodelled dynamics, stopper-rod mechanism wear and upward steel flow in the mold. Good disturbance rejection is required to maintain the desired level in the presence of the disturbances typically associated to the clogging/unclogging phenomenon and measurement noise. Although from the control point of view two inputs seem to be available, i.e., the stopper position and the extracting speed, the only one actually available is the first, since variations in the extracting speed V may deteriorate the product.

The stopper-rod mechanism and its actuator can be modelled as a single first-order dynamic system. The model of the flow through the nozzle together with the clogging/unclogging phenomenon will be considered in the next section. Concerning the level $y(t)$ in the mold, from the balance of matter flowing in ($Q_i(t)$) and out ($Q_o(t)$) we get: $\dot{y}(t) = \frac{Q_i(t) - Q_o(t)}{C}$, where C is the cross section area.

As far as the measurement of the mold level is concerned, it will be assumed that an eddy current device with an accuracy of ± 3 mm is available (for a description of other sensing devices see [10, 11]).

3. THE CLOGGING/UNCLOGGING MODEL

The flow of molten steel through the nozzle causes an aluminium oxide (Al_2O_3) deposit which hence tends to clog. This deposit keeps on growing, thus reducing the magnitude of inflow material into the mold till a sudden unclogging occurs. In [9] a mathematical model of this phenomenon has been proposed which has proved to be quite effective. Specifically, the clogging/unclogging phenomenon has been accounted for by means of a disturbance acting

on the stopper opening signal (through a suitable filter). The input $p(t)$ corresponding to such a disturbance is shown in Figure 2 along with the equivalent first-order linear perturbed plant model. The two parameters A_c and T_c characterizing $p(t)$ can be inferred from historical

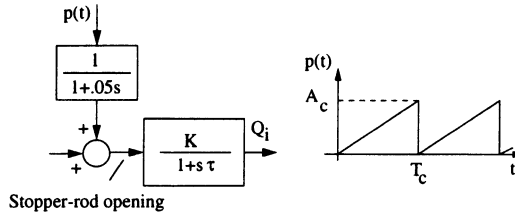


Figure 2: Equivalent linear model of the clogging/unclogging phenomenon

data. Admissible values for them [9] are: $A_c \in [5, 15] \times 10^{-3}$ m and $T_c \in [500, 7000]$ s. The nominal values adopted for the first-order system parameters in [9] are $K_{nom} = 1.1$ and $\tau_{nom} = 0.9$, although stopper-rod mechanism wear can make these parameters vary sensibly. In this paper the above-mentioned variations are quantified as $K \in [.7, 1.3]$ and $\tau \in [.6, 1.3]$.

4. VALUE SETS

From the considerations in the previous sections it follows that the plant can be regarded as a linear time-invariant system subject to time-independent structured uncertainties; precisely, if we denote by $q \in Q$ the vector of real uncertain parameters, the uncertain plant transfer function can be written as

$$P(s, q) = \frac{N_P(s, q)}{D_P(s, q)}, \tag{1}$$

where $N_P(s, q)$ and $D_P(s, q)$ are coprime polynomials whose coefficients are continuous functions of q .

In the considered case, by neglecting the exogenous disturbances and letting C be the section area of the mold, 0.08 be the time constant of the stopper-rod actuator with unity gain, the transfer function from the stopper-rod command to the mold level is given by (see Figure 3)

$$P(s, q) = \frac{1}{(1 + 0.08s)} \frac{K}{(1 + \tau s)} \frac{1}{sC}, \tag{2}$$

with $q = [\tau \ K]$, $N_P(s, q) = K$ and $D_P(s, q) = 0.08C\tau s^3 + (\tau + 0.08)Cs^2 + Cs$.

Now, for linear systems affected by time-independent structured uncertainties, it is possible to verify the stability of feedback configurations by means of an extension of the Nyquist criterion which requires the notion of *value set* $P(j\omega, Q) \subseteq \mathbf{C}$; this, for any fixed $\omega \in \mathbb{R}$, is defined by:

$$P(j\omega, Q) \doteq \{P(j\omega, q) : D_P(j\omega, q) \neq 0, q \in Q\}. \tag{3}$$

In other words, the value set is a bidimensional representation of the uncertainty affecting the system. Now, the following result holds ([12, 13]).

Theorem 4.1 (Robust Nyquist stability criterion) *The negative unity-feedback system with uncertain loop transference $P(s, q)$ is stable for all $q \in Q$ if and only if the Nyquist stability criterion is satisfied for at least one $q \in Q^1$ and $-1 + j0 \notin P(j\omega, Q)$ for all $\omega \in \mathbb{R}$.*

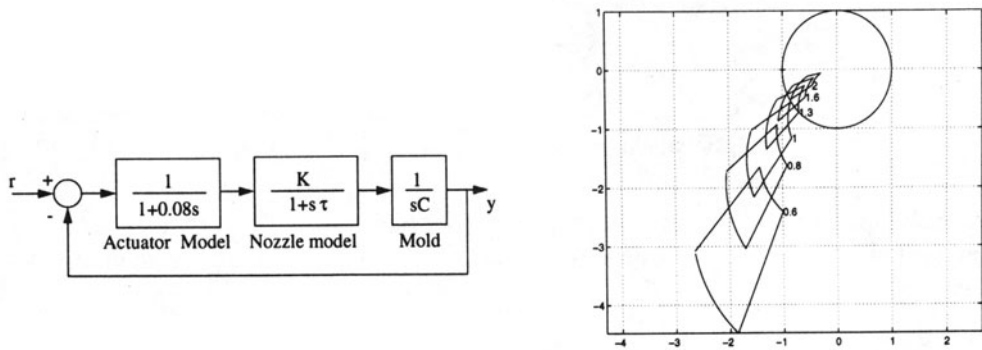


Figure 3: Closed-loop system with uncertain plant and value sets for different values of ω

This result can be extended to nonunity-feedback loops in an obvious way and, as we shall see in the next Section, can advantageously be used for synthesis purposes.

5. CONTROLLER TUNING AND SIMULATIONS

The control loop of the plant outlined in Section 2 together with the clogging/unclogging model described in Section 3 is illustrated in Figure 4, where PID controller and the low-pass output filter are also shown. The output measurement noise is accounted for by means of a white-noise process uniformly distributed in $[-3, +3]$ mm.

The parameters of the PID controller (with filtered derivative action) and the low-pass filter were derived as follows. First, the PID parameters were tuned to ensure good stability margins for every admissible value of the parameters τ and K . Second, the parameters were locally optimized to obtain a better disturbance rejection. Finally, a low-pass filter was added in the feedback path so as to attenuate the effects of the measurement noise without introducing a too big negative phase shift at critical frequencies. As a result of the above procedure, the following PID controller and low-pass filter were obtained:

$$G_C(s) = \frac{0.900s^2 + 0.979s + 0.938}{0.025s^2 + s}, \quad F(s) = \frac{0.1953s^2 + 58.5874}{0.01s^3 + 0.3519s^2 + 4.2831s + 58.5874}$$

¹This means that there exists $q \in Q$ such that the corresponding closed-loop system is stable

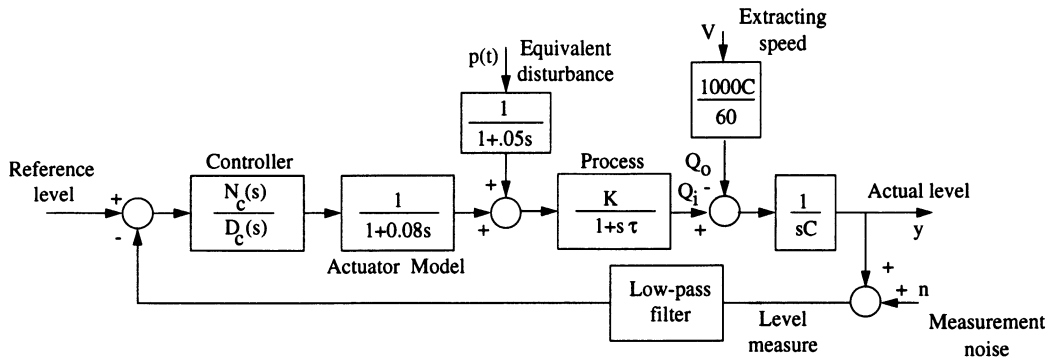


Figure 4: Block diagram of the closed-loop control scheme

The values sets corresponding to the loop transfer function $L(s, q) = G_C(s)P(s, q)F(s)$ are depicted in Figure 5. Finally, Figure 6 shows the simulated mold level with unclogging parameters (cf. 3) $A_c = 15 \text{ mm}$ and $t = 550 \text{ s}$.

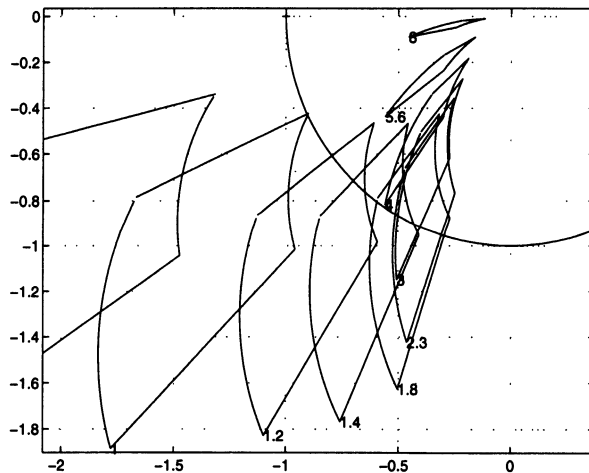


Figure 5: Value sets of $L(s, q)$ for various values of ω

6. CONCLUSIONS

The problem of controlling the molten metal level in continuous casting processes has been considered. The main requirements to be satisfied are robust stability versus parametric uncertainties and good disturbance rejection. The adopted approach meets both these requirements, as simulation results have shown. In particular, overshoot and settling time of

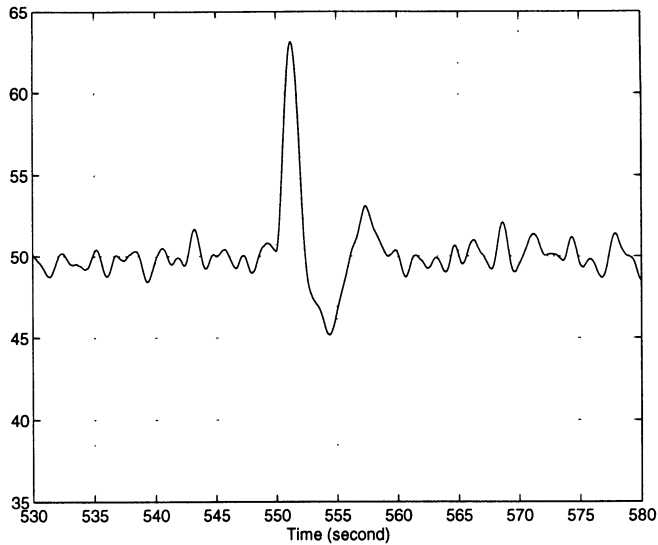


Figure 6: Simulated mold level

the response to the equivalent unclogging disturbance have turned out to be much smaller than those obtained using different approaches.

REFERENCES

1. Y. Matoba, T. Yamamoto, M. Tokuda, T. Watanabe, and H. Tomono, "Instrumentation and control technology for supporting high-speed casting", in *Proc. of 9th PTD Process Technol. Conf.*, 1990, pp. 101–109.
2. K. Asano, T. Kaji, H. Aoki, M. Ibaraki, and S. Moriwaki, "Robust molten steel level control for continuous casting", in *Proc. 35th Conf. Decision Contr.*, Kobe, Japan, 1996, pp. 1245–1250.
3. T. Kurokawa, Y. Kato, and T. Kondo, "Development of CC mold level adaptive control systems", *Current Advances in Materials and Processes*, vol. 5, no. 2, p. 354, 1992.
4. H. Kitada, O. Kondo, H. Kusachi, and K. Sasame "H[∞] control of molten steel level in continuous caster", *IEEE Trans. Contr. Syst. Technol.*, vol. 6, n.2, pp. 200–207, March 1998.
5. R. De Keyser, "Predictive mold level control in a continuous steel casting machine", in *Proc. 13th IFAC World Congr.*, San Francisco, 1996, Vol. M, pp. 487–492.

6. S.F.Graebe, G.C.Goodwin, and G.R.Elsey, "Control design implementation in continuous steel casting", *IEEE Contr. Syst. Magazine*, vol. 15, no. 4, pp. 64–71, 1995.
7. K.Omura, Y.Otsuka, and M.Konishi, "Diagnostic expert system for mold level control equipment in continuous caster", in *Proc. of 6th Int. Iron and Steel Congr.*, Nagoya, Japan, 1990, pp. 62–68.
8. G.Bartolini et Al., "Continuous casting of semifinished steel products", in *The Making, Shaping and Treating of Steel*, 10th edition, AISE Foundation, Pittsburgh, 1985, ch. 21, pp. 741–772.
9. M.Dussud, S.Galichet, and L.P. Foulloy, "Application of fuzzy logic control for continuous casting mold level control", *IEEE Trans. Contr. Syst. Technol.*, vol.6, no.2, pp.246–252, March 1998.
10. D.T.Llewellyn, *Steels, Metallurgy and Applications*, Butterworth–Heinemann, Oxford 1992, pp. 10–11.
11. W. R. Irving *Continuous Casting of Steel*, The Institute of Materials, London, 1993, pp. 178–181.
12. B.Ross Barmish, *New Tools for Robustness of Linear Systems*, MacMillan, New York, 1994.
13. F.Blanchini and R.Tempo, "Robustness analysis with real parametric uncertainty", in W.S.Levine Ed., *The Control Handbook*, CRC Press, Boca Raton, 1996, pp. 495–505.

AUTOMATIC ALIGNMENT OF WORKPIECES FOR ROBOTIC MANIPULATION USING A CONVEYOR BELT AND FIXED FLAT FENCES

R. Caracciolo and P. Gallina
University of Padua, Padua, Italy

A. Gasparetto
University of Udine, Udine, Italy

KEY WORDS: Alignment, Pushed, Sliding, Orientation.

ABSTRACT: This paper presents an automatic system for alignment of workpieces for robotic manipulation operations. The system consists of a sequence of fixed flat fences, suitably oriented across a conveyor belt, so that a workpiece on the belt will slide along each fence and leave the last one finding itself aligned with a desired orientation. In this way there is no need to provide the robotized system with feedback sensors in order to determine position and orientation of the workpiece to be manipulated, but the grasping task can be performed using an open-loop strategy. A prerequisite to the system design is the development of a simple but robust mathematical model which allows to compute the "exit angle", i.e. the orientation of the workpiece when it leaves the last fence, as a function of the number and orientation of the fences. It is thus straightforward to determine the characteristics of the fences (number and orientation) in order to realize a desired alignment of the piece. Several simulation and experimental tests have been carried out, which confirm the effectiveness of the system.

1. INTRODUCTION

Extensive research has been done in the last decades about the automatic planning of robotized manipulation operations. Most of the problems in this field have been solved

robotics). However, the use of closed-loop complex sensor systems considerably increases the cost of the robotized system, which might eventually turn no more profitable, especially if the operations to be performed are quite repetitive. Moreover, employing complex sensors heavily affects the operating speed of the overall robotic system. Our aim is therefore to implement simple, robust open-loop sensorless strategies to perform robotized manipulation tasks. In this paper, we deal with the problem of grasping workpieces lying on a table. Such a problem may be solved using a closed-loop strategy, e.g. a vision system which recognizes the piece to be manipulated, and computes its position and orientation so that the robot can grasp it correctly. However, in many cases it would be convenient to employ a sensorless, open-loop strategy, namely to feed the piece onto the table so that it is always aligned in a predefined way, i.e. presents the same orientation to the manipulator. In this way only one grasping motion has to be programmed, thus greatly reducing the cost of the system and the operational load.

In this paper, a strategy for automatic alignment of workpieces able to slide on their work surface will be considered. Such an open-loop system uses a belt to convey the pieces up to the worktable. The workpiece will slide along a sequence of fixed flat fences, suitably positioned and oriented across the conveyor belt, so that it will leave the last fence finding itself aligned with a desired orientation, depending on the number and orientation of the fences.

The problem of determining the "exit angle" (defined as the orientation of the piece when it leaves the last fence) as a function of the number and orientation of the fences is not an easy one, since several unpredictable factors (e.g. surface irregularities, dust, etc.) can affect the result. Hence, a suitable and robust model of the system should be considered, (in according with theoretical analysis of "pushing" followed by Mason) in order to get adequate equations describing the workpiece motion. From the model equations, it is then possible to get an expression for the "exit angle" as a function of the number and orientation of the fences. Moreover, several simulations have been carried out, using both Working Model and Matlab software packages, to test the effectiveness of the model in predicting the exit angle of the workpiece. Experimental tests have also been done, on a real conveyor belt across which a sequence of flat fences, suitably oriented, has been fixed. The tests consisted in measuring the exit angle of a workpiece and comparing it with the result predicted in simulation. The tests showed an excellent consistency between the simulations and the experimental results, in spite of the physical inaccuracies of the experimental testbed and of the assumptions made on the model.

With regard to the state of the art in the field, the problem we consider in this paper has already been studied by some authors [1÷7]. Among the others, Mason [3,4], Peshkin and Sanderson [5,6] identified sliding operations as fundamental to robotic manipulation, and developed a theory of the motion of a pushed, sliding workpiece in a very general case. Some of the results of their work will be taken here, but we want to consider a less general case, which allows to reduce the complexity of the model and consequently of the overall system. In this way, it is much easier to implement an algorithm which yields the orientation

of the fences as a function of the desired "exit angle", and this turns out to be very suitable for real-time operations.

2. MATHEMATICAL MODEL OF THE SYSTEM

A mathematical model which reproduces the mechanical behavior of the workpiece - belt - fence system has been designed. The model is rather simple, so as not to require a heavy amount of computation and to be effective in real-time operations. Furthermore, it needs to be rather robust, so as to compensate for unpredictable factors that could affect the behavior of the real system.

2.1. ASSUMPTIONS

The assumptions made in the model are the following:

- the value of the dynamic friction coefficient between workpiece and conveyor belt is assumed constant with respect to the relative velocity between the two. As a matter of fact, the relative velocities involved do not induce significant stick-slip phenomena;
- the contact between the piece and the belt occurs on a finite number of points;
- the pressure force is assumed constant on a contact area ΔA_c , and equal to: $p_c = W / A_c$, where W is the total weight of the piece and A_c the total contact area;
- the workpieces are considered to be convex polygons; however, it would not be difficult to extend the model in order to consider also non-convex polygons;
- the inertia forces are neglected, due to the low speed of the conveyor belt.

Such assumptions are commonly made by most researchers in this field [1÷7].

2.2. MOTION OF THE WORKPIECE

The mechanical equations of the system are directly derived by Newton's laws. In this case the external forces are unknown, namely: the contact force F_c between the workpiece and the fence, and the field of friction forces between the workpiece and the belt. The friction forces depend on the instantaneous motion of the piece, because the infinitesimal friction force in a contact point acts against the instantaneous motion of the same point, and have absolute value $p_a = \mu_a p_c$, where μ_a is the friction coefficient between the piece and the belt. Thus, in order to determine the external forces it is necessary to calculate the center of instantaneous rotation (CIR) of the piece to which the field of the friction forces is associated.

In order to determine the mechanical equations, we suppose to instantaneously stop the conveyor belt, and to write the equilibrium equations neglecting the inertial forces according to one of the assumptions listed in the foregoing.

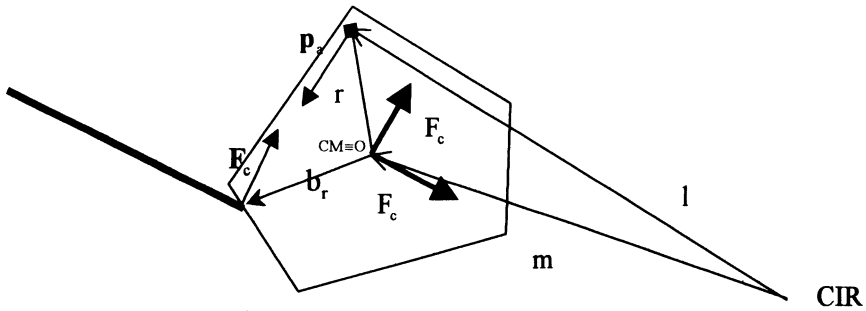


Figure 1 - The workpiece motion

Referring to Fig. 1, we take a reference frame *Ots*, fixed with respect to the piece, with origin in the center of mass of the piece and s-axis parallel to the direction of the contact force between the piece and the fence. The unknowns of the problem are the vector **m** that defines the position of the CIR with respect to the center of mass of the piece, as well as the absolute value of the contact force F_c .

The friction force acting on any contact point A is given by:

$$\mathbf{p}_s = \frac{\mathbf{l} \times \boldsymbol{\omega}}{|\mathbf{l}|} (p_c \cdot \Delta A_c) \tag{1}$$

where $\mathbf{l} = \mathbf{r} - \mathbf{m}$, and $\boldsymbol{\omega}$ is a unit vector indicating the sense of rotation. Note that the value of the friction coefficient has not been included, because it does not affect the computation.

The equation expressing the equilibrium to translation is:

$$\mathbf{F}_c + \sum \mathbf{p}_s = \mathbf{0} \tag{2}$$

and the equilibrium with respect to rotation about the CM is expressed by:

$$\mathbf{b}_r \times \mathbf{F}_c + \sum \mathbf{r} \times \mathbf{p}_s = \mathbf{0} \tag{3}$$

Eqs. 1, 2 and 3 make a system of three non-linear equations with three unknowns. The system can be solved numerically and the value of **m** (i.e. the coordinates of the CIR with respect to the CM of the workpiece for each contact configuration with an end of the fence) can be eventually obtained.

2.3. DEFINITION OF A STABLE FACET

A facet of a workpiece is said to be stable if one of its facet keeps sliding along the fence for all its length. A facet turns out to be stable if the center of mass of the piece lies inside a triangle bounded by the facet itself and the boundaries of the friction cones. The stability condition may be expressed through a simple geometrical relationship.

3. COMPUTATION OF THE EXIT ANGLE

In order to achieve our ultimate goal, namely to determine the number and the orientation of the fences across the conveyor belt so as the workpiece will find itself aligned with a desired orientation on the worktable, the "exit angle" must be computed. We define "exit angle" of the workpiece the orientation it has in the instant when it leaves a fence of the sequence. In order to determine such a value, the whole motion of the piece while it keeps in contact with a fence must be studied. The whole motion consists of two parts:

- supposing that the contact facet is stable, the piece slides along the fence until its center of mass reaches the line representing the direction of the friction force between the fence and the piece itself;
- the piece starts to rotate about its instantaneous CIR. We assume that during this motion the piece keeps in touch with the end of the fence (one-point contact) until it definitely leaves the fence.

We refer to Fig. 2 to study the motion of the workpiece and to compute the value of the exit angle.

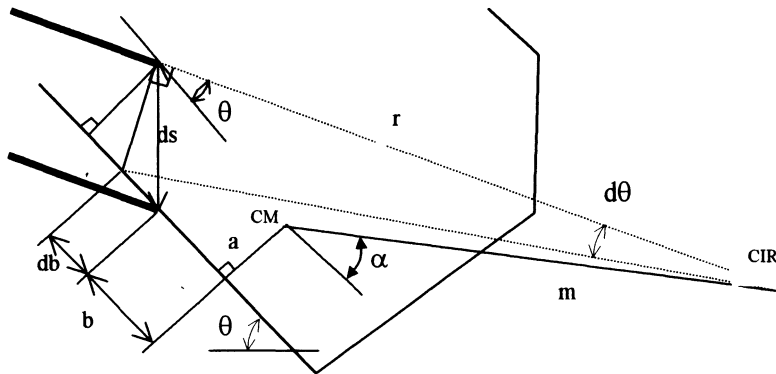


Figure 2 - Computation of the "exit angle"

The results of the computation do not change if we consider the piece fixed and the fence moving with respect to the piece. Referring to Fig. 2, we call ds an infinitesimal motion of the fence; during this motion also a rotation occurs, about the CIR of the workpiece.

Calling db the infinitesimal motion along the workpiece facet, we can write:

$$db = ds \cdot \cos\left(\frac{\pi}{2} - \theta\right) - ds \cdot \sin\left(\frac{\pi}{2} - \theta\right) \cdot \tan \beta \tag{4}$$

and, by substituting (5) into (4), we get:

$$db = ds \cdot \sin \theta - ds \cdot \cos \theta \cdot \frac{a + m \cdot \sin \alpha - ds \cdot \cos \theta}{b + m \cdot \cos \alpha - ds \cdot \sin \theta} \tag{6}$$

Then, calling $d\theta$ the infinitesimal rotation about the CIR, we can write:

$$r \cdot d\theta = \sqrt{\left[ds \cdot \sin\left(\frac{\pi}{2} - \theta\right) \right]^2 + \left[ds \cdot \sin\left(\frac{\pi}{2} - \theta\right) \cdot \tan \beta \right]^2} = ds \cdot \cos \theta \cdot \sqrt{1 + \tan^2 \beta} \quad (7)$$

$$r = \sqrt{[b + m \cdot \cos \alpha + ds \cdot \sin \theta]^2 + [a + m \cdot \sin \alpha - ds \cdot \cos \theta]^2} \quad (8)$$

By substituting (8) into (7) and recalling (5), we obtain the value for $d\theta$.

$$d\theta = \frac{ds \cdot \cos \theta}{b + m \cdot \cos \alpha + ds \cdot \sin \theta} \quad (9)$$

In order to compute the exit angle θ_{exit} , we recursively add the increments db until their sum reaches the whole length of the facet b ; correspondingly, we add the increments $d\theta$. The last value of θ obtained when the iterations stop is the value of θ_{exit} .

$$\begin{array}{ll} b_{i+1} = b_i + db & \text{until } b_{i+1} \geq b \\ \theta_{i+1} = \theta_i + d\theta & \text{then } \theta_{i+1} = \theta_{exit} \end{array} \quad (10)$$

Once the result for the exit angle of a fence is obtained, it is possible to study the behavior of the workpiece during its contact with the following fence. First of all, it should be determined which facet of the piece will be stable during the following contact. The answer can be obtained using simple geometric considerations. Then, the above procedure can be repeated in order to compute the next exit angle until the last fence of the sequence is reached. The last exit angle will yield the alignment of the piece onto the worktable.

4. EXPERIMENTAL TESTS

Simulations were carried out first using the dynamic simulator Working Model, then using the well-known Matlab software. The mechanical equations obtained from the foregoing discussions have been implemented and numerically solved.

Then, an experimental apparatus was realized, so as to have a real testbed for the system. A conveyor belt is actuated by a small motor (see Fig. 3), The belt speed is 0.1 m/s. A sequence of flat adjustable fences positioned across the belt completes the experimental system.

Extensive tests have been carried out, consisting in measuring the exit angle of different types of workpieces given a known configuration of the fences, and to carry out a statistical study of the results. The results of the tests, shown in Tab. 1, are very encouraging, because the repeatability error is low. The discrepancy between the average values of the real exit angles and the values obtained by simulation are mainly due to inaccuracies of the model, namely:

- the conveyor belt was assumed to be a uniform body providing a constant friction coefficient all over its surface;

- the friction between the end of the fence and the workpiece was neglected. This accounts for the fact that the real exit angles (see Tab. 1) are all larger than the values obtained by simulation;
- the stick-slip phenomenon was neglected.

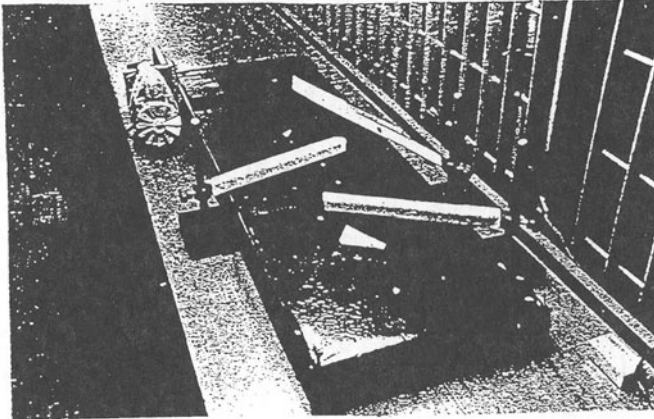


Figure 3 - The experimental apparatus consisting of a conveyor belt with adjustable flat fences

FACET	Calculated angle(degree)
1	52.2474
2	64.2854
3	71.7931

FACET	Measure-ment 1	Measure-ment 2	Measure-ment 3	Measure-ment 4	Measure-ment 5	Measure-ment 6	Measure-ment 7	Measure-ment 8	Measure-ment 9
1	58	57.5	57.5	57.5	57.5	59.5	57	57	57.7
2	66	64.5	65.5	66	68	67	65	65.5	65.9
3	72	72	71	72	72.5	73	72	72	72.1

Table 1 - Simulation and experimental results for a triangular workpiece

5. DESIGN OF THE FENCES

Once the theory for computation of the exit angle has been developed, it is straightforward to build a simple algorithm that determines the number and the orientation of the fences to be set across the conveyor belt in order to align the workpiece with a desired orientation at the end of the belt. What is needed is just to consider the equations in Section 3 and to solve them considering the exit angle as imposed, so as to get the value of the slant angles of the fences with respect to the motion of the conveyor belt.

6. CONCLUSIONS

In this paper the problem of automatically align a workpiece to be manipulated by a robot has been studied. A solution to this problem would enable one to use an open-loop sensorless strategy instead of complex, expensive sensor systems such as vision systems. The use of a conveyor belt across which a sequence of fixed flat fences has been collocated is proposed. In order to get a simple algorithm which could be suitable for real-time applications, some assumptions have been made to simplify the mathematical model of the system. A simple, robust model based on Newton's laws has been built; from this model, the exit angle of the workpiece as a function of the number and the inclination of the fences can be computed. Conversely, from the same relationships it is possible to determine some rules for fence design, namely the number and the inclination of the fences as a functions of the desired alignment of the workpiece. The results of experimental tests have been presented, showing that the repeatability of the system is good and the discrepancy between simulations and experimental results can be overcome updating the model so that it takes into account the friction between the workpiece and the end of the fence.

7. REFERENCES

1. Brost, R. C., "Analysis and Planning of Planar Manipulation Tasks", *Ph.D. thesis, Carnegie Mellon University*, 1991
2. Goldberg, K. Y., "Orienting Polygonal Parts without Sensors", *Algorithmica*, vol. 10, n. 2, August 1993
3. Mason, M. T., "Manipulator Grasping and Pushing Operations", *Ph.D. thesis, MIT*, 1992.
4. Mason, M. T., "Mechanics and Planning of Manipulator Pushing Operations", *The Int. Journal of Robotics Research*, vol. 5, n. 3, 1986
5. Peshkin, M. A. and Sanderson, A. C., "Planning Robotic Manipulation Strategies for Workpieces that Slide", *IEEE Journal of Robotics and Automation*, vol. 4, n. 5, 1988
6. Peshkin, M. A. and Sanderson, A. C., "The Motion of a Pushed, Sliding Workpiece", *IEEE Journal of Robotics and Automation*, vol. 4, n. 6, 1988
7. Singer, N. C. and Seering, W. "Utilizing Dynamic Stability to Orient Parts", *ASME Journal of Applied Mechanics*, vol. 54, 1987

A CONVERGENT ALGORITHM FOR L_2 OPTIMAL MIMO MODEL REDUCTION

A. Ferrante

Politecnico di Milano, Milano, Italy

W. Krajewsky

Polish Academy of Sciences, Warsaw, Poland

A. Lepschy

University of Padua, Padua, Italy

U. Viaro

University of Udine, Udine, Italy

KEYWORDS: Linear multivariable systems, model reduction, L_2 norm.

ABSTRACT: Often, the exact model of industrial processes turns out to be too complex for simulation and controller design. It is therefore mandatory to simplify the mathematical description of the process and/or the one of the controller. A particularly attractive simplification criterion is related to the minimization of the L_2 norm of the approximation error. This paper presents an algorithm for solving the L_2 -optimal MIMO model reduction problem. It is shown that its convergence to the minima of the approximation error norm is guaranteed. The algorithm proves to be fast and efficient compared to other algorithms suggested in the literature to the same purpose.

1. INTRODUCTION AND PROBLEM STATEMENT

The problem of model reduction is a fundamental topic in systems and control theory, and many reduction methods and algorithms of different computational complexity have been proposed during the last decades. This is due essentially to two reasons. First, in many cases the procedure for finding a mathematical description of a complex

industrial process leads to a model of too high dimension to be analyzed (especially in the presence of real-time signal processing constraints). Second, but not less important, many techniques for designing robust optimal controllers (see, e.g. [1] and references therein) do not guarantee a bound on the dimension of the obtained controller which may be too complex and expensive; it is therefore convenient to derive a suboptimal reduced-order controller as “close” as possible to the optimal one.

In this paper, we consider the classical approach based on the minimization of the L_2 norm of the output error, i.e., of the difference between the impulse responses of the original and the reduced-order model. This L_2 norm has a direct physical interpretation (energy) which explains the attention devoted to it by many authors (see, e.g., [2], [3], [4], [5], [6], [7], [8], [9], [10]).

Concerning stable continuous-time multivariable systems, the problem can be stated in frequency domain as follows: given the original $m_o \times m_i$ transfer matrix $F(s)$, find an $m_o \times m_i$ transfer matrix $G(s)$ of preassigned lower order which minimizes the (squared) L_2 -norm of $E(s) := F(s) - G(s)$, i.e.,

$$\|E\|_2^2 = \frac{1}{2\pi} \int_{-\infty}^{\infty} \text{tr} [E(j\omega)E^*(j\omega)] d\omega, \quad (1)$$

where the star indicates complex conjugate transpose.

A drawback of such an approach is that it leads to nonlinear equations with respect to the parameters of the reduced-order model. Furthermore, most algorithms are computationally demanding and their convergence (to local minima) is not always guaranteed.

In the following, an efficient algorithm based on a procedure recently presented by the present authors in [10] is suggested.

Let us denote the original stable $m_o \times m_i$ transfer matrix by

$$F(s) = \frac{N(s)}{d(s)}, \quad (2)$$

where $d(s)$ is the least common denominator (l.c.d.) of degree ν of all input-output transfer functions and $N(s)$ is the $m_o \times m_i$ polynomial matrix formed from the corresponding numerators of degree at most $\nu - 1$.

Similarly, let us denote by

$$G(s) = \frac{M(s)}{c(s)}, \quad (3)$$

the approximating transfer matrix whose l.c.d. $c(s)$ has a preassigned degree $\rho < \nu$.

According to [8], the necessary conditions for $G(s)$ to be the L_2 -norm optimal approximant of $F(s)$ are

$$N(s)c(s) - M(s)d(s) = Q_1(s)c(-s), \tag{4}$$

$$\text{tr}\{Q_1^T(s)M(-s)\} = q_2(s)c(-s), \tag{5}$$

where $Q_1(s)$ is an $m_o \times m_i$ matrix of polynomials of degree at most $\nu - 1$ and $q_2(s)$ is a polynomial of degree at most $\nu - 2$.

To solve the above nonlinear equations, an iterative procedure has been proposed in [10] which can be summarized as follows: starting from some $M^{(0)}(s), c^{(0)}(s)$, solve recursively the equations:

$$N(s)c^{(h+1)}(s) - M^{(h+1)}(s)d(s) = Q_1^{(h+1)}(s)c^{(h)}(-s), \tag{6}$$

$$\text{tr}\{(Q_1^{(h+1)})^T(s)M^{(h)}(-s)\} = q_2^{(h+1)}(s)c^{(h)}(-s), \tag{7}$$

till a specified stopping criterion is satisfied.

Equations (6) and (7) refer to the $(h+1)$ -th step in which the quantities with exponent $(h+1)$ are computed from those with exponent (h) evaluated in the preceding step.

2. DESCRIPTION OF THE ALGORITHM

By equating the coefficients of the equal powers of s on both sides of (6) and (7), a set of *linear* equations in the (current) unknown coefficients of $c^{(h+1)}(s), M^{(h+1)}(s), Q_1^{(h+1)}(s)$ and $q_2^{(h+1)}(s)$ can be derived; this takes the form:

$$A(x^{(h)})x^{(h+1)} = b, \tag{8}$$

where:

$x^{(h+1)}$ is a properly ordered vector formed from the above-mentioned unknowns, b is a constant vector whose elements only depend on the original system parameters, and

$A(x^{(h)})$ is a matrix whose entries depend both on the (known) original system parameters and on the reduced model parameters estimated in the preceding step, i.e., the elements of $x^{(h)}$.

The iterative procedure using (8), described in [10], does not ensure the convergence to the (local) minima of index (1); however, even if the algorithm does not converge to a minimum, it provides the model corresponding to the least value of (1) among all iterations and this is usually quite close to a locally optimal model.

Now, using a notation consistent with (8), the necessary conditions (4) and (5) give rise to the *nonlinear* set of equations:

$$A(x)x = b, \quad (9)$$

which, by assuming that $A(x)$ is nonsingular, can be rewritten in the form of a fixed-point equation as:

$$x = f(x) \quad (10)$$

with

$$f(x) := A(x)^{-1}b. \quad (11)$$

It follows that (8) can be considered as a recursive algorithm to find the fixed points \hat{x} of $f(x)$.

As is known, starting from an initial estimate sufficiently close to \hat{x} , the algorithm is guaranteed to converge to \hat{x} if, and only if, its Jacobian:

$$J(x) := \frac{\partial f}{\partial x}(x) \quad (12)$$

at \hat{x} is a stability matrix (all its eigenvalues lay inside the unit circle centred at the origin).

When this is not the case, by assuming the invertibility of $I - J(x)$ (which is generically true), resort can be made to the new function:

$$g(x) := [I - J(x)]^{-1}[f(x) - J(x)x] \quad (13)$$

and to the recursion

$$x^{(h+1)} = g(x^{(h)}) \quad (14)$$

which is equivalent to:

$$[I - J(x^{(h)})]x^{(h+1)} = f(x^{(h)}) - J(x^{(h)})x^{(h)}. \quad (15)$$

In fact, $g(x)$ is one particular member of the family of functions derived in [11], which have the same fixed points \hat{x} as $f(x)$ and whose Jacobians assume preassigned values at $x = \hat{x}$. In particular, expression (13) for $g(x)$ corresponds to the choice:

$$\frac{\partial g}{\partial x}(\hat{x}) = 0, \quad (16)$$

which ensures quadratic convergence to \hat{x} [12].

The problem essentially consists in evaluating, at each step, $f(x^{(h)})$ and $J(x^{(h)})$ appearing in (13).

The most efficient way to compute $f(x^{(h)})$ is probably the one suggested in [10]. To evaluate $J(x^{(h)})$, let us apply the implicit function theorem to

$$\Phi(x, y) := A(x)y - b = 0, \tag{17}$$

where

$$y = f(x). \tag{18}$$

In this way, we get:

$$J(x) = \frac{\partial f}{\partial x}(x) = - \left[\frac{\partial \Phi}{\partial y} \right]^{-1} \cdot \frac{\partial \Phi}{\partial x}, \tag{19}$$

where

$$\frac{\partial \Phi}{\partial y} = A(x) \tag{20}$$

and

$$\frac{\partial \Phi}{\partial x} = \frac{\partial [A(x)y]}{\partial x}. \tag{21}$$

With the above notation, equation (15) can be rewritten as:

$$\left[\begin{array}{c} A(x^{(h)}) + \frac{\partial [A(x)y]}{\partial x} \Big|_{\substack{x = x^{(h)} \\ y = y^{(h)}}} \end{array} \right] x^{(h+1)} = A(x^{(h)})y^{(h)} + \left[\begin{array}{c} \frac{\partial [A(x)y]}{\partial x} \Big|_{\substack{x = x^{(h)} \\ y = y^{(h)}}} \end{array} \right] x^{(h)}, \tag{22}$$

where $y^{(h)} = f(x^{(h)})$. The crucial point for computing $x^{(h+1)}$ via (22) is clearly the evaluation of:

$$\frac{\partial [A(x)y]}{\partial x} \Big|_{\substack{x = x^{(h)} \\ y = y^{(h)}}}. \tag{23}$$

This can be performed in a very efficient way by exploiting the sparseness of the matrices involved, which makes the algorithm not demanding from the computational point of view.

3. CONCLUDING REMARKS

The automation of manufacturing systems often entails the availability of mathematical models for real-time signal processing, which requires a linearization and simplification of the relevant differential equations. In particular, this problem may arise both in the description of the controlled process and in the design of the corresponding controller (when the adopted synthesis procedure leads to high-order compensators [1]).

The model approximation criterion considered in this paper is based on the minimization of the “energy” (squared L_2 norm) of the difference between the original impulse response and that of the reduced-order model. Such a performance index is particularly meaningful from the technical point of view but is very cumbersome from the algorithmic point of view since the available optimization procedures are computationally demanding.

In [10] the present authors have suggested an efficient technique to solve the above-mentioned problem but the related procedure does not converge in some cases.

The algorithm presented in this paper maintains the remarkable computational simplicity of the procedure in [10] and, at the same time, ensures the (quadratic) convergence to the minima of the index. Essentially it requires the inversion of two $(\nu + \rho) \times (\nu + \rho)$ matrices.

The software implementing the algorithm has been tested on numerous models of industrial processes with satisfactory results. It is available on request.

REFERENCES

- [1] M. A. Dahleh and I. D. Bobillo. *Control of Uncertain Systems: A Linear Programming Approach*. Prentice-Hall, Englewood-Cliffs, NJ, 1995.
- [2] L. Meier and D.G. Luenberger, “Approximation of linear constant systems”, *IEEE Trans. Aut. Contr.*, vol. AC-12, pp.585-588, 1967.
- [3] D.A. Wilson, “Model reduction for multivariable systems”, *Int. J. Contr.*, vol. 20, pp.57-64, 1974.
- [4] A. Ferrante, W.Krajewski, A. Lepschy and U. Viaro, “A new algorithm for L_2 -optimal model reduction”, in: S. Banka, S. Domek and Z. Emirsajlow, eds.. *Proceedings of the International Symposium on Mathematical Models in Automation and Robotics*, 1998, Miedzyzdroje, Poland (Wydawnictwa Politechniki Szczecińskiej, 1998) pp. 224-229.
- [5] A. Ferrante, W. Krajewski, A. Lepschy and U. Viaro, “Convergent Algorithm for L_2 Model Reduction”, *Automatica*, 1998. (To appear).
- [6] W. Gawronski and J.N. Juang, “Model reduction for flexible structures”, In W. Leondes. *Control and Dynamic Systems*, vol. 36, Academic Press, pp. 143-222, 1990.

-
- [7] D.C. Hyland and D.S. Bernstein, "The optimal projection equations for model reduction and the relationships among the methods of Wilson, Skelton and Moore", IEEE Trans. Aut. Contr., AC-30, pp.1201-1211, 1985.
 - [8] W. Krajewski, A. Lepschy and U. Viaro, "Optimality conditions in multivariable L_2 model reduction", J. Franklin Inst., vol. 330, pp.431-439, 1993.
 - [9] J.T. Spanos, M.H. Milman and D.L. Mingori, "A new algorithm for L_2 optimal model reduction", Automatica, 28, pp. 897-909, 1992.
 - [10] W. Krajewski, A. Lepschy, M. Redivo-Zaglia and U. Viaro, "A program for solving the L_2 reduced-order model problem with fixed denominator degree", Numerical Algorithms, vol. 9, pp.355-377, 1995.
 - [11] A. Ferrante, A. Lepschy and U. Viaro, "Forcing convergence of fixed-point recursive algorithms: a system-theoretic approach", *Proc. MTNS 98*. (To appear).
 - [12] D. G. Luenberger. *Optimization by Vector Space Methods*. John Wiley & Sons, New York, 1969.

ANALYTICAL DETERMINATION OF THE POSITION LOOP GAIN FOR CNC MACHINE TOOLS

Z. Pandilov and V. Dukovski

University Sv. Kiril i Methodij, Skopje, Macedonia

KEY WORDS: Position loop gain, Analytical determination, Feed drive, CNC machine tool

ABSTRACT: One of the most important factors which influences the dynamical behavior of the feed drives for CNC machine tools is position loop gain or Kv-factor. It directly influences the contouring accuracy of the machine tool. Usually position loop gain is experimentally tuned on the already assembled CNC machine tool. This paper gives one approach towards its analytical determination. The difference between analytical calculated and experimentally obtained Kv-factor is smaller than 5%, which is completely acceptable.

1. INTRODUCTION

The most important variable which describes the behavior of a position control loop for CNC machine tools feed drives is position loop gain or Kv-factor. This is the ratio of the command velocity (feed rate) v to the position control deviation (following error, tracking error, lag) Δx [1,2,3,4]

$$Kv[s^{-1}] = \frac{v[\text{mm/s}]}{\Delta x[\text{mm}]} \quad \text{or} \quad Kv\left[\frac{\text{m/min}}{\text{mm}}\right] = \frac{v[\text{m/min}]}{\Delta x[\text{mm}]} \quad (1)$$

$$Kv[s^{-1}] = \frac{1000}{60} \cdot Kv\left[\frac{\text{m/min}}{\text{mm}}\right] \quad (2)$$

From the magnitude of the K_v -factor depends tracking or following error. In multi-axis contouring the following errors along the different axes may cause form deviations of the machined contours. Generally position loop gain K_v should be high for faster system response and higher accuracy, but the maximum gains allowable are limited due to undesirable oscillatory responses at high gains and low damping factor. Usually K_v factor is experimentally tuned on the already assembled machine tool [1,5]. This paper presents approach for analytically calculation of the position loop gain K_v . A combined 6-th order digital-analog model of the position loop is presented. In order to ease the calculation, the 6-th order system is simplified with a second order model. With this approach it is very easy to calculate the K_v factor for necessary position loop damping. The difference of the replacement of the 6-th order system with second order system is presented with the simulation program MATLAB. Analytically calculated K_v factor is function of the nominal angular frequency ω and damping D of the feed drive electrical parts (motor and regulator), nominal angular frequency ω_m and damping D_m of the mechanical transmission elements, as well as sampling period T .

2. COMBINED DIGITAL-ANALOG MODEL OF THE FEED DRIVE POSITION CONTROL LOOP AND ANALYTICAL DETERMINATION OF THE K_v FACTOR

Fig. 1 presents digital-analog model of the CNC machine tool feed drive position control loop, where s represents Laplace operator.

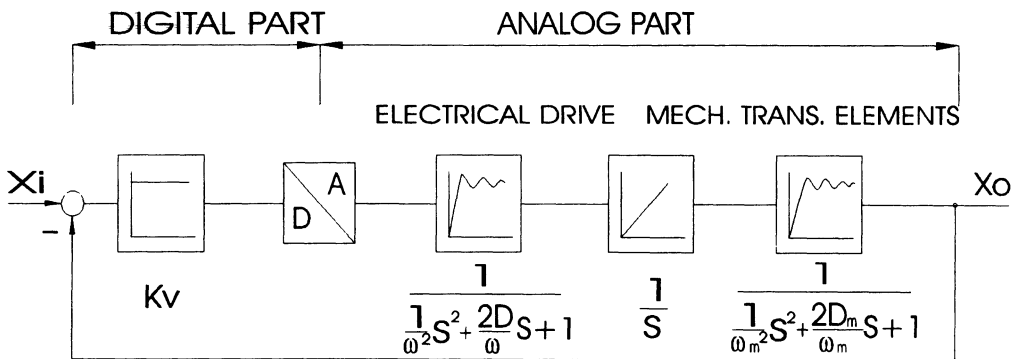


Fig. 1 Combined digital-analog model of the feed drive position control loop

Similar models are presented in [1,6,7], but the transfer function of mechanical transmission elements is not taken in consideration. Because of the existence of the digital part in the presented model we must use z -transformation for analysis. With some approximations and substitutions it is possible to analyze presented model in s -domain (with Laplace transformation). Digital-analog converter is substituted with zero order holder (z.o.h.) and sampler [8]. The new model is presented in fig.2.

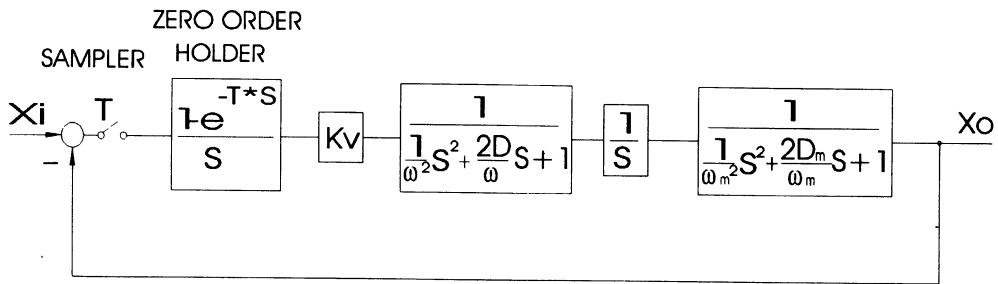


Fig.2 Modified model of the feed drive position control loop presented in fig. 1

According [8,9] we can approximate sampler and zero order holder (z.o.h.) in Laplace domain with the following transfer function:

$$G(s) = \frac{1 - e^{-Ts}}{T \cdot s} \tag{3}$$

With the Padè approximation of the first order for the e^{-Ts} we get:

$$e^{-Ts} \approx \frac{1 - \frac{T}{2} \cdot s}{1 + \frac{T}{2} \cdot s} \tag{4}$$

where T is sampling time (period).
In that case G(s) becomes:

$$G(s) = \frac{1 - e^{-Ts}}{T \cdot s} \approx \frac{1}{1 + \frac{T}{2} \cdot s} \tag{5}$$

With these simplifications feed drive position control loop may be presented with following model (fig.3).

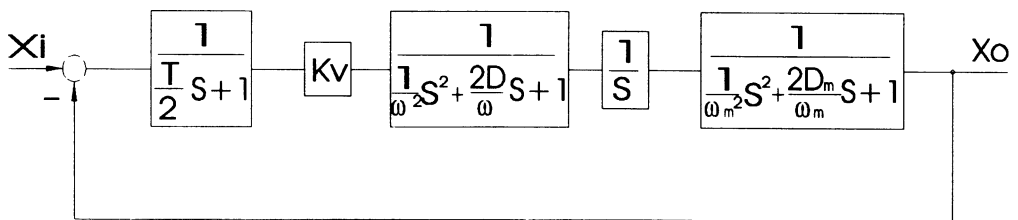


Fig.3 Analog model of the feed drive position control loop

The model in fig.3 may be analyzed in s-domain with Laplace transformation. The transfer function of the feed drive position control loop presented in fig.3 is:

$$\frac{X_o(s)}{X_i(s)} = \frac{K_v \cdot \frac{1}{\frac{T}{2} \cdot s + 1} \cdot \frac{1}{\frac{1}{\omega^2} \cdot s^2 + \frac{2D}{\omega} \cdot s + 1} \cdot \frac{1}{s} \cdot \frac{1}{\frac{1}{\omega_m^2} \cdot s^2 + \frac{2D_m}{\omega_m} \cdot s + 1}}{1 + K_v \cdot \frac{1}{\frac{T}{2} \cdot s + 1} \cdot \frac{1}{\frac{1}{\omega^2} \cdot s^2 + \frac{2D}{\omega} \cdot s + 1} \cdot \frac{1}{s} \cdot \frac{1}{\frac{1}{\omega_m^2} \cdot s^2 + \frac{2D_m}{\omega_m} \cdot s + 1}} \quad (6)$$

$$\frac{X_o(s)}{X_i(s)} = \frac{K_v}{\left(\frac{T}{2} \cdot s + 1\right) \cdot \left(\frac{1}{\omega^2} \cdot s^2 + \frac{2D}{\omega} \cdot s + 1\right) \cdot \left(\frac{1}{s}\right) \cdot \left(\frac{1}{\omega_m^2} \cdot s^2 + \frac{2D_m}{\omega_m} \cdot s + 1\right) + K_v} \quad (7)$$

$$\frac{X_o(s)}{X_i(s)} = \frac{b_0}{a_6 \cdot s^6 + a_5 \cdot s^5 + a_4 \cdot s^4 + a_3 \cdot s^3 + a_2 \cdot s^2 + a_1 \cdot s + a_0} \quad (8)$$

where:

$$\begin{aligned} a_6 &= \frac{T}{2\omega^2\omega_m^2}, \quad a_5 = \left[\frac{1}{\omega^2\omega_m^2} + \left(\frac{2D_m}{\omega^2\omega_m} + \frac{2D}{\omega\omega_m^2} \right) \cdot \frac{T}{2} \right], \\ a_4 &= \left[\left(\frac{2D_m}{\omega^2\omega_m} + \frac{2D}{\omega\omega_m^2} \right) + \left(\frac{1}{\omega^2} + \frac{4DD_m}{\omega\omega_m} + \frac{1}{\omega_m^2} \right) \cdot \frac{T}{2} \right], \\ a_3 &= \left[\left(\frac{1}{\omega^2} + \frac{4DD_m}{\omega\omega_m} + \frac{1}{\omega_m^2} \right) + \left(\frac{2D}{\omega} + \frac{2D_m}{\omega_m} \right) \cdot \frac{T}{2} \right], \\ a_2 &= \left[\left(\frac{2D}{\omega} + \frac{2D_m}{\omega_m} \right) + \frac{T}{2} \right], \quad a_1 = 1, \quad a_0 = K_v \quad \text{and} \quad b_0 = K_v. \end{aligned}$$

Having informations about the magnitude of the variables ω , D , ω_m , D_m , and T in real feed drive position control loops, we can conclude that a_6, a_5, a_4, a_3 have tendency towards zero ($a_6, a_5, a_4, a_3 \rightarrow 0$). So in that case we can simplify 6-th order system with the second order system [8,10]. Simplified transfer function of the feed drive position control loop is:

$$\frac{X_o(s)}{X_i(s)} = \frac{b_0}{a_2 \cdot s^2 + a_1 \cdot s + a_0} \quad (9)$$

where $a_2 = \left(\frac{2D}{\omega} + \frac{2D_m}{\omega_m} + \frac{T}{2} \right)$, $a_1 = 1$, $a_0 = K_v$ and $b_0 = K_v$.

In that case

$$\frac{X_o(s)}{X_i(s)} = \frac{K_v}{\left(\frac{2D}{\omega} + \frac{2D_m}{\omega_m} + \frac{T}{2}\right) \cdot s^2 + \cdot s + K_v} \quad (10)$$

To check the correctness of substitution the 6-th order with the second order system, simulation of the system transfer function response on step function with simulation program MATLAB was performed. Numerical values of the parameters of the examined system were:

$\omega=1000 \text{ s}^{-1}$, $D=0.7$, $\omega_m=663 \text{ s}^{-1}$, $D_m=0.17$, $T=0.006 \text{ s}$ and $K_v=100 \text{ s}^{-1}$.

Following transfer function were compared:

-6-th order system transfer function

$$\frac{X_o(s)}{X_i(s)} = \frac{100}{6.82 \cdot 10^{-15} \cdot s^6 + 1.33 \cdot 10^{-11} \cdot s^5 + 1.57 \cdot 10^{-8} \cdot s^4 + 9.72 \cdot 10^{-6} \cdot s^3 + 4.91 \cdot 10^{-3} \cdot s^2 + s + 100}$$

-second order system transfer function

$$\frac{X_o(s)}{X_i(s)} = \frac{100}{4.91 \cdot 10^{-3} \cdot s^2 + s + 100}$$

Fig. 4. gives responses of the position control loop transfer function of 6-th and 2-nd order on step function.

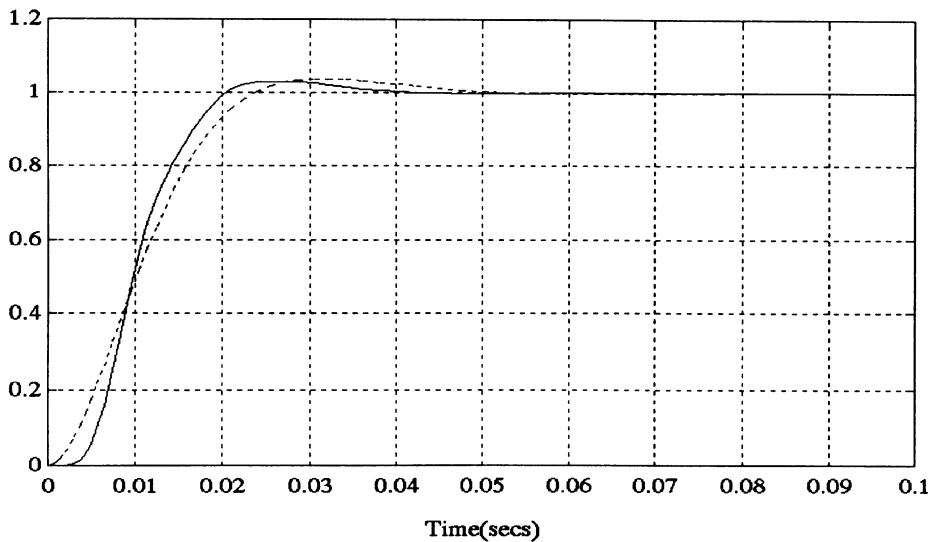


Fig. 4 (————) Time response of the 6-th order system
(- - - - -) Time response of the 2-nd order system

From fig.4 it is obvious that the differences caused by substitution are minimal. It makes substitution completely acceptable. Second order system enables very easy and fast calculation of the Kv-factor for necessary position control loop damping.

We can write the second order system transfer function in the following form:

$$\frac{Xo(s)}{Xi(s)} = \frac{1}{\frac{1}{\omega_n^2} \cdot s^2 + \frac{2\zeta}{\omega_n} \cdot s + 1} \quad (11)$$

where ξ is position control loop damping ($0 < \xi < 1$), and ω_n is nominal angular frequency of the position control loop. We will transform equation (10) in the form of equation (11).

$$\frac{Xo(s)}{Xi(s)} = \frac{Kv}{\left(\frac{2D}{\omega} + \frac{2D_m}{\omega_m} + \frac{T}{2}\right) \cdot s^2 + \cdot s + Kv} = \frac{1}{\frac{\left(\frac{2D}{\omega} + \frac{2D_m}{\omega_m} + \frac{T}{2}\right)}{Kv} \cdot s^2 + \frac{1}{Kv} \cdot s + 1} \quad (12)$$

Comparing (11) and (12) we can obtain:

$$\omega_n = \sqrt{\frac{Kv}{\frac{2D}{\omega} + \frac{2D_m}{\omega_m} + \frac{T}{2}}} \quad \text{and} \quad \zeta = \frac{1}{2} \cdot \sqrt{\frac{1}{Kv \left(\frac{2D}{\omega} + \frac{2D_m}{\omega_m} + \frac{T}{2}\right)}} \quad (13)$$

In order to have required position control loop damping ζ , Kv-factor should be calculated with the following equation:

$$Kv = \frac{1}{4\zeta^2 \left(\frac{2D}{\omega} + \frac{2D_m}{\omega_m} + \frac{T}{2}\right)} \quad (14)$$

Equation (14) gives direct analytical relationship between Kv-factor and ω , D , ω_m , D_m , T and ζ , which are already known variables, or can be calculated very easy.

With the equation (14) it is possible to estimate CNC machine tool feed drive position loop gain Kv without performing experiments.

Correctness of the equation (14) was checked on real feed drive position control loop of CNC milling machine FGS 32-CNC. Position loop damping $\xi=0.7$ is preferable according [11]. That is the value which gives minimal contouring errors. Other numerical values of the examined system were: $\omega=1000 \text{ s}^{-1}$, $D=0.7$, $\omega_m=663 \text{ s}^{-1}$, $D_m=0.17$, and $T=0.006 \text{ s}$.

With the substitution in the equation (14) the position loop gain value $Kv=103.85 \text{ s}^{-1}$ was calculated. Experimentally tuned value of Kv-factor on examined machine tool axis was

$K_v=100 \text{ s}^{-1}$. The difference between analytically calculated and experimentally obtained value of K_v -factor is around 4%, which is completely acceptable.

3. CONCLUSION

The equation (14) enables very fast, simple and precise analytical determination of position loop gain K_v as a function of already known position control loop parameters (ω -nominal angular frequency of the feed drive electrical parts, D -damping of the feed drive electrical parts, ω_m -nominal angular frequency of the mechanical transmission elements, D_m -damping of the mechanical transmission elements and T -sampling time). In that way we can avoid long-time experimental tuning of the K_v -factor on machine tool. Also analytical calculation of the K_v factor gives possibility to estimate the accuracy of the system in the design phase.

REFERENCES

1. Stute G., Böbel K., Hesselbach J., Hodel U., Stoff P.: Electrical feed drives for machine tools. Edited by Hans Gross, John Wiley & Sons, 1983.
2. Weck M.: Handbook of Machine Tools, Volume 3, Automation and Controls. Chichester, John Wiley & Sons, 1984.
3. Bollinger J., Stute G., Van Brussel H., Dinsdale J.: Digital Controls and Feed Drives state-of-the-Art and new Developments, Annals of the CIRP Vol.29/2/1980, 497-506.
4. Weck M., Ye G.: Sharp Corner Tracking Using IKF Control Strategy, Annals of the CIRP Vol. 39/1/1990, 437-441.
5. Palcev A.V., Electrical and Hydraulic drives for NC machine tools and industrial robots. ENIMS, Moscow, 1982, 21-30, (In Russian).
6. Müller P.: Steuerungen und Antriebe für die Hochgeschwindigkeitsbearbeitung, Werkstatt und Betrieb 120(1987)9, 704-706.
7. Gose H., W. Papiernik: Digitale Regelsysteme für CNC-Werkzeugmaschinen, wt-Z. ind. Fertig. 75(1985) No.9, 579-582.
8. Gose H.: CNC-geregelte, discrete Lageregelkreise bei numerischen Mehrachsenbahnsteuerungen, wt-Z. ind. Fertig. 67(1977), No.8, 455-459.
9. Harder L., Isaksson A. J.: Robust PI-control of cutting forces in turning, Proceedings of 31 MATADOR Conference, Manchester, U.K., 1995, pp.261-266.

10. Von Andreas Laika: Ermittlung des Zeitverhaltens von Lageregelkreisen aus den Frequenzgängen ihrer Bauelemente, VDI-Z 119 (1977) Nr.6, 315-318.
11. Aun-Neow Poo, Bollinger J. , Younkin G.: Dynamic Errors in Type I Contouring Systems, IEEE Transactions of Industry Applications. Vol.IA-8, No.4, 1972,477-484.

COMPUTER AIDED TOLERANCE CHARTING

A. Del Taglia and S. Perugini
University of Firenze, Firenze, Italy

KEYWORDS: Tolerance Charting, Process Planning, CAD

ABSTRACT: This research has aimed to design and to implement a Computer Aided Tolerance Charting System and to integrate it into a CAD environment, in order to obtain a fast and reliable analysis tool for assessing Process Plan performance. Pertinent literature is discussed briefly, and the major problems arising in Tolerance Charting – description and editing of the Process Plan within the CAD environment, modeling of machining errors and charting computation – are presented. Finally, a solution for the problems is proposed, with an example of application.

1. INTRODUCTION

Tolerance Charting is a well known technique used to assess the Process Plan performance. When the Process Planner chooses the process, the machine tools, the tools and the process parameters, he must respect a constraint: the product quality. In other words, the resulting dimensions, shape and surface finish must meet the designer specifications. Moreover this goal must be met with a minimum machining cost. For this reason machining tolerances should be as large as possible; more precisely, they should be larger on expensive machining operations and tighter on cheaper operations. Unfortunately machining tolerances present complex problems; they are dependent on the process variables, but also demonstrate a complicated, non-explicit dependency. However, it is possible to predict expected machining errors on manufactured work by applying an analytical tool, in this case Tolerance Charting. It allows a post-analysis stage; therefore changes can be made in the process plan or process parameters in order to meet the design tolerances with a pre-determined margin. For this reason a process plan that gives machining tolerances looser

Published in: E. Kuljanic (Ed.) *Advanced Manufacturing Systems and Technology*,
CISM Courses and Lectures No. 406, Springer Verlag, Wien New York, 1999.

than required must be reformulated because it is unfeasible, while a process plan that gives excessively tight machining tolerances must be changed in order to decrease the machining cost. Such reformulations produce an optimized process plan: the process planning, that is the synthesis stage, is followed by the analysis stage contained in the tolerance charting. As N. Shu has shown [1], to achieve a good result in a synthesis problem, a good and fast analytical tool must be used. In fact, as figure 1 demonstrates, when there is an open loop gain $SA \gg 1$, *Output* is dependent only on *Analysis* performance. Figure 1 also shows that despite a poor process planning procedure, good results can be achieved if a good and fast tolerance charting system is available; it evaluates the process plan and drives the process planner to generate a better one in an iterative procedure.

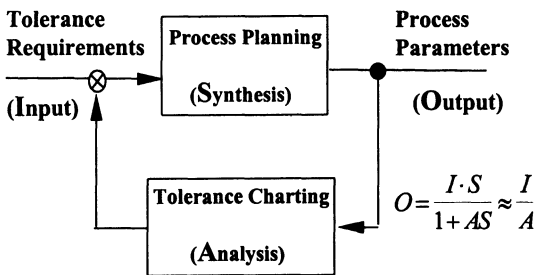


Figure 1. The Synthesis and Analysis loop (adapted from N.P.Shu [1])

Tolerance charting, introduced in the '50ies, is based on a manual procedure [2]. Two pioneering works [3, 4] provide evidence for its relationship to process planning; these works also presented ideas that research has not yet completely exploited. In particular, [3] sets out the ideas of tree structure and incidence matrices organization for process plan representation, the analysis of machining errors, and the concept of machining cost related to the desired machining accuracy.

Other works on Tolerance Charting [5, 6, 7, 8, 9] present solutions based on computer programs and in some cases [5, 10] a Computer Aided Tolerance Charting integrated with a CAD system. In addition these papers present an interesting discussion of the related literature [11], tolerance transfer [9, 12] and tolerance optimization [7, 8 11, 13]. The differences among the works in the literature cited, consist in the way the main problems of Tolerance Charting systems, are faced and solved. These are mainly the data representation, the tolerance balancing objective, and the optimization method used. Nonetheless, nearly all the literature considers machining errors to be a fixed quantity characteristic of the machine used regardless of the machining sequence.

2. BASIC ASSUMPTIONS

During our work, we have made several observations:

- firstly, the error modeling, normally used in the works related to Tolerance Charting, is very rough; the error is given simply as a function of the machine tool accuracy and machining type. Clearly, to present a complete modeling of machining errors would be very complicated and would require a modeling for various components: machining process, machine tool, fixture, workpiece and tool structures, and system dynamics.

Furthermore such modeling would have to consider the thermal effects on structures. Despite these difficulties, we argue that it is possible to adopt an intermediate approach. Taking into account the different components of the manufacturing errors, and evaluating them with overall factors, we determine the order of magnitude of the error, maintaining at the same time the link with the process plan choices. Furthermore, a resultant error depends on many simple errors; thus it seems too conservative to establish a worst case analysis by simply providing the total sum of all these errors. We prefer, therefore, view the error as a stochastic variable that takes into account the statistical distributions of the single errors.

- secondly, based on the literature analyzed, we find all procedures used to “optimize” or “balance” the tolerances, are quite useless. None of these procedures attempt to relate tolerance broadening to process plan modification. However, even if this element had been considered, it would have affected only the machining parameters and not the operation sequence. Consequently we believe that the best way to obtain process optimization is by using an iterative process that consists both of process plan synthesis and process plan analysis, as shown in figure 1.

- thirdly a charting procedure should include three significant factors: be easy to make, be fast, and be completely integrated with a CAD system. To achieve this, it is necessary for the Process Plan formulation to be carried out inside the same CAD system in the following steps: the data regarding the workpiece design and the process plan are extracted from the respective databases; the data are arranged in the computer memory in a dynamic structure; for each dimension to be checked, the complete operation sequence is found that moves from the rough surface to the finished surfaces; errors are determined and accumulated; finally, results are given for machining tolerances and their statistical parameters.

3. ANALYSIS OF MACHINING ERRORS

Errors due to machine tool accuracy

The greater part of machining errors are determined by the positioning accuracy and repeatability of the machine tool, due to feed errors, geometrical errors, presence of backlash, etc. But it is also true that some errors are time-dependent as they are the result of thermal deformations of the machine tool structure. Modeling of this errors is quite complicated and quantitative information is difficult to obtain. A rough estimation of this error is made, according to ISO, as follows: - a constant part A, characteristic of the machine tool is considered; - a part B·L, proportional to the traveled distance L, is added; the error is limited by a maximum value C, corresponding to the maximum observed error. The machine tool error ϵ_M is thus expressed by the following relation:

$$\epsilon_M = \min \{ (A+BL), C \}$$

Errors due to fixturing

These errors arise due to the imperfect repeatability of the workpiece position in the fixture and to the fixture error. Such errors are always present on the dimension and geometry of two surfaces if these are not machined with the same reference surfaces and on the same

fixture or if, after the machining of the first surface, the workpiece is unclamped and clamped again. For instance if the two planes P1 and P2 in figure 3 are machined moving the workpiece from the fixture (machine P1, then unclamp the workpiece, then clamp again, then machine P2), the distance and parallelism of the two planes are affected by the repeatability error of the clamping in the fixture; if the two machining operations are performed with different fixtures (but in respect to the same reference surfaces), the two fixture accuracy errors will also affect the machining error.

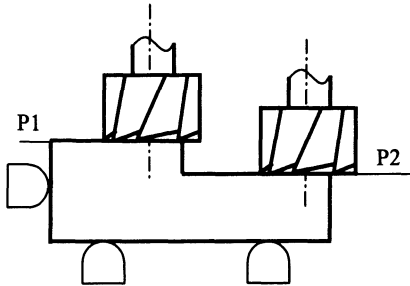


Figure 3. Errors are different if two surfaces are machined:

- with/without int. workpiece unclamping
- dimensional
- with the same tool with/without int. tool change
- with different tools

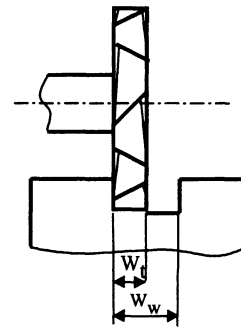


Figure 4. Influence of the tool error

Errors due to the tool

The errors introduced by the tool may have different sources; therefore it is convenient to analyze them one by one:

- pre-setting error: occurs in pre-setting phase. The tool is measured in a pre-setting machine or directly on the machine tool; the tool pre-setting errors are transformed into machining errors by the Numerical Control unit that uses wrong data to program the tool path.
- positioning error: each time a tool is changed in the machine spindle or turret, a repeatability error occurs. The position is never exactly the same and depends on the tool holder accuracy and cleanness of the contact surfaces.

These two errors do not cause a machining error if the two surfaces (say P1 and P2 of figure 3) are machined by the same tool and the tool is not removed in the meanwhile. If the tool is the same but is removed in the meanwhile, only the positioning error will influence machining error. However both errors will cause machining errors if the tool is not the same.

- dimensional error: this error may cause machining errors if different surfaces of the same tool are used to machine different surfaces in the workpiece. As figure 4 shows, the two sides of a groove are machined by the two sides of a circular milling tool; in this case the groove width W_w is affected by the error on the tool width W_t .
- wear error: in normal conditions, the tool undergoes to progressive wear; hence it removes less material than that specified in the machining instructions, and consequently

gives a systematic error that may or may not produce a dimensional error depending on the surfaces orientation.

Errors due to machine tool deformation

The mechanical structure formed by the tool, tool-holder, machine tool, fixture and workpiece is subjected to elastic deformations due to the cutting force. These deformations produce a machining error whose orientation is the same as that given by wear. The importance of the error depends on many parameters; primarily these are the system stiffness, the cutting forces intensity and direction. The cutting force intensity is determined only by the material properties, chip cross section and tool geometry; the cutting force direction influences in two different ways the generation of machining errors: because the stiffness of the structure is different in different directions, the same force causes different deformations depending on its direction; furthermore, the cutting force direction causes the direction of the relative displacement of the tool respect to the workpiece; the machining error is the component perpendicular to the workpiece surface of the relative displacement. The value of the error cannot be assessed with a high degree of accuracy as a lot of information would be necessary. Nonetheless, the order of magnitude may be obtained by evaluating the stiffness of workpiece, fixture, tool and machine tool, the material specific cutting force and chip cross-section. For this purpose, two coefficients have been introduced: - C_d that is a multiplier of the resultant system stiffness and gives information whether all the structural elements works in their maximum stiffness direction ($C_d=1$) or not ($C_d<1$); - C_t that is a multiplier of the resultant system deformation, and is maximum when the deformation is perpendicular to the workpiece surface ($C_t=1$) and minimum when the deformation is tangent to the workpiece surface ($C_t=0$).

The operator does not give all the numerical values of the error parameters; instead, these are normally retrieved from a technological data base, depending on the selected machine tool, fixture and workpiece material. However, in a few cases the operator is requested to indicate a category (e.g. for workpiece stiffness) where each category is associated to a numerical value.

An important characteristic of the tool wear error and machine deformation error is that they have non-zero mean value; this causes the machining error on one operation to influence errors in subsequent operations. For instance, if a roughing operation is affected by an error due to tool wear or to structure deformation, less material is removed than desired; thus in the subsequent finishing operation, the larger depth of cut contributes to a further error.

4. DATA STRUCTURE AND CAD INTERFACE

The data needed for Tolerance Charting come from information related to the Process Plan and the Design. Normally the latter information is available in numerical format that is stored in the CAD Data Base; thus it no longer needs to be taken from the blueprints.

Process Plan information, however, is rarely available in numerical format. More often than not, it is found in paper form related to process sheets, and operations and tools records. Such records are used mainly for transmitting information to NC programmers, to the tool room for tool preparation etc. In short this information is typically human-to-human communication. Hence this type of record is not useful for computer based Tolerance Charting needs. In this case, data must be accessed automatically and therefore must in a format suitable for computer-to-computer communication. It might seem that NC programs are capable of solving this problem, especially when NC programming is performed with the aid of a CAM system that allows the necessary integration with CAD. We have rejected this form of operation because we believe that the Tolerance Charting process, as has been shown in the introduction of this paper, is as more useful as more early is performed. After the NC program has been produced, a lot of work has been done and, if the tolerance charting calculation asks for a process plan review, this work (and money) is lost. For this reason we think that also the process plan design phase should be informatized. To this end we have developed a procedure, integrated into the CAD system, that allows the Process Planner in defining machining operations inside the CAD environment; the process plan is automatically available in computer format at the end of this procedure.

The steps followed by the Process Planner work are the following:

- the part model is opened in the CAD system and the process planning program is run as a Macro instruction inside the CAD itself;
- for each machining operation the operator selects:
 - the surface to be machined
 - the reference surface
 - the fixture code
 - the machine tool code
 - the tool code
 - the machining parameters
 - the machining conditions

the surfaces are chosen with the pointer device (e.g. mouse, track ball); the CAD system returns an internal code used to identify the surface in the CAD Data Base; furthermore a label is automatically given to every surface, in order to identify it both in the drawing and in the process plan: this label is a progressive alphabetical letter starting from "A"; the letter is followed by a number indicating the number of machining operation made on the surface; e.g. A1 means roughing of surface A, and A2, A3, are the successive machining operations.

- measuring instructions can also be introduced. A measuring instruction is characterized by a special machine code that is associated to the measuring accuracy. The result of this operation is that the error stack-up process is interrupted which means and the surface position, at that moment, is considered known, albeit with the uncertainty given by the measuring accuracy. Therefore the depth of cut used for error computation will

not be that given by the process plan, but is computed taking into account the accumulated error;

- other operations, as inspection, deburring, manual operations can be input; however, only those operations that are relevant to tolerance charting have an operation code and are used in the further processing (intermediate tool presetting, tool wear measurement and compensation, workpiece unclamping, tool unmount and mount). All the other, including comments and remarks, are introduced only for process plan completeness;
- at the end of his work, the operator gives an "Exit" instruction and the control returns to the CAD system.

All the data that are input or retrieved during this phase are stored in a document that is a Chronological Process Plan, as shown in figure 5. Each record corresponds to an operation characterized by an operation number, and a code of the operation type. This is followed by all the related parameters. This process plan representation contains all the necessary information and maintains the precedence relations between operations. This structure is useful independently of the tolerance charting, because it is a document that, together with the workpiece drawing, could be used, for example, for NC programming.

The procedure for tolerance charting also requires information about which dimensions are to be verified. This information is stored in a table that contains, for each dimension, the related surfaces, the nominal value and the allowed tolerances. The table is created automatically at the end of the process plan definition. The procedure is the following: for every toleranced dimension found in the CAD model, the automatic procedure searches the related surfaces in the Process Plan file; if both surfaces are present as machined surfaces, a record in the table is added; the record contains the surfaces labels, the nominal dimension, and the design tolerance.

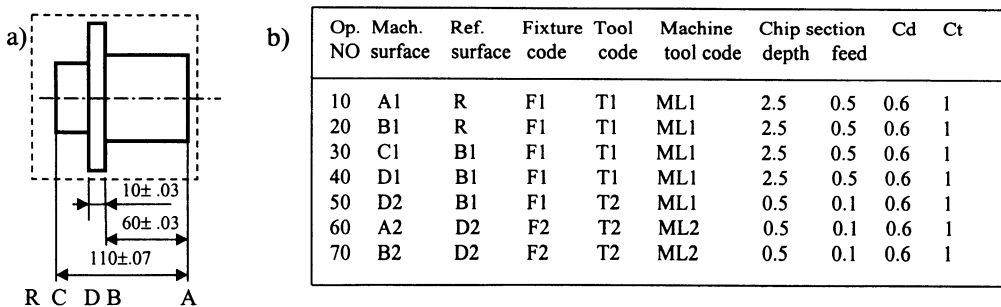


Figure 5. A simple Process Plan: Chronological representation
 a) workpiece drawing b) Process Plan

5. THE TOLERANCE CHARTING PROCEDURE

After the phase of data preparation, the Tolerance Charting procedure begins. The first step consists of the building of another type of organization for the Process Plan data. Starting

from the Chronological Process Plan representation, the Hierarchical Process Plan is obtained. This is a different description of the process plan, and is represented by a tree graph, that relates every machined surface to its reference surface (parent). Figure 6a gives a representation of a Hierarchical Process Plan and figure 6b shows its internal representation as a dynamic structure; the last pointer is used to link each record to its parent, and the other organizes the last machined surfaces in a ring structure. During the construction of this structure, the errors computation is also performed. For each machining operation, all the error components described in section 3 are calculated and stored in the corresponding record; these error components will be used afterwards to find the machining tolerances.

The computation of the resulting tolerances proceeds as follows:

- starting from each dimension to be verified, the occurrence of both surfaces involved is found on the process tree, at the maximum depth (search starting from the bottom);
- by exploring the tree, a common parent is found, and a sub-tree is extracted;
- the common parent is a reference surface from which the two branches that reach the surfaces start; the two branches identify the sequence of operations performed to obtain the surfaces;
- following both the branches the single error components are accumulated, and a total error is found;
- only the active components are considered and summed; for instance, fixture errors and tool errors may compensate themselves if two surfaces are machined with the same reference and fixture, without moving the workpiece and with the same tool; or the tool wear error or machine deformation error compensate if the machined surfaces are accessed from the same side.

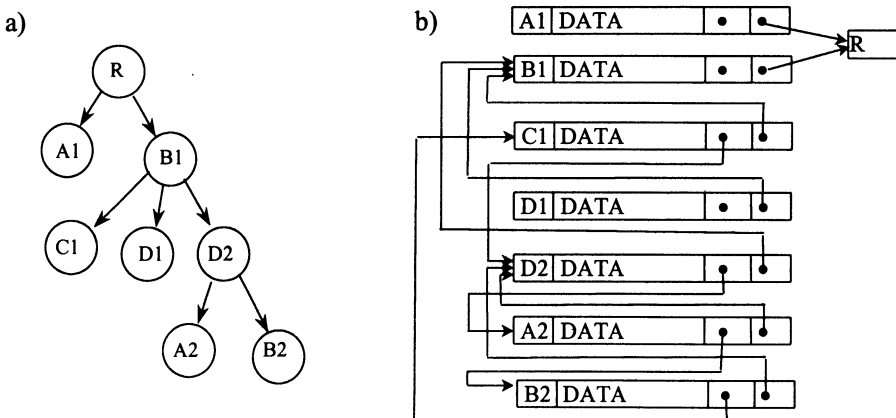


Figure 6. Hierarchical representation of the Process Plan

a) tree structure b) data structure

At the end, the results are reported in the table containing the dimensions to be verified; to each record the following results are added:

- the centre of tolerance of the obtained dimension;
- the lower and upper tolerance of the obtained dimension;
- the probability that the obtained dimension is outside the design tolerances.

Figure 7 shows the completed table containing the results of tolerance charting; the first five columns are input data, while the last four columns are produced by the program.

Input Data					Results			
S1	S2	Nom.Value	L.Tol	U.Tol	Centre Tol.	Lower Tol.	Upper Tol.	Defect Probability
A	C	110.00	-0.07	0.07	110.02	-0.02	0.02	0.
A	B	60.00	-0.03	0.03	60.00	-0.01	0.01	0.
B	D	10.00	-0.03	0.03	10.00	0.01	0.01	0.

Figure 7. Input data and results of the Tolerance Charting process

5. CONCLUSIONS

This procedure for tolerance charting permits a fast verification of the process plan performance, in terms of respect of the specified design tolerances. Being integrated into a CAD environment together with the process plan definition procedure, editing of the process plan and editing of the CAD model may be easily performed. This allows for a new calculation of machining errors and of manufacturing tolerances to be obtained automatically and in a short time. Consequently it is possible to have process plan optimization through an iterative procedure. The limitations of the described procedure are mainly the following: - only dimensional tolerances are treated; - all the toleranced dimensions must be collinear; - the procedure has been implemented in conjunction with a specific CAD system. Nevertheless this approach is sufficiently general to be easily extended to other types of tolerances. However the integration with a different CAD system requires the translation of the interface routines in the specific language, if any, that allows user written routines to perform read/write operations on the CAD Data Base.

6. REFERENCES

1. Shu N.P., 1990, The Principles of Design; Oxford Series on Advanced Manufacturing, Oxford University Press, 1990.
2. Wade O., 1983, Tolerance Control; Tool and Manufacturing Engineers Handbook, Vol. I Machining, Society of Manufacturing Engineers (SME), Dearborn, Michigan.

3. Bjørke Ø., Haugrud B., 1968, *Mathematical Methods in Planning of Machining Operations*; *Annals of the CIRP*, Vol. XVI, pp. 399-407.
4. Fainguelernt D., Weill R., Bourdet P., 1986, *Computer Aided Tolerancing and Dimensioning in Process Planning*; *Annals of the CIRP*, Vol. 35/1/1986.
5. Tang G.R., Fuh Y.M. Kung R., 1993, *A List Approach to Tolerance Charting*; *Computers in Industry*, 1993, Vol. 22, pp. 291-302.
6. Ji P., 1993, *A tree Approach to Tolerance Charting*; *Int. J. Prod. Res.* Vol. 31 No. 5 pp. 1023-1033.
7. Ngoi B.K.A., 1992, *Applying Linear Programming to Tolerance Chart Balancing*; *Int. J. Adv. Manuf. Technol.*, 1992 Vol.7, pp. 187-192.
8. Ngoi B.K.A., Teck O.C., 1993, *A Complete Tolerance Charting System*; *Int. J. Prod. Res.* Vol. 31 No. 2 pp. 453-469.
9. Ngoi B.K.A., Fang S.L., 1994, *Computer-Aided Tolerance Charting*; *Int. J. Prod. Res.* Vol. 32 No. 8 pp. 1939-1954.
10. Britton G.A., Whybrew K., Tor S.B., 1996, *An Industrial Implementation of Computer-Aided Tolerance Charting*; *Int. J. Adv. Manuf. Technol.*, 1996 Vol.12, pp. 122-131.
11. Irani S.A., Mittal R.O., Lehtihet E.A., 1989, *Tolerance Chart Optimization*; *Int. J. Prod. Res.* Vol. 27 No. 9 pp. 1531-1552.
12. Li J.K., Zhang C., 1989, *Operational Dimensions and Tolerance Calculation in CAPP Systems for Precision Manufacturing*, *Annals of the CIRP*, Vol. 38/1/1989.
13. Wei C.C., Lee Y.C., 1995, *Determining the Process Tolerances Based on the Manufacturing Process Capability*; *Int. J. Adv. Manuf. Technol.*, 1995 Vol.10, pp. 416-421.

A DATA ACQUISITION SYSTEM TO MONITOR AND IMPROVE THE PINCH AND ROLL PROCESS OF COMPRESSOR BLADE MANUFACTURE

R.A. Belinski and J.S. Gunasekera
Ohio University, Athens, OH, USA

KEY WORDS: Blade Forming, Pinch, Rolling, Monitoring, Data Acquisition

ABSTRACT: This paper is concerned with a scientific study of the pinch and roll process that is currently used to produce compressor blades for jet engines. It is several decades old and has some shortcomings. The process has to be improved in order to insure the ongoing competitiveness of the pinch and roll process against other blade forming technologies. A major shortcoming is the cost in both time and material involved in the setup of the machine for a production run. This process requires a large amount of time of skilled personnel and scraps several parts for each setup process. Another shortcoming is the variation of the quality aspects of the parts produced by the pinch and roll process. The variations in machine setups and between different machines cause the pinch and roll process to produce a range of output product deficiencies. The development and installation of a data acquisition system (DAQ) specifically designed for the process has overcome these shortcomings. The DAQ system provides setup assistance tools as well as process monitoring capabilities. The DAQ system can monitor several factors that characterize the behavior of the machine and the subsequent part quality. The information obtained by the sensors on these factors can be used to provide information about “good” and “bad” parts in the form of “part signatures”, which are the waveforms of the monitored factors. This information has been used to improve and understand the current process and can be incorporated in any future press designs. The DAQ system has shown the greatest benefits concerning the setup procedures. Improvements in both the efficiency and the effectiveness of these procedures have reduced costs while enhancing part quality.

Published in: E. Kuljanic (Ed.) *Advanced Manufacturing Systems and Technology*,
CISM Courses and Lectures No. 406, Springer Verlag, Wien New York, 1999.

1. INTRODUCTION

A method of jet engine compressor blade fabrication is the pinch and roll process. This process was developed as an alternative to the then current method of manufacture, which was to machine and mill the blade directly from raw stock [1]. This process was extremely wasteful in both labor and material. Off the shelf alternatives were also inadequate. Forging equipment could not meet the required tolerances due to the inherent airfoil shape of the blade. Traditional rolling processes were also eliminated because of the platform located at the root of the blade. (This platform is later machined into a dovetail for final assembly into the engine.) As a result of these problems, the pinch and roll process was developed. The Pinch and Roll process is a two step forming operation, which utilizes two dies. First, a forging operation is performed on the root section of the blade that squeezes the part. This is called the pinching segment. Secondly, the dies simultaneously rotate in opposite directions to impart the proper thickness and contour to the compressor blade. The operation of the pinch and roll machine can be studied in Figure 1. Section (A) shows the placement of the blade in the shuttle of the machine before the process is executed. The forward movement of the shuttle into the dies is shown in section (B). Section (C) is a diagram of the actual pinch process. The dies squeeze the part near the root area during this operation. The last section, (D) of, shows the rolling operation. As the dies rotate, the shuttle (and the blade) moves outward away from the dies.

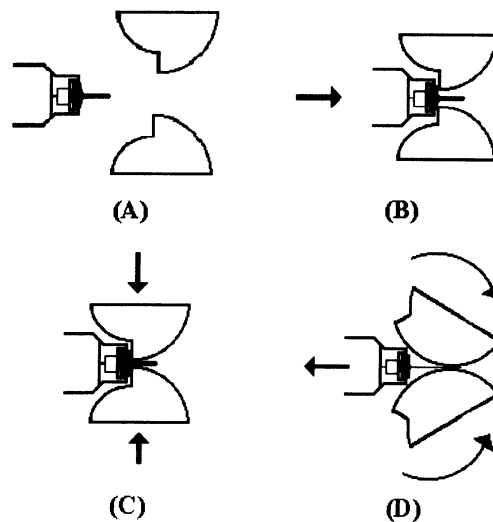


Fig. 1: The Pinch and Roll Process

The dies are rotated by the action of a single hydraulic cylinder by means of free differential linkage. This produces a two-degree of freedom system for the roll actuator mechanism. This means that the two dies are not constrained to rotate at the same rate or position. Because of this, the two dies may be at different angles at any time during the rolling proc-

ess. This process is used on blades of various materials. The type of material dictates if the process is run at room temperature or at elevated temperatures.

A set of two different dies is used in the process. One die has a convex shape and the other die has a concave shape. These shapes are the respective mating contours of the concave and convex sides of the desired blade. The dies are designed with a tapered shape so as to impart an airfoil shape of reduced thickness at the free end of the blade.

To improve the quality aspects and to reduce the associated setup costs of the process, the creation of a data acquisition system was undertaken. The setup process is a major shortcoming of the pinch and roll process. This process requires a large amount of time of skilled personnel and scraps several parts for each setup process. Another shortcoming is the variation of the quality aspects of the parts produced by the pinch and roll process. The variations in machine setups and between different machines cause the pinch and roll process to produce a range of output product deficiencies. To elevate these problems, the DAQ system provides setup assistance tools as well as process monitoring capabilities that can be used as diagnostic tools.

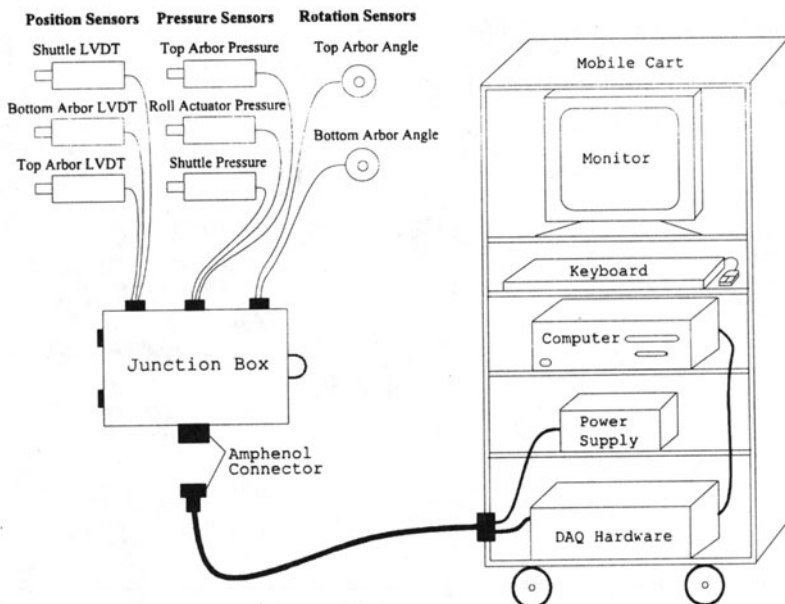


Fig. 2: DAQ System

2. THE DATA ACQUISITION SYSTEM

The data acquisition system consists of several parts. The sensors and their accompanying fixtures are located on the pinch and roll press. Other hardware, such as the computer and the terminal board, are located on a mobile cabinet so that they can service multiple

presses. The arrangement of the equipment in the cabinet and the different sensors and the junction box located on the press are shown in Figure 2. The mobile cabinet is connected to the sensors by means of an Amphenol connector, which allows quite connections between several presses.

The DAQ system consists of 8 transducers. The location of each sensor is numbered accordingly to the channel address of the sensor and is numbered 0 through 7. Fig. 3 shows the locations of the sensors, with their channel numbers on a drawing of the machine. Table 1 shows the location and the description of each of the sensors. All of these sensors combine to provide information necessary to completely describe the displacement and pressures that occur during the process. This allows the establishment of "good" and "bad" part signatures. These signatures can be utilized as warnings of the onset of process drift and as diagnostics of machine malfunctions. The data obtained from these sensors also can be used to replace trial and error set up processes, which are extremely expensive in terms of time, material and labor. To have a data acquisition system perform all of these tasks, efficient, effective, and intuitive software is required.

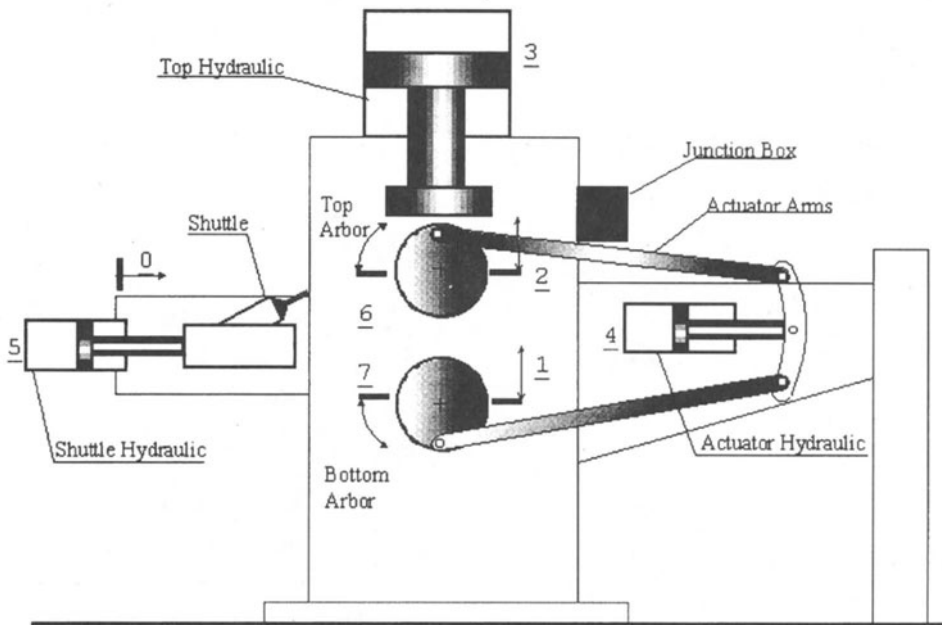


Fig. 3: Sensor Locations on the Pinch and Roll press

3. DATA ACQUISITION SOFTWARE

The data acquisition software programs initialize the DAQ system and direct the computer to manipulate voltage signals to produce output in meaningful units such as pressure, distance and angles. The programs then handle data output and storage. To aid in the pro-

programming for the DAQ system, LabVIEW, from National Instruments Corporation, was the software environment selected to generate and operate the programs needed for the DAQ system. LabVIEW uses a graphical programming language, G; to create programs in block diagram form. LabVIEW programs are called virtual instruments (VIs) because they appear and operate like actual instruments.

There were several separate LabVIEW programs produced for the instrumentation assembled on the pinch and roll press. Each of these programs (virtual instruments) performs a specific task and uses several or all of the sensors. The first program is the monitoring program called DAQ. The DAQ virtual instrument requires the user to input the two die radii, the DAQ scan rate, and the number of scans to acquire. When the process is run, the DAQ program produces screen output and also saves the data to spread sheet files. This saved data can be examined using another virtual instruments (called RECALL) or by spreadsheet programs such as EXCEL. The operation of the RECALL program is simple and is started by pressing the run button. This action is followed by opening of a dialog window that allows the user to browse for the data file of the process run to be investigated.

Table 1: Sensor Locations and Descriptions

Location and Name	Description
0. Shuttle Movement "in and out"	LVDT (linear varying displacement transducer) mounted on the shuttle, measures the displacement of the shuttle relative to the frame of the machine.
1. Lower Arbor Relative to Machine	LVDT mounted the frame of the machine, measures the displacement of the lower arbor relative to the machine.
2. Upper Arbor Relative to Lower Arbor	LVDT mounted the upper arbor, measures the displacement of the lower arbor relative to the upper arbor.
3. Top Hydraulic Cylinder "down"	Pressure transducer connected to the top hydraulic cylinder. This measures the pressure of the hydraulic fluid that forces the two dies are together.
4. Roll Hydraulic Cylinder "roll out"	Pressure transducer connected to the roll actuator cylinder. This measures the roll actuator pressure that supplies the torque during the rolling operation.
5. Shuttle Hydraulic "in"	Pressure transducer connected to the shuttle cylinder. This measures the pressure that is used to hold the shuttle forward to push the blade against the dies.
6. Top Die Angular Movement	A RVIT (rotary varying inductance transducer) that is attached to top arbor to measure the angular change of the top arbor relative to the machine.
7. Bottom Die Angular Movement	A RVIT that is attached to bottom arbor to measure the angular change of the bottom arbor relative to the machine.

The front panels of both the DAQ program and the RECALL program includes three graphic chart windows to display the output data. The horizontal scale of these charts is that of time in seconds. Each of these charts displays a separate type of data. The top chart includes the positional output generated from the linear varying displacement transducer

(LVDT) sensors. These represent the information of the positions (in inches) of the various parts of the machine. This positional chart can be seen in Figure 4. On the right of the chart is the legend that identifies that separate sensor's data. Located below the legend box is a palette of manipulative tools to aid in the investigation of the chart. This palette contains zoom tools and scale manipulators. The colors and line type of any of the the sensor traces can also be modified.

The middle chart in Figure 4 is the output of the pressure sensors. The units for this chart are in pounds per square inch and this chart shows the pressure levels for the three important hydraulic actuators during the process. This chart is most useful for hydraulic system monitoring, especially for the indication of the onset of problems such as seal and pump failures.

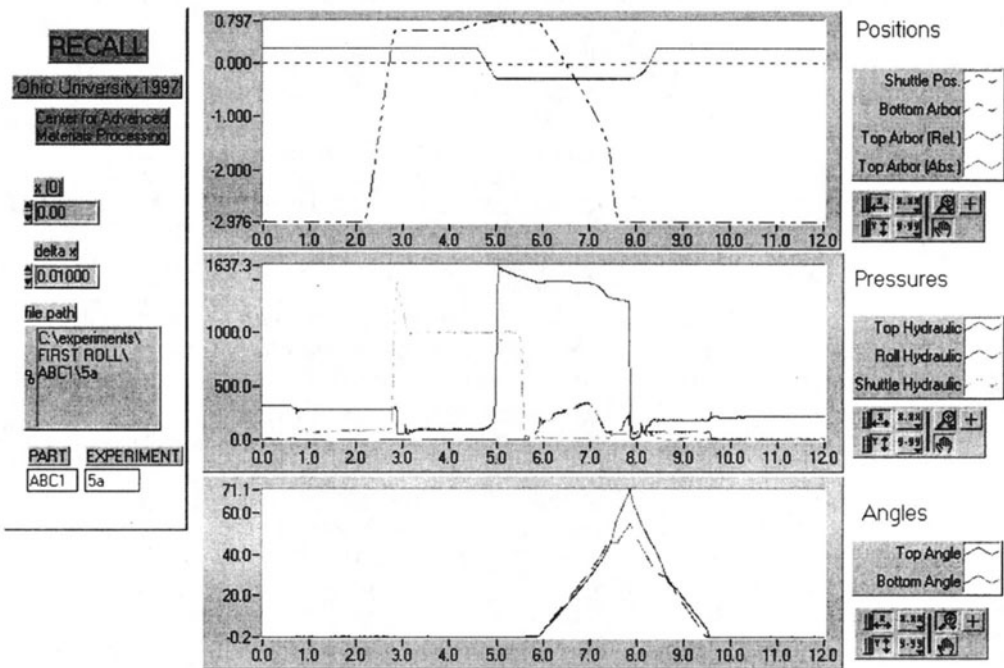


Fig. 4: Front panel of the RECALL virtual instrument

The bottom chart of Figure 4 provides a graph of the angular position (in degrees) of the arbors as related to time. All of these charts can be zoomed in or out, moved around, and scaled independently by using the tools palette as mentioned earlier. The default condition for these charts is for automatic range adaptation. This means that if the time length of scan or the vertical range changes run to run, the program will automatically fit the axis. These attributes allow easy investigation of the displayed data.

Another important program is the SETUP virtual instrument. The SETUP program is utilized to aid in the setup procedure of the pinch and roll machine. It is also used in the setup and zeroing of the DAQ system. This program only manipulates the data that comes from the three displacement sensors (LVDTs) and the two rotational sensors (RVITs). The SETUP front panel is shown in Figure 5.

The SETUP program executes a continuous loop that evaluates the output from the position sensors and manipulates this output to produce screen indicators that help the machine setup crew perform their tasks quicker and more accurately. This is accomplished by the use of light banks. A light bank consists of 3 lights, one of which is green and the other two are red. The green light means that the measurement is in specifications. The red lights dictate that the response is out of specification, and to what side is that response out. This provides the user with a continuous source of feedback while making machine adjustments. Besides the positional information, machine specific calculators are included to help prevent mathematical errors during the process. One of these calculators solves the complex preload system for the pinch and roll press, which was previously misunderstood. The SETUP program also provides the user with accurate information about the die/arbor rotations, which is necessary for the pinching stage of the process.

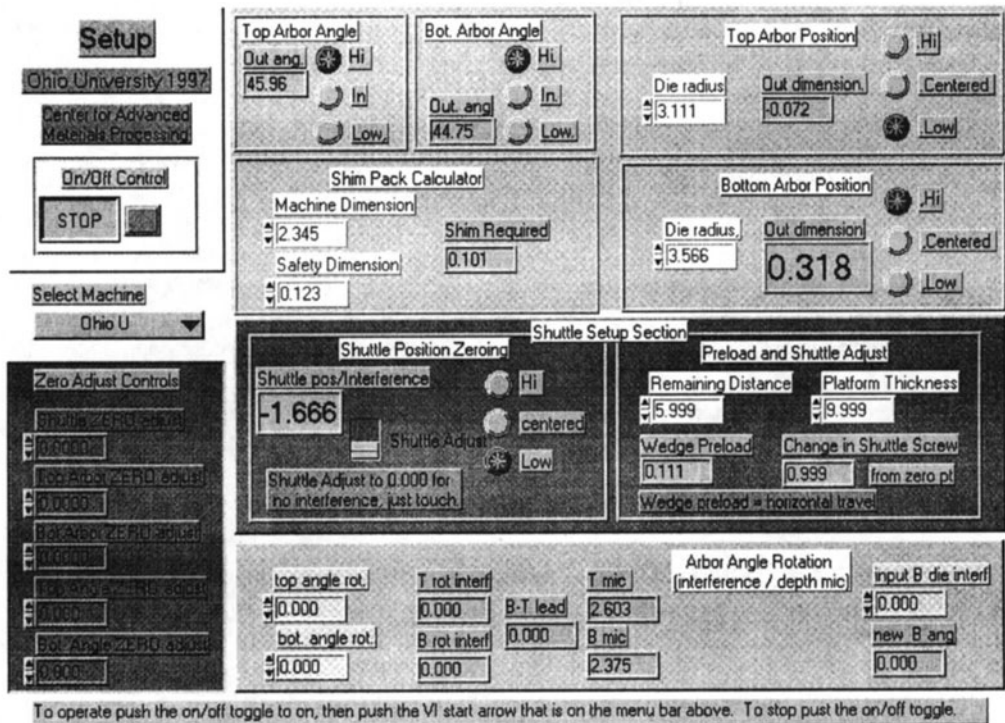


Fig. 5: SETUP Front Panel

4. OUTPUT, FINDINGS AND RESULTS

The DAQ output provided much insight into the pinch and roll process. The development of “good” and “bad” process signatures from the waveforms of the monitored factors allows quick and precise determination of process problems. The DAQ also was essential for understanding the complex workings of the pinch and roll press. Systems such as the shuttle preload system were not understood completely and therefore not utilized to their potential. The shuttle position and the shuttle hydraulic system plots allow for a detail investigation of the interaction of this system with the rest of the press during the pinching process, which involves simultaneous movement between the two dies and the shuttle that holds the part. As the die close onto the part the shuttle travels forward to push the part into the cavity formed by the closing dies. The proper movement of the part and the force developed by the shuttle system has to occur at the proper time and place in order to insure the required part characteristics. Previously, this was misunderstood, and was obtained only with a hit or miss procedure.

The waveforms were also evidence of other machine movements that were not known. When the two die close during the pinching process, the bottom die is depressed. This moves the part centerline from its optimum position for the rest of the process. The DAQ waveforms also showed that the top die was separating from the bottom die during the roll out process. The position plots quantified this “lifting” process that was previously thought unlikely. The pressure plot for the hydraulic cylinder responsible for counteracting this separation force demonstrated a hump at this point in the process. This was due to the backing of the piston in the cylinder, which compressed the entrained air in the hydraulic fluid. The hydraulic system sensor also pointed out that a pressure spike occurred increasing the pressure in the cylinder to 1.6 times the set value.

The most important information gathered by the DAQ system waveforms concerned the rotation of the dies and the arbors. Since the two dies are connected through a free differential, the simultaneous rotation of the set is not insured. The die having the greatest resistance to rotation slows until the other die’s resistance equals it. The two dies can swap the lead-lag rolls during the process. The die set is also not usually a matched set that possesses the same radii for both dies. This also causes unequal die rotation problems. For similar arc lengths, the small radius die must rotate a larger angle than the larger radius die. The DAQ system showed that the free differential was partially compensating for this phenomenon.

This information has been used to improve the current process and can be incorporated in to future press designs. The information gained by the data acquisition system has also been used to perform two and three-dimensional simulations of the process. These simulations take into account the die lifting and the unequal die rotation waveforms in order to produce extremely accurate models. The high accuracy of these models allows the virtual design and testing of die configurations that can improve the quality and the cost of the pinch and roll process.

The pinch and roll process DAQ system has shown great benefits concerning the setup procedures. The previous system of trial and error required 6 to 8 hours, one specially trained setup technician, and over ten parts (which were then scraped). The use of the DAQ setup routines allows this process to be accomplished by the same technician in 40 minutes using only three or four parts. These parts are also within specifications enough that they are not scraped out. This saves considerable cost when multiple passes are considered. The setup system also improves the quality, accuracy, and the consistency of the setups also further reducing cost.

REFERENCES

1. Pinch and Roll – Technical Information for Cold Forming Material and Processes, General Electric Company Reference Manual, General Electric – Rutland Vermont 1985
2. LabVIEW Manuals, National Instruments Corporation, Austin TX, 1996
3. Johnson, Gary W.: LabVIEW Graphical Programming: Practical Applications in Instrumentation and Control, McGraw-Hill, New York, 1994

THE HARMONIC FITTING APPROACH FOR CMM MEASUREMENTS OPTIMIZATION

E. Capello and Q. Semeraro
Politecnico di Milano, Milano, Italy

ABSTRACT: The dimensional inspection of a manufactured part by means of a Coordinate Measuring Machine (CMM) consists in the measurement of a set of points on the part and in the estimation of a "substitute geometry". The accuracy of the estimated substitute geometry depends on the number of the sampled points. The present work deals with the problem of the selection of the optimal number of measured points when the Least Square Method is adopted. The theory of the Harmonic Fitting (HF) will be presented for a flange element and it will be demonstrated that using the HF approach the analytic solution of the estimate error as a function of the number of measured points can be identified, thus evaluating the accuracy of the estimate. It will be shown that the usual statement that the accuracy increases as the number of measured points increases is not always true.

Key words: CMM, LSM fitting, sampling errors, flange element, Harmonic Fitting.

1. INTRODUCTION

The core process of the dimensional inspection of a manufactured part is the *substitute geometry* evaluation, where an analytic geometry is fitted to the measured data. The substitute geometry estimation is the basis for the verification of part conformity to specifications [1]. Data fitting is usually performed using the Least Square Method (LSM) [2] [3]. The accuracy of the estimated parameters \mathbf{p} that characterises the substitute geometry depends on several factors. The measurement uncertainty and the number of sampled points are the most rele-

vant ones. The difference between the estimated parameters vector \mathbf{p}' and the "real" one \mathbf{p} will be defined as the *estimate error*:

$$\boldsymbol{\varepsilon} = \mathbf{p}' - \mathbf{p} \quad (1)$$

These errors can be divided into two components: the first is related to the measurement uncertainty (*measurement error* $\boldsymbol{\varepsilon}^m = \mathbf{p}' - \tilde{\mathbf{p}}$), the second is related only to the sampling of a limited number of points (*sampling error* $\boldsymbol{\varepsilon}^s = \tilde{\mathbf{p}} - \mathbf{p}$). Obviously $\boldsymbol{\varepsilon} = \boldsymbol{\varepsilon}^m + \boldsymbol{\varepsilon}^s$. While the measurement error $\boldsymbol{\varepsilon}^m$ can be directly ascribed to the measurement process and can be modelled as a random variable with gaussian probability density distribution, the cause and the distribution of the sampling error $\boldsymbol{\varepsilon}^s$ are not known [4].

The paper presents the Harmonic Fitting approach which can be used to directly relate this kind of error to the machining process. Closed analytical formulae are derived in order to evaluate the sampling error as a function of the number of sampled points. In particular, the HF approach is applied to a flange element, where a plane geometry has to be estimated.

An accurate determination of the substitute plane is the basis for a reliable dimensional inspection. An incorrect determination of this plane may lead to an erroneous rejection or acceptance of the manufactured part, thus directly affecting the costs of the inspection [7]. Therefore the optimal number of sampling points derives from a compromise between accuracy and time/cost of inspection.

2. SUBSTITUTE GEOMETRY ESTIMATION USING THE LSM

A common geometry that has to be dimensionally controlled is the flange element. Points are sampled on a thin wall (see figure (1)) and deviations normal to the plane are measured. A total of N points are measured at locations x_h, y_h ($h = 0 \dots N-1$). It is always possible, with an appropriate positioning of the axes origin, to obtain that $\sum_{h=0}^{N-1} x_h = \sum_{h=0}^{N-1} y_h = \sum_{h=0}^{N-1} x_h y_h = 0$.

The measured value of z at x_h, y_h is z_h while the respective in plane measure is:

$$z(x_h, y_h) = ax_h + by_h + c \quad (2)$$

The deviation between the measured point and the estimated plane is $\delta_h = z(x_h, y_h) - z_h$ and coefficients a, b, c are chosen to minimize the mean square distance:

$$\Omega = \frac{1}{N} \sum_{h=0}^{N-1} \delta_h^2 = \frac{1}{N} \sum_{h=0}^{N-1} (ax_h + by_h + c - z_h)^2 \quad (3)$$

The minimisation problem can be solved by vanishing the gradient. This problem can be expressed in matrix notation:

$$\begin{bmatrix} \sum_{h=0}^{N-1} x_h^2 & 0 & 0 \\ 0 & \sum_{h=0}^{N-1} y_h^2 & 0 \\ 0 & 0 & N \end{bmatrix} \begin{bmatrix} a \\ b \\ c \end{bmatrix} = \begin{bmatrix} \sum_{h=0}^{N-1} z_h x_h \\ \sum_{h=0}^{N-1} z_h y_h \\ \sum_{h=0}^{N-1} z_h \end{bmatrix} \quad (4)$$

where $\mathbf{p} = [a \ b \ c]^T$. The solution is straightforward. However, from this solution the dependence of \mathbf{p} on the number of sampled points cannot be established. The proposed HF

is an equivalent solution but in the frequency domain and it should be preferred as closed formulae can be derived to evaluate the influence of the number of sampled points.

3. ESTIMATION USING THE HARMONIC FITTING APPROACH

3.1 Harmonic Fitting equations

If we consider the sampled points x_h as a discrete signal, phase and amplitude of harmonics can be calculated using the Discrete Fourier Transform (DFT):

$$X_h = \frac{1}{N} \sum_{k=0}^{N-1} x_k \exp(-j2\pi \frac{hk}{N}) \tag{5}$$

where $j = \sqrt{-1}$. The transform is periodic in the sense that $X_h = X_{N+h} = X_{-h}^* = X_{N-h}^*$ where * indicates the complex conjugate. Because of the particular origin placement it can be stated that $X_0 = Y_0 = 0$. Moreover, from the Parseval's theorem it can be derived that:

$$\sum_{h=0}^{N-1} x_h^2 = N \sum_{h=1}^{N-1} X_h X_h^* = N \sum_{h=1}^{N-1} |X_h|^2; \quad \sum_{h=0}^{N-1} y_h^2 = N \sum_{h=1}^{N-1} |Y_h|^2 \tag{6}$$

and for the sampled measures:

$$\sum_{h=0}^{N-1} z_h x_h = N \sum_{h=1}^{N-1} Z_h X_h^* = N \sum_{h=1}^{N-1} Z_h^* X_h \tag{7}$$

since $X_0 = 0$. Finally, problem (4) can be expressed in terms of frequency as:

$$\begin{bmatrix} \sum_{h=1}^{N-1} |X_h|^2 & 0 & 0 \\ 0 & \sum_{h=1}^{N-1} |Y_h|^2 & 0 \\ 0 & 0 & 1 \end{bmatrix} \begin{bmatrix} a \\ b \\ c \end{bmatrix} = \begin{bmatrix} \sum_{h=1}^{N-1} Z_h X_h^* \\ \sum_{h=1}^{N-1} Z_h Y_h^* \\ Z_0 \end{bmatrix} \tag{8}$$

and in matrix form:

$$\mathbf{B} \cdot \mathbf{p} = \mathbf{f} \tag{9}$$

The solution is therefore:

$$\begin{bmatrix} a \\ b \\ c \end{bmatrix} = \begin{bmatrix} \left(\sum_{h=1}^{N-1} Z_h X_h^* \right) / \left(\sum_{h=1}^{N-1} |X_h|^2 \right) \\ \left(\sum_{h=1}^{N-1} Z_h Y_h^* \right) / \left(\sum_{h=1}^{N-1} |Y_h|^2 \right) \\ Z_0 \end{bmatrix} \tag{10}$$

This solution is equivalent to the one obtained from (4) but the coordinates of all sampled points are expressed in terms of harmonics. In this way it is possible to explain the influence of the number of sampled points on the evaluated parameters. In fact, when the number of sampled points decreases the *aliasing* problem affects the harmonics and, through equations (10), the estimated parameters.

3.2 The effect of aliasing on the Harmonic Fitting

As known, aliasing arises when a band limited signal is sampled at a frequency lower than

double its limit frequency [8] [9]. For the discrete case, this frequency condition becomes a condition on the number of sampled points: The number should be higher than twice the maximum harmonic order present in the signal. If a lower number of points is sampled, due to the periodicity of the harmonics H_h an "overlapping" of harmonics occurs and more than one harmonic is summed to form the aliased harmonics \tilde{H}_h (see Figure (2)):

$$\tilde{H}_h = H_h + A_h \tag{11}$$

where A_h are the high order harmonics that are summed because of harmonics overlapping. When a surface is band limited at the order N ($H_h = 0; h > N$) and it is sampled with a number $M < 2N$ of points the effect of aliasing can be summarized in the following equations:

$$A_h = \sum_{p=1}^{P_h} H_{pM-h}^* + \sum_{q=1}^{Q_h} H_{qM+h}; \text{ where } P_h = \lceil \frac{N+h}{M} \rceil; Q_h = \lceil \frac{N-h}{M} \rceil \tag{12}$$

where $\lceil \rceil$ denotes integer truncation. Therefore different \mathbf{f} and \mathbf{B} matrixes dominate the solution:

$$\tilde{\mathbf{B}} = \begin{bmatrix} \sum_{h=1}^{M-1} |\tilde{X}_h|^2 & 0 & 0 \\ 0 & \sum_{h=1}^{M-1} |\tilde{Y}_h|^2 & 0 \\ 0 & 0 & 1 \end{bmatrix}; \tilde{\mathbf{f}} = \begin{bmatrix} \sum_{h=1}^{M-1} \tilde{Z}_h \tilde{X}_h^* \\ \sum_{h=1}^{M-1} \tilde{Z}_h \tilde{Y}_h^* \\ \tilde{Z}_0 \end{bmatrix} \tag{13}$$

The estimated parameters are:

$$\tilde{\mathbf{p}} = \tilde{\mathbf{B}}^{-1} \tilde{\mathbf{f}} \tag{14}$$

and the estimate error is therefore:

$$\epsilon^s = \tilde{\mathbf{p}} - \mathbf{p} = \tilde{\mathbf{B}}^{-1} \tilde{\mathbf{d}} - \mathbf{B}^{-1} \mathbf{d} \tag{15}$$

Therefore the difference between the estimated and the true parameters can be ascribed to the aliasing affect on both the \mathbf{B} and \mathbf{f} matrixes and depend on the $x - y$ shape of the flange (\mathbf{B} matrix) and on the harmonics of the generated surface (\mathbf{f} matrix). When there is no aliasing effect on the \mathbf{B} matrix (as in the circular case discussed later) the error can be totally ascribed to the generated surface.

4. THE CIRCULAR FLANGE CASE

In the case of a circular flange the derived equations can be sensibly simplified. In fact, for circular flanges $r_k = r \forall k$ and therefore:

$$X_h = \left\{ \begin{array}{ll} \frac{r}{2} & h = 1 \\ \frac{r}{2} & h = N - 1 \\ 0 & \text{elsewhere} \end{array} \right\}; Y_h = \left\{ \begin{array}{ll} -\frac{r}{2}j & h = 1 \\ \frac{r}{2}j & h = N - 1 \\ 0 & \text{elsewhere} \end{array} \right\} \tag{16}$$

and consequently:

$$\mathbf{B} = \begin{bmatrix} \frac{r^2}{2} & 0 & 0 \\ 0 & \frac{r^2}{2} & 0 \\ 0 & 0 & 1 \end{bmatrix}; \quad \mathbf{d} = \begin{bmatrix} \operatorname{Re}(Z_1 X_1^*) \\ \operatorname{Im}(Z_1 Y_1^*) \\ Z_0 \end{bmatrix} \quad (17)$$

When the circular flange is measured with a number of points greater than three no aliasing occurs in the X_h and Y_h transforms and these harmonics remain unchanged. The aliased matrixes are therefore:

$$\tilde{\mathbf{B}} = \mathbf{B}; \quad \tilde{\mathbf{d}} = \begin{bmatrix} \operatorname{Re}(\tilde{Z}_1 X_1^*) & \operatorname{Im}(\tilde{Z}_1 Y_1^*) & \tilde{Z}_0 \end{bmatrix}^T \quad (18)$$

Considering the effect of the aliasing, at the end one obtains:

$$\epsilon^s = \tilde{\mathbf{p}} - \mathbf{p} = \mathbf{B}^{-1} \cdot (\tilde{\mathbf{d}} - \mathbf{d}) = \mathbf{B}^{-1} \cdot \begin{bmatrix} \frac{2}{r} \operatorname{Re}(A_1) & -\frac{2}{r} \operatorname{Im}(A_1) & A_0 \end{bmatrix}^T \quad (19)$$

that is the sampling error can be ascribed only to the effect of the harmonics that are reflected on the harmonics of order 0 and 1:

$$\begin{aligned} A_0 &= 2 \sum_{p=1}^{P_0} \operatorname{Re}(Z_{pM}); & P_0 &= \left\lceil \frac{N}{M} \right\rceil; \\ A_1 &= \sum_{p=1}^{P_1} Z_{pM-1}^* + \sum_{q=1}^{Q_1} Z_{qM+1}; & P_1 &= \left\lceil \frac{N+1}{M} \right\rceil; & Q_1 &= \left\lceil \frac{N-1}{M} \right\rceil \end{aligned} \quad (20)$$

These equations state that the sampling error that arises from a limited sampling is generated by high-order harmonics of the surface that overlap on harmonics of order 0 and 1. Hence, an accurate selection of the sampled points should avoid the overlapping of high amplitude harmonics on the harmonic of order 0 and 1.

5. SURFACE GENERATION STATISTICS AND HF

5.1 Surface generation process

The geometric deviations (and the consequent surface harmonics) are related to the machining process used to generate the part. It can be assumed that these errors are the sum of several elementary deviations that can be related to specific phenomena (i.e. vibrations of machine tool, material spring back, etc.). Each elementary phenomena, with the pertinent elementary geometric deviation, contributes to the generation of total machining error. An example of such division can be found in [10] and in [11] for circular profiles

It is useful for the HF approach to classify the elementary phenomena and their machining errors into three classes:

1. **Space dependent phenomena:** These phenomena mainly derive from:

- *geometric errors of the moving elements of the machine tool;*
- *deformation of workpiece, tool or machine tool due to forces;*
- *residual stresses relief.*

These kind of machining errors are generally repeatable in the sense that parts machined with the same fixture system and with similar cutting forces present analogous surface structure, both in terms of deviation and position. Consequently, the harmonics of the surfaces are well defined, both in terms of amplitude and phase.

2. **Time dependent phenomena:** These phenomena can be related to the time domain rather than to the space one. An example of such phenomena is the run-out of a rotatory tool. These phenomena usually generate a surface pattern that can be described in amplitude but its position on the workpiece cannot be predicted. Therefore, the surface harmonics are generally repeatable in amplitude but not in phase. This leads to the impossibility of estimating the harmonics phase in an average sense.
3. **Random phenomena:** These phenomena are completely random, both in terms of amplitude and phase (or position on the workpiece). Therefore the harmonics that can be ascribed to this kind of phenomena cannot be predicted both in terms of amplitude and phases. They represent a sort of random "noise" that is superimposed to the more deterministic part of the spectrum.

The above classification and attribution of generated surface harmonics to specific phenomena is useful since the complete exploitation of the HF approach requires a statistical description of the harmonics.

5.2 The statistical approach

The first step in the statistical description of the sampling error is the statistical description of surface harmonics. This description can be obtained from a machined and measured set of surfaces. The joint probability density function of the harmonics $f(\mathbf{A})$ can be obtained. The joint probability distribution function $f(\epsilon^s)$ of the sampling error can be derived from $f(\mathbf{A})$ using the HF equations (10) together with the aliasing equations (12).

Care should be taken in the harmonic estimation. In fact, the phase can be accurately described in a statistical sense only for the space dependent-phenomena (type (1.) in the above discussion) and when the orientation of the workpiece has been tracked from the machine tool to the CMM. This is a special case that is not generally applicable.

In a more general case the phase has to be considered as a random variable with uniform distribution over $[0, 2\pi]$. In this case it can be demonstrated that the mean value of the sampling error is zero and an increase in the sampling error variance can be observed [6].

The probability of having a sampling error inside range $(-\bar{\epsilon}^s, \bar{\epsilon}^s)$ is then:

$$P(|\epsilon^s| \leq \bar{\epsilon}^s) = \int_{-\bar{\epsilon}^s}^{\bar{\epsilon}^s} f(\epsilon^s) d\epsilon^s \quad (21)$$

and is a function of the number of sampled points. It should be noticed that if the phase of the harmonics can be predicted, also the position of the sampling grid can be optimized.

6. CONCLUSIONS

The Harmonic Fitting approach (HF) aims to the conscious selection of the optimal number

of sampled points. When this approach is used, the following conclusions can be stated:

- The knowledge of the influence of the sampled point number on the probability distribution of the sampling error is the basis for a fully conscious selection of the optimal number of sampled points. Optimization criteria can be the maximum probability (equation (21)) or the minimum expected cost, as described in [7].
- Since the sampling error depends on the geometric characteristics of the generated surface, a piece of information should be available from the surface generation process in order to determine the sampling error probability distribution. This information is the statistical description of the surface harmonics which is the "fingerprint of the process".
- The proposed HF approach is the junction element between the probability distributions of the surface harmonics and the probability distributions of the sampling errors.
- Using the HF approach the influence of the number of sampling points on the sampling error distribution can be highlighted and directly evaluated using equations (10) and (12).
- The general statement that an increase in the number of sampled point leads to an increase of estimate accuracy is not always true. The sampling error can increase or decrease depending on the harmonics that overlap on the harmonics involved in the Harmonic Fitting (harmonics of order zero and one in the circular flange case).

Acknowledgments

The authors wish to thank Carl Zeiss S.p.A. for the technical support.

References

- [1]Hocken, R.J.; Raya, J.;Babu, U.; "Sampling Issues In Coordinate Metrology; Manufacturing Review", vol. 6, n.4, (1993).
- [2]Shunmungam, M.S.; "New Approach for Evaluating Form Errors of Engineering Surfaces"; Computer Aided Design, (1987).
- [3]Shunmungam, M.S.; "On Assessment of Geometric Errors"; Int. J. Prod. Res., vol. 24, n.2, 413-425, (1986).
- [4]Yau, H.T.; "Uncertainty Analysis in Geometric Best Fit"; Int. J. of Mach. Tools and Manuf., vol. 38, no. 10-11, 1323-1342, (1998).
- [5]Lin, Z.-C.; Chen, C.-C.; "Study of the automatic planning of measurement points with basic element features"; Int. J. Prod. Res., vol. 35, no. 11, 3157-3178, (1997).
- [6]Capello, E.; Semeraro, Q.; "The effect of sampling in circular substitute geometries"; Int. J. of Mach. Tools and Manuf., vol. 39, no. 1, 55-85, (1999).
- [7]Capello, E.; Semeraro, Q.; "Economic Optimisation of CMM Inspection of Circular Elements"; Second International ICSC Symposium IIA'97, Nimes, France, (1997).
- [8]Marple, S.L.Jr.; Digital Spectral Analysis with Applications; Prentice Hall, (1987).
- [9]Otnes, R.K.; Enochson, L.; Applied Time Series Analysis; John Wiley and Sons, (1978).
- [10]Damir, M.N.H.; "Appropriate Harmonic Models for Roundness Profiles"; Wear, vol. 57, (1979).
- [11]Niето, F.J.; Etxabe, J.M.; Giménez, J.G.; "Influence of contact loss between workpiece and grinding wheel on the roundness errors in centreless grinding"; Int. J. of Mach. Tools and

Manuf., vol. 38, no. 10-11, 1371-1398, (1998).

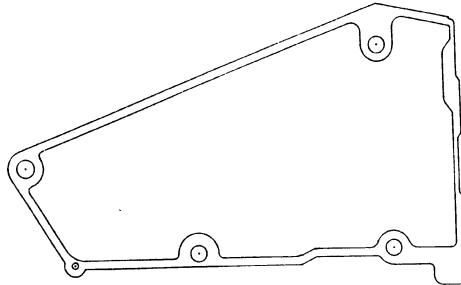


Figure 1. - Example of flange geometry to be measured by CMM.

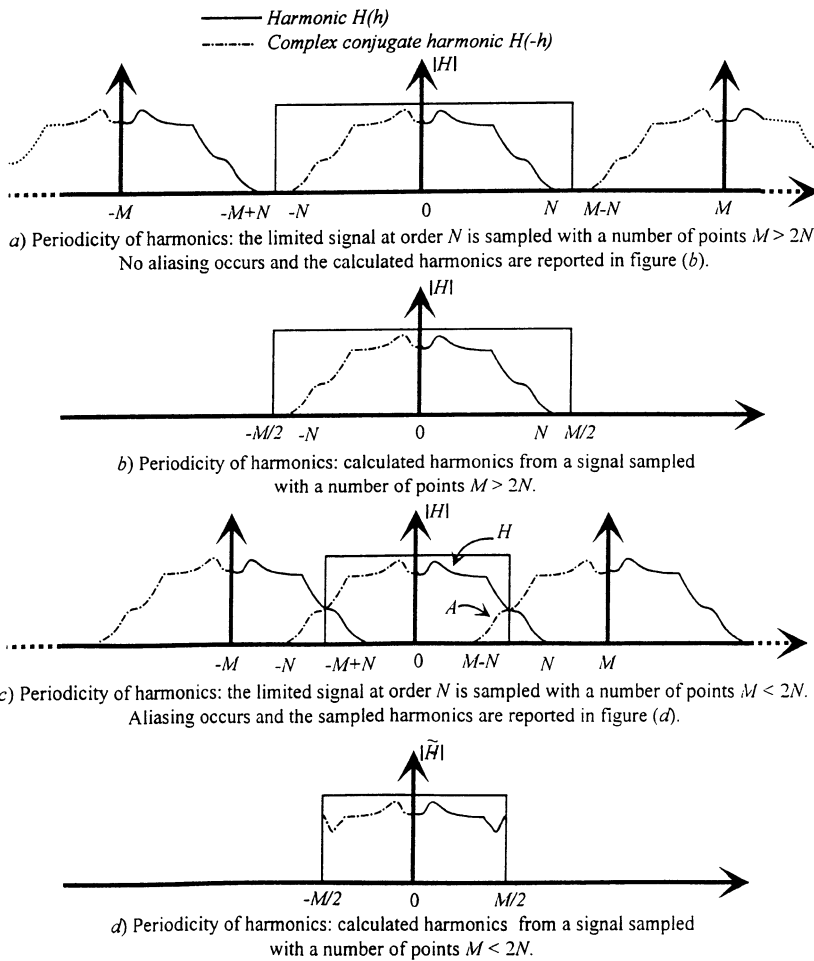


Figure 2. – Effect of aliasing on calculated harmonics.

VISION SYSTEM CALIBRATION AND SUB-PIXEL MEASUREMENT OF MECHANICAL PARTS

M. Lanzetta and G. Tantussi
University of Pisa, Pisa, Italy

KEY WORDS: Measurement, Visual Inspection, Camera Calibration, Sub-pixel Algorithm

ABSTRACT: In this article a measuring system based on artificial vision techniques is described. Even if this problem is not new, several aspects, including sub-pixel algorithms, system programming and lighting, that are addressed in this paper, are still under study. Among them, the vision system calibration is focused. The theoretical model and the practical details of a fast method for 2-D problems are described, by comparing 3-D techniques already in the literature. The main features of the developed system are: cheap and easy to use. An example application is provided for the overall performance assessment.

1. INTRODUCTION

Even if many 3-D vision applications are available in the literature [1], most of industrial applications are still in 2-D. In metrology, non-contact techniques, including artificial vision, have a rapid diffusion both in the literature and in the industrial environment and have been widely approached; in particular, measuring machines based on optical techniques are commercially available. However, there are several open problems [2]: the main drawback of these methods is the low accuracy due to the optical distortion and to the low resolution of available sensors that requires the system calibration and the use of methods to increase

the nominal spatial resolution, commonly addressed to as sub-pixel algorithms. In this paper we describe a simple, inexpensive and reliable vision system for metrology based on the integration of some of the more promising and fast techniques available in the literature.

2. CALIBRATION TECHNIQUES

The vision system calibration is a key factor to achieve the maximum overall performance and is necessary in all cases when absolute measurement on images is performed [2, 3]. It allows finding the correspondence between image points and workspace. The calibration program is executed ones after the system set-up, in order to determine the model parameters that are used every time an image is grabbed for part measurement purposes. The necessary parameters are [1, 3]: external, internal

and optical distortion. The external parameters describe the camera position: translation $T_{3 \times 3}$ and orientation $R_{3 \times 3}$ in some world co-ordinate system. The internal parameters are: the Image Centre (IC), that is the intersection between the image plane and the optical axis, the focal length f , to determine the perspective projection, the image or pixel aspect ratio AR and the scale factor s (s_x or s_y , if $AR \neq 1$) [mm/pixels]. The optical distortion caused by the lenses can be reduced below the maximum acceptable error in two ways: with software methods, increasing the hardware requirements and the processing time, or with more expensive optical devices, for instance by the use of a telecentric objective [4]. The maximum acceptable error in the case of digital imaging is one pixel or the sub-pixel algorithm accuracy, if any (§ 3). Several authors have proposed different techniques that can be characterised as follows [3]: methods based (i) on known world points, (ii) on the geometric relationships within the image, like the vanishing point of parallel lines, (iii) or assuming special hypotheses on perspective or requiring a particular system configuration (stereo view, hand-eye, etc.), or (iv) based on motion, from an image sequence, like in robot or active vision. However developers of artificial vision applications usually do not have the skill, patience and interest in laborious calibration methods. Therefore camera calibration must be simple and as quick as possible. Considering that the examined problem is in 2-D, as in many industrial applications, in order to exploit all available information, the system calibration is performed on a plane approximately perpendicular to the camera axis using a known pattern. Grids or spheres are common to many techniques, like [5] and [6]. The 2-D applications of these 3-D approaches are compared and discussed here in all the calibration steps in § 2.1 and 2.2, providing the parameters obtained for the used system. Concerning the external parameters, the translation and rotation matrices are represented, in the particular configuration used, by an identity matrix $R \equiv I_{3 \times 3}$ and by the vector $T \equiv (0, 0, T_2)$. For the internal parameters and the optical distortion, the following methods have been used.

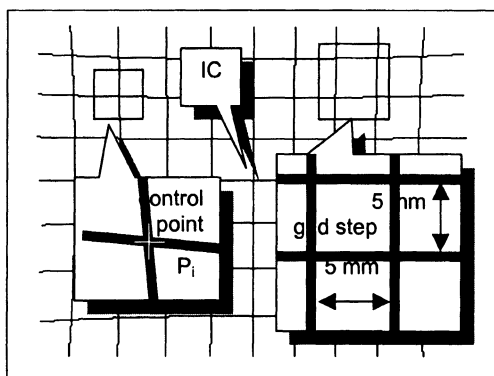


Figure 1 – Sample grid with cushion (negative) distortion

2.1 The grid method

This method is the 2-D application of [5]. A sample binary grid (Figure 1 and 2) is used whose intersection points represent the *control points* of this method. The IC is calculated first as it is weakly influenced by the more relevant optical distortion component, which is radial. Even if in 2-D problems a very accurate location of the IC is not necessary, it can be automatically found with a small effort. We assume that its position

is zoom-independent. Consequently a zoom change produces a radial displacement of all image points using the IC as the pole. By changing the zoom, a general point P_i moves to position P_{i+1} , and so forth (left detail of Figure 2). The straight lines displayed in Figure 2 (left) are determined with the least-squares method. A convergence study gave as a result that 5 positions of 60 control points provide the necessary and maximum accuracy. The IC is calculated by minimising its distance function Δ from all the straight lines, whose coefficients in the *implicit* equation are p_i , q_i and r_i :

$$\Delta = \sqrt{\frac{1}{N} \sum_{i=1}^N d_i^2} \quad \text{where} \quad d_i = \frac{|p_i Y_{IC} + q_i X_{IC} + r_i|}{\sqrt{p_i^2 + q_i^2}} \quad (1)$$

Equation (1) is numerically solved to find the IC co-ordinates $(X_{IC}, Y_{IC}) \equiv (230, 390)$. After setting the zoom in order to maximise the field of view with respect to the observed object, the magnification factor is assessed as the ratio $T_z/f = 15.337$, using the control points belonging to the less distorted image area (column 1 of Table I). By evaluating this ratio instead of the two values separately, the singularity coming from the 2-D application of the grid method is solved. The aspect ratio AR, has been determined as the average ratio between the square sides of the grid on all the images grabbed to find the IC; $AR = 0.9514$ has been determined considering the non-distorted (central) control points. To find the optical distortion, the tangential distortion is neglected and to assess the radial distortion, regression is performed between the measured and the actual Euclidean distance of control points from the IC as in [7]. A 2nd order interpolation equation is found, dividing the image in four concentric areas (Figure 3).

2.2 The sphere method

This method [6] is based on geometrical and optical considerations. The projection on the image plane of a sphere whose centre does not belong to the optical axis is an ellipse whose main axis is radial and contains the IC (Figure 2, right). A rear illuminated black

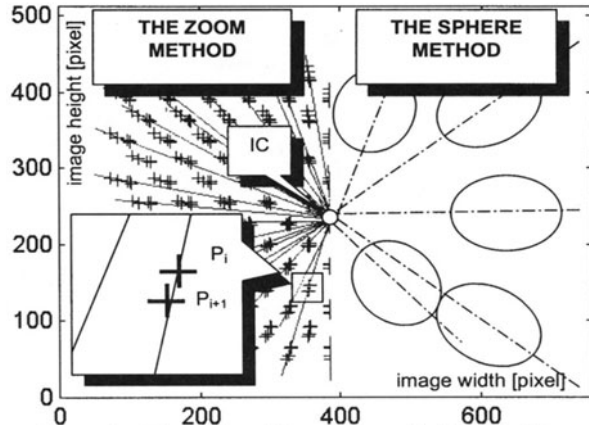


Figure 2 – The grid and the sphere methods to find the Image Centre (IC)

sphere with known radius and tolerance has been used. The principal axes of ellipses are determined with the least-squares method and for the IC again equation (1) is used: IC \equiv (235, 399). Geometric relations between the focal length and the ellipse features (eccentricity, principal axis, and boundary position) can be expressed [6]. With this method, the aspect ratio AR is given by the ratio between the two axes of each ellipse. The sphere method for 2-D problems has generally a lower accuracy than the grid method as a consequence of several practical disadvantages:

- black spheres with low tolerances are more difficult to find than laser printing a black grid. However a sharper grid (Figure 1 and 2) has been obtained with a plotter, a 0.1 mm pen and a *transparent* sheet for rear illumination;
- the sample positioning and lighting is also more critical;
- focusing a sphere requires a higher field depth than a 2-D object;
- the mathematical computation of the ellipse implicit equation is heavier than the grid points regression and errors on parameters are higher;
- the axis intersection region (near the IC in Figure 2) is larger with this method, because of image processing errors (edge detection with out-of-focus); however the error compensation due to the problem symmetry reduces the impact of this error source.

The direct consequence of the experimental comparison is that the 2-D application of the grid method is easier and yields a higher accuracy than the sphere method and for these reasons it has been integrated in the developed system.

2.3 The optical distortion symmetry method

The basic idea of this new method to find the IC is the sample image symmetry: the lens should produce a symmetrical distortion with respect to the two image axes. The four functions representing the actual distance of control points located in the four quadrants d_a versus the measured distance d_m , using the correct IC, are symmetrical two by two. For low cost lenses, the radial symmetry centre could be not coincident with the IC, but for the above reasons it represents a good estimation of it. This method is more suitable for wide-angle lenses, but it cannot be applied to the used system, as the optical distortion is lower than the convergence step and the algorithm becomes unstable, because the error estimating the branch symmetry calculating the polynomial of Figure 3 is of the same order of the

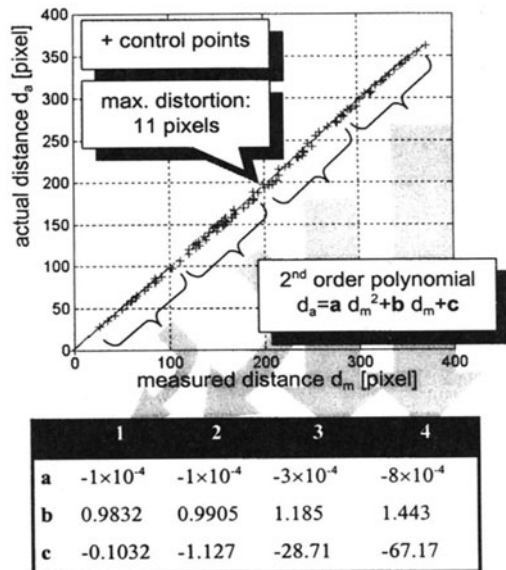


Figure 3 (above) – Interpolation of control points

Table I (below) – Polynomial coefficients in the four concentric areas

iterative accuracy increase at each step. A geometrical interpretation is that, with our system, the four branches match in an area that is greater than the error to estimate.

3. SUB-PIXEL MEASUREMENT

The nominal spatial resolution R_N is the ratio between the field of view and the sensor resolution. For a higher accuracy and consequently a higher measurement reliability, a better (lower) resolution R_N is necessary that can be obtained with the following methods:

- by increasing the sensor resolution;
- by reducing the field of view, divided in smaller areas, with a relative movement between camera and object, like in [2];
- with a sub-pixel method, such as the one described, or with multiple acquisitions.

Assuming a Gaussian distribution of errors, when using N_p points, the position accuracy is increased and R_N is reduced by $\alpha = \sqrt{N_p}$.

More details concerning the impact of the edge width on resolution can be found in [2]. This method can be applied (i) to flat object or (ii) when the boundaries belong to one or more planes perpendicular to the optical axis, if their edges can be represented with geometric primitives. The main steps of the algorithm are summarised in Figure 4:

- a. image acquisition with rear illumination [8];
- b. edge-detection, obtained with a binarisation and a convolution;
- c. optical correction and segmentation;
- d. least-squares interpolation of primitives [9].

A binarisation threshold is easy to find on a *bimodal* histogram (Figure 4a.). However a lighting or threshold change may affect the edge width and position because of light *scattering* effects. This problem is solved by using a *reference* dimension on the observed part and by finding the binarisation threshold with an exhaustive method, until the correct dimension is achieved. After edge-detection, data are *compressed* and the boundary co-ordinates only are kept instead of the whole image, as calibration involves those data only. The necessary memory is reduced, in the described example, from an 8 bit (256 grey-level) 756x567 image, to n_p couples of 10 bit co-ordinates. The interpolation function depends on the geometric primitive, whose main parameters are obtained using the *implicit* equations, e.g. a straight line or a circle for a segment or an arc respectively.

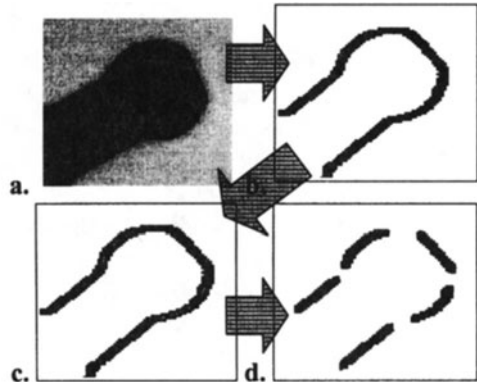


Figure 4 – The main steps of the algorithm

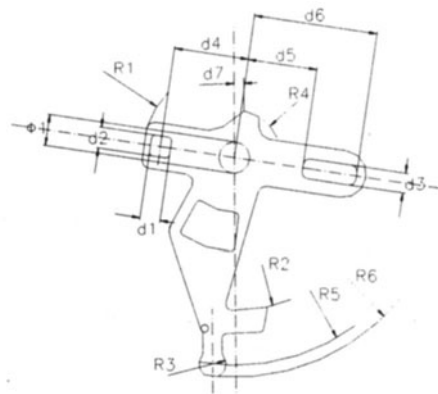


Figure 5 – Benchmark: «blocking lever» (dimensions in Table II)

example, from an 8 bit (256 grey-level) 756x567 image, to n_p couples of 10 bit co-ordinates. The interpolation function depends on the geometric primitive, whose main parameters are obtained using the *implicit* equations, e.g. a straight line or a circle for a segment or an arc respectively.

4. THE LEARNING PROGRAM

The inspection planning is manually performed by self-learning as in most commercial packages. The operator provides the system with the critical dimensions and their position by splitting the contour of the grabbed image into geometrical primitives with a graphical interface and a pointing device according to a decision tree. Every primitive is selected through a set of points to define a window depending on the primitive being searched and according to optimal search criteria. Regarding the system engineering, programming can be automated using CAD data as described in [9]. The primitive selection (*segmentation*) could also be automated finding the *knot-points* between two primitives with the method in [10]. The system is able to measure a part in any position within the field of view with a pattern matching technique, like in [3], therefore it can be used directly on-line without special fixtures. A template of the part to be measured is stored in memory in order to find the actual displacement and the angle of rotation with respect to the template. The present part position and orientation information can be used to shift and rotate the *search mask* containing the user-programmed windows. This method is preferable with respect to rotating the image, because the accuracy reduction due to pixel calculation (up to ± 0.5 pixel) may affect the measurement, while the same error is acceptable when rotating the search mask.

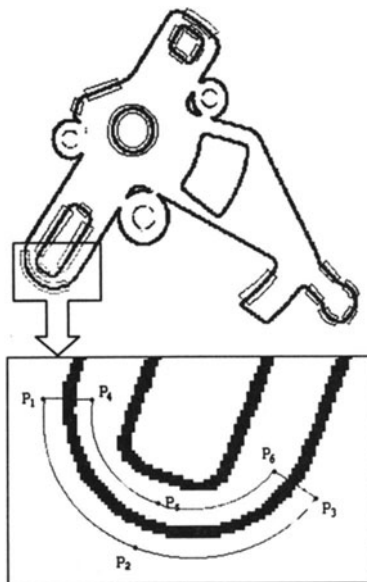


Figure 6 – The inspection mask. Detail of the search window for an arc, defined by six points

5. AN EXAMPLE APPLICATION AND THE EXPERIMENTAL SET-UP

The described system has been designed to be exploited for mechanical part measurement in a transfer pressing line for 100% part and process control purposes. At present a statistical control is performed (i) with a go-nogo calliper by an operator, and (ii) with a CMM for the remaining critical dimensions. If an error is detected, all parts manufactured and stored in a buffer since the previous control are rejected. As an example, a sheared part (Figure 5) has been used to test the system, made of the following components: a PC with a Matrox Image frame grabber, and a monochrome CCD matrix camera with a resolution of 756×567 pixels at 256 grey levels, with zoom lens. The best lighting performance has been obtained with a rear illumination, using a Fresnel lens instead of a simple surface diffuser. Such collimated light source with parallel rays has the following advantages: (i) it avoids reflections on the vertical surfaces for thick sheet parts; (ii) for 3-D objects, where edges are not in the same plane, it reduces the disturbances due to shadows and to the curved surface reflections. Using a fixed threshold binarisation, the light distribution should be as uniform as possible. This can be obtained with a proper lamp positioning or by software means, using a solid sample to find the correction coefficients. The effect of the external environmental lighting can be reduced increasing the rear illumination intensity and re-

ducing the exposure time with a shutter, in order to keep a high signal-to-noise ratio. Tests have shown that a change of light intensity produces a measurement error of about 0.02 mm on ϕ_1 (Table II) for a grey-level threshold change from 50 to 110.

6. RESULTS

Table II – The vision system performance

In Table II, the nominal dimensions D and the tolerances t of the observed part are compared with those coming from the vision system D_m and those taken with standard workshop methods D_a . In the examined case, with a field of 100×75 mm, $R_N = 0.13$ [mm/pixel] and it is not sufficient with the requirements in Table II. For this reason, the sub-pixel algorithm implemented was necessary. The low system resolution is enhanced in detail of Figure 6. Some dimensions* in Table II depend on the position of a single point and not of a primitive. Their estimation could be easily improved by locating points as the intersection of primitives. Apart from them, the maximum absolute error of

Ref.	D [mm]	t [mm]	D_m [mm]	D_a [mm]	E [mm]	% error
ϕ_1	8.1	$\begin{pmatrix} +0.1 \\ 0 \end{pmatrix}$	8.14	8.15	-0.01	-0.1
d_1	5.2	$\begin{pmatrix} +0.1 \\ 0 \end{pmatrix}$	5.26	5.29	-0.03	-0.6
d_2	5.4	$\begin{pmatrix} +0.1 \\ 0 \end{pmatrix}$	5.46	5.42	0.04	0.7
d_3	5.1	$\begin{pmatrix} +0.1 \\ 0 \end{pmatrix}$	5.16	5.14	0.02	0.4
d_4	19.4	$\begin{pmatrix} +0.1 \\ -0.1 \end{pmatrix}$	19.36	19.34	0.02	0.1
d_5	18	$\begin{pmatrix} 0 \\ -0.2 \end{pmatrix}$	17.92	17.90	0.02	0.1
d_6	32	$\begin{pmatrix} +0.2 \\ 0 \end{pmatrix}$	32.02	30.06	-0.04	-0.1
d_7	2.7	$\begin{pmatrix} +0.1 \\ 0 \end{pmatrix}$	2.80	2.77	0.03	1.1
R_1	24	$\begin{pmatrix} +0.1 \\ -0.1 \end{pmatrix}$	24.02	24.05	-0.03	-0.1
R_2	39	$\begin{pmatrix} +0.1 \\ -0.1 \end{pmatrix}$	38.80*	38.92	-0.12	-0.3
R_3	3.5	$\begin{pmatrix} 0 \\ -0.1 \end{pmatrix}$	3.48	3.49	-0.01	-0.3
R_4	12.3	$\begin{pmatrix} +0.1 \\ 0 \end{pmatrix}$	12.26*	12.34	-0.08	-0.7
R_5	53	$\begin{pmatrix} +0.1 \\ -0.1 \end{pmatrix}$	52.84*	52.94	-0.1	-0.2
R_6	56	$\begin{pmatrix} 0 \\ -0.2 \end{pmatrix}$	55.86	55.90	-0.04	-0.1

the vision system is $E_{max} = 0.04$ mm. The calibration techniques used have reduced the optical distortion (Figure 3) from a maximum of 1.43 mm to acceptable values, as shown by the values of E . The system repeatability, calculated as the maximum error E measuring ten times the circle ϕ_1 is $E_{rep} = 0.02$. The system resolution, expressed as the minimum detectable dimension change, has been assessed measuring parts with different values of ϕ_1 and is $E_{res} = 0.02$. The angular accuracy is a direct consequence of linear accuracy. In all cases $E \ll t$, then the described optical measuring method can be applied for part inspection without sorting errors.

7. CONCLUSIONS

The main features of the described system are: cheap, fast and reliable. Low cost, required for industrial applications, is obtained by software means, which is an inexpensive method to increase the performance of commercial hardware in addition to adopting higher resolution cameras. The cycle-time (10 s) is not far from the production-rate (4 s) and could be easily reduced by software optimisation or with special purpose hardware. The system reliability has been assessed by direct comparison on measured parts. A sub-pixel algorithm,

including optimal hardware calibration to stress the overall performance of standard cameras and lenses has been implemented. The described system, obtained by comparing the performance of available techniques from the literature, has attained the goal of 0.3 pixel resolution. A new technique, which could not be tested with the used system, has also been proposed.

ACKNOWLEDGEMENTS

The authors wish to thank Ing. Carlo Scarabeo for his contribution to this work and Ing. R. Sbrana and Mr. P. Gasperini from Atoma Roltra S.p.A. – Pisa (Magna Group) for providing the material and their technical support.

REFERENCES

- [1] Lanzetta, M.: 3-D Vision in Production Processes, Part I - State of the Art (in Italian), *Automazione e Strumentazione*, n. 2, Year XLVI (February 1998), 155-164.
- [2] Lanzetta, M.: Rasterisation of 2-D profiles with Unlimited Resolution through Artificial Vision Techniques: an Application to the Wood Industry, *Proceedings of the 10th International ADM Conference*, Florence Italy, September 17th-19th (1997), 311-316.
- [3] Lanzetta, M.: Stereo Vision with Neural Networks (in Italian), *Automazione e Strumentazione*, n. 7, Year XLIV (July/August 1996), 107-116.
- [4] N.N.: 55 Telecentric, Accurate Machine Vision, brochure of Computar, Japan.
- [5] Li, M.; Lavest, J.-M.: Some Aspects of Zoom-Lens Camera Calibration, Report from CVAP, KTH Stockholm Sweden, TRITA-NA-9503, CVAP172 (February 1995).
- [6] Stein, G.P.: Internal Camera Calibration using Rotation and Geometric Shapes, M.Sc. Thesis, MIT Boston Massachusetts (February 1993).
- [7] Lonardo, P.; Bruzzone, A.: Application of image analysis to mechanical metrology, *Proceedings of III AITEM Conf.*, Fisciano (SA) Italy, September 17th-19th (1997), 459-466.
- [8] Schroeder, H.E.: Practical Illumination Concept and Technique for Machine Vision Applications, in *Robot Sensors*, vol. 1 – Vision, Springer Verlag (1986), 229-244.
- [9] Chen, J.-M.; Ventura, J.A.: Shape analysis of complex profiles, *Int. J. Mach. Tools Manufact.*, vol. 35, n. 3 (1994), 399-429.
- [10] Wu, Q.M.; Rodd, M.G.: Boundary segmentation and parameter estimation for industrial inspection, *IEE Proceedings-E*, vol. 137, n. 4 (July 1990), 319-327.

ANALYSIS OF THE ACCURACY OF THE CAD MODEL RECONSTRUCTION OF SPIRAL BEVEL GEARS BY CMM'S DIGITISATION

V. Carbone, E. Savio, J. Yang and L. De Chiffre
University of Padua, Padua, Italy

KEY WORDS: Gear manufacturing, reverse engineering, free-form surfaces, inspection.

ABSTRACT: This paper presents the procedure that DIMEG has set-up and tested for the reverse engineering of spiral bevel gears and related tools, with particular reference to the accuracy analysis applied to reconstructed CAD models. The work is part of a research project whose objective is the joint optimisation of forging and machining operations in gear manufacturing. Within the project the CAD model of prototypes, semi-finished and final products and related tools are required for simulation, manufacturing and testing. Some of these applications require an accurate mathematical representation of existing physical objects, and for this reason a particular effort was spent on the verification of the accuracy of the reconstructed CAD model. The procedure can be split up into three main steps: i) digitisation of functional surfaces on a reference tooth, using a coordinate measuring machine (CMM) equipped with contact probe, ii) reconstruction of complete solid model in CAD environment, and iii) verification of CAD model on CMM. Results of the accuracy analysis, advantages and limitations of this procedure are presented and discussed.

1. INTRODUCTION

In today's manufacturing organisations the pressure on product cost is driving most of the process re-engineering initiatives. Cost reduction programs are common for all manufacturing processes involving medium to high production volumes, especially when

mature technologies such as forging and machining are involved. As well known, in most cases both of these technologies are used, since forging impresses the overall general shape of the component that is subsequently machined on its functional surfaces. The amount of removed material is a relevant cost driver for the machining process, to be minimised by pre-forming the workpiece; on the other hand, forging capabilities are limited by workpiece geometry, material flow resistance, press force and surface finish constraints. Therefore, extensive studies on the optimum combination of the manufacturing operations are required [1-5].

The present work is part of a research project on gear manufacturing. The objective is the joint optimisation of forging and machining operations for the manufacturing of spiral bevel gears, using near-net shape forging and Gleason conventional cutting technology.

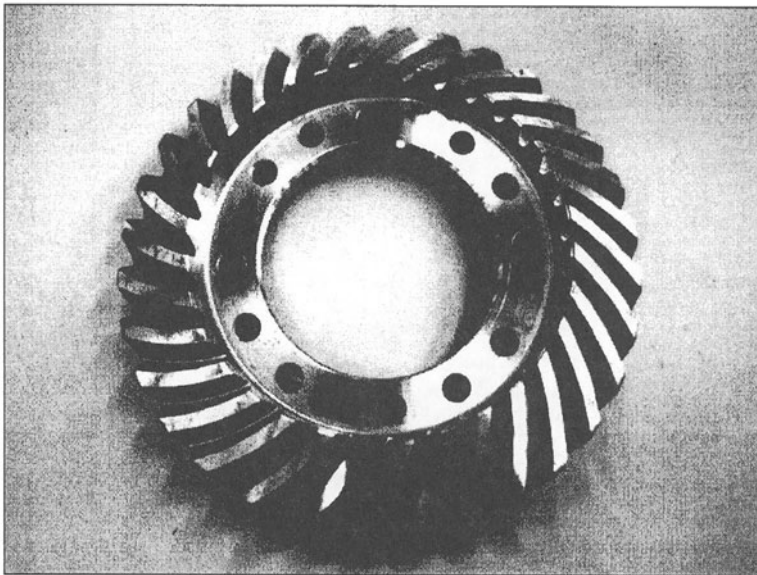


Fig. 1: Semi-finished spiral bevel gear (Courtesy of SIAP-CARRARO)

Current production routings are based on the following main steps: hot forging of disk-shaped parts, rough machining and then finish machining. The idea is to substantially reduce or eliminate the rough machining operation with the near-net shape forging of parts; technical and economical feasibility are therefore mainly constrained by the forging process.

2. PROBLEM DEFINITION

The research is focusing on the definition of feasible open-die hot forging operations, using both physical and numerical simulation. Investigations are carried out using an integrated computer-aided engineering system which includes conventional CNC machining, CAE

simulations and CMM verification of prototypes, semi-finished and final products as well as related tools; 3D CAD modelling is therefore necessary for all the “objects” needed by the project.

In gear design and engineering it is not common to create a 3D CAD model of the gears to be designed. As well known, the designer defines the functional parameters of the gear (module, pressure angle, number of teeth, addendum modification, helix angle, etc.) and then those data are used as input for setting up the gear cutting machines and for quality inspection. The problem is that these parameters describe only the final geometry of the gear; they are not useful for the geometrical representation of the various parts (prototypes, semi-finished gears, tools) to be manufactured, engineered, tested and verified during the research project. Furthermore, in some cases CAD modelling operations based on functional data are difficult or impossible, due to the geometrical complexity of the gear and/or the limitations of the CAD system; this was the situation encountered in modelling spiral bevel gears, in particular regarding free-form surfaces representing the tooth flanks.

On the other hand, some of the parts to be modelled are physical prototypes that can be used as reference for reconstructing the CAD model with reverse engineering techniques. Some of the analyses require a very accurate mathematical representation of these parts, and for this reason a particular effort must be spent on the verification of the accuracy in the reconstructed CAD model.

For all these reasons, investigations have been conducted for setting up a procedure to be used in reconstructing the CAD model of parts (prototypes, gears, tools) with geometrical features similar to spiral bevel gears.

3. THE APPROACH

Different reverse engineering systems are now available, based on different physical principles. Accuracy is a key parameter for selecting the appropriate one; in the present work an integrated CAD/CMM system has been used, based on a coordinate measuring machine (CMM) with contact probe.

Integration between CAD and CMM enable to generate mathematical models from physical objects with high accuracy. Basically, the CMM is used for the acquisition of points (digitisation) on the object's surface and then these data are imported in the CAD environment, either as triplets of coordinates or as partial reconstructed surfaces.

The digitisation operation is critical for the whole reconstruction process, and many authors are proposing different approaches. Sarkar and Menq [6] work with a procedure based on scanning surfaces and afterwards dividing the point cloud into areas without sharp shape changes. In Yau [7] a two step digitising procedure is adopted, based on a rough model created in the first step and then refined in the second. Lin [8] proposes a method that includes a surface lofting algorithm for smooth-surface reconstruction from 3D measurement data.

Concerning the reconstruction of surfaces, two different approaches can be identified. In the first, the digitised points in (x,y,z) format are imported in the CAD environment; these raw data are used as input for CAD routines that transform the points cloud into higher level mathematical representations (i.e. B-spline surfaces), as shown in Fig.2 a).

In the second approach, the digitisation process generates directly a partial surface CAD model in CMM environment; this is made possible by the availability of CAD-like software applications fully integrated on the CMM control system. With these applications the functional surfaces of a part can be digitised and reconstructed in one single step, using semi-automatic iterative operations, available in CMM environment.

Past research work carried out at DIMEG revealed that the former approach is not suited for parts having complex features, sharp edges and difficult accessibility when a contact probe is used; for the procedure aimed at the reconstruction of parts similar to the spiral bevel gear, the latter approach has been adopted. As shown in Fig. 2 b), tooth flanks and top were reconstructed directly in CMM environment only for one reference tooth; the complete solid CAD model was created afterwards, importing the three surfaces in the CAD system. The proposed approach can save total measuring and modelling time using a minimum number of significant point on the functional surfaces.

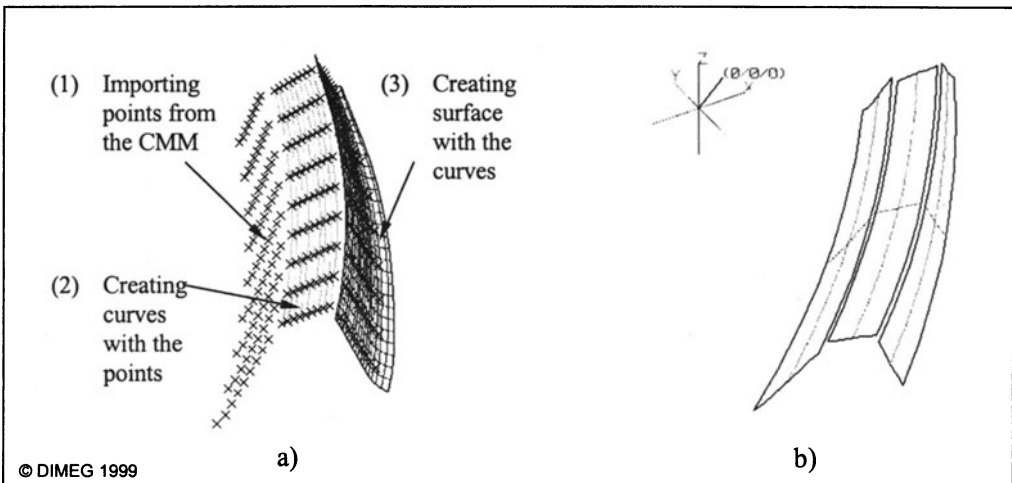


Fig. 2: Approaches to surface reconstruction

4. DESCRIPTION OF THE PROCEDURE

The CAD/CMM system

The digitalisation was performed on a ZEISS coordinate measuring machine equipped with a contact probe head and HOLOS, a software for the measurement of free-form surfaces and for reverse engineering. The uncertainty u_1 of the CMM is $2.2 \mu\text{m} + L/300$ and the probing uncertainty is $1.5 \mu\text{m}$ [9].

The CAD system used was Pro/Engineer by PTC with the specific module Pro/Surface.

Step 1: Digitisation on the CMM

A single reference tooth was digitised with the CMM; its complex functional surfaces, the two flanks and the top, were reconstructed with grids of 9×9 points. Cubic polynomial

functions were chosen, as commonly advised for most CAD/CAM systems [7]. The surface model was then post-processed to the IGES format and imported in the PRO/E environment.

The parameters of regular features, such as the cylindrical and conical surfaces, were measured using UMESS software; these surfaces were not reconstructed in CMM environment, since this operation is much faster and effective if done using the CAD system.

Step 2: CAD modelling

The generation of the gear tooth geometry is based on the contour of the final part. In principle, the three-dimensional geometry of gear wheels can be described using the features “transverse profile”, “guide curve” and “basic body”[10]. The gear geometry, for example, is described by parameters like module, pressure angle, number of teeth, addendum modification, helix angle etc.; with these parameters the CAD system is able to create the tooth profile [11].

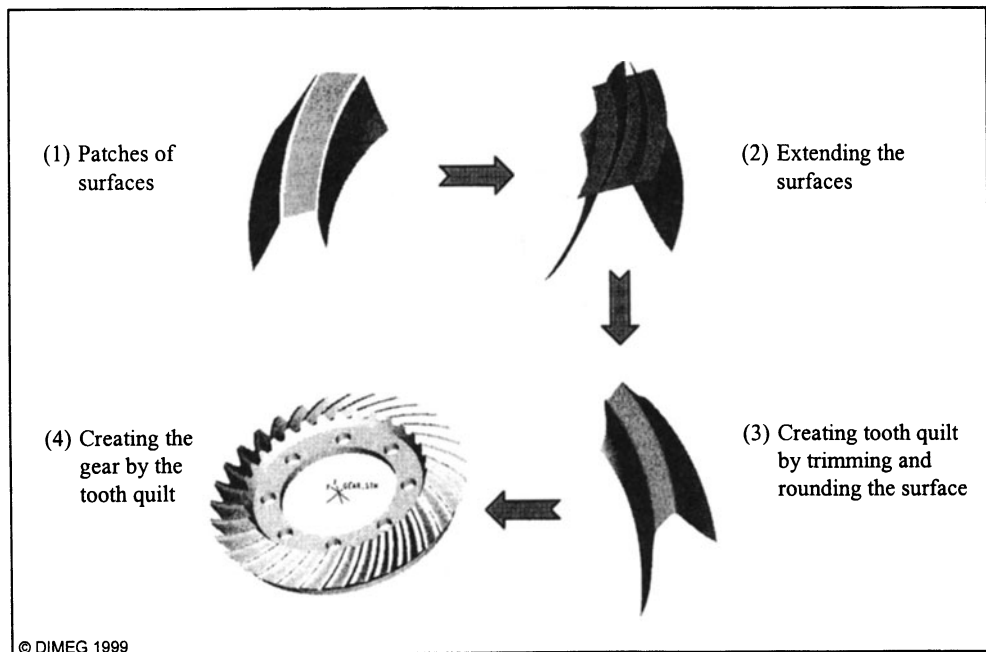


Fig. 3: CAD modelling operations

However, spiral bevel gears manufactured using Gleason cutting technology are very difficult to represent with the available CAD modelling functions. On the other hand, the availability of “masters” in the form of physical objects allows the reconstruction of the CAD model with reverse engineering techniques; the operations, as shown in Fig. 3, were the following:

- (1) a partial surface model of a single tooth was imported in the CAD environment, using standard formats such as IGES or VDA;
- (2) in order to create a closed tooth quilt, the three surfaces were extended and intersected;
- (3) the tooth surfaces were trimmed and joined, creating a complete tooth profile quilt;
- (4) using the parameters measured on the CMM with UMESS, the regular geometries of the gear body were created. The tooth profile quilt was then patterned in the proper positions; the teeth were cut out from the solid body using the teeth profile quilt and a complete solid CAD model of the spiral bevel gear was obtained.

Step 3: Verification on the CMM

Once the CAD model has been reconstructed, it is necessary to evaluate how well the model represents the original physical object. This is an inspection task, consisting on the measurement of the object with the CMM on the basis of the CAD model; the result is represented by the deviations between the points on the CAD model and the points probed on the part.

The inspection process was carried out as follows:

- a) a first rough part alignment was done using the regular surfaces (inner plane and cylindrical surfaces); this alignment was then improved using the functional surfaces of four teeth at 90 degrees;
- b) surfaces to be inspected were measured point by point with regular grids;
- c) best fitting was applied to the measurement data, using the least squares algorithm; the surface fitting involved all the six degrees of freedom. The deviations for the complete CAD model were then calculated.

5. EVALUATION OF THE CAD MODEL ACCURACY

In order to use the reconstructed CAD model for the planned engineering applications, it is important to evaluate the accuracy of the model with respect to the original part. Since the number of data points measured in Step 3 of the procedure is significantly greater than the number of points used for the reconstruction, there will be found deviations between these measured points, distributed on the whole gear, and the nominal surfaces. These deviations can be used as an index for a quantification of the “quality” of the reconstruction process.

The “error” affecting dimensional accuracy of free-form surfaces can be imagined as composed by: i) the form error and ii) tilting or translation of the surfaces in respect to nominal features. There have been considerable studies on the analysis of surfaces reconstructed from 3D measurement data [12-13] ; many sources of errors are influencing the final result and they need to be analysed in order to minimise the final error.

The average error e_{av} is defined as the average deviation between the measured points and the CAD model:

$$e_{av} = \frac{1}{m} \sum_{j=1}^m e_j \quad e_j = |P_a - P_n(u_j)|$$

where m is the number of measured points, e_j represents the shortest distance between the j -th measured point P_a and the nominal CAD point P_n .

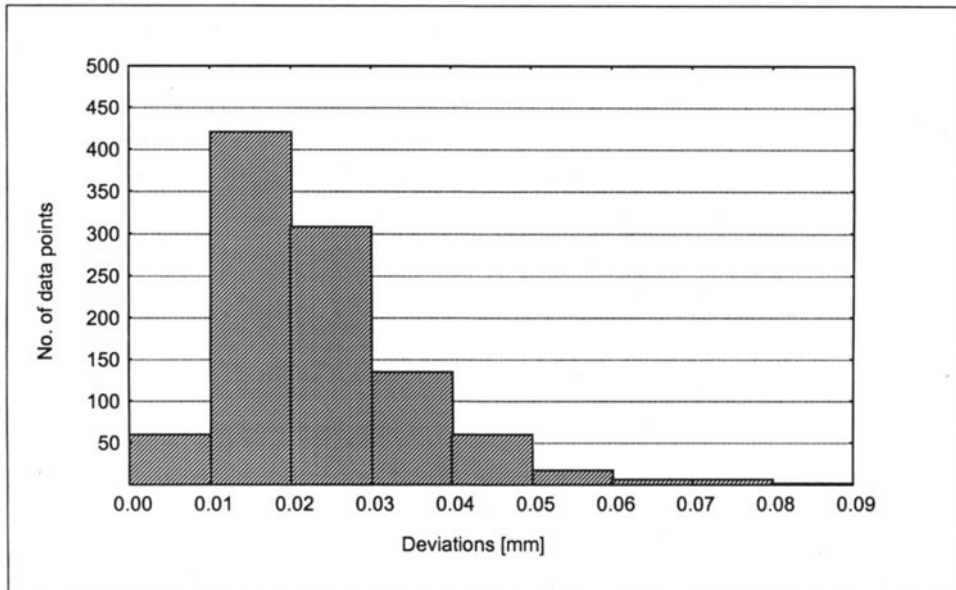


Fig. 4: Distribution of the deviations between CAD model and measured points

Fig. 4 shows the result of an inspection conducted with regular grids of 9×3 points on the teeth flanks of the whole gear. In this case, the average error is 0.023 mm, the standard deviation is 0.017 mm, and 90 % of the deviations are less than 0.04 mm.

The accuracy can be improved with further digitisation and reconstruction; however, the target tolerance of 0.05 mm is substantially satisfied and this means that the proposed procedure is effective for the required applications.

6. CONCLUSIONS

In this paper a procedure for reverse engineering of spiral bevel gears has been presented. The approach consisted on the digitalisation and partial reconstruction of functional surfaces by means of a coordinate measuring machine equipped with contact probe. The partial surface model was completed in CAD environment and a solid model of the whole gear was created. This model was then verified on the CMM with respect to the original physical component. An evaluation carried out on all the teeth flanks gave good results, in accordance with the target accuracy.

The procedure can be used for reverse engineering of other parts having rotational symmetry, sharp edges and complex free-form surfaces, i.e. for geometrical modelling of the various parts (prototypes, gears and related tools) to be manufactured, engineered, tested and verified during the research project.

ACKNOWLEDGEMENTS

The work presented in this paper is part of a research project carried out by DIMEG and SIAP-CARRARO GROUP. The authors wish to thank the company for its support and collaboration.

REFERENCES

1. Suh, N., Basic Concepts in Design for Producibility, Keynote Paper, CIRP 1988.
2. Altan, T., Miller, R. A., Design for Forming and other Near Net shape Manufacturing Processes, Annals of the CIRP Vol. 39/2/90, p. 609, 1990.
3. Lange, K., Some Aspects of the Economic Production of Complex Bulk Components by Cold Forging and Machining, 26th ICFG Plenary Meeting, Osaka, 1993.
4. Knight, W.A., Poli, C.R.; Computer-Aided Part Design for Economical Fabrication by Forging, Proc. of the 11th Conf. On Prod. Research Technology, 1984.
5. Boothroyd G., Knight W., Fundamental of Machining and Machine Tools, Cap. 13 : Design for Machining, 2nd Ed., Marcel Dekker, 1989.
6. Sarkar B., Menq C-H., Smooth-surface approximation and reverse engineering, Computer Aided Design, vol. 23, n° 9, pp.623-628, 1991.
7. Yau H-T., Reverse engineering of engine intake ports by digitization and surface approximation, Int. J. Mach. Manufact. Vol. 37, n°6, pp. 855-871, 1997.
8. Lin C. Y., Liou C. S., Lai J. Y., A surface-lofting approach for smooth-surface reconstruction from 3D measurement data, Computers in Industry, 34, pp. 73-85, 1997.
9. VDI/VDE 2617, Accuracy of coordinate measuring machines. Characteristics parameters and their checking. Part. 2.1, 3. Verein Deutscher Ingenieure, Dusseldorf, Germany, 1989.
10. Wiarda M., Computer-aided design and manufacturing of tools for precision forging, Conference Transactions of the Int. Conf. on Forging and Related Technologies, 27-28 April 1998, Birmingham, UK.
11. Doege E., Bohnsack R. and Romanowsky C., Tool technologies for near net shape forgings, Conference Transactions of the Int. Conf. on Forging and Related Technologies, 27-28 April 1998, Birmingham, UK.
12. Pahk H. J., Kim Y.H., Development of Computer-Aided Inspection System with CMM for Integrated Mold Manufacturing, Annals of the CIRP, Vol. 42, n°1, pp. 557-560, 1993.
13. Yau H-T., Menq C-H., A unified least-squares approach to the evaluation of geometric errors using discrete measurement data, Int. J. Tools Manufact. Vol. 36, n°11, pp. 1269-1290, 1996.

ON A METHODOLOGY FOR PLASMA SPRAYED CERAMIC COATINGS MICROHARDNESS MEASUREMENT

T. Gutema, P. Bracali and R. Groppetti
University of Parma, Parma, Italy

KEYWORDS: Vickers Microhardness, Plasma Spray, Partially Stabilised Zirconia (PSZ), Ceramic Coatings.

ABSTRACT: The dispersion of Vickers microhardness values of Plasma Sprayed (PS) ceramic coatings is often quite high, due to unhomogeneous phase distribution, defects and porosity. Specific experiments have been planned and executed on Plasma Sprayed Partially Stabilised Zirconia (PSZ) coatings, in order to analyse the variation of hardness along coating thickness and the dependence of the measurements on test load and porosity level. A contribution to a methodology and a preliminary protocol definition for measurement and statistical analysis, to be followed to obtain significant and repeatable results, have been studied and proposed. Consequently, microhardness test load, coating test area and statistical analysis technique to be applied, have been studied, validated and proposed.

1. INTRODUCTION

Vickers microhardness measurements are affected by the influence of elastic-plastic behaviour and grain size effects for metals and unhomogeneous phase distribution, local defects and porosity for ceramic coatings. However Vickers microhardness measurement of Plasma Sprayed (PS) ceramic coatings presents more difficulties than metals. The hardness is usually measured on a polished cross section of the specimen using test loads from 1 to 5 N. On account of the unhomogeneous phase distribution, defects and porosity, the dispersion of the measured microhardness values is often quite high and the dispersion may

range up to 15% for ceramic coatings [1]. Moreover the indentations have poor outlines due to the indentation damage and this results in measuring errors and poor repeatability. In addition to this, the hardness values along the thickness are not constant, and only few contributions have addressed the specific topic of the hardness as a function of the thickness. Some analyses, made on the hardness of plasma sprayed coatings, give qualitative indications: Kobayashi and Kitamura have conducted a gas tunnel type Plasma Spraying of Zirconia, analysed the distribution of Vickers microhardness on the cross section, and concluded that higher values have been obtained at the surface side of the coating [2]. Heimann gave also some indication on an increasing trend of the hardness with coating thickness [3]. Blann and Hoffmann demonstrated the repeatability and consistency of Vickers indentation diagonal readings on PS ceramic coatings with low porosity, by means of the execution of systematic microhardness tests, and the dependence of hardness variation on the porosity, which is greater in higher porosity coatings [4]: thus the placement of the indentations requires a specific care so that solid areas are chosen.

In order to define and propose a methodology and a preliminary protocol for measurement execution and result reporting, specific experiments were planned and executed on a PS ceramic coating of industrial interest for thermal barrier, wear resistance, biomedical applications and for specific structural and porosity properties, as Plasma Sprayed Partially Stabilised Zirconia (PSZ) coating, to study the variation of microhardness along coating thickness cross section, microhardness measurement dependence on test load and porosity level.

2. EXPERIMENTAL

Four samples (A, B, C, D) of partially stabilised zirconia (PSZ) coatings with different porosity (1%, 4%, 1.5%, 4%, respectively), have been considered (Table 1). Vickers microhardness measurements were executed on coating cross sections, prepared following standard metallographic procedures. Test load used were 1, 3 and 5 N: consequently, 12 different conditions were studied.

Test load [N]	PSZ coating sample porosity			
	A [1%]	B [4%]	C [1.5%]	D [4%]
1	A1	B1	C1	D1
3	A3	B3	C3	D3
5	A5	B5	C5	D5

Table 1: Vickers microhardness experimental plan on PSZ coatings.

For each condition, Vickers microhardness tests were executed on different cross sections of the coating. In particular, the entire coating cross section was divided in 5 bands for 1 or 3 N test load, and 3 bands for 5 N test load, because of the larger indentation sizes. For each band a series of measures was executed.

2.1 Result significance

The most important hypothesis to be verified is the significance of Vickers microhardness variation on the coating cross section at different distances from the interface. In order to decide whether the data, collected from each band, provide a significant estimation of the variation of the microhardness values on the coating cross section, statistical analysis has to be executed. Microhardness variation as function of test loads has been also studied. The sample values obtained in each series of each data set obtained in the experiment have been therefore tested for normality either graphically or using Pearson χ^2 test. Once the normality of the distribution has been proved, a statistical test has been applied for rejection of outliers. To this effect, different tests, as Q-Test, test of Dixon and Chauvenet criterion, can be used. In the present analysis, the Chauvenet criterion has been applied. After rejection of the outliers, the main hypothesis to be verified is whether the microhardness mean value measured on a cross section depth is statistically the same as that obtained on another cross section depth. In the domain of every data set, the bands are indicated with an index ranging from 1 to m. The null hypothesis H_0 to be verified in every data set is therefore $\mu = \mu_1 = \mu_2 = \dots = \mu_m$.

If the mean values $\mu_1, \mu_2 \dots \mu_m$ belong to a larger common population, whose mean value is μ , the variances of each data series $\sigma_1, \sigma_2 \dots \sigma_m$ should be equal to the overall variance σ . This condition can be verified with the Cochran test or with the more general Bartlett criterion. The present analysis utilises the latter test, that is based on the comparison of the value of the Bartlett variable with an appropriate χ^2 value. This is a precondition to conduct Fisher-Snedecor test (F test) that can be used to decide whether the series of measures belong to a larger common population [5].

In fact the mean values $\mu_1, \mu_2 \dots \mu_m$ in the expression of H_0 can be estimated by the series sample means, but the difference among-means is not considered significant unless it is large compared with the random within-series variation [6].

If F test leads to the conclusion that the results do not belong to a common distribution and the variation among the series is significant, the further step can be the analysis of the trend. In this case it is important to determine if every mean value is significantly different from any other mean or if some couples of means result compatible, so that a new hypothesis on the classification of the data can be suggested. To compare couples of means many solutions have been proposed in the literature: the Fisher LSD (least significant difference) test, the Duncan test for multiple means comparison, and the Tukey HSD (honestly significant difference) test, that could be generally applied even if the number of observation is not the same in every series.

3. RESULT ANALYSIS

The following study investigates the significance of the variation of the PSZ coatings hardness measured values depending on the coating thickness depth and on the test load, and the dependence of the statistical parameters of the distributions on the involved measuring variables.

3.1 Initial data analysis

The initial analysis has been performed on the 12 data sets obtained from the hardness measurements. The series variation is then investigated with statistical procedures in order to identify the data trend.

3.1.1 Measured values and relative plots

The measured microhardness values are plotted against coating thickness for the 12 data sets. The coating thickness is measured from the interface towards the outer surface. Some examples are depicted in Fig. 1. From the observation of the plots, the hardness data values present large dispersion. The trend of the data plots reveals that in most of the cases, the hardness values near the interface and near the coating surface are lower than at the central band. In some cases the trend is flat.

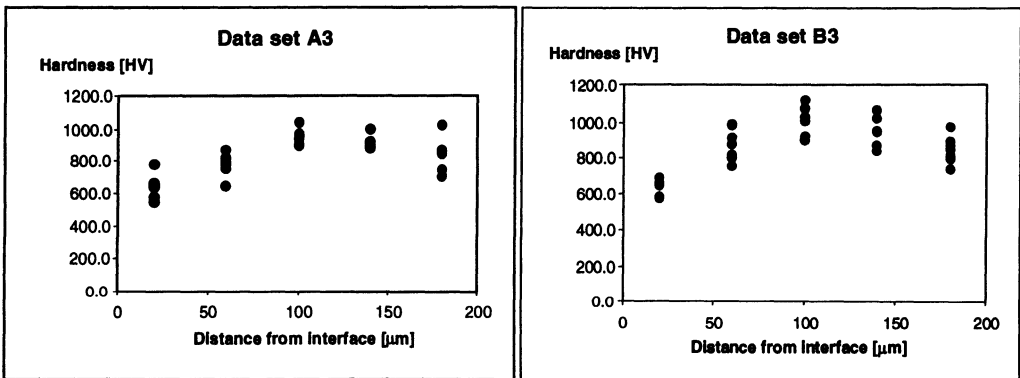


Fig.1: Data plot of hardness as a function of coating thickness for two different PSZ coating samples.

3.1.2 Normality test and rejection of outliers

The sample values obtained in this experiment are therefore tested for normality either graphically or using χ^2 test within each data set. All data sets were found to be normally distributed.

Then the rejection analysis was made on each series applying the Chauvenet criterion. Some of the data sets have presented outliers: in particular set A1 presented 3 outliers, sets A3 and A5 2 outliers and sets B3 and B5 only one outlier each. In the other cases no outliers were identified. As seen from this analysis, the rejected values were few. Most of the values discarded were in the case of sample A.

3.1.3 Hardness variation on coating cross section

As described previously, the hardness values of the coating were evaluated on different sections along the thickness of the coating. The analysis has been carried out on the data sets in which the outliers were rejected.

Before executing ANOVA to demonstrate the null hypothesis on the mean values, a necessary precondition is to determine if the variances of the different series are statistically comparable. This has been executed by using Bartlett test, which is based on the comparison of the value of the Bartlett variable with a particular χ^2 distribution, to obtain a probability value P(B). Results are presented in Table 2.

Data set	B	P(B)	Result
A1	2.71	0.607	Verified
A3	7.59	0.108	Verified
A5	3.51	0.173	Verified
B1	12.64	0.013	Suspicious
B3	1.12	0.891	Verified
B5	2.77	0.250	Verified
C1	5.62	0.229	Verified
C3	4.40	0.355	Verified
C5	0.45	0.799	Verified
D1	4.60	0.331	Verified
D3	6.09	0.193	Verified
D5	2.17	0.705	Verified

Table 2: Results of Bartlett test.

Data set	F	P(F)	Result
A1	16.15	0.000	Not verified
A3	13.74	0.000	Not verified
A5	27.17	0.000	Not verified
B1	6.80	0.001	Not verified
B3	14.60	0.000	Not verified
B5	43.80	0.000	Not verified
C1	1.10	0.377	Verified
C3	4.84	0.005	Not verified
C5	1.77	0.204	Verified
D1	34.88	0.002	Not verified
D3	3.89	0.014	Suspicious
D5	1.14	0.345	Verified

Table 3: Results of F test.

As shown in Table 2, all the data sets except one have comparable variances and are verified for further analysis with F test. Suspicious condition is not sufficient to reject the hypothesis, thus all the values are considered acceptable.

At this point, the variability of the coating hardness values along the thickness is to be verified using F test. The source of variance is considered to be within-series and among-series and the series sample means are compared.

The analysis of variance has been done on all the 12 data sets. As indicated in Table 3, results show that in data set C1, C5 and D5 the null hypothesis is verified, while D3 has resulted suspicious. In all other cases the hypothesis is not verified and the variation is considered significant.

Once the F test is performed, the variability of the data is observed from the trend of the data plots (Fig. 1). The trend reveals that in most of the cases, the hardness values near the interface and near the coating edge are lower than at the central band. In few cases the trend is flat. In any case, fluctuation of hardness data is observed at the two vicinities and as a result the central band seems to present consistent data. Based on this observation, three regions of the coating are identified: near the interface, central part and near the outer surface.

From the above analysis, it can be concluded that three regions of the coating are subjected to a different cooling rate and might present different microstructures. In light of this, the

five regions of the coating identified for the previous analyses with 1 or 3 N test load are grouped into three parts and investigated for microhardness value differences. This observation is verified with a proper statistical procedures as follows.

3.2. Hardness variation in three regions of the coating cross section

Once the hardness variation has been demonstrated by means of ANOVA and after analysing the trend of the data plots, the coating cross section has been divided into three regions, each of which may be characterised by a single hardness value.

3.2.1 Significance of the differences between couples of mean values

In the data sets obtained by 1 or 3 N test load, band I which is representative of coating near the substrate interface consists of the first two series, band II which is representative of the central part, consists of the third and fourth series, and finally band III that represents the coating near the outer border, of the fifth series. In the data sets that utilise a test load of 5 N instead, the new bands correspond to the three series described during the previous analyses.

To study the difference between couples of series means Tukey HSD test can be applied. It is based on the comparison of the HSD variable with the absolute value of the difference Δ_m between the two mean values under examination.

HSD test is performed in three cases: within band II to compare the third and fourth data series, data in band II with band I, and data in band II with band III.

The aim of the first test is to show that the central band contains two data series that are statistically comparable in each data set obtained with a test load of 1 and 3 N. As seen in Table 4, HSD test has proved that this band can be characterised by a unique value of hardness in all the eight cases.

Data set	HSD test 1			HSD test 2			HSD test 3		
	HSD	Δ_m	Result	HSD	Δ_m	Result	HSD	Δ_m	Result
A1	160.6	49.0	Verified	176.0	370.2	Not verified	176.0	81.5	Verified
A3	151.8	123.7	Verified	138.6	312.6	Not verified	138.6	108.6	Verified
A5	-	-	-	129.6	180.1	Not verified	129.6	143.1	Not verified
B1	235.9	129.8	Verified	235.9	338.4	Not verified	235.9	22.2	Verified
B3	144.4	137.9	Verified	158.2	368.2	Not verified	144.4	161.9	Not verified
B5	-	-	-	80.3	218.4	Not verified	73.3	190.9	Not verified
C1	126.5	10.3	Verified	126.5	76.8	Verified	126.5	20.5	Verified
C3	108.5	21.5	Verified	108.5	49.8	Verified	108.5	146.2	Not verified
C5	-	-	-	130.0	45.2	Verified	130.0	33.2	Verified
D1	139.8	100.1	Verified	139.8	15.8	Verified	139.8	1.5	Verified
D3	106.4	25.9	Verified	106.4	9.6	Verified	106.4	133.1	Not verified
D5	-	-	-	73.3	6.4	Verified	73.3	35.3	Verified

Table 4: HDS test results.

The HSD test between the data series in band II and band I is executed to check the statistical homogeneity of the data in the central region and near the interface.

The results demonstrate that in the cases where F test has shown insignificant variability, HSD test has also shown the same conclusion. In particular in data sets C5, D5 and C1 the hardness of the bands is not significantly different. If these three cases are omitted, the data in most of the remaining cases show differences in hardness values of the two zones.

Statistical homogeneity of the data in the central region and those near the edge has been checked with the third HSD test. The results between the data series in band II and band III are somehow similar to the results in the preceding case, if not for a more number of insignificance cases.

With a comprehensive analysis of the results provided by ANOVA and HSD tests, some conclusions about the data trend can be deduced. In the data plots, three different trends have been identified: a pronounced concavity downward, an increasing trend and an approximately flat distribution. However, considering all data sets, the hardness near the interface and towards the outer border presents a very large dispersion, while the values obtained in the central region do not exhibit this peculiarity.

3.2.2 Standard deviation in the 3 bands

The calculation, executed on data sets, clearly revealed the variation of the standard deviation both with the thickness and the test load. In 8 out of 12 cases the standard deviation is lower for the central band compared to the other two bands. This phenomenon could be correlated with the measurement problems met during data acquisition. In fact, in most cases a redistribution of the porosity in the proximity of the indentations and the cushion shape of the indentations observed could contribute to the reading error.

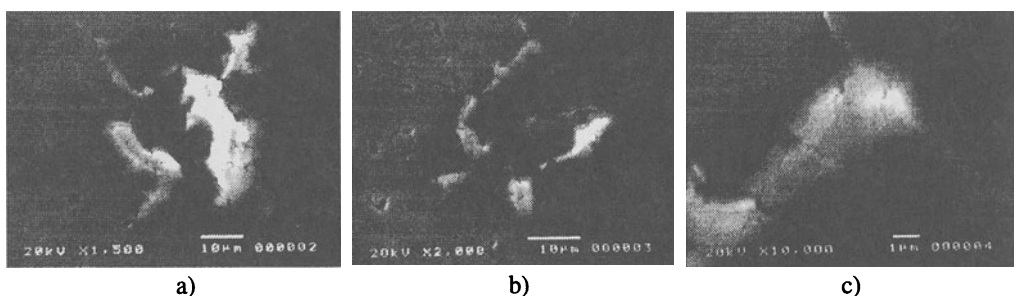


Fig.2: SEM micrographs of Vickers microhardness indentations of Partially Stabilized Zirconia (PSZ) coating: a) near interface zone, b) near outer surface, c) magnification of a detail of b).

For 1 N test load micro-crack propagation has been noticed (see Fig. 2 - b, c) although this was less evident in the central band. In the interfacial and central zones the diagonals of the indentations presented measurement difficulties due to the relative error introduced in reading small indentations [7]. In the case of 5 N test load, most of the indentations resulted in damaged outlines, macro-crack propagation, deformed and cracked indentations (see Fig. 2 - a). Therefore some tests had to be discarded and more number of tests were required to get the same number of data as in the case of 1 or 3 N test loads. These effects were evident

especially near the interface and near the outer surface. 3 N test load gave the best results, with limited microcracks propagation in the interface and surface regions. The central zone presented the most distinct indentation outlines [8].

3.2.3 Minimum number of observations to obtain a fixed error

In the domain of the experiments, it could be concluded that 3 N is the test load that gives the best statistical accuracy of the hardness, and the test should be conducted in the central band of the coating.

This assumption can be demonstrated showing that the minimum number of observations required to obtain a fixed confidence level if the test are executed following the suggested procedure, is inferior if compared with the standard procedure which does not consider the measuring region along the coating thickness. In fact when a Gaussian model is used to interpret an obtained statistical distribution, it allows the determination of the probability that a single measured value lies within an interval corresponding to a fixed relative error.

Taking into account firstly the distribution of band II, and then the entire data set, for a probability of 0.980 and a relative error of 5 %, results shown in table 5 have been obtained.

Data set	n	
	Entire	Band II
A3	61	7
B3	61	17

Data set	n	
	Entire	Band II
C3	19	4
D3	19	8

Table 5: Minimum number of observation to obtain a relative error of 5%.

The data obtained for the sets, that use a 3 N test load, highlight the advantages of the proposed measuring methodology and procedure. In order to establish a relationship between the hardness test results obtained for the entire coating thickness cross section (given by the overall mean value for each data set) and the results performed only in the central band (given by the mean value in band II), the relative difference has been evaluated. For this experiment using the proposed measuring procedure, the hardness results provided always higher values than the overall mean. The ratio between the two values ranged from 0 to 16%, but in most cases the ratio was about 5%. This value characterises the graph shape, being lower for flat distributions, and relatively higher for curved trends.

3.3 Variation with test load and sample properties

The standard deviation has been found to vary with the test load for each data set. In most cases higher loads give lower variance. Considering the microhardness mean values, the general tendency is again the decrease of the values with the load mainly due to indentation elastoplasticity [7]. Analysing the plots and the statistical results, hardness differences among the four samples considered could not be imputed to the difference in content of porosity. On the other hand, the porosity values considered ($1 \div 4$ %) are not significantly different to cause sensible variations of the microhardness properties.

4. CONCLUSIONS

Based on the observations and analyses presented above, the following proposed procedure is indicated as a contribution to define a preliminary protocol for microhardness measurement of Plasma Sprayed ceramic coatings:

- i. 3 N test load;
- ii. tests conducted in the central band of the coating avoiding thus mixing up of measured hardness values in the region close to the interface and to the outer surface;
- iii. position on the coating section selected such that the indentation lies on a less porous region;
- iv. once the test load and test positions are selected, the measured results should undergo standard statistical treatments;
 - a) the minimum number of observations required could be taken equal to 20, to provide only 5 % error on the mean value. This number is defined on the limited samples considered and is not a general conclusion;
 - b) rejection of outliers using criterion of Chauvenet;
 - c) the microhardness data obtained after rejection can be represented with the mean value and the standard deviation.

The statistical treatment mentioned above has been deduced using the following guidelines:

- on each data set, the microhardness data relative to different positions along the coating thickness can be grouped into different series;
- outliers must be rejected using certain statistical criteria like the criterion of Chauvenet.
- The sample is treated to follow a Gaussian distribution but should be checked for example with the χ^2 test;
- ANOVA should be conducted in order to decide if the microhardness variation along the thickness is significant; this step involves the verification of Bartlett condition and F test;
- if the last step shows the significance of the variation, HSD test can be used to achieve a new data classification, based on statistical criteria;
- the minimum number of microhardness tests, required to obtain the results within a limited dispersion range, can be calculated using the Gaussian model to interpret the data distribution.

Such a procedure is believed to increase the consistency in exchange of information on microhardness, and it helps to reduce experimental time. It also averts against misinterpretation of the microhardness properties of Plasma Sprayed ceramic coatings.

ACKNOWLEDGEMENTS

The authors acknowledge the co-operation of A. Basili and A. Attolini for the microhardness measurement execution, and the funding of CNR (National Research Council of Italy) and the support of SM s.r.l. Lombardore (Torino), Italy.

REFERENCES

1. G. Reiners, H. Kreye and R. Schwetzke, Properties and characterization of thermal spray coatings, Proceedings of the 15th International Thermal Spray Conference, Nice, France, 25 - 29 May 1998.
2. A. Kobayashi and T. Kitamura, Characteristics of high hardness zirconia coatings formed by gas tunnel type plasma spraying, Thermal Spray: Practical Solutions for Engineering Problems, ASM International, Ohio, USA, 1996.
3. Robert B. Heimann, Denise Lamy, Terry N. Sopkow, Parameter Optimization of Alumina-Titania Coatings by a Statistical Experimental Design, Thermal Spray Research and Applications, Proceedings of the Third National Thermal Spray Conference, Long Beach, Ca, 20-25 May 1990.
4. G. A. Blann, M. Hoffmann, Characterization of thermally sprayed coatings using manual vs. automatic microhardness testing, Thermal Spray: Practical Solutions for Engineering Problems, ASM International, Ohio, USA, 1996.
5. E. L. Crow, F. A. Davis, M. W. Maxfield, Statistics Manual, Dover Publications, New York, 1960.
6. C. F. Dietrich, Uncertainty, Calibration and Probability - The Statistics of Scientific and Industrial Measurement, Adam Hilger IOP Publishing Ltd, Bristol, 1991.
7. R. Groppetti, T. Gutema, Contribution to Nano- and Microhardness Measurements on Metal Kerfs Obtained by Precision Abrasive Water Jet Cutting, ISMTII '96, Hayama, Japan, pp. 105-112, Sep. 30, 1996.
8. T. Gutema, P. Bracali, R. Groppetti, S. Bertini, A. Scrivani, Characterisation of plasma sprayed ceramic coatings for advanced industrial applications, United Thermal Spray Conference 1999, Düsseldorf, Germany, March 17 - 19, 1999.

PRINCIPLES OF TORQUE MEASUREMENTS FOR ROTATING MICROSYSTEMS

W. Brenner, G. Haddad, G. Popovic, A. Vujanic and E. Chatzitheodoridis
Technische Universitaet Wien, Wien, Austria
R. Duffait and P. Wurmsdobler
CETEHOR, Besançon, Francia

KEYWORDS: Torque measurement, Rotational speed measurement, Cable brake method, Measurement cross element, CETEHOR device, CSEM devices, HAFAM device

ABSTRACT: In this paper, the torque-rotational speed characteristics of rotating inicrosystems and the principles involved are examined. Furthermore, some devices on the market and some realisations in the scope of TMR-proiect "Handling and Assembly of Functionally Adapted Microcomponents, HAFAM" are presented.

1. INTRODUCTION

The optimisation of kinetic chains, including actuators and driven elements, requires the knowledge of the energy balance of all components and the evaluation of losses. The latter is especially important for the development of microsystems, because for small sizes these power losses can reach significant values. The reasons are the introduction of high nonlinear behaviour caused by the size reduction, and the lowering of the geometrical precision induced by when the limits of the technical possibilities are reached.

The measurement operation assigns a value to a physical quantity [1]. A measurement chain for this operation includes the following elements (Fig. 1):

- Sensors for delivering a signal in accordance with the value of the quantity to be measured

- Elements for signal processing
- Elements for data display, storage or use (e.g. insertion of the measurement chain into a feedback control or machining process).

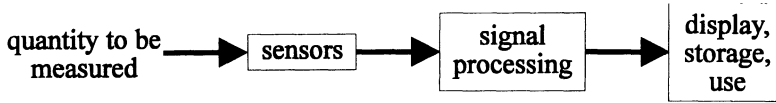


Fig. 1: General structure of a measurement chain

1.1. Torque- rotational speed characteristics

The main characteristic of a motor is its usable power in Watt which is available at the output shaft. For driving a mechanism there are two quantities to be considered: the usable torque C_U and the rotational speed in rad/s (ω) or in rpm (N). These quantities also define the output power $P_U = C_U \cdot \omega$. For a driven element, the resistant torque together with the rotational speed ω gives the required power to drive it.

1.2. Test device for the torque-rotational speed characteristics

The general structure of such a device consists of the regular elements of a measurement chain (Fig. 2). Since the goal is the measurement of the dynamical characteristics, it is necessary to join the components so that the resistance and the torque-rotational speed (including brake or driving device, inertial load, etc.) can be estimated.

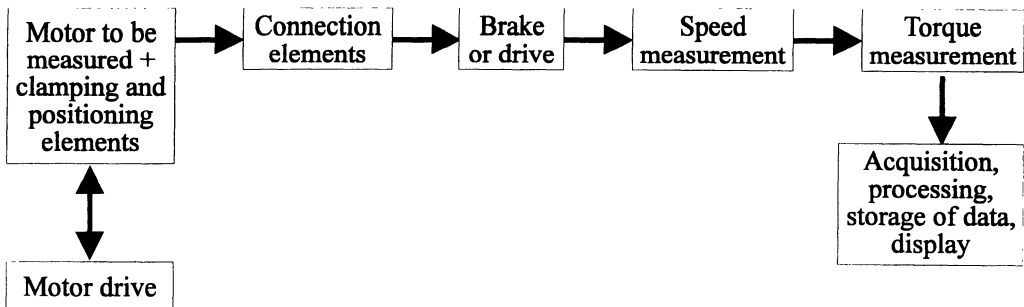


Fig. 2: General structure of a test bench for torque-rotational speed characteristics.

The purposes of the device developed for the measurement of the torque-rotational speed characteristics are the following:

- Measurement of torque versus speed in the steady-state, useful for motors and driven components like bearings, micro gears, etc.
- Measurement of transient phases (starting or stopping phase, step mode): torque versus time, rotor position versus time or, torque versus rotor position (only for motors).

For the measurement of torque versus speed, the input parameters are the signal shapes of the electric input variables. For the measurement of transient phases, the value of the inertial load is a very important parameter.

The schematic representations of these configurations are shown in the figures 3 a) and b).

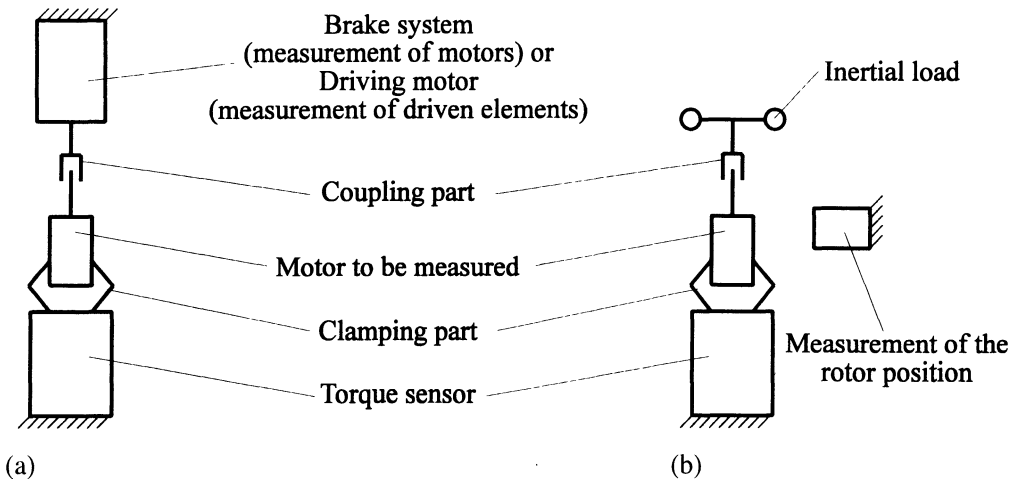


Fig. 3: Structure of a measurement device for torque-rotational speed characteristics
a) Stable speed state
b) Transient phases

1.3. Commonly used brake devices

The brake device is a very important element of such a test bench. It must guarantee a stable speed at a predetermined point of operation. Generally the brake system is based on dry friction (e.g. cable brake, eddy current brake etc.) or on viscous friction. Among the different systems, there are also the following [2]:

1.3.1. Dry friction brake

- **Prony brake:** The Prony brake consists of a set of jaws squeezing the output shaft. A dynamometer (or, for the large systems, a weight at the end of an arm) allows the balancing of the brake at an angular position relative to the torque to be measured. Since the braking torque is not perfectly constant this system is more appropriate for the characterisation of high-torque machines with low rotational speeds. Consequently, it will not be examined in this paper.
- **Tape brake:** This device is very simple and it is well adapted for the micromotors. A tape or a wire is rolled up on a pulley, which is fixed at the output shaft. On the one end of the wire a dynamometer is fixed while at the other end a weight provides the necessary braking torque. A version of this device was developed by the IFWT (Fig. 4).

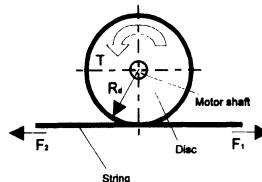


Fig. 4: Cable brake of the IFWT

A string is wound around an aluminium disc in a single loop. The force along the string is determined using leaf springs and strain gauges. CETEHOR developed a similar version of this system (Fig. 5). The slide friction is obtained by spacing the two pulleys and adjusting the wire strain.

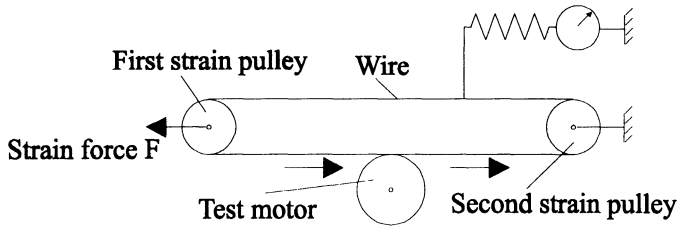


Fig. 5: CETEHOR brake system

This kind of brake is convenient for torque values, which are within a range of some μNm to 2 Nm. The suitable choice of a friction material will guarantee a constant value of the friction torque during the measurement.

- Powder brake: This principle is based on the braking effect caused by magnetic powder which is located in the gap between the stationary and the moving parts. The braking effect can be adjusted by changing the value of the magnetic field. The braking torque is approximately proportional to the current flowing through the induction coil. Another electromechanical brake system, which is well adapted for high-speed micromotors, is the Eddy current brake system.

1.3.2. Viscous brake system

This principle is based on the use of the viscosity of a fluid or of a force field. There are for example systems such as, system which use a set of ribs immersed into a liquid or hydraulic-brake systems. The device developed by IFWT of the TU Vienna uses the friction effect of a conical shaped brake body, which is fixed on the motor shaft and immersed into a brake liquid with a known viscosity (Fig. 9).

1.4. Uncertainty sources

Systematic uncertainties arise from usual measurement chains: misalignments of the shaft, distortion or displacement of the system to be measured within its support or relatively to the measurement sensor, fitness and sensor linearity, uncertainty of measurement method and data processing.

Moreover, there are uncertainty sources which are more specific to the measurement of the torque-rotational speed characteristics. They are caused by the inaccuracy of the brake or driving system or, in the case of a motor, by the power supply. Among them, we can mention the following:

- Instability of the braking or driving effect and, consequently, of the rotational speed. For the dry friction brake the instability is for example due to the variations of the friction

coefficient in relation with the variation of the friction coefficient with the heating of the friction materials.

- Instability of the power supply (micromotor characterisation). This error source is however only imputable to the test bench, if it includes an integrated power supply, and the driving elements for the motor to be measured.

Note: The amount of the uncertainty by torque measurement depends on the shape of the mechanical characteristics of the element to be measured.

2. DEVICE-EXAMPLES AND -REALISATIONS

2.1. CSEM devices

The magnitude of the torque acquired during measurements is in the range of some μNm (watch motor of the Lavet type at the second pointer with torque of less than $15 \mu\text{Nm}$) to about 10 mNm . The rotational speeds are very low. Figures 6 a) and b) show two test benches of CSEM (Neuchâtel, CH) available on the market for the watch industry. The Engretest is more adapted for the characterisation of small gears.

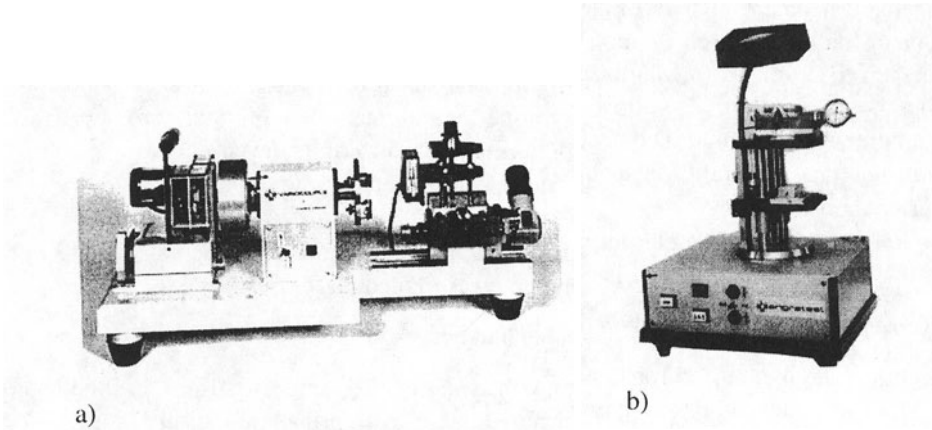


Fig. 6: Measurement devices from CSEM, Neuchâtel (Switzerland)
a) Variocouple, b) Engretest (Photos doc CSEM)

For both devices the measurement can only be made for less than 10 revolutions of the output shaft.

2.2. Universal device for small torque (Fig. 7)

This device is in development by CETEHOR (Fig. 7). It is the object of a European collaboration in the frame of the HAFAM. The partners for the development of this device are:

- Torque sensor: IFWT (Institut für Feinwerktechnik) of the Technical University and MTE Meßgeräte Entwicklung-und-Vertriebs GmbH of Vienna (Austria)
- Rotor optical position micro sensor: UNINOVA (Instituto de Desenvolvimento de Novas Tecnologias) of the University of Lissabon (Portugal)

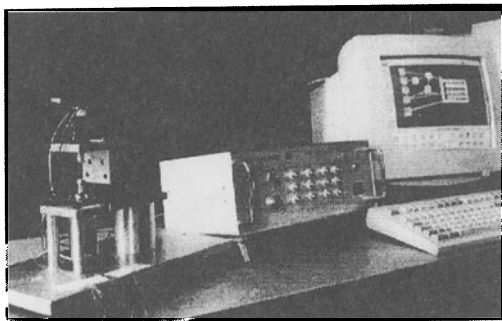


Fig. 7: Measurement device for small torque (development in the frame of the HAFAM program)

- IMM (Institute of Microsystemtechnics of Mainz) for clamping elements
- Structure of the bench and electronics: CETEHOR

The measurement range and the required facilities are the following:

- Mechanical characteristics of driving- and driven elements. The measurement range depends on the used sensor and starts from 50 μNm , with a resolution of 0.05 μNm and goes up to 20 mNm (resolution 20 μNm). The speed of rotation can reach 6000 rpm. The chosen structure also allows the torque measurement of motors at zero speed (for example when the motor is defected or during the course of its development).
- Transient phases: torque versus time, rotor position versus time or torque
- Current consumption
- Digital programmable input/output also allowing various functions such as driving step motors and automatic start of programmed measurement processes.

2.3. Torque measurement based on the cable brake method [4]

The cable brake is a closed force system, consisting of the cable (or string) and the cable disc. The force along the string is determined using leaf springs and strain gauges. The steel leaf springs are rectangular. The dimension of the leaf spring is governed by its material, the measured range of force and the range of deformation. The spring retainer clamps while the leaf spring and one of the holders are movable in the X-direction with a micrometer. Thus, the string strength can be adjusted very precisely.

When the disc is not moving, the force in the string is constant, and no force is applied to the disc. When the disc is rotating and the string is stretched, the string causes friction and brakes the disc. Two different forces can be measured at the two ends of the string (Fig. 8). The force difference is applied to the disc because of the friction between string and disc. This friction force acts upon the disc's circumference, creating a friction torque with respect to the middle point of the disc. The force difference can be measured and it is possible to calculate the friction torque applied to the disc (and to the motor) with the known disc radius.

The torque T can be deduced by a simple equation $T = (F_2 - F_1) \cdot (R_d + R_s)$. Where R_d and R_s are the disc radius and string radius respectively.

The rotational speed of the motor is monitored with an optical counter.

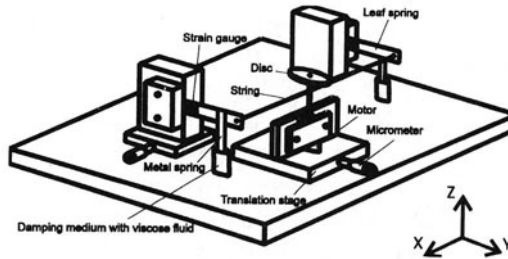


Fig. 8: Torque measurement with the aid of leaf springs and strain gauges

2.4. Torque measurement with the aid of the so-called measurement cross element [4]

The motor to be tested (Fig. 9) is mechanically clamped in a prismatic motor mount. The motor mount and the motor can be slid into the motor's axial direction by means of a shifting device. A step motor and a spindle are used to make the shift in $2 \mu\text{m}$ steps. The motor shaft is braked by immersing an interconnected braking device in a brake fluid of known viscosity.

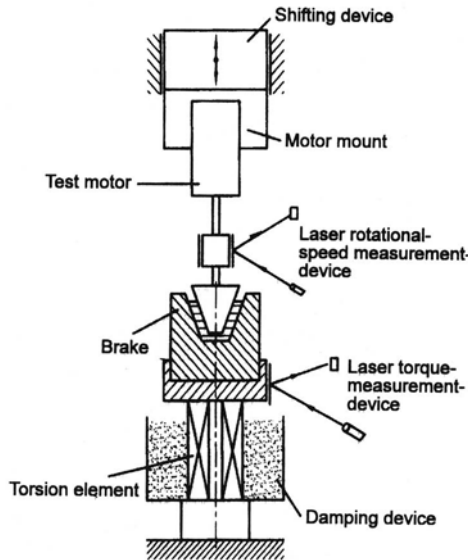


Fig. 9: Torque measurement with the aid of the so-called measurement cross

The brake fluid container is fixed on a rigid element with low torsion resistance (the so-called measurement cross [3]). The resultant braking torque exerts a torsional force on the measurement cross, and this is measured by means of a contactless measuring device (a laser system with a PSD optoelectronic sensor). The vibration occurring during the measurement procedures is absorbed by a damping device. The measurement of the

rotational speed of the motor to be tested is also contactless, being performed by a laser system. To this end, a reflecting prism is fitted onto the motor shaft or integrated into the brake for very small motors. The prism reflects a laser beam onto a circular array of photodiodes. When the motor shaft, which is fitted to the prism and the braking device, is rotated, all the photodiodes are successively illuminated. This way is possible not only to measure the rotational speed but also to record rotational speed fluctuations or step width in the case of step motors.

The measuring procedure is automatic. The brake which is fitted onto the motor shaft is progressively immersed into the brake fluid container by a computer-controlled step motor and then withdrawn. A characteristic curve of the rotational speed and torque can be automatically acquired in this way.

3. CONCLUSION

The two test benches of CSEM available on the market have been developed for the watch industry. The range of torque measurements is between some μNm to some 10 mNm. For both devices the measurement can only be made for less than 10 revolutions of the output shaft.

The device which will be developed by CETEHOR should measure torque between $50\mu\text{Nm}$ to 20 mNm with a resolution of $0.05\mu\text{Nm}$. The speed of rotation ranging up to 6000 rpm could also be measured.

The miniature cable brake permits the measurement of torque of miniature motors in the μNm range with a resolution of $1\mu\text{Nm}$ and rotational speeds up to 50,000 rpm.

The torque sensor with the aid of the so-called measurement cross element permits uninterrupted recording of rotational speed, torque and characteristics of miniature and micromotors. It is therefore possible to record micromotor characteristics at the sub- μNm range and rotational speeds up to 500,000 rpm.

ACKNOWLEDGEMENT

This work was supported by the TMR-Project "Handling and Assembly of Functionally Adapted Microcomponents (HAFAM)".

REFERENCES

1. Bavelard, G. et al: La métrologie en PME-PMI, Pratique de la mesure dans l'industrie, Chap. 4, Les chaînes de mesure, par P. LEBLOIS, Réseau CTI, AFNOR
2. Duffait, R. and Nogarede, B.: Mesure des faibles couples dans les microsystèmes, 8th International Metrology Congress, 20-23.10.1997, Besancon, p. 171-177
3. Austrian patent no. AT 393167 B
4. Haddad, G. et al: Testing of micromotors and rotating microsystems, Proceeding of 5th International Conference on Rotor Dynamics 1998, Darmstadt, Germany, p. 746-755

LOW-COST VISUAL CONTROL FOR HANDLING AND ASSEMBLY OF MICROSYSTEMS

**M. Jakovljevic, D. Petrovic, W. Brenner, G. Popovic, E. Chatzitheodoridis,
A. Vujanic, R. Martins and E. Fortunato**
Technische Universitaet Wien, Wien, Austria

KEYWORDS: Microsystems, image processing, handling, quality control

ABSTRACT

An environment capable of on-line visual quality and motion control is presented. The resolution of the visual system is better than $3\mu\text{m}$. The objects are held in a flexible paletting system and need not lie on predefined position. The data from the visual system may be sent to the motor control and can correct the position of the gripping system. The visual motion and quality control actively take a part in the control loop of the setup.

1. INTRODUCTION

The market tendency toward micro-mechatronic products consisting of a number of microdevices is leading not only to the development of new applications, but also to improvement of the characteristics and competitiveness of macroscopic systems. Those systems in the micrometer range may be found in low- and high-volume applications and may be fabricated by using bulk and surface silicon micromachining [1] techniques. On the other hand, microsystems may be fabricated in other technologies which do not rely on semiconductor technologies. Such microsystems consist of the parts fabricated in technologies as LIGA [2] and may be even more complicated containing different materials as metals, polymers, glass etc. The objectives of handling and assembly in this area are to cover a wide spectrum of different components, materials and shapes at a microscopic level with adequate accuracy. In the micrometer range any manual quality control even in small

Published in: E. Kuljanic (Ed.) *Advanced Manufacturing Systems and Technology*,
CISM Courses and Lectures No. 406, Springer Verlag, Wien New York, 1999.

quantities is hard to evaluate. In addition, the parts must be absolutely free of defect for later application in medical/life support and similar systems. Therefore automated quality control must be introduced which causes the overall microsystem costs to be downscaled.

For a number of reasons such as low costs, reliability, flexibility, speed and accuracy the microparts may be controlled visually. In the field of microsystem handling control, another reason for their application is of great importance. The repeatability and accuracy of macroscopic mechanical systems lays approximately in the $3\mu\text{m}$ and $1\mu\text{m}$ range, respectively. In order to lower the costs of the mechanics and drive control, the visual quality control system may be incorporated in the control loop as intelligent sensing system (see Figure). In this case the system may have twofold functionality which significantly contributes to the end product – a flexible assembly line for microsystem applications.

2. SPECIFICATION

The parts to be assembled lay in a sub-millimeter range. The image processing must be developed to fit the need of reliable pattern recognition and image processing, which act as an input parameter for a control system. In the scope of navigation for a handling system the position and orientation of microparts should be given. In addition such a visual system must be able to simultaneously check the quality and the consistency of the parts. The accuracy must lie almost in the sub-micron range. Obviously, novel techniques must be used in order to permit the work with such components. The aim of this work, in the scope of the European Community Project - HAFAM, is to develop reliable and inexpensive environment for supporting of handling, testing and assembly in the field of microsystem technology.

The properties of the visual control subsystems for handling will be estimated at first. The visual system consists of the light, lenses, camera, processing unit, framegrabber unit and communication facilities for handling control.

The light is in most cases so important as the image processing itself. Bad light conditions will cause even the best processing algorithms to fail, and perfect light may make a primitive and probably faster algorithm to work perfectly. The setup depends on the measurement needs or position estimation of objects. It consists of different types of adjustable lights roughly divided into direct diffuse light, sidelight and background light. The palleting system or part holder must be so designed that the light can reach the part effectively in any position.

The lens possesses a few properties which must be considered, such as distortion, focal length and working distance. Telecentric lenses with appropriate dimensions are available for parts with an outer dimension of less than $1000\mu\text{m}$. The distortion is very low and focusing is not a problem since the parts remain in the area of telecentricity and focus (limited to the millimeter range). The working distance is, depending on the lens, in the

range from 10 to 50 centimeters. Ample working distance is convenient, because of the space needed for the light system.

The camera's speed and resolution are an issue, as they directly influence the properties of the system. The use of high-resolution (2048x2048 or higher) cameras may be attractive, but this causes the amount of information which must be processed to explode. In standard PC system (200Mhz Pentium) significant amount of time is required (~1 secs) to load the picture loading operation. Therefore, standard (and cheap) solutions must be used. Standard EIA cameras combine lower resolution (768x576) with high speed (ca. 20 images per second). By incorporating appropriate lenses, the measurement may be in the range of micrometer resolution which is satisfactory for most applications. In addition, the position of the micropart may be estimated with satisfactory resolution for handling.

The framegrabber loads the pictures and translate analogue signals into digital data. Standard framegrabbers in various designs are preferred because of the low cost. The processing system must be based on Windows NT workstations. This will provide additional flexibility and faster performance in the years to come. In comparison with high-speed special solutions programming of the system is better supported and the performances are expected to double every two to three years.

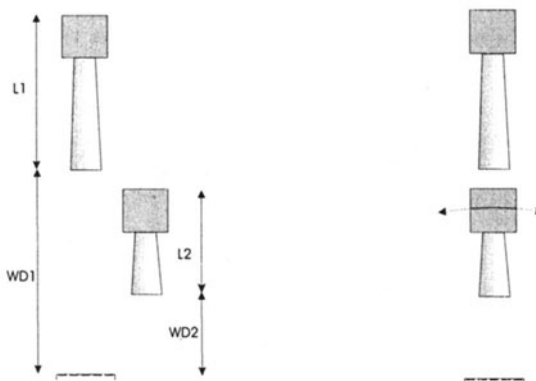


Figure 1. a) Position for rough estimation of the part positions (left) b) Fine measurement and position control (right)

3. SETUP

The basic idea of the visual control system is presented in the Figure 2. It consists of two equivalent cameras (Pulnix TM7) with different optics. The first one is fixed in position and able to cover the area of the palleting system (85mmx65mm). It determines the approximate position of the part in the palette and may have a fault-protection/testing function. The system is able to control the position of lower camera with one mirror and a

generated grid pattern. The second one is a measuring camera and takes the digitized image of the part in the field of $1200 \times 900 \mu\text{m}$. It must be mobile for positioning over the region of interest determined by the first camera. Both cameras have precise telecentric [3] lenses for measurement tasks. The working distances and the lengths of the cameras with lens are $WD1=420\text{mm}$, $L1=550\text{mm}$, $WD2=70\text{mm}$, $L2=320\text{mm}$.

The main light for measurement tasks, position determination and rough shape estimation is a diffuse backlight. It is the best option for precise measurements. The edges are easily recognized. The sidelight is important for image processing by using the shadow, which is dependent on the topology of the micropart. The roughness and different kinds of holes, hills or channels on the surface may be recognized with this light. As a third kind of light, normal frontal diffuse light is used for fine recognition of details not visible with other kinds of light. Various wavelengths may be applied depending on the application.

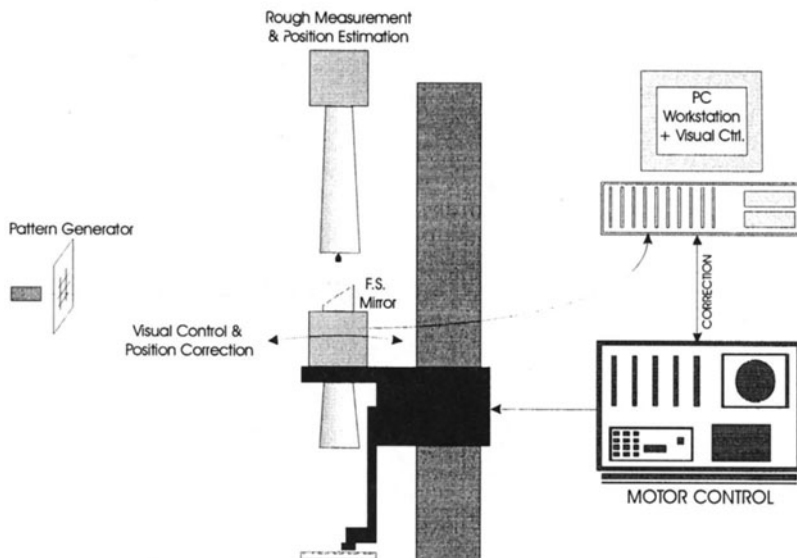


Figure 2. Schematic of the setup

Since the environmental vibration can be successfully suppressed, the vibration caused by motors and interrupted handling motion may be a problem in a high-speed application. The picture may be digitised only if positioned stably after subsidence of the vibration delay in within ten to hundred milliseconds. The application and the speed of the handling again determine the vibration delay and a designer must be prepared for compromise. This problem may be decreased by better mechanical design. Obviously, the maximum acceleration shock ($<7G$) [4] for cameras and optics is a limiting factor. The palette system has been developed to reduce the costs of image processing. It consists of transparent glass plate with a circular depression ($500\mu\text{m}$) with radius of 2mm . The microparts are not

expected to be at the defined place, and they may be randomly positioned within the circle. Therefore, the cost of mechanical positioning in assembly line will be reduced.

The accuracy of the optical system may be brought down to $3\mu\text{m}$ with the given optics. The software system must consider subpixeling and reduce the resolution down to the 1-2 micrometres. The subpixeling algorithm [5] employs the smooth transition of the black and white intensities on the edges to calculate in a range smaller than the pixel width (in our case theoretically $1.56\mu\text{m}$, but practically around $3\text{-}4\mu\text{m}$).

4. CONTROL LOOP

A diagram of the control flow is presented in the Figure 3. Depending on the application mode the handling control may be absolute or relative. The absolute procedure leads the handling system to the right point without any extended visual testing procedure. On the other hand, the relative procedure is an iterative process for repetitive correction of the position with required accuracy.

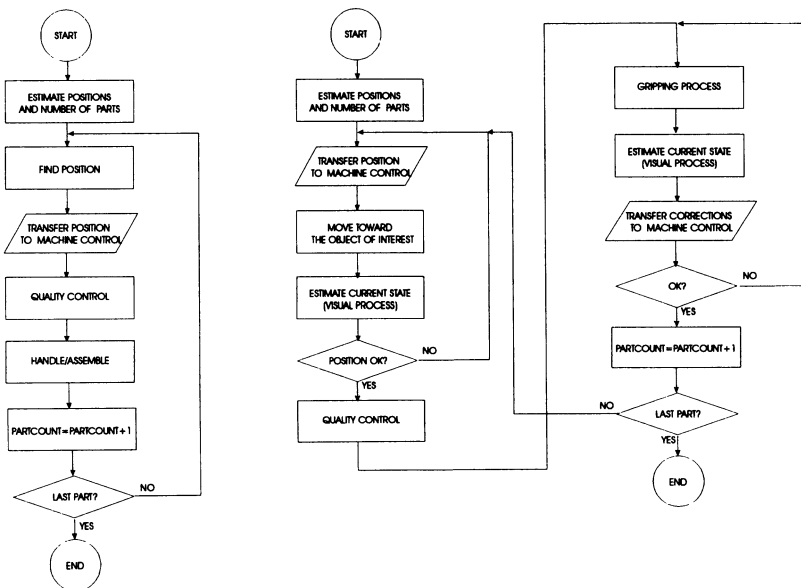


Figure 3. Control loop with absolute (left) and relative (right) procedure.

5. SOFTWARE

The software is built to support the most important functions for simple programming of different applications in Visual C++ and consists of several modules for determining a shape, position and dimensions of the system. Matrox MIL V5.1 libraries [6] have been used for our system. This image processing software library has well-developed functions

for different fields of application. The interfacing module has been built for the purpose of taking advantage of the tens of man-years invested in commercial image processing libraries without losing the necessary flexibility and independence of hardware platforms. This piece of software takes care about the compatibility with different models of frame grabbers. This facilitates future extensions. In addition, more important functions have been optimized and adapted to increase speed.

The modules are divided into three groups:

- Position estimation
- Shape recognition
- Measurement

The rest of the functions were taken over from MIL libraries. This seems to be a good way to reconcile the complexity and the speed. The determination of position is organized in several steps: rough position estimation, precise position estimation and a determination of object rotation. These functions are critical for the system's speed, particularly if evaluated in the control loop. Mostly they are line- or pixel- oriented and do not check an area of the image. The area is checked later in smaller regions of interest.

The shape recognition is based on similar principles. Normally, a slow 2D-Fourier transformation has to be used for very complex objects, but the MEMS parts are mostly very simple and may be covered by simpler functions.

The measurement of the dimensions is a topic of special interest. We are not interested only in obtaining the dimension expressed in pixels but also to obtain the subpixeling position of the edge. This is easy to do in the laboratory, but difficult on the assembly line. The environmental light may play a role, and the reflection from the handling system as well. The light conditions may vary significantly in different positions making any precise determination of dimension inaccurate. We use a blend of statistic processing and fuzzified rules to support our subpixeling algorithm. Depending on the amplitude, shape and intensity of the signal on edges, we are able to correct the calculated values and to achieve greater accuracy in the subpixel range.

Operation	Time (ms)
Rough position estimation for all parts ²	>30
Position estimation ¹	>5
Precise position estimation with angle ¹	>40
Measurement ¹	>5 ms
Shape recognition ¹	>25ms
Subpixeling edge estimation (line algorithm)	0.25-0.3
With additional constraints and simple fuzzy rules 0.5-2ms	0.5-2

¹depending on the object and measurement complexity

²depending on the number of objects

Figure 4. The speed of processing (200Mhz Pentium PC)

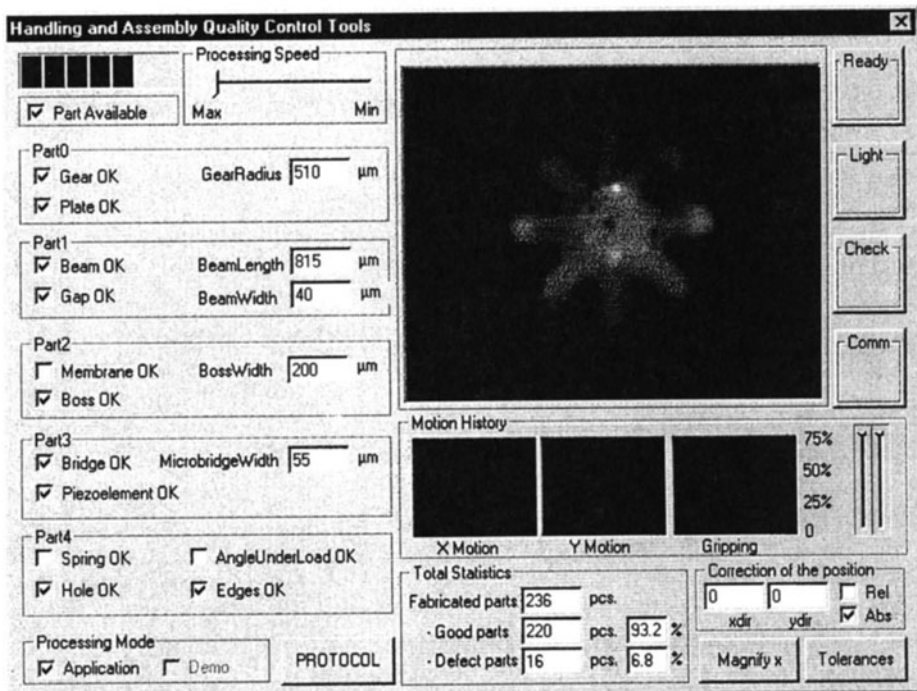


Figure 5. Application Interface (microgear $D=500\mu\text{m}$, sidelight)

6. CONCLUSION

The programmable low-cost system for simple quality control, which is also capable of providing a support for handling control, has been presented. The objective of this work in recognizing today's possibilities for integrated visual control in automated microsystem assembly lines. The imperative of integrating visual control in the assembly environment is even stronger in the field of microsystem fabrication technologies. The sensors must be more accurate, the motors and controls must be reliable even in submicrometer range. The gap between pure macroscopic mechanical control and microscopic grippers will demand more complex control and microsensors, which are hard to fabricate. To lower the cost of overall systems, intelligent and flexible control of the position and physical dimension is needed. The quality of the microparts will be important problem in the near future, after the microtechnologies reach a certain level of maturity.

Twofold on-line visual quality and motion control may reduce the fabrication costs together with the costs of the assembly equipment and control in the field of microsystems fabrication technology.

REFERENCES

1. Petersen;K.E.:Silicon as Mechanical Material, Proceedings of the IEEE, Vol.70, No.5, May '82.
2. Heuberger; A.: Mikromechanik, Springer-Verlag, 1989.
3. <http://www.silloptics.com/>
4. "Tm7 Technical Manual", Pulnix Inc., U.S.A., 1996
5. Jahne, Bernd.: "Digital Image Processing", 4th ed., Springer Verlag, 1997
6. "Mil v5.1 Library", Matrox Imaging Inc., Canada., 1998

**STABILITY ANALYSIS OF ROTATING DISCS
THE CIRCULAR SAW CASE**

P. Chabrier

ARC Soissons Villeneuve Saint Germain Soissons, France

P. Martin

ENSAM, Metz, France

KEY WORDS: Sawing disc, Residual stress, Cutting stability

ABSTRACT: Circular saws are rotating discs which become thinner and thinner according to production imperatives. Because of their cutting solicitations, they must be prepared in tension so as to avoid apparition of vibrations. In the work reported here, we make a synthesis of theoretical background on prestressed discs. It is shown the importance of tensioning operation and cutting conditions on disc behaviour. All of these results are validated by an experimental study conducted on wood sawing.

1. PRESENTATION OF CIRCULAR SAWBLADES

For many years, important developments have occurred in design, preparation and maintenance of circular saw. This tool is widespread for sawing different materials as stone, wood, metal and all of their derivatives. However, circular saws production involves a complex series of stages from steel sheet to final product. An example of a typical production cycle is like the following :

- initial state, natural or treated steel sheet usually in 75Cr1 (Din 2003) or 80CrV2 (Din 2235)
- shaping, whose widespread process is now laser cutting
- heat treatment with two stages. First, oil tempering about 870°C to transform martensite in austenite. The intermediate hardness must be near to 63 HRC. Then there

Published in: E. Kuljanic (Ed.) *Advanced Manufacturing Systems and Technology*,
CISM Courses and Lectures No. 406, Springer Verlag, Wien New York, 1999.

is an annealing about 450°C to obtain a final hardness between 40 and 45 HRC, which is function to the tool application. For information, hardness is a customer specification, but this is not the case of grain structure.

- plane grinding which defines final thickness
- straightening, to eliminate residual bumps and deeps
- tensioning to introduce residual stress in the blade core
- bore diameter, usually H7 or H8
- external diameter by turning or grinding.

At this stage, the work of core manufacturer is finished. In order that circular sawblade cuts, several operations remain, but depend on final use. Usually, we have,

- tipping cutting material (carbide stellite diamond)
- sharpening.

Complexity of circular saw production process makes that this is a tool of high technicity.

Moreover, this is blade core which defines tool quality in terms of stability and durability. But evolution of customer needs and production imperatives make that core becomes thinner and thinner. Therefore, straightening and tensioning, which are the most important operations improving sawblade cutting behaviour, must be controlled.

2. STRAIGHTENING AND TENSIONNING OPERATIONS

Straightening is an automatic operation where blades are lightly compressed between large roller, so as to eliminate bumps and deeps remaining from plane grinding. Tensioning involves carefully hammering or more frequently squeezing the blade between narrow rolls in a zone about half to thirds of the way from the centre to the periphery. In the contact zone, the metal is very slightly thinner: a plastic deformation appears, which induces axisymmetric and in-plane stresses [1]. It is said that blade is prestressed. Thus, in the plane of the saw, the metal in the tensioned region is actually in compression (fig. 1) while the metal at the rim of the saw is slightly stretched and is in tension [2].

In technical terms, we said that the blade becomes soft or that an dishing effect appears. This phenomenon is evident when the blade is mounted on a spindle and collared by flanges : the greater the degree of tensioning, the greater the dishing effect. When the saw is running at the desired peripheral speed, the metal at the rim stretches under the centrifugal forces while the metal nearer the collar can expand correspondingly, counterbalancing the strains induced by rolling. The sawblade straightens, and can cut accurately when running at the correct peripheral speed: the faster the rim speed is, the greater tensioning is required. Mechanically, the aim of tensioning is to introduce internal stress in the disc so as to increase its rigidity during running. But how to quantify level of tensioning required? Two methods are one of interest :

- bending test, the most popular in sawblade production. A lateral force of amplitude known is applied near the blade rim while sawblade deviation is recorded at 90° from the application force point. This is a comparative method.

- vibration analysis, used in majority by scientists. This method allows us to evaluate residual stresses at the plastic zone boundaries, by computing new natural frequencies.

3. CIRCULAR SAW VIBRATIONS

The most general saw vibration can be considered to be a sum of individual saw vibration modes [3]. Each mode has a specific shape and amplitude and it oscillates at a specific frequency ω_{mn} termed natural frequency. Each mode shape consists of an integer combination of nodal circle m , and nodal diameter n . The natural frequencies depend upon the saw geometry, clamping ratio, material properties, and the membrane stresses in the plane of the saw. These stresses arise from rotation, tension and thermal effects.

The critical speed determines the maximum stable saw rotation speed of the saw. At operating speeds near the critical speed, vibrational resonance occurs; applying a small force produces large, transverse displacements which results in inaccurate sawcut. A physical explanation of the critical speed for rotating discs has been established [4] and requires the concept of a propagating transverse wave. Critical speed can be explained by describing saw vibration in terms of two travelling waves for each vibration mode, moving around the sawblade at the same speed or frequency.

For the stationary observer of a rotating saw, the frequency of the wave travelling in the same direction as the saw will be increased by the saw rotational speed, whereas the frequency travelling in the opposite direction will be reduced. With the increase of a rotation speed, frequencies of the backward travelling waves for different vibration modes will approach zero at various rotational speeds and will appear as a standing wave. The particular rotational speed at which the first backward wave frequency becomes zero (corresponding to a vibration mode), is called the critical speed (fig. 2).

The aim of tensioning is to shift natural frequencies and its critical speed through introduction of a membrane stress state. However, there are many more parameters affecting critical speed. We can mention the most important which are :

- thickness sawblade
- collar diameter.

All of these parameters have been introduced in a finite element analysis so as to compute sawblade behaviour in terms of natural frequencies and bending deflection. We take into account effects of centrifugal forces, tensioning, temperature and lateral cutting forces [5].

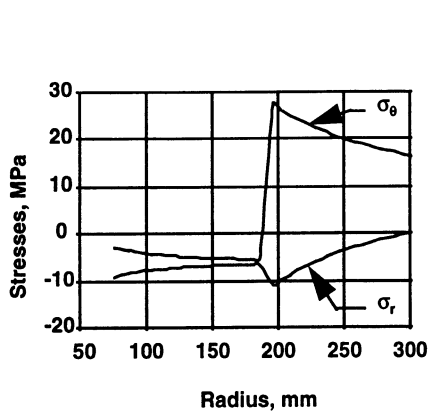
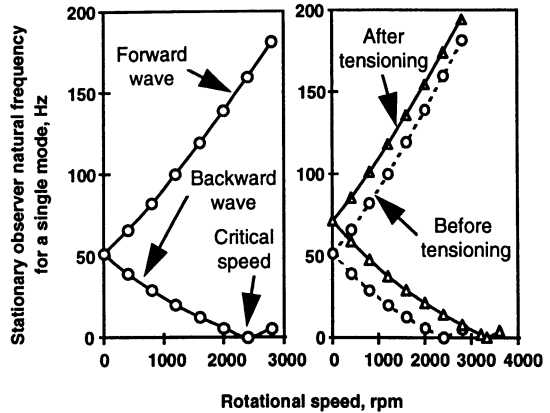


Figure 1: stresses arising from roll tensioning



Figures 2 : critical speed and influence of tensioning on natural frequencies

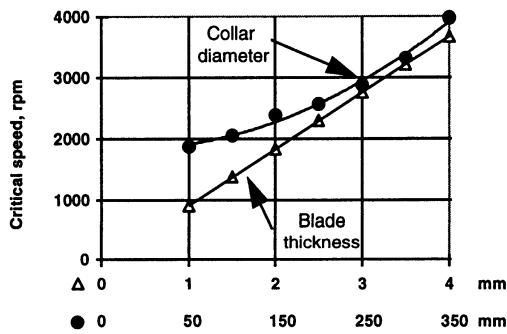


Figure 3: influence of collar diameter and blade thickness on critical speed.

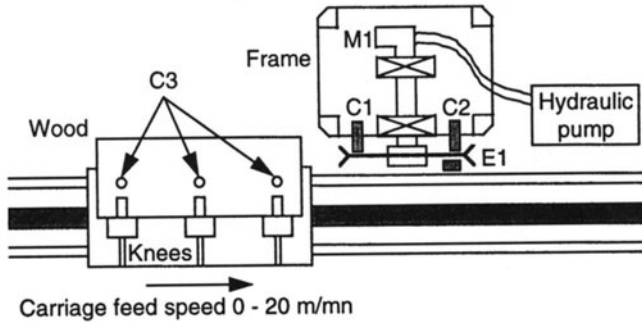
4. EXPERIMENTAL APPROACH

So as to validate our numerical work, we decided to apply it to wood sawing. The most complicated problem. Of course blade is submitted to centrifugal forces and lateral cutting forces, but in addition we have different heating [6]:

- a central predominant heating originating from heat conduction of bearings (rim speed is about 90 m.s-1)
- a peripheral heating, originating from wood / steel friction during cutting, which conducts to a thermal expansion of the metal at the rim.

In the others problems, cutting is under watering, which eliminates temperature parameter.

Therefore, we have developed an experimental laboratory device of characteristics given in figure 4. Blades are held by flanges of 150 mm in diameter. We worked on six carbide tipped circular sawblades (table 1) divided in two thickness classes (A and B). For each category, we have chosen three level of tensioning (1: slow, 2: normal, 3: strong). All of these blades have been characterised by modal analysis and bending test so as to determine their first critical speed (stability parameter).



C1, C2 : eddy current sensors, C3 : tridirectional piezoelectric force sensor
 E1 : electromagnet to excite blade, M1 : 40 HP hydraulic drive, (0 - 4000 rpm)

Figure 4: schematic sketch of experimental set-up

Circular saws tested				
Outside diameter : 600 mm				
Bore diameter : 110 mm				
Number of teeth : 32				
Rake angle : 20°				
Clearance angle : 15°				
Radial slots : 4 external slots, 55 mm long and 1 mm wide				
Blades	Thickness	Tensioning	Crit. speed	
A	A1	2.6 mm	Slow	2450 rpm
	A2	2.6 mm	Normal	2600 rpm
	A3	2.6 mm	Strong	2800 rpm
B	B1	3.2 mm	Slow	2950 rpm
	B2	3.2 mm	Normal	3100 rpm
	B3	3.2 mm	Strong	3450 rpm

Table 1 : characteristics of blades tested

Then, we have computed by FEM residual stresses arising from tensioning. Fig. 5 shows good agreement between theoretical and experimental results.

Then, we aim to compare sawblade behaviour during cutting. We cut in the grain direction 2 m long, 27 mm thick, spruce boards (Picea Abies) with seldom little knots. These boards had been naturally seasoned to an average moisture content of 12%. Cutting speed and feed speed were respectively 55 m/s and 10 m/mn. Moreover, we recorded blade deviation near the cutting zone (sensor C1, on fig. 4). Fig. 6 gives an example of raw signal recorded. For each blade, five trials have been done.

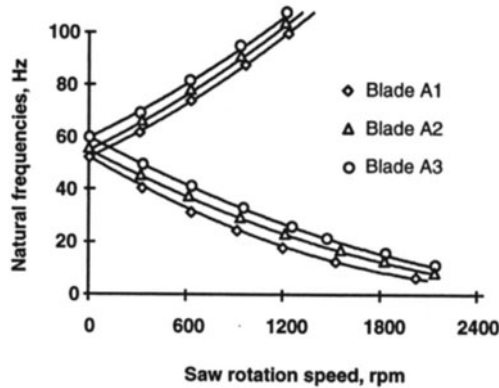


Figure 5 : Influence of tensioning on critical speed (theoretical curves and experimental points)

As we see it in figure 7, for sawblades B, the greater the level of tensioning, the more the blade stable. It is not right for blades A. A2 is unstable during cutting: resonance occurs. For this blade, there is a modal coincidence between one blade frequency and rim speed : this is a condition of resonance which results in inaccurate sawcut.

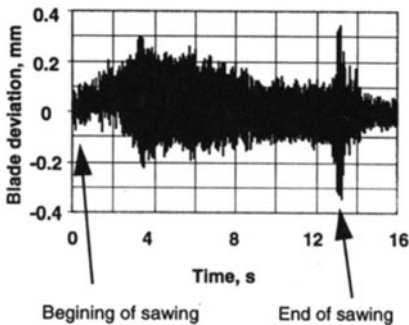


Figure 6 : example of signal recorded

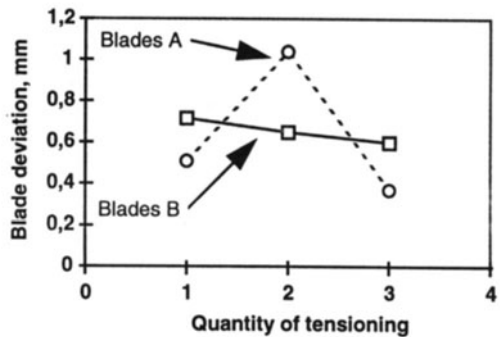


Figure 7: tensioning influence on cutting behaviour

Finally, we see that thinner blades are more stable than thicker. Very surprising phenomenon also explained by excitation frequencies.

5. CONCLUSION

Circular sawblades are tools of high technicity. Understanding their cutting behaviour requires concept of propagating transverse waves. A synthesis of theoretical background on vibrations and prestressing discs is first made in this paper.

Besides this knowledge has been validated on sawing experiments, conducted on a wood machine developed in consequence. The results, in good agreement with theory, can be helpful for saw manufacturers and sawfillers.

In the future we shall go on, by designing a new experimental device to mechanically test circular sawblades by integrating sound analysis. The study is currently being under the way.

REFERENCES

1. Schajer, G.S., 1984, Understanding saw tensioning, *Holz als Roh-und Werkstoff*, 42:425-430.
2. Nicoletti, N., Fendeleur, D., Nilly, L., Renner, M., 1996, Using finite element to model circular saw roll tensioning, *Holz als Roh-und Werkstoff*, 54:99-104.
3. Mote, C.D., Szymani R., 1977, Principal developments in thin circular saw vibration and control research, Part 1, *Holz als Roh-und Werkstoff*, 35(5):189-196.
4. Schajer, G.S., 1986, Simple formulas for natural frequencies and critical speeds of circular saws, *Forest Product Journal*, 36(2):37-43.
5. Chabrier, P., Martin, P., 1997, Analyse par la méthode des éléments finis du comportement dynamique d'un disque précontraint : application aux scies circulaires, *Actes du 13ème Congrès Français de Mécanique*, 4:233-236.
6. Nishio, S., Marui, E., 1995, Effects of slots on the lateral vibration of a circular sawblade during sawing, *Mokuzai Gakkaishi*, 41(8):722-730.

ON THE PRESSURE DISTRIBUTION AT THE CONTACT BETWEEN SMALL END OF A CONROD AND GUDGEON PIN

F. De Bona

University of Udine, Udine, Italy

A. Strozzi and P. Vaccari

University of Modena, Modena, Italy

KEY WORDS: Stresses, Connecting Rod, Gudgeon Pin

ABSTRACT: The contact pressure profile between the small end of a connecting rod and the gudgeon pin is investigated, having in mind the evaluation of the peak stresses in the small end. An analytical expression for the maximum bending moment in the small end is traceable in the pertinent literature, which is based upon a contact pressure profile of the form $p=k*\cos(\theta)^2$. A series of plane finite element (F.E.) studies have been carried out, aimed at clarifying the reliability of the analytical pressure profile. The numerical findings show a pressure distribution which appreciably differs from the analytical predictions, and which remains essentially uniform along the contact arc. Such a pressure profile produces stresses in the small end which are noticeably lower than the analytical values. As a consequence the analytical modelling, although approximate, is conservative, and therefore its practical validity remains unaltered. On the other side, high performance connecting rods require accurate calculations, which must be based upon realistic pressure profiles, an observation which motivates the current study. Preliminary three-dimensional finite element studies are also included, which essentially confirm the plane analysis.

1. INTRODUCTION

In this section the basic knowledge is summarised concerning the stress state in the small end of a connecting rod (conrod), with particular regard to the pressure distribution between the small end of the conrod and the gudgeon pin. It is in fact observed that the

Published in: E. Kuljanic (Ed.) *Advanced Manufacturing Systems and Technology*,
CISM Courses and Lectures No. 406, Springer Verlag, Wien New York, 1999.

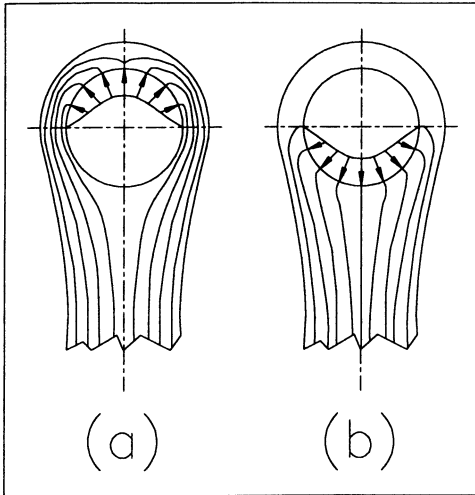


Figure 1

the stress flow lines in the small end at the TDC and when the conrod is pulled under the effects of the inertial forces, whereas Figure 1 (b) describes the stress flow lines still at the TDC, but when the conrod is pushed by the combustion forces. In Figure 1 (a), the contact between small end and gudgeon pin occurs along the upper half edge of the small end and, therefore, the stresses affect the whole of the small end. Conversely, in Figure 1 (b) the contact between small end and pin takes place along the lower half border of the small end and, therefore, the load transfers directly from small end to gudgeon pin without really stressing the small end. The above observations rationalise the conclusion that the small end is more severely stressed when it is at the TDC and when the conrod is in tension under the effects of the inertial forces, although the maximum loads acting on the conrod are the combustion forces and not the inertial loads.

It has been observed at the beginning of this section that the determination of the stress state in the small end of the conrod presupposes a detailed knowledge of the contact pressure profile between pin and small end. In the following, the contact pressure profiles traceable in the pertinent literature are briefly reviewed. The most commonly accepted pressure profile is that reported in [1,2]:

$$p = p_0 \cos^2 \vartheta \quad (1.1)$$

where the origin of the angular coordinate θ coincides with the centre of the contact arc between piston pin and small end, Figure 2 (a). This pressure distribution reaches its maximum value p_0 at the contact arc centre, it then diminishes gradually to vanish at an angular distance of $\pi/2$ from the contact centre. Figure 2 (a) indicates that, according to this model, the maximum stresses in the small end of the conrod affect section *B-B* where, by interpreting the small end in terms of a curved beam [1], a bending moment and a normal force predominate. The peak stress occurs at the inner fibre of section *B-B*, where both

evaluation of the stress state in the small end of the conrod and in the gudgeon pin requires a detailed knowledge of the contact pressure profile between pin and small end. Limiting ourselves to the mechanical analysis of the small end of the conrod, it is noted that the stresses reach their peak value in the small end as the conrod is at the top dead centre (TDC) and is in tension under the effects of the inertial forces. In fact, in this conrod position the stresses in the small end are found to be higher than those still relative to the TDC, but to the situation in which the conrod is in compression due to the combustion forces.

Figure 1 details the two afore-mentioned situations. In particular, Figure 1 (a) depicts

these stress components are compressive. According to [1], the ovalising bending moment M_0 and normal force N at section $B-B$ may be estimated by the following formulae:

$$M_0 = 0.08 P r_m \quad ; \quad N = P / 2 \tag{1.2}$$

where P indicates the total tensile load acting on the conrod, and r_m represents the mean radius of the small end of the connecting rod, Figure 2 (a).

An alternative pressure distribution is favoured in [3], where the pressure profile is assumed to remain constant throughout the contact arc between small end and gudgeon pin, Figure 2 (b). Following [3], and assuming a semi-angular extent of 135° of the curved beam part of the small end, [1], the ovalising bending moment M_0 and normal force N at section $B-B$ are expressed by formulae:

$$M_0 = 0.021 P r_m \quad ; \quad N = P / 2 \tag{1.3}$$

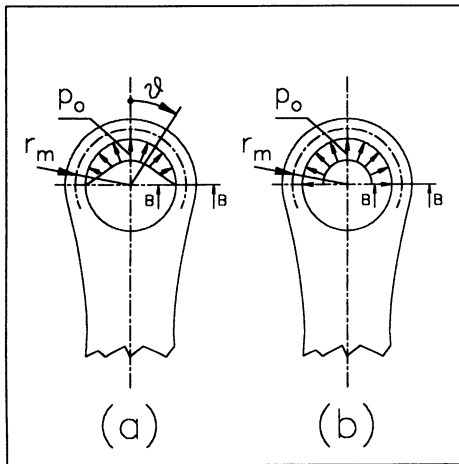


Figure 2

Additional studies on the contact pressure profile are presented in [4], where photoelastic and numerical results are compared. A photoelastic analysis effected for a variety of small end geometries is presented in [5]. A three-dimensional photoelastic study is presented in [6,7] for the contact between gudgeon pin and small end of connecting rod, particularly addressing the stresses in the gudgeon pin. Design formulae for the gudgeon pin are presented in [8], which are based on the ovalisation of the pin, and which are therefore connected to an assumed specific pressure distribution between small end and gudgeon pin. Finally, in [9] preliminary photoelastic and numerical studies on the

actual pressure profile at the contact between small end and gudgeon pin are presented. On the whole these additional studies indicate pressure profiles between small end and gudgeon pin which are intermediate between the two extreme distributions illustrated in Figure 2, favoured in [1] and in [3], respectively. As a consequence, the peak stresses in the small end of a conrod are evaluated in this paper by adopting only three models, namely the pressure profile according to [1], that favoured in [3], and the pressure profile deriving from the direct solution of the contact between small end and gudgeon pin. This last problem is solved numerically with the aid of a finite element program. The above comparison is carried out for a range of small end geometries, with the aim to clarify whether a simplified pressure profile produces sufficiently accurate peak stresses in the

small end, that is, whether the peak stresses in the small end can be estimated with simple models, without resorting to lengthy finite element modellings.

2. DISCUSSION OF A PLANE MODELLING

In this section the development of a plane model is discussed which is as consistent as possible with the three-dimensional fashion of the contact problem between gudgeon pin and small end. Figure 3 (a) depicts the realistic contact pressure profile between gudgeon pin on one side, and small end and piston housings on the other side, as shown in [2]. Contact pressure peaks occur at the contact transition zone of the gudgeon pin between small end and piston, which confer to this contact problem a strongly three-dimensional fashion. Such stress gradients agree with the photoelastic readings of the ovalising stresses presented in [4]. Figure 3 (b), instead, describes the classical simplification of the contact pressure adopted to evaluate conservatively the pin bending stress σ_g , said "global stress", as reported in [1]. Finally, Figure 3 (c) depicts the idealisation employed to estimate the

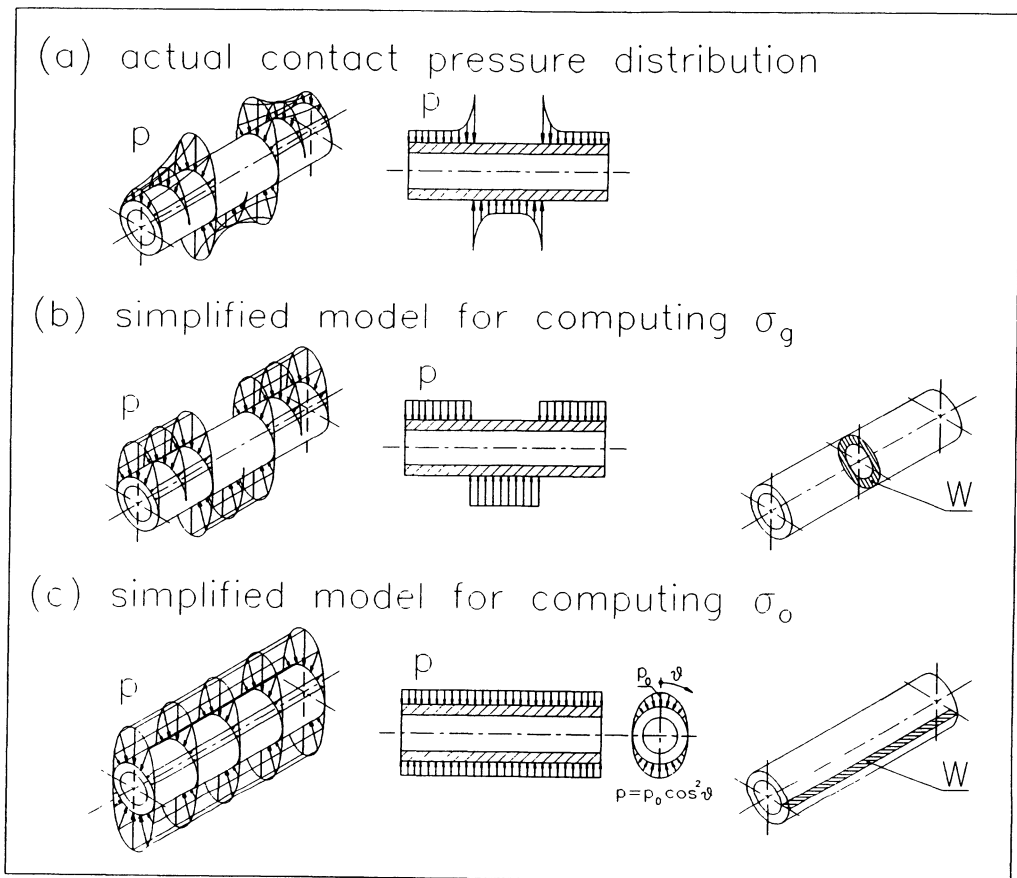


Figure 3

pin ovalising stresses σ_o , [1]. The same modelling is also used to derive the gudgeon pin squeeze as a result of its ovalisation, as reported in [8]. This modelling is typically plane, since the gudgeon pin contact pressure is assumed to remain constant for each cross section of the pin. It is also observed that each pin section is self-equilibrated. Such properties classify model (c) as the most consistent plane simplification of the three-dimensional contact problem between gudgeon pin and small end of the connecting rod, and this idealisation will be adopted in the plane study presented in this paper. As a consequence, in this plane simulation the gudgeon pin is supposed to be loaded along the upper half border by the contact pressure, and to be loaded along the lower half border by the same contact pressure, which mimics the pressure exerted between gudgeon pin and piston housing.

The correctness of the contact pressure (1.1) between small end of the conrod and gudgeon pin is explored in the following, in the limits of the plane modelling just discussed. To this aim, the deformed shapes of the small end and of the gudgeon pin are compared at the TDC, both when the conrod is compressed and when it is pulled. In particular, it is examined whether the deformed shapes of small end and gudgeon pin are compatible or otherwise. Figure 4 (a) represents the plane models of the gudgeon pin and small end, in the absence of loads. Figure 4 (b) illustrates the deformed shape of the small end at the TDC when the conrod is pulled. Under the effect of a contact pressure whose maximum falls at the contact centre, and which diminishes laterally, the small end ovalises vertically, by increasing its vertical diameter. Instead the gudgeon pin, under the effects of the contact pressure shown in Figure (b), ovalises laterally by increasing its horizontal diameter. The two deformed shapes, of the gudgeon pin and of the small end, are therefore incompatible, so that the contact pressure (1.1) appears to be unrealistic. The actual pressure must in fact possess a profile such that the deformed shapes of gudgeon pin and small end are consistent. It may be speculated that a contact pressure profile nearly uniform along the whole contact arc, [3], produces deformed shapes for gudgeon pin and small end which are

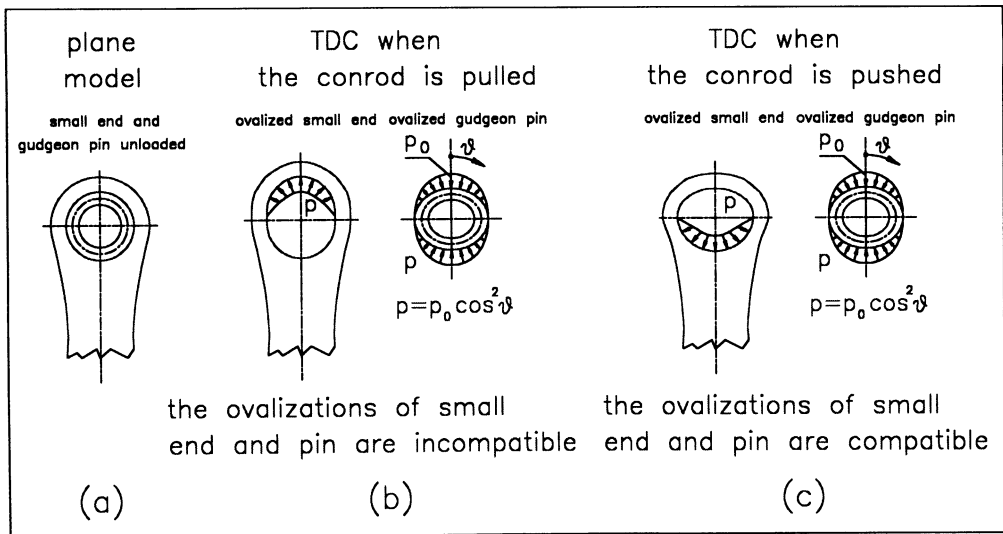


Figure 4

more consistent than those obtained by adopting the pressure profile (1.1). Under the effects of a uniform pressure distribution, the gudgeon pin behaves similar to an externally pressurised pipe, so that it is subject to a compression force more than to a bending moment. As a consequence, the pin essentially does not ovalise, and a similar deformed shape characterised by a limited ovalisation is expected for the small end. It may be concluded that a uniform pressure distribution produces deformations in the gudgeon pin and in the small end which are mutually compatible. This compatibility suggests that the actual pressure profile is not far from being uniform.

Figure 4 (c) finally illustrates the deformed shape of the small end at the TDC when the conrod is pushed. This time the ovalisations of both pin and small end exhibit an increase of the horizontal diameter, so that the two deformations are mutually consistent. As a consequence, the contact pressure profile (1.1) is more realistic in the TDC when the conrod is pushed than when the conrod is pulled, [3]. On the other hand, the situation when the conrod is pulled is more relevant, since in this position the small end is more stressed. Having clarified that the contact pressure (1.1) is not realistic in the TDC when the conrod is pulled, it is necessary to define the correct pressure profile and, in addition, which approximate pressure distribution better estimates the peak stresses in the small end. To this aim, in the following sections various plane finite element studies are carried out, followed by preliminary, fully three-dimensional numerical studies.

3. PLANE FINITE ELEMENT STUDY

This section presents various finite element numerical stress studies of the small end

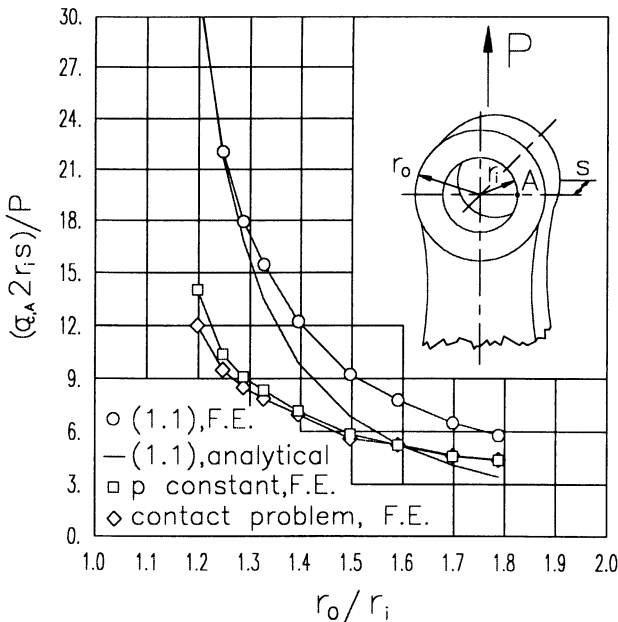


Figure 5

modelled as a plane problem, which in particular show that the dry pressure profile (1.1) is conservative, since it overestimates the actual stress field in the small end. The contact pressure distribution of the numerical approach has been derived by solving the contact problem between pin and small end with the aid of finite elements. As a consequence, such a contact pressure exhibits a realistic profile, in the limits of the plane model adopted in this section. This contact pressure distribution has been found to remain almost uniform along the contact arc, as conjectured

in section 2 . This result is essentially independent of the relative radial thickness adopted for the small end of the conrod.

Figure 5 depicts the circumferential stress at point A , $\sigma_{c,A}$, evaluated for a wide range of small end geometries which covers the whole technically significant geometries, that is, for outer to inner radii ratios ranging from 1.2 to 1.8 . The lower figures are more typical of a two stroke engine, whereas the higher values address four stroke engines. Four curves are presented in Figure 5 . The top cure refers to a small end loaded by a pressure profile according to (1.1) , and solved numerically with the finite element method. The second cure is relative to the same contact pressure distribution, but the analytical formulae (1.2) are employed to evaluate $\sigma_{c,A}$. The third curve adopts a constant pressure profile along the small end loaded arc, as in Figure 2 (b). Finally, the fourth curve describes the circumferential stress at point A when the contact pressure is determined by actually solving numerically the contact problem between small end and gudgeon pin.

It clearly emerges that the constant pressure profile constitutes an accurate model for computing $\sigma_{c,A}$ along the whole range of practically relevant outer to inner radii ratios of the small end. It is also noted that the contact pressure distribution expressed by formula (1.1) produces a circumferential stress at point A which becomes appreciably conservative for the small end geometries typical of two stroke engines. As a consequence, the traditional formulae (1.2), which are based upon such a pressure profile, conserve their practical validity, although the constant pressure model is more suitable than the $k \cdot \cos(\theta)^2$ distribution when a refined calculation of the small end is required, as in the case of high performance engines. It is concluded that the circumferential stress at point A may be accurately evaluated without directly solving the contact problem between small end and gudgeon pin, since a uniform contact pressure distribution furnishes extremely accurate stress values.

It is finally noted that the circumferential stress at point A computed by adopting formulae (1.3) reported in [3] for the bending moment and normal force would be heavily underestimated, so that a misprint is suspected in [3]. For this reason, the corresponding circumferential stress has not been reported in Figure 5.

4. PRELIMINARY THREE-DIMENSIONAL FINITE ELEMENT STUDY



Figure 6

This section presents some preliminary dry, fully three-dimensional finite element studies addressing the contact between small end and connecting rod, in order to assess the plane modelling employed in section 3. Figure 6 illustrates a mesh adopted for the mechanical analysis of the small end and gudgeon pin. Figure 7 shows the stress state in the small end at the TDC when the conrod is pulled. For reasons of symmetry, only one quarter of small end has been investigated. From an attentive investigation of the stress contour lines, it clearly emerges that the stress state remains essentially constant along the small end axial direction,



Figure 7

whereas a very localised stress concentration is perceivable at the edge of the small end. This stress concentration is due to the fact that the contact pressure exhibits a peak in the vicinity of the sharp corner assumed at the edge of the small end. Such a contact pressure peak may be reduced, or even removed, by properly rounding the sharp edge of the small end. Current research addresses the determination of the most suitable fillet radius.

In the limits of the afore observations, it may be concluded that the plane model adopted in section 3 for the mechanical analysis of the small end is realistic, apart from a limited small end portion in the vicinity of the small end edge.

5 CONCLUSIONS

A dry, plane, finite element study has been carried out for the contact pressure and peak circumferential stress in the small end of a connecting rod. It has been shown that traditional approaches are overconservative. Preliminary three-dimensional studies have confirmed the validity of the plane modelling.

ACKNOWLEDGEMENTS

The authors would like to acknowledge the contribution of Ing. F. Bonacini with particular regard to the finite element investigation.

REFERENCES

1. Giovannozzi, R.: *Costruzione di Macchine*, Patron, 1965.
2. Garro, A.: *Progettazione Strutturale del Motore*. Levrotto&Bella, 1992.
3. Kolkin, A. Demidov, V.: *Design of Automotive Engines*. MIR Publications.
4. Wearing, J.L., Arnell, P.P., Patterson, C.: A Study of the Stress Distribution in a Lug loaded by a Free Fitting Pin. *J. Strain Analysis*, 20 (1985) 217-224.
5. Manzella, G.: Sul Proporzionamento dei Collegamenti ad Occhio. *Tecnica Italiana*, 3 (1948) 6-14.
6. Fessler, H. , Padgham, H.B: A Contribution to the Stress Analysis of Piston Pins. *J. Strain Analysis*, 1 (1968) 422-428.
7. Fessler, H. and Hyde, T.H.: Stress Distribution in Gudgeon Pins. *J. Strain Analysis*, 32 (1968) 375-386.
8. Neale, M. J.: *Tribology Handbook*, Newnes-Butterworths, 1973.
9. Strozzi, A., Corradini, L, Chinni, L. Vignocchi, D.: Comparative Analysis of the Contact Pressures between Gudgeon Pin and Small End in High Performance Engines. *High-Tech Engines and Cars, 4th International Conference, Modena, Italy, (1998)*.

FATIGUE IN HARD METALS AND CERMETS
AN IMPORTANT DAMAGE PROCESS IN TOOL LIFE LIMITING

H.G. Sockel, P. Kindermann, P. Schlund, S. Kursawe, M. Herr and Ph. Pott

University of Erlangen-Nurnberg, Erlangen, Germany

U. Schleinkofer and W. Heinrich

Kennametal Hertel AG, Germany

K. Gorting

Plansee AG, Austria

KEY WORDS: Hardmetals, Cermets, Fatigue, Testing of Fatigue,

ABSTRACT

The behaviour of hardmetals and cermets under cyclic bending has been investigated by a new experimental method. Both coated and uncoated materials have been tested, at temperatures varying between 25°C and 900°C. The results show a strong fatigue effect. The endured stress amplitudes and lifetimes are strongly reduced under cyclic loads in comparison to the behaviour under static loads. Strong negative influences come from temperature and hard coatings. The conclusions advise the engineer to take fatigue into account in strength and lifetime calculations.

1. INTRODUCTION

Hardmetal and cermet tool materials are very well known in the area of production engineering. They have their most important field of technical application in the area of cutting tools [1,2]. In this field they cover the area between HSS-materials with very high toughness and ceramic materials including diamond and cBN with very high hardness [2]. Since their initial development between 1920 and 1930 they have found increasing fields of application as cutting tools due to the fact that the toughness and the hardness can be changed in relatively large ranges by changing the composition and microstructure. This

allows the adaptation of the materials to special cutting processes with their characteristic loading profiles.

In their application the materials are subjected to wear and to different thermo-mechanical loads, at 25°C and at elevated temperatures up to about 1200°C at the cutting edge [4,5]. The mechanical loads consist of static, monotonically increasing and cyclic loads. The complete exploitation of the intrinsic wear resistance of the tool material requires that the lifetimes under the mechanical loads are higher than under the wear load alone. Until 1992, the mechanical properties of hard metals and cermets were largely characterised by hardness, bending strength, and toughness measurements, and thus only the material response to static or quasi static loading conditions was investigated. The material response to cyclic loading was generally not investigated, due to the absence of any simple, inexpensive laboratory test. In consequence of this experimental difficulty there was very little knowledge in the literature about the fatigue of these materials before 1992 [4,6]. A short survey is given in reference [7].

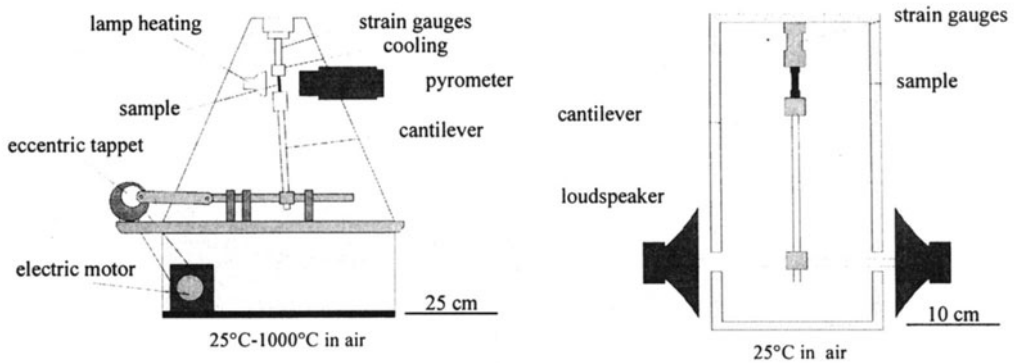


Fig. 1: Schematic representation of the apparatus used for bending tests at temperatures between 25°C and 1000°C,

In order to rectify this situation, systematic investigations of the behaviour of these materials under cyclic loads were started using a newly available experimental testing technique. This paper presents the experimental method and most important results about the fatigue behaviour from a phenomenological point of view.

2. EXPERIMENTS AND MATERIALS

The above mentioned experimental problems in the investigation of the behaviour under cyclic loads were overcome by the application of a modified apparatus which was developed and applied for the study of fatigue of ceramic materials by Fett and Munz in 1990 [8]. The machines used are shown schematically in Fig. 1. The use of big machines with

control of strain and stress would have been very expensive and would not have allowed a sufficiently high number of samples to be tested in order to obtain statistically reliable data. The simple apparatus used allows cyclic bending tests to be carried out in which only the stress is controlled. The stress control alone is sufficient for these materials because they exhibit between 25°C and 900°C no plastic regime, but only an elastic regime which is limited by fracture. The machines used are relatively small and not very expensive. Therefore several of these machines could be built in order to be able to investigate a relatively high number of samples in a limited time. A further development of the apparatus of Fett and Munz in the last 3 years allows the investigations to be carried out at temperatures between 25°C and 1000°C in air [9]. In both types of machines tests under static, monotonically increasing, and cyclic loads can be carried out. The frequencies in the cyclic tests are 22 Hz at 25°C and 2 to 5 Hz at higher temperatures.

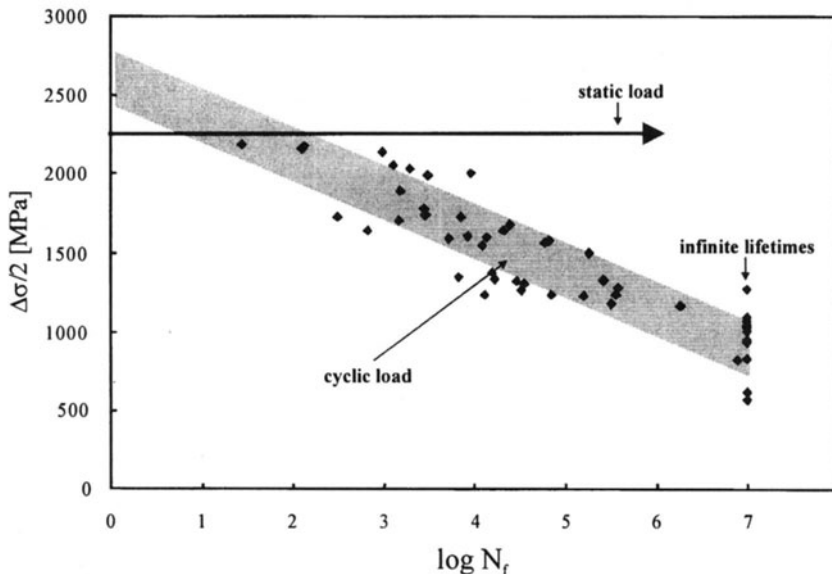


Fig. 2: Wöhler-plot of the stress amplitude versus the cycles until failure for the hard-metal P4M at 25°C,

The initial aim of the systematic studies under cyclic loads was a phenomenological description of the behaviour under these loads. Beyond this in the second step microstructural investigations by SEM, TEM, and SAM had the aim to find the damage processes occurring during fatigue.

The investigated materials were provided by Kennametal Hertel. They had the following compositions in wt.%: hardmetal P4M: WC 86, Co 6, (Ta,Nb)C 5, TiC 3, cermet HT7:

Ti(C,N) 53, WC 13, (Ta,Nb)C 8, TiN 5, Mo₂C 3, Co 12, Ni 6, hardmetal G10: WC 93, Co 7, hardmetal G30: WC 85, Co 15.

3. RESULTS AND DISCUSSION

In the following section some of the main results will be presented and discussed. This will be done with emphasis on the phenomenological description of the mechanical behaviour. Some information about the mechanisms in the microstructure will be mentioned, but not discussed in detail.

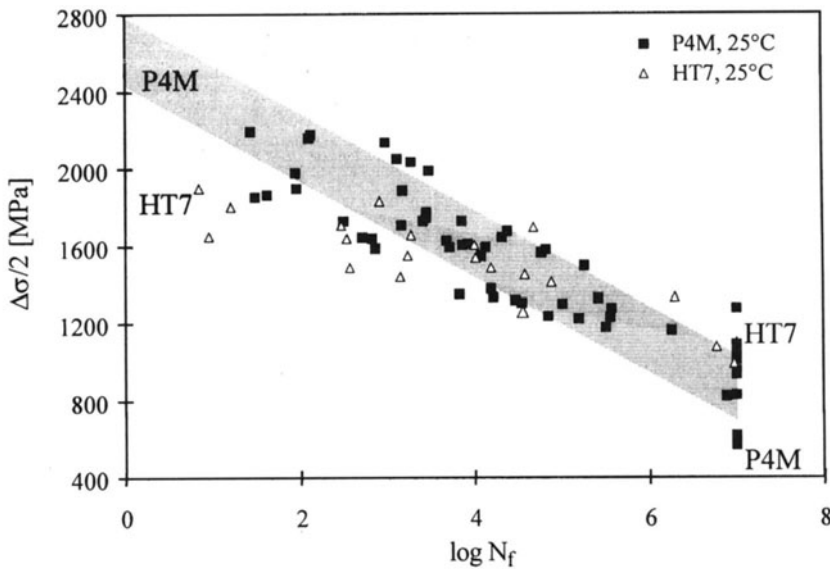


Fig. 3: Wöhler-plot of the stress amplitude versus the cycles until failure for the hardmetal P4M and the cermet HT7 at 25°C,

Fig. 2 shows the results for tests under static and cyclic loads at 25°C for the hardmetal P4M in a Wöhler plot. The bending strength is given in the Wöhler plots at $N_f = 0$. The tests under static loads with stresses of up to 90% of the bending strength lead to infinite lifetimes. In contrast to this behaviour the endured stress amplitudes under cyclic loads decrease strongly with the cycles until failure. That means that fatigue effects occur in the material. Microstructural investigations indicate the damage mechanisms under cyclic loads: subcritical surface cracks grow under cyclic loads until they reach the critical crack size and critical crack growth with failure occurs. Such a damage mechanism is not observed under static loads at low temperatures. Here no subcritical crack growth can be observed during the measured lifetimes.

From these results and from results of earlier works [10,11] it can be concluded that the behaviour under cyclic loads cannot be deduced from the behaviour under static or monotonically increasing loads. This behaviour under cyclic loads has to be determined experimentally and has to be taken into account in the design of components subjected to cyclic loads during use. The loss of strength by fatigue is relatively strong. From the data in Fig. 2 it can be seen that only stress amplitudes below about 40% of the bending strength can be applied if at least 10^7 cycles are required before failure of the component in the technical application.

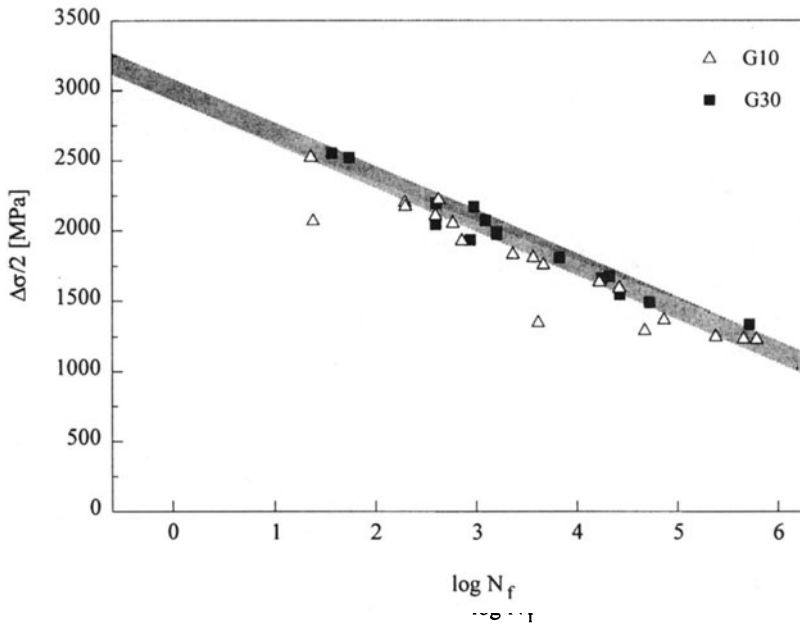


Fig. 4: Wöhlerplot of the stress amplitude versus cycles until failure for hardmetals G10 and G 30 at 25°C,

Fig. 3 shows the results obtained from hardmetal P4M and cermet HT7 after testing under cyclic loading conditions at 25°C. Again, these support the conclusion that the behaviour under cyclic loads cannot be derived from that under static or quasi static loads. The hardmetal has a bending strength which is about 35% higher compared with the cermet. However, if we consider the fatigue behaviour, we remark that the hardmetal loses its strength much faster with increasing number of cycles N_f compared to the cermet. Compared to the cermet the hardmetal exhibits a higher strength under static loads, but a lower resistance against fatigue. This is important for applications with cycles $N_f > 10^5$. If however the application requires only $N_f < 10^5$ then the hardmetal shows a higher strength than the cermet. It has already been mentioned that subcritical crack propagation is the main damage mechanism under cyclic loading. From investigations of critical crack propagation in

hardmetals it is known that the binder phase, which represents between 5 to 30 wt.% of the material is responsible for about 80% of the total fracture energy [12,13]. From this fact one would expect a strong influence of the binder content on the bending strength and the strength under cyclic loads. In Fig. 4 the behaviour of two hardmetals under cyclic loads is shown. They differ only in the binder content. G10 has a cobalt-content of 7.0, G30 of 15 wt.%. The hardmetal G30 with the higher cobalt-content exhibits higher strength under cyclic loads at low N_f . However, the difference in the behaviour of the two hard metals is relatively small and would have been expected to be greater. It also seems that their difference becomes smaller with increasing N_f . This is obviously caused by the fact that we have different damage processes with increasing crack length with influence on the subcritical crack propagation.

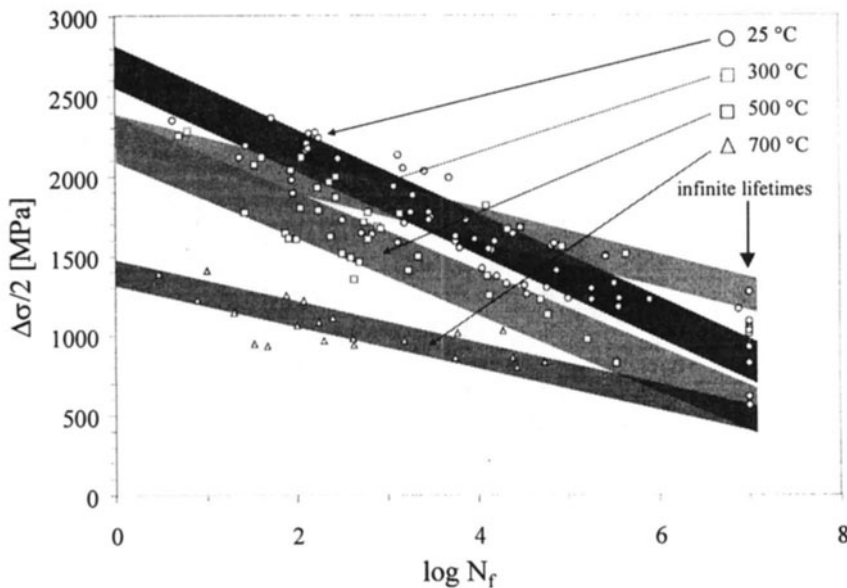


Fig. 5: Wöhler-plot of the stress amplitude versus the cycles until failure for the hardmetal P4M for different temperatures,

In the behaviour under cyclic loads the influence of temperature is of special interest. The occurrence of higher temperatures up to about 1200°C in the cutting process has been mentioned already. The behaviour of the hardmetal P4M under cyclic loads is shown for several temperatures in Fig. 5. For all temperatures one finds the similar behaviour that the strength decreases with N_f . If one considers first the curves for 25°C, 500°C, and 700°C it can be remarked that the lifetimes for a given stress amplitude are reduced very strongly, by several orders of magnitude, with the increase of temperature. The curve for 300°C does not fit into the changes of the other curves with temperature. The temperature dependence

of the strength becomes more clear when the fatigue sensitivity is plotted versus temperature. This fatigue sensitivity is defined as the slope of the curves for constant temperature in a special Wöhler plot, in which the stress amplitude is normalised by the corresponding stress amplitude for $N_f = 0$. The fatigue sensitivities obtained for P4M and HT7 are plotted versus temperature in Fig. 6. The fatigue sensitivity changes strongly for both materials with temperature. Obviously different processes with influence on the subcritical crack propagation are responsible for these decreases and increases. Microstructural investigations lead to the following responsible processes. P4M shows a decrease between 25°C and 300°C which is caused by a decrease in the amount of Co transformed from the fcc to the less ductile hcp structure during cyclic loading. The following increase is due to an increasing influence of the oxidation of the Co-binder at the crack tip [14]. The decrease above 500°C is caused by the brittle-ductile-transition of special ceramic phases. The cermet HT7 shows no change in the fatigue sensitivity between 25°C and 500°C. This is due to the fact that the Co-Ni-binder exhibits no phase transformation and therefore no influence on the subcritical crack propagation. The following decrease between 500°C and 700°C is caused again by the brittle-ductile-transition of special ceramic phases. The process responsible for the increase above 700°C is the oxidation of the Co-Ni-binder along subcritical cracks.

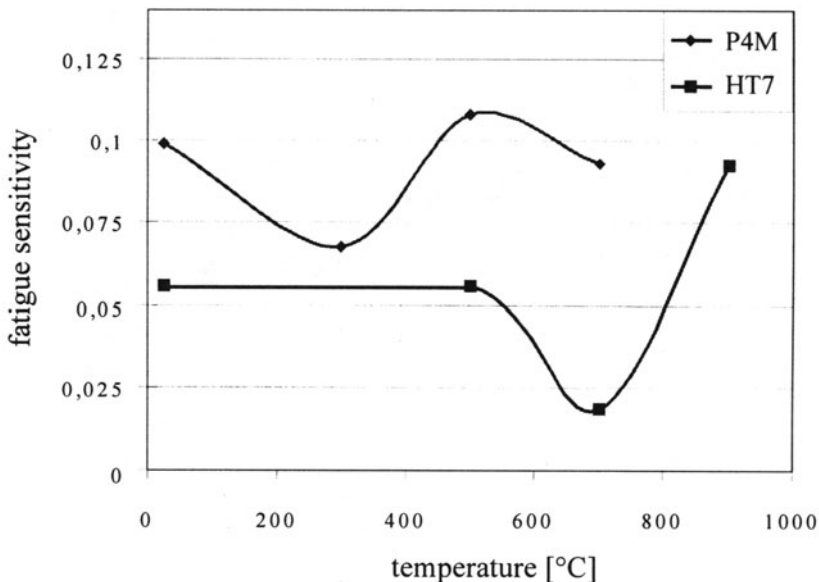


Fig. 6: Fatigue sensitivity versus temperature for the hardmetal P4M and the cermet HT7,

It should be emphasised here that although difficult and very time-consuming, the investigations into the microstructural processes influencing subcritical crack propagation at different temperatures are absolutely essential for the further improvement of the fatigue

properties of these materials. The knowledge of these processes is the basis for the development of concrete strategies for improvements in the future.

The influence of coatings on the fatigue behaviour can be treated here only very shortly. Details are given in reference [15]. More than 50% of hardmetal and cermet cutting tools are coated by hard materials such as TiN, Ti(C,N), TiAlN, and Al_2O_3 in order to increase the wear resistance. Therefore the influence of these coatings on the fatigue behaviour is of special interest. Fig. 7 shows the results of the behaviour of P4M with different coatings under cyclic loads. It can be remarked that the strength at 25°C is in general reduced when the material is coated with a brittle material. Very strong reductions of the strength are observed for CVD-coatings. The lifetimes of the uncoated material for a given stress amplitude are reduced by several orders of magnitude by the coating. These strong influences of the coatings have different reasons. Microstructural investigations lead to the conclusion that the following phenomena can play a role in the influence of the coating on the fatigue behaviour: residual stresses in the coating and the substrate, crack formation in the coating, propagation of the cracks in the coating in the substrate, and damaging of the substrate at the surface during the coating process.

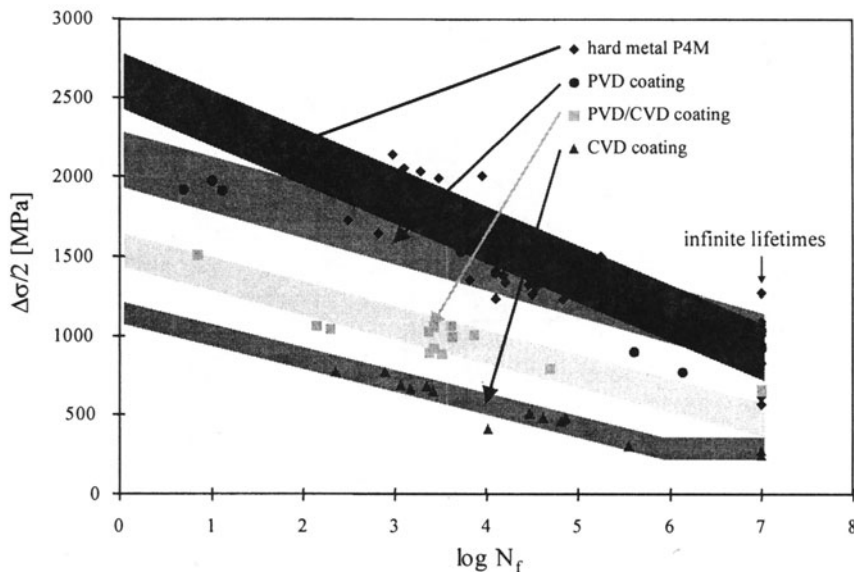


Fig. 7: Wöhler-plot of the stress amplitude versus cycles until failure for the hardmetal P4M without and with different hard coatings at 25°C,

4. CONCLUSIONS

The investigations of the behaviour of hardmetals and cermets under cyclic loads lead to the following main results. The materials show a strong fatigue effect. Compared to the behaviour under static loads the endured stress amplitudes under cyclic loads are reduced strongly. This occurs at 25°C and the fatigue effect becomes more strong at higher temperatures. Beside the temperature the other strong negative influence on the fatigue is caused by coatings of hard materials. In all mentioned cases the strongly reduced endured stress amplitudes in cyclic loading lead to very strong reductions of lifetimes by orders of magnitudes. This means that the designing engineer has to take into account this fatigue behaviour in his strength and lifetime calculations. For this he has to use experimental data about the fatigue behaviour because it cannot be deduced from the behaviour under static or quasi static loads. A modelling of the fatigue based on the obtained microstructural damage processes is in progress. It will be an additional help for the designing engineer.

ACKNOWLEDGEMENTS

The authors thank Prof. H. Mughrabi and Ms. V. Pugsley for the critical reading of the manuscript.

REFERENCES

1. Santhanam, A.T., P. Tierney, and J.L. Hunt : Cemented Carbides, Metals Handbook, ASM International, Ohio, 1990.
2. Kiefer, R. and F. Benesovsky: Hartmetalle, Springer Verlag, Wien, 1965.
3. Schintlmeister, W., E. Garber, W. Wallgram, and L. Schmid: Hartmetalle und deren Beschichtung für die spanende Formgebung, Tagungsband der Internationalen Pulvermetallurgischen Tagung, Dresden, Deutschland, 23.-25. 10. 1989.
4. Schedler, W.: Hartmetall für den Praktiker, VDI-Verlag, Düsseldorf, 1988.
5. Bhaumik, S.K., R. Balasubramaniam, G.S. Upadhyaya, and M.L. Vaidya: Oxidation behaviour of hard and binder phase modified WC-10-Co cemented carbides, Journal of Materials Science 11(1992) 1457-1459.
6. Almond, E.A. and B. Roebuck: Fatigue-crack growth in WC-Co hardmetals, Metals Technology (1980) 83-85.
7. Schleinkofer, U., H.-G. Sockel, P. Schlund, K. Görting, and W. Heinrich: Behaviour of cemented carbides under cyclic mechanical loads, Materials Science and Engineering

A109(1995) 1-8.

8. Fett, T., G. Martin, D. Munz, and G. Thun: Determination of $da/dN-\Delta K_I$ curves for small cracks in alumina in alternating bending tests, *Journal of Materials Science* 26(1991) 3320-3328.
9. Kindermann, P., P. Schlund, H.-G. Sockel, M. Herr, W. Heinrich and K. Görting: High-temperature fatigue of cemented carbides under cyclic loads, *International Journal of Refractory Metals & Hard Materials*, accepted for publication.
10. Schleinkofer, U., H.-G. Sockel, K. Görting, and W. Heinrich: Microstructural processes during subcritical crack growth of hard metals and cermets, *Materials Science and Engineering A209(1996)* 103-110.
11. Schleinkofer, U., H.-G. Sockel, K. Görting, and W. Heinrich: Fatigue of hard metals and cermets – new results and a better understanding, *International Journal of Refractory & Hard Materials* 15(1997) 103-112.
12. Sigl, L.S., H.E. Exner, and H.F. Fischmeister: Characterisation of fracture relevant parameters in WC-Co hardmetals, *Inst. Phys. Conf. Ser.* 75(1986) 631-643.
13. Sigl, L.S.: PhD-Thesis, Universität Stuttgart, F. R. Germany, 1986.
14. Kindermann, P., U. Schleinkofer, H.-G. Sockel, W. Heinrich, and K. Görting: Development of the microstructure in cemented carbides between 25°C and 1000°C and the relationship to their properties in the technical application, *Proceedings of the 1998 Powder Metallurgy World Congress* 4(1998) 57-62.
15. Schlund, P., P. Kindermann, H.-G. Sockel, U. Schleinkofer, W. Heinrich, and K. Görting: Mechanical behaviour of PVD- and CVD-coated hard metals, *International Journal of Refractory Metals & Hard Materials*, accepted for publication.

RESIDUAL STRESSES AFTER INDUCTION SURFACE HARDENING AND GRINDING

J. Grum

University of Ljubljana, Ljubljana, Slovenia

KEY WORDS: Residual Stresses, Induction surface hardening, Grinding

ABSTRACT: A number of research studies have shown that besides the design itself an important role is here played also by the stress state created in the material by carelessly planned manufacturing technologies. Internal stresses which are, since the completion of manufacturing, termed residual stresses very much reflect the manufacturing procedures and machining conditions.

Residual stresses are analyzed in terms of different induction surface hardening conditions and then also after finish grinding in terms of different machining conditions.

1. INTRODUCTION

In the last decade research and development activities in manufacturing technology have been very closely and unavoidably related to computer technology. The quality of a product, however, depends very much on the selection of material and on the consequences which the machining processes have on products.

A systems analysis about the machinability of materials has to include also investigations of their mechanical and physical properties as well as all the various effects that different machining processes leave on the workpiece surface. An integral research of material machinability should offer a full insight into the properties of material or product and should include material machinability with surface integrity of the material workpiece and tool.

The importance of surface integrity for surface quality and reliability in operation has been a generally accepted fact for quite some time. In all industrial countries the changes in the surface layer of the workpiece after the application of various machining processes are the subject of numerous investigations. A lot of progress has been made in the field of developing measuring methods, but there is still much confusion in the field of results evaluation and systematization. This could be explained by the fact that a great amount of

data has to be dealt with which are however not resting on the same experimental basis and thus possess only an intrinsic value. A good knowledge of surface integrity can undoubtedly help the engineer to make the right selection of machining conditions thus contributing to the longer life time of material.

The investigation of grinding mechanisms have led to a description of what happens during abrasive - metal interactions and how the grinding energy is dissipated. Excessive grinding temperature causes thermal damage in the surface layer of the workpiece [1-4].

Due to friction conditions between the grinding wheel and the specimen and due to the presence of a coolant/lubricant, this effect is joined by the effect of microhardening and tempering of the surface layer. These changes which take place only in the thin layers directly under the surface are strongly dependent on the machining conditions and kind of material [5-10].

The percentage of heat distribution into the grinding wheel and workpiece is principally the same, therefore the safety margin to the critical heat energy in the workpiece is even higher under this condition. Conventional testing methods such as metallographical inspection, X-ray diffraction, residual stress, and microhardness measurement are time consuming and cannot be used for the real time testing. Therefore, there is a considerable need for non-destructive testing techniques [2,11].

2. EXPERIMENTAL PROCEDURE

Workpiece material

For manufacturing crankshafts a heat-treatable steel 4140 AISI, was used. This steel is very appropriate for statically and dynamically loaded parts of car engines and machines especially because of its high hardness achieved after hardening (57 HRC). The steel is characterized by good hardenability and is thus suitable for manufacturing machine parts with large cross-sections in which after refinement a very high strength can be obtained. After tempering the steel does not show a tendency to brittleness and therefore no special heat treatment procedures are required. This steel is also suitable for surface hardening (flame hardening, induction surface hardening) and displays a very good resistance to wear. However, special attention has to be paid in the phase of product design and great care should be given to the design of radius and transition areas to prevent notch effects under dynamical loads. The steel is adapted for the use in a wide range of temperatures and preserves high toughness even at low temperatures.

- Induction surface hardening always leaves compressive residual stresses in the surface layer which makes machine components more resistance to dynamical loads. Compressive residual stresses in the surface layer after induction surface hardening prevent the occurrence of cracks in dynamically loaded components and prevent the growth of existing cracks on the workpiece surface if these are present due to surface hardening or surface hardening and grinding.
- Induction surface hardening is appropriate for more small-sized workpieces (not necessarily) since by well chosen technology of heating and cooling or quenching we can ensure a hardened surface layer and a refined core. Thus we can create a required wear resistance of the machine component on a certain location as well as required load bearing capacity of the component suffering only a slight loss of toughness of the core.

Table 1 gives a comparison of designations of this steel in various national standards. A chemical composition of the steel is given in Table 2. The designation indicates that this is an alloyed heat-treatment CrMo steel with a medium carbon content. The steel is designed for dynamically loaded structural parts as well as for specific machine parts such as: gear wheels, traveling wheels, car semi-axes, Cardan-joint elements and similar. Molybdenum yields a desirable fine microstructure after hot working as well as heat treatment contributing to a good strength- to- toughness ratio. Thanks to its fine-grained microstructure it also reaches a relatively high toughness in the heat-treated condition.

Table 1. Designation of alloyed heat-treatment steel 4140 according to some national standards

GERMANY		ENGLAND	USA	RUSSIA
W.No. DIN 17007	Designation DIN 17006	BS	AISI	ГОСТ
1.7225	42CrMo4	En 19	4140	-

Table 2. Chemical composition of the heat-treatment Cr-Mo steel 4140.

CHEMICAL COMPOSITION OF STEEL 4149 (AISI)						
ELEMENT [%]						
C	Si	Mn	P	S	Cr	Mo
0.38	0.15	0.50	max.	max.	0.90	0.15
-	-	-	0.035	0.035	-	-
0.45	0.40	0.80			1.20	0.30

Table 3. Mechanical properties of the alloyed heat-treatment steel concerned.

DIAMETER D [mm]	YIELD STRESS $R_{p0.2}$ [N/M M ²]	TENSILE STRENGT R_m [N/mm ²]	ELONGATION A_5 [%] min.	CONTRACTION Z [%] min.	TOUGHNESS ρ_3 [J] min.
up to 16	885	1080-1280	10	40	34
16-40	765	980-1180	11	45	41
40-100	635	880-1080	12	50	41

The steel contains between 0.38 and 0.45 % of carbon which makes it a typical heat-treatment steel and, with regard to the other alloying elements, also ideal for flame hardening or induction surface hardening. The steel is not susceptible to brittleness after tempering at normal temperature's and duration of heat treatment; therefore, there are no special manufacturer's requirements regarding steel quenching and tempering. The steel shows very high toughness values at ambient temperature and keeps them also in operating conditions, i.e. even considerably below an average ambient temperature. Strength of the steel concerned as well as its surface hardness and consequently wear resistance may be increased by heat treatment and thermochemical treatment. Table 3 presents mechanical properties of heat-treatable steel AISI 4140, such as yield point ($R_{p0.2}$), tensile strength (R_m), extension (A), and impact toughness according to Charpy (ρ_3). The data on the properties are related to the characteristic masses of parts which are defined by the diameter of the cylindrical part. In table 3, steel AISI 4140 has three characteristic groups of diameters, i.e. up to 16 mm, from 16- 40 mm, and from 40-100 mm. Thus in our case

presenting a crankshaft with a diameter ranging between 40 - 100 mm, we can estimate the magnitude of the yield point to be $R_{p\ 0.2} = 635\ \text{N/mm}^2$ and the magnitude of tensile strength to be $R_m = 880 - 1080\ \text{N/mm}^2$. Tensile strength of the steel concerned varies between 880 and $1280\ \text{N/mm}^2$ and a minimum toughness value ρ_3 amounts to around 41 J.

The steel is very sensitive to notch effects in dynamically loaded parts due to unsuitably shaped notches and transitions on a machine part. The table gives values which are a basis of evaluation of fatigue strength for various types of load. Fatigue strength of a material σ_D is lowest under torsional load and varies, for the diameters mentioned, i. e. 40 to 100 mm, from 255 to $310\ \text{N/mm}^2$. Fatigue strength under torsional load is three or four times lower than the tensile strength of steel under static load.

Table 4 presents fatigue strength values for steel AISI 4140 under different loads, that is under bending, alternate compression-tension, and torsional load. In the best case fatigue bending strength for steel 4140 (AISI) ranges between $530 \dots 380\ \text{N/mm}^2$, which means that the steel has to be very carefully machined and heat treated, and ensures compressive residual stresses in the hardened surface layer. These compressive residual stresses on the surface should be if possible higher than could be the tensile strength on the surface due to external loads.

Table 4. Fatigue strength in different stages of quenching and tempering structural steel 4140 (AISI).

TENSILE STRENGTH $R_m / \text{N/mm}^2$	FATIGUE STRENGTH		
	BENDING $\sigma_D / \text{N/mm}^2$	COMPRESSION- TENSION $\sigma_D / \text{N/mm}^2$	TORSION $\sigma_D / \text{N/mm}^2$
1180	530	420	325
980	470	375	285
880	430	345	255
780	380	305	255

Residual stresses after induction surface hardening

One of the main features of induction surface heating compared with conventional heating procedures is that heat is generated in the workpiece itself. In conventional heating procedures the heat input achieved is only $5 - 200\ \text{kJ/m}^2\ \text{sek}$ energy per unit of area in unit of time whereas in induction surface heating this energy input is $300\ \text{MJ/m}^2\ \text{sec}$. In induction surface heating, heat penetrates into the workpiece by the aid of high frequency alternating current, the choice of frequency depending on heating requirements [13-14]. Induction surface hardening is most often used for surface hardening of machine components and has the following main advantages over other procedures:

- Heating procedure is not strictly governed by hardening temperature. All that matters is that the heating process does not end at a too low temperature as some time is necessary for the transformation into austenite. Upwards the temperature of heating is limited by the solidus-line temperature since the process is to be carried out while the material is in solid condition. Thanks to a short heating up time, there is no danger

that at higher austenitization temperatures the austenite grains would grow, which also means that there is no danger of formation of coarse and brittle martensite.

- Thanks to the nature of the procedure, after induction surface hardening the machine part especially if shaped symmetrically are less susceptible to undesirable deformations. The volume changes in the machine part after hardening the surface layer can be very accurately predicted or estimated. The volume changes after induction surface hardening of thin layers are so small that quite often the function of the machine part is not affected.
- The induction surface hardening procedure enables the engineer, by simply adapting the shape of the induction coil, to ensure a desired shape of the hardened profile of the surface layer. Likewise, the engineer can surface harden only that machine part of the surface (local hardening) on which a certain increased level of hardness and wear resistance are wanted. One of the main advantages of induction surface hardening is that it makes possible to harden a surface layer only on certain places, at defined penetration depth and shape.
- These advantages make it possible that the induction hardening can be fully automated and is especially suitable for large series of workpieces.

Crankshafts were taken from production after induction surface hardening with the heat treatment and machining conditions as specified in the technology sheet. The residual stresses on the main crankshaft bearings were measured on the bearing location in the middle (A), on the extreme left side (C) and on the extreme right side (G).

Figure 1 shows residual stress distribution after induction surface hardening in the central bearing location (A) and on the extreme left side (C). For both location residual stresses were measured on two samples. The distribution of residual stresses on the location (A) is as expected very similar on both samples, the highest compressive stress ranging between 1020 to 1060 N/mm² in the depth around 250 μ m and then slowly dropping to a depth of 3.5 mm.

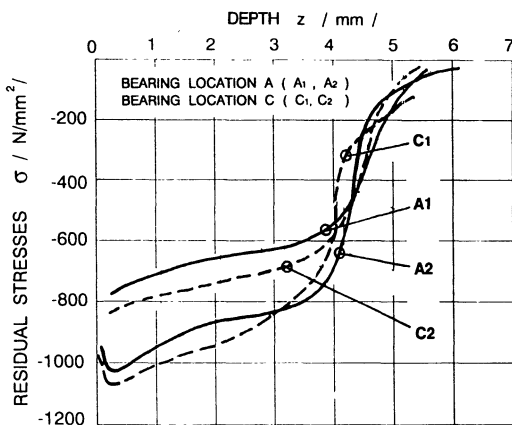


Figure 1. Residual stress profile after induction surface hardening on the sample A of the mean bearing location in the middle of the crankshaft and on the sample C on the extreme left side.

The residual stresses distribution after induction surface hardening on the bearing location (C) is very similar to that in the central bearing location (A) only that its absolute values are slightly lower and that a distinct fall in the residual stresses can be noted as early as around the depth of 3 mm reaching its minimum value already at a depth around 5.0 mm.

It can be seen that the residual stress distribution is just as favourable as in the central location only that its absolute values are slightly lower. Our belief is that the difference in the residual stress distribution can be related to the period of overheating on the austenitization temperature which resulted in a thinner layer in austenitization and thus also a thinner hardened surface layer.

Residual stresses after induction surface hardening and finish grinding

The last phase in the manufacturing of crankshafts is fine grinding where in order to achieve the desirable condition of the surface and the surface layer, i.e. we have to ensure:

- suitable dimensions of the particular bearing locations with respect to the allowable deviations;
- suitable surface roughness;
- that the grinding stresses are compressive or lowest tensile so that the favourable stress profile obtained by induction surface hardening of the surface layer is maintained;
- smallest changes possible in the microstructure and thus also smallest changes in the hardness and microhardness profiles in the heat-affected zone after grinding.

How is it possible to assure a desirable surface and surface layer quality after induction surface hardening and fine grinding? Finding an answer to this question requires a very good knowledge of the process of grinding on the micro level as well as all mechanical and heat effects acting on the layer of the workpiece including the type and condition of the grinding wheel. An all-inclusive consideration of the numerous influences of the kind and condition of the tool on the changes on the surface and in the surface layer of the workpiece in the given machining conditions can be based on the descriptions of "Surface Integrity" [10,12].

For the grinding process the following conditions have been selected :

- different kinds of grinding;
- different grinding conditions (gentle, conventional, abusive).

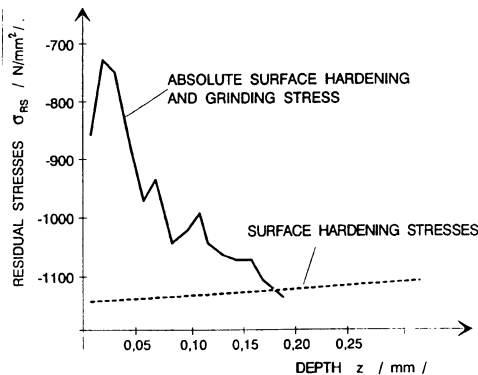


Figure 2. Subsurface residual stress profile after induction surface hardening and grinding (absolute stress) on bearing location A

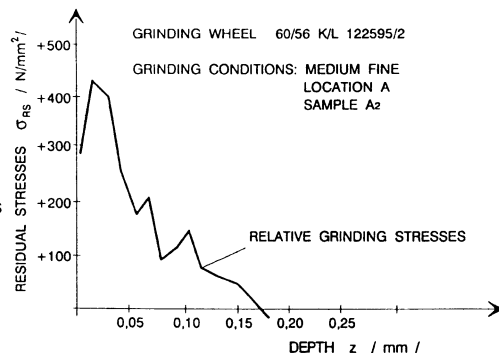


Figure 3. Subsurface profile of relative grinding stress on bearing location A

Under different machining conditions of grinding, different temperature cycles were obtained on the surface and in the depth of the heat-affected zone which has effected microstructural changes and changes in the microhardness and residual stresses. Thus on the surface a maximum temperature higher than the temperature of melting of the workpiece material was obtained. The depth of the remelted layer is only a few micrometres and makes a very fine ledeburite microstructure containing fine cementite spread in residual austenite.

The newly formed microstructure has a slightly lower hardness than martensite. The residual stresses in the thin surface layer will be tensile due to plastic deformation of the surface layer in grinding caused by tensile forces in the contact zone of the workpiece material and to this should be added also the tensile stresses induced by the occurrence of residual austenite. In conventional grinding conditions, on bearing location A relative grinding tensile forces amount to $+ 425 \text{ N/mm}^2$ and then change the sign in the depth around $175 \mu\text{m}$, as shown in figure 2. The relative grinding stress is obtained by measuring the residual stress after induction surface hardening and then by measuring on the same spot after induction-hardening and grinding and then calculating their difference. In figure 3 we can see the measured absolute residual stress profile after induction surface hardening and grinding, and the measured residual stress profile after induction surface hardening. Figure 3 shows the absolute residual stress profile after hardening and grinding on bearing location A as well as the average residual stress after induction surface hardening, and then the relative grinding stress can be calculated. The results confirm as predominant the residual stresses, stresses induced by the plastic deformation of the material and a lesser influence of tensile stresses caused by the formation of residual austenite. On the basis of the measurements of residual stresses after induction surface hardening and/or induction surface hardening and grinding, we can conclude that:

- for residual stresses after induction surface hardening and grinding, the conditions of abusive grinding are a more favourable choice. They lower to a lesser extent the desirable compressive residual stresses after induction surface hardening;
- grinding conditions can be chosen also so that the melting temperature of the workpiece material (gentle-grinding conditions) is not exceeded. Then the favourable compressive stresses after induction surface hardening are lowered only due to plastic deformation of the workpiece material during the process and thus relatively low tensile residual stresses are thus obtained. However, we should take into account that this will significantly lower the productivity.
- special attention should be paid to the selection of the kind of the grinding wheel in terms of grinding wheel material, binding agent, hardness and pore density, since by a right selection we can contribute to higher cutting efficiency concerning the plastic deformation of the workpiece material. In this way we can keep the grinding tensile stresses as low as possible and make the compressive residual stresses induced by induction surface hardening the prevailing kind.

3. CONCLUSIONS

Induction surface hardening creates very desirable residual stress state. Residual stresses are always of compressive nature and are usually present to the depth of the induction surface hardened layer. A major difficulty in induction surface hardening is, however, to ensure a very slight/slow variation in microhardness and the existence of compressive residual stresses in transition areas to the microhardness of the core material. By gently grinding varying the hardness and existence of compressive stresses in the transition area it is possible to diminish the notch effect induced by stress concentration. Additional grinding of induction surface hardened surface deteriorates the stress state in the surface layer, since grinding has always induced tensile stresses. By a right selection of machining conditions and grinding wheel taking into account its properties, the engineer will contribute to lesser

tensile residual stresses and will avoid deteriorating the favourable residual stress state after induction surface hardening.

REFERENCES

1. Shaw, M.C. : Fundamentals of Wear, *Annals of the CIRP*, 1971, Vol 19, 553 - 544
2. Neailey K.: Surface Integrity of Machined Components - Residual Stresses and Fatigue, *Machined Surfaces, Metals and Materials*, March 1988, 141-145.
3. Neailey K.: Surface Integrity of Machined Components - Microstructural Aspects, *Machined Surfaces*, February 1988, 93-96.
4. Snoeys, R., Maris, M., Peters, J. (1978). Thermally Induced Damage in Grinding, Key - Note - Papers, *Annals of the CIRP*, 1987, Vol 27, No. 2, 571 - 581
5. Althaus, P. G.: Residual Stresses in Internal Grinding, *Industrial Diamond Review*, No. 3, 1985 124 - 127
6. Moris, M., Snoeys, R. : Heat Affected Zone in Grinding Operations, *Proceedings of the Fourteenth International Machine Tool Design and Research Conference*, (Koenigsberger F., Tobias S. A., Eds.) Manchester, 1973, 569 - 669
7. Triemel J.: Grinding with Cubic Boron Nitride, *Proceedings of the Fourteenth International Machine Tool Design and Research Conference*, (Koenigsberger F., Tobias S. A., Eds.) Manchester, 671-676
8. Tönshoff H. K., Grabner T.: Cylindrical and Profile Grinding with Boron Nitride Wheels, *Proceedings of the 5th Int. Conf. on Production Engineering Keynote Paper*, Tokyo 1984, 326-344
9. Grum, J., Žerovnik, P.: Residual Stresses in Tool Steels after Heat Treatment and Subsequent Grinding, *Proceedings of the 5th Yugoslav Symposium on Heat Treatment of Metals*, Vrnjačka Banja, 1989, 289-293
10. Grum, J., Ferlan D.: Residual Internal Stresses After Induction Hardening and Grinding, *17th ASM Heat Treating Society Conference Proceedings, Including the 1st International Induction Heat Treating Symposium*, Eds.: D.L. Milan, D. A. Poteet Jr., G.D. Pfaffmann, V. Rudnev, A. Muehlbauer, W. A. Albert, ASM Int. Metals Park, Ohio, 1998, 629-639
11. Scholtes, B.: Residual Stresses Introduced by Machining, *Advances in Surface Treatments*, (A. Niku-Lari, Ed.), Published in Cooperation with the Institute for Industrial Technology Transfer, Vol. 4, Pergamon Press, Oxford, 1987, 59-71
12. Field, M., Kahles, J. F. Cammet, J.T.: Review of Measuring Method for Surface Integrity, *Annals of the CIRP*, Vol. 21, No. 2, 1971, 219 - 237
13. Lozinski, M. G.: *Industrial Applications of Induction Heating* Pergamon Press, Oxford, 1969
14. Stevens, N. : *Induction Hardening and Tempering*, *Metals Handbook*, Ninth Edition, Volume 4, Heat Treating, American Society for Metals, Metals Park, Ohio, 1981, 451 - 483

MICRO-DYNAMIC BEHAVIOUR OF A NANOMETER POSITIONING SYSTEM

S. Zelenika

Sincrotrone Trieste, Trieste, Italy

F. De Bona

University of Udine, Udine, Italy

KEYWORDS: High-Precision Positioning, Mechanical Non-linearities, Adaptive Control

ABSTRACT: The identification of the main mechanical macro and micro-dynamics non-linearities which are present in precision positioning systems is performed in this work. The employed compensation technique makes use of a dual-mode control law in which high precision is achieved by using an adaptive pulse width control typology. The obtained positioning accuracy is within the interval of uncertainty of the measurements performed by using a laser interferometric system.

1. INTRODUCTION

In the design of high-precision positioning systems, a solution based on sliding and rolling devices is frequently adopted [1]. It is well known, however, that in this case the precision of actuation is significantly influenced by the presence of two types of mechanical non-linearities which are usually referred to respectively as "macro-dynamics" phenomena (stiction, Coulomb friction, viscous friction, backlash) and "micro-dynamics" phenomena (presliding displacements, i. e. displacements that occur even for loads smaller than those needed to overcome stiction [2-4]). While several references dealing with the macro-dynamics behaviour can be found in literature [5-7], the micro-dynamics behaviour has not yet been clearly characterized, particularly concerning its influence on the precision of positioning devices [8]. Moreover, despite the fact that there are several ways by which backlash and friction can be minimized already in the design phase [8-9], in the case of high-precision applications this type of compensation is seldom sufficient to reduce adequately the obtainable interval of uncertainty of the displacements. It is thus often necessary to use a

feedback signal of the actual position and suitably chosen closed-loop control laws.

PID (Proportional, Derivative, Integral) control is one of the most commonly used control laws in precision positioning systems [8, 10-12]. The applicability of this control law to nanometer-precision positioning is however limited. In fact, when a PD control law with high gains is used to increase the damping and the stiffness of the system in order to reduce stick-slip, residual steady-state errors will always be encountered [8, 11, 13]. If an integral term is added to reduce these errors, the presence of mechanical non-linearities causes stability problems and thus for velocities approaching zero the positioning system will always present limit cycles around the reference position [1, 5]. It has been shown [12] that, even if with extensive experimental measurements a deep knowledge of the model of the system has been acquired and stabilizing values of the parameters P, I, and D have been identified, a residual limit cycle will always be present due to static friction. Moreover, friction presents a meaningful variability mainly caused by microwear, by position-dependency and by variability of the temperature and lubrication conditions, so that the optimization of the parameters P, I and D performed by using only the deterministic component of the model does not make it possible to compensate the disturbances introduced by its stochastic component [14, 15]. Secondary effects such as frictional memory and rising static friction (influence of the history of motion on the value of the frictional force) can then enhance this effect. Hence, the strategy which is being increasingly adopted nowadays in order to obtain precise sliding and rolling electro-mechanical positioning systems is the usage of adaptive control typologies [8].

Several control laws based on an adaptive algorithm have been proposed in literature, but only the case of positioning system with macro-dynamics non-linearities has been considered, since the positioning precision was such that the influence of the micro-dynamics effects was negligible. It should also be noted that the need to obtain relatively large displacements with high precisions makes it necessary to use dual-mode control laws, where a conventional control law is used to bring the system in the vicinity of the reference position and then an adaptive controller is used to compensate the residual positioning error. The aim of this work is, therefore, twofold. Firstly, to identify experimentally the main mechanical non-linearities of a traditional electro-mechanical positioning system, with particular attention drowned to its micro-dynamics behaviour. Secondly, to explore if an adaptive approach developed to overcome macro-dynamics phenomena can be extended to the case of nanometer positioning which involves also micro-dynamics effects.

2. EXPERIMENTAL SET-UP

Fig.1 shows the system developed for the experimental study. It consists of a DC motor and a gear reducer, connected by means of an elastic joint to a lead screw-nut drive mechanism that converts motor rotation in a translation of a guide with free rolling elements (balls). A spring with a slight preload is used to compensate for backlash. It must be pointed out that standard mechanical components without particular accuracy requirements have been employed.

The position feedback signal is obtained by using a Michelson-type laser-Doppler interferometric system (HP5527A) for non-contact measurements. As shown on Fig.2, a laser head emits two laser beams of slightly different known frequencies with opposite linear perpendicular polarizations; a polarizing splitter reflects the reference beam to a upper corner cube, and then back to a receiver mounted on the laser head. The measuring beam (dotted line) passes through the splitter towards a corner cube and is reflected back to the receiver. In the receiver the measuring and the reference beams interfere; the change in the difference of the beams frequencies, evaluated through the use of heterodyne detection, gives a signal proportional to the relative displacement between the fixed polarizing splitter and the corner

cube that is mounted on the positioning stage. In this optical configuration the measurement technique permits a resolution of 10 nm to be obtained. The system is equipped with an air sensor to compensate for the variations in the refraction index of the surrounding air induced by temperature and pressure changes; a temperature material sensor is also employed to compensate for thermal expansion of the supporting structures. The uncertainty in the stage linear displacement measurements was evaluated according to the procedure described in [16]. In the case of a maximum stage travel of 10 mm an interval of uncertainty of ± 20 nm was then obtained.

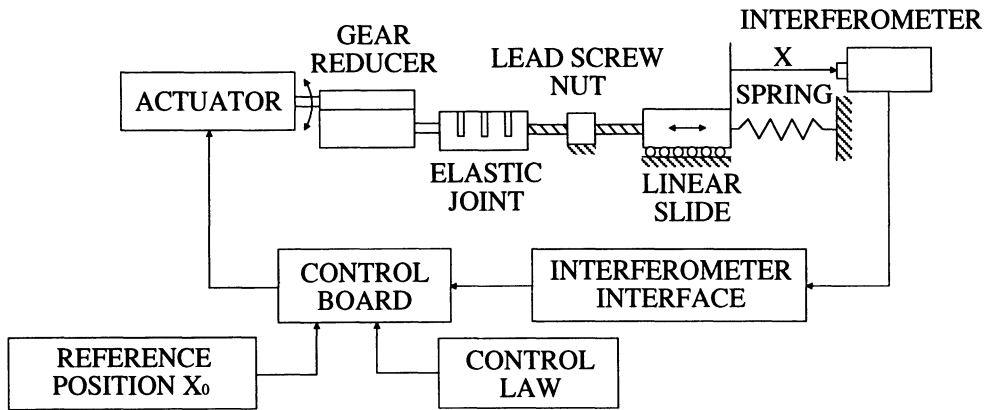


Fig.1 Scheme of the experimental set-up

The use of a programmable board (HP10936A Servo-Axis Board) allows to obtain an analogue signal (max. range $\pm 10V$) which is proportional to the actual displacement (with an adjustable constant of proportionality depending on the reference position). This signal is then read by the control unit. In order to obtain the exchange of data between the Servo-Axis Board and the computer and to increase its rate, a binary interface (HP GPIO, General Purpose Input/Output) is used. This interface allows to have a 16-bit bi-directional exchange of data in the full-duplex mode at rates that can be up to 10 kHz.

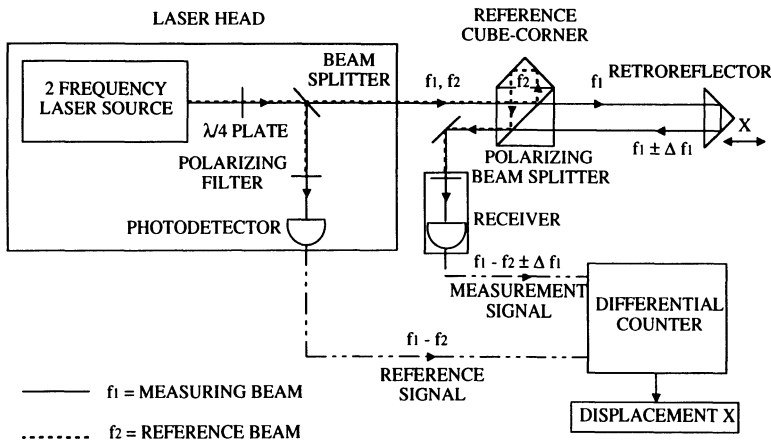


Fig.2 Michelson-type laser-Doppler interferometer

The DS1102 board (dSpace GmbH., Germany) is used to control the motor. This board uses a floating-point digital signal processor (DSP - model TMS320C31 by Texas Instruments) and allows the implementation of linear and non-linear control typologies by using algorithms written in C with libraries including predefined control functions.

3. MICRO-DYNAMICS MECHANICAL NON-LINEARITIES

In the case of positioning systems that should achieve nanometer accuracy the micro-dynamics behaviour has to be considered. In this case the load-displacement characteristics follows a non-linear relationship due to local deformation prior to stiction breakaway. Therefore the experimental identification has to be performed simply by measuring the displacement resulting from the application of a load gradually increased up to the point at which stiction is overcome. In the case of the positioning system considered in this work, the micro-mechanical non-linearities are mainly due to the linear slide. In fact, the presence of balls on V-grooves enhances the influence of micro-asperities elastic and plastic deformations; moreover, as this is the last element of the kinematic chain, its equivalent stiffness has a far bigger influence with respect to that of the other elements.

The following measurement procedure was used: the linear stage, mounted on an optical bench in horizontal position, was loaded in the direction of motion by means of a lubricated pulley and wire system to whose end calibrated weights were gradually added on. The resulting displacement of the stage was measured by means of a Michelson-type laser-Doppler interferometric system. The measurements were performed up to the point at which stiction breakaway occurred. The load-displacement characteristics was also recorded when unloading the system starting from different load levels.

In Fig.3 the load-displacement characteristic obtained by averaging 10 measurements is shown. In the whole measuring range a maximum interval of uncertainty of $\pm 6\%$ was assessed, confirming that, as already noticed in [4], the micro-dynamics phenomena have a relevant stochastic component. This interval of uncertainty was however not reported in the diagram of Fig. 3.

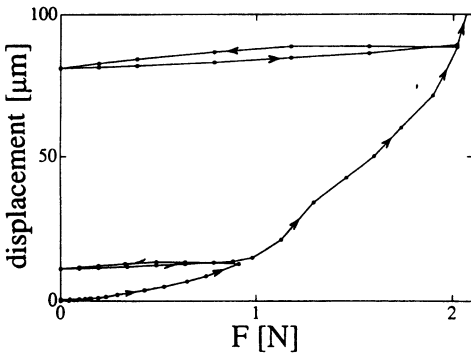


Fig.3 Micro-dynamics non-linearity

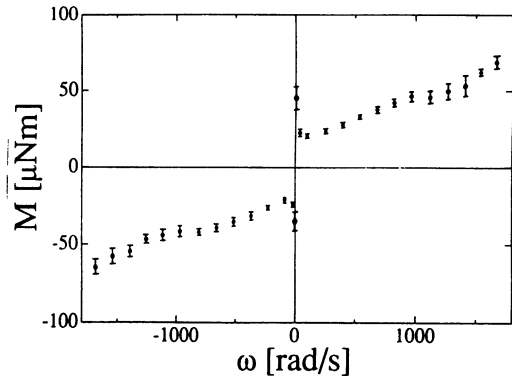


Fig.4 Friction and its dispersion

It can be observed that, before the load reaches the stiction value, a significant displacement is obtained. The measured displacement is a non-linear function of the applied load. When the system is unloaded, it travels back, but the resulting displacement is significantly smaller than the displacement obtained in the loading phase. Moreover, the displacement vs. load characteristic during unloading is almost linear, with a mean slope that remains constant independently from the load at which unloading is started.

The obtained results are meaningfully different from those obtained recently by Futami et al. [3]. In that case, however, the load was applied at high frequency following a sinusoidal law and not pseudo-statically as in this work. On the other hand, the results shown in Fig.3 are in excellent agreement with those reported in an earlier work by Courtney-Pratt and Eisner [4], despite the limits imposed by the poor precision of the measurement techniques available at that time. In their work Courtney-Pratt and Eisner [4] suggested also that the observed non-linear behaviour was mainly caused by phenomena of elasto-plastic deformations which occur at the interface of the bodies in relative motion in the presence of forces that are normal and tangential to the contact surface.

In conclusion, in agreement with the results reported in [4], the micro-dynamics behaviour shown in Fig.3 has a main irreversible component due to plastic deformations of the asperities in the contact area, but also a reversible component due to elastic strains. This elastic component is significant only for very small displacements. If a dynamics loading procedure such as that outlined in [3] is performed, probably only this elastic component can be measured.

4. MACRO-DYNAMICS MECHANICAL NON-LINEARITIES

The most important macro-dynamics mechanical non-linearities are represented by static, Coulomb and viscous friction [5, 8]. In order to establish the dependence of the frictional loads on system motion, a simple measurement procedure suggested in [17] was followed. It can in fact be shown that the angular velocity is proportional to the voltage applied to the motor, while the absorbed current is proportional to the frictional torque. Therefore, the mechanical non-linearities of the system referred to the motor axis can be identified with a measurement of electrical parameters. This approach is more accurate and simpler than the explicit one. In order to evaluate the contribution of all the elements of the electro-mechanical positioning system, at first the procedure was applied to the motor alone, and then it was repeated by adding one by one to the motor the other elements of the kinematic chain; in all the cases the measurement was repeated in 10 different positions. By comparing the frictional loads of the single elements of the positioning system it was established that the main contribution was that of the DC motor. In fact, when the contributions of the downstream elements have to be referred to the motor axis, the corresponding frictional torques must be reduced proportionally to the speed ratios.

Fig.4 shows the dependence of the frictional torque M on the angular velocity w for the whole system. The characteristic Stribeck curve can be clearly observed, where the viscous component is mainly caused by the back-electromagnetic force of the motor. This type of behaviour is typical of positioning systems driven by DC motors and it is in perfect agreement with the most recent tribological models [7, 8, 11, 13, 17, 18].

Fig.4 shows also the frictional torque interval of uncertainty resulting from repeated measurements; the considerable dispersion (up to $\pm 15\%$) is mainly caused by the variability of friction with respect to system position. Similar percentage values of frictional dispersion were reported also in [5], where the case of accurate positioning systems involving only macro-dynamics effects was considered. As pointed out previously, the presence of such a significant disturbance of stochastic nature implies the necessity of adopting an adaptive control law.

5. ADAPTIVELY CONTROLLED PRECISE POSITIONING

Only the case of positioning systems whose precision was at such a level that no micro-dynamics phenomena were involved was studied thoroughly in literature. In fact, in this case several adaptive-type control approaches have been suggested [5, 6-8]. Particularly

interesting is the work of Yang and Tomizuka [5], where a simple control typology with a rigorously established stability was developed. The control strategy used in that work is based on the modulation of the width of an impulse, determined from a comparison of the output of the actual positioning system and that of a reference model. The mechanical model of the positioning system used by Yang and Tomizuka [5] is shown in Fig.5; in this case the dependence between the pulse width t_{imp} and the resulting displacement X is quadratic. Because of the variability of the frictional effects the coefficient of proportionality between the square of the pulse width and the respective displacement has a significant stochastic component and can thus only be determined adaptively by using the classical MRAC (Model Reference Adaptive Control) or STR (Self Tuning Regulator) algorithms [19].

In the case of high-precision positioning, the only work traceable in literature is that of Ro and Hubbel [2]. In that work the micro-dynamics non-linearity is used to obtain precise positioning, but the adopted micro-dynamics model is the non-linear elastic model described in [3] presenting the limits outlined earlier. Moreover, the method devised in [2] is applicable only in the case when the distribution of friction follows a predetermined characteristic, so that the approach can not be applied in a more general frame.

In the case when a simple positioning (as opposed to trajectory tracking) is sought, the adaptive control typologies based on pulse width modulation (PWM) constitutes certainly one of the most efficient solutions [8]. In fact, as everyday experience shows, when small corrective movements are needed to reach the desired position, the application of impulsive loads permits the static friction to be overcome without an excessive overshoot (caused by the rapid reduction of the resistive loads at stiction breakaway).

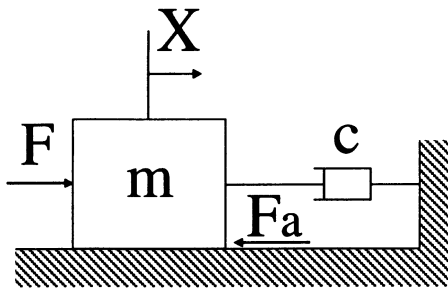


Fig.5 Positioning system model as described in [5]

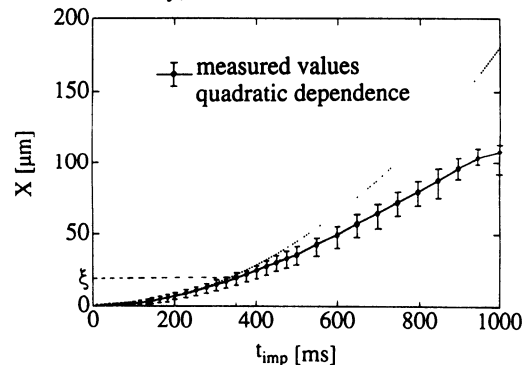


Fig.6 Displacement versus pulse width dependence

Trying to extend the applicability of the method developed in [5] to the case of nano-positioning, it becomes necessary to identify the nature of the dependence of the displacement on pulse width. For this purpose repetitive experimental measurements have been performed by actuating through the DSP board the electro-mechanical system under consideration with constant amplitude impulses and gradually increased width. Comparing the experimental data with Yang and Tomizuka's model [5] (Fig. 6), it can be observed that for pulse widths smaller than 350 ms (and thus displacements smaller than 20 μm) the actual and the analytically obtained characteristics are in an almost perfect agreement, both being quadratic. For larger pulses width and displacements the difference between the two characteristics becomes significant since in the studied case the displacement vs. pulse width dependence becomes almost linear. Thus, if the range of variation of pulses width is limited to values where the quadratic characteristic is valid, the model developed in [5] still holds. However, comparing Fig.3 to Fig.6 it follows that in this range of displacements the linear

slide could be in the micro-dynamics field and therefore the model parameters have a different physical meaning, than those considered in [5]. In fact, if the linear slide is in the micro-dynamics field, its stiction breakaway has not been reached, so that the frictional force F_a does not account for the contribution of the slide, but only for that of the upstream elements (motor, reducer, leadscrew-nut), which is anyway usually the prevailing one. Moreover, for the considered range of displacements the micro-dynamics forces shown in Fig.3 prevail on the elastic reaction of the spring used to compensate for backlash. The micro-dynamics forces are, however, still negligible, compared to frictional forces, due to the effect of speed ratios. The effective contribution of the micro-dynamics forces can thus be considered as a virtual variation of F_a and therefore is already taken into account by the adaptive approach suggested in [5].

The range of applicability of the method can then be easily increased by imposing a dual structure to the control law, where the "rough" controller has to be precise enough to bring the system within the previously determined range of validity of the PWM control. Extensive experimental measurements have allowed to determine that in the studied case it is sufficient to use the simple PID control typology in which the proportional term is kept constant while the I and D terms are set to zero (P control); in other experimental configurations it might be necessary to use a real PD or PID control [8].

Based on the above considerations a control procedure was implemented and its baseline structure was:

- the reference position X_0 is compared to the actual displacement X measured via the interferometric system;
- if the obtained difference is bigger than the range of applicability of the PWM control, the actuation is controlled using the P control up to the point when the electro-mechanical system comes to a rest;
- at this point the actuation is performed by applying impulses of variable width, where the width of the first impulse is determined by using a pre-defined (supposed) value of the coefficient of proportionality K between the displacement and the square of the pulse width;
- the subsequent values of this coefficient are then determined by an adaptive approach using a MRAC-type algorithm. Fig.7 shows the block diagram of the MRAC system as described in [19] and implemented as suggested by [5]; for this purpose the regulator is based on the previously described quadratic characteristic, where the coefficient of proportionality K between the square of the pulse width t_{imp} and the resulting displacement \bar{X} is determined by a parameter adaptation algorithm (PAA). The input signals to this algorithm are the pulse width, the actual displacement and the displacement X' , that is obtained using a linear reference model in which an ideal response of the system is assumed.

Fig.8 shows the experimental results obtained by applying the described procedure in the case of a small reference position ($10 \mu\text{m}$) and rather large one (1mm). For comparison purposes, in the same figure are also given the results obtained by using the simple P control. It can be observed that the application of the P control introduces unacceptable residual errors amplified by the fact that the values of the proportional gain optimised for a determined reference position can not be automatically applied to different reference positions because of the stochastic nature of the phenomena. In the case of the dual-type control law proposed in this work, the system is initially actuated following a P control law, which results in a high slope and a marked overshoot. The adaptive control law is then applied for fine positioning resulting in a considerably smaller velocity of approach bringing the system to the reference position with nanometer accuracy. In fact, several measurements performed with various reference positions by using the proposed approach, allowed to establish that in all the considered cases the positioning error was smaller than the interval of uncertainty of the measurements done by using the laser interferometric system (i.e. the error was within $\pm 20 \text{nm}$).

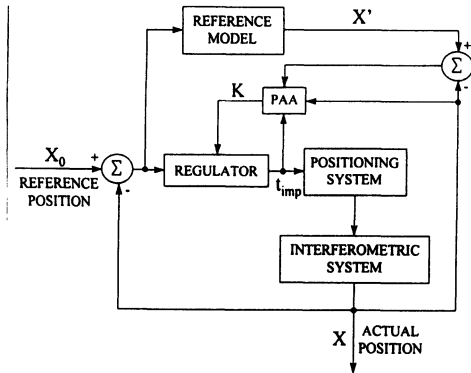
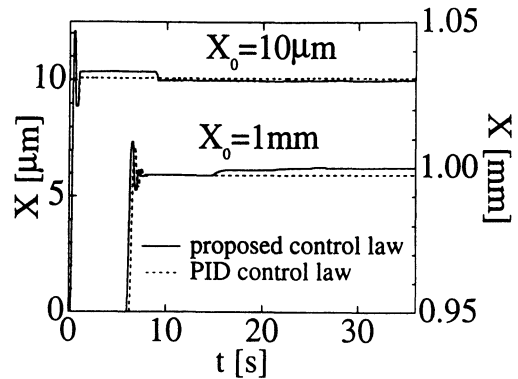


Fig.7 MRAC algorithm

Fig.8 Measured displacement for a $10\ \mu\text{m}$ and for a 1mm reference position

6. CONCLUSIONS AND FUTURE WORK

The experimental characterization of the dynamics of an electromechanical positioning system has confirmed that two kinds of mechanical non-linearities (micro-dynamics and macro-dynamics non-linearities) affect the achievable positioning accuracy. It has then been shown that the control typology developed in [5] to compensate the mere macro-dynamics effects can also be used to compensate for the micro-dynamics non-linearities, if a suitable limitation of the range of displacements is adopted. The experimental results obtained with the mentioned approach using a DSP have confirmed such considerations. Future work should deal with a wider characterization of the micro-dynamics effects, including their dependence on mechanical parameters such as normal loads, types of bearings, lubrication, etc. When fast positioning as well as nanometer accuracy is needed, further improvements might be necessary, in the transition between the coarse and the fine control typology, and in the convergence of the MRAC algorithm.

REFERENCES

1. Slocum, A. H.: Precision Machine Design, Prentice-Hall, Englewood Cliffs, 1992
2. Ro, P. I. and Hubbel, P. I.: Model Reference Adaptive Control of Dual-Mode Micro/Macro Dynamics of Ball Screws for Nanometer Motion, ASME J Dyn Sys, Meas & Contr, 115 (1993), 103-108
3. Futami, S., Furutani, A. and Yoshida, S.: Nanometer positioning and its micro-dynamics, Nanotechnology, 1 (1990), 1, 31-37
4. Courtney-Pratt, J. S. and Eisner, E.: The effect of a Tangential Force on the Contact of Metallic Bodies, Proc Royal Soc, A 238 (1957), 529-550
5. Yang, S. and Tomizuka, M.: Adaptive Pulse Width Control for Precise Positioning Under the Influence of Stiction and Coulomb Friction, ASME J Dyn Sys, Meas & Contr, 110 (1988), 3, 221-227

6. Friedland, B. and Park, Y. J.: On Adaptive Friction Compensation, *IEEE Trans Autom Contr*, 37 (1992) 10, 1609-1612
7. Canudas, C., Astrom, K. J. and Braun, K.: Adaptive Friction Compensation in DC Motor Drives, *Proc IEEE Int Conf Robotics & Autom*, San Francisco (CA, USA), 1986, 1556-1561
8. Armstrong-Helouvry, B., Dupont, P. and Canudas de Wit, C.: A Survey of Models, Analysis Tools and Compensation Methods for the Control of Machines with Friction, *Automatica*, 30 (1994) 7, 1083-1138
9. Hale, L. C. and Slocum, A. H.: Design of Anti-backlash Transmissions for Precision Position Control Systems, *Prec Eng*, 16 (1994) 4, 244-258
10. Rao, G. S. and Ro, P. I.: Control of a Traction Drive System, *Int. Progress in Precision Engineering*, Butterworth-Heinemann, Boston (MA, USA), 1993, 854-857
11. Dupont, P. E.: Avoiding Stick-Slip Through PD Control, *IEEE Trans Autom Contr*, 39 (1994) 5, 1094-1097
12. Armstrong-Helouvry, B. and Amin, B.: PID Control in the Presence of Static Friction: Exact and Describing Function Analysis, *Proc 1994 American Control Conf.*, Baltimore (MD, USA), 1994, 597-601
13. Johnson, C. T. and Lorenz, R. D.: Experimental Identification of Friction and Its Compensation in Precise, Position Controlled Mechanisms, *Proc. IEEE Industry Appl Soc. Ann. Meeting*, Dearborn (MI, USA), 1991, 1400-1406
14. Smith, M. H., Annwamy, A. M. and Slocum A.: Adaptive Control Strategies for a Precision Machine Tool Axis, *Precision Engineering*, 17 (1995) 3, 12-24
15. Olejniczac, O., Bonis, M. and Lahmar, D.: Control of Permanent Magnets Brushless Electrical Motors-Performances of an Internal Model Control Algorithm, *Int. Progress in Precision Engineering*, Butterworth-Heinemann, Boston (MA, USA), 1993, 858-865
16. Steinmetz, C. R.: Sub-micron Position Measurement and Control on Precision Machine Tools with Laser Interferometry, *Precision Engineering*, 12 (1990) 1, 12-24
17. Lee, H. S. and Tomizuka, M.: Robust Motion Controller Design for High-Accuracy Positioning Systems, to be published in *IEEE Trans Ind Elec*.
18. Armstrong-Helouvry, B.: Stick Slip and Control in Low-Speed Motion, *IEEE Trans Autom Contr*, 1993, 38 (1993) 10, 1483-1496
19. Astrom, K. J.: Theory and Applications of Adaptive Control - A Survey, *Automatica*, 19 (1983) 5, 471-486

EMPLOYMENT OF FUZZY LOGIC MODELLING IN QUENCHING OF STEEL RODS FOR REINFORCED CONCRETE AFTER HOT ROLLING

F. Memola Capece Minutolo and B. Palumbo
University of Naples Federico II, Naples, Italy

V. Sergi
University of Salerno, Salerno, Italy

KEY WORDS: fuzzy logic, quenching, reinforced concrete, steel rod.

ABSTRACT: The traditional production of steel rods for reinforced concrete, a long time considered of short technological interest, has been recently modified with the development of new procedures, which enhance mechanical characteristics without adding micro-alloys. In particular, the process outlined in this paper, said tempcore process, enables to graduate mechanical and technological properties of the steel rods, so that these characteristics can vary in assigned limits. The underlying principle of this innovative process lies in surface quenching of the rods on leaving the last stand in the hot rolling mill, followed by self-tempering. Process adjustment still relies on the experience of the production manager, taking as a parameter for assessing process efficiency the temperature reached by the rod on the cooling plate. In this paper, the influence is examined of the process variables (final rod diameter, chemical composition, water flow rate and velocity), on the ultimate rod structure, upon which all mechanical properties, in general, depend. Based on the finding of a previous study, the possibility is examined of applying fuzzy logic techniques to the heat treatment process under examination with a view to rendering it more rational and independent of operator unreliability. The study will have a dual future aim. To evaluate the possibility of predicting the properties of the reinforced concrete rods when chemical composition of steel and final diameter are known, and secondly, to graduate the intensity of the treatment to obtain rods with predetermined properties from steel with known chemical composition.

1. INTRODUCTION

The traditional Italian production of steel rods for reinforced concrete with enhanced adhesion, types FeB3SK and FeB44K, has always been influenced by Ministerial provisions,

Published in: E. Kuljanic (Ed.) *Advanced Manufacturing Systems and Technology*,
CISM Courses and Lectures No. 406, Springer Verlag, Wien New York, 1999.

which solely contemplated the possibility of exceeding the limit values preset for certain mechanical characteristics as well as the observance of other technological and geometric ones.

All this has led to the development of a number of different methods for manufacturing steel rods for reinforced concrete, ranging from the smelting of selected scrap, to the purchasing of billets from different manufacturers, to the rolling of products that would otherwise be scrapped.

Fortunately, the recent demand for products with special characteristics (for example, the so called weldable rod), the increasingly stringent Community standards and the growing fierce competition from manufacturers outside the EU are contributing to underline the importance of process control in addition to conventional product control practices. The Ministerial Decree of 09/01/96 has also introduced some innovations which add to the changed conditions mentioned before. Apart from the before mentioned exceeding of specific lowest values for mechanical properties, the Ministerial Decree also provides, for some of them, that the single trial values found should not exceed the fixed lowest performance value over a fixed amount.

Consequently, all this has led to the consideration that the time is now ripe for the problems associated with the manufacture of steel rods for reinforced concrete, to be tackled with scientific methodologies not based solely on acquired experience. Traditionally, steel rods were regarded as an inferior product and thus not worthy of any particular attention.

The mentioned needs have led to a gradual but steady abandonment of the empirical techniques usually adopted (further cold plastic deformation, addition of micro-alloying elements [1, 2]) in order to obtain the values for the mechanical characteristics as required by law. Alternatively, the past few years have also witnessed the development of a new procedure, called "tempcore" [3, 4, 5] based on a short but intense heat treatment to which the rods are subjected on leaving the last stand in the hot rolling mill. An appropriate graduation of the intensity of such a treatment enables overall improvement of the mechanical characteristics of the rods, without compromising its weldability properties and independently of both the initial chemical composition of the bar and the final diameter of the rod to be obtained.

2. TEMPCORE TECHNOLOGY

The tempcore process exploits the improved mechanical characteristics of the steel that underwent heat treatment. In this process, on leaving the last stand in the hot rolling mill, the rod enters in the tempcore plant. This is made up mainly of a container including some tubes where the bars slide, suitably guided, to avoid any dangerous deflection. Cooling water can be sprayed counter-current on the rod from some nozzles placed in circle along the route. The cooling equidistant sections are separated from one another in order to allow the water to flow away and prevent it from coming into continuous contact with the rod. The speed at which the water is sprayed from the nozzles is adjusted by acting on the general pressure, while the flow is regulated by closing or opening a certain number of cooling sections. This way, an outer ring whose diameter can be suitably changed by

modifying the process parameters, is involved in a quenching process thus acquiring a martensitic structure. Naturally, the central part of the bar remains at a temperature higher than that of the total austenitization and therefore, in the following cooling phase it causes the heat to radiate outward, thus inducing a tempering process in the area previously subject to the treatment. By doing so, it is possible to achieve an overall improvement of strength characteristics (yield point and tensile stress) without reducing its tensile characteristics (elongation) and therefore preserving the ductility of the material.

Thus, it is clear that the mechanical properties of the rod can be modified by changing the process parameters. Such an intervention makes it possible to adjust the extent of the treatment over a certain range and area [6]. This technique obviates the need to conduct a meticulous chemical analysis of the steel in order to obtain a rod of a certain diameter. On the other hand, a certain chemical composition does not necessarily have to be rolled to a particular diameter in order to ensure the desired mechanical characteristics. The process parameters, which are usually adjusted, are water flow rate and its transfer speed. In theory, also the rod speed could be changed but, adjusting this parameter in the continuous rolling mill is difficult to be put into practice and also, in some cases, not financially viable. Other types of process are therefore usually preferred.

3. TEMPCORE PROCESS SIMULATION

The final rod structure after the tempcore treatment will consist of, as showed through the macrograph in figure 1, the typical hardened tempered structure, a normalised structure in the central core and a mixture of the two in the interlying area.



Fig. 1 – Macrograph of the rod section treated with tempcore process.

In order to be able to determine in advance the mechanical characteristics that the rod for reinforced concrete will possess after the tempcore treatment, it is necessary to know the following:

- the cooling speed reached in the various outer rings to determine the thickness that can undergo transformations producing martensitic or bainitic structures;
- the residual enthalpic content when the rod leaves the cooling apparatus which defines the extent of the self-tempering process in the treated area [7].

Since the two phenomena described make it possible, taken together, to determine the definition of the final structure and therefore of the mechanical characteristics of the rod, it

was necessary to make a numerical simulation of the two stages of the cooling process. Namely, the forced boiling inside the heat treatment plant and the process involving heat radiation and natural convection in the open air. To obtain this, the discretization of Fourier's general equation was used with the method of control volumes [8].

The cooling process simulation was performed for all diameters and in various conditions of flow rate of the water sprayed from the nozzles and with varying numbers of cooling sections operating at the same time. The results are shown in table 1, where leaving temperature (T_{end}) means the external temperature of the rod as it could be measured at about 0.5 m from the end of the tempcore plant. The latter was the shortest possible distance where a temperature meter could be located in a production plant. On the other hand, temperature on the cooling plate (T_{plate}) means the external temperature of the rod as it could be measured on the cooling plate about 30 m from the end of the plant. figure 2 records the temperatures relating to different cooling conditions for two different diameters. An accurate analysis of these results makes it possible to claim that the influence on the temperature profile of the two parameters of water flow rate and number of active sections, that is, the interaction time between water jets and rod, are quite different. In particular, the water flow speed does not influence the temperature reached by the plate. However, it influences the temperature at the end of the tempcore plant, although its effect is about half of that attributable to a similar variation in the number of sections working simultaneously.

4. FUZZY CONTROL OF TEMP CORE PROCESS

The first step is to identify the modifiable variables and to determine their effects on the mechanical characteristics of the rod. However, since it is not possible to develop a mathematical model of the process that will take into account all the variables in play and their reciprocal effects, this information and operator experience would normally have to suffice in order to select the process parameters to be used for process control. In light of this, a plausible solution is to address the possibility of using artificial intelligence techniques, such as fuzzy logic, in order to take the acquired knowledge into account without having to use a mathematical model or simulation techniques [9, 10].

Fuzzy logic is a powerful yet straightforward technique that can help solve a variety of problems, especially in the field of process control and decision-making activities. Much of the inherent power of fuzzy logic stems from the possibility to draw conclusions and generate answers on the basis of information that may be inaccurate, ambiguous, incomplete, vague or of a qualitative nature. Such information can also be formulated as deduced linguistic expressions, for example from the every day experience of an operator who, in describing his/her own control strategy, may use instruments such as:

“IF x is equal to y , THEN w is equal to z ”

The basic problem arising from the use of a fuzzy control is to find an adequate group of rules to transform the fuzzy inputs into outputs values in the form of fuzzy sets. This mapping can also be expressed through fuzzy conditional relations; that is a control rule can always be decomposed into a sequence of expressions of the type:

IF ... AND ... THEN ... AND

where the statement following IF is called antecedent and the one following THEN is called the consequent of the specific instantiation of the control rule.

Tab I – Results of the simulation of the cooling process.

V_{H_2O} [ms ⁻¹]	Sect.	$\phi = 12$ mm		$\phi = 20$ mm		$\phi = 30$ mm	
		T_{end} [°C]	T_{plate} [°C]	T_{end} [°C]	T_{plate} [°C]	T_{end} [°C]	T_{plate} [°C]
20	5	659	822	647	829	594	805
	10	513	733	504	752	446	723
	15	418	657	413	686	359	656
	20	351	591	350	630	302	600
40	5	569	787	558	799	504	776
	10	408	681	404	709	357	685
	15	316	598	319	638	284	616
	20	261	530	268	580	242	560
60	5	511	763	503	780	453	758
	10	350	651	351	685	316	665
	15	269	567	277	614	255	597
	20	224	501	235	558	221	545
80	5	469	746	464	767	419	746
	10	313	631	320	670	294	653
	15	243	549	255	600	240	587
	20	205	485	219	545	210	535
100	5	436	733	435	756	396	738
	10	289	617	299	659	279	646
	15	227	536	241	590	231	580
	20	195	475	209	537	204	529

Therefore, in order to apply the fuzzy logic to the tempcore process, it is necessary to evaluate the influence that the main process parameters exert on the final mechanical characteristics of the rod.

Diameter

All other conditions being equal, varying rod diameter necessitates that proportional variations be made to the size of the area subjected to the heat treatment in order to ensure similar values for the mechanical characteristics. However, bearing in mind that the temperature at the end of the hot rolling process (about 950 °C) can keep the steel in the austenitic state but is not sufficient for recrystallization, the austenitic grain size, on which the final ferrite-pearlite structure will depend, is greatly affected by the extent of the forming process, especially in the final rolling stands. Therefore, in order to obtain the same mechanical characteristics in rods of different diameters, the area subjected to the heat

treatment must increase more than proportionally with rod diameter.

Chemical composition

Chemical composition, carbon content in particular, has considerable influence on mechanical characteristics. Such is its importance that in iron and steel industries using conventional technologies it is the only process variable that can be manipulated in order to obtain the mechanical and technological properties required for steel rods for reinforced concrete. The peculiar feature of the tempcore technology is that it allows chemical compositions to be largely neglected and tends toward production characterised by only slightly variable mechanical properties. It must be remembered, however, that as the carbon content increases, the layer subjected to heat treatment must be smaller and the cooling speed at the internal limit of this layer may be lower.

Cooling water flow speed

The already mentioned table I and figure 2 show that the water flow, that is, the number of cooling sections operating at the same time, considerably affects both the temperature profile obtained at the end of the tempcore production line, and the temperature profile on the cooling plate. However, the effect on the latter is much more marked. It is therefore possible to assume that in order to check the temperature at the end of the process, it is convenient to use a suitable modification in the cooling water flow speed which does not substantially alter the temperature profile on the cooling plate. If the cooling plate temperature needs to be changed, it is necessary to change the number of active cooling sections, in spite of the fact that this entails, at the same time, a variation in the temperature at the end of the production line. As a consequence, it will be absolutely inevitable to operate a variation in the opposite direction of the water flow rate.

An example will be provided in order to demonstrate that the fuzzy logic model can be applied to the tempcore process. Let us suppose that we need to produce a rod measuring 18 mm in diameter by using steel with 0.37% carbon content. By analysing the CCT and IT curves for a similar type of steel [11], one can conclude that tempering is obtained for that layer when the cooling speed reaches 500 °C in less than one second. It is also evident from the graphs that the hardness of the tempered area, after tempering at 600 °C is 325 HV and that in the central core with a normalised structure is 210 HV. If one wants the rod to have an average hardness of 245 HV (relating to a tensile stress of about 650 MPa for a mild steel), then one deduces, [6], that the thickness of the area to be treated with heat must be 1.5 mm.

Since the rolling mill process speed for a rod measuring 18 mm in diameter is 10 ms⁻¹, the parameters imposed by the tempcore treatment must be such that on leaving the plant the temperature measured at 1.5 mm from the external surface must be 500 °C and that the plate temperature must be 600 °C.

This means that the external temperature of the rod as it could be measured when leaving the plant is 300 °C. These last two temperatures are the only measurable ones in a production plant. Through the simulation process one finds that in order to obtain these cooling conditions, the water flow rate must be 35 ms⁻¹ and 12 sections need to be active.

It has also been assumed that the four variables considered, that is TE (temperature on leaving the tempcore apparatus), TP (plate temperature), NU (number of active cooling

sections) and VE (flow rate of water sprayed from the nozzles, V_{H_2O}) can have a range of $\pm 50\%$ with respect to the values to be reached. For the fuzzy transformation of the four variables, identical membership functions have been chosen, all triangular and with five classes marked with labels as specified in table II and with a degree of overlap between adjacent classes of 25% [12].

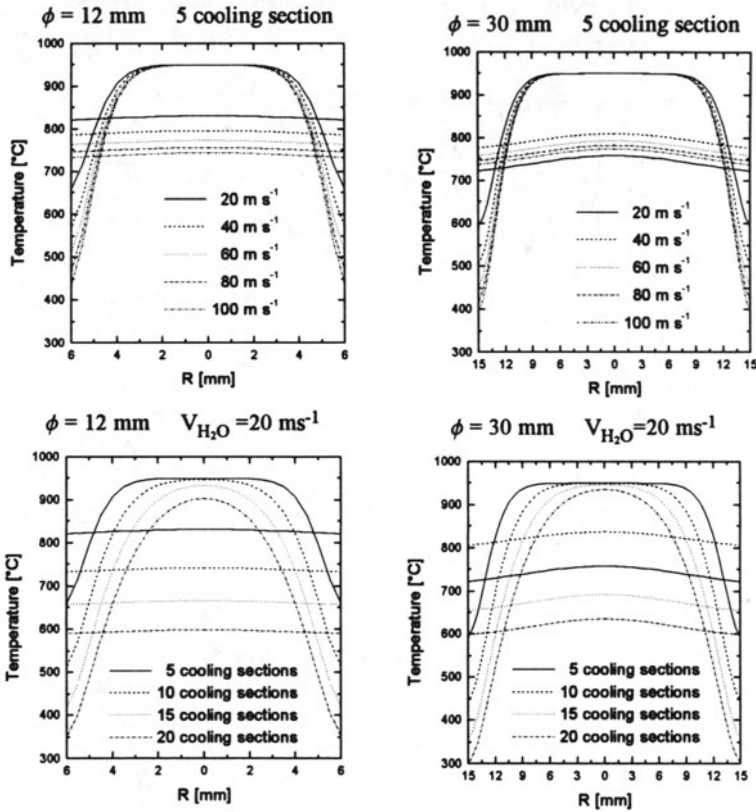


Fig. 2 - Temperature profiles in different cooling conditions.

Tab. II - Labels and meaning of the fuzzy variables.

Labels	NL	NS	AZ	PS	PL
Meaning	Negative Large	Negative Small	Approx Zero	Positive Small	Positive Large

The following tables, III and IV, contain the fuzzy inference rules, bearing in mind that the water flow rate only affects the external temperature when leaving the tempcore apparatus while the number of active cooling sections affects both control variables.

Tab. III - Fuzzy rules for water flow rate control.

TE	NL	NS	AZ	PS	PL
VE	NL	NS	AZ	PS	PL

Tab. IV - Fuzzy rules to control the number of active sections.

TE \ TP	NL	NS	AZ	PS	PL
NL			NL		
NS		NS	NS		
AZ	NL	NS	AZ	PS	PL
PS			PS	PS	
PL			PL		

If one assumes that, in light of the previous experience, one has chosen to have six operating cooling sections and a water flow rate of 50 ms^{-1} , the values of the temperatures at the end of the production line and on the cooling plate will be $345 \text{ }^\circ\text{C}$ and $720 \text{ }^\circ\text{C}$, calculated through the simulation process. Such values are obviously different from estimated values so it is necessary to make a few variations on the selected parameters.

In order to explain the application of the fuzzy logic control, one must suppose to change the number of cooling sections first, by taking into consideration the following two control rules only:

- Rule 1 IF TP = PS AND TE = AZ THEN NU = PS
- Rule 2 IF TP = AZ AND TE = AZ THEN NU = AZ

With the help of figure 3, which includes all the membership functions for all the fuzzy variables in a normalised form with a domain (called the universe of discourse) comprised between ± 2 , it is possible to calculate the membership to each of the single fuzzy sets of the variables:

$$TE = [(345-300)/300]/0.25 = 0.6, TP = [(720-600)/600]/0.25 = 0.8$$

$$\mu_{PS}(TP) = 0.8, \mu_{AZ}(TP) = 0.2 \text{ e } \mu_{AZ}(TE) = 0.4.$$

Once the membership values of each variable included in the antecedent have been fixed, one calculates through an AND operation or through a minimum determination, the truth values of each of the antecedents. In particular for rule 1 the truth value of the antecedent is 0.4 while the truth value is 0.2 for rule 2. The degree of truth of the consequent can be determined using the correlation product inference procedure or the minimum correlation inference procedure, chosen here as an example. Therefore, the membership functions of the consequents are truncated at the truth values of their relative antecedents. In other words, all the rules are assessed at the same time using an OR operation. Hence, the rule application method can be defined as a max-min type of procedure. The final stage in the decision-making process is the defuzzification procedure, that is the passing from the fuzzy sets of data in output to crisp values that can then be used as an input for process control. This is achieved by applying the centre of gravity rule, which means evaluating a weighted

mean value of the fuzzy sets produced:

$$\bar{x} = \frac{\int_D x \cdot \mu(x) dx}{\int_D \mu(x) dx}$$

that calculated in the case examined, gives a value of 0.63 which corresponds to an increase of 16% in the number of nozzles, that is an increase in the number of cooling sections from 6 to 7. The slight increment is due to the fact that, in order to better clarify how the fuzzy procedure works, only two control rules have been considered.

Actually, the control has to be carried out with an iterative procedure by making adjustments alternately to both the speed at which the water is sprayed from the nozzles and to the number of active cooling sections. In the cases examined, the deviation between the expected and measured temperature both in the plate and at the end of the tempcore process, was fixed at $\pm 5\%$. The procedure, after a few iterations, becomes convergent and does not show any instability problem.

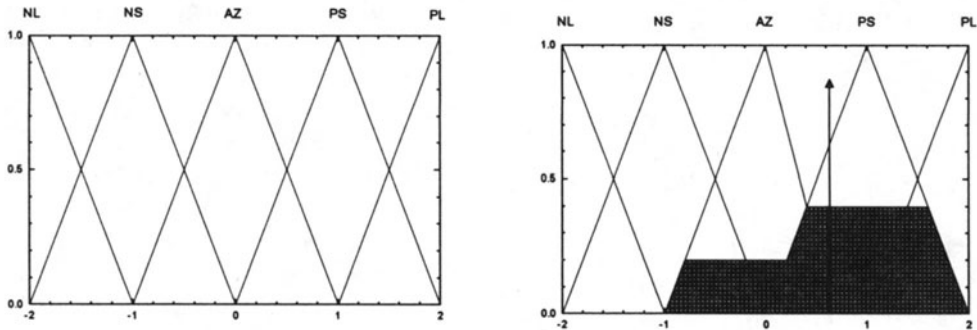


Fig. 3 - An example of fuzzy inference and defuzzification stage.

5. CONCLUSIONS

By making use of experimental results and a simulation model, in a previous paper, it has been possible to verify that the mechanical characteristics of steel rods for reinforced concrete, obtained with a tempcore process, are closely correlated with the structures acquired during the final heat treatment. They in turn depend on the water flow and on the number of cooling sections operating at the same time.

However, the large number of variables in play makes it impossible to use a closed-form mathematical model to describe the dependences and interactions between the process variables and those in the material being processed.

Consequently, in this paper, it was decided to verify the possibility of applying the fuzzy logic method to the process control. This has been tested with the aid of a simplified

numerical model under the assumptions of constant temperature of the steel rod on leaving the last stand in the rolling mill and the same chemical composition of the steel used. Hence the application examined has essentially concerned the choice of optimal process parameters rather than process control.

The results obtained were fairly satisfactory. In the future the simulation process will be expanded by eliminating most, if not all, simplifying hypotheses. In this way it will be possible to test the suitability of the fuzzy logic to the real process control by taking into account, among other things, the normal variations in the rod temperature when it enters the rapid cooling apparatus and in the chemical composition of the steel used. In this case, it will be possible to roll any billet independently of the chemical composition of the steel and the final diameter.

6. REFERENCES

1. Korchynsky M., Wille P., Acciai saldabili di elevata resistenza per tondo per cemento armato con aggiunta di vanadio e azoto, *La Metallurgia Italiana*, n. 11, 1984, pp. 481-491.
2. Sergi V., Applicazione di reti neurali per la previsione delle caratteristiche meccaniche di acciai dolci dopo laminazione, *Applicazione dell'intelligenza artificiale all'ingegneria*, Liguori, 1993, pp. 177-194.
3. AAVV, Tempcore: a New Process for the Production of High Yield Strength Concrete Reinforcing Bars, Centre de Recherches Métallurgiques, Liege, 1972.
4. Zheng H., Abel A., Residual stress effects on the fatigue properties of tempcore reinforcing steel, *Int. Conf. On Analysis of Residual Stresses*, Reims, France, 1997, pp. 177-182.
5. Gori R., Mazzarella O., Russo S., Analisi sperimentale comparativa sul comportamento ciclico di barre di acciaio FeB44K, tempcore e inox per strutture sismo-resistenti in calcestruzzo armato, *Congresso CTE*, Napoli, 7-9 novembre 1996.
6. Giorleo G., Memola Capece Minutolo F., Sergi V., Fuzzy logic modeling and control of steel rod quenching after hot rolling, *Journal of Materials Engineering and Performance*, Vol. 6 (5), October 1997, pp. 599-604.
7. Grossmann M.A., Bain E.C., *Principles of Heat Treatment*, American Society for Metals, 1964.
8. Patankar S.V., *Numerical Heat Transfer and Fluid Flow*, Hemisphere Publishing Co., 1980.
9. Zadeh L.A., *Fuzzy Logic, Computer*, vol. 21/4, 1988, pp. 83-93
10. Bannatyne R., *La logica fuzzy*, *Automazione Energia Informazione*, vol. 81/4, 1994, pp. 412-416.
11. Vandervoort G., *Atlas of Time-Temperature Diagrams for Irons and Steels*, Carpenter Technology Co., 1991.
12. Klir G.J., Yuan B., *Fuzzy Set and Fuzzy Logic: Theory and Applications*, Prentice Hall Inc., 1995.

**HIGH PRECISION ROTATION MECHANISM BASED
ON CROSS-SPRING PIVOTS**
MATHEMATICAL MODELLING AND LASER TRIANGULATION MEASUREMENTS

F. De Bona

DIEGM University of Udine, Udine, Italy

A. Strozzi

University of Modena, Modena, Italy

S. Zelenika

Sincrotrone Trieste, Trieste, Italy

KEYWORDS: Flexible Elements, Cross-Spring Pivot, Geometrical Non-Linearities, Laser Doppler Interferometry

ABSTRACT: This work addresses the parasitic motion of a rotation mechanism based on flexural pivots aimed at precision engineering applications. From the analytical point of view the problem is reduced to the study of large deflections of an elastic frame and a solution based on the Newton-Raphson method is proposed. An experimental assessment performed by using the interferometric technique of laser triangulation permits the limits of applicability of the proposed method to be established.

1. INTRODUCTION

Flexural hinges (Fig.1) are mechanical drives characterized by high stiffness with respect to the translation degrees of freedom (X and Y) and by high compliance with respect to the rotational degree of freedom (ϑ). Usually such devices are constituted by two leaf springs of equal dimensions which cross at their midpoints forming an angle 2α , which justifies this fact that they are generally referred to as cross-spring pivots.

Flexural hinges are commonly used in metrology as dynamometers and in the aerospace field, for several applications where particular working conditions (high temperature, aggressive environment, etc) do not permit conventional sliding and rolling bearings to be used. In these cases the mechanical design of the pivots deals with the evaluation of the leaf spring strength and stiffness as well as with the stability analysis of the overall mechanism [1].

Recently such devices have also been used in precision engineering, nanotechnology and

micromechanics. In fact, flexural hinges are free from backlash and friction and therefore they permit high rotational accuracy to be obtained. In high precision applications a careful structural analysis has to be performed. In fact, as shown in Fig.1, the rotation ϑ is followed by a parasitic translation $\overline{OO'}$. As a consequence the "geometrical" center O (i.e. the crossing point of the tangents to the leaf springs where they are clamped to the moveable block) moves to O'. This parasitic displacement can be characterized by establishing the variation of the amplitude d and of the phase ϕ of the displacement $\overline{OO'}$, versus the rotation angle ϑ .

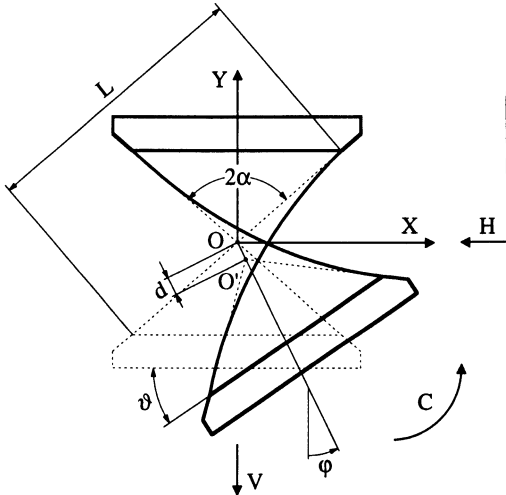


Fig.1: Flexural hinge

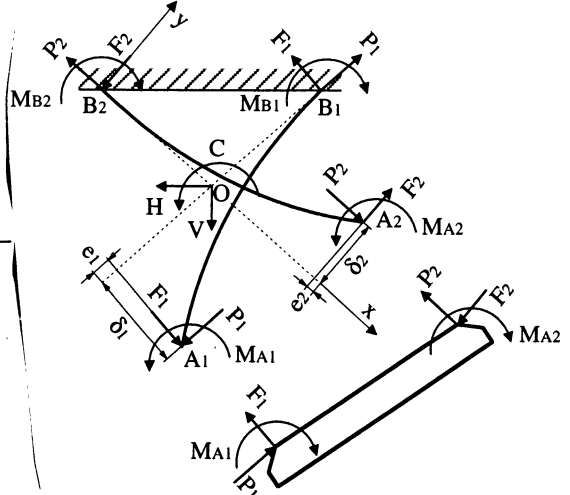


Fig.2: Displacements and reactions

Several methods have been proposed to evaluate the parasitic motion $\overline{OO'}$. In [2] the exact expression of the leaf spring curvature is used and a solution in terms on elliptic integrals is obtained for the case of the hinge loaded only by a pure couple C. In fact, in this case the problem is symmetric and therefore the values of the reactions can be evaluated analytically. Other authors have obtained approximate solutions based on geometrical [3] or kinematic [4, 5] considerations. All the mentioned approaches do not permit the effect of the horizontal load H and of the vertical load V to be taken into account and they give results characterized by a wide scattering. On the other hand, the experimental results available in literature [4, 6, 7] do not make it possible to confirm the reported theories, as the used measurement techniques were characterized by high uncertainty.

In this work a method is proposed that permits the parasitic motions to be evaluated, even when the effect of the lateral loads H and V has to be considered. In order to establish the limit of applicability of the proposed method, an experimental assessment is also performed by using an interferometric technique of laser triangulation.

2. MATHEMATICAL MODEL

The hinge parasitic motion can be evaluated following the approach suggested in [1]; in that case the analysis was limited to the determination of the hinge stiffness around the undeflected position ($\vartheta=0$). In this work the overall working range of angular motion will be considered, so that the assumption of small deflections does not hold any more and consequently the problem becomes strongly non-linear.

In the usual configuration of Fig.1, where the undeflected spring-strips cross at their midpoints,

the equilibrium equations of the moving block are the following (Fig.2):

$$V = (P_1 + P_2) \cos \alpha + (F_1 - F_2) \sin \alpha \tag{1}$$

$$H = (P_1 - P_2) \sin \alpha - (F_1 + F_2) \cos \alpha \tag{2}$$

$$C = M_{A_1} + F_1 \frac{L}{2} - P_1 \delta_1 + M_{A_2} + F_2 \frac{L}{2} - P_2 \delta_2 \tag{3}$$

The compatibility equations for the leaf springs edges A₁ and A₂ are:

$$(\delta_1 - \delta_2) \cos \alpha + (e_1 + e_2) \sin \alpha = L \sin \alpha (1 - \cos \vartheta) \tag{4}$$

$$(\delta_1 + \delta_2) \sin \alpha - (e_1 - e_2) \cos \alpha = L \sin \alpha \sin \vartheta \tag{5}$$

The leaf-spring equilibrium equations can be written by considering the flexural contribution of the axial load and the approximate expression for the curvature; moreover it is supposed that the two leaf springs possess the same mechanical characteristics (L, I, E). It follows:

$$EI \frac{d^2y}{dx^2} = P_{1(2)}y + M_{A_{1(2)}} - F_{1(2)}x \tag{6, 6'}$$

where subscripts 1 and 2 refer to leaf spring 1 and leaf-spring 2 respectively. According to [1], Eqs. (1-6) can be written in dimensionless form by adopting the following notation:

$$\lambda_{1(2)} = \frac{e_{1(2)}}{\vartheta^2 L} \quad \xi_{1(2)} = \frac{2\delta_{1(2)}}{\vartheta L} - 1 \quad h = \frac{HL^2}{EI} \operatorname{cosec} \alpha \quad v = \frac{VL^2}{EI} \operatorname{sec} \alpha$$

$$f_{1(2)} = \frac{F_{1(2)}L^2}{EI} \quad 4\beta_{1(2)}^2 = \frac{P_{1(2)}L^2}{EI} \quad m_{A_{1(2)}} = \frac{M_{A_{1(2)}}L}{EI}$$

Integrating twice Eqs. (6, 6') and putting the expressions of the spring strip edge displacements and rotations equal to those of points A₁ and A₂ of the moveable block, it follows:

$$f_{1(2)} = \vartheta \left(2\beta_{1(2)}^2 + 2\xi_{1(2)} \frac{\beta_{1(2)}^3}{\beta_{1(2)} - \tanh \beta_{1(2)}} \right) \tag{7, 7'}$$

$$m_{A_{1(2)}} = \vartheta \left(\beta_{1(2)} \operatorname{coth} \beta_{1(2)} - \xi_{1(2)} \frac{\beta_{1(2)}^2 \tanh \beta_{1(2)}}{\beta_{1(2)} - \tanh \beta_{1(2)}} \right) \tag{8, 8'}$$

The expression for the length variation of the leaf spring as obtained in [8] is used:

$$e_{1(2)} = \int_0^L \frac{1}{2} \left(\frac{dy}{dx} \right)^2 dx \tag{9, 9'}$$

and consequently, by substituting Eqs (6, 6') in (9, 9') and integrating, it follows:

$$\lambda_{1(2)} = \frac{1}{16\beta_{1(2)}} \left[\beta_{1(2)} (3 - \coth^2 \beta_{1(2)}) + \coth \beta_{1(2)} \right] + \frac{1}{4} \xi_{1(2)} \quad (10, 10')$$

A system of 11 equations (1, 2, 3, 4, 5, 7, 7', 8, 8', 10, 10') in the 11 unknowns $\lambda_1, \lambda_2, \xi_1, \xi_2, \beta_1, \beta_2, m_{A1}, m_{A2}, f_1, f_2, \vartheta$ is thus obtained. The parameters $\lambda_1, \lambda_2, \xi_1$ e ξ_2 can now be expressed as function of β_1 e β_2 ; by substituting the thus obtained expression in Eqs. (1, 2) and making the assumption that: $2\alpha=90^\circ$, it is possible to write:

$$\begin{aligned} & 4\beta_{1(2)}(4 + \vartheta^2) \left(\beta_{2(1)} \cosh \beta_{2(1)} - \sinh \beta_{2(1)} \right) \left[\frac{1}{2} (v \pm h) - 4\beta_{1(2)}^2 \right] \pm \\ & \pm \cosh \beta_{2(1)} \left(\mp 32\beta_{2(1)}^3 \beta_{1(2)} + 16\beta_{2(1)}^3 \beta_{1(2)} \vartheta \mp 4\beta_{2(1)}^3 \beta_{1(2)} \vartheta^2 + 2\beta_{2(1)}^3 \beta_{1(2)} \vartheta^3 \pm \right. \\ & \pm 32\beta_{2(1)}^3 \beta_{1(2)} \cos \vartheta - 16\beta_{2(1)}^3 \beta_{1(2)} \vartheta \cos \vartheta + 32\beta_{2(1)}^3 \beta_{1(2)} \sin \vartheta \pm 16\beta_{2(1)}^3 \beta_{1(2)} \vartheta \sin \vartheta - \\ & - 32\beta_{2(1)}^2 \beta_{1(2)} \vartheta \tanh \beta_{2(1)} - 8\beta_{2(1)}^2 \beta_{1(2)} \vartheta^3 \tanh \beta_{2(1)} \pm 4\beta_{2(1)}^3 \vartheta^2 \coth \beta_{1(2)} - \\ & - 2\beta_{2(1)}^2 \beta_{1(2)} \vartheta^3 \coth \beta_{2(1)} \mp 2\beta_{2(1)}^3 \beta_{1(2)} \vartheta^2 \operatorname{cosech}^2 \beta_{1(2)} + \beta_{2(1)}^3 \beta_{1(2)} \vartheta^3 \operatorname{cosech}^2 \beta_{2(1)} \mp \\ & \left. \mp 2\beta_{2(1)}^3 \beta_{1(2)} \vartheta^2 \operatorname{cosech}^2 \beta_{1(2)} \cosh 2\beta_{1(2)} + \beta_{2(1)}^3 \beta_{1(2)} \vartheta^3 \operatorname{cosech}^2 \beta_{2(1)} \cosh 2\beta_{2(1)} \right) = 0 \end{aligned} \quad (11, 11')$$

where the upper and lower sign refer to Eqs. (11) and (11') respectively. These expressions hold if the leaf springs are under tensional loads; if compressive forces have to be considered, parameter β becomes imaginary and therefore the substitution $\beta=i\omega$ has to be introduced in Eqs.(11) and (11').

The derived non-linear system of equations with the variables β_1 e β_2 (ω_1 and ω_2 in the case of compression) as unknowns, can be solved following a Newton-Raphson method. The calculation can be arranged according to an iterative approach: if V and H are known, v and h can also be evaluated; for a certain value of ϑ the system of equations (11, 11') is solved and the values of β_1 e β_2 are calculated. The values of $\lambda_1, \lambda_2, \xi_1$ e ξ_2 and of the deflections e_1, e_2, δ_1 e δ_2 can then be obtained. From Eq. (7, 7') and (8,8') the values of f_1, f_2 and of m_{A1} e m_{A2} can also be determined. Finally Eq. (3) gives the value of the couple applied to the hinge, that has to be compared with the actual value C. The procedure is then repeated up to the point when convergence is reached. Simple geometrical considerations allow one to obtain the values of the displacements in the X and Y directions and hence the amplitude and the phase of $\overline{OO'}$.

$$\frac{d_X}{L} = \frac{\vartheta(\xi_1 + 1)}{2} \cos \alpha + \lambda_1 \vartheta^2 \sin \alpha + \frac{\sin(\alpha - \vartheta) - \sin \alpha}{2} \quad (12)$$

$$\frac{d_Y}{L} = \frac{\vartheta(\xi_1 + 1)}{2} \sin \alpha - \lambda_1 \vartheta^2 \cos \alpha - \frac{\cos(\alpha - \vartheta) - \cos \alpha}{2} \quad (13)$$

$$\frac{d}{L} = \sqrt{\left(\frac{d_X}{L} \right)^2 + \left(\frac{d_Y}{L} \right)^2} \quad \varphi = \arctan \left(\frac{d_X/L}{d_Y/L} \right) \quad (14)$$

3. EXPERIMENTAL ASSESSMENT

A cross-spring pivot with the following mechanical characteristics has been built: L=115 mm,

$t=0,5$ mm, $b=15$ mm, $\alpha=45^\circ$ (t =spring-strip thickness, b =spring-strip width); in order to minimize the effects induced by the compliance of the constraints, a ratio $t/L \ll 1$ was chosen, in accordance with the results presented in [6]. The leaf springs were made of beryllium-copper alloy ($E=131$ GPa, $\sigma_R=1251$ MPa, $\sigma_{0,2}=1124$ MPa), the other parts of the mechanism were made of AISI 304 steel. Following the approach suggested in [1] the maximum working range of the angle ϑ ($\pm 30^\circ$) and the values of the vertical load V (-70 N, $+12.5$ N) defining the stability range were established.

The measurement of the parasitic motion $\overline{OO'}$ can be performed by considering the rigid motion of the moveable block in the X-Y plane. This motion can be characterized by the values of the coordinates of a single point of the block versus the rotation angle ϑ . The accurate measurement of a trajectory in a 3D space is generally performed using laser tracking techniques. This approach is used in metrology, to calibrate measurement robots [9], and it has also been recently applied in micromechanics to characterize high precision manipulators [10]. In the latter case the trajectory of a retroreflector connected to the moveable element was obtained from the measurement of the variation of its distance from three laser interferometers; the tracking of the retroreflector was obtained by using a photodiode quadrant detector. In the case of flexural hinges the laser tracking technique can be considerably simplified. In fact, only a 2D measurement has to be performed; moreover, as the overall range of the amplitude d is limited, a suitable orientation of the retroreflector permits its displacement to be measured without re-orienting the laser beams. It should be noted that, since in this case there are no errors induced by the photodiode quadrant detector electronic drift, the achievable accuracy is higher.

The measurement principle is schematically represented in Fig.3; two in-plane laser beams forming a well known angle γ ($\gamma \approx 25^\circ$) are reflected by a corner cube whose optical centre K coincides with the geometrical centre of the hinge O . Two single beam interferometers [11] permit the two components X' and Y' of the displacement $\overline{OO'}$ to be measured so that the values of X and Y can be easily determined. As a consequence of the optical properties of the cube corner (see [12]) the displacement measurement is not affected by the rotation ϑ of the movable block around point O . The angle ϑ is measured at the same time by using a differential laser interferometric system [12].

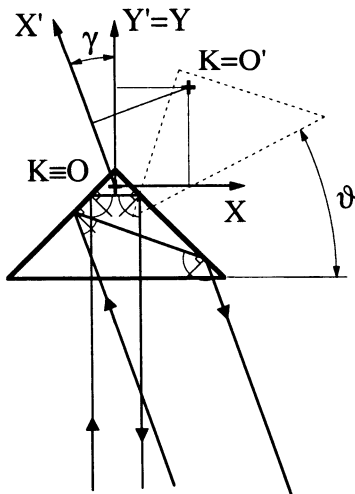


Fig.3: Measurement principle

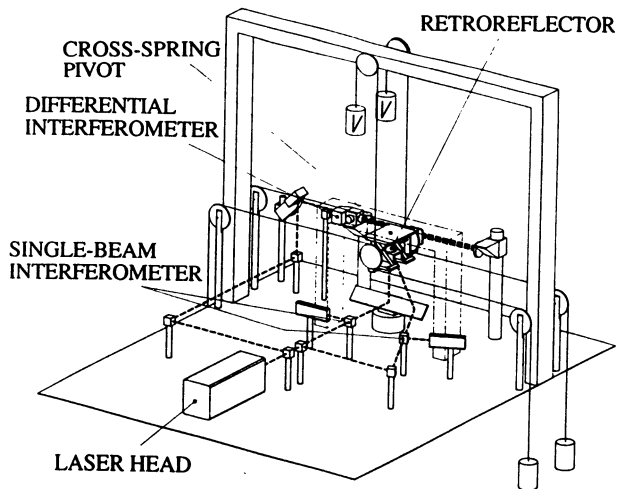


Fig.4: Scheme of the measurement system

Fig.4 shows the set-up of the measurement system, which is essentially constituted by a two

frequency laser head (HP5517A), two single beam interferometers (HP10705A) with their receivers (HP10780C) and a differential interferometer (HP10715A). The values of X' , Y' and ϑ were obtained by using a fringe counting board (HP5507A) interfaced to a PC. The hinge can be loaded with couples and forces by means of a simple system based on calibrated weights connected by wires to the pivot center. At first the system was loaded by the sole force V , and then the measurement was performed by simply increasing the applied torque and measuring at the same time X' , Y' , and ϑ .

A resolution of 10 nm for linear displacements and of 0.2 μ rad for angular displacements was achieved. The measurement interval of uncertainty is mainly due to systematic errors (alignment and assembly errors, uncertainty in the evaluation of γ); random errors (variation of the refractive index of light, dead-path error, etc. [11]) are negligible.

4. RESULTS AND DISCUSSION

Fig.5 shows the dependence of the amplitude d and of the phase ϕ on the rotation angle ϑ , when the hinge is loaded only with a couple C ($V=H=0$).

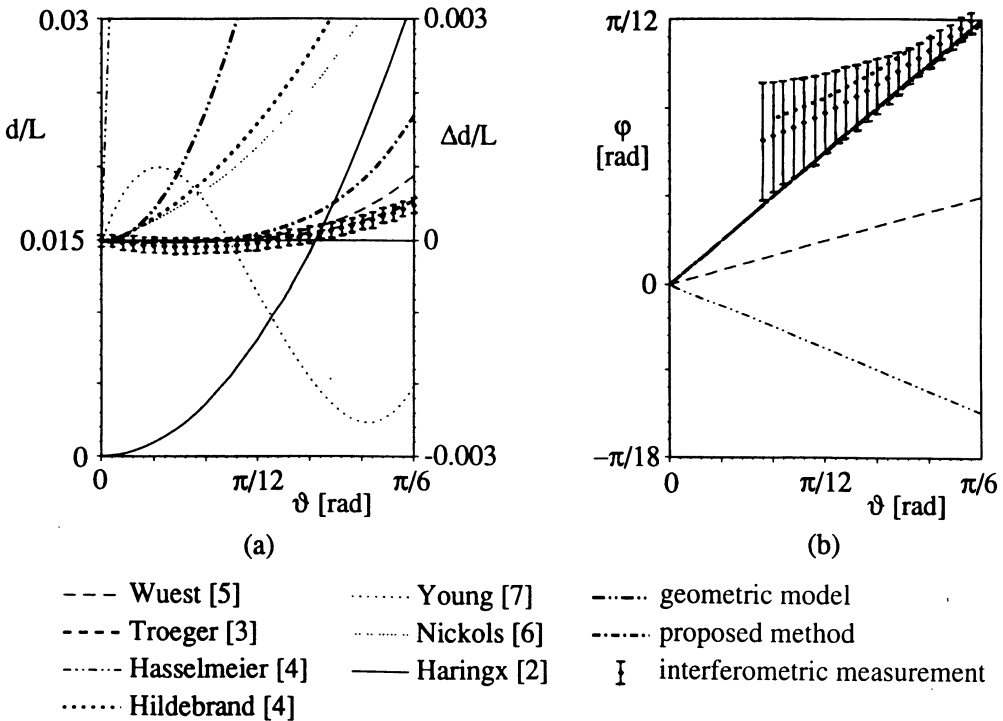


Fig.5: Diagram of d/L , $\Delta d/L$ (a) and ϕ (b) versus ϑ in the case: $V=H=0$

The results obtained by applying the analytical and the experimental methods available in literature ([2], [3], [4], [5], [6], [7]) are compared to those achieved with the proposed method and with the interferometric measurements; in the latter case the interval of uncertainty evaluated as described in the previous section is also represented.

The results achieved can be more easily compared if the difference $\Delta d/L$ is taken into account, between the values of d/L obtained with each of the considered method and those got with the method described in [2]. In the case when the pivot does not undergo lateral loads, the solution proposed in [2] should be the most accurate, since in that paper the exact curvature expression was used in the equilibrium equation of the leaf-springs. Therefore in this particular case ($H=V=0$) the values of $\Delta d/L$ correspond to the error introduced by the considered method. In Fig.5 it can be noted that the results of the interferometric measurements are in good agreement with those obtained in [2]. The method proposed in this work gives acceptable results, even if less accurate than those obtained in [3] and in [5]; on the other hand, methods [3] and [5] introduce appreciable errors in the values of the phase φ . All the other methods result in very large errors, both in the amplitude and in the phase.

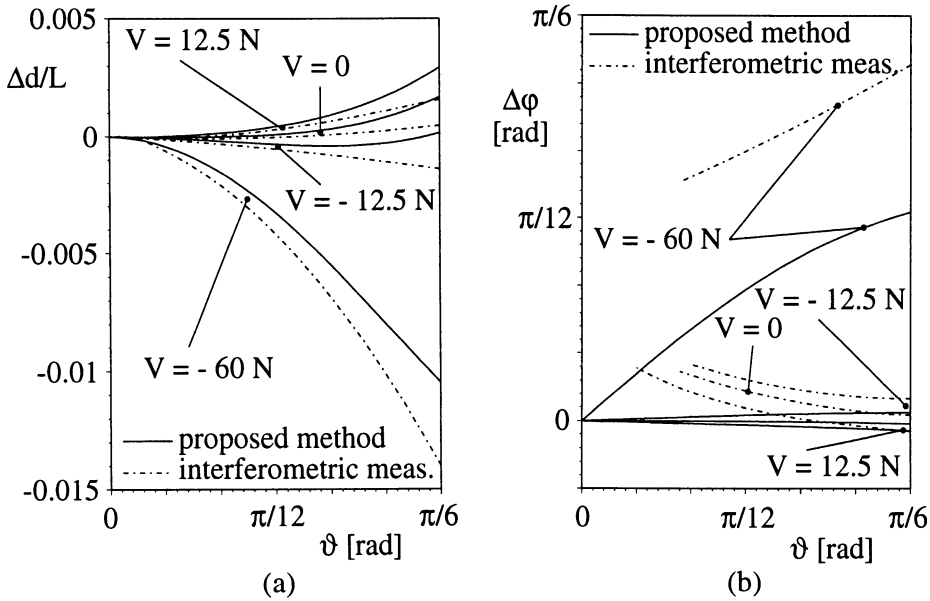


Fig.6: Diagram of $\Delta d/L$ (a) and $\Delta\varphi$ (b) versus ϑ for different values of V

The validity of the analytical method proposed in this work is enhanced if the effect of the lateral loads is considered. In fact, flexural hinges generally support mechanical elements characterized by considerable weights, while the rotation is generally obtained by loading the hinge with a force instead of a pure couple; this has great importance from the mechanical design point of view. Fig.6 shows the values of $\Delta d/L(\vartheta)$ and of $\Delta\varphi(\vartheta)$ (same meaning as $\Delta d/L$) obtained with the proposed method and experimentally for different values of V . In these cases the intervals of uncertainty were not reported, but they are similar to those reported in Fig.5. It can be noticed that the proposed method permits the influence of the lateral loads to be established clearly. Only in the case of large rotations and in the case of values of V close to the instability condition, the theoretical results become significantly different from those obtained experimentally. This behaviour can be easily rationalized observing that the approximate expression for the curvature used in Eqs. (6) and (6') introduces errors that increase with increasing axial loads and leaf spring deflections [8]. It can be concluded that the proposed method allows the mechanical behaviour of the leaf-spring to be adequately described, if the difference between the approximate and the exact expression of the curvature is limited.

5. CONCLUSIONS

The evaluation of the parasitic motion of a crossing-spring pivot under lateral loads can be performed only if the non-linear behaviour of the leaf springs is considered; a first approach, suggested in this work, is that of considering the equilibrium equations, where the contribution of the axial loads is taken into account, but the approximated expression of the curvature is used. This results in a adequate solution if the most common case of limited lateral loads and angular rotations is considered. A more accurate approach could be obtained using the exact equilibrium equations (where the exact expression of the curvature is used); this approach would however give rise to additional computational problems. In fact in this case an expression in terms of elliptic integrals is obtained and therefore in applying the Newton-Raphson method the Jacobian has to be evaluated following lengthily numerical procedures [13]. Probably in the latter case the obtainable solution would not exhibit significant advantages with respect to a F.E.M. approach.

REFERENCES

1. Wittrick, W. H.: The Properties of Crossed Flexure Pivots and the Influence of the Point at which the Strips Cross, *Aer. Quart.*, II (1951), 272-292
2. Harings, J. A.: The Cross-Spring Pivot as a Constructional Element, *Appl. Sci. Res. A*, 1 (1949) 4, 313-332
3. Troeger, H.: Considerations in the Application of Flexural Pivots, *Aut. Con.*, 17 (1962) 4, 41-46
4. Hildebrand, S.: Obliczanie i Zachowanie sie w Pracy Spreznych Krzywosci, *Pomiary-Automatyka-Kontrola*, 11 (1958), 501-508
5. Wuest, W.: Blattfedergelenke fur Messgerate; *Feinwerktechnik*, 54 (1950) 7, 167-170
6. Nickols, L. W. and Wunsch, H. L.: Design Characteristics of Cross-Spring Pivots, *Eng.*, 10 (1951), 473-476
7. Young, W. E.: An Investigation of the Cross-Spring Pivot, *J. Appl. Mech.*, *Trans. ASME*, 11 (1944), A-113 - A-120
8. Timoshenko, S. T. and Gere, J. M.: *Theory of Elastic Stability* - 2nd ed., McGraw-Hill, New York, 1961
9. Gilby, J. H. and Parker, G. A.: Laser-Tracking System to Measure Robot Arm Performance; *Sensor Rev.*, Ottobre (1982), 180-184
10. Nakamura, O., Mitsuo, G.: Laser Interferometric Calibration of Microscan Mechanisms by Using Three Laser Beams, *Precision Engineering*, 15 (1993) 1, 39-43
11. Slocum, A.: *Precision Machine Design*; Prentice-Hall, Englewood Cliffs, 1991
12. Peck, E. R.: Theory of the Corner-Cube Interferometer, *J. Optical Soc. of America*, 38 (1948) 12, 1015-1024
13. De Bona, F., Zelenika, S.: A Generalized Elastica Approach to the Analysis of Large Displacements of Spring-Strips, *Proc. Instn Mech Engrs, Part C*, 211 (1997), 509-517

END-OF LIFE EVALUATION OF PRODUCTS

T. Andes and W.A. Knight
University of Rhode Island, RI, USA

KEYWORDS: Ecodesign, Disassembly, Recycling.

ABSTRACT: The design of products for ease of disassembly and end-of-life processing to recover and recycle potentially valuable materials is influenced by the possible end-of-life destinations for the component parts and sub-assemblies. The most appropriate choice of end-of-life processing for specific components is influenced by a number of factors, including the use of surface coatings, fillers, types of assembly methods, compatibility of materials and so on. This paper presents an evaluation scheme, which determines the suitable end-of-life destinations for the components within a product. The procedure utilizes a series of classification charts and numerical ratings, such that each item is given a numerical score for the possible end-of-life destinations. In this way, the overall material recovery potential of a proposed product design can be evaluated.

1.0 INTRODUCTION.

Public opinion and increased legislation is placing more emphasis on the end-of-life disassembly of products to recover and recycle materials [1-3]. The efficiency of material recovery is influenced by the appropriate end-of-life destinations of constituent parts and materials. The possible end-of-life destinations include various methods of recycling, waste-to-energy incineration, landfill disposition and so on. The appropriate choice of end-of-life destination for a particular component is determined by several factors including, surfaces coatings, fillers, materials compatibility, assembly methods and so on. This means that the initial selection of materials and material combinations in a product has a great influence on the suitable end-of-life destinations for products. Thus a procedure to guide designers in the selection of materials for efficient end-of-life processing is required and this paper outlines a scheme which uses a series of classification charts and numerical ratings to evaluate the suitable end-of-life destinations for materials and products. The

Published in: E. Kuljanic (Ed.) *Advanced Manufacturing Systems and Technology*,
CISM Courses and Lectures No. 406, Springer Verlag, Wien New York, 1999.

aim is for a relatively simple easy to use procedure to guide users towards material selections with improved material recovery potentials. The procedure can be used to evaluate the end-of-life disposition performance of products and as a means of assigning end-of-life destinations for design for environment (DFE) analysis procedures [4,5].

2.0 END-OF-LIFE DESTINATIONS

The end-of-life destinations considered in the evaluation procedure are as follows:

Recycling

- Direct Recycling – the reuse of material as feedstock for new components with the material processed ‘as-is’.
- Segregated Recycling – the reuse of the material as feedstock for new component, but mixed materials must be segregated, pre-treated and each material processed or disposed of independently.
- Secondary Recycling – lower grade recycling, such as regrinding to use the material as a filler or to create a composite material.

Reprocessing

- Chemical/Thermal Reprocessing – processes to recover the basic material constituents, including, for plastics, such processes as glycolysis, hydrolysis and pyrolysis, as well as recovery methods for other materials.
- Incineration (regular) - waste-to-energy incineration without special environmental controls.
- Incineration (special) - waste-to-energy incineration, with special environmental control to handle toxic materials or emissions.
- Unique process – specialized processes used for hazardous waste treatment, etc., such as the processing of CFCs.

Landfill

- Landfill (normal waste)
- Landfill (hazardous waste)

There are two other possible end-of-life destinations for products. However these can only be determined by the user for individual items.

- Reuse – Items recovered can be reused, as is, directly in other assemblies
- Remanufacture - reclaimed items from retired products are remanufactured and reused for secondary markets.

3.0 CLASSIFICATION OF MATERIALS AND ADDITIVES.

The evaluation procedure uses a series of classification charts to assign numerical values to rank the end-of-life destinations. The classification first divides materials into three main material categories: polymers, metals and other miscellaneous materials. A table for each category contains a list of materials, together with a numerical rating on a scale of zero to 100, which indicates a ranking of the end-of-life destination for the basic materials. Figure 1 shows a portion of the table for polymers (plastics). Each main table has associated tables of additives that may influence the suitability of the possible end-of-life

destinations. These tables include surface coatings, fillers and other additives. Each additive is assigned a numerical factor between zero and 1.0, with a value of 1.0 indicating no effect on the ranking of the corresponding end-of-life destination. Figure 2 shows a portion of the additive table for plastics. An assumption is made that the effect of two or more additives to a material is cumulative in the effect on the destination ranking.

Finally there are two compatibility tables for materials, which assign factors between zero and 1.0. These factors are used when more than one material exists in the item being considered. The two tables are for the overall compatibility of the main material groups and for the compatibility of mixed plastics. As more information becomes available an individual material capability table should replace the first of these tables.

4.0 END-OF-LIFE RANKING METHODOLOGY

Considerable thought was given to how to rank each material for each end-of-life destination. There are three main factors that influence end-of-life destination for a given material: environmental impact, the technological practicality of material recovery, and economics. Several ranking schemes that combined environmental and economic effects were considered, but for simplicity it was decided that the main consideration would be processing economics and relative material values (demand). The level of technological practicality can be measured by economic means. The less practical the processing technology is, the more it will cost to use. Environmental impact can also be measured economically, through the imposition of tariffs, elevated disposal costs due to decreasing landfill space and environmental harm and so on. With this in mind, the preference rankings generated are based on the economics of end-of-life processes (which incorporates the economics of environmental impact) and end-use market demand (value) of recovered materials. The total ranking is out of 100 points, with half the points devoted to each of these two economic drivers.

The impact of combining materials and additives on end-of-life disposal was also investigated. The two primary areas of impact that were investigated were effects on reprocessing (cost) and effects on end-use market demand. The impact that each additive has on a material's ranking is defined by an effect factor (from 0.0 to 1.0) which is used to modify the basic material end-of-life ranking. The total points for the effect factor are proportioned evenly between the relative economics of processing and material market demand.

The rankings and factors have been assigned initially based on published data [6-9] and from discussions with product dismantlers and recycling companies. A wide range of facilities involved with material reprocessing and disposal were contacted to supplement the published information. Many of the rankings and factors of the system are based on the experiences of these facilities. Some of the rankings should be regarded as tentative at this stage to be updated, as more research data becomes available.

		End-of-Life Ranking								
		Recycle			Reprocess				Landfill	
Material	Code	Direct Recycling	Segregated Recycling	Secondary Recycling	Chemical/Thermal Reprocessing	Incineration (regular)	Incineration (special)	Unique Process	Landfill (regular)	Landfill (special)
ABS	P1	70	50	60	75	75	60	10	85	40
ASA, SAN	P2	50	40	60	75	75	60	10	85	40
EPM/EPDM	P3	50	40	60	75	75	60	10	85	40
HDPE	P4	90	70	60	75	80	65	10	85	40
LDPE	P5	90	70	60	75	80	65	10	85	40
PA	P6	50	40	60	75	80	65	10	85	40
PBT	P7	50	40	60	75	75	60	10	85	40
PC	P8	70	50	60	75	75	60	10	85	40

Figure 1 Portion of the Classification Table for Polymers.

		End-of-Life Ranking								
		Recycle			Reprocess				Landfill	
Coatings, Additives, Fillers	Code	Direct Recycling	Segregated Recycling	Secondary Recycling	Chemical/Thermal Reprocessing	Incineration (regular)	Incineration (special)	Unique Process	Landfill (regular)	Landfill (special)
Antioxidants	AP1	0.90	0.90	1.00	0.95	0.85	0.85	1.00	1.00	1.00
Antistatic agents	AP2	0.90	0.90	1.00	0.95	0.85	0.85	1.00	1.00	1.00
Biostabilizers	AP3	0.90	0.90	1.00	0.95	0.95	0.95	1.00	1.00	1.00
Chemical blowing agents	AP4	0.70	0.50	0.80	0.70	0.85	0.85	1.00	1.00	1.00
Metal Coatings	AP19	0.30	0.60	0.75	0.90	0.75	0.75	1.00	1.00	1.00
Labels, compatible plastics	AP22	0.95	0.95	0.90	0.90	1.00	1.00	1.00	1.00	1.00

Figure 2 Portion of the Additives Classification for Polymers.

5.0 EXAMPLE OF ANALYSIS OF A MATERIAL

Below is a step-by-step example of the ranking of an individual material.

		End-of-Life Ranking											
		Recycle			Reprocess					Landfill			
		Direct Recycling	Segregated Recycling	Secondary Recycling	Chemical/Thermal Reprocessing	Incineration (regular)	Incineration (special)	Unique Process	Landfill (regular)	Landfill (special)			
Step #	Primary Material	Coatings, Additives, Fillers											
Step #1	P8				70.0	50.0	60.0	75.0	75.0	60.0	10.0	85.0	40.0
Step#2	P8	AP4			49.0	25.0	48.0	52.5	63.8	51.0	10.0	85.0	40.0
Step#3	P8	AP4	AP19		14.7	15.0	36.0	47.3	47.8	38.3	10.0	85.0	40.0
Step#4	P8	AP4	AP19	AP22	14.0	14.3	32.4	42.5	47.8	36.3	10.0	85.0	40.0

Key: P8 = PC AP4= Chemical Blowing Agent AP19= Metal Coating AP22=Labels, compatible plastics

Figure 3 Main Table Showing Analysis of a Material.

- STEP #1. The code for the primary material is input into a Main Table (Figure 3). The rankings for each end-of-life destination are input the corresponding Materials Table (Figure 1).
- STEP #2. The code for the first additive that is present is input into the Main Table. The corresponding effect factors from the Additives Table (Figure 2) are multiplied by the rankings in the Main Table for each respective end-of-life category.
- STEP #3. Step #2 is repeated for the second additive present with the primary material.
- STEP #4. Step #2 is repeated for the third additive present with the primary material.

The bottom line in Figure 3 gives the final end-of-life preferences. It can be seen that the end-of-life destination with the highest preference (85.0) is Landfill (regular). However, if a disposal option other than landfill was being considered, the results suggest that either incineration or reprocessing have the next highest levels of preference.

6.0 RECOMMENDING AN END-OF-LIFE DESTINATION

The final step is the interpretation of the results. The strength of the proposed end-of-life classification system is that it indicates which end-of-life destinations are possible by providing a level of preference for each. Therefore, the user should look at the results and see which end-of-life destinations have the highest levels of preference. Two different biases can be given to the interpretation of the results as follows:

Economic Strategy

One strategy for an end-of-life recommendation is based mostly on economic considerations; that is the end-of-life rankings derived. The recommended end-of-life

destination is the destination with the highest level of preference. If two or more destinations have similar values, then the most environmentally friendly option would be selected (the destination closest in the Main Table to the left; end-of-life destinations are listed in the tables from left to right in approximate order of environmental preference).

Environmental Strategy

The other recommended strategy focuses more on environmental impact and excludes landfill as a possibility as this is least environmentally friendly destination. The highest level of preference with this exclusion is then recommended.

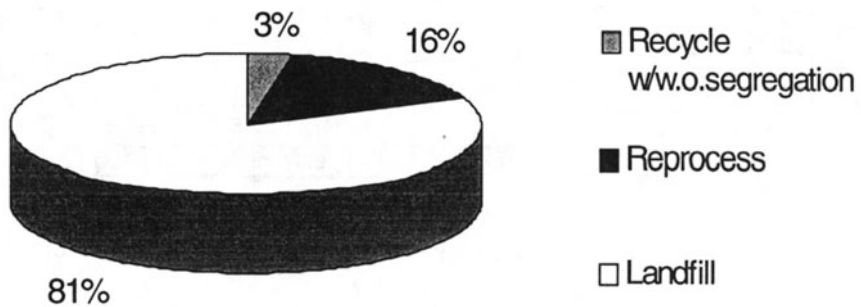


Figure 4 End-of-Life Destinations for Personal Computer

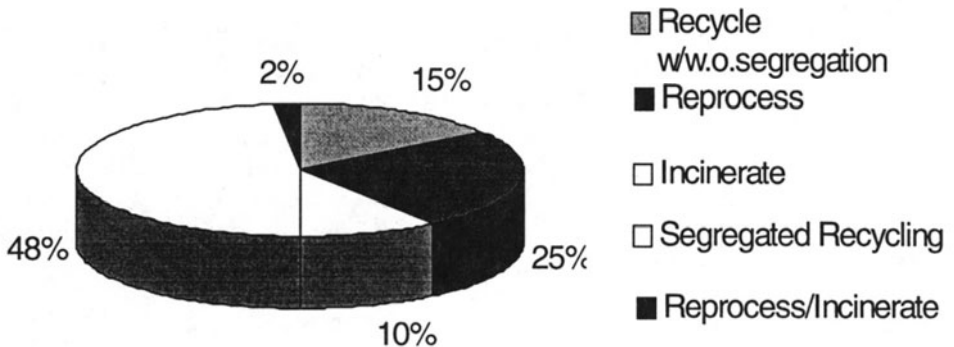


Figure 5 End-of-Life Destinations for Personal Computer –No Landfill

7.0 ANALYSIS RESULTS.

Several case studies have been conducted using this evaluation scheme and the results of two of these are summarized below. The products analyzed are a personal computer processing unit (IBM PS/2) and a 1995 truck instrument panel. In each case the

product was disassembled and the materials identified for each item. End-of-life destination rankings for each item were determined as outlined in Section 4.0. The overall results of these analyses are summarized in Figures 4 through 7, which show the distribution by weight of the recommended end-of-life destinations for the two products. Figures 4 and 6 give the results based on the full range of destinations (economic strategy) and Figures 5 and 7 give the results neglecting landfill disposal (environmental strategy). For these result summaries, when two end-of-life destinations have the same final ranking a combined category is shown.

From the results in Figures 4 and 6, it can be seen that, based on processing economics and market demand for materials, landfill disposal is recommended for most items in each product. This essentially verifies current practice for disposal of durable goods. If landfill disposal is not considered as an option, then the end-of-life destinations with the highest rankings become more varied (Figures 5 and 7). Based on this more environmentally friendly strategy, more than 60 percent of the components by weight are recommended to be recycled in each case.

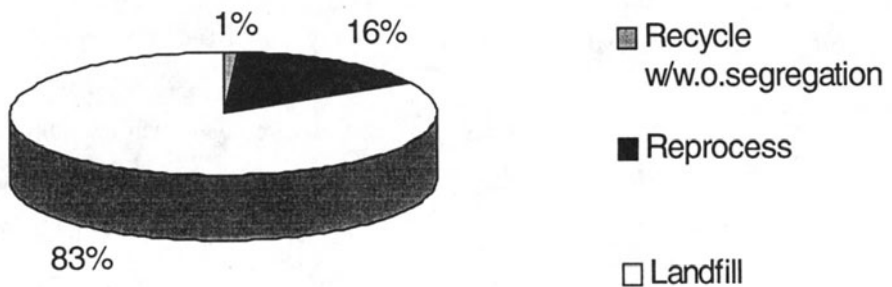


Figure 6 End-of-Life Destinations for Truck Instrument Panel.

8.0 CONCLUDING REMARKS.

A procedure for evaluating and ranking end-of-life destinations for materials and products has been outlined. This procedure can be used for assessing the end-of-life disposition performance of products and as a means of assigning end-of-life destinations for design for environment (DFE) analysis procedures. The numerical ratings at present have been assigned based mainly on current processing economics and the relative recovered value of materials. Alternative rankings based more on environmental considerations could be developed. The present numerical rankings should be continually updated as different material recovery processes become available and as the infrastructure and demand for recycled materials develops. Future expansion of the classification should be focused on an extended material compatibility table and the associated ranking factors.

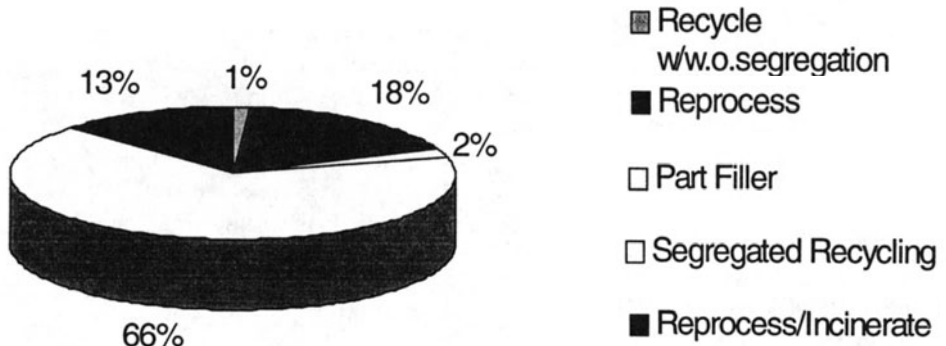


Figure 7 End-of-Life Destinations for Truck Instrument Panel – No Landfill

REFERENCES.

1. Alting, L and Boothroyd, G, 1992, Design for Assembly and Disassembly, *Annals of CIRP*, 41/2,: 625-638.
2. Jovane, F. et al, 1993, A Key Issue in Product Life Cycle: Disassembly, *Annals of CIRP*, 42/2: 651-658.
3. Johnson, M.R. and Wang, M.H., 1995, Planning Product Disassembly for Material Recovery, *Int. Journal of Production Research*, 3/11: 3119-3142.
4. Rapoza, B., Harjula, T, Knight, W.A. and Boothroyd, G., 1996, Design for Disassembly and Environment, *Annals of CIRP*, 45/1: 109-114.
5. Sodhi, M and Knight, W.A., 1998, Design for Disassembly and Bulk Recycling, *Annals of CIRP*, 47/1: 115-118.
6. GE Plastics, Design for Recycling, DFR ENG 6M/0392, no date.
7. Lund, H.F., 1992, *The McGraw-Hill Recycling Handbook*, McGraw-Hill, New York.
8. Stesial, R.I., 1996, *Recycling and Resource Recovery Engineering*, Springer, New York.
9. Bisio, A.L. and Xanthos, M., 1994, *How to Manage Plastics Waste*, Hanser Gardner Publications, Cincinnati.

A METHOD FOR ESTIMATING THE PROFITABILITY OF A PRODUCT DISASSEMBLY OPERATION

S.K. Das

New Jersey Institute of Technology, NJ, USA

KEY WORDS: Disassembly, Economic Analysis, Cost Estimation

ABSTRACT: Disassembly is the process of physically separating the parts in a product. End-of-life product disassembly is slowly growing into a common and worthwhile industrial practice. There are several reasons for this, including, (i) the recovery of valuable and reusable parts or subassemblies, (ii) product separation to facilitate the downstream material recovery process, (iii) the removal of hazardous or toxic materials, (iv) to remanufacture the product for another useful life, and (v) to destroy the proprietary parts or subassemblies. In combination these reasons also help the environmental and ecological detriments associated with product disposal. The process of disassembly tends to be predominantly manual, and the overall economics is still not well understood. In this paper our goal is to introduce a method which will support the “direct disposal?” versus “disassemble?” decision making process. We present a model to compute the disassembly return on investment. This model considers the costs associated with product sortation into disassembly families, disassembly operation costs, and the market value of the output streams. We use this model to generate both a threshold for the disassembly return on investment, and also the maximum allowable disassembly labor time. The model is constructed from empirical evidence gathered from several industrial disassembly facilities. This model can be used to evaluate new and old designs.

1. INTRODUCTION

The process of disassembly attempts to breakup a product into several pieces, with the expectation that the pieces together have a net value greater than the discarded product. But

Published in: E. Kuljanic (Ed.) *Advanced Manufacturing Systems and Technology*,
CISM Courses and Lectures No. 406, Springer Verlag, Wien New York, 1999.

unlike an assembly process the net value added percentage in disassembly is significantly less. This implies that for a disassembly activity to be profitable, the labor time, equipment needs, energy needs, skill needs, and space requirements must be relatively small. During product design, designers are rarely concerned with the disassembly or the reuse of parts. Consequently, disassembly tends to be an expensive process and is usually not a viable end of life option. The process of disassembly tends to be predominantly manual, and the overall economics is still not well understood. There is much reported research on the life cycle analysis (LCA) of products [1]. These LCA models attempt to capture all costs associated with production, usage, and disposal of the product. They usually account for a disposed product's costs either as a whole or in parts. But, since the cost to disassemble the part is not obvious, disassembly is not easily justified in these models.

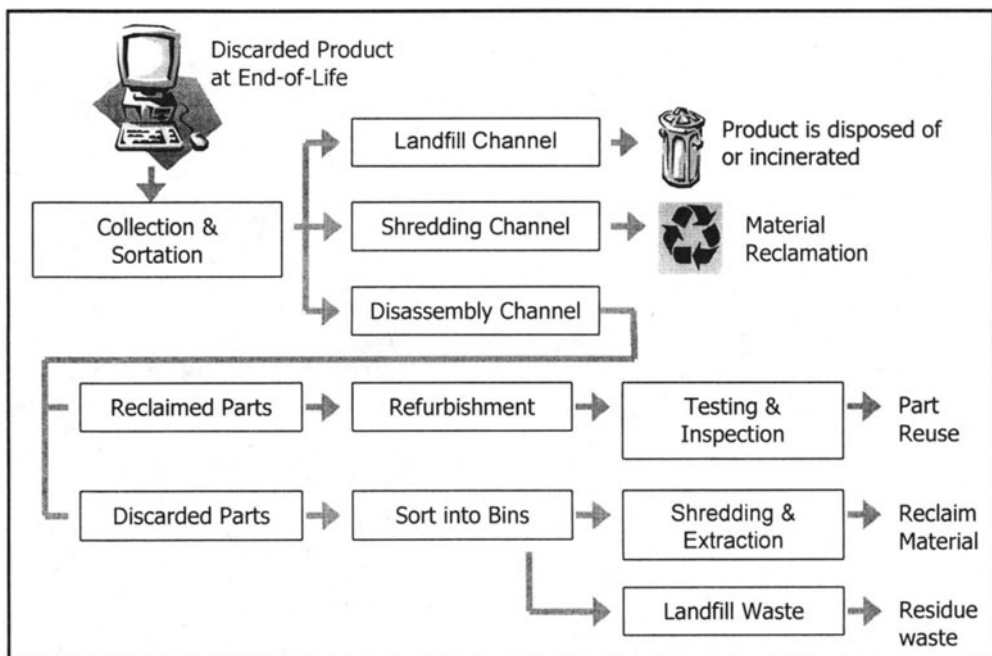


Fig. 1: The Product Disposal Channels

The lack of an effective approach for estimating the product end-of-life disassembly effort is one of the primary reasons limiting a more widespread interest in product disassembly. As a result products with a good number of reusable/recyclable parts are disposed of or recycled in their entirety. For example in the case of computers and copiers, parts such as CRT glass, keyboard caps, drive motors, transformers, and steel casings, could all be given a new life if they could be disassembled efficiently. In the long run disassembly issues must be addressed and resolved during the product design process. This requires the availability of tools that can readily and accurately estimate the future disassembly cost. Present

research is primarily concerned with estimating end-of-life value, and there is a lack of effective tools for cost and effort estimation.

At the end of its life a product may be processed in one of three possible channels as shown above in Figure 1: (i) direct disposal to a landfill site, (ii) shredded with subsequent material recovery followed by landfill disposal of the residual waste, and (iii) partial or full disassembly to facilitate recovery of assets and materials. Ecologically, the best channel is the third. In this paper our goal is to introduce a method which will support a recycling facility in deciding whether a product can be profitably processed in the disassembly channel. We present a model to compute the disassembly return on investment. This model considers the costs associated with product sortation into disassembly families, disassembly operation costs, and the market value of the output streams. We use this model to generate both a threshold for the disassembly return on investment, and also the maximum allowable disassembly labor time. The model is constructed from empirical evidence gathered from several industrial disassembly facilities. This model can also be used to evaluate new designs to see the extent to which they satisfy ecodesign principles.

2. CAUSES OF HIGH DISASSEMBLY COSTS

Disassembly generates two output streams, reclaimed parts and discarded parts. Discarded parts are sorted into commodity bins which have some material commonality constraints. Table 1 lists some example output bins and their average market price in the US.

Table 1: Common Commodity Output Bins from a Disassembly Facility

	Commodity	Vendor	Possible Outcome	Price/lb
1	Steel	Ferrous Dealer	Industrial uses, landfill	\$ 0.02
2	UPS	Ferrous Dealer	Industrial uses, landfill	\$ 0.02
3	Magnets	Ferrous Dealer	Industrial uses, landfill	\$ 0.02
4	Aluminum High	Non-Ferrous Dealer	Al for Industry	\$ 0.49
5	Aluminum Mix	Non-Ferrous Dealer	Alum, landfill	\$ 0.19
6	Copper High	Non-Ferrous Dealer	Cu	\$ 0.67
7	Copper Mix	Non-Ferrous Dealer	Cu, Landfill	\$ 0.08
8	Gold Ends	Precious Metal Dealer	Industrial gold, landfill	\$ 0.93
9	Softfoam	Packaging Vendor	Home insulation and carpet	
10	CRTS	Glass Vendor	reused, landfill, glass	
11	Recycle Plastic	Plastics Vendor	countertops, showerstalls	\$ 0.02
12	Hard Mix Plastic	Plastics Vendor	Tiles, decking, landfill, etc	\$(0.11)

Each output stream involves several activities, including 1. Collection, 2. Sorting, 3. Product Handling, 4. Disassembly Instructions, 5. Part Separation, 6. Part Handling, 7. Part Cleaning, and 8. Part Testing and Inspection. Our research confirms that these activities are inherently expensive due to several cost drivers, the most important of which are:

- Non-homogenous product stream - This make it difficult to achieve economies of scale and leads to a labor intensive activity and a high setup effort.

- Use of quick assembly principles - This often leads to a higher disassembly effort. For instance permanent fasteners, nesting parts interference fits, etc.
- Use of destructive separation methods (e.g., saws, hammers, and cutter) - These are labor intensive activities.
- Part outfeed is cumbersome - This usually means manual material handling is needed.
- Unknown material properties and value - It thus not obvious to the disassembly facility, which part goes where and what is worth disassembling.
- Cleaning involves abrasive and toxic materials
- Wear and tear is not uniform - This means not all parts are okay, so the disassembly yield is low.
- Process planning is not well defined – There are no efficient methods for generating process plans
- Material composition of parts is not obvious to the bin sorter
- Material extraction technologies limit the level of purity in each output bin

A disassembly facility is usually equipped with a few tools, and air gun and shear cutter being the most common. Since fasteners are the primary opposition to the separation process, the most labor intensive part of the disassembly process is unfastening.

3. DISASSEMBLY ECONOMICS

We model disassembly as a multi-step process. During each step some reusable parts or discarded parts may or may not be generated. To generate these parts the worker performs one of two classes of activities: 1. Unfastening Processes - where a fastening device is removed in an operation, which reverses the assembly fastening action. 2. Disassembly Processes – All other activities that facilitate the separation of the product into its parts. The first step in the economic analysis is project what the outputs of the disassembly process for a given product will be. This is done by disassembly planner who is familiar with the bill-of-materials of the product and the fastening and joining structure of the product. Let $i = 1, \dots, N$ be the commodity output bins in the facility and $j = 1, \dots, M$ the reusable parts reclaimed from the product. Then we introduce the following notation:

W_i	the net generated weight of bin i output per unit product
V_i	the market value of bin i per unit weight
R_j	the reuse value of reclaimed part j

Note that the part reuse value is net of any cleaning, refurbishment, and inspection costs. Estimation of these variables can be done from experience data or historical norms. For instance in the case of personal computers, we can expect that 45% of the aluminum content will enter the Aluminum High bin, 25% the Aluminum Mix bin, and 30% the general waste bin. More accurate numbers are derived from developing a detailed disassembly process plan for the product. Pnueli and Zussman [5], Johnson and Wang [3] and Penev and Ron [6] among others have suggested methods for deriving a product disassembly plan.

There are three primary cost elements involved. First there is the direct labor time associated with the disassembly. There are several approaches by which this can be done. Kroll [4] developed a method for estimating the disassembly time using work measurement analysis. Vujosevic et al [7] also used a work measurement tool to estimate disassembly times in developing a simulator for maintainability analysis. Alternatively, a few products can be disassembled and a labor estimate derived using time and motion analysis. The second cost element is the disassembly effort. This includes the associated tooling and fixturing needs, part accessibility, worker skill and instructions, process hazards, and force requirements. Das et al [2] propose a scheme for estimation the disassembly effort index (DEI) for a product, and this is amenable to our economic analysis. To compute the DEI score as a function of seven factors, which are (i) time (ii) tools (iii) fixture (iv) access (v) instruct (vi) hazard and (vii) force requirements. The DEI score ranges from zero upwards, with zero indicating no effort. The third element is the material sorting and logistics cost associated with the disassembly activity. We introduce the following notation to represent these costs.

- α the labor cost rate per unit time including all direct time related costs
- β the overhead or effort cost rate per unit index
- C the sorting and logistics cost associated with the product
- T the total disassembly time of the product
- Δ the DEI score for the product

Observe that β is representative of the indirect and overhead cost and can be estimated by calibrating past cost performance of the facility with the DEI scores. For instance, if the indirect and overhead cost for five previously processed products can be estimated. Then, we can compute the DEI score for these five and subsequently derive a trial β for each. The average of these would then provide a calibrating β . The profitability of the disassembly operation then is a function of the associated costs and values generated. We propose the following measure for the disassembly return on investment.

$$\text{Disassembly Return on Investment} = R_d = \frac{\sum V_i + \sum R_i - \psi}{\alpha T + \beta \Delta + C} - 1 \tag{1}$$

where, ψ represents the greater value from processing the product in either the shredding channel or the landfill channel. Often ψ will be negative implying a cost. For a given scenario one could determine a threshold level for R_d , and that could be used to decide whether disassembly is an attractive alternative.

4. AN EXAMPLE ANALYSIS

The DeskJet computer printer shown in Figure 2 was disassembled and evaluated. This class of product has a useful life of 3 to 4 years and is disposed of in relatively large quantities. Normally the entire product would be landfilled “as is”. the product can be disas-

sembled using the nine step plan shown in table 2. In table 3 the output bins from the disassembly operation are listed.

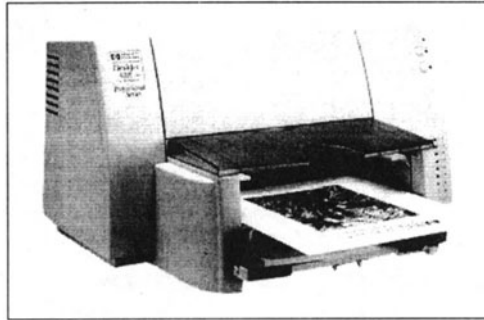


Fig. 2: The DeskJet Printer

Table 2: The Disassembly Plan for the DeskJet Printer

Step #	Description
1	Release snaps and pull out front tray assembly
2	Use chisel level to remove side carriage cover
3	Unscrew and remove top fasteners (x2)
4	Release bottom snaps and remove printer upper housing
5	Release latches and remove printer cartridge (x2) from cradle
6	Unscrew (x3) and remove power supply and connection unit
7	Using scissors cut out ribbon wire to cartridge cradle
8	Unscrew (x2) and then use lever to remove circuit board
9	Use lever to break bottom printer housing from carriage assembly

We found that for the proposed plan $T = 1.20$ mins and $\Delta = 104$. There is one reusable part, which is the power supply unit, and for it the projected market value is $R_1 = \$1.90$. For the four output bins market prices are $V_1 = \$0.02/\text{lb}$, $V_2 = \$0.02/\text{lb}$, $V_3 = \$0.95/\text{lb}$, and $V_4 = \$-0.03/\text{lb}$. Other cost parameters are as follows $C = \$1.07$, $\alpha = \$10.70/\text{hr}$, $\beta = \$0.014/\text{unit score}$, and $\Psi = \$0.12$.

Table 3: Disassembly Output from the Printer

Bin #	Contents	W_i
1.	Recyclable Plastic	8.0 lbs.
2.	Steel	9.0 lbs.
3.	Electronic Circuit Board	0.64 lbs.
4.	Landfill Waste	1.67 lbs.

The R_d for the example printer therefore is 10.75%. Note that R_d is representative of the gross margins and hence is a direct measure of the profitability. R_d is sensitive to a variety of factors. The most significant issue is the market related values, since these are changing constantly. Many disassemblers are reluctant to maintain output inventory since it could

adversely affect their profitability. Another key issue is where to stop the disassembly. The above plan assumed completed disassembly. Figure 3 charts the change in R_d with each disassembly step. Clearly, if we had stopped after step 6 then R_d would have been optimal. A disassembler therefore needs to plot the curve and determine the optimal stopping point.

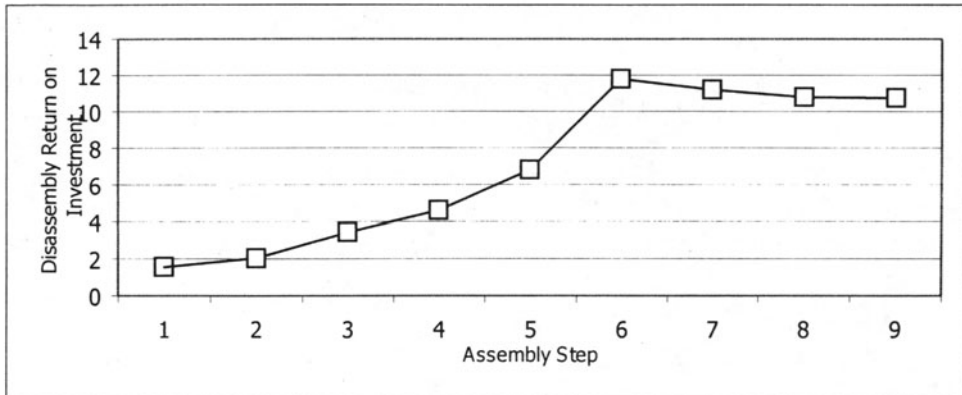


Fig. 3: R_d and the Disassembly Steps

5. SUMMARY

A method to assist a recycling facility decide whether disassembly is profitable has been proposed. Such an analysis will help increase the percentage of disposed products that enter the disassembly channel. The economic model requires the user to first have a disassembly plan, and market prices for the output commodities. We can continue to expect that disassembly will become a more widespread activity, and can foresee the construction of large-scale facilities processing high volumes of disposed products. We are already seeing the early phases of this evolution in Europe and the United States. Such an evolution cannot be simply driven from an environmental concern, but must also be profitable and/or cost effective. There continues to be the need for models to support this economic analysis. Most of the facilities that we studied were manual operations, but one can expect more automation in the future.

REFERENCES

1. Carnahan, J.; Thurston, D.: Trade-off modeling for product and manufacturing process design for the environment, *Journal of Industrial Ecology*, Vol. 2(1), (1998), pp. 79-92
2. Das, S.K.; Yedlarajah, P.; Narendra, R.: An approach for estimating the end-of-life product disassembly effort and cost, NJIT Technical report, Newark, NJ, USA, 1998
3. Johnson, M.; Wang, M.: Planning product disassembly for material recovery opportunities, *International Journal of Production Research*, Vol. 33(11), (1995), pp. 3119-3142

-
4. Kroll, E.: Application of work-measurement analysis to product disassembly for recycling, *Concurrent Engineering Research and Applications*, Vol. 4(2), (1996), pp. 149-158
 5. Penev, K.; de Ron, A.: Determination of a disassembly strategy, *International Journal of Production Research*, Vol. 34(2), (1996), pp. 495-506
 6. Pnueli, Y.; Zussman, E.: Evaluating end-of-life value of a product and improving it by redesign, *International Journal of Production Research*, Vol. 35(4), (1997), pp. 921-942
 7. Vujosevic, R.; Raskar, R.; Yetukuri, N.; Jyotishankar, M.; Juang, S.: Simulation, animation, and analysis of design disassembly for maintainability analysis, *International Journal of Production Research*, Vol. 33(11), (1995), pp. 2999-3022

ESTABLISHING THE ECODESIGN STRATEGY

M. Kljajin

University J. Jurjia, Slavonski Brod, Croatia

KEY WORDS: Ecodesign, Strategy, Environment, MET Matrix

ABSTRACT: This paper elaborates steps of establishing the ecodesign strategy for the selected product to be redesigned. It also establishes how much latitude the project team needs, and whether it should proceed incrementally (evolution) or more drastically (revolution). To benefit full from such innovations, it is important to consider which ecodesign routes are the best from both the environmental and the corporate perspective. In one step therefore the paper focuses on establishing the most promising ecodesign strategy for the project. The problem which was defined in the design brief in earlier steps is now analysed in greater detail. There are three very important questions to answer: «What can the company do?», «What does the company want to do?» and «What must the company do?». Based on the analysis of the environmental product profile and the company's drivers for ecodesign, priorities are set concerning the most suitable ecodesign strategy to follow in the project. The paper ends with a specification of the environmental requirements for the planned product.

1. INTRODUCTION

Ecodesign can lead to the birth of new ideas. To benefit full from such innovations, it is important to consider which ecodesign routes are the best from both the environmental and the corporate perspective. Therefore it has to be focused on establishing the most promising ecodesign strategy for the project. There are three questions:

Published in: E. Kuljanic (Ed.) *Advanced Manufacturing Systems and Technology*,
CISM Courses and Lectures No. 406, Springer Verlag, Wien New York, 1999.

- 1) What can the company do? - This depends on the existing environmental product profile.
- 2) What does the company want to do? - This relates to the internal drivers, or the objectives and possibilities available within the company.
- 3) What must the company do? - This is dictated by the external drivers, in other words, by the need to include the environmental requirements of other players such as competitors, customers and government.

Based on the analysis of the environmental product profile and the company's drivers for ecodesign, priorities are set concerning the most suitable ecodesign strategy to follow in the project.

2. ESTABLISHING THE MOST SUITABLE ECODESIGN STRATEGY

The different routes that can be followed in ecodesign are called ecodesign strategies. A classification of ecodesign strategies is as follows:

- 1 Ecodesign strategy - Selection of low-impact materials (clean materials, renewable materials, low energy content materials, recycled materials, recyclable materials).
- 2 Ecodesign strategy - Reduction of material usage (reduction in weight, reduction in transport/volume).
- 3 Ecodesign strategy - Optimisation of production techniques (alternative production techniques, fewer production steps, low/clean energy consumption, less production waste, few/clean production consumables).
- 4 Ecodesign strategy - Optimisation of the distribution system (less/clean/reusable packaging, energy-efficient transport mode, energy-efficient logistics).
- 5 Ecodesign strategy - Reduction of impact in the user stage (low energy consumption, clean energy source, few consumables needed, clean consumables, no wastage of energy or consumables).
- 6 Ecodesign strategy - Optimisation of initial lifetime (reliability and durability, easy maintenance and repair, modular product structure, classic design, strong product-user relations).
- 7 Ecodesign strategy - Optimisation of the end-of-life system (reuse of product/components, remanufacturing/refurbishing, recycling of materials, safe incineration).

A procedure of establishing an ecodesign strategy is illustrated in Fig. 1 which can be used to select systematically the most suitable combination of ecodesign strategies for a particular project. The procedure contains five activities. It starts with the analysis of the environmental product profile, followed by analysis of the internal and external drivers for ecodesign. Based on these analyses, improvement options are generated. To select the most suitable improvement options, a feasibility study is executed. Finally, the improvement options which are expected to be the most promising are presented as the project's ecodesign

strategy. All these steps must be implemented by the team members, one of whom should represent management. The team should preferably include staff from the marketing, purchasing, logistics and production departments. The results of each step can be, recorded on a work sheet.

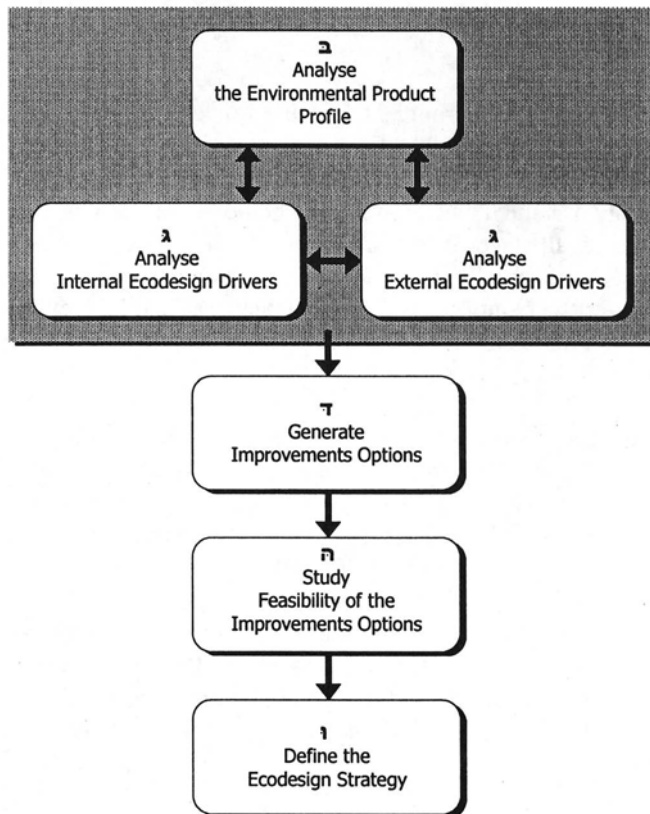


Fig. 1: Establishing an ecodesign strategy

3. ANALYSE THE ENVIRONMENTAL PRODUCT PROFILE

A good understanding of the main environmental problems the product causes during its total life cycle is essential to ecodesign. To obtain this, the project team should first decide the exact subject for the environmental profile. In ecodesign it is not enough to consider just the physical product; the whole product system needed to ensure the product's proper functioning must be considered as well. In what follows, the term «product» is used to mean the product system as a whole. After this, the team should decide on how it wishes to establish the environmental profile of the existing product. Several methods, qualitative and quantitative, are available to do this. This section describes two such qualitative tools:

the MET Matrix and the Ecodesign Checklist. Note that the term «qualitative» does not assume that an environmental profile can be made without using figures or without searching for the required data. If the project team decides to analyse the environmental product profile in more detail, it can make use of computer tools which have been developed for this purpose.

4. THE MET MATRIX

When establishing a product's environmental profile it is essential to take into account all the types of environmental problem that a product system produces throughout its life cycle. The MET Matrix is a means of organising such an analysis. The letters MET stand for Material cycle, Energy use and Toxic emissions. The power of the matrix is that it helps a project team to focus on all stages of the product life cycle (vertically), and on the various environmental effects (horizontally) a product has in the subsequent life cycle stages. To prevent stumbling over the complexity of environmental effects, the environmental problems are grouped into three main areas: the Material cycle (input/output), Energy use (input/output) and Toxic emissions (output) (Table 1).

The column on materials is intended for notes on environmental problems concerning the input and output of materials. This column should include figures about the application of materials which are non-renewable or create emissions during production (such as copper, lead and zinc), incompatible materials and inefficient use or non-reuse of materials and components in all five stages of the product life cycle.

The energy consumption during all stages of the life cycle is listed in the column on energy use. Include energy consumption for the product itself, and of transport, operating, maintenance and recovery as well. Inputs of materials with an extremely high energy content are listed in the first cell of this column. Exhaust gases produced as a result of energy use are included in this column.

The column on toxic emissions is dedicated to the identification of toxic emissions to land, water and the air in the five life cycle stages.

Table 1: MET Matrix (in general)

Life cycle stage		Material cycle (Input/Output)	Energy use (Input/Output)	Toxic emissions (Output)
Production and supply of materials and components				
In-house production				
Distribution				
Utilisation	Operation			
	Servicing			
End-of-life system	Recovery			
	Disposal			

Defining the environmental product profile using the MET Matrix, it is recommended to split the analysis into three separate activities: defining the product system boundaries, performing a needs analysis and performing a functional product analysis. *First* the team defines what exactly belongs to the product system being studied and what does not. For ecodesign it is essential not to focus on the physical product only, but to consider also the products and consumables which are necessary for the product to function properly over its total lifetime. *Secondly*, the team performs a needs analysis with respect to the product system just defined. There are two central questions: how does the actual product fulfil the needs it is meant to fulfil, and can a product system be developed that fulfils the same needs in a radically more effective and efficient way? *Thirdly*, a functional product analysis is made, focusing on the physical product and its separate components, using the MET Matrix.

A functional product analysis starts with a discussion of the product's functionality, its weak and its strong aspects (which parts or functions tend to cause the product to fail), the product's actual lifetime and its energy consumption. The product is then taken to bits, the weights of the various sub-assemblies and components are measured, the type and amount of materials and components used are listed, and the connections between them identified.

To perform the functional product analysis systematically, the team should fill out the MET Matrix for the main product, considering its environmental effects at all stages of its life cycle. Ensure that auxiliary materials used in all stages of the life cycle are taken into account. If a certain sub-assembly or component turns out to be a serious environmental bottleneck, it can be investigated in a separate MET Matrix. Examine all the cells of the matrix and highlight those where there are environmental bottlenecks on the MET Matrix of work sheet. Use as many figures in the matrix as possible to prevent working with vague statements.

To avoid forgetting any environmental impacts, use the Ecodesign Checklist which is described below. This checklist will ensure that the project team asks the most relevant questions related to the product life cycle.

5. THE ECODESIGN CHECKLIST

The Ecodesign Checklist provides support for the qualitative environmental analysis by listing all the relevant questions that need to be asked when establishing environmental bottlenecks during the product life cycle. The checklist can thus be used to complement the MET Matrix described above. The checklist also suggests improvement options for areas where environmental problems are identified. The product life cycle has been divided into five life cycle stages as it shown in the Ecodesign Checklist (Table 2).

Table 2: Ecodesign Checklist (in general)

↓	Questions	Answers
	The Ecodesign Checklist needs analysis:	
0	How does the product system actually fulfil social needs?	
0.1	What are the product's main and auxiliary functions?	
0.2	Does the product fulfil these functions effectively and efficiently?	
0.3	What user needs does the product currently meet?	
0.4	Can the product functions be expanded or improved to fulfil users' needs better?	
0.5	Will this need change over a period of time?	
0.6	Can we anticipate this through (radical) product innovation?	
	Life cycle stage 1: Production and supply	
1	What problems can arise in the production and supply of materials and components?	
1.1	How much, and what types of plastic and rubber are used?	
1.2	How much, and what types of additives are used?	
1.3	How much, and what types of metals are used?	
1.4	How much, and what other types of materials are used?	
1.5	How much, and which type of surface treatment is used?	
1.6	What is the environmental profile of the components?	
1.7	How much energy is required to transport the components and materials?	
	Life cycle stage 2: In-house production	
2	What problems can arise in the production process in your own company?	
2.1	How many, and what types of production processes are used (including connections, surface treatments, printing and labelling)?	
2.2	How much, and what types of auxiliary materials are needed?	
2.3	How high is the energy consumption?	
2.4	How much waste is generated?	
2.5	How many products don't meet the required quality norms?	
	Life cycle stage 3: Distribution	
3	What problems arise in the distribution of the product to the customer?	
3.1	What kind of transport packaging, bulk packaging and retail packaging are used (volumes, weights, materials, reusability)?	
3.2	Which means of transport are used?	
3.3	Is transport efficiently organised?	
	Life cycle stage 4: Utilisation	
4	What problems arise when using, operating, servicing and repairing the product?	
4.1	How much, and what type of energy is required, direct or indirect?	
4.2	How much, and what kind of consumables are needed?	
4.3	What is the technical lifetime?	
4.4	How much maintenance and repairs are needed?	
4.5	What and how much auxiliary materials and energy are required for operating, servicing and repair?	
4.6	Can the product be disassembled by a layman?	
4.7	Are those parts often requiring replacement detachable?	
4.8	What is the aesthetic lifetime of the product?	
	Life cycle stage 5: Recovery and disposal	
5	What problems can arise in the recovery and disposal of the product?	
5.1	How is the product currently disposed of?	
5.2	Are components or materials being reused?	
5.3	What components could be reused?	
5.4	Can the components be disassembled without damage?	
5.5	What materials are recyclable?	
5.6	Are the materials identifiable?	
5.7	Can they be detached quickly?	
5.8	Are any incompatible inks, surface treatments or stickers used?	
5.9	Are any hazardous components easily detachable?	
5.10	Do problems occur while incinerating non-reusable product parts?	

The questions to ask are given in the left-hand columns of the tables opposite; some improvement options could be suggested in the right-hand columns. The checklist starts with a needs analysis, which is a series of questions concerning the functioning of a product as a whole. The needs analysis is followed by five sets of questions that are relevant to the subsequent stages of the product's life cycle. The main question asked in a needs analysis is to what extent does the product fulfil its main and auxiliary functions. This question should be answered before focusing on the environmental bottlenecks in the various stages of the product's life cycle.

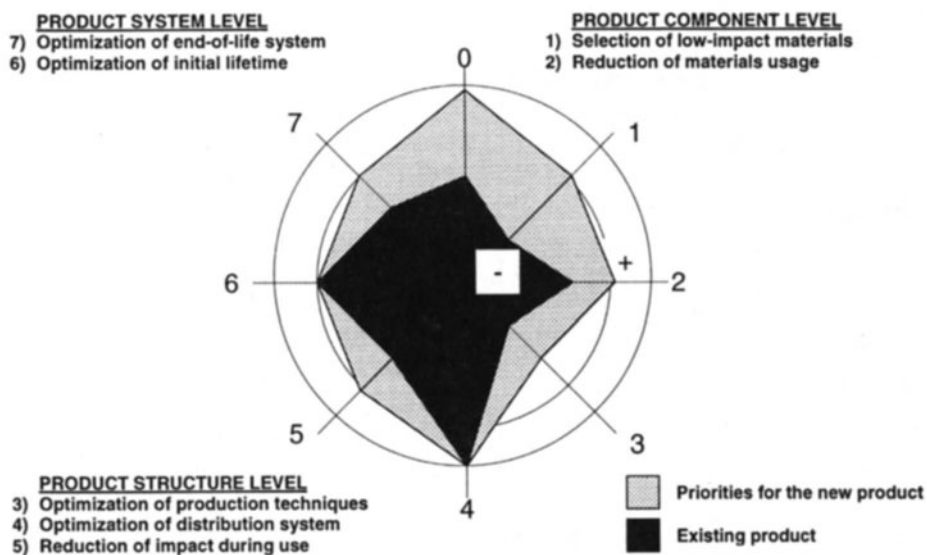


Fig. 2: The ecodesign strategy wheel

6. CONCLUSION

During the analysis of the environmental product profile, many improvement options will have come up spontaneously. These improvement options have been filled out on work sheet, grouped according to a classification of seven ecodesign strategies. The recommended classification of ecodesign strategies, called the ecodesign strategy wheel, is illustrated in Figure 2. To generate even more improvement options, the project can also go the other way around by using the ecodesign strategy wheel as an option-generating tool. The model visualises the strategies that can be followed for ecodesign. Some relate mostly to product components, some to product structure and others to the product system.

The ecodesign strategy wheel visualises which strategies can be followed for ecodesign in general. The model shows which design solutions can lead to improvement of the environmental profile of a product, without describing the resulting separate environmental ef-

fects. At this moment in the step-by-step plan, the ecodesign strategy wheel is used as a general framework, provoking new improvement options. Later, the project team can use the ecodesign strategy wheel of Figure 2 to visualise and communicate the established ecodesign strategy inside and outside the company. First the environmental profile of the old product is sketched on a rough five-point scale for reference. Then the ecodesign priorities for the new product are added. The result is a clear picture of the level of ecodesign ambition for a certain ecodesign project. The resulting surface visualises the ecodesign strategy which is established after evaluation of the proposed ecodesign strategy from both the environmental and the business perspective; the bigger the difference between the two surfaces, the higher the ambitions for ecodesign are set.

The options for improvement, clustered in accordance with the ecodesign strategy wheel, are subsequently assessed for their anticipated environmental merit, their technical, organisational and economic feasibility, and their market opportunities. Which options are in accordance with the internal and external drivers for ecodesign? Ecodesign priorities must be established by the entire team; all representatives of management and the marketing, purchasing, research and development, and production departments should have their say. To set the ecodesign priorities systematically, the work sheet Ecodesign Priority Matrix can be used. List the options and give each option a priority rating plus the some labels to indicate whether the option should be realised in the short or long term. The technical feasibility and the market opportunities are estimated using the techniques that are normally applied in the company.

The last activity deals with concluding and visualising the results of establishing the most promising ecodesign strategy for the project. The establishment of ecodesign priorities can be drawn up and visualised by adding two activity lines to the ecodesign strategy wheel: short-term activities versus long-term activities. This makes it easy to communicate the ecodesign strategy both internally and externally. A two-track policy is stimulated: in the short term the company can be motivated by options for improvement which are easy to carry out; this gives rise to sufficient motivation to tackle other matters, the costs of which will be recovered only after additional investments have been made. Finally, the ecodesign strategy which is established for the short term is included in the list of requirements for the product to be redesigned. The environmental requirements should be described quantitatively as far as possible. This will facilitate at a later stage the mutual comparison of various product concepts or detailed solutions. In practice, the analysis of environmental problems and thinking creatively about options for improvement is best done in groups. Such a group consists of the project team and possibly other stakeholders.

REFERENCES

1. Steinhilper, R.; Hieber, M.; Osten-Sacken, D.: Decision Management Systems for Downcycling/Upycling/Eco Design - Interdisciplinary Experiences, Proceedings of the

4th CIRP International Seminar on Life Cycle Engineering 1997, Chapman and Hall, London 1997, 324-334.

2. Steinhilper, R.: Eco-Design und Eco Innovation - Pionierleistungen und Praxisbeispiele, Niedersachsen, Umweltministerium, Tagung Abfallvermeidung bei Produktgestaltung und -nutzung, Hannover 1997, 37-51.
3. Steinhilper, R.: Product Recycling and Eco-Design: Challenges, Solutions and Examples, Institution of Electrical Engineers - IEE, London, International Conference on Clean Electronics Products and Technology (CONCEPT), Edinburgh IEE, 1995 (IEE conference publication, 416).
4. Steinhilper, R. (Ed.): Umwelt- und recyclinggerechte Produktentwicklung/Eco Design, Haus der Technik e.V. - HDT, Essen 1995.
5. ...: Environmental Life Cycle Management: A Guide To Better Business Decisions, National Office of Pollution Prevention and the Hazardous Waste Branch of Environment Canada, April 1997.
6. Pahl, G.; Beitz, W.: Engineering Design - A Systematic Approach, Second Edition, Springer-Verlag, Berlin-Heidelberg-New York 1996.
7. Brezet, H.; van Hemel, C.: Ecodesign – A promising approach to sustainable production and consumption, United Nations Publication, UNEP, 1997.

QUALITY IMPROVEMENT AND DESIGN OF EXPERIMENTS
AN INDUSTRIAL APPLICATION

E. Gentili, M. Formentelli and G. Trovato
University of Brescia, Brescia, Italy

KEY WORDS: Quality Improvement, Design of Experiments, Industrial Application.

ABSTRACT: Quality improvement is an important feature in seamless tube production because of the critical way in which they are used. In order to obtain this improvement big investments are needed for building new furnaces and new quenching equipments. Taking into account the present economical situation in Italy, managers prefer a limited investment with a short term pay back time. We decided to pursue quality improvement using the chances given by the "DOE" [1].

1. INTRODUCTION

The steel plant we considered is one of the most important in Italy in the seamless tube production. Products must meet BS 5750, API Q1 and ASME NCA-3800 standards. The kinds of steel most frequently requested by customers are AISI 4140, AISI 4130, 25 CrMo4, 25CrMo6 and C43. The tubes are produced for car, motorbike and oil use and they are treated in a homogeneous and repetitive way in lots of weight between 20 and 100 kN. Fig.1 shows the flowchart of the hadening and tempering plant able to treat 35 kN/h.



Figure 1 – Flowchart of the plant

The heating system of the hardening module include five circular inductors, of a maximum power of 1200 kW at a frequency of 2000 Hz. Two serial heads equipped with water nozzles compound the quenching system: the first one is tangential (bolts of water forming a hole of variable diameters), the second one is radial.

The handling device pushes the tubes inside the furnace, leaving no space between the subsequent pieces subjected to a rotational and translational speed. The rotational speed allows a more uniform cooling during the quenching phase. The nozzles of the quenching heads are distributed in circular groups on orthogonal plans in respect of the tube axis. In the two first tangential heads it is possible to change the water hole diameter, according to the tube diameter, and the amount of water for each head. In the radial head only the amount of water can be governed. The total water capacity is 100 m³/h.

The tempering furnace presents feeding rolls and several pipes in which natural gas and air are used. The atmosphere inside the furnace has to be such so as to eliminate surface oxidation. Tubes are inserted in blocks and in parallel, using the full length of the furnace. The heat comes from the floor and the ceiling but not from the side walls and refractory barriers separate different heating zones, allowing the right temperatures for heat treatment needs. The tempering phase is simpler than the hardening one because good provisional models for the final mechanical properties exist. The important parameters are only the tempering temperature and the time while the tubes remain at the temperature: they are well controlled so the process seems to be problem free. In effect positioning the tubes in a parallel group gives the possibility of a heterogeneous temperature between the central and lateral parts. A second critical aspect is the repeatability in the time of the thermal treatment independently from the operation state and external factors.

2. SELECTION OF THE STEEL TYPE AND OF THE RESPONSE VARIABLES

We have considered different hardening and tempering steels: AISI 4140, AISI 4130, 25CrMo4, 25CrMn6 and C43. We have chosen the AISI 4130, less hardenable than the AISI 4140, in order to carry out our experiments. This steel is used to produce precision seamless tubes, cold-drawn and tempered for oil tools. The production process includes pickling, tapering, cold-drawing, normalising, roller straightening, front and tail cutting, facing and quality control.

Our aim is to reach a structure as martensitic as possible. This problem does not arise with the AISI 4140 steel and because of this reason it has not been chosen for our experiments. The AISI 4130 can produce some changes in the outer diameter and thickness of the tubes after quenching especially if martensite and bainite represent each 50% of the structure.

We have considered the output variables taking into account the requirements of the customer. The first set of output variables includes the mechanical properties of the hardened and tempered tube: ultimate tensile stress R_m (>677 N/mm²), proof stress R_s ($542 - 643$ N/mm²) and percentage elongation ($>19.5\%$). Tests must conform to the ASTM A370 standard. The second output variable is the hardness on perpendicular layers of the tube. Customer requirements impose a minimum hardness $HRC_{min} = 16.0$, a maximum hardness $HRC_{max} = 22.0$ and a difference inferior to 4 points of the average hardness in the

four sectors at the same distance from the edge. The third set of output variables considers dimensions and defects. Customers require tolerances for the outer diameter and for the thickness of the tubes and the absence of hardening cracks and surface defects.

Consequently we have considered the mechanical characteristics and hardness of the tube after tempering, their dimensional variations after hardening and tempering, the hardness on section of the tube after hardening. The control of the last variable is not a customer requirement, but it is useful for evaluating the depth in hardening and enables a test on the product in an intermediate phase of the process.

The measuring procedure of the mechanical characteristics and of the hardness of the tube after tempering requires the cut of a specimen 600 mm long from the tube tail using a water cooled blade. From this piece we cut two longitudinal and opposite (at 180°) specimens (according to the ASTM A370 standard) for the tensile stress and a ring 40mm thick with parallel faces and with a surface adequately finished for hardness test (API SCT standard). The measuring procedure of the size change in the tubes after hardening and tempering requires the use of micrometer calipers to measure the outer and the inner diameters at a distance of 200 mm from the ends of the tube and along three generating lines at 120°. These were precedently punched with the letters A,B,C to enable the measurement in the same positions after the heat treatment. Size data have been collected at front and tail ends before and after hardening and only at the tail after tempering, because the front specimen was cut just after hardening.

The measuring procedure of the hardness on the radial section after hardening requires to cut a 800 mm long specimen from the point of the tube using a oxyhydrogen flame. We used the central part, far away from the cut area, to produce a 40 mm thick ring, with parallel faces and with the surface appropriately finished for hardness tests (API SCT standard).

3. CHOICE OF THE EXPERIMENTAL DESIGN

At first we examined the controllable and uncontrollable factors of the plant. Some controllable parameters are the same in the hardening and in the tempering process: kind of steel and identification code of the casting, diameter and thickness of the tube, feeding speed.

In the hardening process we have also the adjustment parameters of the induction furnace (power, voltage, frequency) influencing the peak temperature of the tube in the austenitizing phase, the water flow through the nozzles of the two hardening heads, the diameter of the water hole produced by the tangential hardening head, the mechanical characteristics of the incoming tube (controllable by a preliminary normalising process and the temperature of the tube out-coming from the hardening heads (parameter non easily controllable). The other controllable factor in the tempering phase is the temperature of the heating areas.

There are two uncontrollable factors in the hardening phase: the water pressure and the temperature of the incoming water. There are also two uncontrollable factors in the tempering phase: the uniformity of the temperature between the centre and the walls of the

furnace and the mechanical characteristics of the hardened tube. In effect the aim of the experiments was to find a better way to control this parameter.

The number of the controllable factors and the difficulties in operating precise adjustments encouraged us to consider only two levels of the factors. Our experiments were costly not only because of workers, energy, laboratory tests, etc., but also because of disturbances inducted in the production regularity of the plant. Consequently we decided to adopt only three factors (at two levels) with two replicates (2^3 factorial experiment with 16 runs).

At the moment, the tempering process is easier to control than the hardening one because we have a better knowledge of the effect of the factors on the quality of the product. Thus we have chosen the three factors from the controllable parameters of the hardening process and we have maintained the same level of controllability of the tempering phase.

The three factors of the experiment are: the austenitizing temperature, the diameter of the water hole on the head of the tangential quenching unit, the water flow through the nozzles of the two quenching heads. We can make the following points:

- 1) we were able to determine the austenitizing temperature adjusting the parameters of the induction furnace,
- 2) we used a preliminary normalising process to guarantee the mechanical characteristics of incoming tubes,
- 3) we did not consider the temperature of the out-coming tube from the quenching heads because all the tests guaranteed that the tubes reached the level M_f , The temperature of 720° of the tempering furnace and the working speed of the tubes of 16 m/h (equivalent to a permanence time in the furnace of 3.6 h) respected the production of 3500 kg/h that the plant must maintain because of economical considerations.

We used the experience of the person responsible for the hardening process to choose the austenitizing temperature and thus we reached the two levels varying the power and the voltage of the heating inductors. To measure the temperature of the tube, we used an optical pyrometer, positioned at the exit of the last inductor and just in front of first quenching head.

The maximum diameter of the water hole on the head of the tangential quenching unit corresponded to the inner diameter of the tube: the responsible for the process used an empirical rule and took into account a strong decrease in the efficiency of the quenching using bigger diameters. The adjustment of the parameter was made using a calibrated lever.

The control of the water flow through the nozzles of the two hardening heads was made regulating the first set of nozzles of the tangential quenching head (Table 1), whereas the opening of the second set of nozzles of the same head and of the ones of the radial head were kept constant.

High level	100%	100%	50%
Low level	0%	100%	50%

Table 1 - Control of the water through the first set of the nozzles of the tangential quenching head

4. THE EXPERIMENT

We denoted the controllable factors as follows:

- A denoted the austenitizing temperature,
- B denoted the water hole diameter on the head of the tangential quenching unit,
- C denoted the water flow through the nozzles of the two quenching heads.

Table 2 shows the signs of the effects of the 2^3 design with two replicates.

We chose the order of the 16 runs and the tubes to be used in every run using a randomised criterion. We marked all the tubes punching their front and tail ends, identifying specimens with a special ink able to permit a complete traceability during the experiment.

Number Run	Treatment Combination	Factorial Effect		
		A	B	C
1	b	-	+	-
2	b	-	+	-
3	bc	-	+	+
4	abc	+	+	+
5	ac	+	-	+
6	abc	+	+	+
7	ab	+	+	-
8	c	-	-	+
9	a	+	-	-
10	bc	-	+	+
11	ab	+	+	-
12	(1)	-	-	-
13	a	+	-	-
14	(1)	-	-	-
15	c	-	-	+
16	ac	+	-	+

Table 2 - Signs of the effects of 2^3 design with 2 replicates

As the plant is designed for a continuous process, in order to have the time needed to change the parameters during the hardening process we used an auxiliary tube. The total experiment took 100 minutes.

We controlled the hardness of the tubes along the same generating lines (front and tail ends) and after we cut a portion from the front end of every tube to make the specimens for hardness tests.

The 16 tubes were positioned in parallel during the tempering process and the temperature and feeding speed were respectively 720°C and 16 m/h.

After tempering we measured only the tail end of the tube and we cut the specimens from this portion, having used the front portion of the tube during the first phase. We chose randomly the three generating lines at 120° and the order of the tubes to be measured, as well as the position of the tubes during the tempering phase and the order of the hardness tests.

5. ANALYSIS OF THE RESULTS

We collected 32 data of the tubes mechanical characteristics after hardening and tempering, 96 data of size variations after hardening and the same amount after tempering, and 576 data of hardness on section of tubes after hardening and after tempering. All the hardened tubes showed an increase of the outer and inner diameters and a decrease of the thickness. During tempering the outer and inner diameters decreased and the thickness was constant. So, after the hardening and tempering processes both diameters increase, while the thickness of the tube decreases. Table 3 and Table 4 present the analysis of variance respectively for the outer and inner diameters expansions of the tube tails after hardening.

Variable of output: Outer diameter expansion						
Tube treatment: Hardening						
Test position on the tube: Tail						
Variance source	Effect	Sum of squares	Freedom Degrees	Mean square	F ₀	F _{0.99,1.8}
A	0.0712	0.0203	1	0.0203	53.262	11.26
B	-0.0387	0.0060	1	0.0060	15.754	11.26
C	0.0312	0.0039	1	0.0039	10.245	11.26
AB	-0.0212	0.0018	1	0.0018	4.738	11.26
AC	0.0687	0.0189	1	0.0189	49.590	11.26
BC	0.0187	0.0014	1	0.0014	3.688	11.26
ABC	0.0162	0.0010	1	0.0010	2.770	11.26
Total		0.0564	15			
Error		0.0030	8	0.0004		

Table 3

Variable of output: Outer diameter expansion						
Tube treatment: Hardening						
Test position on the tube: Tail						
Variance source	Effect	Sum of Squares	Freedom Degrees	Mean square	F ₀	F _{0.99,1.8}
A	0.1200	0.0576	1	0.0576	68.776	11.26
B	-0.0700	0.0196	1	0.0196	23.403	11.26
C	0.0575	0.0132	1	0.0132	15.7910	11.26
AB	-0.0425	0.0072	1	0.0072	8.6268	11.26
AC	0.0900	0.0324	1	0.0324	38.686	11.26
BC	0.0000	0.0000	1	0.0000	0.0000	11.26
ABC	0.0225	0.0020	1	0.0020	2.4179	11.26
Total		0.1388	15			
Error		0.0067	8	0.0008		

Table 4

The ANOVA test [2-7] shows the great importance of the hardening temperature of the tube (factor A). The water hole diameter on the head on the tangential quenching unit (factor B) is important, but not as much as factor A. The water flow through the nozzles of the two quenching heads (factor C) has no importance on the increase of diameters. The interaction AC shows some importance only on the increase of the outer diameter at the tail end. The analysis of variance shows a small importance of the three factors in the change in thickness of tubes after hardening. The tempering produced a reduction of the outer and inner diameters (about 0.05 mm) leaving the thickness unchanged.

Experiments showed that the hardness is always bigger on the outer edge of the wall of the tubes both after hardening and tempering and this is coherent with our expectations.

Only the austenitizing temperature (factor A) is important in the hardening process and the analysis of variance shows its importance for the layers inside the wall of the tubes. The hardening in the outer edge is independent from the controllable factors. The limited quenching capacity of the plant produces a decreasing hardness passing from the outer to the inner diameter of the tubes. However the higher level of the austenitizing temperature gives a stronger hardness to the inner layers and produces a more homogeneous hardness along all the tube. Factor A is the only one influencing the hardness of the tube after the tempering process and table 5 shows the results obtained using the analysis of variance for the data of hardness measured at the tail end and at half the thickness of the tubes.

Variable of output:		Hardness variances				
Data concerning:		Average HRC at half thickness of the tubes				
Tube treatment:		Hardening plus tempering				
Test position on the tube:		Tail				
Variance source	Effect	Sum of Squares	Freedom Degrees	Mean Square	F ₀	F _{099.1.8}
A	1.1223	5.0438	1	5.0438	74.359	11.26
B	0.2396	0.2296	1	0.2296	3.3849	11.26
C	-0.0229	0.0021	1	0.0021	0.0310	11.26
AB	-0.3979	0.6333	1	0.6333	9.3373	11.26
AC	0.3896	0.6071	1	0.6071	8.9503	11.26
BC	-0.4271	0.7296	1	0.7296	10.7563	11.26
ABC	0.1604	0.1029	1	0.1029	1.5175	11.26
Total		7.8911	15			
Error		0.5426	8	0.0678		

Table 5

The analysis of variance of the average values of the proof stress R_p , of the ultimate tensile stress R_m , of the percentage elongation $A_{\%}$ and of the percentage contraction in area $Z_{\%}$ after the tempering process shows they are independent from the controlled parameter of the hardening process. The tempering phase has therefore masked the effect of these above stated parameters.

6. CONCLUSIONS

The water flow through the nozzles of the two quenching heads (factor C) does not influence the quality of the tube, showing no effect on the dimensional and mechanical characteristics. To minimise the use of water and consequently the operating costs, we can close the first set of nozzles and open 50% the second set of the tangential head and open the radial quenching head at the 50%.

We must consider that the austenitizing temperature (factor A) influences the dimensional variations, the depth of hardening and the hardness of the quenched tube. To minimise the tube expansion we had to choose an austenitizing temperature of 900°C. but to optimise the depth of hardening we selected a temperature of 1000°C. We had the advantage of a greater and more uniform hardness of the tube, but we had to compensate the expansion during the tube drawing.

Factor B influences dimensional variations. The water hole diameter of 55 mm gave a smaller expansion of the outer diameter (0.28 mm) and of the inner diameter (0.50 mm) after tempering than using a water hole diameter of 30 mm (respectively 0.35 and 0.60 mm). This choice gave an average hardness of the inner edge of the quenched tube of 48.4 HRC and an average difference of the hardness between outer and inner diameter of 1.2 HRC. The average hardness difference between outer and inner edge of the quenched and tempered tube was 0.8 HRC. The tube expansion was compensated during the drawing process.

To reach the customer requirements we chose a tempering temperature of 710°C and a treatment length of 3.6 hours, which produced a harder tube and a proof stress less than 655 N/mm².

ACKNOWLEDGEMENTS

The Authors wish to acknowledge the generous support offered by MURST in the realisation of this work. Special thanks to Mrs Mary Flynn who checked the manuscript.

REFERENCES

1. Fisher, R.A.: *The Design of Experiments*, 4th ed., Oliver & Boyd, Edinburgh, 1947
2. Montgomery, D.: *Introduction to Statistical Quality Control*, J. Wiley, New York, 1985
3. Chatfield, C.: *Statistics for Technology*, Chapman & Hall, Londra, 1992
4. R.G. Petersen,: *Design and Analysis of Experiments*, M. Dekker, New York, 1985
5. Garcia-Diaz, A.,: *Principles of Experimental Design*, Chapman & Hall, London, 1995
6. Barker T.B.: *Quality by Experimental Design*, Dekker, New York, 1994
7. Ghosh S., Rao C.R: *Design and Analysis of Experiments*, Elsevier, Amsterdam, 1996

QUALITY METHODS FOR DESIGN OF EXPERIMENTS

F. Galetto

Polytechnic of Turin, Turin, Italy

KEY WORDS: Quality Management, Design Of Experiments, Taguchi Method

ABSTRACT: Too often managers know little about Statistics and Probability; nevertheless often they make decisions using blindly methods imported from Japan, just because they are Japanese methods (e.g. Taguchi Methods). The paper shows that Logic and the Scientific Approach are able to provide the right route toward the good methods for Quality. With actual industrial applications and theory we show some pitfalls managers are making by using *a*-scientific methods. Managers have a new job: learning Quality through MBITE, Scientific Approach, Intellectual Honesty, Rational Management, TQM², FAUSTA VIA,

1. INTRODUCTION

Quality is a "very talked" and "in fashion" subject: many top managers are giving this matter great attention, especially due to Quality System Certification (according to ISO 9001/9002/9003 Standards) and to Quality Awards (e.g. Malcolm Baldrige QA, European QA) and Quality Prizes (e.g. Deming Prize); many gurus are providing their precepts for making Quality.

Recently TQM (Total Quality Management) has taken the chair in the Quality evolution; at its first appearance, in 1957, the concept was devised by A.V. Feigenbaum and named TQC (Total Quality Control); after that Feigenbaum spread his ideas all over the world. Today, unfortunately, too many people refer to it as *Total Quality, a statement with no sense at all* : in [31] only one, out of 32 papers (600 pages), used TQM: the editor had to give an Editor's Note "*TQM* is synonym for *total quality*, the term used in this book"; the wrong term got the "citizenship" against the right one!

All this in spite of the fact that in the document ISO/TC 176/SC 1 N 95 of 6th December 1990 it was stated: "*total*" is related to "*management*" and not to "quality".

That is the Quality Culture that is around. [yes, written this way, with Q and C interchanged]. If one uses Logic, the "science of drawing the right conclusions", he sees how far we are from Quality.

TQC is a concept 40 years old! Feigenbaum (1961) stated "*prevention*" as more important than problem "*correction*". Unfortunately he did not use the important idea of prevention very much.

It is very interesting that scholars, like W.E. Deming [3,4] and J. Juran, from 1950 onwards, for more than 40 years were teaching Quality ideas, *without using* the adjective "*total*": they used, in a simpler way, "Quality Control". As a matter of fact, there is absolutely *no need of this adjective*.

Juran, in his Quality Control Handbook (2nd ed.), mentioned Total Quality Control only three times (in 3 notes, referring to Feigenbaum). **Deming never** used the adjective "total".

Absolutely fundamental for Deming is Statistical Thinking [3, 4] that permits manager understand the following fundamental principles:

1. *Scientific Statistical Approach is needed to draw logic conclusions and take sensible decisions, based on actual data, generated in designed experiments*
2. *The absence of statistical approach before, during and after the experiments typically results in relatively uninformative output of questionable general validity.*
3. *Scientific statistical approach of any experiment entails*

3.1. *statistical design*, 3.2. *correct statistical conduct*, 3.3. *scientific statistical analysis of the data*.

Deming began teaching Japanese about Statistical Thinking on 1949, that is 50 years ago.

Deming always said that this fundamental idea was due to W. A. Shewhart [32, 33].

Many managers still lack it: they have a new job: learning how to use Quality methods for Quality. *Quality of methods used for making Quality is very important* and managers are asked to break the "Disquality Vicious Circle" and reduce the Disquality Costs [9, 10, 11, 19, 20, 21, 22].

2. THE GIQA: PREVENTION VERSUS IMPROVEMENT

In 1984 Galetto developed a model for Quality, called IQA, Integral Quality Approach: it integrated various developments of Integral Theory of Reliability, devised in 1973; then, 1973, the Quality System was considered "integration of all company functions for making Quality", well in advance to TQM; since then it has been provided to Italian Companies and to Italian students: the core of IQA have been **Prevention** [a point that only in 1994 *-years late-* was inserted into ISO 9000 Series of Standards] and the **Scientific Approach** [still absent (1998) in the ISO 9000]; the Scientific Approach is very much bigger and more important than in Juran and Deming philosophies. IQA, presented in several papers and Conferences, it is not generally known by people writing on TQM.

TQM and TQM Masters have recently entered higher education, but did Quality enter?

If you look at those course programs, you can see that they generally lack some very important subjects like Reliability (system prediction and testing, FMECA, FTA), Design Of Experiments, and Prevention; but there is something worse: if you look at the course teaching, you can see that they teach wrong ideas to students in very important fields like reliability analysis, hypotheses testing, data analysis, improvements tools, confusion of Problem Solving with Prevention, ...

Prevention with "future consequences of present decisions" [the *future*], in the Company Space-Time continuum, has always been the characteristic of GIQA [10, 12, 18, 19, 20, 21, 22]. Quality Management, according to GIQA, asks managers to commit to mobilising all level of management for Quality, Prevention and Continuous Improvement, using Quality Methods for Quality.

If TQM, as said in several papers and books, is "about continuous improvement" it is apparently clear that the *so called "total quality"* is only a part of GIQA.

As a matter of fact, those papers and books relate the improvement to "problem solving" and to the use of the PDCA (Plan Do Check Act cycle, called by many people the "Deming cycle", while W. E. Deming calls it "PDSA, Plan-Do-Study-Act, the Shewhart cycle"): this is very different from **problem prevention**. Neither the "project by project improvement" process, based on J. M. Juran [23] ideas: **tackling the so called "quality problems" is not prevention**. It is clear that one can

plan for product features without planning for prevention: there are thousands of companies acting this way and lacking prevention. The **Kaizen** process of M. Imai is **not prevention**, as well. ISO Standards 9001 and 9002 are not better: see paragraph "4.14 Corrective and preventive action". It one of the biggest flaws in the ISO Standards.

All that does not mean that Quality Improvement is not important: improvement is important and saves a lot of money, through the application of the PDCA cycle.

Quality Improvement is very different from Problem Prevention.

In this respect, it is very important that managers realise that "**Customer Needs Satisfaction**" is quite different from "Customer Satisfaction". Therefore it is still more important that managers realise that "**Customer/User/Society Needs Satisfaction**" is very different from "Customer Satisfaction". "*Total Quality Managers*" (the managers of *Total Quality!!!*) do not understand this big difference: they are not managers, according to the rational definition of "Manager" given in [19, 20, 21, 22]. Such Managers behave according the "Business core System" [fig. 2].

Too many "**ISO-drugged managers**" and too many Companies are still lacking Quality Management on Quality: it is the most huge problem against Quality achievement. To overcome this drawback there is a MUST: ***Quality Education on Quality for Managers***. [19, 20, 21, 22]

This is certainly the most important goal of the course "Industrial Quality Management" at Turin Polytechnic, based on real Quality experience (30 years) of the author, both in Industry (as Quality Manager in big Corporations), in University (Padova, Genoa, Turin) and as a Quality consultant.

To differentiate GIQA from TQM the following symbol was devised ϵQ_{GE}^{IO} which stands for the "**epsilon Quality** made by Intellectual honest people who always use experiments (*Gedanken Experimente*) to find the truth" [G. E. was a statement used by Einstein; but Galileo too, the Italian scientist, was used to "mental experiments", the most important tool for Science; **epsilon Quality** conveys the idea that Quality is made of very many prevention and improvement actions]. GIQA uses very important ideas: the Scientific Approach, MBITE, FAUSTA VIA, TQM²:

- MBITE stands for Management By If ... Then ... Else ..., acronym devised to remind managers of their obligations for prevention and long-term commitment, through the **ITE approach to decisions**. **It is the fundamental basis for Prevention**: i.e. making full use of the thinking ability.
- FAUSTA VIA (the profitable route to Quality) stands for Focus, Assess and Understand Scientifically the needs, Scientifically Test ideas and hypotheses, Activate the solutions (Preventive or Corrective); then Verify their effectiveness and Implement extensively on all other similar cases; eventually Assure the satisfaction of the Customer, User and Society **needs**. [fig. 1]
- TQM² stands for Testify Quality of Management in Management: Prevention and Improvement are both needed and **must be shown** by Managers.

In the GIQA it is important to define with Quality the word Quality. In order to provide a practical and managerial definition, since 1985 F. Galetto was proposing the following definition : **Quality is the set of characteristics of a system that makes it able to satisfy the needs of the Customer, of the User and of the Society**. None other definition (to the author's knowledge) highlights the importance of the **needs** of the three actors: **the Customer, the User and the Society**.

They are still not considered in the latest document, the ISO 8402:1994!!! [def. 1.9 "customer"]

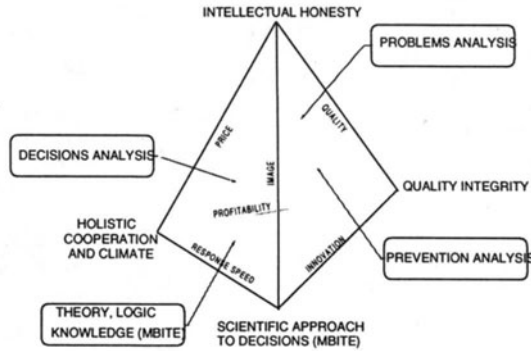
3. DESIGN OF EXPERIMENTS (DOE) IN THE GIQA VERSUS TAGUCHI METHODS

Any decision about Quality of product and processes is usually based on data, collected through tests on samples; there is always some risk of making a wrong decision because of the random variation always present. Managers want this risk to be acceptably small: the risk becomes smaller as the number of observation increases.

the profitable route to Quality

F. Galetto

F focus
A assess
U understand
S scientifically
T test
A activate
V verify
I implement
A assure



F. Galetto

.... again and again

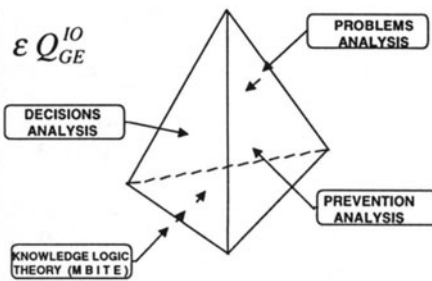
ϵQ_{GE}^{10}



Quality Essence
 (the core is Prevention)

F. Galetto

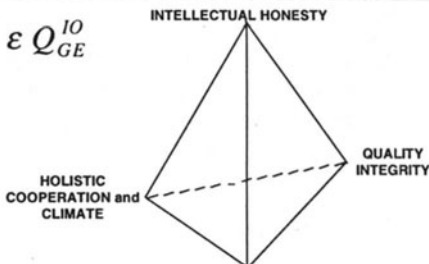
ϵQ_{GE}^{10}



RATIONAL MANAGER TETRAHEDRON

F. Galetto

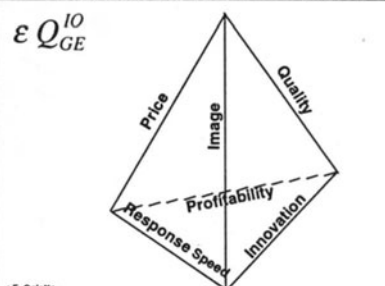
ϵQ_{GE}^{10}



SCIENTIFIC APPROACH TO DECISIONS (M B I T E)
 MANAGEMENT TETRAHEDRON

F. Galetto

ϵQ_{GE}^{10}



COMPETITIVENESS TETRAHEDRON

F. Galetto

Figure 2. the Business core System

It is clear that the more data we get, the more the cost of testing is. It necessary to keep the cost of testing to a minimum consistent with the maximum risk of a wrong decision, that the manager is prepared to accept. DOE is a way to get the optimum testing effort: the least cost for the accepted

risk. DOE permits to obtain more information for less cost than can be obtained by traditional experimentation.

In DOE the first point to be tackled is the choice of the "dependent" (response) variable on which we will collect the data and to define the independent variables (the factors) that may affect the response [which factors are to be varied and choice of the levels of any factor (quantitative or qualitative), controlled factors or uncontrolled factors, fixed or random]. We refer to the variables in terms of which the experiment is conceived as structural or design factors, in order to distinguish them from the extraneous or *environmental factors* that will inevitably be present as background sources of variability. If an environmental factor can be isolated and if it is recognised as worth controlling, it may be placed on the same footing as the structural factors and incorporated into the design (this kind of design is now called "Combined Array" [2, 26] to distinguish it from the "Product Array" (early 80ies) of Taguchi; you can see in ref. 7 that this idea, with no name given to it, was used, by F. Galetto, at least 5 years before (1975, at FIAT), i.e. more than 20 years ago). Otherwise, such factors are combined with the un-assignable causes of variation (uncontrollable factors) to provide a within-replicate estimate of the experimental error.

The second is the way factor levels are to be combined (treatment combinations or test states) with the order of experimentation, in random order, and the number of observation to be taken: the random type of selection tends to even out any variation associated with the uncontrollable factors. Randomisation is used to secure that analysis of data can really provide an unbiased estimator of the experimental error: *only replications provide* a true estimation of the experimental error.

The third point is the collection and the analysis of data. Since every phenomenon generates data that are not the same (due to some disturbing "random error"), in order to extract the "true behaviour" of the phenomenon we need to separate the random error from the collected data. To do that, scientific methods must be used. One of these is the ANOVA based on the Normal Equations and the Gauss-Markov Theorem. As said above, replications are absolutely needed for the experimental error estimation: such an estimate is very important for any significance decision.

The scientific method for DOE based on the Normal Equations and the Gauss-Markov Theorem is called G-Method: it is one of the many methodologies proposed by GIQA, the only Quality Philosophy that really *strives for Prevention*. [9, 10, 12, 18, 19, 20, 21, 22] The ***"Prevention spirit" will be again missing in the VISION 2000, the future ISO 9000 Series of Standards!!!***

As a competitor one can find the Taguchi Methods [we can not describe them, due to "space problem"; see 22, 29, 34, 35]; they are called up on by managers and scientists to support them in making decisions; these methods are very appealing for them as they are claimed to be less expensive (i.e. less testing is needed) and easier (i.e. no knowledge is needed). If one designs experiments and analyses with Taguchi Methods he will find out that the scientific analysis of data provides different conclusions. Since the scientific analysis is scientifically correct, it follows that a huge amount of money was wasted, using Taguchi.

Quality of Quality Methods [that is Quality of the methods, used in the Quality field, for making Quality (of products and services)] is often disregarded by the "so-called quality professionals" because knowledge is required to judge Quality, according with the "Knowledge Matrix" [12, 16, 19, 20, 21, 22]. The right tools can be used if managers do use correctly the "Knowledge Matrix".

Based on an actual industrial application we will show most of the important differences between the proposed methods for DOE and the pitfalls managers are making, because they do not use the FAUSTA VIA (the profitable route to Quality). Managers, at every level, have to meditate upon these facts, decide to learn, and to climb the ladder of knowledge: from

ignorance \Rightarrow awareness \Rightarrow simple knowledge \Rightarrow know-how \Rightarrow full understanding.

Looking at the Business core System and at the Knowledge Matrix, it is apparent that a golden rule has to be understood by managers: tests have to be designed in order to get the information needed to take good decisions and to prevent problems and failures. Statistics provides suitable tools for "Design of Experiments" (DOE) in order to get maximum of information at stated costs and risks.

According to professor D. C. Montgomery [28], "in the early 1980s, professor G. Taguchi introduced his approach to using experimental design ...".

Actually, before 1980 many people in the West, and myself [7], made many applications on DOE.

The important method named DOE (Design of Experiments), born in the 30ies due to Fischer and Yates, has been applied to many fields (agriculture, medicine, chemistry, mechanics, electronics). The merit of Taguchi Methods popularity pertains to Ford Motor Co.; in 1982 Ford introduced the methods to its suppliers. ASI (American Suppliers Institute) was founded with the support of Ford; MIT edited Taguchi books. Extremely accurate advertising gave popularity to TM and *often people use blindly Taguchi Methods*. Thousand of people (managers, quality managers, quality consultants, professors) claim that Taguchi Methods are good; actually, the *people I met* knew little about Design of Experiments and Reliability theory and methods. (ASI experts as well!!)

To show the drawbacks of such methods we will use an application to parameter design: the paper was priced as "*best technical paper*" by ASQC, in 1986!!! [2]. I knew about it in 1986 when it was presented to 80 Top-manager of FIAT, at Marentino. We will compare the Taguchi approach with the scientific approach and conclusions provided by the G-Method [13, 14, 15, 16, 17, 18, 19, 22], a method of DOE based on the Scientific Approach, originated by Galileo, and on the Gauss-Markov theorem (that states optimum properties of linear estimators). Mathematics, Logic and Physics can prove that Taguchi approach is wrong especially when he writes "... when there is interaction, it is because insufficient research has been done on the characteristic values". Many examples of the pack of lies of the "Taguchians" can be shown, using the G-method, (G stands for good, general, guaranteed, golden, based on Gauss-Markov theorem, or Galileo-wise); the G-method, based on the Scientific Approach, uses the "normal equations" of analysis of variance and of covariance [13, 15, 17, 21]. By the use of the G-method it comes out that Taguchi Methods are a bad version of the good techniques of DOE, as it was mentioned at the plenary session of EOQC Conference (1989) by J. Juran [14]: **there are many cases that show the benefits of managerial and scientific conduct of testing activities. The pitfalls of a counter-conduct are very costly.** Taguchi distinguishes between "controlled factors" [he calls their treatment combinations as "inner array"] and "noise factors" [he calls their treatment combinations as "outer array"]: "controlled factors" are those that we want to use to get the "optimum response" The design then of the structural factors is the combination of the two arrays [see 2, the Byrne-Taguchi case]. Since generally the number of test states and the replications are very large, the outer ed inner arrays are reduced, according to certain rules, and a reduced design is carried out [fractional design].

It is obvious that it is absurd and un-managerial pretending that fractional designs provide you with the same information of complete designs: you can not estimate neither the factors effect, nor the interaction effect; they are inevitably entangled: you have generated the ALIAS Structure. Moreover, generally only one application is made of each treatment combination and therefore the estimator of the experimental error is not available.

This point is hidden by Taguchi lovers [13, 14, 17, 22, 25]. That is a huge cost of disquality.

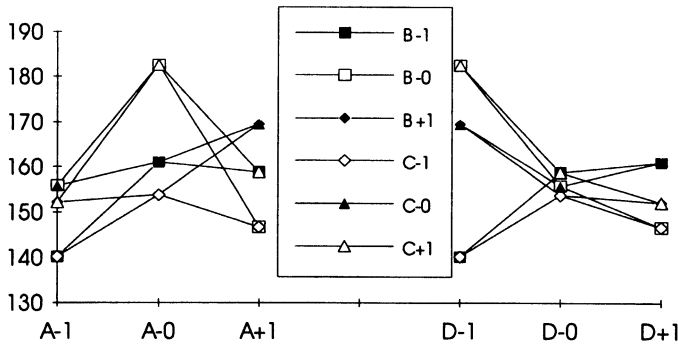
Since every phenomenon generates data that are not the same (due to some disturbing "random error"), in order to extract the "true behaviour" of the phenomenon we need to separate the random error from the collected data. This is precluded by the use of Taguchi-Methods (S/N ratios).

To overcome this point Taguchi postulates that interactions are zero [are not present, have no effect] and then the SS (Sum of Squares) of interactions is used to estimate the experimental error.

The Case "*best technical paper*" of Byrne-Taguchi [2]: the experiment was carried out to find a method to assemble an elastomeric connector to a nylon tube such that the pull-off force (the "response variable") could be maximum. 4 "controllable factors" (3 levels) and 3 uncontrollable "noise factors" (2 levels) were identified. Both kinds of factors were "controlled" during the test: "structural factors". Following the Taguchi parameter design method, one experimental design was selected for the controllable factors A, B, C, D (inner "L9 orthogonal array") and another for noise factors E, F, G (outer "L8 orthogonal array"). The combined array comprised 72 test states [coding -1, 0, 1; "standard" 1, 2, 3 used by Taguchi]; the pull-off force was observed for each state: the 72 collected data and the 9 S/N (Signal to Noise ratio) are in the table. Analysing the S/N, Byrne and Taguchi found the optimum state $A_2B_1C_2D_1$, **neglecting the interactions between the factors**. The following graph shows that is not so wise to neglect interactions.

Since there are 72 data, you can know better your process by analysing the significance of interactions, if the original data, not the S/N, are processed: the significant interactions between

the "controlled factors" are highlighted in the table ("bolded capital letters") and the significant interactions between the "controlled factors and the noise factors" are highlighted in the table ("italic bold capital letters"); moreover "noise factors" are more significant than controlled factors.



E	1	1	1	1	-1	-1	-1	-1
F	1	1	-1	-1	1	1	-1	-1
G	-1	1	-1	1	-1	1	-1	1

A, B; C, D factors				E, F, G "outer factors" response								S/N
A	B	C	D	19.1	20	19.6	19.9	16.9	9.5	15.6	24.025	
-1	-1	-1	-1	21.9	24.2	19.8	19.7	19.6	19.4	16.2	25.522	
-1	0	0	0	20.4	23.3	18.2	22.6	15.6	19.1	16.7	25.335	
-1	1	1	1	24.7	23.2	18.9	21	18.6	18.9	17.4	25.904	
0	-1	0	1	25.3	27.5	21.4	25.6	25.1	19.4	18.6	26.908	
0	0	1	-1	24.7	22.5	19.6	14.7	19.8	20	16.3	25.326	
0	1	-1	0	21.6	24.3	18.6	16.8	23.6	18.4	19.1	25.711	
1	-1	1	0	24.2	23.2	19.6	17.8	16.8	15.1	15.6	24.832	
1	0	-1	1	28.6	22.6	22.7	23.1	17.3	19.3	19.9	26.152	
1	1	0	-1									

source	df	SS	MS	Fc	F10%	signif	source	df	SS	MS	Fc	F10%	signif
A	2	50.58	25.29	11.85	4.32	*							
B	2	13.38	6.69	3.14	4.32								
C	2	68.59	34.30	16.07	4.32	*	E	1	275.7	275.7	129.2	4.54	*
D	2	23.67	11.84	5.55	4.32	*	F	1	161.7	161.7	75.75	4.54	*
A*B	4	92.27	23.07	10.81	4.11	*	A*G	2	26.57	13.28	6.22	4.32	*
A*C	4	37.06	9.26	4.34	4.11	*	D*E	2	21.75	10.87	5.09	4.32	*
A*D	4	81.97	20.49	9.60	4.11	*	D*F	2	15.45	7.73	3.62	4.32	
B*C	4	74.25	18.56	8.70	4.11	*	D*G	2	7.86	3.93	1.84	4.32	
B*D	4	119.2	29.79	13.96	4.11	*							
C*D	4	63.96	15.99	7.49	4.11	*	Res	4	8.54	2.135			

The so called "product array design" structure (product of the inner by the outer array) led to a very large experiment of 72 test states that did not permitted the estimation of the interactions (so the authors were forced to neglect them!). *If they had used* the G-method [see 7, as one of the first applications] they could have designed a "combined array" of the "structural factors" that would have been more likely to improve process understanding and decisions.

A simpler analysis (with similar information on the significance of factors and interactions) was done [using a pocket computing machine] immediately after the Marentino conference and sent to all the manager: the outcome of that was a very fast application of Taguchi Method at FIAT-Auto, the car factory: managers are not able to take Quality decisions, and therefore they waste money!!!

The residual error is not computed as difference of the estimated factors and interactions from the corrected total sum of squares SS, in the ANOVA table. **But there is an important hoax always hidden by Taguchi and his lovers.** When you carry out a part of all the test you should do (this is called "fractional replication design") you can NOT obtain the same information of the complete design: you can not separate factors effect and interactions effects; they are **inevitably entangled**. The experimental "inner array" is a "fractional factorial 3^{4-2} design" in the controlled factors A, B, C, D. There are several ways to get it; a recent and very interesting method is mentioned in [26] and shown in [30]: find the solution to the following system of equations (factors are x_i)

$$x_2^3 - x_2 = 0, \quad 4x_4 + 9x_1^2x_2^2 + 3x_1x_2^2 - 6x_2^2 - 3x_1^2x_2 + 3x_1x_2 + 2x_2 + 4 - 2x_1 - 6x_1^2 = 0$$

$$x_1^3 - x_1 = 0, \quad 4x_3 - 9x_1^2x_2^2 - 3x_1x_2^2 + 6x_2^2 - 3x_1^2x_2 + 3x_1x_2 + 2x_2 - 4 + 2x_1 + 6x_1^2 = 0$$

The solution provides you with the treatment combinations, not the confounding pattern as, on the contrary, is written in [26]: it is said there that "the left-side two equations confound the 1st and the 3rd order interaction of each factor, as it is taken for granted for 3 level factors design. The right-side two equations confound the 4th (3rd) factor with a complex combination of interactions (of the 1st two factors)". The authors do not provide the "alias structure", as always do the "Taguchi lovers" [25]. **If they had used** the G-method they would had found that every factor is "entangled" with various interactions (we use the symbol & for the "entanglement relation" and ... for not shown higher order interactions): **A&B*C&B*D&C*D&ABC&...; B&A*C&A*D&C*D&...; C&A*B&A*D&B*D&...; D&A*B&A*C&B*C&...**

"Entanglement" is an "equivalence relation", in a logical sense. More precisely, there is also the **ALIAS structure** (the symbol @ stands for "equivalent to"), neglected by Byrne and Taguchi:

$$\boxed{(A+B)@C*D@... (A+C)@B*D@... (A+D)@B*C@... (B+C)@A*D@... (B+D)@A*C@... (C+D)@A*B@...}$$

This means that changing "additively" any two factors is exactly the same as changing "interactively" the other two factors and As a consequence you can not choose the best levels of factors as though they were independent, "a magic feature of Taguchi orthogonal arrays".

You can show all that using the G-Method [14, 16, 17, 21, 22]; in chapter 9 of ref. 22 it is mentioned a method that allows you to find the bias of the estimate of the parameters of a "reduced model"; the same idea can be used for finding the alias structure: let X be the design matrix, Y the vector of the random variable associated with the test states and β the vector of the parameters ("full model"; let's partition the tests states into two sets, with related vectors Y_1 and Y_2 , and the full model into two vectors β_1 (the "reduced model") and β_2 ; the design matrix and $S=X'X$ are partitioned accordingly into four sub-matrices X_{ij} and S_{ij} . Assuming that S is non-singular the required estimator of the vector β is

$$\begin{bmatrix} \hat{\beta}_1 \\ \hat{\beta}_2 \end{bmatrix} = \begin{bmatrix} S_{11}^{-1}(I + S_{12}NS_{21}S_{11}^{-1}) & -S_{11}^{-1}S_{12}N \\ -NS_{21}S_{11}^{-1} & N \end{bmatrix} \begin{bmatrix} X'_{11}Y_1 + X'_{21}Y_2 \\ X'_{12}Y_1 + X'_{22}Y_2 \end{bmatrix} \text{ where } N = (S_{22} - S_{21}S_{11}^{-1}S_{12})^{-1}$$

From this it is easily seen that

- when a full design is carried out and a reduced model is considered the estimator of β_1 is biased
- when a **fractional design** is carried out only a reduced model β_1 , ALIASED, can be estimated. It is not scientific and not managerial say the contrary [9, 10, 11, 12, 14, 16, 19, 20, 21, 22]. The right tools can be used if managers do use correctly the "Knowledge Matrix" [22].

The same G-Method allows you to find the resolution of a given design: for example, you can show that the 54-runs "combined array, allocating for three 3-level factors [X, W, Z] and four 2-level ones [A, B, C, D]" design in [27] does not appear to be a "resolution V design", unless you define "resolution" differently from the usual way [1, 15, 17, 22, 28, 29]: as a matter of fact A is entangled with **A*B & C*W &**

IF skilful people make such kind of pitfalls, what can we expect from **incompetent** ones? **These** last use Taguchi Methods and claim: "TM work", BUT they did not read Taguchi books [35]: it very amazing asking them "Did you read Taguchi books [35]?". I **always** had the reply NO!!!

Why people act that way? I have been looking for the answer for at least 15 years: I found it during last holidays in [36]: the truth does not influence them: **only their conviction is reality!!!**

Using Statistics correctly for the Byrne-Taguchi case, the optimum point is therefore different from the one found by Byrne-Taguchi, due to interactions (as seen from the previous graph).

The significance of factors and interactions is hidden (if not forbidden) by the analysis of S/N; moreover, firstly the noise factors E and F are much more important than the controlled factors A, B, C, D, secondly the interactions A*G, D*E, D*F between some controlled factors and the noise factors E, F, G are more important than the controlled factors A, B, C, D: therefore it is better to act as Rational Managers with the FAUSTA VIA (the profitable route to Quality) [fig. 1].

Using Logic, a Rational Manager is not dazzled by "the robust design methodology, following the modern Total Quality philosophy, ... (where) Taguchi proposes to use different types of response, characterised by great simplicity ... today possible even for inexperienced people thanks to the diffusion of advanced statistical software ..." [27]. In the same paper the problem of the alias structure is hoaxed-missed again! The entanglement can be found by the G-method.

Unfortunately, at least 90% of the papers on application of TM do not provide you with the alias structure. ***This attitude unfortunately cheats people and robs them of their right to know.***

If skilful people slip into such pitfalls what can you expect from unskilled managers who act like "tamed monkeys monkeying their incompetent consultants and teachers"?

For ten years, since 1988, Levi [17, 24, 25] and Galetto [11, 12, 13, 14, 15, 16, 18, 19, 20, 21, 22] have been suggesting to be cautious in using blindly some Taguchi ideas. At that date the name "G-method" was invented, but many applications of it were made before [22].

We can not mention here all the wrong Taguchi applications that have been carried out since then: let's content ourselves of the few (out of the many) cases reported in the references. [2, 14, 15, 16, 17, 21, 29, 34, 35]. **Form the previous case, and the other many wrong that you can find in the literature, it is evident that a lot of disquality was generated and a huge amount of money was wasted. Were they unfortunate? Absolutely not, they were a-scientific.**

Does Taguchi Method work ??? NO, it is really robust in FAILURE!!!

"Signal/Noise ratios" used in connection with the so called Robust Design are nonsense from a scientific point of view: these are multifunctional transformations of the data, and at the end the transformed data must be normally distributed if, logically, the F ratio resulting from ANOVA and shown in the "Quality Engineering using Robust Design" books should have any statistical sense). In many cases interactions are important; therefore it is quite non-managerial pretending, before any test, to say (Taguchi) "... when there is interaction, it is because insufficient research has been done on the characteristic values.", or to say, after a test (Phadke), "... if we observe that for a particular objective function the interactions among the control factors are strong, we should look for the possibility that the objective function may have been selected incorrectly".

All the cases I had the opportunity to analyse show that

facts and figures are useless, if not dangerous, without a SOUND theory. (F. Galetto).

It is silly saying: "I was in Japan and learned: data are important; I speak with **facts and figures**". Interactions are really very important, according the fundamental principle F1 of GIQA [19, 20].

4. CONCLUSIONS

Managers have to learn Logic, DOE, Statistical Thinking to make good decisions. Quality is number one Management goal, not only for product and services, but **for Quality methods as well**. DOE is one of the most powerful methodologies for making Quality and preventing problems. Managers must know the DOE fundamental ideas. If they do not do that, they are doomed to waste Company money and to spoil Company reputation.

Any transformation is always difficult for human beings; they seem to resist new ideas especially when it is required to use, **in a better way**, rationality, intellectual honesty, Logic, ... Experience shows that good ideas work in practice in any case people put them into practice with coherence

and intellectual honesty (TQM²). Management must encourage a climate for change and show with facts their dedication to Quality [TQM²], because building Quality brings better profits. All that is for managers, the Managing Director (or the C.E.O.) included; M.D.s must permit their first-line managers, *the Quality manager included*, to feel secure to express their ideas on Quality management, with respect to company Quality commitment (see the Management Tetrahedron and the Rational Manager Tetrahedron): again TQM². "Quality of methods for Quality is important", there are methods misleading (Taguchi M., Bayes M., ...): it is better that MANAGERS BE EDUCATED ON QUALITY, always thinking to Deming statements in *Out of Crisis*.

- *Experience alone, without theory, teaches management nothing about what to do to improve quality and competitive position, nor how to do it.*
- *It's a hazard to copy. It is necessary to understand the theory of what one wishes to do or to make.*
- ***The result is that hundreds of people are learning what is wrong.***
- ***I make this statement on the basis of experience, seeing every day the devastating effects of incompetent teaching and faulty applications.***

REFERENCES

1. BOX E. P., JONES S. P., (1992), Designing Products That Are Robust to the Environment, *TQM*, 3,
2. BYRNE D, TAGUCHI S. (86), The Taguchi approach to parameters design, *ASQC86 and Quality Progress* dec. 87
3. DEMING W.E. (1986), *Out of the Crisis*, Cambridge Press, "**L'azienda di qualità**", traduzione piena di errori!!!
4. DEMING W.E. (1997), *The new economics for industry, government, education*, Cambridge Press.
5. FEIGENBAUM A.V. (1993), *Total Quality Control*, 3a ed., McGraw-Hill.
6. FISHER R. A. (1935) *The Design of Experiments* - Oliver and Boyd, Edimburgo
7. GALETTO F. (79), Une application des plans d'experiences dans l'industrie automobile, *SIA*, Paris
8. GALETTO F. (84), L'insegnamento della affidabilità all'Università", *Congr. AICQ*, Milano
9. GALETTO F. (1986), "Quality/Reliability: How to get results", *EOQC (Automotive Section)*, Madrid.
10. GALETTO F. (87), Quality/Reliability, The IVECO way, Management. Dev. Rev., Brussels
11. GALETTO F. (1988), "L'industria ha bisogno di buoni tecnici in qualità", *Un. di Padova*, Bressanone
12. GALETTO F. (1988), "Quality and Reliability. A must for Industry.", *19th ISATA*, Montecarlo
13. GALETTO F. (89), Metodi Taguchi: elementi di meditazione, *Un. di Padova*, Bressanone
14. GALETTO F. (89), Quality of methods for quality is important, *EOQC Conference*, Vienna
15. GALETTO F. (90), Basic and managerial concerns on Taguchi Methods, *ISATA*, Florence
16. GALETTO F. (1993), DOE. Importanti idee sulla Qualità per i manager, *DEINDE*, Torino
17. GALETTO F., LEVI R. (93), Planned Experiments-Key factors for product Quality, *3rd AMST 93*, Udine
18. GALETTO F. (96), Managerial Issues for Design of Experiments, *4th AMST 96*, Udine
19. GALETTO F. (97), GIQA(Golden Integral Quality Approach): from Mgt of Quality to Q.ty of Mgt, *TQM*, in press
20. GALETTO F. (1997), La vera sfida: dal Mgt della Qualità alla Qualità del Mgt, *XIX Conv. N.le AICQ*, Assago
21. GALETTO F. (97), "Qualità dei metodi: <<La verità vi farà liberi>>", *XIX Conv. Naz.le AICQ*, Assago
22. GALETTO F. (1997), *Qualità. Alcuni metodi statistici da Manager*, CUSL, Torino.
23. JURAN, GRINA F. M., (1993), *Quality Planning and Analysis*, 3rd ed., McGraw-Hill, N.Y. (**big errors**)
24. LEVI R. (1988), Pianificazione ed analisi degli esperimenti nella ricerca applicata, Firenze - *ATA*, 163-171
25. LEVI R. (1991), Piani sperimentali e metodi Taguchi: luci e ombre, *ATA*, vol 44, n. 11, 777- 781
26. LEVI R., LOMBARDO A. (97) Nuove frontiere nella programmazione degli esperimenti, *Convegno SIS*, 210-215
27. LOMBARDO A. (1997), Product-Array and Combined Array for Robust Design, *Statistica Applicata*, vol 9, n. 1
28. MONTGOMERY D.C. (96), *Introduction to Statistical Quality Control*, Wiley & Sons (**wrong def. of "Quality"**)
29. PHADKE M.S. (1989), *Quality Engineering using Robust Design*, Prentice Hall.
30. PISTONE G., WYNN H. P. (1996) Generalised confounding with Groebner bases, *Biometrika* 83 (1)
31. ROBERTS (Ed.) (1995) *Academic Initiatives in Total Quality for Higher Education*, ASQC Press
32. SHEWHART W.A. (1931), *Economic Control of Quality of Manufactured Products*, D. Van Nostrand
33. SHEWHART W.A. (36), *Statistical Method from the Viewpoint of Quality Control*, Graduate School, Washington
34. TAGUCHI G. (1986), *Introduction to Quality Engineering*, ASI, Dearborn.
35. TAGUCHI G. (1987), *System of Experimental Design*, vol. 1 & 2, UNIPUB/Kraus Publications, N.Y.
36. WATZLAWITCK P. (1976) *La realtà della realtà*, Astrolabio, Roma
37. WINCH C. (1996) *Quality and Education*, Blackwell Publishers, Oxford, UK

DYNAMIC INSPECTION POLICY IN MANUFACTURING SYSTEMS SUBJECTED TO LINEAR WEAR PROCESS

M. Braglia, C. Festa and E. Gentili
University of Brescia, Brescia, Italy

KEY WORDS: Maintenance, Inspection Policy, Manufacturing System, Optimisation

ABSTRACT: The aim of this paper is to correlate the quality control policy with the deterioration process of a production system. The aim is to consider how the wear process of the system influences the choice of control policy parameters of the items produced, and how these parameters have to be changed according to the need of maintaining optimal working conditions. For a failure rate $\gamma(t)$ of the production system increasing linearly with the time it can be (analytically) shown how these parameters have to be changed (at different times t) in order to maintain optimal working conditions. In particular, a specific objective function of the loss time t owing either to defective units or to the production shut-down (in order to make an inspection) will be developed and will allow us to vary the parameters over the time.

1. INTRODUCTION

Several papers have recently been published on planned maintenance and they show the advantage of a possible cost reduction over a long period. Unexpected failures in the production process induce a lower productivity level and product quality, with a consequent reduction of the expected profit in the long term.

An important maintenance scheme regards the *inspection models*. It involves a choice of the optimal inspection scheduling of a system that cannot be monitored continuously.

Published in: E. Kuljanic (Ed.) *Advanced Manufacturing Systems and Technology*,
CISM Courses and Lectures No. 406, Springer Verlag, Wien New York, 1999.

Every inspection has a cost, partly due to the stops in production. The basic model described in [1] considers failures detectable only by inspection. The failure of the system is not catastrophic but provokes a partial degrade to the *out-of-control* functioning.

We can divide inspection models in two principal sub-classes [2]:

1. Models looking to plan an optimal scheduling of the production system inspections using statistical hypothesis of the ageing process plant;
2. Models able to decide immediately for the inspection using a statistical product control at the end of the plant. In this case, we have “partially observable Markov decision models”. It is impossible to control all the pieces because of the cost or of the time involved. The above models are very similar to acceptance sampling policies in production and/or procurement.

Our paper refers to inspection models of class “2” and is an extension of the work [3]. This regarded the determination of the optimal quality management (control) in a production system with a constant wear rate. The purpose was to determine the optimal set of values (k, n, c) able to maximise the long term expected profit. The three values (k, n, c) represent the size of the lot produced, the size of the sampled lot and the acceptance number, respectively.

This work introduces a failure rate $\gamma(t)$ of the production system increasing linearly with the time, instead of a constant failure rate. The goal function to be minimised is based on the computation of the lost time producing defective items and inspecting the productive system. Suitable weights take into account the cost due to the different kinds of lost time and allow an economical analysis.

Our paper will show the need to change dynamically the choice of the parameters optimising the control process management accordingly with the plant wear and with the need of maintaining the optimal (working) conditions.

The model uses information inherent in the wear process of the production system as well as the data from the plant control system. It is a first attempt to unify the above two classes of inspection policies.

2. THE MODEL

We consider a manufacturing system characterised by two possible states. When the process is in the in-control state the probability of producing defective units is given by p_1 , while in the out-of-control state this probability is given by p_2 , with $p_2 > p_1$. We consider a production system subject to wear: in particular $\gamma(t)$ is the system failure rate linearly increasing with the time, i.e.:

$$\gamma(t) = \alpha_s + 2\beta t$$

where

$$\alpha_s = \alpha + \beta(s-1)\frac{k}{\lambda}.$$

α_s represents the (mean) value of the failure rate at the beginning of the generic production of lot s . The corresponding reliability is given by

$$R(t) = e^{-\alpha_s t - \beta t^2} \tag{1}$$

The jobs arrive at the production system according to a Poisson process and the amount of processing time is stochastic with a known probability distribution function $f(\cdot)$. In this plant it is impossible to keep under control the functioning conditions of the system and the state of the system can only be known making inspections after the system shut-down.

In order to find the right instant of time to stop the process for inspection, a (k, n, c) policy [3] is adopted. Briefly (see Figure 1), in (k, n, c) inspection policy, a predetermined number of n units from each lot of k elements produced is inspected. If the number of non conforming units is greater than a prescribed minimum c , the production process is stopped and an inspection is carried out. If no failure cause is found (i.e. we have a false alarm) the production process is simply continued without any change. Otherwise the process is shut down for an additional time to carry out a maintenance operation, until the maintenance operation is concluded. The searching and maintenance times are defined by a pdf $s(\cdot)$ with mean θ and variance σ_s^2 and a pdf $m(\cdot)$ with mean g and variance σ_g^2 , respectively. Finally, we can assume that, thanks to the maintenance operation, the failure probability per unit time $\gamma(t)$ is returned to the initial value $\gamma(0)$ at the end of the maintenance operation itself. In other words, besides re-starting the process in the in-control state, we reset the initial wear condition of the system.

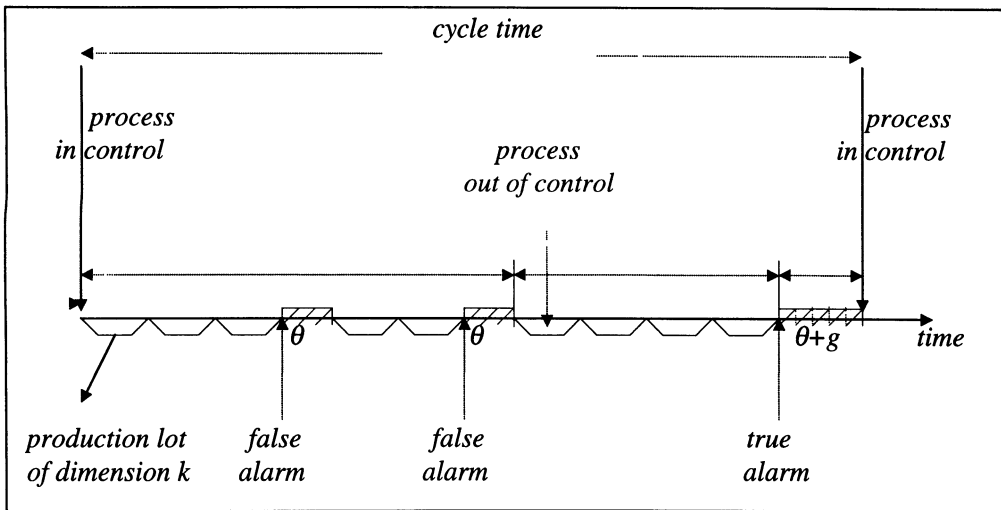


Fig. 1: Production cycle scheme

The quantities of interest of our model that must be calculated are the following:

1. the probability q_1 of giving a false alarm when the process is in-control is given by:

$$q_1 = \sum_{i=c+1}^n \binom{n}{i} p_1^i (1-p_1)^{n-i};$$

2. the probability q_2 of giving a true alarm when the process is indeed out-of-control, is given by:

$$q_2 = \sum_{i=c+1}^n \binom{n}{i} p_2^i (1-p_2)^{n-i};$$

3. if a system failure occurs in a sampling interval s , the probability that it occurs while the j -th job is in process (i.e. during the time interval $[x, x+y]$), is given by:

$$A_{js} = \frac{1}{B_s} \int_0^\infty \int_0^\infty (R(x) - R(x+y)) f(y) f^{j-1}(x) dx dy \tag{2}$$

where the reliability $R(\cdot)$ is given by eqn. (1). Note that $f^{j-1}(x)$ is the $(j-1)$ -th convolution of the distribution function $f(x)$ and represents the probability that the total processing time required to produce the first $(j-1)$ jobs is x . In this model we consider the case where the production system is characterised by an exponential service time with $f(x) = \mu e^{-\mu x}$, for $x \geq 0$. Then the k -th convolution of $f(x)$ is given by the following a gamma pdf

$$f^k(x) = \frac{e^{-\mu x} (\mu x)^{k-1} \mu}{(k-1)!}$$

with $\rho = \lambda / \mu < 1$. Moreover,

$$B_s = \int_0^\infty (1 - R(z)) f^k(z) dz \tag{3}$$

is the probability of failure occurring in a sampling interval s and represents the normalisation term of eqn. (2).

Integrating the two equations (2) and (3) we obtain (see Appendix)

$$B_s = 1 - \left(\frac{\mu}{\alpha_s + \mu} \right)^k \left(1 - \beta \frac{k(k+1)}{(\alpha_s + \mu)^2} \right) \tag{4}$$

$$A_{js} = \frac{1}{B_s} \left(\frac{\mu}{\alpha_s + \mu} \right)^{j-1} \left(1 - \frac{\mu}{\alpha_s + \mu} \right) + \frac{\beta}{B_s} \left(\frac{\mu}{\alpha_s + \mu} \right)^j \left(\frac{j(j+1)}{(\alpha_s + \mu)^2} - \frac{j(j-1)}{\mu(\alpha_s + \mu)} \right). \tag{5}$$

We can note that for $\beta = 0$ (i.e. if we do not consider the wear of the system with constant failure rate γ) we obtain the same results presented in [3]. Then, the β terms represent the corrections due to presence of wear process of the manufacturing system.

4. if a failure occurs while the j -th job in a given sampling interval s is in process, the probability of detecting it through this sample is given by [3]

$$q_{12s} = \sum_{j=1}^k A_{js} \sum_{m=0}^{j-1} \frac{\binom{j-1}{m} \binom{k-j+1}{n-m}}{\binom{k}{n}} \sum_{w+t=c+1}^n \binom{m}{w} p_1^w (1-p_1)^{m-w} \binom{n-m}{t} p_2 (1-p_2)^{n-m-t}.$$

3. THE COST FUNCTION

Let us consider a generic production cycle. The aim is to determine the optimal limit value c that minimises the expected loss processing time owing to an incorrect choice of the parameter c . An incorrect choice of c may give two possible contributes to the objective function:

1. [probability of no failure occurrence] [probability of giving a false alarm when the process is in-control] [loss time τ_1];
2. [probability that a failure occurs] [probability of non-giving a true alarm when the process is out-of-control] [loss time τ_2].

We can immediately estimate τ_1 that is equal to the loss time for a searching operation that was not necessary ($\tau_1 = \theta$). As regards τ_2 , it can not be immediately derived because the loss due to the second case may continue for several successive lots. In other words, many lots of k elements can be processed before the out-of-control state is detected. If T_c represents the loss time due to an incorrect choice of c , it follows that:

$$\begin{aligned} T_c &= (1 - B_s) q_1 \theta + B_s (1 - q_{12s}) q_2 \tau_2 + B_s (1 - q_{12s}) (1 - q_2) q_2 2 \tau_2 + \\ &\quad + \dots + B_s (1 - q_{12s}) (1 - q_2)^{i-1} q_2 i \tau_2 + \dots = \\ &= (1 - B_s) q_1 \theta + B_s (1 - q_{12s}) q_2 \tau_2 \sum_{i=0}^{\infty} (i+1) (1 - q_2)^i \end{aligned}$$

where

$$\tau_2 = (p_2 - p_1) \frac{k}{\lambda}$$

represents the loss time “in excess” compared with usual (i.e. with a probability p_1 of producing a defective unit) caused by the processing, in the out-of-control state, of a greater number of non conforming units in any successive lot, after the s -th lot, owing to the failure non detection. The equation can also be written in the following form:

$$T_c = T_\theta + T_\tau = (1 - B_s) q_1 \theta + B_s \tau_2 (1 - q_{12s}) \frac{1}{q_2}$$

where T_θ is the loss time due to inspections which were not necessary, and T_τ is the loss time due to the production of an excessive number of defective units. The two terms of T_c have not in general the same importance. In order to evaluate it, the two contributes of T_c

may be weighted with two numerical coefficients c_i and c_p . Based on the above, the general form of the equation is given by:

$$T_c = c_i(1 - B_s)q_1\theta + c_p B_s \tau_2(1 - q_{12s}) \frac{1}{q_2}.$$

The value of the two coefficients may be estimated considering the costs associated with the two different loss times. The loss time for false inspections T_θ includes, besides the operating costs to detect a failure for each false alarm, the costs due to the non-production caused by the system shut-down. To the loss time in producing defective units, may be added either the costs of scrapping defective sampled units or the costs of outgoing defective units (i.e. the post-sale failure costs). Thanks to these coefficients, it turns out that the objective function assumes an economic nature.

4. EXPERIMENTAL RESULTS

In order to verify whether the control policy (k,n,c) has to be changed during the wear process of the manufacturing system, we consider the set of parameters reported in Table 1.

K	n	θ	c_i	c_p	α	φ	p_1	p_2	μ	λ
85	8	30	0.6	1	0	$4 \cdot 10^{-6}$	0.05	0.25	4	2

Tab.1: Experimental data

Moreover, note that during the choice of the numerical values, we have taken into account the following aspects of the analytical model: (i) the binomial distribution has been used in the expressions of q_1 , q_2 , and q_{12s} . It turns out that the lot size k and the sample size n have to satisfy the inequality $n < k/10$. Otherwise, the hypergeometric distribution should be used; (ii) λ and μ values give the system's operating conditions in which the production system is not saturated (i.e., $\rho < 1$).

Since k and n values are considered to be constant, a variance in the (k,n,c) policy may result in a change in the acceptance number c over time. Table 2 shows the experimental results, in terms of T_c , according to what was obtained in the previous sections. Notice that the mean time between failure (MTBF), given by (for a Weibull distribution)

$$MTBF = \gamma + \eta \Gamma \left(1 + \frac{1}{\beta} \right),$$

is also reported.

As expected, the acceptance number c must be changed several times during a system cycle before the MTBF. In particular, while the first lot is processed, with a failure rate $\gamma(0)=0$ (i.e., the system is not subject to wear), it is worth making an inspection only if there are at least four defective units among the eight sampled ones. As lots are produced, the optimal control policy requires the limit control c to pass to more and more restrictive values until

$S=8$ where one defective unit causes the production shut-down in order to carry out an inspection. We want also to note that during the lot $S=34$ the minimising c value becomes equal to 0.

	S=1	S=2	S=3	S=4	S=5	S=6
c=0	6.054	6.031	6.008	5.986	5.963	5.941
c=1	1.047	1.103	1.158	1.213	1.267	1.321
c=2	0.149	0.314	0.478	0.640	0.802	0.962
c=3	0.141	0.659	1.174	1.684	2.191	2.694
c=4	0.568	2.791	4.997	7.188	9.362	11.521
	S=7	S=8	S=9	S=10	S=11	S=12
c=0	5.918	5.896	5.874	5.852	5.830	5.809
c=1	1.374	1.427	1.479	1.531	1.583	1.634
c=2	1.121	1.278	1.435	1.590	1.744	1.896
c=3	3.194	3.689	4.181	4.670	5.154	5.635
c=4	13.664	15.791	17.902	19.999	22.079	24.145

MTBF

Tab.2: Values of T_c with the varying of the lot S and the acceptance level c .

5. CONCLUSIONS

This paper analytically shows how, it is necessary to vary the parameters of the sampling plan (k, n, c) over the time in order to maintain optimal working conditions as the production wear goes on. In particular, the case of failure rate increasing in a linear way with the time it has been treated.

Future work should consider the development of the appropriate and more complex theory relevant to the more general case of a failure rate which grows with the time according to Weibull distribution.

ACKNOWLEDGEMENTS

This work has been supported by CNR and INFM funds. Dr. Braglia is a member of INFM - Section of Parma (Department of Physics, University of Parma, Italy). This paper has been written in memory of Prof. G.L. Braglia.

REFERENCES

1. Barlow, R.E., Hunter, L.C., Proschan, F.: Optimum checking procedures, Journal of the Society for Industrial and Applied Mathematics, 4 (1963), 1078-1095.
2. Valdez-Flores, C., Feldam, R.M.: A survey of preventive maintenance model for stochastically deteriorating single-unit, Naval Research Logistics, 36 (1989), 419-446.

3. Hsu, L.F., Tapiero, C.S.: An economic model for determining the optimal quality and process control quality in a queue-like production system, *International Journal of Production Research*, 28 (1990), 1447-1457.

APPENDIX

Now, we report the approximations imposed relevant to A_{js} and B_s calculation. Because the expression of the failure rate adopted is $\gamma(t) = \alpha_s + 2\beta t$, we can write that:

$$\begin{aligned}
 s = 1 \quad t = 0 \quad \alpha_1 &= \gamma(0) = \alpha, \\
 s = 2 \quad t = \frac{k}{\lambda} \quad \alpha_2 &= \gamma\left(\frac{k}{\lambda}\right) = \alpha + 2\beta \frac{k}{\lambda} = \alpha + 2\beta(2-1) \frac{k}{\lambda}, \\
 s = 3 \quad t = 2\frac{k}{\lambda} \quad \alpha_3 &= \gamma\left(2\frac{k}{\lambda}\right) = \alpha + 2\beta 2 \frac{k}{\lambda} = \alpha + 2\beta(3-1) \frac{k}{\lambda},
 \end{aligned}$$

...
and in general,

$$\alpha_s = \alpha + 2\beta(s-1) \frac{k}{\lambda}.$$

Considering the following integral:

$$A_{js} = \frac{1}{B_s} \int_0^\infty \int_0^\infty \left(e^{-\alpha_s x - \beta x^2} - e^{-\alpha_s(x+y) - \beta(x+y)^2} \right) f(y) f^R(x) dx dy,$$

where

$$B_s = \int_0^\infty \left(1 - e^{-\alpha_s z - \beta z^2} \right) f^k(z) dz, \quad f(y) = \mu e^{-\mu y}, \quad \text{and} \quad f^R(x) = \frac{e^{-\mu x} (\mu x)^{R-1} \mu}{(R-1)!}$$

with $R=j-1$.

Given that, if $x < 0,1$ and supposing a small value of β (i.e., $\beta x^2 < 0.1$), we can approximate to first order the exponential in the following way:

$$e^x = \sum_{k=0}^\infty (-1)^k \frac{x^k}{k!} = 1 - x + \frac{x^2}{2!} - \frac{x^3}{3!} + \dots \approx 1 - x,$$

then

$$A_{js} = \frac{1}{B_s} \int_0^\infty \int_0^\infty \left(e^{-\alpha_s x} (1 - \beta x^2) - e^{-\alpha_s(x+y)} (1 - \beta(x+y)^2) \right) f(y) f^R(x) dx dy,$$

and

$$B_s = \int_0^\infty \left(1 - e^{-\alpha_s z} (1 - \beta z^2) \right) f^k(z) dz.$$

Finally, developing the two integrals we obtain the equations (5) and (6) reported in the text.

AN SPC APPROACH TO THE ANALYSIS OF PROCESS CAPABILITIES OF A FLEXIBLE MANUFACTURING SYSTEM

M. Russo and D. Freguia
Danieli & C., Buttrio (UD), Italy
R. Guggia and R. Meneghello
University of Padua, Padua, Italy

KEY WORDS: Quality, SPC, Process Capabilities Indexes

ABSTRACT: Quality control extended to the entire life cycle, from design to final product inspection, is a prerequisite for technical and economical success.

The paper presents some activities aimed at analysing a Flexible Manufacturing System (FMS) machining process by means of Statistical Process Control (SPC) tool applied to dimensional characteristics of a Chock Support of a Rolling Mill Cartridge Stands.

The paper focuses on the analysis of Process Capabilities Indexes of data collected through an extensive Coordinate Measuring Machine (CMM) measurement campaign, at the end of machining operations. On the basis of measurement results, causes of variations have been identified. As a result, new fixtures and locking procedures have been designed with a view to achieve a process, under statistical control, capable to meet geometrical specifications required by the product functionality.

1. INTRODUCTION.

Statistical techniques are excellent tools for providing information on processes or machines. To improve products or processes many analysis and problem solving techniques are available. The Statistical Process Control (SPC) technique, applied in this study, allows an efficient and effective control of process as well as machine parameters.

A process is said to be operating in statistical control when the only sources of variation are common causes but a state of statistical control it's an achievement arrived at by elimination, one by one, by determined effort, of special causes of excessive variation. The first aim of a process control system is to provide a statistical signal when special causes of variation are present. Control charts are among the tools used to detect these special causes.

Published in: E. Kuljanic (Ed.) *Advanced Manufacturing Systems and Technology*,
CISM Courses and Lectures No. 406, Springer Verlag, Wien New York, 1999.

As long as the process remains in statistical control it will continue to be predictable with obvious benefits in consistency of quality, productivity and cost.

Once the process performance is predictable, its capability can be assessed.

Capability represents a measure of the actual performance of the process (or machine) when compared with specified tolerance limits. Thus it is utilised to assess influences on product variability due to the machine itself or the MACHINE-METHODS-MATERIALS-MAN-AMBIENT system.

In this work, an example of the combined approach of both Control Charts and Capabilities Indexes is presented.

2. INDUSTRIAL CONTEXT

The research work has been carried out at Danieli & C., a company specialised in the design and manufacture of systems and machines for the steelmaking and rolling industry.

The production departments are:

- Heat-treatments of raw and semifinished products
- Machining
- Structural steelwork
- Assembly

This case study consists in the analysis of the Yasda YBM 1000 FMS machining system.

3. THE APPROACH

The main purpose of the measurement campaign is that of:

- developing a procedure to quantify process capabilities indexes of the FMS chip forming machining applied to the selected component;
- comparing the effects of two fixture devices on geometrical product characteristics;

The procedure carried out to fulfil this purpose is structured into the following steps:

1. *identification* of product/process parameters to be monitored;
2. *definition* and selection of samples size and items (number of lots and samples for each lot);
3. *execution* of measurement campaign;
4. *analysis* of data, indexes calculation and optimisation opportunities;

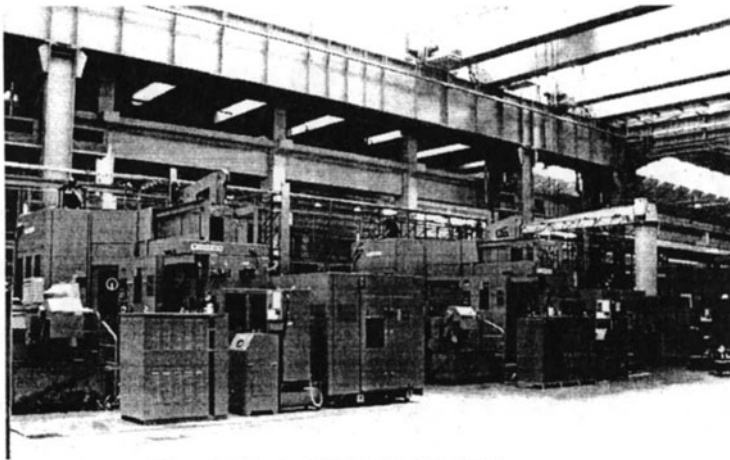


Fig. 1. Yasda FMS YBM1000 System.

Identification

The study focuses on the machining operations of the “Chock Supports” relevant to the “Cartridge stands” in figure 2. These chocks have considerable dimensions if compared with the centesimal tolerances required which ensure functional ability of the component; the central bore diameter nominal value is $\varnothing 390$ mm, H7 toleranced (0 to +0,057mm), and the side bores distance nominal value is 560 mm, H7 toleranced (0 to +0,070 mm).

Machining operations are performed on a FMS Yasda system (Fig. 1): process phases and relevant work-cycles have been optimised.

The process control point, i.e. the geometrical inspection phase, has been consequently defined: measurements are carried out at the end of all machinings.

Definition

The Yasda machine processes lots of different products; lots are generally small (100 pieces max. can be reached). The work time for the component selected is approximately 10 days for 50 pieces.

Ten lots have been considered; each lot counts 30 pieces. The sample represent approximately 15% of the entire lot; it means that each sample counts 5 components. The pieces are checked in a consecutive row within the lot (sample).

Execution

After machining operations, workpieces have been progressively numbered and time, date, drawing #, job #, and work order # have been recorded on a form by the Yasda operator. A Coordinate Measuring Machine has been utilised for the workpiece inspection and data collection. This system allows CNC programming of measurement cycles which assures the required repeatability of the inspection procedure.

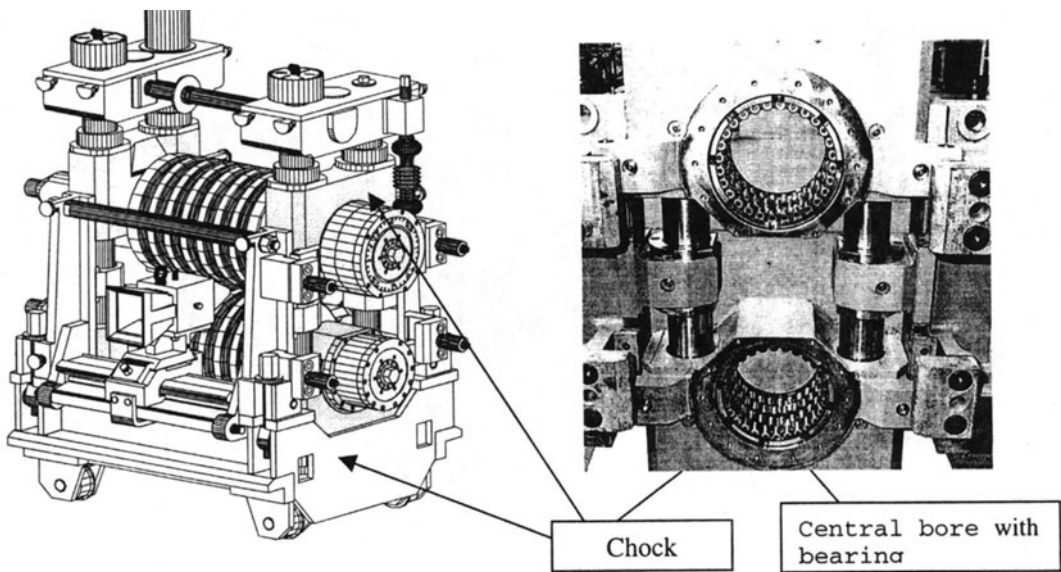


Figure 2. Representation of the Chock Support

The measurement cycle has been defined according to ISO 1101 requirements; adequate single-point probings have been homogeneously distributed on the surface of geometrical features, identified in step 1, whose relevant actual parameters values have been evaluated.

Analysis

Collected data are split into classes; for each of these classes the frequency is calculated and completed with the relevant histogram. The frequency distribution curve is then analysed by means of the Skewness (Sk) and Kurtosis (K) indexes to verify Normal distribution (Gaussian): this is a prerequisite to an effective capability analysis.

The actual values for Sk and K are to be verified according to the following intervals:

$$-0,5 \leq Sk \leq +0,5 \quad \text{and} \quad 2,5 \leq K \leq 3,5.$$

The capability analysis is based on capability indexes derived from control charts.

Control charts utilised are \bar{X} (sample average) and R (sample range) charts; data values of \bar{X} and R are plotted versus sequence of samples through time (fig. 4). For the entire study period the $\bar{\bar{R}}$ and $\bar{\bar{X}}$ are calculated:

$$\bar{\bar{R}} = \frac{R_1 + R_2 + \dots + R_{10}}{10}$$

$$\bar{\bar{X}} = \frac{\bar{X}_1 + \bar{X}_2 + \dots + \bar{X}_{10}}{10}$$

The main purpose of control charts analysis is to identify any evidence that the process average or the process variability are not operating within statistical control: the \bar{X} chart shows process location of the variable average value. The R chart highlights trends and patterns in the range of the variable.

Process Capability Indexes are a mean to indicate the process variability relative to specifications. Indexes Cp (amplitude capability) and Cpk (position capability) are defined as:

$$Cp = \frac{AmplitudeTp}{6\sigma} \quad Cpk = \frac{USL - \bar{X}}{3\sigma} \quad \text{or} \quad Cpk = \frac{\bar{X} - LSL}{3\sigma}$$

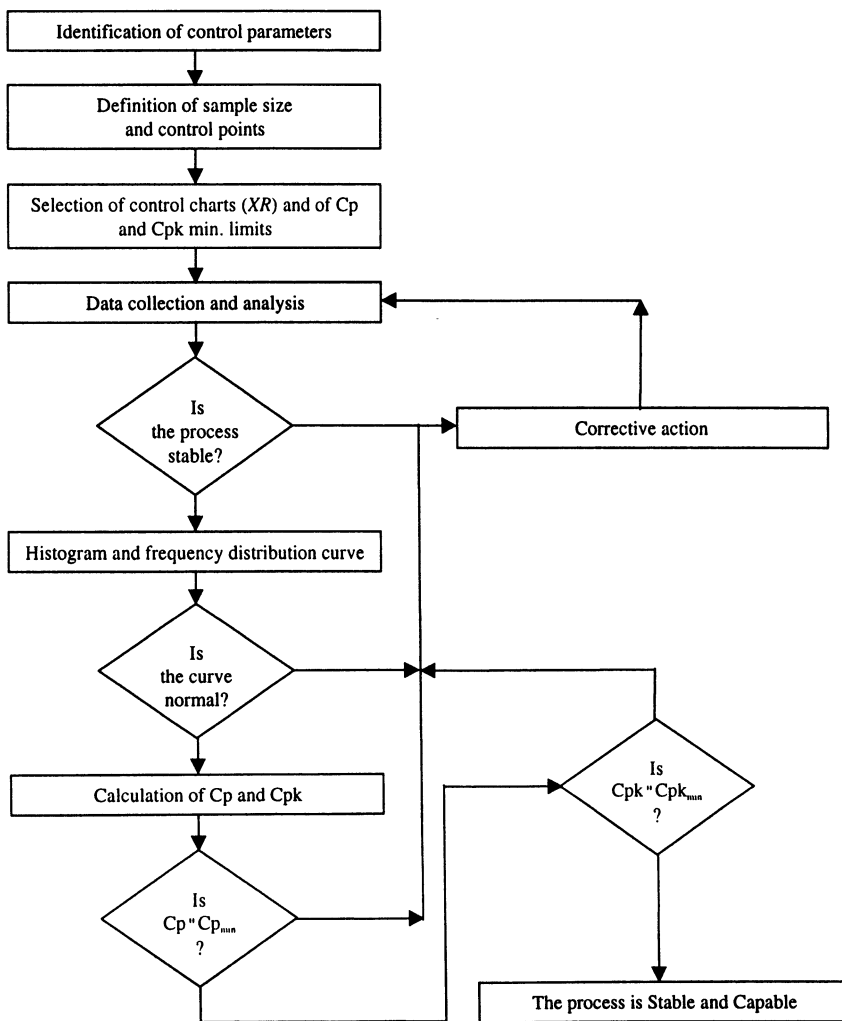


Figure 3. Representation of the implemented procedure.

With T_p = design tolerance, USL = Upper specification (tolerance) limit, LSL = Lower specification limit, \bar{X} = average values of the measured variable (X), σ = actual standard deviation of X. The lower value for Cpk is used.

Usually the 'target' (acceptable) process variability is pre-assigned to the Cp and Cpk indexes: a minimum value of 1,33 was adopted for both indexes.

The selected Cp represents the minimum value acceptable to define the "Capability" process; values comprised between 1 and 1,33 are in any case acceptable but they indicate that, as they move closer to 1, the process variability (frequency distribution curve) tends to cover the whole functional tolerance range. Values lower than 1 are absolutely unacceptable and the causes for the variability shall have to be removed.

A Cp equal to 1,33 indicates that the 6σ -range lies within 75% of the design tolerance T_p ; this means that the unknown part of the distribution could lie within the design tolerance and this is a safety margin.

With Cpk equal to 1,33 the distribution curve is centred versus the tolerance; in case of lower values, the process is either off-centre or it has a high variability; values comprised between 1 and 1,33 can be accepted but are considered to be extreme cases.

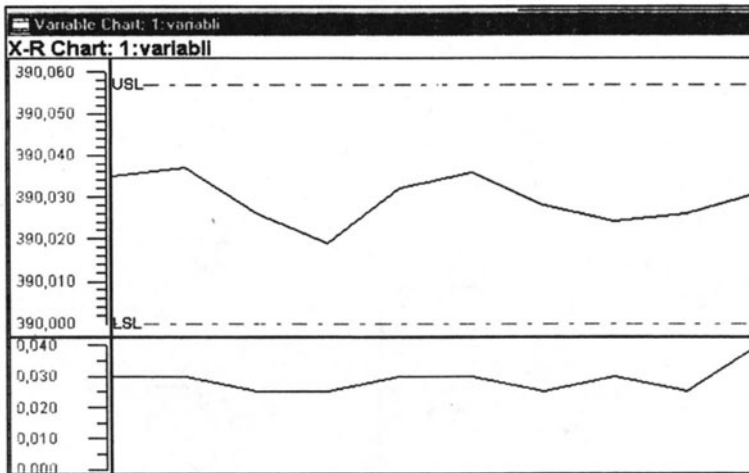


Fig. 4 Example of control chart data

4. RESULTS

Initial study

Measured data, obtained from workpieces machined by the Yasda FMS in its standard set-up, show a not-normal distribution of control parameters (fig. 5). In particular, Sk and K relevant to the central bore diameter are:

Sk=0,1 and K=1,99.

Control charts highlight an unexpected variability in the production process confirmed by having $C_p=0,76$ and $C_{pk}=0,74$ (Fig. 5); in this case the FMS-workpiece-ambient system is operating under negligible systematic causes: thus, it does not require any adjusting operation; as concerns variability, some unknown accidental effects act as amplifying the expected production spread: the cause might be erroneously locked parts as well as excessive machining single-operations tolerances.

A careful on-field inspection pointed out that the workpiece locking system was inadequate: more suitable fixtures and different locking torques were selected and applied. Moreover, Yasda operators were given a more thorough training on the work methods and the tool management was improved as regards both the wear extent and the replacement of bits.

Second study

The second data measurement cycle, run after these corrective actions, is presented in fig. 6:

it shows a Normal distribution of central bore diameter (Sk and K indexes within the limits).

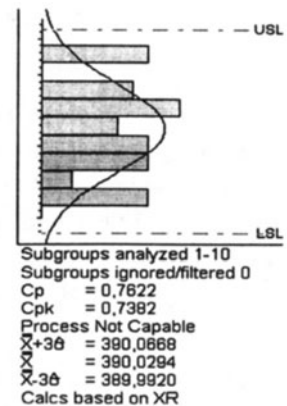


Fig. 5 . Results of initial study

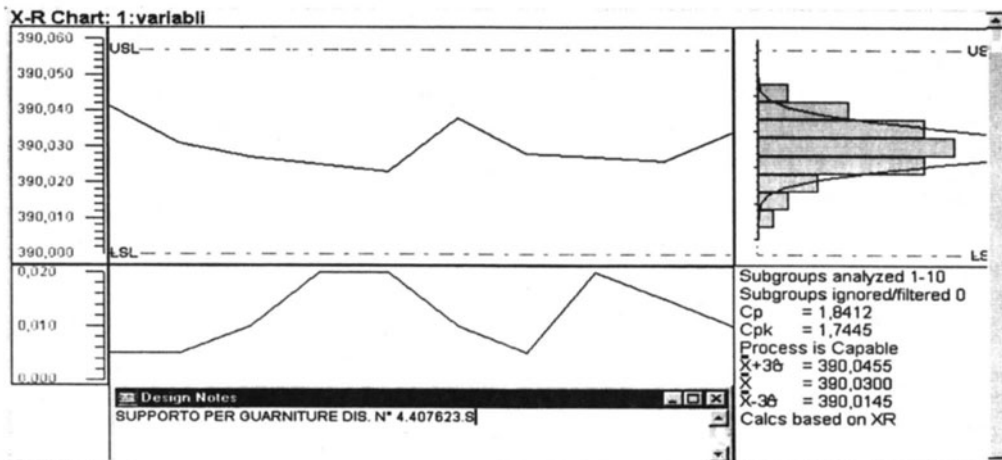


Fig. 6: results of the study after corrective actions

\bar{X} chart confirms the centred location (between tolerance limits) of the average bore $\bar{\bar{X}}$ diameter: equal to 390,029 mm and equal to 390,030 mm respectively in the initial and second study.

R chart reveals a clear improvement in the process variability, from 0,040mm to 0,020mm, while 6σ -range reduces from 0,075mm to 0,031mm.

The calculation of C_p and C_{pk} gives the following values:

$C_p = 1,84$ and $C_{pk} = 1,74$.

5. CONCLUSIONS

A process capability study on the machining of Chock Support for Rolling Mill Cartridge Stands was presented. The application of statistical techniques led to the identification and the quantitative assessment of most critical manufacturing parameters. Results coming from statistical analysis of the production data were used to design some process modifications; a new measurement campaign were then performed and a comparison with previous configuration was made. We can now say that the new configuration allows to maintain the control of the process as well as to achieve capability indexes as required by tolerance specifications.

REFERENCES

1. Montgomery D. C., Introduction to statistical quality control, Wiley, New York, 1996.
2. Krimmel O., Martinsen K., Tonnessen K., Rasch F.O., Increasing Efficiency by Analysing the Interface between ForMing and Machining, Proceedings AMST'99, (E. Kuljanic ed.), CISM Springer Verlag Series 406, 427-436, 1999, Springer Verlag Wien New York

PARTIAL MIXED EFFECTS SPLIT-PLOT DESIGN UNDER UNKNOWN SPATIAL DEPENDENCE

R. Guseo

University of Padua, Padua, Italy

KEY WORDS: Split-plot design, mixed effects, non-equicorrelated error terms.

ABSTRACT: It is well-known that sequential nested treatments give rise to unknown dependent error effects. Factorial designs assume independence of error term so that each experiment must be performed one at a time. Grouping experimental units is a common practice, therefore, statistical analysis must be conveniently modified.

For instance, in determining the effect of annealing temperature, factor A, in breaking strength of experimental metal alloys, the laboratory ovens are arranged with each different metal samples, factor B, (one for each alloy). The temperature levels assigned to each oven are different. The experiment may be replicated (blocking factor) during three different tours (shifts).

This is not a factorial design with blocking factors, because annealing is performed simultaneously (whole-plots) on different metal samples (sub-plots).

Standard split-plot design is based upon fixed effects and a special additive version of independent error term components (equicorrelation) under normality.

In many situations the effects of factors A and B may be no longer assumed fixed and, moreover, the spatial arrangement of sub-plots may not agree with the simple symmetric equicorrelation structure of residuals.

The paper is devoted to the combined statistical analysis under partial mixed effects and unknown spatial dependence.

Under these extended assumptions, it is proved that the usual standard significance tests

for block and factor A effects are exact in probability. The corresponding standard tests for main effects of B and interaction $A \times B$ are not F -distributed, nevertheless, a simple robust procedure may be applied.

1. INTRODUCTION

Basic *split-plot* design replication with fixed effects within random blocks is a well-known extension of traditional factorial designs due to an actual hierarchical application of factors to experimental units. For instance, a first factor (whole) is simultaneously applied to a set of experimental samples and a second factor is applied to smaller experimental units, e. g., samples or subplots. This nested application of factors give rise to special dependencies among residual errors.

This paper is devoted to the examination of robustness properties of basic split-plot analysis under mixed effects (partial) of main factors and unknown non-equicorrelated spatial dependence of residual errors.

The main results, paragraphs 4 and 5, state that the traditional split-plot analysis is practically stable or robust. There are only minor differences on non-centrality parameters and, therefore, on the power of statistical procedure.

2. BASIC FIXED EFFECTS SPLIT-PLOT UNDER COMPLETE BLOCKS

Let us consider a basic situation with two main factors, A , B , and a blocking factor. Economical and physical reasons suggest a remarkable modification of the standard factorial design, due to a natural hierarchy between factors A and B .

For instance, in determining the effect of annealing temperature, factor A , in breaking strength of experimental metal alloys, it is much more convenient to cluster some different metal samples, or different alloys that define factor B , in order to avoid an expensive randomized change of the temperature of a laboratory oven as established in a standard factorial design.

In this example, the annealing temperature has a leading role and factor B levels are nested within a special common level of factor A simultaneously applied to a cluster (whole-plot) of experimental units (sub-plots).

The blocking factor may be assigned to different experimental sessions in order to control environmental effects such as different tours or different laboratories, etc..

The residual normal stochastic errors are not i.i.d. as claimed by a regular factorial. The standard split-plot design assume *equicorrelation* among errors of responses of experimental units belonging to the same whole-plot.

Following the terminology of previous example, independence assumption of errors linked to breaking strength of metal alloys, simultaneously treated with a common annealing temperature, is no longer acceptable. Spatial positioning of metal samples in a standard split-plot design affect the correlation of errors with an assumed uniform

pattern (equicorrelation).

The basic fixed effects split-plot model under complete random blocks is

$$y_{ijk} = \mu + t_i + \alpha_j + \beta_k + (\alpha\beta)_{jk} + \varepsilon_{ijk}, \tag{1}$$

where $i = 1, 2, \dots, r$ is the block index; $j = 1, 2, \dots, a$ is the level index of factor A ; $k = 1, 2, \dots, b$ is the level index of factor B ; y_{ijk} is the observed response. The explanatory components of model (1) are: μ , the grand mean response; t_i , the random effect of the i -th block T_i , $T_i = T \sim \mathcal{N}(0, \sigma_T^2)$; α_j , the fixed effect of the j -th level of factor A , $\sum_{j=1}^a \alpha_j = 0$; β_k , the fixed effect of the k -th level of factor B , $\sum_{k=1}^b \beta_k = 0$; $(\alpha\beta)_{jk}$, the fixed level of the interaction $A \times B$ at levels j for A and k for B , $\sum_{j=1}^a (\alpha\beta)_{jk} = \sum_{k=1}^b (\alpha\beta)_{jk} = 0$.

The residual error term, ε_{ijk} , defines a stochastic normal experimental error of zero mean and common variance σ^2 , $\varepsilon_{ijk} \sim \mathcal{N}(0, \sigma^2)$, but, unlike canonical factorial model, the correlation among errors is

$$E(\varepsilon_{ijk} \cdot \varepsilon_{i'j'k'}) = \begin{cases} \rho\sigma^2 & \text{if } i = i', j = j', k \neq k'; \\ \sigma^2 & \text{if } i = i', j = j', k = k'; \\ 0 & \text{elsewhere.} \end{cases}$$

Independence between T and ε_{ijk} , $T \perp \varepsilon_{ijk}$, is a common and realistic assumption.

3. BLOCK MIXED EFFECT SPLIT-PLOT UNDER SPATIAL DEPENDENCE

Spatial positioning of experimental units (sub-plots) in a standard split-plot design affect the correlations among errors of the same whole-plot with a simple and uniform unknown equicorrelation pattern.

In order to model *locally* this dependence as a function of distance between subplots, some papers recently appeared treating special cases. See, for instance, references displayed in [1] and [2]. In a previous paper, [1], the standard dependence assumption of a fixed effect split-plot design was generalized in order to examine which part of standard split-plot analysis may be robustly performed. The extension was based upon $E(\varepsilon_{ijk}\varepsilon_{i'j'k'}) = \sigma^2 q_{kk'}$, where $\mathbf{Q} = (q_{kk'})$ is an *unknown* full rank correlation matrix.

Here we consider a further extension with reference to the nature of hierarchical factors A and B . We suppose that they are random effects with, possibly, non null mean effects. This extension is quite reasonable in many situations, specially when a deterministic control of a factor level is not available and, in particular, the planned change of regime between two levels is not perfectly deterministic with a stochastic dependence structure that does not depict the new local effect of factor as an independent one.

Here we assume that this type of dependence among levels of the same factor is unknown and stable (uniform) among them.

Let us define a vectorized version of model (1), coherent with implicit hierarchical order of effects, i. e., $\mathbf{y}^* = (y_{111}, y_{112}, \dots, y_{11b}, y_{121}, y_{122}, \dots, y_{12b}, \dots, y_{ra1}, y_{ra2}, \dots, y_{rab})'$, based upon the Kronecker product \otimes ,

$$\mathbf{y}^* = (\mathbf{1}_r \otimes \mathbf{1}_a \otimes \mathbf{1}_b)\mu + (\mathbf{I}_r \otimes \mathbf{1}_a \otimes \mathbf{1}_b)\mathbf{t} + (\mathbf{1}_r \otimes \mathbf{I}_a \otimes \mathbf{1}_b)\mathbf{a} + (\mathbf{1}_r \otimes \mathbf{1}_a \otimes \mathbf{I}_b)\mathbf{b} + (\mathbf{1}_r \otimes \mathbf{I}_a \otimes \mathbf{I}_b)\mathbf{v} + \boldsymbol{\epsilon}^*, \tag{2}$$

where, $\mathbf{t} \sim \mathcal{N}_r(\mathbf{0}, \sigma_T^2 \mathbf{I}_r)$ is a random block effect with zero mean, $\mathbf{a} \sim \mathcal{N}_a(\boldsymbol{\alpha}, \sigma_A^2 \boldsymbol{\Sigma}_a)$, $\boldsymbol{\Sigma}_a = (1 - \rho_a)\mathbf{I}_a + \rho_a \mathbf{J}_a$ is a random effect factor A , $\mathbf{b} \sim \mathcal{N}_b(\boldsymbol{\beta}, \sigma_B^2 \boldsymbol{\Sigma}_b)$, $\boldsymbol{\Sigma}_b = (1 - \rho_b)\mathbf{I}_b + \rho_b \mathbf{J}_b$ is a random effect factor B , \mathbf{v} summarises the fixed effects of interaction $A \times B$ and $\boldsymbol{\epsilon}^* \sim \mathcal{N}(\mathbf{0}, \sigma^2 \mathbf{V})$, $\mathbf{V} = (\mathbf{I}_r \otimes \mathbf{I}_a \otimes \mathbf{Q})$.

It may be proved that $\mathbf{t}^* = (\mathbf{I}_r \otimes \mathbf{1}_a \otimes \mathbf{1}_b)\mathbf{t} \sim \mathcal{N}(\mathbf{0}, \sigma_T^2 ab \mathbf{W}_T)$, $\mathbf{W}_T = (\mathbf{I}_r \otimes \mathbf{U}_a \otimes \mathbf{U}_b)$ and $\mathbf{U}_n = \frac{1}{n} \mathbf{J}_n = \frac{1}{n} \mathbf{1}_n \mathbf{1}'_n$; $\mathbf{a}^* = (\mathbf{1}_r \otimes \mathbf{I}_a \otimes \mathbf{1}_b)\mathbf{a} \sim \mathcal{N}(\boldsymbol{\alpha}^*, \sigma_A^2 r b \mathbf{W}_A)$, with $\mathbf{W}_A = (\mathbf{U}_r \otimes \boldsymbol{\Sigma}_a \otimes \mathbf{U}_b)$ and $\boldsymbol{\alpha}^* = (\mathbf{1}_r \otimes \mathbf{I}_a \otimes \mathbf{1}_b)\boldsymbol{\alpha}$; $\mathbf{b}^* = (\mathbf{1}_r \otimes \mathbf{1}_a \otimes \mathbf{I}_b)\mathbf{b} \sim \mathcal{N}(\boldsymbol{\beta}^*, \sigma_B^2 r a \mathbf{W}_B)$, with $\mathbf{W}_B = (\mathbf{U}_r \otimes \mathbf{U}_a \otimes \boldsymbol{\Sigma}_b)$ and $\boldsymbol{\beta}^* = (\mathbf{1}_r \otimes \mathbf{1}_a \otimes \mathbf{I}_b)\boldsymbol{\beta}$. Mutual stochastic independence of vectors \mathbf{t}^* , \mathbf{a}^* , \mathbf{b}^* and $\boldsymbol{\epsilon}^*$ is assumed.

If \mathbf{a}^* and \mathbf{b}^* are degenerate random vectors on $\boldsymbol{\alpha}^*$ and $\boldsymbol{\beta}^*$ we attain the model examined in [1]. Moreover, if \mathbf{Q} equals $(1 - \rho)\mathbf{I}_b + \rho \mathbf{J}_b$ then the basic fixed effects split-plot design under complete random blocks is attained.

Let us examine now which is the behaviour of the usual sum of squares statistics in order to arrange a correct analysis of variance under these extensions.

The main purpose is to evaluate to which extent the usual analysis, based upon the basic fixed effects split-plot under complete random blocks, may be performed exactly or by the means of a robust approximation.

4. RANDOM BLOCKS AND FACTOR A EFFECTS ANALYSIS

The random effect of the block factor T is evaluated via SSR , i. e.,

$$SSR = \sum_i y_{i..}^2 / ab - y^2 / rab = \sum_{ijk} (t_i - t./r + \epsilon_{i..} / ab - \epsilon_{...} / rab)^2, \tag{3}$$

where a dot denotes a sum over the corresponding index, e. g., $t. = \sum_{i=1}^r t_i$, and the involved random vectors are \mathbf{t}^* and $\boldsymbol{\epsilon}^*$.

Let us define $\mathbf{e}^* = \boldsymbol{\epsilon}^* + \mathbf{t}^*$ and $\mathbf{R} = [(\mathbf{I}_r - \mathbf{U}_r) \otimes \mathbf{U}_a \otimes \mathbf{U}_b]$, with $\text{rank } r(\mathbf{R}) = r - 1$, then, $SSR = \mathbf{e}^{*'} \mathbf{R} \mathbf{e}^*$ and $\mathbf{e}^* \sim \mathcal{N}(\mathbf{0}, \sigma^2 \mathbf{V} + \sigma_T^2 ab \mathbf{W}_T)$.

Let us fix $\tilde{\mathbf{R}} = \mathbf{R} / \phi$ with ϕ defined later on. Note that $\mathbf{R} \mathbf{V} = (\mathbf{I}_r - \mathbf{U}_r) \otimes \mathbf{U}_a \otimes \mathbf{U}_b \mathbf{Q}$ and $\mathbf{R} \mathbf{W}_T = (\mathbf{I}_r - \mathbf{U}_r) \otimes \mathbf{U}_a \otimes \mathbf{U}_b$, then

$$\tilde{\mathbf{R}} \text{Var}(\mathbf{e}^*) = \frac{1}{\phi} \{ (\mathbf{I}_r - \mathbf{U}_r) \otimes \mathbf{U}_a \otimes \mathbf{U}_b (\sigma^2 \mathbf{Q} + \sigma_T^2 ab \mathbf{I}_b) \}. \tag{4}$$

Let us evaluate if a real number ϕ exists such that $\tilde{\mathbf{R}} \text{Var}(\mathbf{e}^*)$ is an idempotent matrix. Firstly, consider that

$$\mathbf{U}_t \mathbf{S} \mathbf{U}_t = \frac{s}{t} \mathbf{U}_t, \quad s = \mathbf{1}'_t \mathbf{S} \mathbf{1}_t, \tag{5}$$

and s denotes the sum of all entries of matrix \mathbf{S} .

The squared version of matrix (4), with $\mathbf{S} = \sigma^2 \mathbf{Q} + \sigma_T^2 ab \mathbf{I}_b$, is equal to

$$\begin{aligned} (\tilde{\mathbf{R}}\text{Var}(\mathbf{e}^*))^2 &= \frac{1}{\phi^2} \{(\mathbf{I}_r - \mathbf{U}_r) \otimes \mathbf{U}_a \otimes \mathbf{U}_b \mathbf{S} \mathbf{U}_b \mathbf{S}\} \\ &= \frac{1}{\phi^2} \left\{ (\mathbf{I}_r - \mathbf{U}_r) \otimes \mathbf{U}_a \otimes \frac{s}{b} \mathbf{U}_b \mathbf{S} \right\}, \end{aligned} \tag{6}$$

and, therefore, idempotency is attained for $\phi = \frac{s}{b} = \left(\frac{\sigma^2 s_b}{b} + \sigma_T^2 ab \right)$, and $s_b = \mathbf{1}'_b \mathbf{Q} \mathbf{1}_b$.

By a well-known theorem on normal quadratic forms, see e. g. [3] p. 57, it follows that

$$\frac{SSR}{\phi} = \mathbf{e}^{*\prime} \tilde{\mathbf{R}} \mathbf{e}^* \sim \chi^2_{[r-1,0]}, \tag{7}$$

and, in particular, the mean value of $MSR = SSR/(r - 1)$ is $E(MSR) = \phi = \frac{\sigma^2 s_b}{b} + \sigma_T^2 ab$.

Note that, under the null hypothesis on block effects,

$$SSR \stackrel{H_0}{\sim} \frac{\sigma^2 s_b}{b} \chi^2_{[r-1,0]}. \tag{8}$$

The random effect of the factor A is evaluated by the quadratic form SSA ,

$$SSA = \sum_j y_{.j.}^2 / rb - y_{...}^2 / rab = \sum_{ijk} \left(a_j - \frac{a.}{a} + \varepsilon_{.j.} / rb - \varepsilon_{...} / rab \right)^2, \tag{9}$$

a function of random vectors \mathbf{a}^* and $\boldsymbol{\epsilon}^*$.

Let us define $\mathbf{e}^* = \mathbf{a}^* + \boldsymbol{\epsilon}^*$, $\mathbf{F}_A = [\mathbf{U}_r \otimes (\mathbf{I}_a - \mathbf{U}_a) \otimes \mathbf{U}_b]$, with $\text{rank } r(\mathbf{F}_A) = a - 1$, and $\tilde{\mathbf{F}}_A = \frac{\mathbf{F}_A}{\psi}$ with a real ψ defined later on, then $SSA = \mathbf{e}^{*\prime} \mathbf{F}_A \mathbf{e}^*$ and $\mathbf{e}^* \sim \mathcal{N}(\boldsymbol{\alpha}^*, \sigma^2 \mathbf{V} + \sigma_A^2 rb \mathbf{W}_A)$.

Consider the product matrix

$$\tilde{\mathbf{F}}_A \text{Var}(\mathbf{e}^*) = \frac{1}{\psi} \left\{ \mathbf{U}_r \otimes (\mathbf{I}_a - \mathbf{U}_a) \otimes \mathbf{U}_b (\sigma^2 \mathbf{Q} + \sigma_A^2 rb (1 - \rho_a) \mathbf{I}_b) \right\}. \tag{10}$$

Following a proof similar to steps (4 - 8), its squared version is idempotent if and only if $\psi = \frac{s}{b} = \left(\frac{\sigma^2 s_b}{b} + \sigma_A^2 rb (1 - \rho_a) \right)$ and then,

$$\frac{SSA}{\psi} = \mathbf{e}^{*\prime} \tilde{\mathbf{F}}_A \mathbf{e}^* \sim \chi^2_{[a-1, \frac{1}{2\psi} rb \sum_{i=1}^a \alpha_i^2]}, \tag{11}$$

where, the non centrality parameter is $\frac{1}{2} E(\mathbf{e}^{*\prime} \tilde{\mathbf{F}}_A \mathbf{e}^*) = \frac{1}{2\psi} rb \sum_{i=1}^a \alpha_i^2$ and the mean value of $MSA = SSA/(a - 1)$ is $E(MSA) = \psi \left[1 + \frac{2\lambda}{a-1} \right] = \psi + \frac{rb}{a-1} \sum_{i=1}^a \alpha_i^2 = \left[\frac{\sigma^2 s_b}{b} + \sigma_A^2 rb (1 - \rho_a) + \frac{rb}{a-1} \sum_{i=1}^a \alpha_i^2 \right]$.

Note that, under the null hypothesis, $H_0 : \alpha_j = 0$ and $\sigma_A^2 = 0$ (or $\rho_a^2 = 1$), $j = 1, 2, \dots, a$,

$$SSA \stackrel{H_0}{\sim} \frac{\sigma^2 s_b}{b} \chi_{[a-1,0]}^2. \tag{12}$$

The sum of squares that may be compared with SSR and SSA is

$$\begin{aligned} SSEA &= \sum_{ij} y_{ij}^2/b - \sum_j y_{.j}^2/rb - \sum_i y_{i.}^2/ab + y_{...}^2/rab \\ &= \sum_{ijk} (\varepsilon_{ij.}/b - \varepsilon_{.j.}/rb - \varepsilon_{i..}/ab + \varepsilon_{...}/rab)^2 \\ &= \mathbf{e}^{*'} \tilde{\mathbf{F}}_{EA} \mathbf{e}^*, \end{aligned} \tag{13}$$

where $\mathbf{e}^* = \boldsymbol{\epsilon}^*$, $\mathbf{F}_{EA} = (\mathbf{I}_r - \mathbf{U}_r) \otimes (\mathbf{I}_a - \mathbf{U}_a) \otimes \mathbf{U}_b$, with $\text{rank } r(\mathbf{F}_{EA}) = (r-1)(a-1)$, and $\tilde{\mathbf{F}}_{EA} = \mathbf{F}_{EA}/\varphi$.

Idempotency of $\tilde{\mathbf{F}}_{EA} \text{Var}(\mathbf{e}^*)$ is attained for $\varphi = \frac{\sigma^2 s_b}{b}$, then

$$SSEA \sim \frac{\sigma^2 s_b}{b} \chi_{[(r-1)(a-1);0]}^2, \tag{14}$$

and $E(MSEA) = \frac{\sigma^2 s_b}{b}$.

It is easy to prove that $SSEA$, SSR and SSA are mutually independent. Therefore, the traditional split-plot analysis is exact in testing block and random factor A effects and is based upon Snedecor's F distributions.

5. RANDOM FACTOR B AND INTERACTION $A \times B$ ANALYSIS

The random effect of factor B is recognised by SSB ,

$$SSB = \sum_k y_{..k}^2/ra - y_{...}^2/rab = \sum_{ijk} \left(b_k - \frac{b}{b} + \varepsilon_{..k}/ra - \varepsilon_{...}/rab \right)^2, \tag{15}$$

a quadratic form based upon \mathbf{b}^* and $\boldsymbol{\epsilon}^*$. Let us define $\mathbf{e}^* = \mathbf{b}^* + \boldsymbol{\epsilon}^*$, $\mathbf{F}_B = \mathbf{U}_r \otimes \mathbf{U}_a \otimes (\mathbf{I}_b - \mathbf{U}_b)$ with $\text{rank } r(\mathbf{F}_B) = b - 1$, and $\tilde{\mathbf{F}}_B = \mathbf{F}_B/\gamma$ so that $SSB = \mathbf{e}^{*'} \mathbf{F}_B \mathbf{e}^*$ and $\mathbf{e}^* \sim \mathcal{N}(\boldsymbol{\beta}^*, \sigma^2 \mathbf{V} + \sigma_B^2 r a \mathbf{W}_B)$.

Unfortunately, there does not exist a real number γ such that the product $\tilde{\mathbf{F}}_B \text{Var}(\mathbf{e}^*)$ give rise to an idempotent matrix,

$$\tilde{\mathbf{F}}_B \text{Var}(\mathbf{e}^*) = \frac{1}{\gamma} \left\{ \mathbf{U}_r \otimes \mathbf{U}_a \otimes (\mathbf{I}_b - \mathbf{U}_b) [\sigma^2 \mathbf{Q} + \sigma_B^2 r a (1 - \rho_b) \mathbf{I}_b] \right\}. \tag{16}$$

Nevertheless, the mean value and the variance of SSB may be easily determined via a simple theorem in [3] p. 55. In particular, the expected value of SSB is

$$E(SSB) = \text{tr}\{\mathbf{F}_B(\sigma^2 \mathbf{V} + \sigma_B^2 r a \mathbf{W}_B)\} + \boldsymbol{\beta}^{*'} \mathbf{F}_B \boldsymbol{\beta}^*$$

$$\begin{aligned}
 &= \text{tr}\{\mathbf{U}_r \otimes \mathbf{U}_a \otimes (\mathbf{I}_b - \mathbf{U}_b)[\sigma^2 \mathbf{Q} + \sigma_B^2 ra(1 - \rho_b)\mathbf{I}_b]\} + ra \sum_{k=1}^b \beta_k^2 \\
 &= \sigma^2 \left(\text{tr} \mathbf{Q} - \frac{s_b}{b} \right) + \sigma_B^2 ra(1 - \rho_b)(b - 1) + ra \sum_{k=1}^b \beta_k^2, \tag{17}
 \end{aligned}$$

and, therefore,

$$E(MSB) = \frac{\sigma^2}{b - 1} \left(\text{tr} \mathbf{Q} - \frac{s_b}{b} \right) + \sigma_B^2 ra(1 - \rho_b) + \frac{ra}{b - 1} \sum_{k=1}^b \beta_k^2. \tag{18}$$

The variance of SSB is

$$\text{Var}(SSB) = 2 \left\{ \text{tr}[\mathbf{F}_B(\sigma^2 \mathbf{V} + \sigma_B^2 ra \mathbf{W}_B)]^2 + 2\boldsymbol{\beta}^* \mathbf{F}_B(\sigma^2 \mathbf{V} + \sigma_B^2 ra \mathbf{W}_B) \mathbf{F}_B \boldsymbol{\beta}^* \right\}. \tag{19}$$

Under the null hypothesis $\text{Var}(SSB/H_0)$ is

$$\text{Var}(SSB/H_0) = 2\sigma^4 \text{tr}[(\mathbf{I}_b - \mathbf{U}_b)\mathbf{Q}]^2. \tag{20}$$

The random effect of B , measured by SSB , may be compared with $SSEAB$,

$$\begin{aligned}
 SSEAB &= \sum_{ijk} y_{ijk}^2 - \sum_{ij} y_{ij.}^2/b - \sum_{jk} y_{.jk}^2/r + \sum_j y_{.j.}^2/rb \\
 &= \sum_{ijk} (\varepsilon_{ijk} - \varepsilon_{ij.}/b - \varepsilon_{.jk}/r + \varepsilon_{.j.}/rb)^2, \tag{21}
 \end{aligned}$$

a quadratic form based upon vector $\boldsymbol{\epsilon}^*$.

Let us define $\mathbf{F}_{EAB} = (\mathbf{I}_r - \mathbf{U}_r) \otimes \mathbf{I}_a \otimes (\mathbf{I}_b - \mathbf{U}_b)$ a matrix with rank $r(\mathbf{F}_{EAB}) = (r - 1)a(b - 1)$ and $\mathbf{e}^* = \boldsymbol{\epsilon}^*$. It may be proved that $\mathbf{e}^* \sim \mathcal{N}(\mathbf{0}, \sigma^2 \mathbf{V})$ and

$$SSEAB = \mathbf{e}^{*'} \mathbf{F}_{EAB} \mathbf{e}^*. \tag{22}$$

Given $\tilde{\mathbf{F}}_{EAB} = \mathbf{F}_{EAB}/\delta$, there does not exist again a real δ such that

$$\tilde{\mathbf{F}}_{EAB} \text{Var}(\mathbf{e}^*) = \frac{\sigma^2}{\delta} \{ (\mathbf{I}_r - \mathbf{U}_r) \otimes \mathbf{I}_a \otimes (\mathbf{I}_b - \mathbf{U}_b) \mathbf{Q} \},$$

is an idempotent matrix.

With simple computations it may be proved that

$$E(SSEAB) = \sigma^2(r - 1)a \left(\text{tr} \mathbf{Q} - \frac{s_b}{b} \right) \tag{23}$$

and, therefore,

$$E(MSEAB) = \frac{\sigma^2}{b - 1} \left(\text{tr} \mathbf{Q} - \frac{s_b}{b} \right), \tag{24}$$

with variance

$$\text{Var}(SSEAB) = 2\sigma^4 a(r - 1)\text{tr}((I_b - U_b)Q)^2. \tag{25}$$

6. CONCLUDING REMARKS

Under the null hypothesis on the effects of factor B , the ratio $R_B = MSB/MSEAB$ may be examined following the robust results in [1]. With a similar argument the fixed effect due to interaction between factors A and B may be detected via the quadratic form $SSAB$.

The table **Tab. 1** summarises the ANOVA for a partially mixed effects split-plot design under unknown spatial dependence. The F ratio of the first part are exactly distributed according to a Snedecor's F . The ratios R of the second part are only an approximation and may be compared with the robust thresholds in [1].

Tab. 1 ANOVA: Partial mixed Split-Plot with two Factors and Complete Blocks			
Source	$MS()$	$E(MS)$	Ratio
BLOCK	$R = \frac{SSR}{(r-1)}$	$\frac{s_b\sigma^2}{b} + ab\sigma_T^2$	F_R
FACT. A	$A = \frac{SSA}{(a-1)}$	$\frac{s_b\sigma^2}{b} + \sigma_A^2 rb(1 - \rho_a) + rb \sum_j \frac{\alpha_j^2}{(a-1)}$	F_A
ER. (A)	$EA = \frac{SSEA}{((a-1)(r-1))}$	$\frac{s_b\sigma^2}{b}$	
FACT. B	$B = \frac{SSB}{(b-1)}$	$\frac{\sigma^2}{b-1} (\text{tr}Q - \frac{s_b}{b}) + \sigma_B^2 ra(1 - \rho_b) + ra \sum_k \frac{\beta_k^2}{(b-1)}$	R_B
IN. $A \times B$	$AB = \frac{SSAB}{((a-1)(b-1))}$	$\frac{\sigma^2}{b-1} (\text{tr}Q - \frac{s_b}{b}) + r \sum_{jk} \frac{(\alpha\beta)_{jk}^2}{((a-1)(b-1))}$	R_{AB}
E. ($A \times B$)	$EAB = \frac{SSEAB}{(a(b-1)(r-1))}$	$\frac{\sigma^2}{b-1} (\text{tr}Q - \frac{s_b}{b})$	

REFERENCES

- Guseo, R.: Split-plot design: a robust analysis, in E. Kuljanic (Ed.) *Advanced Manufacturing Systems and Technology*, CISM Courses and Lectures No. 372, Springer Verlag, Wien New York, (1996), 849-856.
- Kuri, A.I., Mathew, T. e Sinha, Bimal K.: *Statistical Tests for Mixed Linear Models*, Wiley, New York, 1998.
- Searle, S.R.: *Linear Models*, Wiley, New York, 1971.

SOME COMMENTS ABOUT RUN ORDERS IN PERFORMING TWO-LEVEL FACTORIAL DESIGNS

C. Mortarino

University of Padua, Padua, Italy

KEY WORDS AND PHRASES: Correlated observations, Trend resistant run order.

ABSTRACT: The problem of finding trend resistant run sequences in performing factorial designs has been raised in past years and solutions have been provided to create trend resistant run orders with minimum number of level changes (in order to reduce experimental costs). With these sequences estimates of factors effects are not affected (biased) by the eventual presence of a trend component into the model.

A simultaneous question is introduced by correlation among observed responses. When a V-robust dependence pattern might be assumed it was proved that ordinary least squares estimates are totally efficient if a two level fractional factorial design is performed.

The aim of this paper is to make evidence on the link existing between those two different types of robustness (against an additive trend component and against correlation among observations). Moreover it is here proved that, even if both nuisance sources are present, ordinary least squares estimates are unbiased and totally efficient.

1. INTRODUCTION

Suppose an experiment is to be performed according to a given fractional factorial

design. In some cases, the time order in which the runs or treatment combinations are performed need not be randomized. Instead, certain systematic run orders may be preferred. For example, if the runs are carried out in some time or space sequence, each observation may be affected by a trend which is a function of time or position. In the presence of a time trend, a nonrandomized run order may improve the efficiency with which factor effects are estimated.

The cost of conducting an experiment is often of practical importance. A second run order criterion may be a cost function based on the number of times each factor changes level. The practical interpretation is that it costs a certain amount to change the levels of each factor, for example to reset a measurement instrument, change the fertilizer on a field trial, restart an industrial plant and so on. The literature makes available some algorithms for creating run sequences which may balance between those two dual objectives. In section 2. main references will be given together with a quick outline of that approach.

Simultaneously there might be the problem of correlation among responses measured on different runs. In [1] is recalled the definition of V-robust dependence pattern and is there stated also the main result proved in [2], namely coincidence between OLSE and WLSE for parameters of a multiresponse linear model when a two level fractional factorial design is performed. In section 3. the notation (here and there) used will be described in order to provide a suitable tool to explain the link existing between those two different types of assumption.

In section 4. it is proved that, when the special sequences proposed in order to make estimates robust with respect to a time trend effect are performed, V-robustness dependence pattern leads again to coincidence between OLSE and WLSE of factor effects parameters and those estimates are also robust with respect to trend effects.

Finally, section 5. will compare the approach here followed to combine trend resistance with correlated responses with approaches followed by [3] and [4].

2. TREND RESISTANT RUN ORDERS

In experiments that must be carried out in a time sequence, some practical considerations may point to the use of a systematic run order instead of a complete randomization (the widespread advice given to experimenters).

First of all, a randomized sequence might have big costs due to the total number of level changes enforced. For some factors, level changes may need themselves time (temperature modification, alloy or amalgam composition, for example) or may force to long waiting time to reach again the original system steadiness. Since in almost every real experimental procedure a waste of time entails big costs, level changes

should be carefully taken into account in experimental planning. This is, actually, the reason why randomization has been often overlooked in practical experimentation. Run sequences with a small number of level changes may represent an interesting solution (provided that, of course, these sequences are created following “statistical principles” in addition to empirical ones).

Furthermore, since observations may be affected by a time trend effect, a run order counteracting this adverse effect could be essential to avoid misleading results. If a polynomial time trend perturbs observations, factors effect estimates calculated without considering it will be heavily biased. For this reason it is very important to find out if some run sequences might eliminate that bias effect.

This two-objective problem has been recently examined in the statistical literature: [5] provides a very clear survey of results by that time available. The *foldover* method and the DW method are there described and compared. Those procedures allow the construction of run sequences with a small number of level changes and such that

$$\mathbf{X}'\mathbf{T} = \mathbf{O} \quad (1)$$

(here \mathbf{X} is the model matrix while \mathbf{T} encloses some trend effect). Condition (1) states that effects to be estimated (columns of \mathbf{X}) are *orthogonal* with respect to time trend effects (usually linear or quadratic trends are examined) so that estimates are not biased at all by trend.

In particular, the outcome of the foldover method and the DW method is not a single run sequence, but those methods generate a whole *class* of equivalent sequences (with respect to trend resistance). The choice of a specific element of that class can be done using the cost (number of level changes) criterion.

This approach has been completed by more recent works ([6], [7], among the others), where the same twofold criterion is applied to find out sequences of asymmetrical factorial designs and also asymmetrical orthogonal arrays.

A further related research topic is recently represented by [8], where optimality of certain block designs is proved even in presence of linear trend.

3. CORRELATED RESPONSES

In [1] the problem of correlation among responses measured on different runs is discussed with examples of situations where this problem arises. In that paper the V -robust dependence pattern is recalled for the more complex context of a multiresponse model. Multiresponse observations naturally stem from real application where a single item is classified according to many features (in other words, many responses are simultaneously measured on the same experimental unit). In this paper, for the

sake of simplicity, only the uniresponse model will be considered, but the same results could be proved for the more general case as well.

Let

$$\mathbf{y} = \mathbf{X}\boldsymbol{\beta} + \boldsymbol{\varepsilon} \quad (2)$$

be the linear model to be examined. Here \mathbf{y} denotes the n -vector of observed responses from a fractional factorial experiment with n runs, $\mathbf{X}_{n \times p}$ is the matrix containing columns corresponding to effects to be estimated, either main effects or interaction effects, $\boldsymbol{\beta}_{p \times 1}$ is the vector of parameters of interest. Correlation among different observations is modelled by assuming that $\boldsymbol{\varepsilon}_{n \times 1}$ is a vector of random errors with zero mean, $E(\boldsymbol{\varepsilon}) = \mathbf{0}$, and covariance matrix

$$\text{Var}(\boldsymbol{\varepsilon}) = \boldsymbol{\Sigma}.$$

That covariance matrix is assumed to be V -robust with respect to \mathbf{X} (this dependence pattern essentially links covariance between responses measured in two runs to the difference of factors setup used for those two runs). From this assumption an important result follows:

$$\text{WLSE}(\boldsymbol{\beta}) = (\mathbf{X}'\boldsymbol{\Sigma}^{-1}\mathbf{X})^{-1}\mathbf{X}'\boldsymbol{\Sigma}^{-1}\mathbf{y} = (\mathbf{X}'\mathbf{X})^{-1}\mathbf{X}'\mathbf{y} = \text{OLSE}(\boldsymbol{\beta}), \quad (3)$$

the weighted least squares estimator (WLSE) for $\boldsymbol{\beta}$ (which is the best linear unbiased estimator) is equal to the ordinary least squares estimator (OLSE), whose calculation can be performed independently from $\boldsymbol{\Sigma}$. Equality (3) can be proved since V -robustness of $\boldsymbol{\Sigma}$ with respect to \mathbf{X} leads to

$$\boldsymbol{\Sigma}\mathbf{X} = \mathbf{X}\boldsymbol{\Lambda} \quad (\text{and } \mathbf{X}'\boldsymbol{\Sigma}^{-1} = \boldsymbol{\Lambda}^{-1}\mathbf{X}'), \quad (4)$$

where $\boldsymbol{\Lambda}$ is a $p \times p$ diagonal matrix whose nonzero elements are eigenvalues for $\boldsymbol{\Sigma}$.

4. MAIN RESULT

Problems discussed in previous sections might not raise only separately. For this reason, it would be interesting to analyse the impact of combining into a single model a trend effect on the mean value of \mathbf{y} and a correlation effect among its components. The model here assumed for \mathbf{y} is then the following:

$$\mathbf{y} = \mathbf{X}\boldsymbol{\beta} + \mathbf{T}\boldsymbol{\alpha} + \boldsymbol{\varepsilon}. \quad (5)$$

The time trend effect on the mean value of the responses is modelled via the product $T\alpha$. Parameters in α are here treated as noise parameters and their estimation is consequently neglected. Observe that since the run sequence here performed has been chosen to be resistant against time trend components, matrix T must satisfy link (1). Finally, as in (2), $\epsilon_{n \times 1}$ is a vector of random errors with zero mean, $E(\epsilon) = \mathbf{0}$, and covariance matrix $\text{Var}(\epsilon) = \Sigma$.

The following theorem can now be proved.

Theorem. *Consider model (5). If Σ is assumed to be V -robust with respect to X , then assuming (1), OLSE for interesting parameters, β , produce the best linear estimators (and estimates are also robust with respect to trend effects).*

Proof.

Denoting by Z the matrix obtained by adding T 's columns to matrix X ,

$$Z_{n \times (p+t)} = [X, T],$$

and denoting by γ the $(p+t)$ -vector obtained by stacking elements of β and α ,

$$\gamma = [\beta', \alpha']',$$

it is well known that

$$\text{WLSE}(\gamma) = (Z'\Sigma^{-1}Z)^{-1}Z'\Sigma^{-1}y. \quad (6)$$

Using (4) and (1), it is possible to prove that the product matrix within brackets is a block diagonal matrix:

$$\begin{aligned} Z'\Sigma^{-1}Z &= \begin{bmatrix} X' \\ T' \end{bmatrix} \Sigma^{-1} [X \ T] \\ &= \begin{bmatrix} X'\Sigma^{-1}X & X'\Sigma^{-1}T \\ T'\Sigma^{-1}X & T'\Sigma^{-1}T \end{bmatrix} \\ &= \begin{bmatrix} \Lambda^{-1}X'X & \Lambda^{-1}X'T \\ T'X\Lambda^{-1} & T'\Sigma^{-1}T \end{bmatrix} \\ &= \begin{bmatrix} \Lambda^{-1}X'X & O \\ O' & T'\Sigma^{-1}T \end{bmatrix}. \end{aligned} \quad (7)$$

By substituting (7) into (6) and using again (4), it follows immediately that

$$\begin{aligned}
 \text{WLSE}(\boldsymbol{\beta}) &= (\boldsymbol{\Lambda}^{-1} \mathbf{X}' \mathbf{X})^{-1} \mathbf{X}' \boldsymbol{\Sigma}^{-1} \mathbf{y} \\
 &= (\mathbf{X}' \mathbf{X})^{-1} \mathbf{X}' \mathbf{y} \\
 &= \text{OLSE}(\boldsymbol{\beta}). \quad \square
 \end{aligned}$$

Previous result states robustness of $\text{OLSE}(\boldsymbol{\beta})$ against two possible simultaneous model misspecifications: an additive trend effect and a correlation pattern among response components. Ordinary least squares estimates are generally appropriate for model (2) with $\text{Var}(\boldsymbol{\varepsilon}) = \sigma^2 \mathbf{I}_n$. Previous theorem proves that this method preserves its good properties (unbiasedness and full efficiency) even if (5) is the “true” model from which observations stemmed.

For this reason, if trend effect or V -robust dependence (but also both of them) are suspected to have an impact on a practical experimental procedure, a carefully chosen run sequence of a two level fractional factorial design might be a useful (and, as argued in previous sections, sparing) solution.

5. A COMPARISON WITH DIFFERENT APPROACHES

The approach here followed to consider a model with both trend effect on the mean value of \mathbf{y} , the response vector, and correlation among different components of \mathbf{y} , is not, of course, the only possible one.

In [3] trend resistant run sequences are investigated when time effect is modelled via a first order autoregressive model. In this case, the sequence $\{\omega_i\}$ of error terms is a first order autoregressive process with

$$\omega_i = \rho \omega_{i-1} + a_i,$$

where the a_i are independent, zero mean random shocks. The authors of that paper deduce that run orders are trend robust if the factors change level many times. This is, of course, conflicting with the cost criterion described in previous sections and shows how entangled might become in practice this multiple criterion problem.

Steinberg, in [4], adopted a model structured as

$$\mathbf{y} = \mathbf{X}\boldsymbol{\beta} + \mathbf{t} + \mathbf{u}, \quad (8)$$

where \mathbf{u} is a stochastic vector with zero mean value and $\text{Var}(\mathbf{u}) = \sigma^2 \mathbf{I}_n$ and \mathbf{t} is an ARIMA time series model:

$$\Phi(B)(1 - B)^m t_i = \Theta(B)a_i,$$

where B is the *backshift operator* ($Bt_i = t_{i-1}$), $\Phi(B)$ and $\Theta(B)$ are polynomials and the a_i are uncorrelated random shocks with zero mean and common variance $\tau^2\sigma^2$.

In this way both correlation and trend are embedded into \mathbf{t} . Model (8) generalizes the standard assumption of a polynomial trend which was used in the others cited papers dealing with run order.

However, as pointed out by Steinberg himself, this model requires, in order to be estimated, that the structure of the ARIMA model (polynomials $\Phi(B)$ and $\Theta(B)$) is known (or at least well estimated) and also that a good estimate of τ^2 is available. Parameter τ^2 represents here the variance component ratio that controls the trade off between trend and noise.

Different structures for the ARIMA model have little impact on final estimates, which are instead heavily affected by τ^2 . Steinberg reports good results obtained with a generalized cross validation procedure in order to estimate τ^2 and the ARIMA model.

This procedure proves to be very powerful but very complex to implement and there are situations when the whole method can not be applied at all: since some degrees of freedom are necessary to estimate those extra parameters, nearly saturated fractional factorials are excluded.

For this reason, result proved in section 4. may represent a solution for all situations when the procedure suggested by Steinberg can not be applied. Furthermore, the approach here suggested stems from a *robustness* reasoning: a standard, simple, well known procedure can be thoroughly used beyond its classical assumption domain (whether the different assumption structure *is perceived or not*).

REFERENCES

1. Mortarino, C.: Robustness of canonical analysis for some multiresponse dependent experiments, in: Kulianic, E. ed., AMST '96 - Advanced Manufacturing Systems and Technology, Springer Wien New York, 1996, 857-864.
2. Guseo, R., Mortarino, C.: Multiresponse dependent experiments: robustness of fractional factorial designs, Note di Ricerca, Dipartimento di Scienze Statistiche, Università di Udine, 3 (1995).
3. Cheng, C.S., Steinberg, D.M.: Trend robust two-level factorial designs, *Biometrika*, 78 (1991), pp. 325-336.
4. Steinberg, D.M.: Factorial experiments with time trends, *Technometrics*, 30 (1988), pp. 259-269.

5. Cheng, C.S.: Construction of run orders of factorial designs, in: Ghosh, S. ed., *Statistical Design and Analysis of Industrial Experiments*, Marcel Dekker, New York, 1990, 423–439.
6. Bailey, R. A., Cheng, C.S., Kipnis, P.: Construction of trend-resistant factorial designs, *Statistica Sinica*, 2 (1992), 393–411.
7. Jacroux, M.: On the construction of trend resistant asymmetrical orthogonal arrays, *Statistica Sinica*, 6 (1996), 289–297.
8. Jacroux, M., Majumdar, D., Shah, K.R.: On the determination and construction of block designs in the presence of linear trends, *Journal of the American Statistical Association*, 92 (1997), 375–382.

STATISTICAL ECONOMIC DESIGN OF AN X CONTROL CHART

G. Celano and S. Fichera
University of Catania, Catania, Italy

KEYWORDS: Quality control, X control chart, ats, genetic algorithm.

ABSTRACT: The paper presents the economic design of an X control chart preserving the statistical proprieties of the chart. The classical algorithms of economic design are based on the minimisation of a cost function which depends on the sample size n , the width of control limits k , and the time interval between samples h : the statistical proprieties, represented by ATS_1 and ATS_2 are obtained values. It is possible to achieve a control chart that reaches the economic goal but has an insufficient ATS_1 or ATS_2 . For this reason an appropriate design is necessary before the chart is used. In this paper a new approach, based on an evolutionary algorithm, to solve this problem is proposed. The design of the chart has been developed considering the objective function, which directly handles on α and β values and permits to consider both economic and the statistical properties. The proposed approach has been compared to a well-known heuristic algorithm, a sensitivity analysis has been carried out too. The obtained results show the effectiveness of the evolutionary algorithm.

1 INTRODUCTION

The model developed by Duncan [1] considers the costs associated with the implementation of X control chart, proposed by Shewart [2], and defines a cost function which depends on the sample size n , the width of control limits k , and the time interval between samples h . The n , h and k , values that minimise the cost functions are chosen to utilise the chart in the production process. The heuristic algorithms to minimise the cost

function and to find the optimal design of the chart proposed by many authors consider the statistical proprieties of the chart as output values. But as pointed out by Woodall [3], control charts based on economically optimal design generally have poor statistical properties and the values of ARL_0 and ARL_1 obtained by the chart parameters are not optimised accordingly to a statistical point of view. In order to resolve this problem Saniga [4] proposed a constrained model, while Del Castillo et al. [5] considered an interactive multiobjective algorithm on the basis of a simplified procedure. Simpson and Keats [6] have developed a trade – off analysis which shows as large gains in statistical properties are attainable with little increase in costs; a multiobjective evolutionary algorithm, which uses n , k and h as variables and a fitness function which depends both on costs and statistical properties, has been presented by Celano. In this paper an evolutionary algorithm that can consider both the economic and statistical objective has been developed: the variables of the objective function are α and β values and the parameters of the chart are obtained from them. The performance of the proposed algorithm has been tested by computer simulation utilising the examples reported in literature and the results have been compared with one of the best conventional algorithm. A sensitivity analysis has been carried out to evaluate the relationship between the cost when the process is out of control and the economic and the statistical proprieties of the chart.

2 ECONOMIC MODEL

In order to design an X control chart with respect to economic criteria it is necessary to make some basic assumptions about the behaviour of the process. It is characterised by a single in control state, which can be represented by the mean μ of a process parameter when no assignable causes are present; it may have $s \geq 1$ out of control states: each one of them is associated with a particular assignable cause. The assignable causes occur during an interval of time accordingly a Poisson distribution: so, assuming that the process begins in an in control state, the length of in control period is an exponential random variable. The last assumption implies that the transitions between the two possible states of the process are instantaneous. The process is not self correcting, so, if a transition to an out of control state has occurred, it can be returned to the in control condition only after an operator intervention; moreover, during the search of the assignable cause, the process is allowed to continue the production of items. The process is divided into cycles constituted by the following phases: production, monitoring and adjustment; each cycle begins with the production process in the in control state and continues until there is the appearance of an out of control signal on the control chart. Following an adjustment in which the process is returned to the in control state, a new cycle begins. Let $E(T)$ be the expected length of a cycle and $E(C)$ the expected net income gained during a cycle.

In the classical model [1] the optimisation of costs associated with the implementation of X control charts is realised by choosing the variables n , k and h minimising the expected loss per hour $E(L)$. The Duncan's model parameters are defined with the following symbols:

- λ is the number of occurrences per hour of an assignable cause: it represents the parameter of the exponential distribution that models the length of in – control period;
- δ represents the number of standard deviations σ in the shift of the mean μ_0 of a quality

characteristic to value $\mu_0 + \delta\sigma$ or $\mu_0 - \delta\sigma$;

- V_0 is the net income per hour of operation in the in control state;
- V_1 is the income per hour of operation in the out of control state;
- a_4 is the loss incurred per hour of operation own to the production of nonconforming items: $a_4 = V_0 - V_1$;
- a_1 is the fixed component of sampling cost;
- a_2 is the variable component of sampling cost;
- a_3 is the cost of finding an assignable cause;
- a'_3 is the cost of finding an assignable cause when none exists;
- g is the time required to take a single item and interpret the results;
- D is the time required to find an assignable cause after a point plotted outside the control limits;

The expected length $E(T)$ of a cycle is equal to:

$$E(T) = \frac{1}{\lambda} + h \cdot ARL - \tau + g \cdot n + D \tag{1}$$

where $\frac{1}{\lambda}$ is the mean time interval that the process remains in control state and $h \cdot ARL - \tau$ is the length of out of control period; the first term represents the number of samples required to produce an out of control signal times the time interval between samples. The Average Run Length with process in out of control state is

$$ARL = \frac{1}{1 - \beta} = \left(\int_{-\infty}^{k - \delta\sqrt{n}} \phi(z) dz + \int_{k - \delta\sqrt{n}}^{\infty} \phi(z) dz \right)^{-1} \tag{2}$$

The second term of $h \cdot ARL - \tau$

$$\tau = \frac{\int_{jh}^{(j+1)h} \lambda \cdot e^{-\lambda t} (t - jh) dt}{\int_{jh}^{(j+1)h} \lambda \cdot e^{-\lambda t} dt} = \frac{1 - (1 + \lambda h) \cdot e^{-\lambda h}}{\lambda \cdot (1 - e^{-\lambda h})} \tag{3}$$

is, given the occurrence of an assignable cause between j and $j+1$ sample, the expected time of occurrence of the cause within this interval. The term $g \cdot n$ is the time required taking a sample and interpreting the results and D is the time required finding an assignable cause.

The expected number of false alarms N_{fa} may be defined as α times the number of samples taken before the shift:

$$N_{fa} = \alpha \cdot \left[\sum_{j=1}^{\infty} j \cdot \int_{jh}^{(j+1)h} \lambda \cdot e^{-\lambda t} dt \right] = \frac{\alpha \cdot e^{-\lambda h}}{1 - e^{-\lambda h}} \tag{4}$$

where α is the reciprocal of the in control Average Run Length

$$\alpha = \frac{1}{ARL_0} = 2 \cdot \int_{-\infty}^k \phi(z) dz \tag{5}$$

The expected net income per cycle $E(C)$ has the following expression:

$$E(C) = V_0 \cdot \frac{1}{\lambda} + V_1 \cdot \left(\frac{h}{1-\beta} - \tau + g \cdot n + D \right) - a_3 - \frac{\alpha \cdot a_3' \cdot e^{-\lambda h}}{1 - e^{-\lambda h}} - (a_1 + a_2 \cdot n) \cdot \frac{E(T)}{h} \quad (6)$$

First and second term of this expression are the gains obtained respectively during in control and out of control periods; the remaining ones represent the costs associated to the search of assignable causes, to false alarms and to sampling.

Assuming that the sequence of production – monitoring – adjustment can be represented as a renewal reward stochastic process, the expected net income per hour $E(A)$ can be determined by dividing $E(C)$ by $E(T)$:

$$E(A) = \frac{E(C)}{E(T)} \quad (7)$$

rearranging the terms of this expression, it may be written:

$$E(A) = V_0 - E(L) \quad (8)$$

where the expected loss per hour $E(L)$ is equal to:

$$E(L) = \frac{a_4 \cdot [h/(1-\beta) - \tau + g \cdot n + D] + a_3 + a_3' \cdot \alpha \cdot e^{-\lambda h} / (1 - e^{-\lambda h})}{1/\lambda + h/(1-\beta) - \tau + g \cdot n + D} + \frac{a_1 + a_2 \cdot n}{h} \quad (9)$$

The function $E(L)$ must be minimised in order to pursue the economic goal, whereas the statistical objectives are reached by maximising the value of the average time signal in control state (ATS_1) and minimising the average time signal in out of control state (ATS_2).

ATS_1 and ATS_2 are defined as:

$$ATS_1 = h * ARL_0 \quad ATS_2 = h * ARL_1 \quad (10)$$

As variables of the function $E(L)$ we have chosen α and β so that we can directly consider the statistical aspects of the problem, while h has been calculated through the formula obtained by the economic optimisation .

3 EVOLUTIONARY ALGORITHM

Genetic algorithms (GAs) simulates the evolution of a population, based on the rule of the survival of the fittest for the given environment [7]. The pool of chromosomes forming the actual population contains differing genetic material and the main genetic operator, the crossover operator, works selecting pairs of solutions from an actual population, and combining them to produce new solutions. It develops a set of solutions with individuals in reciprocal competition and the evolution of that population is obtained transferring the beneficial adaptations gained during the search from the chromosomes of the parents to the ones of the offspring. The genetic operators for the control chart design have been selected and worked out on the basis of a previous experience of the authors, particularly, a decimal encoding of individuals has been adopted, as well as a preference for genetic operators which directly ensures solution feasible procedure. Moreover, an elitist strategy has been chosen during the evolutionary process, consisting in preserving the best chromosome

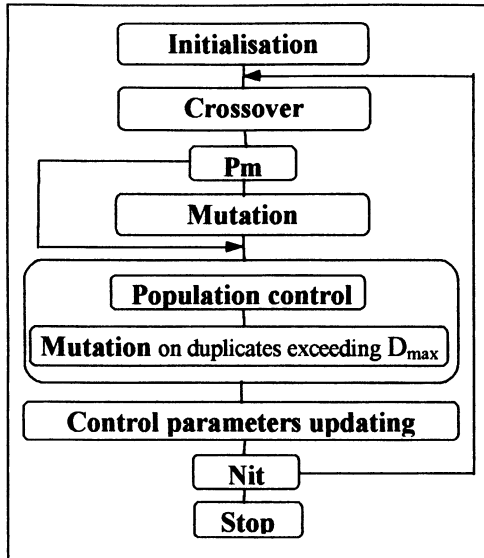


Fig. 1 Genetic algorithm

from disruption caused by the application of the mutation operator. In order to avoid premature convergence, due to a quick increase of the number of copies of «the fittest individuals», a population control technique that, over a given number, mutates the duplicates of current chromosomes in the actual population has also been embedded in the developed GA. The architecture of the proposed evolutionary algorithm is sketched in Fig. 1. After the initialisation, the evolutionary process is carried out, based on the selection at each iteration of two parents on a fitness basis and on the application of the crossover operator. Similarly, mutation is performed. The appropriate chromosomal diversity in the current population is assured by using, after the application of the conventional genetic operators, a population

control operator which applies the mutation operator to the copies of each individual which exceeds a given level.

3.1 Genetic operators

Representation. For the problem investigated the decimal encoding of individuals has been adopted. Each individual consists of a decimal string of two elements, α and β , that represents a feasible solution because the chart parameters n , h and k are obtained from α and β , through the following relations:

$$n = \left(\frac{z+k}{\delta} \right)^2 \quad h = \sqrt{\frac{\alpha \cdot a'_3 + a_1 + a_2 \cdot n}{\lambda \cdot a_4 \left(\frac{1}{1-\beta} - \frac{1}{2} \right)}} \tag{11}$$

where k and z are respectively the values of the normal standard variable corresponding to α and β .

Fitness. To evaluate the individual effectiveness three ways are considered depending on the configuration of the algorithm. When the economic objective is considered the fitness value, F , coincide with the expected loss per hour (9). If the objective are the statistical proprieties the fitness values depending from ATS_1 e ATS_2 :

$$F = W_1 * ATS_1 + \frac{W_2}{ATS_2} \tag{12}$$

In the multiobjective configuration the fitness is a function of the economic and the statistical goals:

$$F = E(L) * \left(W_1 * ATS_1 + \frac{W_2}{ATS_2} \right) \tag{13}$$

W_1 W_2 are coefficients, which values ranging from 0.1 and 1.

Crossover. Considering that two genes only constitute an individual, crossover operator is performed mixing the genes of two chosen individual. Fig 2

Mutation. This operator is randomly applied during iterations with probability P_m ; an individual is casually chosen on a fitness basis, and substituted with a new one generated by the mutation operator. Mutation is constructing a new sequence through random drawing;

α_1	β_1	parent 1				
α_2	β_2	parent 2		α_1	β_1	Parent
α_1	β_2	offspring 1		α_2	β_2	Offspring
α_2	β_1	offspring 2				
Crossover			Mutation			

Fig. 2 Genetic operators

Population control. In order to avoid premature convergence of the algorithm, due to a quick increase in the copies of the fitter individuals, an operator that discards duplicates exceeding D_{max} is applied at each iteration. The duplicates are identified on a fitness basis and the discarded individuals are substituted with their “offspring” generated by the mutation operator.

Control Parameters Updating and Stop test. To perform intensification-diversification cycles of the evolutionary process, after N_{ip} iterations without improvements, the mutation probability is increased by ΔP_m ; on the contrary, when a new minimum is found, P_m is reset to the initial value. The previously described operators are iteratively applied until the ending criterion, the maximum number of iterations N_{itmax} , is fulfilled.

4 SIMULATION RESULTS

Three configurations of the evolutionary algorithm have been considered corresponding the three different fitness functions described in 3.1: the economic design algorithm, EDA, the statistical design algorithm SDA, and the multiobjective design algorithm MDA. In order to assess the effectiveness of the proposed technique, the algorithms have been tested on a set of 5 problems reported in literature [1] [8]. The following setting of control parameters has been employed: $N_s=50$, $P_m=0.01$, $D_{max}=2$, $N_{it}=50000$. The results of the three algorithms, together with the ones obtained by one of the best conventional algorithm [8], CA, based on economic optimisation, are resumed in Table 1. The $E(L)$ average of EDA compared with the conventional algorithms shows a significant improvement. The control chart designed on the basis of the SDA results shows excellent statistical proprieties but an unacceptable increment of cost until the 476 % of the example 1. The MDA results show little increase in cost, the 7.1 % in average, but at the same time a significant improvement of statistical proprieties, the increment of 88,3% of ATS_1 and the

decrease of 7,3% ATS_2 .

Example	algorithm	E(L)	ATS_0	ATS_1	n	h	k
1	CA	624,26	101,04	1,81	3	0,97	2,59
	EDA	624,26	101	1,82	3	0,96	2,59
	SDA	3598,16	13597,8	0,1	20	0,1	4,48
	MDA	642,24	254,55	1,6	4	0,84	2,94
2	CA	10,38	447,01	0,85	5	0,76	2,99
	EDA	10,37	308	0,83	5	0,77	3,02
	SDA	14,01	1,32E6	0,76	25	0,76	5
	MDA	11,97	695,7	0,82	3	0,42	3,43
3	CA	608,86	131	1,7	5	1,3	3,2
	EDA	541,79	161,3	1,86	2	1	2,74
	SDA	1626,15	1,74E6	1	25	1	5
	MDA	557,25	327,7	1,82	2	0,75	3,05
4	CA	594,13	171,6	2,7	2	1,6	2,6
	EDA	563,2	174	3,00	3	2,54	2,44
	SDA	2935,62	1,74E6	1	25	1	5
	MDA	616,62	246,5	2,58	2	1,34	2,78
5	CA	647,5	371,8	2,1	17	1,9	2,8
	EDA	627,6	156	1,9	11	1,45	2,6
	SDA	983,19	1,22E6	1,4	25	0,7	5
	MDA	658,09	185,3	1,77	8	0,89	2,82

Table 1 Simulation results

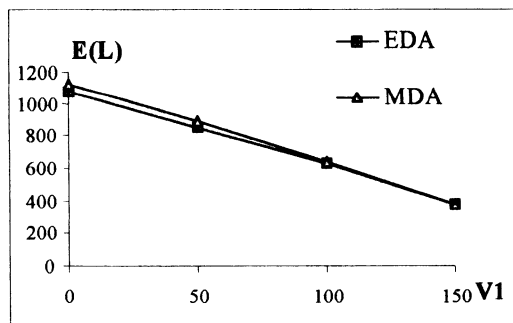


Fig. 2 Expected loss per hour

To evaluate the effectiveness of the MDA algorithm in different process environments a sensitivity analysis is carried out considering the results of the economic and the multiobjective algorithms, $E(L)$, ATS_1 and ATS_2 , in relation with the value V_1 , particularly it ranges from 0, this mean there is no gain when the process is out of control, until the gain 75% of V_0 . The Fig. 3, 4 and 5 show respectively the relation between $E(L)$, ATS_2 , ATS_1 and V_1 . The costs

calculated with the two algorithms have small difference ranging from the 5% and 2,23% corresponding to V_1 equal 0 and 75%. Instead the ATS_1 and ATS_2 have relevant shifting. The increment of ATS_1 range between the 169% and the 85%, whereas the decrease of ATS_2 ranges from the 15% and the 11%. These results obtained confirm the effectiveness of the multiobjective algorithm. But they also point out that, when the products realised during an out of control are defective and it is no possible any recycle, the cost difference are double in comparison with there is at least an earn of the 50%. In this condition the

statistical advantage remain significant: the 169% for ATS_1 and the 15% for ATS_2 .

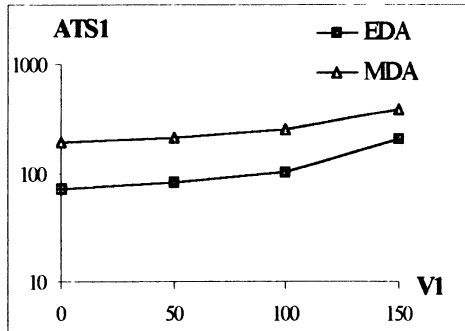


Fig. 3 Average time signal in control

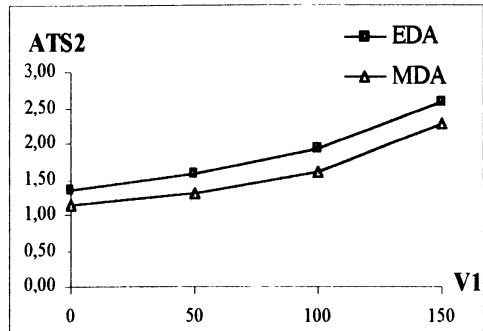


Fig. 4 Average time signal out control

5 CONCLUSION

The present paper deals with \bar{X} control chart design. A multiobjective approach is proposed to pursue contemporaneously an economic objective and a statistical objective. The results obtained with the developed method show that is possible, for every kind of process, to gain a great improvement of the statistical properties of the chart with a relative small increase in costs. In this way is possible to have sensible charts which present the signal of a special cause in a very short time and consequently the production of possible non conforming items is considerably reduced.

ACKNOWLEDGEMENT

This research has been supported by MURST.

REFERENCE

1. Duncan, A. J.: The economic design of \bar{x} charts used to maintain current control of a process. *Journal of American Statistical Association*, 51, 1956, 228-242.
2. Shewhart, W. A.: *Economic Control of Quality of Manufactured Product*. Van Nostrand, New York, 1931.
3. Woodall, W. H.: Weaknesses of the economic design of control charts. *Technometrics*, 28(4), 1986, 408-409.
4. Saniga, E. M.: Economic statistical control-chart designs with application to \bar{x} and r charts. *Technometrics*, 31(3), 1989, 313-320.
5. Del Castillo, E., Mackin, P. and Montgomery, D. C.: Multiple-criteria optimal design of \bar{x} control charts. *IIE Transactions*, 28, 1996, 467-474.
6. Simpson, J. R., Keats, J. B.: Trade - off analysis versus constrained optimization with an economic control chart model. *IIE Transactions*, 27, 1995, 765-772
7. Michalewicz, Z.: *Genetic Algorithms + Data Structures = Evolution Program*, Springer-Verlag, New York, 1994.
8. Montgomery, D. C.: Economic designs of an \bar{x} control chart. *Journal of Quality Technology*, 14 (1), 1982, 40-43.

INFLUENCING FACTORS AND CASE STUDIES IN DESIGN FOR QUALITY MANUFACTURABILITY

S.K. Das and B. Veerapanini
New Jersey Institute of Technology, NJ, USA

KEY WORDS: Design, Quality, Manufacturability

ABSTRACT: The quality manufacturability (QM) of a design is defined as the likelihood that defects will occur during its manufacture in a standard plant. Clearly, some designs are more likely to have a lower production yield rate and/or higher quality management cost as compared to an alternative design. The reason for this is that in any production facility there is an inherent defect occurrence process, the strength of which is dependent both on the product's design and process capability. This relationship between the defect occurrence process and the design is the basis for QM. The output of the DFQM method is the QM-Index matrix, which indicates the QM of each part in the assembly. In this paper we present standardized influencing factors that are used to derive the QM-Index Matrix. Quality assurance groups can use DFQM for evaluating a design even before prototype manufacturing. Design groups on the other hand can use this method as part of their design analysis in the virtual environment. DFQM will help improve the quality yield of a plant, and also lead to a shorter product cycle time. Two case studies of an automobile door handle and a cellular phone are presented.

1. INTRODUCTION

The primary objective of a designer is to develop designs that first satisfy a certain functionality, and second are economical to manufacture. Following this, there are several secondary objectives to be met. One such objective is to create designs that have a high level of quality manufacturability (QM). The QM of a design is defined as the likelihood that

Published in: E. Kuljanic (Ed.) *Advanced Manufacturing Systems and Technology*,
CISM Courses and Lectures No. 406, Springer Verlag, Wien New York, 1999.

quality defects will occur during its manufacture. Creating designs with a high QM ensures that a minimal effort is expended in maintaining and achieving quality specifications on the production floor. Further, the need for product redesign is reduced. Improving QM involves executing a design analysis to answer the following questions: (i) what quality defects will possibly occur during the manufacture of a given design (ii) what is the significance of these defects, and (iii) how will these defects effect customer satisfaction and functionality? Traditionally, these questions can not be reliably answered until initial manufacturing has begun. In this paper we discuss a new method, called DFQM, to help designers answer these questions early in the design cycle. This permits the designer to improve the QM in a virtual environment. This new method can be implemented in the form of a computer based tool which is able to model and simulate the manufacturing “defect occurrence process”, and hence predict likely quality problems.

An assembled product is comprised of several parts which are held together via some fastening mechanism. In the simplest case we may have a product with just two parts, while at the other extreme we have an automobile or aircraft which is assembled from thousands of parts. It is well known that many of the quality problems in an assembled product originate during the assembly process itself. The process of positioning, inserting, and fastening several different parts to form one product, inherently results in assembly defects. Often the occurrence of these defects is a function of the design itself. This implies that there are some designs that are more likely than others to have assembly defects are. In order to develop a generally applicable QM analysis tool, we need to first identify general classes of quality defects. Our research indicates there are six general classes of manufacturing defects in assembled products. These are,

- | | |
|-------------------------------|------------------------------|
| 1. Missing or misplaced parts | 2. Part misalignments |
| 3. Part interferences | 4. Fastener related problems |
| 5. Assembly non-conformity | 6. Damaged parts. |

Note that all of these defects are physical in nature. These defects will manifest themselves in a functional defect, depending on the type of product. For example, a misalignment may cause a motor to heat up, while in the case of a door it may cause water leakage.

DFQM models the linkage between the above defects and a variety of design features. These models identify which design features and relationships promote the occurrence of assembly defects, and under what conditions. In this paper our focus is on these “causing” design features. We introduce the features and present a standardized format for measuring them in a QM context. The results presented here are part of a larger research initiative in the DFQM area. Details of the DFQM method, which complement the results reported here, are reported in Das et al [2] and Tamboo [8] (1994).

2. QUALITY MANUFACTURABILITY AND DFM

DFM is an approach for designing products so that, (i) the design is quickly transitioned into production, (ii) the product is manufactured at minimum cost, (iii) the product is

manufactured with a minimum effort in terms of processing and handling requirements, and (iv) the manufactures product attains its designed level of quality. Several techniques for DFM have been developed and implemented in industry. Typically, a technique will focus on one or more of the above listed objectives. There is not much research on evaluating a design from a manufactured quality perspective. Techniques such as Taguchi methods and robust design methods [5, 7, 1], Ishikawa or cause/effect diagrams, and quality function deployment [3] are usually used to better only the design quality of a product. Morup [4] introduces design for quality (DFQ) as a quality driven form of integrated product and process development, but the emphasis is more on functionality than manufacturability. DFQM is a new approach that focuses exclusively on evaluating the design of assembled products from a manufactured quality perspective. DFQM analysis is also applicable in a global supply chain environment. Smith and Whitehall [6] observe that design and manufacturing groups tend to be geographically distant from each other, with little interaction. Taylor [9] proposes a model for design for global manufacturing and assembly (DFGMA). He considers the costs of production setup and design setup for different global sites. DFQM would help reduces these costs.

3. THE QUALITY MANUFACTURABILITY ANALYSIS SCHEME

The analytical process in DFQM is structured as a sort of reverse cause-effect analysis. That is we are identifying causes, and then predicting effects or quality defects during assembly. This is similar in structure to the failure mode effects analysis (FMEA) method. But while FMEA provides the user with a blank worksheet, DFQM already models the causes and effects, and the user is only required to identify the presence of the causes. The flowchart in Figure 1 identifies the three key elements of the approach and their relationship, and their definition follows.

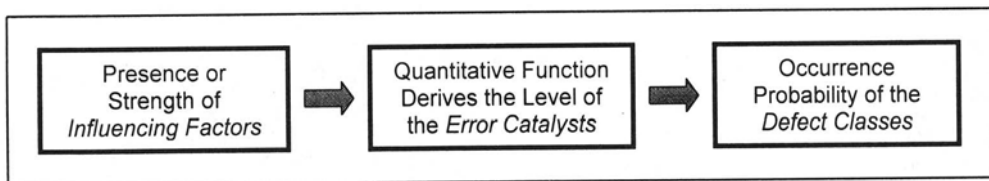


Fig. 1: Logical Elements of DFQM

- *Influencing Factor Variables* - A variable or feature of the design or assembly process which can lead to one or more of the defect classes. Factors may relate to the physical attributes of the design, or the manufacturing process.
- *Defect Classes* - An assembly quality defect commonly seen in manufactured products. Each defect differs in terms of what causes them, and their specific orientations.
- *Error Catalysts* - These describe design-assembly situations that promote the occurrence of quality defects. The logic of the error catalyst function describes factor conditions that are undesirable. The prevailing level of each factor variable is used by the er-

ror catalyst function to create a likelihood estimate of a defect occurring. For each defect classes there are several error catalysts.

In improving the QM a designer must first evaluate the intensity level of each error catalyst. The level is given by an accompanying function, and is defined on a 0 to 1 scale. When the intensity is 1, then conditions are such that it is highly likely the associated specified defect will occur during practice, Conversely, when the intensity is 0 then its highly unlikely to occur. When the error catalysts are strong, then the designer must change the design so as to weaken the error catalysts. In the ideal design all the error catalysts will be 0 or inactive.

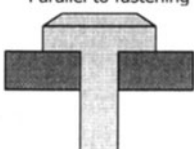
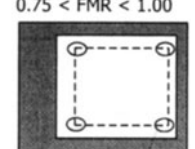
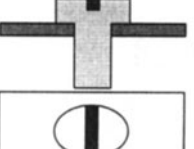
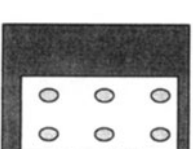
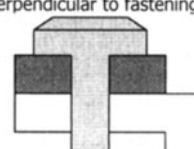
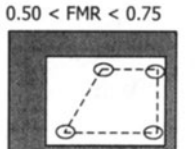
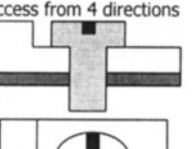
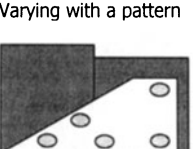
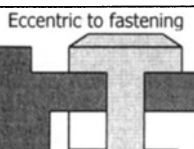
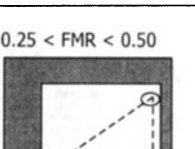
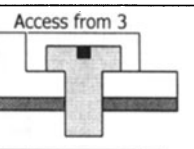
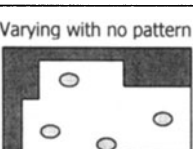

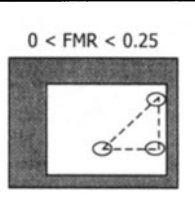
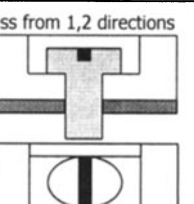
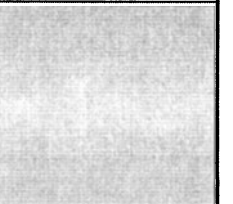
	Dir. Of Separation Force A	Force Mapping Ratio B	Fastener Accessibility C	Spacing D
1	Parallel to fastening 	$0.75 < FMR < 1.00$  Fastener Location	Access from 5 directions 	Constant with a pattern 
2	Perpendicular to fastening 	$0.50 < FMR < 0.75$ 	Access from 4 directions 	Varying with a pattern 
3	Eccentric to fastening 	$0.25 < FMR < 0.50$ 	Access from 3 	Varying with no pattern 
4		$0 < FMR < 0.25$ 	Access from 1,2 directions 	

Fig. 2: Standard Chart for Fastening System

4. STANDARDIZED FACTOR VARIABLES

A variety of factors could influence the occurrence of quality defects. We have identified some of the primary factors, and then standardized them for use in the DFQM method. There are in total three categories of factors, each of which is described below.

	ABUTMENTS	INSERTED	OVERLAPPING				Without Locators
			With Locators		Self Locating		
			3. Fully	4. Partly	5. Fully	6. Partly	
A Same Base							
B Different Bases Horiz					Same as C5	Same as C6	Same as C7
C Different Bases Vertical							

Fig. 3: Standard Chart for Positional Relationship Between Mating Pairs

4.1. FASTENING SYSTEM

In our research we found the fastening system to be a key determinant of product quality. Fastening systems are defined in four dimensions from a QM perspective: (i) direction of the separation force (ii) force mapping ratio (iii) fastening accessibility and (iv) inter fastener distance. The force mapping ratio is the between the fastener enclosed area and the part mating area. The standards for measuring each of these is shown in Figure 2. In all cases the QM deteriorates as we move down the table. Generally the best case for QM is (A1-B1-C1-D1) and the worst case is (A3-B4-C4-D3).

4.2. POSITIONAL RELATIONSHIPS

Many defects originate from the difficulty in assembling two mating parts. We thus find that the positional relationship of parts is an important determinant of quality. This relationship is measured in two dimensions: (i) the commonality of the base on which the two parts rest and (ii) the ease with which the parts are located. Figure 3 illustrates the range of standard positions. The base is the part on which a part rests. Example locators are pins, grooves, or notches. The relationship between QM and the position is not monotonic across the table. There are some dominant QM related positions. For example, A1 tends to be best, while C1 and C7 tend to be the worst. Column 5 is a recommended design strategy since it eliminates the need for locating devices, while still having a low chance of error.

	Physical Support A	Connective B	Limiting or Guiding C
1 No Motion		Electrical Junction 	
2 Joint Motion			Same as C1
3 Relative Motion		Car Door 	

and represent the mating pair

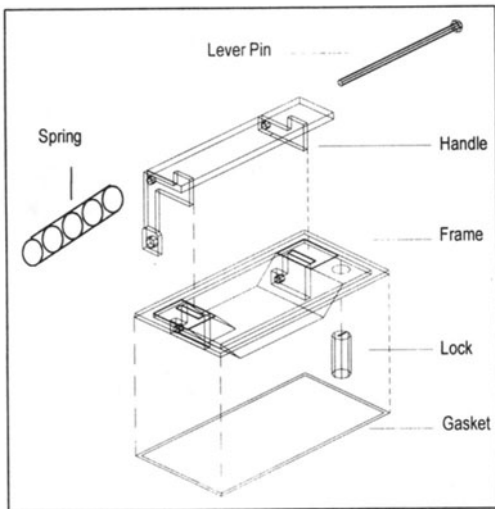
Fig. 4: Standard Chart for Functional Relationship

4.3. FUNCTIONAL RELATIONSHIP

Another key determinant of quality is the functional relationship between mating parts. This relationship is measured in two dimensions: (i) the nature of the motion between the parts and (ii) what function is transmitted. Figure 4 illustrates the range of functional relationships. Physical support implies one part provides primary support for the other. Connective implies the mating link provides a desired functionality (e.g., electrical, force

transmission). Limiting implies one part restricts the position of the other. The effect of the functional relationship on the QM is dependent on a variety of factors. For instance, when two parts have relative motion and are connective then the chance of misalignment is high.

The logic of the DFQM method is captured in the error catalysts. For a given design, every part is described as per the above standard definitions, and this is used to generate the QM-Index matrix. The rows in this matrix represent the parts and the columns the defect classes. Each matrix entry therefore evaluates the QM of a part in the context of the corresponding defect class. The matrix entries are computed by the error catalyst functions. The following case studies illustrate the utility of the matrix.



Part	Defect Class					
	1	2	3	4	5	6
Handle	0.1	0.5	0.3	0.0	0.0	0.0
Frame	0.0	0.0	0.0	0.0	0.0	0.1
Gasket	0.4	0.0	0.0	0.3	0.0	0.1
Lock	0.0	0.0	0.0	0.0	0.0	0.0
Spring	0.4	0.0	0.0	0.1	0.1	0.3
Lever Pin	0.0	0.3	0.1	0.0	0.4	0.4

Fig. 5: Design of an Automobile Door Handle Fig. 6: QM-Index Matrix for the Handle

5. AUTOMOBILE DOOR HANDLE CASE STUDY

The design of the handle is shown in Figure 5. The assembly sequence is as follows, first the frame is fixed, then the handle, gasket, spring, lever pin, the welding operation, and finally the lock are inserted. Consider the mating between the handle and the lever pin. Then the fastening system is A2-B1-C3-D1. The positional relationship is B2 and the functional relationship is C3. Figure 6 shows the QM-Index matrix for the handle. The defect numbers are listed in section 1. A major problem with the design is that the assembly cannot be done strictly in the Z-axis. Hence manual assembly or a dual axis assembly machine is needed, which sets the stage for quality problems. Another problem is that the spring must be positioned before the end of the lever pin can be welded on to the frame and handle. There has to be an external fixture to hold the spring since the frame is contoured and has no natural resting positions. The rubber gasket is flexible and is attached to the frame by interference pins, further, it is a functionally non-critical part. This could lead to a misplace-

ment error. The legs of the handle are inserted through two slots in the frame with no positional elements. This sets the stage for a misalignment between the handle and frame. The lever pin passes through four holes, two in the frame and two in the handle, and there are no positioning or guide elements. This could also lead to a misalignment between the frame, handle and lever pin.

6. CELLULAR PHONE CASE STUDY

The design of the phone is shown in Figure 7, there are a total of twelve parts. Figure 8 shows the QM-Index matrix for the door handle. The analysis indicates that there is no design feature that could lead to catastrophic levels of assembly defects. We observe that there is little to no likelihood of nonconformance or interference type defects. The only moving parts in the phone are the antenna and keypad. None of these appears to be problem sources. There are several potential problems related to the remaining defect classes. Parts with the most significant defect sources are (i) Mylar Dome (ii) LCD (iii) Upper Housing (iv) Receiver (v) Keypad (vi) LCD Lens and (vi) Antenna. The receiver has no positioning elements and is assembled on the upper housing in a negative Z-axis. This could lead to misalignments or a fastening failure. The Mylar dome, which is a flexible sheet, also has no positioning elements and is likely to be missing or misaligned. The positioning elements on the keypad and microphone are symmetrical and a 180-degree misalignment is possible. The antenna is inserted into the assembly with a non Z-axis assembly and then tightened. The possibility of over tightening this part is quite high as the antenna has an odd shape; this defect could be reduced by snap fitting the antenna on to the lower housing instead of threading it.

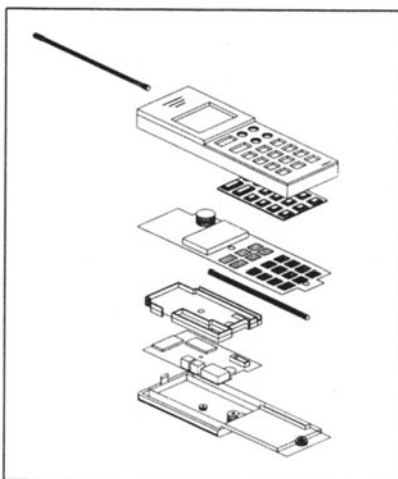


Fig. 7: Design of a Cellular Phone

Part	Defect Class					
	1	2	3	4	5	6
Cir Board 1	0.0	0.0	0.0	0.2	0.0	0.1
Cir Board 2	0.0	0.0	0.0	0.2	0.0	0.1
Chassis	0.0	0.0	0.0	0.2	0.0	0.0
Mylar Dome	0.4	0.1	0.0	0.0	0.0	0.0
LCD	0.0	0.2	0.0	0.0	0.0	0.0
Microphone	0.1	0.0	0.0	0.0	0.0	0.0
Lower Hsng	0.0	0.0	0.0	0.0	0.0	0.2
Upper Hsng	0.0	0.3	0.0	0.0	0.0	0.1
Receiver	0.6	0.4	0.0	0.2	0.0	0.1
Key Pad	0.3	0.3	0.0	0.0	0.0	0.0
LCD Lens	0.0	0.2	0.0	0.1	0.0	0.0
Antenna	0.0	0.0	0.1	0.2	0.0	0.2

Fig. 8: QM-Index Matrix for the Cell Phone

7. SUMMARY

The manufacture of high quality products is a necessity in today's market place. But short life cycles, large product mixes, plus short design lead times often make it difficult to achieve this requirement. It is important that designers be able to develop products that require a minimal monitoring and inspection effort, that is they are robust to the variations and limitations inherent in a normal plant. The proposed DFQM method introduces a procedure by which designers can evaluate the design from a manufacturing quality perspective. The DFQM method predicts only quality defects that occur during the assembly process, it cannot and does not have the intelligence to predict quality defects that occur during part fabrication processes. Further, the methodology does not focus on defects on a functional level but rather at a physical level.

REFERENCES

1. Chen, L.: Designing Robust Products with Multiple Quality Characteristics, *Computers & Operations Research*, Vol. 24(10), (1997), pp. 937-944
2. Das, S. K.; Datla, V.; Gami, S.: DFQM – An Approach for Improving the Quality of Assembled Parts, to appear in *International Journal of Production Research*, 1998
3. Hauser, J.; Clausing, D.: The House of Quality, *Harvard Business Review*, May, (1988), pp. 63-73
4. Morup, M.: A New Design for Quality Paradigm, *Journal of Engg Design*, Vol. 3(1), (1992), pp. 63-80
5. Phadke, M.S.: *Quality Engineering Using Robust Design*, Prentice Hall, Englewood Cliffs, NJ, USA, 1989
6. Smith, J.A.; Whitehall, F.: In Search of Quality – What Designers Can Do, *Machine Design*, Nov., (1997), pp. 85-88
7. Taguchi, G.; Elsayed, E.A.; Hsiang, T.: *Quality Engineering in Production Systems*, McGraw-Hill Book Company, New York, 1989
8. Tamboo, A.: *Design for Quality Manufacturability Analysis of Missing/Misplaced Parts & Part Interferences*, Unpublished M.S. Thesis, New Jersey Institute of Technology, USA, 1994
9. Taylor, G.D.: Design for Global Manufacture and Assembly, *IIE Trans*, Vol. 29, (1997), pp. 585-597

**VIRTUAL LEARNING ENVIRONMENT BASED
ON ADVANCED INFORMATION TECHNOLOGIES**
A NEW APPROACH TOWARD HUMAN EMPOWERMENT FOR TOTAL QUALITY

A. Alto and M. Dassisi
Politecnico di Bari, Bari, Italy

KEYWORDS: Information Technologies, Training; Total Quality

ABSTRACT

Total Quality revolution of the last decade put the issue of personnel training as a mandatory commitment for companies, to assure human resources more flexibility and self-consciousness on the production problems. Training activities are quite often delegated to external consultants or to non-professional internal skilled personnel, which applies naive approach in teaching. The original ideas that inspired the ESPRIT project n.28974, named "Total Quality Management on-line", are here presented. The project, currently in process within a consortium of several 1st and 2nd tier automotive suppliers, addresses the problem of continuous education on Total Quality topics using the most advanced Information Technologies. The present paper sketches the main features of a virtual learning environment which is proposed as a new approach to this aim.

NOTE: The paper was originally conceived by both Authors during fruitful discussions held in 1998. Unexpected decease of Professor Attilio Alto prevented him to contribute to the writing of the final version.

It is a wish of the coauthor to maintain the name of Professor Attilio Alto to pay homage to his memory, to his innovative spirit and constant attention devoted to ethic and social aspects of the scientific research and educational activity throughout his life.

Published in: E. Kuljanic (Ed.) *Advanced Manufacturing Systems and Technology*,
CISM Courses and Lectures No. 406, Springer Verlag, Wien New York, 1999.

1. INTRODUCTION

The revolution taking place in Europe, Total Quality (TQ), is primarily focusing attention about people and teamwork (*esprit de corps*) to achieve the common goals of business. 'People building', through formation and motivation, and 'management by training' are the fundamental bricks of this industrial renaissance to foster latent talent emergence from employees in new ideas and achievements. Continuous learning is made at all levels, particularly within automotive companies, addressing several topics: technical skill improvement; relationship capacities; work-group; problem finding and solving attitudes.

One of the most crucial point of this activity is the trade-off between the effectiveness of the traditional training programmes and methods and the investment to be sustained. This problem may become even more significant for multi-site companies, which do have also multi-cultural topics to face, sometimes related to different countries.

Advanced Information Technologies (IT) may represent a turning-point for training; they may in fact increase efficiency of training in two ways: 1) customisation of the training programs either in terms of training contents or availability of access to information; 2) more objective and controlled learning processes. But to do so, new approaches have to be developed since IT training tools developed so far, even though with spectacular graphical effects, use a passive approach for training (see for instance the electronic book and encyclopaedia), leaving to the trainee the responsibility of the learning results.

Based on these arguments, in the paper are sketched the basic ideas and the feature for a new approach to train personnel for an interactive learning environment, based on IT and oriented to the training on Total Quality mainly thought for automotive 1st and 2nd tier suppliers.

The original ideas presented here were the basis of the ESPRIT 28974 project named "Total Quality Management on-line", operated by the Authors within a consortium of several 1st tier automotive suppliers (Bosch, GKN, SKF, Lucas Varity) and representative of 2nd tier suppliers (CLEPA and San Valeriano) as well as multimedia companies (Grifo Multimedia and Synergie).

2. TRAINING NEEDS FOR TOTAL QUALITY

The problem of total quality within companies is to transform quality feeling (our common sense) in an operative attitude (tools, methods and behaviours) to solve small daily problems at all level within the company. Quality implementation is nothing else than an application of series of common sense actions: but how much is difficult to apply them.

Training plays a fundamental role in this process. The basic objective for total quality training may be thus formulated as follows: the development for company personnel - in all functions and at all levels - of those attitudes, that knowledge, and those skills in

quality which may contribute to production of company products at minimum cost consistent with full customer satisfaction. This objective is not a trivial task, since several different types of knowledge exist, which may be *tacit* or *explicit* according to [1], as well as *company specific* or *common technical knowledge*.

In the present time, companies are getting used to invest heavily in continuous training programmes to this aim. Independently of the company size, every person in the organisation is entitled to training: s/he may be practitioners but, also, personnel changing positions and so on. Most enlightened companies produce also annual training plans.

A standard approach for training in industry is to take volunteers from all level of the organisation (from supervisor to manager) and trainee them in the practical approach to be used. These people become then facilitators (mentors) with the job to cascade the knowledge learned in a series of courses and on-the-job sessions. The most experienced person on the subject, on the other hand, is not always the best person to teach the common technical knowledge; sometimes s/he is not either the best to teach even the company specific one! Outside consultant may thus be profitably employed. The problem in this case is, of course, how to transfer company specific knowledge as well as the tacit one.

Quality training programs has to be tailored for each company, depending also on the skill profile and capacity of the employee to be addressed. Each time a training phase has to be restarted, new efforts have to be devoted by companies: a course costs an average of 7 times the cost per hour of personnel for one-of-a-kind course, tailored for a specific need. This is a significant investment of money and time! Furthermore, uncertain outcomes may result, either in terms of learning results (not all the persons are able to teach and it is not always assure the availability of experts everywhere and anytime in the company!) or in terms of time spent to reach a specific target, which might depend also on the specific epoch experienced by the company (overloading; critical phases; etc.). As a result, the cultural level on quality of personnel might result not constant. Another aspect has to be taken into account at this regard, which is becoming important with the emerging forms of distributed companies and the co-makership approach widely adopted in the automotive sector (up to the distributed virtual enterprise which is behind the corner): tailoring courses for multi-plant and/or multi-cultural company, means not only the need to translate words but also the need to translate concepts following the local habits and idioms. Selling the TQ programmes in the large, distributed companies call naturally for a great deal of flexibility in the training plan. As compared with the single plant, TQ programmes the multi-plant company may require a wider degree of initial participation in plan development and also much more extensive way-paving before application may be initiated. A larger organisation has to be involved to support the associated expense, devoting more attention to preparation of extensive quality control of training materials to be used in the early phases of the introduction the programme.

All these aspects rise the problem of training effectiveness and the return on investment in training, which are becoming very strong points to address [2].

Unfortunately keeping an accurate track of training is not a common practice within companies. Nowadays, in fact, one more frequently finds the training given to staff to have been informal and perhaps in the nature of supervised 'on the job' experience. Although this is the appropriate way to teach some skill (particularly for the company specific knowledge and the tacit knowledge), the real problem with this is that all-too-often one finds that this approach is unstructured, and there is no record to demonstrate that is ever completed. There is less difficulty where the training is achieved by attending formal courses (evidence; certificate by the training organisation).

Accurate objective methods for evaluating the actual impact of training on the trainee in the mentoring process are needed. The number of days devoted for training per year per head is, to the Authors opinion, too aggregate digit to have a clear measure of the training outcomes. Training need assessment may be one possible premise (not a solution) to this problem, allowing a clear statement of the training targets (objective list of all the topics and cultural profile per each skill level) [3].

3. THE VIRTUAL LEARNING ENVIRONMENT

The 'virtual learning environment' (VLE) sketched in the paper is thought as to face training needs of European automotive supply industries. The basic philosophy of the approach is to create a common standard for training on quality topics, thus stimulating co-operation attitudes amongst big companies and SME's at the learning and knowledge transfer stage.

The idea behind VLE is to train personnel on real case problems, giving her/him the possibility of an open interaction of the trainee with different knowledge sources: s/he, under appropriate guidance, should be also allowed to simulate the use of quality techniques in a stand alone fashion, to access to a testimonial case database or even to interact with other people sharing the same problem or the same experience working in different plants, by giving her/him the chance to 'call for a real-time help'. In this direction, several learning methodologies has to be used combined with the most advanced Information Technologies available (web-based; virtual reality; etc.).

We propose here to set a network (open network, i.e. the Web, or closed network, i.e. company intranet) to create a 'virtual learning environment', where trainee's needs should be satisfied forwarding help-tokens in the network. This space might allow also the settlement of a sort of temporary '*virtual quality circle*', by means of appropriate regulation of the interaction between experienced people willing (or appointed to) answer the token.

The framework of VLE sketched here should consists of three parts, as explained in further detail in the next sub-paragraphs:

- The Simulator, with local stand-alone simulation learning features, covering the relevant aspects of quality systems and quality tools for general employee training, mainly addressing common technical knowledge.

- The Case Database, which can be accessible either in local or in remote fashion using standard web-based technologies, integrating company/project specific cases and/or documents to support training, mainly addressing explicit knowledge.
- The Virtual Interactive Open-Space, based on the new Web technologies, oriented to on-the-job teaching and on-line interactive problem solving, mainly addressing common technical, explicit and even tacit knowledge.

A general user interface and a set of web-oriented facilities for management of training session as well as a set of services for synchronous and asynchronous communication supporting collaborative learning should complete the VLE. The user-friendly interface should facilitate the navigation within the environment and the access to all the facilities of the VLE (e.g. access to a video conference session without initialisation problems upon verification of true need of access; etc.). It can be realised, for instance, on the basis of graphic metaphors recalling a training centre, with rooms and offices where "virtual" training takes place.

Advanced didactical methods and techniques have also to be employed to support multilingual and multicultural curricula as well as to stimulate learning, as explained in the next paragraphs.

The VLE should adopt the most advanced Information Technologies: a careful attention should be paid in using these latter, taking into account the degree of confidence of industrial personnel with IT, as well as the fact that it should be the user to control the process of knowledge improvement and management not vice versa. For instance, virtual reality simulators should carefully used because of some statistics reveal 1/3 of the users to suffer from kinetosis.

In the same way, the number of degree of freedom in exploring didactical contents has to be carefully controlled as to avoid the 'get lost' syndrome.

3.1 THE SIMULATOR

The VLE here sketched should allow the trainee to learn by himself using simulation sessions; s/he should also be allowed to play the role of several skill levels within the company, allowing s/he to explore a virtual firm with appropriate guide to give help and answers during the navigation.

The idea is to represent a "virtual enterprise", to give a lively simulation of the plant environment, based on graphical interfaces, embedding interactive multimedia tutorial and toolkit for understanding how implementing quality system quality tools.

Appropriate didactical approaches has to be designed to adapt knowledge (explicit and/or common technical one) to the new training approach, in order to favourite the "learning by exploring" approach and, at the same time, assuring a smoother increase of the didactical complexity during the learning sessions, to fit the specific training needs of industrial personnel.

3.2 THE CASE DATABASE

Simulation of real operation condition is not enough for customised learning; the trainee has to face practical problem-solving situations. To this aim we propose to build a case database, with a structured access according to an interactive decision-making process, under the control of appropriate software agents.

For software agent we intend here a software tool designed to perform a specific function and acting as a controller running under the main application environment but hidden to the user.

The knowledge base, to our view, should embed explicit company-specific knowledge. Very accurate approach has to be devised in structuring cases, as this may affect the efficiency of training sessions. Database access has to be made in fact through a question & answer mechanism, thus acting as a virtual on-the-job learning.

The database, at regimen, should be an on-line buffer of testimonial cases, to be updated dynamically via question/answer sessions with experts, and also linked to Simulator's applications. Users seeking answers to questions can search directly for the relevant information in the database or, if not available, ask questions to experts responding to the question. Answers coming back to the knowledge base, may become dynamically available in the future for everybody having access to it. The experts can be both corporate or external experts appointed specifically for training purposes.

Initial data base building process should be as follows: 1) data collection from existing sources (concern database; dis-quality records according to standard procedures; etc.) 2) homogenisation of them according to a common didactical structure; 3) implementation of the database; 4) creation of 'data marts', i.e. smallest part of the database which should be accessible in read-only mode by trainees concerning a specific quality subjects.

The database should be made such as each record represents a cube with n-dimension, where the n-dimension should represent the n-unit in which the firm is divided: production, marketing, administration, and so on, as to allow the user to understand what total quality means involving all the functions of the business.

3.3 THE VIRTUAL INTERACTIVE OPEN-SPACE

As to favourite group-ware training and also to assure a true problem-solving approach, a virtual interactive communication open space should be implemented to support collaborative learning through asynchronous and synchronous communication tools.

This virtual communication space should be realised setting a network (either open or closed one) and using advanced IT technologies oriented towards virtual live-sessions of training, discussion and interaction between different people (we call this "*Virtual Quality Circle*"). The open space, on the other hand, should give the opportunity to the trainee to communicate asynchronously or synchronously, based on a common problem or theme concerning quality, with previously designated subject-matter experts and share their expertise independently from the country or even the company of origin.

Partners, even suppliers or client, sharing the same technologies, should greatly take advantage from this interaction.

The asynchronous communication tool is intended, in this ideal sketch of VLE, here to facilitate collaboration and knowledge transfer independently of their spatial or temporal location of experts. It should also allow an ongoing audit trail of significant events, meetings and communications regarding one or more topics with links to supporting documents, training and resources.

The synchronous collaboration tool instead is here intended to enable on-line collaboration, tutoring or training using vis-a-vis debates by means of facilities for application sharing, common web browsing, multi-point Internet telephone, question and answer mode and video conferencing.

A special software agent (i.e. automatic tracking procedure with statistical records) has to be provided to allow measurement of the training sessions. Special care should be devoted in setting the agents for 'hollow' interactions, such as videoconferencing or unstructured mailing communications!.

4. EMBEDDED TEACHING STRATEGIES

People empowerment is reached by a clear definition of what and when things are required from them; people should be allowed the ability to grasp the situation for themselves and understand the guidelines in which they can operate. Explaining at trainee's request new jargon, new procedures, new routines and even new languages would simplify understanding and consequently increase the involvement, interest and contribution increases. As stated before, much of quality learning process - especially in attitudes, but to an appreciable extent also in knowledge and skill - take places very informally and almost imperceptibly during the course of a man's regular working day. Part of it is forced upon him during the finger-burning of on-the-job experience; a great deal of it comes about as a result of the daily contacts between the man and his superior; part of it results from the exposure of the man to his fellows workers.

Stimulating learning by means of curiosity in the VLE is an important aspect to be considered. Education is a product and the teacher should serve much the same function in producing educated people as does the supervisor in manufacturing products. The new emerging paradigm in teaching is, in fact, the Total Quality teaching [4]. Today's tutor is expected to design work enignment that stimulate interest, award systems that stimulate initiative and expectations that challenge and then coach each trainee individually to success.

To do so, VLE here proposed should allow to access to a variety of experts (or knowledge sources) easily and quickly, with a constant and reliable support oriented to problem-solving; s/he should have also the opportunity to compare and contrast the different opinions of the different experts. This aspect would be addressed by the virtual interactive open space.

The VLE didactical architectures should embed these concepts and be designed to bring trainees to the point that they want to know something, searching amongst different topics which has thus to be appropriately structured.

A mixed teaching strategy is here suggested, particularly for the Simulator of the VLE, to overcome the standard passive approaches in training. The trainee should thus be allowed to move without any pre-defined scheme: appropriate software agents have to recognise his/her actions and assist him/her to learn something which is near his/her implicit requirements; some recurring mistakes, actions or questions might allow the software agents to intervene appropriately to the user's need.

To leverage the processes of 'natural learning', VLE must offer answers on an as-needed basis allowing a certain degree of freedom. This means trainee must be allowed to try things out and fail in a simulation fashion. It also means trainees must be given answers only after they have generated questions and/or have attempted to solve it several times unsuccessfully.

Sometime, trainees might not know how to formulate questions neither he know exactly how to ask something before knowing it: multiple key-points access to simulation scenarios can be adopted to address this problem.

Much of human reasoning is case-based rather than rule-based: the database architecture should address this idea. When people solve problems, they frequently are reminded of previous problems they have faced. We are constantly accumulating cases and comparing those cases to the cases we have already accumulated in a effort to understand the next case that will appear. This should be the way cases and knowledge are build in the database.

In the "learning by doing" approach the trainee experiences failures, times when s/he realises that s/he needs new information in order to progress. Such are the times when 'case-based teaching' can provide the knowledge that trainee needs. Because isolated facts are difficult for trainees to integrate into their memories, useful knowledge is typically best presented in the form of stories or, better, metaphors.

5. LEARNING EFFECTIVENESS ASSESSMENT

Training is now a *must* statement, it has to be done for every company: but how much it is effective?. The widely accepted concepts of "measure it to control it" has also to be applied also to training since this activity is becoming a very important investment for companies. It is very hard to correctly measure the training effects and to demonstrate that is training to make the difference. In several situations, standard measures commonly adopted are: productivity; customer complaints; scraps; etc. The problem is that many of the measurable outcomes at work are influenced by different factors as well as training.

We suggest to address this specific problems within the VLE using appropriate strategies and implementing these using specific software agents. Several things might be eligible for measuring:

- 1) reaction of participants to training; for instance measure of training satisfaction . To derive in-progress information about the training session as well as at the very end of it has become a quite standard practice since the last two decades. Questionnaire and/or multiple answer tests are the most used one; recently the interview technique has been introduced. This basis might be sometime invalidated by subjective trainee factors.
- 2) Learning, i.e. the difference between pre and post-course knowledge and skill. Learning, unless practised and reinforced, is too soon forgotten. The true efficiency of the learning process, which is a result of two factors -the ability of the trainee to rapidly understand and the capacity of the teacher to stimulate attention and curiosity to learn- should be checked after a certain period of time since the learning phase. This period should be longer enough as to allow the enthusiasm to settle down and to see if the contents of the course has taken place in the standard practice of everyday's habits. A follow up tracking procedure has to be settled down based on a training need assessment to this aim.
- 3) Behavioural changes, which can be measured later (three-months) and is best judged or rated by subordinated of the trainees. Other objective measures are revenue generation, end-user or customer satisfaction (most popular but difficult to relate only to training), speed of process at the work unit.
- 4) Costs, which should be broken down into segments: direct labour (teachers); direct labour (trainee). The cost data not necessary provide a reliable measure of the training effectiveness, since costs may represent a too aggregate information. Furthermore, accurate operating quality-cost report should be available from the existing accounting system.

The VLE should contain customised built-in '*software agent*', which should be an intelligent software able to perform specific tasks in background on the interactions between trainee and VLE. According to the above, objective indicator of learning efficiencies and, if it is possible of effectiveness, should and can be provided within the modules of VLE.

The idea of software agents here suggested is to assess learning effectiveness based on accurate tracking of each session during the learning stage, using either statistics automatically collected during the interaction of the user with the applications. For the specific session these can be frequency of mistakes, time to answer, learning paths followed, etc. Tracking the session should be made with the agreement of trainee, since this fact might strongly influence the success in using the VLE.

A different approach should be provided where using 'hollow' approaches for interaction, such as videoconferencing, in which the evaluation become very difficult: it should be delegated using standard approaches to skilled personnel as well as to a subjective questionnaire to be completed by answer of the trainee.

5. DISCUSSION

The virtual learning environment sketched in the paper is thought to address selectively different skill levels with a problem-solving guided approach. The exploration of practical cases has to be favoured and explained at trainee's demand in their resolution via appropriate software agents. Trainee may enter the environment with a specific request or question; a guided path should allow him to access the proper tools, didactic material and or experts (e.g. corresponding personnel in another site) as to allow her/him multi-faced possibility to solve given training (hopefully real) problem.

Mainly four principles should be respected in building the environment:

- 1) concentrate upon practical, meaningful quality material and case studies;
- 2) training material should be made consulting the line organisation to the fullest extent possible, especially in regards to the scope and the kinds of material to be used in the programs;
- 3) continuous improvement should be strongly encouraged, through several means, since the solution to the industrial problems are always changing and thus education contents and education for educators too;
- 4) individual approach (tailored upon the specific level of personnel to fit the specific needs) since interests and objectives differ widely among organisation levels: middle-upper management; practitioners; skilled workmen and assembly operators; shop personnel and so on.

6. CONCLUSIONS

Training is not a cost but an investment, an enablement, indeed a necessity. But is this investment worth it? Does training affect the bottom line? The VLE architecture sketched in this paper moves into the direction of improving the efficiencies as well as the effectiveness of training activities by means of a new approach to the training activities. It may address also a very critical problem faced in industry: motivation of personnel in using the quality culture and attitude. It allows in fact 1) the opportunity to understand according to proper needs, avoiding declaring any personal fault to anyone; 2) to 'dress the daddy's clothes', allowing trainee to play different roles, thus promoting cross-cultural exchanges between higher and lower skill levels.

ACKNOWLEDGEMENTS

The authors wish to thank Dr. A. Ulloa Severino - Grifo Multimedia s.r.l., Tecnopolis - 70010 Bari -Italy - for the support given in discussing contents in paragraph 3

REFERENCES

1. Dankbaar, B., Bouwman, B. December "The training network of the European automotive supply industry: training and knowledge transfer", Coppa Consultancy, The Netherlands, 1998, 1-20
2. Chase, N., "Raise your training ROI", Quality On Line, <http://qualitymag.com/0997f3.html>, 1997, 1-16
3. Swist, J., "Conducting a training needs assessment", AMX International Inc., 1997, 1
4. Mc Vey, R.S., "Total quality teaching as Analogous to Total Quality management", <http://fairway.ecn.purdue.edu/asec/sect95/1A/1A4.html>, 1995, 1-8

AUTHOR INDEX

	Page		Page
Alberti N.	53	Durante S.	207
Andes T.	799	Ferrante A.	651
Andreadis G.	273	Festa C.	843
Antonelli D.	353, 393	Fichera S.	485, 875
Appunkuttan K.K.	301	Filice L.	385, 611
Atik A.	39	Filippi S.	573
Barcellona A.	353	Fioretti M.	323
Bariani P.F.	323	Formentelli M.	825
Basile V.	385	Fragomeni J.	329
Belinski R.A.	677	Franco A.	545
Bergamin A.M.	573	Fratini L.	369, 377
Berger L.-M.	125	Freguia D.	851
Bertagnolio A.	97	Galetto F.	833
Blanchini F.	635	Gallina P.	643
Blank P.	125	Gasparetto A.	445, 643
Borsellino C.	163, 361, 611	Gatto A.	565
Bouzakis K.D.	215, 273, 437	Gentili E.	825, 843
Bracali P.	711	Giannopoulos G.	437
Braglia M.	843	Giardini C.	257, 461
Brenner W.	721, 729	Giovagnoni M.	445
Brnic J.	337	Gorting K.	753
Brookes E.J.	107	Grasso V.	485
Bugini A.	257	Grendel H.	65
Canadija M.	337	Groppetti R.	711
Capello E.	687	Grum J.	603, 619, 763
Caracciolo R.	643	Guggia R.	851
Carbone V.	703	Gunasekera J.S.	677
Casalino G.	583	Gunther G.	65
Celano G.	875	Guseo R.	859
Ceretti E.	145, 257, 461	Gutema T.	711
Chabrier P.	737	Haddad G.	721
Chatzitheodoridis E.	721, 729	Heinrich W.	753
Chryssolouris G.	197, 289	Henriques E.P.	223
Colosimo B.M.	627	Hofer E.P.	249
Comoglio M.	207	Hung N.P.	171, 179
Cukor G.	241, 265, 315	Ippolito R.	187, 231
Custro A.	377	Iuliano L.	231
Dabala' M.	419	Jakovljevic M.	729
Dal Negro T.	323	Jakupec S.	529
Das S.K.	807, 883	James R.D.	107
De Bona F.	745, 771, 791	Jovane F.	25
De Chiffre L.	703	Jurkovic M.	265, 521
De Toni A.	477	Karpuschewki B.	117, 145
Del Taglia A.	667	Kindermann P.	753
Deshpande A.S.	301	Kljajin M.	815
Di Lorenzo R.	345, 369	Knight W.A.	799
Dini G.	545	Krajewsky W.	651
Donnarumma A.	515	Krell A.	125
Duffait R.	721	Krimmel O.	427
Dukovski V.	659	Kuljanic E.	11, 241, 445, 591

	Page		Page
Kursawe S.	753	Rabazzana F.	207
Kustagi V.K.	301	Randjelovic S.	401
La Commare U.	485	Rasch F.O.	427
La Spada A.	485	Ren X.	107
Lanzetta M.	545, 695	Richter V.	125
Lepschy A.	651	Romano D.	97, 393
Levi R.	97	Ruisi V.F.	155, 163, 361, 611
Lim S.W.	171	Russo M.	851
Ljubetic J.	315	Santochi M.	545
Lo Casto S.	155, 377	Savio E.	703
Lo Valvo E.	309	Sawodny O.	249
Lucchini E.	155	Sbaizero O.	155
Ludovico A.D.	583	Schiefer E.	39
Maccarini G.	257, 461	Schleinkofer U.	753
Magrini M.	419	Schlund P.	753
Marinsek G.	557, 591	Schmidt B.C.	453
Martin P.	281, 737	Schneider M.	137
Martins R.	729	Schulz H.	39
Martinsen K.	427	Sciamanda M.	187
Masan G.	469	Semeraro Q.	687
Maschio S.	155	Sergi V.	781
Meausoone P.J.	281	Settineri L.	187
Memola Capece Minutolo F.	781	Smoljan B.	411, 493
Meneghetti A.	477	Socket H.G.	753
Merchant M.E.	3	Sorby K.	507
Mesquita R.M.D.	223	Staffieri A.	573
Miani C.	573	Stoiljkovic V.	401
Miani F.	445, 573, 591, 635	Strozzi A.	745, 791
Miani S.	635	Sturm R.	619
Micari F.	53, 345, 385, 611	Tantussi G.	545, 695
Micheletti G.F.	81	Tonnessen K.	427
Mikac T.	521	Tonshoff H.K.	65, 117, 469, 537
Milcic B.	529	Trovato G.	825
Monno M.	627	Tsirbas K.	197
Mortarino C.	867	Turkalj G.	337
Mourtzis D.A.	197, 289	Udiljak T.	529
Mrsa J.	493	Vaccari P.	745
Mussig B.	453	Vedovato G.	419
Nassimbeni G.	499	Veerapanini B.	883
Ostendorf A.	537	Vezzetti E.	231
Palumbo B.	781	Viaro U.	635, 651
Pandilov Z.	659	Vujanic A.	721, 729
Paolasini S.	557	Warnecke H.J.	1
Pappalardo M.	515	Weinert K.	137
Paraskevopoulou R.	215	Winkler J.	117, 145
Pekic Z.	521	Wurmsdobler P.	721
Peper C.	537	Xeromerites E.D.	289
Perrone G.	485	Yang J.	703
Perugini S.	667	Zannis S.	197
Petrovic D.	729	Zanzero M.	573
Piacentini M.	163	Zelenika S.	771, 791
Pilgrim J.	453	Zhong Z.W.	171, 179
Popovic G.	721, 729	Zuljan D.	603